Modeling Macro-scale Clay Behavior at Micro-scale Clay Particle Interfaces

Laura M. Kösoğlu

Dissertation submitted to the faculty of the Virginia Polytechnic Institute and State University in partial fulfillment of the requirements for the degree of

Doctor of Philosophy

In

Civil Engineering

George M. Filz, Chairman
Thomas L. Brandon
Joseph E. Dove
Michael F. Hochella, Jr.
James K. Mitchell

March 28, 2011
Blacksburg, VA

Keywords: Clay, creep, secondary compression, friction, AFM

Modeling Macro-scale Clay Behavior at Micro-scale Clay Particle Interfaces

Laura M. Kösoğlu

ABSTRACT

Clay consolidation has generally been considered from a macro-scale perspective by measuring the macro-scale compression of a clay soil over time. Clay particles in consolidation tests experience shear and normal forces at the inter-particle level due to force applied to the soil at the macro-scale. These shear and normal forces cause the particles to slide at the micro-scale and produce macro-scale changes in soil volume and shape. By considering the inter-particle interactions at the micro-scale, the shear force - normal force - velocity relationship can be described by the Rate Process Theory (RPT). This research investigated the use of the RPT for analyzing sliding at individual clay particle contacts during secondary compression to describe macro-scale clay behavior.

The novel micro-scale friction experiments conducted in this research demonstrated that an Atomic Force Microscope (AFM) can be used to obtain coefficient of friction (μ) measurements for montmorillonite. This method allows for the measurements to be performed over spatial scales of a few microns, can be done under dry conditions or a wide range of aqueous solutions, and requires no calibration beyond making a few microscopic measurements of the probe. Control tests of silica on mica ($\mu = 0.29 \pm 0.02$) agree with literature values where limits indicate one standard deviation. μ values for wet and dry sodium montmorillonite were determined to be 0.20 ± 0.03 and 0.72 ± 0.03, respectively.

The micro-scale AFM and macro-scale triaxial shear, ring shear, and direct shear experimental data of μ as a function of sliding velocity were found to match well with those calculated using common RPT parameter values. The activation energy for the macro-scale triaxial shear and corresponding micro-scale friction regime experiments fall within the expected range for pure montmorillonite of 84–109 kJ/mol. Additionally, the micro-scale and macro-scale experimental results fall within the expected range for the number of bonds per unit of normal force of 10^7–10^9 bonds/N.

A discrete element method (DEM) model was developed to calculate thin, disk-shaped clay particle movement in three dimensions during compression using the RPT as a contact model. The DEM compression results were compared to macro-scale consolidation experiments conducted on the same reference clay as the micro-scale AFM experiments. The influences on the compression of the number of bonds at each clay contact per unit of normal contact force and the activation energy were quantified. Increasing the activation energy decreased the compression, as expected. Similarly, increasing the number of bonds per unit of normal force at the contacts decreased the compression, as expected. Realistic clay fabrics with varying particle sizes, particle size distributions, and aspect ratios led to a compression model with behavior similar to the macro-scale laboratory compression tests.

This research provides evidence of the close correspondence between macro-scale and micro-scale μ measurements and contributes to multi-disciplinary understanding of factors that control friction between clay particles and deformation of clay masses. The results from this work can be applied to a wide range of time-dependent phenomena such as clay secondary compression, shear deformation, and fault dynamics behavior.

ACKNOWLEDGEMENTS

I would like to thank my advisor, Professor George M. Filz, for his guidance throughout my doctoral studies. I have been honored to work with such a distinguished researcher, devoted teacher, and a true professional over the years. He is a role model for me as I continue my career.

I would also like to recognize the professors who served on my committee: Professors Thomas L. Brandon, Joseph E. Dove, Michael F. Hochella, Jr., and James K. Mitchell. Their interest and input in my research have been very helpful.

Thanks also go to Professor Barry R. Bickmore from the Department of Geological Sciences at Brigham Young University. His genuine excitement about my research and encouragement were invaluable as I ventured outside of my own discipline. I also wish to thank Diane Moore from USGS for her helpful comments.

I would like to thank Professor Özer Çinicioğlu at Boğaziçi University in İstanbul, Türkiye who allowed me to work in his laboratory to conduct experiments overseas.

Funding for this research was provided by the U.S. National Science Foundation (Grant No. DGE-0504196) and the Charles E. Via, Jr. Department of Civil and Environmental Engineering at Virginia Tech. Without this financial support, this study would not have been possible.

Thanks also go to my parents, John R. Hannum and Eleanore P. Hannum, brothers, Matthew J. Hannum and Daniel J. Hannum, and sister-in-law, Meghan A. Hannum, who have all been incredibly supportive of me as I have pursued my Ph.D. studies.

Finally, I would like to thank my husband, Mehmet Alpaslan Kösoğlu, who pursued his Ph.D. in Mechanical Engineering at Virginia Tech at the same time. I am thankful for his support and love over the years.

TABLE OF CONTENTS

LIST OF FIGURES

CHAPTER 5: INTEGRATION OF FRICTION AND CLAY MINERALOGY

CHAPTER 6: MICRO-SCALE EXPERIMENTS - MATERIALS AND METHODS

CHAPTER 7: MICRO-SCALE EXPERIMENTS - RESULTS AND DISCUSSION

CHAPTER 8: MACRO-SCALE EXPERIMENTS

CHAPTER 9: DISCRETE ELEMENT METHOD - MODEL SET-UP

CHAPTER 10: DISCRETE ELEMENT METHOD - MODEL RESULTS AND DISCUSSION

LIST OF TABLES

Chapter 1

Introduction

This chapter discusses the motivation for this research in Section 1.1 and the interdisciplinary focus in Section 1.2. The research objective and research outline are provided in Sections 1.3 and 1.4, respectively.

1.1 Motivation

Loading of saturated clays results in compression due to the transfer of stress from the water phase to the solid phase associated with hydrodynamic expulsion of water from the clay, known to geotechnical engineers as primary consolidation. Volume changes can also result from the continuing adjustment and breakage of clay particles, which can occur under constant effective stress and is termed secondary compression. A sample compression curve depicting the representation of these phases is shown in Fig. 1.1.

While Terzaghi's consolidation theory (Terzaghi, 1923) for standard one-dimensional consolidation tests is currently used to estimate field consolidation settlement, it is well known (Shirako *et al*., 2006) that the actual consolidation behavior differs from that predicted by Terzaghi's theory. Terzaghi's theory assumes that the soil fabric behaves as an elastic body, and creep is not incorporated. The difference between observed field compression and those values predicted by theory is attributed to secondary compression (Shirako *et al*., 2006).

Secondary compression can be important for normally consolidated clay and organic soil, such as fibrous peat. Soils with greater organic content experience greater secondary compression settlement (Leonard and Girault, 1961). Settlement from preloading clay can lead to unexpectedly large magnitudes of secondary compression (Adachi *et al*., 1986; Crawford and Morrison, 1996). It can also be difficult to determine the coefficient of consolidation from laboratory tests on soils exhibiting large secondary compression (Lambe and Whitman, 1969).

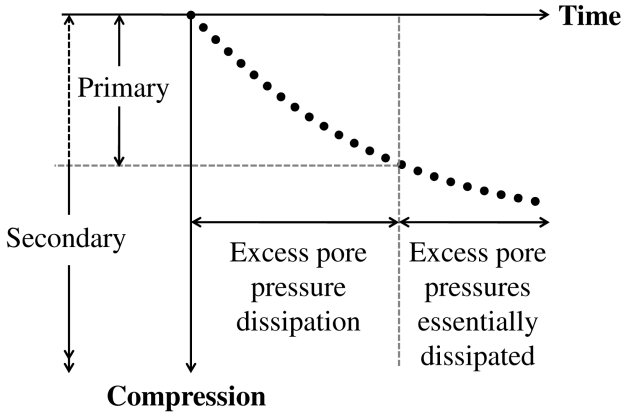

Fig. 1.1: Compression as a function of time depicting primary consolidation and secondary compression.

Another complicating factor in settlement analyses is when secondary compression occurs simultaneously with primary consolidation. After spending much time studying consolidation, Taylor (1948) came to the conclusion that secondary compression occurs during primary consolidation as well as after the completion of

primary consolidation. Olson (1998) compared the measured hydraulic conductivity during consolidation tests to the values calculated based on Terzaghi's consolidation theory. The ratio of measured to calculated hydraulic conductivity varied from 1.9 to 4.4 for San Francisco Bay Mud. The ratios for other clays are also provided by Olson (1998), who attributed the difference between the measured and calculated values to secondary compression. Water expulsion from the soil does not prevent particle readjustment and secondary compression from occurring simultaneously.

In the field, where clay layers can be relatively thick, primary consolidation can take months or years to complete. For these cases, large secondary compression effects are even more likely to occur during the primary consolidation phase. Understanding secondary compression from a theoretical basis may lead to a more complete understanding of primary consolidation. This study hypothesizes that secondary compression is related to the friction between the clay particles.

Besides secondary compression, the friction between minerals also plays a fundamental role in the study of fault dynamics. The behavior and shear strength of discontinuities in geological masses vary as a function of the residual friction angle (Price, 2009). The residual friction angle is related to the resistance of the failed shear surface after considerable movement. The friction coefficient, μ, is also used to determine the angle at which a fault should form (Bunds, 2001). A range of earthquake phenomena have been explained based upon time-dependent "rate and state" friction laws that incorporate empirical parameters, often considering both field data and laboratory rock friction experiments (Scholz, 1998). Multiple lines of evidence suggest that the strength of many faults is significantly weaker than would be expected based upon the friction

values determined for rocks in laboratory experiments (Zoback, 2000; Holdsworth, 2004), although multiple hypotheses continue to be tested (Zoback *et al*., 2010).

The presence of relatively weak minerals, such as phyllosilicates with low μ values, may contribute to overall fault weakness. While it has long been recognized that the fine-grained broken and chemically altered gouge material along the active traces of faults often contains clay minerals (Wu *et al*., 1975; Solum *et al*., 2006; Schleicher *et al*., 2009; Solum *et al*., 2009), experimental evidence suggests that large volume percentages or localized concentrated zones of clay minerals might be required to account for field observations (Tembe *et al*., 2006; Carpenter *et al*., 2009). Detailed observations of materials from depth in an actively creeping section of the San Andreas fault (the San Andreas Fault Observatory at Depth or SAFOD project, Zoback *et al*., 2010) led to a variety of relevant findings. Talc, known to have extremely low friction coefficient values, was discovered in cuttings of serpentinite from rocks that are believed to be currently creeping (Moore and Rymer, 2007). Additionally, localized <100 nm thick coatings of several clay minerals, including illite-smectite and chlorite-smectite, crystallized relatively recently (~4-8 Ma) on the surfaces of gouge grains (Schleicher *et al*., 2010). These observations present the possibility that networks of low-friction phyllosilicates could be responsible for weakening of the San Andreas and other faults (Kopf and Brown, 2003; Colletini *et al*., 2009). Another complication is that while laboratory experiments and modeling suggest the friction coefficient of phyllosilicates is lowest when the preferred orientation of the basal planes is maximized (Wintsch *et al*., 1995; Kock and Huhn, 2007; Collettini *et al*., 2009), field studies suggest that clay fabrics are not oriented except perhaps at very localized scales (Solum *et al*., 2009; Wenk *et al*.,

2010). Thus, friction measurements of smectite and mixed-layer clay minerals can contribute to the evolving understanding of fault slip.

These applications consider friction as a macro-scale phenomenon. The value of the friction coefficient is often assumed to be scale-independent (Gao *et al.*, 2004), but this may not always be the case. Therefore, it is sometimes useful to investigate the friction coefficient as a function of spatial scale to test hypotheses about the mechanisms controlling friction. For example, Kuhn and Mitchell (1993) provided evidence that clay creep may be controlled at the molecular scale by the arrangement of silica tetrahedra rather than by the macro-scale surface roughness of the clay particles. Similarly, Dieterich and Kilgore (1994) attributed frictional forces in rocks to small-scale forces operating at contact points. However, no method was then available to measure friction at microscopic scales.

1.2 Interdisciplinary Focus

Support for this work was provided, in part, by the U.S. National Science Foundation (NSF) under grant No. DGE-0504196. The NSF Integrative Graduate Education and Research Traineeship (IGERT) program supports Virginia Tech's Exploring Interfaces through Graduate Education and Research (EIGER) Ph.D. fellowships. Support was also provided by the Via Foundation of the Charles E. Via, Jr. Department of Civil and Environmental Engineering at Virginia Tech.

One of the goals of EIGER is to explore critical interfaces without discipline-specific boundaries and to aid in interdisciplinary research. This research considers the interfaces between clay particles undergoing compression. Both macro-scale and micro-

scale compression were considered to develop a better understanding of the mechanisms at play. A novel method was developed through interdisciplinary collaboration to measure the friction coefficient between micro-scale clay coated surfaces.

1.3 Research Objective

The objective of this research is to evaluate a theoretical relationship among shear force, normal force, and velocity at the interfaces between clay particles and use this relationship to determine the magnitude of macro-scale compression of a clay soil mass.

1.4 Research Outline

The scope of work for this research consists of eight tasks in four phases, as shown in Fig. 1.2.

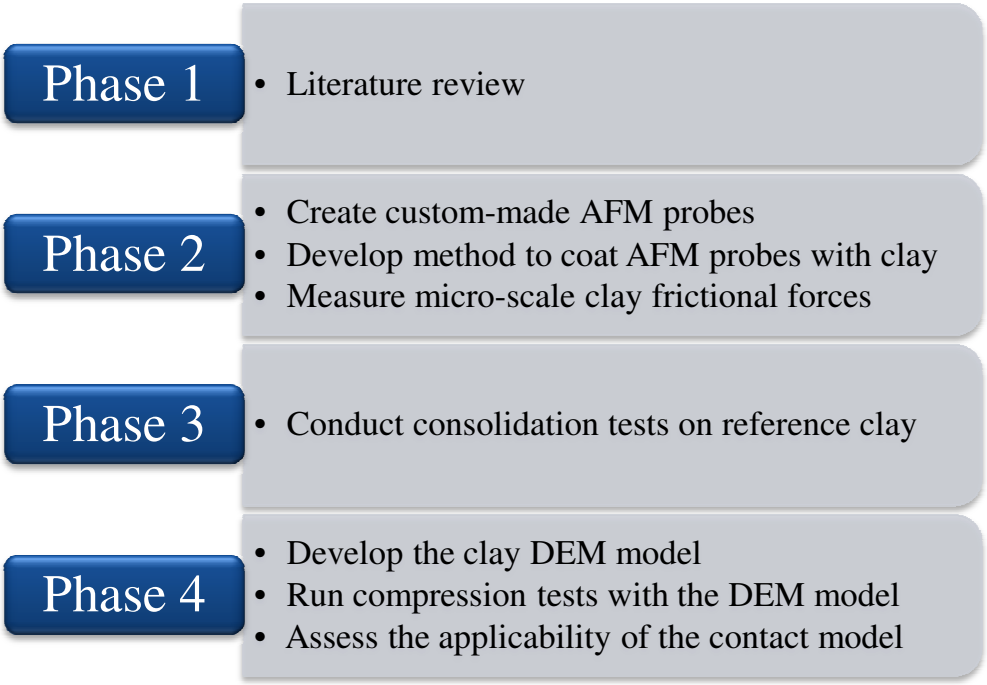

Fig. 1.2: Research outline

Chapter 2

Brief Review of Consolidation and Secondary Compression Theories

This chapter provides an overview of different consolidation (Section 2.1) and secondary compression (Section 2.2) theories.

2.1 Overview of Consolidation Theories

Starting with Terzaghi's linear elastic theory in 1923, various consolidation theories have been proposed over the years to describe both the time rate and magnitude of consolidation and compression of soil. These theories will be briefly discussed as they are critical to the understanding of consolidation and historically significant to the field of geotechnical engineering.

Using three rheological elements (spring, dashpot, and slider) and arranging them in parallel or series, a large variety of models to describe clay consolidation and compression are possible. A spring represents linear or nonlinear elastic behavior, and the elastic deformation occurs instantly after stress application. In rheological models, elastic springs have immediate and total recovery upon stress removal. When the lateral strain is constant, such as for a consolidation test, the slope of the stress (σ) – strain (ε) plot is the constrained modulus (M). Fig. 2.1 depicts the $\sigma - \varepsilon$, σ – time (t), and $\varepsilon - t$ relationships for a spring.

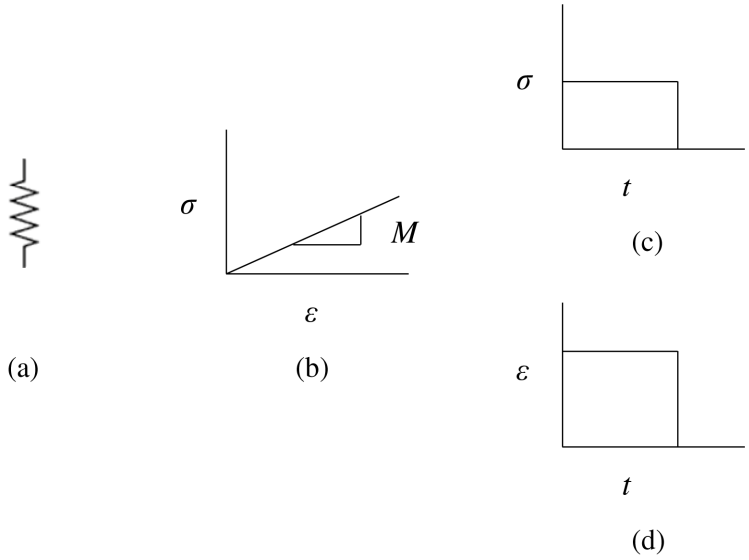

Fig. 2.1: Rheological model spring behavior; (a) Symbol, (b) $\sigma - \varepsilon$, (c) $\sigma - t$, (d) $\varepsilon - t$.

A dashpot is a piston moving freely in a cylinder filled with liquid with a small hole in the cylinder to allow the liquid to escape. Dashpots are used to model materials that exhibit viscous behavior. Fig. 2.2 depicts the $\sigma - \dot{\varepsilon}$, $\sigma - t$, and $\varepsilon - t$ relationships for a dashpot.

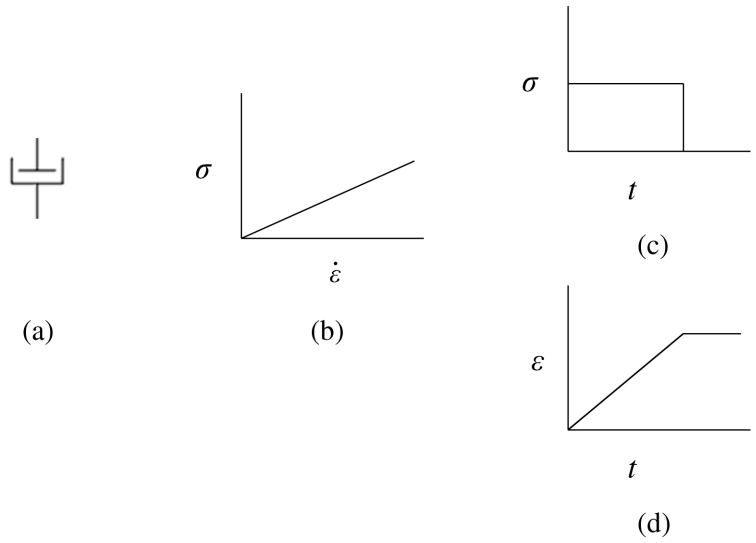

Fig. 2.2: Rheological model dashpot behavior; (a) Symbol, (b) $\sigma - \dot{\varepsilon}$, (c) $\sigma - t$, (d) $\varepsilon - t$.

Sliders represent plastic behavior. No change in length occurs until the applied stress exceeds the yield stress, σ_y. After that stress is reached, the slider will slip to an unlimited extent even if the stress remains constant. The strain is unrecoverable upon stress removal. Fig. 2.3 depicts the $\sigma - \varepsilon$, $\sigma - t$, and $\varepsilon - t$ relationships for a slider.

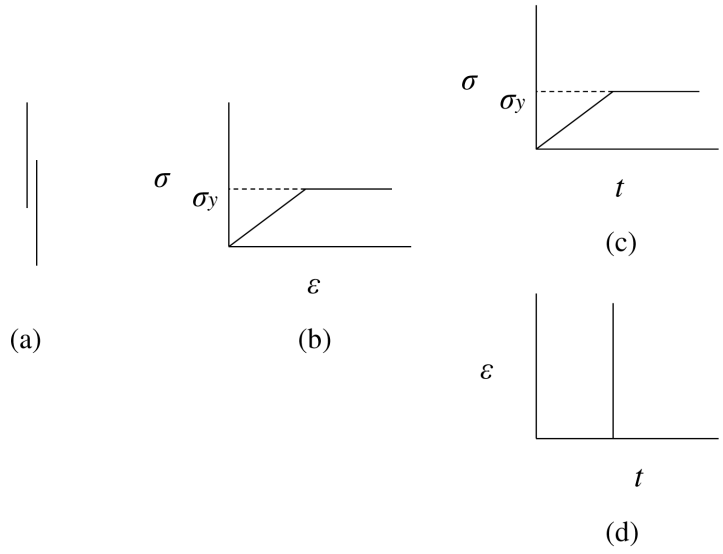

Fig. 2.3: Rheological model slider behavior; (a) Symbol, (b) $\sigma - \varepsilon$, (c) $\sigma - t$, (d) $\varepsilon - t$.

Terzaghi's model (1923) was based on the assumption that consolidation can be modeled as time-independent linear elastic compression. For a given spring constant and applied stress, the soil will compress according to Hooke's law of linear elasticity where strain is proportional to stress. This model is depicted in Fig. 2.4a. All of the models in Fig. 2.4 are effective stress models and do not include dissipation of excess pore water pressure during primary consolidation.

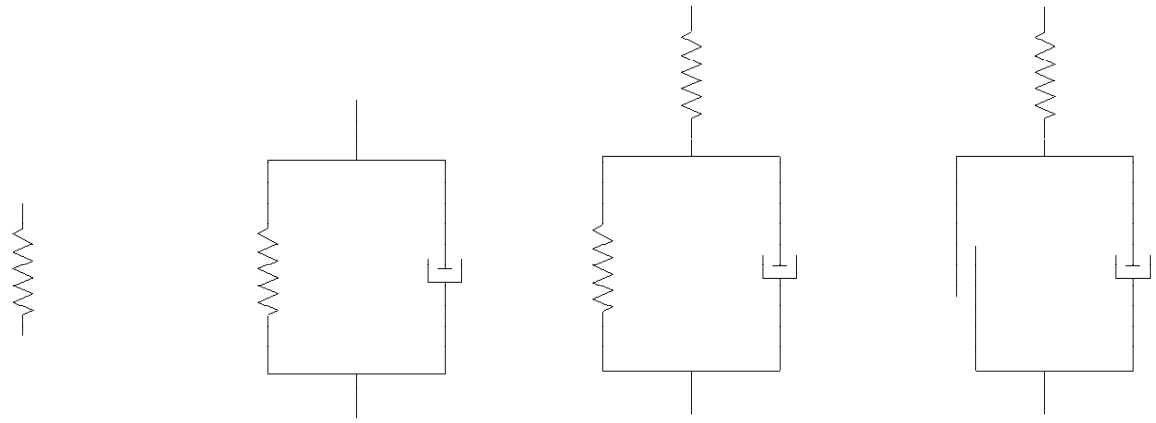

(a) (b) (c) (d)

Fig. 2.4: Summary of discussed effective stress rheological models of compression; (a) Terzaghi (1923), (b) Taylor (1942), (c) Taylor and Merchant (1940), (d) Garlanger (1972).

There are several assumptions for Terzaghi's one-dimensional consolidation theory:

1. The clay is homogeneous, and the degree of saturation is 100%.
2. Drainage occurs at the top and/or bottom of the compressible layer.
3. The compression and the water flow occur in one dimension.
4. Darcy's law applies.
5. The soil grains and pore water are incompressible.

6. The load increment results in low strains so that the coefficient of permeability, k, and the coefficient of compressibility, a_v, are constant.
7. Secondary compression does not occur.

In 1942, Taylor modified the Terzaghi model to include a viscoelastic component (spring and dashpot in parallel), as shown in Fig. 2.4b. The dashpot behavior is controlled by the viscosity of the pore fluid. When a load is applied, the dashpot initially supports the load and then over time gradually transfers the load to the spring. Over time with constant applied stress, the strain rate approaches zero, the stress on the dashpot approaches zero, and the stress on the spring approaches the total applied stress to the system. Taylor and Merchant (1940) developed another model to include a spring in series with the viscoelastic component. The resulting elastic-viscoelastic model is shown in Fig. 2.4c. Both springs and the dashpot behave in a linear fashion.

Garlanger (1972) proposed an elastic-viscoplastic model (Fig. 2.4d) to capture both the elastic and plastic behavior of soil. For this model, there are two sets of constitutive equations: one when the applied stress is less than the yield stress of the slider and one when the applied stress is greater than the yield stress of the slider.

2.2 Overview of Secondary Compression Theories

Secondary compression can be a significant aspect of clay behavior. Three-dimensional finite element creep analyses conducted on the foundation soils of the leaning tower of Pisa (Bai *et al.*, 2008) determined that creep effects caused 1.7º of the

tower's famous 5.5º tilt. Creep effects also account for approximately 1 m of settlement of the tower.

Gibson and Lo (1961) used the Taylor and Merchant (1940) model to estimate the time rate of secondary compression strain for large values of time where excess pore pressures due to loading have dissipated, meaning at times greater than the time indicating the end of primary consolidation, t_p:

$$\varepsilon(t) = \Delta\sigma\left(a_1 + a_2\left(1 - e^{-\left(\frac{a_3}{a_2}\right)(t-t_p)}\right)\right), \quad t > t_p$$

where $\Delta\sigma$ = applied consolidation stress

a_1, a_2, a_3 = empirical parameters determined from test data

This method was found to accurately estimate secondary compression for certain secondary compression curve shapes especially when the coefficient of secondary compression, C_α, was constant. However, the method has generally been found to require excessively long duration consolidation tests to determine the empirical values of a_1, a_2, and a_3, or the assumption that the ratio of a_3/a_2 is constant must be made, which may not be accurate (Dhowian, 1991).

Juárez-Badillo (1985) proposed a general time-dependent equation for the soil volume change associated with creep:

$$e = \frac{e_f}{1 + \left(\frac{t}{t^*}\right)^{-\xi}}$$

where e_f = final void ratio at $t = \infty$

t^* = characteristic time for which $e = 0.5e_f$

ξ = shear fluidity (reciprocal of viscosity) of the clay

While the model is quite simple compared to the model proposed by Gibson and Lo (1961), it does require knowledge of the final void ratio, which can often only be estimated given time constraints. Also, the shear fluidity of the clay is required, which is not typically measured.

Stolle *et al.* (1999) proposed another model for clay creep based on parameters determined from standard laboratory tests. If the normal effective stress is increased from σ_0 to σ, then the total strain after time, t, is given by:

$$\varepsilon = A\ ln\left(\frac{\sigma}{\sigma_0}\right) + C\ ln\left[1 + \left(\frac{\sigma}{\sigma_{p0}}\right)^{B/C}\frac{t}{\tau}\right]$$

$$A \approx \frac{C_s}{2.3(1+e_0)} \qquad B \approx \frac{C_C - C_s}{2.3(1+e_0)} \qquad C \approx \frac{C_\alpha}{2.3(1+e_0)}$$

where σ_{p0} = preconsolidation pressure

τ = time scale determined by fitting the equation to the macro-scale consolidation test data

C_s = swelling index

C_c = compression index

C_α = secondary compression index

One of the theoretical limitations of the creep model proposed by Stolle *et al.* (1999) is that it does not take into account temperature. It has been shown (Mitchell *et al.*, 1968; Smyth, 1983; Boudali *et al.*, 1994; He *et al.*, 2002) that temperature affects the creep rate of soil. Therefore, a temperature correction factor might need to be applied to the model parameters to account for this effect.

Yin (1999) proposed a hyperbolic function to describe the non-linear creep strain, $\Delta\varepsilon$, of clay:

$$\Delta\varepsilon = \frac{\psi_o' ln[(t + t_o)/t_o]}{1 + (\psi_o'/\Delta\varepsilon_1) ln[(t + t_o)/t_o]}$$

where t_o = time at which secondary compression starts

t = time after secondary compression starts

$\Delta\varepsilon_1$ = creep strain limit

ψ_o' = initial value (at $t = 0$) of the ratio of ψ to specific volume

$\psi = C_\alpha$ / ln 10

C_α = secondary compression coefficient

Methods of determining the parameters in the hyperbolic model using curve fitting techniques are described in more detail in Yin (1999). Robinson (2003) experimentally verified that a hyperbolic function best described the secondary-compression as a function of time relationship for kaolinite, red soil, silty soil, and peat.

Hinchberger and Qu (2009) proposed an elastic-viscoplastic constitutive model to calculate clay creep. A state-dependent viscosity parameter was used to incorporate the

response of a rate-sensitive clay fabric where weak cementation bonds may form between particles and affect the clay micro-structure. This model was tested on Saint-Jean-Vianney clay and found to describe the clay's creep behavior.

The focus of the current study is on the use of Rate Process Theory (RPT) to describe secondary compression. Time is incorporated indirectly into the theory through deformation-dependent mechanisms that are based on changes in soil structure. Chapter 3 provides greater detail on RPT.

Chapter 3

Rate Process Theory

This chapter provides the derivation of the Rate Process Theory in Section 3.1 and the theory applied to clay creep in Section 3.2.

3.1 Rate Process Theory Derivation

The theoretical model used in this study is based on the Rate Process Theory (RPT) developed by Eyring (1936) in the discipline of physical chemistry. The diffusion of gases, chemical reactions, flow of liquids, and soil particle contact zone behavior are described as rate processes because they all involve the relative movement of atoms or molecules (Keedwell, 1984).

During the application of a shear stress to a material, there is a net relative movement of atoms in the direction of the applied stress (Keedwell, 1984). The general premise of the theory is that each contact zone is made up of an assembly of atoms and

molecules, termed “flow units.” These flow units, which are in the process of being deformed, are constrained from movement due to energy barriers which separate adjacent equilibrium positions, as shown in Fig. 3.1. For the flow units to be displaced to new positions, they must become “activated” by acquiring sufficient energy to surmount the energy barrier. The movement is inhibited by the free energy of activation, ΔF, which is a measure of bonding strength (Kuhn and Mitchell, 1993). When a shear force is applied, the original energy barrier becomes distorted in two ways. First, the energy barrier shifts horizontally by δ, which is the elastic distortion of the material structure. Second, the energy barrier height decreases in the direction of the applied shear force due to the additional force and increases in the opposite direction, as shown by the change from Curve A to Curve B (Fig. 3.1). As a result, the structure will shift in the direction of the applied shear force if the supplied energy exceeds the activation energy.

The kinetic energy of an atom varies with temperature, and the flow units, which are on the atomic scale, are in oscillatory motion about a mean position. The Boltzmann constant relates energy at the molecular level with temperature at the bulk level. To convert energy to frequency, the Planck constant is used. The mean frequency of oscillation, ω, is:

$$\omega = \frac{kT}{h}$$

where k = Boltzmann constant = 1.38×10^{-23} J/K

T = absolute temperature [K]

h = Planck constant = 6.62×10^{-34} J-s

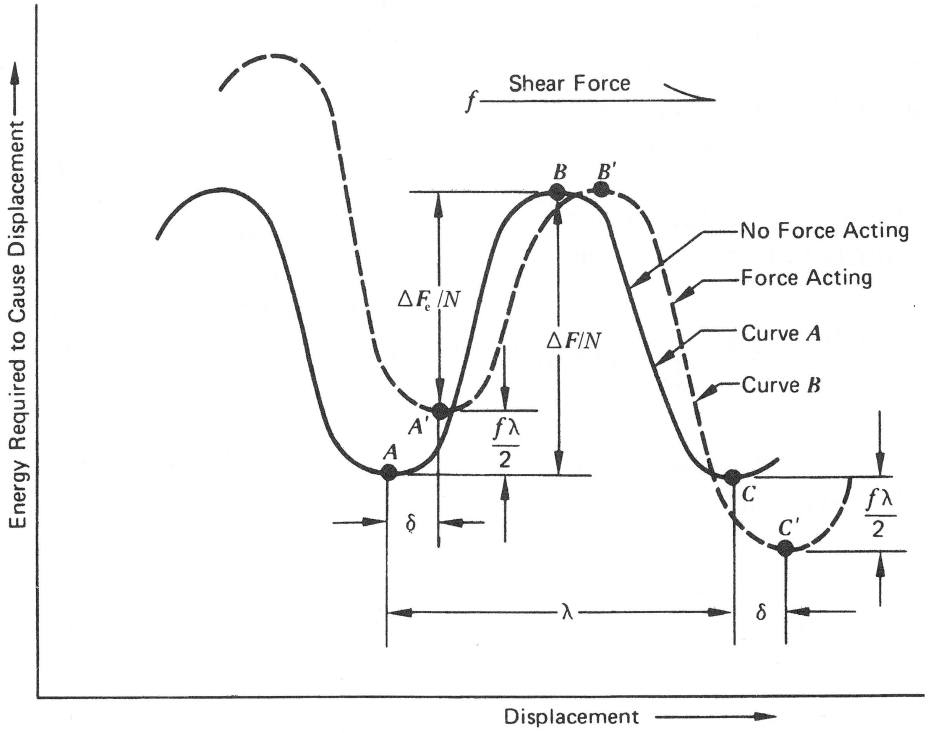

Fig. 3.1: Energy barriers separating equilibrium positions and effect of a shear force on energy barriers (Mitchell and Soga, 2005).

The division of thermal energies among the flow units is given by the Boltzmann distribution function. The probability of an energy state being greater than an arbitrary energy value of ΔE is:

$$p(\Delta E) = e^{-\frac{\Delta E}{kT}}$$

Therefore, the frequency of bond rupture or activation, υ, is ω multiplied by the probability of achieving an energy state greater than ΔE.

$$\upsilon = \frac{kT}{h} e^{-\frac{\Delta E}{kT}}$$

For a bond rupture to occur, an atom must move by $\lambda/2$, where λ is the distance between successive equilibrium positions, as discussed in greater detail below. Essentially λ is related to the mean spacing of atoms. When the clay is in an unstressed state, bond ruptures have equal probability of occurring in all directions, and therefore the net movement of the clay is zero. If a shear stress is applied to the clay, the chance of bond rupture in the direction of the force increases, as explained in the earlier energy barrier discussion. Since the movement of the flow unit is assisted by the applied force, the energy required for bond rupture, E, is reduced to:

$$E = \Delta E - \frac{f\lambda}{2}$$

where f = average applied force per flow unit

As shown in Fig. 3.1, the energy barrier height will essentially decrease by $f\lambda/2$ in the direction of the force and increase by $f\lambda/2$ in the opposite direction of the force. Thus, the energy barrier in the direction of the force and opposite to the direction of force are $\Delta E - f\lambda/2$ and $\Delta E + f\lambda/2$, respectively. Therefore, the net frequency of activation or net frequency of bond rupture in the direction of the applied force is:

$$v_{net} = \frac{kT}{h}\left(e^{\frac{-\left(\Delta E - \frac{f\lambda}{2}\right)}{kT}}\right) - \frac{kT}{h}\left(e^{\frac{-\left(\Delta E + \frac{f\lambda}{2}\right)}{kT}}\right)$$

$$v_{net} = \frac{2kT}{h}\left(e^{-\frac{\Delta E}{kT}}\right) sinh\left(\frac{f\lambda}{2kT}\right)$$

The activation energy, ΔF, is the minimum energy per mole required for bond rupture. Given that $k = R/N$, where R is the universal gas constant equal to 8.31 J/(mol-K) and N is the Avogadro constant, $\Delta F/R$ can be substituted for $\Delta E/k$ such that:

$$\upsilon_{net} = \frac{2kT}{h}\left(e^{-\frac{\Delta F}{RT}}\right) sinh\left(\frac{f\lambda}{2kT}\right)$$

The net frequency of activation or net frequency of bond rupture, υ_{net}, is the frequency with which a flow unit is displaced a distance λ between successive equilibrium positions in the direction of applied force. The strain rate is thus:

$$\dot{\varepsilon} = X\upsilon_{net} = X\frac{2kT}{h}\left(e^{-\frac{\Delta F}{RT}}\right) sinh\left(\frac{f\lambda}{2kT}\right)$$

X is proportional to the number of flow units in the direction of deformation, which may be both time and structure-dependent. For most solid deformation problems, $f\lambda/2kT$ is greater than one (Mitchell *et al.*, 1968). Therefore, the strain rate can be approximated with:

$$sinh\left(\frac{f\lambda}{2kT}\right) \approx \frac{1}{2}e^{\left(\frac{f\lambda}{2kT}\right)}$$

as

$$\dot{\varepsilon} = X\frac{kT}{h}\left(e^{-\frac{\Delta F}{RT}}\right)\left(e^{\left(\frac{f\lambda}{2kT}\right)}\right)$$

The sliding velocity, $\dot{s}$, is the net frequency of activation multiplied by the distance between equilibrium positions.

$$\dot{s} = \lambda v_{net} = \frac{2kT\lambda}{h}\left(e^{-\frac{\Delta F}{RT}}\right) sinh\left(\frac{f\lambda}{2kT}\right)$$

3.2 Rate Process Theory Applied to Clay Creep

To relate the RPT to clay, three questions need to be answered:

1. What is the distance, λ, between successive equilibrium positions for the clay?
2. What is the average applied force per flow unit, f, for the clay?
3. What is the free energy of activation, ΔF, for the clay?

Previous research (Andersland and Douglas, 1970; Christensen and Wu, 1964) has shown that the flow units which participate in soil creep have atomic dimensions, such as individual oxygen atoms moving across the cleavage plane. Wei *et al.* (2000) conducted AFM lateral force microscopy experiments to visualize the lattice of muscovite mica, and a representative AFM image is shown in Fig. 3.2. Erlandsson *et al.* (1988) have shown that λ can be taken as the distance between atomic holes in the hexagonal arrangement of SiO_4 tetrahedra, making λ = 0.53 nm. This value is different from the value used by Kuhn and Mitchell (1993), who took λ equal to the diameter of an oxygen ion, making λ = 0.28 nm. As noted by Mitchell and Soga (2005) and explained

below, even if λ is changed, the relative proportion of λ to the number of flow units per unit area, S, will still be the same.

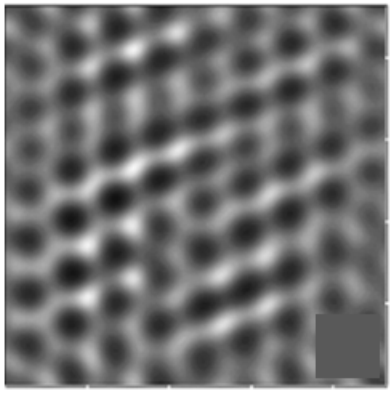

Fig. 3.2: Muscovite mica surface. Lighter areas correspond to locations of greater friction. The square image is 4.64 nm by 4.64 nm (Wei *et al.*, 2000).

The next parameter of interest is the average applied force per flow unit, f, which is:

$$f = \frac{f_t}{n}$$

where f_t = tangential contact force

n = number of bonds at the contact

In previous work (Kuhn and Mitchell, 1993), n has been defined as:

$$n = n_1 f_n$$

where n_1 = number of bonds per unit of normal contact force

f_n = normal contact force

This yields the following RPT formula for sliding velocity at the particle contacts:

$$\dot{s} = \frac{2kT\lambda}{h}\left(e^{-\frac{\Delta F}{RT}}\right) sinh\left(\frac{\lambda}{2kT}\frac{f_t}{n_1 f_n}\right)$$

Efforts have been made (Mitchell *et al*., 1969) to estimate the value of n_1 based on macro-scale creep tests at different effective stresses. Mitchell *et al*. (1969) proposed that the number of bonds formed between two particles is proportional to the compressive force transferred at their contact. The average applied force per flow unit, f, for the clay can be defined as:

$$f = \frac{\tau}{S}$$

where τ = shear stress on the clay

S = number of flow units per unit area

Mitchell *et al*. (1969) assumed that the number of flow units equals the number of inter-particle bonds. On the plane of maximum shear stress, f is defined as:

$$f = \frac{D}{2S}$$

where D = deviator stress under triaxial stress conditions

Therefore, the strain rate can be calculated by:

$$\dot{\varepsilon} = X\frac{kT}{h}\left(e^{-\frac{\Delta F}{RT}}\right)(e^{\alpha D})$$

where $\alpha = \frac{\lambda}{4SkT}$

The parameter α can be determined from the slope of the plot of log strain rate vs. stress. The strain rate is measured at the same time after the start of creep for several different stress increments. α is constant for a given value of effective consolidation pressure. Once α is determined experimentally, λ/S can be determined. Finally, S can be determined, using the appropriate value of λ. The relationship between S and the effective consolidation pressure, p_0, has been found to be constant for normally consolidated soils (Mitchell *et al*., 1969), such that:

$$S = S_1 p_0$$

where S_1 = number of bonds per unit area per unit of mean effective stress

Mitchell *et al*. (1969) determined the values of S_1 to be nearly constant for a given soil. The range of values of S_1 for different soil types was found to be 1 x 10^9 to 1 x 10^{10}

bonds/N. Therefore, adjusting for the revised value of λ discussed above, this yields the range of values of S_1 to be 1.9 x 10^9 to 1.9 x 10^{10} bonds/N.

Mitchell *et al.* (1969) took the average number of bonds per contact as proportional to the number of bonds formed along a plane. Additionally, the average f_n at a contact was assumed to be proportional to p_0 (Cundall and Strack, 1983). Therefore, n_1 should be proportional to S_1 such that:

$$n_1 = cS_1$$

where c = proportionality factor

Kuhn and Mitchell (1993) used the Discrete Element Method (DEM) to estimate the parameter, c. Using assemblies of two dimensional disks, they determined the proportionality factor, c, to be 0.2. Therefore, n_1 ranges from 3.8 x 10^8 to 3.8 x 10^9 bonds/N. Values at both the upper and lower range were used in the current study.

The last parameter, the free energy of activation, ΔF, is a measure of bond strength. This parameter has been studied extensively by Mitchell *et al.* (1969) and Andersland and Douglas (1970). The following observations were made (Mitchell and Soga, 2005):

1. ΔF is relatively large and is much greater than the activation energy of the viscous flow of water.

2. The following changes to the soil have no significant effect on ΔF: changes in water content (even complete drying), adsorbed cation type, consolidation pressure, void ratio, and pore fluid.
3. Sand and clay have similar ΔF values.
4. Clay in suspension such that a continuous structure cannot be formed deforms with a ΔF equal to that of water.

The typical range of ΔF values for soils undergoing creep deformation is 80-180 kJ/mol (Mitchell and Soga, 2005). Values of ΔF can be determined by measuring the experimental activation energy, ΔF_e, using Dorn's Method (Tietz and Dorn, 1956). Dorn's Method is a useful method to determine ΔF_e since the strain rates need to be determined at two different temperatures for identical soil structures. In this procedure, the soil creeps under a constant deviator stress, D_1, at temperature, T_1. The temperature is then increased rapidly to T_2 while D_1 is held constant. Just before the temperature increase, the strain rate, $\dot{\varepsilon}_1$, is determined. Immediately after the temperature increase, the strain rate, $\dot{\varepsilon}_2$, is determined. ΔF_e is thus determined by:

$$\Delta F_e = \frac{2.3RT_2T_1}{T_2 - T_1} log\left(\frac{\dot{\varepsilon}_2 T_1}{\dot{\varepsilon}_1 T_2}\right)$$

Finally, the activation energy used in the sliding velocity equation requires ΔF, which is greater than ΔF_e. ΔF_e and ΔF are related by:

$$\Delta F_e = \Delta F - \frac{f\lambda N}{2}$$

where N = Avogadro constant = 6.02 x 10^{23} mol^{-1}

Chapter 4

Review of Applicable Clay Mineralogy

This chapter provides a review of clay mineralogy that is discussed later in this research. It is divided up by crystal structure (Section 4.1), layer charge (Section 4.2), and electrostatic separation energy (Section 4.3).

4.1 Crystal Structure

Rate Process Theory (RPT), described in Chapter 3, is a micro-scale model based on fundamental properties of the clay crystal structure. As discussed in Chapter 5, macro-scale friction experiments on a wide variety of clays have demonstrated that the coefficient of friction of clay varies depending on the clay structure, layer charge, and electrostatic separation energy, among other factors. Therefore, a review of such crystal structures and terms are discussed in this chapter.

4.1.1 Sheet Silicates

Sheet silicates, or phyllosilicates, consist of hexagonal arrangements of silica tetrahedra, as shown earlier (Fig. 3.2) using an AFM. Sheet silicates include the clay minerals, mica group, serpentinite group, and chlorite group.

Phyllosilicates are typically classified as either 1:1 or 2:1 layer silicates. 1:1 indicates that one silica tetrahedral sheet is bonded to one octahedral sheet. Kaolinite and serpentine are examples of 1:1 phyllosilicates. 2:1 layer silicates have two silica tetrahedral sheets surrounding one octahedral sheet. Examples of 2:1 phyllosilicates are micas, vermiculite, and montmorillonite.

Phyllosilicates are also categorized by the type of octahedral sheet they contain. Octahedral sheets that contain predominantly trivalent cations such as Al^{+3} and Fe^{+3} are called dioctahedral sheets because only two out of every three of the octahedral sites are filled. Phyllosilicates are classified as trioctahedral when they contain predominantly divalent cations such as Mg^{+2} and Fe^{+2}, resulting in all three octahedral sites being occupied.

Another phyllosilicate classification is the number of isomorphous substitutions in the mineral structure and whether the substitution occurs in the tetrahedral or octahedral sheet. Isomorphous substitution occurs when one ion in the crystal structure is replaced by another ion of similar charge and radius without changing the crystal form. When one cation is replaced by another of lower valence, there is a deficiency of positive charge. In the tetrahedral sheet, Si^{+4} can be replaced by Al^{+3}, and in the octahedral sheet, Al^{+3} or Fe^{+3} can be replaced by Mg^{+2}. The net negative electric charge created by the isomorphous substitution is compensated by the adsorption of cations on the surface. This

phenomenon leads to the development of the diffuse double layer between adjacent silica sheets. Generally, isomorphous substitution is not significant in 1:1 phyllosilicates, meaning that these minerals have a very low permanent layer charge.

4.1.1.1 Clay Minerals

The clay mineral group consists of a variety of phyllosilicates such as montmorillonite, kaolinite, illite, talc, pyrophyllite, vermiculite, halloysite, and palygorskite. Montmorillonite, kaolinite, talc, and pyrophyllite are discussed in further detail in this research, and therefore will be introduced in this section.

4.1.1.1.1 Montmorillonite

Montmorillonite is part of the smectite group, which also contains nontronite and beidellite. Montmorillonite is a 2:1 dioctahedral sheet silicate with an idealized chemical formula of $(Na)_{0.33}(Al_{1.67}Mg_{0.33})Si_4O_{10}(OH)_2$. Typically, isomorphous substitution occurs in the octahedral sheet for montmorillonite. Cations may be present between the layers to balance charge deficiencies created by the ionic substitutions discussed earlier. Montmorillonite is also characterized by a high swell potential.

Montmorillonite is common in poorly drained or dry soils that have been weathered from magnesium rich rocks (Schaetzl and Anderson, 2005). The crystal structure for montmorillonite is shown in Fig. 4.1. All of the crystal structure figures in this chapter were generated using CrystalMaker v6.1, a software program by CrystalMaker Software Ltd.

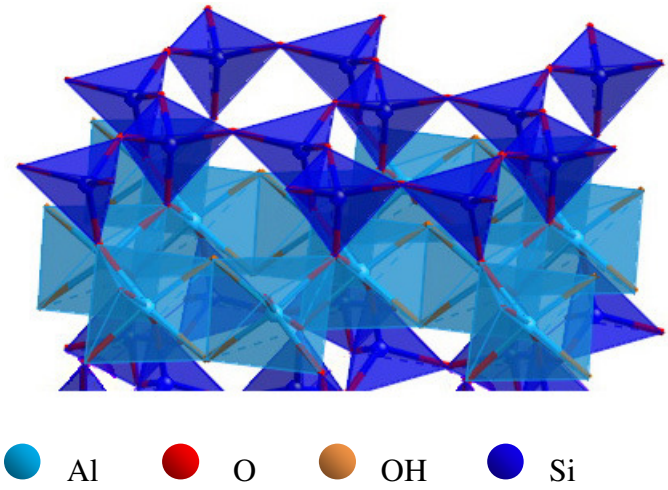

Fig. 4.1: Montmorillonite crystal structure.

4.1.1.1.2 Kaolinite

Kaolinite is part of the kaolin group, which also contains dickite and nacrite. Kaolinite is a 1:1 dioctahedral sheet silicate with a formula of $Al_2Si_2O_5(OH)_4$. Kaolinite typically has little to no isomorphic substitution and therefore has negligible layer charge. However, adjacent 1:1 layers are held together by hydrogen bonds between the hydroxide of the octahedral sheet and the oxygen of the tetrahedral sheet, leading to low swell potential. Kaolinite typically forms from the weathering of other aluminosilicates in slightly acidic, well-drained, and highly weathered soils in which silica, calcium, and magnesium have been removed by leaching (Dixon, 1989). The crystal structure for kaolinite is shown in Fig. 4.2.

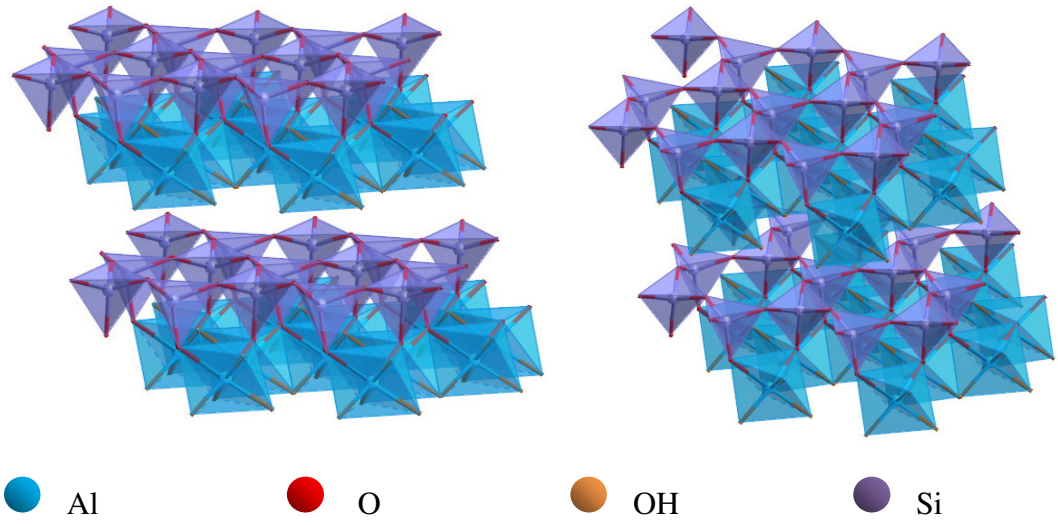

Fig. 4.2: Kaolinite crystal structure.

4.1.1.1.3 Talc

Talc is a trioctahedral 2:1 sheet silicate mineral with an octahedral sheet composed of magnesium. The ideal formula unit is $Mg_3Si_4O_{10}(OH)_2$. No isomorphic substitution occurs and the 2:1 layers are uncharged. Therefore, the interlayer bonding between tetrahedral sheets is mostly controlled by weak dispersion forces (Schaetzl and Anderson, 2005). The weak interlayer forces allow the layers to easily shear past each other, leading to a low coefficient of friction. Talc may contribute to fault weakness, as discussed in Chapter 1.

Talc has a low swell potential (Kleijn and Oster, 1982) and primarily forms from the hydration and carbonation of serpentine. The crystal structure for talc is shown in Fig. 4.3.

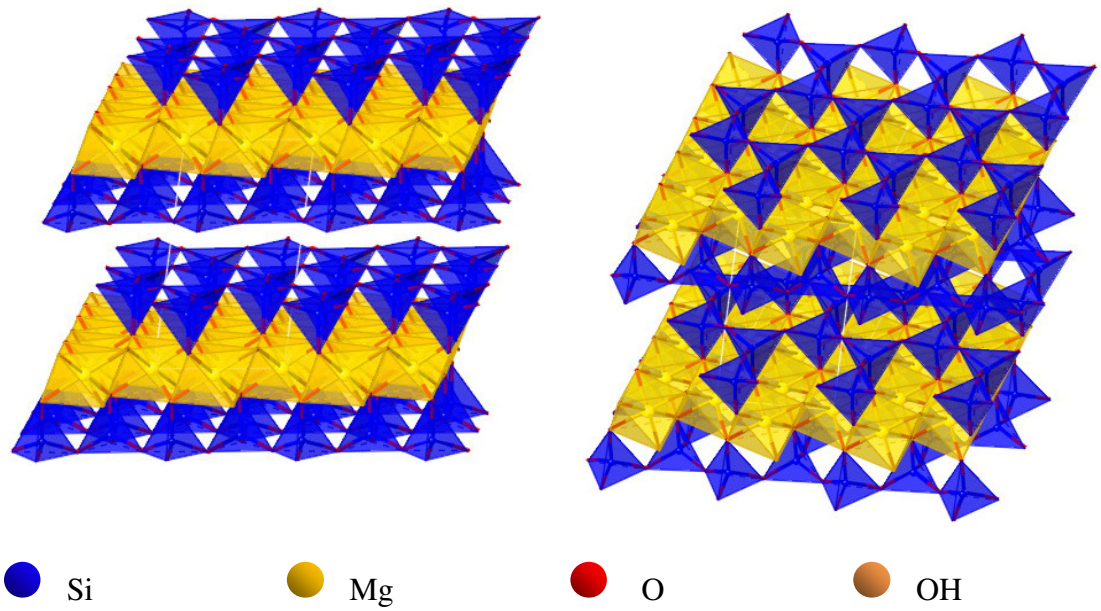

Fig. 4.3: Talc crystal structure.

4.1.1.1.4 Pyrophyllite

Pyrophyllite is a dioctahedral 2:1 sheet silicate mineral with an octahedral sheet composed of aluminum. The ideal formula unit is $Al_2Si_4O_{10}(OH)_2$. Each stack of three intralayers is electrically neutral. Even though montmorillonite and pyrophyllite have similar crystal structures, pyrophyllite has a low swell potential (Kleijn and Oster, 1982). The difference is that substitution in the octahedral sheet of montmorillonite is balanced by interlayer cations, which attract water molecules. The weak interlayer van der Waals bonds can be easily overcome due to the interlayer water, leading to swelling in montmorillonite (Moore and Lockner, 2004).

Pyrophyllite is found in aluminum rich metamorphic rocks or as a result of hydrothermal alteration of acidic volcanic rocks (Kogel *et al.*, 2006). Pyrophyllite exists in two ordered forms, or "polytypes." The most commonly occurring is a two layer monoclinic form, pyrophyllite-2M, but a single-layer triclinic form, pyrophyllite-1Tc,

also occurs. Many disordered varieties also occur. The crystal structure of Pyrophyllite-1Tc is shown in Fig. 4.4, and the crystal structure of Pyrophyllite-2M is shown in Fig. 4.5.

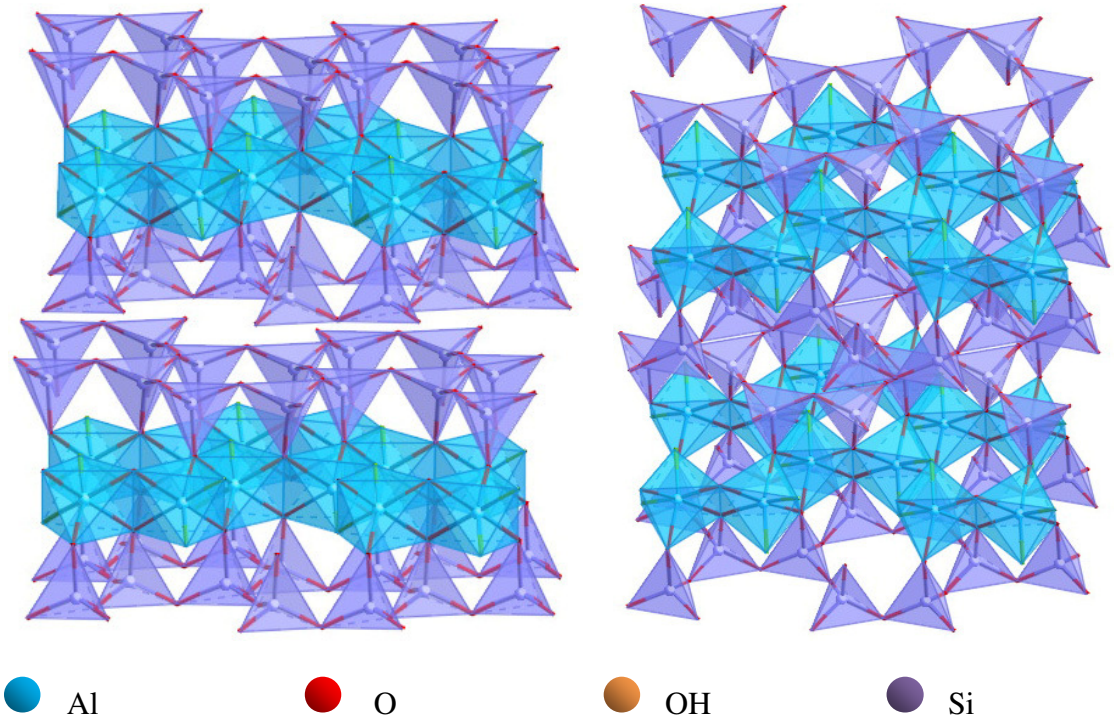

Fig. 4.4: Pyrophyllite-1Tc crystal structure.

4.1.1.2 Mica Group

The mica group is a group of phyllosilicates characterized by perfect basal cleavage. Muscovite, margarite, biotite, phlogopite, lepidolite, and glauconite are in the mica group. The first three of those listed will be discussed in this section as they pertain to this research.

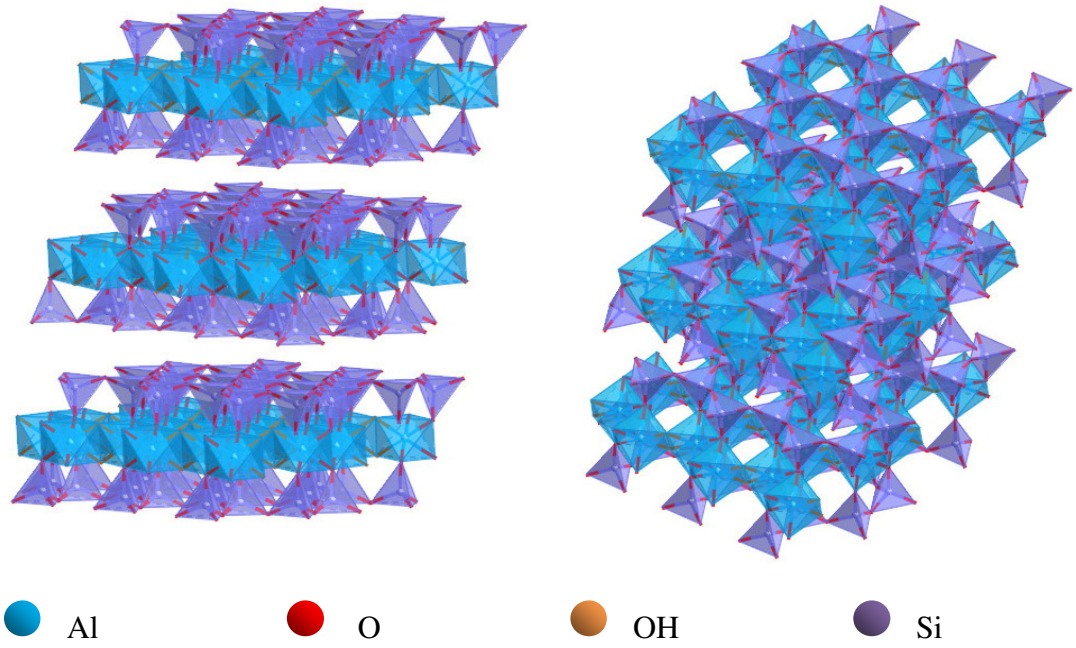

Fig. 4.5: Pyrophyllite-2M crystal structure.

4.1.1.2.1 Dioctahedral Mica

This section discusses the dioctahedral micas muscovite and margarite.

4.1.1.2.1.1 Muscovite

Muscovite is one of the most common mica minerals, and it can be found in a wide variety of rocks. Muscovite is a 2:1 sheet silicate that forms thin, virtually-transparent flakes. One quarter of the tetrahedral sites is occupied by aluminum, and the remaining sites are occupied by silicon. The ideal formula unit is $KAl_2(Si_3Al)O_{10}(OH)_2$.

Isomorphic substitution of lower valence cations for higher valence cations occurs in the tetrahedral and/or octahedral sheet. The layer charge is approximately 1.0 mol per formula unit. The negative charge is balanced by interlayer potassium ions (Moore and Lockner, 2004), which are strongly bound by electrostatic forces. Due to the high layer

charge and interlayer cations, muscovite has a very low swell capacity, unlike montmorillonite. Muscovite is found in granitic igneous rocks and metamorphic rocks. The most common polytype is the 2M1 form, as shown in Fig. 4.6.

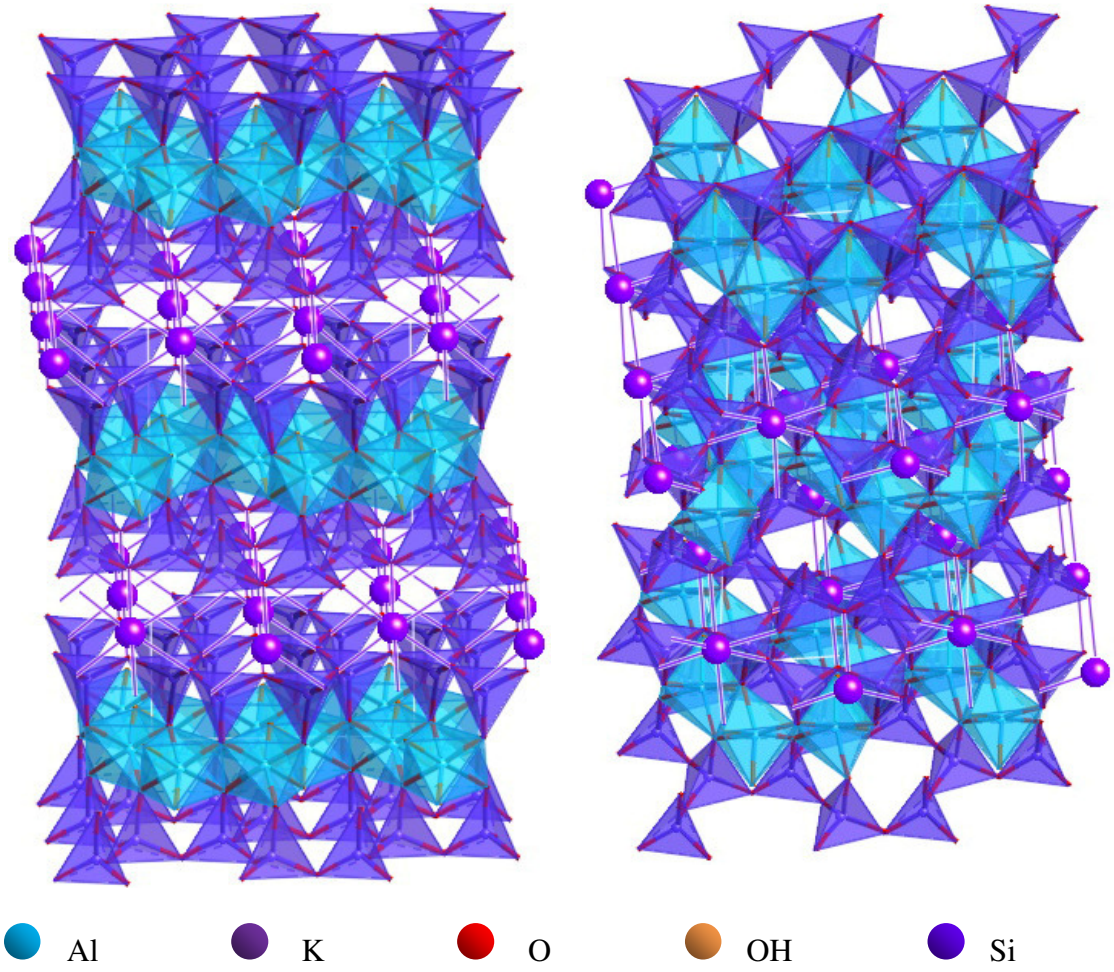

Fig. 4.6: Muscovite-2M1 crystal structure.

4.1.1.2.1.2 Margarite

Margarite is a dioctahedral 2:1 sheet silicate with a structure (Fig. 4.7) analogous to that of muscovite. One half of the tetrahedral sites are occupied by aluminum, and the remaining sites are occupied by silicon. The ideal formula unit is $CaAl_2(Si_2Al_2)O_{10}(OH)_2$.

Margarite is an unusual mica in that it has calcium as the interlayer cation to balance the layer charge. This makes the mineral harder, and its cleavage sheets are more brittle. As a result, margarite is referred to as a brittle mica.

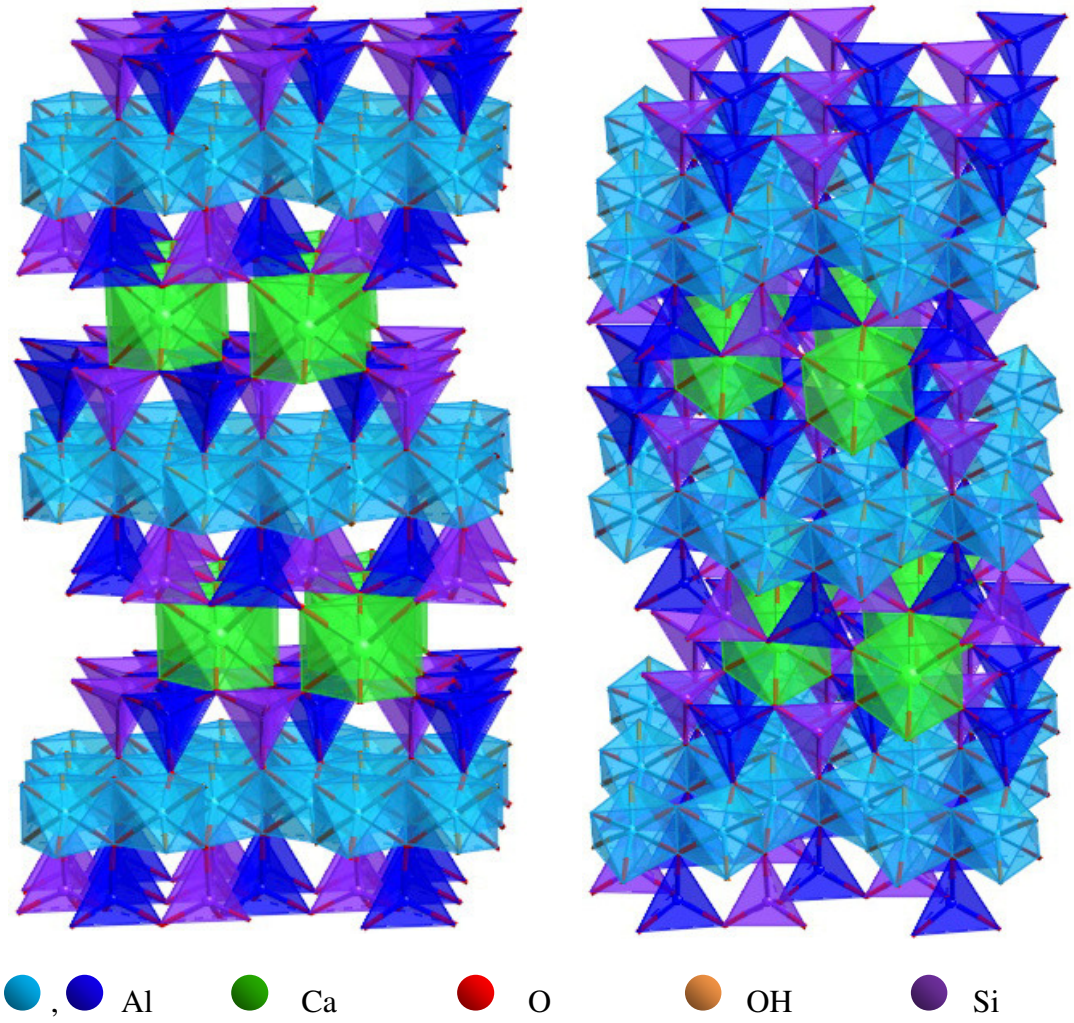

Fig. 4.7: Margarite crystal structure.

4.1.1.2.2 Trioctahedral Mica

Biotite is a 2:1 sheet silicate with a crystal structure consisting of trioctahedral sheets containing magnesium and iron. The ideal formula unit is

$K(Mg,Fe)_3(Si_3Al)O_{10}(OH)_2$. Isomorphic substitution occurs in the tetrahedral sheet. One of four Si^{+4} can be replaced by Al^{+3}, and the charge is balanced by adding one monovalent interlayer cation, such as K^+ (Moore and Lockner, 2004). Like muscovite, biotite has a layer charge of 1.0 mol per formula unit caused by aluminum substituting for silicon in the tetrahedral sheet. The presence of iron in the octahedral sheet causes biotite to weather faster than muscovite (Schaetzl and Anderson, 2005). The biotite crystal structure is shown in Fig. 4.8.

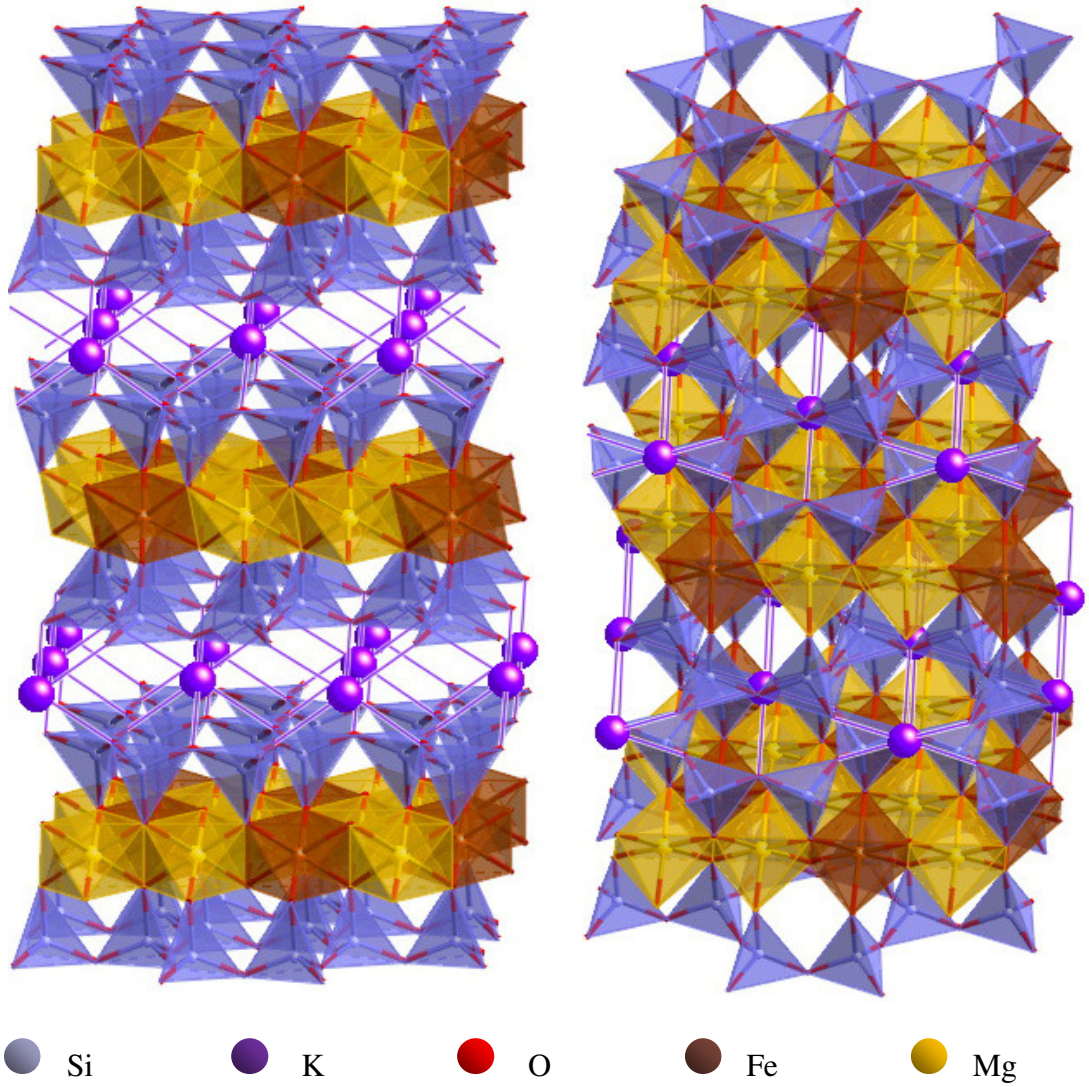

Fig. 4.8: Biotite crystal structure.

4.1.1.3 Serpentinite Group

The serpentine minerals are 1:1 trioctahedral minerals, and there are three polymorphs: lizardite, antigorite, and chrysotile, which all have the approximate composition of $Mg_3Si_2O_5(OH)_4$. Lizardite is the most abundant polymorph and generally has the appearance of very fine, platy crystals. Stacking variations of the crystalline structure lead to different polytypes such as 1T and 2H1. The crystal structure of Lizardite-1T is shown in Fig. 4.9, and the crystal structure of Lizardite-2H1 is shown in Fig. 4.10. Serpentine minerals usually have magnesium in the octahedral sheet, although cobalt, chromium, nickel, and aluminum can also be present. Serpentines form through the hydrothermal alteration of olivine, pyroxene, and peridotite, and they tend to weather easily (Schaetzl and Anderson, 2005).

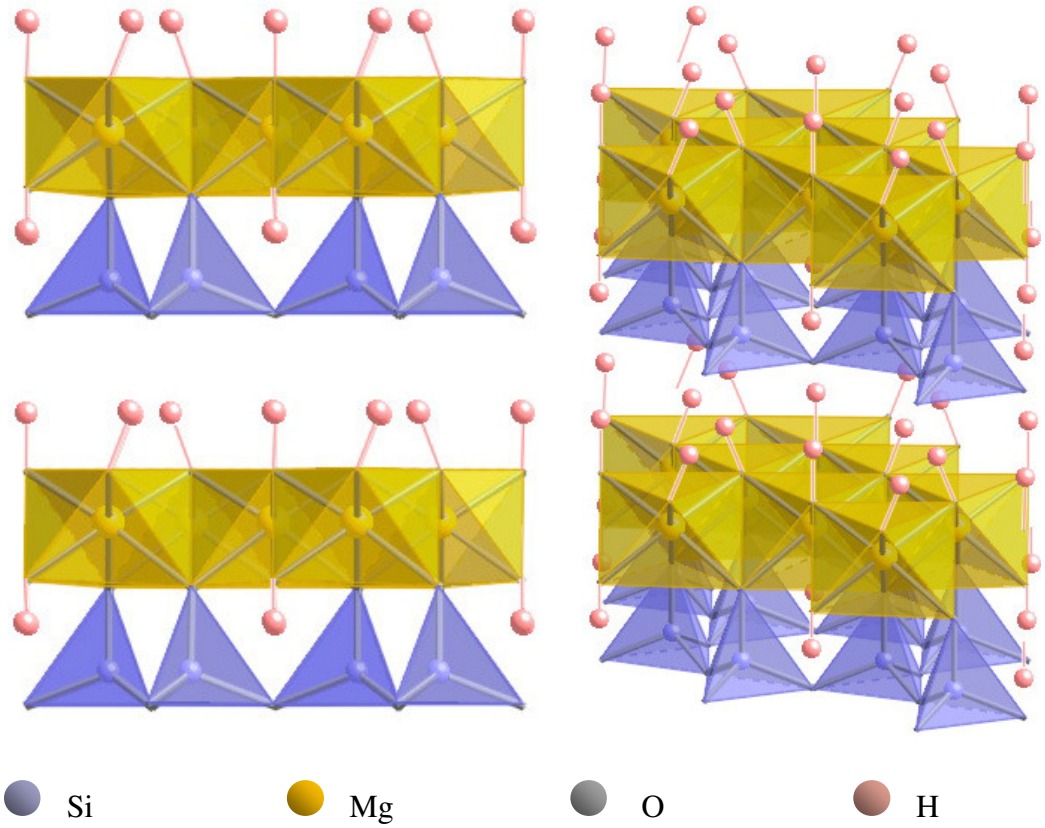

Fig. 4.9: Lizardite-1T crystal structure.

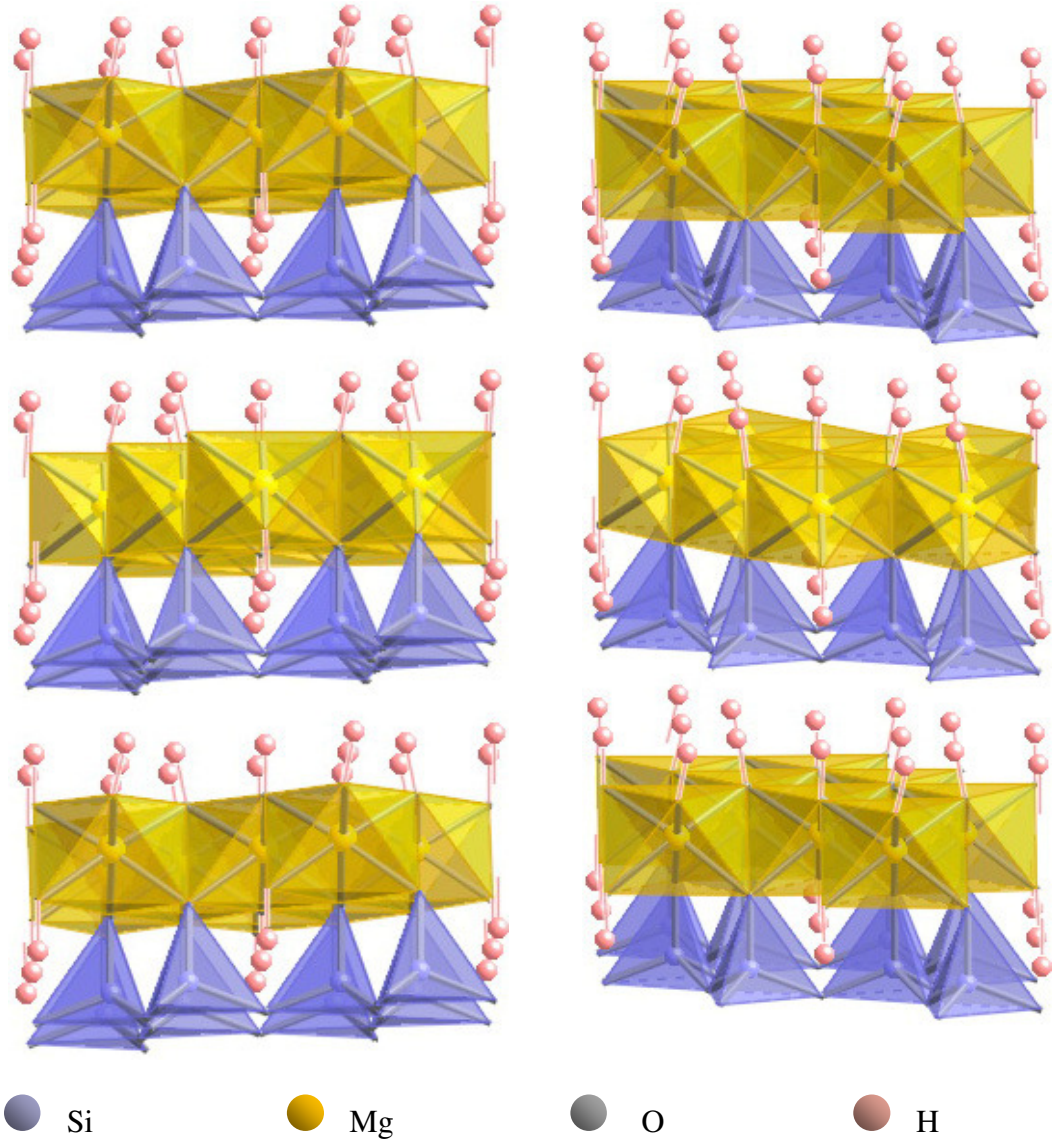

Fig. 4.10: Lizardite-2H1 crystal structure.

4.1.1.4 Chlorite Group

The chlorite group is a group of 2:1 phyllosilicates minerals that are usually trioctahedral. The octahedral sheet is predominately composed of magnesium or iron. The ideal formula unit is $(Mg,Fe,Al)_6(Si,Al)_4O_{10}(OH)_8$. Chlorite is sometimes called a 2:1:1 phyllosilicate because there is an extra positively charged interlayer octahedral

sheet between adjacent 2:1 layers to balance the layer charge. This interlayer sheet effectively blocks other interlayer ions. The crystal structure for chlorite is shown in Fig. 4.11. Chlorite forms from mafic (magnesium or iron rich) igneous and metamorphic rocks (Schaetzl and Anderson, 2005).

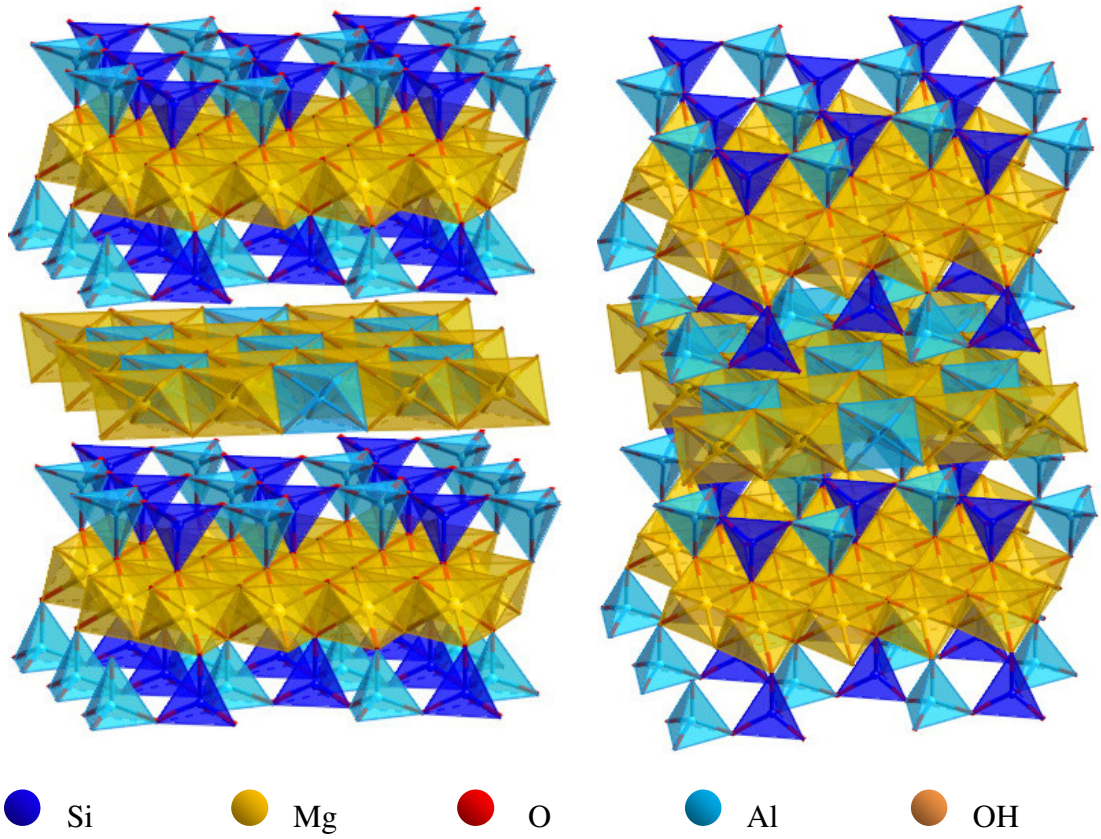

Fig. 4.11: Chlorite crystal structure.

4.1.2 Hydroxides

Hydroxides consist of a plane of cations sandwiched between two layers of hydroxyl ions. Dipole-dipole bonds form between the hydroxyls in adjacent layers

(Moore and Lockner, 2004). Gibbsite and brucite sheets are fundamental components of many of the minerals described earlier.

4.1.2.1 Gibbsite

Gibbsite, or aluminum hydroxide, is dioctahedral and has an ideal composition of $Al(OH)_3$. The crystal structure is shown in Fig. 4.12.

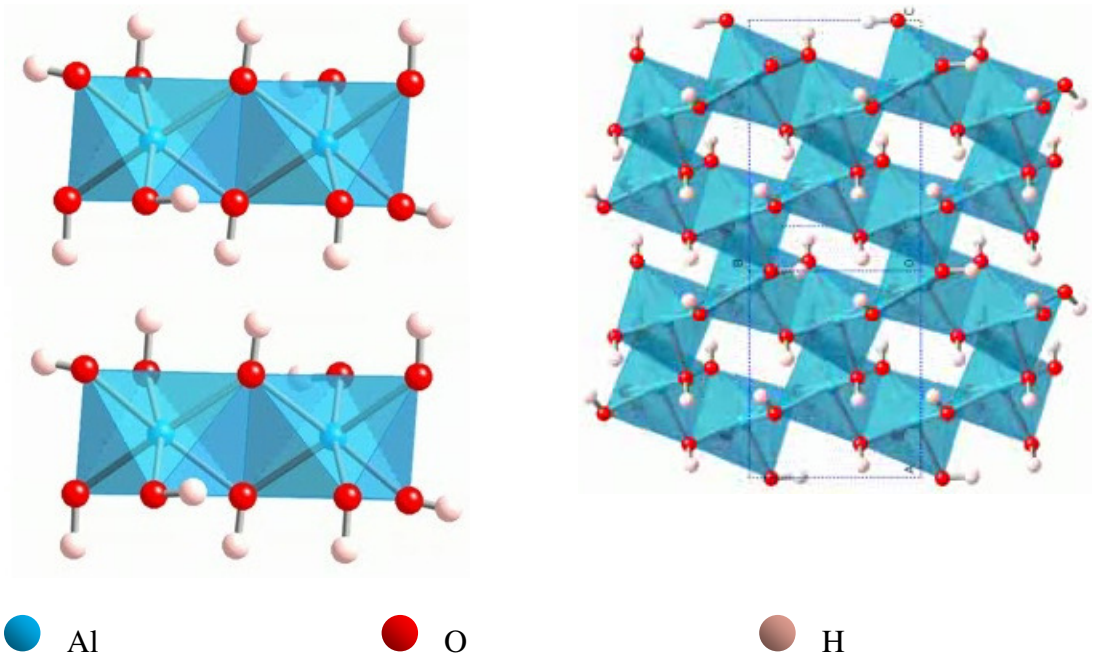

Fig. 4.12: Gibbsite crystal structure.

4.1.2.2 Brucite

Brucite, or magnesium hydroxide, is trioctahedral and has an ideal composition of $Mg(OH)_2$. The crystal structure is shown in Fig. 4.13.

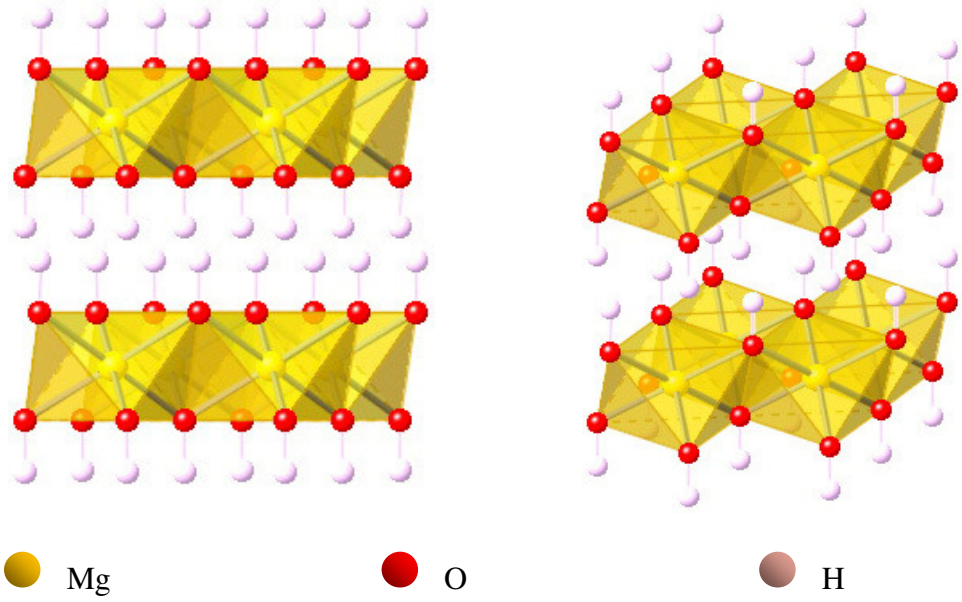

Fig. 4.13: Brucite crystal structure.

4.2 Layer Charge

Clays can be classified by the value of the permanent layer charge. Isomorphic substitution and vacancies can lead to a negative layer charge in a mineral, as discussed in Section 4.1.1. For 1:1 phyllosilicates, the layer charge is usually nearly zero due to the lack of isomorphic substitution. Figs. 4.14 and 4.15 depict the total negative layer charge per formula unit for dioctahedral and trioctahedral 2:1 phyllosilicates, respectively. While not depicted, brittle micas such as margarite and clintonite have layer charges of two or greater.

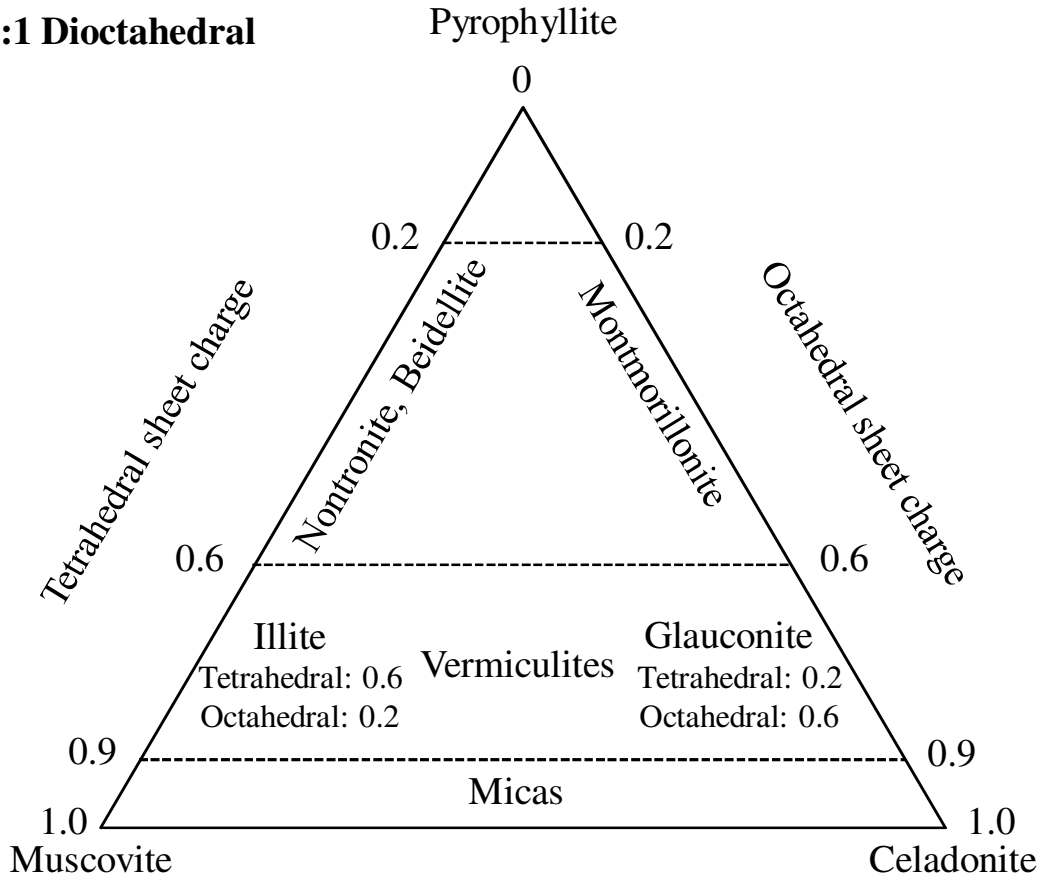

Fig. 4.14: Layer charge and charge location for dioctahedral 2:1 clays (adapted from Schaetzl and Anderson, 2005, from Zelazny and White, 1989).

4.3 Electrostatic Separation Energy

The total lattice energy of a crystal is composed of the electrostatic energy, van der Waals attractive force, and a repulsion term generally believed to have a magnitude similar to the van der Waals term (Moore and Lockner, 2004).

Giese (1974, 1978, 1980) and Bish and Giese (1981) calculated the change in electrostatic separation energy, or interlayer bonding energy, for a variety of minerals. This was accomplished by calculating the potential energy for the structure and for a structure with the same interatomic distances and angles within the layers but with the

layers separated by a relatively large distance, such as 0.9 nm. The difference in energies is the electrostatic separation energy and is a measure of the strength of the interlayer bonding.

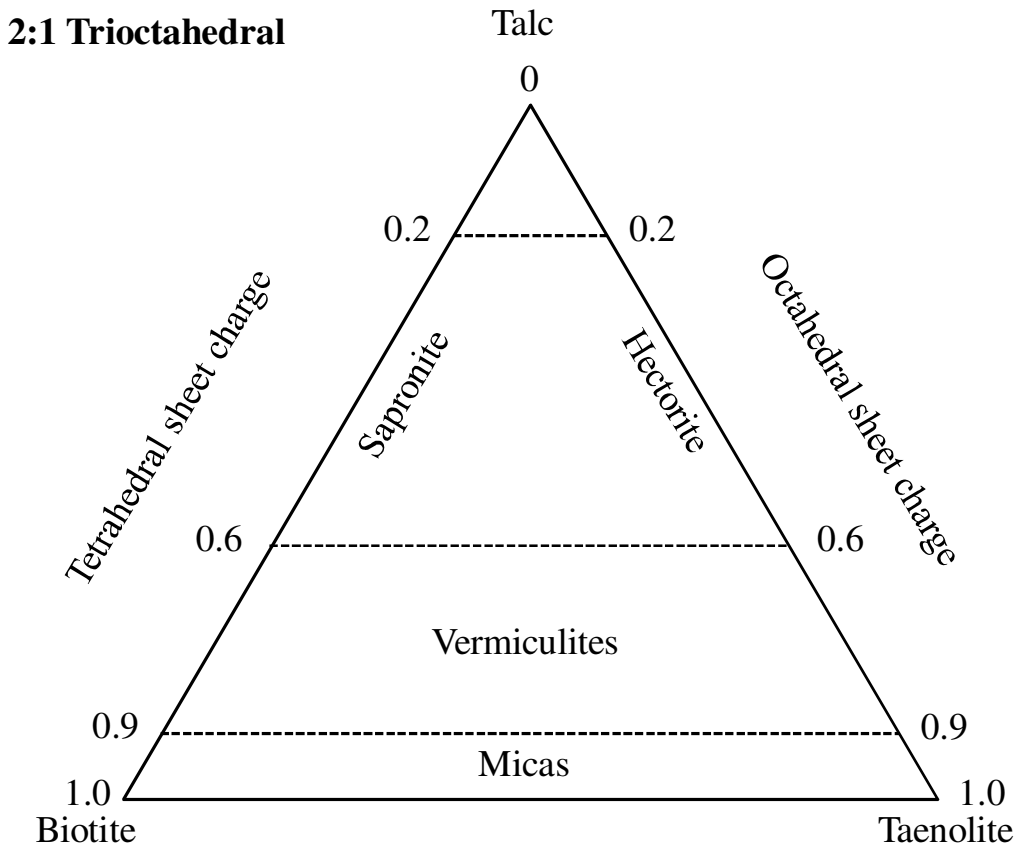

Fig. 4.15: Layer charge and charge location for trioctahedral 2:1 clays (adapted from Schaetzl and Anderson, 2005, from Zelazny and White, 1989).

The strongest bonding (50-200 kcal/mol) was calculated for dioctahedral and trioctahedral 1:1 structures, brittle micas, and hydroxides. Intermediate bonding (10-50 kcal/mol) was calculated for most dioctahedral and trioctahedral micas. Weak bonding

(0-10 kcal/mol) was calculated for zero layer charge 2:1 structures such as talc and pyrophyllite.

The relative separation energies vary with separation distance. For small separation distances, talc and pyrophyllite have greater electrostatic separation energies and are therefore more strongly bonded than muscovite is. To achieve any swelling, the energy at the lower separation distances must first be overcome. Therefore, the relatively high energies at low separation distances result in non-expanding behavior because swelling cannot initiate (Giese, 1978).

Chapter 5

Integration of Friction and Clay Mineralogy

This chapter discusses the friction data obtained from a variety of macro-scale laboratory tests. A brief overview of challenges of estimating clay creep is provided (Section 5.1), which is followed by a discussion of wet and dry friction coefficients obtained at different sliding velocities and pressures from laboratory tests (Section 5.2).

5.1 Challenges of Clay Creep Estimation

The complexity of clay fabric presents a challenge in developing a model for clay creep estimations. Kaolinite tends to form plate-like particles and flocculate in cardhouse structures creating edge-to-face formations. The fabric after sedimentation in a marine environment is a cardhouse structure with edge-to-face associations. This structure can

cause structural problems in the case of "quick clays" where the shearing resistance at the particle contacts decreases due to a decrease in the ion concentration of the pore fluid. As a result, remolding the soil can cause the cardhouse structure to collapse and turn the soil into a viscous fluid (Maio *et al*., 2004).

Montmorillonite tends to be even more challenging in terms of understanding clay creep than kaolinite because the particle shapes vary immensely. Montmorillonite particles tend to be smaller than kaolinite particles and wavy in texture in three dimensions. Typical sizes are 10-1000 nm in width and about 1 nm in thickness with aspect ratios varying from 60-500 (Ploehn and Liu, 2006). While the cardhouse structure of edge-to-face flocculation is well established in kaolinite, it is not established in montmorillonite. Rather face-to-face and shifted-face-to-face aggregation is predominant.

5.2 Previous Research

A variety of studies have measured the wet and dry coefficients of friction for different clays from a macro-scale perspective. The types of tests, test conditions, and clays vary by study. This section will discuss and compare previous research on macro-scale clay friction.

5.2.1 Macro-scale Wet Coefficient of Friction

The results from various studies using specialized triaxial shear, direct shear, and torsional ring shear tests to determine the wet coefficient of friction of clays are described in the following subsections.

5.2.1.1 Triaxial Tests

Numerous studies have measured the coefficient of friction, μ, using specialized triaxial shear experiments. In general, the experimental setup for these tests consists of two cylindrical rock blocks which are cut at inclined surfaces of 30-35º to the axial loading axis and stacked. The block dimensions are usually on the order of 6.35 cm long by 2.54 cm in diameter. The top block is usually Berea sandstone, which has a permeability of approximately eight orders of magnitude greater than the clay being tested. This top section establishes a hydraulic connection from the clay to the fluid pressure generator and pore pressure transducers. The bottom section consists of granite or in some cases impermeable silica to prevent water infiltration.

The clay being studied is mixed with distilled or deionized water to achieve a paste-like consistency. A thin layer of the clay, usually about 1 mm in thickness, is spread between the upper and lower block sections along the incline.

Many of the tests discussed in this section studied both wet and dry friction. To measure the wet and dry friction in the same test, a piston was moved axially at a constant rate to achieve a constant shearing velocity. After some distance of axial displacement, such as 2.5 mm, the piston movement was stopped, and the sample was inundated with distilled water. The pore pressure was increased, allowed to equilibrate, and then shearing continued to some maximum shear displacement of approximately 9 mm in most cases. The confining pressure and pore pressure were controlled throughout the experiments.

Morrow *et al.* (1982) conducted triaxial shear experiments on montmorillonite, illite, and kaolinite. The clays were tested in saturated, drained conditions. The sliding

velocity along the gouge-filled saw cut, or along the incline between the rock blocks, was 0.073 μm/s. The total shear displacement was approximately 9 mm. Montmorillonite was determined to have a saturated μ of 0.13 at 200 MPa confining pressure. Under the same conditions, illite and kaolinite had saturated μ values of 0.44 and 0.34, respectively.

Morrow *et al.* (1992) later conducted triaxial shear experiments on saturated montmorillonite and illite. The montmorillonite samples used were high quality sodium montmorillonite, as was the case in most of the studies discussed in this chapter. The clays were tested in saturated, drained conditions. The shear displacement rate was initially 0.01 μm/s. Morrow *et al.* (1992) found that as the shear displacement increased up to a maximum of 7 mm, the wet μ for illite became less dependent on the effective confining pressure (cell pressure minus the pore water pressure), while the wet μ for montmorillonite became more dependent. The maximum μ at a shear displacement of approximately 7 mm for montmorillonite was found to be 0.20, 0.25, and 0.32 at extremely high effective confining pressures of 100, 200, and 300 MPa, respectively. Illite was found to have a maximum μ of 0.43 at a shear displacement of approximately 7 mm, regardless of effective confining pressures varying from 100 to 300 MPa. Morrow *et al.* (1992) speculated that the increase in montmorillonite μ with effective confining pressure is due to loosely bound interlayer water which is squeezed out by greater pressures. Illite does not expand and thus presumably does not exhibit this phenomenon. Morrow *et al.* (1982) found that Tejon Pass Fault gouge, comprised mainly of montmorillonite and mixed layer (montmorillonite/illite) clays, also exhibits this trend. Lupini *et al.* (1981) also found a similar trend when studying montmorillonite using ring shear tests.

After this 7 mm of displacement, the samples were then displaced 1 mm more at a greater sliding velocity of 1 μm/s. For a 200 MPa effective confining pressure, the wet μ for illite and montmorillonite were 0.47 and 0.28, respectively, indicating velocity-strengthening behavior. This velocity strengthening effect is supported by other studies (Saffer *et al.*, 2001; Saffer and Marone, 2003; Moore and Lockner, 2007).

Moore *et al.* (1997) conducted similar triaxial friction experiments on chrysotile, lizardite, and antigorite, which are all minerals of the serpentinite group described in Section 4.1.1.3 and are commonly found in fault gouge. The effective confining pressure for these tests was 100 MPa, and the tests were run to approximately 4 mm of shear displacement at a sliding velocity of 1.2 μm/s. The wet μ values under these conditions were 0.23, 0.46, and 0.48 for chrysotile, lizardite, and antigorite, respectively. The low μ value for chrysotile is attributed to the mineral's comparatively high adsorbed water content.

Morrow *et al.* (2000) also conducted triaxial shear experiments on a wide variety of minerals in saturated, drained conditions. The tests were conducted at effective confining pressures of 100 MPa and sliding velocities of 0.50 μm/s. The total shear displacement was approximately 9 mm. The wet μ values for these minerals are shown in Table 5.1. The wet μ values for chrysotile, lizardite, and antigorite are quantitatively similar to those determined by Moore *et al.* (1997).

Moore and Lockner (2004) also conducted triaxial shear experiments in saturated, drained conditions. The tests were run at 100 MPa effective confining pressures and sliding velocities of 0.58 μm/s. The total shear displacement was 9 mm. The wet μ values for these minerals are shown in Table 5.2. Moore and Lockner (2004) showed that both

the wet and dry μ values (see Section 5.2.2) of 2:1 phyllosilicates generally follow very well defined trends with respect to certain crystallochemical factors. Moore and Lockner (2004) found that a near linear relationship exists between wet μ and tetrahedral layer charge, as defined in Section 4.2. The slope depends on whether the mineral is dioctahedral or trioctahedral. They also found that the wet μ correlates fairly well with electrostatic separation energy, which was introduced in Section 4.3, for 2:1 phyllosilicates.

Table 5.1: Macro-scale coefficient of friction values for different minerals. The effective confining pressure is 100 MPa, and the sliding velocity is 0.50 μm/s (Morrow *et al.*, 2000).

Mineral	Wet μ	Dry μ
Kaolinite	0.55	0.77
Antigorite	0.50	0.77
Muscovite	0.46	0.50
Lizardite	0.41	0.80
Chlorite	0.39	0.60
Brucite	0.30	0.45
Montmorillonite	0.23	0.52
Chrysotile	0.23	0.44
Talc	0.20	0.24

Table 5.2: Macro-scale coefficient of friction values for different minerals. The effective confining pressure is 100 MPa, and the sliding velocity is 0.58 μm/s (Moore and Lockner, 2004).

Mineral	Wet μ	Dry μ
Margarite	0.67	0.80
Kaolinite	0.51	0.84
Gibbsite	0.51	0.75
Muscovite	0.44	0.57
Lizardite	0.42	0.82
Chlorite	0.38	0.67
Biotite	0.32	0.48
Brucite	0.30	0.49
Pyrophyllite	0.28	0.56
Talc	0.20	0.36

The results from Morrow *et al.* (2000) for montmorillonite fit into Moore and Lockner's (2004) near linear trend of wet μ vs. tetrahedral layer charge for a 2:1 dioctahedral phyllosilicate. Comparing the experiments conducted under similar conditions by Morrow *et al.* (2000) and Moore and Lockner (2004), montmorillonite, a swelling mineral, and pyrophyllite and talc, non-swelling minerals, have similar wet μ values. Pyrophyllite and montmorillonite have very similar crystal structures. The main difference is that minor substitution in the octahedral sheet of montmorillonite leads to the attraction of interlayer cations to balance the charge. As a result, water molecules are attracted to the cations, and this water leads to swelling. Evidence that minerals with and

without interlayer water have similar wet μ values is significant because the swelling properties of montmorillonite may not affect its wet μ value under high pressures.

Montmorillonite was studied more extensively by Moore and Lockner (2007) using the same experimental set-up and methods under saturated and drained conditions. The tests were run at 100 MPa effective confining pressure, varying sliding velocities, and run to shear displacements of approximately 9 mm. For sliding velocities of 0.058, 0.58, and 5.8 μm/s, the wet μ values were 0.145, 0.155, and 0.165, respectively. At 150 MPa effective confining pressure and at sliding velocities of 0.058, 0.58, and 5.8 μm/s, the wet μ values were 0.175, 0.18, and 0.20, respectively.

Tembe *et al.* (2010) also conducted triaxial shear experiments on montmorillonite and illite. The clays were tested under saturated and drained conditions. The tests were run to 9 mm shear displacement, and the effective confining pressure was 40 MPa. The sliding velocity was 1.0 μm/s. The wet μ values were 0.12 and 0.30 for montmorillonite and illite, respectively.

5.2.1.2 Direct Shear Tests

Direct shear tests can also provide information on the saturated, drained μ for soils. In this test, soil is placed inside a box between two porous stones to facilitate drainage. The box is divided into upper and lower sections. First, a vertical normal stress is applied to consolidate the sample. An axial strain gauge monitors vertical deformation, as would be done in a consolidation test. Second, a constant rate of horizontal displacement is applied to the lower box, which is monitored by a shear displacement gauge. The shearing velocity is kept at a low enough value that pore water pressures will

not build up. The shear force required to keep the top box stationary is measured using a load cell. From this shear force, the shear stress is determined using the known contact area.

The triaxial shear tests described in Section 5.2.1.1 do not necessarily provide residual μ values for soils because of the limited shearing displacement of approximately 9 mm. Direct shear tests allow the soil to be sheared to very large displacements because the shear direction can be reversed. Typically, shearing in a direct shear box is reversed every 5 mm of displacement to minimize the effect of a decreasing contact area as the boxes become less overlapped (Terzaghi *et al.*, 1996). The sample is sheared repeatedly until the minimum strength is obtained and maintained for at least three shear cycles.

Maio and Fenelli (1994) conducted direst shear tests on montmorillonite. The montmorillonite was mixed with distilled water to a water content near the soil's liquid limit and consolidated. The saturated montmorillonite was sheared at a velocity of 0.083 μm/s. At effective normal pressures of 0.22, 0.32, and 0.42 MPa, the residual μ values were 0.06, 0.06, and 0.07 to 0.11, respectively.

Brown *et al.* (2003) also conducted direst shear tests on montmorillonite. The montmorillonite samples were first saturated with sea water and consolidated. The influences of NaCl concentration on μ is discussed by Maio and Fenelli (1994) and Moore and Lockner (2007). Then, the saturated montmorillonite was sheared at 0.1 μm/s. At a very high effective normal stress of 30 MPa, the residual μ value was 0.12.

Saffer *et al.* (2001) conducted direst shear tests on montmorillonite. The montmorillonite samples were mixed to 11% water content and consolidated. The tests were run to 20 mm of displacement. At an effective normal stress of 50 MPa, the residual

μ value was 0.15 at a shearing velocity of 1 μm/s. For an effective normal stress of 45 MPa and shearing velocities of 1 and 10 μm/s, the residual μ was 0.15 and 0.16, respectively. The reduced water content at the beginning of the study may have lead to partially saturated conditions that could have affected the reported μ values.

Saffer and Marone (2003) later conducted more direct shear tests on montmorillonite. For 100 MPa effective normal stress and shearing velocities of 2, 20, and 200 μm/s, the residual μ was 0.080, 0.095, and 0.105, respectively.

5.2.1.3 Ring Shear Tests

Torsional ring shear tests provide an advantage over direct shear tests in determining residual μ values because unlimited shear displacements can be obtained without changing shearing direction. In the experimental setup of the studies discussed in this section, the soil was confined by an upper and lower ring with porous stones on the top and bottom to permit drainage. First, a vertical stress was applied to the soil. Second, the lower ring was rotated while the upper ring remained stationary. The torque applied was measured, and the shear stress was calculated. The lower half of the sample continued to rotate until a minimum strength was determined.

Lupini *et al.* (1981) conducted ring shear tests on montmorillonite. The montmorillonite was mixed with distilled water and consolidated. The saturated montmorillonite was then sheared at 5.0 μm/s at 0.18 and 0.35 MPa effective normal stresses, and the residual μ values were 0.089 and 0.103, respectively.

Stark and Eid (1994) also conducted an extensive ring shear testing program on more than 30 cohesive soil samples. The samples were mixed with distilled water prior to

shearing at velocities of 0.3 µm/s. Stark and Eid (1994) developed a relationship between drained residual μ and liquid limit based on the ring shear tests they conducted. Extrapolating the correlation for the highly plastic clay SWy-2, which is a reference sodium montmorillonite (liquid limit = 520% from Marcial *et al*., 2002), yields a μ of 0.07 at an effective normal stress of 0.4 MPa.

Brown *et al.* (2003) also conducted ring shear tests on montmorillonite in conjunction with the direct shear tests described in Section 5.2.1.2. The montmorillonite was saturated with seawater and sheared at 1.5 µm/s for at least 70 mm or until no further changes in shear stress occurred. At an effective normal stress of 1.5 MPa, the residual μ value was 0.10.

Tiwari and Marui (2005) conducted ring shear tests on montmorillonite. The montmorillonite was mixed to a water content near its liquid limit and consolidated. The saturated montmorillonite was then sheared at 8.3 µm/s at 0.25 MPa effective normal stress, and the residual μ value was determined to be 0.066. Varying the shearing velocity from 0.17 to 17.0 µm/s only led to a change in the residual μ of 0.004.

5.2.1.4 Summary of Wet Coefficient of Friction Data

Fig. 5.1 depicts the wet μ values for montmorillonite as a function of sliding velocity for the studies discussed above. It is evident from the results that the triaxial shear experiments may not have reached a minimum residual μ value given the limited shear displacement in the tests. It is also apparent that the minimum wet μ value for montmorillonite is approximately 0.06, and the maximum residual wet μ value is 0.16, regardless of velocity. This range is in quantitative agreement with the residual wet μ

values for montmorillonite proposed by Mitchell and Soga (2005) of 0.07-0.18. Correlation of wet μ with sliding velocity in terms of the Rate Process Theory and the micro-scale results is discussed in Section 7.4.

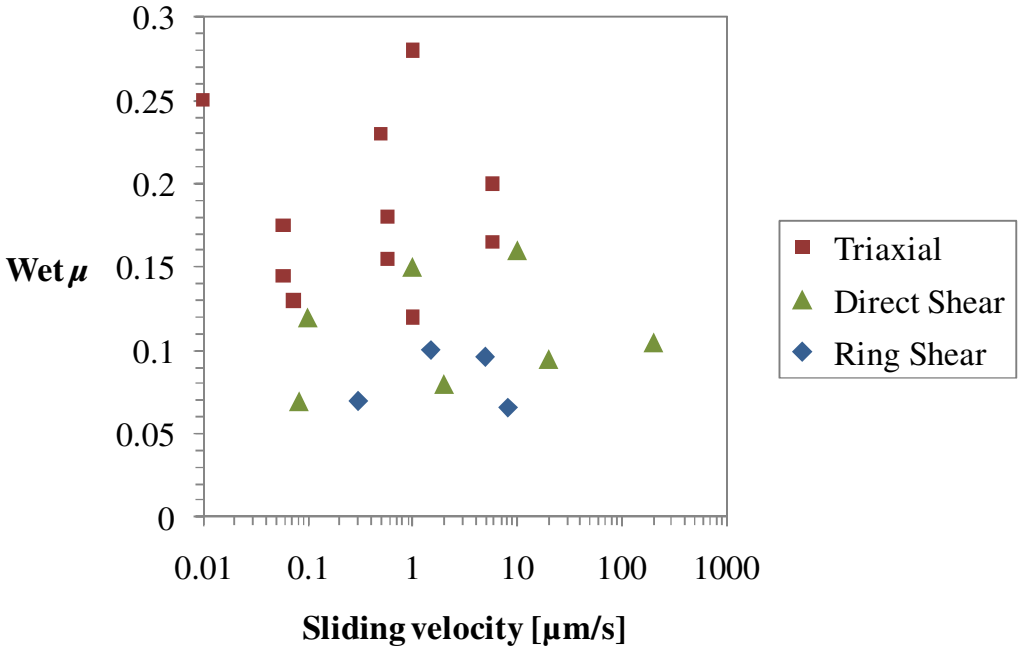

Fig. 5.1: Coefficient of friction as a function of sliding velocity for saturated friction tests on montmorillonite.

The normal stress applied to the clay may also affect the measured μ. Very high normal stresses may produce greater μ values as interlayer water is squeezed out, as demonstrated by Morrow *et al.* (1982), Morrow *et al.* (1992), and Lupini *et al.* (1981). The effect of normal stress on μ is shown in Fig. 5.2.

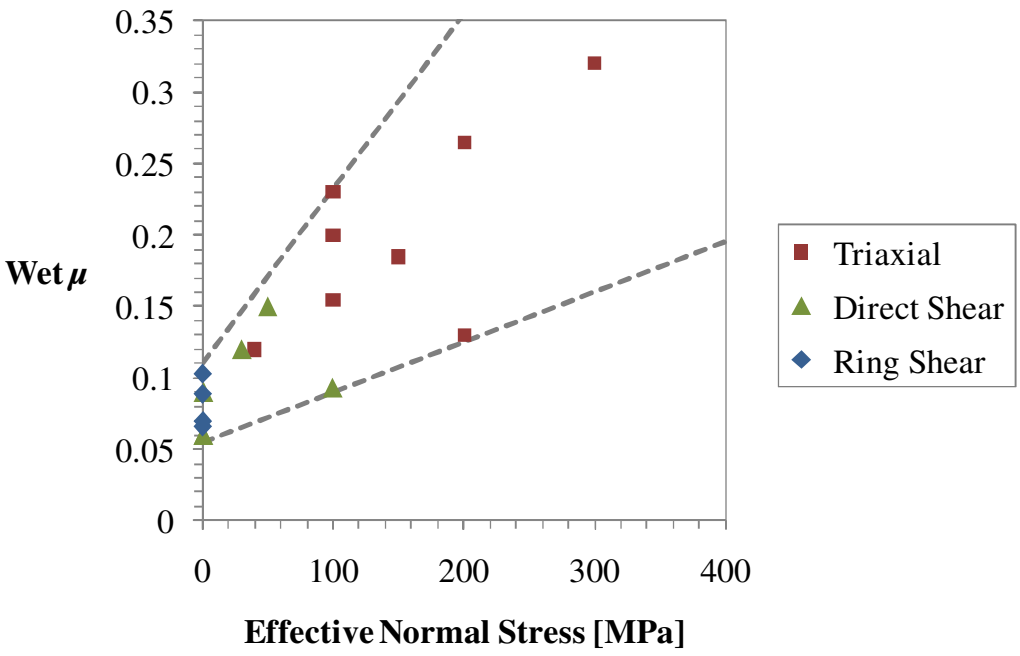

Fig. 5.2: Coefficient of friction as a function of effective normal stress for saturated friction tests on montmorillonite.

5.2.2 Macro-scale Dry Coefficient of Friction

For the dry triaxial shear experiments, the same procedure was followed as described in Section 5.2.1.1. The main difference is that the samples in the cylindrical assembly were oven-dried, sometimes in a vacuum, for at least 24 hours before shearing, and water was not introduced into the system.

Morrow *et al.* (1982) conducted triaxial shear experiments on dry Tejon Pass Fault gouge, which is comprised mainly of montmorillonite and mixed layer (montmorillonite/illite) clays. The sliding velocity along the gouge-filled saw cut was 0.073 μm/s, and the total shear displacement was approximately 9 mm. The gouge was determined to have a dry μ of 0.74 at 200 MPa confining pressure.

Morrow *et al.* (1992) later conducted triaxial shear experiments on dry montmorillonite and illite samples. The shearing velocity was 1 μm/s, and the shear displacement was approximately 7 mm. At a 300 MPa effective confining pressure, the dry μ values for montmorillonite and illite were 0.60 and 0.73, respectively.

Moore *et al.* (1997) conducted dry triaxial friction experiments on chrysotile, lizardite, and antigorite. As was shown by their experiments described in Section 5.2.1.1, chrysotile had a wet μ which was significantly less than the wet μ values of lizardite and antigorite, despite the minerals all being from the same mineral group. The low μ value for chrysotile was attributed to chrysotile's ability to adsorb water. Moore *et al.* (1997) tested this hypothesis by heating a chrysotile sample to 175-200 ºC under vacuum for 120 hours and then shearing the sample at a sliding velocity of 0.23 μm/s at 100 MPa effective normal stress. At approximately 1.5 mm of displacement, the dry μ value for chrysotile was 0.62, which is similar to the dry μ values of lizardite and antigorite, indicating that the adsorbed water content of the clay may affect its wet μ value.

Morrow *et al.* (2000) conducted dry triaxial shear experiments on a wide variety of minerals. The tests were conducted at effective confining pressures of 100 MPa and sliding velocities of 0.50 μm/s. The total shear displacement was approximately 4 mm. The dry μ values for these minerals are shown in Table 5.1. The dry μ for montmorillonite was determined to be 0.52.

Morrow *et al.* (2000) found that the impact of saturation on the μ value varied depending on the mineral's tendency to adsorb or take on interlayer water, as was suggested by the friction results provided by Moore *et al.* (1997) on chrysotile. Morrow *et al.* (2000) determined that immediately following sample saturation, the percent

decrease in μ due to wetting of chrysotile, lizardite, and antigorite was 64%, 51%, and 39%, respectively. Montmorillonite had a 60% reduction of μ immediately after saturation.

Morrow *et al.* (2000) also found that the dry μ for the different minerals tested was related to the mineral bond strength or electrostatic energy. Minerals with lower separation energy, such as talc, had lower dry μ values due to these weak bonds. Minerals with strong hydrogen bonds, such as kaolinite and lizardite, exhibited greater dry μ values.

Moore and Lockner (2004) also conducted dry triaxial shear experiments on a variety of minerals. The tests were run at 100 MPa effective confining pressures and sliding velocities of 0.58 μm/s. The total shear displacement was 9 mm. The dry μ values for these minerals are listed in Table 5.2.

Similar to the findings of Morrow *et al.* (2000), Moore and Lockner (2004) also found a near linear relationship between dry μ and electrostatic separation energy. The dry μ values are also quantitatively similar between the studies. The main difference between the results is the dry μ of talc. The talc sample used by Morrow *et al.* (2000) may have been exposed to room humidity prior to testing, causing the dry value to be similar to the wet value, as indicated by Moore and Lockner (2004).

While montmorillonite was not tested by Moore and Lockner (2004), pyrophyllite, which has a similar crystal structure, was tested. Moore and Lockner (2004) found great variation in the dry μ results for pyrophyllite, with values anywhere from 0.38 to 0.70. Moore and Lockner (2004) speculated that exposure to room humidity may have lead to this variability.

Moore and Lockner (2007) conducted dry triaxial shear experiments on montmorillonite. The tests were run at 100 MPa effective confining pressures, varying sliding velocities, and run to shear displacements of approximately 9 mm. For sliding velocities of 0.058, 0.58, and 5.8 μm/s, the dry μ values were 0.73, 0.75, and 0.77, respectively.

Fig. 5.3 shows the dry μ values of montmorillonite as a function of sliding velocity for the triaxial tests discussed. These tests were conducted with limited displacements and at very high normal stresses. The maximum dry μ value of montmorillonite of 0.77 is supported by the work of Byerlee (1978), who tested a wide variety of minerals and found the maximum dry μ value was approximately 0.85 at normal effective stresses less than 200 MPa. The lower μ values found by Morrow *et al.* (1992, 2000) are indicative of how the μ of phyllosilicates can vary depending on the interlayer bond strength or electrostatic separation energy. A discussion of the dry μ as a function of sliding velocity in terms of the Rate Process Theory and the micro-scale results is provided in Section 7.4.

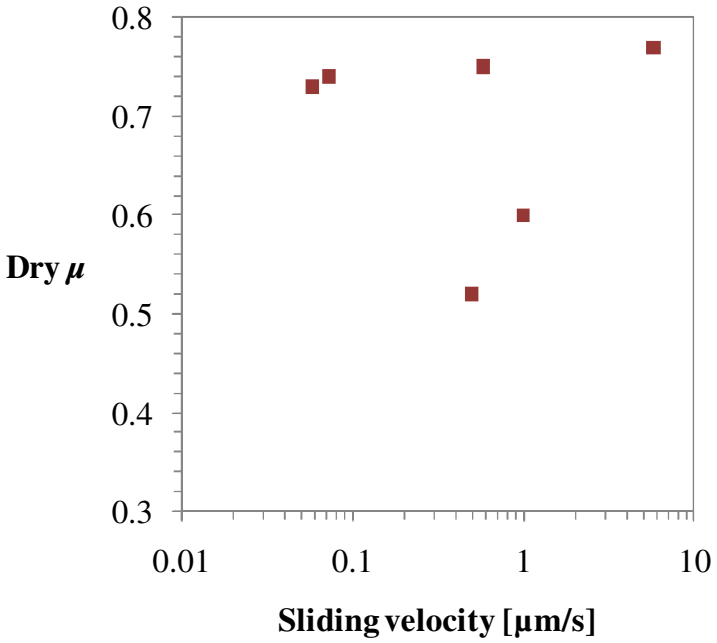

Fig. 5.3: Coefficient of friction as a function of sliding velocity for dry friction tests on montmorillonite.

Chapter 6

Micro-scale Experiments – Materials and Methods

This chapter provides an overview of the equipment and materials used in the micro-scale experiments (Section 6.1) as well as the experimental methodology (Section 6.2). The micro-scale data analysis method is presented in Section 6.3.

6.1 Equipment Development

This section covers in detail all of the equipment and materials used for the micro-scale friction experiments conducted in this study. This includes substrates, Atomic Force Microscope (AFM) probes, electronic equipment, and other materials.

6.1.1 Substrates

In this study, a substrate refers to any flat surface which is tested in an AFM for either topographic scans or force measurements. A substrate may also simply serve as a base for either micro-spheres or glue, which is discussed in Sections 6.1.2.2 and 6.2.1. The substrate was glued to a metal AFM puck using Cytec Conap Products Easypoxy K-20 Epoxy. The puck is necessary because it provides support for the substrate, and it is magnetically attached to the AFM piezo-electric scanner to prevent the substrate from shifting laterally during experiments. Several of such pucks are shown in Fig. 6.1. For the experiments conducted in this study, the maximum substrate size was 1 cm in diameter.

Fig. 6.1: Metal AFM pucks. Each puck has a 1 cm diameter.

On top of these metal pucks, one of two substrates was glued: a pure silica glass coverslip (Fig. 6.2a) or a sheet of freshly cleaved muscovite mica from Maine (Fig. 6.2b). The muscovite was cut to fit the metal AFM puck using a utility knife. Only the center area of the substrate was used in experiments, and therefore uncovered puck edges around the substrate were not a concern. Photographs of the assembled glass and mica substrates are shown in Figs. 6.3a and 6.3b, respectively.

(a) 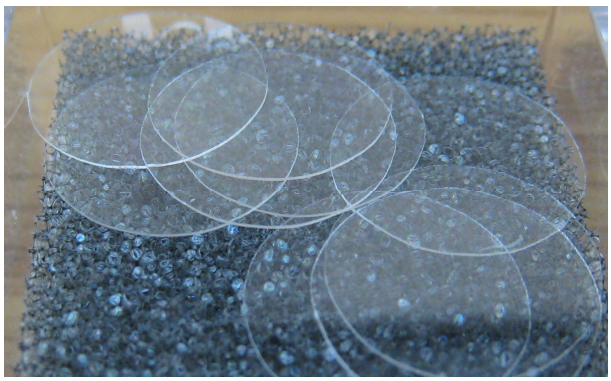 (b) 

Fig. 6.2: Substrates used (a) Glass coverslips. Each glass coverslip has an 8 mm diameter, (b) Muscovite mica.

(a) 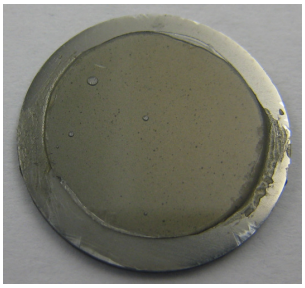 (b) 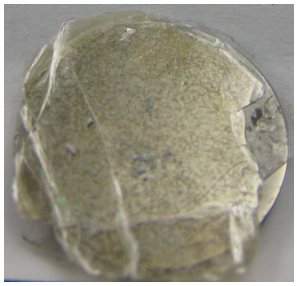

Fig. 6.3: Types of substrates attached to metal AFM pucks: (a) Glass coverslip, (b) Muscovite mica.

6.1.2 AFM Probes

The AFM probes were constructed using tipless AFM cantilevers and glass micro-spheres. The probe construction method is described in the following subsections.

6.1.2.1 Cantilevers

Standard AFM tips are relatively sharp with a probe tip diameter on the order of 20 nm and a height of 20 μm. The sharp tips are extremely useful for imaging purposes, as shown in Sections 6.2.2.3, 7.1, and 7.2.3, but they are not ideal for force measurements. The contact area of the tip is often irregularly shaped, which makes a

constant radius of curvature difficult to determine. Additionally, the contact area of a standard, sharp AFM tip is relatively small, which can result in unacceptably low signal-to-noise ratios in force measurements. Finally, a sharp tip is easy to damage when conducting friction measurements.

To mitigate the problems associated with using standard AFM tips for friction measurements, custom AFM probes were designed and produced in house. These probes consisted of silica glass micro-spheres glued to the ends of tipless AFM cantilevers (MikroMasch USA, San Jose, California, series NSC12 or CSC12, Al-coated). A schematic showing the arrangement of six cantilevers on a chip and the chip dimensions is shown in Fig. 6.4. A photograph of five such chips is shown in Fig. 6.5.

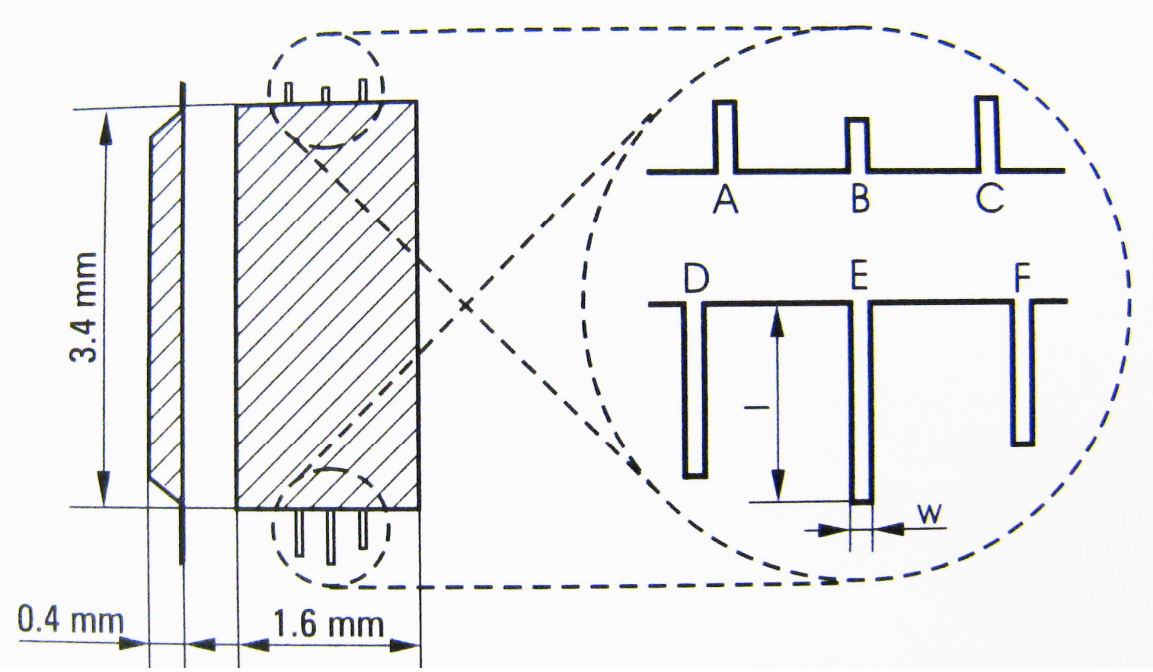

Fig. 6.4: Schematic of six tipless rectangular cantilevers on a NSC12 or CSC12 silicon chip (MikroMasch USA, 2010). *l* and *w* refer to length and width, respectively. Designations A-F refer to different cantilever lengths, and subsequently, different spring constants.

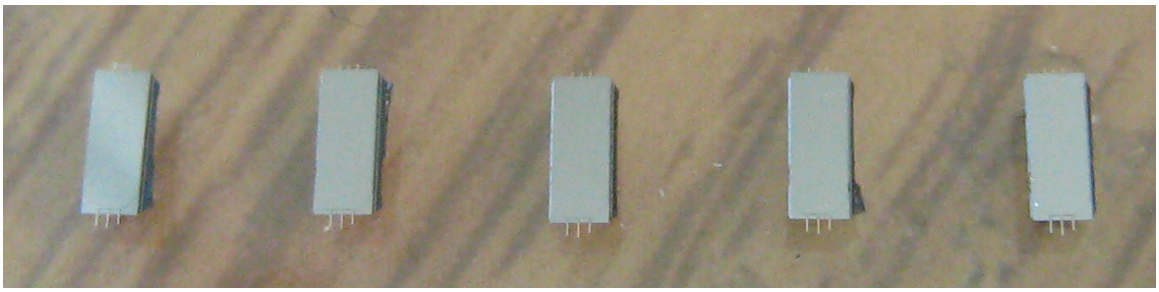

Fig. 6.5: Five NSC12 silicon chips. There are six cantilevers per chip.

The manufacturer specifications of the different lengths, widths, thicknesses, resonant frequencies, and spring constants are shown in Tables 6.1 and 6.2. The dimensions were verified using an Environmental Scanning Electron Microscope (ESEM) (Philips XL30 ESEM-FEG, FEI Company, Hillsboro, Oregon), and the resonant frequencies and spring constants were verified using a closed loop scanner Dimension 3100 AFM (Veeco, Santa Barbara, California).

6.1.2.2 Micro-spheres

The glass spheres that were used in this study were silicon oxide micro-spheres manufactured by Corpuscular, Inc. (Cold Spring, New York). The diameters tested were 10, 52, and 104 μm. The diameters of the micro-spheres were also verified using an ESEM. ESEM images of the 52 and 10 μm diameter spheres attached to the ends of tipless cantilevers are shown in Fig. 6.6. The 104 μm diameter spheres were determined to be too large to attach to the AFM tipless cantilevers using the method of assembly described in Section 6.2.1, and therefore ESEM images were not obtained.

Table 6.1: CSC12 cantilever manufacturer specifications.

Cantilever Type	A			B			C		
	Min	Typical	Max	Min	Typical	Max	Min	Typical	Max
Length, ±5, μm		110			90			130	
Width, ±3, μm		35			35			35	
Thickness, μm	0.7	1.0	1.3	0.7	1.0	1.3	0.7	1.0	1.3
Resonant frequency, kHz	65	105	150	95	155	230	50	75	105
Spring constant, N/m	0.25	0.95	2.5	0.45	1.75	5.0	0.15	0.6	1.5

Cantilever Type	D			E			F		
	Min	Typical	Max	Min	Typical	Max	Min	Typical	Max
Length, ±5, μm		300			350			250	
Width, ±3, μm		35			35			35	
Thickness, μm	0.7	1.0	1.3	0.7	1.0	1.3	0.7	1.0	1.3
Resonant frequency, kHz	9.5	14	19	7	10	14	14	20	28
Spring constant, N/m	0.01	0.05	0.1	0.01	0.03	0.08	0.02	0.08	0.2

Table 6.2: NSC12 cantilever manufacturer specifications.

Cantilever Type	A			B			C		
	Min	Typical	Max	Min	Typical	Max	Min	Typical	Max
Length, ±5, μm		110			90			130	
Width, ±3, μm		35			35			35	
Thickness, μm	1.7	2.0	2.3	1.7	2.0	2.3	1.7	2.0	2.3
Resonant frequency, kHz	165	210	240	240	315	405	120	150	190
Spring constant, N/m	3.5	7.5	12.5	6.5	14	27.5	2.5	4.5	8.5

Cantilever Type	D			E			F		
	Min	Typical	Max	Min	Typical	Max	Min	Typical	Max
Length, ±5, μm		300			350			250	
Width, ±3, μm		35			35			35	
Thickness, μm	1.7	2.0	2.3	1.7	2.0	2.3	1.7	2.0	2.3
Resonant frequency, kHz	23	28	34	17	21	24	33	41	49
Spring constant, N/m	0.2	0.35	0.7	0.1	0.3	0.4	0.35	0.65	1.2

(a)

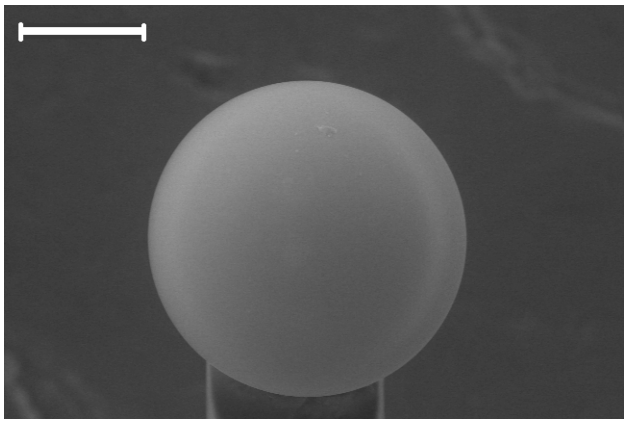

(b)

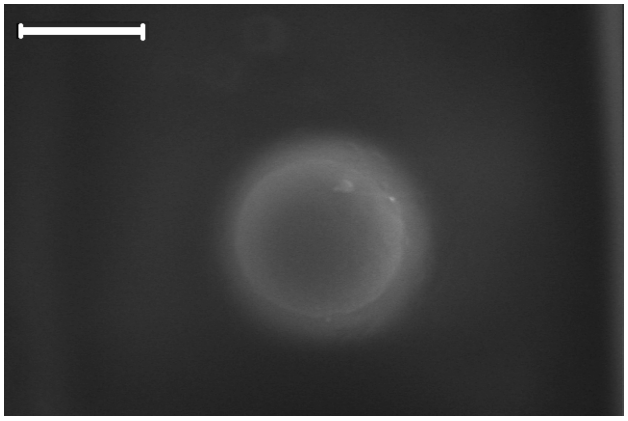

Fig. 6.6: ESEM images of micro-spheres attached to AFM cantilevers: (a) 52 μm diameter (scale bar is 20 μm), (b) 10 μm diameter (scale bar is 10 μm).

The micro-spheres were shipped in deionized water. To make the micro-spheres available for use with the AFM, a piece of trimmed-to-size, freshly cleaved muscovite was epoxied to an AFM puck and heated on a hotplate at 100°C. The vial containing the micro-spheres was shaken by hand, and a pipette was used to extract 50 μL from the vial and to drop the suspended micro-spheres onto the heated puck. The puck was then allowed to air-dry and cool.

6.1.3 Equipment and Material List

The following equipment and materials were used in this study:

- Veeco Dimension 3100 AFM (Fig. 6.7)
- Philips XL30 ESEM FEG
- Cytec Conap Products Easypoxy K-20
- Loctite Marine Epoxy
- AFM fluid cell
- Metal AFM pucks
- Glass AFM coverslips
- Muscovite mica
- SWy-2 sodium montmorillonite
- Polysciences polyethyleneimine
- AFM chip holder gel case
- NanoProbe SPM tips, wafer #455
- Fisher Scientific hotplate
- Denver Instrument M-120 balance
- Fisher Scientific sonic dismembrator 100
- Corpuscular, Inc. micro-spheres (Fig. 6.6)
- MikroMasch NSC12 or CSC12 (Figs. 6.4 and 6.5)
- BioForce Nanosciences UV/ozone cleaner
- Nikon Eclipse 6600 POL optical microscope
- Sorvall Superspeed RC2-B automatic refrigerated centrifuge
- Halcyonics active vibration isolation system (Fig. 6.7)
- Barnstead/Thermolyne Labquake shaker
- Watson Marlow, Inc. peristaltic pump 323

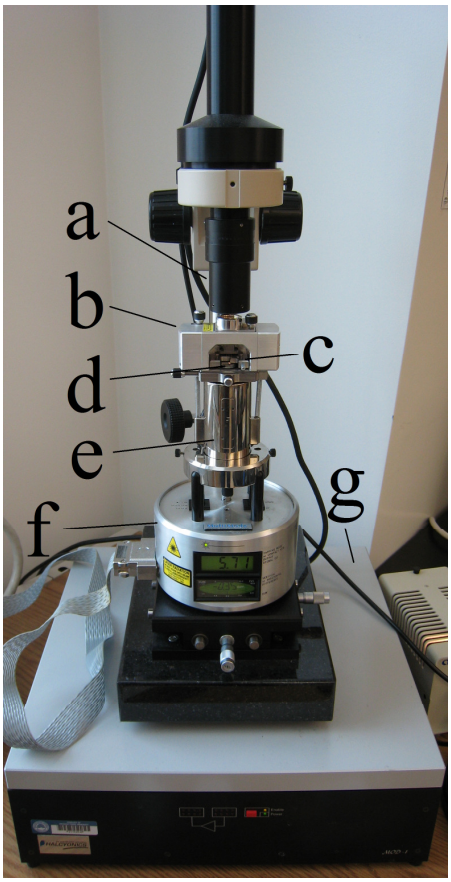

Fig. 6.7: AFM setup. a. Microscope, b. SPM head with laser and photodiode, c. Chip holder, d. Substrate, e. Piezo-electric scanner, f. Signal sum display, g. Vibration isolator.

- VWR Scientific model 1510E incubator
- Barnstead NanoPure Diamond water purification system
- Utility knife
- Plastic toothpicks
- Plastic vials
- Glass flasks

6.2 Experimental Methodology

This section covers the methods used to construct the probes, prepare the clay, coat the substrate and probes with the clay, and obtain AFM force curves.

6.2.1 AFM Probe Construction

The AFM probes were assembled using the following procedure. The AFM chip and chip holder were first cleaned in a UV/ozone cleaner (BioForce Nanosciences, Ames, Iowa) for 20 minutes to remove organic surface contaminants. A piece of trimmed-to-size, freshly cleaved muscovite was then epoxied to a metal AFM puck. The muscovite puck and the AFM chip in the chip holder were then loaded into the AFM. The cantilever of interest was located using the AFM optical microscope, and a small amount of mixed Loctite Marine Epoxy was dabbed onto the muscovite using a plastic toothpick. Using the AFM as a micromanipulator, the cantilever of interest was moved over the glue spot and lowered onto the glue. Care was taken so that only the very tip of the free end of the cantilever touched the epoxy, and the cantilever was lowered slowly to prevent it from crashing into the muscovite and bending excessively. Once the end of the cantilever was

coated in wet epoxy, the tip was raised sufficiently to allow removal of the muscovite puck. The micro-sphere coated muscovite puck was then quickly loaded into the AFM, and a lone micro-sphere was located using the AFM optical microscope. The glue-coated tip of the cantilever was slowly lowered onto the center of the micro-sphere. Once contact was made, the cantilever was raised slowly, and the micro-sphere was attached to the probe. The chip was removed from the AFM chip holder and placed in a numbered grid gel case. The glue was allowed to solidify for 24 hours prior to friction measurements to ensure a strong bond. ESEM images of several constructed probes are shown in Fig. 6.8. The dark area on the tip of the cantilever is the glue.

(a) 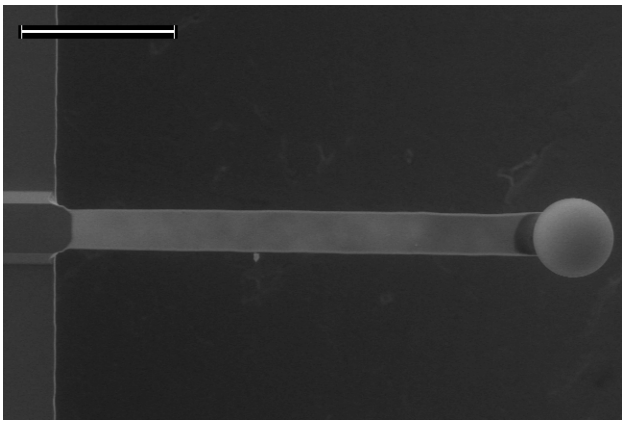 (b) 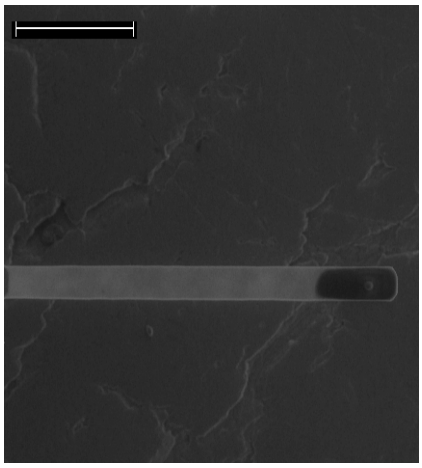

Fig. 6.8: ESEM images of constructed probes. (a) CSC12, cantilever E, 52 µm diameter micro-sphere, scale bar is 100 µm, (b) CSC12, cantilever E, 10 µm diameter micro-sphere, scale bar is 100 µm.

Upon closer inspection of the probe made with a 10 µm diameter micro-sphere, it was determined that the micro-sphere was too small for the purpose of this study. The micro-sphere became fully coated in epoxy, as shown in Fig. 6.9, every time the probes

were constructed. Based upon the difficulties associated with using the 104 and 10 µm diameter micro-spheres, the 52 µm diameter micro-spheres were chosen.

(a)

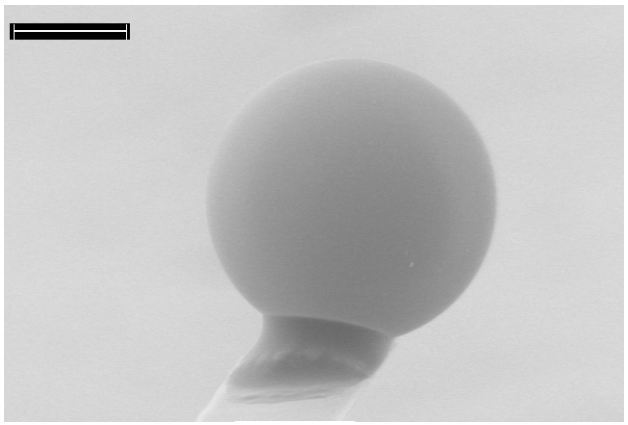

(b)

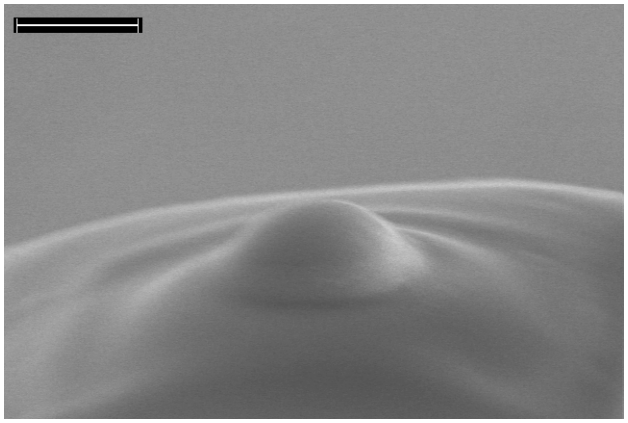

Fig. 6.9: ESEM image showing the amount of epoxy on the micro-sphere after probe assembly. (a) 52 µm diameter micro-sphere, scale bar is 20 µm, (b) 10 µm diameter micro-sphere, scale bar is 5 µm. The 10 µm diameter micro-sphere is coated in epoxy.

6.2.2 Clay Preparation

The method developed in this study for measuring micro-scale friction required attaching clay particles to the micro-spheres. Montmorillonite was chosen for this study because the clay particles consist of thin flexible crystallites (Moll, 2001) which would tend to conform to the shape of the micro-sphere better than plate-like particles such as

kaolinite would. Additionally, kaolinite, which has essentially no permanent layer charge, did not attach to glass surfaces sufficiently to image in previous studies (Bickmore *et al.,* 1999).

The montmorillonite used in this study (Fig. 6.10) was a Wyoming sodium montmorillonite reference clay (SWy-2) obtained from the Source Clays Repository at Purdue University. The properties of the clay (Table 6.3) have been highly studied. The layer charge without exchangeable cations falls into the expected range for montmorillonite of 0.25-0.40. SWy-2 possesses a high cation exchange capacity.

Fig. 6.10: Photograph of SWy-2.

Table 6.3: SWy-2 properties.

Property	Value	Reference
Specific gravity (g/cm^3)	2.70	Parker *et al.* (1980)
Specific surface area (m^2/g)	810	Parker *et al.* (1980)
Cation exchange capacity (meq/100 g)	85	Borden and Giese (2001)

Using x-ray diffraction, the mineralogy of the as-shipped SWy-2 was measured by Chipera and Bish (2001) as consisting of 75% smectite, 8% quartz, 16% feldspar, and 1% gypsum, mica and/or illite, and possibly kaolinite and/or chlorite. However, once the SWy-2 was size-sorted to less than 2 µm, the sample contained 95% smectite, 4% quartz, 1% feldspar, gypsum, mica and/or illite, and possibly kaolinite and/or chlorite (Chipera and Bish, 2001). Given the vast improvement in purity, the clay was first size-sorted prior to coating the probes. The method used to sort the clay is described in Section 6.2.2.1.

6.2.2.1 Size Sorting

The montmorillonite was sorted such that only particles smaller than 2 µm were used. A centrifuge method was used to sort the clay, which required a slurry of the clay to be prepared. 2.0 g of clay was added to 50 mL of deionized water and dispersed with a sonic dismembrator. An integrated form of Stokes' Law, as shown below, was used to calculate the time required in seconds for the sedimentation of particles of a particular diameter and specific gravity under centrifugal acceleration (Svedberg and Nichols, 1923).

$$t = \frac{nlog\frac{R}{S}}{3.81N^2r^2\Delta S}$$

where n = viscosity of the liquid at the existing temperature (poises)

R = radius of rotation of the top of the sediment in the tube (cm)

S = radius of rotation of the surface of the dispersion in the tube (cm)

N = revolutions per second

r = particle radius (cm)

ΔS = difference in specific gravity between the particles and the dispersion

After the clay dispersion was centrifuged for the required time, the supernatant was separated from the vial and dried in the incubator.

6.2.2.2 Interlayer Ion Saturation

The SWy-2 was sodium-saturated using the following procedure. A small mass (0.5 g) of the size sorted SWy-2 obtained using the procedure described in Section 6.2.2.1 was added to a 15 mL plastic vial filled with 1.0 M NaCl and dispersed with a sonic dismembrator. The vial was then put in a shaker for at least 12 hours. The vial was then centrifuged at 9000 rpm for 20 min. The supernatant in the vial was then discarded. The vial was then filled with deionized water, dispersed again with a sonic dismembrator, and then put in the shaker for at least 4 hours. The vial was then centrifuged at 9000 rpm again for 20 min. The supernatant was discarded, and the vial was again filled with deionized water, dispersed with a sonic dismembrator, and then put in the shaker for another 4 hours. Finally, the vial was centrifuged at 9000 rpm for 20 min, and the supernatant was discarded. The montmorillonite was transferred to a heat resistant dish and dried in the incubator for 12 hours. For calcium and potassium-saturation, the same procedure was followed except the solution used was 1.0 M $CaCl_2$ and KCl, respectively.

6.2.2.3 AFM Images of Montmorillonite

The AFM was used to image the particle topography after size sorting. A dilute dispersion (0.05 g/L) of clay was used for this step to image individual clay particles. Complete substrate coverage was not necessary for this step. Section 6.2.3 provides more information on the clay coating procedure.

A standard sharp-tipped AFM probe (NanoProbe SPM tips, wafer #455) was used for imaging purposes. AFM topographical images of the clay particles on a 2.5 μm scale are shown in Fig. 6.11. Some of the features of the clay particles are depicted, such as 1 nm thick layers of clay undergoing stacking and folding. It is reasonable to surmise that during the friction experiments conducted in this study, stacking and folding of the clay particles also occurred. The method used to determine the coefficient of friction (see Section 6.3.2) is based on the difference in behavior as the micro-sphere rotates and slides across the clay-coated surface and back. Such small features, as shown in Fig. 6.11, would not be expected to alter the coefficient of friction measurements obtained from a relatively enormous 52 μm diameter micro-sphere sliding across the clay surface.

6.2.3 Substrate Coating

To attach the clay to the substrate, a procedure developed by Bickmore *et al.* (1999) was modified for this application. A glass coverslip was epoxied onto an AFM sample puck. Polyethyleneimine (PEI) ($(C_2H_5N)_n$, Polysciences, Warrington, Pennsylvania) was diluted 1:2000 by mass with deionized water. The puck was then cleaned in the UV/ozone cleaner for 20 minutes, immersed in the PEI solution for 30 seconds, continuously rinsed with deionized water for 5 minutes, oven-dried for 1 hour,

and allowed to cool. A 0.1 g/L dispersion of clay was prepared using a sonic dismembrator for 10 minutes. The puck was then heated on a hotplate to >100°C, and 100 µL of the clay dispersion was pipetted onto the heated puck and left for 1 minute to flash boil the clay onto the substrate. The puck was then continuously rinsed with deionized water for 20 seconds and dried with compressed air. Finally, the coated puck was cleaned in the UV/ozone cleaner for 20 minutes. The coating coverage (Fig. 7.1) was verified with the AFM in tapping mode to obtain topographic images of the coating coverage, which were compared to images taken of the plain silica glass. The change in thickness of the coating was step-wise in 1 nm increments, indicating the clay coating consisted of individual clay layers.

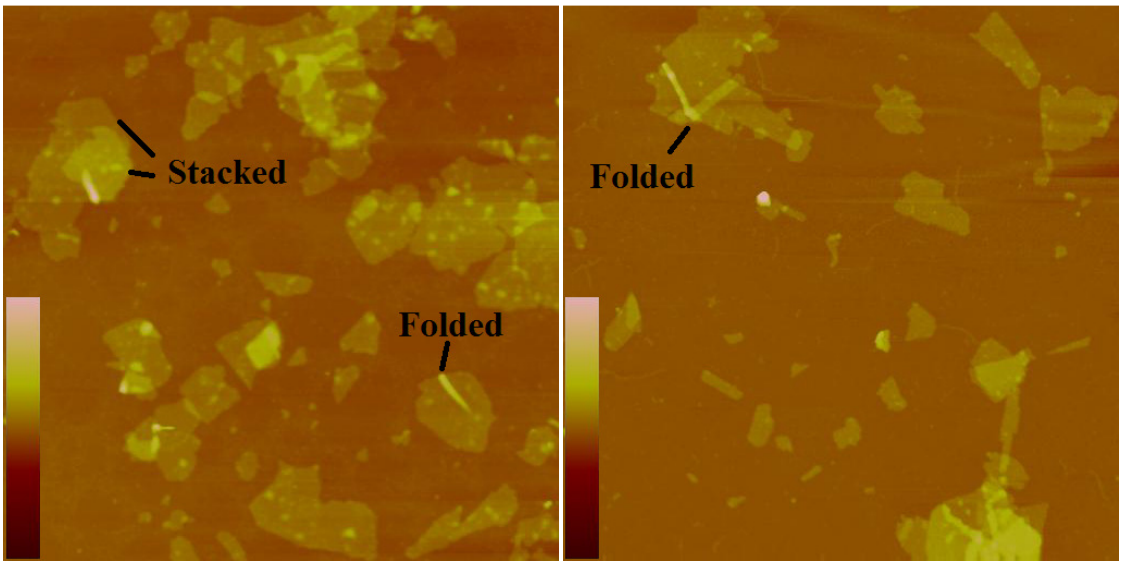

Fig. 6.11: AFM topographical image of individual SWy-2 particles. The topographic scales are 20 nm and each square image is 2.5 x 2.5 µm.

6.2.4 Probe Coating

To coat the AFM spherical glass probes with SWy-2, a similar procedure was used, but the procedure needed to be modified slightly because of the small size of the AFM probes. The AFM chip was put into the AFM fluid chip holder and cleaned in the UV/ozone cleaner for 20 minutes. The AFM chip was then removed from the chip holder using tweezers and submerged into a small beaker containing the same PEI dilution for 30 seconds. The chip was then removed and immersed into a second beaker containing deionized water and held with tweezers in the water for 5 minutes. The chip was not allowed to drop into either beaker given the delicate probe on the end. The chip was then placed back into the fluid chip holder, oven-dried for 1 hour, and allowed to cool. A more concentrated, 1.0 g/L clay dispersion was made by mixing the clay in deionized water and dispersing with a sonic dismembrator for 10 minutes. The chip was then removed from the chip holder and held in the clay dispersion for 30 seconds using tweezers. The chip was then removed and immersed into a second beaker containing deionized water and held with tweezers in the water for 2 minutes. The chip was then placed back into the fluid chip holder, oven-dried for 5 minutes, and allowed to cool. Using an optical microscope, it was verified that the micro-sphere was still attached to the cantilever. Finally, the AFM chip was put into the AFM chip holder and cleaned in the UV/ozone cleaner for 20 minutes. While it was not possible with the equipment available to image the clay coverage on the spherical probes, another substrate was prepared using this method, and the AFM was used to obtain topographic images (Fig. 7.2) of the clay coating.

6.2.5 Atomic Force Microscope

This section will explain the methodology used to obtain topographic images and force curves for the clay under wet and atmospheric conditions.

6.2.5.1 Imaging

Topographic images of a surface were obtained using the AFM in tapping mode. Topographic information is measured by scanning a sharp-tipped AFM probe across a substrate in a raster pattern. The probe tip is lightly tapped on the surface to minimize lateral forces which may cause sample disturbance or probe breakage. During this scanning, the photodiode detects the change in light intensity from the laser focused on the reflective back of the probe tip. The light intensity is a measure of the path length of the reflected beam. Changes in light intensity provide a measure of the change in the path length between the cantilever and the photodiode, and as a result, a measurement of the vertical height of the substrate. AFM images can also be obtained with the substrate submerged (Fig. 7.2).

6.2.5.2 Force Curves

Force curves were obtained using the AFM in contact mode. In this mode, the piezo-electric scanner was moved vertically to bring the AFM tip in contact with the substrate. A force curve is defined as the plot of the normal force at the free end of the AFM cantilever as a function of the separation, which is the vertical distance between the free end of the cantilever and the substrate. Force curves are thus generally “L-shaped”

plots (Fig. 6.12), and provide information on the maximum normal force applied to the substrate.

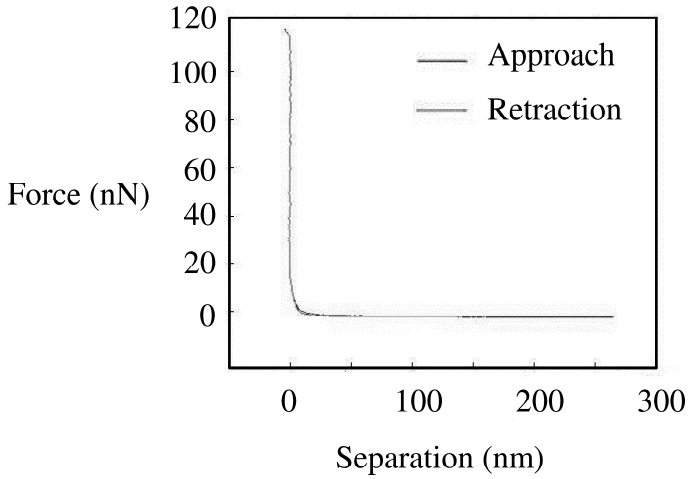

Fig. 6.12: Force vs. separation on approach and retraction for glass on mica. The approach and retraction curves overlap as expected. The maximum normal force applied is 115 nN.

To generate the force curves in this study, cantilever deflection [V] as a function of vertical piezo-electric scanner distance [nm] measurements were first recorded. After reaching a user-specified deflection, the piezo-electric scanner reversed, leading to the retraction part of the plot. A sample of such a plot is shown in Fig. 6.13. In this plot, the initial starting point is where the tip and substrate were not yet in contact, and therefore there was no force. The piezo-electric scanner continued to extend on the approach portion of the curve until it reached a predefined cantilever deflection and then retracted. Hysteresis, where the approach and retraction curves do not follow the exact same deflection-distance relationship, often occurs due to frictional forces. The constant compliance region is defined as the linear portion of the deflection-distance curve. The

curve is calibrated such that the slope of the constant compliance region equals one. This calibration ensures that the force curve will have the force applied at a separation distance of zero, meaning the probe and substrate are in contact.

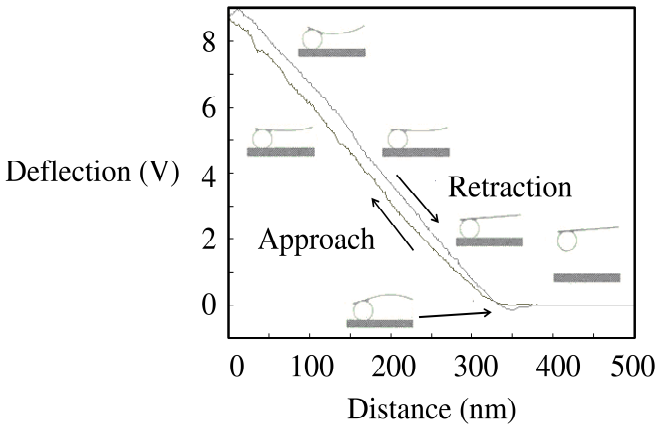

Fig. 6.13: Deflection vs. displacement for montmorillonite shearing on montmorillonite in a wet environment. Schematics of cantilever deflection are greatly exaggerated for explanation purposes.

This calibration adjusts the deflection axis such that the cantilever deflection [nm] is plotted. The normal force vs. distance can also be plotted to determine the variation in normal force as the piezo-electric scanner moved. This is accomplished by multiplying the deflection [nm] by the effective spring constant of the cantilever. Finally, to plot the normal force as a function of separation (force curve), the vertical deflection of the free end of the cantilever is subtracted from the piezo-electric scanner height, thereby generating the classic "L-shaped" plot where the force is plotted at approximately zero separation distance.

6.2.5.3 Wet and Dry Friction

Experiments in which the wet coefficient of friction was to be obtained were conducted in an AFM fluid cell. This fluid cell is similar to an AFM chip holder. However, it is made of acrylic and provides an opening for the cantilever and substrate to come in contact when submerged. Given the delicate nature of the setup, a peristaltic pump was used to introduce water into the system and to remove it after the experiment concluded to prevent equipment damage. The dry experiments were conducted under atmosphereic conditions.

6.3 Micro-scale Data Analysis

This section covers the methods used to calculate the spring constant of the cantilevers and the coefficient of friction and sliding velocity of the clay-coated surfaces during the micro-scale friction experiments.

6.3.1 Effective Spring Constant

The dimensions of the assembled probes were characterized using the ESEM. Fig. 6.14 shows a diagram of a probe marked to illustrate the dimensions measured. L_0 is the flexible length of the cantilever from the base to the edge of the glue spot holding the glass micro-sphere and L_1 is the distance from the edge of the glue spot to the midpoint at which the micro-sphere is attached. L_2 is the diameter of the micro-sphere. One must also obtain the angle θ of the cantilever from the horizontal from the AFM manufacturer ($\theta < 0$). This angle can be estimated as -10 to -15° in most cases (Attard *et al.*, 1999, 2007).

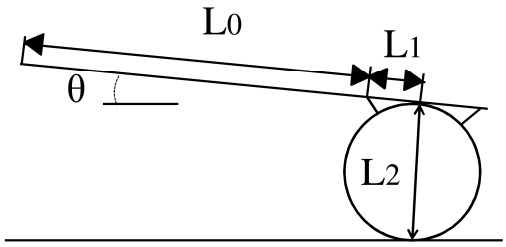

Fig. 6.14: Schematic of probe dimensions measured with an ESEM.

The method used to determine the coefficient of friction, μ, did not require calibration other than the probe dimensions and θ. However, measurements of the normal force between the probe and substrate required the normal spring constant of the cantilever. The normal spring constant of the cantilever was measured using the thermal method with a Dimension 3100 AFM modified with closed loop scanning capability prior to the attachment of the micro-sphere. A closed loop scanner allows for much greater precision in collecting force curves, and it is necessary for this method.

The calibrated spring constant (k_{cal}) was then corrected for the attachment of the micro-sphere. The effective spring constant (k_{eff}) is calculated as:

$$k_{eff} = \frac{k_{cal}}{cos^2\theta}\left(\frac{L_{cal}}{L_0}\right)^3$$

where L_{cal} = full cantilever length when the thermal method is used to obtain k_{cal}

6.3.2 Coefficient of Friction and Sliding Velocity

The AFM has long been used to image clay particle morphology (Blum, 1994; Bosbach *et al.*, 2000; Bickmore *et al.*, 2001, 2002; Piner *et al.*, 2003) and has even been

used to measure the pore structure of wet clay (Selvam *et al.*, 2006). Nishimura *et al.* (2002) used the AFM colloidal probe technique to measure normal forces between the basal surfaces of clays. The AFM has also been used to measure micro-scale frictional forces by tracking the torsion of the cantilever during scanning (Ruan and Bhushan, 1994; Bhushan *et al.*, 1995; Jones *et al.*, 2004; Gao *et al.*, 2004; Bhushan, 2005; Gnecco *et al.*, 2005). However, this technique requires painstaking calibration of both the torsional spring constant of the cantilever and the lateral sensitivity of the photodetector.

In this study, force curves were used to determine μ using the axial method developed by Attard *et al.* (2007). Given the uncertainty in determining the spring constant of the cantilevers, the axial method was used in this study because k_{eff} is not required to determine μ. The classic lateral method requires the torsional spring constant to determine μ, which would lead to uncertainty in the error introduced. The axial method provides results very similar to results obtained by the lateral method, as was demonstrated by Attard *et al.* (2007). Attard *et al.* (2007) measured the wet μ of silica glass on mica as 0.28 with the axial method and 0.31 with the lateral method.

The axial method uses the difference between the slopes of the approach and retraction portions of the plot of the deflection [V] vs. distance [nm] plot (Fig. 6.13) to determine μ. The slope of interest starts at the point of intersection between the approach and retraction curves. When the probe touches the surface, the cantilever bends, causing the probe to rotate and slide. The rotation and sliding are impeded by frictional forces, resulting in hysteresis between the constant compliance regions of the approach and retraction curves. Stiernstedt *et al.* (2005) and Attard *et al.* (2007) derived equations that provide μ in terms of L_0, L_1, L_2, θ, and the difference in slope in the constant compliance

regions. The sliding velocity during the probe-substrate interaction can also be calculated from these parameters and the approach and retraction velocities. The following parameters are defined:

$$a = L_1 cos\theta + L_2 sin\theta$$

$$b = L_1 sin\theta - L_2 cos\theta$$

$$c = \frac{2}{3} L_0^3 cos\theta + L_0^2 a$$

$$d = L_0^2 cos\theta + 2L_0 a$$

$$f = \frac{2}{3} L_0^3 sin\theta + L_0^2 b$$

$$h = L_0^2 sin\theta + 2L_0 b$$

$$i = ccos\theta + ad$$

$$j = fcos\theta + ah$$

The ratio of the horizontal displacement of the probe on the substrate, y_2, to the vertical piezo-electric scanner drive distance, z_2, which is also equal to the ratio of their velocities $\dot{y_2}$ and $\dot{z_2}$, is:

$$\frac{y_2(t)}{z_2(t)} = \frac{\dot{y_2}}{\dot{z_2}} = \frac{csin\theta + bd}{ccos\theta + ad}$$

From this equation, the sliding velocity, $\dot{y_2}$, is determined. A final term is defined to capture the change in slope from the deflection in terms of photodiode voltage [V], ΔV,

vs. distance [nm], Δz_2. If $\alpha_{\pm} = \Delta z_2/\Delta V_{\pm}$ [nm/V] with the slopes of the constant compliance region on either the approach (+) or retraction (-) portions, then:

$$e = \frac{{\alpha_+}^{-1} - {\alpha_-}^{-1}}{{\alpha_+}^{-1} + {\alpha_-}^{-1}}$$

The coefficient of friction, which is the ratio of the horizontal friction force to the vertical surface force, $\mu = \left|F_y/F_z\right|$, is given by:

$$\mu = \frac{ih - jd + \sqrt{(ih - jd)^2 + 4ihjde^2}}{2jhe}$$

Chapter 7

Micro-scale Experiments – Results and Discussion

This chapter presents and discusses the results from the micro-scale experiments. The clay coverage obtained using the procedure described in Sections 6.2.3 and 6.2.4 is presented in Section 7.1. The control tests that were conducted prior to the clay friction tests are discussed in Section 7.2. The different probes that were used throughout the tests are depicted and described in Section 7.3. Finally, Section 7.4 includes all of the friction results for both the wet and dry montmorillonite friction tests and compares them to macro-scale experiments and RPT calculations.

7.1 Clay Coverage

To determine the coverage of montmorillonite, the AFM imaging capability was used. To minimize the lateral force on the glass substrate, tapping mode was used in this study for imaging, as is common practice (Section 6.2.5.1). AFM images of the montmorillonite-coated glass using the substrate coating procedure and plain silica glass are shown in Fig. 7.1. AFM images of the montmorillonite-coated glass using the probe coating procedure are shown in Fig. 7.2. These images are blurrier given that they were obtained in a fluid cell with the substrate submerged. Significant loss of clay particles due to the water was not apparent.

7.2 Control Tests

Several control tests were conducted to ensure that the procedure generated accurate μ values and sufficient clay coverage. These tests will be discussed in the following subsections.

7.2.1 Silica Glass on Muscovite Mica

Attard *et al.* (2007) tested the axial method for measuring μ against the standard lateral method. They measured the wet μ of silica glass on mica as 0.27 ± 0.01 (36 µm diameter silica glass probe, axial method), 0.29 ± 0.03 (16 µm diameter silica glass probe, axial method) and 0.31 ± 0.01 (36 µm diameter silica glass probe, lateral method) where limits indicate standard error on the mean. These results show that the two methods provide comparable results. Given the uncertainty in determining the spring

constant of the cantilevers, the axial method was used in this study because the effective normal spring constant is not necessary to determine μ.

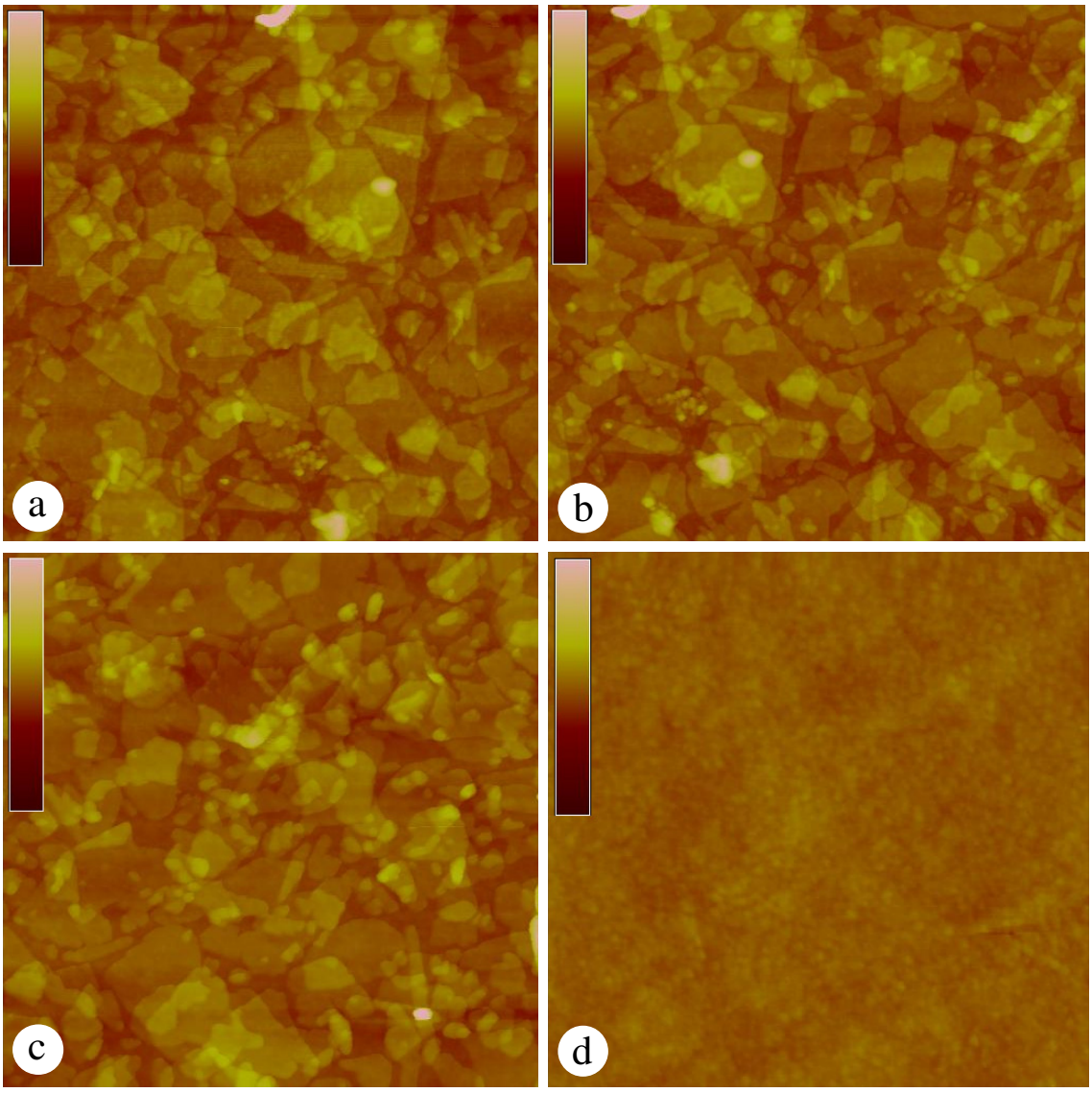

Fig. 7.1: (a), (b), (c) AFM images of SWy-2 coverage on glass at different locations using the substrate coating procedure with topographic scale 20 nm. Each square image is 2 μm by 2 μm. (d) AFM image of silica glass coverslip with topographic scale 10 nm. Square image is 1.1 μm by 1.1 μm.

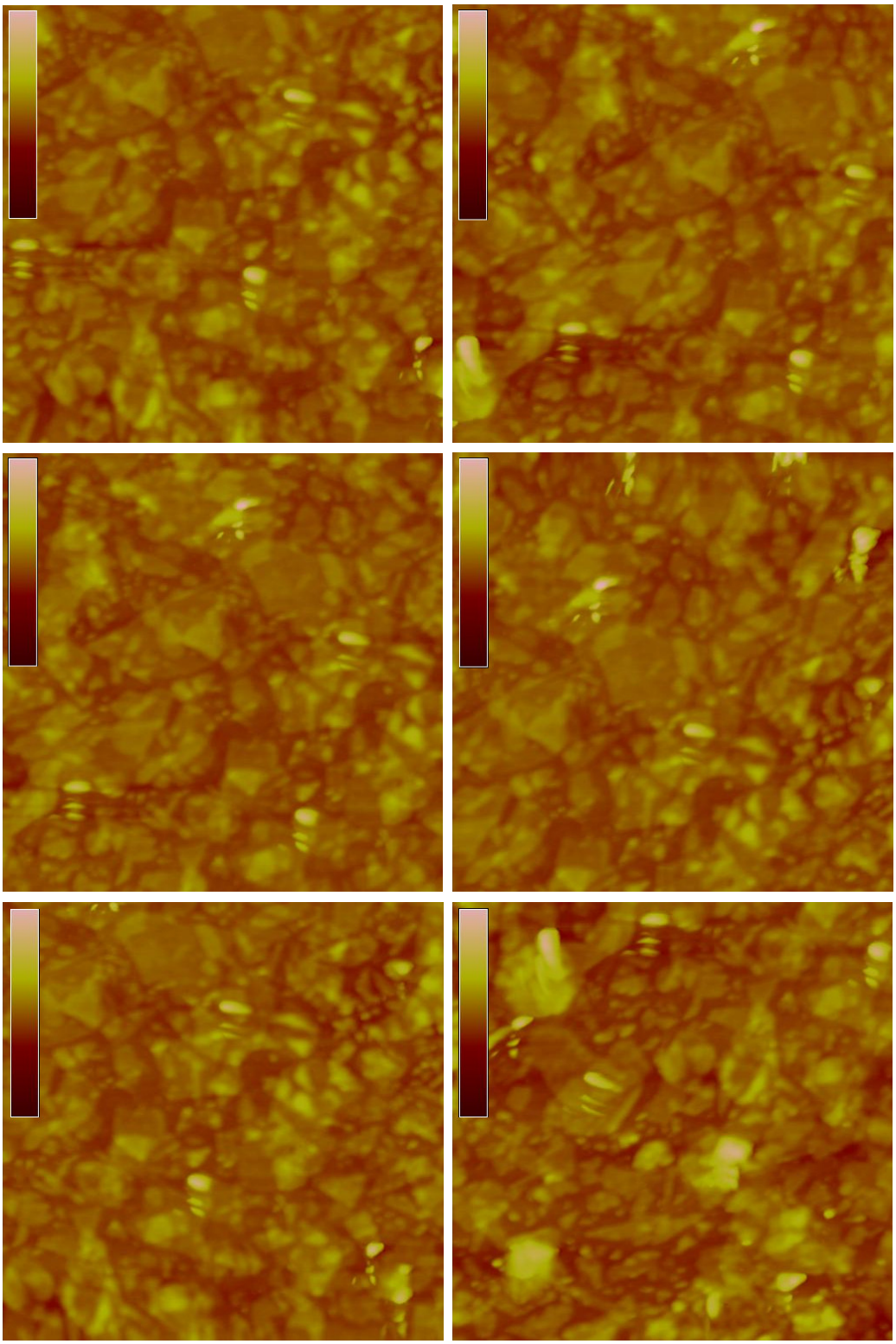

Fig. 7.2: AFM images of SWy-2 coverage on glass using the probe coating procedure with topographic scale 20 nm. Each square image is 2 μm by 2 μm. The images were taken while the substrate was submerged in the fluid cell.

AFM friction experiments were conducted in this study to determine the wet μ of silica glass on mica, and it was determined that $\mu = 0.29 \pm 0.02$ (limits always indicate one standard deviation in this study's results; deflection-distance curves in Appendix C), which matches well with the range of values determined by Attard *et al.* (2007). Probe 1, described in Section 7.3, was used in these experiments.

7.2.2 PEI Removal

Another control test was conducted to ensure that potential leftover PEI used to glue clay particles to the probe and substrate was removed using the UV/ozone cleaner. Theoretically, PEI which remained could stick to the opposing surface and lead to erratic behavior and incorrectly high μ values. Friction experiments were conducted before the PEI was applied, after the PEI was applied, and after the PEI was removed. The results (Table 7.1) show that the UV/ozone cleaner removed excess PEI effectively. Probe 2, described in Section 7.3, was used in the PEI control tests.

Table 7.1: PEI removal control test results (deflection-distance curves in Appendix D).

	Wet μ
Before PEI application	0.29 ± 0.01
After PEI application	0.47 ± 0.02
After PEI removal	0.28 ± 0.01

7.2.3 UV/Ozone Cleaning Effect on Clay Coverage

The final control test that was conducted was to ensure that the UV/ozone cleaning process did not affect the clay coverage. The clay-coated substrates were imaged

before and after cleaning, rinsing with de-ionized water, and drying (Fig. 7.3). It is evident from the topographic scans that the coverage was not affected by the UV/ozone cleaner.

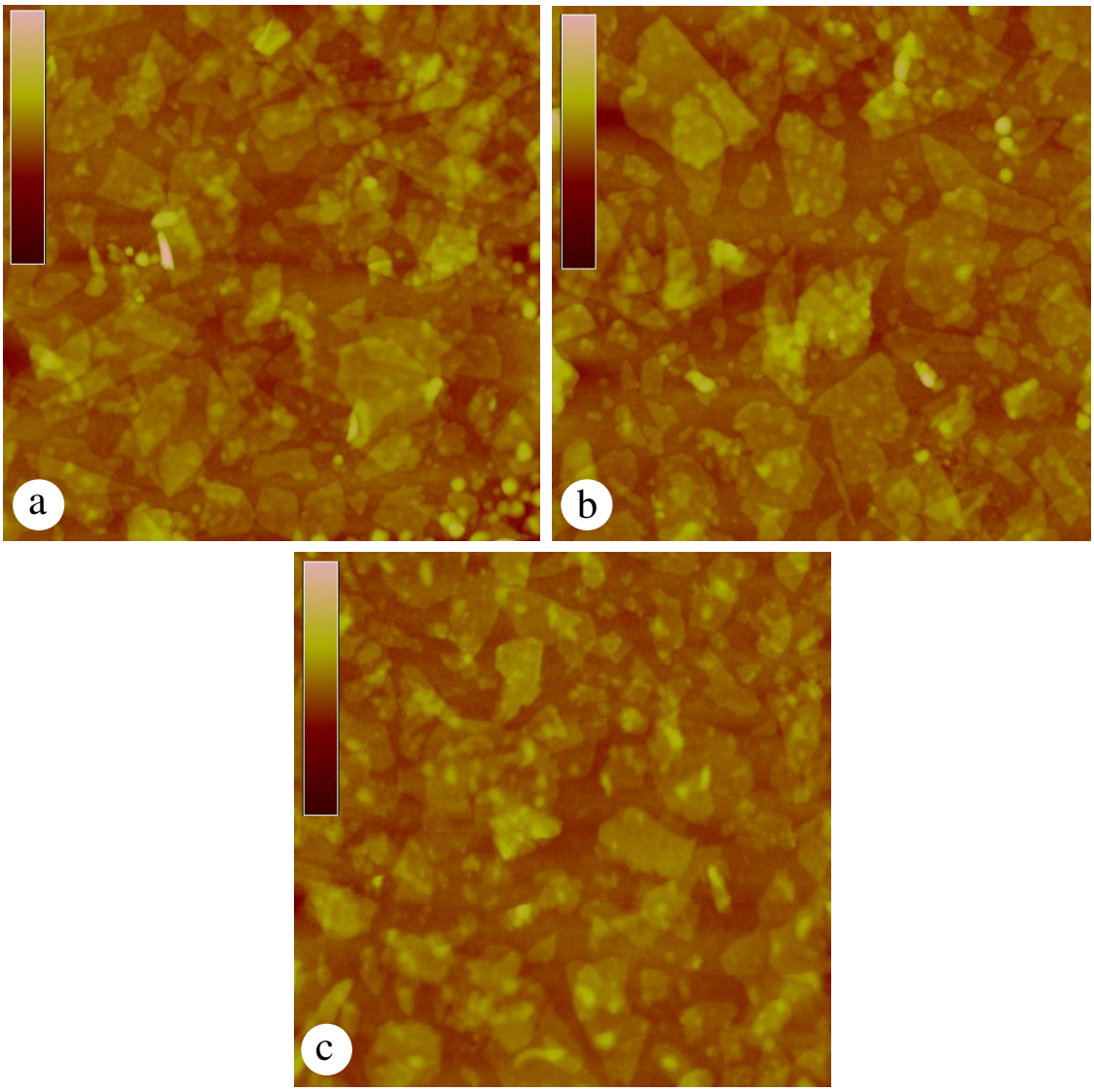

Fig. 7.3: (a), (b) AFM images of SWy-2 coverage on glass at different locations before UV/ozone cleaning (c) AFM image of SWy-2 coverage on glass after UV/ozone cleaning. No change in coverage is apparent. Topographic scales are 20 nm. Each square image is 2 μm by 2 μm.

7.3 Probe Properties and Images

While testing cantilever E (Fig. 6.8), the longest cantilever with the lowest spring constant, it was determined that the micro-sphere on the end of the cantilever was rolling around tremendously, leading to unusable force curves. The axial method requires clearly defined regions of approach and retraction with constant slope values to be useful. Cantilevers A, C, and F were used in this study. The properties for the probes are shown in Table 7.2. The analysis procedure to determine the effective spring constants of the constructed probes is explained in Section 6.3.1. ESEM images of the probes are shown in Figs 7.4 – 7.8.

Table 7.2: Probe properties.

Probe	Chip Type	Lever	k_{cal} [N/m]	k_{eff} [N/m]	Resonant Frequency [kHz]	L [μm]	L_0 [μm]	L_1 [μm]	L_2 [μm]	w [μm]
1	NSC	F	0.2000	0.69	41.5	250.0	185.0	41.91	47.03	32.95
2	CSC	C	0.0779	0.39	47.4	130.0	85.07	23.11	51.63	28.67
3	CSC	A	0.3896	2.2	91.6	101.9	64.41	21.75	50.89	27.18
4	CSC	A	0.1604	0.49	68.6	95.89	73.92	8.26	52.34	24.61
5	CSC	A	0.0907	0.18	61.9	97.94	86.78	3.97	55.37	25.28

7.4 Force Curves

This section discusses the results obtained for the different micro-scale friction experiments. The results are divided up by experiment condition: dry sodium-saturated montmorillonite, wet sodium-saturated montmorillonite, wet calcium-saturated montmorillonite, and wet potassium-saturated montmorillonite.

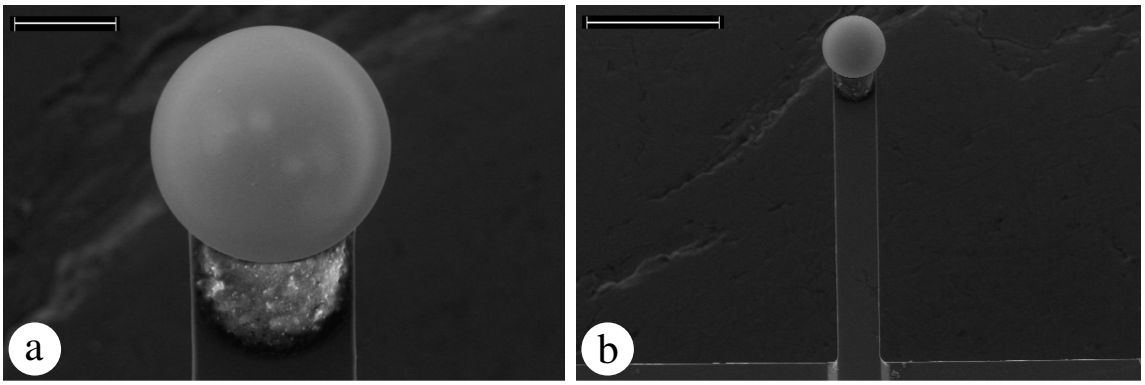

Fig. 7.4: ESEM images of Probe 1. (a) Scale 20 μm, (b) Scale 100 μm.

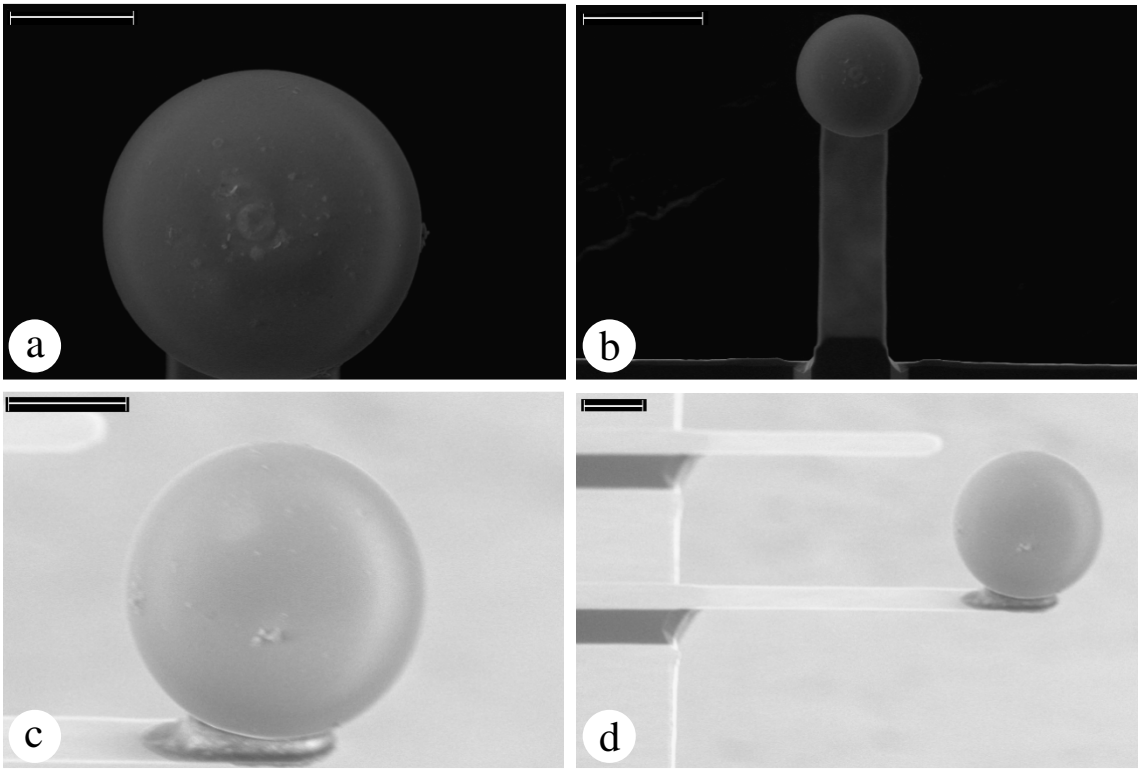

Fig. 7.5: ESEM images of Probe 2. (a), (c), (d) Scale 20 μm, (b) Scale 50 μm. Differences in contrast are a function of the tilt angle used when capturing images with the ESEM.

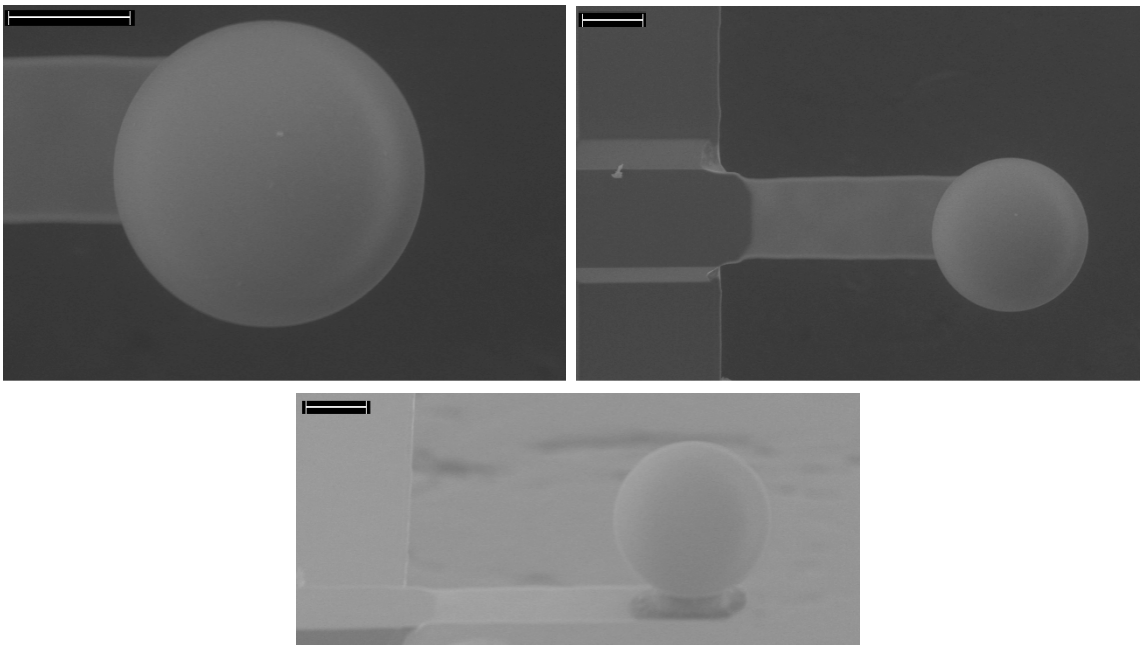

Fig. 7.6: ESEM images of Probe 3. Scale is 20 μm in all images. Differences in contrast are a function of the tilt angle used when capturing images with the ESEM.

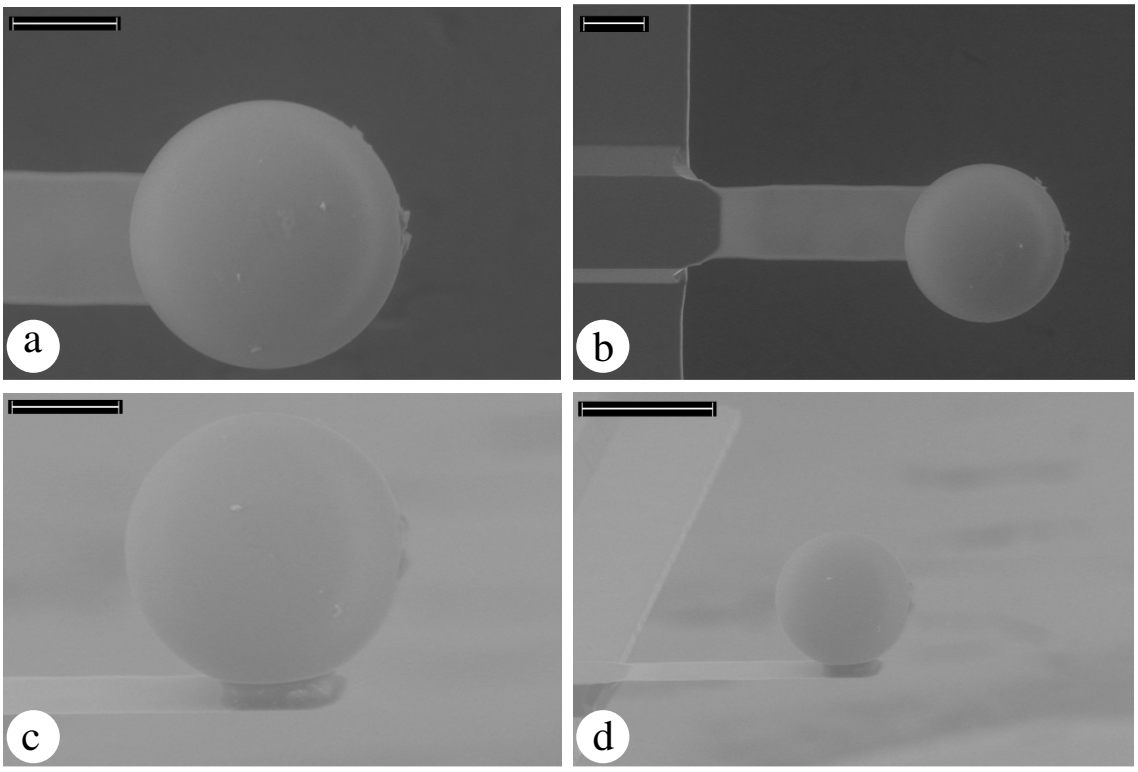

Fig. 7.7: ESEM images of Probe 4. (a), (b), (c) Scale 20 μm, (d) Scale 50 μm. Differences in contrast are a function of the tilt angle used when capturing images with the ESEM.

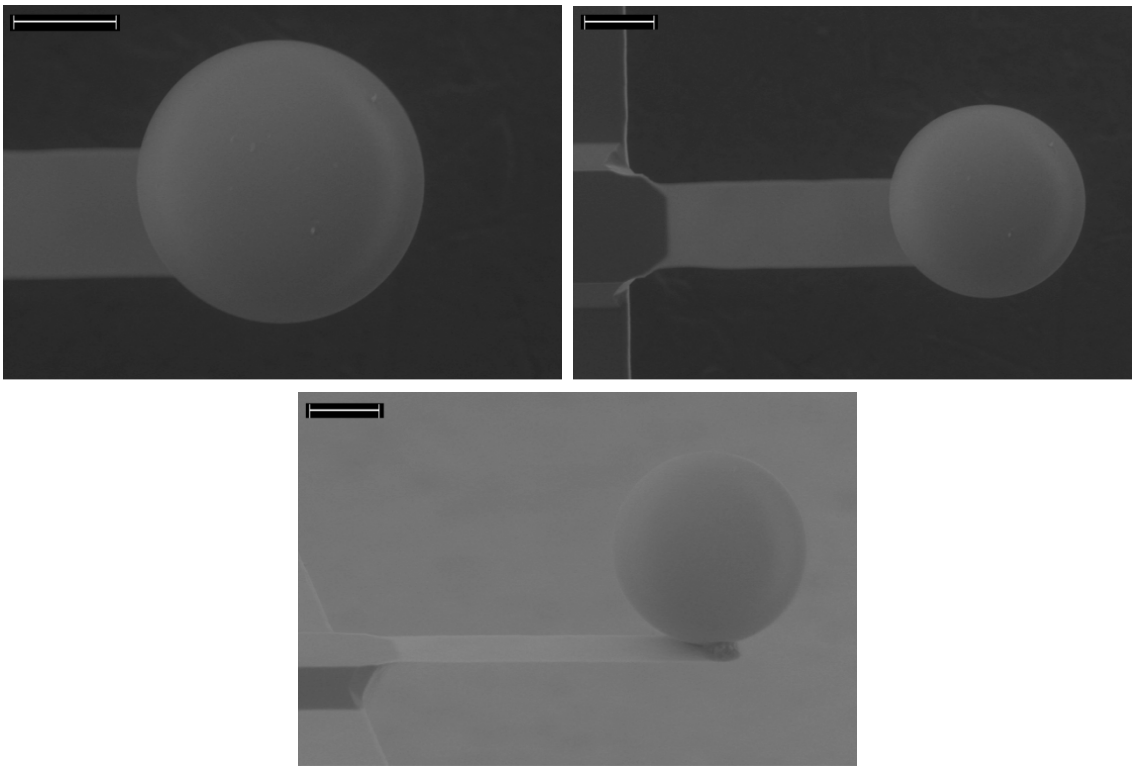

Fig. 7.8: ESEM images of Probe 5. Scale is 20 μm in all images. Differences in contrast are a function of the tilt angle used when capturing images with the ESEM.

7.4.1 Dry Sodium-saturated Montmorillonite

Probe 1 was used to measure the dry friction between two sodium-saturated montmorillonite coated surfaces. Different locations on the substrate were used to verify the accuracy of the friction measurements obtained. The μ value between sodium-saturated dry montmorillonite was determined to be 0.72 $\pm$ 0.03 (deflection-distance curves in Appendix E), which is in quantitative agreement with the macro-scale dry μ of 0.74 and 0.75 measured by Morrow *et al.* (1982) and Moore and Lockner (2007), respectively, for similar sliding velocities (see Section 5.2.2). The sliding velocities tested in the micro-scale experiments were 0.115 μm/s and 0.533 μm/s, and the maximum applied normal force was 180 nN. A histogram of the results is shown in Fig. 7.9.

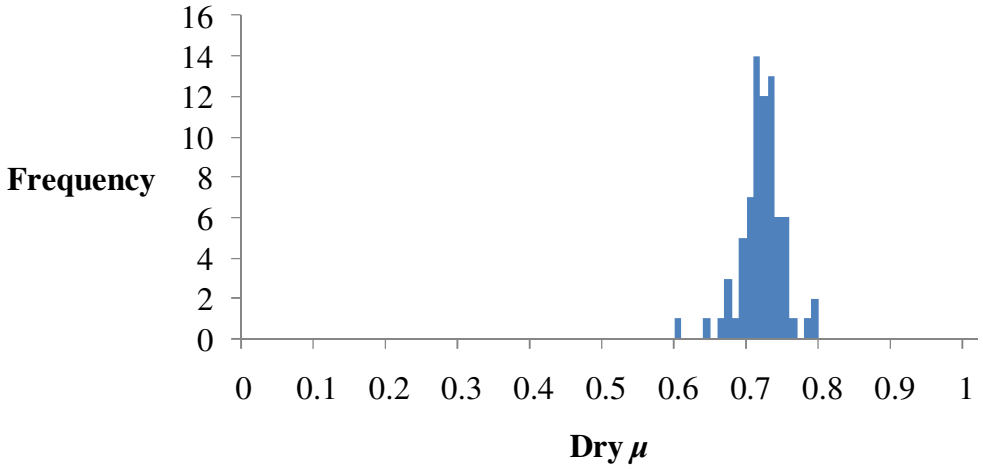

Fig. 7.9: Histogram of dry coefficient of friction frequency for sodium-saturated montmorillonite (bin width = 0.01, 74 measurements).

A summary plot of the dry micro-scale friction coefficient results as a function of sliding velocity compared to previous macro-scale research (Section 5.2.2) is given in Fig. 7.10. The results from this study and from Morrow *et al.* (1982) and Moore and Lockner (2007) are greater than those obtained by Morrow *et al.* (1992) and Morrow *et al.* (2000), which may have been affected by room humidity (Moore and Lockner, 2007). Additionally, Moore and Lockner (2007) indicated that due to the thin grain texture of montmorillonite, the grains may preferentially curl and fold during shear rather than sliding along basic clay units, leading to a greater dry friction coefficient than would be expected based on the electrostatic separation energy.

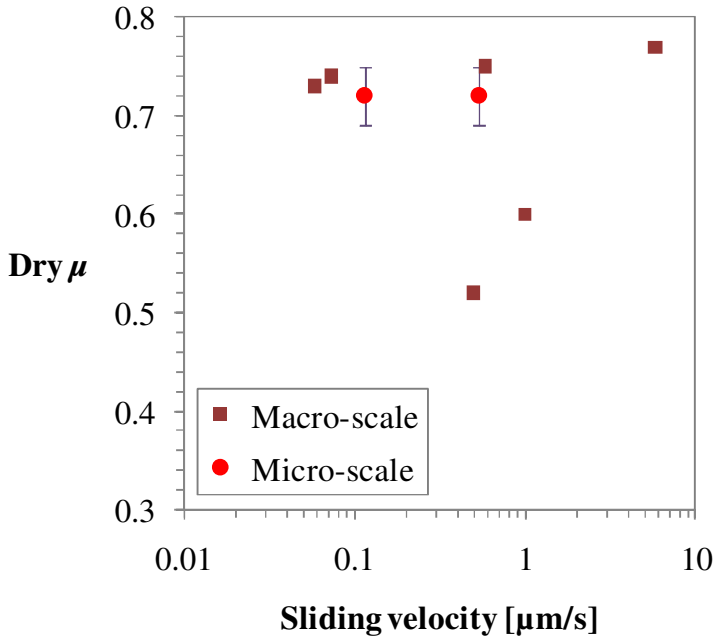

Fig. 7.10: Coefficient of friction as a function of sliding velocity for micro-scale and macro-scale dry friction tests on montmorillonite.

Given that the contact area of the micro-sphere probes and sample surfaces were at most a few microns across, the factor controlling clay friction under dry conditions can involve distances no larger than that. Drying montmorillonite tends to form particles which are less than a few microns across. Montmorillonite is unique among 2:1 phyllosilicates in that under certain conditions, such as Na^+ saturated interlayers and low ionic strength, the individual layers may completely disperse in aqueous fluid. When such a dispersion is dried, the layers may come back together in a somewhat haphazard fashion. While the layers preferentially aggregate face-to-face along their basal surfaces, they may be misaligned horizontally, have different sizes, and so on. Since the individual platelets are quite flexible, they bend to fit their surroundings, with the result that the aggregates often form in a shape more like an American football than a deck of cards. The frictional strength of most minerals follows Byerlee's Law, as described in Section

5.2.2, where the maximum dry μ is approximately 0.85. However, phyllosilicates are a major exception to the rule, ostensibly because of the parallel planes of weaker bonds between layers (Moore and Lockner, 2004). If the orientations of montmorillonite layers in dried samples are sub-parallel, their frictional strength may be related to more than just the ease with which individual layers can slide past one another, and their overall behavior may more closely approximate Byerlee's Law. The extremely large range for montmorillonite μ values in macro-scale experiments (0.06 - 0.78, Moore and Lockner, 2007) could perhaps be explained by differences in normal stress, displacement magnitude, shear rate, hydration state, pore pressure, and thickness and geometry of particles formed during drying.

7.4.2 Wet Sodium-saturated Montmorillonite

Probe 3 was used to measure the wet friction between two sodium-saturated montmorillonite coated surfaces. Different locations on the substrate were used to verify the accuracy of the friction measurements obtained. The μ value between sodium-saturated wet montmorillonite in the micro-scale tests was determined to be 0.20 ± 0.03 (deflection-distance curves in Appendix F), which is in quantitative agreement with the macro-scale wet μ of 0.23 and 0.18 measured by Morrow *et al.* (2000) and Moore and Lockner (2007), respectively, for similar sliding velocities. The sliding velocity tested in the micro-scale experiments was 1.2 μm/s, and the maximum applied normal force was 800 nN. A histogram of the results is shown in Fig. 7.11.

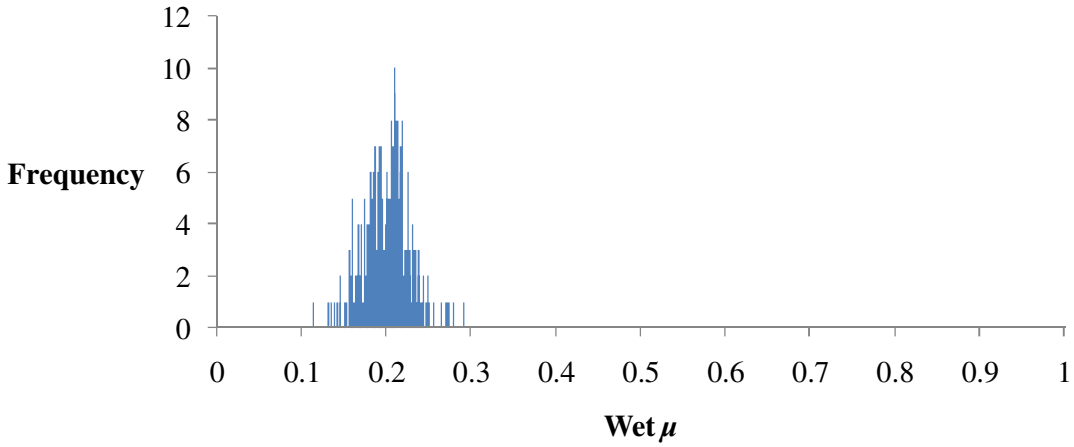

Fig. 7.11: Histogram of wet coefficient of friction frequency for sodium-saturated montmorillonite (bin width = 0.001, 341 measurements).

7.4.3 Wet Calcium-saturated Montmorillonite

Probe 4 was used to measure the wet friction between two calcium-saturated montmorillonite coated surfaces. The μ value between calcium-saturated wet montmorillonite was determined to be 0.07 $\pm$ 0.02 (deflection-distance curves in Appendix G), which is in quantitative agreement with the macro-scale wet μ of 0.07 and 0.08 measured by Stark and Eid (1994) and Saffer and Marone (2003), respectively, for similar sliding velocities. The sliding velocity tested in the micro-scale experiments was 1.3 μm/s, and the maximum applied normal force was 140 nN. A histogram of the results is shown in Fig. 7.12.

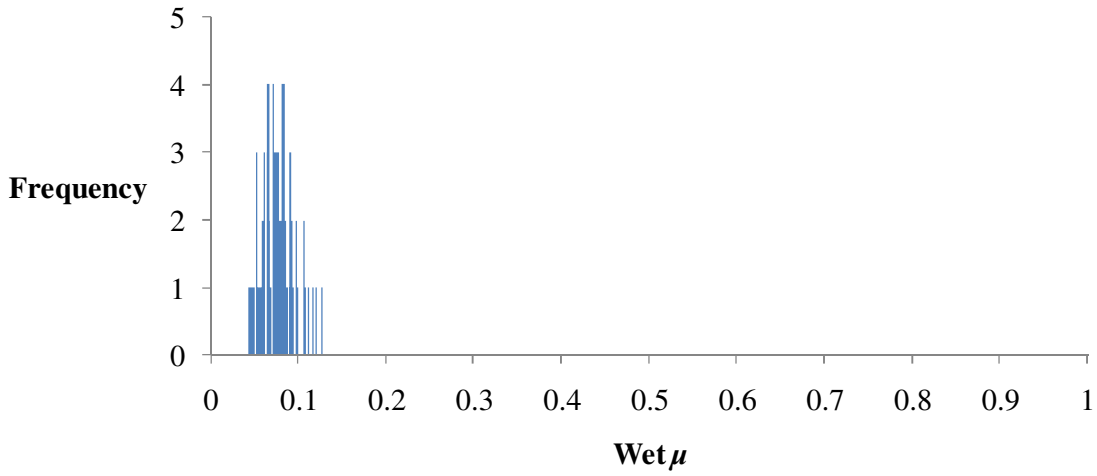

Fig. 7.12: Histogram of wet coefficient of friction frequency for calcium-saturated montmorillonite (bin width = 0.001, 91 measurements).

7.4.4 Wet Potassium-saturated Montmorillonite

Probe 5 was used to measure the wet friction between two potassium-saturated montmorillonite coated surfaces. Different locations on the substrate were used to verify the accuracy of the friction measurements obtained. The measured μ values between potassium-saturated wet montmorillonite surfaces exhibited a bimodal distribution, with peaks of μ values at 0.07 ± 0.01 and 0.23 ± 0.02 (deflection-distance curves in Appendix H). The lower of these two values is consistent with the results obtained from the wet friction experiments conducted on calcium-saturated montmorillonite, and the higher value is consistent with the results from the wet friction experiments on sodium-saturated montmorillonite. The sliding velocity tested in the micro-scale experiments was 1.2 μm/s, and the maximum applied normal force was 70 nN. A histogram of the results is shown in Fig. 7.13.

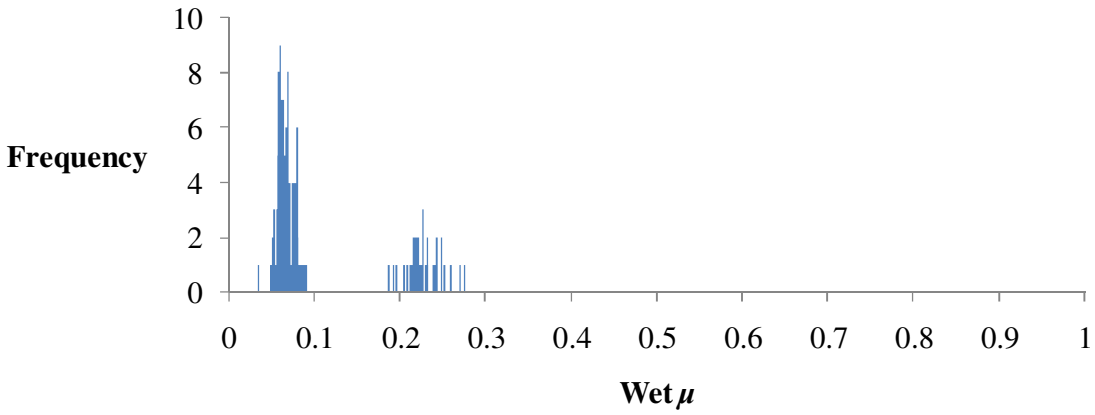

Fig. 7.13: Histogram of wet coefficient of friction frequency for potassium-saturated montmorillonite (bin width = 0.001, 167 measurements).

7.4.5 Summary of Wet Micro-scale Friction

A summary plot of the wet micro-scale results compared to previous macro-scale research (Chapter 5) is given in Fig. 7.14. The wet micro-scale μ correlates well with the macro-scale wet μ. While it was not possible to test a wide range of sliding velocities in the micro-scale tests given equipment limitations, the results obtained do seem reasonable when compared to macro-scale specialized triaxial shear tests, direct shear tests, and ring shear tests. From a macro-scale perspective, it is known that for the residual μ to be obtained, sufficient sliding must occur such that the grains realign along the shear plane. The specialized triaxial shear experiments were generally limited to a total displacement of 9 mm, while the ring shear and direct shear experiments could be sheared to relatively large displacements as needed. This mechanism may also explain the two different friction regimes apparent in the micro-scale tests. While the actual grain alignment at the contact point of the probe and substrate is unknown, it is reasonable to surmise that in some cases, the grain alignment may have been uniform enough to yield a μ similar to a residual μ, as was found in the direct shear and ring shear tests ($\mu \approx 0.10 \pm 0.03$).

However, in other cases, such as the triaxial shear experiments ($\mu \approx 0.18 \pm 0.05$), the displacements were not large enough and the grains were not aligned sufficiently to produce residual μ values.

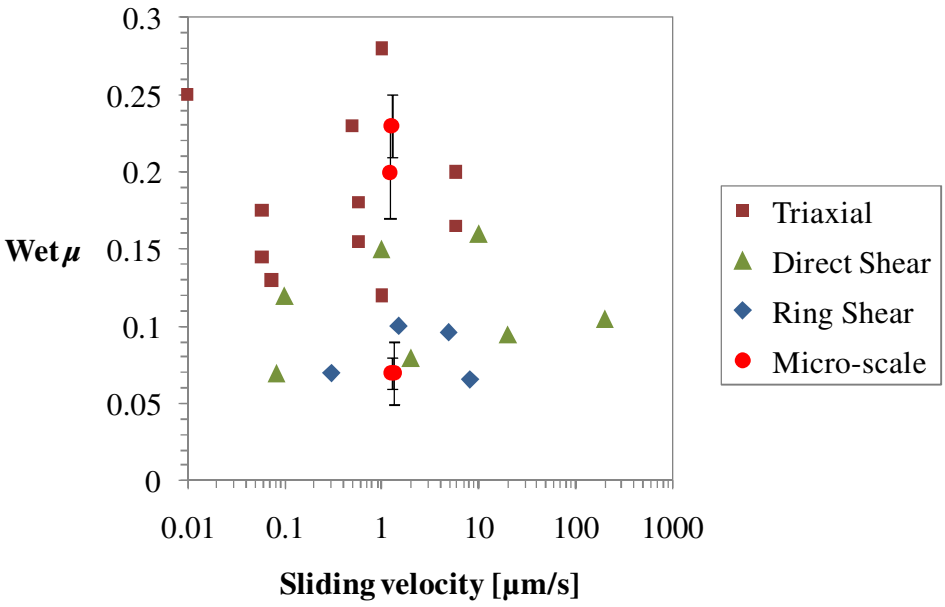

Fig. 7.14: Coefficient of friction as a function of sliding velocity for micro-scale and macro-scale wet friction tests on montmorillonite.

The AFM friction experiments conducted in this study occurred on the micro-scale (1-100 µm) because micro-spheres were used for the AFM tips. No attempt was made to obtain the size of the contact area during the friction experiments. However, an estimate of the horizontal displacement magnitude at the probe-substrate interface, y_2, can be made using the equations described in Section 6.3.2. Based on the experimental deflection-distance curves, the average vertical piezo-electric scanner displacement, z_2, is on the order of 300 nm. Therefore, using typical probe dimensions, the calculated value of y_2 is approximately 150 nm. This displacement is equivalent to sliding over

approximately 280 equilibrium positions, represented by the center-to-center distance of λ = 0.53 nm between holes in the arrangement of silica tetrahedra.

The clay particles were size-sorted to less than 2 μm in size, as described in Section 6.2.2.1. As shown in Fig. 6.11, the particles were in many cases larger than 150 nm. Therefore, the displacement distances in the AFM tests were about equal to the size of one clay particle.

Because the μ values from the AFM tests are based on the slopes of the approach and retraction portions of the deflection-displacement plots, as well as the probe dimensions, the calculated μ values should be essentially the same, whether the sliding occurred over 25 nm or 150 nm. However, there are practical limitations to using very small sliding distances because if the sliding distance is too small, accurate slope values would not be obtained from the data, and the calculated μ values would not be reliable. Considering this limitation, sliding over just a few equilibrium positions in an attempt to obtain an "atomic-scale" μ was not possible with the experimental method used.

The close correspondence between the micro-scale and macro-scale μ values suggests that the same factors that control the micro-scale experiments may also control the macro-scale experiments, despite the very large change in scale.

The micro-scale and macro-scale wet and dry friction experiments can be compared to Rate Process Theory (RPT), which was described in Chapter 3. Choosing typical RPT parameters, families of curves can be generated (Figs. 7.15 and 7.16) depicting the change in μ as a function of sliding velocity. The activation energy, ΔF, for the macro-scale specialized triaxial shear and similar micro-scale friction regime experiments fall within the range expected for pure montmorillonite of 84 – 109 kJ/mol

(Ripple and Day, 1966). However, the ring shear, direct shear, and corresponding micro-scale friction regime experiments with residual μ values have activation energies lower than expected (55 – 80 kJ/mol). It is reasonable to surmise that alignment of grains reduced the energy required to initiate sliding, leading to a lower activation energy in these cases.

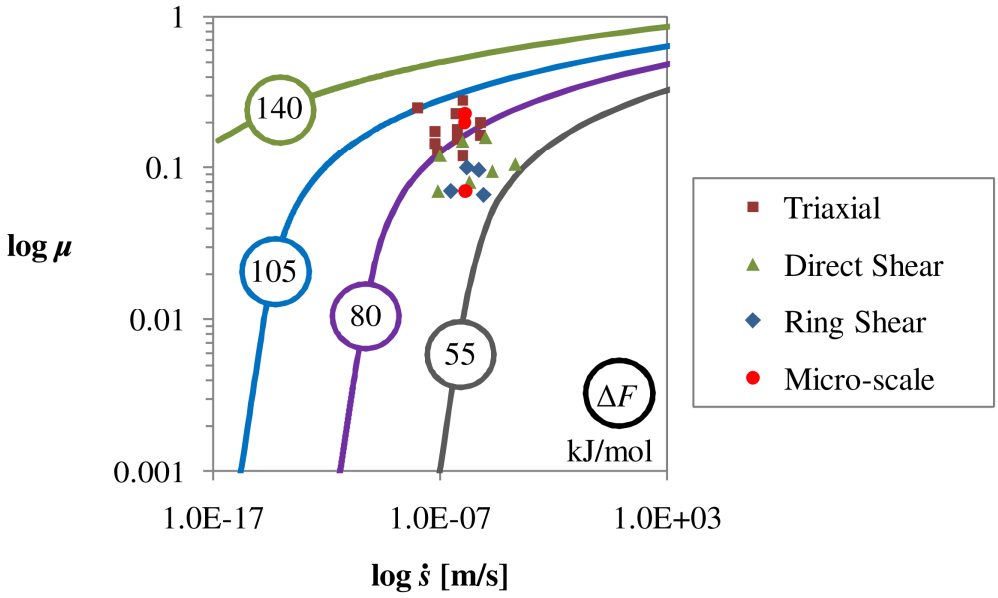

Fig. 7.15: Coefficient of friction as a function of sliding velocity for micro-scale and macro-scale wet friction tests on montmorillonite compared with RPT ΔF values. n_1 = 10^9 bonds/N, T = 298 K, λ = 0.53 nm.

The RPT μ values calculated using a typical range of the number of bonds per N of force (n_1) of 10^7 – 10^9 bonds/N correspond very well with both the micro-scale and macro-scale experimental results. This range is based on the method described in Chapter 3. The range of n_1 values most consistent with the micro-scale and macro-scale experiments is 10^8 – 10^9 bonds/N.

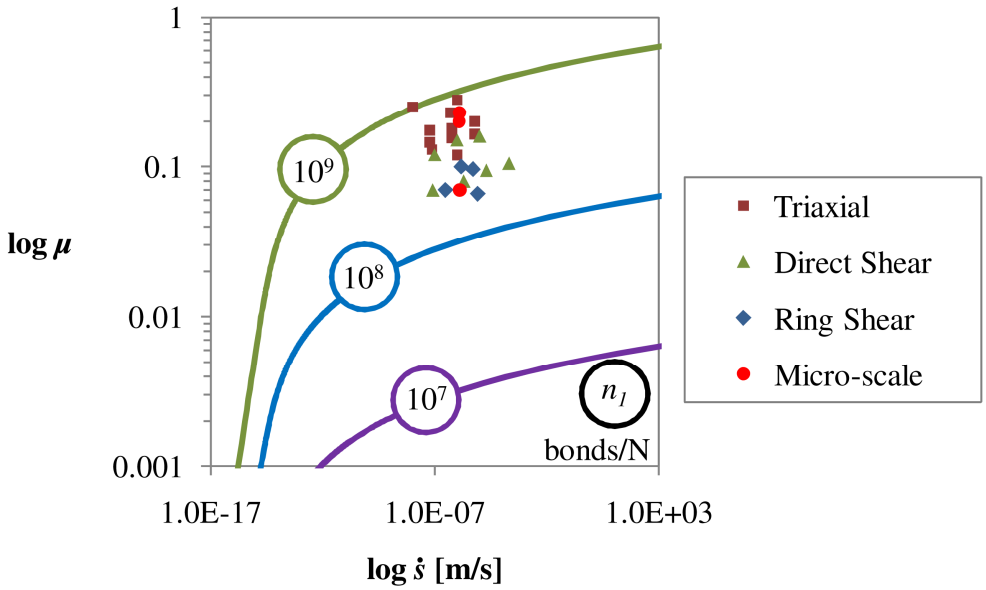

Fig. 7.16: Coefficient of friction as a function of sliding velocity for micro-scale and macro-scale wet friction tests on montmorillonite compared with RPT n_1 values. ΔF = 105 kJ/mol, T = 298 K, λ = 0.53 nm.

Chapter 8

Macro-scale Experiments

This chapter describes the macro-scale experiments conducted for this study. The clay used in the consolidation experiments was the same that was used in the micro-scale friction experiments (sodium montmorillonite reference clay SWy-2). The equipment used (Section 8.1), experimental methodology (Section 8.2), and results and discussion (Section 8.3) are provided in this chapter.

8.1 Equipment Development

The following equipment was used:

- Consolidometer (consolidation ring, 2 porous stones, filter paper, spacer disk, load block)
- Deformation dial indicator reading to 0.01 mm
- Loading device

- Stopwatch or timer
- Thermometer
- Deionized water
- Spatula
- Ceramic mixing bowl

8.2 Experimental Methodology

Consolidation tests (ASTM D 2435-96) were conducted on the clay to determine the consolidation parameters and also to obtain macro-scale secondary compression magnitudes. The following load increments were used: 25, 50, 100, 200, 400, 800, 1600, and 3200 kPa. The tests were run for weeks at a time to obtain long-term settlement data. The initial water content of the clay was 397%, and the final water content was 53%.

8.3 Results and Discussion

The compression as a function of the log of time data is shown in Fig. 8.1. As the load increases, the magnitude of compression decreases as expected. The void ratio as a function of consolidation pressure is shown in Fig. 8.2. The results were also compared to the consolidation tests conducted by Marcial *et al.* (2002) on a similar Wyoming montmorillonite reference clay (Na-Ca MX80). The purpose of that work was to determine the behavior of montmorillonite undergoing high stress (up to 30 MPa) consolidation.

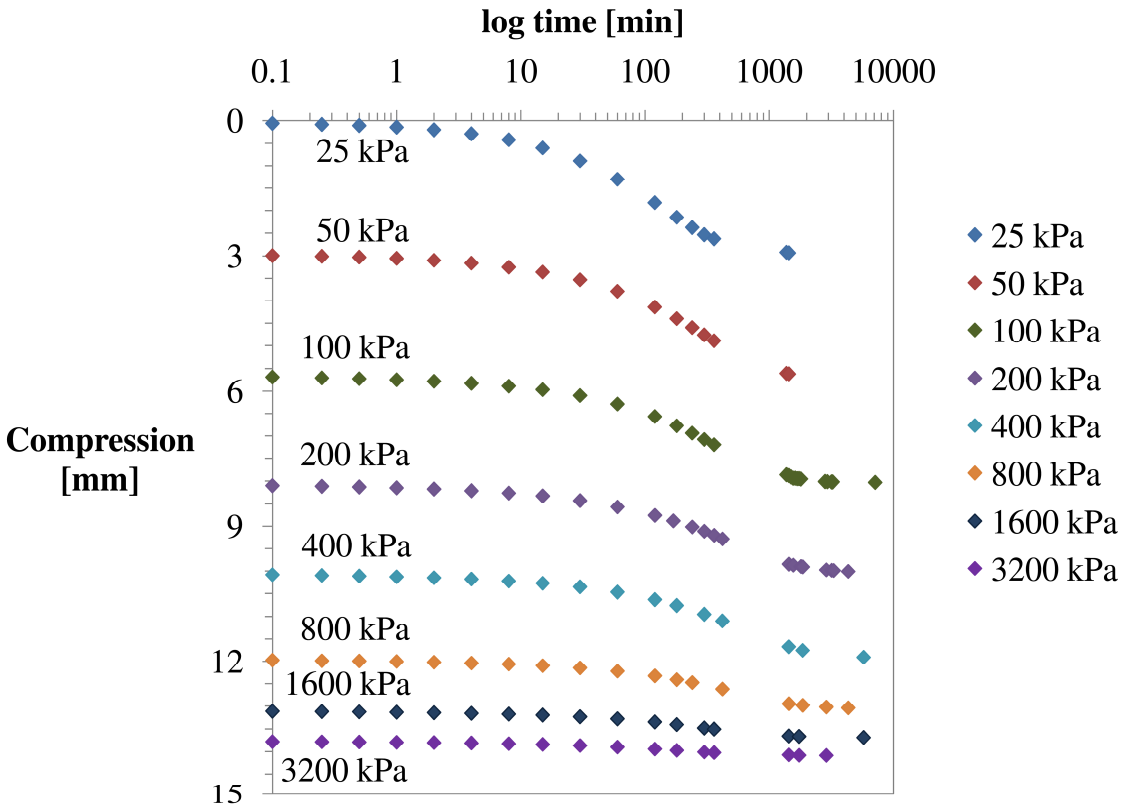

Fig. 8.1: Compression vs. log time.

The coefficient of compressibility, $a_v = -\Delta e/\Delta p$, is 0.038 ksf^{-1} at 1000 kPa, and the corresponding coefficient of volume compressibility, $m_v = a_v/(1+e_o)$, is 0.0035 ksf^{-1} based on an initial void ratio of 10.02. Therefore, the constrained modulus, $1/m_v$, is approximately 300 ksf. The specific gravity, G_s, was determined to be 2.4 based on void ratio, water content, and assumed 100% saturation at the end of the consolidation test.

The coefficient of secondary compression, $C_\alpha = \Delta\varepsilon/\log(t_2/t_1)$, was found to be 0.015 for pressures of 100 – 800 kPa. The strain was calculated by dividing the change in thickness by the original sample thickness.

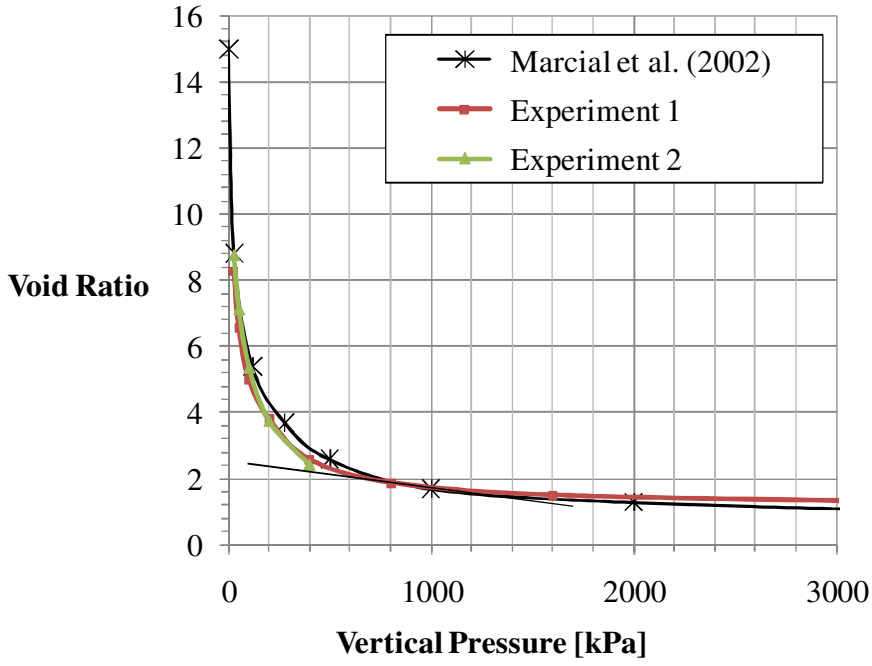

(a)

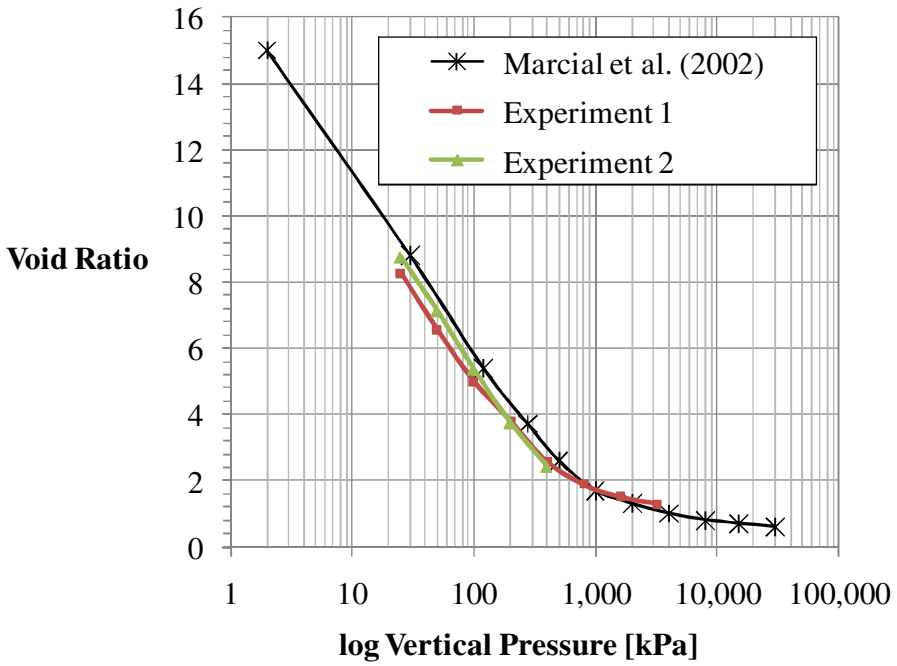

(b)

Fig. 8.2: (a) Void ratio vs. vertical pressure. (b) Void ratio vs. log vertical pressure.

Chapter 9

Discrete Element Method – Model Set-up

This chapter introduces the theory behind the Discrete Element Method (DEM) in Section 9.1. Previous research using DEM to model soils is provided in Section 9.2. The general model parameters used for this study are described in Section 9.3.

9.1 Theory

DEM is a useful numerical tool for modeling the movement and interactions of particles within a granular assembly. DEM is a finite difference method that calculates the movement of particles over time. Advanced DEM simulations permit user-defined particle shapes and geometries, user-defined loads, and user-defined contact models. All DEM analyses conducted in this study are computed in three-dimensions, as this is the

most rigorous type of analysis. However, for explanation purposes, the two-dimensional case of two circles or disks colliding, as presented by Cundall and Strack (1979) and shown in Fig. 9.1, will be discussed in this section.

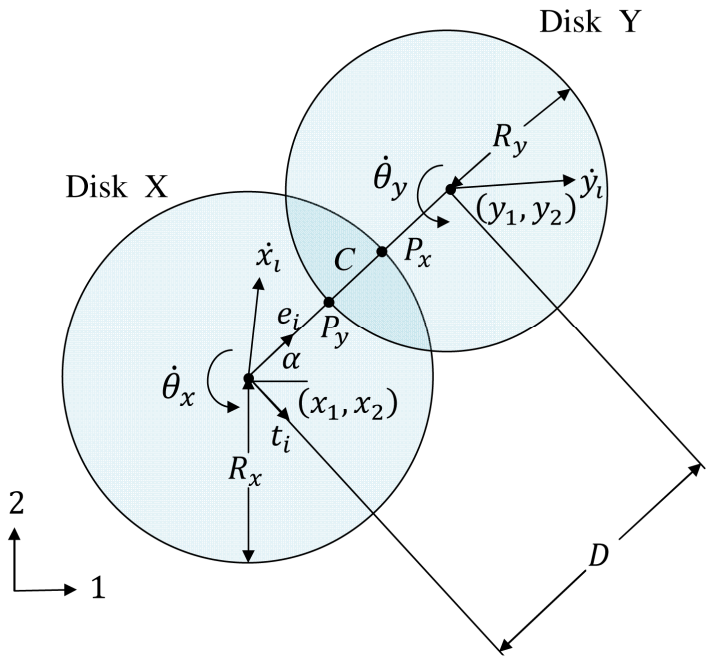

Fig. 9.1: Schematic depicting the collision of disks X and Y in two dimensions. The particles do not overlap in the simulation, but the calculated overlap is used to determine contact forces.

In DEM calculations, contact detection is determined by comparing the distances between the centers of two adjacent disks. When the distance, D, between the centers of the disks is less than the sum of their radii, $R_x + R_y$, contact has occurred (Fig. 9.1). While the particles do not actually overlap during the simulation, it is through this theoretical overlap, C, that new velocities and positions are calculated.

Points P_x and P_y define the points of intersection of the line connecting the centers of the disks to the boundaries of disks X and Y, respectively. The unit vector pointing from the center of disk X to the center of disk Y is e_i and is defined as:

$$e_i = (cos\alpha, sin\alpha)$$

where i = 1, 2

α = angle between the horizontal and the line between disk centers

When collision has occurred, the relative velocity of point P_x with respect to P_y is given by:

$$\dot{X}_i = (\dot{x}_i - \dot{y}_i) - \left(\dot{\theta}_x R_x + \dot{\theta}_y R_y\right) t_i$$

where t_i = unit vector obtained by a 90° clockwise rotation of e_i

$\dot{\theta}$ = angular velocity

This relative velocity is resolved into normal and tangential components, $\dot{n}$ and $\dot{s}$, respectively.

$$\dot{n} = \dot{X}_i e_i = (\dot{x}_i - \dot{y}_i) e_i - \left(\dot{\theta}_x R_x + \dot{\theta}_y R_y\right) t_i e_i = (\dot{x}_i - \dot{y}_i) e_i$$

$$\dot{s} = \dot{X}_i t_i = (\dot{x}_i - \dot{y}_i) t_i - \left(\dot{\theta}_x R_x + \dot{\theta}_y R_y\right) t_i t_i = (\dot{x}_i - \dot{y}_i) t_i - \left(\dot{\theta}_x R_x + \dot{\theta}_y R_y\right)$$

The relative displacement increments in the normal, Δn, and the tangential, Δs, directions, can now be determined.

$$\Delta n = \dot{n}\Delta t = [(\dot{x}_i - \dot{y}_i)e_i]\Delta t$$

$$\Delta s = \dot{s}\Delta t = \left[(\dot{x}_i - \dot{y}_i)t_i - \left(\dot{\theta}_x R_x + \dot{\theta}_y R_y\right)\right]\Delta t$$

The next step is to determine the contact force. When two disks collide, two components of the contact force result, which are the normal force, F_N, and shear force, F_S. Increments of these forces are calculated using the following equations:

$$\Delta F_N = k_N \Delta n$$

$$\Delta F_S = k_S \Delta s$$

where k_N = normal particle stiffness

k_S = shear particle stiffness

There are several models to calculate the normal and shear forces using the above general equations. One of the most widely used is the Hertz-Mindlin model for spheres (Mindlin and Deresiewicz, 1953) due to its accurate and efficient force calculation. In the Hertz-Mindlin model, the stiffness is a function of the particle overlap, such that the spring stiffness is a function of the degree of compression of the spring.

At each time step, the force increments ΔF_N and ΔF_S are added to the sum of all force increments, F_n and F_s, determined from previous time steps.

$$(F_n)_N = (F_n)_{N-1} + \Delta F_N$$

$$(F_s)_N = (F_s)_{N-1} + \Delta F_S$$

where indices N and $N-1$ refer to times t_N and t_{N-1} such that:

$$\Delta t = t_N - t_{N-1}$$

For $(F_n)_N$, compression is taken as positive, which is opposite to the direction of the unit vector e_i. For $(F_s)_N$, force generating a counterclockwise rotation is taken as positive, which is opposite to the direction of the unit vector t_i.

The tangential force is limited by a Coulomb-type friction law to allow for unlimited and unrecoverable sliding at the contact. The maximum shear force is calculated as:

$$(F_S)_{max} = F_n \mu_S + c = F_n(tan\varphi_u) + c$$

where μ_S = the coefficient of static friction between the two disks

φ_u = interparticle friction angle of the disks

c = cohesion at the inter-particle contact

The normal and shear forces for each contact are then resolved into components. The sum of these contact force components plus any body forces, such as gravitational

forces or applied forces, is calculated to yield the total net force components acting on disk X, given as:

$$\sum F_{xi} = \left(\sum F_{x1}, \sum F_{x2}\right)$$

The resultant moment acting on disk X is also determined from all of the shear forces acting on disk X as:

$$\sum M_x = \sum F_S R_x$$

The particle translational acceleration and rotational acceleration can then be calculated:

$$\sum F_{xi} = m_x \ddot{x}_i$$

$$\sum M_x = I_x \ddot{\theta}_x$$

where m_x = mass of disk X

$\ddot{x}_i$ = translational acceleration of disk X

I_x = moment of inertia of disk X

$\ddot{\theta}_x$ = angular acceleration of disk X

If particle X is composed of M number of disks, the moment of inertia for particle X is calculated as:

$$I_x = \sum_j \left(\frac{1}{2} m_j R_j^2 + m_j d_j^2 \right)$$

where m_j = mass of disk j

R_j = radius of disk j

d_j = distance between the center of disk j and the axis of rotation, taken as the center of mass of the particle

Numerical integration of the accelerations needs to then be performed over a time step to compute new velocities. In addition, integration is required to calculate the particle displacement increments from which the new particle coordinates are obtained. Taking $\ddot{x}_i$ and $\ddot{\theta}_x$ as constant over the time step, Δt, the new translational and angular velocities are determined as:

$$(\dot{x}_i)_{N+\frac{1}{2}} = (\dot{x}_i)_{N-\frac{1}{2}} + \left(\frac{\sum F_{xi}}{m_x} \right)_N \Delta t$$

$$(\dot{\theta}_x)_{N+\frac{1}{2}} = (\dot{\theta}_x)_{N-\frac{1}{2}} + \left(\frac{\sum M_x}{I_x} \right)_N \Delta t$$

Further integration yields the new position and rotation of disk X:

$$(x_i)_{N+1} = (x_i)_N + (\dot{x}_i)_{N+\frac{1}{2}}\Delta t$$

$$(\theta_x)_{N+1} = (\theta_x)_N + (\dot{\theta}_x)_{N+\frac{1}{2}}\Delta t$$

This process is followed for every disk. Having obtained new positions and velocities for each of the particles, the cycle of updating contact forces and particle locations is then repeated. It is necessary to check each time step for new contacts or for contacts that no longer exist. As a result, the speed of computation is heavily influenced by the number of disks in the simulation. The preceding derivation was conducted in two-dimensions, while the model used in this study was three-dimensional, which resulted in an even greater drain on processing power and memory. Additionally, each clay particle is composed of hundreds of spheres, as discussed in Section 9.3.3, resulting in an extremely computationally intensive model.

Another factor that affects the computation time is the time step and total simulation time. Setting a time step which is too large can result in two particles moving from distant locations to a large apparent overlap in one time step. The particle forces and energies which are then calculated will be very large due to the large apparent overlap, resulting in the particles being assigned very large, incorrect velocities. The particle system may then become unstable. However, setting a time step which is too small results in an extremely low computational speed without any benefit.

The optimum time step is often determined by using the Rayleigh time step, which is the method incorporated in the EDEM software used in this study. The Rayleigh time step is the time that it takes for a shear wave to propagate along the surface of an

elastic body. When a force is applied to an elastic body, Rayleigh waves propagate along the surface with a velocity of:

$$v_R = \alpha \sqrt{\frac{G}{\rho}}$$

where α = root of $(2-\alpha^2)^4 = 16(1-\alpha^2)\left[1-\frac{1-2\upsilon}{2(1-\upsilon)}\alpha^2\right]$

$$\approx 0.1631\upsilon + 0.876605$$

G = shear modulus

ρ = density

υ = Poisson's ratio

The highest frequency of Rayleigh wave propagation is determined by the smallest sphere in the system (Sheng *et al.*, 2003). Therefore the Rayleigh time step is calculated as:

$$t_R = \frac{\pi R_{min}}{v_R} = \frac{\pi R_{min}}{\alpha}\sqrt{\frac{\rho}{G}}$$

where R_{min} = minimum particle radius

In actual DEM practice, Δt is usually taken as some fraction of the Rayleigh time step, t_R. Typically for systems with high coordination numbers, such as four or greater, $\Delta t = 0.2t_R$ is used, and for lower coordination numbers, $\Delta t = 0.4t_R$ is usually acceptable.

9.2 Previous Research

Previous research has typically focused on sand because the particles can be approximated as spherical grains (Oquendo *et al.*, 2009; Kwok and Bolton, 2010). However, clays cannot be approximated in such a manner given their plate-like structure. Clay particles, such as montmorillonite, typically exhibit length to thickness aspect ratios on the order of 60 to 500 (Ploehn and Liu, 2006). By using spherical particles, the particle assemblies are unrealistic for clays, and the results may not be applicable to what is observed experimentally. Other research (Kuhn and Mitchell, 1993) has considered clay particles as ovals, which is more accurate than the spherical approximation, but only two-dimensional analyses were considered due to computational limitations. Kwok and Bolton (2010) determined that, with all other parameters the same, converting a spherical RPT DEM analysis from two dimensions to three dimensions increased the creep by several orders of magnitude, which indicates that three dimensional analyses are essential for accurate modeling of creep.

Three dimensional DEM analysis of clay particle movement is a relatively new topic and very limited research has been published so far. One of the first published research papers on the use of a three-dimensional DEM model for clay compression was conducted by Yao and Anandarajah (2003). These researchers modeled each kaolinite clay particle as a thin rectangular prism with length and width dimensions of 0.5 µm x

0.5 µm. Thicknesses of 37 and 60 nm were tested. The model consisted of 400 of these particles, similar to this study's research. The starting configuration was with the particles placed randomly and without contact with other particles, also similar to this study.

Yao and Anandarajah (2003) noted that typical kaolinite size thicknesses are in the range of 25-74 nm. For the thinner (37 nm) particle assemblies, the final void ratios were significantly greater than those measured during a one-dimensional compression lab test on kaolinite. This difference highlights the importance of particle size on a DEM simulation, and led the authors to speculate that kaolinite thicknesses used in their lab tests were closer to 60 nm.

Another three dimensional DEM analysis of clay (Katti *et al.*, 2009) modeled the swelling of sodium montmorillonite, which is the same type of clay used in this study. The researchers wanted to determine how particle size affects clay swelling. Following the research by Yao and Anandarajah (2003), they developed their particles as thin rectangular prisms. The particle dimensions were 0.1 µm x 0.1 µm x 0.00092 µm, and all of the particles were of this uniform size. The length to thickness aspect ratio of 109 is realistic for montmorillonite particles.

In terms of RPT, Kuhn and Mitchell (1993) and Kwok and Bolton (2010) tested the theory using DEM. The limitations of these studies are explained above. The modeling focus of this current study was to consider three dimensional, disk-shaped particles undergoing compression with the interactions at the contact interfaces controlled by RPT. To the author's knowledge, DEM analyses incorporating all three features have not been performed previously.

9.3 DEM Model Parameters

DEM Solutions EDEM v. 2.2 was used as the software for the DEM analyses. This section describes the basic model parameters such as the model geometry, steel container properties, clay properties, clay particle placement, and consideration of water films. The model was load controlled. The ratio of f_t to f_n, which is the coefficient of friction, μ, was limited to a maximum of 0.20 in the analyses, which is a reasonable value for montmorillonite based on micro-scale tests (Section 7.4).

9.3.1 Model Geometry

The clay particles were placed randomly within a hollow steel cylinder with an inner diameter of 250 μm and height of 90 μm (Simulation Set 1) or an inner diameter of 236 μm and height of 180 μm (Simulation Sets 2–3). A steel base contained the particles during compression. Wall friction (μ = 0.20) was assigned to achieve a more realistic model. Gravity was not included because weight effects of the clay in the small model size were not expected to lead to significant compression of the soil mass compared to the externally applied load.

9.3.2 Steel Properties

The steel material had the properties shown in Table 9.1. The Poisson's ratio, elastic modulus, and density were based on typical properties for steel (AISC, 2001). The density was scaled up by 10^{18} to decrease the simulation time, as explained in Section 9.3.3.

Table 9.1: Steel properties.

Poisson's ratio	0.30
Elastic modulus [GPa]	207
Density [kg/m^3]	7861

9.3.3 Clay Properties

The particle shape template was created using Autodesk Inventor Professional 2010 and then imported into EDEM. Two types of particles were tested. Particle 1 was a disk-shaped particle that had a length of 29.6 μm, width of 24.0 μm, and thickness of 2.0 μm. The average length to thickness aspect ratio was 13.4, and each particle was composed of 537 overlapping spheres (Fig. 9.2a). The aspect ratio was determined by averaging the length and width and then dividing the result by the particle thickness. While even smaller thicknesses would potentially model more common aspect ratios for montmorillonite, computational requirements limited such analyses. Particle 2 was a disk-shaped particle that had a length and width of 8.0 μm and thickness of 2.0 μm. The average length to thickness aspect ratio was 4, and each particle was composed of 37 overlapping spheres (Fig. 9.2b). Both of these particle types had widely varying sizes and size distributions in the different simulations. However, the aspect ratios were fixed.

The clay material had the properties shown in Table 9.2. The Poisson's ratio was based on molecular dynamics work conducted by Manevitch and Rutledge (2004). For the elastic modulus, individual particles needed to be quite stiff, though modeling values of 200 GPa (McNeil and Grimsditch, 1993) was not possible due to software limitations. Therefore, a sufficiently stiff value was chosen for the simulations. The particle density was chosen based on a G_s value of 2.7. The mass of the particles was scaled up by 10^{18} to

decrease the simulation time from years to days, as is common practice in DEM calculations (Thornton, 2000; O'Sullivan *et al.*, 2002; Cui and O'Sullivan, 2006). Tests were conducted to ensure that density scaling did not lead to erroneous results. This was done by running the same model with the clay particle density scaling factor set equal to 10^{12} and to 10^{18}. Both runs yielded the exact same compression magnitude curve (Fig. 9.3), although the 10^{18} scaling factor ran in two-thirds of the time.

(a) 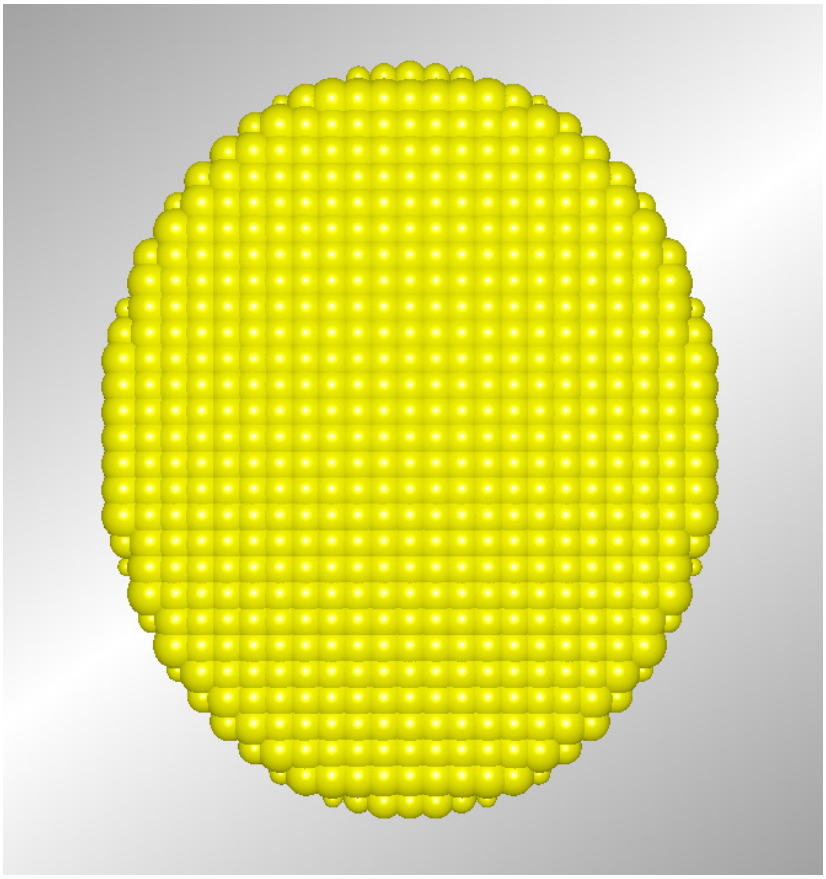

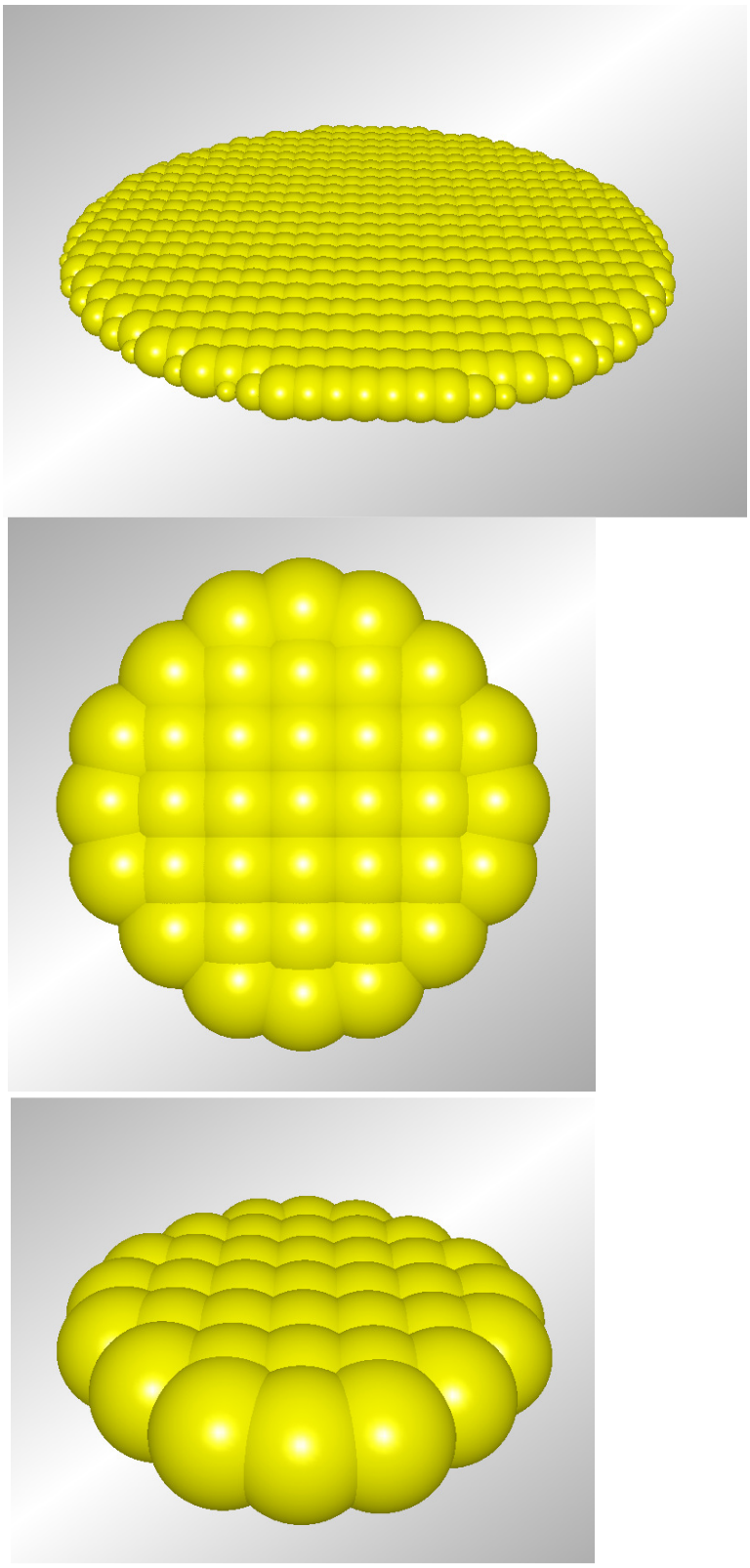

(b)

Fig. 9.2: Plan and isometric views of particle compositions. (a) Particle 1 (composed of 537 overlapping spheres), (b) Particle 2 (composed of 37 overlapping spheres).

Table 9.2: Single clay particle properties.

Poisson's ratio	0.14
Elastic modulus [MPa]	10.0
Density [kg/m^3]	2696

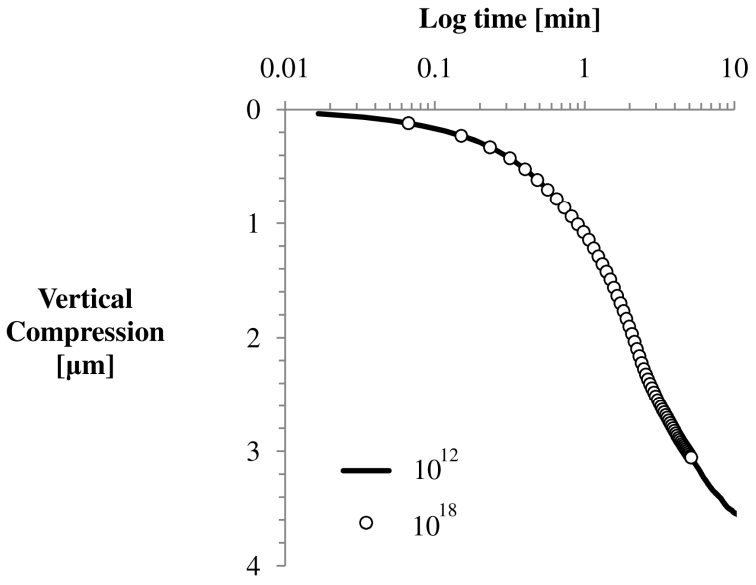

Fig. 9.3: Vertical compression as a function of time for different clay particle density scaling factors. The magnitude of scaling factor does not affect the compression curve results.

9.3.4 Particle Placement

The number of particles of each type with the desired size distribution was specified, and a random placement algorithm was used for particle placement. The particles did not have any contacts at the beginning of the simulations. Since the initial configuration started the particles suspended without any contact with surrounding particles, the model was run with a small (0.02 - 1.0 kPa) applied vertical stress to achieve a more realistic starting assembly.

9.3.5 Water Film

Since clay particle contacts during shear have been shown to be solid-to-solid interfaces (Matsui *et al*., 1980; Koerner *et al.*, 1977), interlayer water films should not affect sliding behavior. However, the water films could potentially inhibit the compression of the clay, especially for a swelling clay such as montmorillonite. Bolt (1956) found a 3-4 nm thick layer of water to be essentially trapped during the compression of Wyoming montmorillonite, which had particle thicknesses of approximately 10 nm.

While a detailed interlayer water analysis was not possible with the DEM code used and the computational resources available, the model particle thicknesses were thick enough to consider each particle as being composed of stacks of basic units of 2:1 layers with trapped interlayer water between. Accounting for the effect of interlayer water resulted in a greater and more realistic void ratio when compared to macro-scale tests, as discussed in Chapter 10, demonstrating that interlayer water may be an important factor to consider in DEM analyses of clay compression.

Chapter 10

Discrete Element Method – Model Results and Discussion

This chapter presents and discusses the results from the numerical model. The results are divided into three simulation sets. Simulation Set 1 focused on analyzing the effects of RPT parameters on the clay compression (Section 10.1). Simulation Set 2 involved modifying the RPT-based contact model (Section 10.2). Simulation Set 3 analyzed the effects of particle geometry and size distribution on the clay compression (Section 10.3).

10.1 Simulation Set 1 – Effects of RPT Parameters

The first set of simulations analyzed the effects of applied stress, number of bonds per unit of normal contact force (n_1), and activation energy (ΔF) on clay compression.

10.1.1 Model

Inter-particle bonding has been shown to resist applied shear force rather than bonding to water films. Particle bonding is effectively solid-to-solid (Mitchell *et al.*, 1968). Evidence of solid-to-solid contacts in clay is also demonstrated by scratches on particle surfaces generated during shear (Matsui *et al.*, 1980) and acoustic emissions observed during laboratory experiments (Koerner *et al.*, 1977). Similar creep behavior and similar ΔF values for wet and dry clay also indicate that deformation is not controlled by the viscous flow of water (Mitchell and Soga, 2005). Therefore, for the DEM analyses conducted in this study, water was not directly included in the model, and the hydraulic resistance to compression was not represented.

The clay model consisted of 397 plate-like particles (type: Particle 1), and each particle was composed of 537 overlapping spheres. Therefore, the entire model consisted of 213,189 spheres. Since the initial configuration consisted of suspended particles without any contact with surrounding particles, the model was run with a small (0.02 kPa) applied vertical stress to achieve a more realistic starting assembly. The void ratio after application of this small initial stress was 5.6.

10.1.2 Results and Discussion

DEM compression analyses were conducted with vertical applied stresses of 200, 400, and 800 kPa. The influence of n_1 on the void ratio, e, vs. log pressure, p, relationship is shown in Fig. 10.1. As expected, clays with a greater number of bonds between particles compressed less for a given load increment. The clays with fewer bonds between particles also experienced a longer time period of compression, as

particles continued to slide past each other into smaller and smaller configurations. The compression also exhibits an approximately linear relationship between e and log p, which is in agreement with the observed response over limited ranges of stress. The low void ratio values are attributed to the tendency of the relatively small number of disk-shaped particles used in this simulation to move towards a flat arrangement. Given that modeling individual clay layers and interlayer water was not within the computational capabilities of the software or workstation used, the effects on void ratio of each DEM particle being comprised of many basic units of clay and interlayer water were accounted for in the post-run analyses. The data presented in Fig. 10.1 is of the raw e values from EDEM without interlayer water.

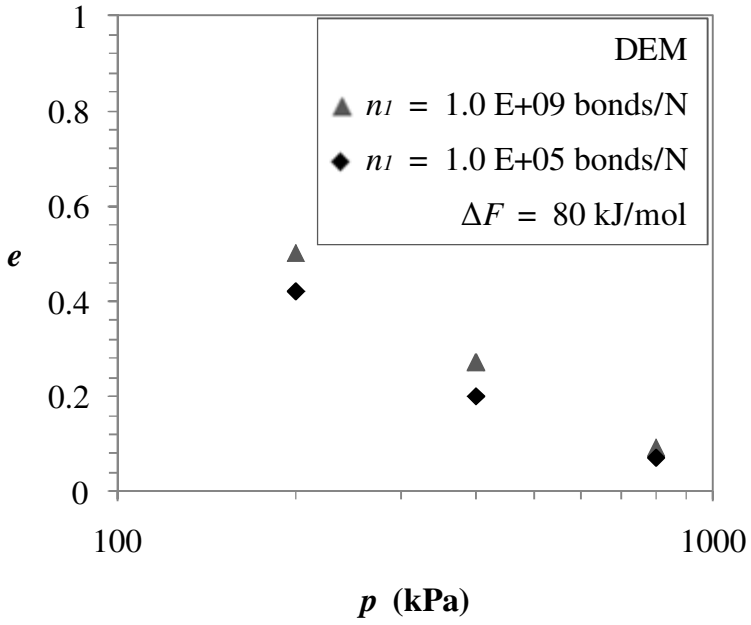

Fig. 10.1: Influence of n_1 on e vs. p.

When there was a greater energy barrier to overcome, the clay also compressed less. Holding n_1 constant at 10^9 bonds/N and varying ΔF from 80 to 140 kJ/mol resulted in a final void ratio at 400 kPa of 0.27 and 0.33, respectively. Fig. 10.2 shows how e increases as the energy barrier increases.

While the RPT equation calculates several orders of magnitude changes in sliding velocity due to changes in n_1 and ΔF, the relatively minimal impact on macro-scale compression is attributed to the dense particle arrangement with multiple contacts between clay particles. Unlike gaseous assemblies of suspended clay particles, an arrangement with multiple contacts per particle represents a more realistic starting configuration for soil compression.

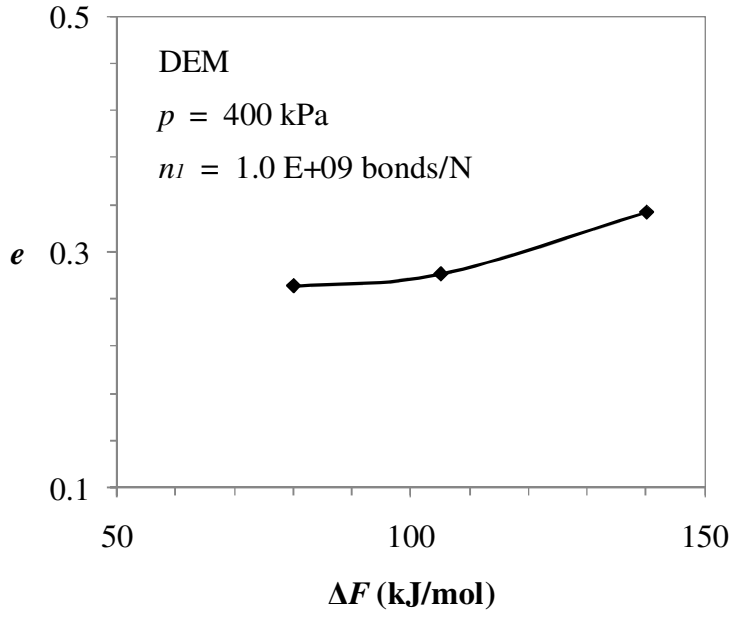

Fig. 10.2: Influence of ΔF on ε.

10.2 Simulation Set 2 – Modification to RPT

During the numerical simulations conducted in Simulation Set 1, it became apparent that the particles collapsed to very dense arrangements even under the small (0.02 kPa) loading. This difficulty is demonstrated by the time-lapse images of the particles undergoing compression, shown in Fig. 10.3. This total collapse of particles occurred in every analysis conducted, which involved varying the n_1 and ΔF parameters over a wide range from 10^5 – 10^9 bonds/N and 80 – 140 kJ/mol, respectively.

Kwok (2008) and Kwok and Bolton (2010) conducted three-dimensional DEM numerical analyses on spheres using RPT and observed that the normal force increases and the tangential force decreases during creep starting at an initial void ratio, e_0, of 0.67. An assembly of uniform spheres has a minimum void ratio of 0.35 and a maximum of 0.92. Therefore, a total collapse of the assembly was not possible in their analyses.

Abbireddy and Clayton (2010) conducted two-dimensional DEM analyses on disk-shaped particles (aspect ratios up to 20) using a spring contact model. They dropped the particles into the domain to achieve the initial assembly. They noted that the maximum initial void ratio achieved was 0.48 and that the disk-shaped particles were predominantly oriented horizontally after being randomly placed and dropped.

The relationship between sliding velocity and the mobilized coefficient of friction defined by the RPT equation (Figs. 7.15 and 7.16) shows that, as an assembly's creep velocities decrease, the mobilized coefficient of friction between particles decreases, which may permit particle collapse. For example, for $n_1 = 10^9$ bonds/N, $\Delta F = 105$ kJ/mol, $T = 298$ K, and $\lambda = 0.53$ nm, the RPT equation for sliding velocity [m/s] reduces to:

$$\dot{s} = 2.5 \times 10^{-15} sinh(64\mu)$$

For the parameters given above, a reduction of $\dot{s}$ from 1 nm/s to 0.1 nm/s corresponds to a 17% reduction in μ.

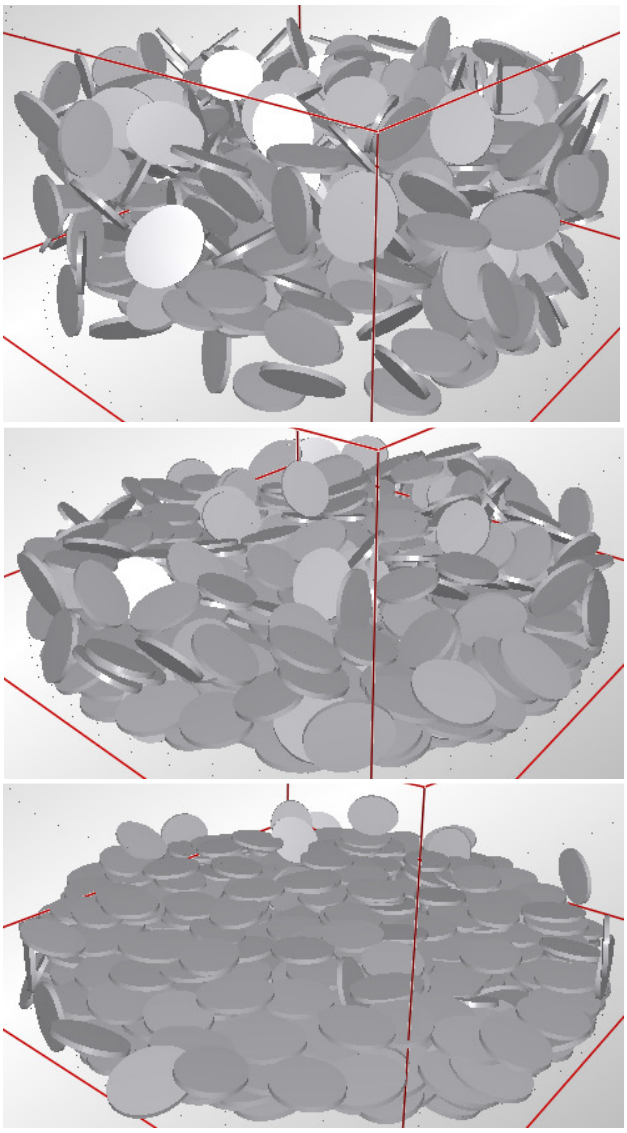

(a)

(b)

(c)

Fig. 10.3: Time-lapse perspective images of continual collapse of a cylindrical particle assembly with the RPT contact model (Simulation Set 1). (a) Initial particle configuration (e_o = 10.5), (b) After application of 0.02 kPa loading (e = 5.60), (c) After application of 800 kPa loading (e = 0.09).

In Simulation Set 2, the goal was to implement a minimum μ, μ_{min}, at which the sliding velocity of the clay particles would equal zero, thereby preventing unrealistic continual particle collapse. The modified RPT theory is:

For $\mu > \mu_{min}$:

$$\dot{s} = \frac{2kT\lambda}{h}\left(e^{-\frac{\Delta F}{RT}}\right) sinh\left(\frac{\lambda}{2kTn_1}(\mu - \mu_{min})\right)$$

For $\mu \leq \mu_{min}$:

$$\dot{s} = 0$$

10.2.1 Model

To test the modified theory against the standard RPT model, the DEM model was modified with a taller and slightly narrower cylindrical ring. The purpose of the height change was to accommodate a greater number of clay particles than studied in prior analyses. The inner diameter and height of the new ring were 236 μm and 180 μm, respectively.

The clay model consisted of 732 plate-like particles (type: Particle 1), and each particle was composed of 537 overlapping spheres. Therefore, the entire model consisted of 393,084 spheres. Since the initial configuration consisted of suspended particles without any contact with surrounding particles, the model was run with a small (1.0 kPa) applied vertical stress to achieve a more realistic starting assembly. The void ratio after application of this initial stress was 2.78 with a μ_{min} of 0.

10.2.2 Results and Discussion

The model was run with μ_{min} varying from 0 to 0.20. The influence of μ_{min} on the e and C_α values for a 200 kPa loading is shown in Fig. 10.4. In this simulation set, n_1 and ΔF were taken as 10^9 bonds/N and 140 kJ/mol, respectively. The standard RPT contact model resulted in a denser configuration, which supports the hypothesis that the standard RPT model leads to a more collapsed assembly. The standard RPT model also had a greater creep rate, as shown by increasing values of C_α. The consolidation tests discussed in Chapter 8 that were conducted on the Wyoming montmorillonite reference clay SWy-2 yielded a C_α value of 0.015 for pressures of 100 – 800 kPa. Therefore, while implementing a μ_{min} value did improve both the e and C_α values in terms of the lab tests, this modification alone was not sufficient to produce realistic results.

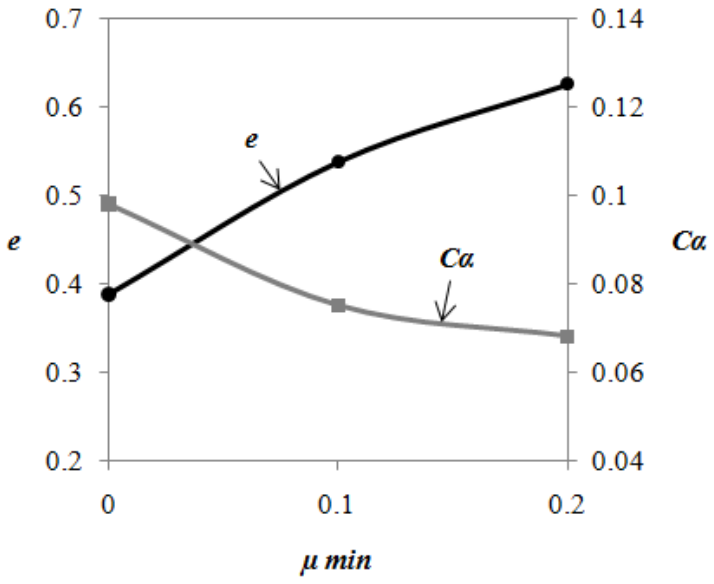

Fig. 10.4: Influence of μ_{min} on e for Simulation Set 2 at an applied stress of 200 kPa. n_1 = 10^9 bonds/N and ΔF = 140 kJ/mol.

10.3 Simulation Set 3 – Effects of Particle Size and Distribution

Simulations Sets 1 and 2 made it apparent that variations to the RPT parameters and the contact model itself would not be sufficient in attaining a numerical model which provided results similar to the macro-scale consolidation tests. The goal of Simulation Set 3 was to model more realistic clay fabrics with variations in particle size, size distribution, and aspect ratio.

10.3.1 Model

The overall geometry of the model in this simulation set was the same as Simulation Set 2. The standard RPT contact model was used with $n_1 = 10^9$ bonds/N and $\Delta F = 105$ kJ/mol. Three separate particle assemblies with varying size distributions were tested over varying pressures. A summary of the three particle assembly properties is shown in Tables 10.1 – 10.3. A normal distribution was used with the mean and standard deviation shown. The aspect ratios (AR) of particle types Particle 1 and Particle 2 (described in Section 9.3.3) were fixed, but their sizes were varied by a scaling factor.

The assemblies were designed such that the initial void ratio was the same in all simulations ($e = 13.0$). However, given that the particles started without contact with other particles, a pressure of 25 kPa was applied to the assemblies. The void ratio after this stress application was taken as the initial starting condition given the more realistic particle arrangement.

Table 10.1: Assembly 1 properties.

	Particle 1 (AR = 13.4)			Particle 2 (AR = 4.0)		
	1a	1b	1c	2a	2b	2c
Number of particles	600	1109	100	0	0	0
Percent of total particles	33.2	61.3	5.5	0	0	0
Scaling factor	0.5	1.0	2.0	-	-	-
Average width (μm)	13.4	26.8	53.6	-	-	-
Average thickness (μm)	1.0	2.0	4.0	-	-	-
Standard deviation of width (μm)	0.05	0.05	0.05	-	-	-
Total number of particles	1809			0		

Table 10.2: Assembly 2 properties.

	Particle 1 (AR = 13.4)			Particle 2 (AR = 4.0)		
	1a	1b	1c	2a	2b	2c
Number of particles	40	120	40	40	120	40
Percent of total particles	10.0	30.0	10.0	10.0	30.0	10.0
Scaling factor	0.5	1.0	2.0	2.0	4.0	6.0
Average width (μm)	13.4	26.8	53.6	16.0	32.0	48.0
Average thickness (μm)	1.0	2.0	4.0	4.0	8.0	12.0
Standard deviation of width (μm)	0.05	0.05	0.05	0.05	0.05	0.05
Total number of particles	200			200		

Table 10.3: Assembly 3 properties.

	Particle 1 (AR = 13.4)			Particle 2 (AR = 4.0)		
	1a	1b	1c	2a	2b	2c
Number of particles	0	0	0	52	156	52
Percent of total particles	0	0	0	20.0	60.0	20.0
Scaling factor	-	-	-	2.0	4.0	6.0
Average width (μm)	-	-	-	16.0	32.0	48.0
Average thickness (μm)	-	-	-	4.0	8.0	12.0
Standard deviation of width (μm)	-	-	-	0.05	0.05	0.05
Total number of particles	0			260		

10.3.2 Results and Discussion

The results in terms of e vs. p for Assemblies 1, 2, and 3 are compared to macro-scale experiments in Fig. 10.5. Water films were accounted for in the results (Section 9.3.5) and taken as a fixed water content, w_{fixed}. Given that the particles were a fixed size, a fixed water content due to water films was chosen to fit the laboratory data. The w_{fixed} was added to the decreasing water content due to clay compression to calculate the total water content (given that the weight of the solids is constant), which is shown in Fig. 10.6. G_s for SWy-2 was taken as 2.4 based on macro-scale consolidation tests. Marcial *et al.* (2002) took G_s for MX80, a sodium-calcium Wyoming montmorillonite, as 2.7. In both Figs. 10.5 and 10.6, a w_{fixed} of 142% was used, and the assembly with the thinnest particles (Assembly 1) best matched the macro-scale tests. The compression ratio, $C_{\varepsilon c}$, at 50 kPa is also consistent between Assembly 1 ($C_{\varepsilon c}$ = 0.61) and the lab experiments ($C_{\varepsilon c}$ = 0.69) taking 25 kPa as the initial condition in both cases, as explained in Section 10.3.1.

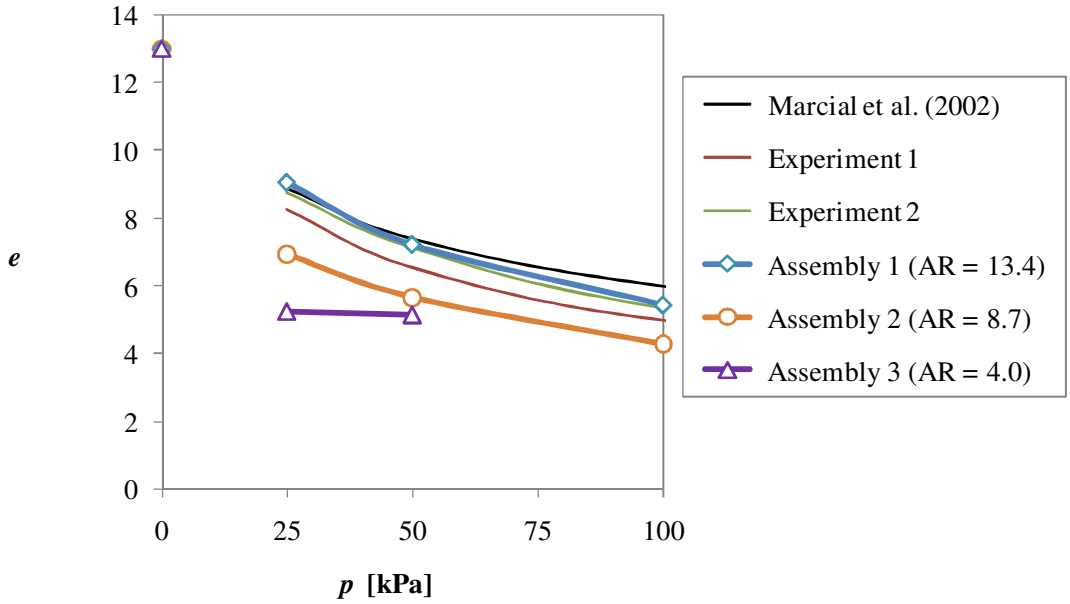

Fig. 10.5: e vs. p for Assemblies 1, 2, 3 and macro-scale experiments (w_{fixed} = 142%).

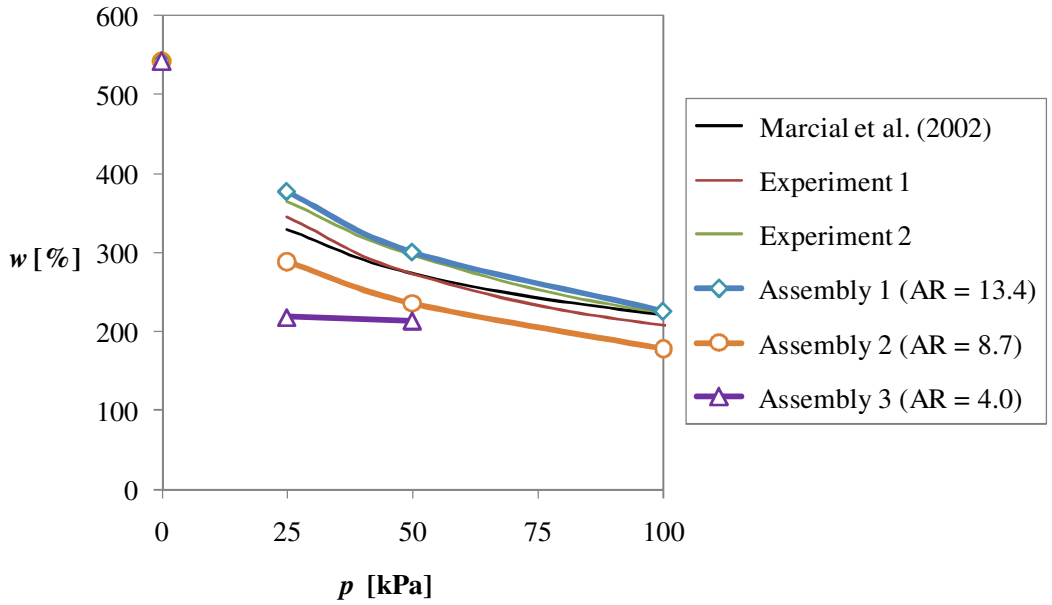

Fig. 10.6: w vs. p for Assemblies 1, 2, 3 and macro-scale experiments (w_{fixed} = 142%).

It is evident from these results that the clay fabric modeled plays a significant role in DEM analyses. After reaching a configuration where particles were in contact with

each other at a pressure of 25 kPa, the assembly with thinner particles compressed more for a given load increment than the assembly with thicker particles. Given that the models are identical except for the particle geometry, this difference is likely due to the thinner particles being able to slide more easily into available void spaces. This behavior is consistent with the expected behavior of normally consolidated clay and sand. Modeling clay particles as spheres would likely lead to significant error in the model.

Figs. 10.7 and 10.8 show the results in terms of e vs. p for Assemblies 2 and 3, respectively. The macro-scale creep tests best match the DEM results for Assemblies 2 and 3 at a w_{fixed} of 176% and 228%, respectively. Fig. 10.9 provides a summary of the w_{fixed} and corresponding e_{fixed} for different particle aspect ratios with a G_s of 2.4.

Significant variations in C_α were also apparent among Assemblies 1, 2, and 3. C_α was obtained from the linear portions of the strain-log time plots, as shown for the 50 kPa load increment in Figs. 10.10 – 10.12. The strain was calculated by dividing the change in thickness by the original sample thickness, as was also done in the macro-scale experiments. A summary of the C_α values from the DEM analyses of Assemblies 1, 2, and 3 for the 50 kPa load increment is given in Fig. 10.13, which also shows the value of C_α for an aspect ratio of one (or sphere), as determined by Kwok and Bolton (2010) to be 4.5×10^{-4} using RPT.

It is apparent from the DEM results that larger *AR*s tend to match best with laboratory tests during primary consolidation, and smaller *AR*s tend to match best with laboratory tests during secondary compression. During compression, the thin montmorillonite particles may tend to bend, interlock, and clump together, resulting in smaller effective *AR* values.

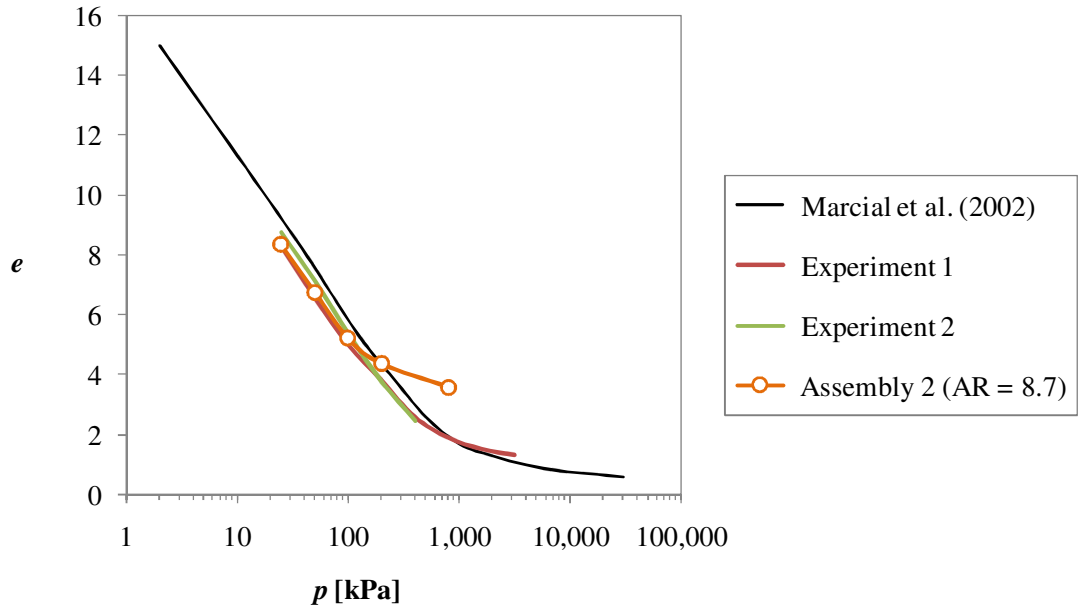

Fig. 10.7: e vs. p for Assembly 2 and macro-scale experiments (w_{fixed} = 176%).

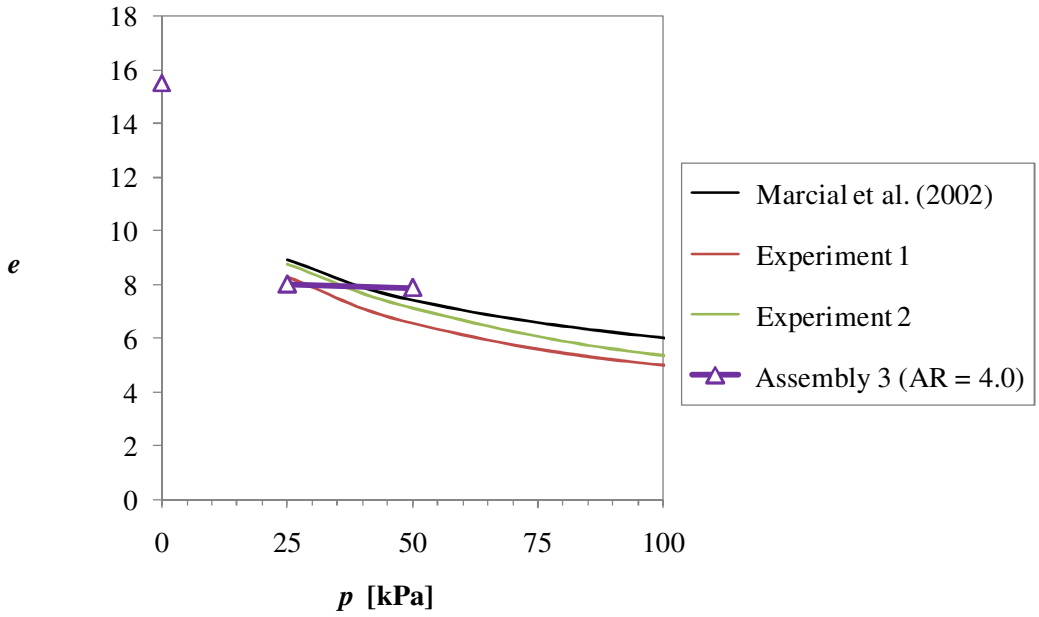

Fig. 10.8: e vs. p for Assembly 3 and macro-scale experiments (w_{fixed} = 228%).

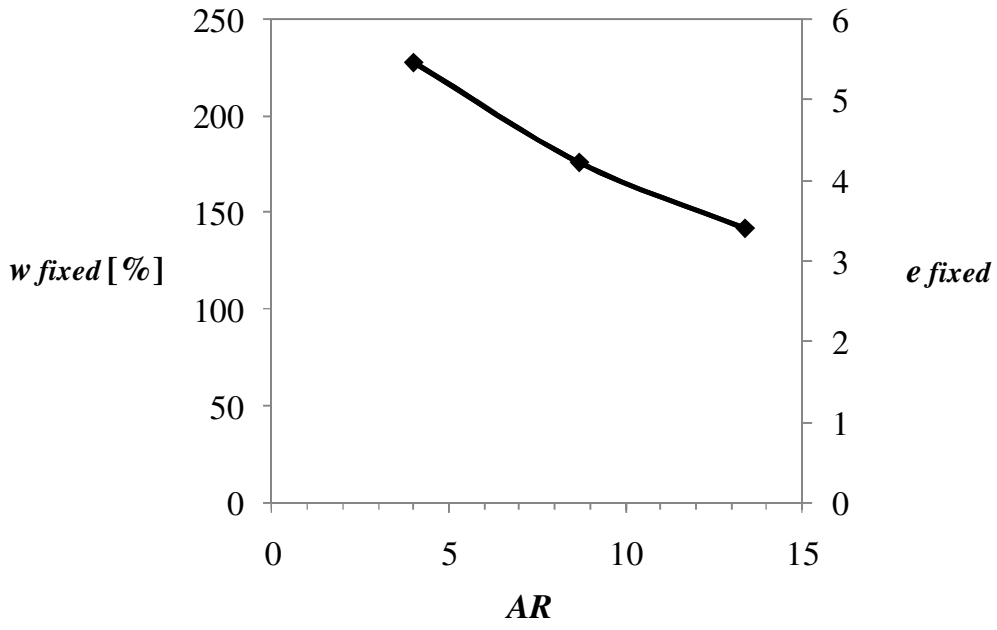

Fig. 10.9: w_{fixed} and e_{fixed} vs. AR.

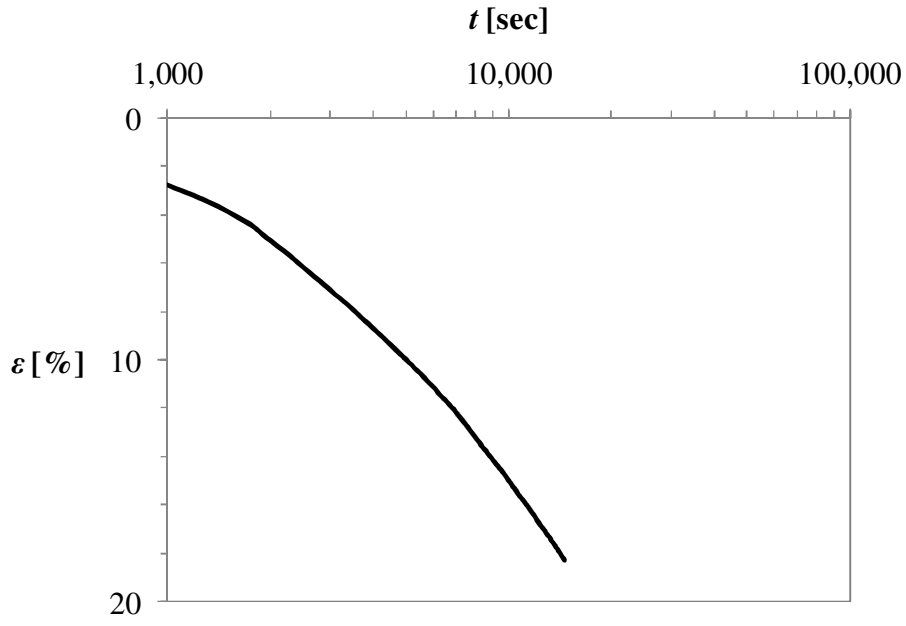

Fig. 10.10: Assembly 1 ε vs. t for 50 kPa load increment.

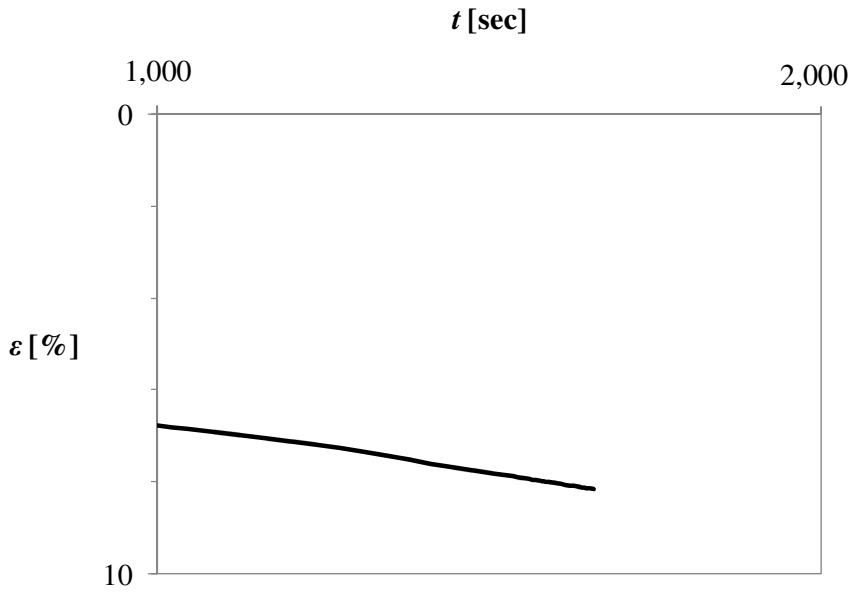

Fig. 10.11: Assembly 2 ε vs. t for 50 kPa load increment.

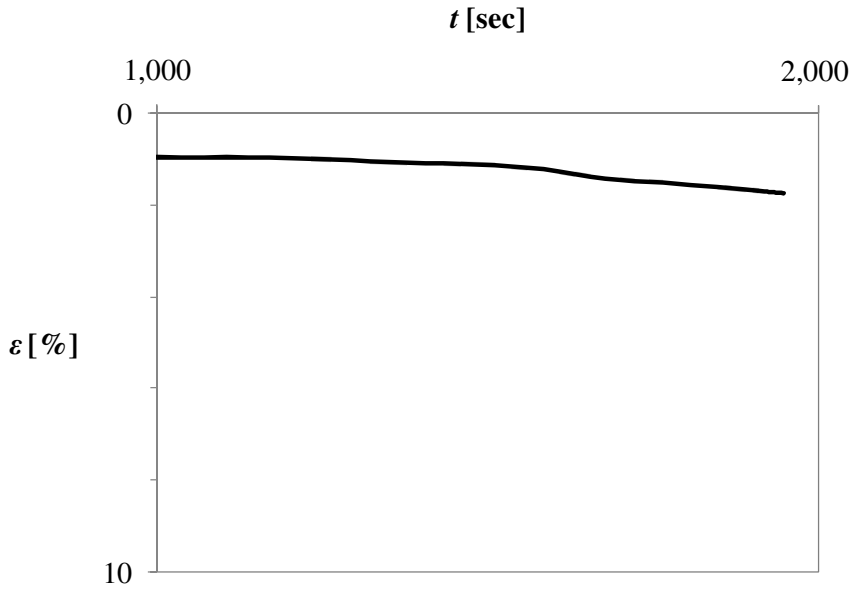

Fig. 10.12: Assembly 3 ε vs. t for 50 kPa load increment.

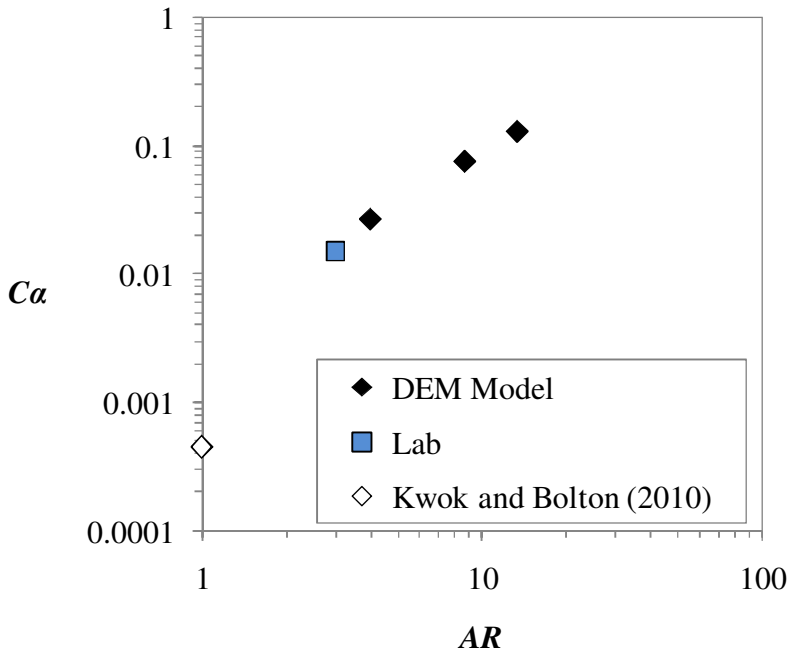

Fig. 10.13: C_α vs. AR.

It is apparent from the DEM results that increasing the number of thin disk-shaped particles yields an assembly that experiences secondary compression at a faster rate and at a greater magnitude. Assemblies consisting of a greater number of thicker particles may compress at a slower rate because the particles may be too thick to fit into the available void spaces. Time-lapse images of the assemblies undergoing compression are shown in Figs. 10.14 – 10.16. The void ratio values in the figure captions take into account interlayer water films. Particle alignment along the vertical and horizontal boundaries in the model is apparent in the figures.

The difference in the compression curves of the assemblies is attributed to the arbitrary initial condition of starting all of the assemblies with the same initial void ratio. Thinner particle assemblies may naturally form fabrics with large void ratios, while the thicker particle assemblies require fewer particles to achieve the same initial void ratio.

Once a load is applied to the assembly and the particles start to contact each other and slide into a more realistic arrangement, then the thinner assemblies compress more and at a faster rate. This observation is consistent with what would be expected when comparing assemblies of disks with assemblies of spheres.

The value of C_α for Assembly 3 (0.026) best matches that obtained from the laboratory tests (0.015). Given that the clay used in the consolidation tests was montmorillonite rather than kaolinite, the particles may not have behaved like a house of cards and instead interlocked, bent, and compressed with smaller effective aspect ratios. The difference in C_α may also be due to the effects of irregularly shaped particles or different size distributions between the idealized model assembly and the laboratory soil. However, given the difficulties associated with developing a DEM model of clay-sized, disk-shaped particles that use RPT to model clay compression, it is encouraging that the *e* and C_α values between the model and the laboratory experiments matched as closely as they do. As computational power increases over time and becomes more widely accessible, modeling of even more complex clay assemblies with more particles and wider distributions of particle sizes and shapes will become possible, perhaps even including pressure dependent amounts of interlayer water within the soil particles.

(a)

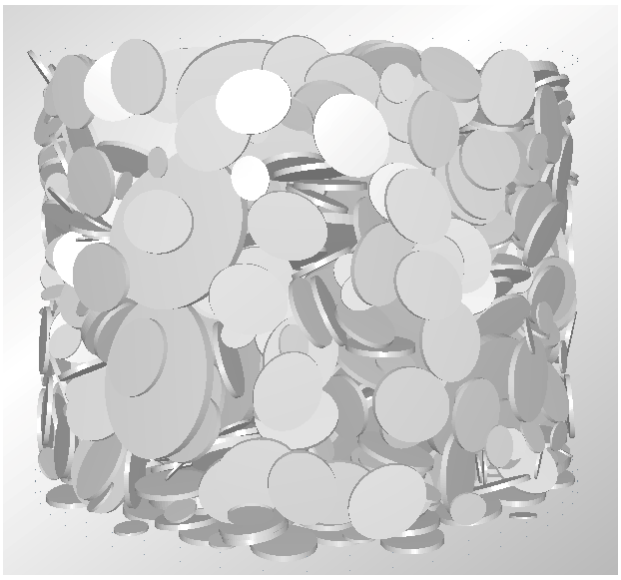

(b)

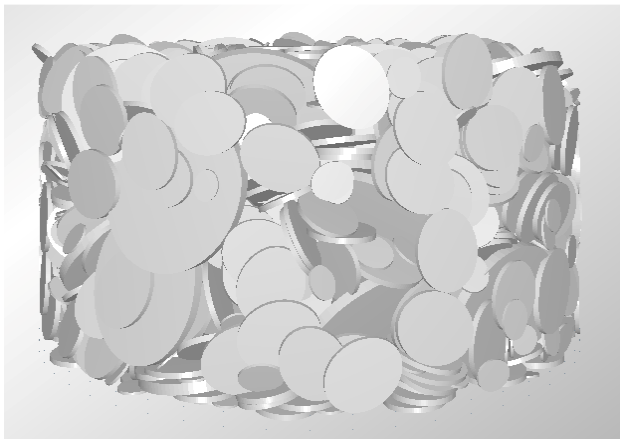

(c)

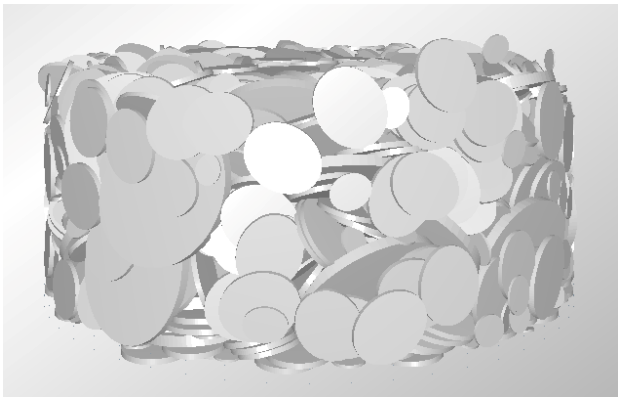

Fig. 10.14: Time-lapse perspective images of compression of Assembly l. (a) Initial particle configuration, (b) After application of 25 kPa loading, (c) After application of 50 kPa loading.

(a)

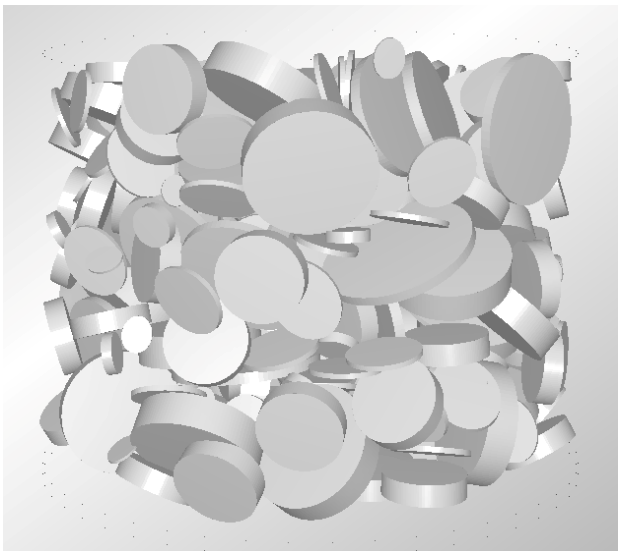

(b)

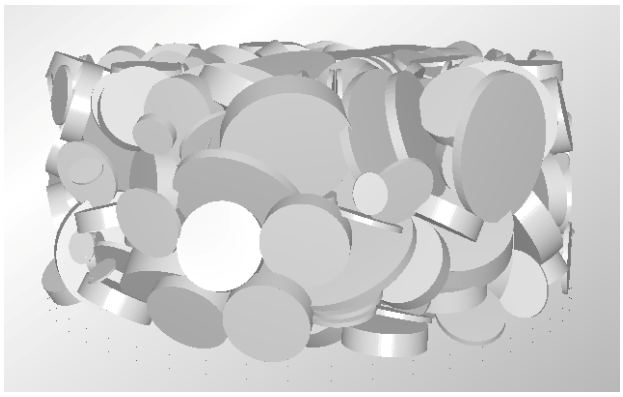

(c)

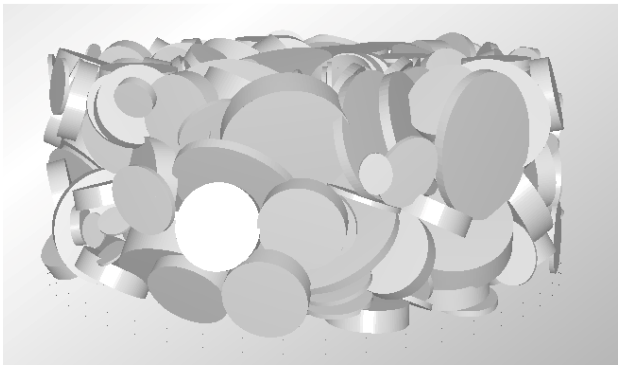

(d)

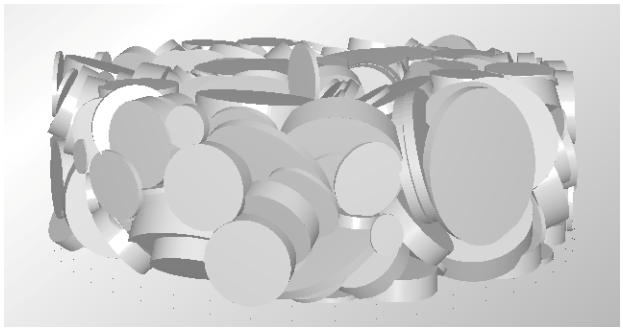

(e) 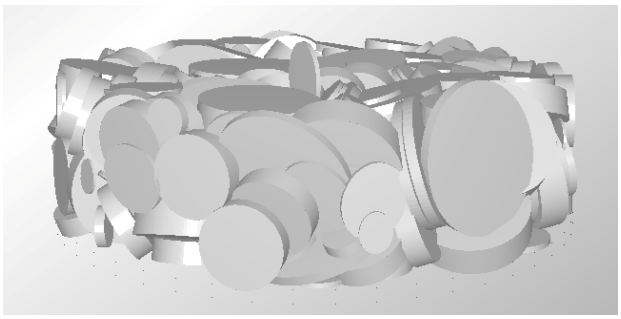

Fig. 10.15: Time-lapse perspective images of compression of Assembly 2. (a) Initial particle configuration, (b) After application of 25 kPa loading, (c) After application of 50 kPa loading, (d) After application of 100 kPa loading, (e) After application of 200 kPa loading.

(a) 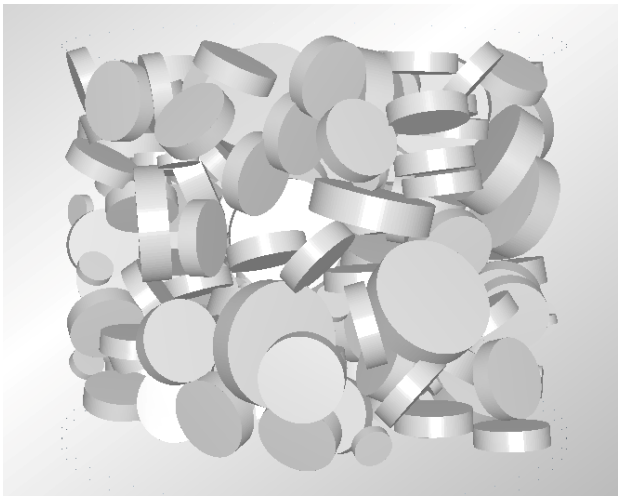

(b) 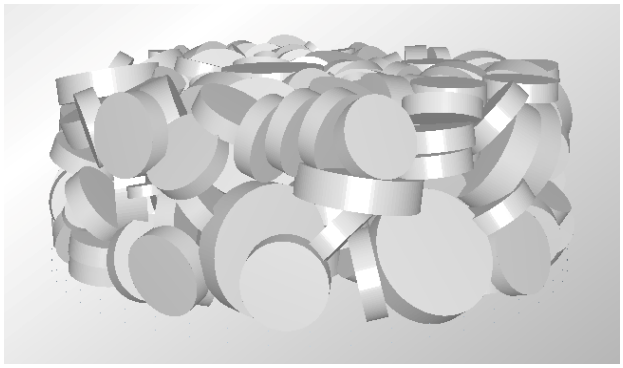

(c) 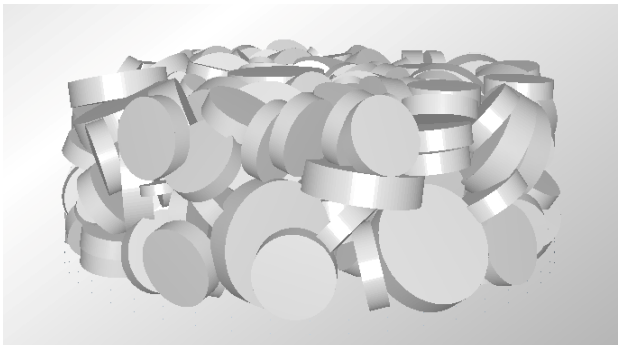

Fig. 10.16: Time-lapse perspective images of compression of Assembly 3. (a) Initial particle configuration, (b) After application of 25 kPa loading, (c) After application of 50 kPa loading.

Chapter 11

Summary, Conclusions, and Recommendations for Future Research

This chapter summarizes the research conducted (Section 11.1), presents conclusions based on the research (Section 11.2), and provides recommendations for future research (Section 11.3).

11.1 Summary

This study aimed to quantify macro-scale clay compression from micro-scale experiments and numerical analyses. The coefficient of friction, μ, of clay at the micro-scale has generally not been studied due to difficulties in obtaining measurements at such small scales within a bulk soil volume undergoing shear. Information on friction at the

micro-scale may provide insight into grain-scale processes that control behavior of bulk samples.

This research investigated the use of the Rate Process Theory (RPT) for describing sliding at individual clay particle contacts during a creep test. The general premise of the theory applied to clay is that each particle to particle contact is constrained from movement due to energy barriers which separate adjacent equilibrium positions on the atomic scale. For the clay particles to be displaced to new positions, they must become activated by acquiring sufficient energy.

This section summarizes the research conducted and is divided into micro-scale experiments, macro-scale experiments, and numerical modeling.

11.1.1 Micro-scale Experiments

This study involved developing a novel method to measure the micro-scale μ of clay. To measure the frictional forces between clay particles, an Atomic Force Microscope (AFM) was used. Customized AFM probes were made in house by gluing 52 μm diameter silica micro-spheres to the ends of tipless cantilevers, and a novel method was developed to coat the micro-spheres with montmorillonite particles using polyethyleneimine (PEI). A similar coating procedure was followed to coat a flat silica substrate, and friction experiments were conducted between the surfaces under aqueous and atmospheric conditions using an AFM. The method allows for measurements to be obtained over spatial scales of a few microns, provides measurements of micro-scale normal and shear forces between minerals, and requires no calibration beyond making a few microscopic measurements of the AFM probe using an Environmental Scanning

Electron Microscope (ESEM). The method provides measurements of micro-scale normal and shear forces between minerals, which can be used for a variety of applications such as in the study of secondary compression, shear deformation, and fault dynamics.

11.1.2 Macro-scale Experiments

Consolidation tests (ASTM D 2435-96) were conducted on the same sodium montmorillonite used in the micro-scale tests to determine the consolidation parameters and also to obtain macro-scale secondary compression magnitudes. A literature review was conducted of macro-scale wet and dry μ for sodium montmorillonite obtained from specialized triaxial shear, ring shear, and direct shear tests over varying sliding velocities.

11.1.3 Numerical Modeling

A discrete element method (DEM) numerical model of clay compression was developed using thin, three-dimensional disks to represent clay particles using a RPT contact model. Three simulation sets were conducted. Simulation Set 1 involved the study of RPT parameters on clay compression. Simulation Set 2 investigated a modified RPT-based model which limited the minimum μ in the model to minimize particle collapse. Simulation Set 3 studied the effect of different particle geometries, sizes, and size distributions on clay compression.

11.2 Conclusions

This section provides a summary of the conclusions from the research and is divided into micro-scale experiments, macro-scale experiments, and numerical modeling.

11.2.1 Micro-scale Experiments

Several control tests were conducted prior to the micro-scale clay friction experiments. Control tests of silica on mica ($\mu = 0.29 \pm 0.02$, where limits indicate one standard deviation) were found to agree with literature values. Control tests were also conducted to ensure that the UV/ozone cleaner fully removed any potential excess PEI on the surfaces. Also, AFM topographic scans of the clay coverage before and after PEI removal were compared to ensure complete clay coverage of the surfaces.

The μ value for wet sodium montmorillonite was determined to be 0.20 ± 0.03. The wet μ values closely matched those from macro-scale specialized triaxial shear experiments where residual μ values were not reached because shear displacements were relatively small. A second friction regime was apparent in the calcium-saturated ($\mu = 0.07 \pm 0.02$) and potassium-saturated ($\mu = 0.07 \pm 0.01$) experiments. The potassium-saturated experiments also exhibited $\mu = 0.23 \pm 0.02$ in certain friction tests, which is similar to the sodium-saturated μ value. It was speculated that since the two friction regimes' μ values matched the macro-scale triaxial shear μ values of 0.18 ± 0.05 and ring shear/direct shear residual μ values of 0.10 ± 0.03, the difference may result from different grain alignment at the probe-substrate interface.

The μ value for dry sodium montmorillonite was determined to be 0.72 ± 0.03. The dry μ values closely matched several macro-scale specialized triaxial shear experiments. Variability in the dry μ value of montmorillonite has been observed in macro-scale tests (Moore and Lockner, 2007) and may be due to differences in normal stress, displacement magnitude, shear rate, and thickness and geometry of particles formed during drying.

11.2.2 Macro-scale Experiments

The micro-scale and macro-scale μ values match well with those calculated for common RPT parameter values at varying sliding velocities. The activation energy for the macro-scale triaxial shear and corresponding micro-scale friction regime experiments fall within the range for montmorillonite of 84 – 109 kJ/mol. Ring shear and direct shear tests, which achieved a residual μ, and the corresponding friction regime of micro-scale μ values achieved activation energies in the range of 55 – 80 kJ/mol. All of the micro-scale and macro-scale experimental results fall within the expected range for the number of bonds per unit of normal force of 10^7 – 10^9 bonds/N.

11.2.3 Numerical Modeling

The numerical model investigated the use of the Rate Process Theory (RPT) for describing sliding at individual clay particle contacts during a creep test. The influences on compression of the number of bonds at each clay contact per unit of normal contact force and the activation energy were quantified using a DEM model. Increasing the energy barrier decreased the compression, as expected. Similarly, increasing the number of bonds per unit of normal force at the contacts decreased the compression, as expected.

Modifications to the RPT to implement a minimum μ value improved the model in terms of complete particle collapse; however, void ratios, e, and coefficients of secondary compression, C_α, were still not sufficiently improved to match macro-scale creep tests.

It was determined that modeling more realistic clay fabrics with varying particle sizes, particle size distributions, and aspect ratios led to a model that more closely

behaved like the macro-scale laboratory compression tests. For assemblies composed of thinner particles, the slope of the e vs. p plot and the e values were consistent between the model and laboratory experiments. The thinner particle assemblies also exhibited a greater C_α value than the thicker particle assemblies. Thinner particle assemblies may be able to compress more and at a faster rate than thicker particle assemblies when dissipation of excess pore pressure does not inhibit the rate of compression because the thinner particles are able to slide into smaller void spaces more easily. It is evident from the results that modeling clays as disks rather than spheres has a significant impact on the compression behavior and that modeling compression in three-dimensions is a necessary computational step to achieve more realistic assemblies.

11.3 Recommendations for Future Research

This section provides a summary of recommendations for future research on micro-scale clay friction and numerical modeling of clay compression.

11.3.1 Micro-scale Experiments

Future work using the AFM method developed could be focused on studying the bimodal μ distribution of potassium-saturated clay. A method to determine if the clay at the micro-scale interface shifts into a uniform grain alignment would be useful to determine if the bimodal distribution is a result of a residual μ being obtained.

It would also be interesting to test a wide variety of clays such kaolinite, illite, serpentinite minerals such as lizardite, and talc. There is great interest in the possibility of faults being controlled by slippage due to talc formation which may generate a plane of

weakness. Another possible investigation is of the micro-scale μ between clay and concrete for applications of sliding along pile foundations. The experimental method developed could easily be adapted to test the micro-scale μ of other clays and materials under a variety of environmental conditions.

11.3.2 Numerical Modeling

DEM models with different boundary conditions such as triaxial compression and direct shear would be interesting to study in the future. An additional study on the impact of initial clay fabric and particle aspect ratio and size distribution would be useful. Modeling of clay tactoids, or American football-shaped particles, would be interesting to study in future work as well as modeling the effective stress transfer to the clay.

To develop a significantly improved DEM model, it may be necessary to model individual basic units of clay and interlayer water films using molecular dynamics. This would require development of a completely new DEM code. Additionally, the model would require more powerful computational resources for the simulations to be completed in reasonable time frames.

RPT for the purpose of describing clay compression has been studied experimentally for over 50 years. While interest in the topic has varied, research on the topic continues to be published. The use of DEM for modeling clay compression using RPT in the future appears promising. Such models will not replace laboratory consolidation tests, but they can provide additional insights into the fundamental mechanisms underlying consolidation, creep, and stress-strain-strength behavior of soils.

Appendix A

References

The references cited in this study are presented in this section.

Abbireddy, C.O.R. and Clayton, C.R.I. (2010). "Varying initial void ratios for DEM simulations." *Géotechnique*, 60(6), 497-502.

Adachi, T., Iwasaki, Y., Sakamoto, M., and Suwa, S. (1986). "A case history: Settlement of fill over soft ground." *Consolidation of Soils: Testing and Evaluation*, ASTM STP 892, 684-693.

American Institute of Steel Construction. (2001). *Manual of steel construction*. AISC, IL.

Andersland, O.B. and Douglas, A.G. (1970). "Soil deformation rates and activation energies." *Géotechnique*, 20(1), 1-16.

Attard, P., Carambassis, A., and Rutland, M.W. (1999). "Dynamic surface force measurement. 2. Friction and the atomic force microscope." *Langmuir*, 15, 553-563.

Attard, P., Stiernstedt, J, and Rutland, M.W. (2007). "Measurement of friction coefficients with the atomic force microscope." *J. Physics: Conference Series*, 61, 51-55.

Bai, J., Chan, D., and Morgenstern, N. (2008). "Numerical analysis of time-dependent behavior for the Leaning Tower of Pisa." *Soils and Foundations*, 48(2), 207-220.

Bhushan, B., Israelachvili, J.N., and Landman, U. (1995). "Nanotribology - friction, wear and lubrication at the atomic-scale." *Nature*, 374, 607-616.

Bhushan, B. (2005). "Nanotribology and nanomechanics." *Wear*, 259, 1507-1531.

Bickmore, B.R., Hochella, M.F., Jr., Bosbach, D., and Charlet, Laurent. (1999). "Methods for performing atomic force microscopy imaging of clay minerals in aqueous solutions." *Clays and Clay Minerals*, 47(5), 573-581.

Bickmore, B.R., Bosbach, D., Hochella, M.F., Jr., Charlet, L., Rufe, E. (2001). "In situ atomic force microscopy study of hectorite and nontronite dissolution: Implications for phyllosilicate edge surface structures and dissolution mechanisms." *American Mineralogist*, 86, 411-423.

Bickmore, B.R., Nagy, K.L., Sandlin, P.E., and Crater, T.S. (2002). "Quantifying surface areas of clays by atomic force microscopy." *American Mineralogist*, 87, 780-783.

Bish, D. L. and Giese, R. F., Jr. (1981). "Interlayer bonding in IIb chlorite." *American Mineralogist*, 66, 1216–1220.

Blum, A.E. (1994). "Determination of illite/smectite particle morphology using scanning force microscopy." In Nagy, K.L., and Blum, A.E., (Eds.), *Scanning Probe Microscopy of Clay Minerals*, Boulder, Clay Minerals Society, 171-202.

Bolt, G.H. (1956). "Physico-chemical analysis of the compressibility of pure clays." *Géotechnique*, 6(2), 86-93.

Borden, D. and Giese, R.F. (2001). "Baseline studies of the Clay Minerals Society source clays: cation exchange capacity measurements by the ammonia-electrode method." *Clays and Clay Minerals*, 49(5), 444-445.

Bosbach, D., Charlet, L., Bickmore, B.R., Hochella, M.F., Jr. (2000). "The dissolution of hectorite: In-situ, real-time observations using atomic force microscopy." *American Mineralogist*, 85, 1209-1216.

Boudali, M., Leroueil, S., and Srinivasa Murthy, B.R. (1994). "Viscous behavior of natural clays." Proc. 13th ICSMFE, 1, 411-416.

Brown, K.M., Kopf, A., Underwood, M.B., and Weinberger, J.L., (2003). "Compositional and fluid pressure controls on the state of stress on the Nankai subduction thrust: A weak plate boundary." *Earth and Planetary Science Letters*, 214, 589-603.

Bunds, M.P. (2001). "Fault strength and transpressional tectonics along the Castle Mountain strike-slip fault, southern Alaska." *Geological Society of America Bulletin*, July 2001, 908-919.

Byerlee, J. (1978). "Friction of rocks." *Pure Applied Geophysics*, 116, 615-626.

Carpenter, B.M., Marone, C., and Saffer, D.M. (2009). "Frictional behavior of materials in the 3D SAFOD volume." *Geophysical Research Letters*, 36, L05302.

Chipera, S.J. and Bish, D.L. (2001). "Baseline properties of the Clay Minerals Society source clays: powder x-ray diffraction analyses." *Clays and Clay Minerals*, 49(5), 398-409.

Christensen, R.W. and Wu, T.H. (1964). "Analysis of clay deformation as a rate process." Proc. 4147, *J. Soil Mech. Found. Engrg. Div.*, 90, SM6, 125-157.

Collettini, C., Viti, C., Smith, S.A.F., and Holdsworth, R.E. (2009). "Development of interconnected talc networks and weakening of continental low-angle normal faults." *Geology*, 85, 567-570.

Crawford, C.B. and Morrison, K.I. (1996). "Case histories illustrate the importance of secondary-type consolidation settlements in the Fraser River delta." *Can. Geotech. J.*, 33, 866-878.

Cui, L. and O'Sullivan, C. (2006). "Exploring the macro- and micro-scale response of an idealised granular material in the direct shear apparatus." *Géotechnique*, 56(7), 455-468.

Cundall, P.A. and Strack, O.D.L. (1979). "A discrete numerical model for granular assemblies." *Géotechnique*, 29, 517.

Dhowian, A.W. (1991). "Secondary compression of sabkha 'saline' soils." *Engineering Geology*, 30, 155-169.

Dieterich, J.H. and Kilgore, B.D. (1994). "Direct observation of frictional contacts; new insights for state-dependent properties." *Pure and Applied Geophysics*, 143(1-3), 283-302.

Dixon, J.B. (1989). "Kaolin and serpentine group minerals." In: Dixon, J.B., Weed, S.B., (Eds.), *Minerals in Soil Environments*, Soil Science Society of America, Madison, WI, 467-525.

Erlandsson, R., Hadziioannou, G., Matte, C.M., McClelland, G.M., and Chiang, S. (1988). "Atomic scale friction between the muscovite mica cleavage plane and a tungsten tip." *J. Chem. Phys.*, 89(8), 5190-5193.

Eyring, H. (1936). "Viscosity, plasticity, and diffusion as examples of absolute reaction rates." *J. Chemical Phys*ics, 4(1936). 283-291.

Gao, J.P., Luedtke, W.D., Gourdon, D., Ruths, M., Israelachvili, J.N., and Landman, U. (2004). "Frictional forces and Amontons' law: From the molecular to the macroscopic scale." *J. Physical Chemistry B*, 108, 3410-3425.

Garlanger, J.E. (1972). "The consolidation of soils exhibiting creep under constant effective stress." *Géotechnique*, 22(1), 71-78.

Gibson, R.E. and Lo, K.Y. (1961). "A theory of soil exhibiting secondary compression." *Norw. Geotech. Inst.*, 78(5), 179–215.

Giese, R. F., Jr. (1974). "Surface energy calculations for muscovite." *Nature*, 248, 580–581.

Giese, R. F., Jr. (1978). "The electrostatic interlayer forces of layer structure minerals." *Clays and Clay Minerals*, 26, 51–57.

Giese, R. F., Jr. (1980). "Hydroxyl orientations and interlayer bonding in amesite." *Clays and Clay Minerals*, 28, 81– 86.

Gnecco, E., Bennewitz, R., Pfeiffer, O., Socoliuc, A., and Meyer, E. (2005). "Friction and wear at the nanoscale," in *Nanotribology and nanomechanics*, B. Bhushan, ed. Springer, 484-532.

He, M., Blum, A.S., Overney, G., and Overney, R.M. (2002). "Effect of interfacial liquid structuring on the coherence length in nanolubrication." Physical Review Letters, 88(15).

Hinchberger, S.D. and Qu, G. (2009). "Viscoplastic constitutive approach for rate-sensitive structured clays." *Can. Geotech. J.*, 46, 609-626.

Holdsworth, R.E. (2004). "Weak faults - rotten cores." *Science*, 303, 181-182.

Jones, R., Pollock, H.M., Geldart, D., and Verlinden-Luts, A. (2004). "Frictional forces between cohesive powder particles studied by AFM." *Ultramicroscopy*, 100, 59-78.

Juárez-Badillo, E. (1985). "General time volume change equation for soils." *Proc., XI Int. Conf. on Soil Mech. and Found. Engrg.*, San Francisco, Vol. 2, 519-530.

Katti, D.R., Matar, M.I., Katti, K.S., and Amarasinghe, P.M. (2009). "Multiscale modeling of swelling clays: a computational and experimental approach." *KSCE J. Civil Engineering*, 13(4), 243-255.

Keedwell, M.J. (1984). *Rheology and soil mechanics*. Elsevier, London.

Kim, Y.T., and Leroueil, S. (2001). "Modeling the viscoplastic behaviour of clays during consolidation: application to Berthierville clay in both laboratory and field conditions." 38, 484-497.

Kleijn, W.B., and Oster, J.D. (1982). "A model of clay swelling and tactoid formation." *Clays and Clay Minerals*, 30(5), 383-390.

Kock, I., and Huhn, K. (2007). "Influence of particle shape on the frictional strength of sediments - a numerical case study." *Sedimentary Geology*, 196, 217-233.

Koerner, R.M., McCabe, W.M., and Lord, A.E., Jr. (1977). "Acoustic emission behavior of cohesive soils." *J. of the Geotechnical Engineering Division*, 103(8), 837-850

Kogel, J.E., Trivedi, N.C., Barker, J.M., and Krukowski, S.T. (2006). *Industrial minerals and rocks.* Littleton, Colorado, Society for Mining, Metallurgy, and Exploration, Inc.

Kopf, A., and Brown, K.M. (2003). "Friction experiments on saturated sediments and their implications for the stress state of the Nankai and Barbados subduction thrusts." *Marine Geology*, 202, 193-210.

Kuhn, M.R. and Mitchell, J.K. (1993). "New perspectives on soil creep." *J. Geotechnical Engineering*, 119(3), 507-524.

Kwok, C.-Y. (2008). "Micromechanical modeling of soil creep." Ph.D. Dissertation, University of Cambridge.

Kwok, C.-Y. and Bolton, M.D. (2010). "DEM simulations of thermally activated creep in soils." *Géotechnique*, 60(6), 425-433.

Lambe, T.W. and Whitman, R.V. (1969). *Soil mechanics*. Wiley & Sons, Inc., NJ.

Leonard, G.A. and Girault, P. (1961). "Study of the one-dimensional consolidation test." *Proc. 5th Int. Conf. on Soil Mechanics and Foundational Engineering*, 1, 213-218.

Lupini, J.F., Skinner, A.E., Vaughan, P.R. (1981). "The drained residual strength of cohesive soils." *Géotechnique*, 31(2), 181-213.

Maio, C., Fenelli, G.B. (1994). "Residual strength of kaolin and bentonite: the influence of their constituent pore fluid." *Géotechnique*, 44(4), 217-226.

Maio, C., Santoli, L., Schiavone, P. (2004). "Volume change behaviour of clays: The influence of mineral composition, pore fluid composition, and stress state." *Mechanics of Materials*, 36, 435-451.

Manevitch, O.L. and Rutledge, G.C. (2004). "Elastic properties of a single lamella of montmorillonite by molecular dynamics simulation." *J. Phys. Chem.*, 108, 1428-1435.

Marcial, D., Delage, P., and Cui, Y.J. (2002). "On the high stress compression of bentonites." *Can. Geotech. J.*, 39, 812-820.

Matsui, T., Ito, T., Mitchell, J.K., and Abe, N. (1980). "Microscopic study of shear mechanisms in soils." *J. Geotechnical Engrg. Div.*, 106(2), 137-152.

McNeil, L.E. and Grimsditch, M. (1993). "Elastic moduli of muscovite mica." *J. Phys.: Condens. Matter*, 5, 1681-1690.

MikroMasch. (2010). "NSC12 ultrasharp cantilevers and gratings specifications."

Mindlin, R.D. and Deresiewicz, H. (1953). "Elastic spheres in contact under varying oblique forces." *J. Applied Mechanics,* 20, 327–344.

Mitchell, J.K., Campanella, R.G., and Singh, A. (1968). "Soil creep as a rate process." *J. Soil Mech. Found. Engrg. Div.*, 94(1), 231-253.

Mitchell, J.K., Singh, A., and Campanella, R.G. (1969). "Bonding, effective stress, and strength of soils." *J. Soil Mech. Found. Engrg. Div.*, 95(5), 1219-1246.

Mitchell, J.K. and Soga, K. (2005). *Fundamentals of soil behavior*. Wiley & Sons, Inc., NJ.

Moll, W.F. (2001). "Baseline studies of the Clay Minerals Society source clays: geological origin." *Clays and Clay Minerals*, 49(5), 374-380.

Moore, D.E., Lockner, D.A., Shengli, M., Summers, R., and Byerlee, J.D. (1997). "Strengths of serpentinite gouges at elevated temperatures." *J. Geophysical Research*, 102(B7), 14,787-14,801.

Moore, D.E. and Lockner, D.A. (2004). "Crystallographic controls on the frictional behavior of dry and water-saturated sheet structure minerals." *J. Geophysical Research*, 109(B3), B03401, 1-16.

Moore, D.E., and Lockner, D.A. (2007). "Friction of the smectite clay montmorillonite: A review and interpretation of data," in *The seismogenic zone of subduction thrust faults*, T. H. Dixon and C. Moore, (Eds.), Margins Theoretical and Experimental Earth Science Series, vol. 2, Columbia University Press, 317-345.

Moore, D.E., and Rymer, M.J. (2007). "Talc-bearing serpentinite and the creeping section of the San Andreas fault." *Nature*, 448, 795-797.

Morgan, J.K. and Boettcher, M.S. (1999). "Numerical simulations of granular shear zones using the distinct element method 1. Shear zone kinematics and the micromechanics of localization." *J. Geophysical Research*, 104(B2), 2703-2719.

Morrow, C.A., Shi, L.Q., and Byerlee, J.D. (1982). "Strain hardening and strength of clay-rich fault gouges." *J. Geophysical Research*, 87(B8), 6771-6780.

Morrow, C., Radney, B., and Byerlee, J. (1992). "Frictional strength and the effective pressure law of montmorillonite and illite clays." In: Evans, B., Wong, T., (Eds.),

Fault mechanics and transport properties of rocks, Academic Press Inc., San Diego, CA, 69-88.

Morrow, C., Moore, D.E., and Lockner, D.A. (2000). "The effect of mineral bond strength and adsorbed water on fault gouge frictional strength." *Geophysical Research Letters*, 27(6), 815-818.

Nishimura, S., Kodama, M., Yao, K., Imai, Y., and Tateyama, H. (2002). "Direct surface force measurement for synthetic smectites using the atomic force microscope." *Langmuir*, 18(12), 4681-4688.

Olson, R.E. (1998). "Settlement of embankments on soft clays." *J. Geotechnical and Geoenvironmental Engineering*, 124(8), 659-669.

Oquendo, W.F., Munoz, J.D., and Lizcano, A. (2009). "Oedometric test, Bauer's law and the micro-macro connection for a dry sand." *Computer Physics Communications*, 180, 616-620.

O'Sullivan, C., Bray, J.D., and Riemer, M.F. (2002). "Influence of particle shape and surface friction variability on response of rod-shaped particulate media." *J. Engrg. Mechanics*, 128(11), 1182-1192.

Parker, J.C., Zelazny, L.W., and Amos, D.F. (1980). "Swelling components of compacted Ca-montmorillonite." *Clays and Clay Minerals*, 28(2), 135-141.

Piner, R.D., Xu, T.T., Fisher, F.T., Qiao, Y., and Ruoff, R.S. (2003). "Atomic force microscopy study of clay nanoplatelets and their impurities." *Langmuir*, 19, 7995-8001.

Ploehn, H.J. and Liu, C. (2006). "Quantitative analysis of montmorillonite platelet size by atomic force microscopy." *Industrial & Engineering Chemistry*, 45, 7025-7034.

Price, D.G. (2009). *Engineering Geology: Principles and Practice* (M.H. de Freitas, ed.). Springer, Berlin.

Ripple, C.D. and Day, P.R. (1966). "Suction responses due to homogenous shear of dilute montmorillonite-water pastes." *Proc. 14th National Conference on Clays and Clay Minerals*, 307-316.

Robinson, R.G. (2003). "A study on the beginning of secondary compression of soils." *J. Testing and Evaluation*, 31(5), 388–397.

Ruan, J.A. and Bhushan, B. (1994). "Atomic-scale friction measurements using friction force microscopy. 1. General-principles and new measurement techniques." *J. Tribology*, 378-388.

Saffer, D.M., Frye, K.M., Marone, C., and Mair, K. (2001). "Laboratory results indicating complex and potentially unstable frictional behavior of smectite clay." *Geophysical Research Letters*, 28(12), 2297-2300.

Saffer, D.M. and Marone, C. (2003). "Comparison of smectite- and illite-rich gouge frictional properties: application to the updip limit of the seismogenic zone along subduction megathrusts." *Geophysical Research Letters*, 215, 219-235.

Schaetzl, R. and Anderson, S. (2005). *Soils: genesis and geomorphology*. Cambridge University Press, NY.

Schleicher, A.M., Warr, L.N., van der Pluijm, B.A. (2009). "On the origin of mixed-layered clay minerals from the San Andreas Fault at 2.5-3 km vertical depth (SAFOD drillhole at Parkfield, California)." *Contributions to Mineralogy and Petrology*, 157, 173-187.

Schleicher, A.M., van der Pluijm, B.A., and Warr, L.N. (2010). "Nanocoatings of clay and creep of the San Andreas fault at Parkfield, California." *Geology*, 38(7), 667-670.

Scholz, C.H. (1998). "Earthquakes and friction laws." *Nature*, 391(1), 37-41.

Selvam, A., See, C.H., Barkdoll, B., Prasad, S., and O'Haver, J. (2006). "Use of atomic force microscopy for examining wet clay." *Clays and Clay Minerals*, 54(1), 25-28.

Sheng, Y., Lawrence, C.J., Briscoe, B.J., and Thornton, C. (2003). "Numerical studies of uniaxial powder compaction process by 3D DEM." *Engineering Computations*, 21(2-4), 304-317.

Shirako, H., Sugiyama, M., Tonosaki, A., and Akaishi, M. (2006). "Secondary compression behavior in standard consolidation tests." *Proc. Schl. Eng. Tokai Univ., Ser. E*, 31(2006), 27-32.

Smyth, W.S.K. (1983). "Consolidation characteristics of Lakehead clay." School of Engineering, Lakehead University, Thunder Bay, Ont.

Solum, J.G., Hickman, S.H., Lockner, D.A., Moore, D.E., van der Pluijm, B.A., Schleicher, A.M., and Evans, J.P. (2006). "Mineralogical characterization of protolith and fault rocks from the SAFOD Main Hole." *Geophysical Research Letters*, 33, L21314.

Solum, J.G. and van der Pluijm, B.A. (2009). "Quantification of fabrics in clay gouge from the Carboneras fault, Spain and implications for fault behavior." *Tectonophysics*, 475, 554-562.

Stark, T.D. and Eid, H.T. (1994). "Drained residual strength of cohesive soils." *J. Geotechnical Engineering*, 120(5), 856-871.

Stiernstedt, J., Rutland, M.W., and Attard, P. (2005). "A novel technique for the in situ calibration and measurement of friction with the atomic force microscope." *Review of Scientific Instruments*, 76, 083710.

Stolle, D.F.E., Vermeer, P.A., and Bonnier, P.G. (1999). "A consolidation model for creeping clay." *Can. Geotech. J.*, 36, 754-759.

Svedberg, T. and Nichols, J. B. (1923). "Determination of size and distribution of size by centrifugal methods." *J. Am. Chem. Soc.* 45, 2910-2917.

Taylor, D.W. and Merchant, W. (1940). "A theory of clay consolidation accounting for secondary compression." *J. Mathematics and Physics*, 19(3), 167-185.

Taylor, D.W. (1942). "Research on Consolidation of Clays." Department of Civil and Sanitary Engineering, Series 82, Massachusetts Institute of Technology, Cambridge, MA, Aug. 1942.

Taylor, D.W. (1948). *Fundamentals of soil mechanics*. Wiley, New York.

Tembe, S., Lockner, D.A., Solum, J.G., Morrow, C.A., Wong, T.-f., and Moore, D.E. (2006). "Frictional strength of cuttings and core from SAFOD drillhole phases 1 and 2." *Geophysical Research Letters*, 33, L23307.

Tembe, S., Lockner, D.A., and Wong, T. (2010). "Effect of clay content and mineralogy on frictional sliding behavior of simulated gouges: Binary and ternary mixtures of quartz, illite, and montmorillonite." *J. Geophysical Research*, 115, B03416, 1-22.

Terzaghi, K. (1923). Die Berechnung der Durchlässigkeitsziffer des Tones aus dem Verlang der Hydrodynomischen Spannungserscheinunpen. *Sitzungsbcrichte, Matematisch Notar-wissenschaftliche Klasse* (Akademie der Wissenschaften, Vienna), Part 2.2, 132, 3/4, 125-138.

Terzaghi, K., Peck, R., and Mesri, G. (1996). *Soil mechanics in engineering practice*. Wiley & Sons, Inc., NY.

Thornton, C. (2000). "Numerical simulations of deviatoric shear deformation of granular media." *Géotechnique*, 50(1), 43-53.

Tietz, T. and Dorn, J. (1956). "Creep of copper at intermediate temperatures." *Transactions*, *Amer. Inst. Mech. Eng.*, 206, 156.

Tiwari, B. and Marui, H. (2005). "A new method for the correlation of residual shear strength of the soil with mineralogical composition." *J. Geotechnical and Geoenvironmental Engineering*, 131(9), 1139-1150.

Wei, Z.Q., Wang, C., and Bai, C.L. (2000). "Surface imaging of fragile materials with hydrophobic atomic force microscope tips." *Surface Science*, 467, 185-190.

Wenk, H.R., Kanitpanyacharoen, W., and Voltolini, M. (2010). "Preferred orientation of phyllosilicates: Comparison of fault gouge, shale, schist." *J. Structural Geology*, 32(4), 478-489.

Wintsch, R.P., Christoffersen R., and Kronenberg, A.K. (1995). "Fluid-rock weakening of fault zones." *J. Geophysical Research*, 100(B7), 13021-13032.

Wu. F.T., Blatter, L., and Roberson, H. (1975). "Clay gouges in the San Andreas fault system and their possible implications." *Pure and Applied Geophysics*, 113, 87-95.

Yao, M. and Anandarajah, A. (2003). "Three-dimensional discrete element method of analysis of clays." *J. Engineering Mechanics*, 129(6), 585-596.

Yin, J.-H. (1999). "Non-linear creep of soils in oedometer tests." *Géotechnique*, 49(5), 699-707.

Zelazny, L.W. and White, G.N. (1989). "The pyrophyllite-talc group." In: Dixon, J.B., Weed, S.B., (Eds.), *Minerals in soil environments*, Soil Science Society of America, Madison, WI, 547-550.

Zoback M.D. (2000). "Strength of the San Andreas." *Nature*, 405, 31-32.

Zoback, M.D., Hickman, S., and Ellsworth, W. (2010). "Scientific drilling into the San Andreas fault zone." *EOS*, 91(22), 197-199.

Appendix B

Nomenclature

The nomenclature used in this study is presented in this section.

A	Empirical parameter for Stolle *et al.* (1999) method
AR	Average aspect ratio
a	Empirical parameter for Stiernstedt *et al.* (2005) method
a_v	Coefficient of compressibility
a_1, a_2, a_3	Empirical parameters for Gibson and Lo (1961) method
B	Empirical parameter for Stolle *et al.* (1999) method
b	Empirical parameter for Stiernstedt *et al.* (2005) method
C	Empirical parameter for Stolle *et al.* (1999) method or particle overlap
C_c	Compression index
C_s	Swelling index

C_α	Secondary compression coefficient
$C_{\varepsilon c}$	Compression ratio
c	Smaller of the disks in contact's cohesion or proportionality factor or empirical parameter for Stiernstedt *et al.* (2005) method
D	Deviator stress under triaxial stress conditions or distance between the centers of two colliding disks
D_1	Initial deviator stress for Tietz and Dorn (1956) method
d	Empirical parameter for Stiernstedt *et al.* (2005) method
d_j	Distance between the center of disk *j* and the axis of rotation, taken as the center of mass of the particle
E	Elastic modulus or energy
ΔE	Energy change
e	Void ratio or empirical parameter for Stiernstedt *et al.* (2005) method
e_f	Final void ratio
e_{fixed}	Fixed void ratio
e_i	Unit vector pointing from the center of disk X to the center of disk Y
e_0	Initial void ratio
F_n	Normal force
$F_{n,f}$	Final normal force
F_S	Shear force
$F_{s,f}$	Final shear force
F_x	Net force on disk X
F_y	Horizontal friction force or net force on disk Y
F_z	Vertical surface force
ΔF	Free energy of activation
ΔF_e	Experimental activation energy

f	Average applied force per flow unit or empirical parameter for Stiernstedt *et al.* (2005) method
f_n	Normal contact force
f_t	Tangential contact force
G	Shear modulus
G_s	Specific gravity
h	Planck's constant or empirical parameter for Stiernstedt *et al.* (2005) method
I_x	Moment of inertia of disk X
i	Empirical parameter for Stiernstedt *et al.* (2005) method
j	Empirical parameter for Stiernstedt *et al.* (2005) method
k	Coefficient of permeability or Boltzmann's constant
k_{cal}	Calibrated spring constant
k_{eff}	Effective spring constant
k_N	Normal particle stiffness
k_S	Shear particle stiffness
L_{cal}	Full length of the cantilever
L_0	Length of the flexible part of the cantilever
L_1	Length of the rigid part of the cantilever to the midpoint of the microsphere attachment
L_2	Microsphere diameter
l	Length
M	Constrained modulus or number of disks
M_x	Resultant moment acting on disk X
M_y	Resultant moment acting on disk Y
m_j	Mass of disk j

m_v	Coefficient of volume compressibility
m_x	Mass of disk X
N	Avogadro constant or revolutions per second or index
n	Number of bonds at the contact or viscosity
Δn	Relative displacement increment in the normal direction
$\dot{n}$	Normal component of the relative velocity
n_1	Number of bonds per unit of normal contact force
P_x, P_y	Points of intersection of the line connecting the centers of the disks to the boundaries of disks X and Y
p	Pressure
p_o	Effective consolidation pressure
R	Universal gas constant or radius of rotation of the top of the sediment
R_j	Radius of disk j
R_{min}	Minimum particle radius
R_x	Radius of disk X
R_y	Radius of disk Y
r	Particle radius
S	Number of flow units per unit area or radius of rotation of the surface of the dispersion
ΔS	Difference in specific gravity
S_1	Number of bonds per unit area per unit of mean effective stress
Δs	Relative displacement increment in the tangential direction
$\dot{s}$	Sliding velocity or tangential component of the relative velocity
T	Absolute temperature
T_1	Initial temperature for Tietz and Dorn (1956) method

T_2	Final temperature for Tietz and Dorn (1956) method
t	Time
t_i	Unit vector obtained by a 90° clockwise rotation of e_i
t_p	Time indicating the end of primary consolidation
t_R	Rayleigh time-step
t_0	Time at which secondary compression starts
t^*	Characteristic time for which $e = 0.5e_f$
ΔV	Change in photodiode voltage
w	Width or water content
w_{fixed}	Fixed water content
X	Parameter proportional to the number of flow units in the direction of deformation
$\dot{X}_i$	Relative velocity of point P_x with respect to P_y
x_i	Horizontal (1) or vertical (2) coordinate of disk X
$\dot{x}_i$	Horizontal (1) or vertical (2) translational velocity of disk X
$\ddot{x}_i$	Horizontal (1) or vertical (2) translational acceleration of disk X
y_i	Horizontal (1) or vertical (2) coordinate of disk Y
$\dot{y}_i$	Horizontal (1) or vertical (2) translational velocity of disk Y
y_2	Horizontal axial displacement of the probe on the substrate
$\dot{y}_2$	Horizontal axial velocity of the probe on the substrate
z_2	Vertical piezo-electric scanner displacement
$\dot{z}_2$	Vertical piezo-electric scanner velocity
α	$\lambda/4SkT$ or angle with horizontal or DEM parameter
α_+	Slope of the constant compliance region on the approach portion
α_-	Slope of the constant compliance region on the retraction portion

δ	Energy curve minimum displacement distance = elastic distortion of the soil
ε	Strain
$\Delta\varepsilon_1$	Creep strain limit
$\dot{\varepsilon}$	Strain rate
$\dot{\varepsilon}_1$	Initial strain rate for Tietz and Dorn (1956) method
$\dot{\varepsilon}_2$	Final strain rate for Tietz and Dorn (1956) method
θ	Angle cantilever makes with the horizontal
$\dot{\theta}_x$	Angular velocity of disk X
$\ddot{\theta}_x$	Angular acceleration of disk X
$\dot{\theta}_y$	Angular velocity of disk Y
$\ddot{\theta}_y$	Angular acceleration of disk Y
λ	Distance between successive equilibrium positions
μ	Coefficient of friction
μ_{min}	Minimum coefficient of friction
μ_s	Coefficient of static friction between the two disks
v_R	Rayleigh waves surface propagation velocity
ξ	Shear fluidity (reciprocal of viscosity) of the clay
ρ	Density
σ	Stress
$\Delta\sigma$	Applied consolidation stress
σ_{po}	Preconsolidation pressure
σ_y	Yield stress
$\dot{\sigma}$	Stress rate
σ'	Effective stress

τ	Shear stress or time scale related to σ_p and the macro-scale consolidation test data
υ	Poisson's ratio or frequency of bond rupture
υ_{net}	Net frequency of bond rupture or activation
φ_u	Inter-particle friction angle of the disks
ψ	C_α / ln 10
$\psi_o^{'}$	Initial value (at t = 0) of the ratio of ψ to specific volume
ω	Mean frequency of oscillation

Appendix C

Glass on Muscovite Mica Deflection-Distance Curves

The deflection-distance curves contained in this section were obtained using the uncoated glass probe and an uncoated mica substrate in an aqueous environment. These experiments served as control tests.

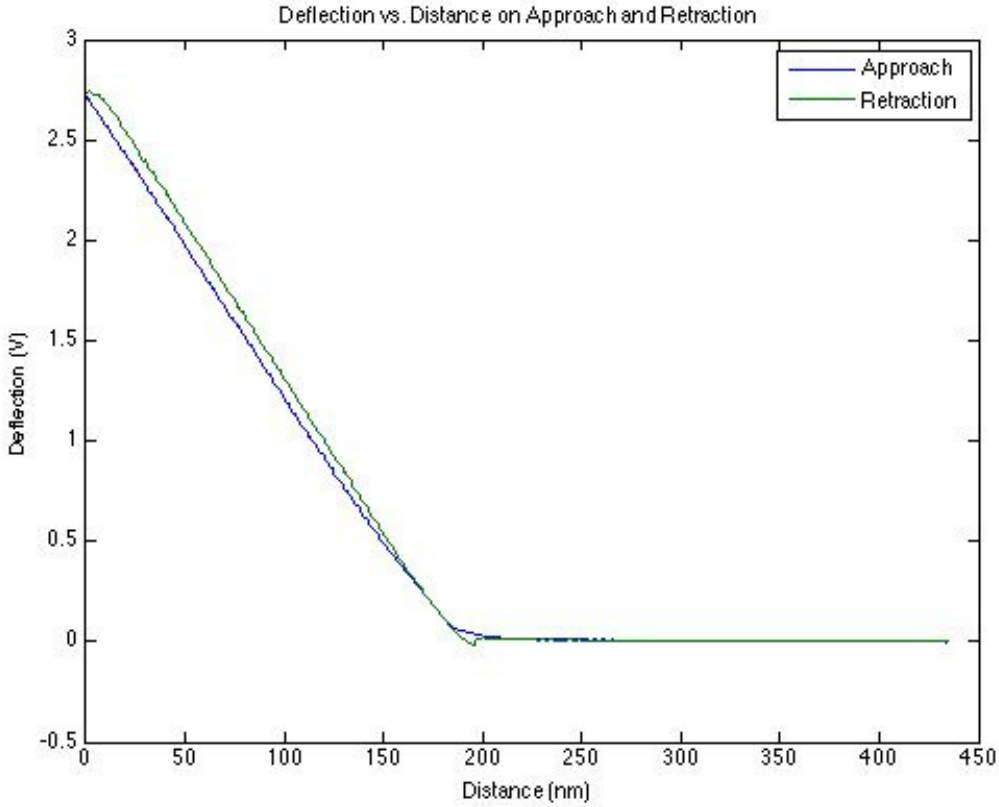
Deflection vs. Distance on Approach and Retraction
Approach
Retraction
Deflection (V)
Distance (nm)
3
2.5
2
1.5
1
0.5
0
-0.5
0
50
100
150
200
250
300
350
400
450

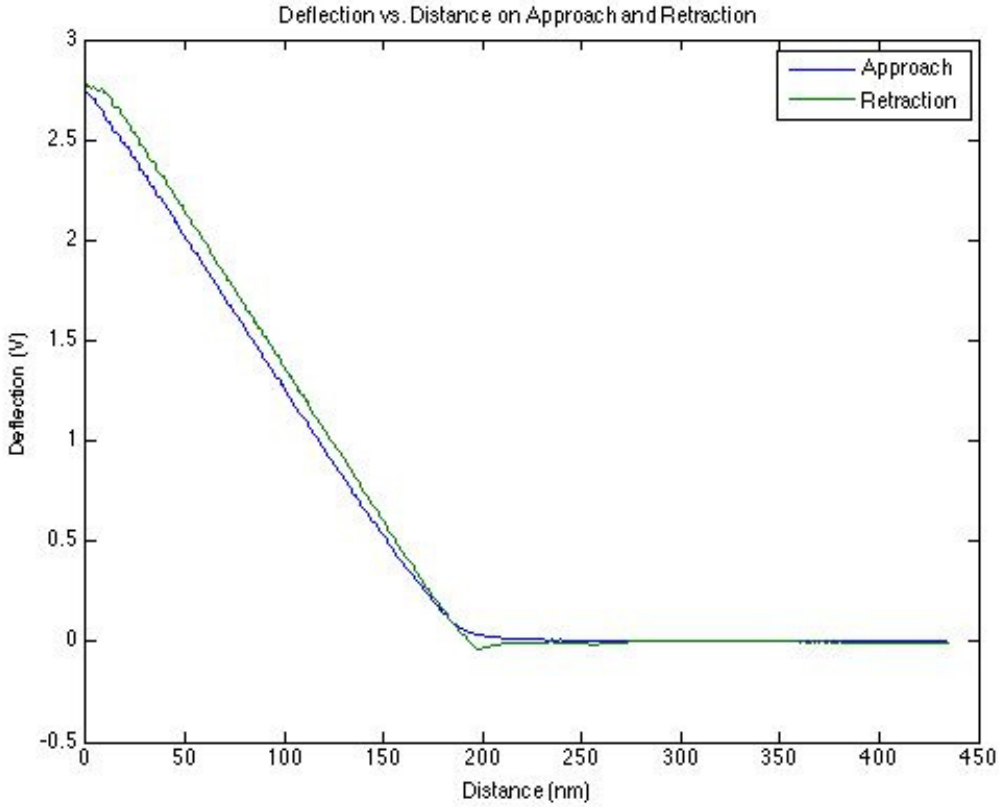
Deflection vs. Distance on Approach and Retraction
Approach
Retraction
Deflection (V)
Distance (nm)
3
2.5
2
1.5
1
0.5
0
-0.5
0
50
100
150
200
250
300
350
400
450

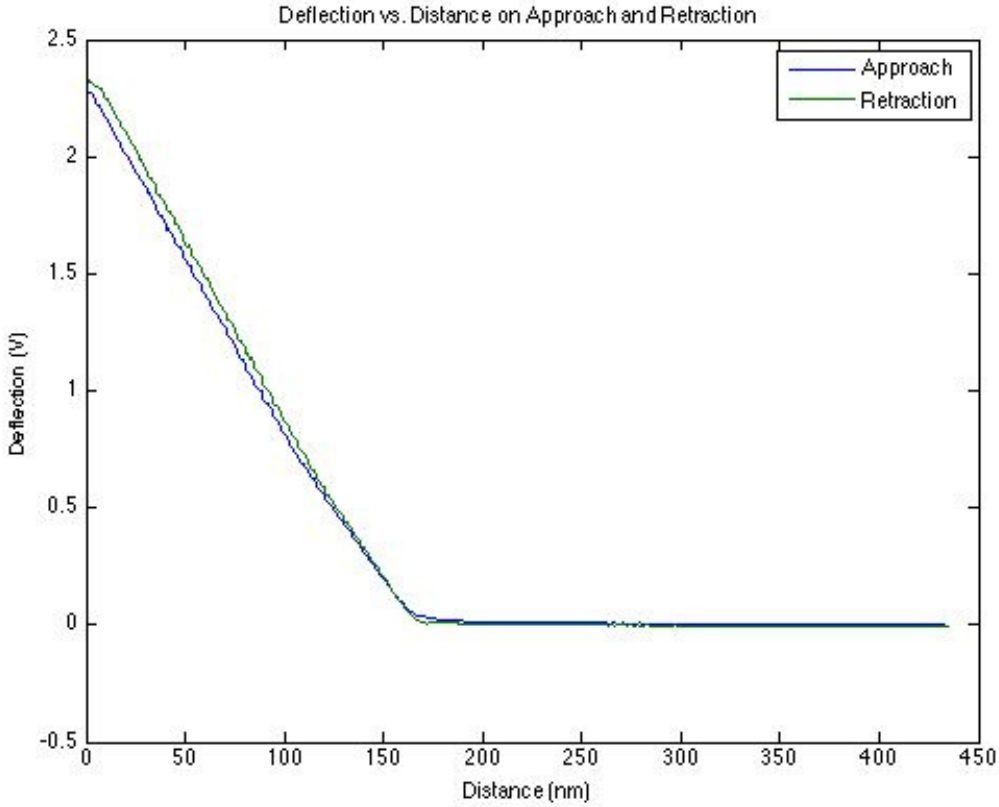
Deflection vs. Distance on Approach and Retraction
Approach
Retraction
Deflection (V)
Distance (nm)
2.5
2
1.5
1
0.5
0
-0.5
0
50
100
150
200
250
300
350
400
450

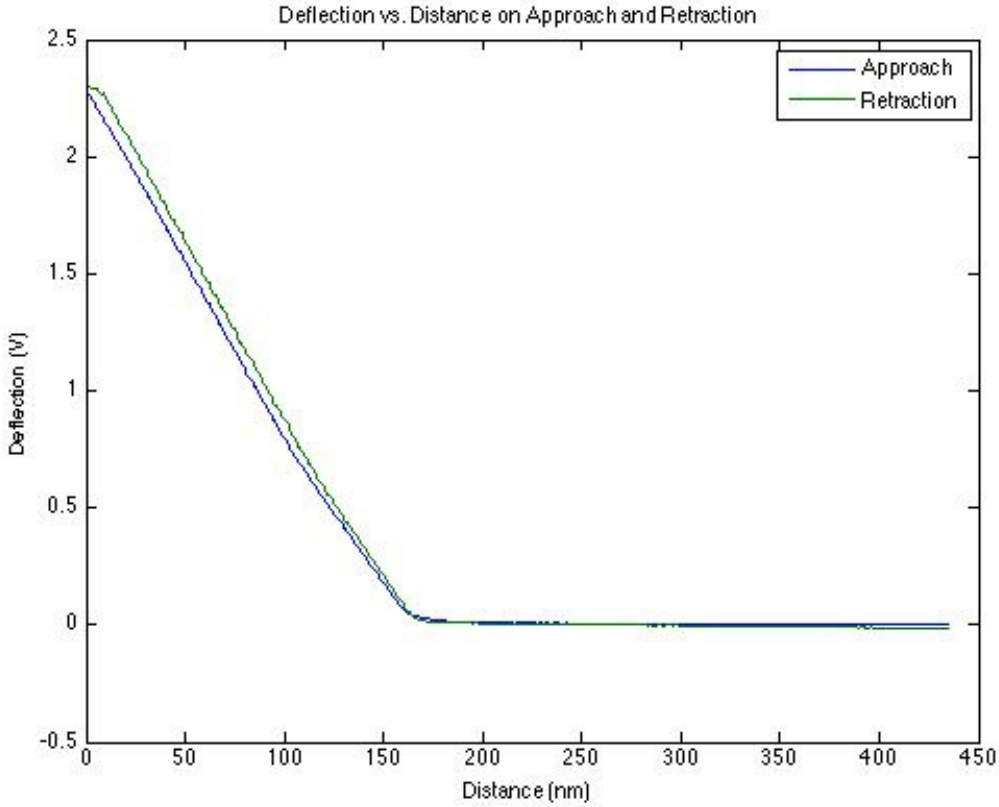
Deflection vs. Distance on Approach and Retraction
Approach
Retraction
Deflection (V)
Distance (nm)
2.5
2
1.5
1
0.5
0
-0.5
0
50
100
150
200
250
300
350
400
450

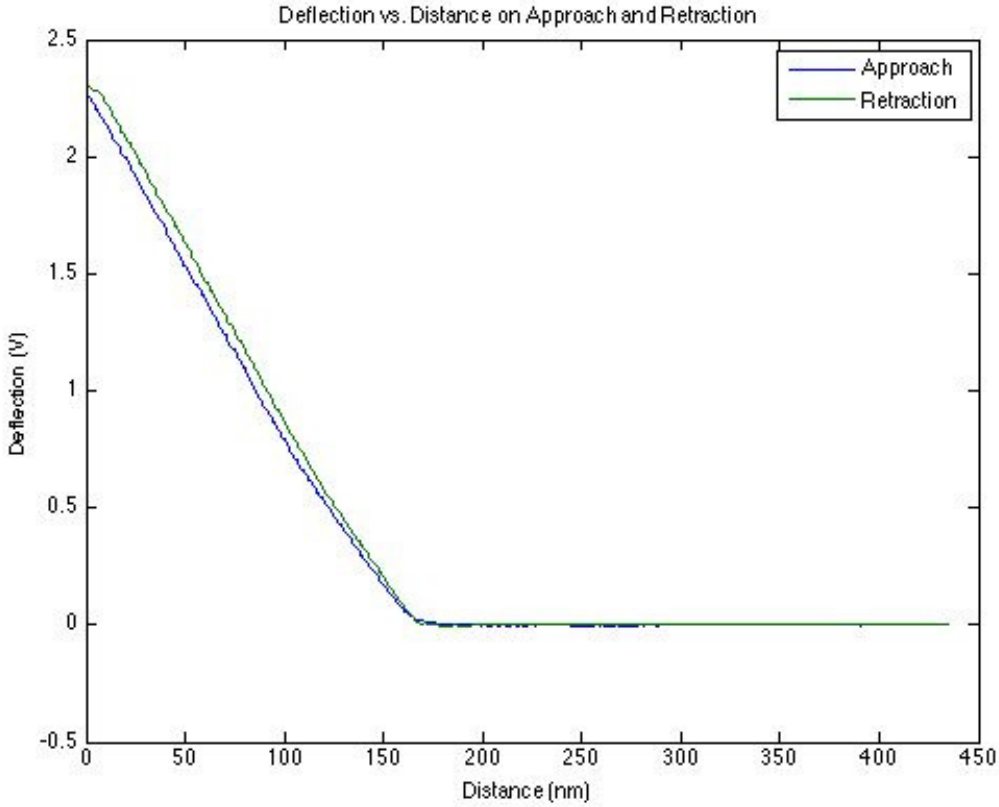
Deflection vs. Distance on Approach and Retraction
Approach
Retraction
Deflection (V)
Distance (nm)
2.5
2
1.5
1
0.5
0
-0.5
0
50
100
150
200
250
300
350
400
450

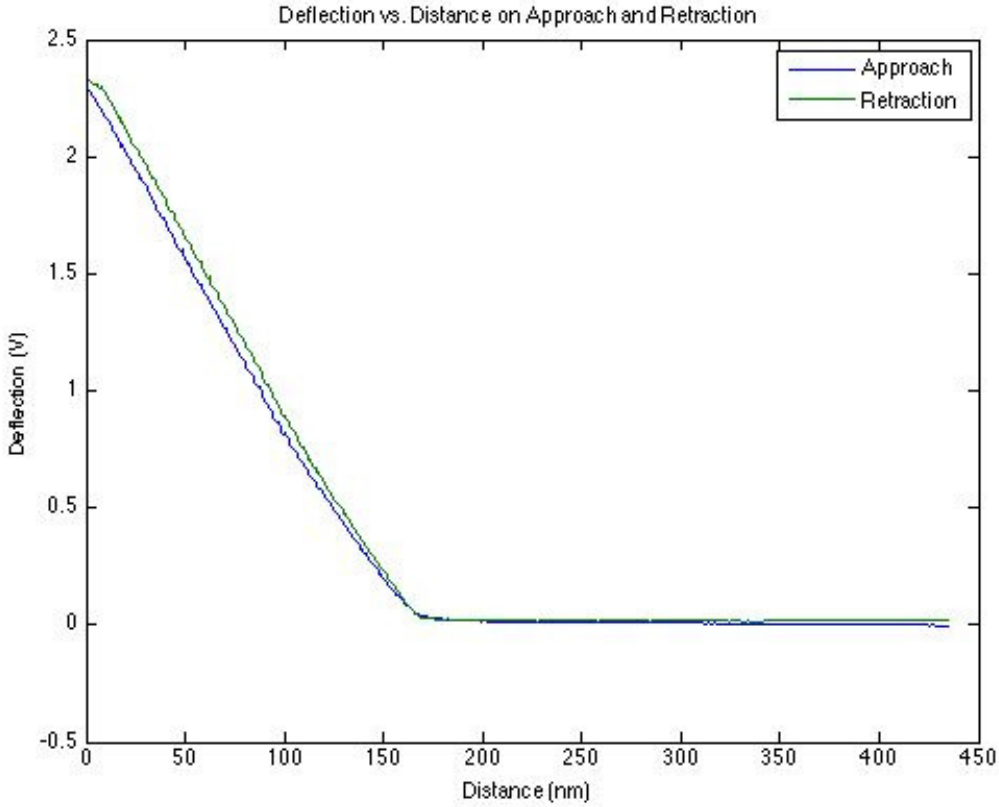
Deflection vs. Distance on Approach and Retraction
Approach
Retraction
Deflection (V)
Distance (nm)
2.5
2
1.5
1
0.5
0
-0.5
0
50
100
150
200
250
300
350
400
450

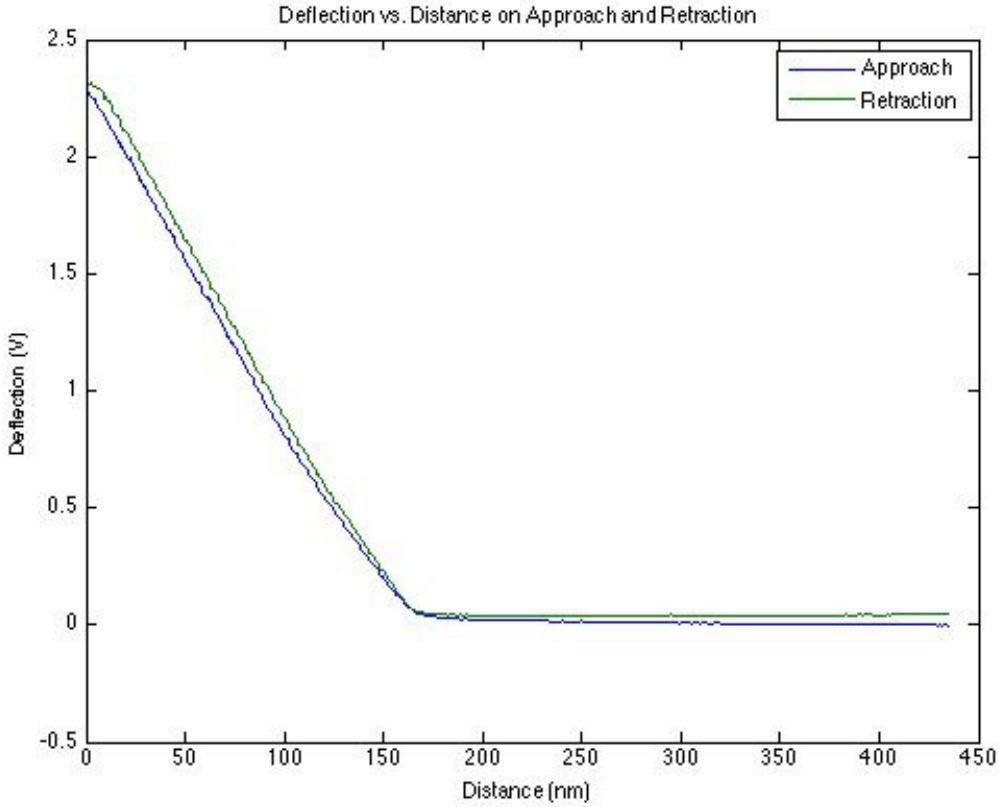
Deflection vs. Distance on Approach and Retraction
Approach
Retraction
Deflection (V)
Distance (nm)
2.5
2
1.5
1
0.5
0
-0.5
0
50
100
150
200
250
300
350
400
450

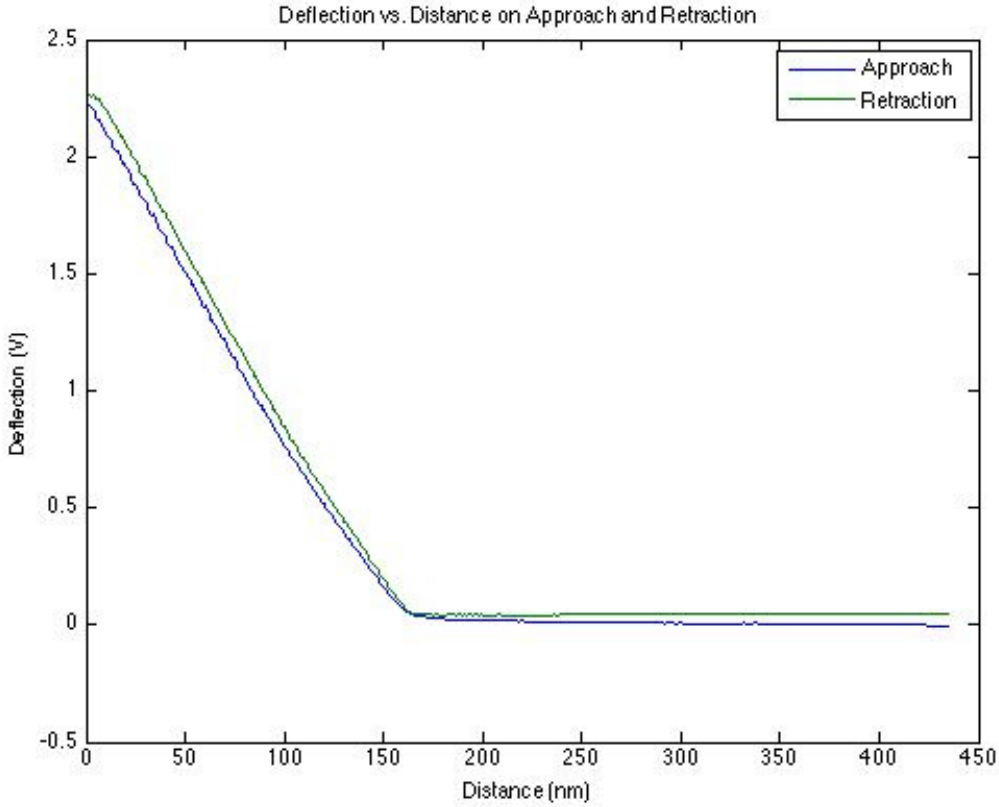
Deflection vs. Distance on Approach and Retraction
Approach
Retraction
Deflection (V)
Distance (nm)
2.5
2
1.5
1
0.5
0
-0.5
0
50
100
150
200
250
300
350
400
450

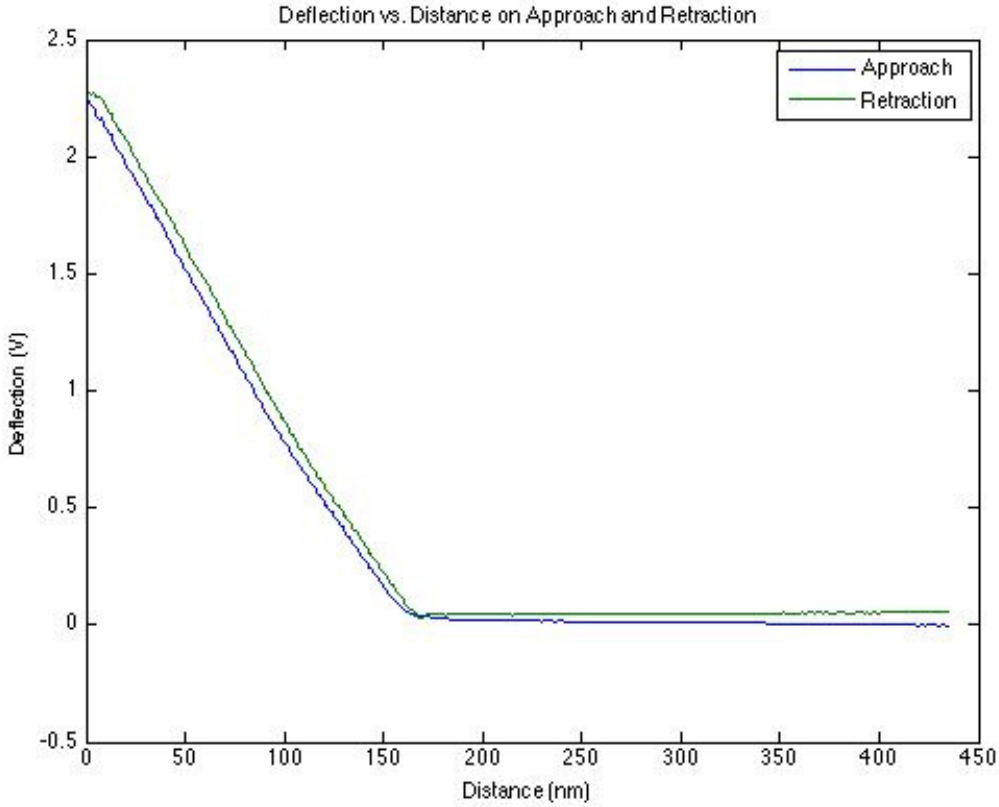
Deflection vs. Distance on Approach and Retraction
Approach
Retraction
Deflection (V)
Distance (nm)
2.5
2
1.5
1
0.5
0
-0.5
0
50
100
150
200
250
300
350
400
450

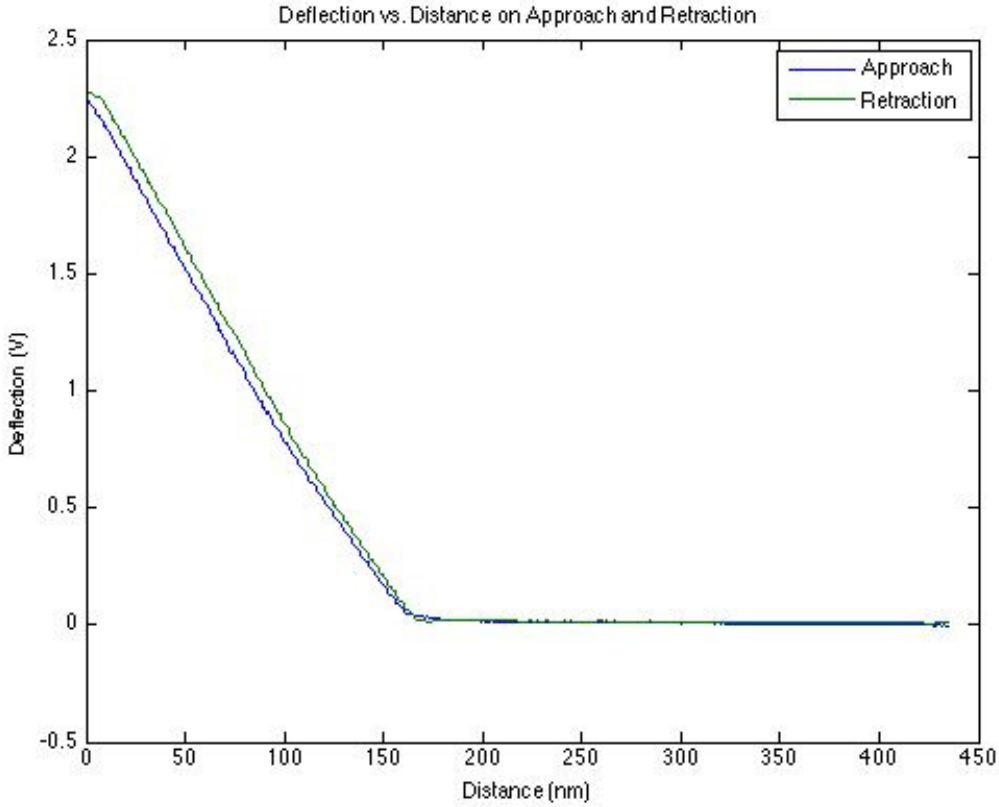
Deflection vs. Distance on Approach and Retraction
Approach
Retraction
Deflection (V)
Distance (nm)
2.5
2
1.5
1
0.5
0
-0.5
0
50
100
150
200
250
300
350
400
450

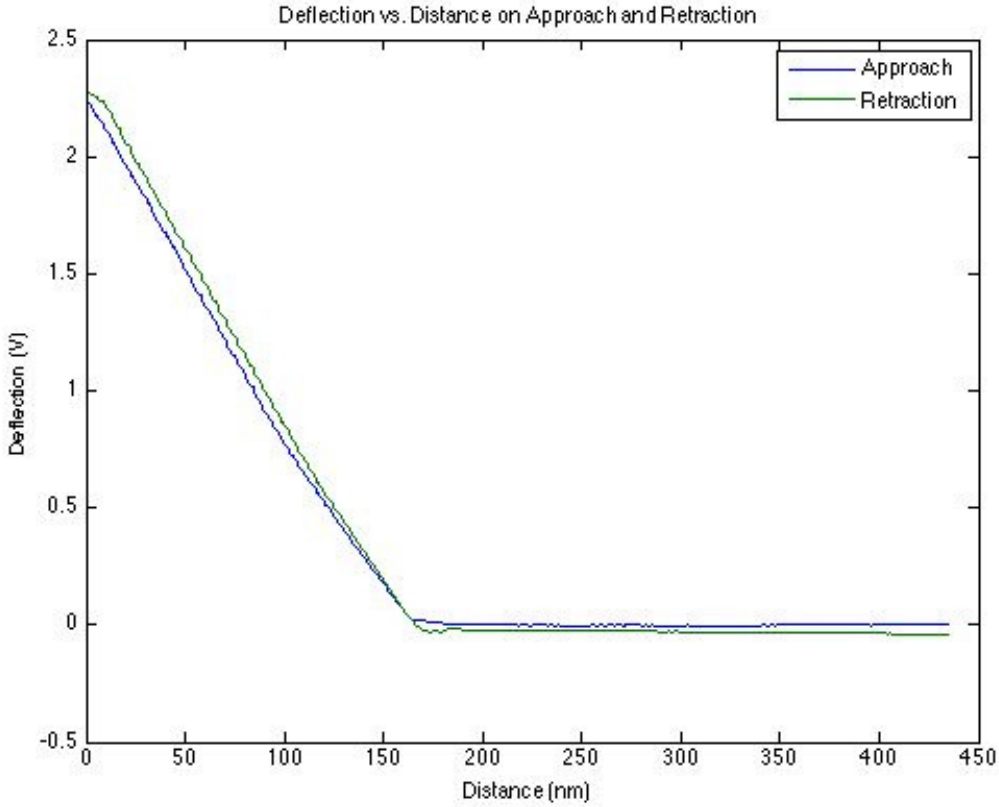
Deflection vs. Distance on Approach and Retraction
Approach
Retraction
Deflection (V)
Distance (nm)
2.5
2
1.5
1
0.5
0
-0.5
0
50
100
150
200
250
300
350
400
450

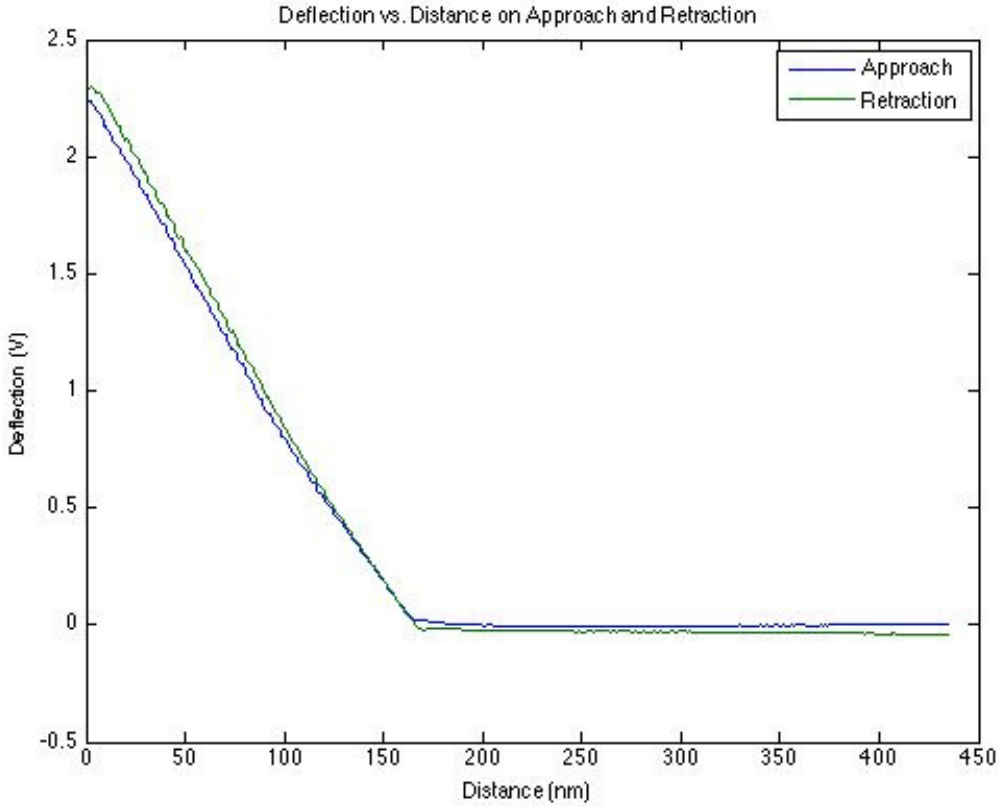
Deflection vs. Distance on Approach and Retraction
Approach
Retraction
Deflection (V)
Distance (nm)
2.5
2
1.5
1
0.5
0
-0.5
0
50
100
150
200
250
300
350
400
450

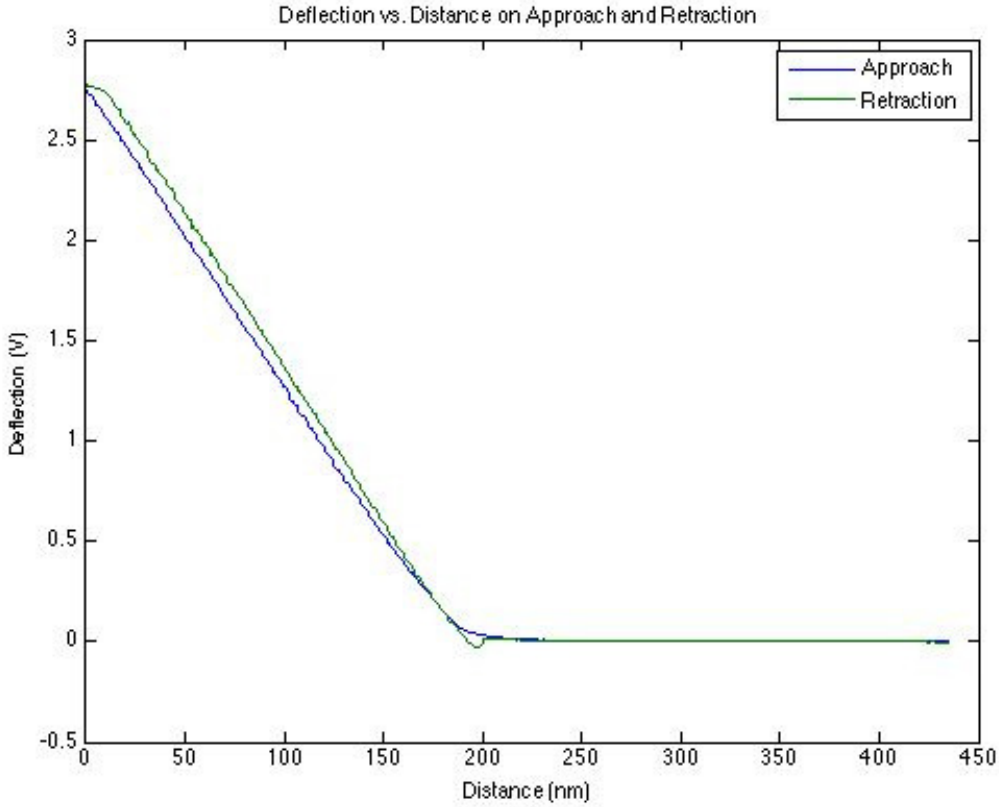
Deflection vs. Distance on Approach and Retraction
Approach
Retraction
Deflection (V)
Distance (nm)
3
2.5
2
1.5
1
0.5
0
-0.5
0
50
100
150
200
250
300
350
400
450

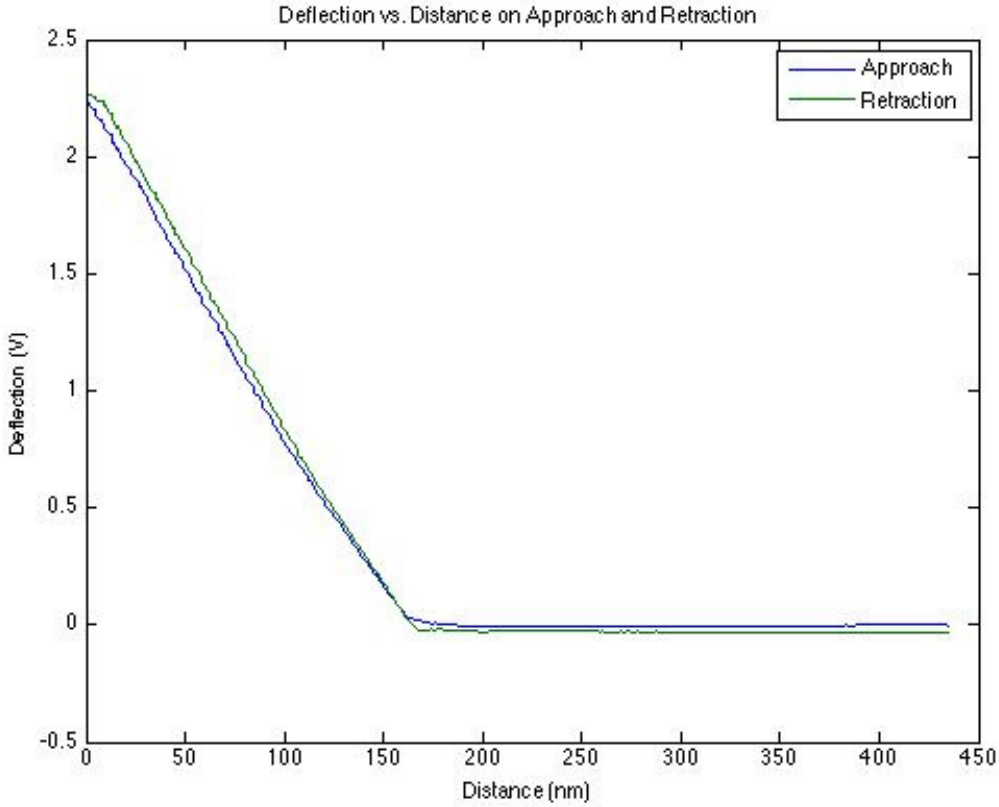
Deflection vs. Distance on Approach and Retraction
Approach
Retraction
Deflection (V)
Distance (nm)
2.5
2
1.5
1
0.5
0
-0.5
0
50
100
150
200
250
300
350
400
450

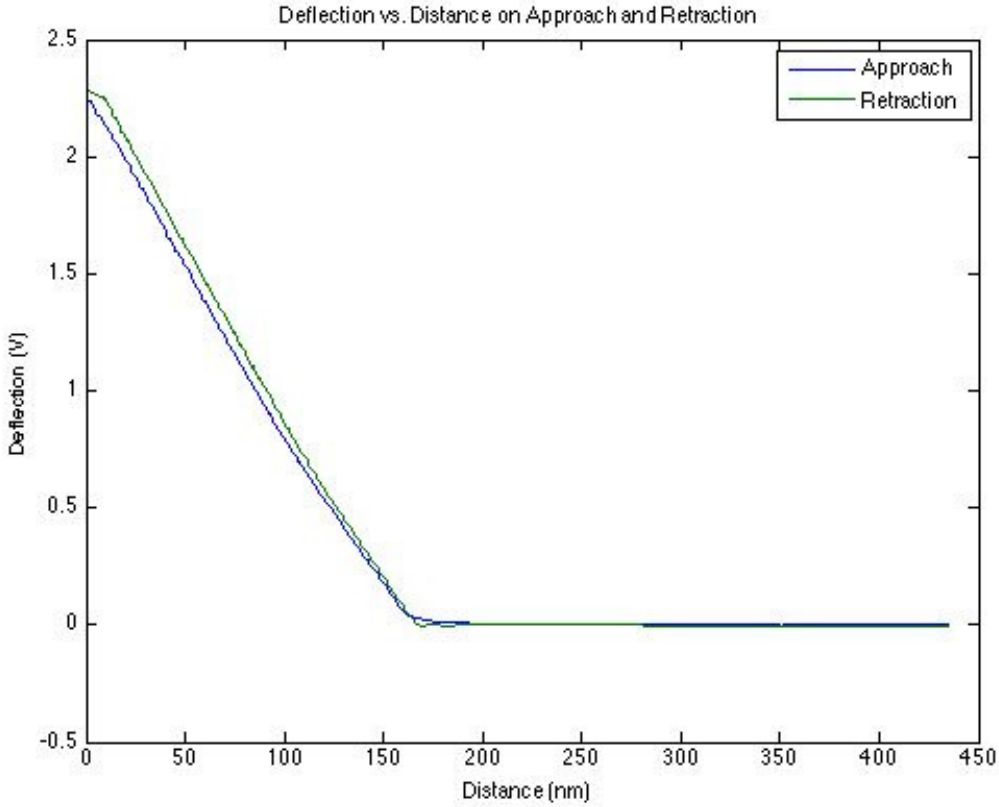
Deflection vs. Distance on Approach and Retraction
Approach
Retraction
Deflection (V)
Distance (nm)
2.5
2
1.5
1
0.5
0
-0.5
0
50
100
150
200
250
300
350
400
450

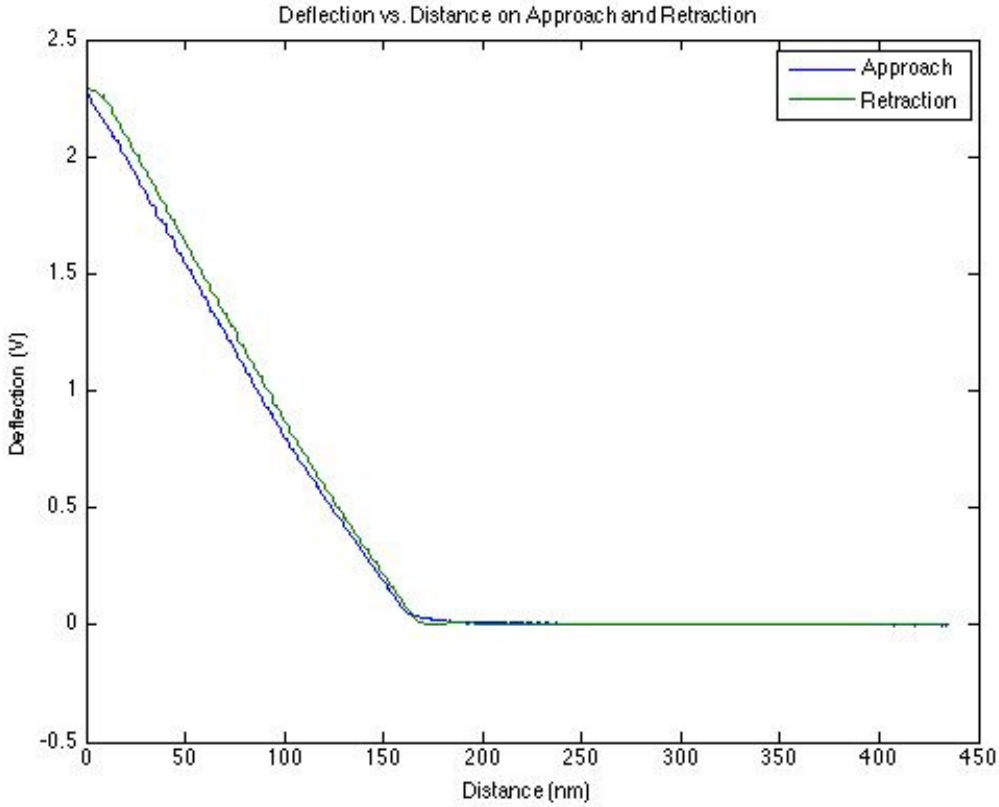
Deflection vs. Distance on Approach and Retraction
Approach
Retraction
Deflection (V)
Distance (nm)
2.5
2
1.5
1
0.5
0
-0.5
0
50
100
150
200
250
300
350
400
450

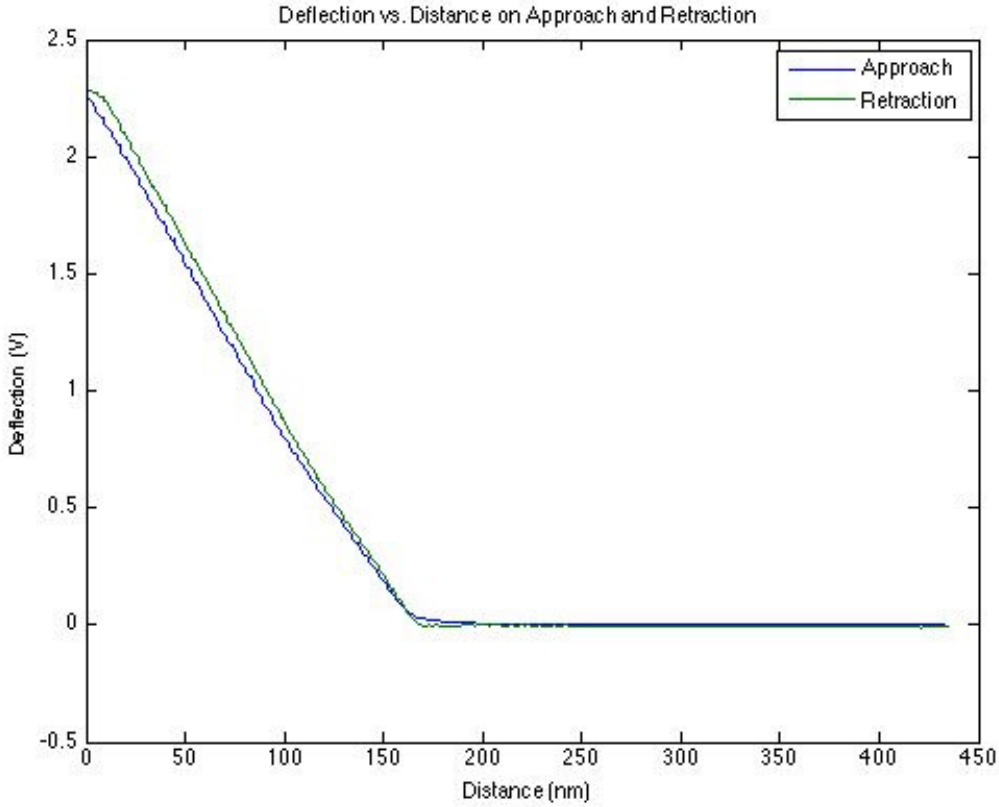
Deflection vs. Distance on Approach and Retraction
Approach
Retraction
Deflection (V)
Distance (nm)
2.5
2
1.5
1
0.5
0
-0.5
0
50
100
150
200
250
300
350
400
450

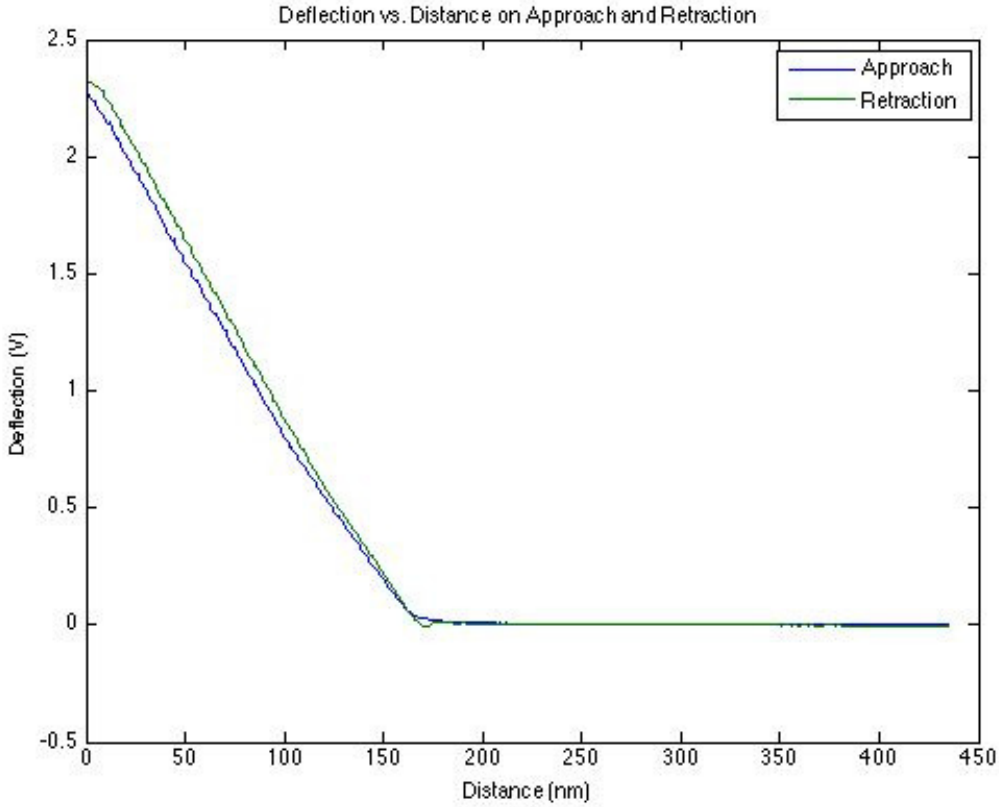
Deflection vs. Distance on Approach and Retraction
Approach
Retraction
Deflection (V)
Distance (nm)
2.5
2
1.5
1
0.5
0
-0.5
0
50
100
150
200
250
300
350
400
450

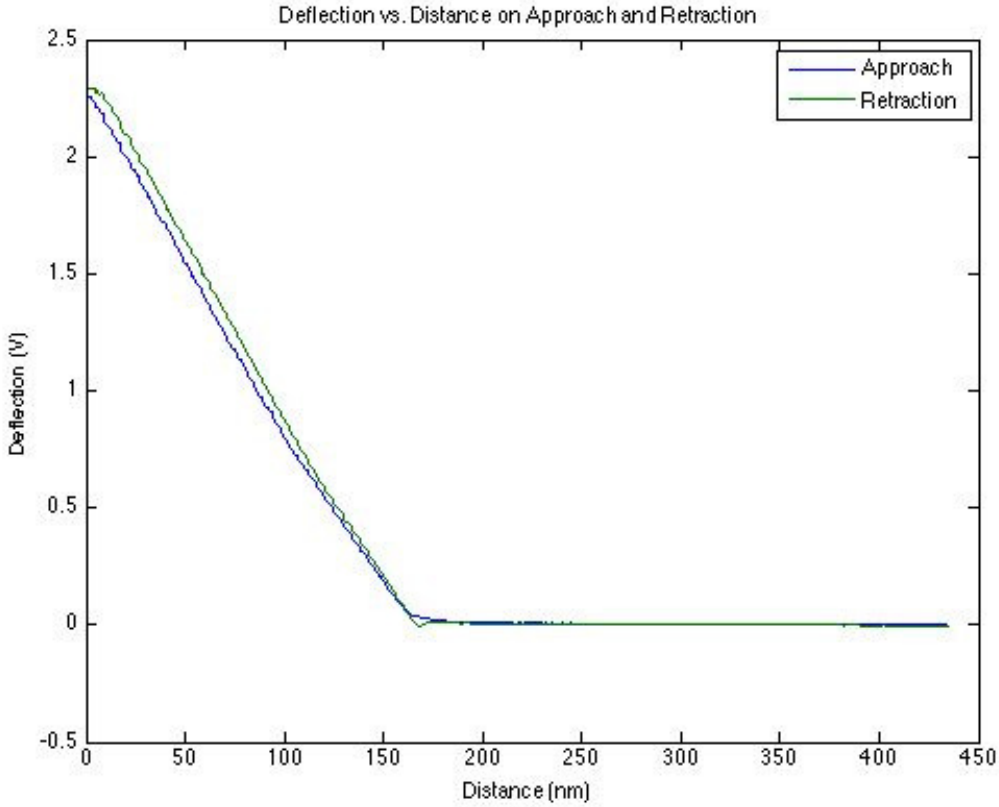
Deflection vs. Distance on Approach and Retraction
Approach
Retraction
Deflection (V)
Distance (nm)
2.5
2
1.5
1
0.5
0
-0.5
0
50
100
150
200
250
300
350
400
450

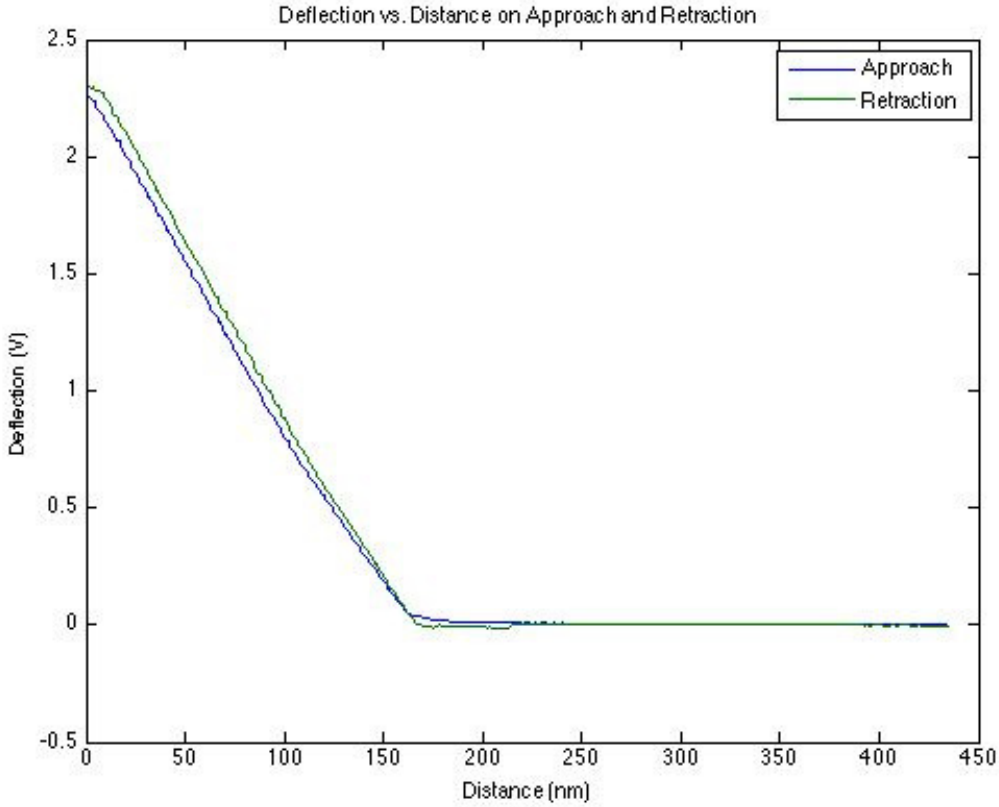
Deflection vs. Distance on Approach and Retraction
Approach
Retraction
Deflection (V)
Distance (nm)
2.5
2
1.5
1
0.5
0
-0.5
0
50
100
150
200
250
300
350
400
450

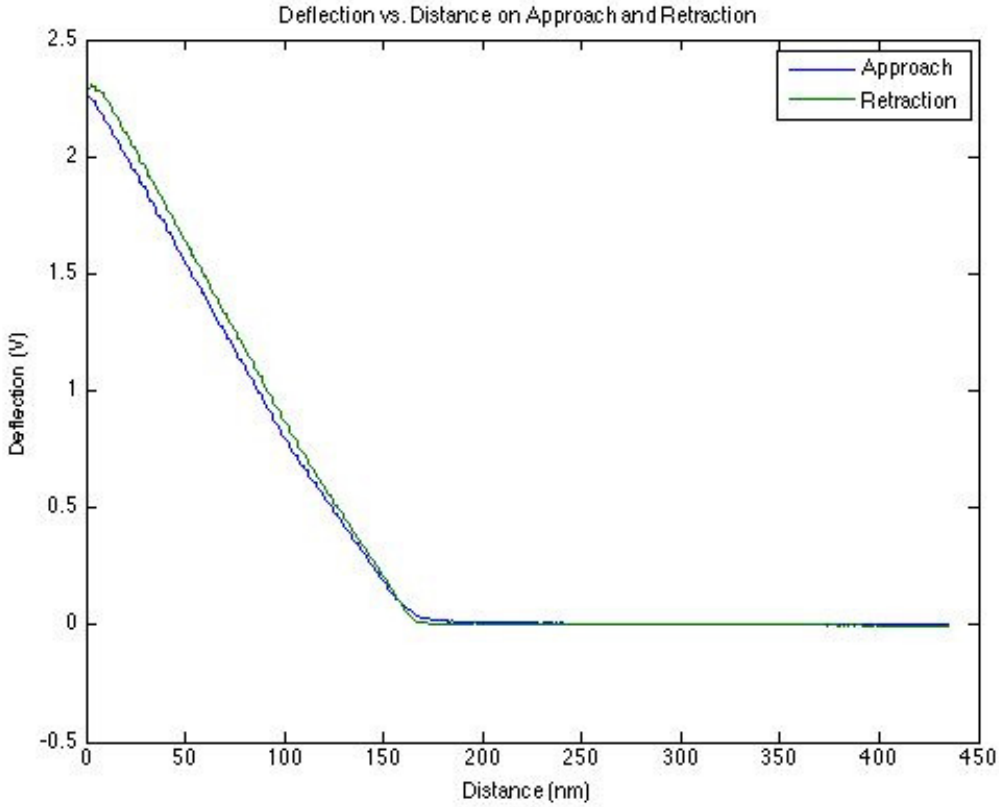
Deflection vs. Distance on Approach and Retraction
Approach
Retraction
Deflection (V)
Distance (nm)
2.5
2
1.5
1
0.5
0
-0.5
0
50
100
150
200
250
300
350
400
450

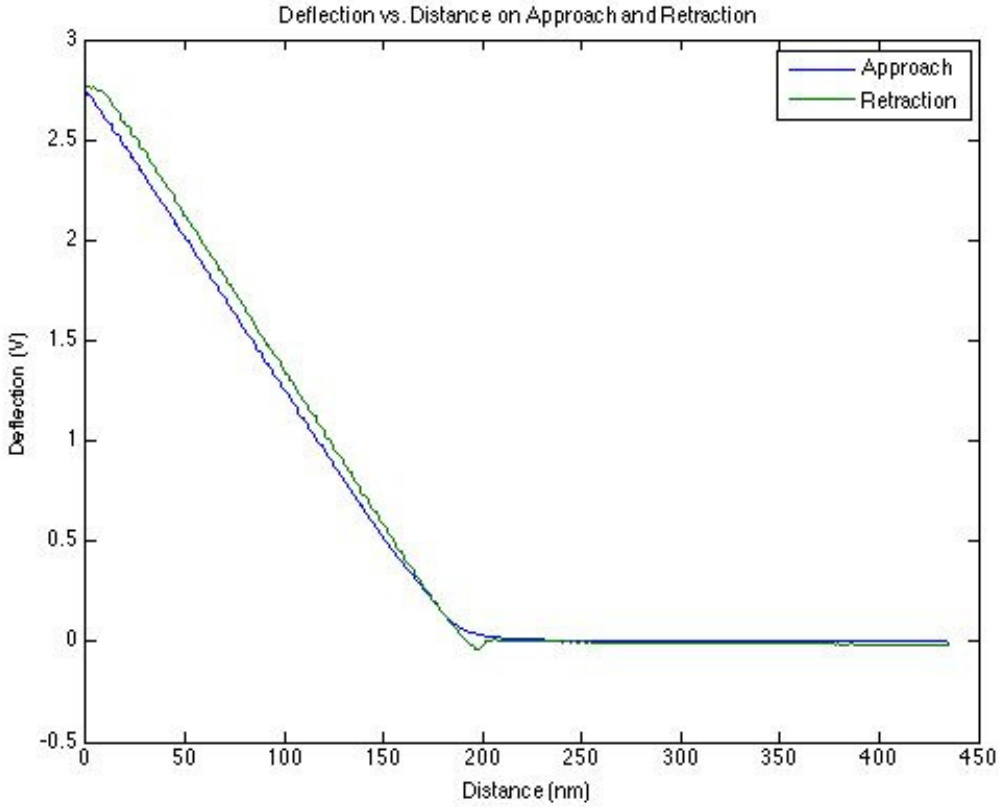
Deflection vs. Distance on Approach and Retraction
Approach
Retraction
Deflection (V)
Distance (nm)
3
2.5
2
1.5
1
0.5
0
-0.5
0
50
100
150
200
250
300
350
400
450

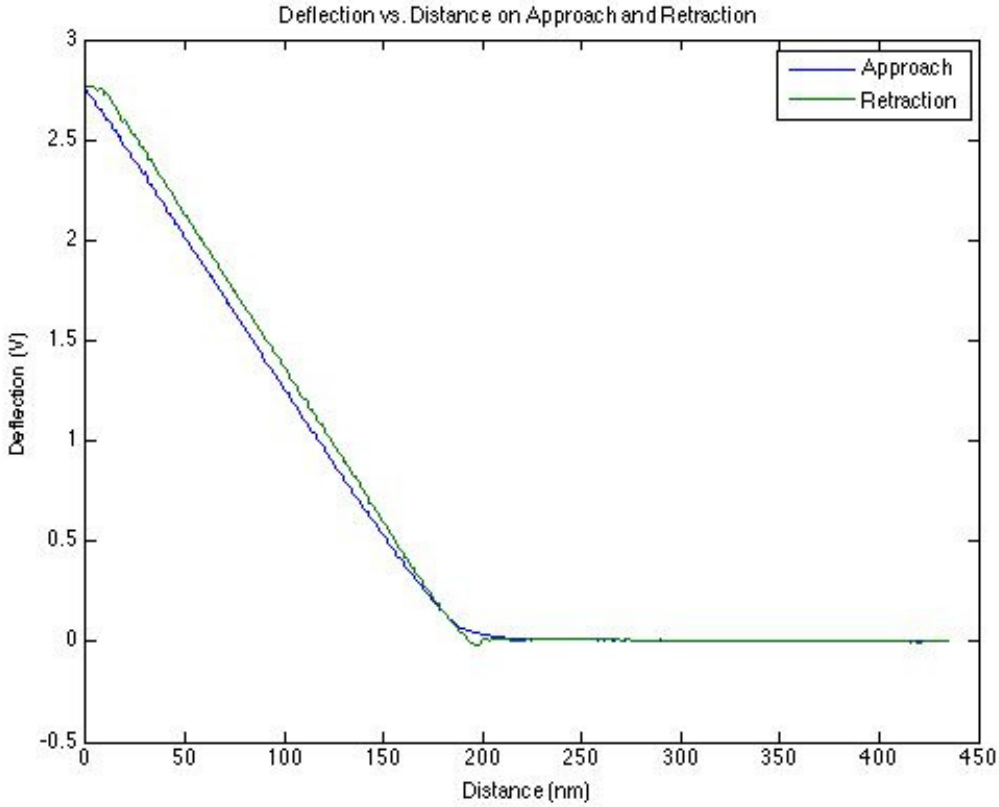
Deflection vs. Distance on Approach and Retraction
Approach
Retraction
Deflection (V)
Distance (nm)
3
2.5
2
1.5
1
0.5
0
-0.5
0
50
100
150
200
250
300
350
400
450

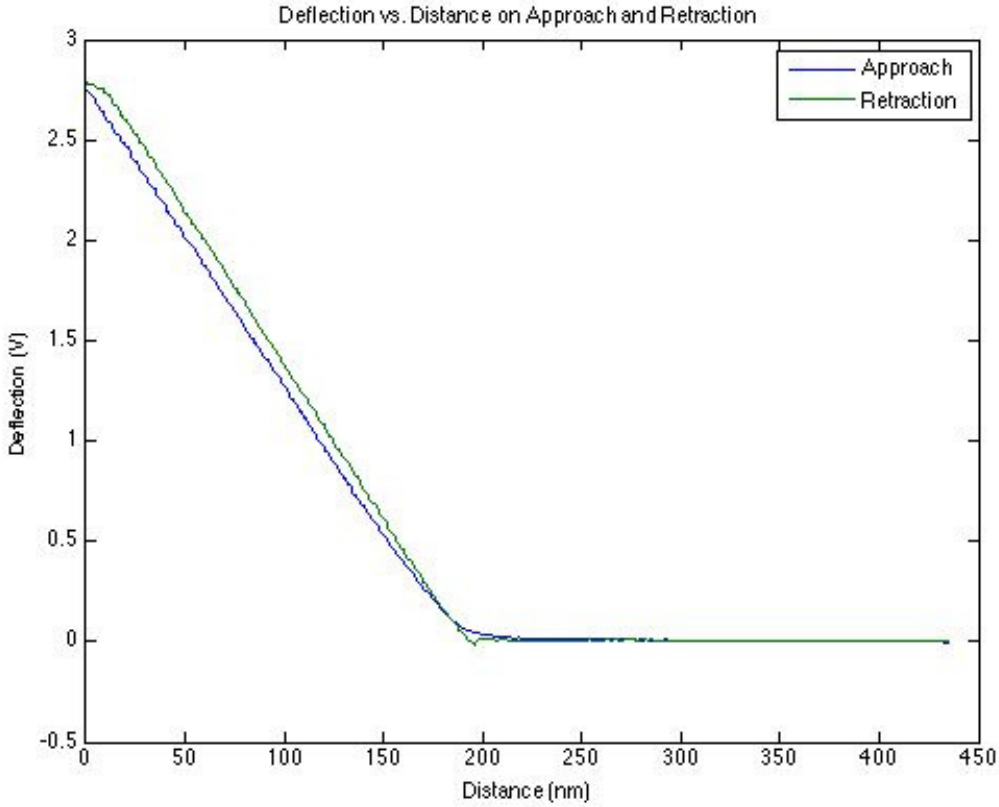
Deflection vs. Distance on Approach and Retraction
Approach
Retraction
Deflection (V)
Distance (nm)
3
2.5
2
1.5
1
0.5
0
-0.5
0
50
100
150
200
250
300
350
400
450

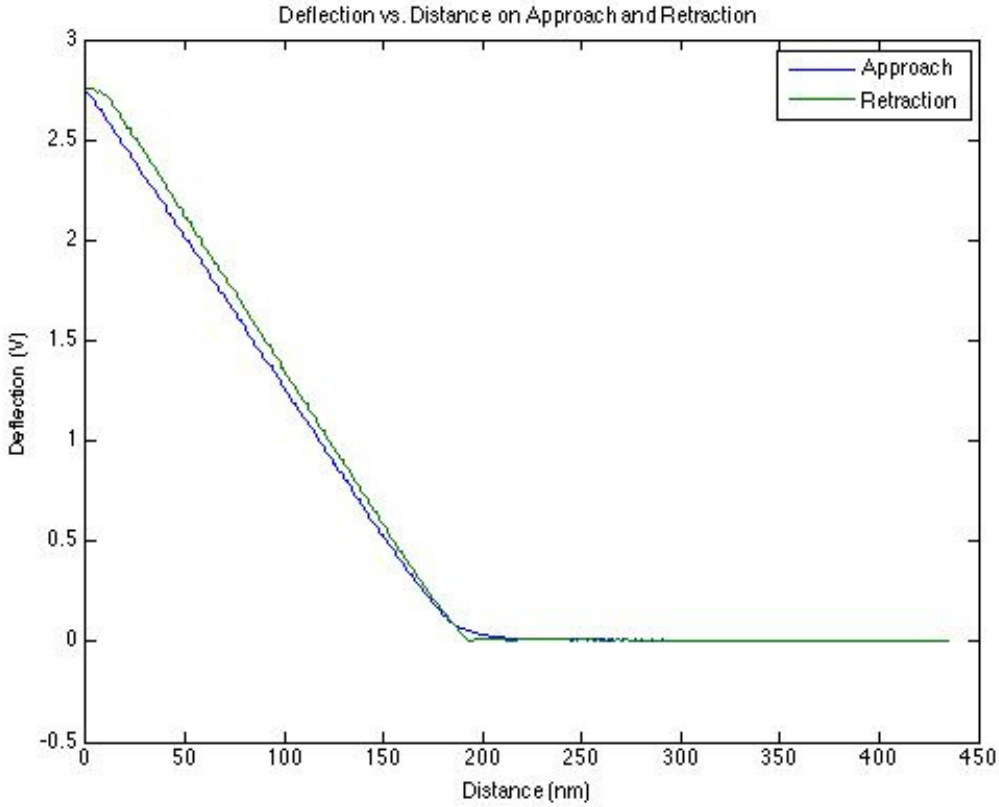
Deflection vs. Distance on Approach and Retraction
Approach
Retraction
Deflection (V)
Distance (nm)
3
2.5
2
1.5
1
0.5
0
-0.5
0
50
100
150
200
250
300
350
400
450

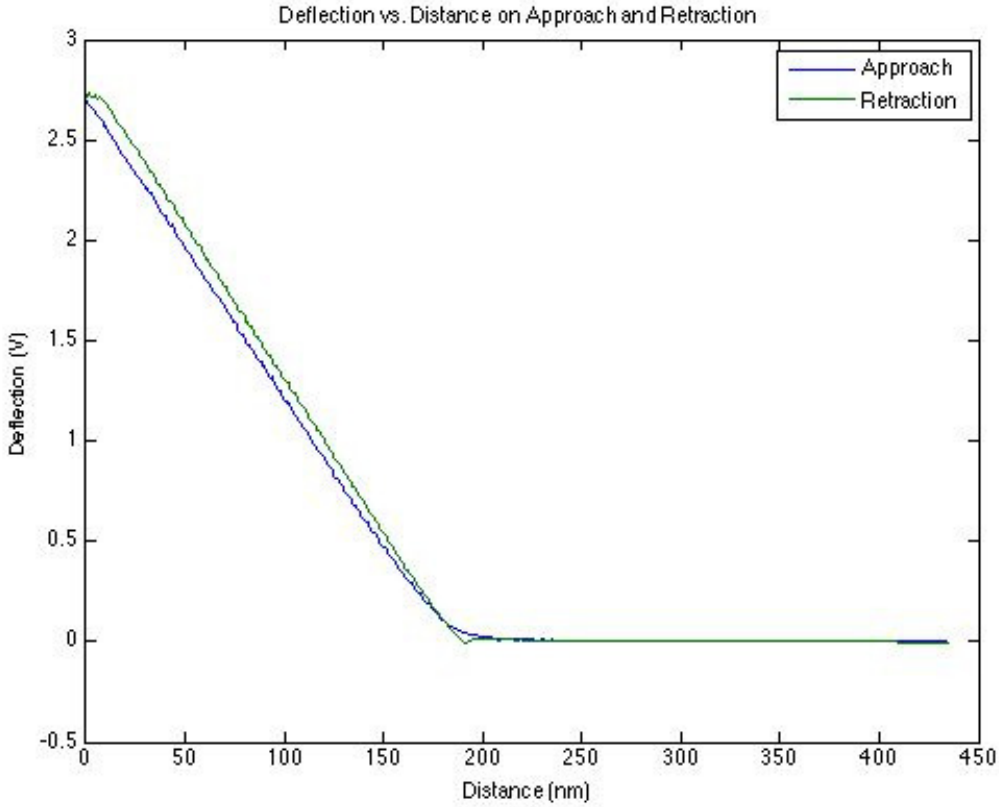
Deflection vs. Distance on Approach and Retraction
Approach
Retraction
Deflection (V)
Distance (nm)
3
2.5
2
1.5
1
0.5
0
-0.5
0
50
100
150
200
250
300
350
400
450

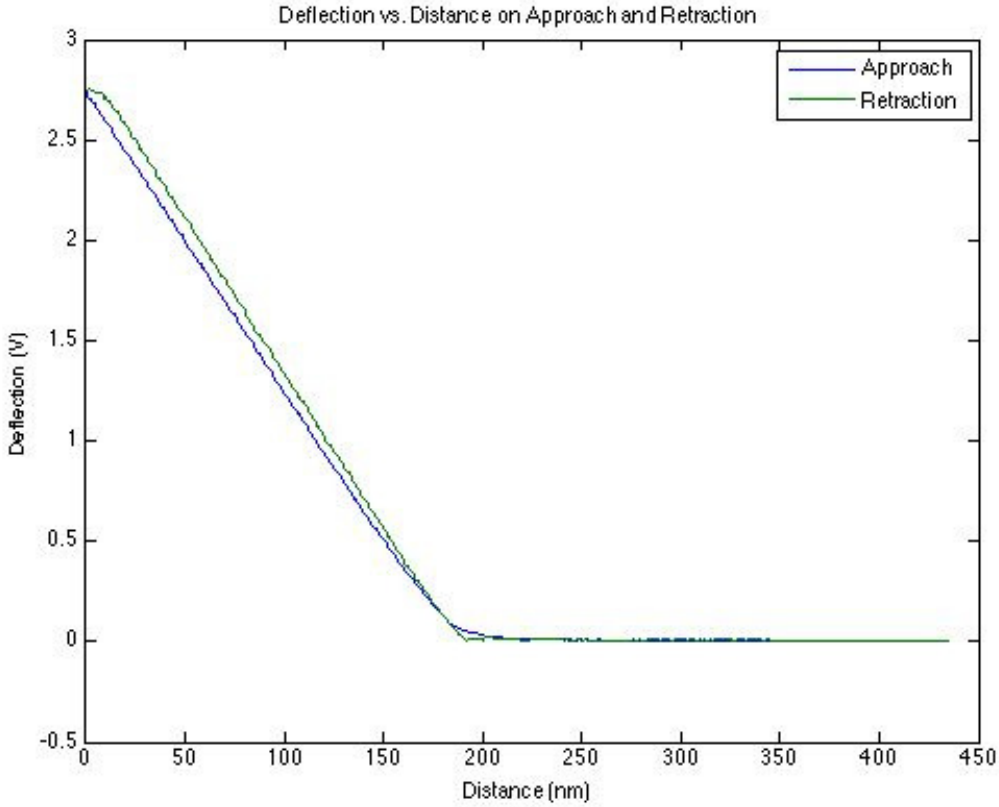
Deflection vs. Distance on Approach and Retraction
Approach
Retraction
Deflection (V)
Distance (nm)
3
2.5
2
1.5
1
0.5
0
-0.5
0
50
100
150
200
250
300
350
400
450

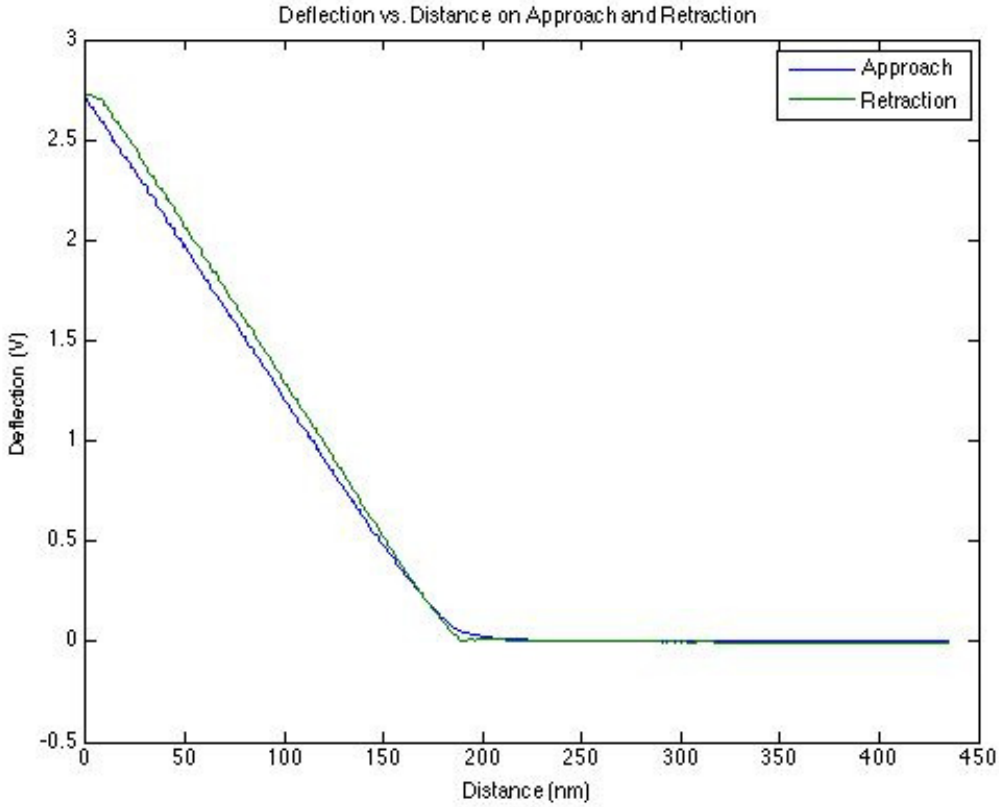
Deflection vs. Distance on Approach and Retraction
Approach
Retraction
Deflection (V)
Distance (nm)
3
2.5
2
1.5
1
0.5
0
-0.5
0
50
100
150
200
250
300
350
400
450

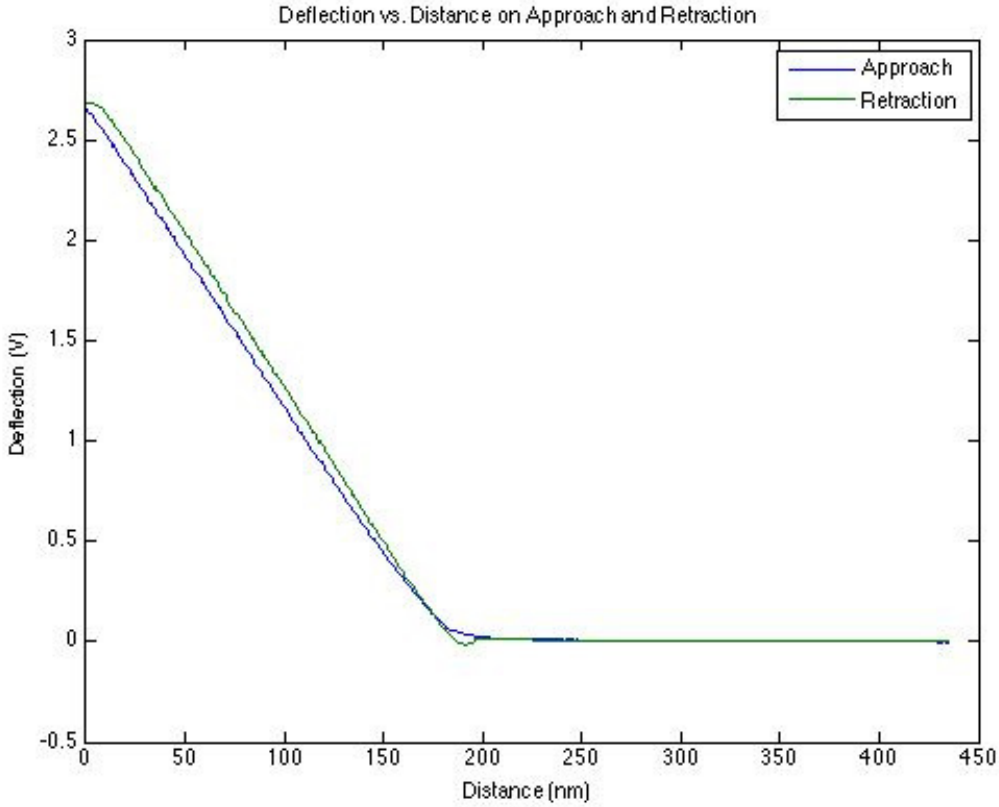
Deflection vs. Distance on Approach and Retraction
Approach
Retraction
Deflection (V)
Distance (nm)
3
2.5
2
1.5
1
0.5
0
-0.5
0
50
100
150
200
250
300
350
400
450

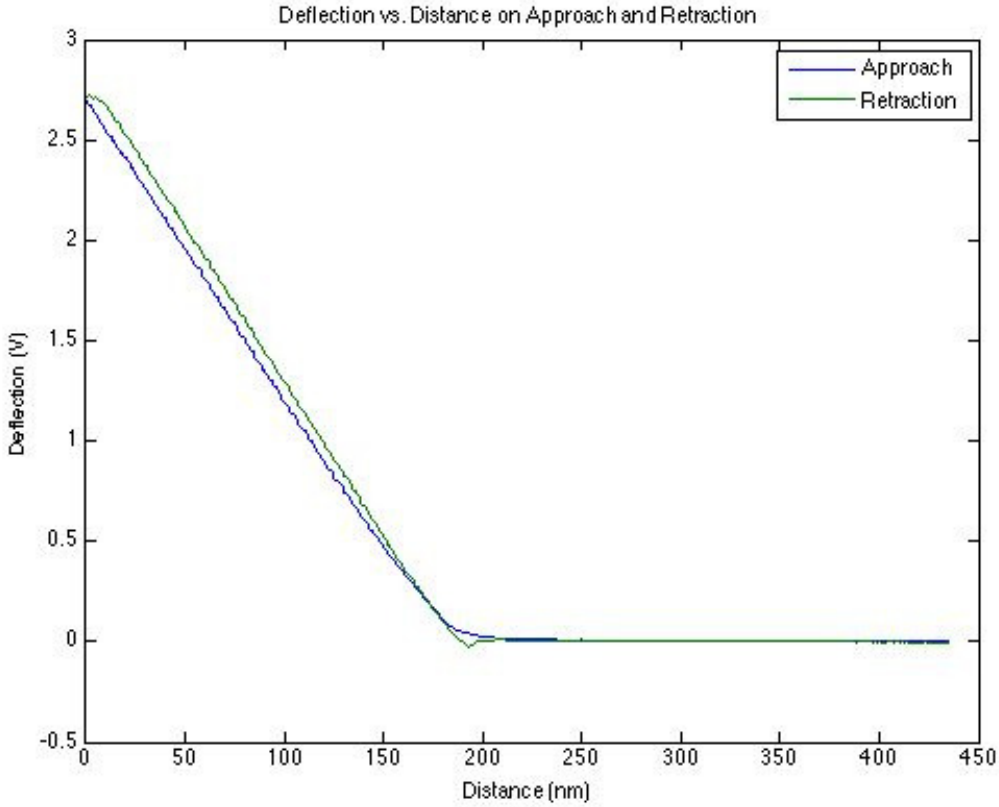
Deflection vs. Distance on Approach and Retraction
Approach
Retraction
Deflection (V)
Distance (nm)
3
2.5
2
1.5
1
0.5
0
-0.5
0
50
100
150
200
250
300
350
400
450

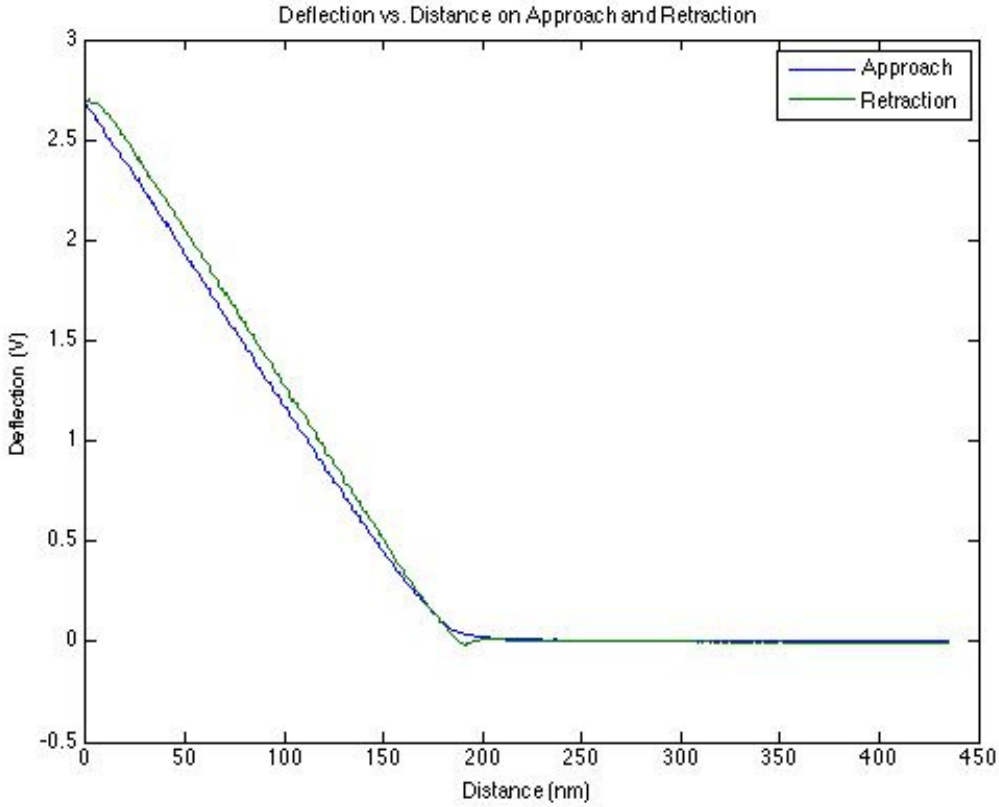
Deflection vs. Distance on Approach and Retraction
Approach
Retraction
Deflection (V)
Distance (nm)
3
2.5
2
1.5
1
0.5
0
-0.5
0
50
100
150
200
250
300
350
400
450

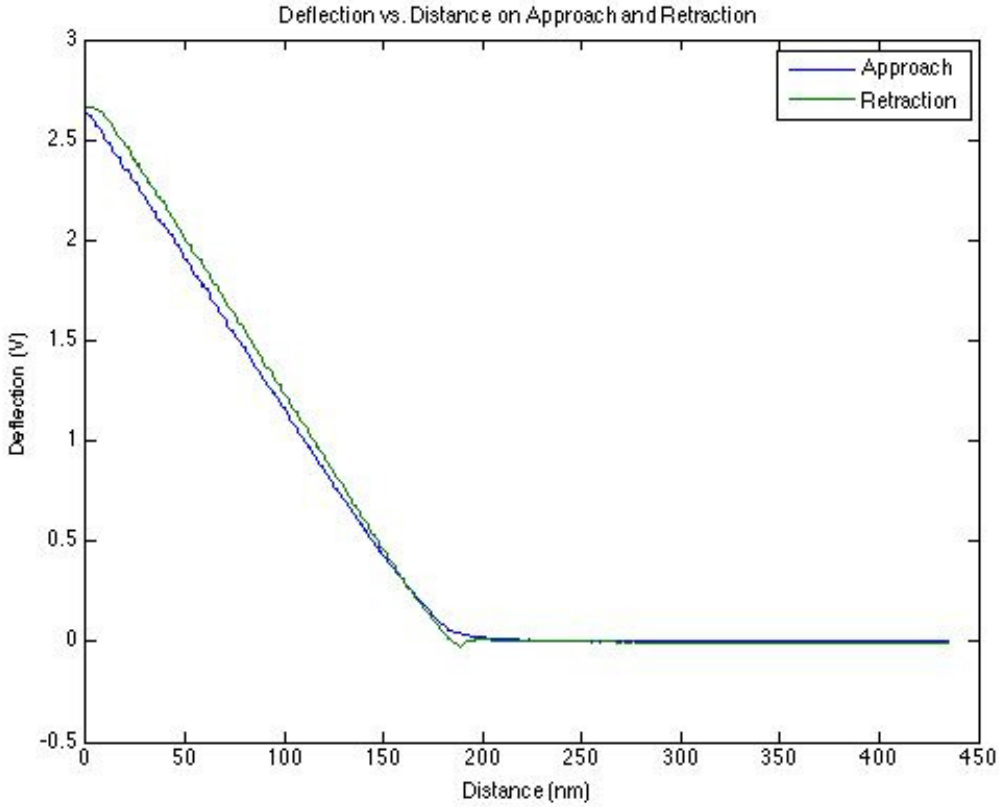
Deflection vs. Distance on Approach and Retraction
Approach
Retraction
Deflection (V)
Distance (nm)
3
2.5
2
1.5
1
0.5
0
-0.5
0
50
100
150
200
250
300
350
400
450

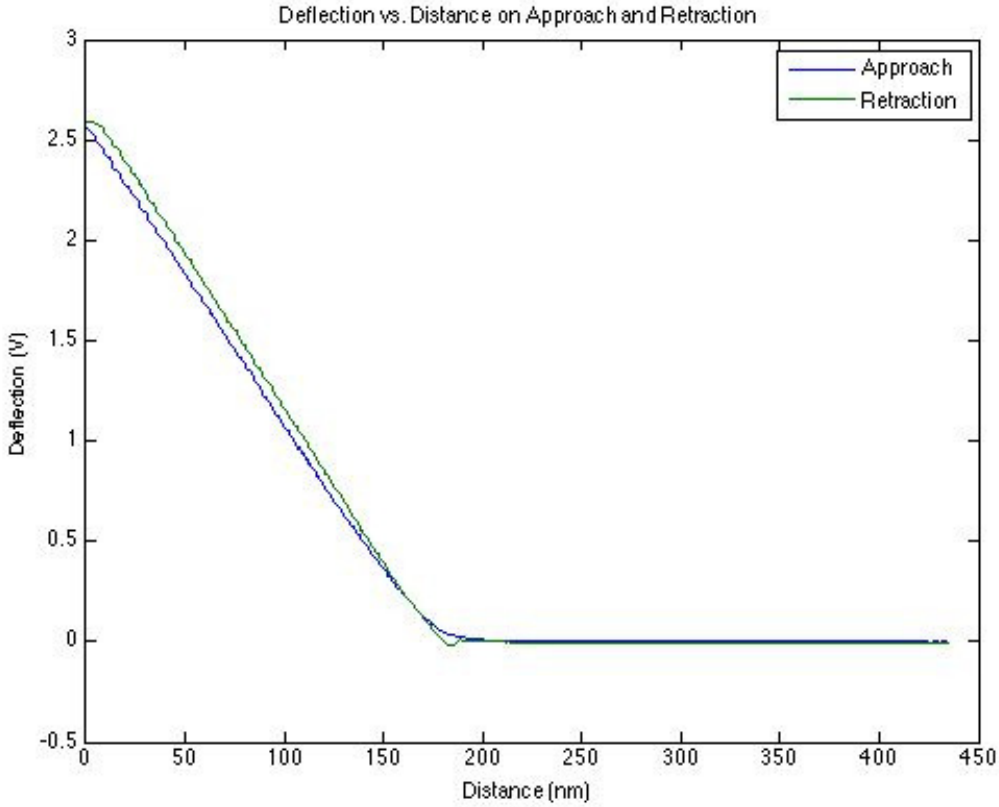
Deflection vs. Distance on Approach and Retraction
Approach
Retraction
Deflection (V)
Distance (nm)
3
2.5
2
1.5
1
0.5
0
-0.5
0
50
100
150
200
250
300
350
400
450

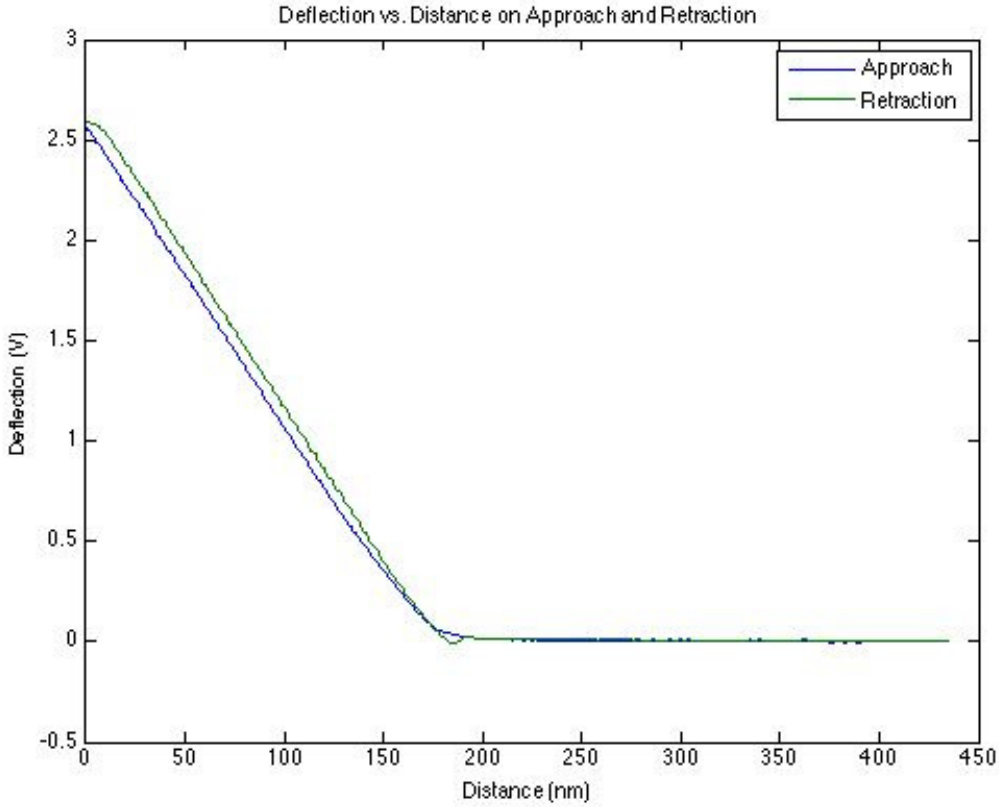
Deflection vs. Distance on Approach and Retraction
Approach
Retraction
Deflection (V)
Distance (nm)
3
2.5
2
1.5
1
0.5
0
-0.5
0
50
100
150
200
250
300
350
400
450

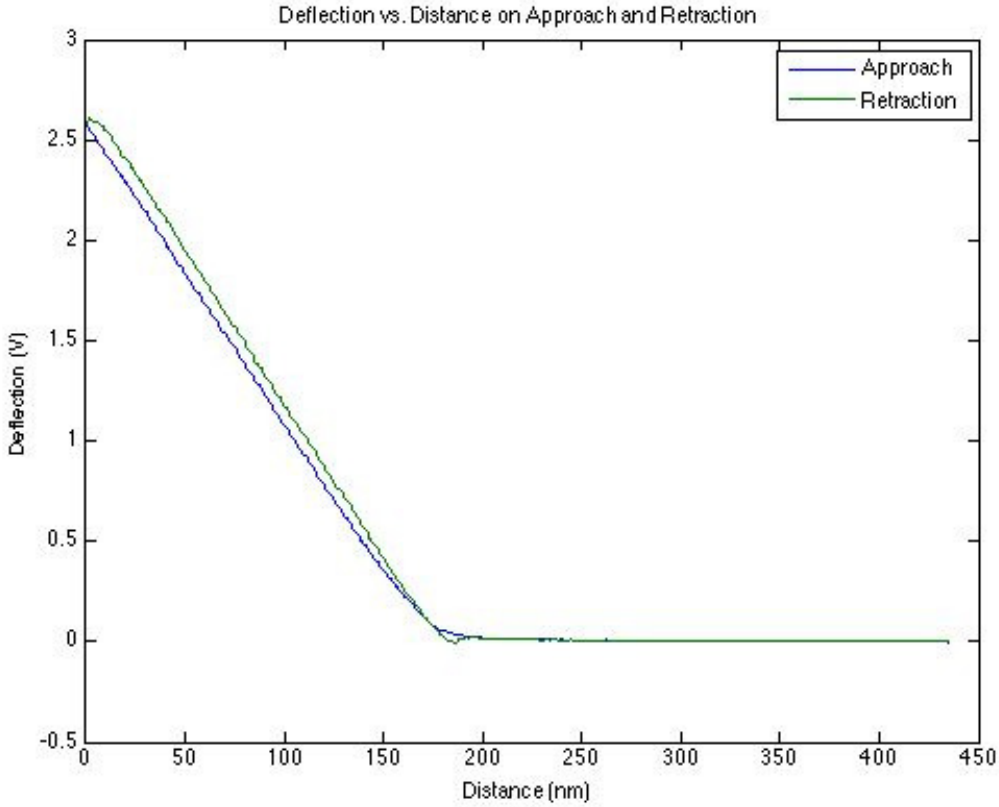
Deflection vs. Distance on Approach and Retraction
Approach
Retraction
Deflection (V)
Distance (nm)
3
2.5
2
1.5
1
0.5
0
-0.5
0
50
100
150
200
250
300
350
400
450

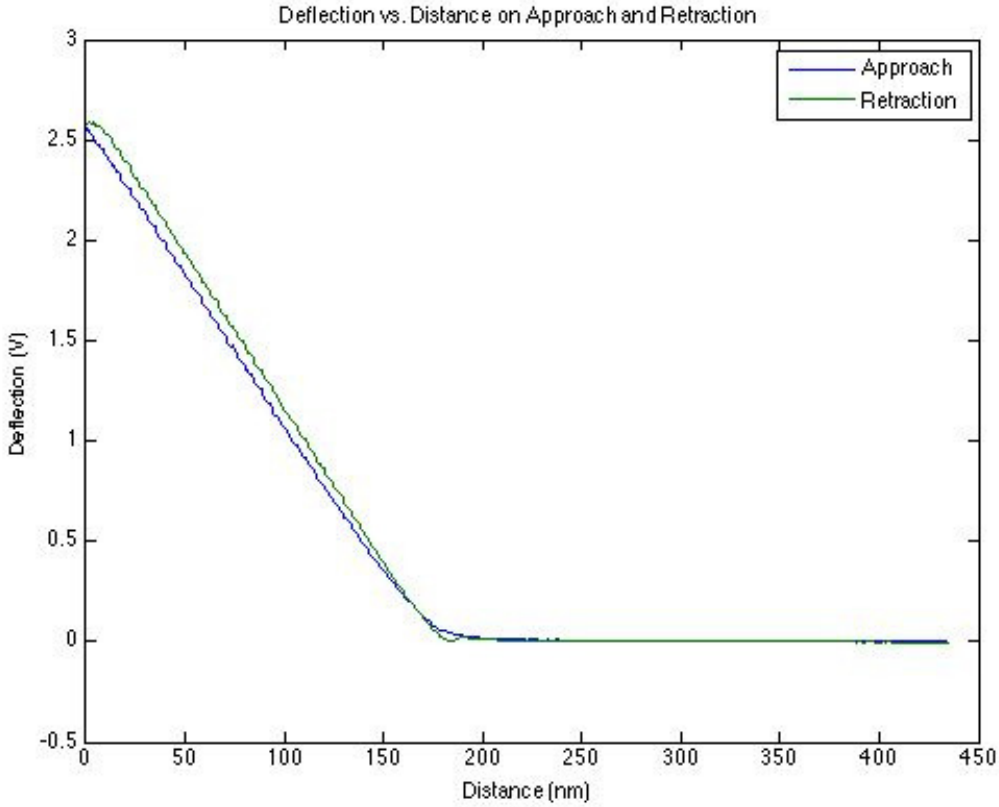
Deflection vs. Distance on Approach and Retraction
Approach
Retraction
Deflection (V)
Distance (nm)
3
2.5
2
1.5
1
0.5
0
-0.5
0
50
100
150
200
250
300
350
400
450

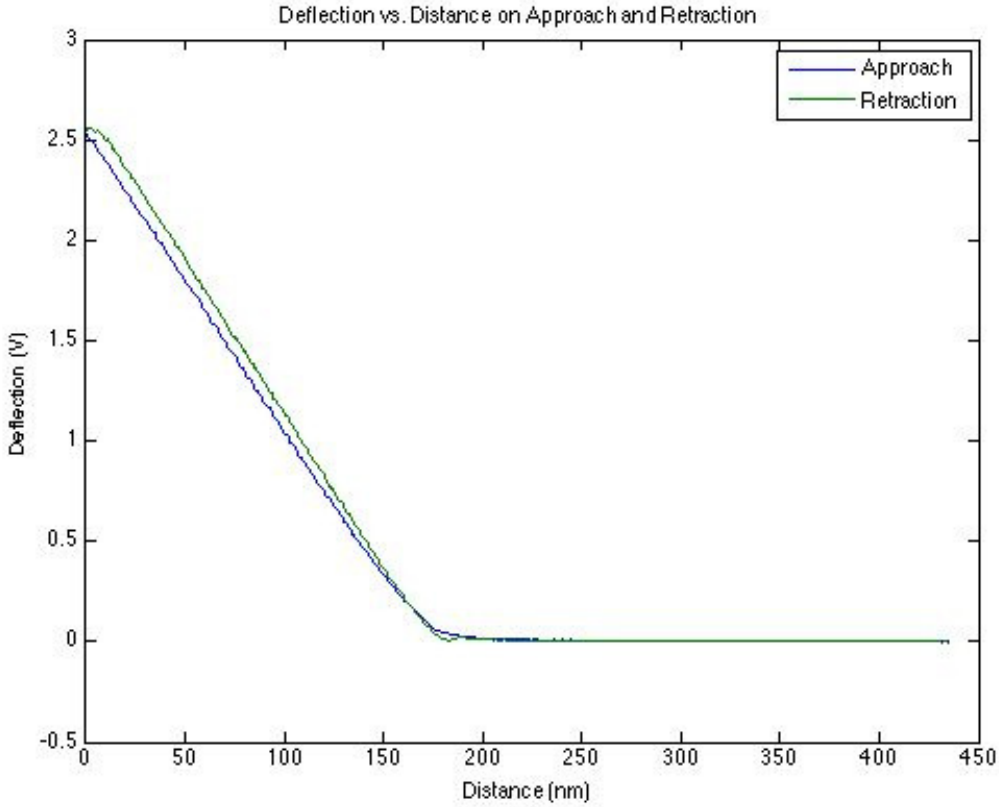
Deflection vs. Distance on Approach and Retraction
Approach
Retraction
Deflection (V)
Distance (nm)
3
2.5
2
1.5
1
0.5
0
-0.5
0
50
100
150
200
250
300
350
400
450

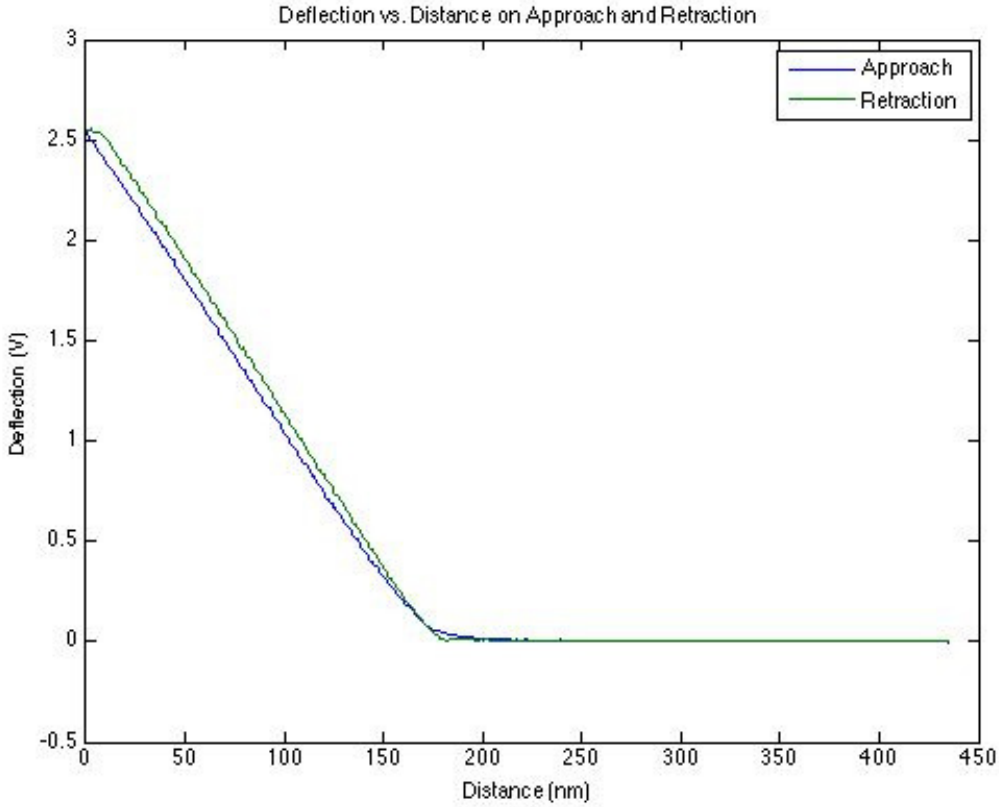
Deflection vs. Distance on Approach and Retraction
Approach
Retraction
Deflection (V)
Distance (nm)
3
2.5
2
1.5
1
0.5
0
-0.5
0
50
100
150
200
250
300
350
400
450

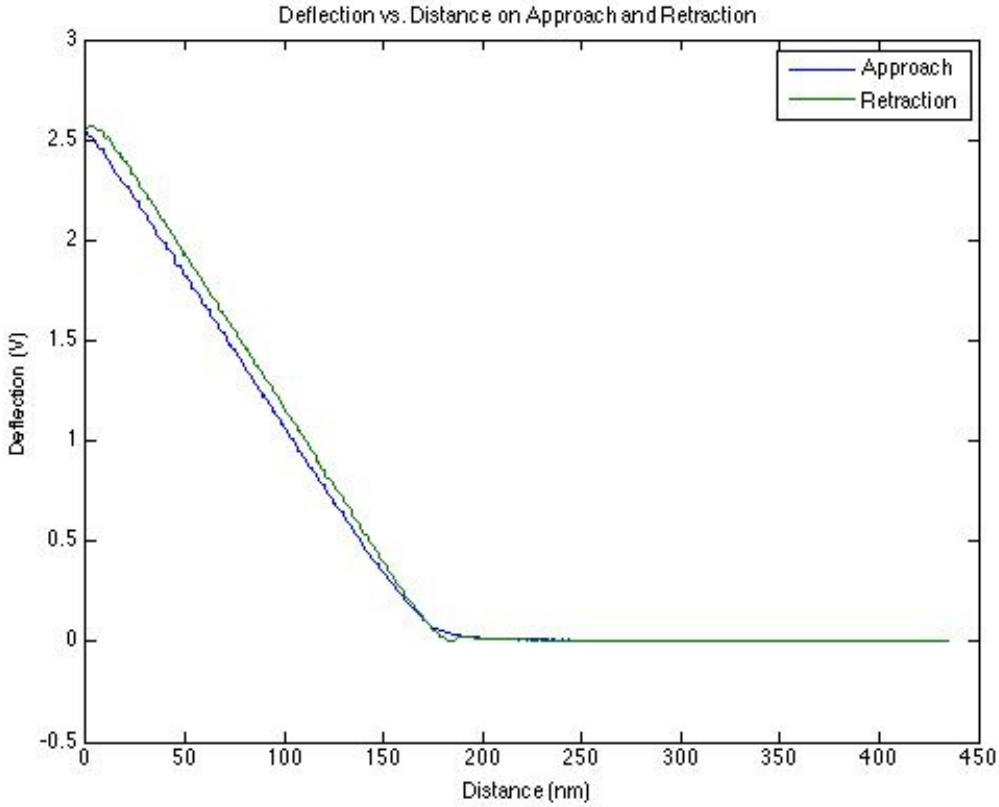
Deflection vs. Distance on Approach and Retraction
Approach
Retraction
Deflection (V)
Distance (nm)
3
2.5
2
1.5
1
0.5
0
-0.5
0
50
100
150
200
250
300
350
400
450

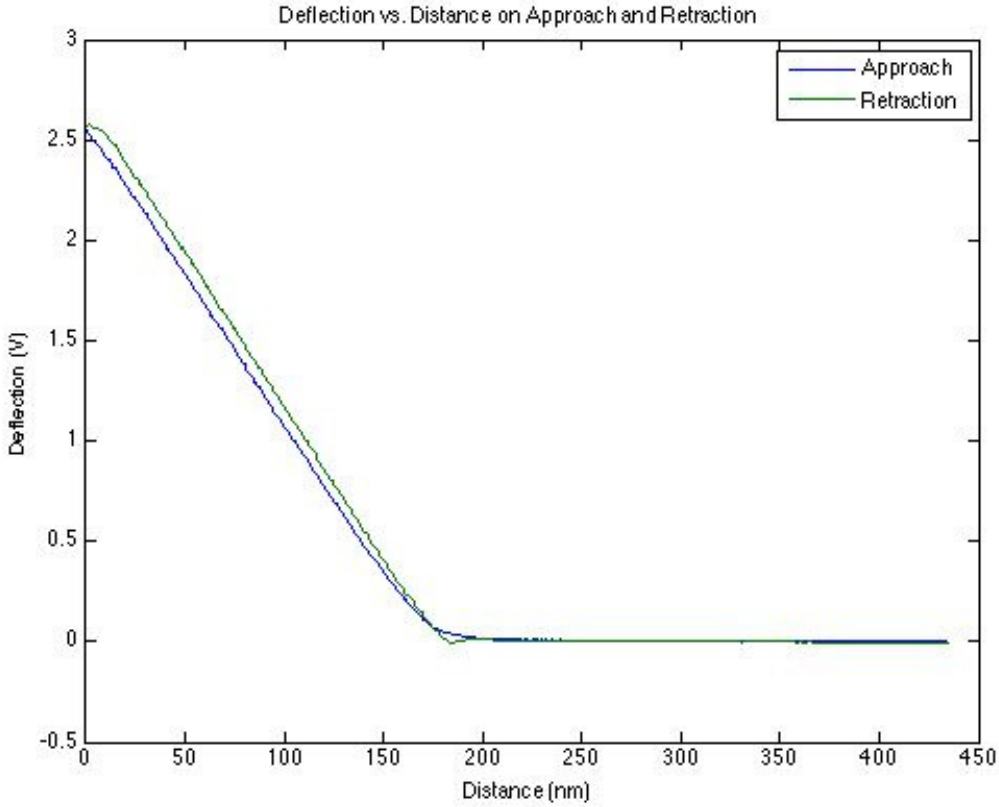
Deflection vs. Distance on Approach and Retraction
Approach
Retraction
Deflection (V)
Distance (nm)
3
2.5
2
1.5
1
0.5
0
-0.5
0
50
100
150
200
250
300
350
400
450

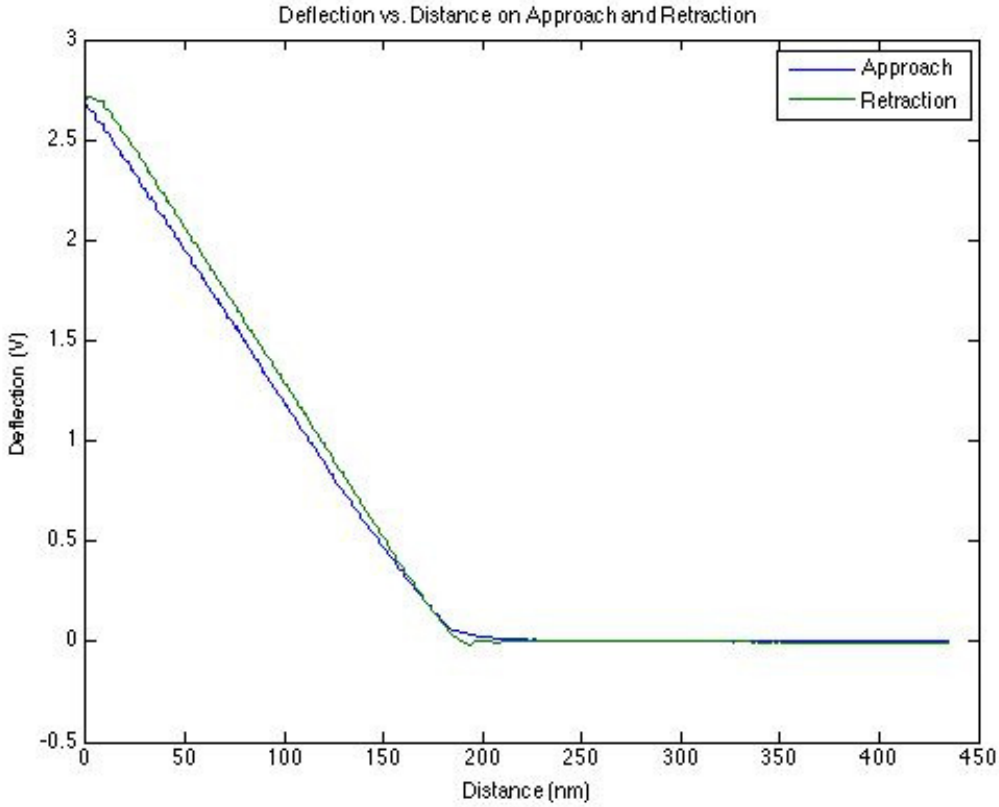
Deflection vs. Distance on Approach and Retraction
Approach
Retraction
Deflection (V)
Distance (nm)
3
2.5
2
1.5
1
0.5
0
-0.5
0
50
100
150
200
250
300
350
400
450

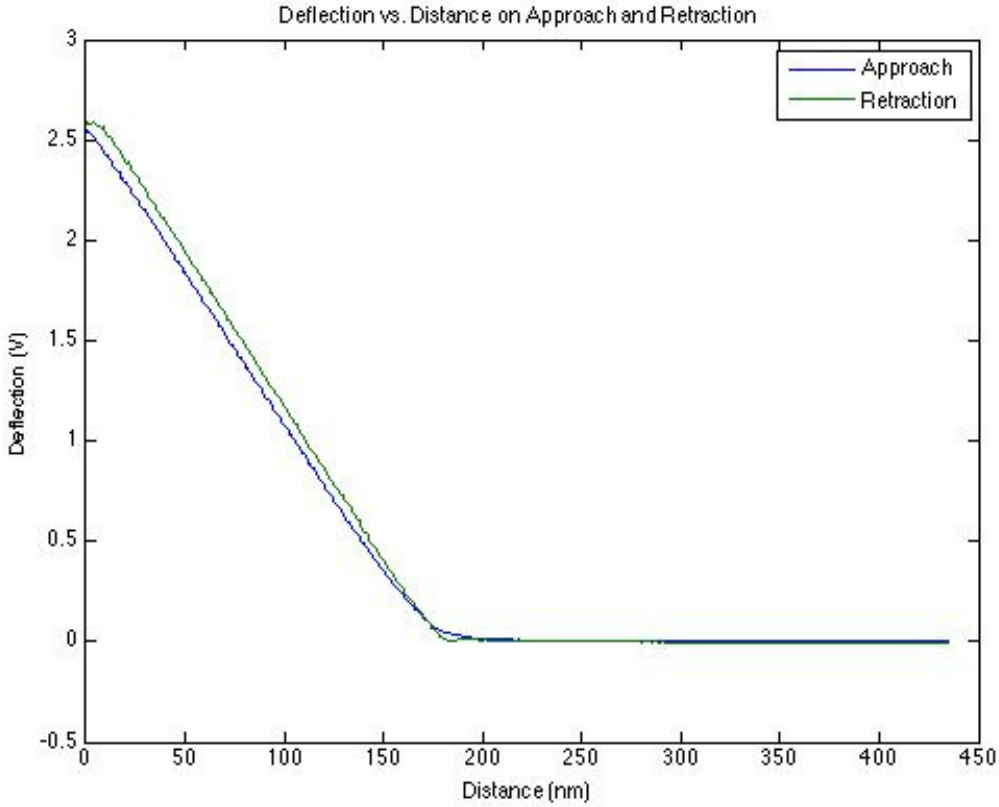
Deflection vs. Distance on Approach and Retraction
Approach
Retraction
Deflection (V)
Distance (nm)
3
2.5
2
1.5
1
0.5
0
-0.5
0
50
100
150
200
250
300
350
400
450

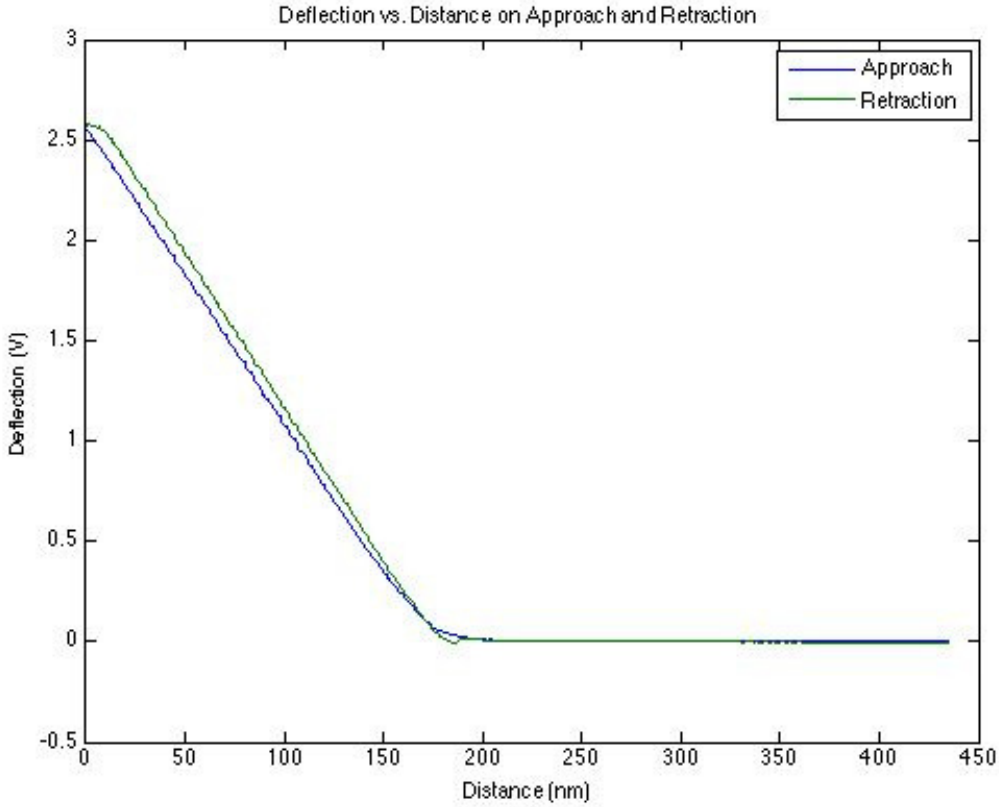
Deflection vs. Distance on Approach and Retraction
Approach
Retraction
Deflection (V)
Distance (nm)
3
2.5
2
1.5
1
0.5
0
-0.5
0
50
100
150
200
250
300
350
400
450

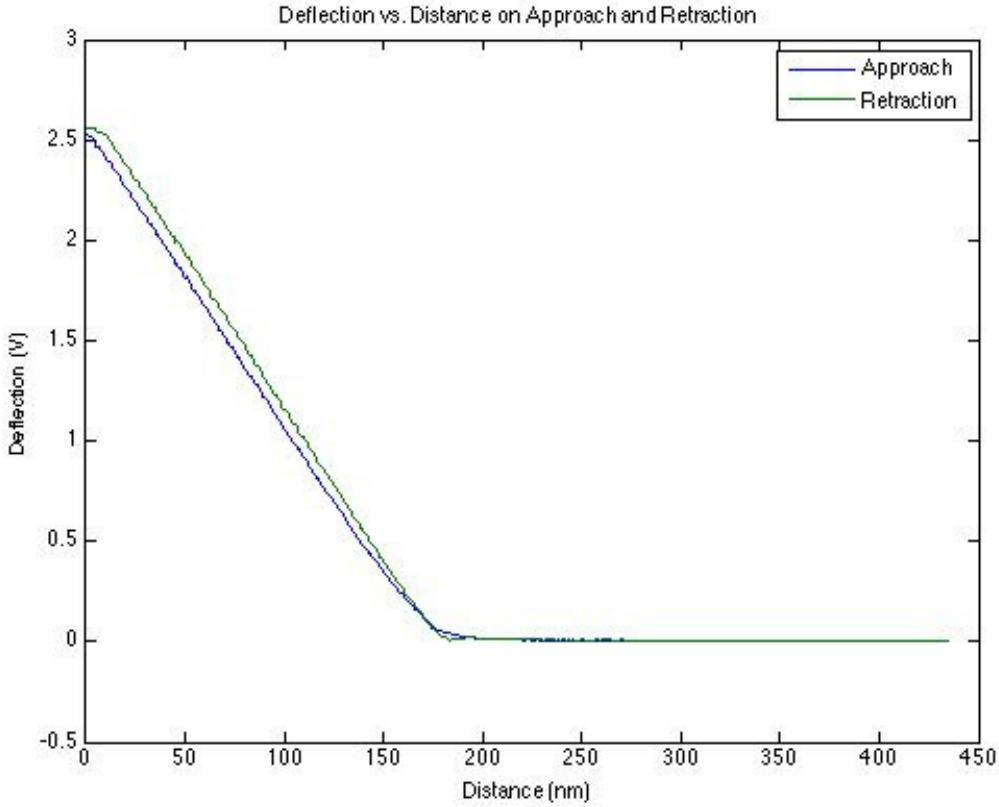
Deflection vs. Distance on Approach and Retraction
Approach
Retraction
Deflection (V)
Distance (nm)
3
2.5
2
1.5
1
0.5
0
-0.5
0
50
100
150
200
250
300
350
400
450

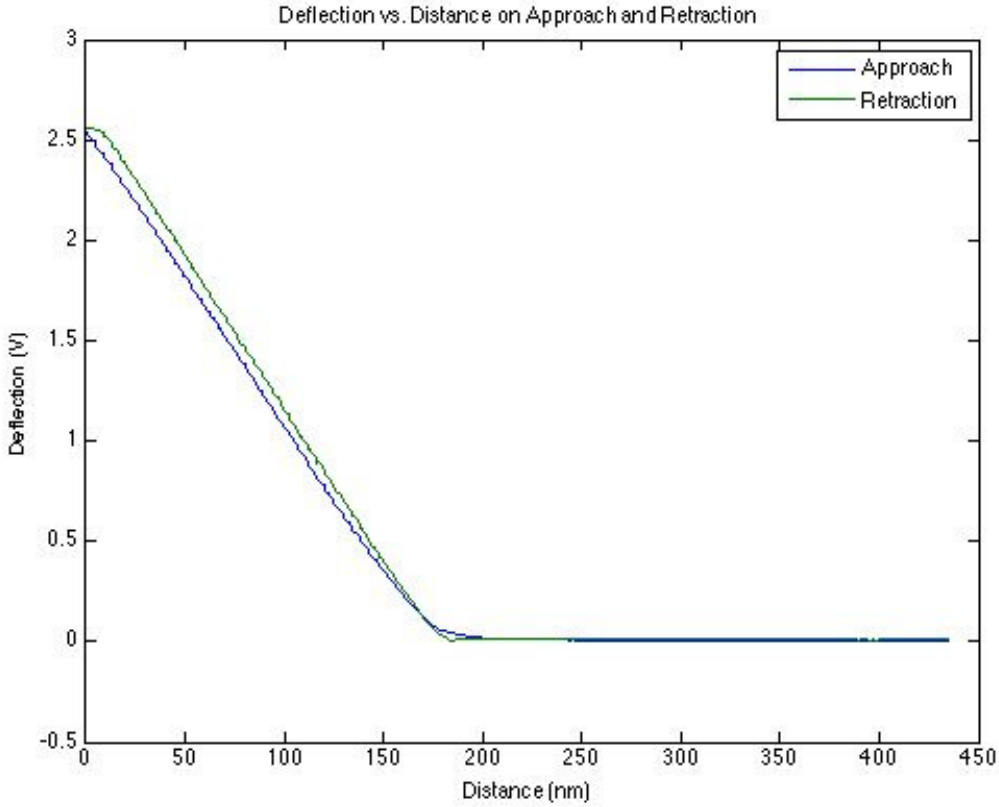
Deflection vs. Distance on Approach and Retraction
Approach
Retraction
Deflection (V)
Distance (nm)
3
2.5
2
1.5
1
0.5
0
-0.5
0
50
100
150
200
250
300
350
400
450

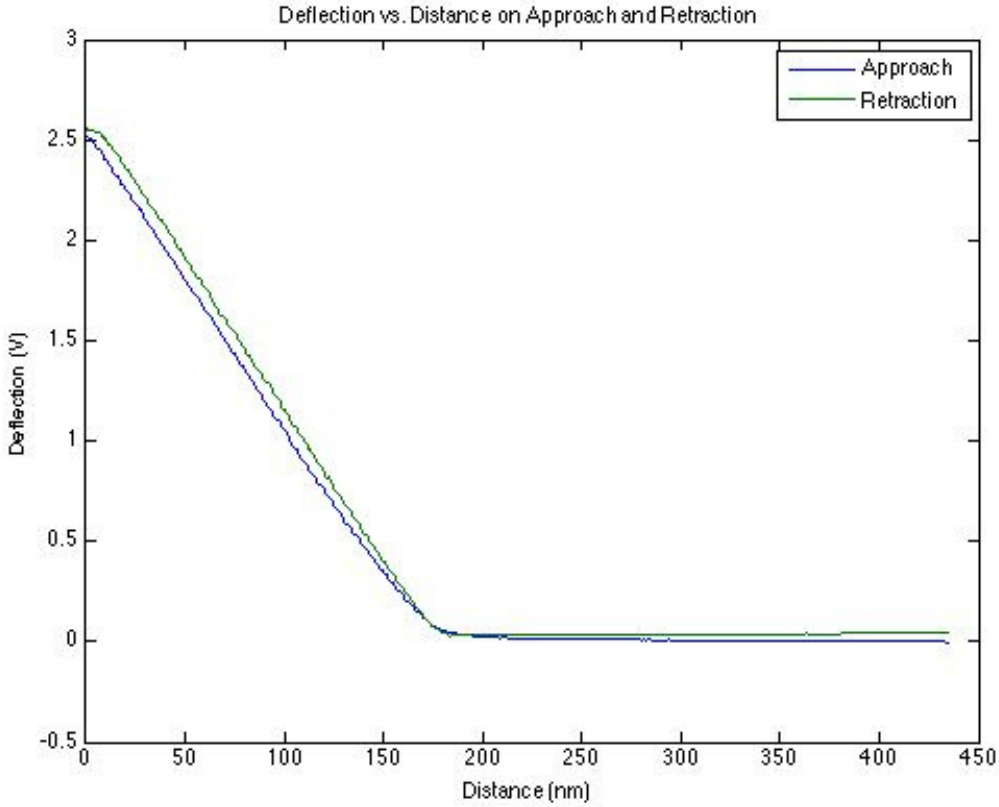
Deflection vs. Distance on Approach and Retraction
Approach
Retraction
Deflection (V)
Distance (nm)
3
2.5
2
1.5
1
0.5
0
-0.5
0
50
100
150
200
250
300
350
400
450

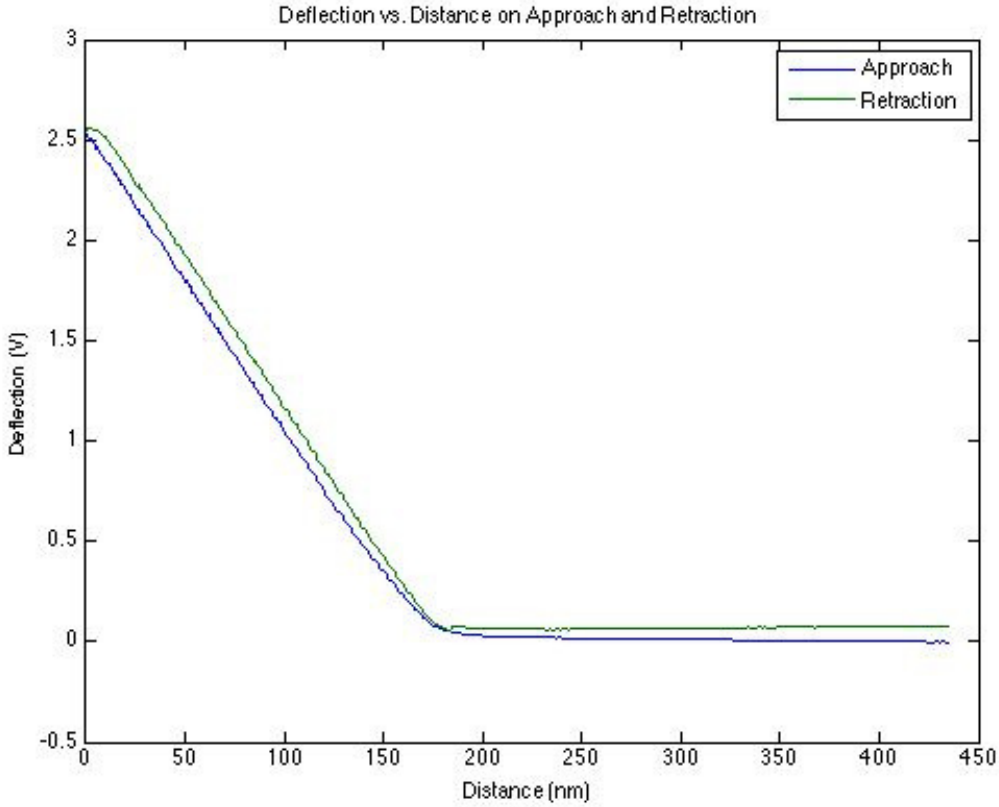
Deflection vs. Distance on Approach and Retraction
Approach
Retraction
Deflection (V)
Distance (nm)
3
2.5
2
1.5
1
0.5
0
-0.5
0
50
100
150
200
250
300
350
400
450

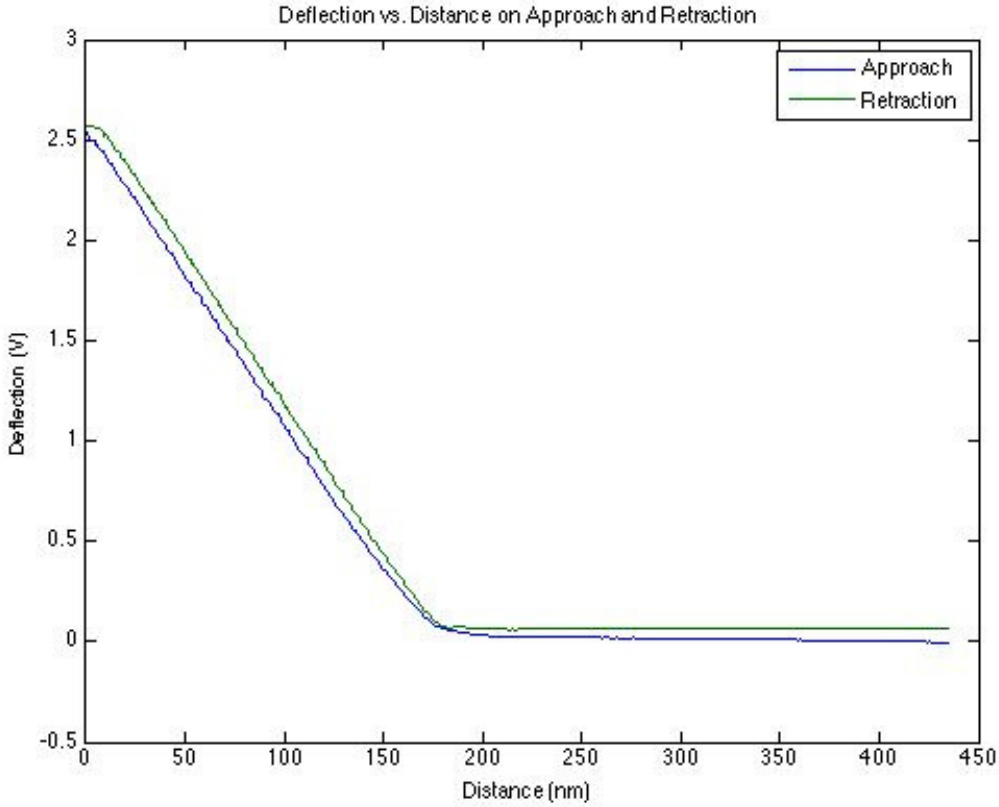
Deflection vs. Distance on Approach and Retraction
Approach
Retraction
Deflection (V)
Distance (nm)
3
2.5
2
1.5
1
0.5
0
-0.5
0
50
100
150
200
250
300
350
400
450

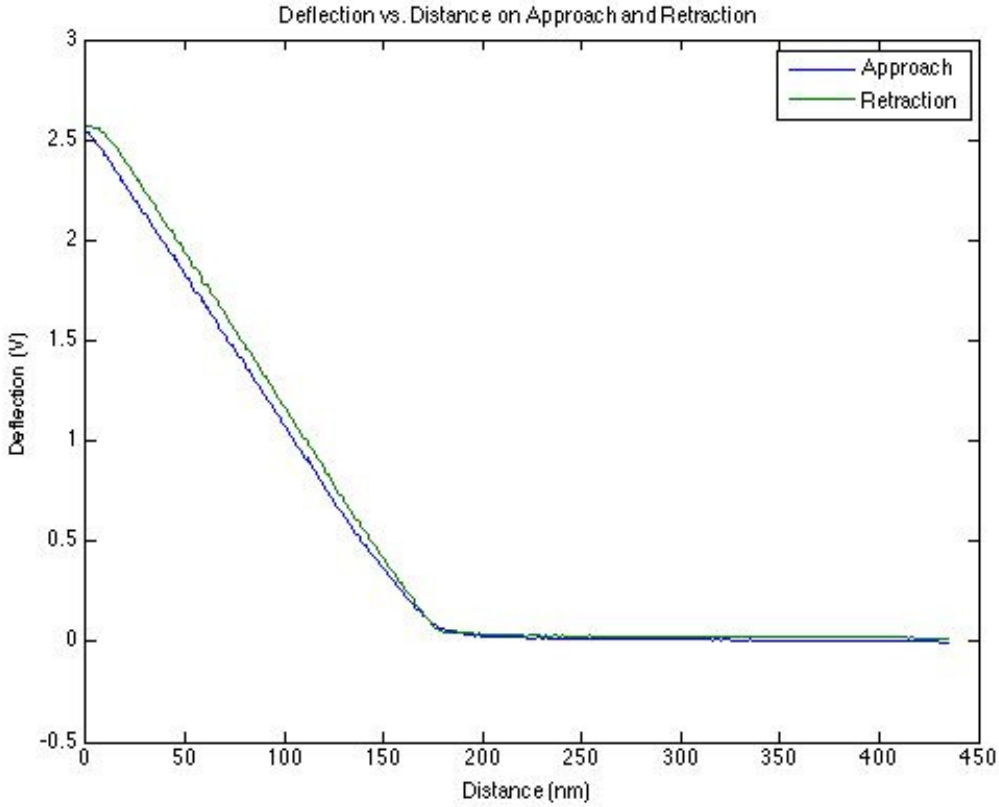
Deflection vs. Distance on Approach and Retraction
Approach
Retraction
Deflection (V)
Distance (nm)
3
2.5
2
1.5
1
0.5
0
-0.5
0
50
100
150
200
250
300
350
400
450

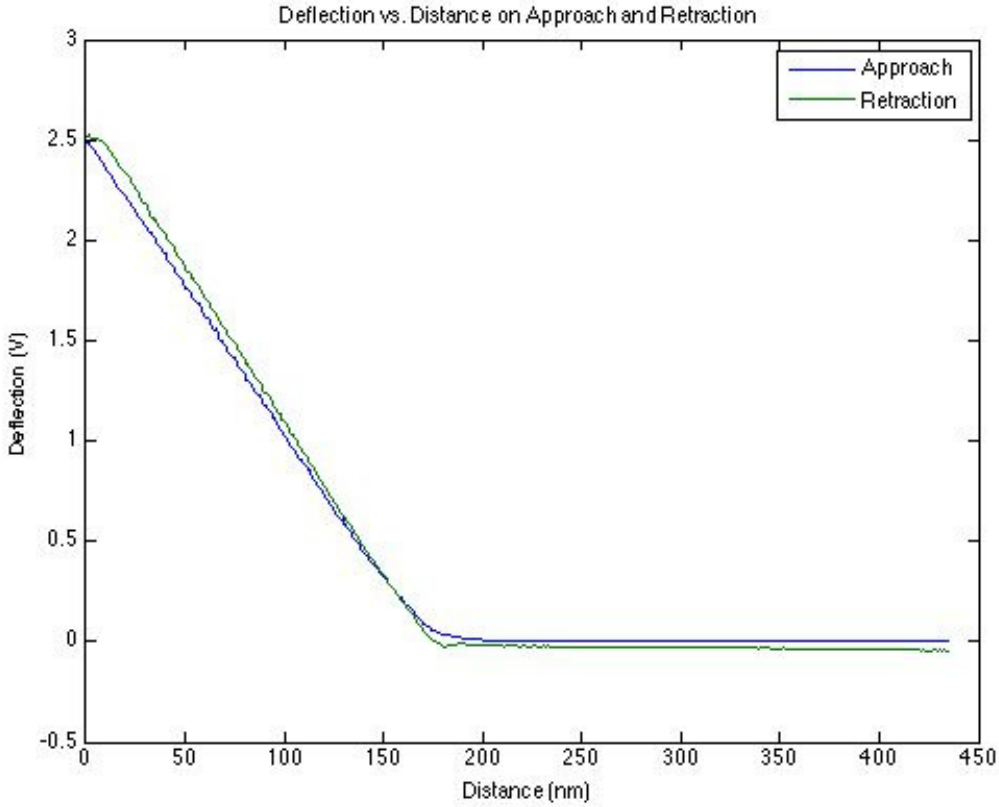
Deflection vs. Distance on Approach and Retraction
Approach
Retraction
Deflection (V)
Distance (nm)
3
2.5
2
1.5
1
0.5
0
-0.5
0
50
100
150
200
250
300
350
400
450

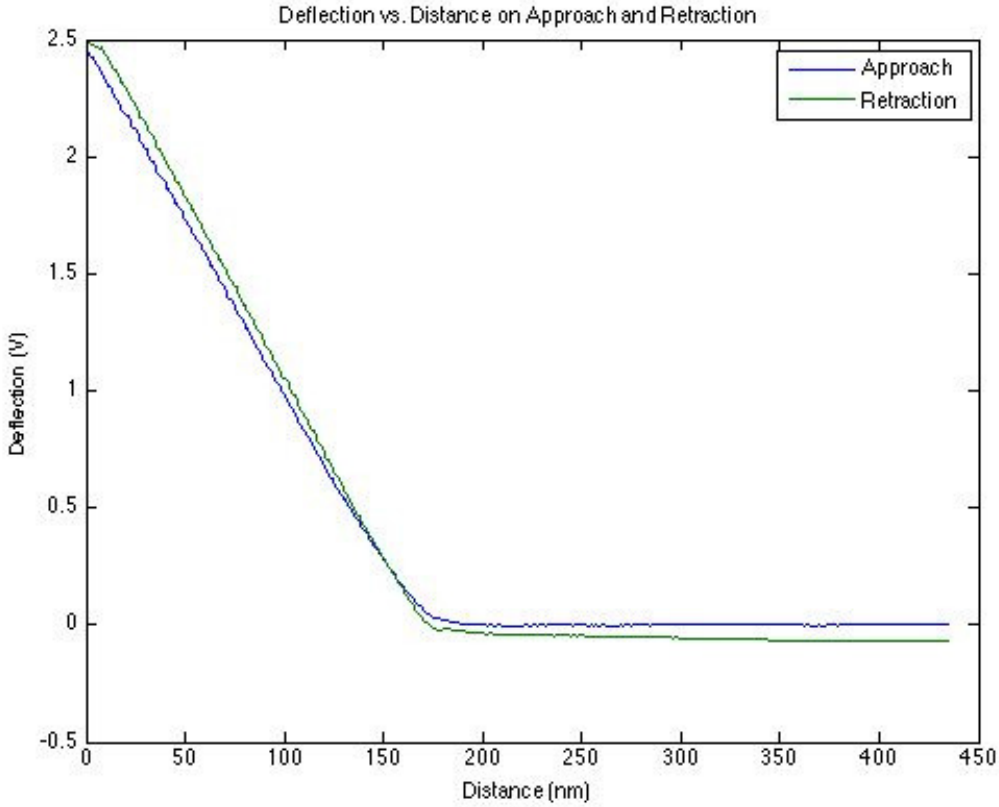
Deflection vs. Distance on Approach and Retraction
Approach
Retraction
Deflection (V)
Distance (nm)
2.5
2
1.5
1
0.5
0
-0.5
0
50
100
150
200
250
300
350
400
450

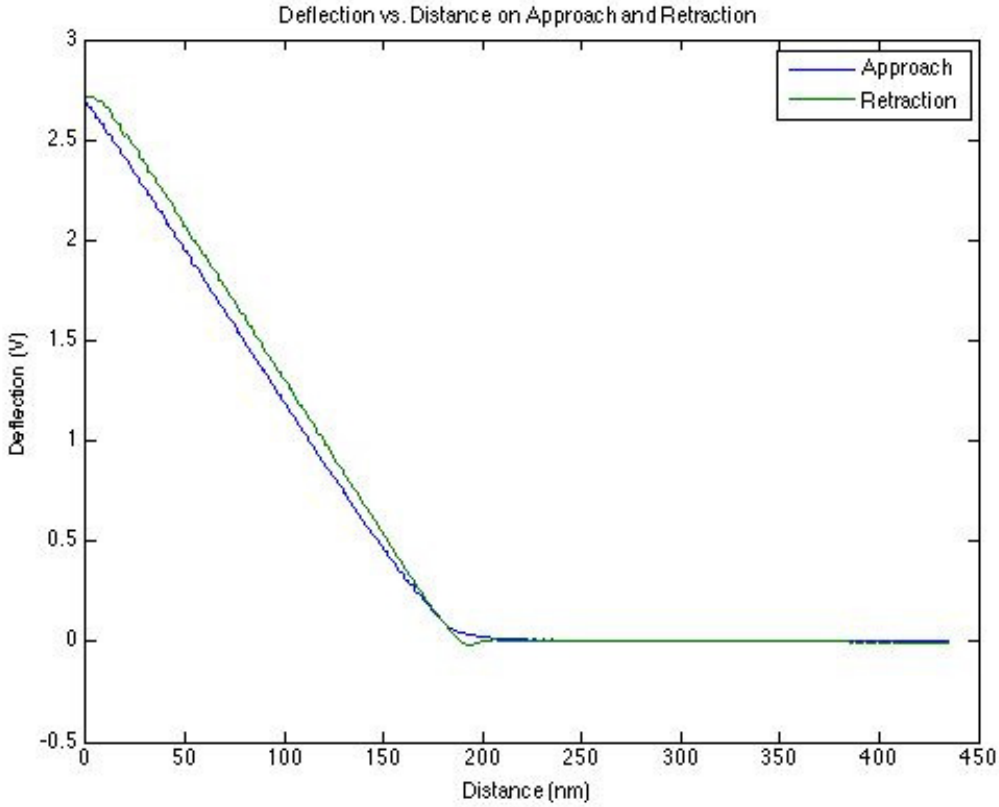
Deflection vs. Distance on Approach and Retraction
Approach
Retraction
Deflection (V)
Distance (nm)
3
2.5
2
1.5
1
0.5
0
-0.5
0
50
100
150
200
250
300
350
400
450

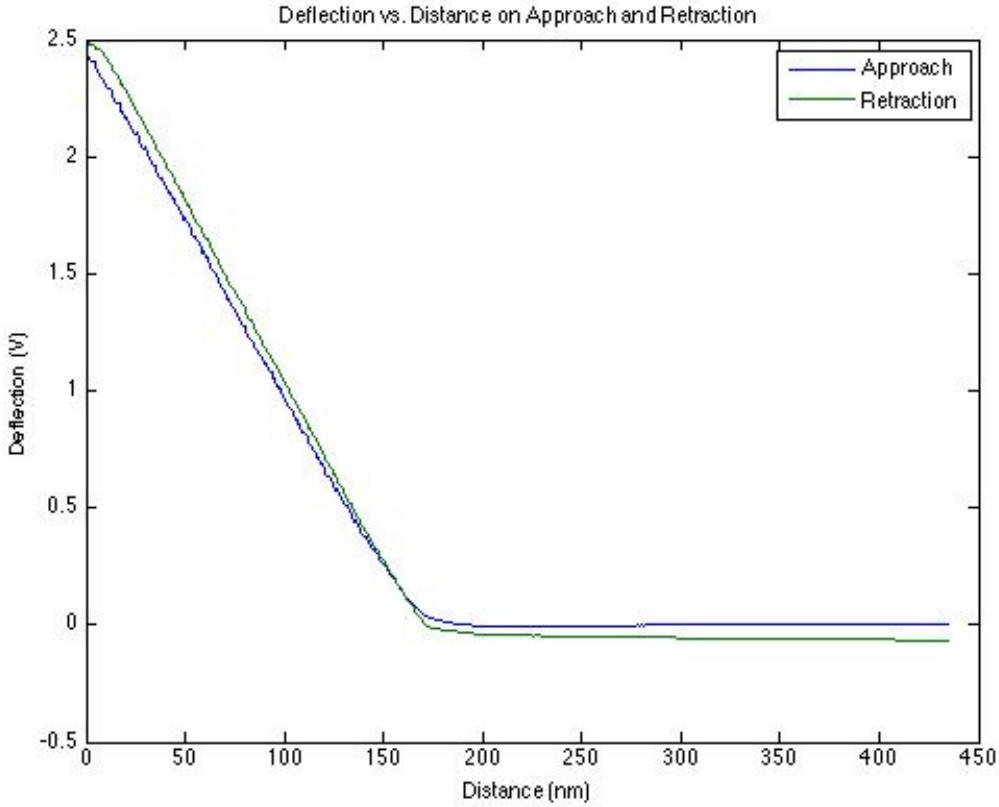
Deflection vs. Distance on Approach and Retraction
Approach
Retraction
Deflection (V)
Distance (nm)
2.5
2
1.5
1
0.5
0
-0.5
0
50
100
150
200
250
300
350
400
450

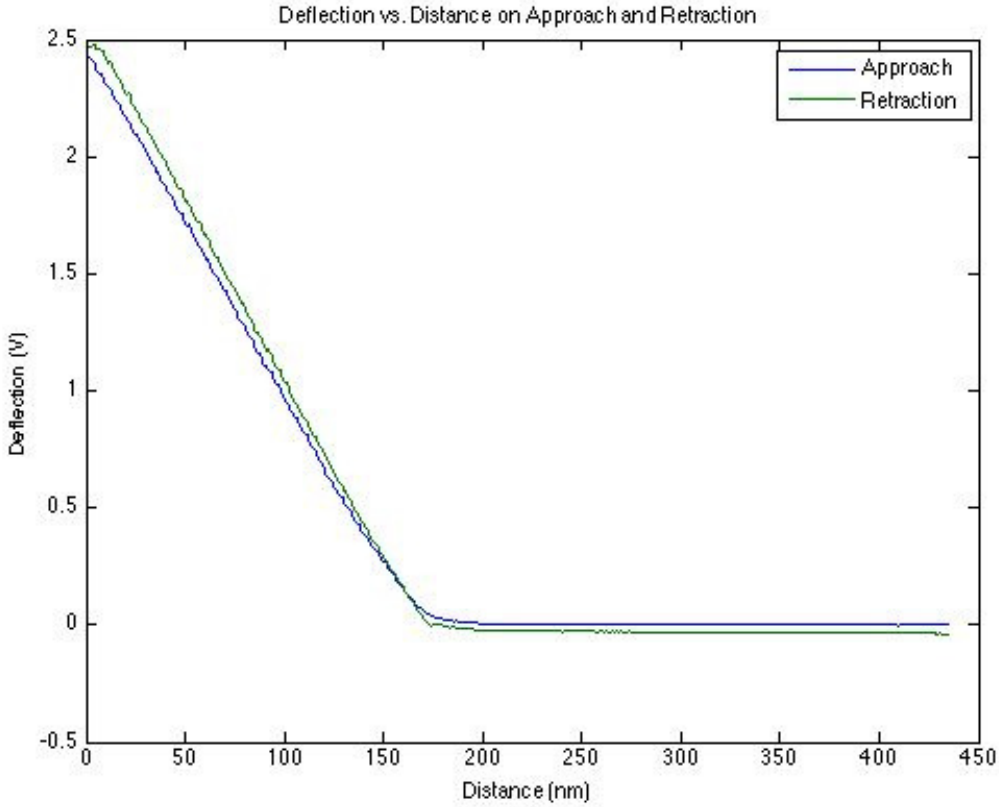
Deflection vs. Distance on Approach and Retraction
Approach
Retraction
Deflection (V)
Distance (nm)
2.5
2
1.5
1
0.5
0
-0.5
0
50
100
150
200
250
300
350
400
450

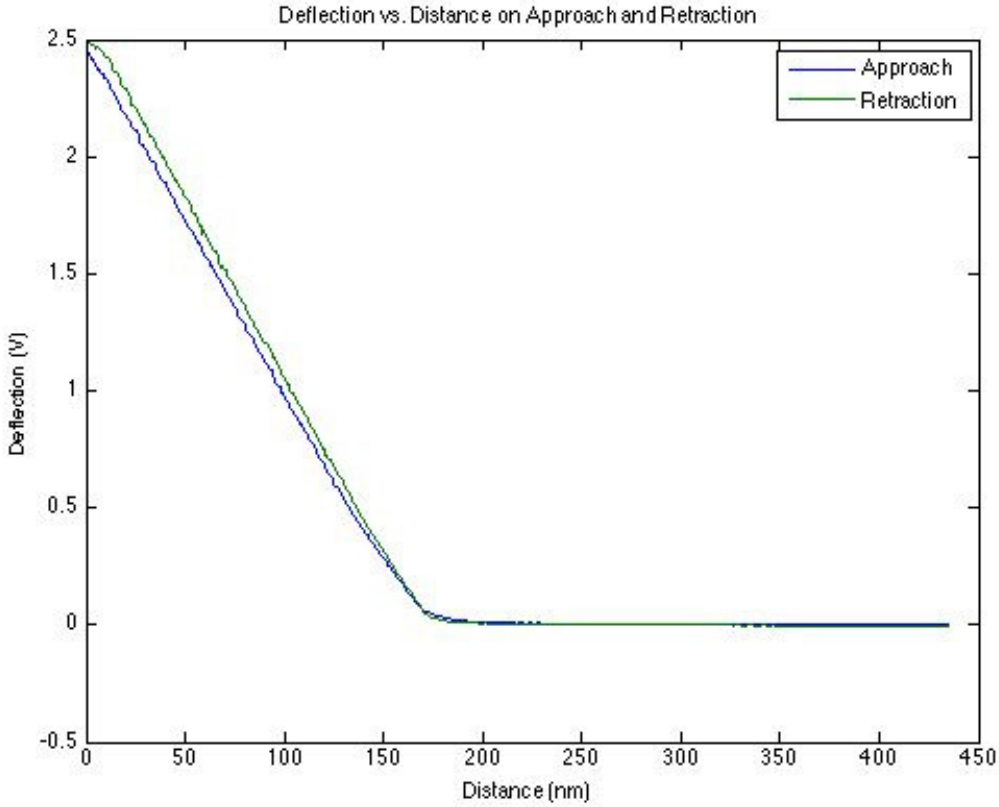
Deflection vs. Distance on Approach and Retraction
Approach
Retraction
Deflection (V)
Distance (nm)
2.5
2
1.5
1
0.5
0
-0.5
0
50
100
150
200
250
300
350
400
450

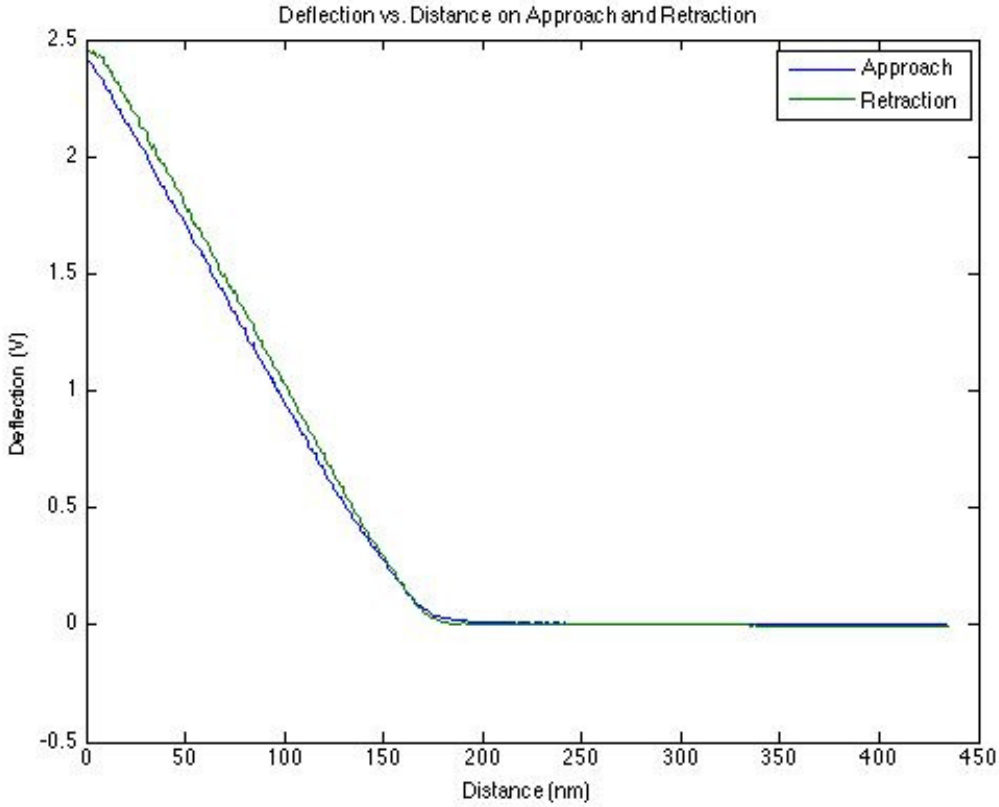
Deflection vs. Distance on Approach and Retraction
Approach
Retraction
Deflection (V)
Distance (nm)
2.5
2
1.5
1
0.5
0
-0.5
0
50
100
150
200
250
300
350
400
450

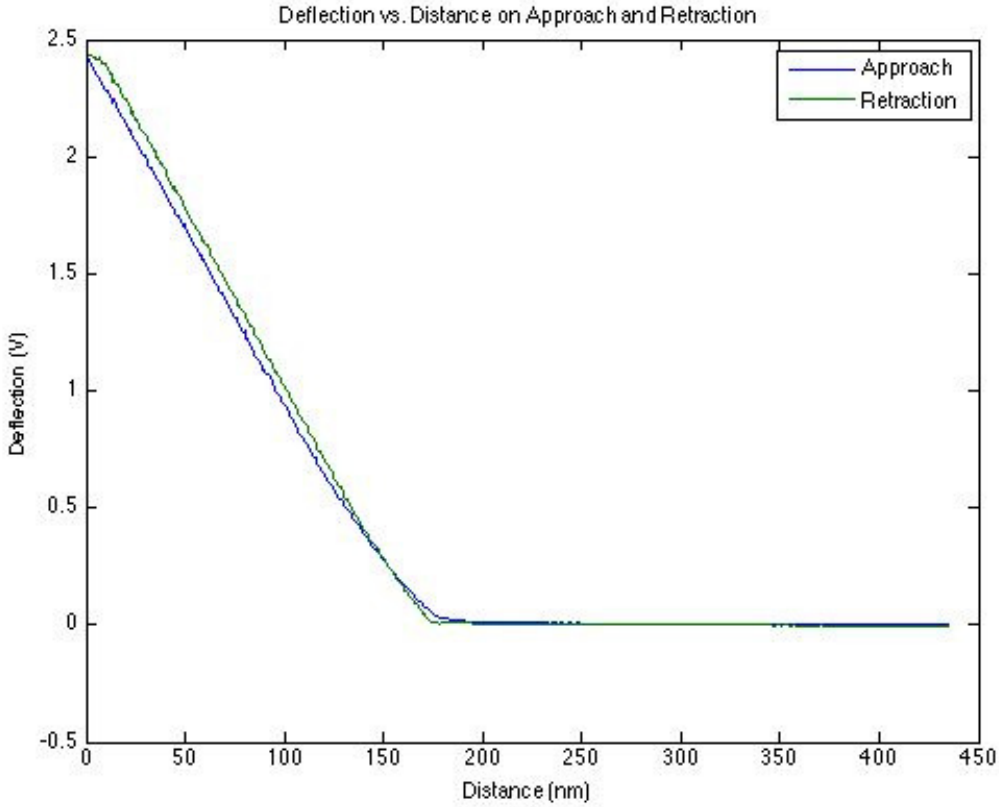
Deflection vs. Distance on Approach and Retraction
Approach
Retraction
Deflection (V)
Distance (nm)
2.5
2
1.5
1
0.5
0
-0.5
0
50
100
150
200
250
300
350
400
450

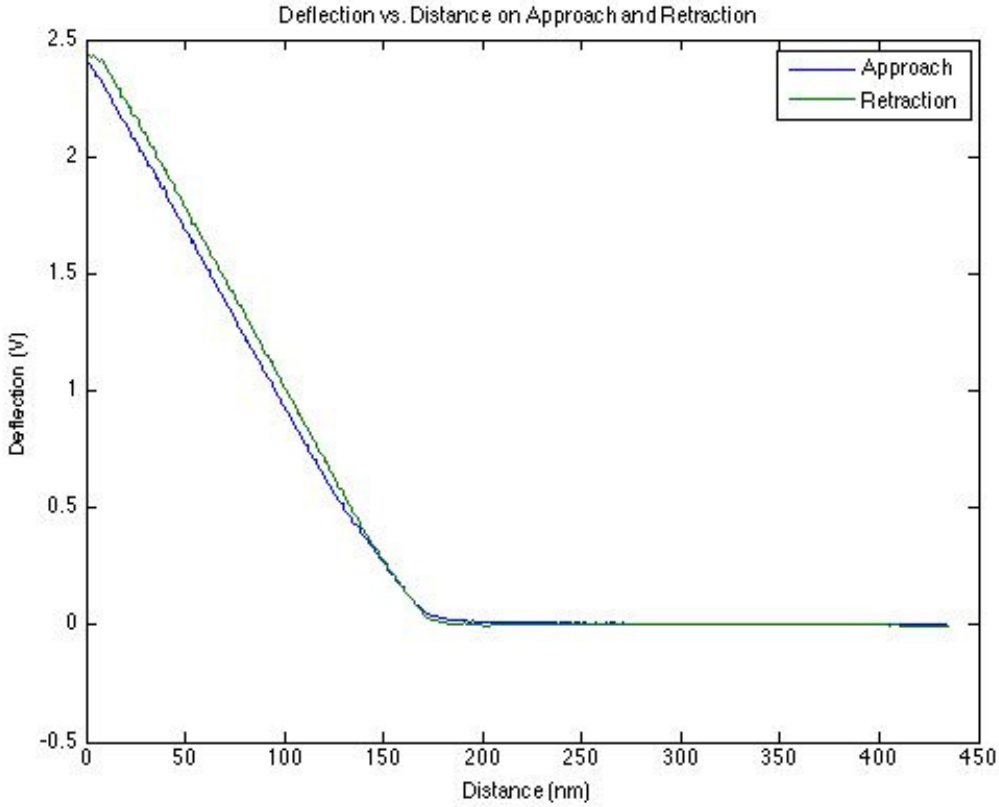
Deflection vs. Distance on Approach and Retraction
Approach
Retraction
Deflection (V)
Distance (nm)
2.5
2
1.5
1
0.5
0
-0.5
0
50
100
150
200
250
300
350
400
450

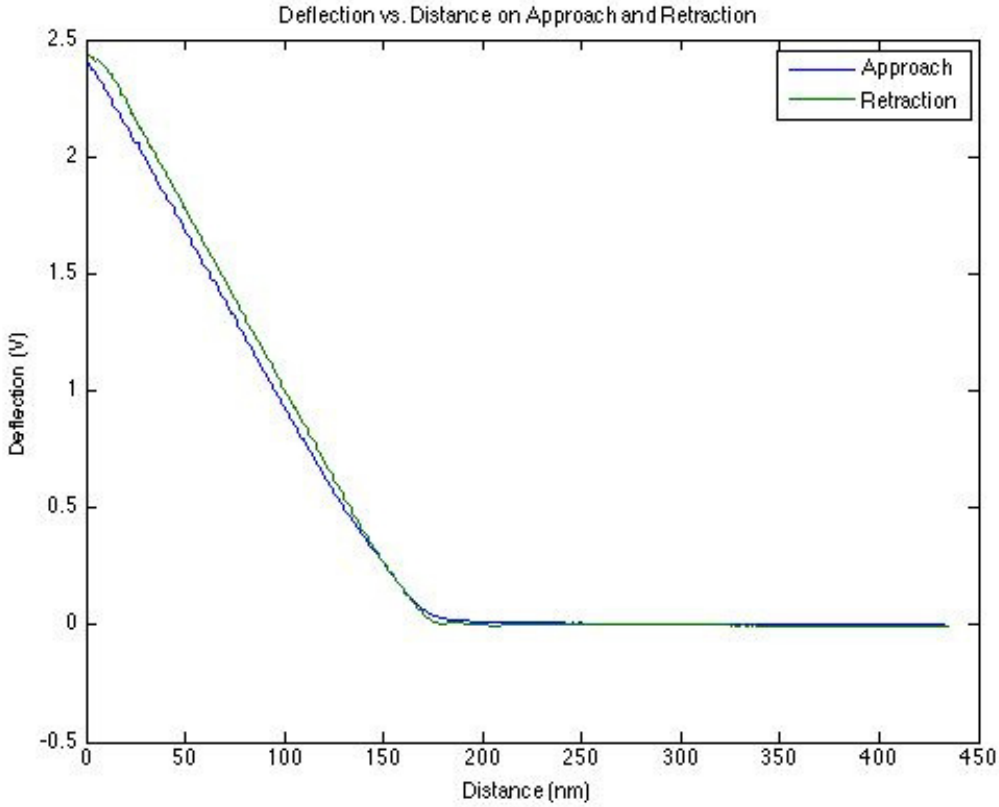
Deflection vs. Distance on Approach and Retraction
Approach
Retraction
Deflection (V)
Distance (nm)
2.5
2
1.5
1
0.5
0
-0.5
0
50
100
150
200
250
300
350
400
450

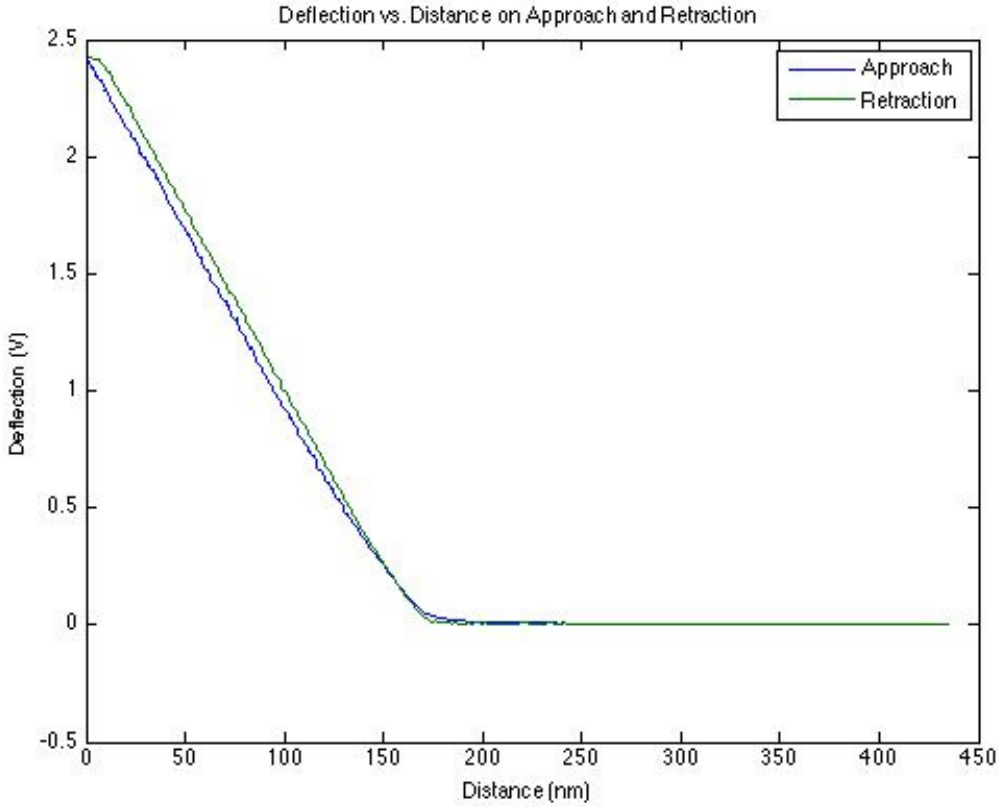
Deflection vs. Distance on Approach and Retraction
Approach
Retraction
Deflection (V)
Distance (nm)
2.5
2
1.5
1
0.5
0
-0.5
0
50
100
150
200
250
300
350
400
450

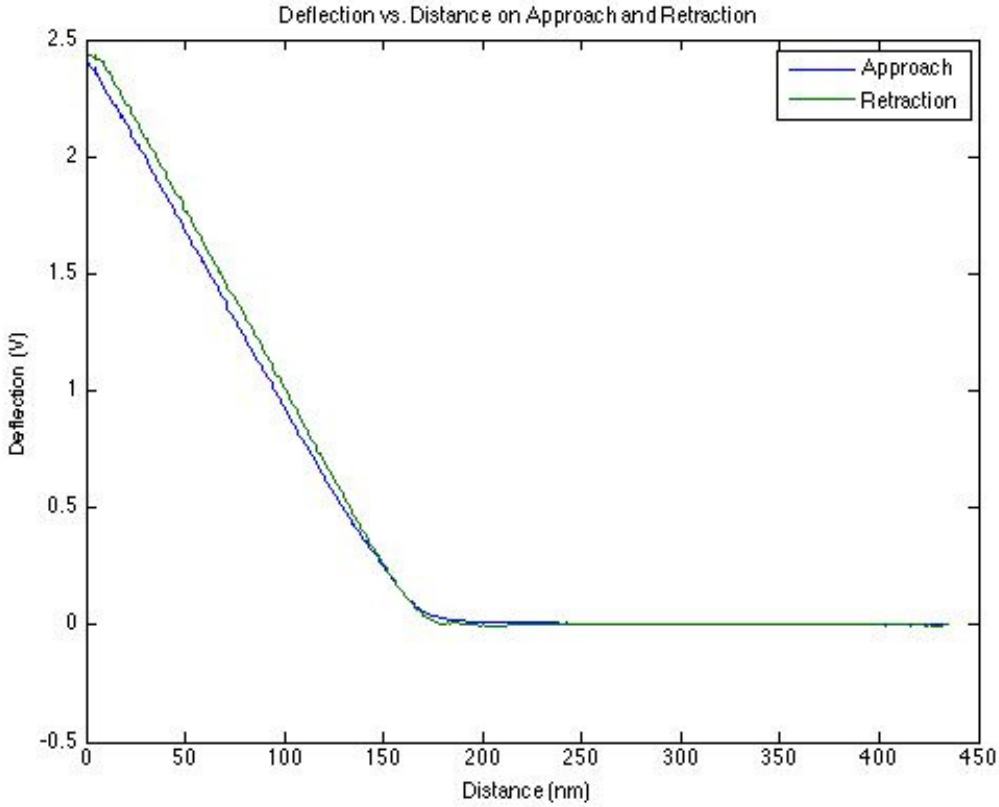
Deflection vs. Distance on Approach and Retraction
Approach
Retraction
Deflection (V)
Distance (nm)
2.5
2
1.5
1
0.5
0
-0.5
0
50
100
150
200
250
300
350
400
450

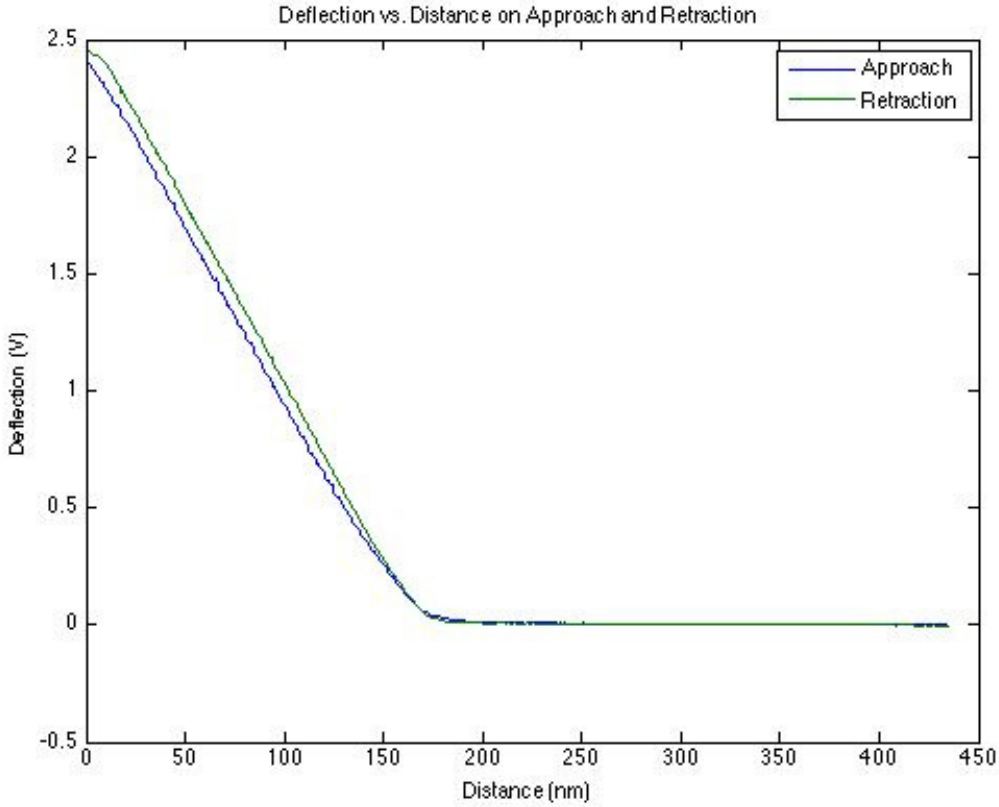
Deflection vs. Distance on Approach and Retraction
Approach
Retraction
Deflection (V)
Distance (nm)
2.5
2
1.5
1
0.5
0
-0.5
0
50
100
150
200
250
300
350
400
450

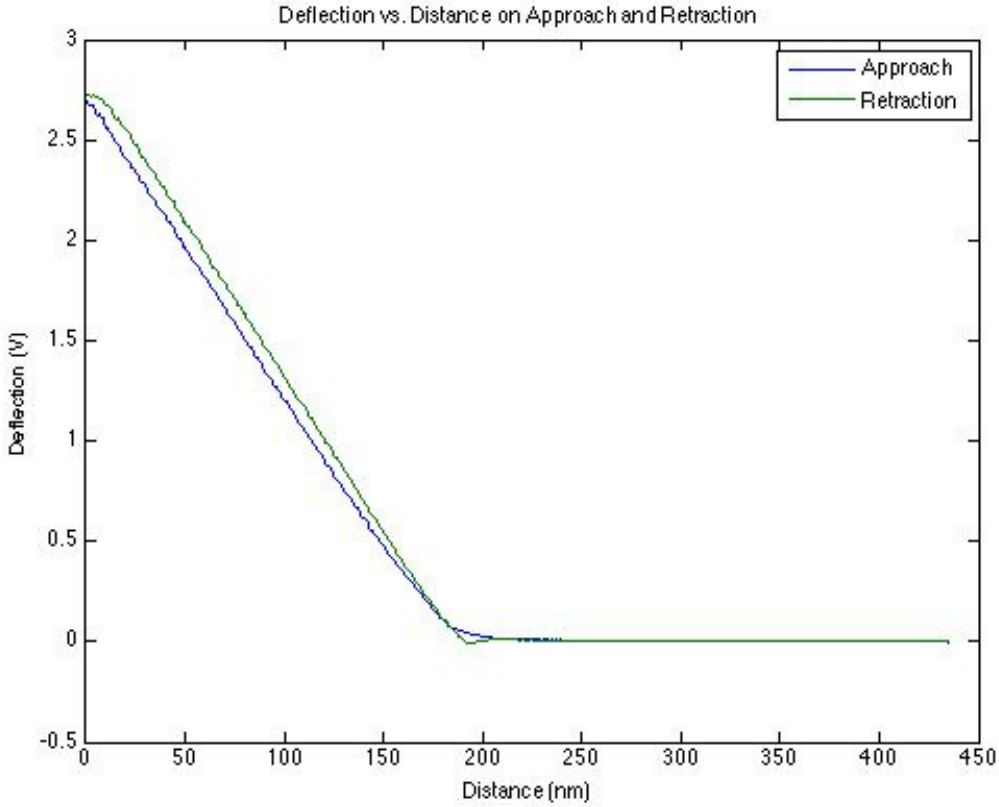
Deflection vs. Distance on Approach and Retraction
Approach
Retraction
Deflection (V)
Distance (nm)
3
2.5
2
1.5
1
0.5
0
-0.5
0
50
100
150
200
250
300
350
400
450

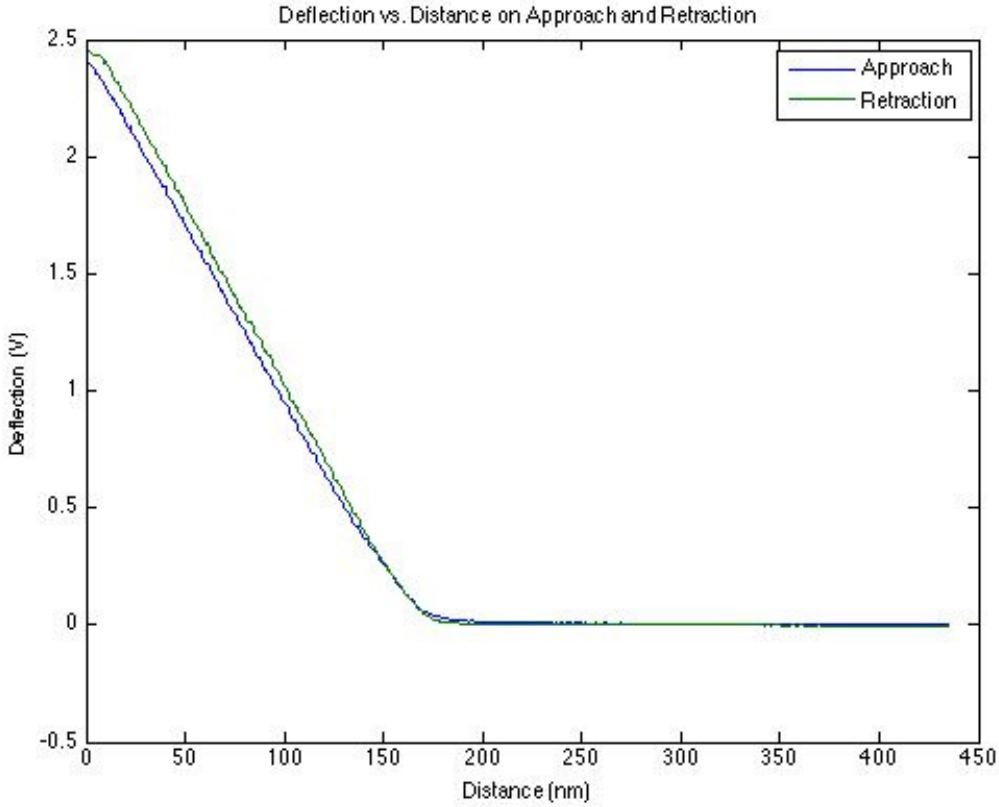
Deflection vs. Distance on Approach and Retraction
Approach
Retraction
Deflection (V)
Distance (nm)
2.5
2
1.5
1
0.5
0
-0.5
0
50
100
150
200
250
300
350
400
450

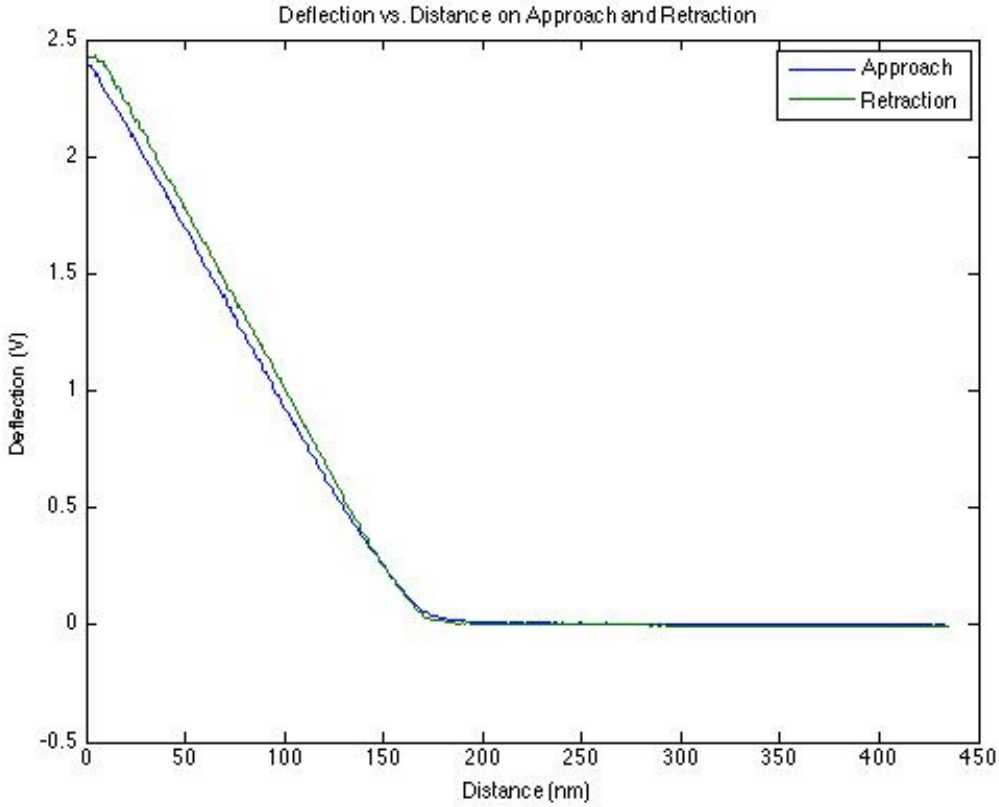
Deflection vs. Distance on Approach and Retraction
Approach
Retraction
Deflection (V)
Distance (nm)
2.5
2
1.5
1
0.5
0
-0.5
0
50
100
150
200
250
300
350
400
450

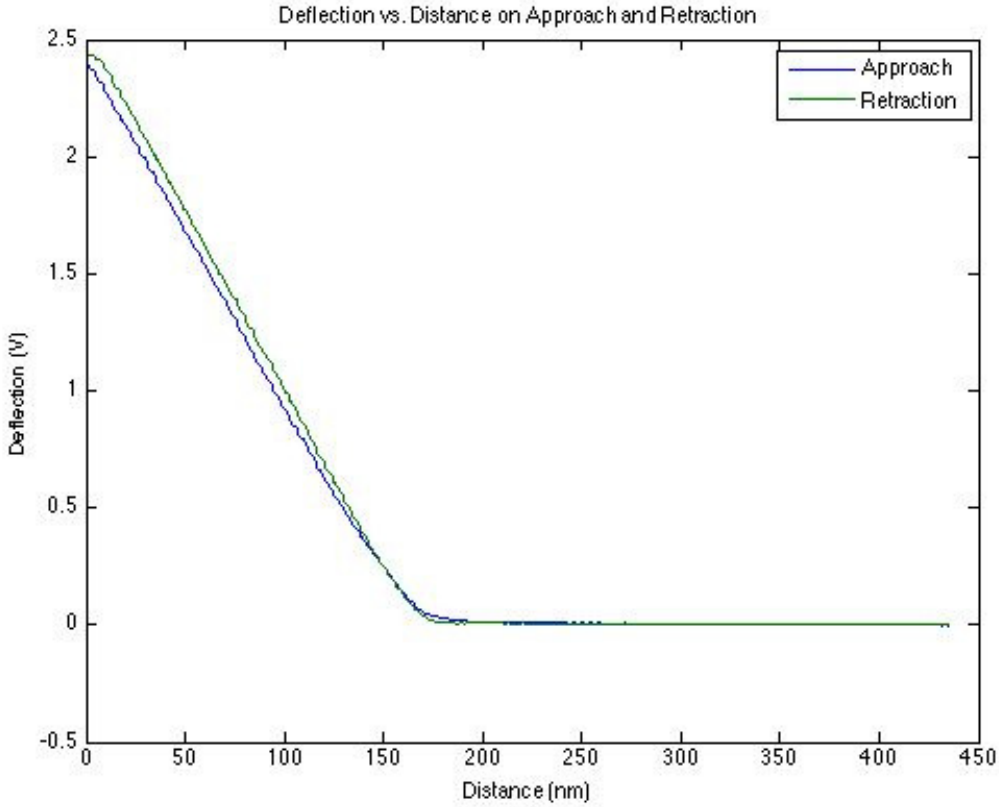
Deflection vs. Distance on Approach and Retraction
Approach
Retraction
Deflection (V)
Distance (nm)
2.5
2
1.5
1
0.5
0
-0.5
0
50
100
150
200
250
300
350
400
450

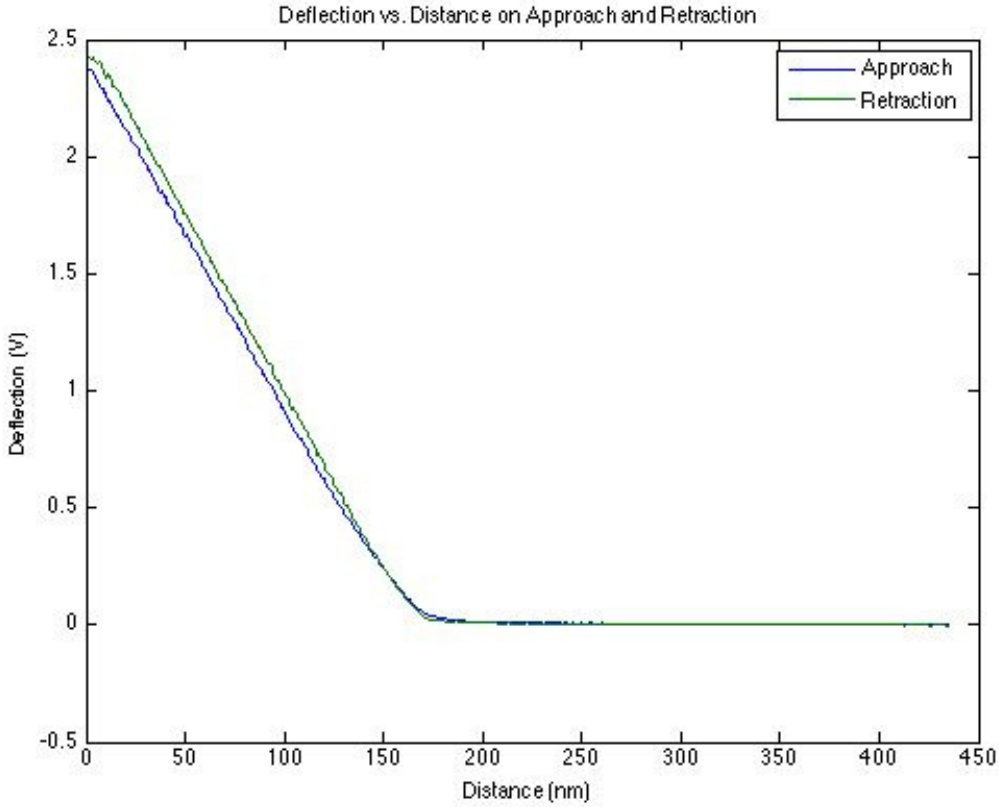
Deflection vs. Distance on Approach and Retraction
Approach
Retraction
Deflection (V)
Distance (nm)
2.5
2
1.5
1
0.5
0
-0.5
0
50
100
150
200
250
300
350
400
450

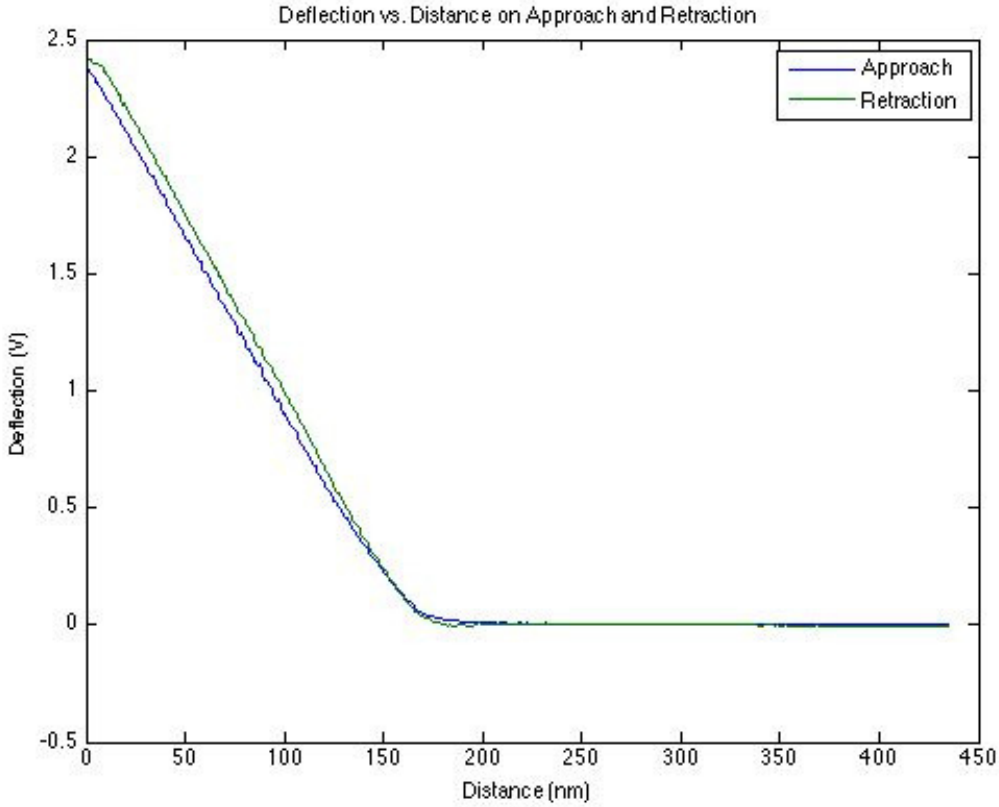
Deflection vs. Distance on Approach and Retraction
Approach
Retraction
Deflection (V)
Distance (nm)
2.5
2
1.5
1
0.5
0
-0.5
0
50
100
150
200
250
300
350
400
450

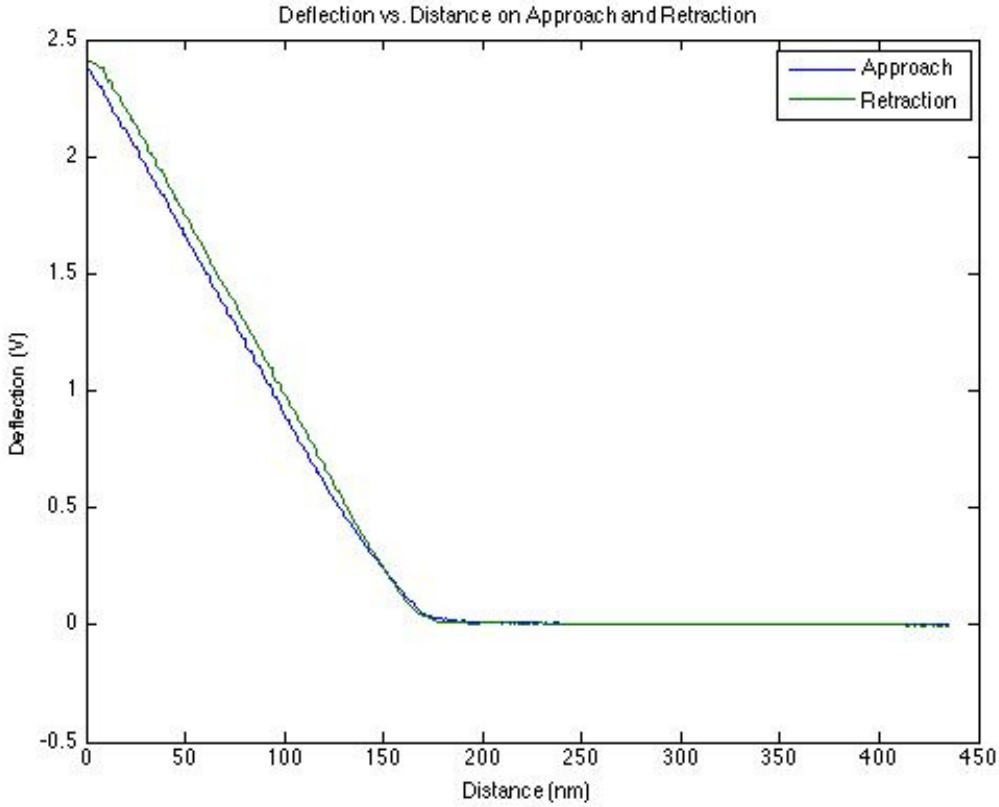
Deflection vs. Distance on Approach and Retraction
Approach
Retraction
Deflection (V)
Distance (nm)
2.5
2
1.5
1
0.5
0
-0.5
0
50
100
150
200
250
300
350
400
450

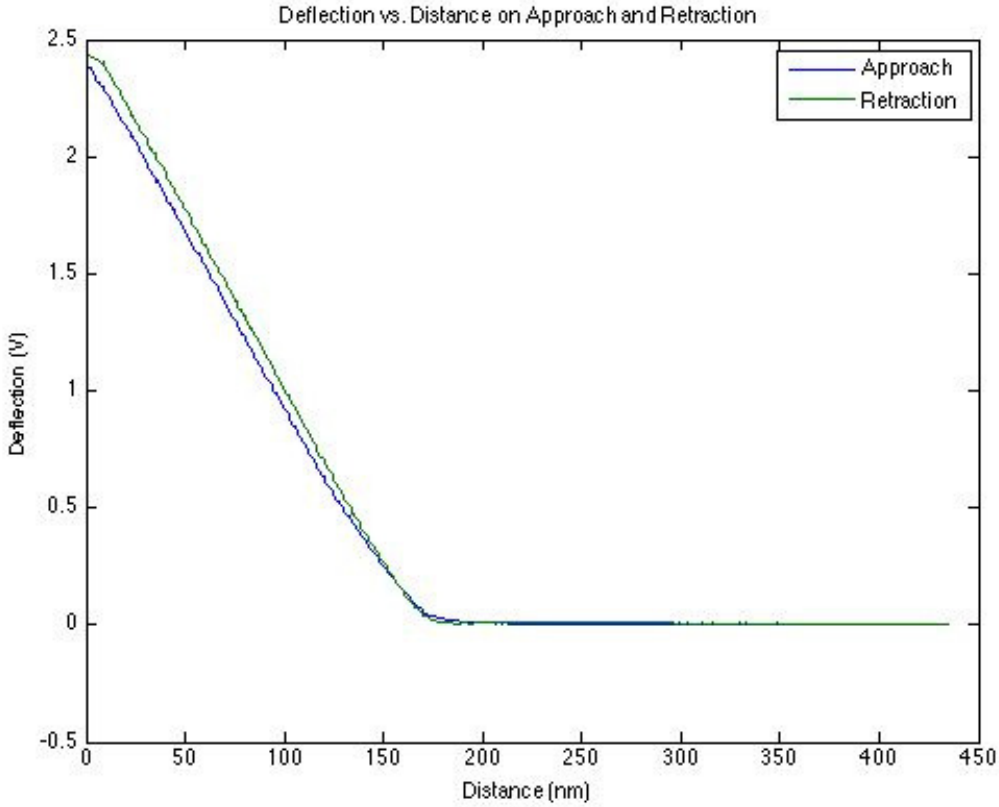
Deflection vs. Distance on Approach and Retraction
Approach
Retraction
Deflection (V)
Distance (nm)
2.5
2
1.5
1
0.5
0
-0.5
0
50
100
150
200
250
300
350
400
450

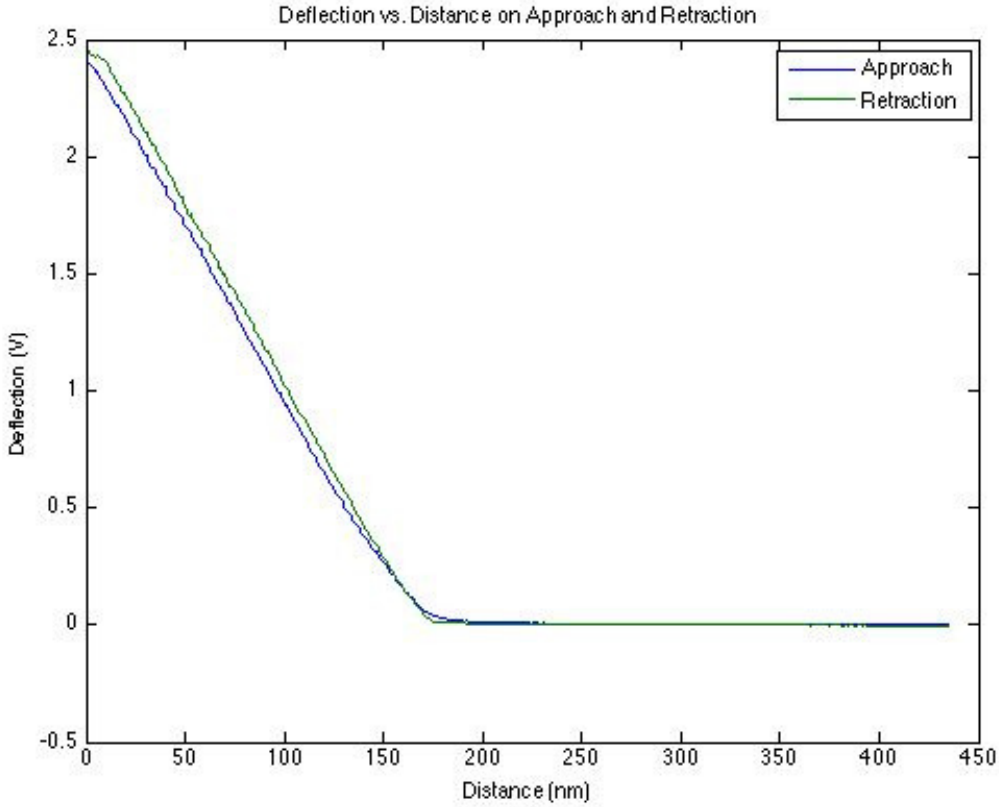
Deflection vs. Distance on Approach and Retraction
Approach
Retraction
Deflection (V)
Distance (nm)
2.5
2
1.5
1
0.5
0
-0.5
0
50
100
150
200
250
300
350
400
450

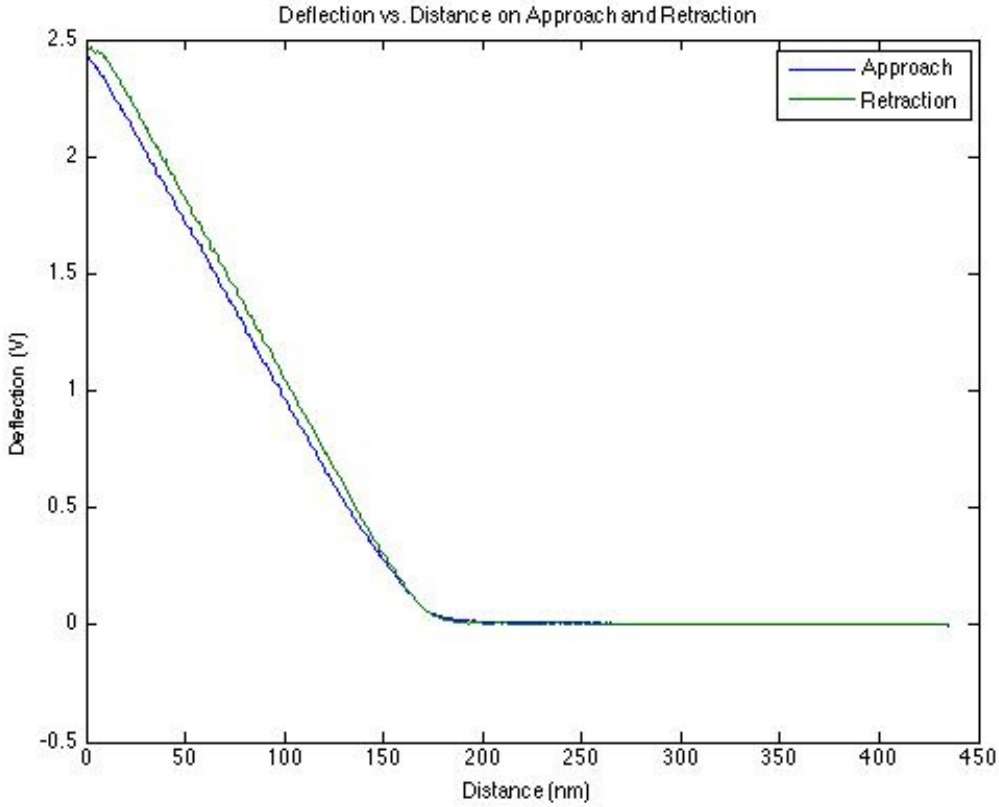
Deflection vs. Distance on Approach and Retraction
Approach
Retraction
Deflection (V)
Distance (nm)
2.5
2
1.5
1
0.5
0
-0.5
0
50
100
150
200
250
300
350
400
450

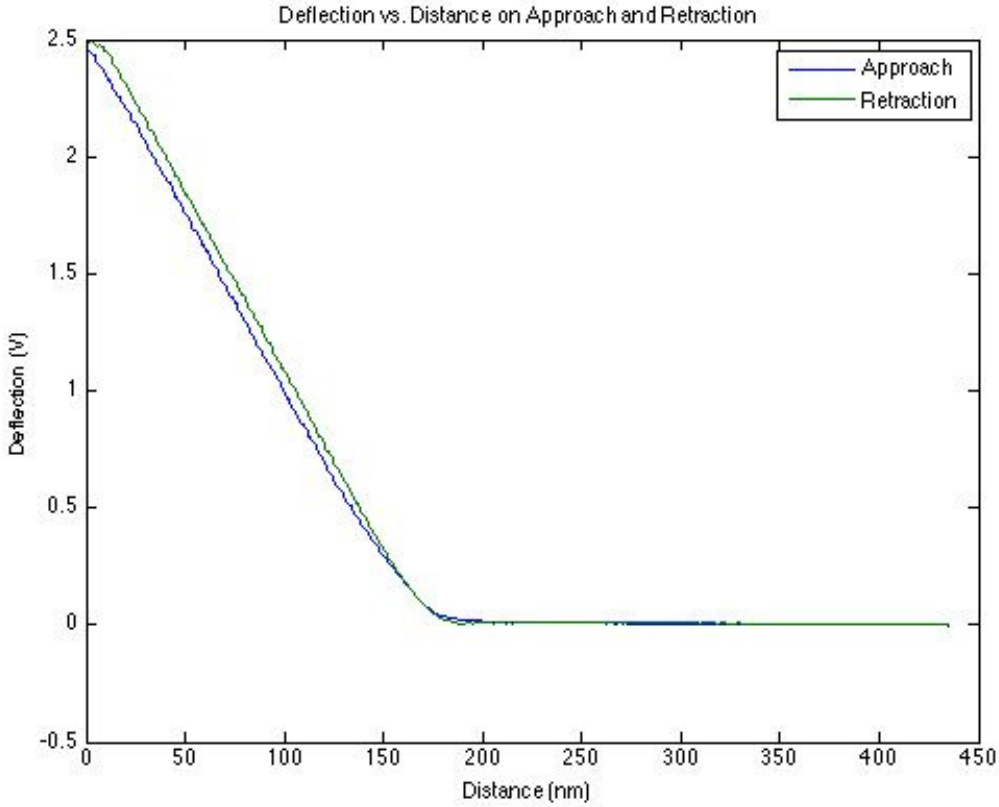
Deflection vs. Distance on Approach and Retraction
Approach
Retraction
Deflection (V)
Distance (nm)
2.5
2
1.5
1
0.5
0
-0.5
0
50
100
150
200
250
300
350
400
450

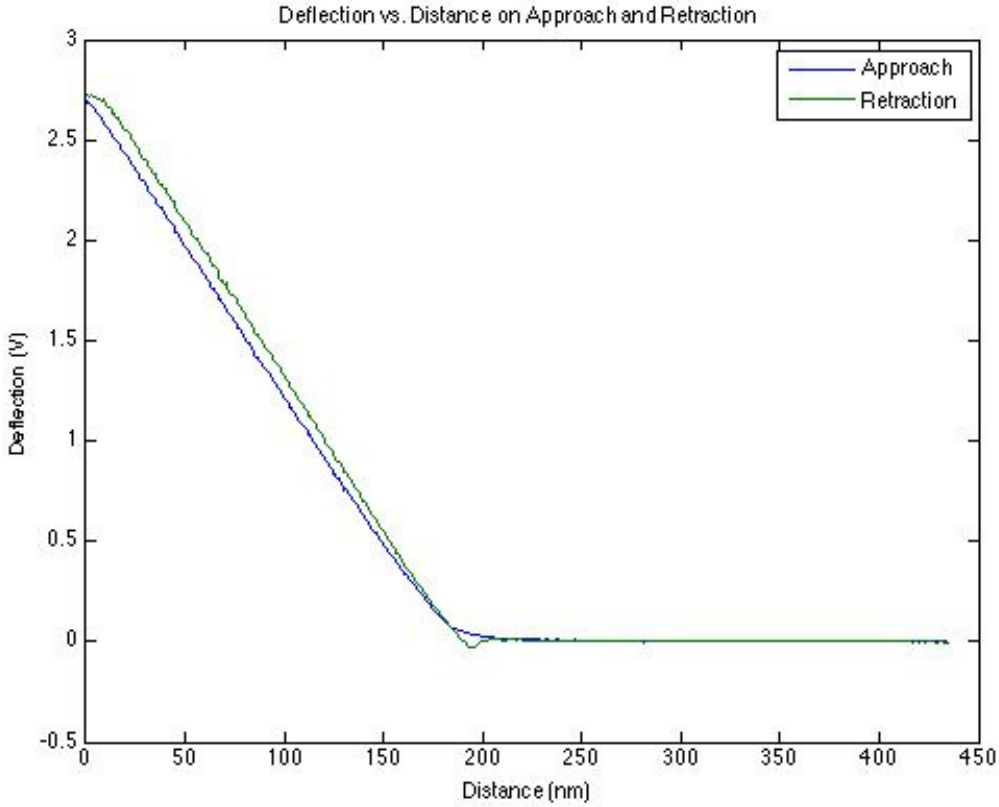
Deflection vs. Distance on Approach and Retraction
Approach
Retraction
Deflection (V)
Distance (nm)
3
2.5
2
1.5
1
0.5
0
-0.5
0
50
100
150
200
250
300
350
400
450

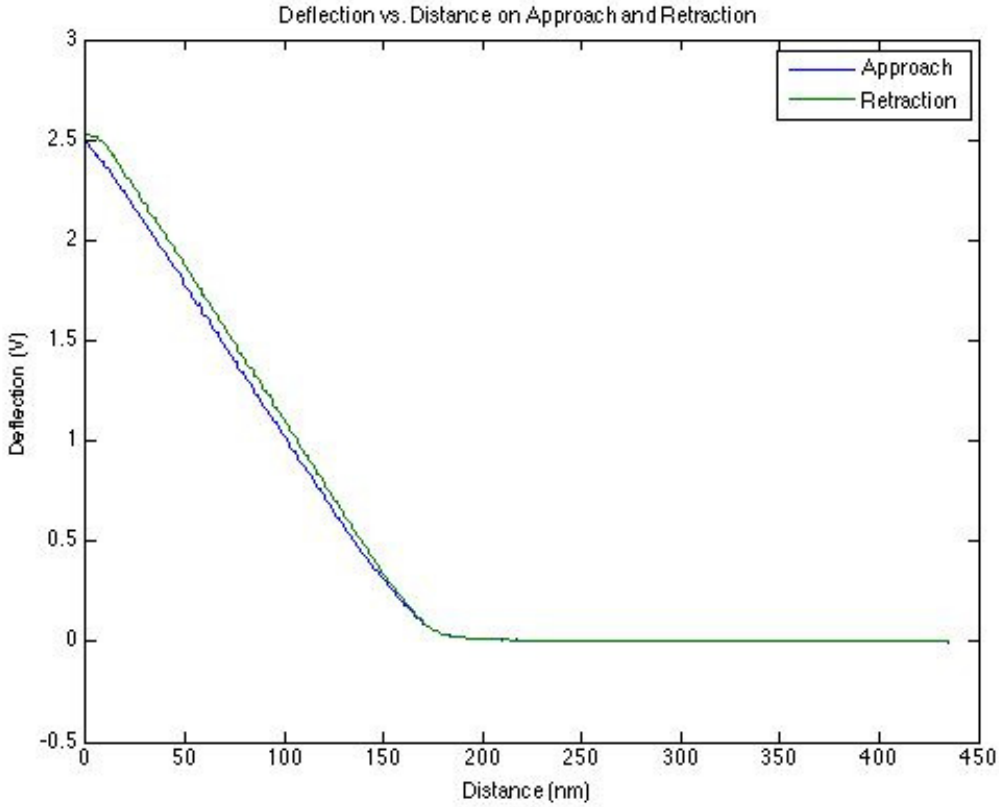
Deflection vs. Distance on Approach and Retraction
Approach
Retraction
Deflection (V)
Distance (nm)
3
2.5
2
1.5
1
0.5
0
-0.5
0
50
100
150
200
250
300
350
400
450

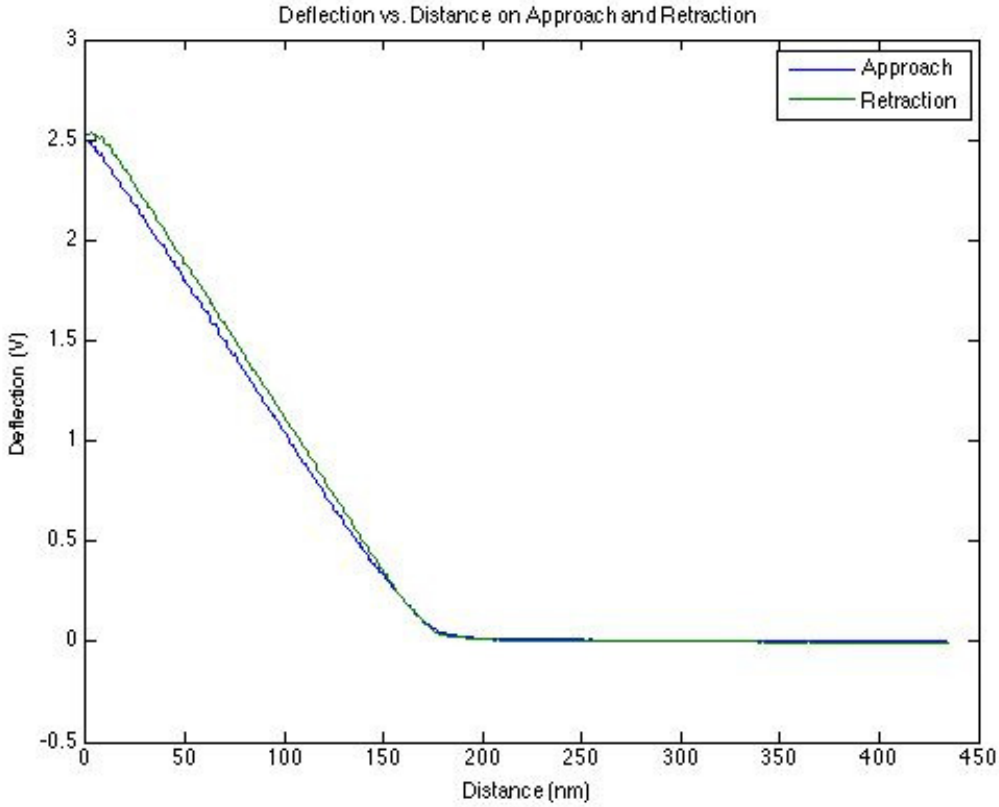
Deflection vs. Distance on Approach and Retraction
Approach
Retraction
Deflection (V)
Distance (nm)
3
2.5
2
1.5
1
0.5
0
-0.5
0
50
100
150
200
250
300
350
400
450

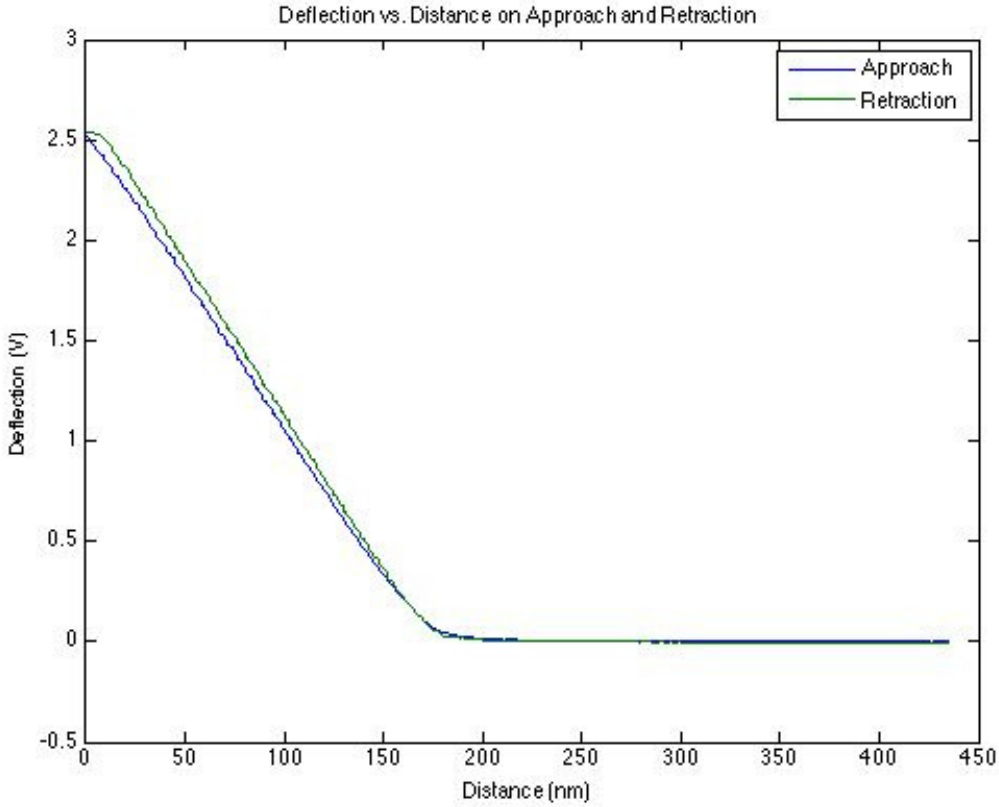
Deflection vs. Distance on Approach and Retraction
Approach
Retraction
Deflection (V)
Distance (nm)
3
2.5
2
1.5
1
0.5
0
-0.5
0
50
100
150
200
250
300
350
400
450

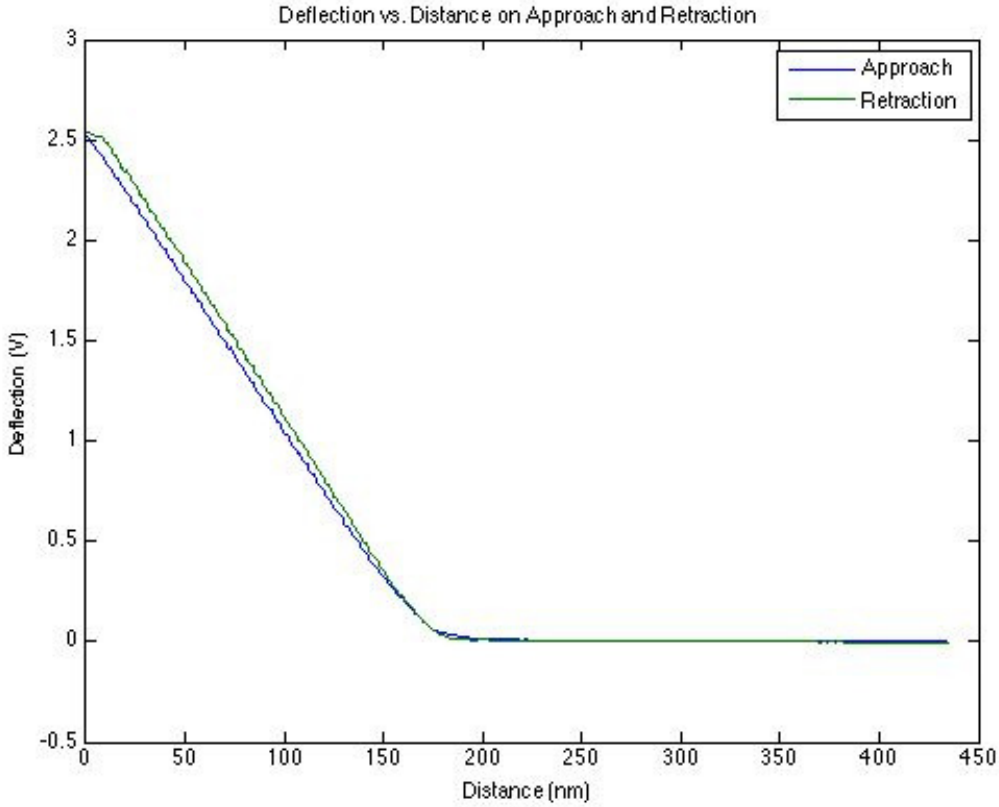
Deflection vs. Distance on Approach and Retraction
Approach
Retraction
Deflection (V)
Distance (nm)
3
2.5
2
1.5
1
0.5
0
-0.5
0
50
100
150
200
250
300
350
400
450

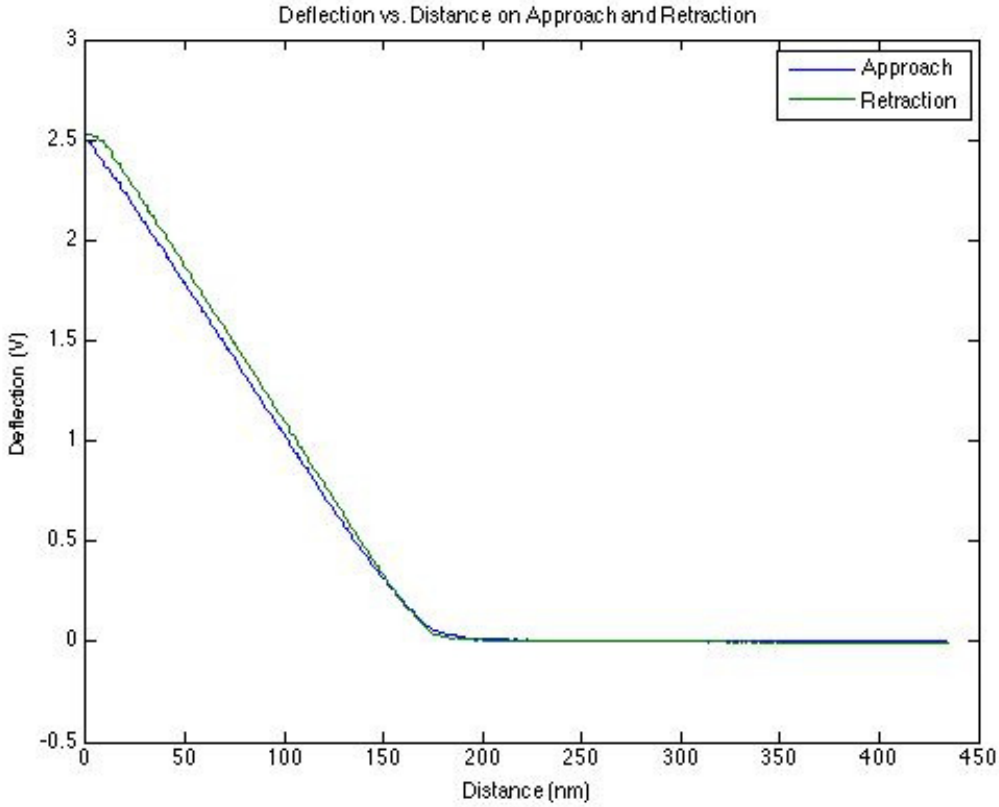
Deflection vs. Distance on Approach and Retraction
Approach
Retraction
Deflection (V)
Distance (nm)
3
2.5
2
1.5
1
0.5
0
-0.5
0
50
100
150
200
250
300
350
400
450

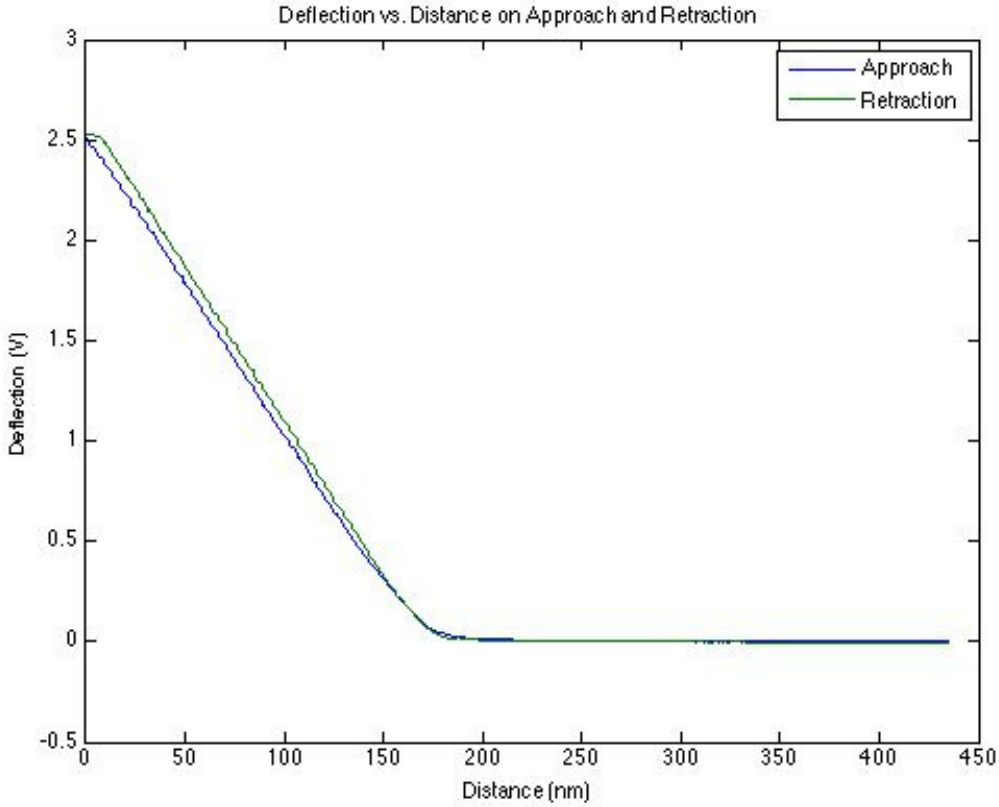
Deflection vs. Distance on Approach and Retraction
Approach
Retraction
Deflection (V)
Distance (nm)
3
2.5
2
1.5
1
0.5
0
-0.5
0
50
100
150
200
250
300
350
400
450

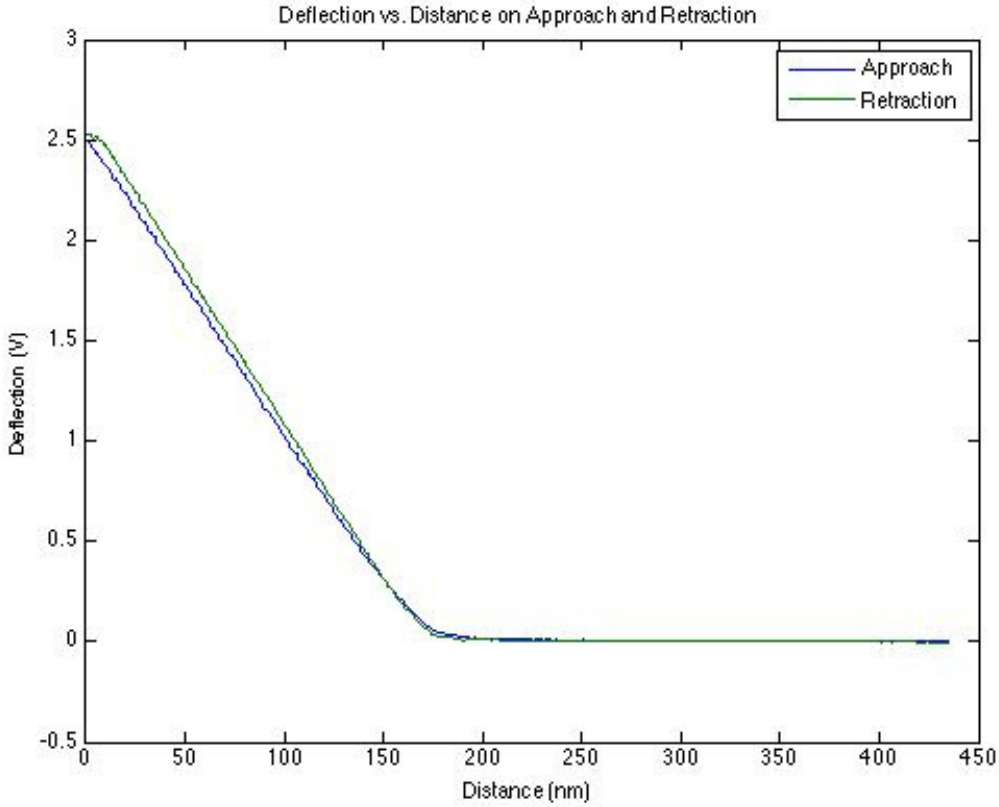
Deflection vs. Distance on Approach and Retraction
Approach
Retraction
Deflection (V)
Distance (nm)
3
2.5
2
1.5
1
0.5
0
-0.5
0
50
100
150
200
250
300
350
400
450

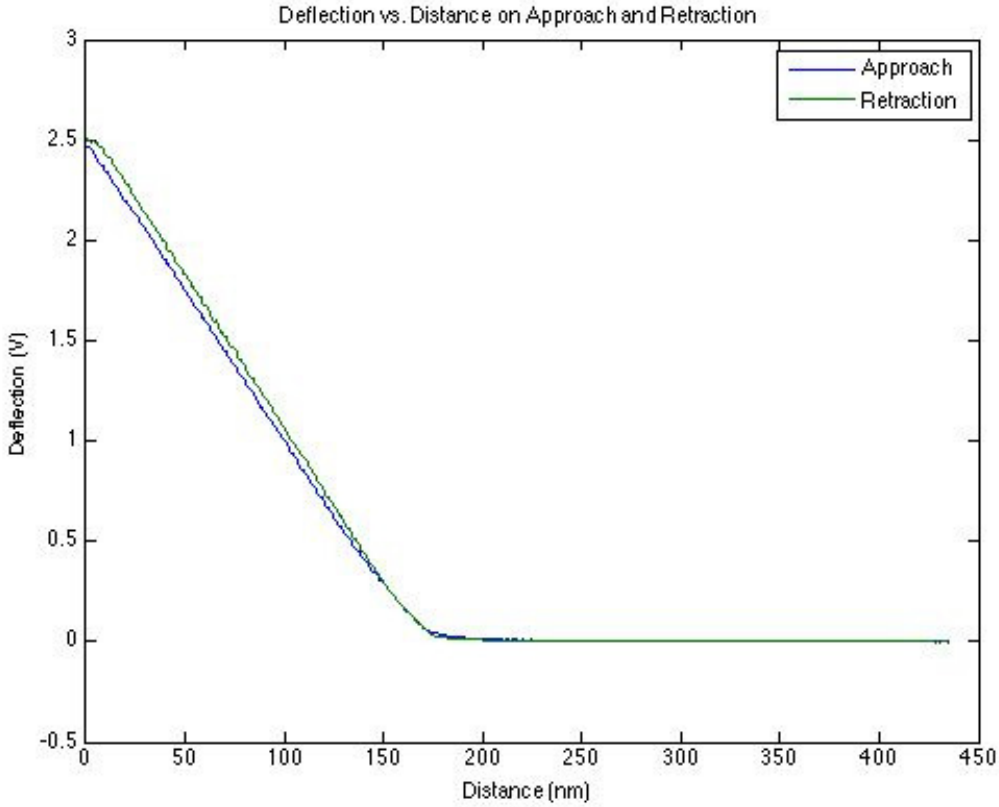
Deflection vs. Distance on Approach and Retraction
Approach
Retraction
Deflection (V)
Distance (nm)
3
2.5
2
1.5
1
0.5
0
-0.5
0
50
100
150
200
250
300
350
400
450

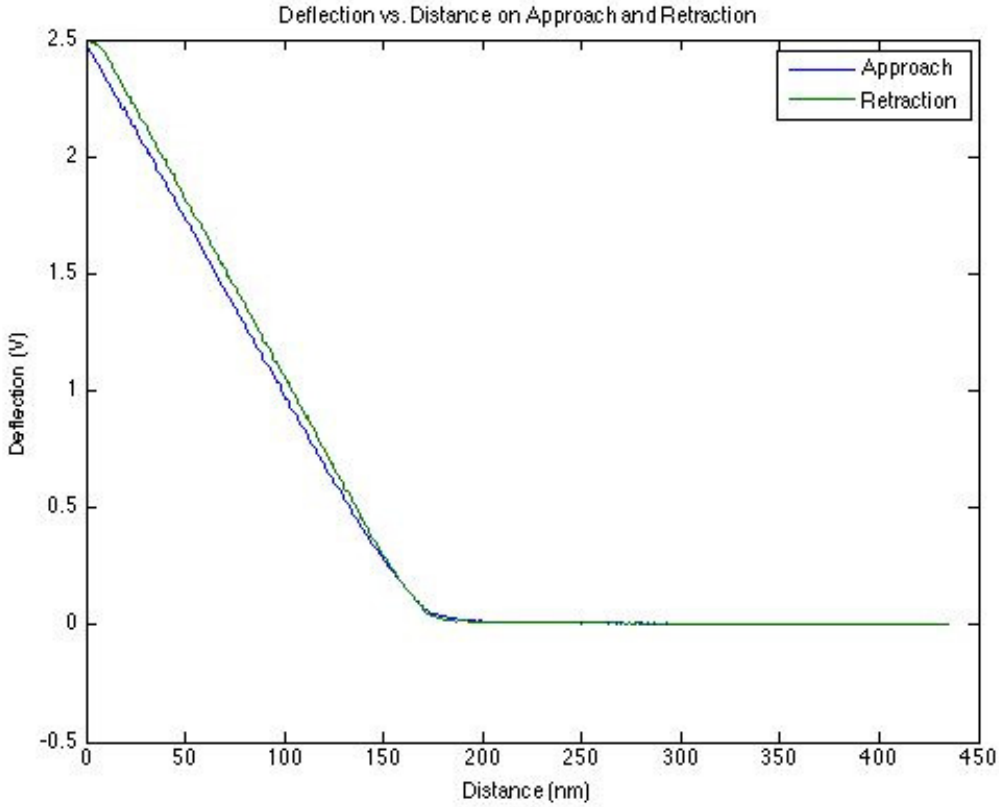
Deflection vs. Distance on Approach and Retraction
Approach
Retraction
Deflection (V)
Distance (nm)
2.5
2
1.5
1
0.5
0
-0.5
0
50
100
150
200
250
300
350
400
450

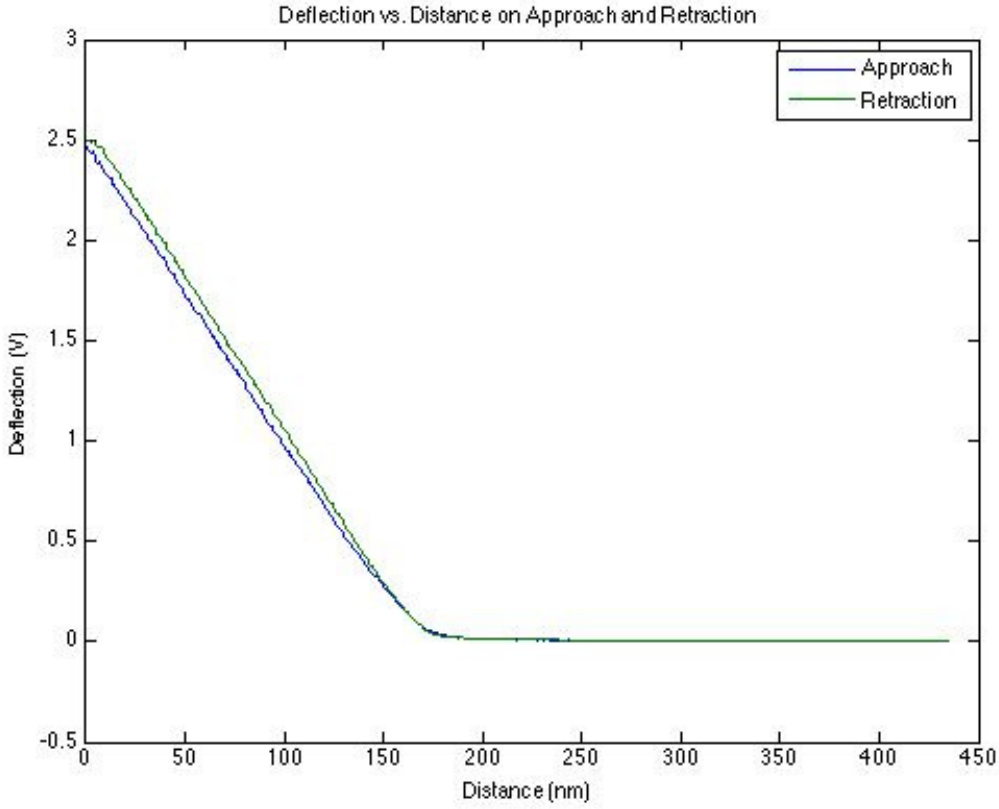
Deflection vs. Distance on Approach and Retraction
Approach
Retraction
Deflection (V)
Distance (nm)
3
2.5
2
1.5
1
0.5
0
-0.5
0
50
100
150
200
250
300
350
400
450

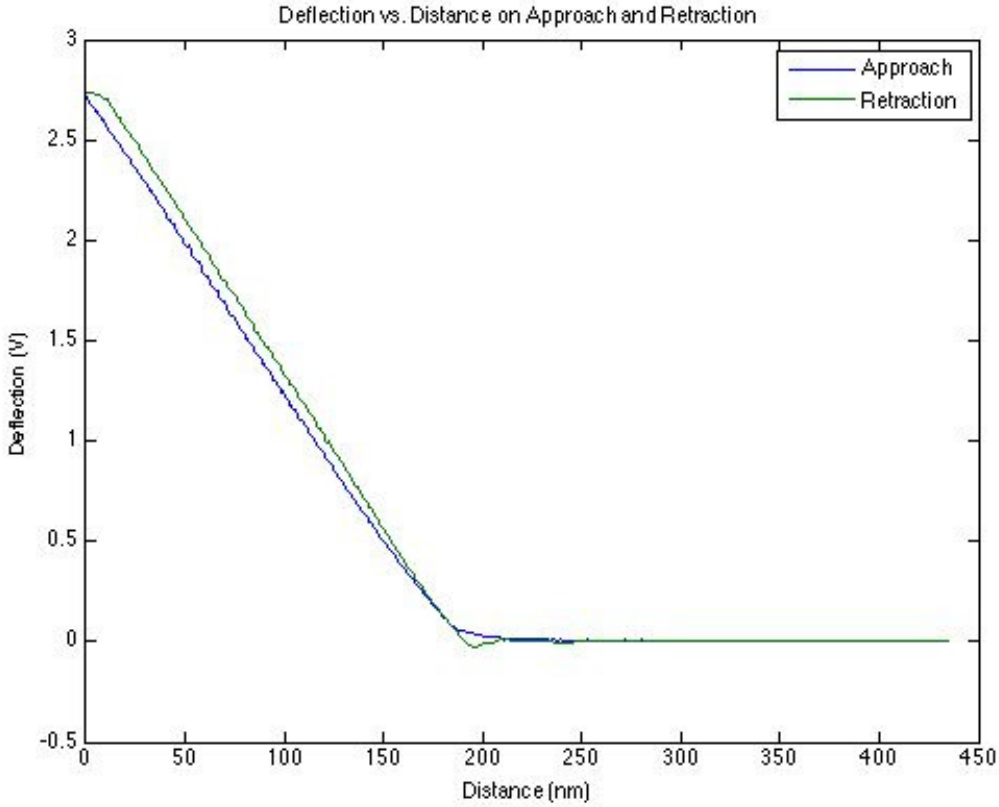
Deflection vs. Distance on Approach and Retraction
Approach
Retraction
Deflection (V)
Distance (nm)
3
2.5
2
1.5
1
0.5
0
-0.5
0
50
100
150
200
250
300
350
400
450

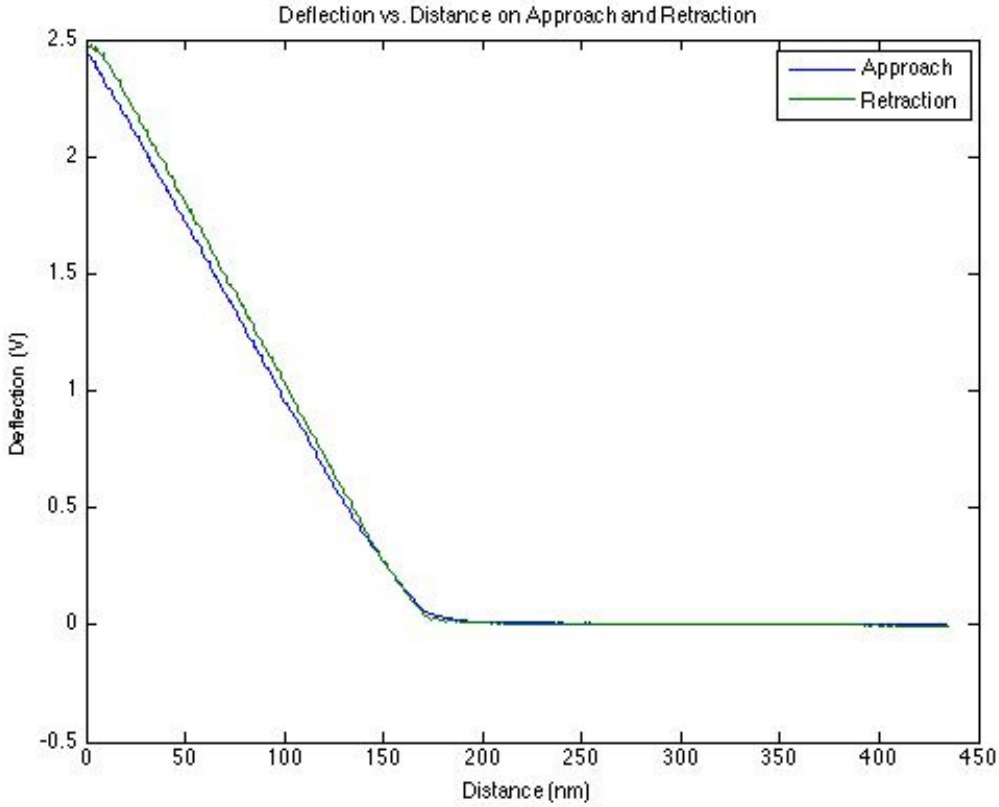
Deflection vs. Distance on Approach and Retraction
Approach
Retraction
Deflection (V)
Distance (nm)
2.5
2
1.5
1
0.5
0
-0.5
0
50
100
150
200
250
300
350
400
450

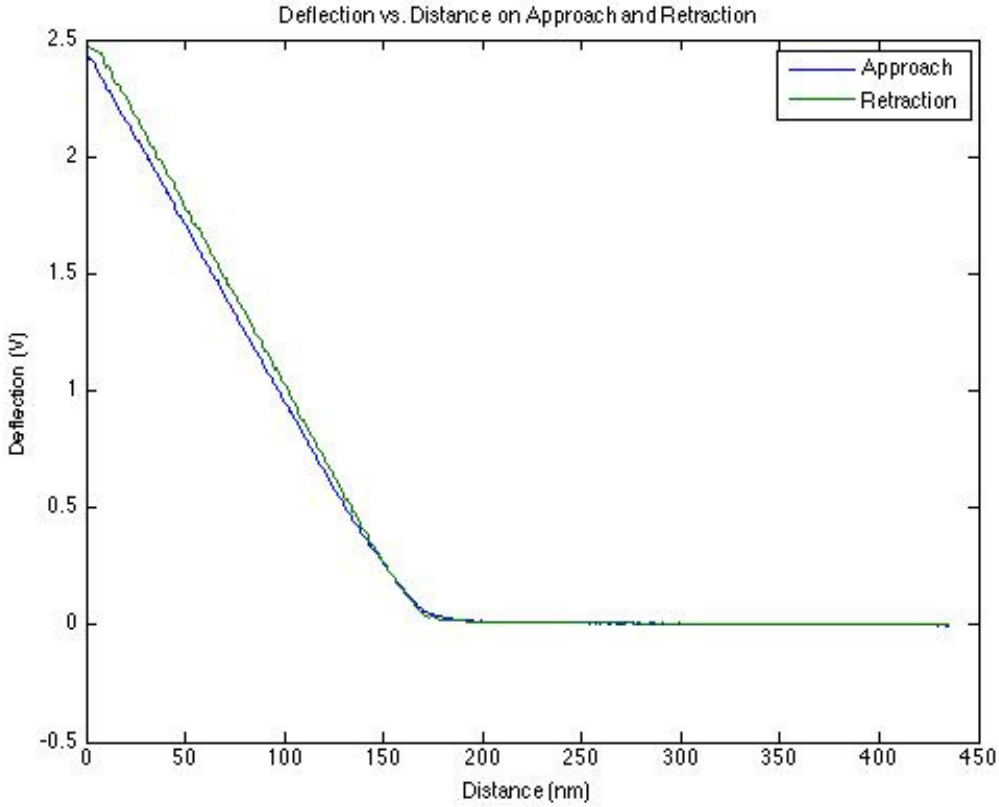
Deflection vs. Distance on Approach and Retraction
Approach
Retraction
Deflection (V)
Distance (nm)
2.5
2
1.5
1
0.5
0
-0.5
0
50
100
150
200
250
300
350
400
450

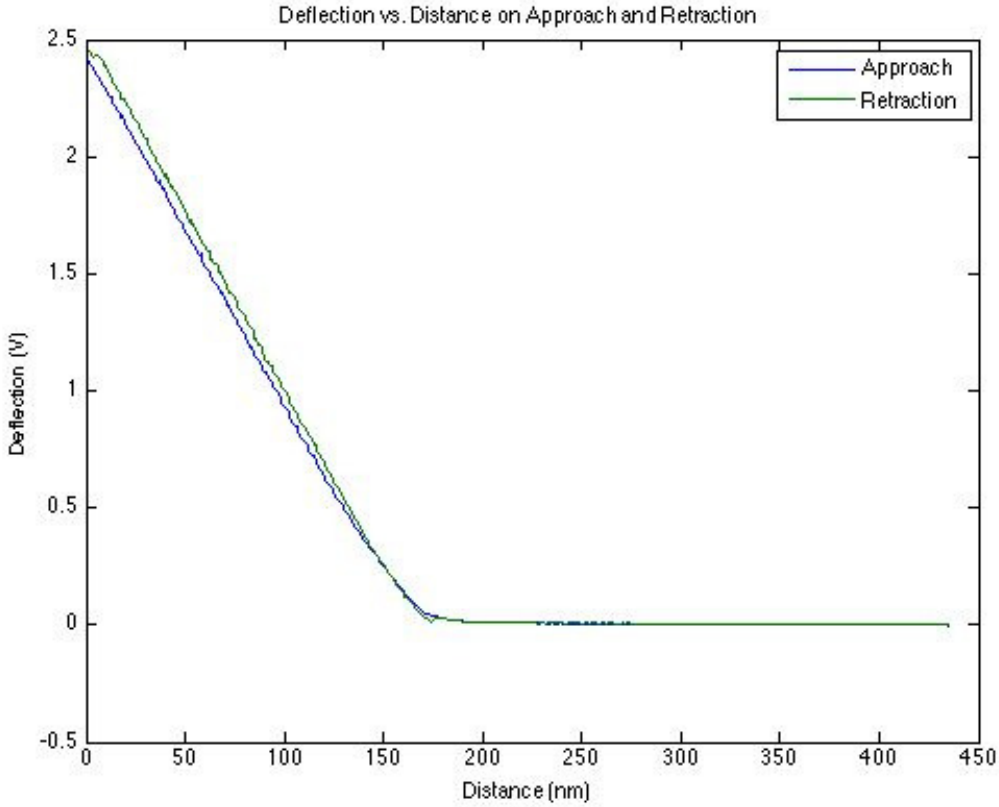
Deflection vs. Distance on Approach and Retraction
Approach
Retraction
Deflection (V)
Distance (nm)
2.5
2
1.5
1
0.5
0
-0.5
0
50
100
150
200
250
300
350
400
450

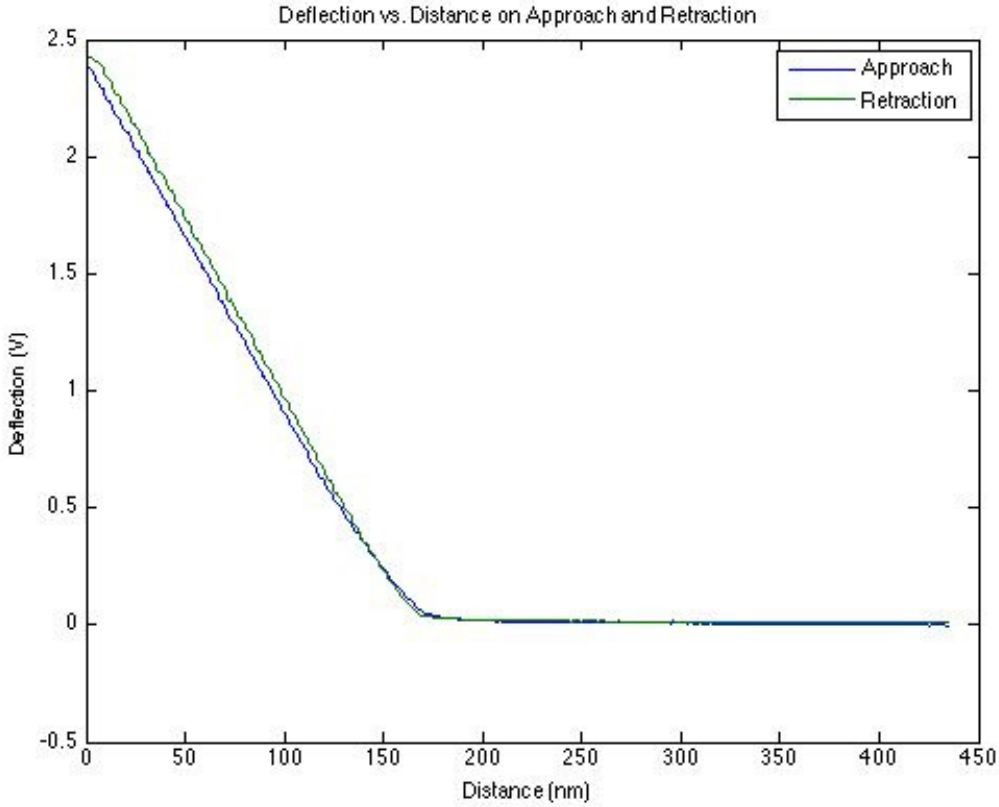
Deflection vs. Distance on Approach and Retraction
Approach
Retraction
Deflection (V)
Distance (nm)
2.5
2
1.5
1
0.5
0
-0.5
0
50
100
150
200
250
300
350
400
450

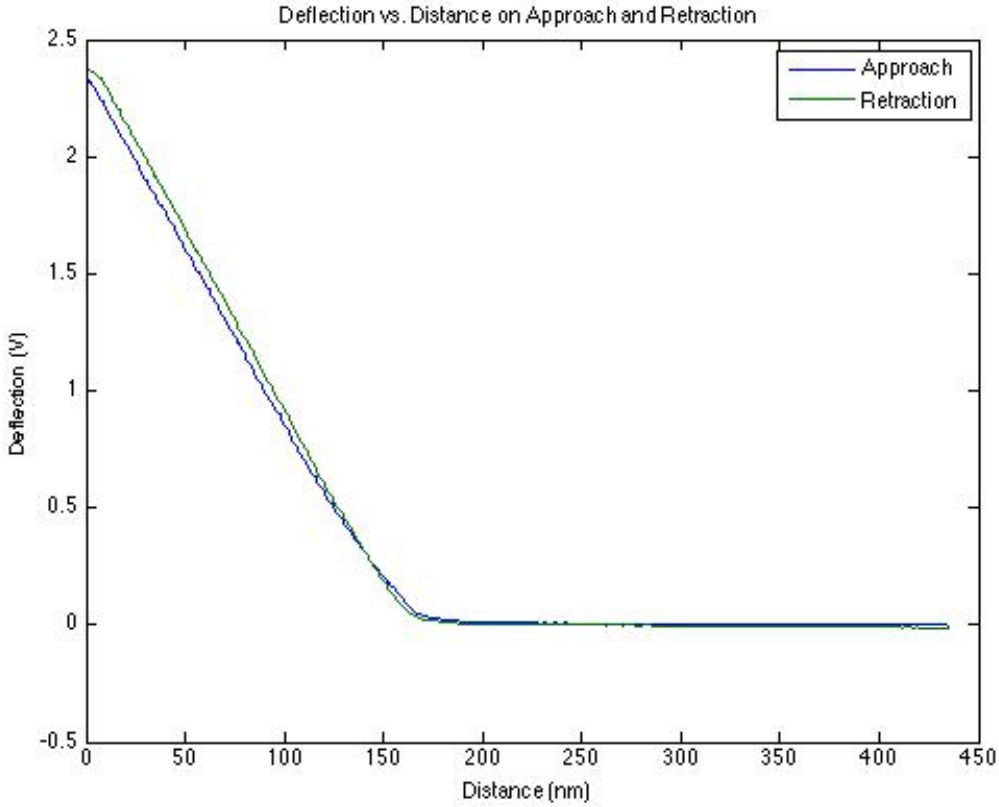
Deflection vs. Distance on Approach and Retraction
Approach
Retraction
Deflection (V)
Distance (nm)
2.5
2
1.5
1
0.5
0
-0.5
0
50
100
150
200
250
300
350
400
450

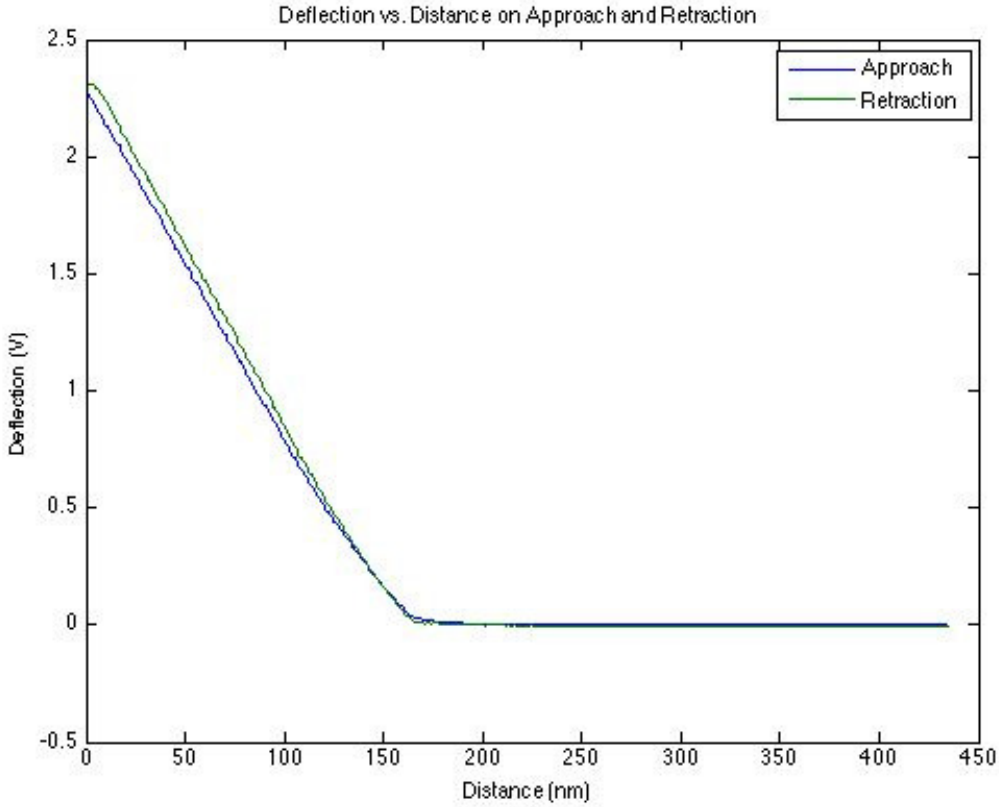
Deflection vs. Distance on Approach and Retraction
Approach
Retraction
Deflection (V)
Distance (nm)
2.5
2
1.5
1
0.5
0
-0.5
0
50
100
150
200
250
300
350
400
450

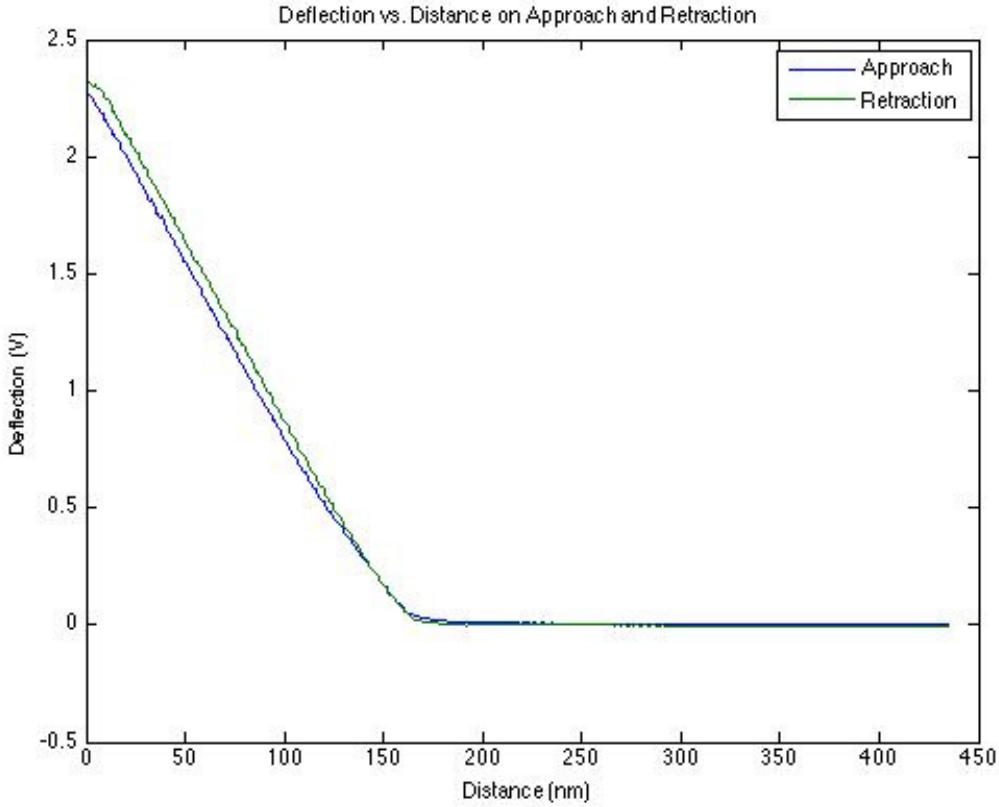
Deflection vs. Distance on Approach and Retraction
Approach
Retraction
Deflection (V)
Distance (nm)
2.5
2
1.5
1
0.5
0
-0.5
0
50
100
150
200
250
300
350
400
450

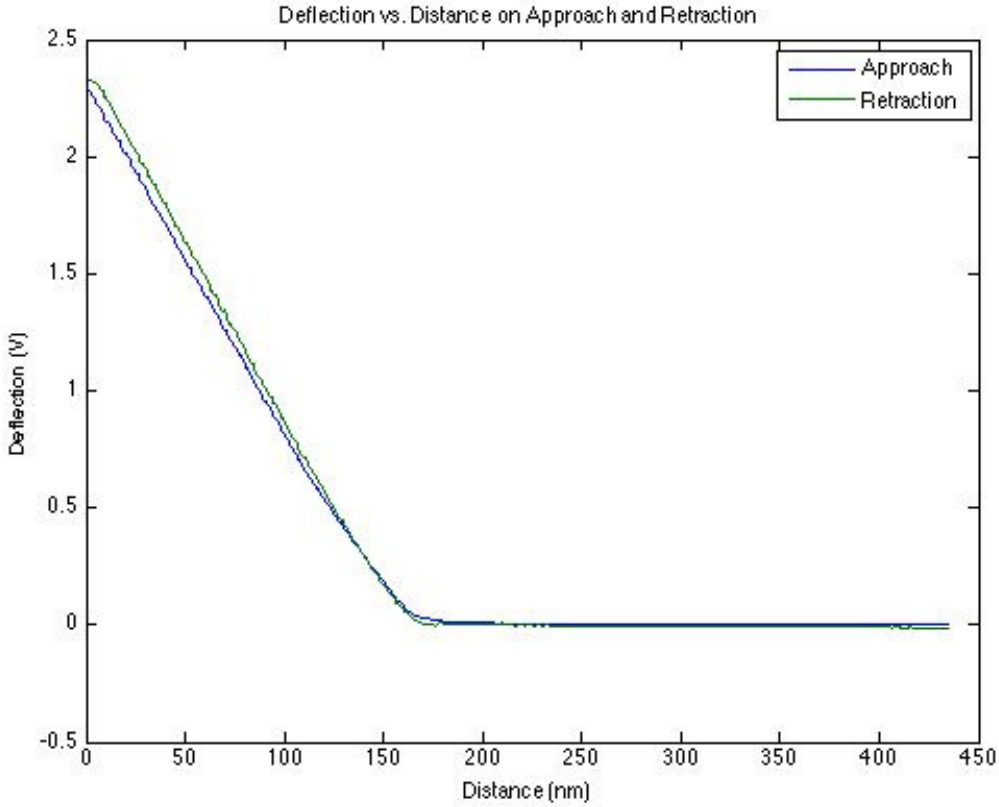
Deflection vs. Distance on Approach and Retraction
Approach
Retraction
Deflection (V)
Distance (nm)
2.5
2
1.5
1
0.5
0
-0.5
0
50
100
150
200
250
300
350
400
450

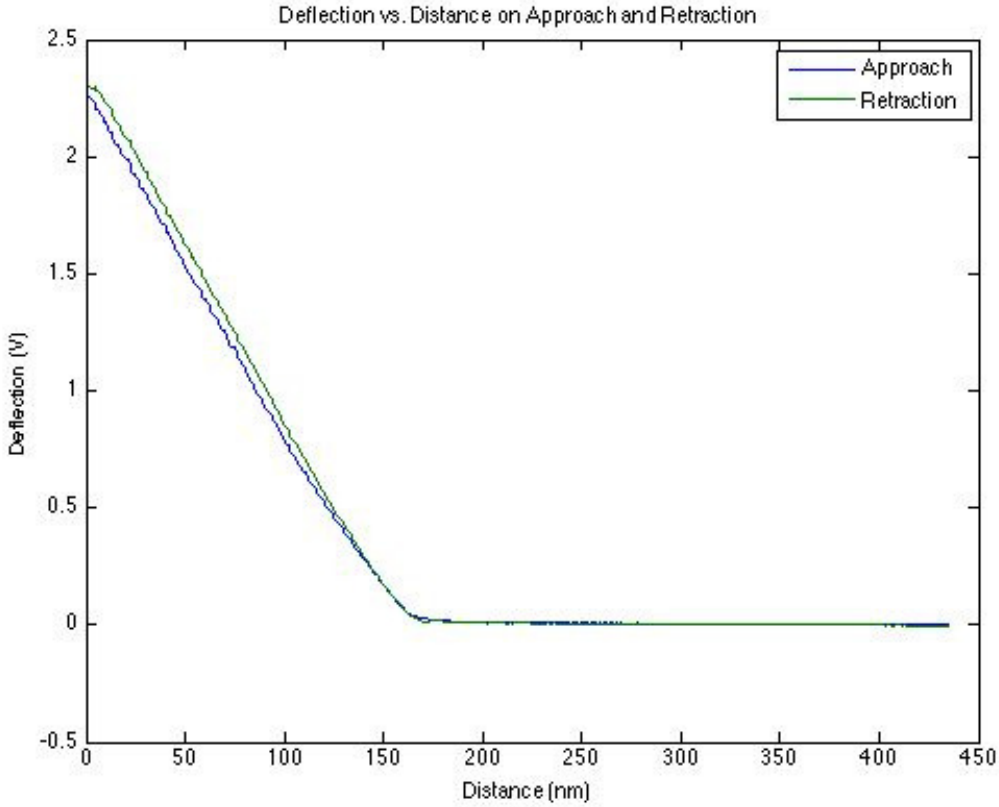
Deflection vs. Distance on Approach and Retraction
Approach
Retraction
Deflection (V)
Distance (nm)
2.5
2
1.5
1
0.5
0
-0.5
0
50
100
150
200
250
300
350
400
450

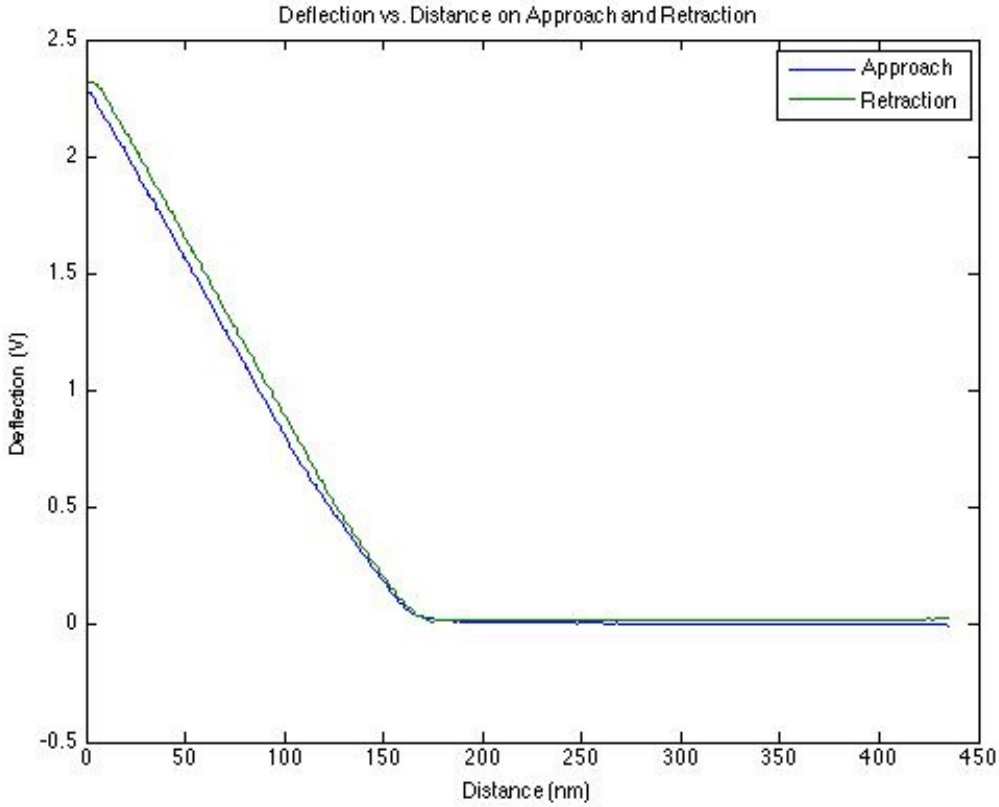
Deflection vs. Distance on Approach and Retraction
Approach
Retraction
Deflection (V)
Distance (nm)
2.5
2
1.5
1
0.5
0
-0.5
0
50
100
150
200
250
300
350
400
450

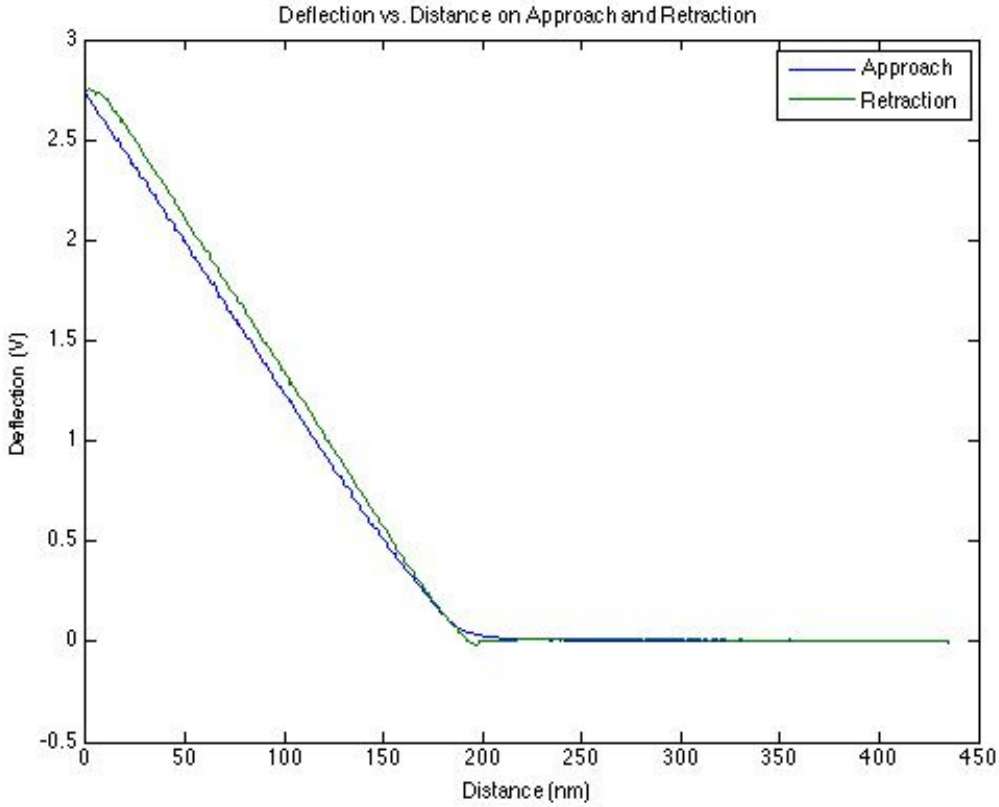
Deflection vs. Distance on Approach and Retraction
Approach
Retraction
Deflection (V)
Distance (nm)
3
2.5
2
1.5
1
0.5
0
-0.5
0
50
100
150
200
250
300
350
400
450

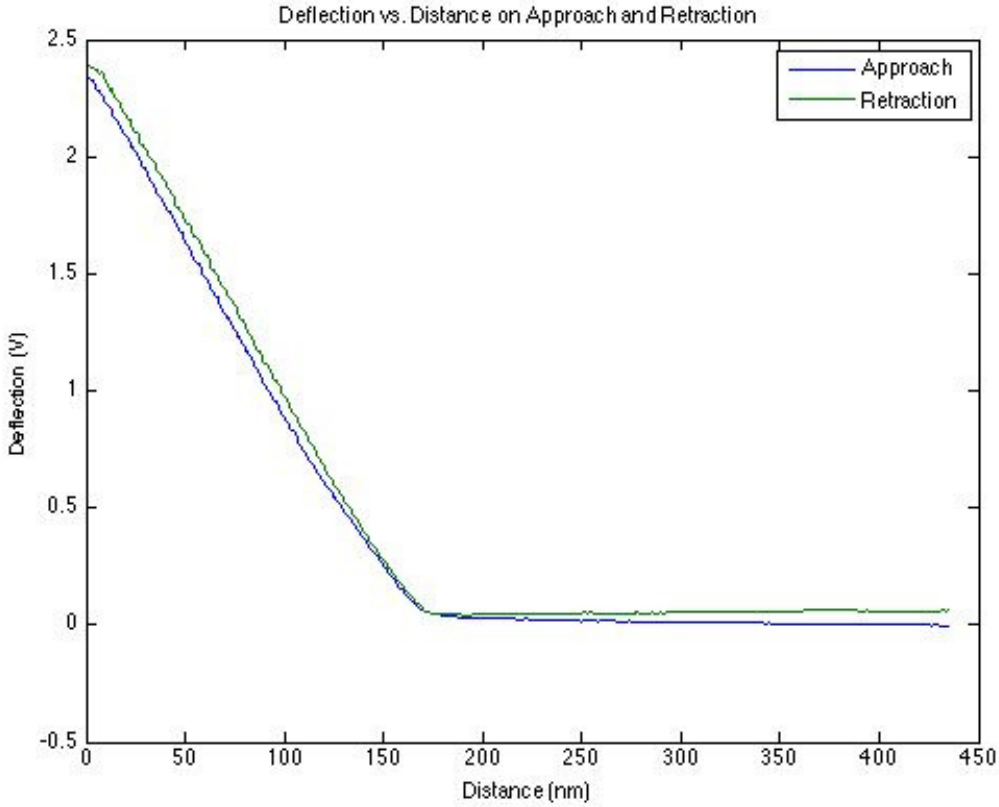
Deflection vs. Distance on Approach and Retraction
Approach
Retraction
Deflection (V)
Distance (nm)
2.5
2
1.5
1
0.5
0
-0.5
0
50
100
150
200
250
300
350
400
450

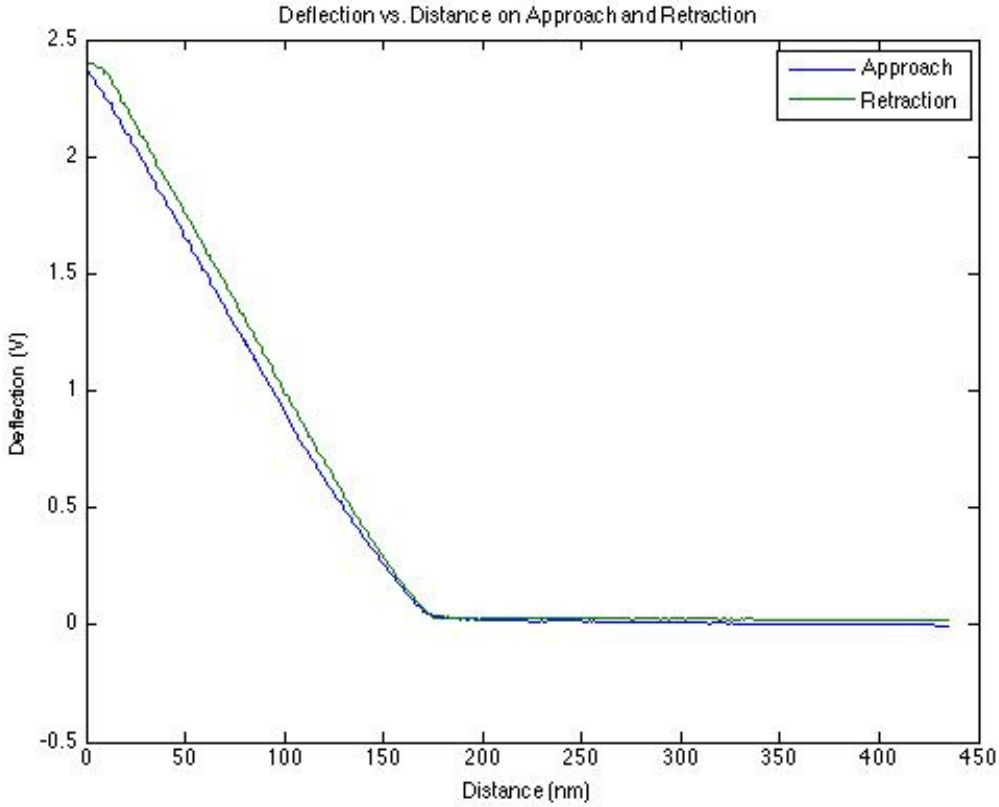
Deflection vs. Distance on Approach and Retraction
Approach
Retraction
Deflection (V)
Distance (nm)
2.5
2
1.5
1
0.5
0
-0.5
0
50
100
150
200
250
300
350
400
450

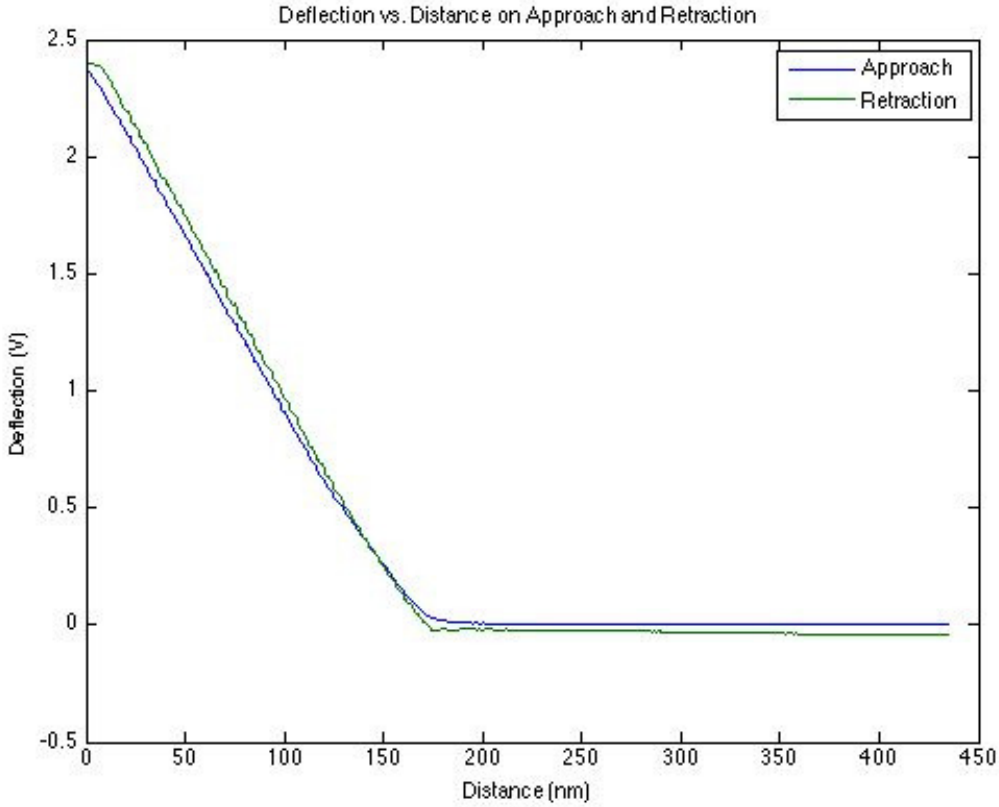
Deflection vs. Distance on Approach and Retraction
Approach
Retraction
Deflection (V)
Distance (nm)
2.5
2
1.5
1
0.5
0
-0.5
0
50
100
150
200
250
300
350
400
450

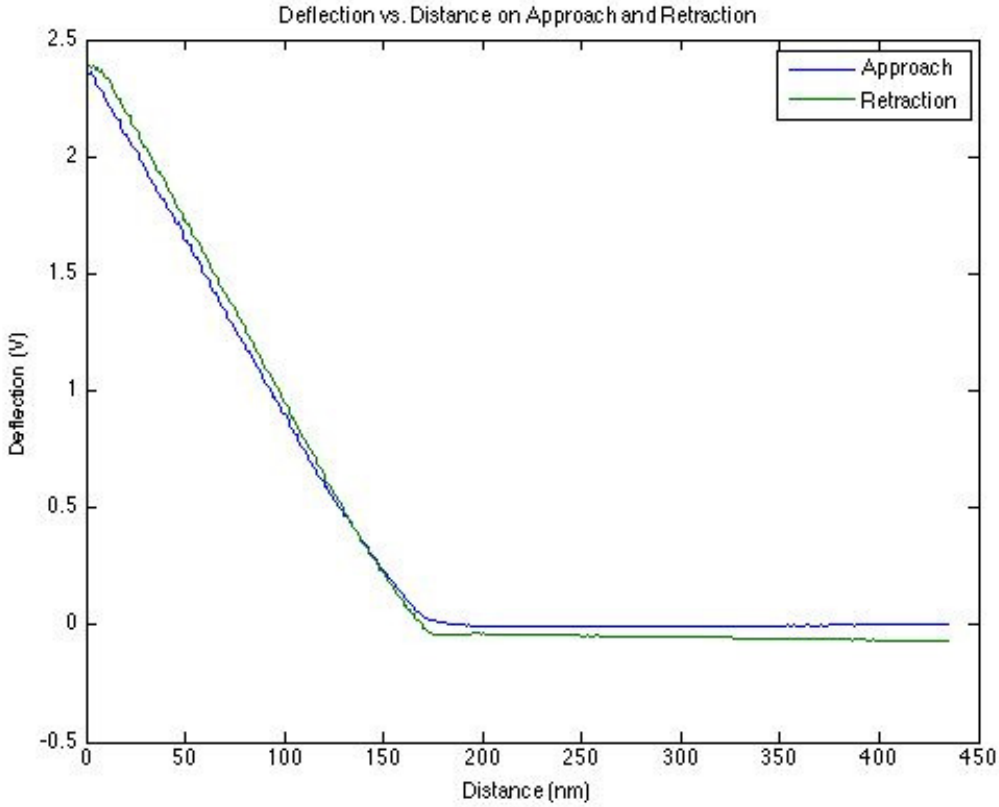
Deflection vs. Distance on Approach and Retraction
Approach
Retraction
Deflection (V)
Distance (nm)
2.5
2
1.5
1
0.5
0
-0.5
0
50
100
150
200
250
300
350
400
450

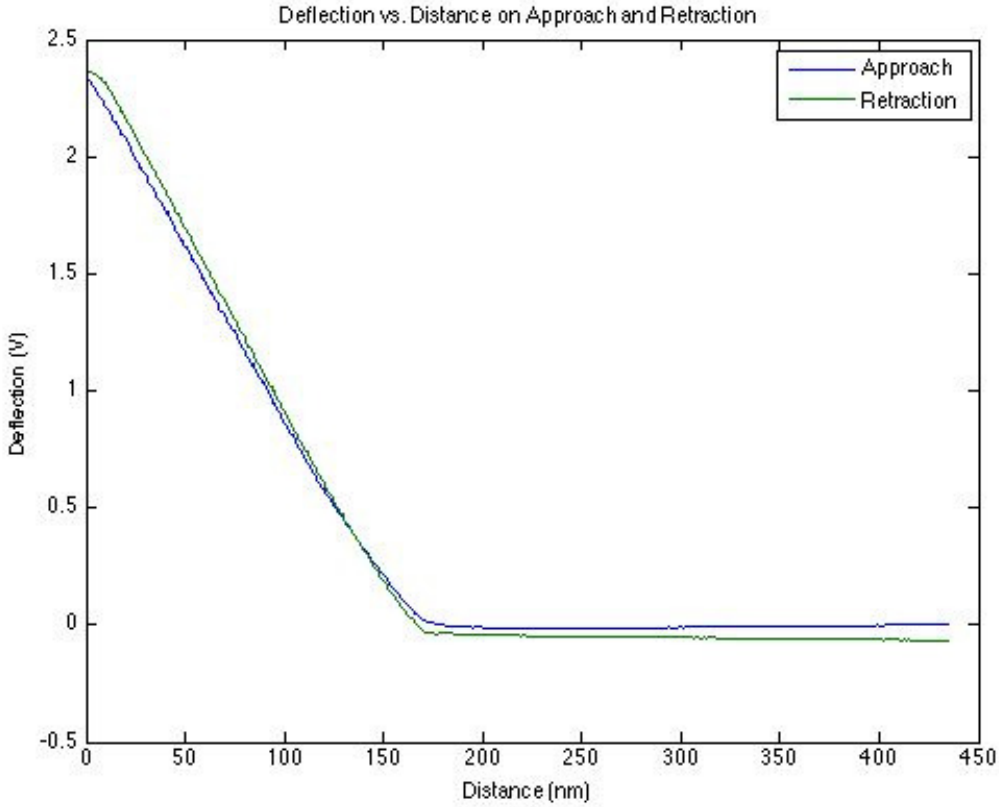
Deflection vs. Distance on Approach and Retraction
Approach
Retraction
Deflection (V)
Distance (nm)
2.5
2
1.5
1
0.5
0
-0.5
0
50
100
150
200
250
300
350
400
450

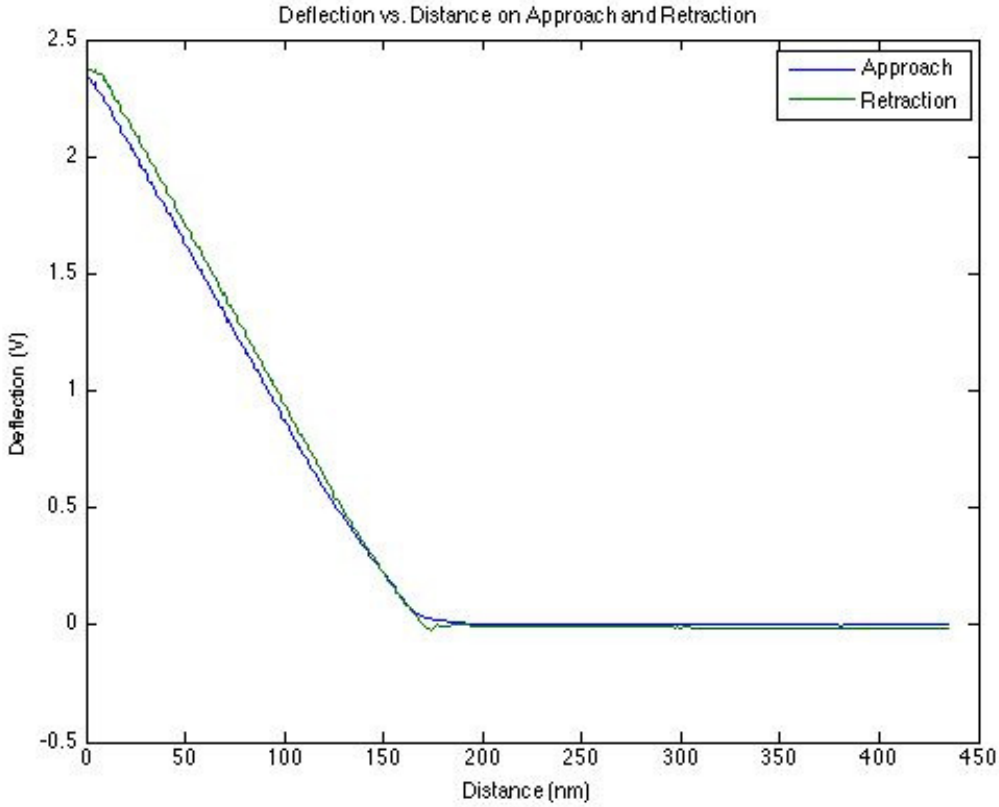
Deflection vs. Distance on Approach and Retraction
Approach
Retraction
Deflection (V)
Distance (nm)
2.5
2
1.5
1
0.5
0
-0.5
0
50
100
150
200
250
300
350
400
450

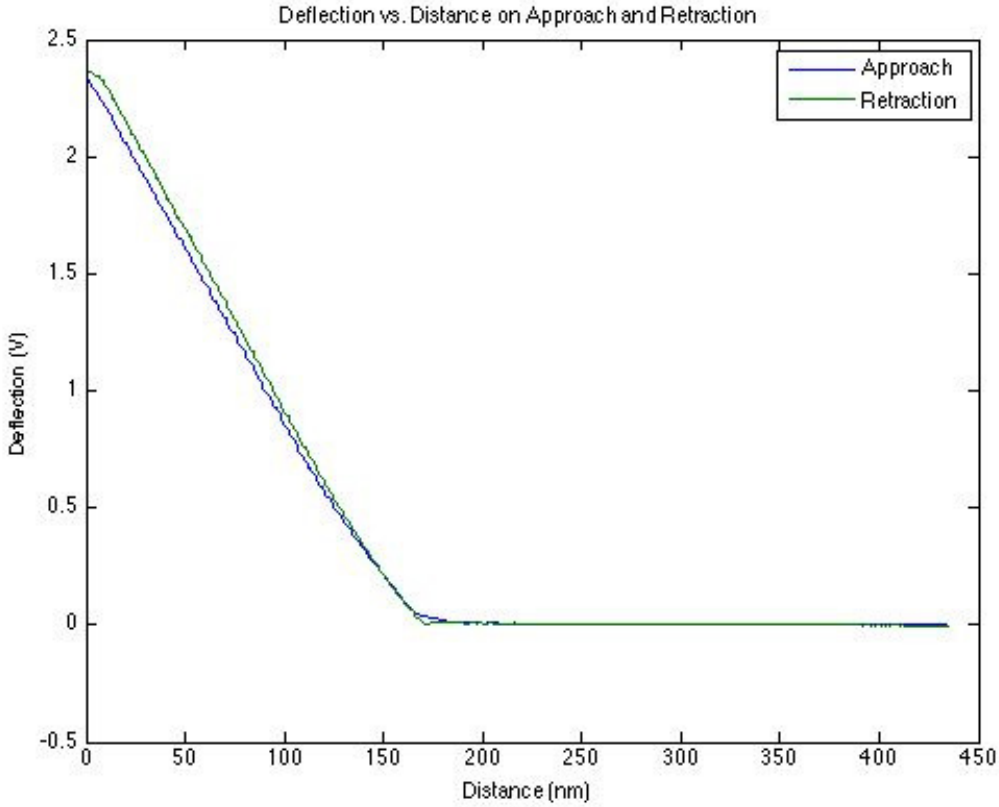
Deflection vs. Distance on Approach and Retraction
Approach
Retraction
Deflection (V)
Distance (nm)
2.5
2
1.5
1
0.5
0
-0.5
0
50
100
150
200
250
300
350
400
450

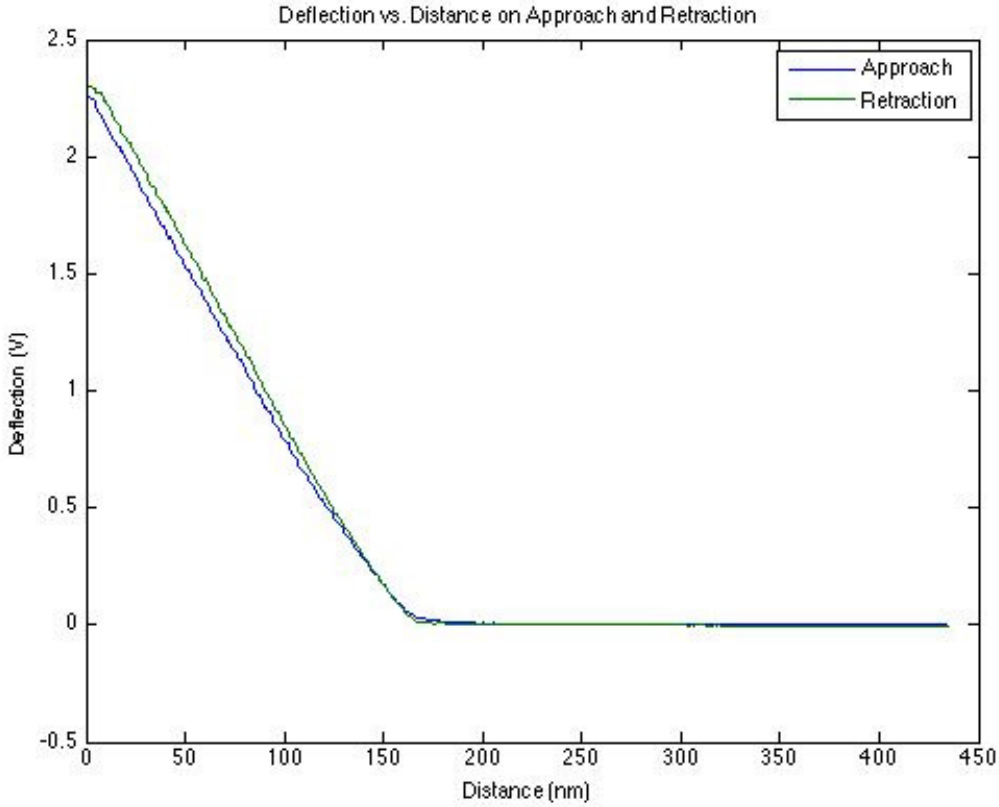
Deflection vs. Distance on Approach and Retraction
Approach
Retraction
Deflection (V)
Distance (nm)
2.5
2
1.5
1
0.5
0
-0.5
0
50
100
150
200
250
300
350
400
450

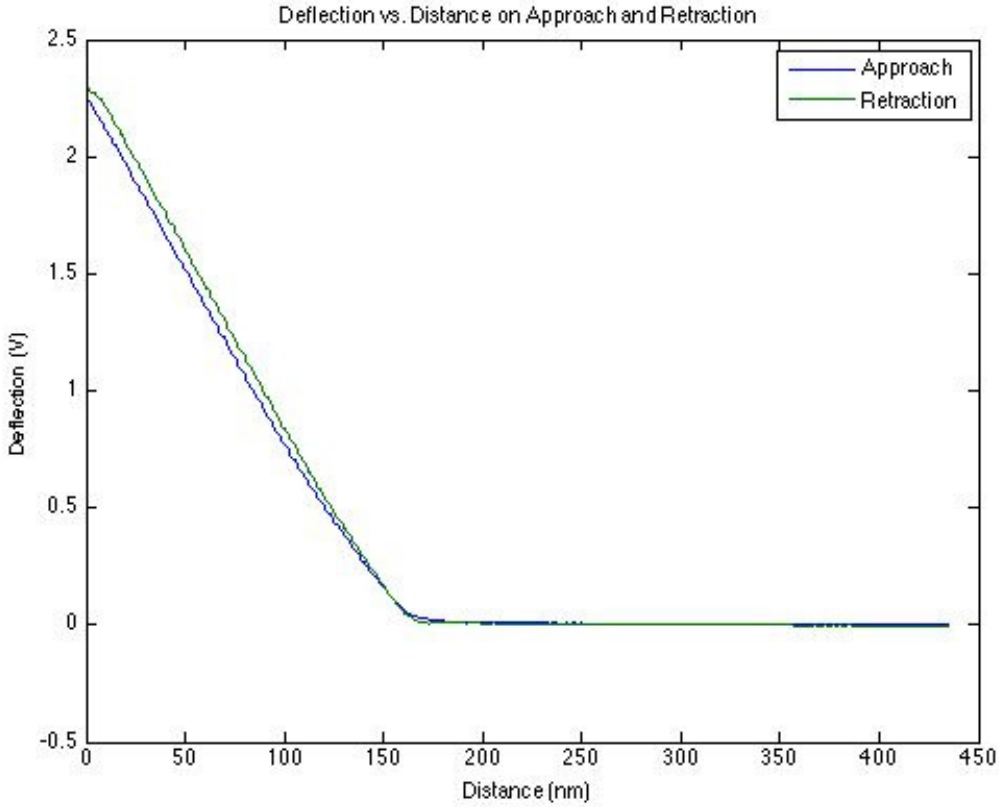
Deflection vs. Distance on Approach and Retraction
Approach
Retraction
Deflection (V)
Distance (nm)
2.5
2
1.5
1
0.5
0
-0.5
0
50
100
150
200
250
300
350
400
450

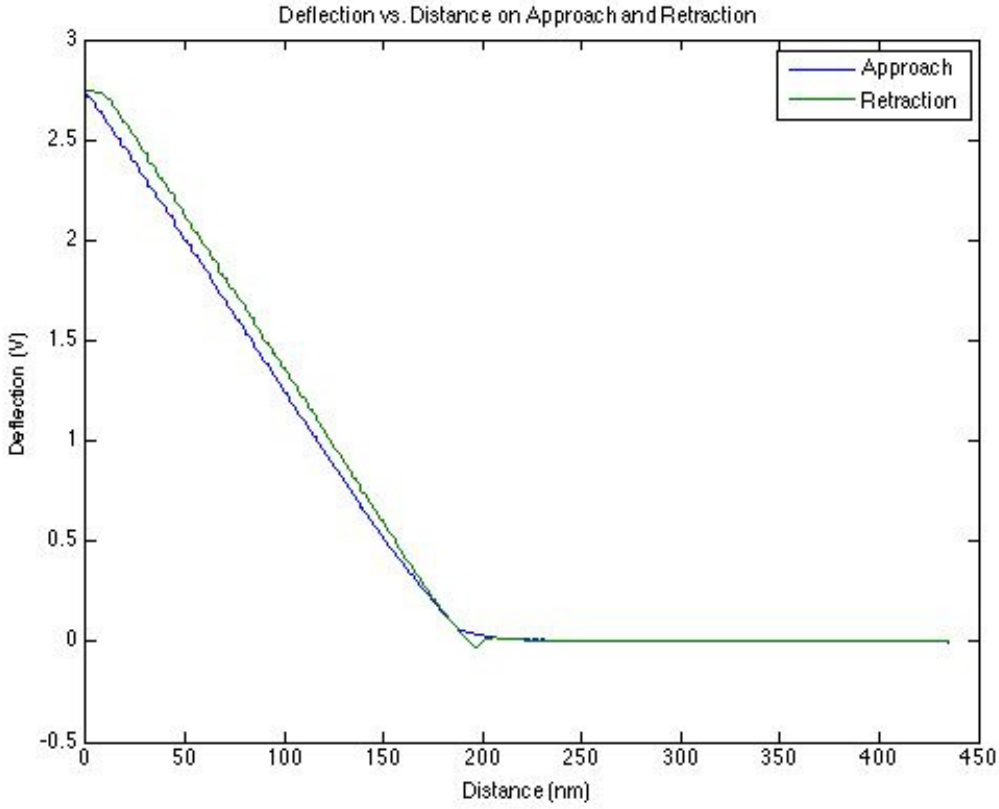
Deflection vs. Distance on Approach and Retraction
Approach
Retraction
Deflection (V)
Distance (nm)
3
2.5
2
1.5
1
0.5
0
-0.5
0
50
100
150
200
250
300
350
400
450

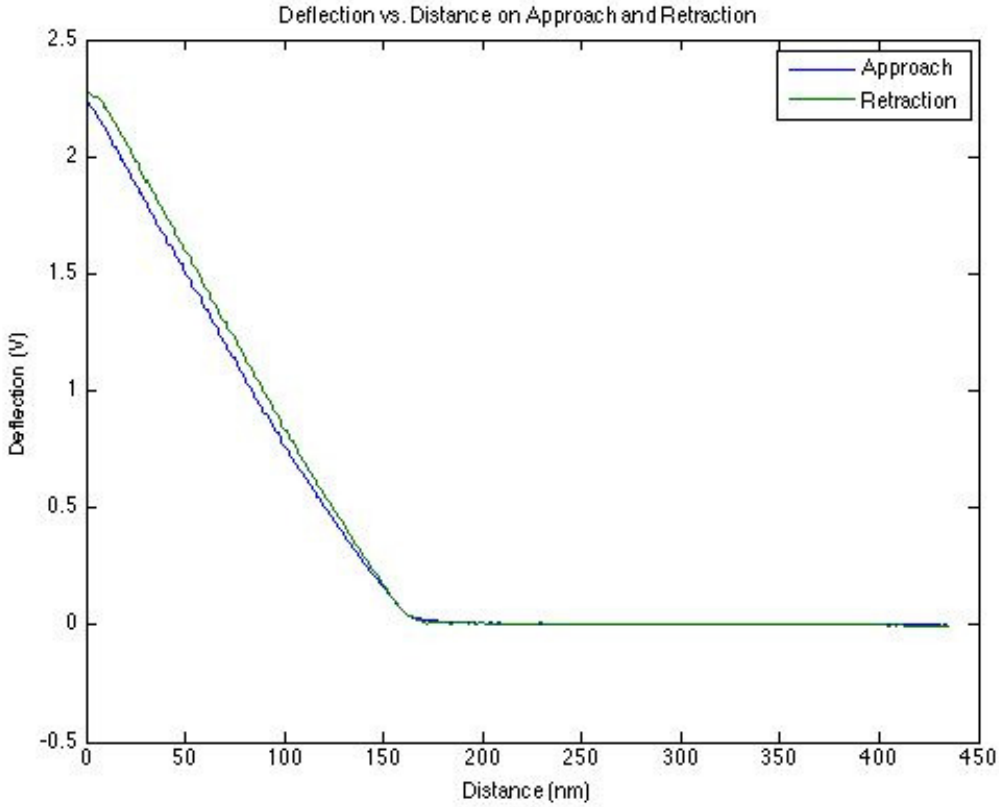
Deflection vs. Distance on Approach and Retraction
Approach
Retraction
Deflection (V)
Distance (nm)
2.5
2
1.5
1
0.5
0
-0.5
0
50
100
150
200
250
300
350
400
450

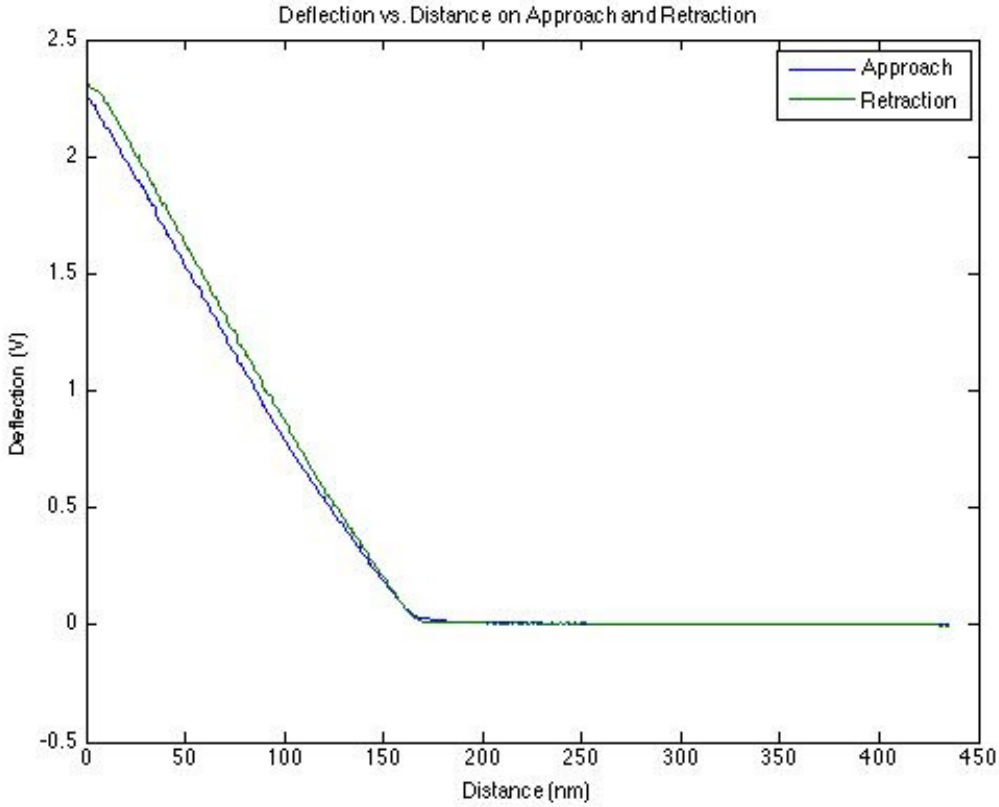
Deflection vs. Distance on Approach and Retraction
Approach
Retraction
Deflection (V)
Distance (nm)
2.5
2
1.5
1
0.5
0
-0.5
0
50
100
150
200
250
300
350
400
450

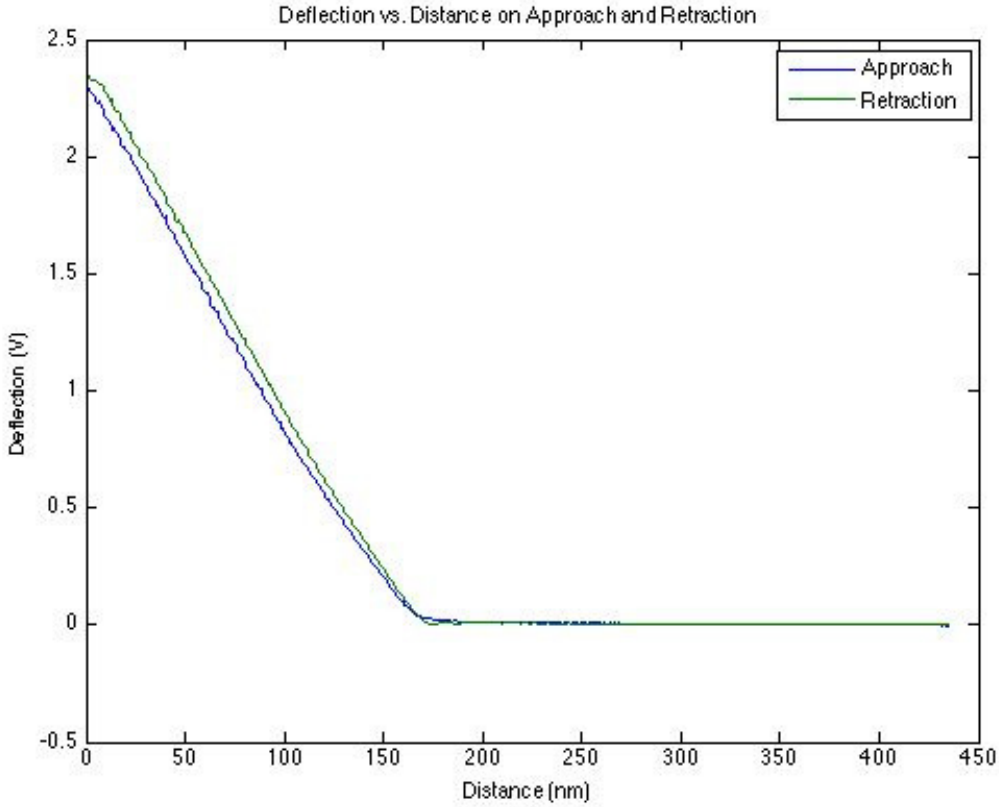
Deflection vs. Distance on Approach and Retraction
Approach
Retraction
Deflection (V)
Distance (nm)
2.5
2
1.5
1
0.5
0
-0.5
0
50
100
150
200
250
300
350
400
450

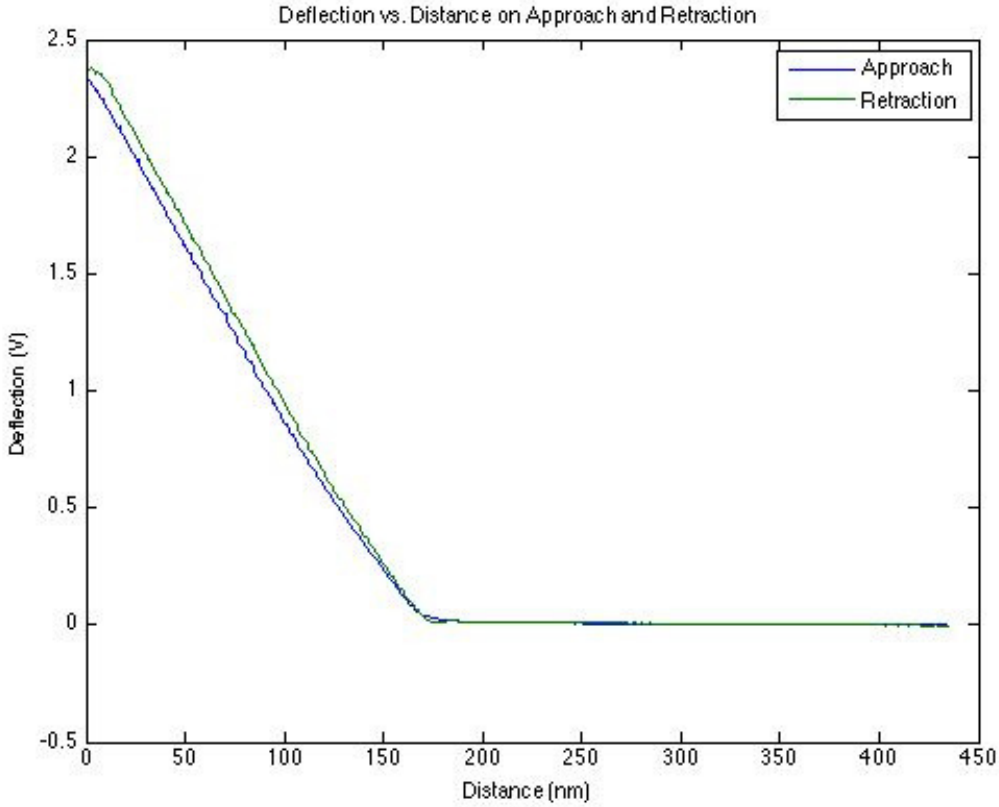
Deflection vs. Distance on Approach and Retraction
Approach
Retraction
Deflection (V)
Distance (nm)
2.5
2
1.5
1
0.5
0
-0.5
0
50
100
150
200
250
300
350
400
450

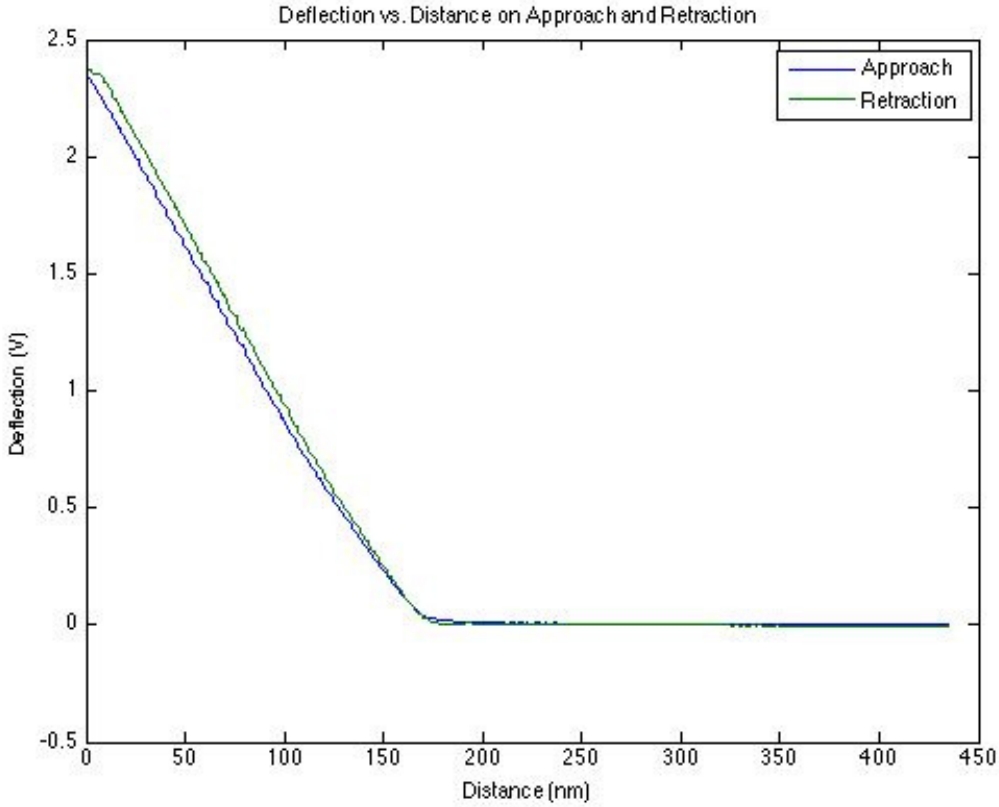
Deflection vs. Distance on Approach and Retraction
Approach
Retraction
Deflection (V)
Distance (nm)
2.5
2
1.5
1
0.5
0
-0.5
0
50
100
150
200
250
300
350
400
450

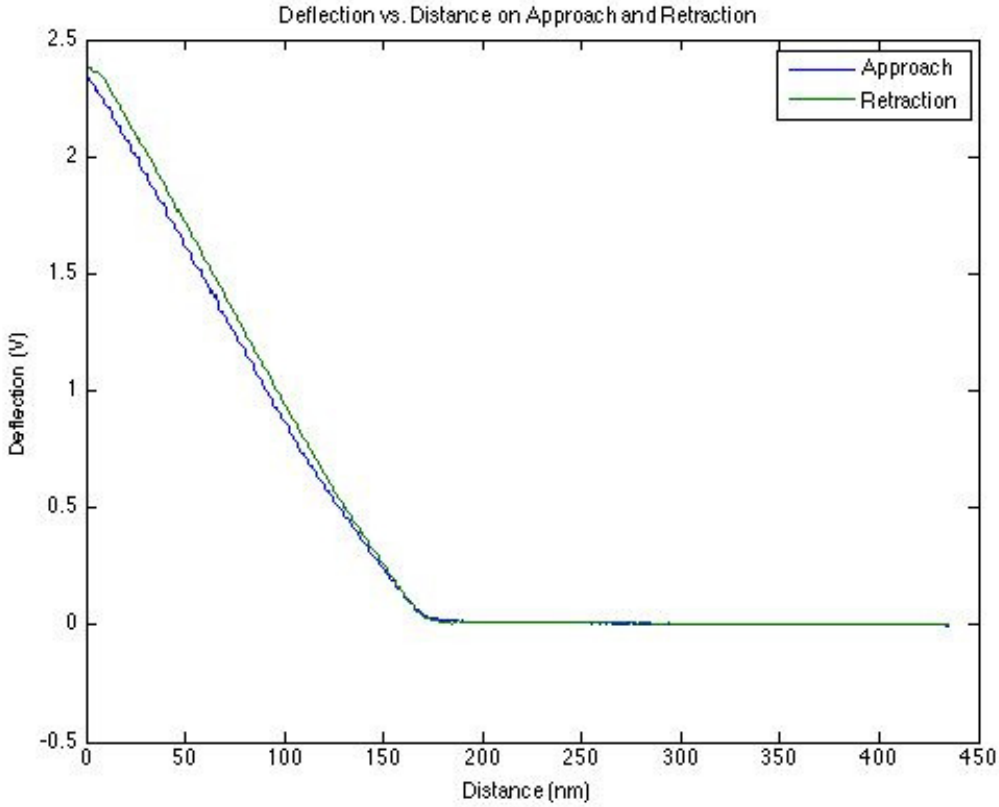
Deflection vs. Distance on Approach and Retraction
Approach
Retraction
Deflection (V)
Distance (nm)
2.5
2
1.5
1
0.5
0
-0.5
0
50
100
150
200
250
300
350
400
450

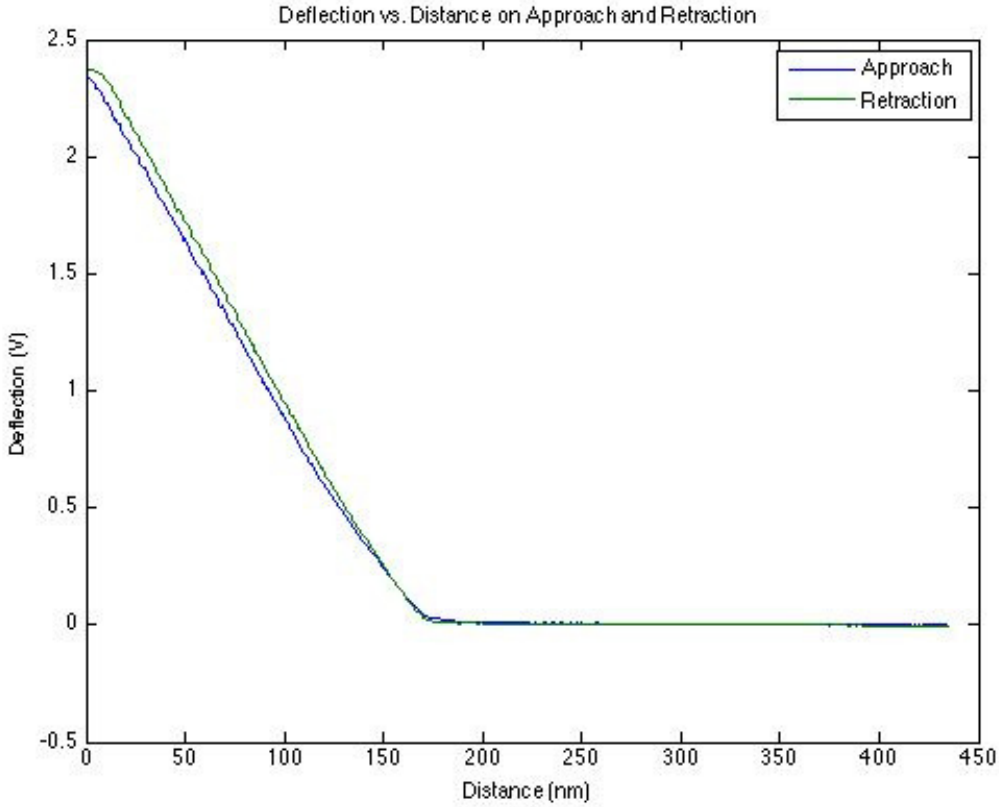
Deflection vs. Distance on Approach and Retraction
Approach
Retraction
Deflection (V)
Distance (nm)
2.5
2
1.5
1
0.5
0
-0.5
0
50
100
150
200
250
300
350
400
450

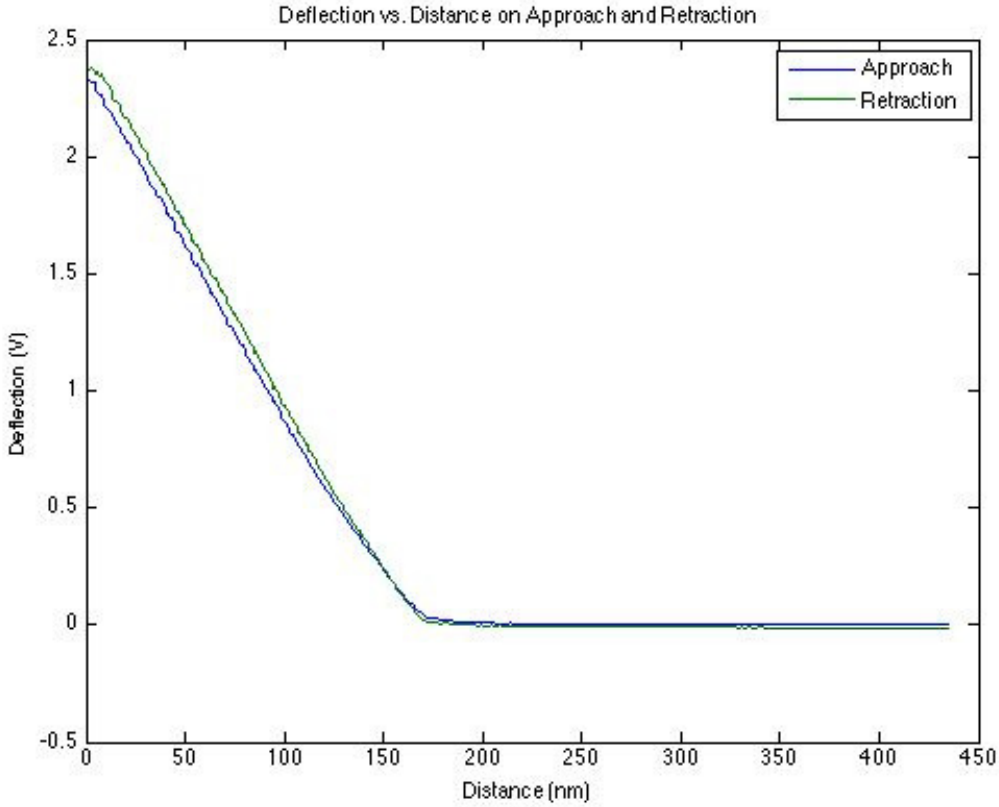
Deflection vs. Distance on Approach and Retraction
Approach
Retraction
Deflection (V)
Distance (nm)
2.5
2
1.5
1
0.5
0
-0.5
0
50
100
150
200
250
300
350
400
450

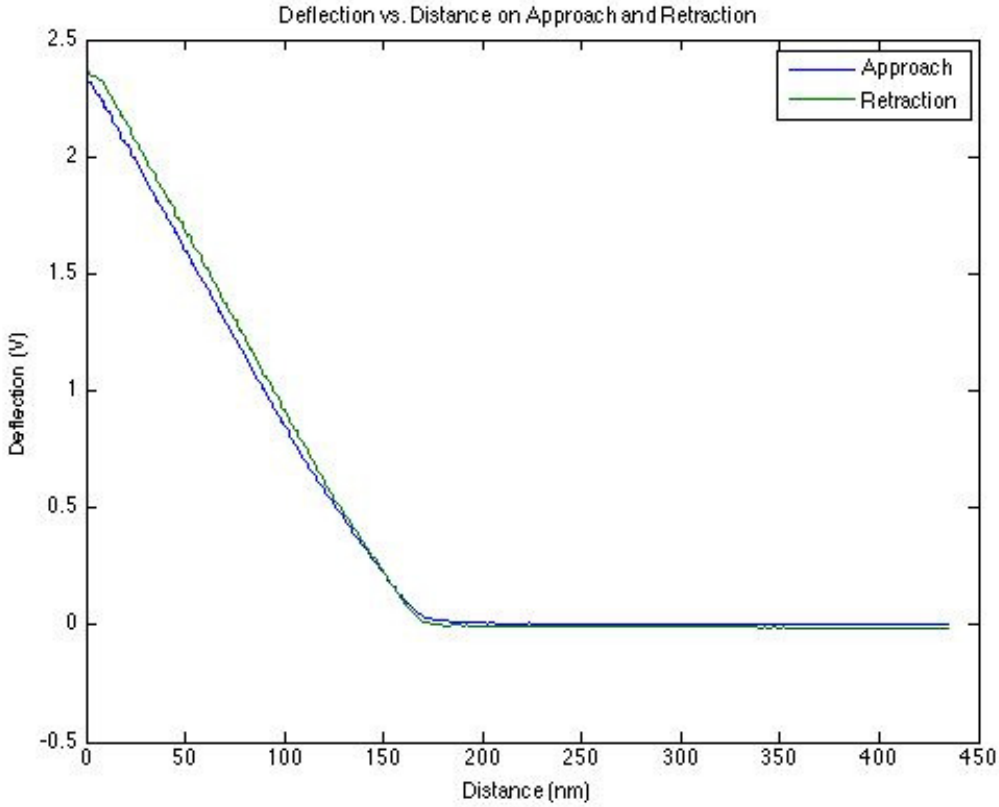
Deflection vs. Distance on Approach and Retraction
Approach
Retraction
Deflection (V)
Distance (nm)
2.5
2
1.5
1
0.5
0
-0.5
0
50
100
150
200
250
300
350
400
450

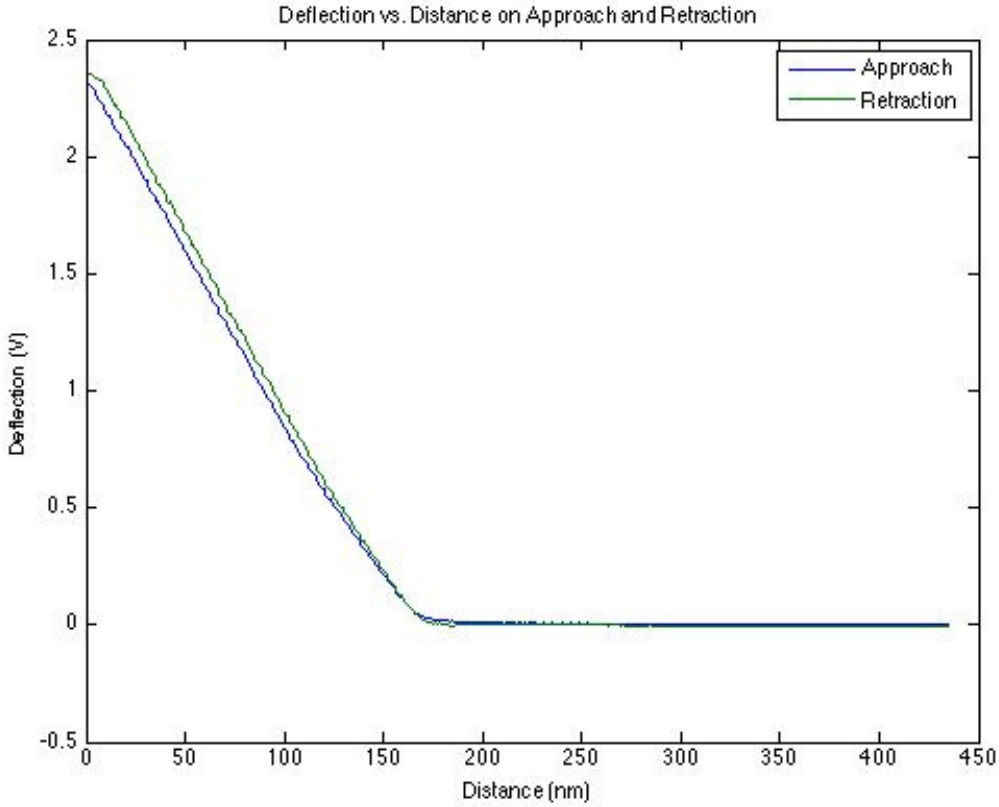
Deflection vs. Distance on Approach and Retraction
Approach
Retraction
Deflection (V)
Distance (nm)
2.5
2
1.5
1
0.5
0
-0.5
0
50
100
150
200
250
300
350
400
450

Appendix D

PEI Removal
Deflection-Distance Curves

The deflection-distance curves contained in this section were obtained using the uncoated glass probe and an uncoated mica substrate in an aqueous environment. These experiments served as control tests to test the use of the UV/ozone cleaner for PEI removal.

Before PEI Application

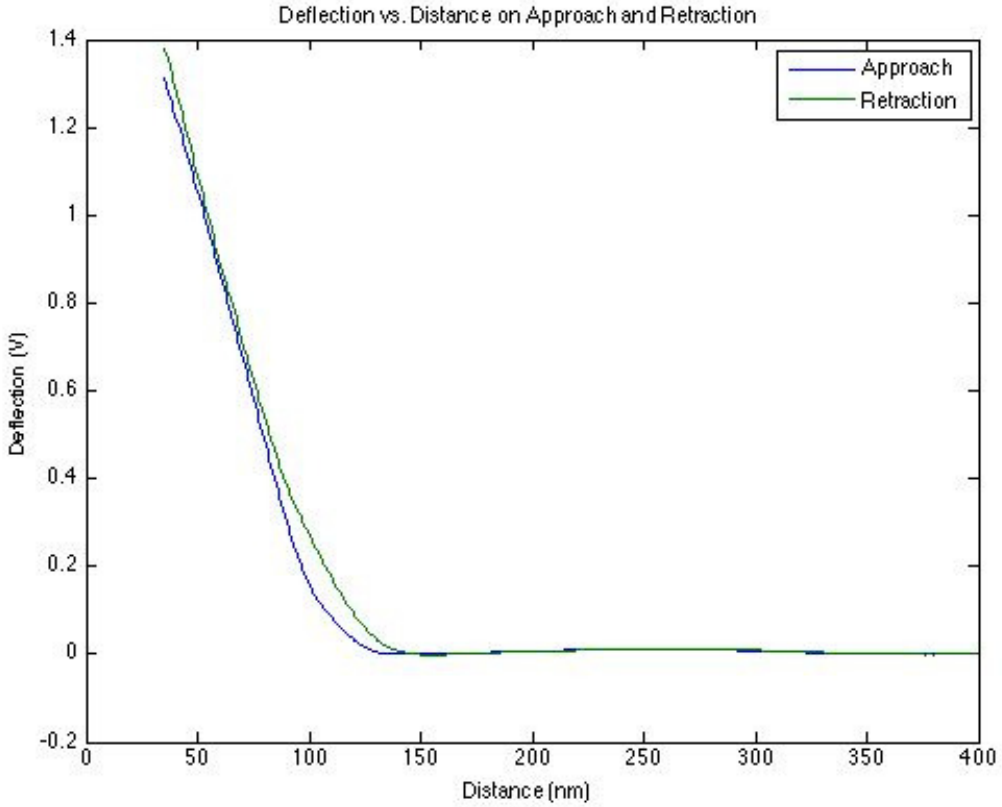

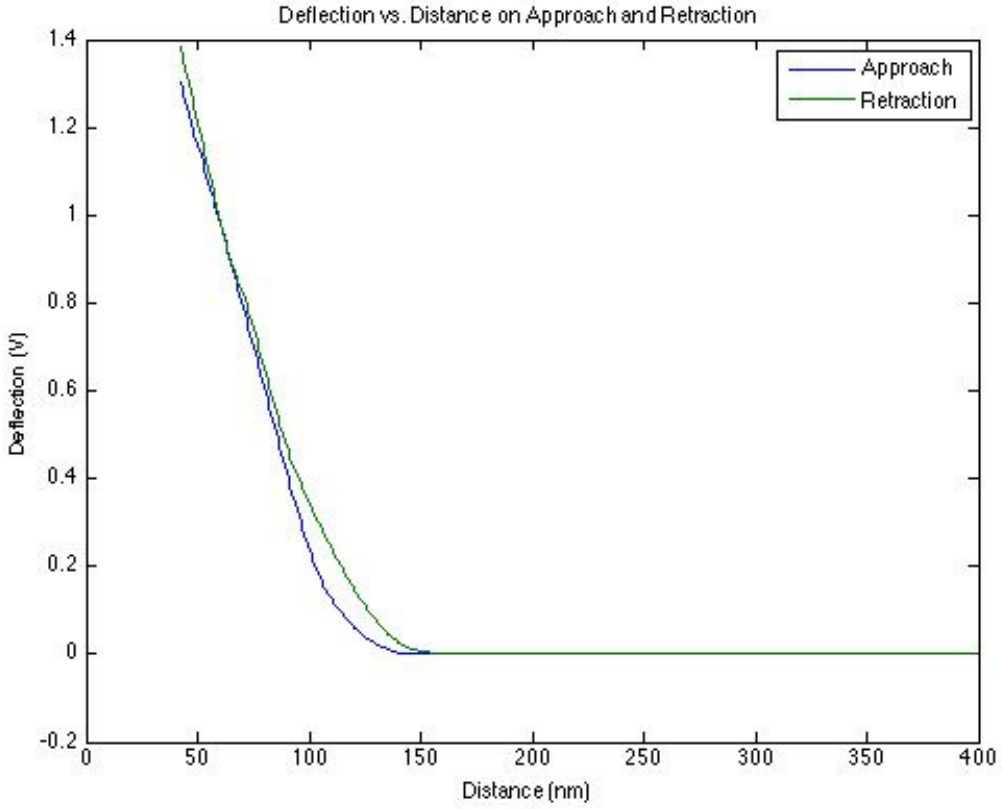

Before PEI Application

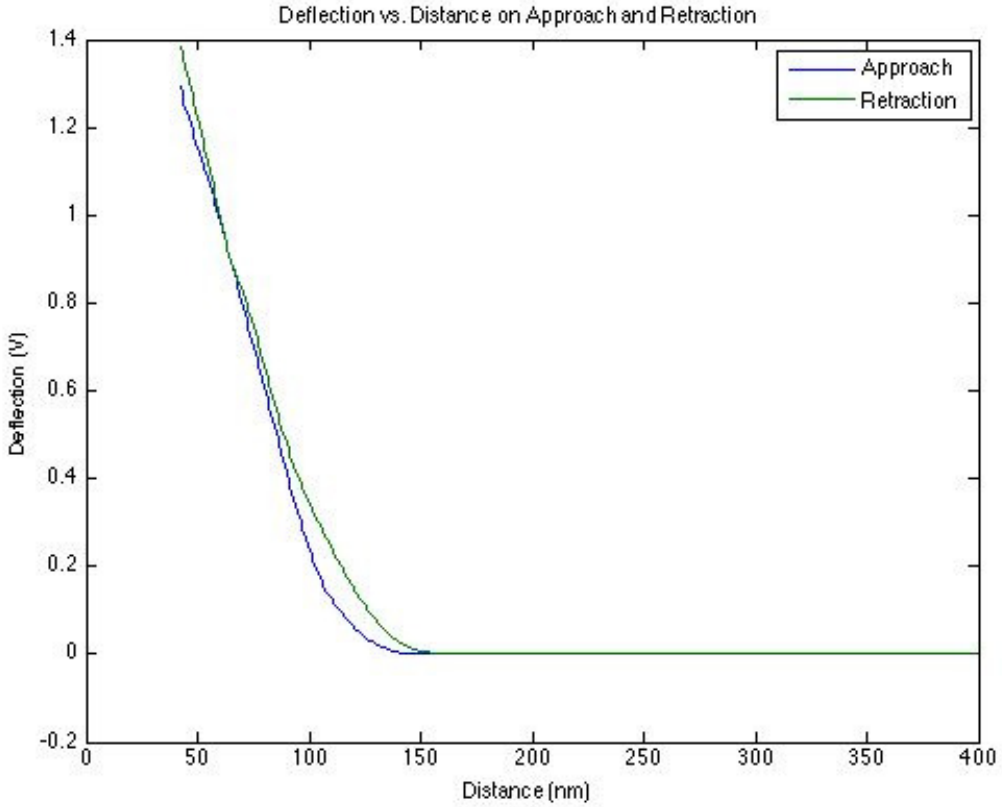

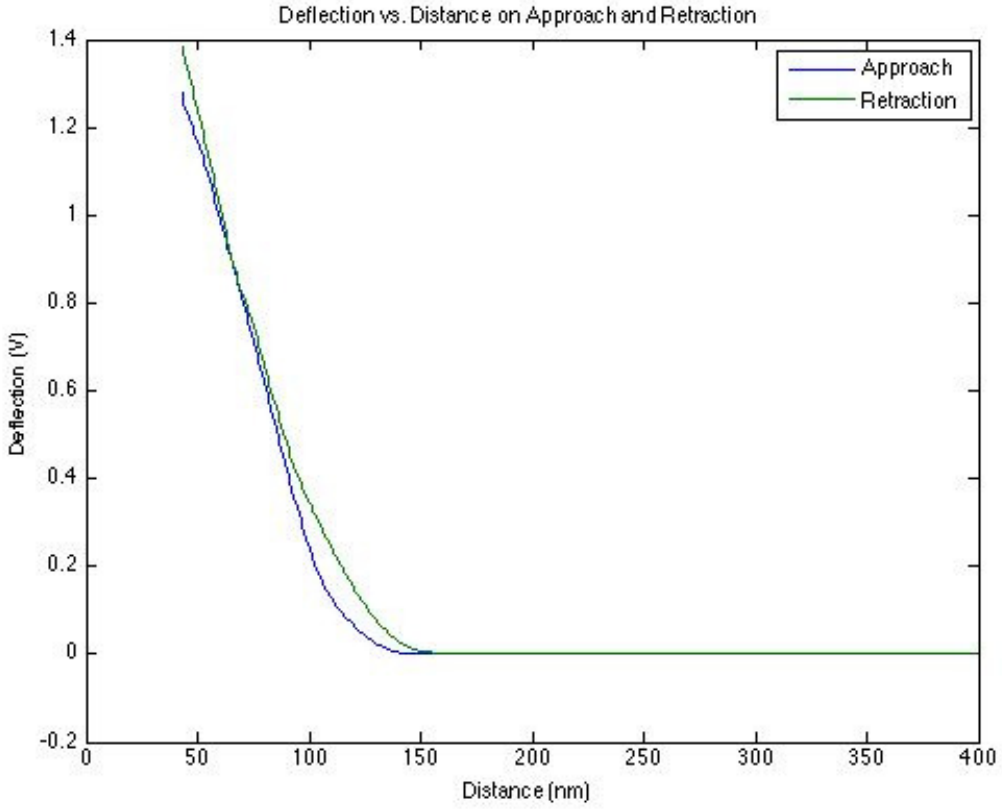

Before PEI Application

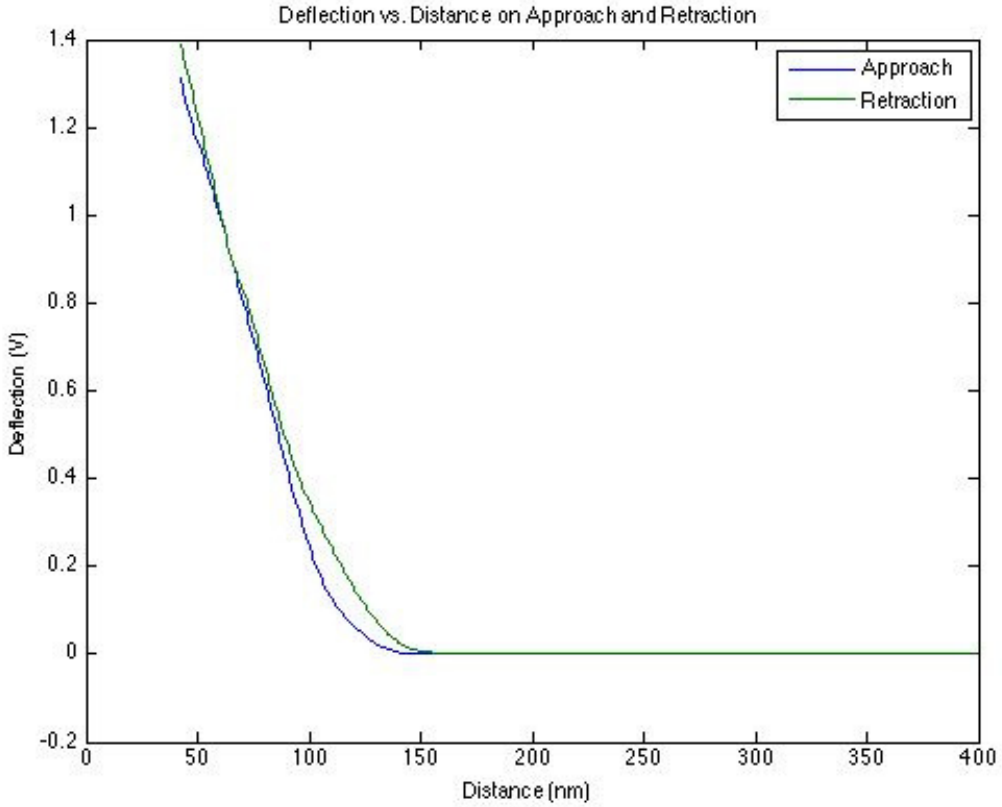

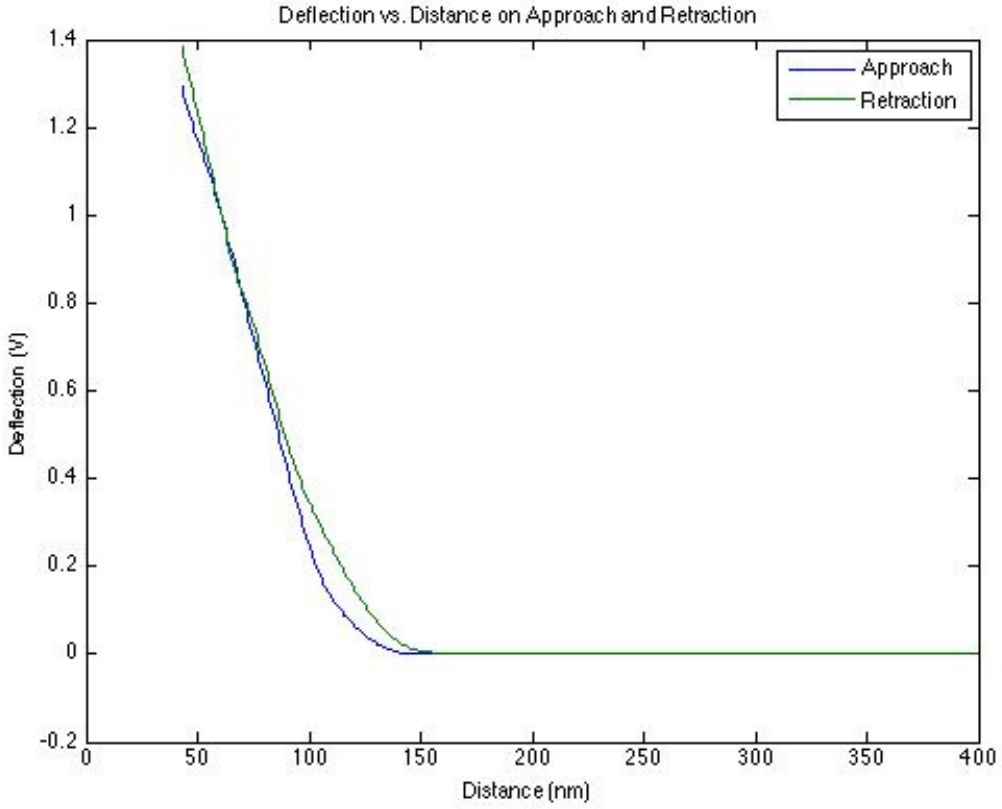

Before PEI Application

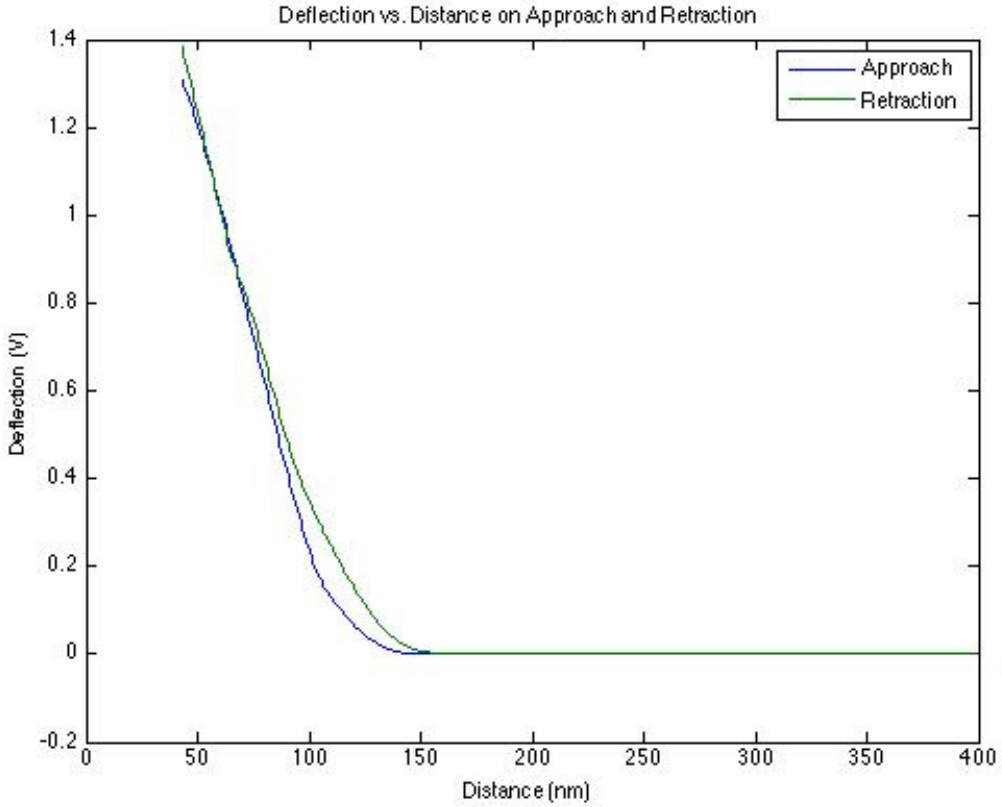

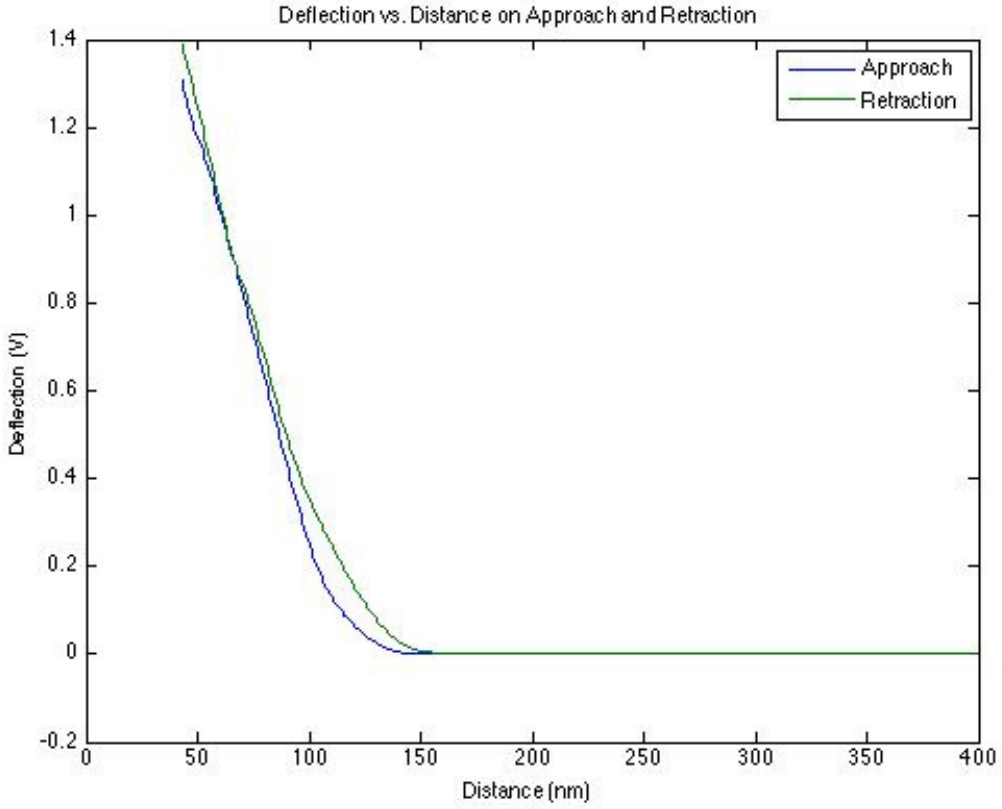

Before PEI Application

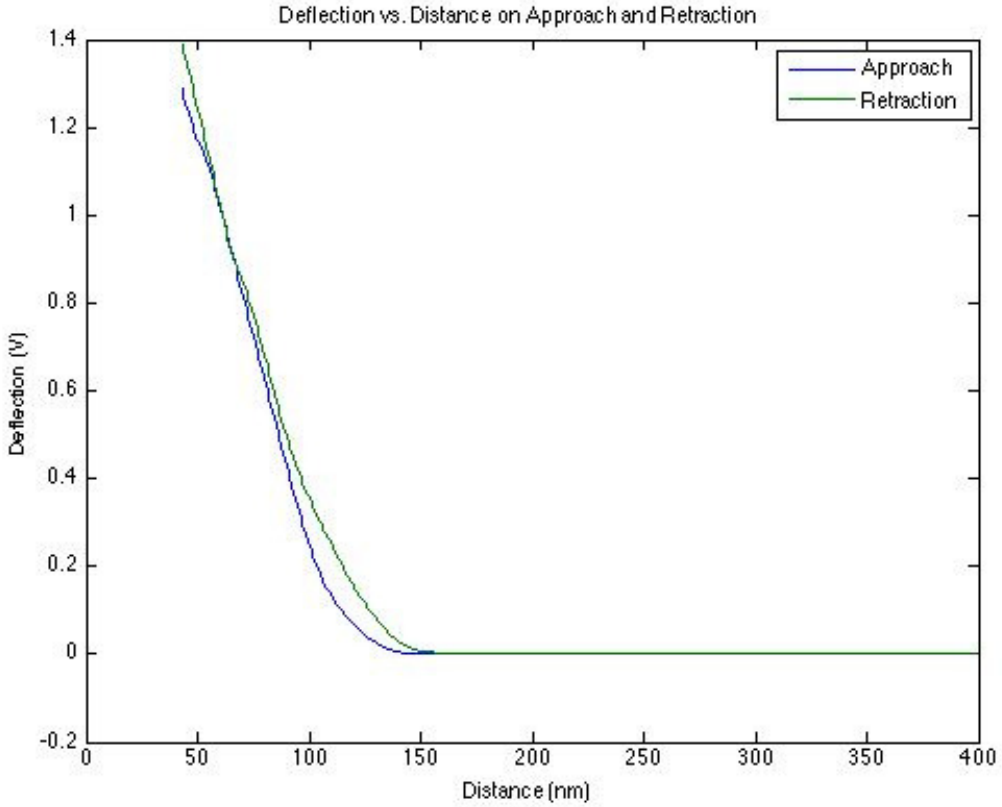

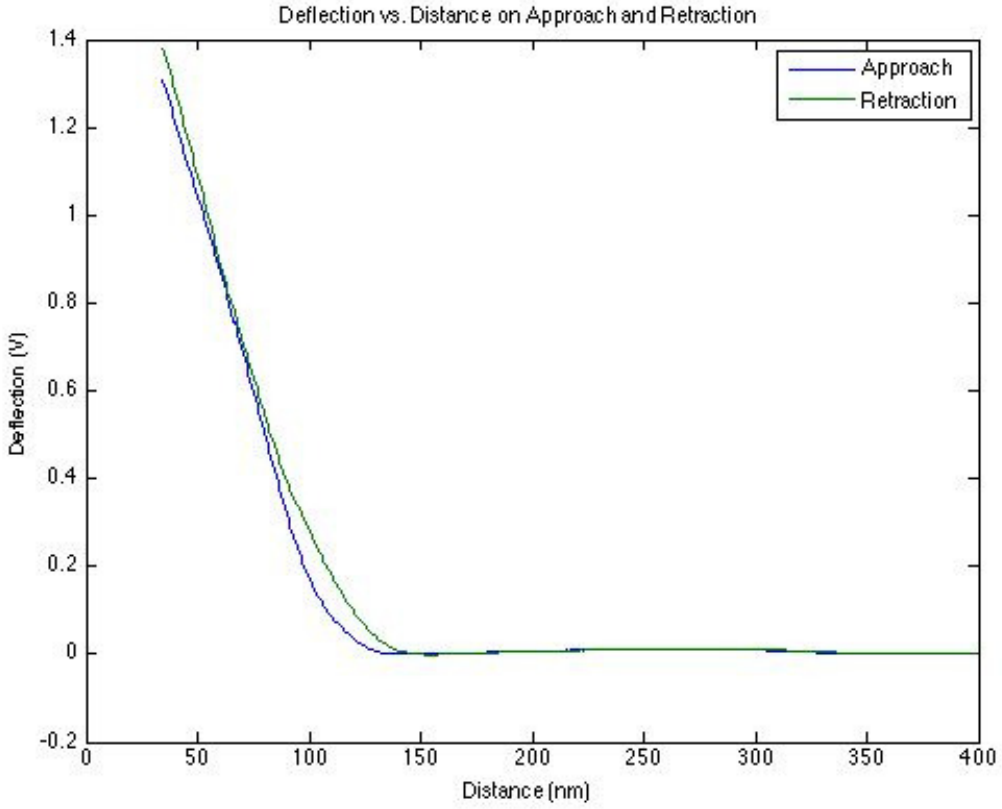

Before PEI Application

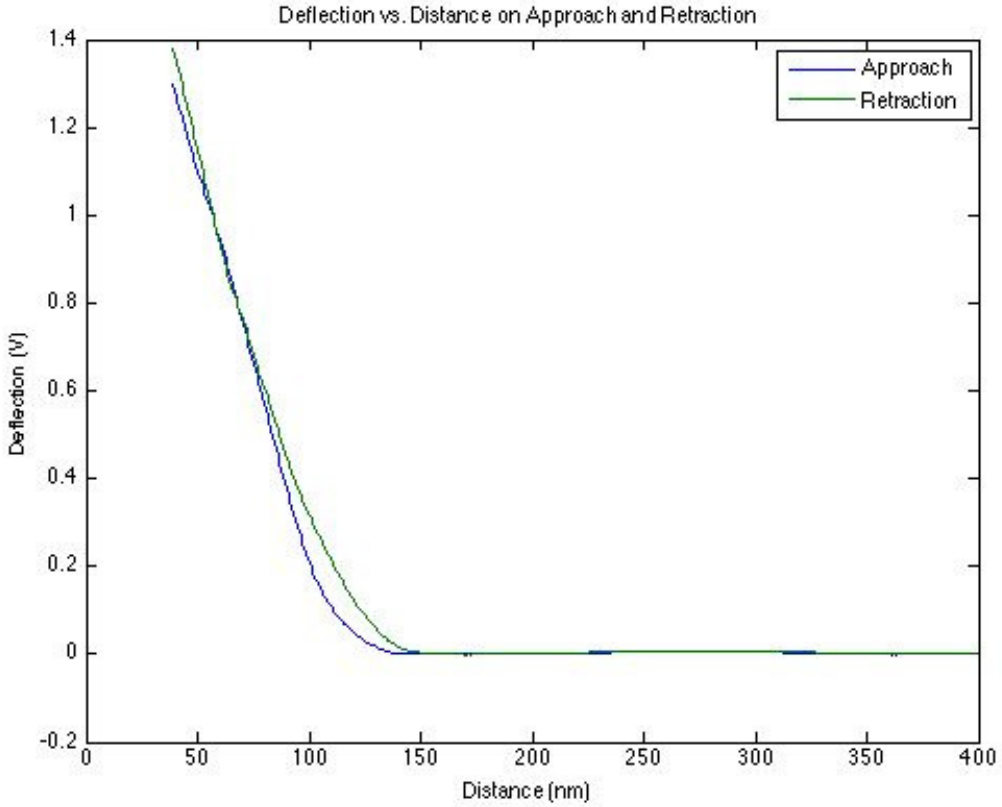

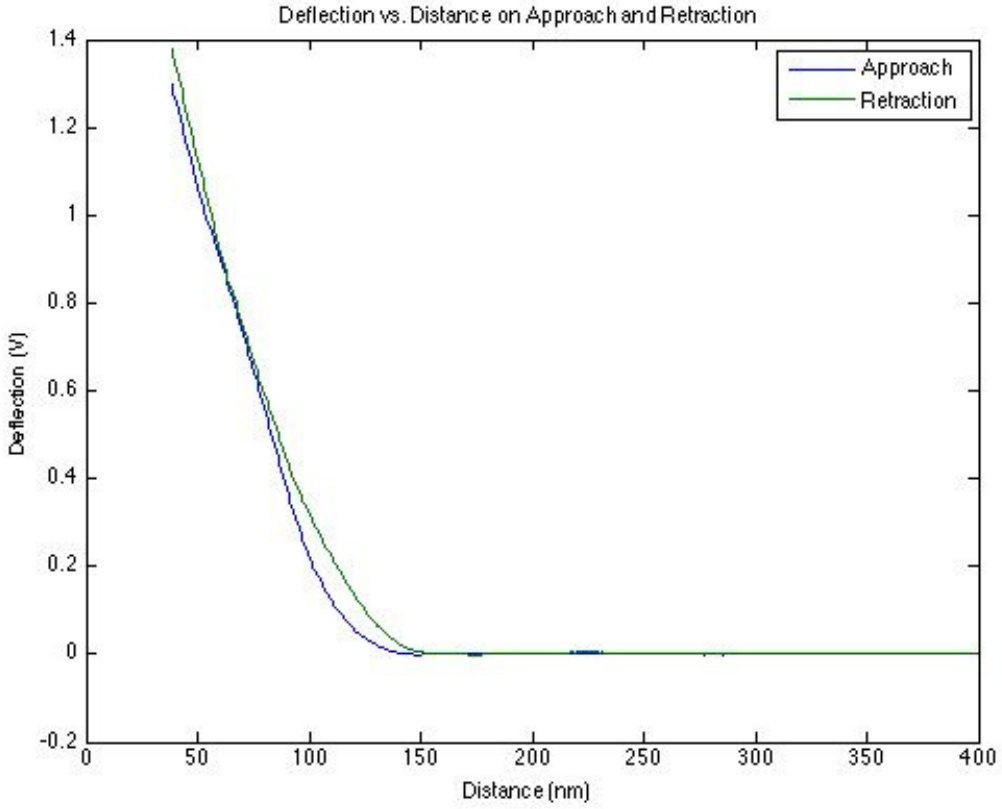

Before PEI Application

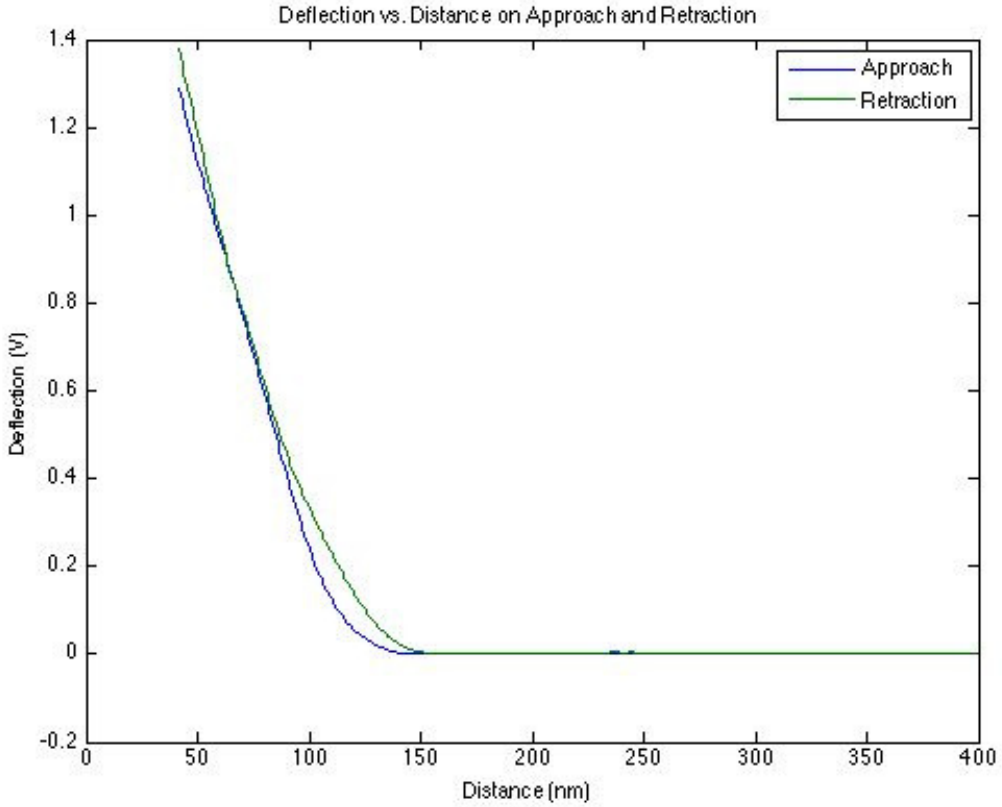

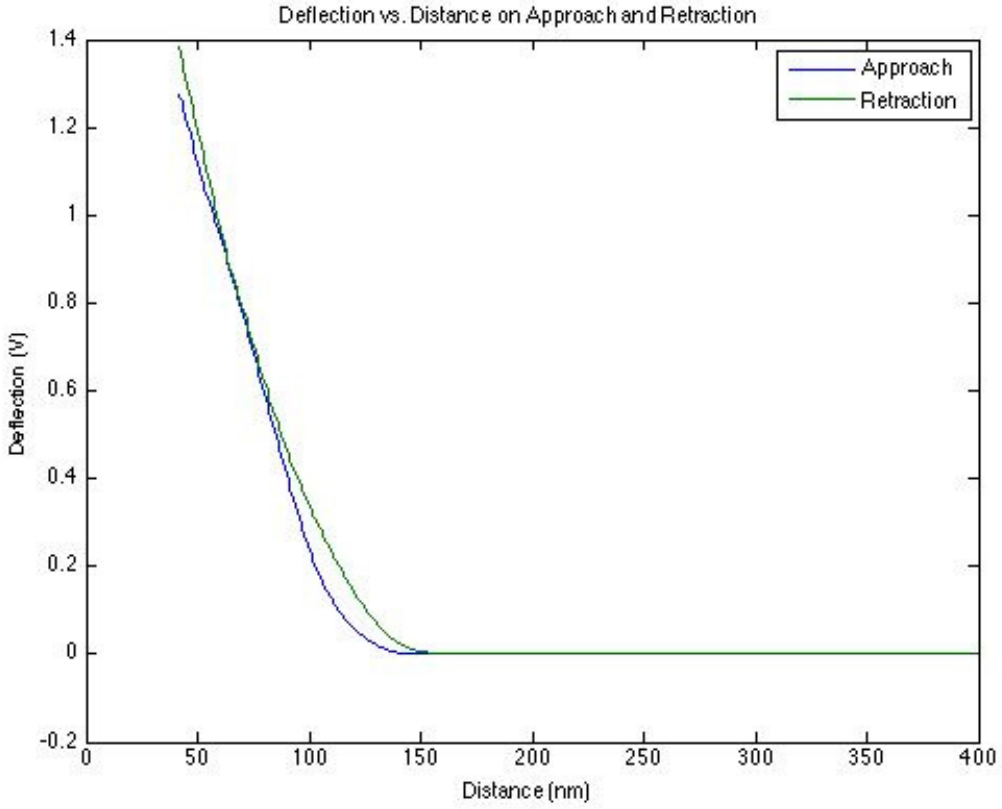

Before PEI Application

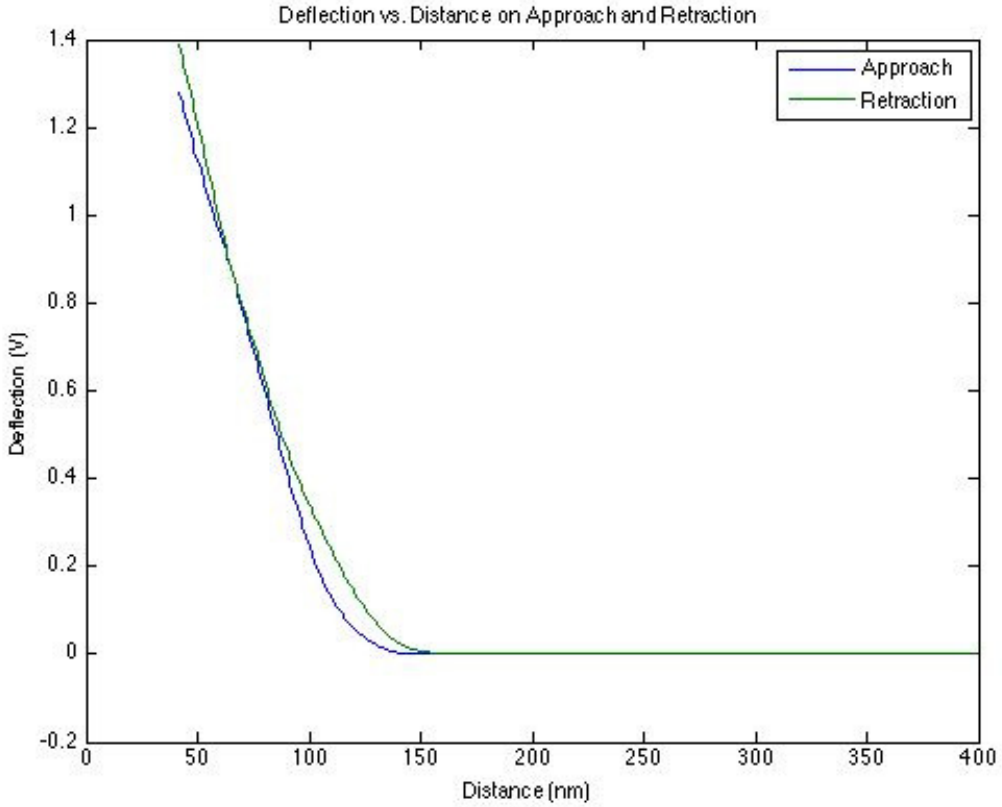

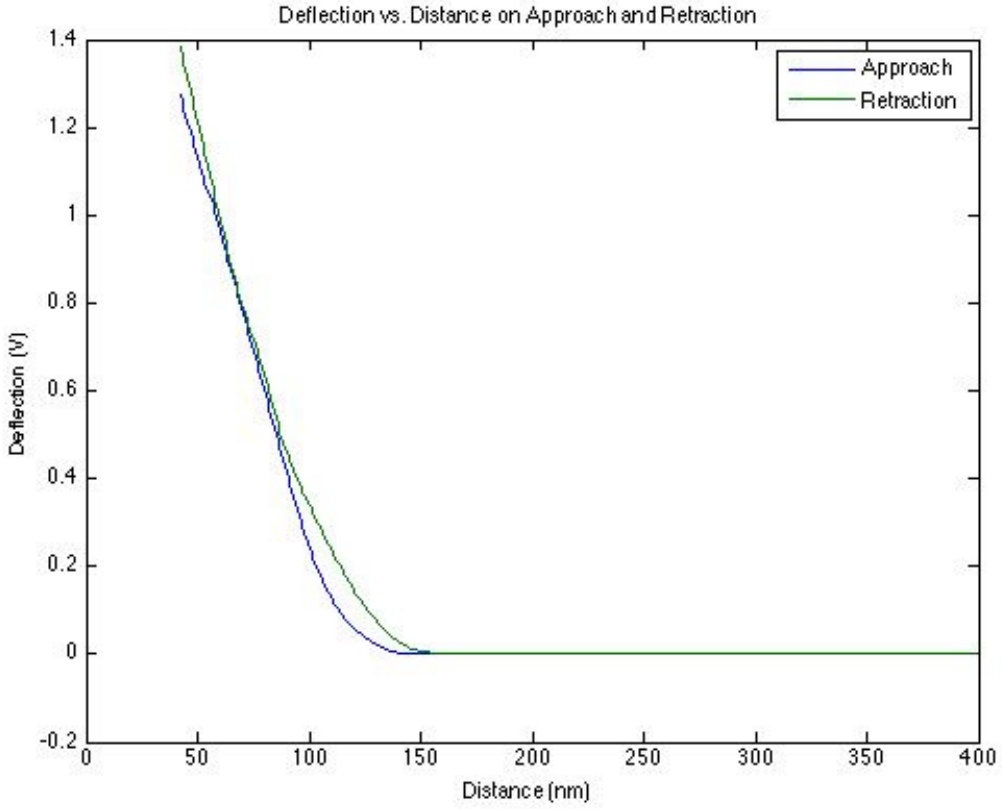

Before PEI Application

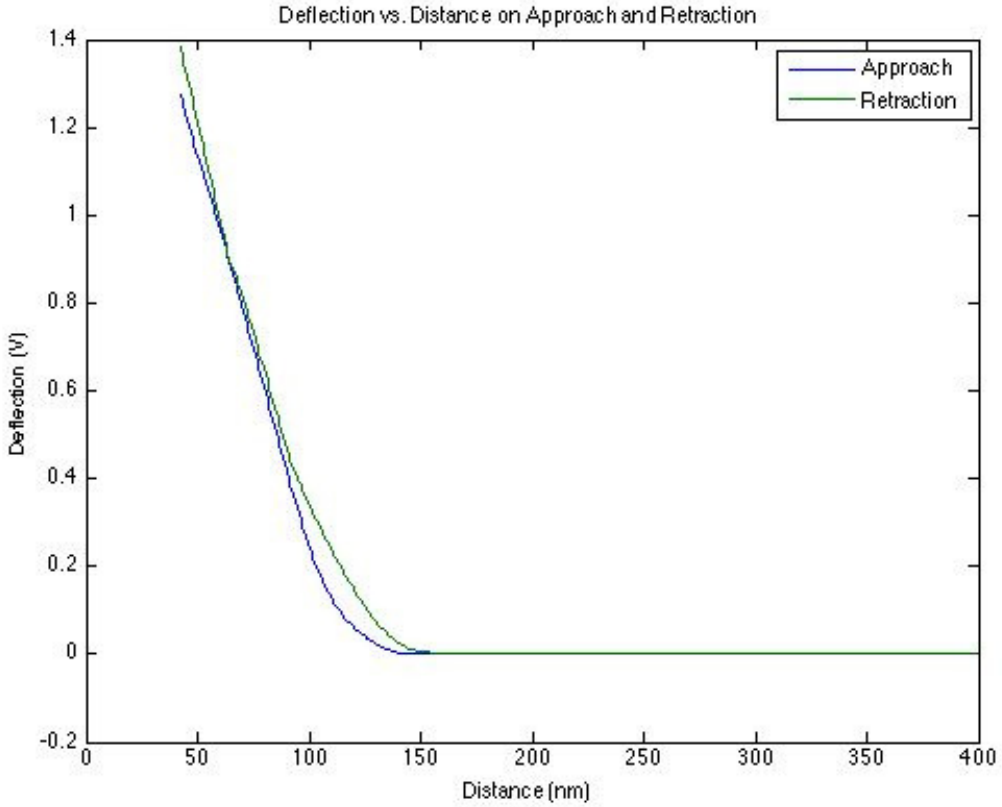

After PEI Application

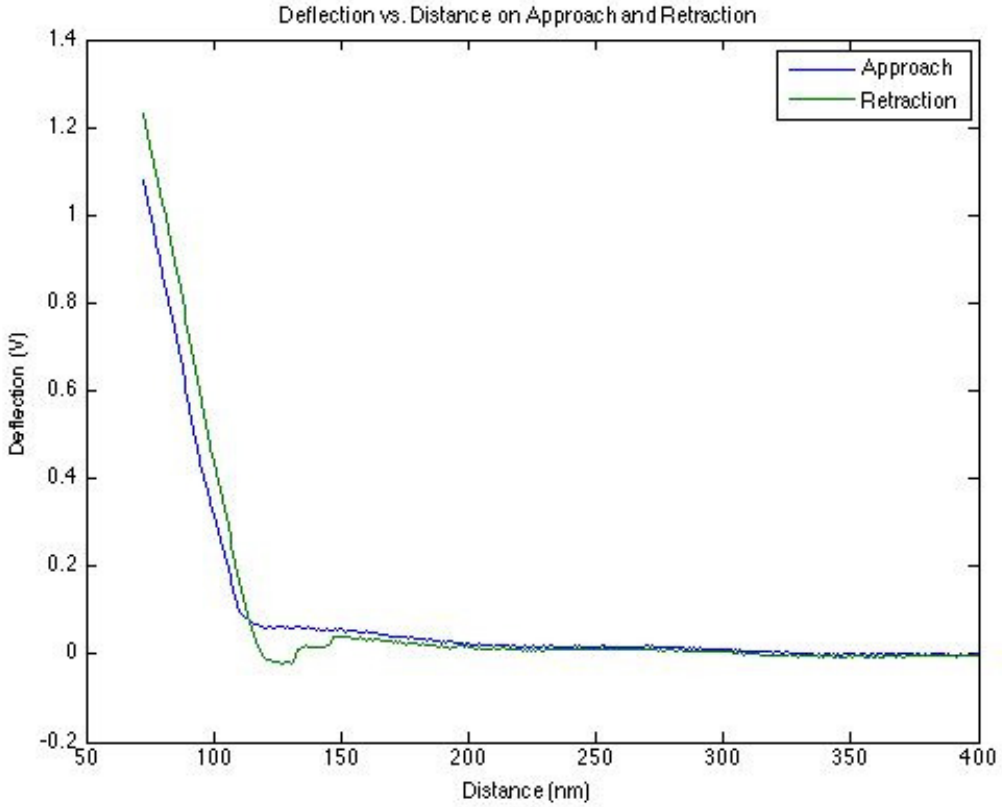

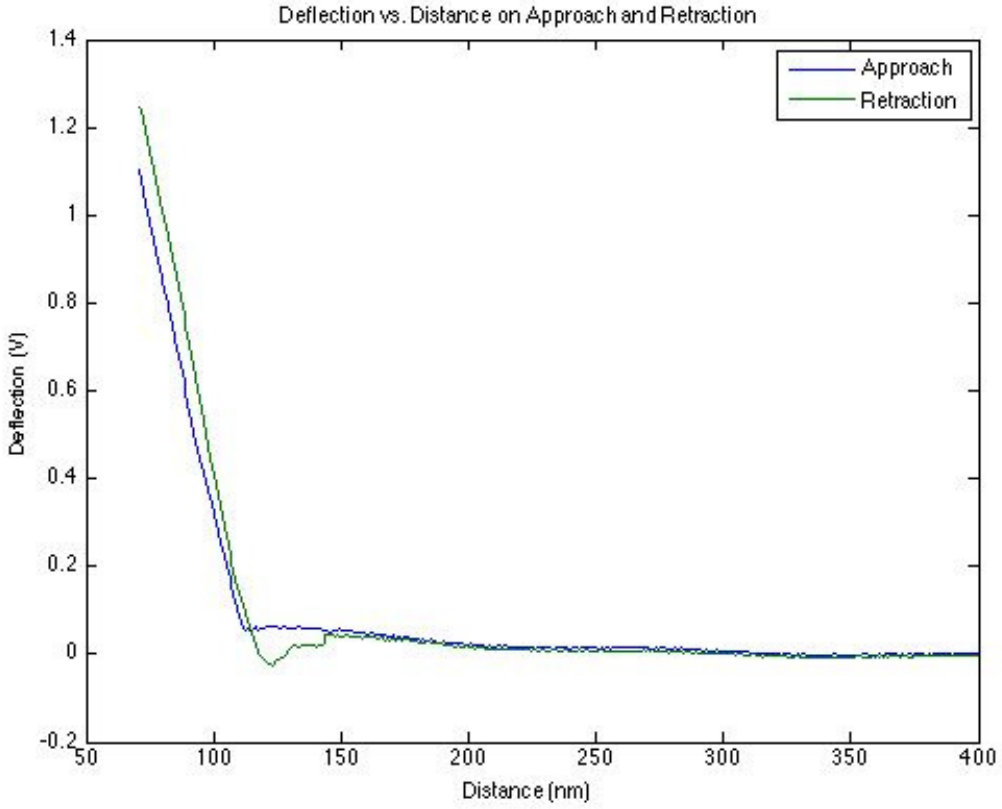

After PEI Application

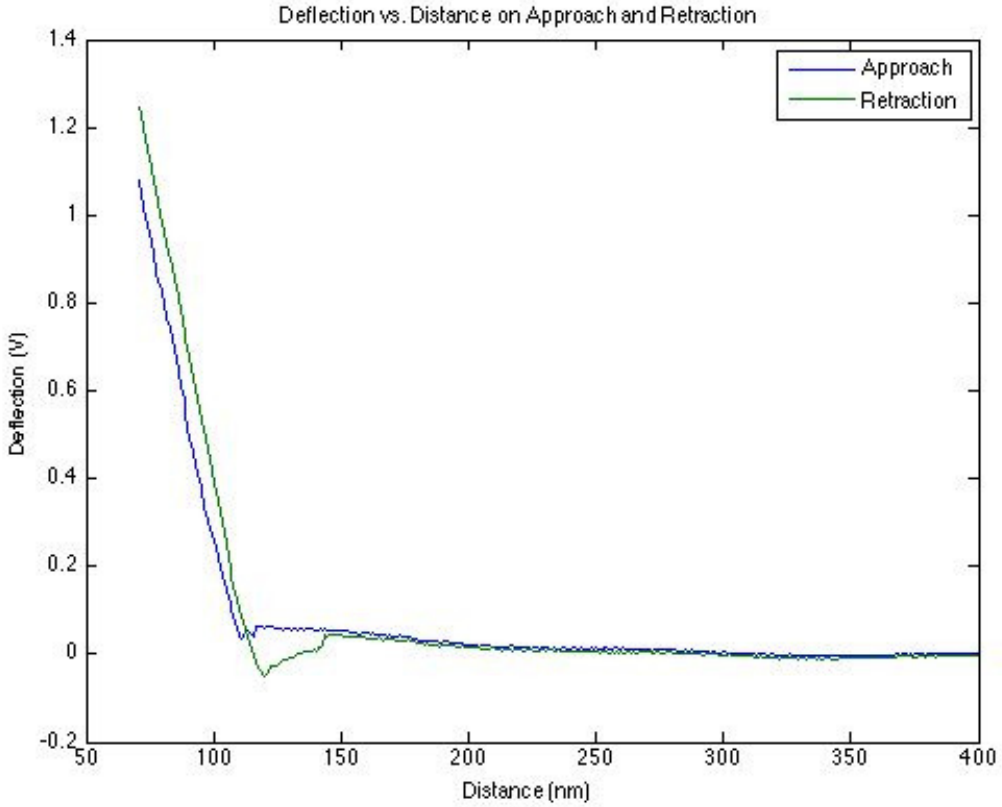

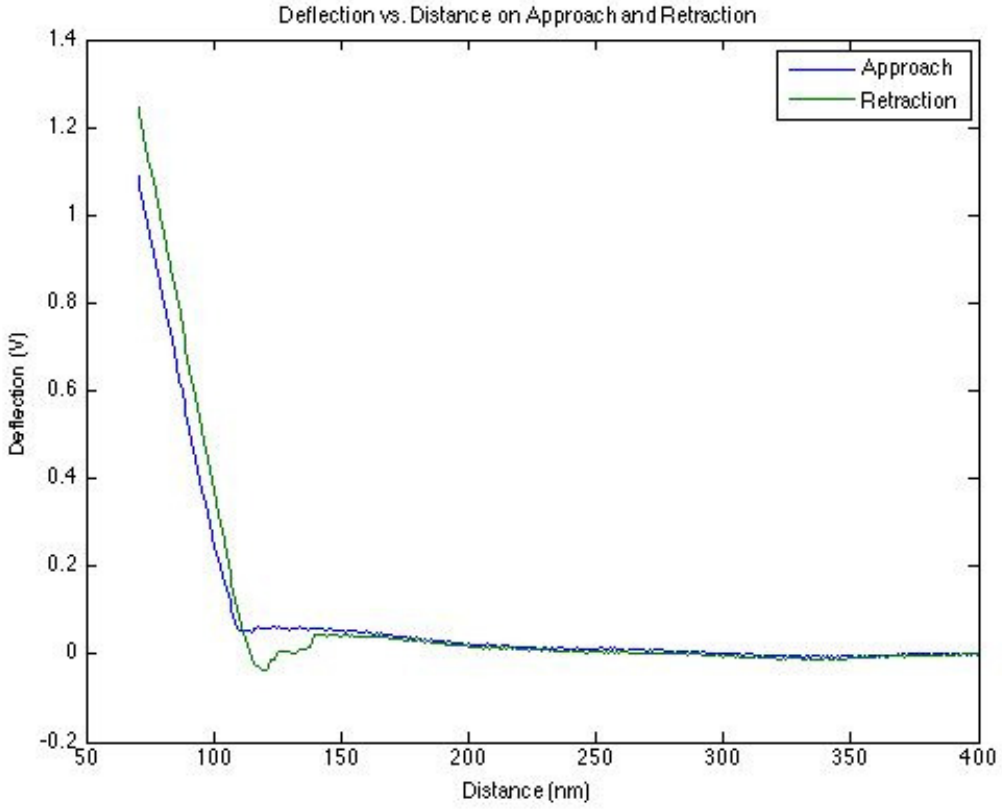

After PEI Application

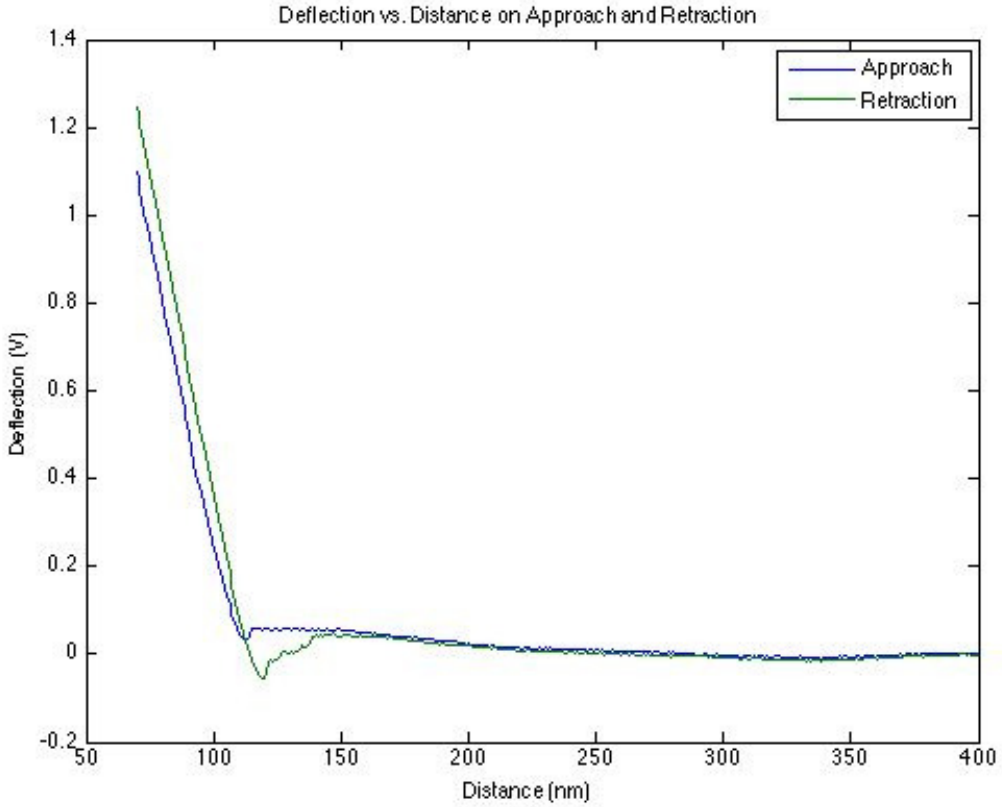

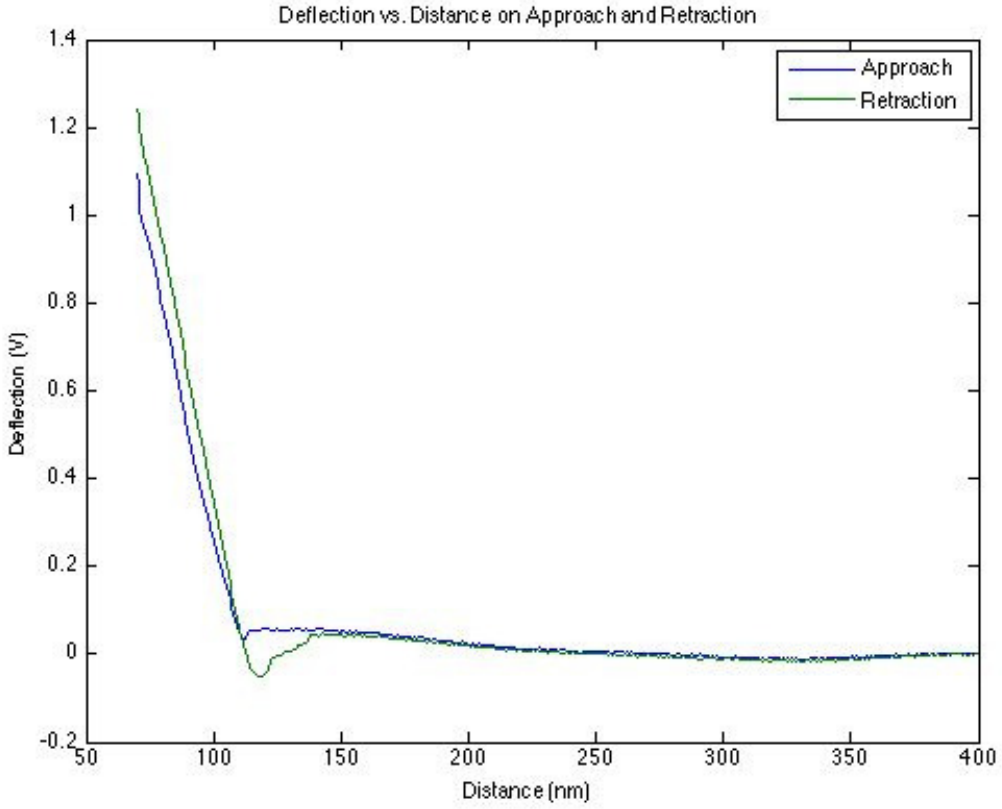

After PEI Removal

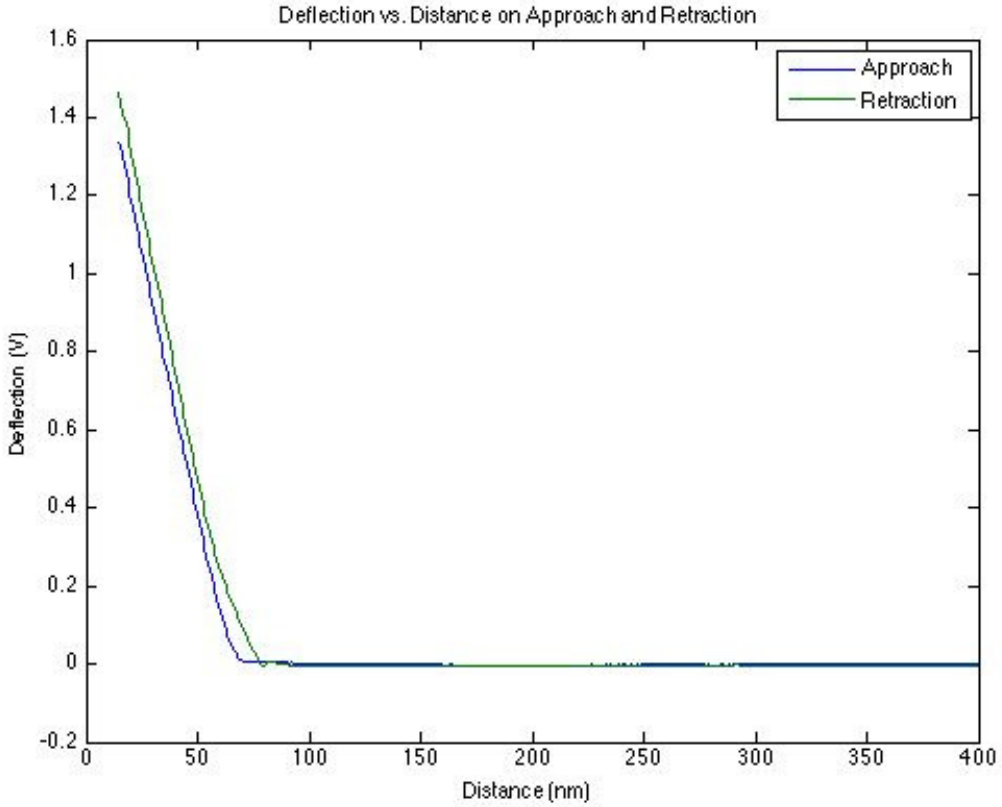

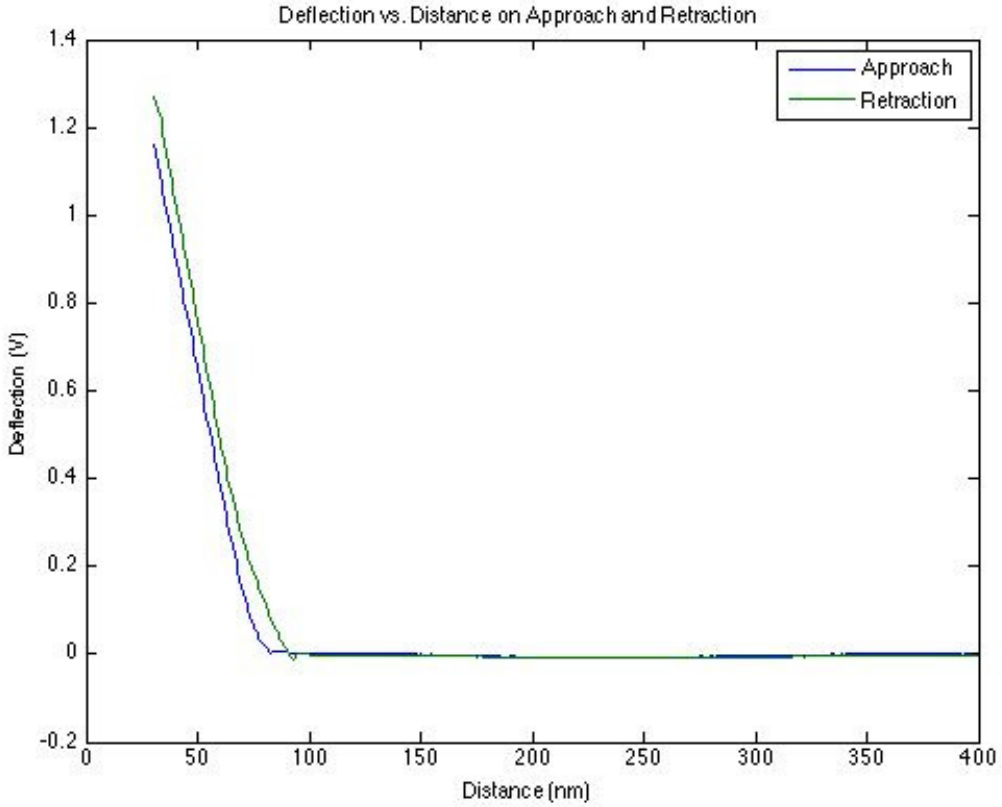

After PEI Removal

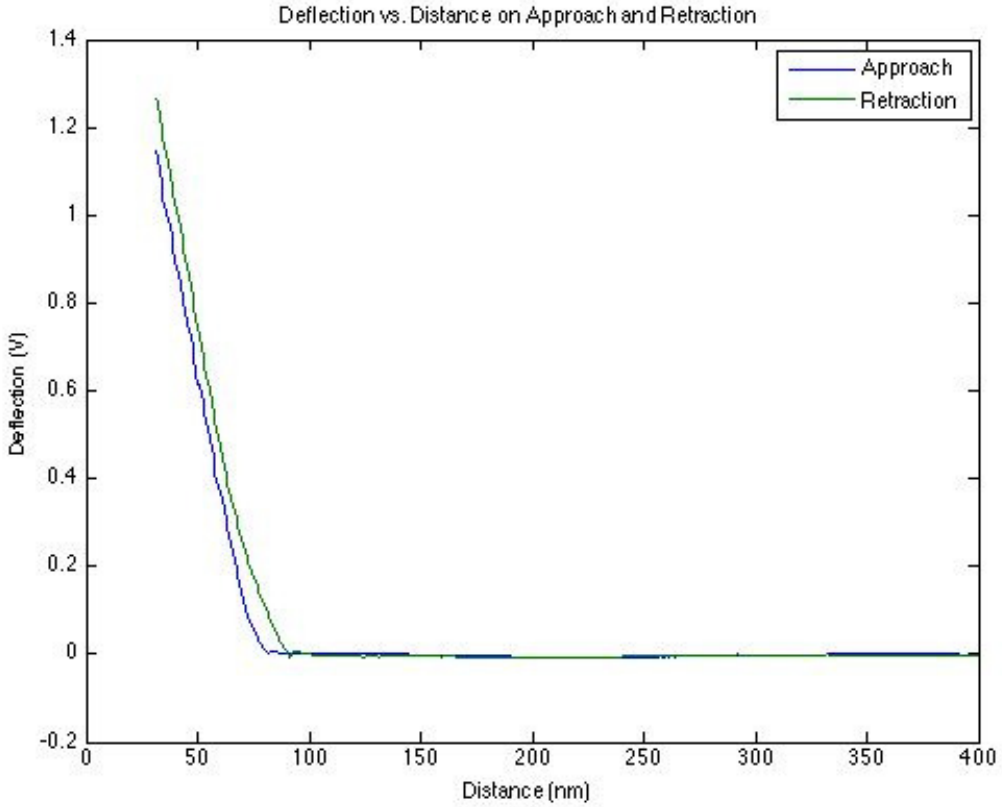

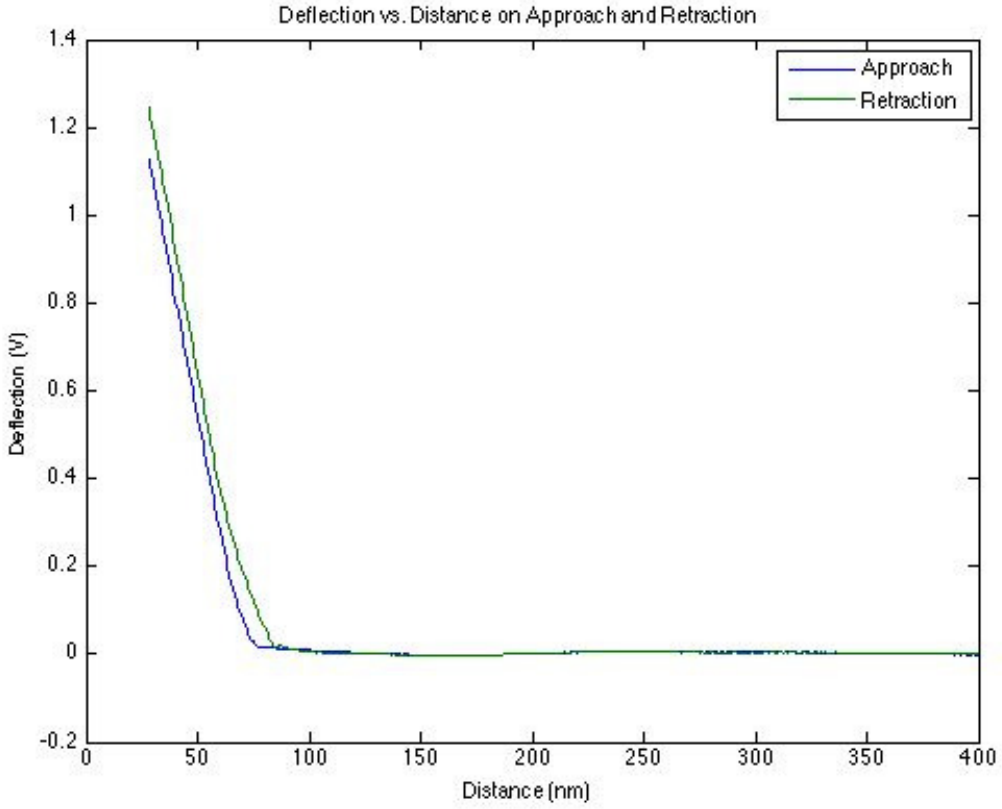

After PEI Removal

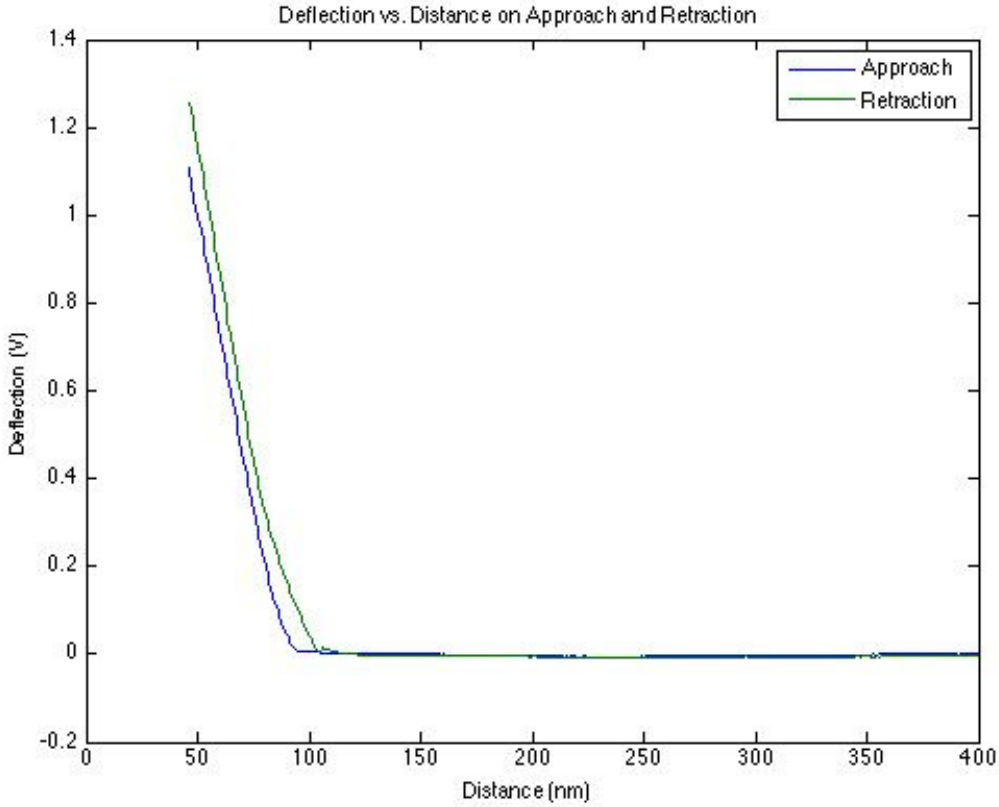

Appendix E

Sodium-saturated Dry Montmorillonite Deflection-Distance Curves

The deflection-distance curves contained in this section were obtained using the clay-coated glass probe and clay-coated glass substrate under atmospheric conditions.

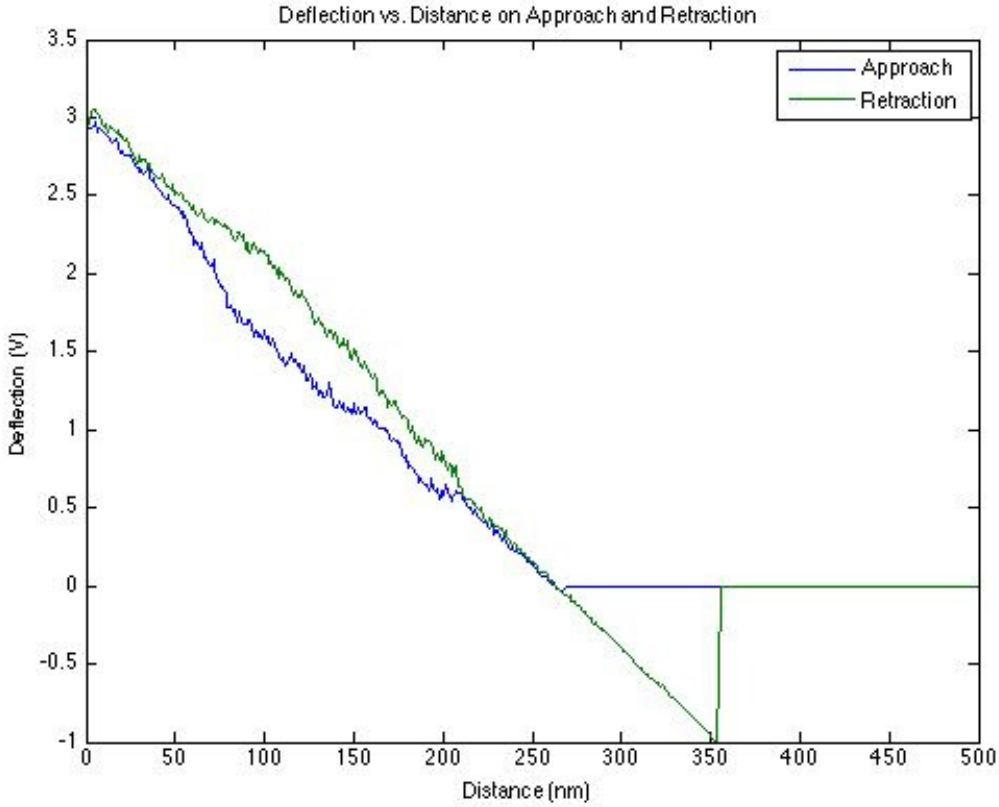
Deflection vs. Distance on Approach and Retraction
Approach
Retraction
Deflection (V)
Distance (nm)
3.5
3
2.5
2
1.5
1
0.5
0
-0.5
-1
0
50
100
150
200
250
300
350
400
450
500

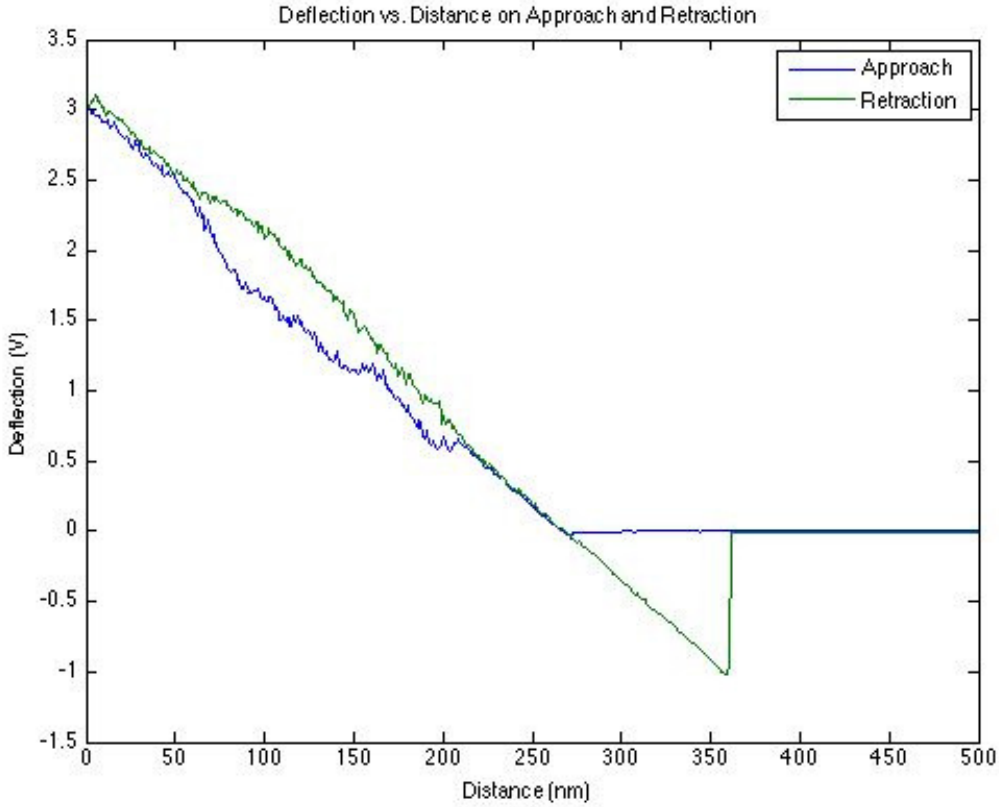
Deflection vs. Distance on Approach and Retraction
Approach
Retraction
Deflection (V)
Distance (nm)
3.5
3
2.5
2
1.5
1
0.5
0
-0.5
-1
-1.5
0
50
100
150
200
250
300
350
400
450
500

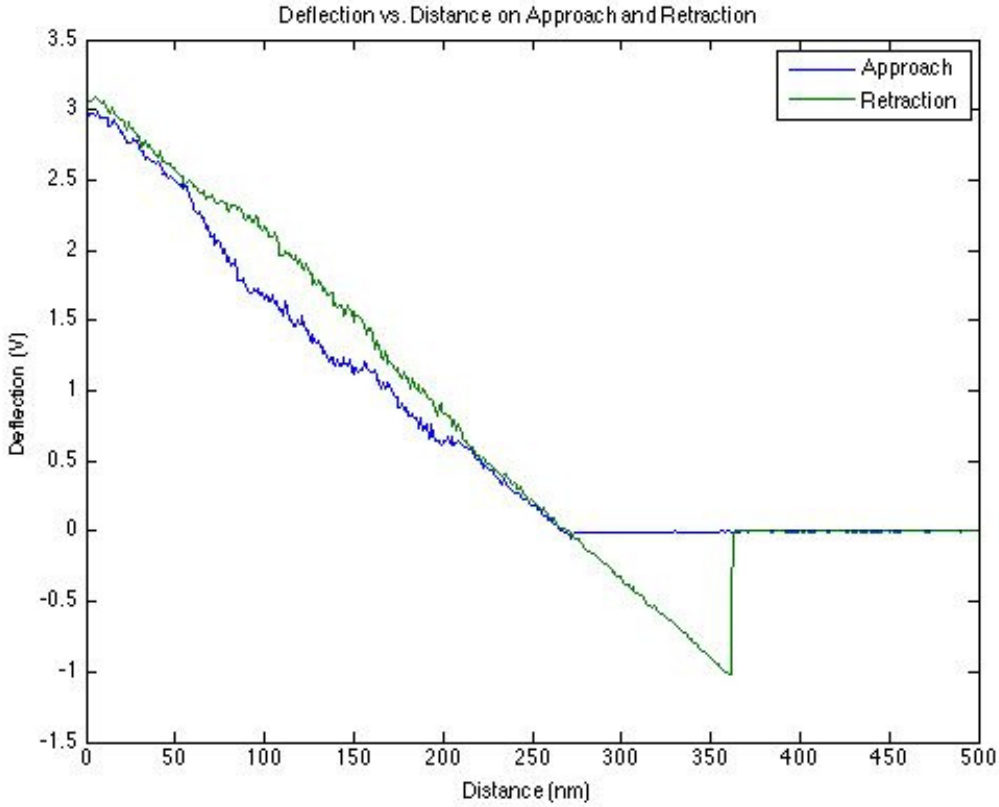
Deflection vs. Distance on Approach and Retraction
Approach
Retraction
Deflection (V)
Distance (nm)
3.5
3
2.5
2
1.5
1
0.5
0
-0.5
-1
-1.5
0
50
100
150
200
250
300
350
400
450
500

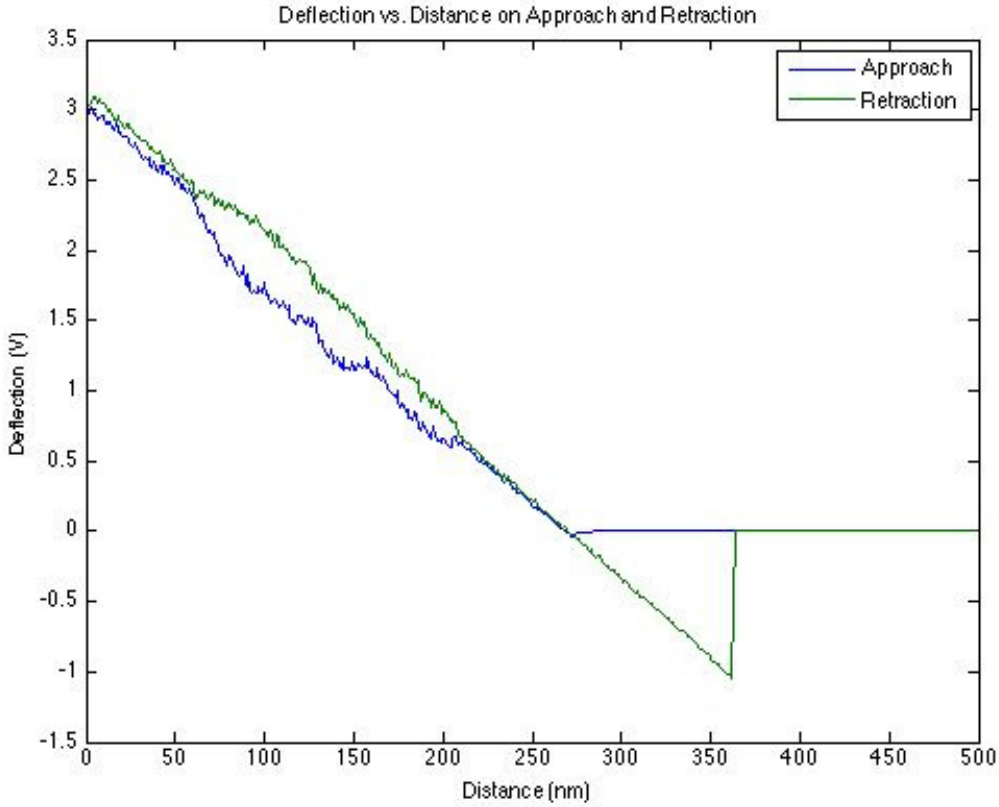
Deflection vs. Distance on Approach and Retraction
Approach
Retraction
Deflection (V)
Distance (nm)
3.5
3
2.5
2
1.5
1
0.5
0
-0.5
-1
-1.5
0
50
100
150
200
250
300
350
400
450
500

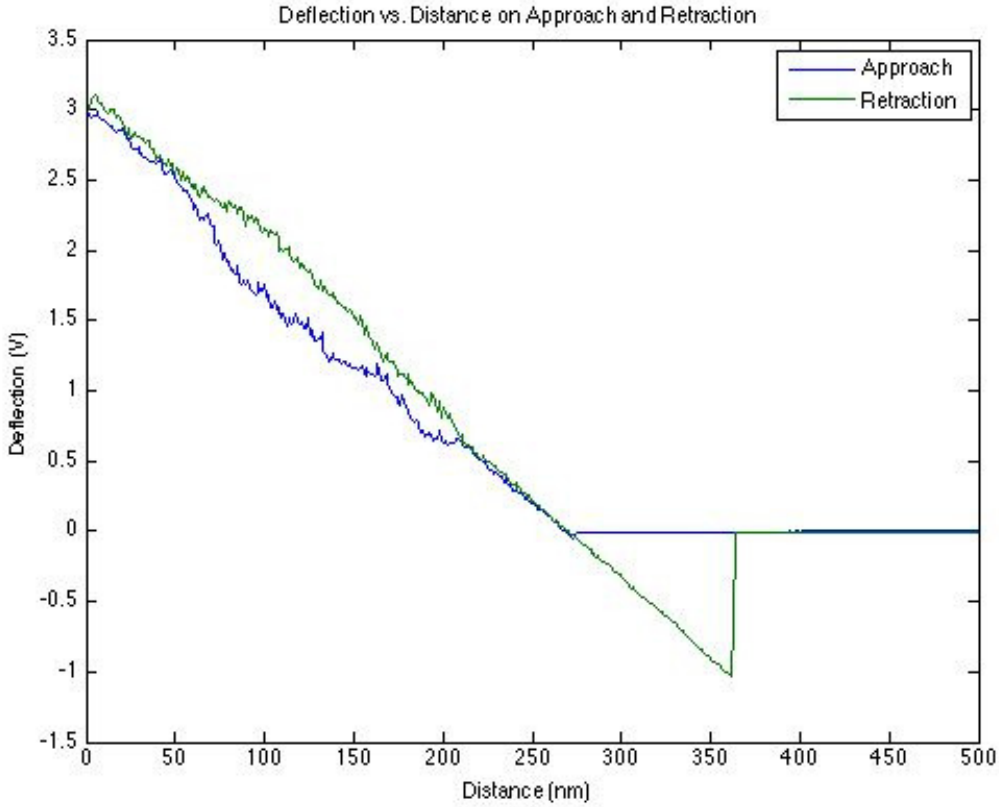
Deflection vs. Distance on Approach and Retraction
Approach
Retraction
Deflection (V)
Distance (nm)
3.5
3
2.5
2
1.5
1
0.5
0
-0.5
-1
-1.5
0
50
100
150
200
250
300
350
400
450
500

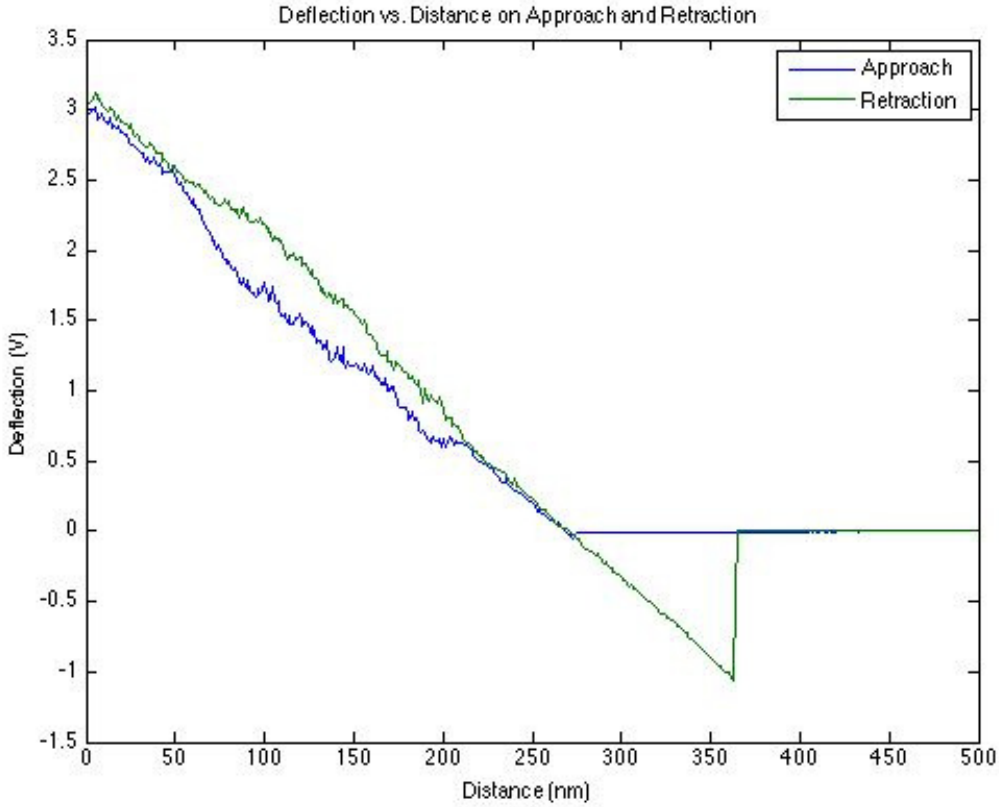
Deflection vs. Distance on Approach and Retraction
Approach
Retraction
Deflection (V)
Distance (nm)
3.5
3
2.5
2
1.5
1
0.5
0
-0.5
-1
-1.5
0
50
100
150
200
250
300
350
400
450
500

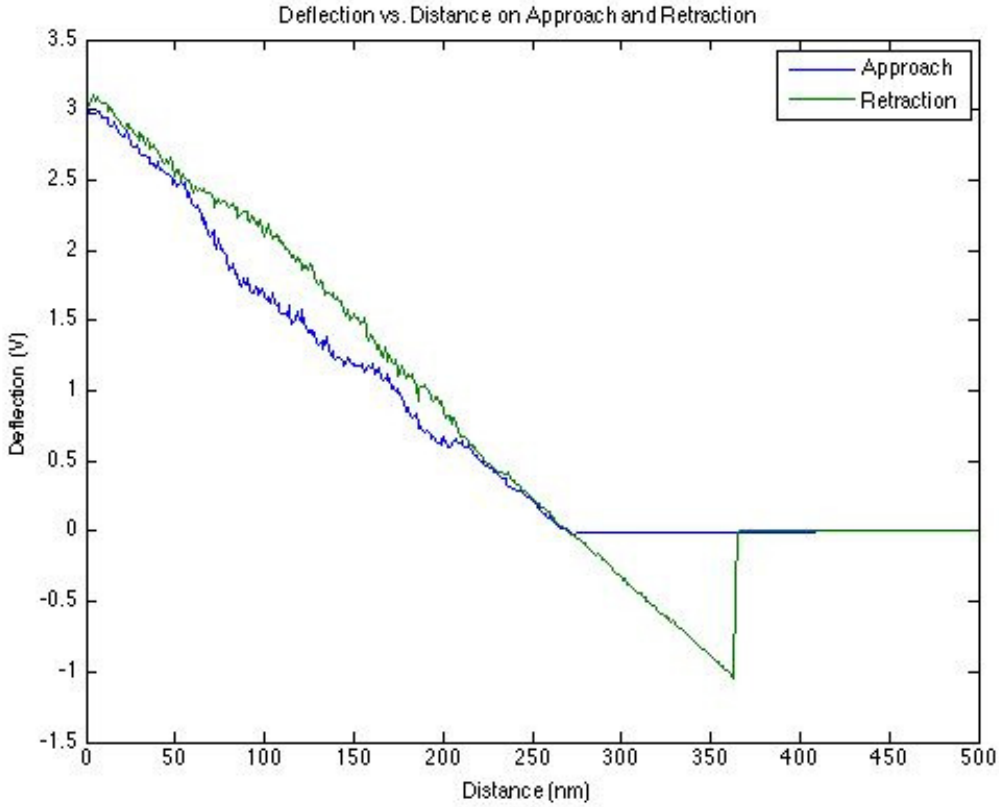
Deflection vs. Distance on Approach and Retraction
Approach
Retraction
Deflection (V)
Distance (nm)
3.5
3
2.5
2
1.5
1
0.5
0
-0.5
-1
-1.5
0
50
100
150
200
250
300
350
400
450
500

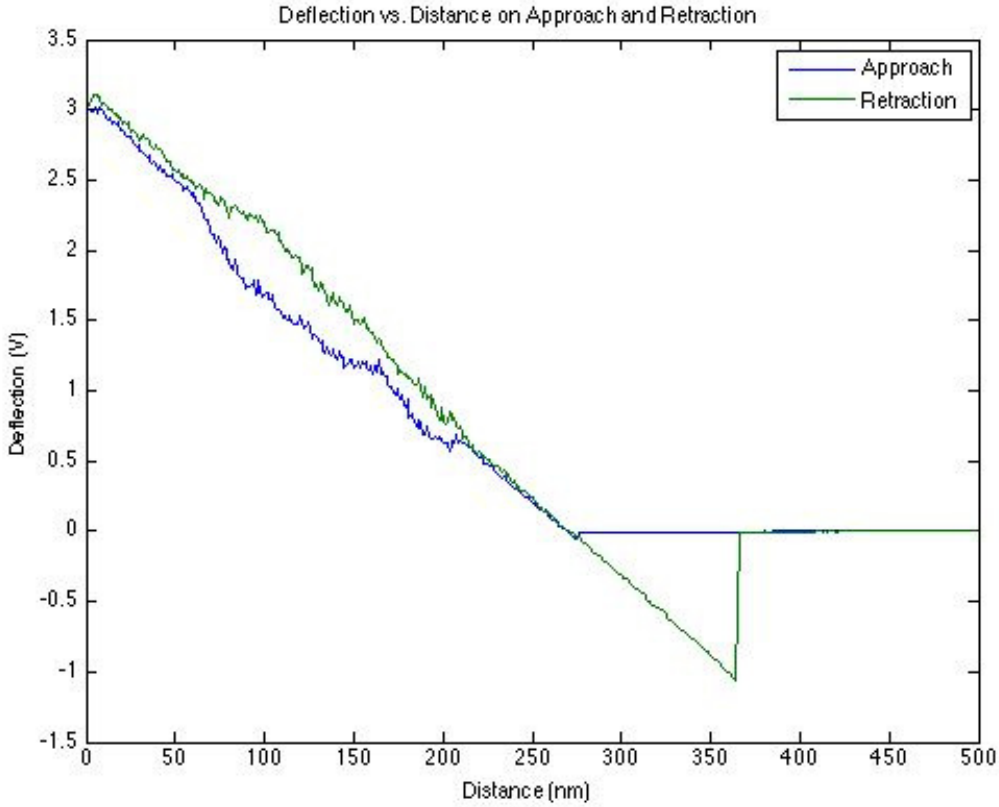
Deflection vs. Distance on Approach and Retraction
Approach
Retraction
Deflection (V)
Distance (nm)
3.5
3
2.5
2
1.5
1
0.5
0
-0.5
-1
-1.5
0
50
100
150
200
250
300
350
400
450
500

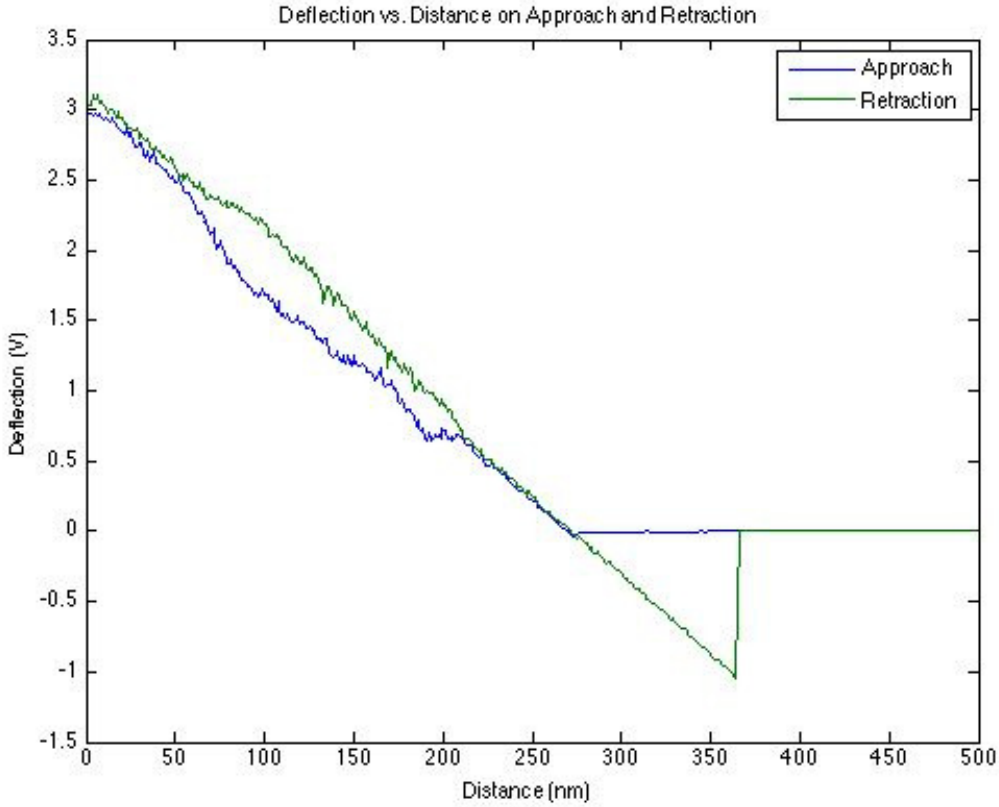
Deflection vs. Distance on Approach and Retraction
Approach
Retraction
Deflection (V)
Distance (nm)
3.5
3
2.5
2
1.5
1
0.5
0
-0.5
-1
-1.5
0
50
100
150
200
250
300
350
400
450
500

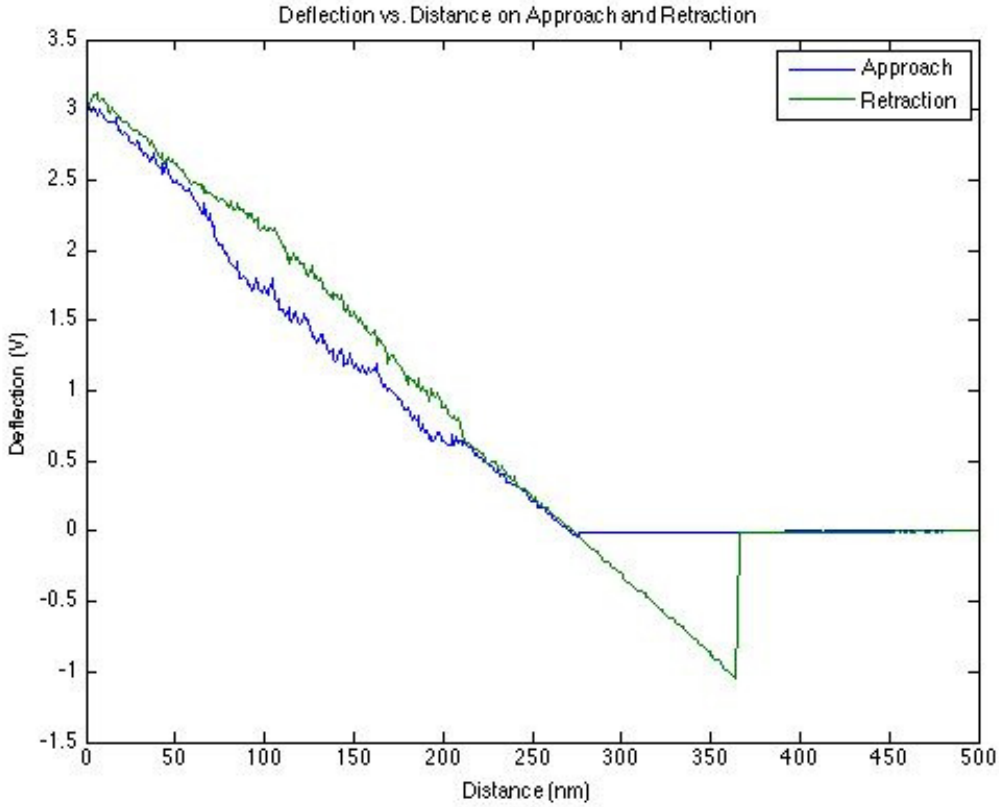
Deflection vs. Distance on Approach and Retraction
Approach
Retraction
Deflection (V)
Distance (nm)
3.5
3
2.5
2
1.5
1
0.5
0
-0.5
-1
-1.5
0
50
100
150
200
250
300
350
400
450
500

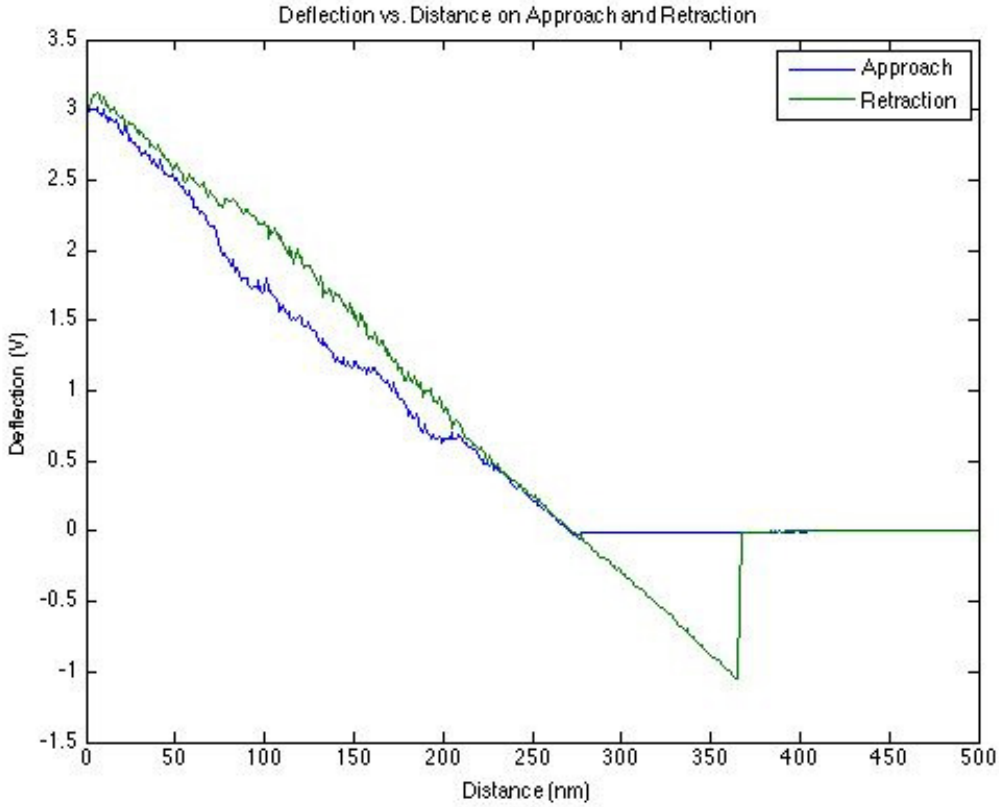
Deflection vs. Distance on Approach and Retraction
Approach
Retraction
Deflection (V)
Distance (nm)
3.5
3
2.5
2
1.5
1
0.5
0
-0.5
-1
-1.5
0
50
100
150
200
250
300
350
400
450
500

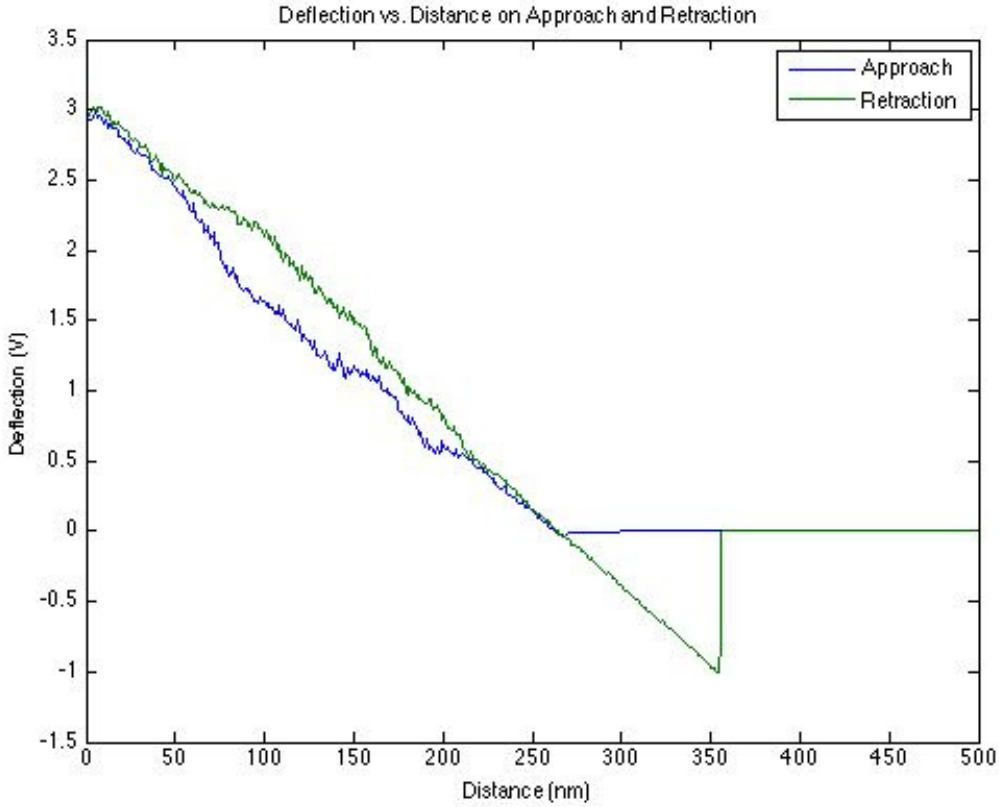
Deflection vs. Distance on Approach and Retraction
Approach
Retraction
Deflection (V)
Distance (nm)
3.5
3
2.5
2
1.5
1
0.5
0
-0.5
-1
-1.5
0
50
100
150
200
250
300
350
400
450
500

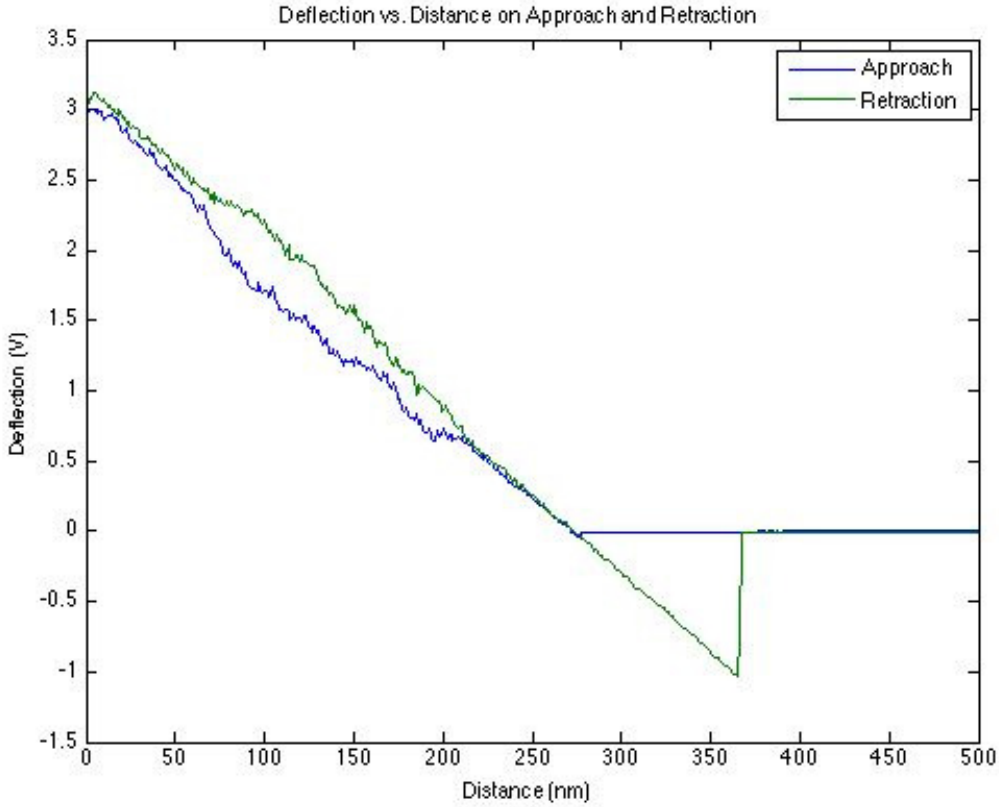
Deflection vs. Distance on Approach and Retraction
Approach
Retraction
Deflection (V)
Distance (nm)
3.5
3
2.5
2
1.5
1
0.5
0
-0.5
-1
-1.5
0
50
100
150
200
250
300
350
400
450
500

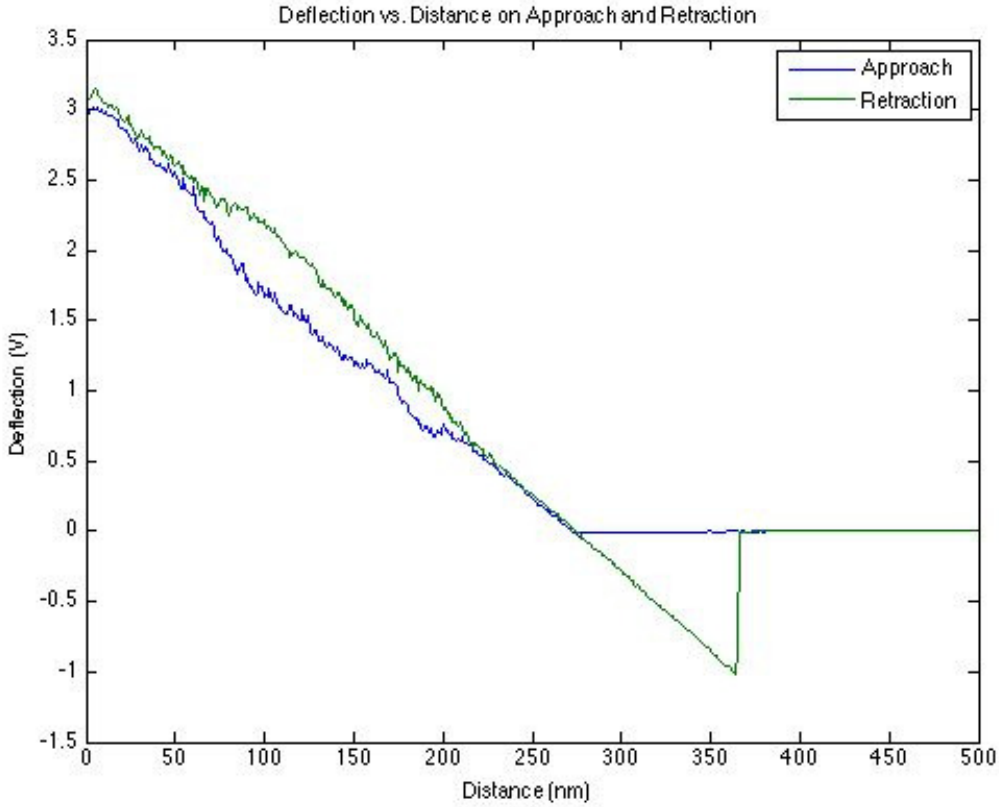
Deflection vs. Distance on Approach and Retraction
Approach
Retraction
Deflection (V)
Distance (nm)
3.5
3
2.5
2
1.5
1
0.5
0
-0.5
-1
-1.5
0
50
100
150
200
250
300
350
400
450
500

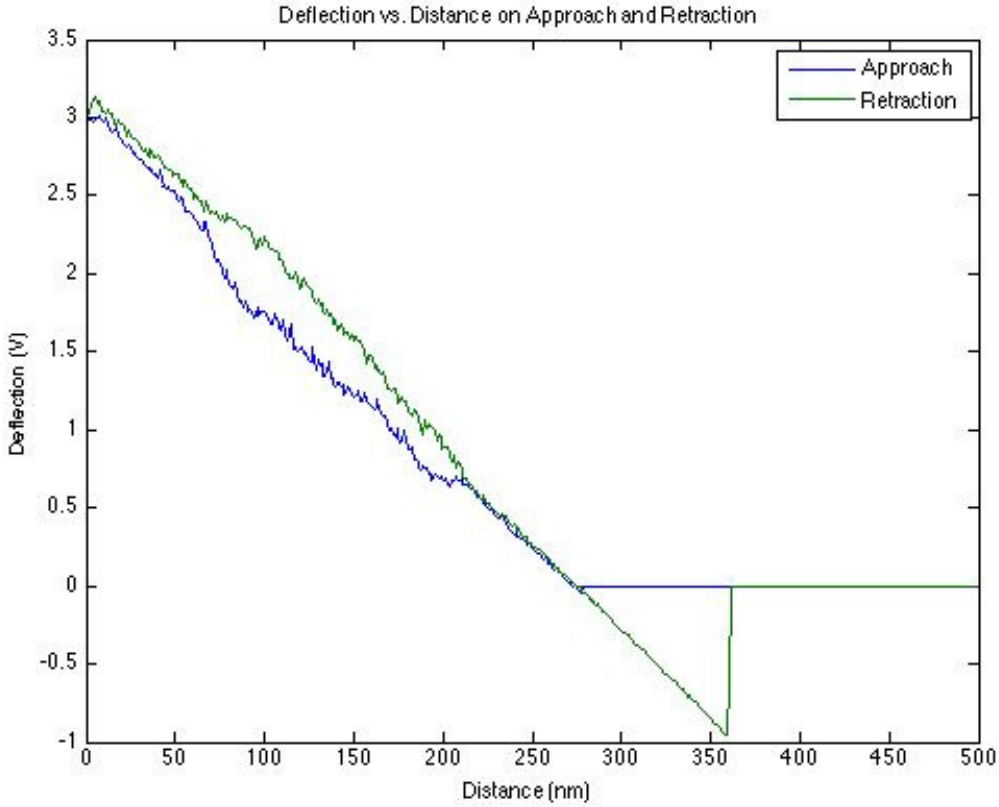
Deflection vs. Distance on Approach and Retraction
Approach
Retraction
Deflection (V)
Distance (nm)
3.5
3
2.5
2
1.5
1
0.5
0
-0.5
-1
0
50
100
150
200
250
300
350
400
450
500

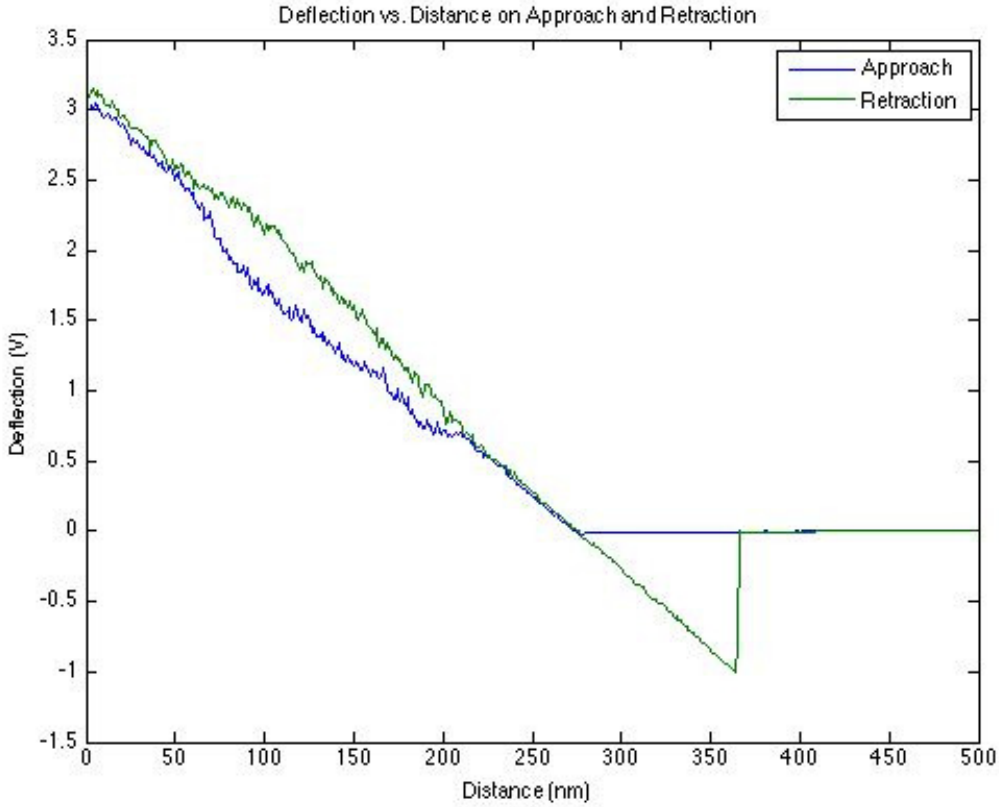
Deflection vs. Distance on Approach and Retraction
Approach
Retraction
Deflection (V)
Distance (nm)
3.5
3
2.5
2
1.5
1
0.5
0
-0.5
-1
-1.5
0
50
100
150
200
250
300
350
400
450
500

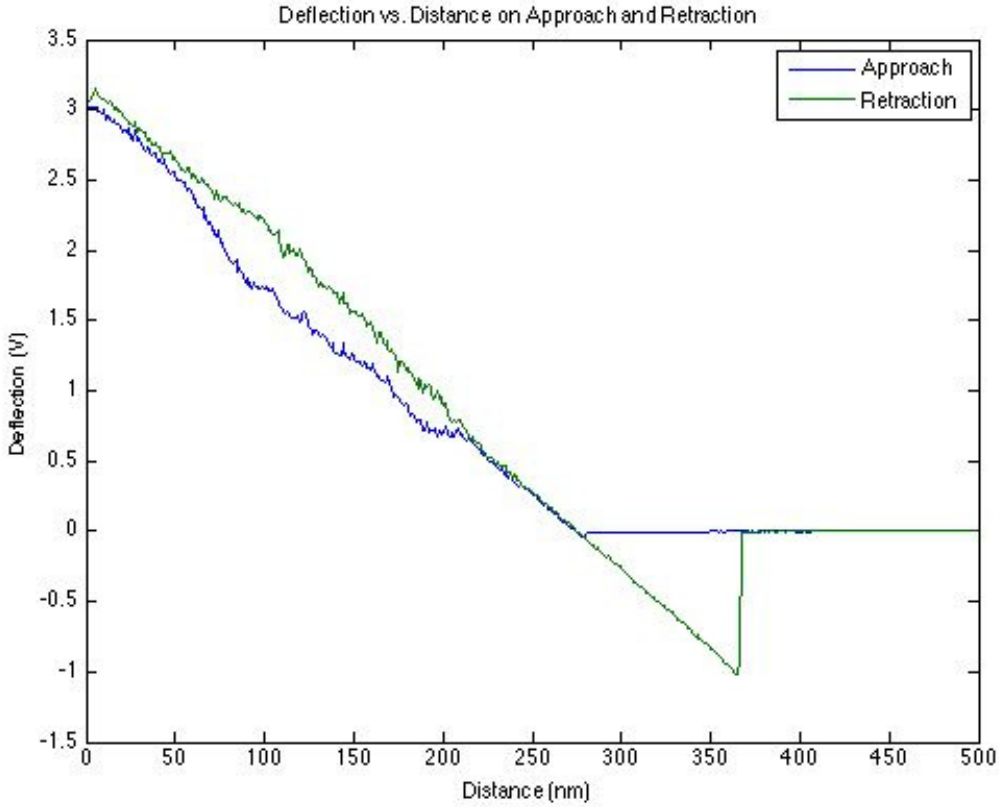
Deflection vs. Distance on Approach and Retraction
Approach
Retraction
Deflection (V)
Distance (nm)
3.5
3
2.5
2
1.5
1
0.5
0
-0.5
-1
-1.5
0
50
100
150
200
250
300
350
400
450
500

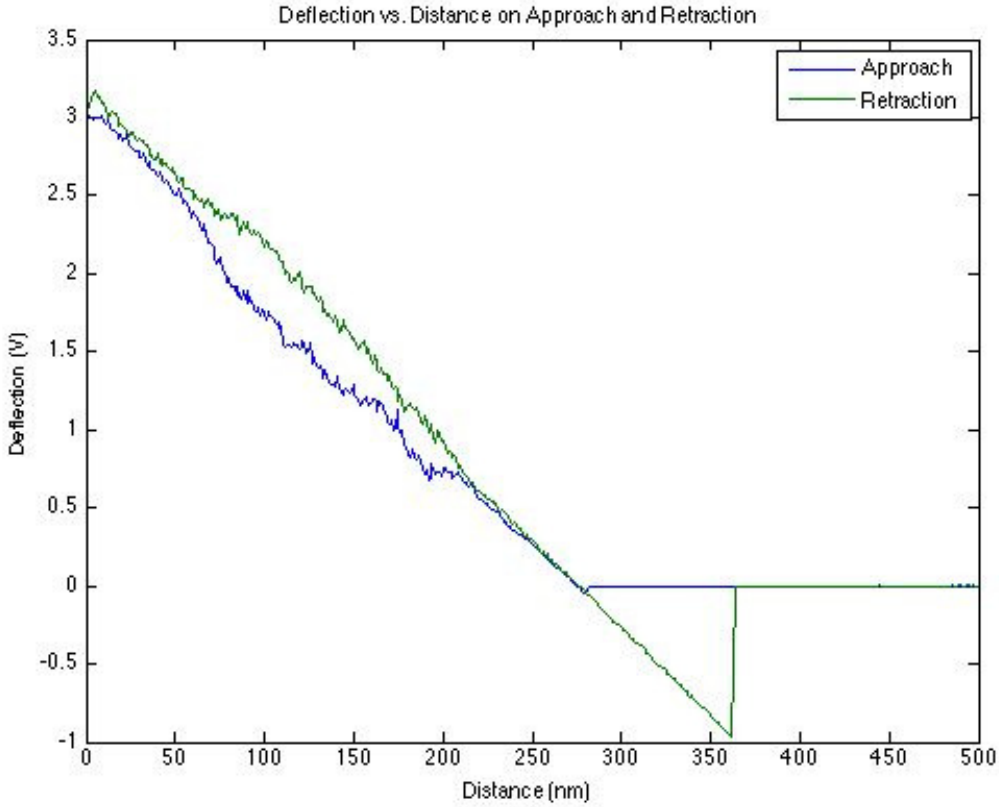
Deflection vs. Distance on Approach and Retraction
Approach
Retraction
Deflection (V)
Distance (nm)
3.5
3
2.5
2
1.5
1
0.5
0
-0.5
-1
0
50
100
150
200
250
300
350
400
450
500

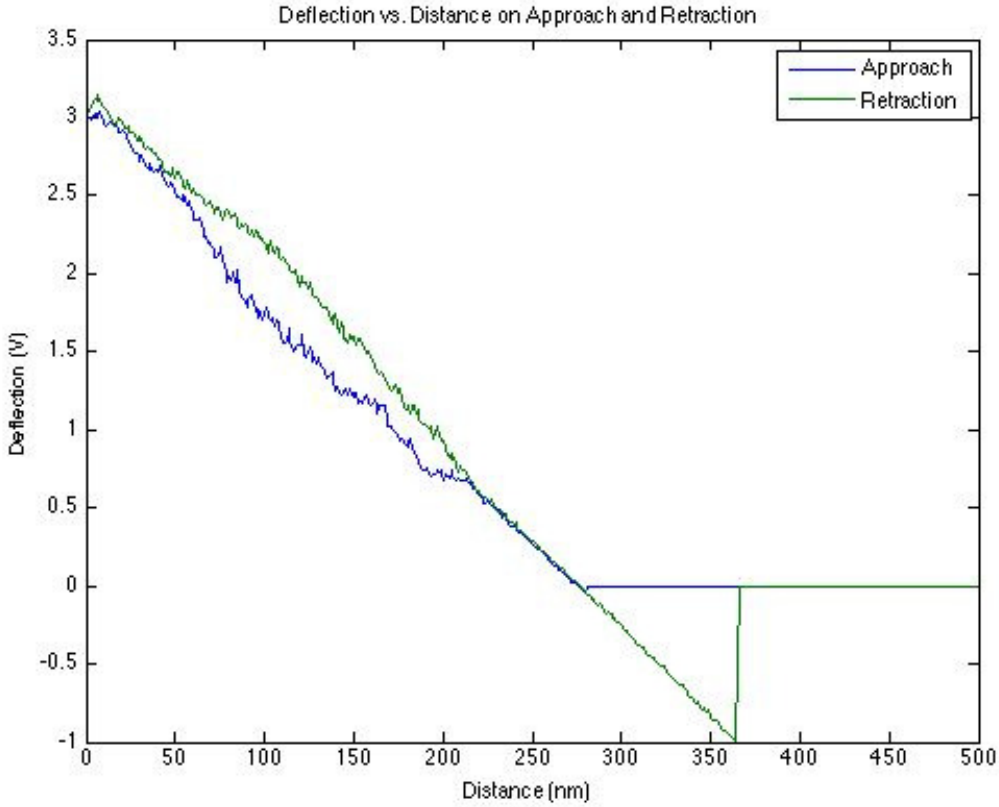
Deflection vs. Distance on Approach and Retraction
Approach
Retraction
Deflection (V)
Distance (nm)
3.5
3
2.5
2
1.5
1
0.5
0
-0.5
-1
0
50
100
150
200
250
300
350
400
450
500

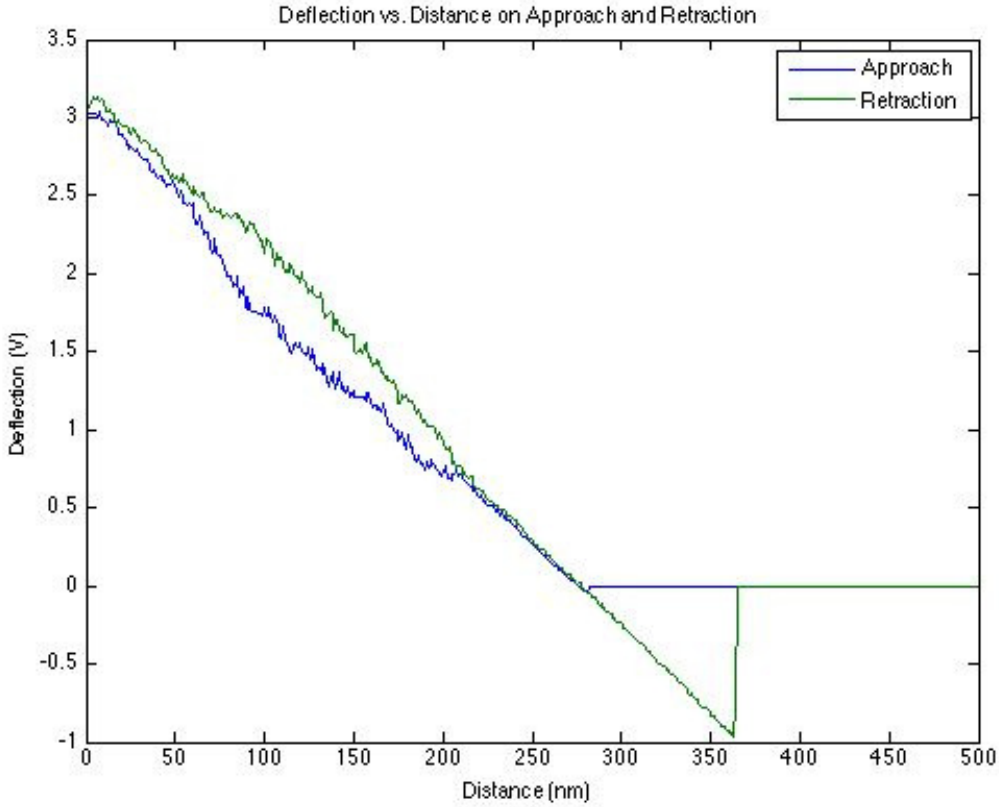
Deflection vs. Distance on Approach and Retraction
Approach
Retraction
Deflection (V)
Distance (nm)
3.5
3
2.5
2
1.5
1
0.5
0
-0.5
-1
0
50
100
150
200
250
300
350
400
450
500

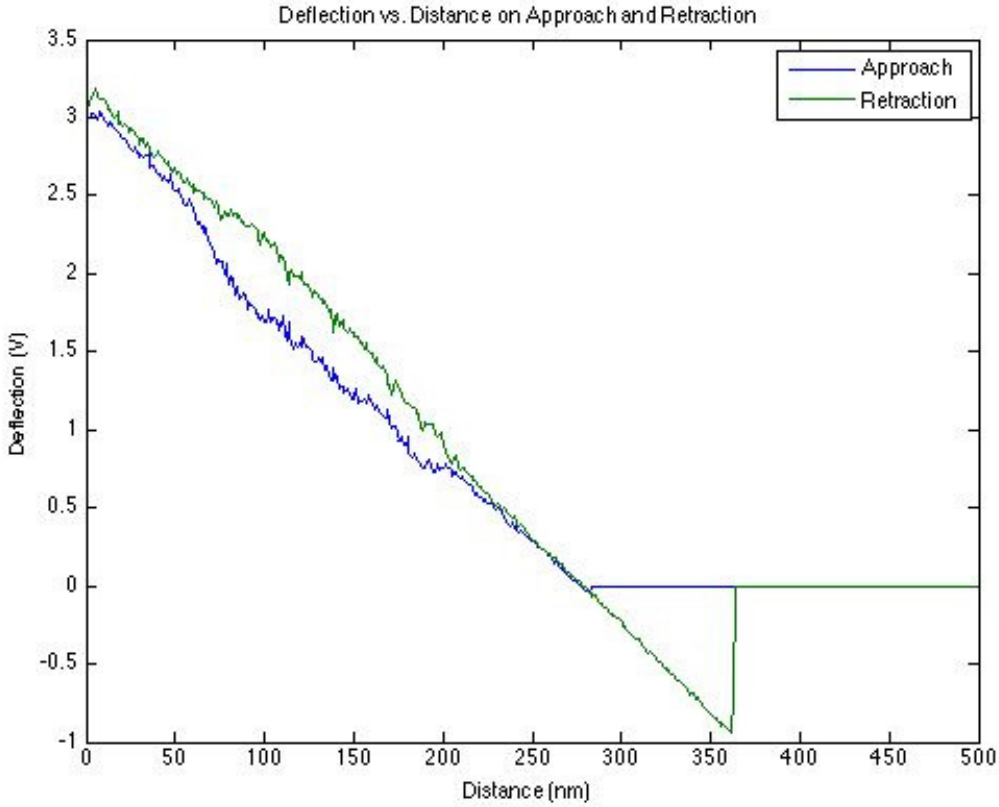
Deflection vs. Distance on Approach and Retraction
Approach
Retraction
Deflection (V)
Distance (nm)
3.5
3
2.5
2
1.5
1
0.5
0
-0.5
-1
0
50
100
150
200
250
300
350
400
450
500

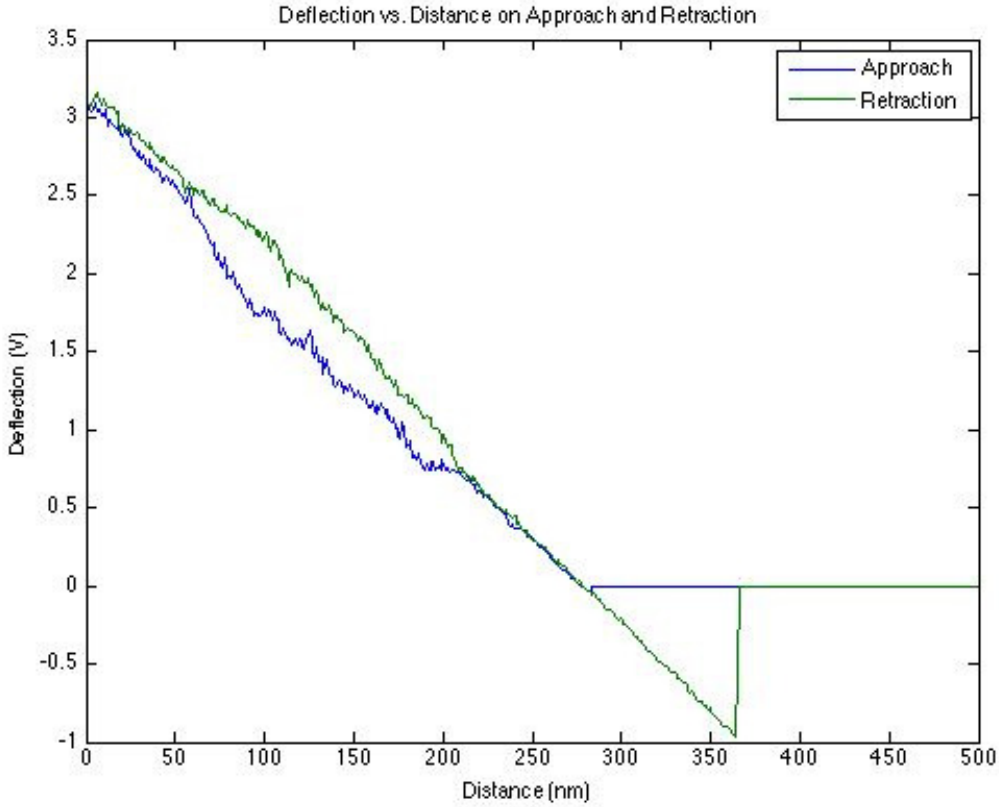
Deflection vs. Distance on Approach and Retraction
Approach
Retraction
Deflection (V)
Distance (nm)
3.5
3
2.5
2
1.5
1
0.5
0
-0.5
-1
0
50
100
150
200
250
300
350
400
450
500

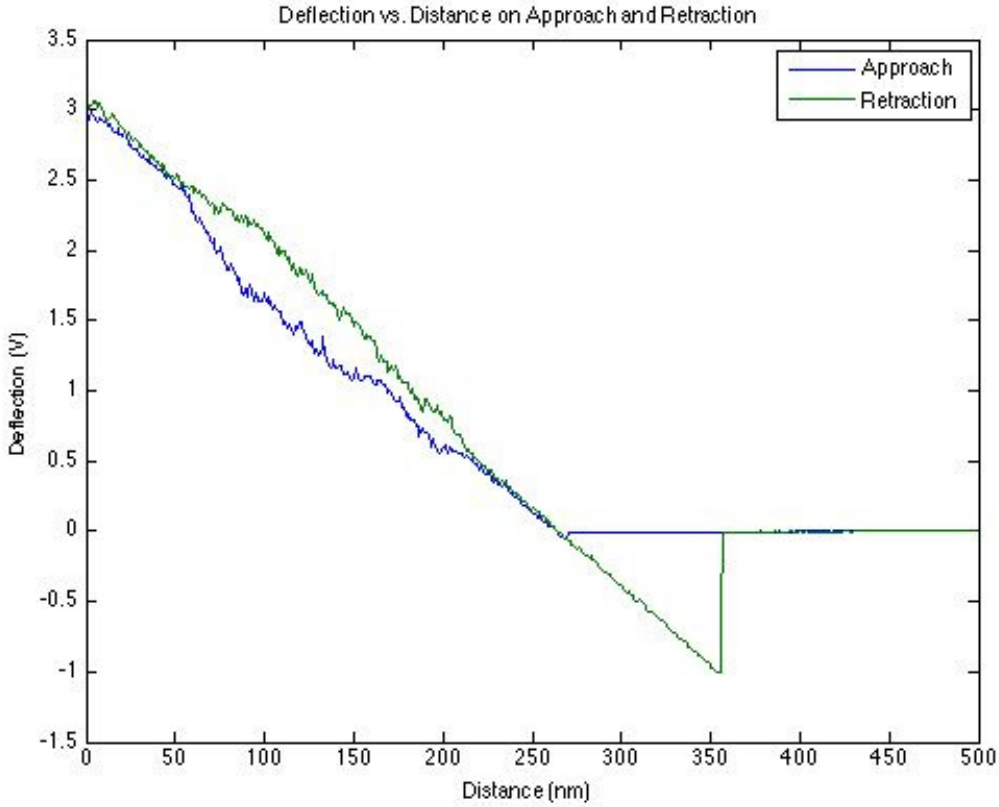
Deflection vs. Distance on Approach and Retraction
Approach
Retraction
Deflection (V)
Distance (nm)
3.5
3
2.5
2
1.5
1
0.5
0
-0.5
-1
-1.5
0
50
100
150
200
250
300
350
400
450
500

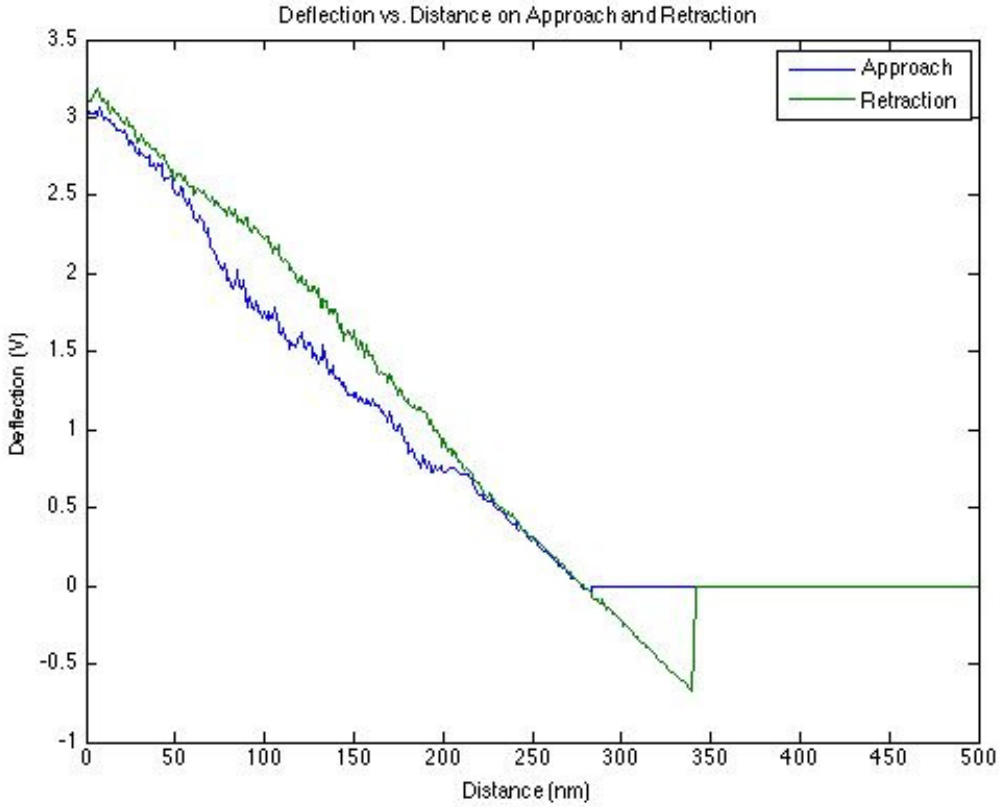
Deflection vs. Distance on Approach and Retraction
Approach
Retraction
Deflection (V)
Distance (nm)
3.5
3
2.5
2
1.5
1
0.5
0
-0.5
-1
0
50
100
150
200
250
300
350
400
450
500

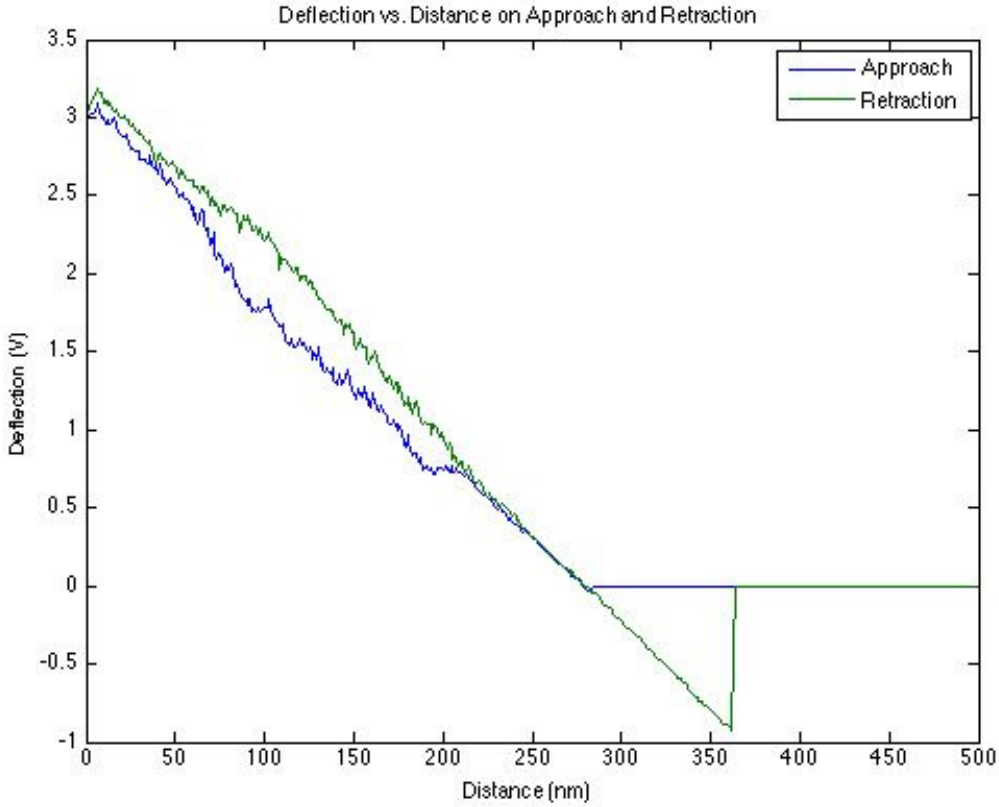
Deflection vs. Distance on Approach and Retraction
Approach
Retraction
Deflection (V)
Distance (nm)
3.5
3
2.5
2
1.5
1
0.5
0
-0.5
-1
0
50
100
150
200
250
300
350
400
450
500

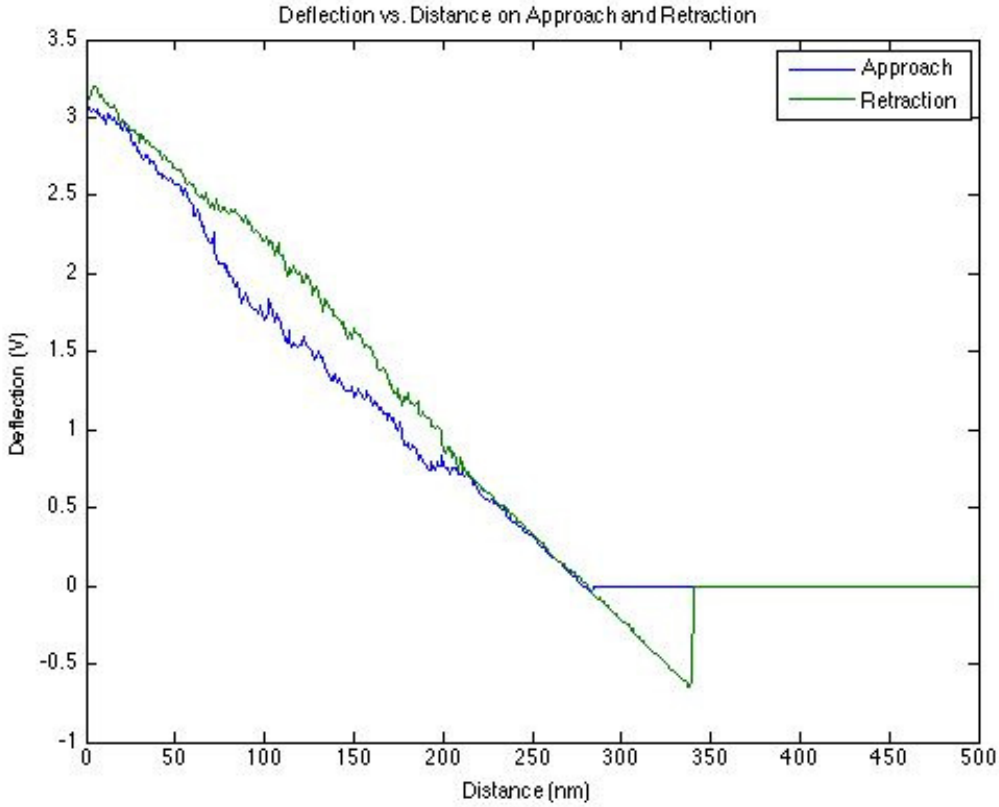
Deflection vs. Distance on Approach and Retraction
Approach
Retraction
Deflection (V)
Distance (nm)
3.5
3
2.5
2
1.5
1
0.5
0
-0.5
-1
0
50
100
150
200
250
300
350
400
450
500

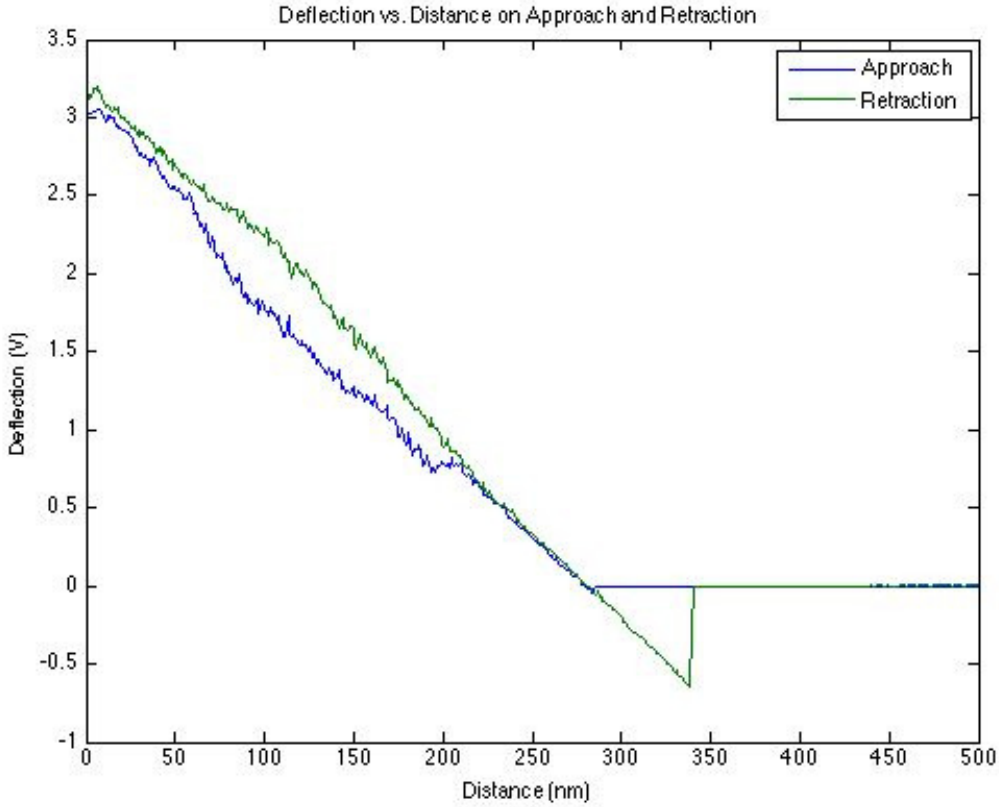
Deflection vs. Distance on Approach and Retraction
Approach
Retraction
Deflection (V)
Distance (nm)
3.5
3
2.5
2
1.5
1
0.5
0
-0.5
-1
0
50
100
150
200
250
300
350
400
450
500

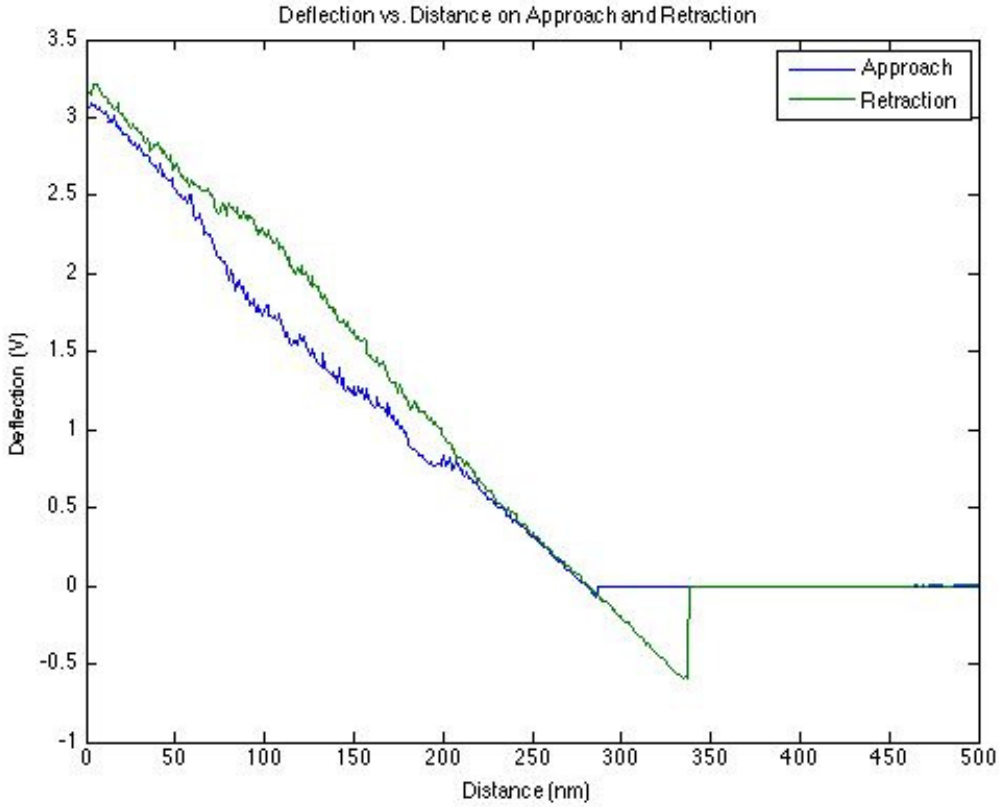
Deflection vs. Distance on Approach and Retraction
Approach
Retraction
Deflection (V)
Distance (nm)
3.5
3
2.5
2
1.5
1
0.5
0
-0.5
-1
0
50
100
150
200
250
300
350
400
450
500

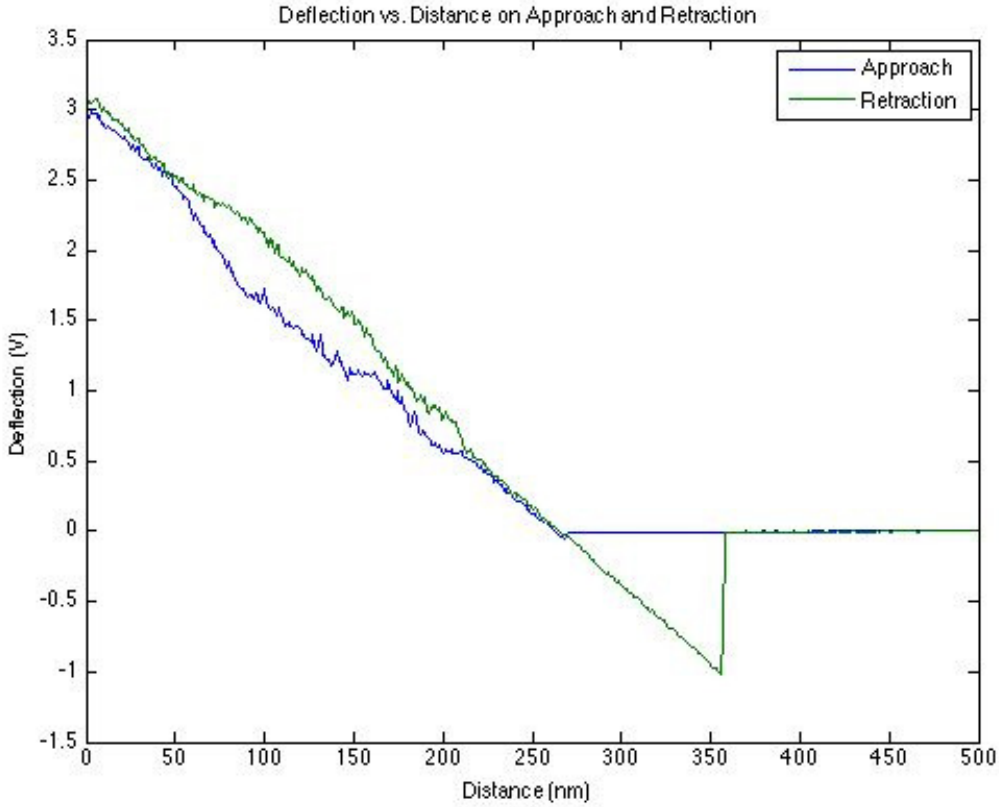
Deflection vs. Distance on Approach and Retraction
Approach
Retraction
Deflection (V)
Distance (nm)
3.5
3
2.5
2
1.5
1
0.5
0
-0.5
-1
-1.5
0
50
100
150
200
250
300
350
400
450
500

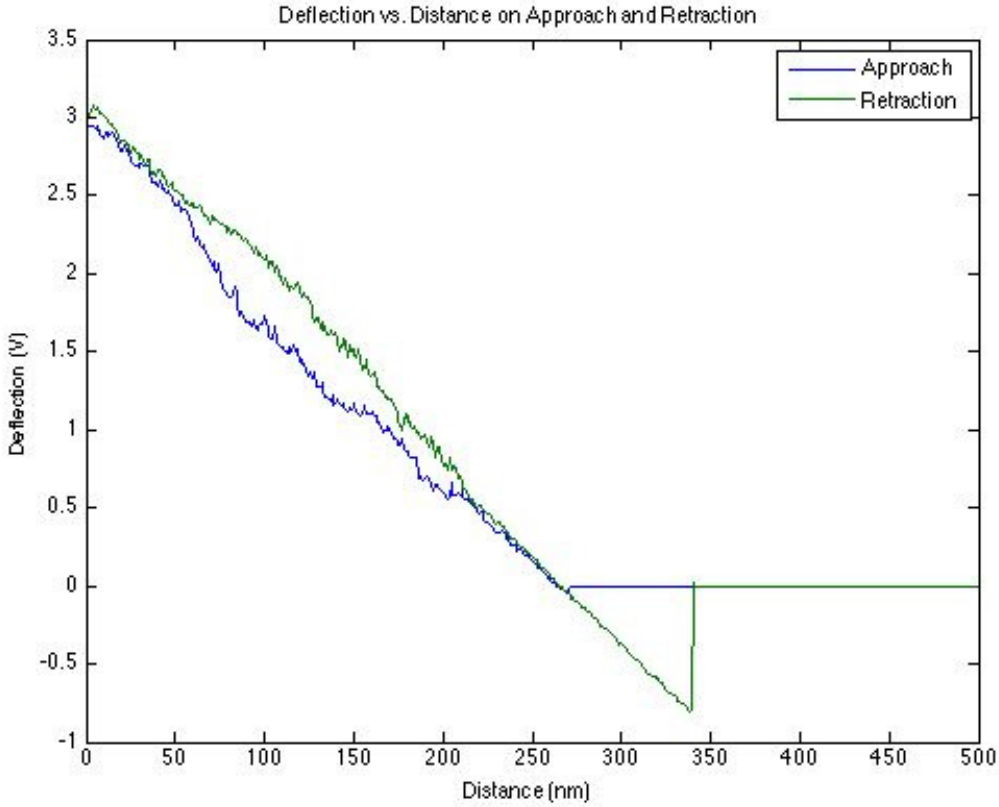
Deflection vs. Distance on Approach and Retraction
Approach
Retraction
Deflection (V)
Distance (nm)
3.5
3
2.5
2
1.5
1
0.5
0
-0.5
-1
0
50
100
150
200
250
300
350
400
450
500

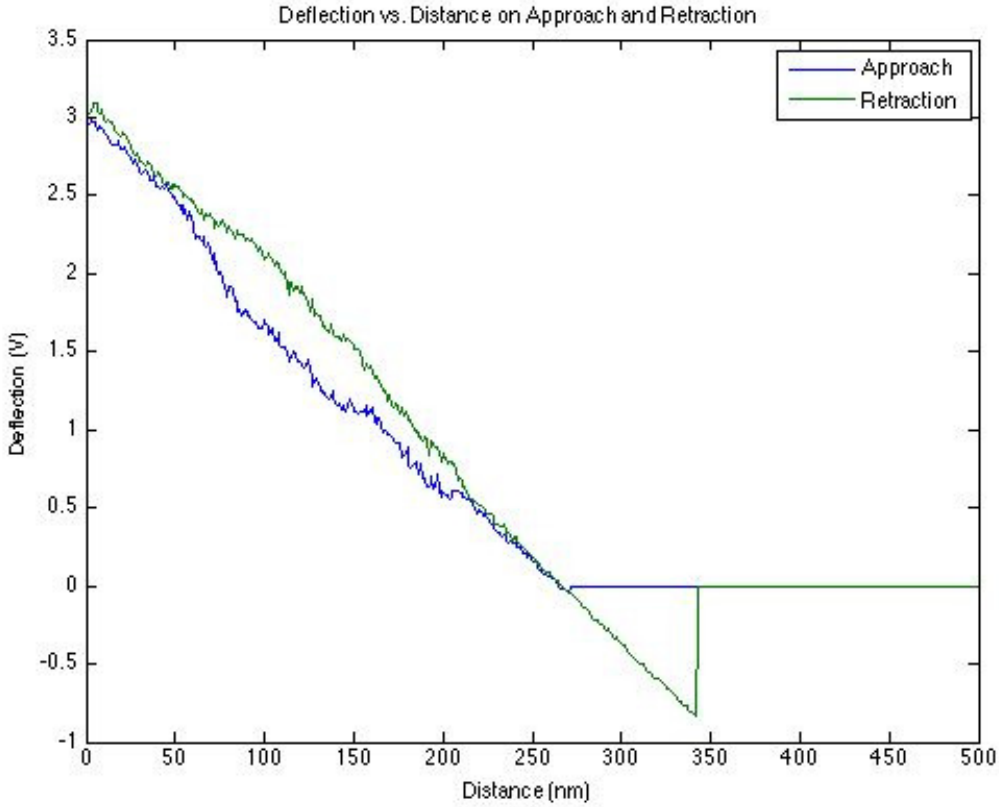
Deflection vs. Distance on Approach and Retraction
Approach
Retraction
Deflection (V)
Distance (nm)
3.5
3
2.5
2
1.5
1
0.5
0
-0.5
-1
0
50
100
150
200
250
300
350
400
450
500

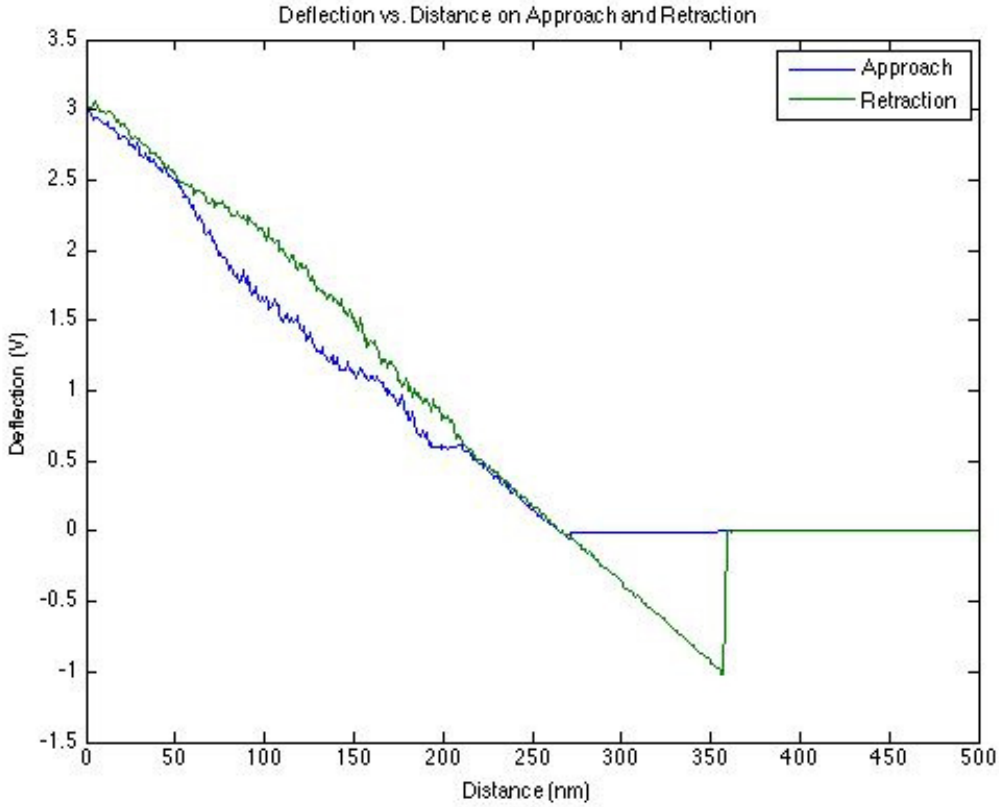
Deflection vs. Distance on Approach and Retraction
Approach
Retraction
Deflection (V)
Distance (nm)
3.5
3
2.5
2
1.5
1
0.5
0
-0.5
-1
-1.5
0
50
100
150
200
250
300
350
400
450
500

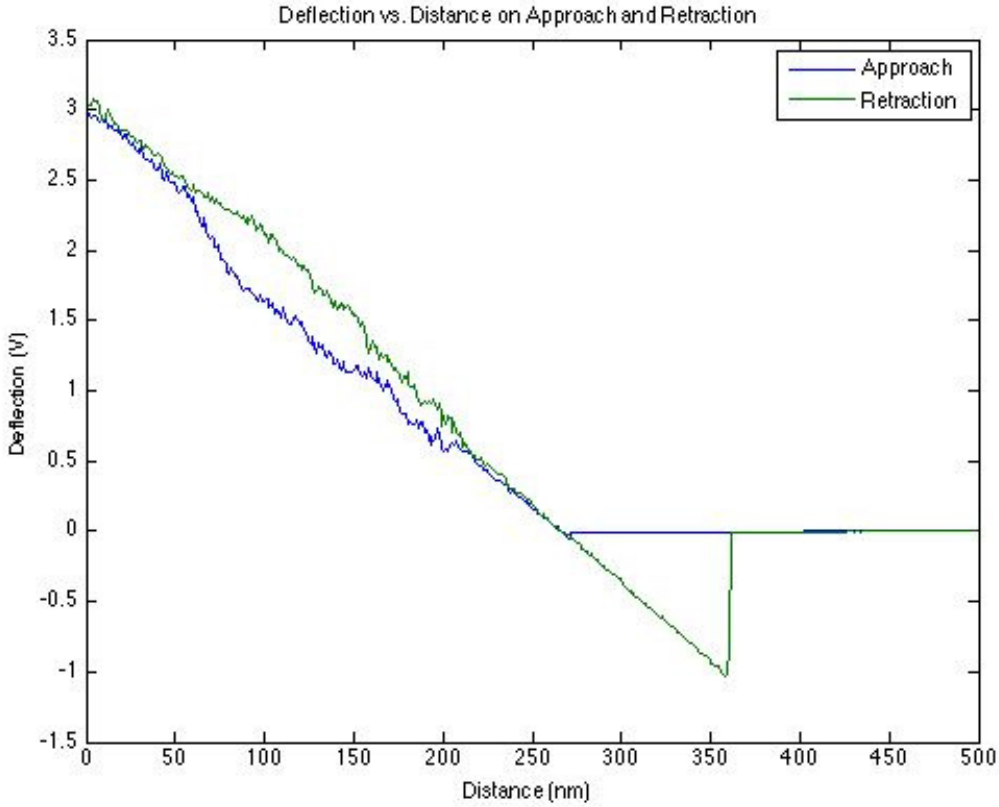
Deflection vs. Distance on Approach and Retraction
Approach
Retraction
Deflection (V)
Distance (nm)
3.5
3
2.5
2
1.5
1
0.5
0
-0.5
-1
-1.5
0
50
100
150
200
250
300
350
400
450
500

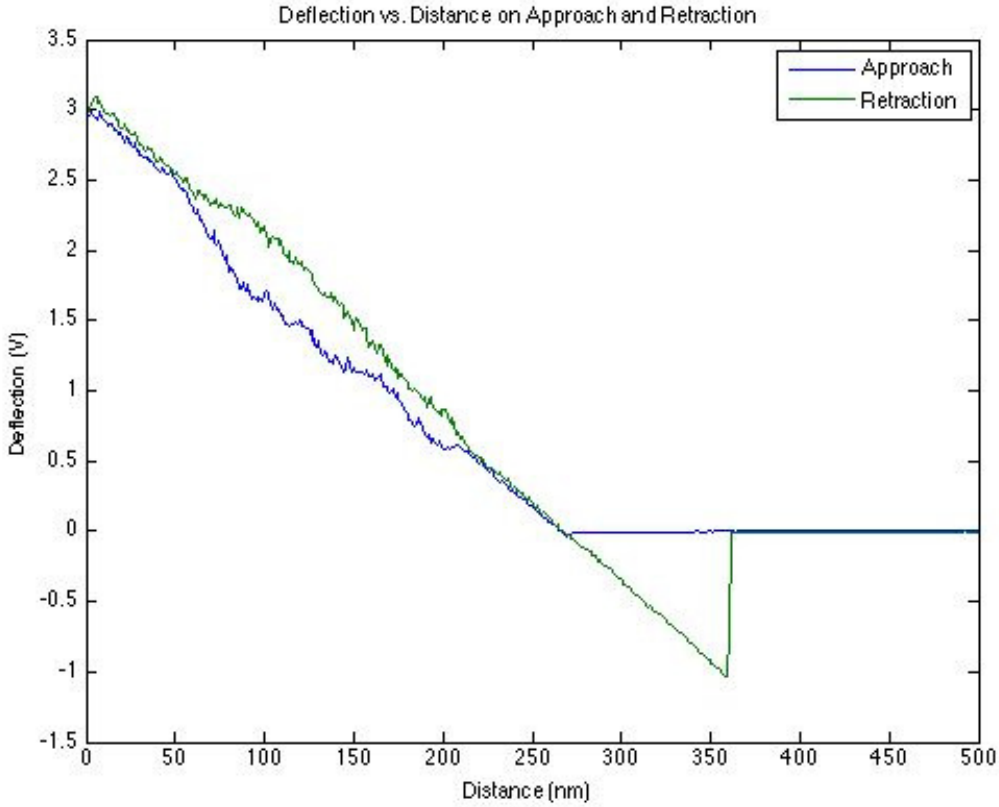
Deflection vs. Distance on Approach and Retraction
Approach
Retraction
Deflection (V)
Distance (nm)
3.5
3
2.5
2
1.5
1
0.5
0
-0.5
-1
-1.5
0
50
100
150
200
250
300
350
400
450
500

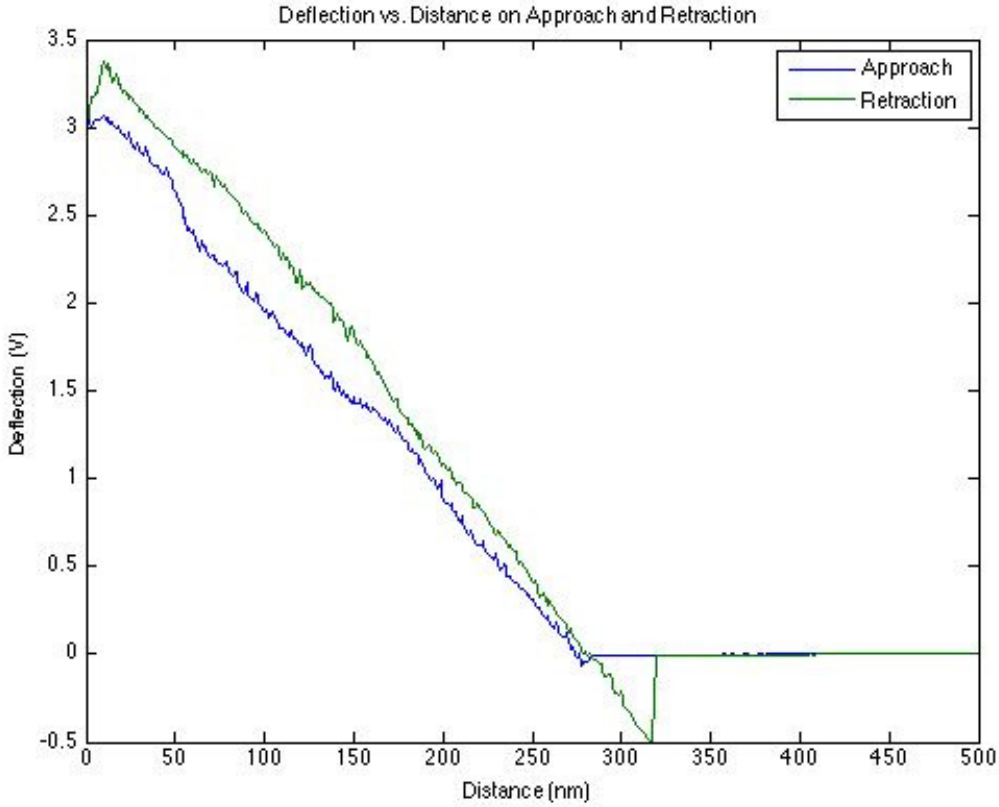
Deflection vs. Distance on Approach and Retraction
Approach
Retraction
Deflection (V)
Distance (nm)
3.5
3
2.5
2
1.5
1
0.5
0
-0.5
0
50
100
150
200
250
300
350
400
450
500

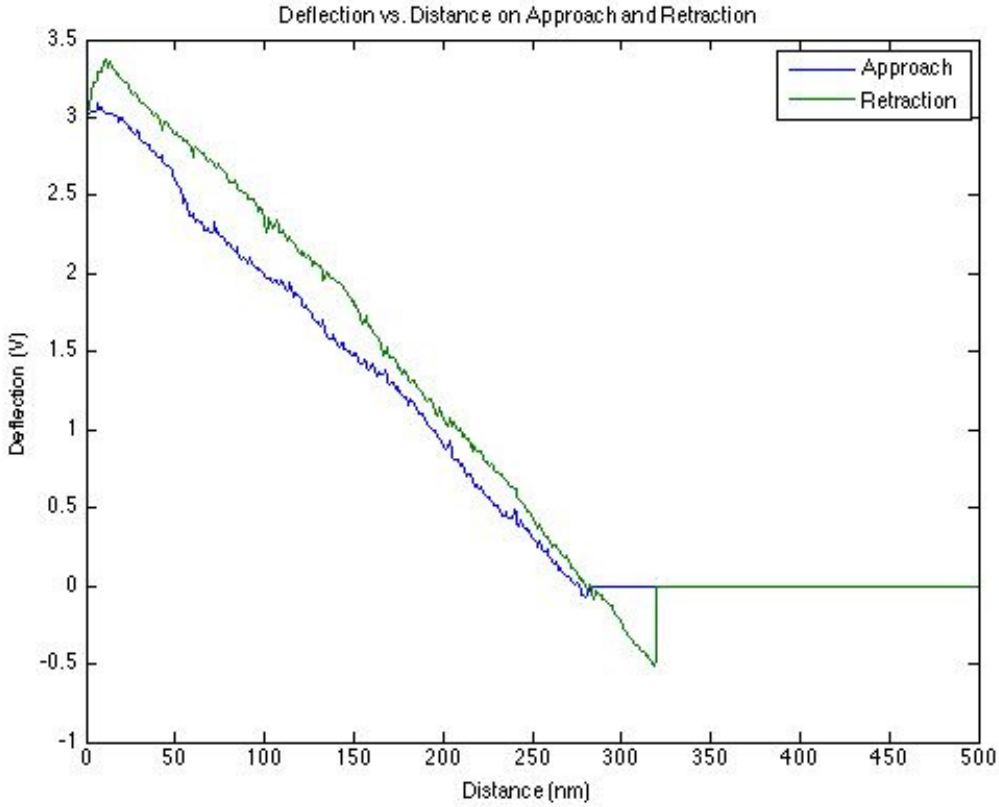
Deflection vs. Distance on Approach and Retraction
Approach
Retraction
Deflection (V)
Distance (nm)
3.5
3
2.5
2
1.5
1
0.5
0
-0.5
-1
0
50
100
150
200
250
300
350
400
450
500

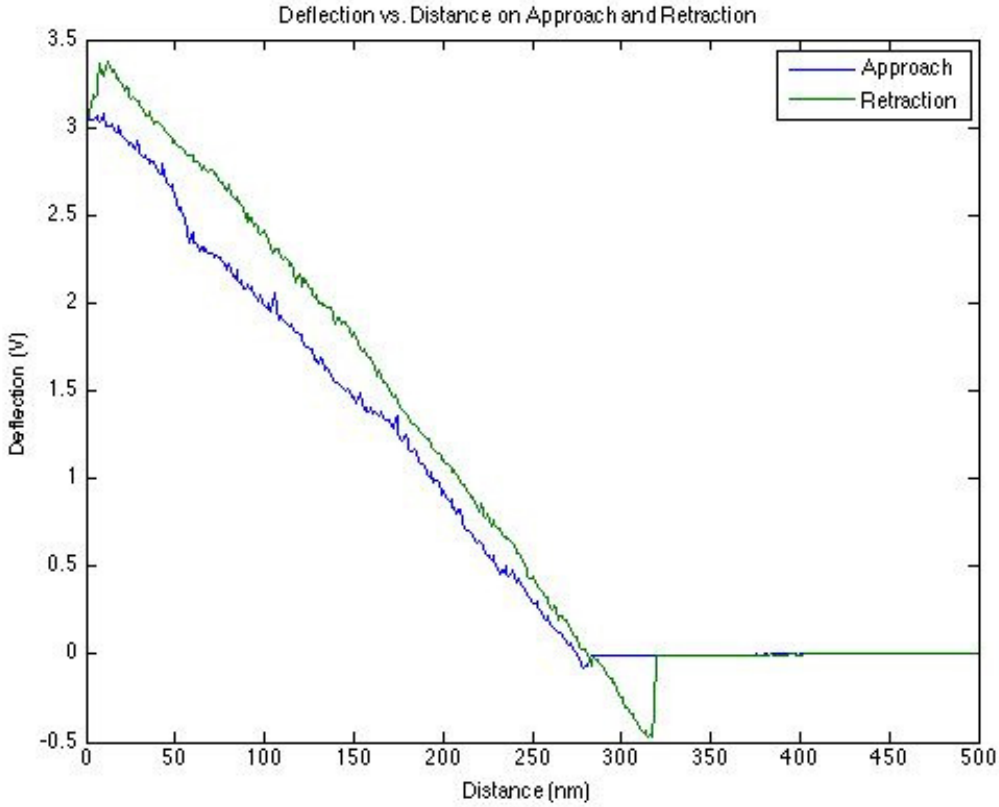
Deflection vs. Distance on Approach and Retraction
Approach
Retraction
Deflection (V)
Distance (nm)
3.5
3
2.5
2
1.5
1
0.5
0
-0.5
0
50
100
150
200
250
300
350
400
450
500

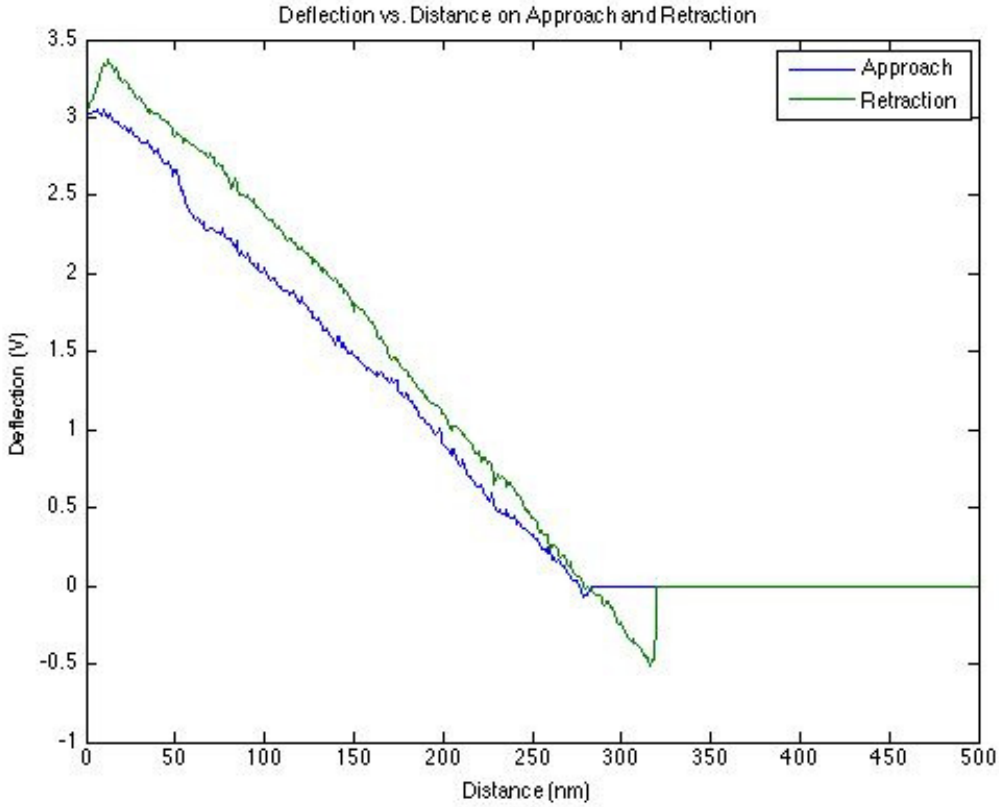
Deflection vs. Distance on Approach and Retraction
Approach
Retraction
Deflection (V)
Distance (nm)
3.5
3
2.5
2
1.5
1
0.5
0
-0.5
-1
0
50
100
150
200
250
300
350
400
450
500

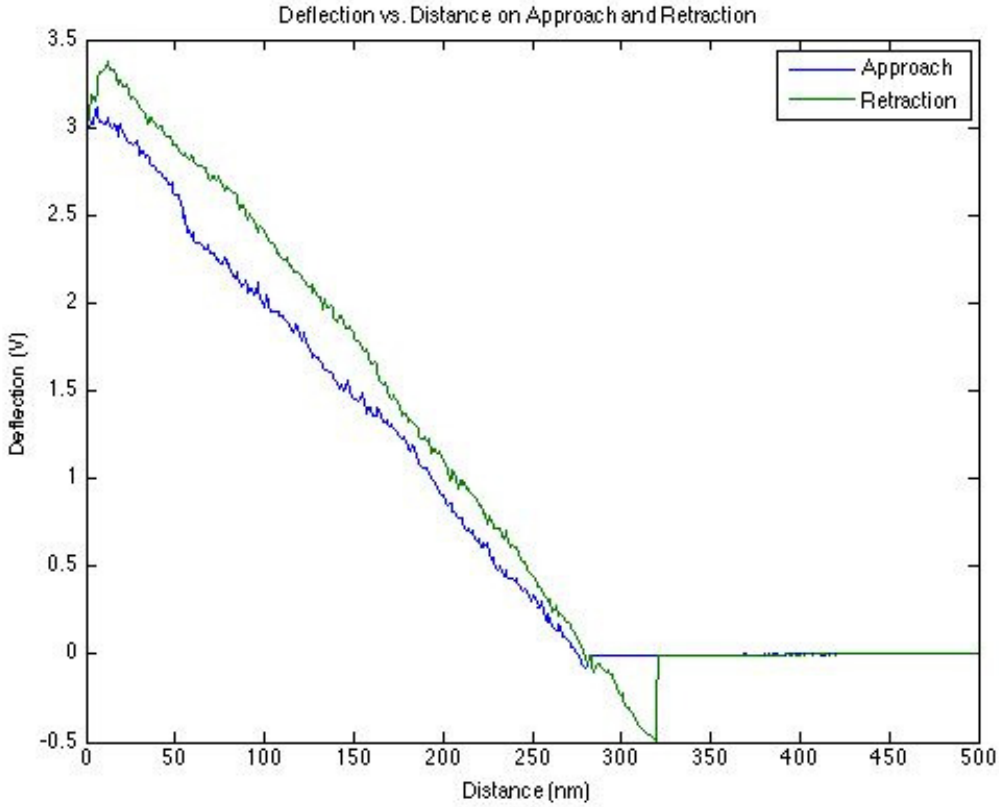
Deflection vs. Distance on Approach and Retraction
Approach
Retraction
Deflection (V)
Distance (nm)
3.5
3
2.5
2
1.5
1
0.5
0
-0.5
0
50
100
150
200
250
300
350
400
450
500

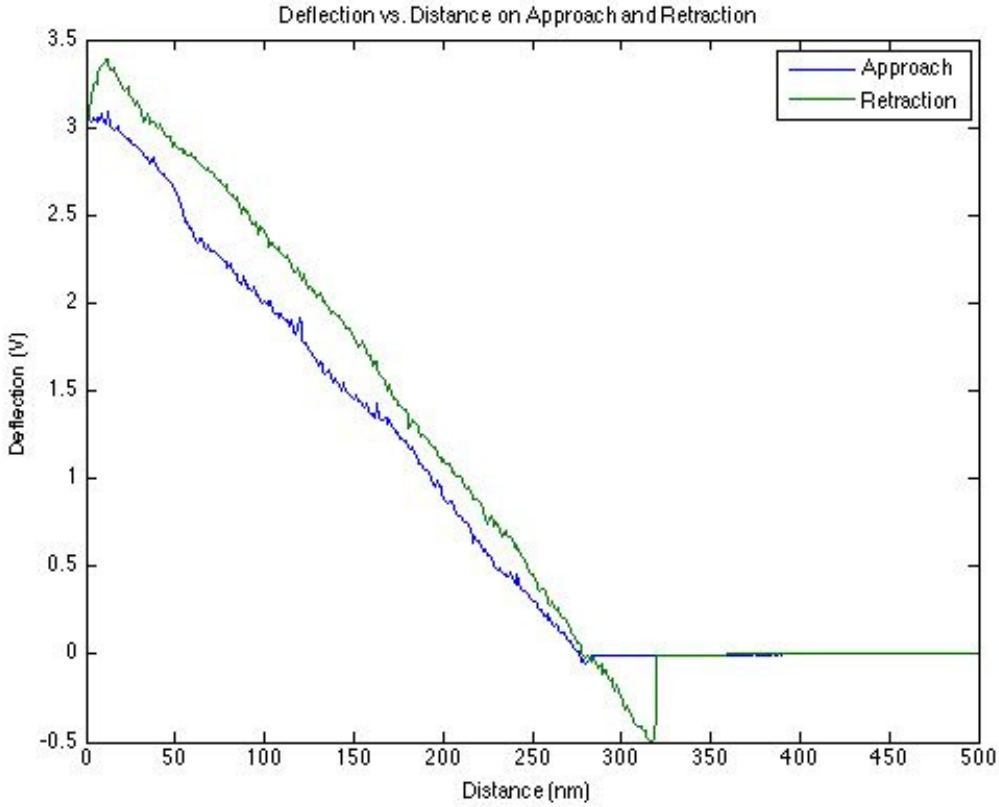
Deflection vs. Distance on Approach and Retraction
Approach
Retraction
Deflection (V)
Distance (nm)
3.5
3
2.5
2
1.5
1
0.5
0
-0.5
0
50
100
150
200
250
300
350
400
450
500

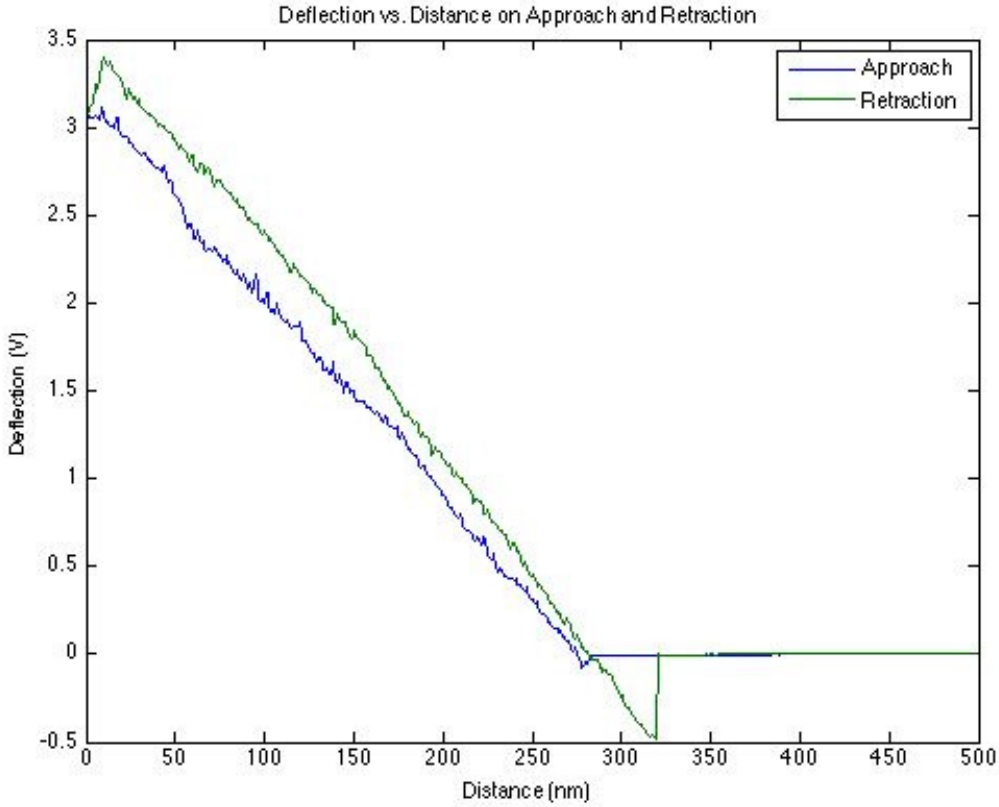
Deflection vs. Distance on Approach and Retraction
Approach
Retraction
Deflection (V)
Distance (nm)
3.5
3
2.5
2
1.5
1
0.5
0
-0.5
0
50
100
150
200
250
300
350
400
450
500

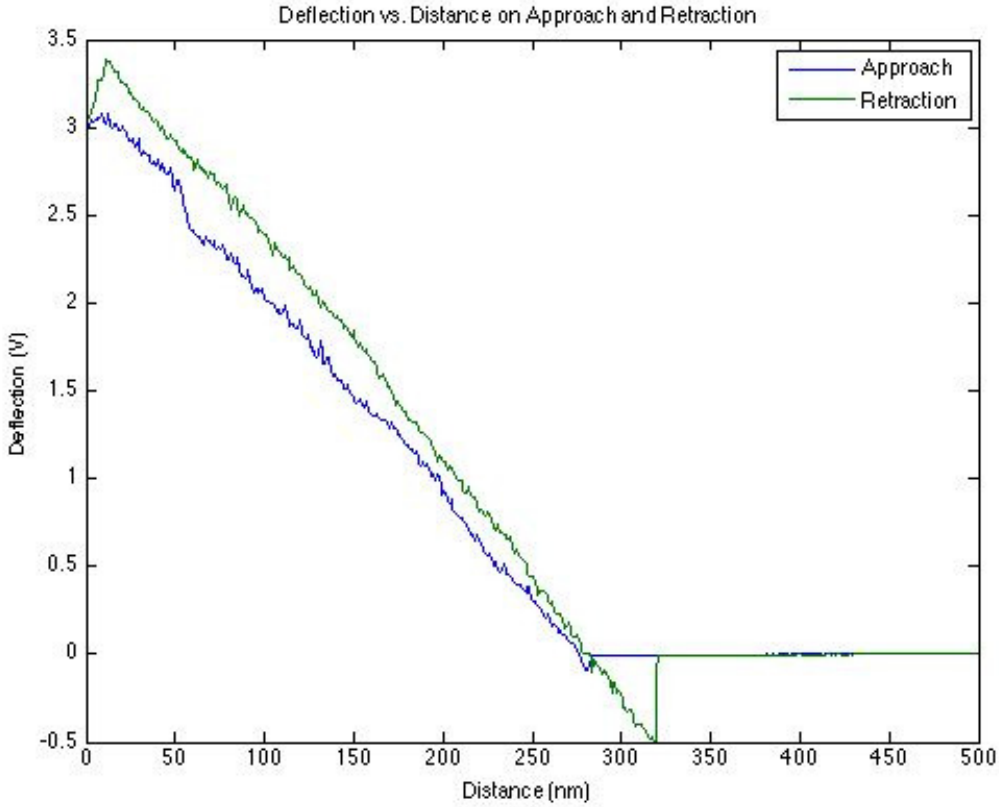
Deflection vs. Distance on Approach and Retraction
Approach
Retraction
Deflection (V)
Distance (nm)
3.5
3
2.5
2
1.5
1
0.5
0
-0.5
0
50
100
150
200
250
300
350
400
450
500

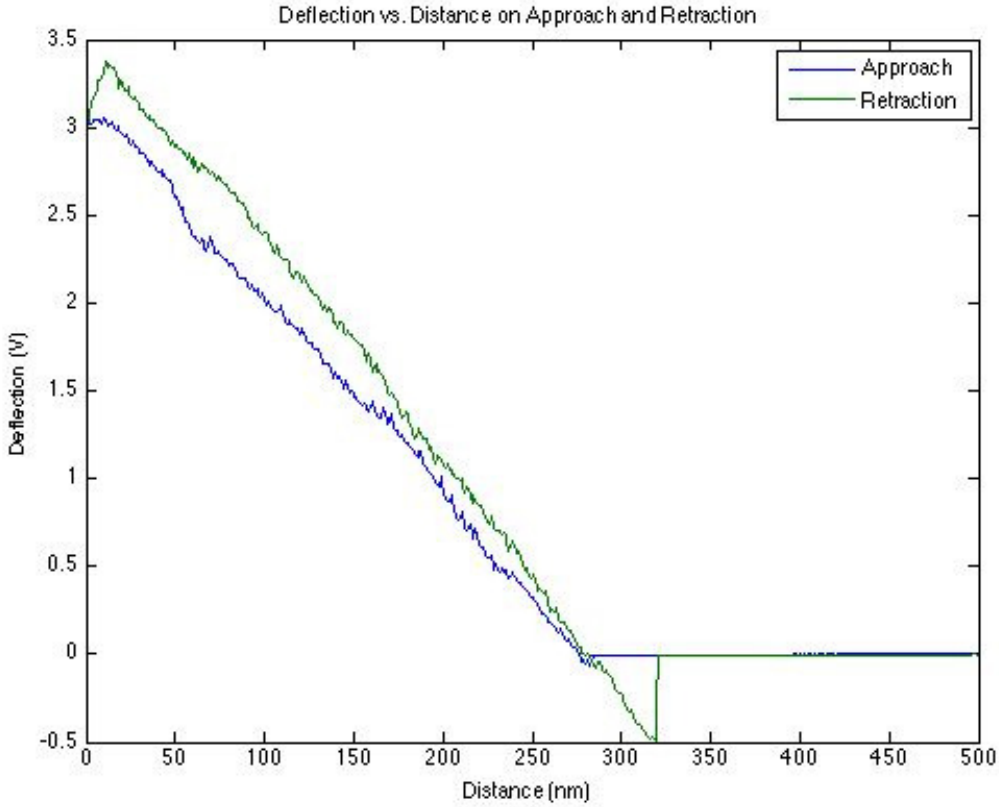
Deflection vs. Distance on Approach and Retraction
Approach
Retraction
Deflection (V)
Distance (nm)
3.5
3
2.5
2
1.5
1
0.5
0
-0.5
0
50
100
150
200
250
300
350
400
450
500

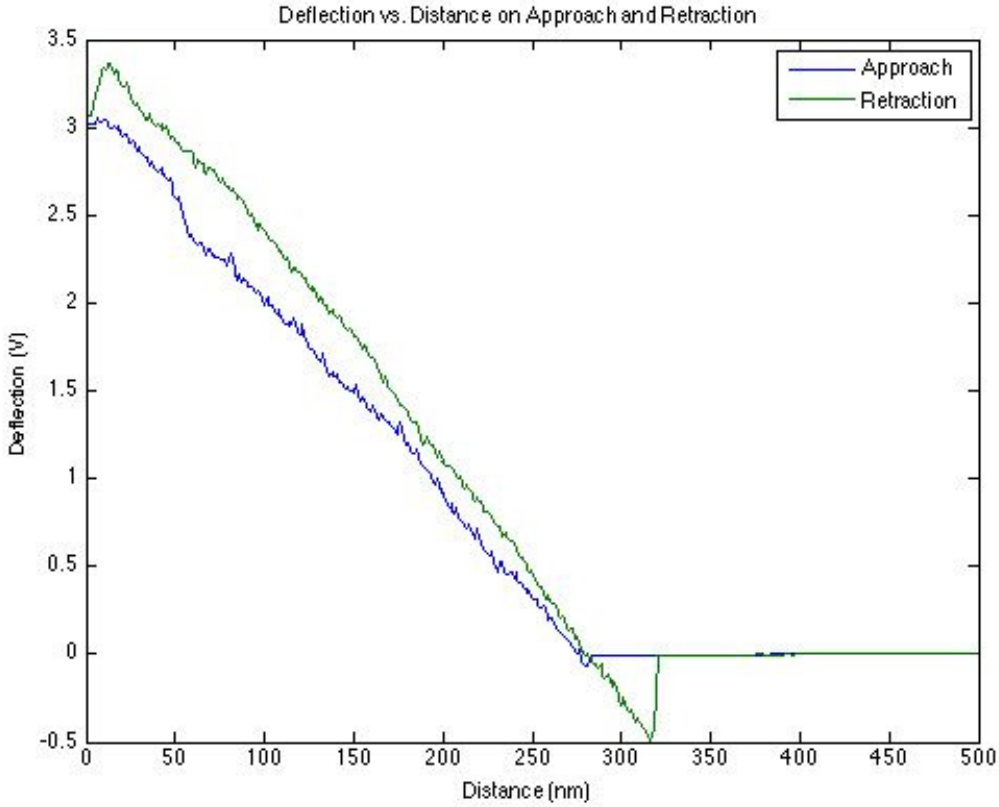
Deflection vs. Distance on Approach and Retraction
Approach
Retraction
Deflection (V)
Distance (nm)
3.5
3
2.5
2
1.5
1
0.5
0
-0.5
0
50
100
150
200
250
300
350
400
450
500

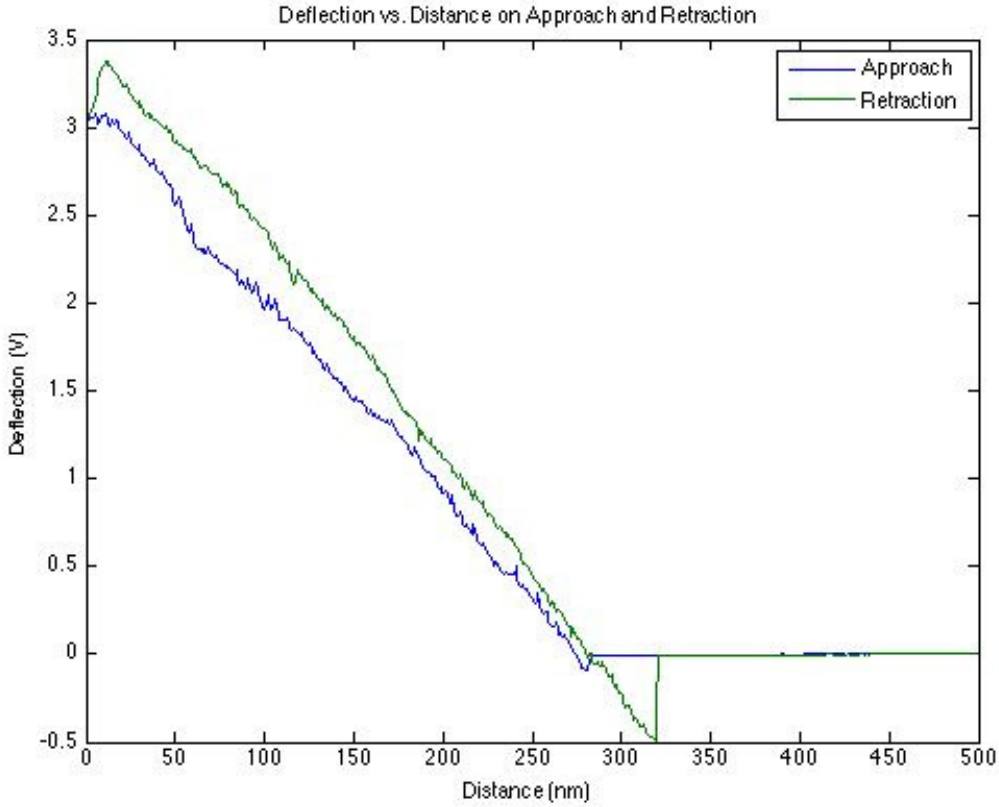
Deflection vs. Distance on Approach and Retraction
Approach
Retraction
Deflection (V)
Distance (nm)
3.5
3
2.5
2
1.5
1
0.5
0
-0.5
0
50
100
150
200
250
300
350
400
450
500

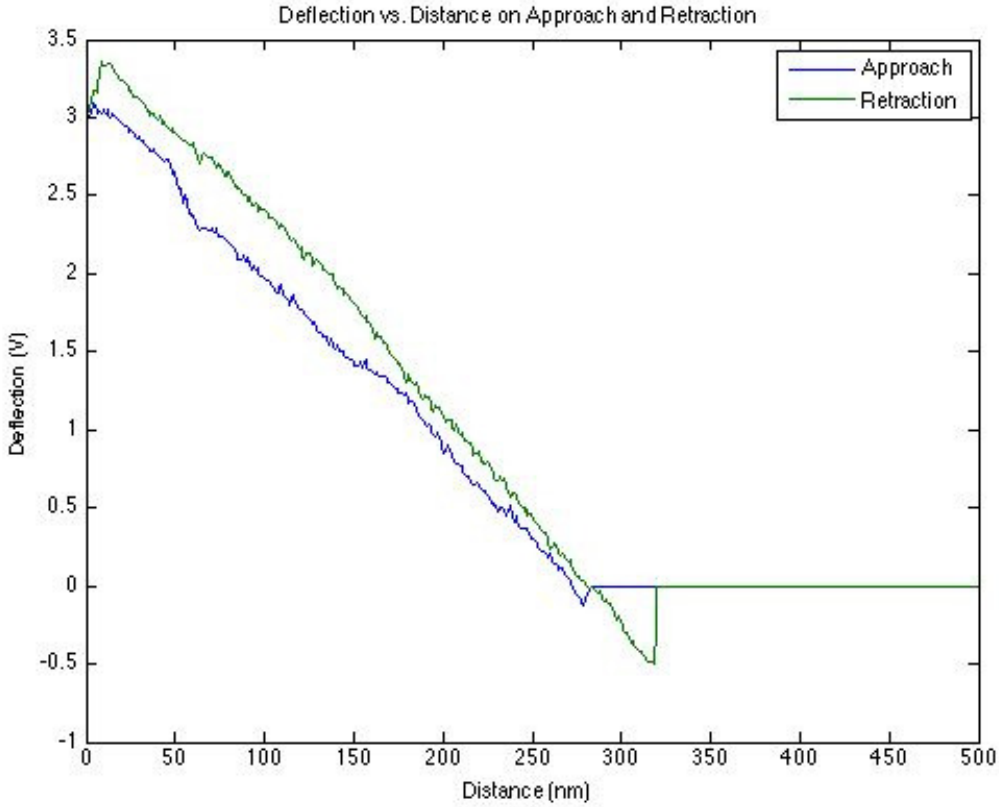
Deflection vs. Distance on Approach and Retraction
Approach
Retraction
Deflection (V)
Distance (nm)
3.5
3
2.5
2
1.5
1
0.5
0
-0.5
-1
0
50
100
150
200
250
300
350
400
450
500

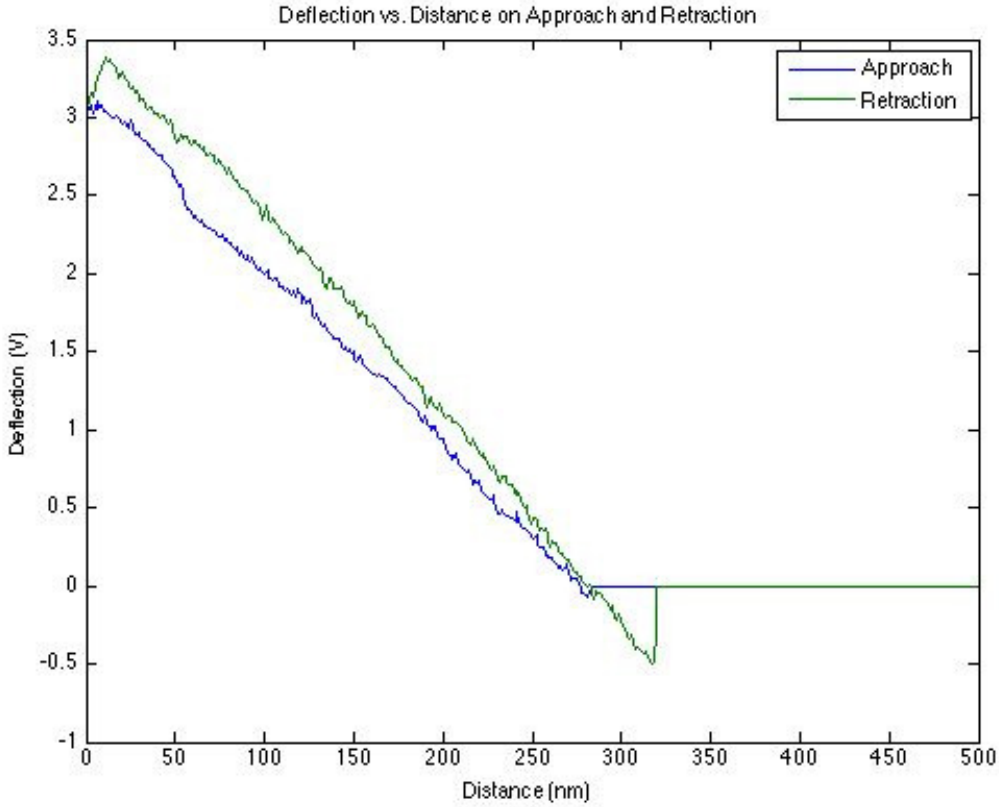
Deflection vs. Distance on Approach and Retraction
Approach
Retraction
Deflection (V)
Distance (nm)
3.5
3
2.5
2
1.5
1
0.5
0
-0.5
-1
0
50
100
150
200
250
300
350
400
450
500

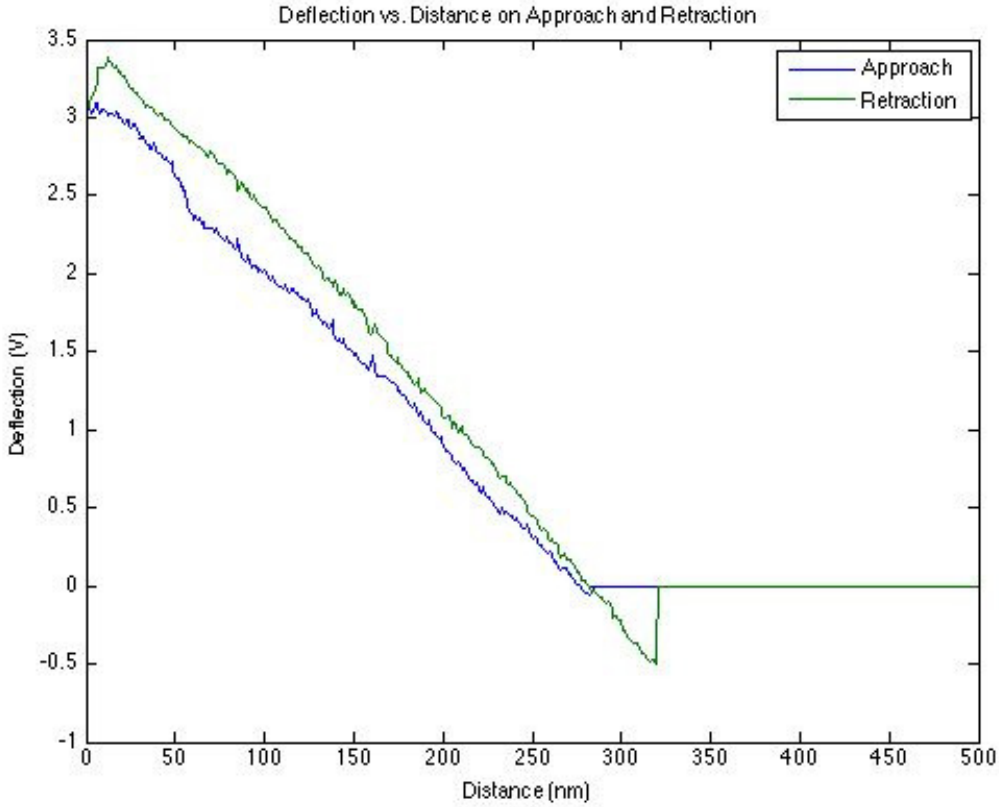
Deflection vs. Distance on Approach and Retraction
Approach
Retraction
Deflection (V)
Distance (nm)
3.5
3
2.5
2
1.5
1
0.5
0
-0.5
-1
0
50
100
150
200
250
300
350
400
450
500

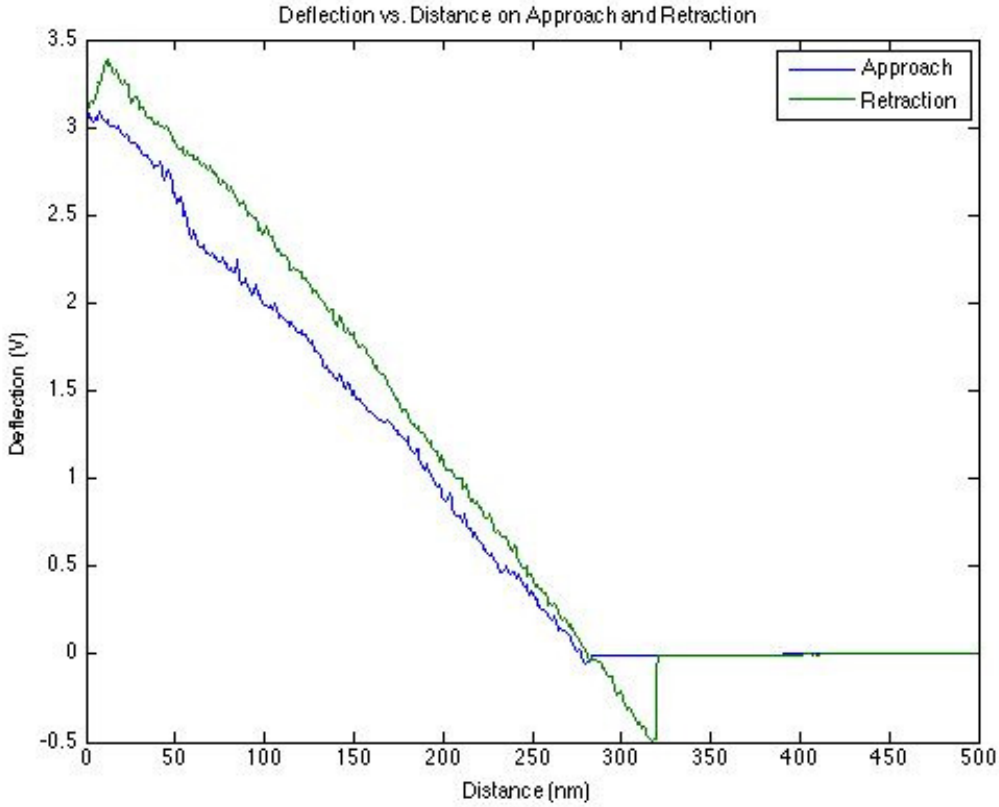
Deflection vs. Distance on Approach and Retraction
Approach
Retraction
Deflection (V)
Distance (nm)
3.5
3
2.5
2
1.5
1
0.5
0
-0.5
0
50
100
150
200
250
300
350
400
450
500

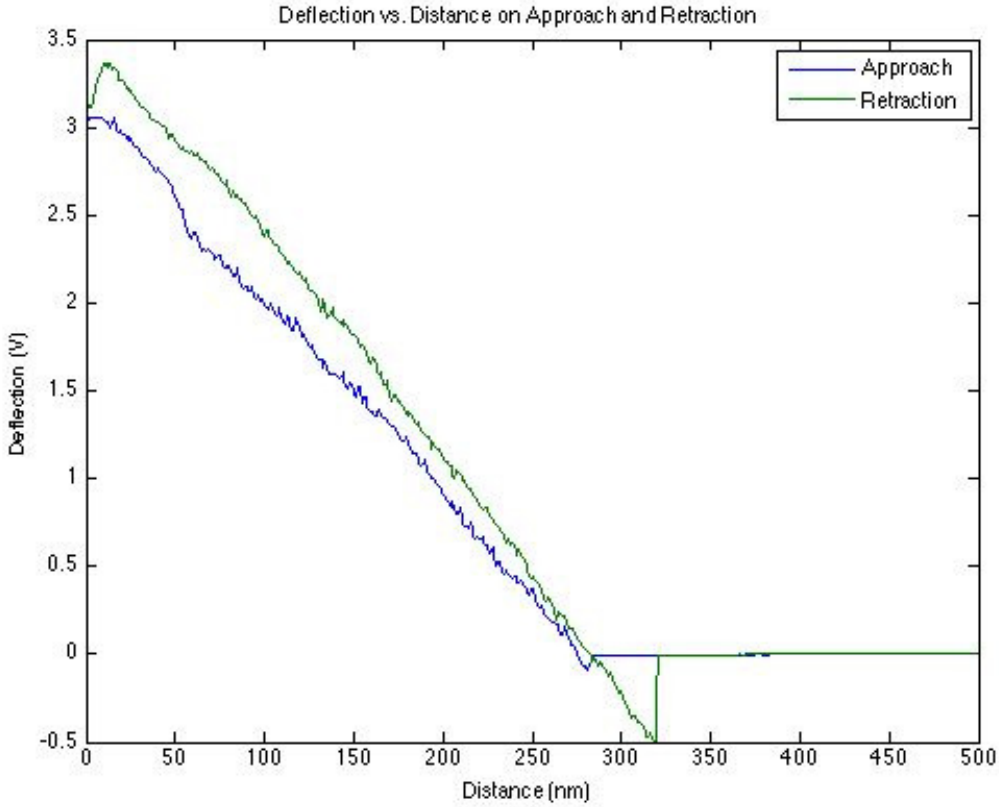
Deflection vs. Distance on Approach and Retraction
Approach
Retraction
Deflection (V)
Distance (nm)
3.5
3
2.5
2
1.5
1
0.5
0
-0.5
0
50
100
150
200
250
300
350
400
450
500

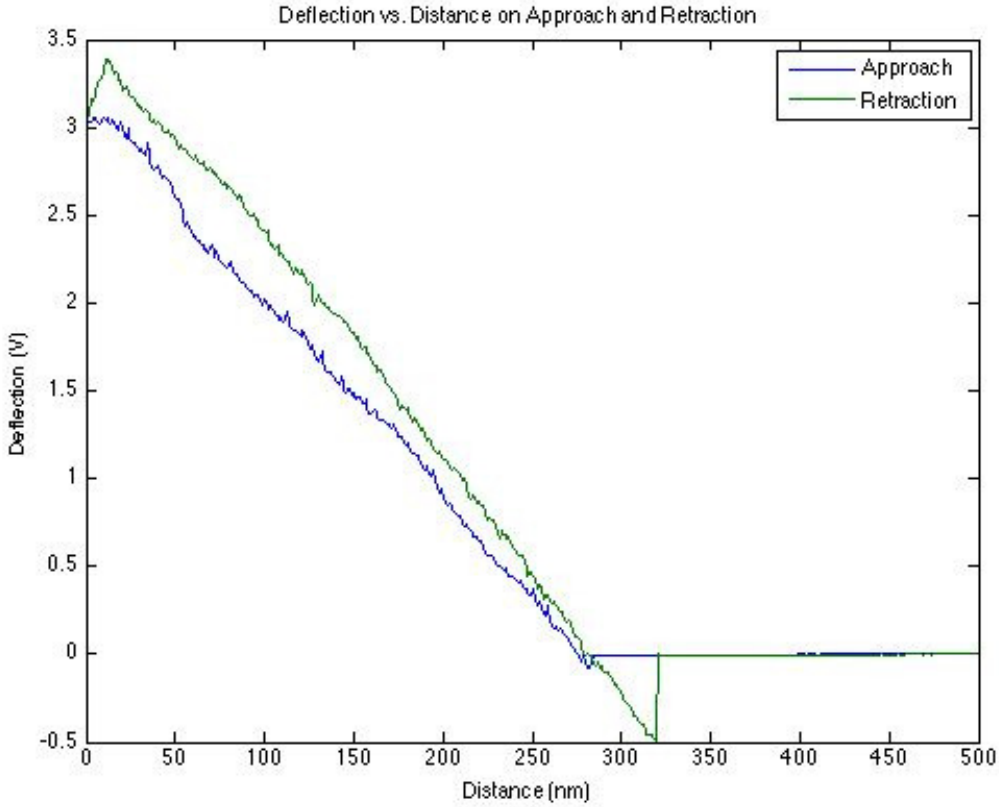
Deflection vs. Distance on Approach and Retraction
Approach
Retraction
Deflection (V)
Distance (nm)
3.5
3
2.5
2
1.5
1
0.5
0
-0.5
0
50
100
150
200
250
300
350
400
450
500

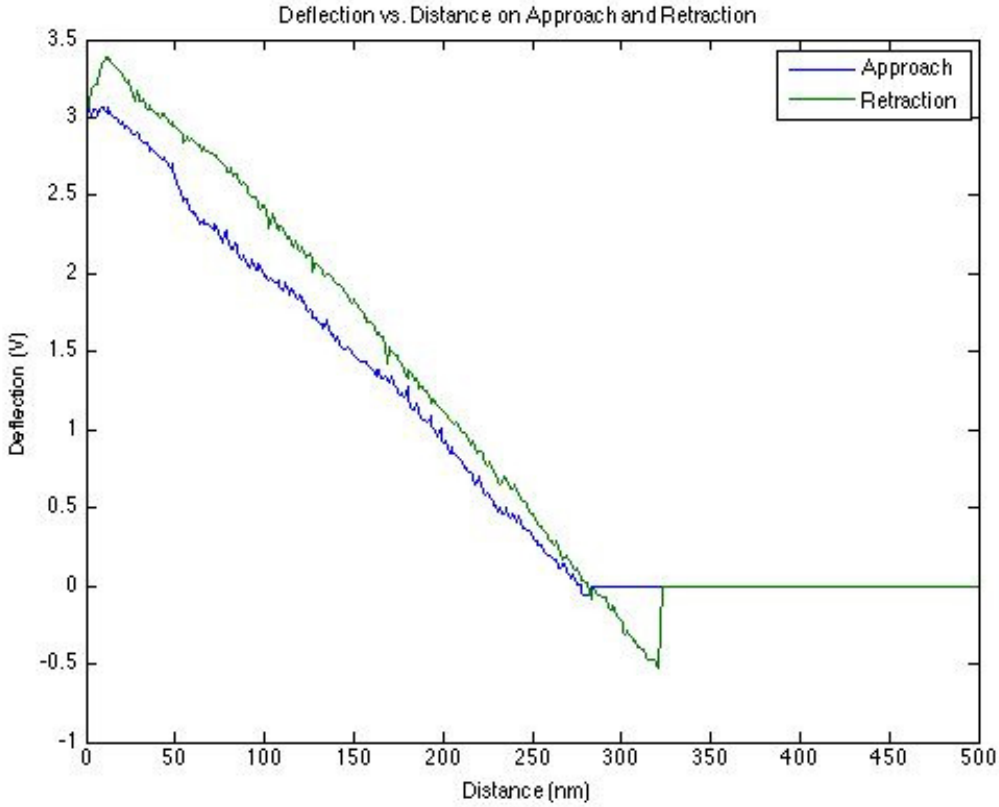
Deflection vs. Distance on Approach and Retraction
Approach
Retraction
Deflection (V)
Distance (nm)
3.5
3
2.5
2
1.5
1
0.5
0
-0.5
-1
0
50
100
150
200
250
300
350
400
450
500

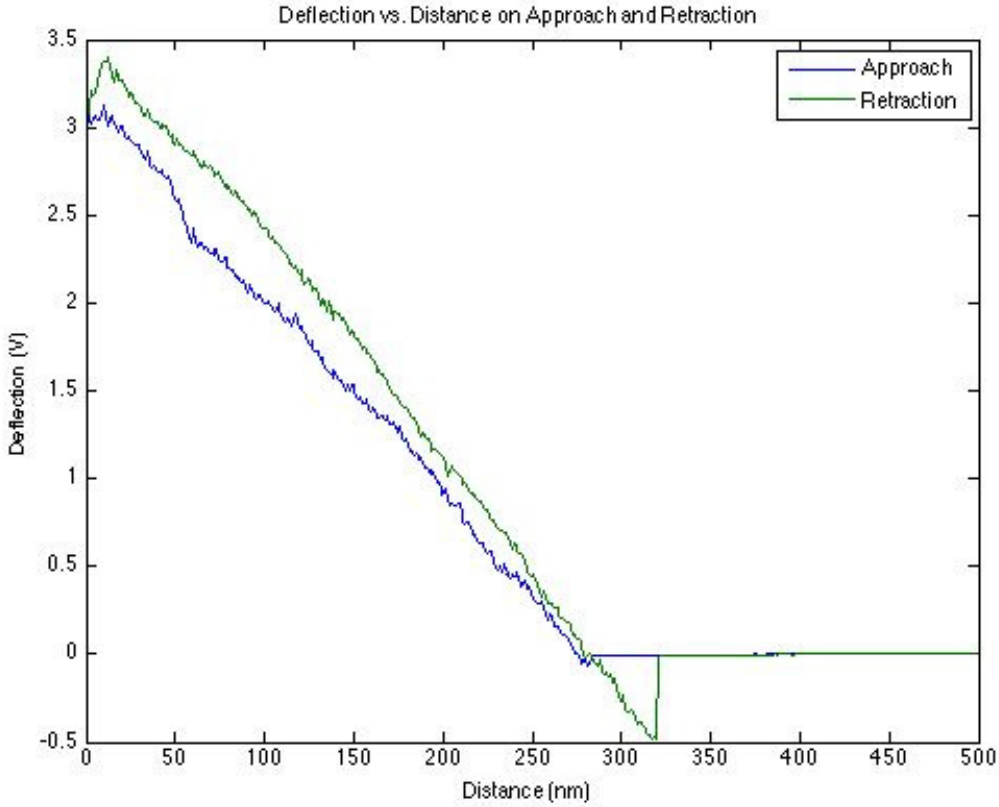
Deflection vs. Distance on Approach and Retraction
Approach
Retraction
Deflection (V)
Distance (nm)
3.5
3
2.5
2
1.5
1
0.5
0
-0.5
0
50
100
150
200
250
300
350
400
450
500

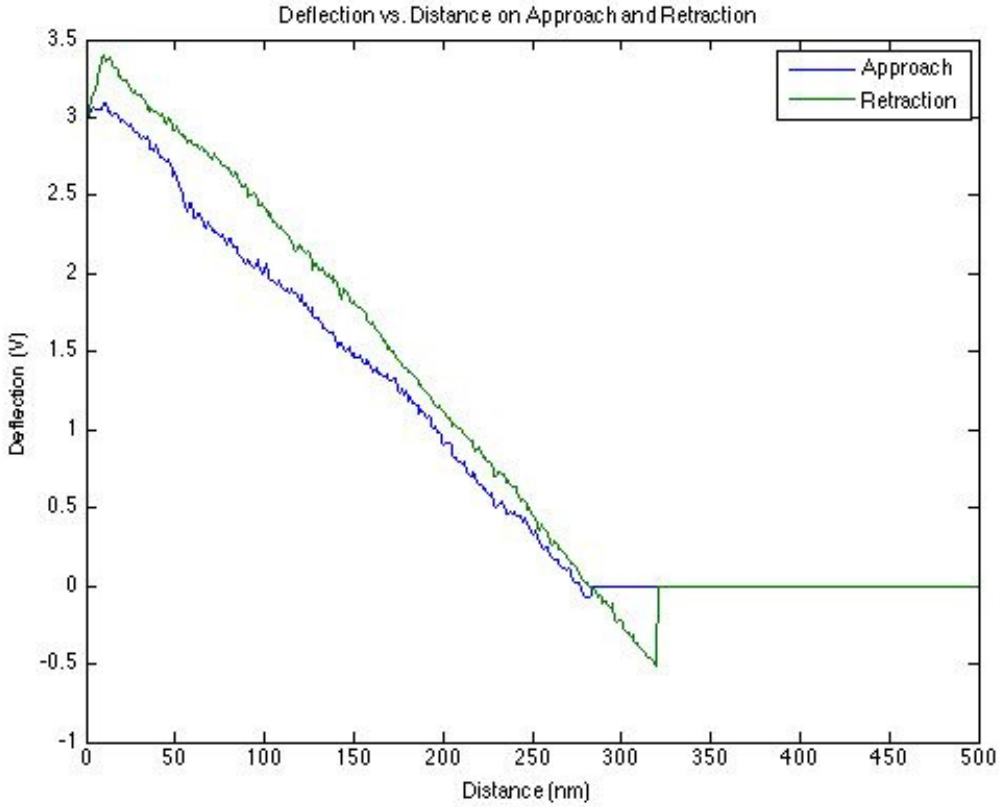
Deflection vs. Distance on Approach and Retraction
Approach
Retraction
Deflection (V)
Distance (nm)
3.5
3
2.5
2
1.5
1
0.5
0
-0.5
-1
0
50
100
150
200
250
300
350
400
450
500

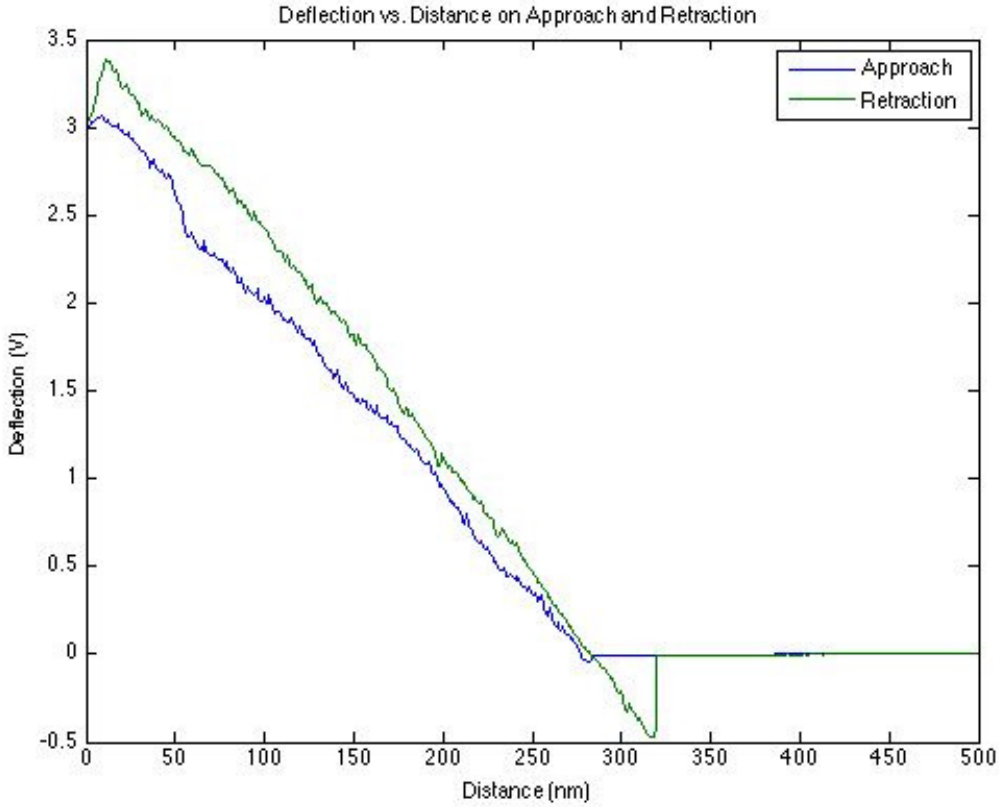
Deflection vs. Distance on Approach and Retraction
Approach
Retraction
Deflection (V)
Distance (nm)
3.5
3
2.5
2
1.5
1
0.5
0
-0.5
0
50
100
150
200
250
300
350
400
450
500

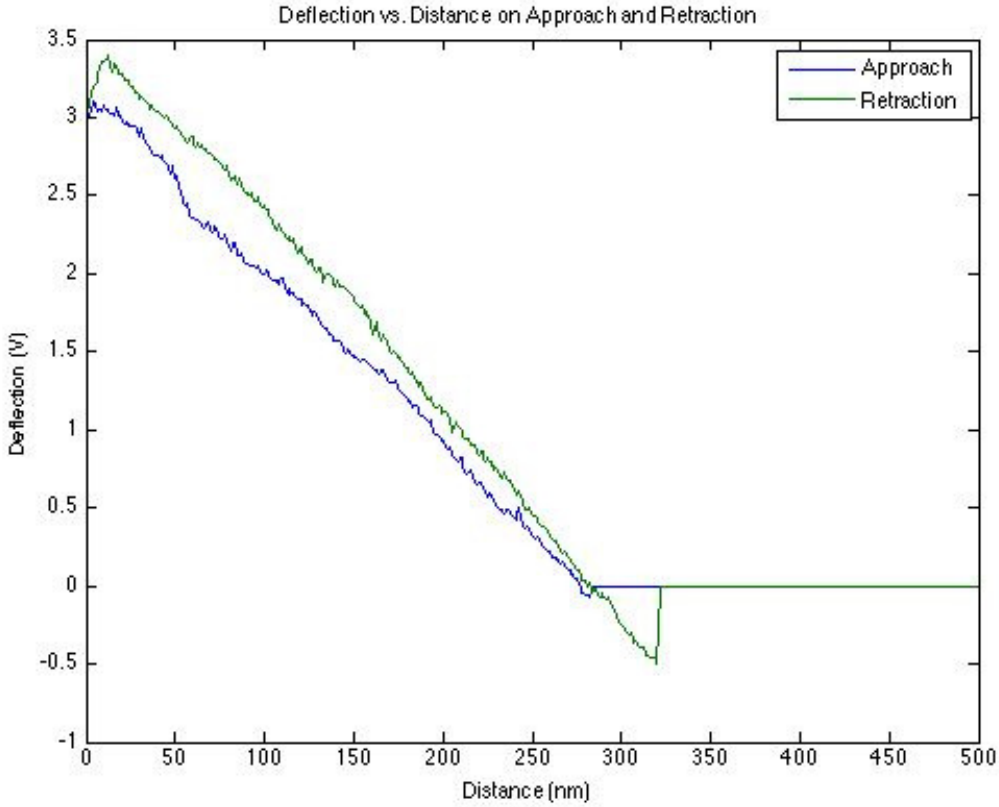
Deflection vs. Distance on Approach and Retraction
Approach
Retraction
Deflection (V)
Distance (nm)
3.5
3
2.5
2
1.5
1
0.5
0
-0.5
-1
0
50
100
150
200
250
300
350
400
450
500

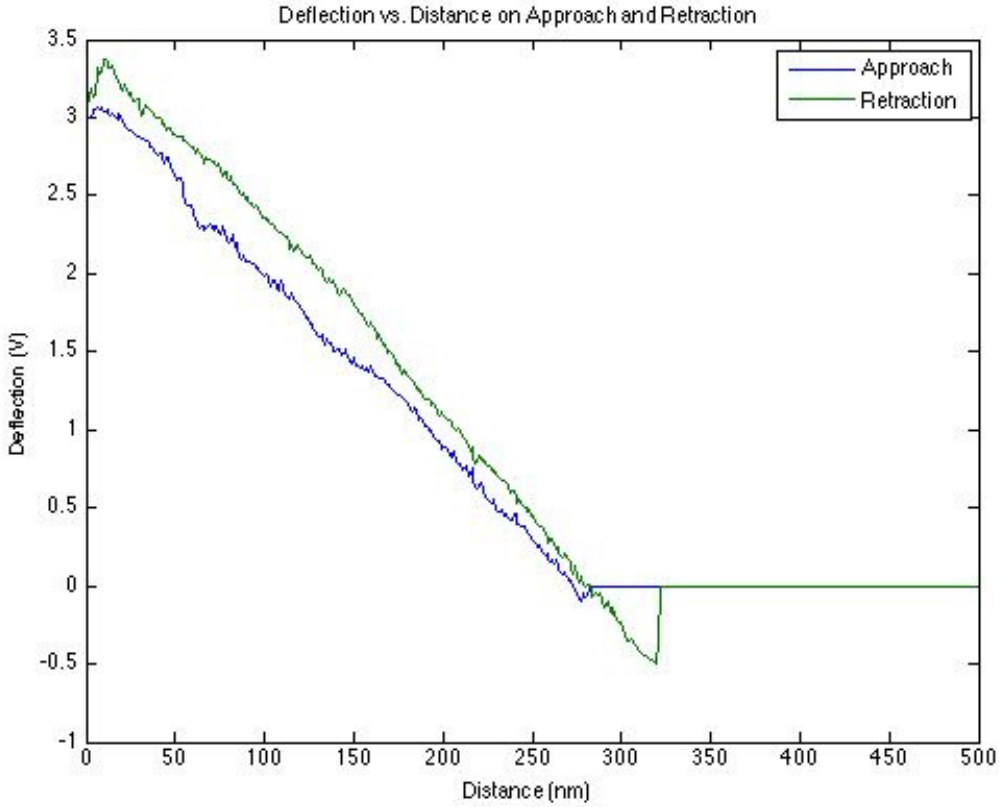
Deflection vs. Distance on Approach and Retraction
Approach
Retraction
Deflection (V)
Distance (nm)
3.5
3
2.5
2
1.5
1
0.5
0
-0.5
-1
0
50
100
150
200
250
300
350
400
450
500

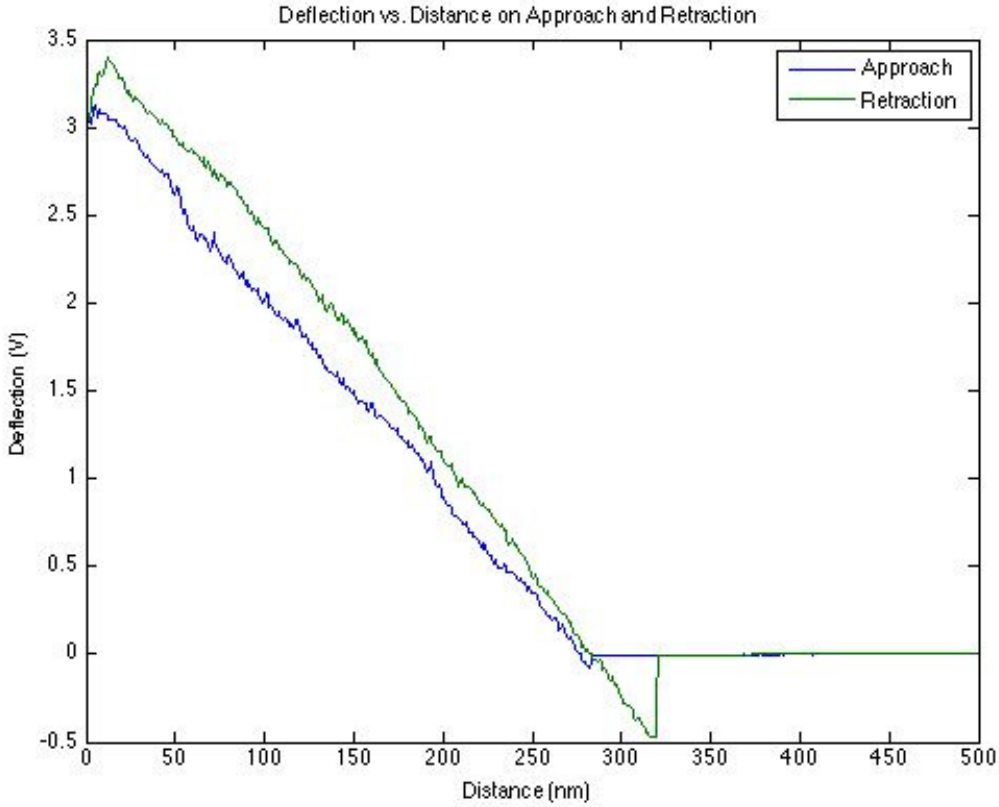
Deflection vs. Distance on Approach and Retraction
Approach
Retraction
Deflection (V)
Distance (nm)
3.5
3
2.5
2
1.5
1
0.5
0
-0.5
0
50
100
150
200
250
300
350
400
450
500

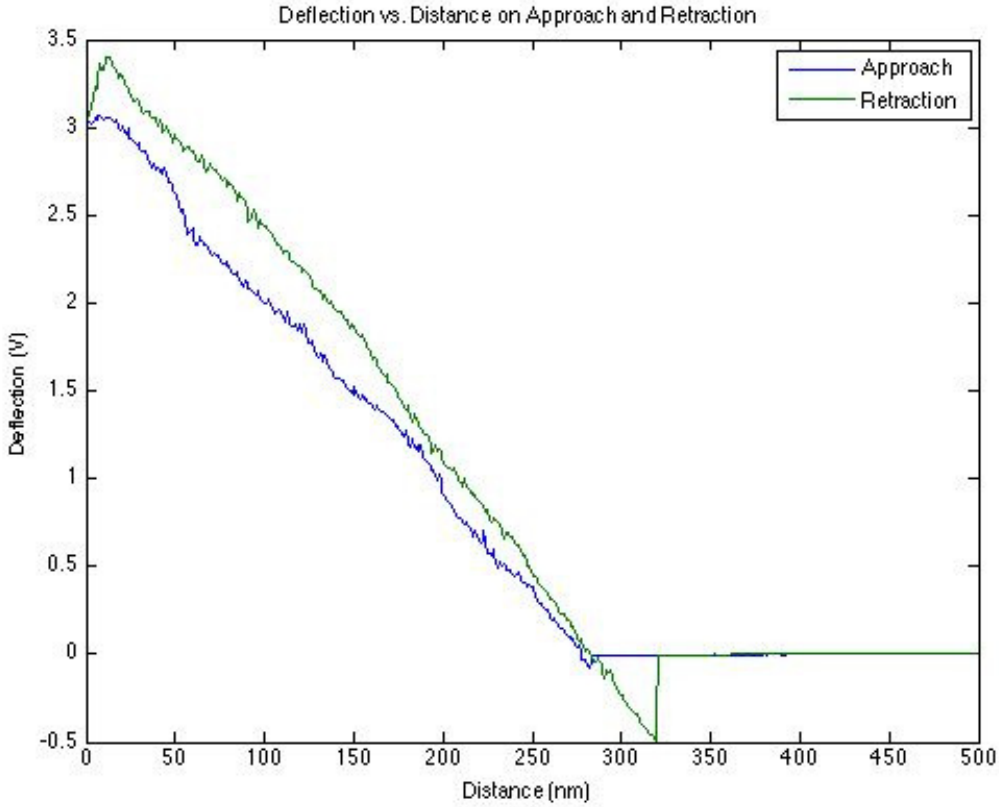
Deflection vs. Distance on Approach and Retraction
Approach
Retraction
Deflection (V)
Distance (nm)
3.5
3
2.5
2
1.5
1
0.5
0
-0.5
0
50
100
150
200
250
300
350
400
450
500

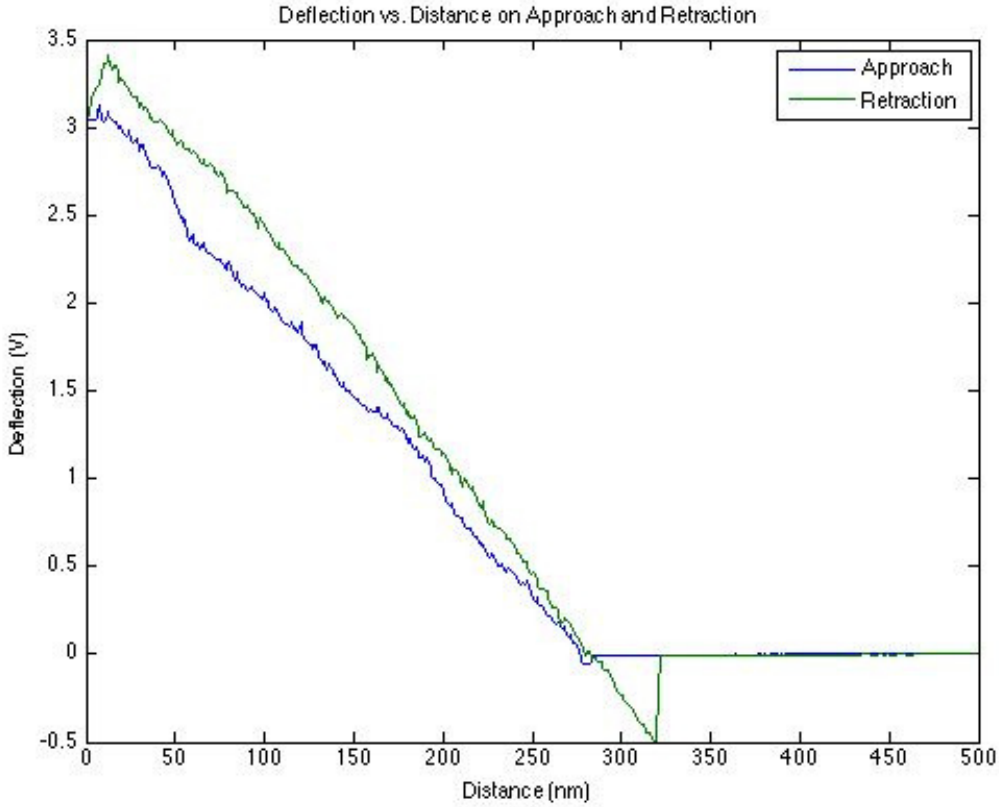
Deflection vs. Distance on Approach and Retraction
Approach
Retraction
Deflection (V)
Distance (nm)
3.5
3
2.5
2
1.5
1
0.5
0
-0.5
0
50
100
150
200
250
300
350
400
450
500

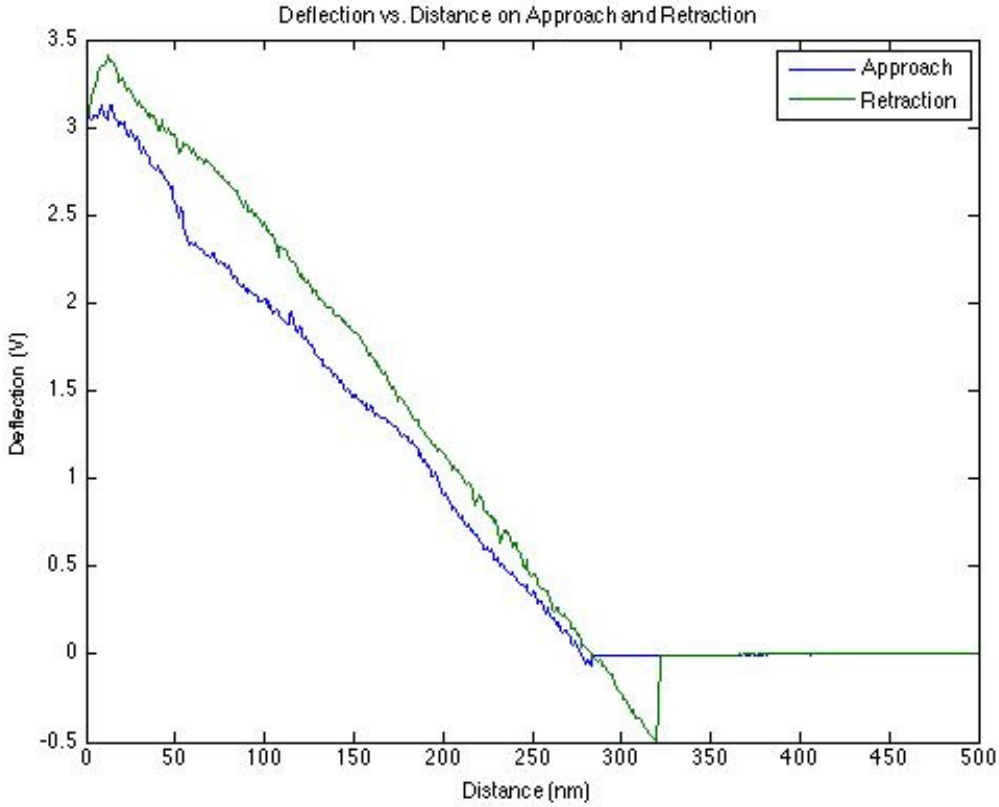
Deflection vs. Distance on Approach and Retraction
Approach
Retraction
Deflection (V)
Distance (nm)
3.5
3
2.5
2
1.5
1
0.5
0
-0.5
0
50
100
150
200
250
300
350
400
450
500

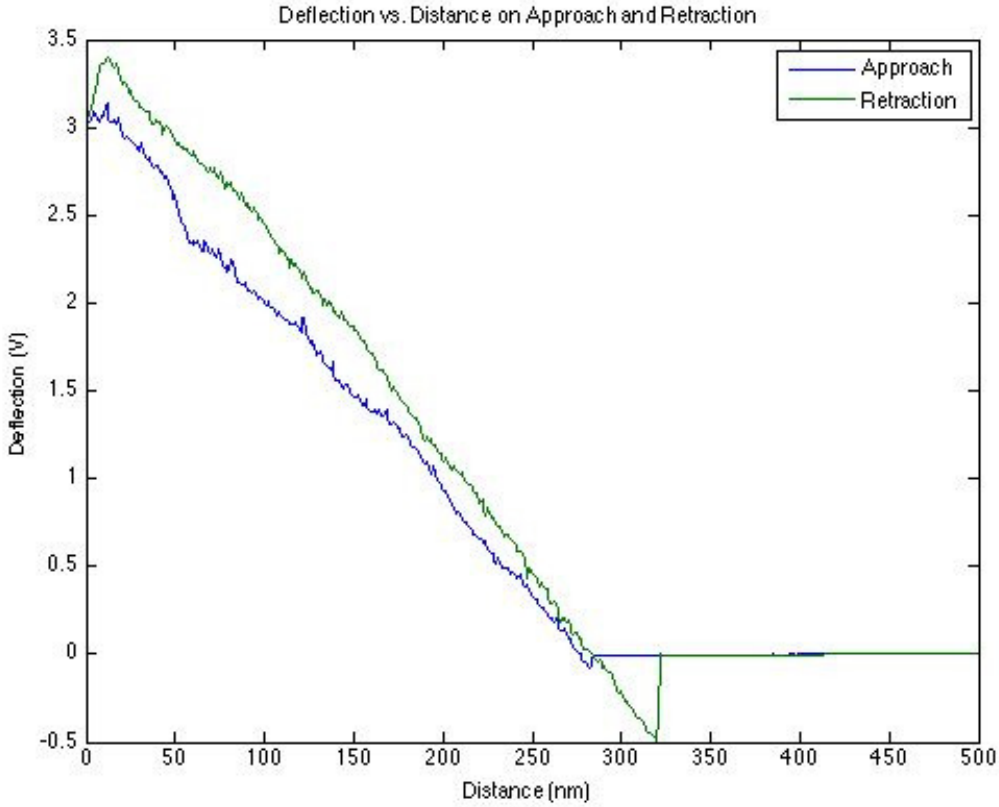
Deflection vs. Distance on Approach and Retraction
Approach
Retraction
Deflection (V)
Distance (nm)
3.5
3
2.5
2
1.5
1
0.5
0
-0.5
0
50
100
150
200
250
300
350
400
450
500

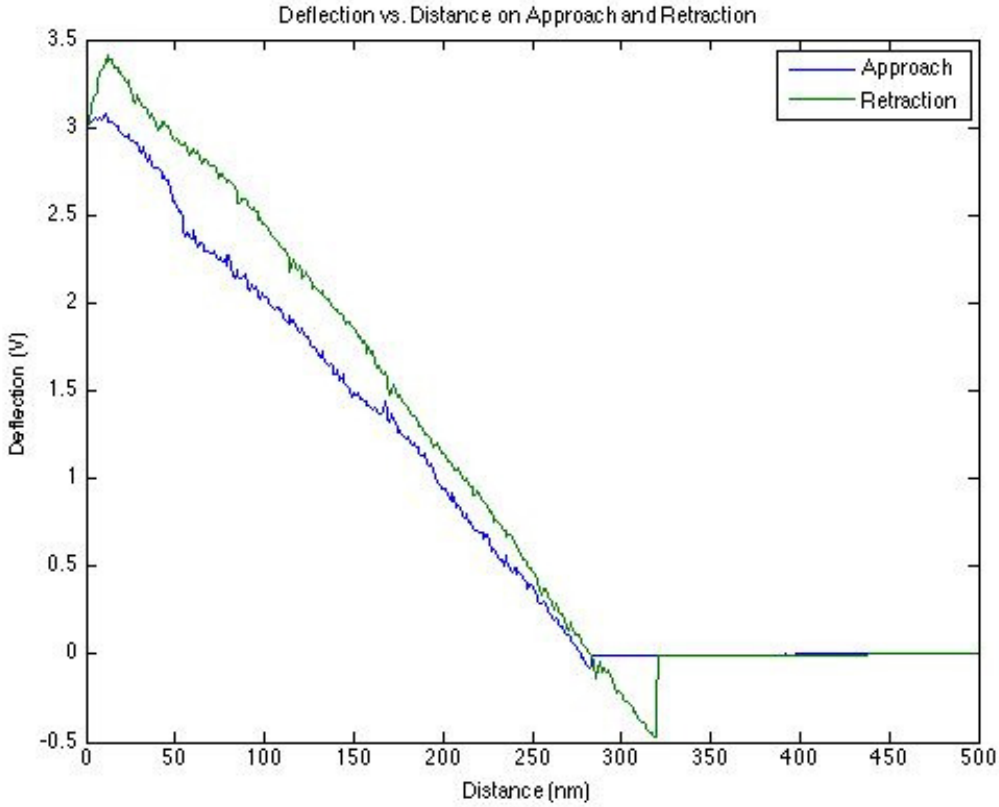
Deflection vs. Distance on Approach and Retraction
Approach
Retraction
Deflection (V)
Distance (nm)
3.5
3
2.5
2
1.5
1
0.5
0
-0.5
0
50
100
150
200
250
300
350
400
450
500

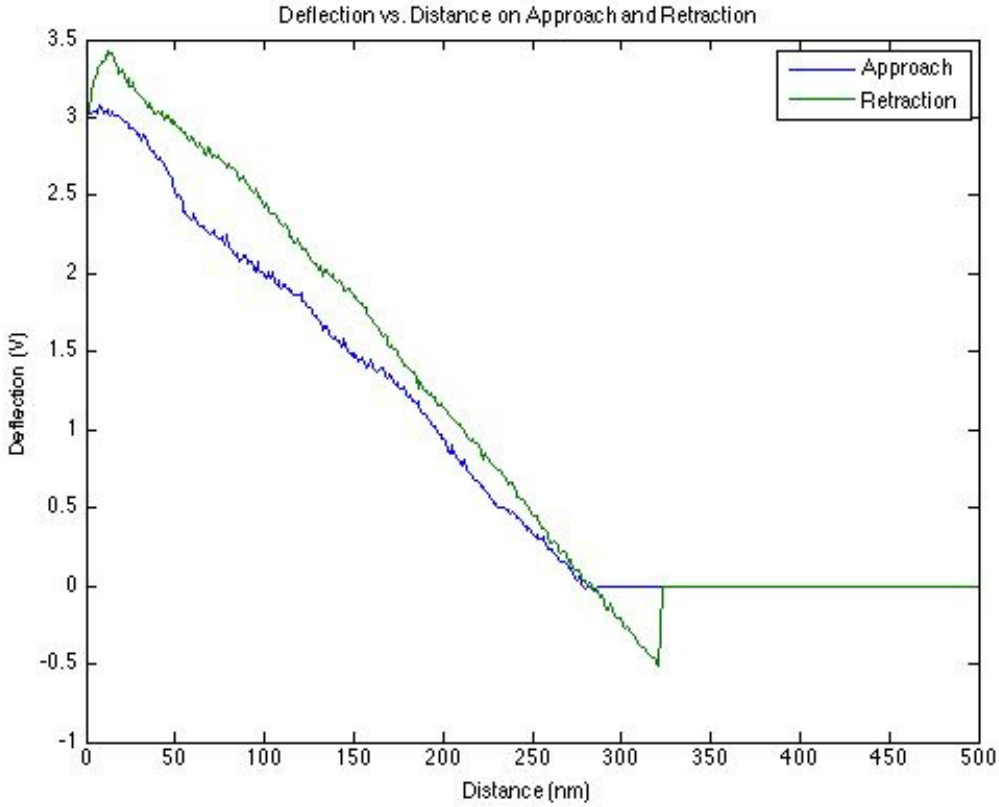
Deflection vs. Distance on Approach and Retraction
Approach
Retraction
Deflection (V)
Distance (nm)
3.5
3
2.5
2
1.5
1
0.5
0
-0.5
-1
0
50
100
150
200
250
300
350
400
450
500

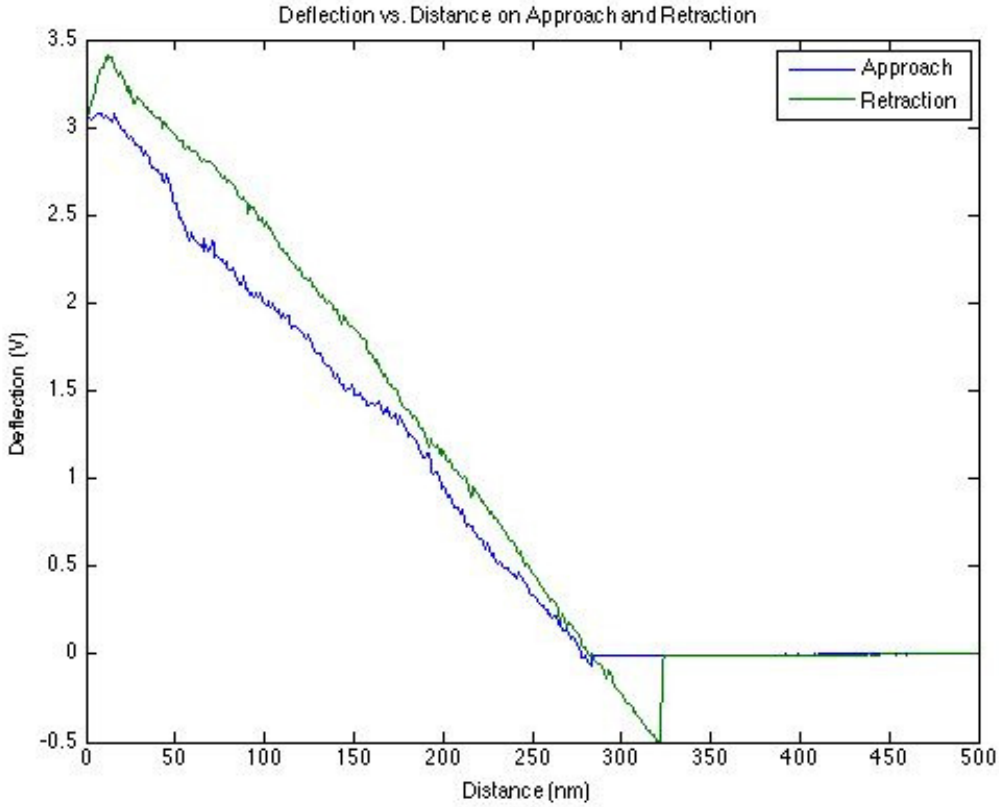
Deflection vs. Distance on Approach and Retraction
Approach
Retraction
Deflection (V)
Distance (nm)
3.5
3
2.5
2
1.5
1
0.5
0
-0.5
0
50
100
150
200
250
300
350
400
450
500

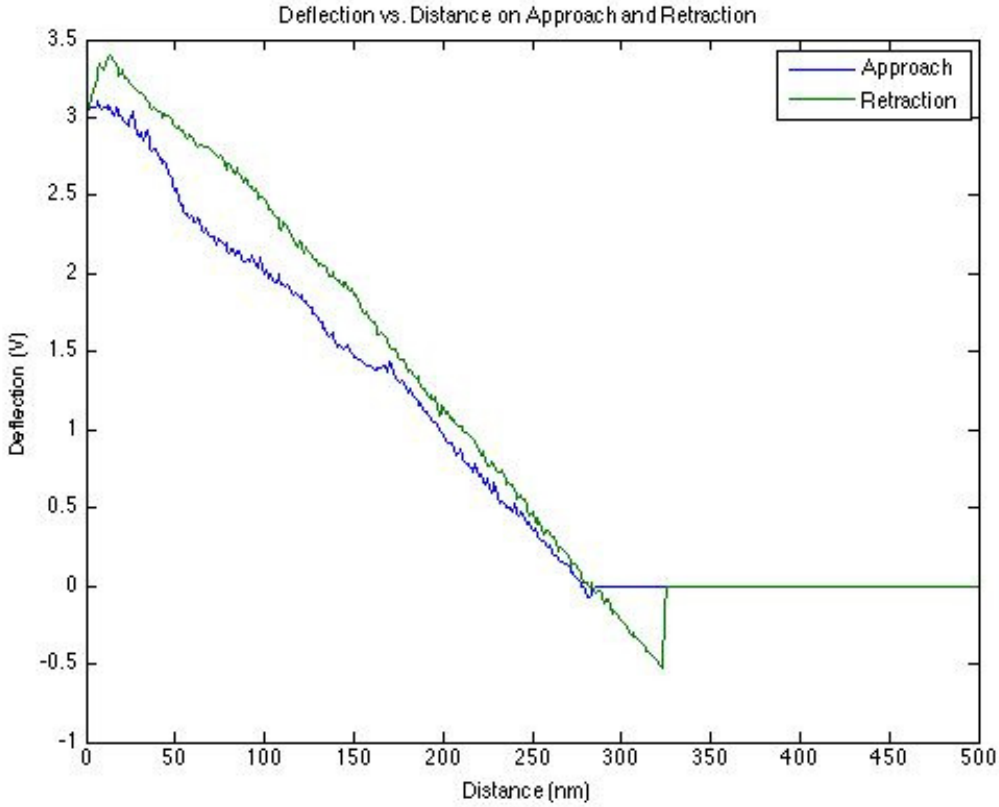
Deflection vs. Distance on Approach and Retraction
Approach
Retraction
Deflection (V)
Distance (nm)
3.5
3
2.5
2
1.5
1
0.5
0
-0.5
-1
0
50
100
150
200
250
300
350
400
450
500

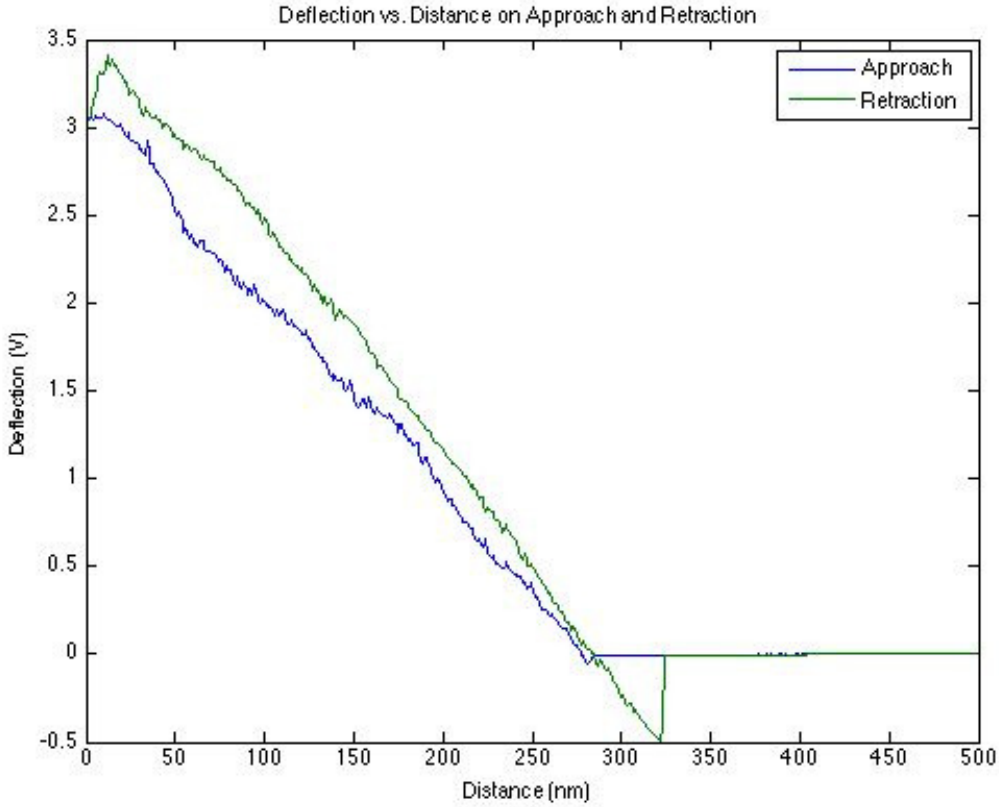
Deflection vs. Distance on Approach and Retraction
Approach
Retraction
Deflection (V)
Distance (nm)
3.5
3
2.5
2
1.5
1
0.5
0
-0.5
0
50
100
150
200
250
300
350
400
450
500

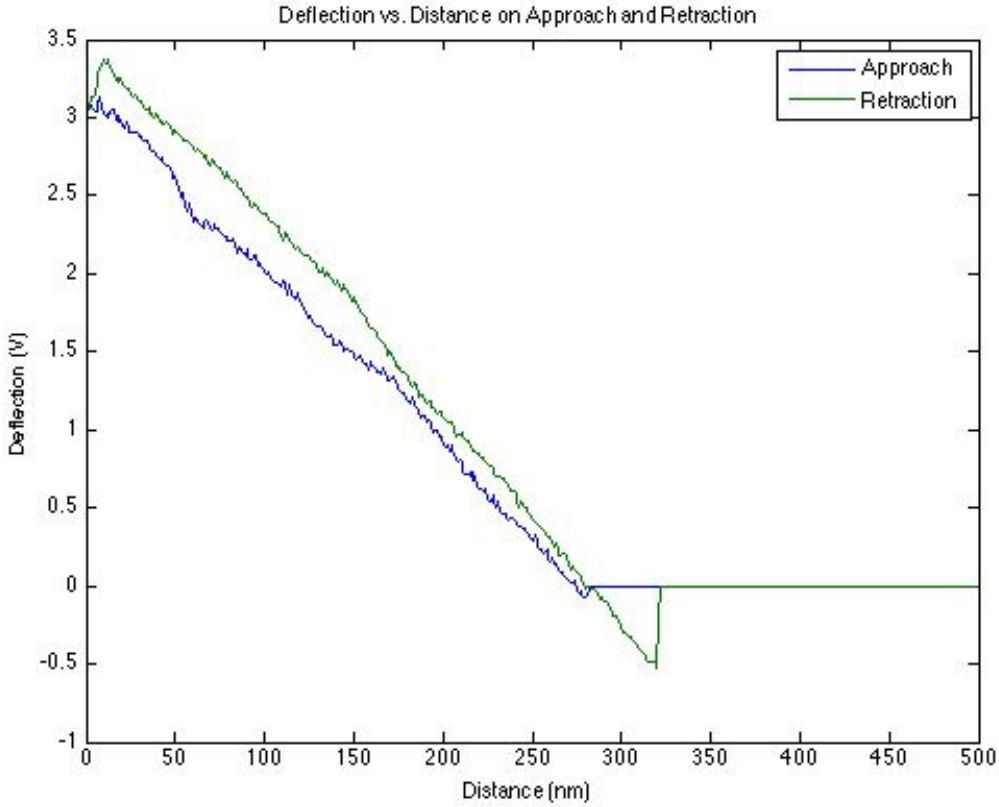
Deflection vs. Distance on Approach and Retraction
Approach
Retraction
Deflection (V)
Distance (nm)
3.5
3
2.5
2
1.5
1
0.5
0
-0.5
-1
0
50
100
150
200
250
300
350
400
450
500

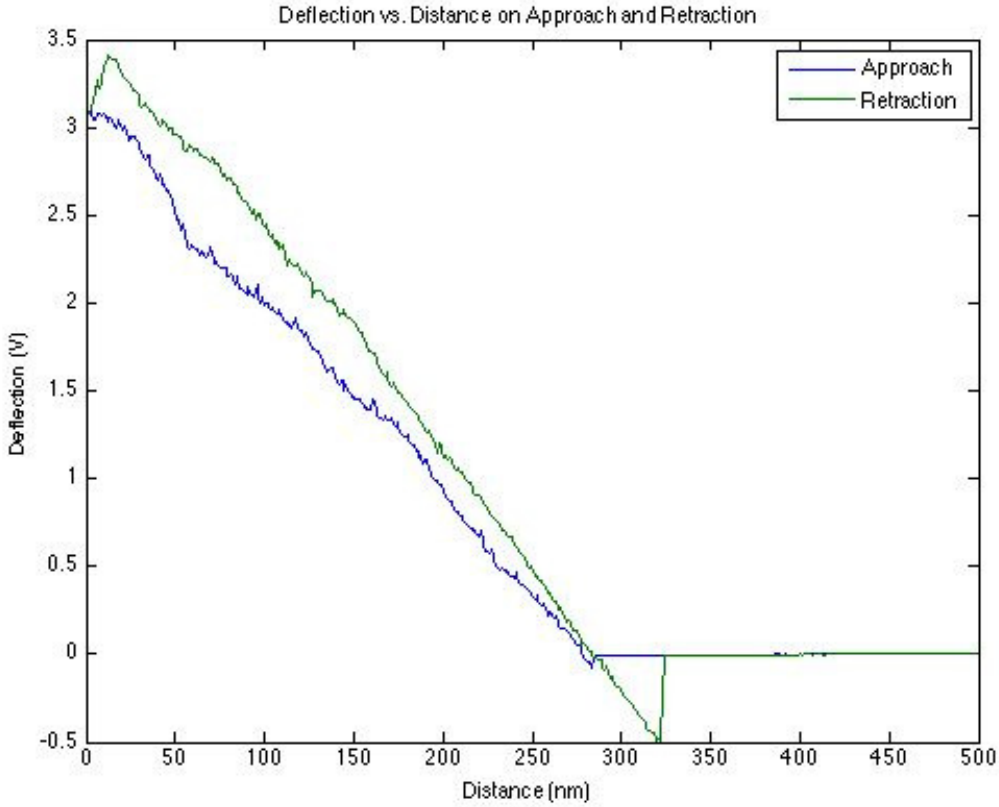
Deflection vs. Distance on Approach and Retraction
Approach
Retraction
Deflection (V)
Distance (nm)
3.5
3
2.5
2
1.5
1
0.5
0
-0.5
0
50
100
150
200
250
300
350
400
450
500

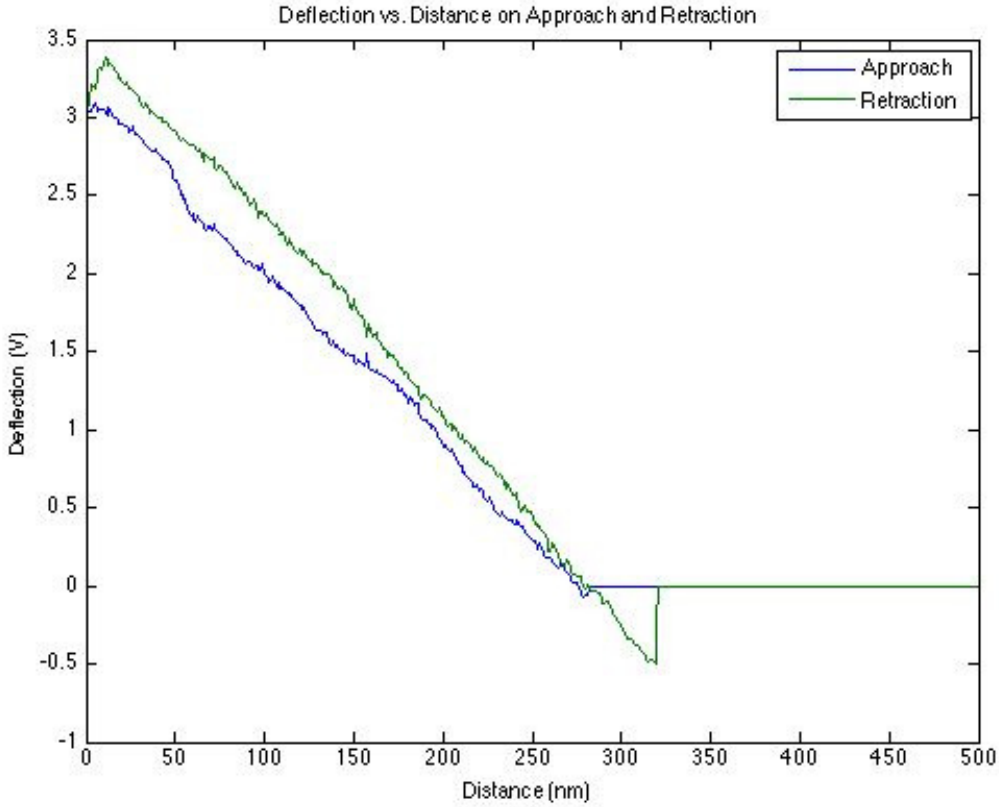
Deflection vs. Distance on Approach and Retraction
Approach
Retraction
Deflection (V)
Distance (nm)
3.5
3
2.5
2
1.5
1
0.5
0
-0.5
-1
0
50
100
150
200
250
300
350
400
450
500

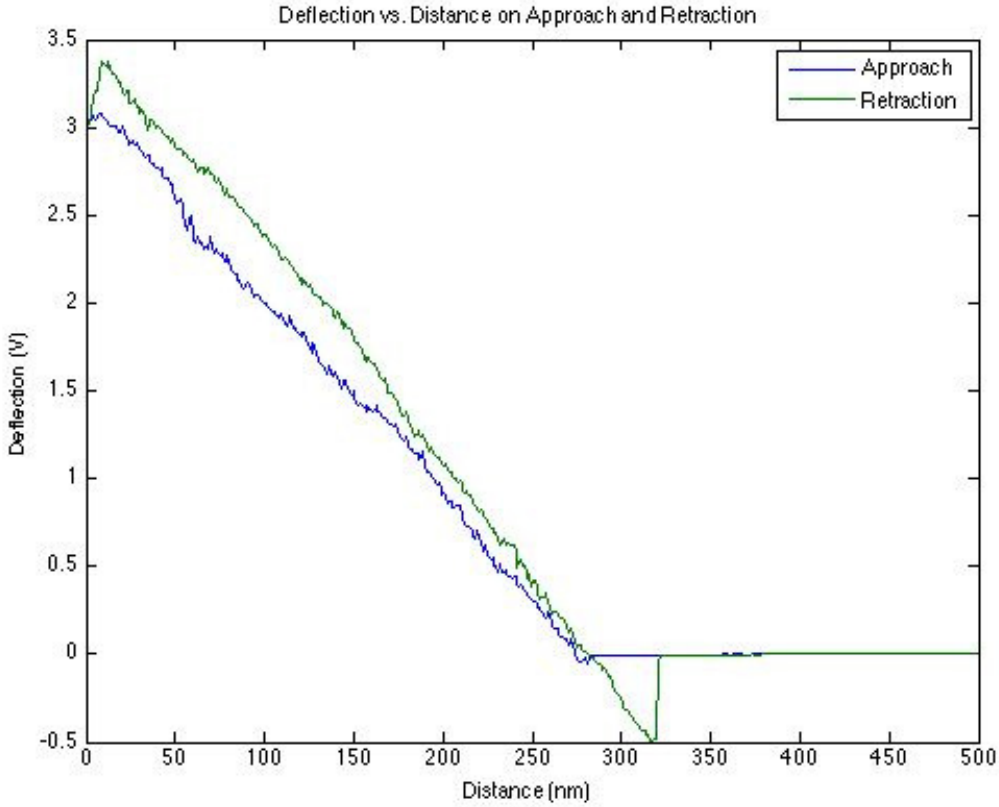
Deflection vs. Distance on Approach and Retraction
Approach
Retraction
Deflection (V)
Distance (nm)
3.5
3
2.5
2
1.5
1
0.5
0
-0.5
0
50
100
150
200
250
300
350
400
450
500

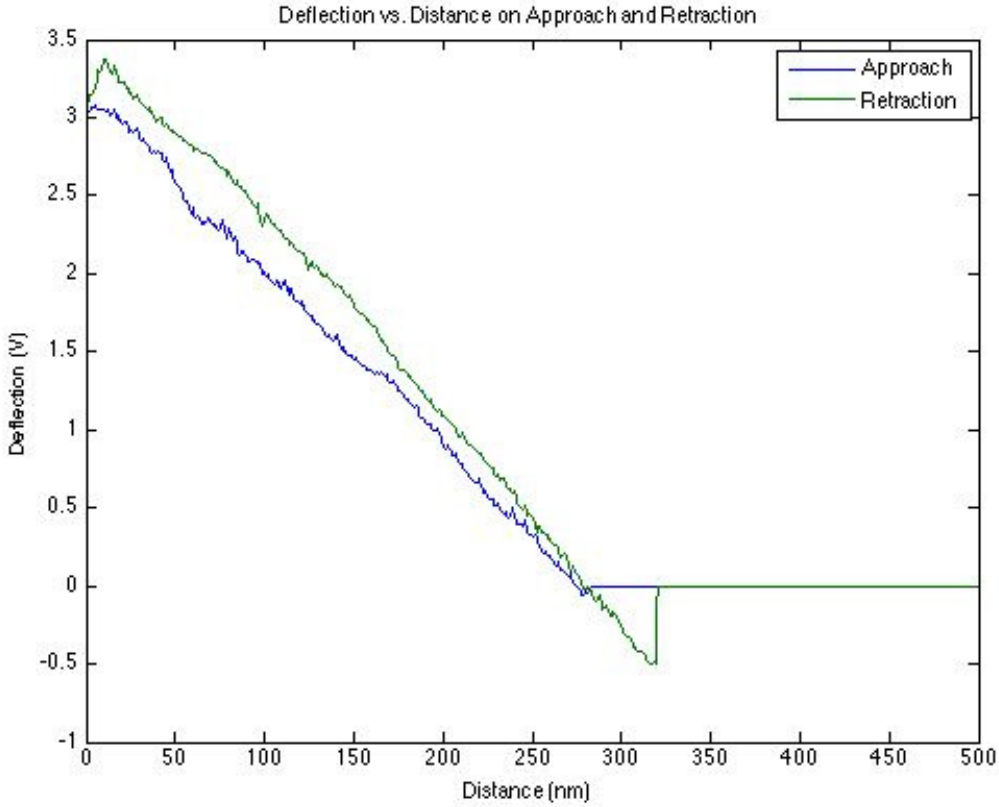
Deflection vs. Distance on Approach and Retraction
Approach
Retraction
Deflection (V)
Distance (nm)
3.5
3
2.5
2
1.5
1
0.5
0
-0.5
-1
0
50
100
150
200
250
300
350
400
450
500

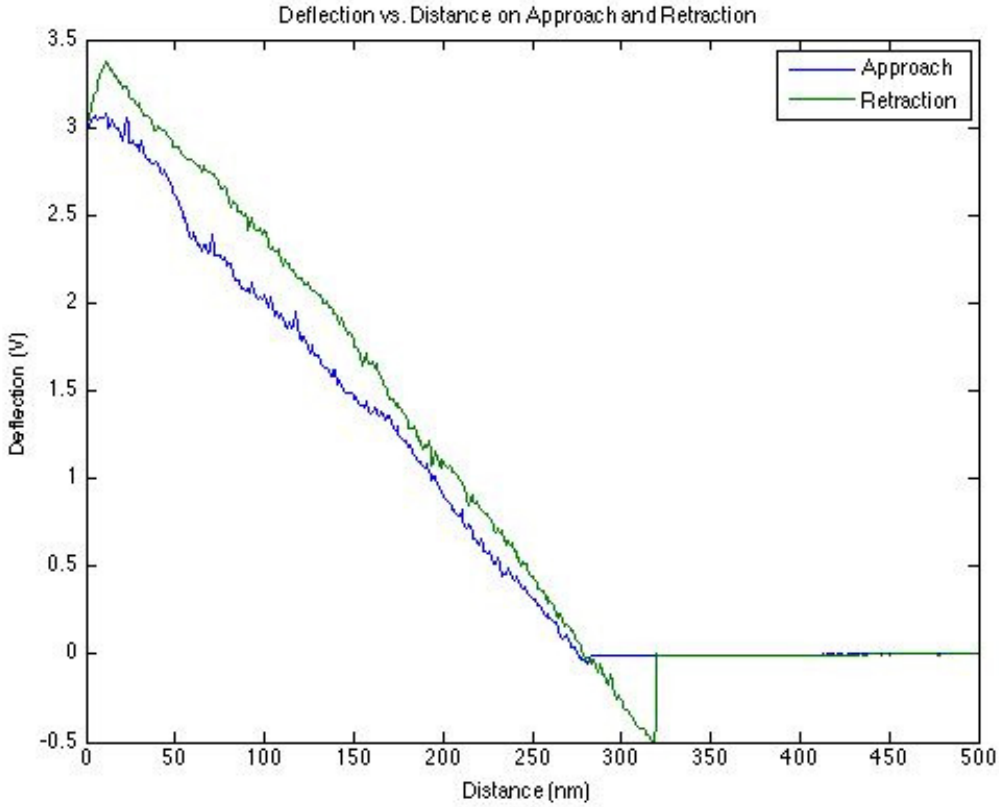
Deflection vs. Distance on Approach and Retraction
Approach
Retraction
Deflection (V)
Distance (nm)
3.5
3
2.5
2
1.5
1
0.5
0
-0.5
0
50
100
150
200
250
300
350
400
450
500

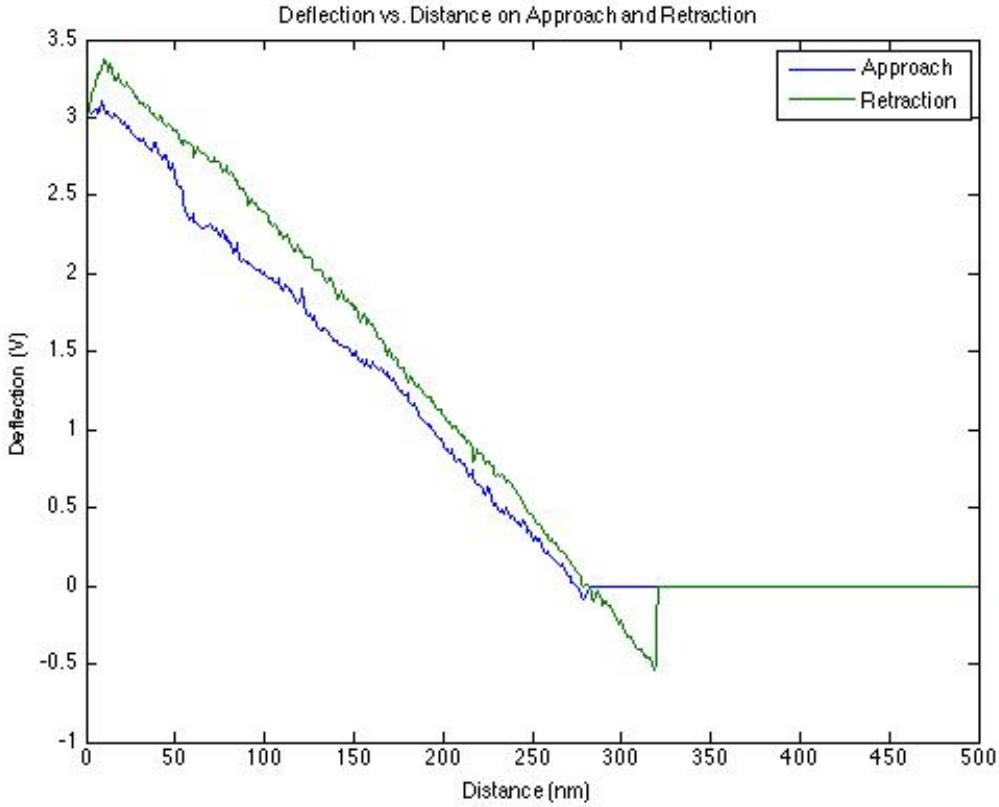
Deflection vs. Distance on Approach and Retraction
Approach
Retraction
Deflection (V)
Distance (nm)
3.5
3
2.5
2
1.5
1
0.5
0
-0.5
-1
0
50
100
150
200
250
300
350
400
450
500

Appendix F

Sodium-saturated Wet Montmorillonite Deflection-Distance Curves

The deflection-distance curves contained in this section were obtained using the clay-coated glass probe and clay-coated glass substrate in an aqueous environment.

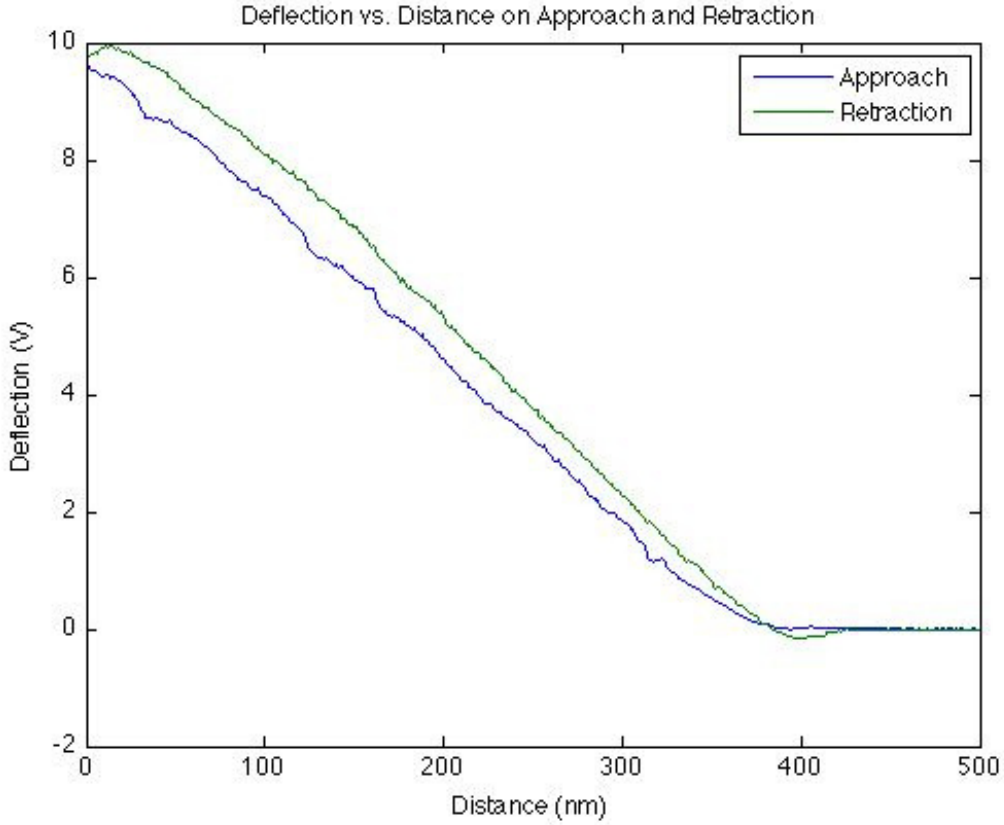
Deflection vs. Distance on Approach and Retraction
Approach
Retraction
Deflection (V)
Distance (nm)
10
8
6
4
2
0
-2
0
100
200
300
400
500

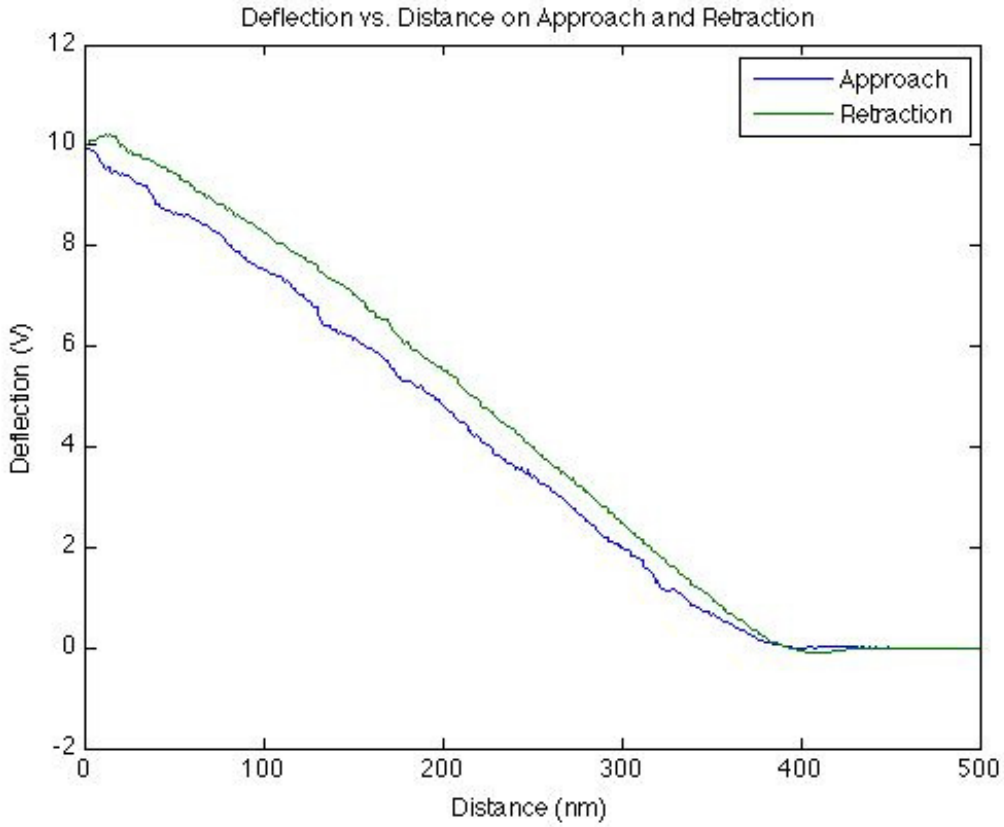
Deflection vs. Distance on Approach and Retraction
Approach
Retraction
Deflection (V)
Distance (nm)
12
10
8
6
4
2
0
-2
0
100
200
300
400
500

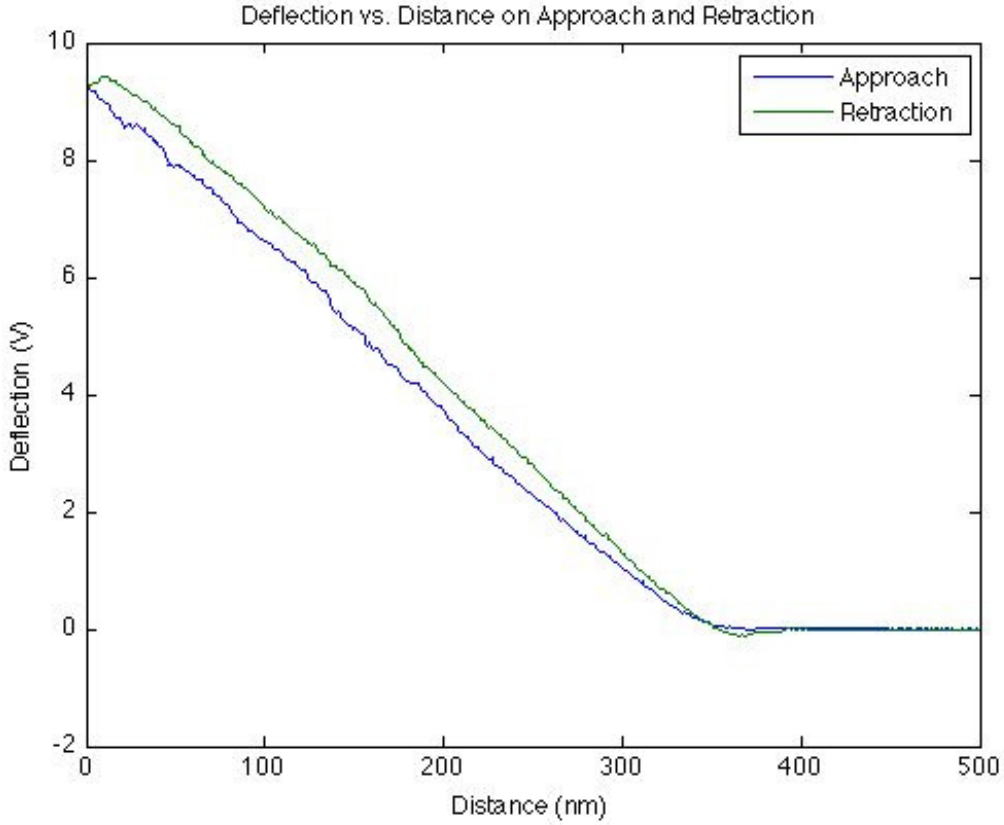
Deflection vs. Distance on Approach and Retraction
Approach
Retraction
Deflection (V)
Distance (nm)
10
8
6
4
2
0
-2
0
100
200
300
400
500

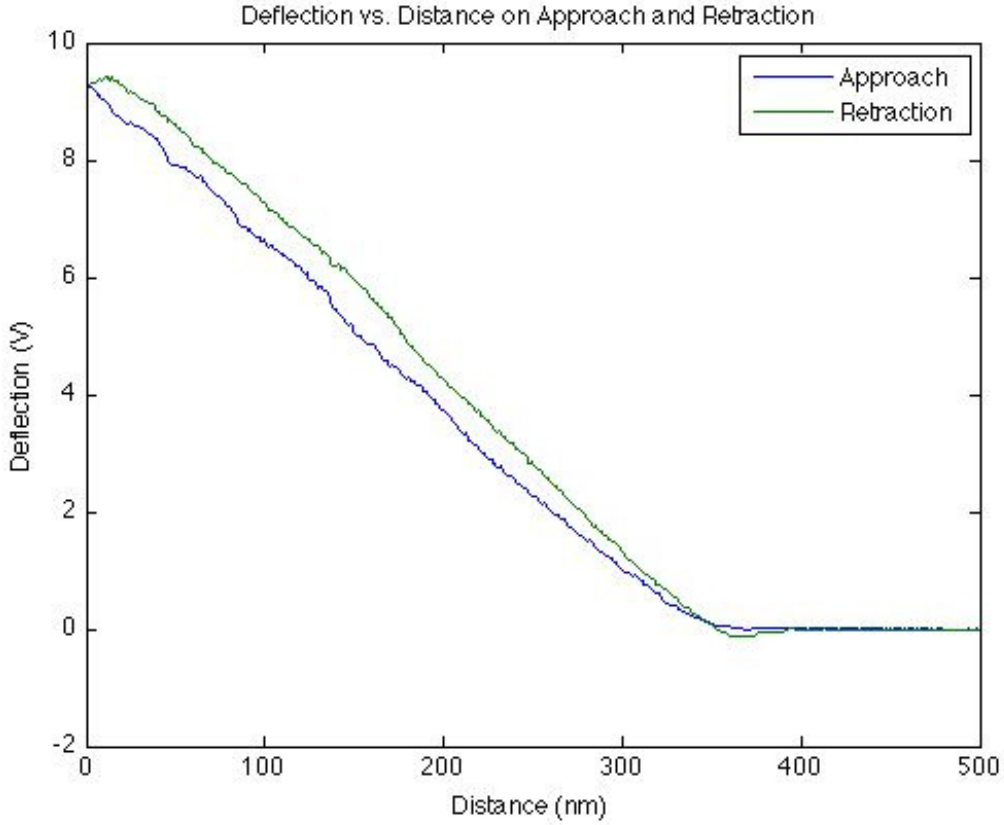
Deflection vs. Distance on Approach and Retraction
Approach
Retraction
Deflection (V)
Distance (nm)
10
8
6
4
2
0
-2
0
100
200
300
400
500

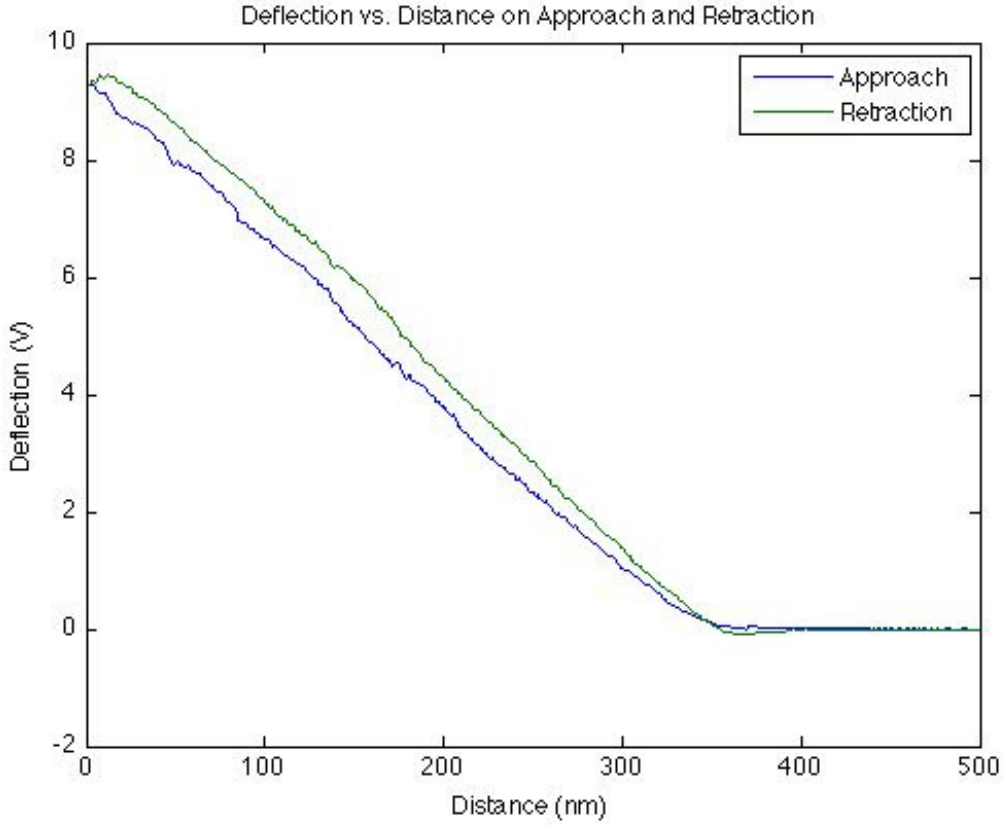
Deflection vs. Distance on Approach and Retraction
Approach
Retraction
Deflection (V)
Distance (nm)
10
8
6
4
2
0
-2
0
100
200
300
400
500

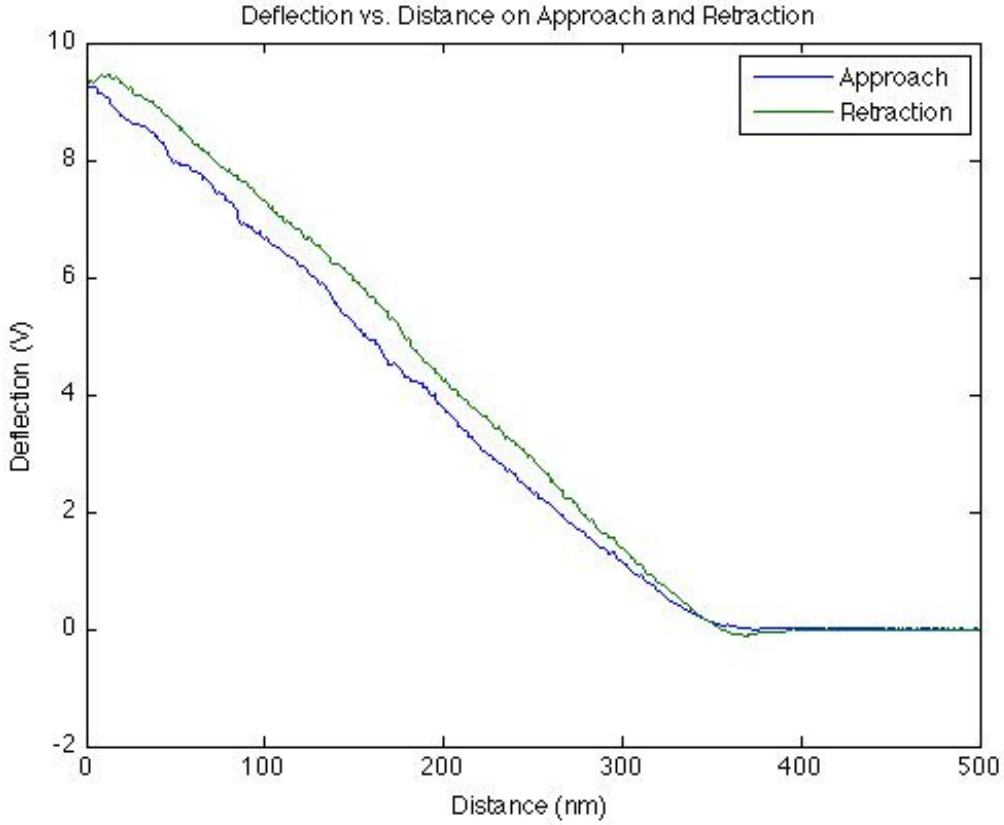
Deflection vs. Distance on Approach and Retraction
Approach
Retraction
Deflection (V)
Distance (nm)
10
8
6
4
2
0
-2
0
100
200
300
400
500

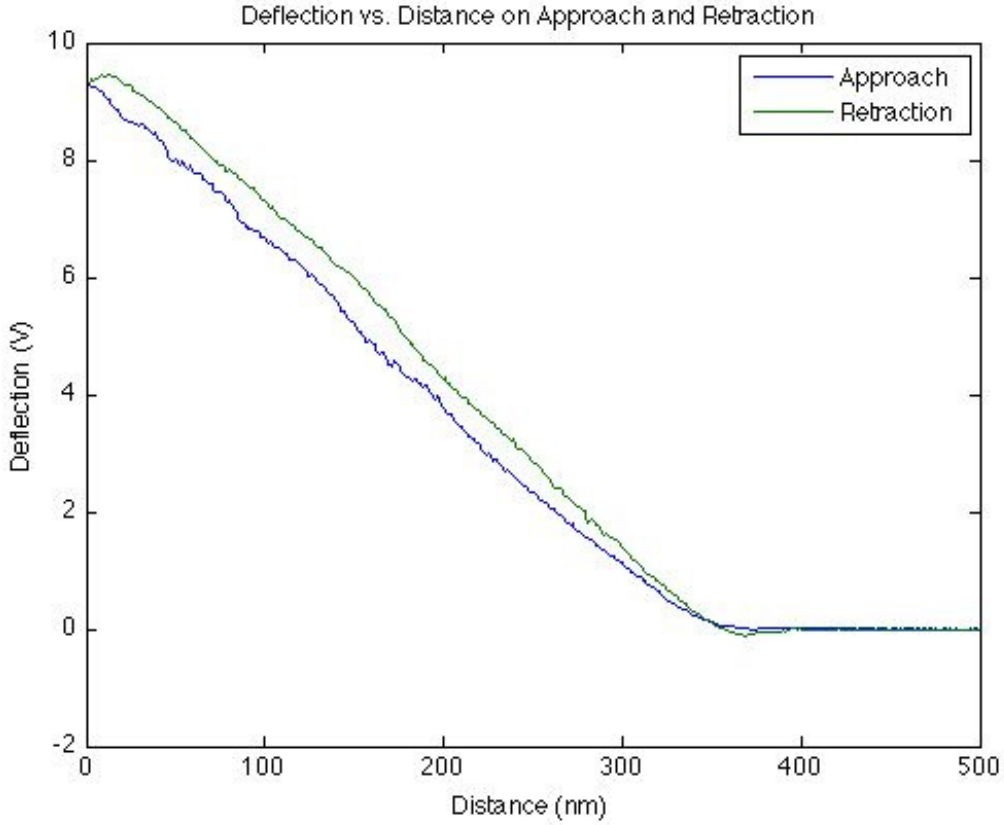
Deflection vs. Distance on Approach and Retraction
Approach
Retraction
Deflection (V)
Distance (nm)
10
8
6
4
2
0
-2
0
100
200
300
400
500

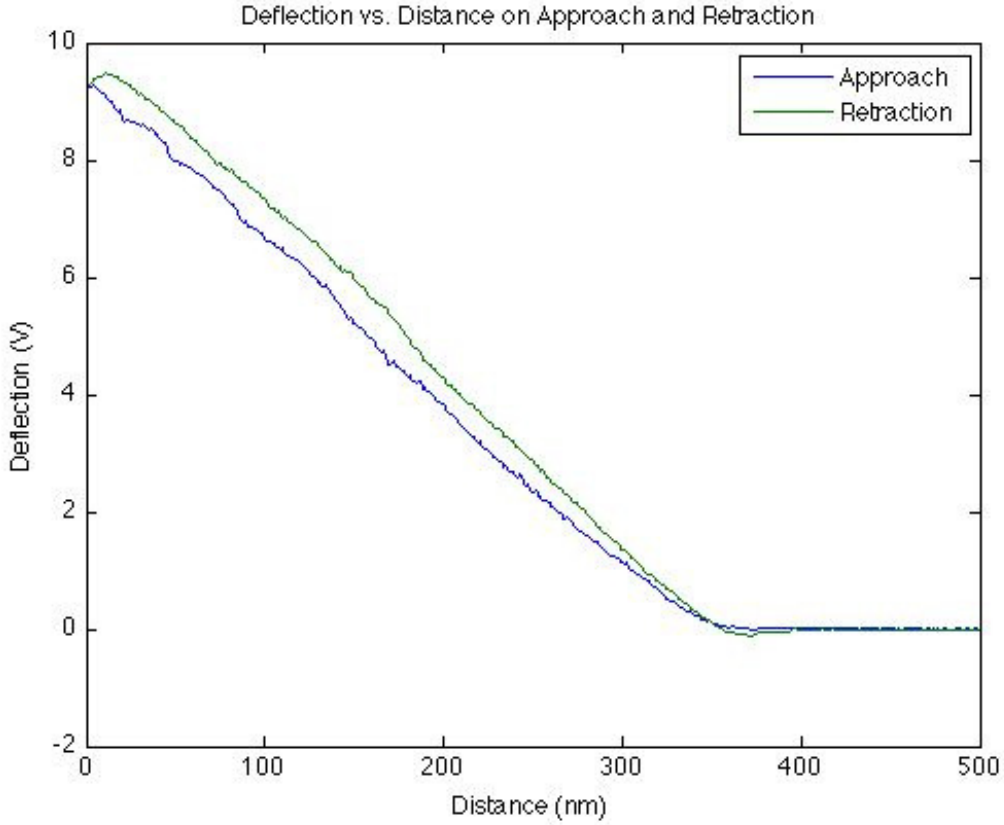
Deflection vs. Distance on Approach and Retraction
Approach
Retraction
Deflection (V)
Distance (nm)
10
8
6
4
2
0
-2
0
100
200
300
400
500

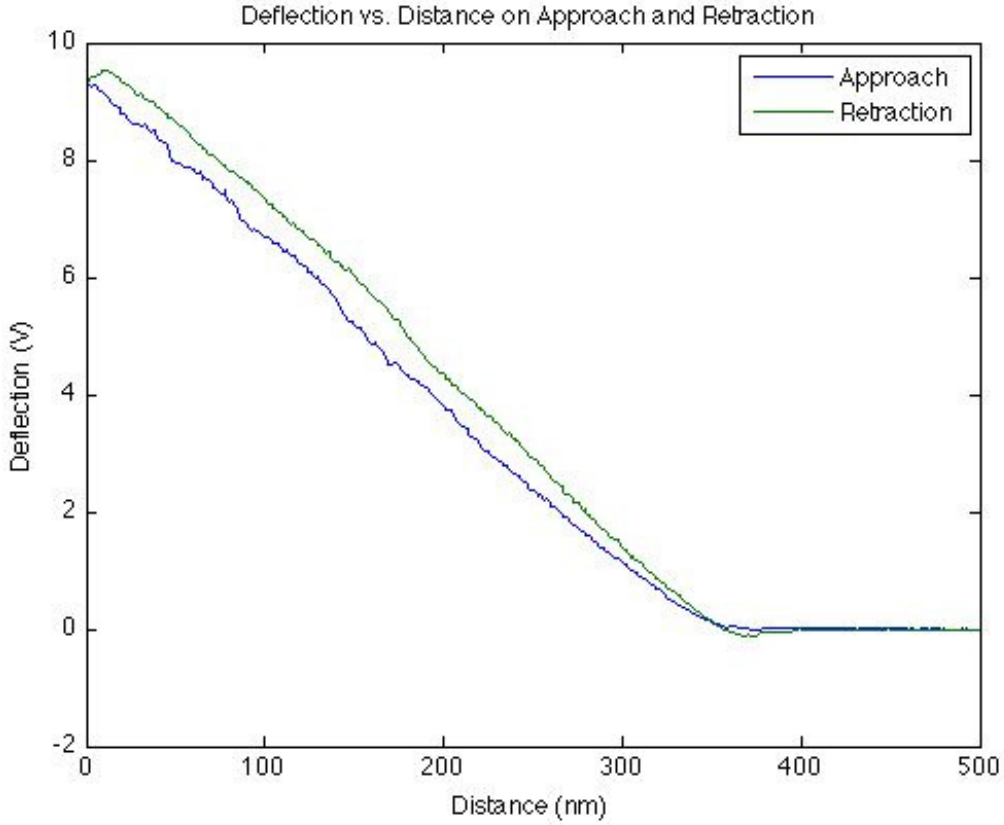
Deflection vs. Distance on Approach and Retraction
Approach
Retraction
Deflection (V)
Distance (nm)
10
8
6
4
2
0
-2
0
100
200
300
400
500

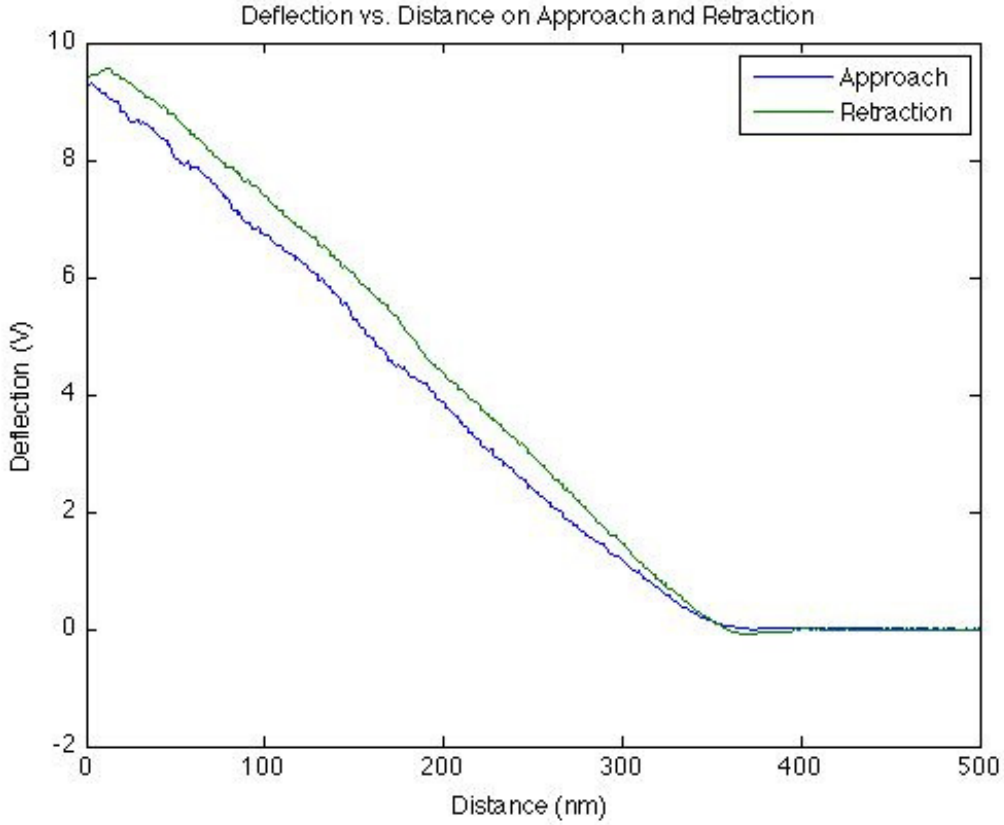
Deflection vs. Distance on Approach and Retraction
Approach
Retraction
Deflection (V)
Distance (nm)
10
8
6
4
2
0
-2
0
100
200
300
400
500

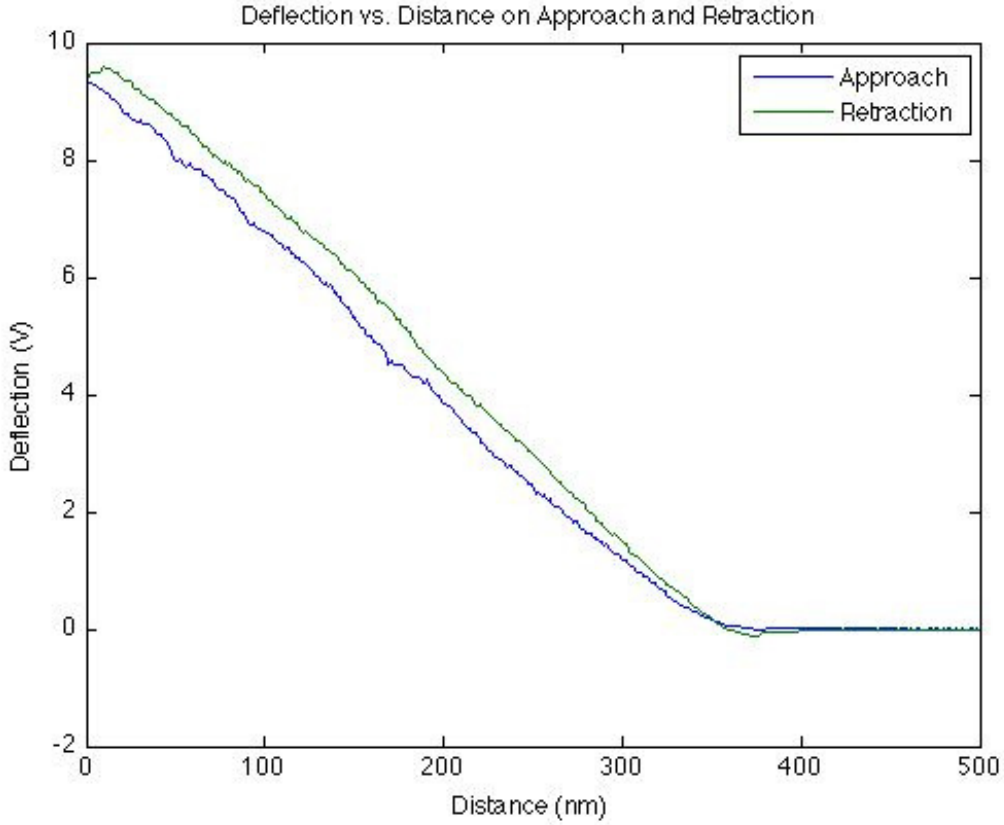
Deflection vs. Distance on Approach and Retraction
Approach
Retraction
Deflection (V)
Distance (nm)
10
8
6
4
2
0
-2
0
100
200
300
400
500

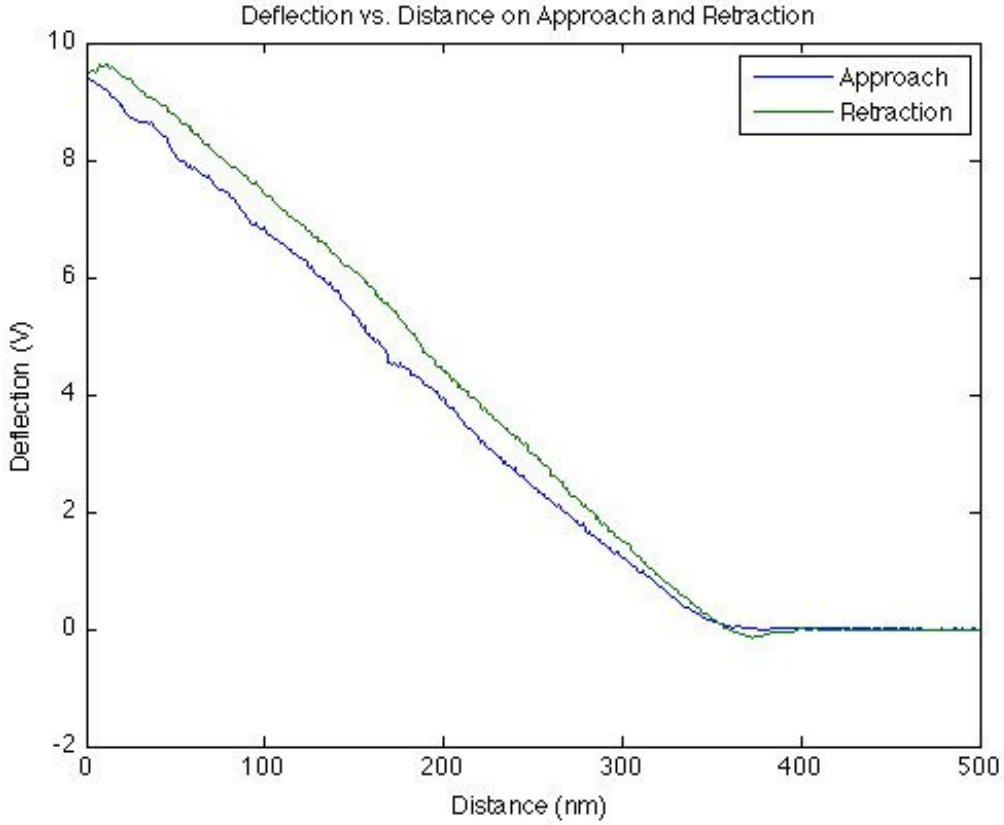
Deflection vs. Distance on Approach and Retraction
Approach
Retraction
Deflection (V)
Distance (nm)
10
8
6
4
2
0
-2
0
100
200
300
400
500

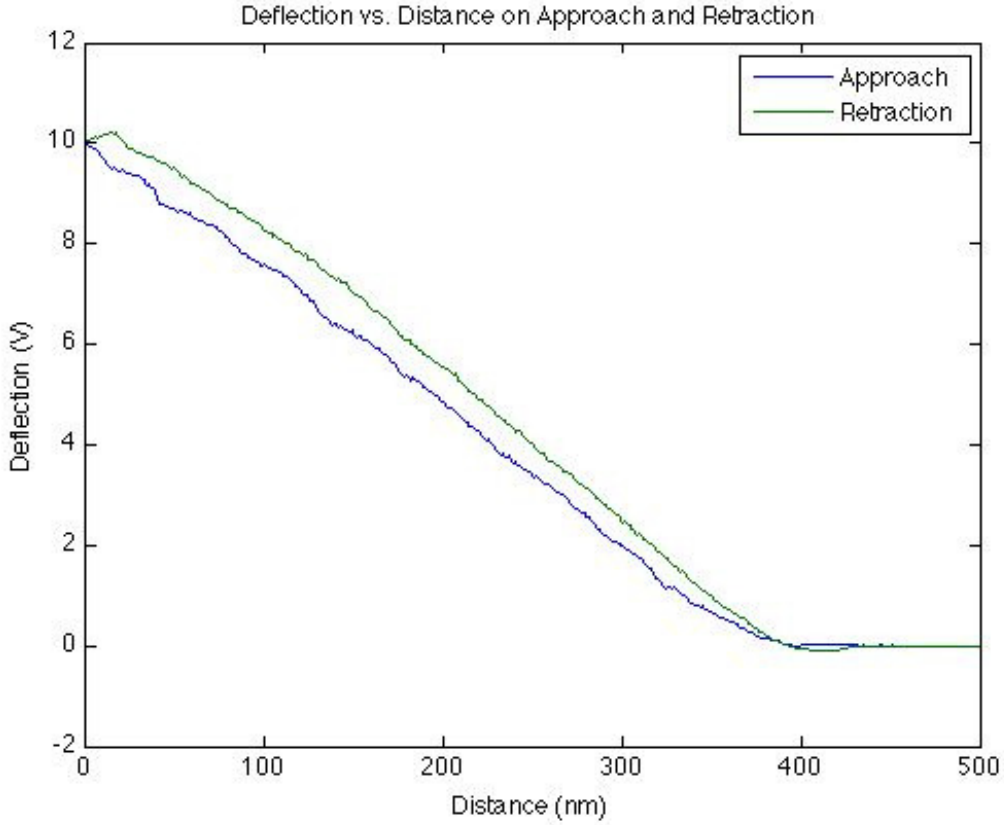
Deflection vs. Distance on Approach and Retraction
Approach
Retraction
Deflection (V)
Distance (nm)
12
10
8
6
4
2
0
-2
0
100
200
300
400
500

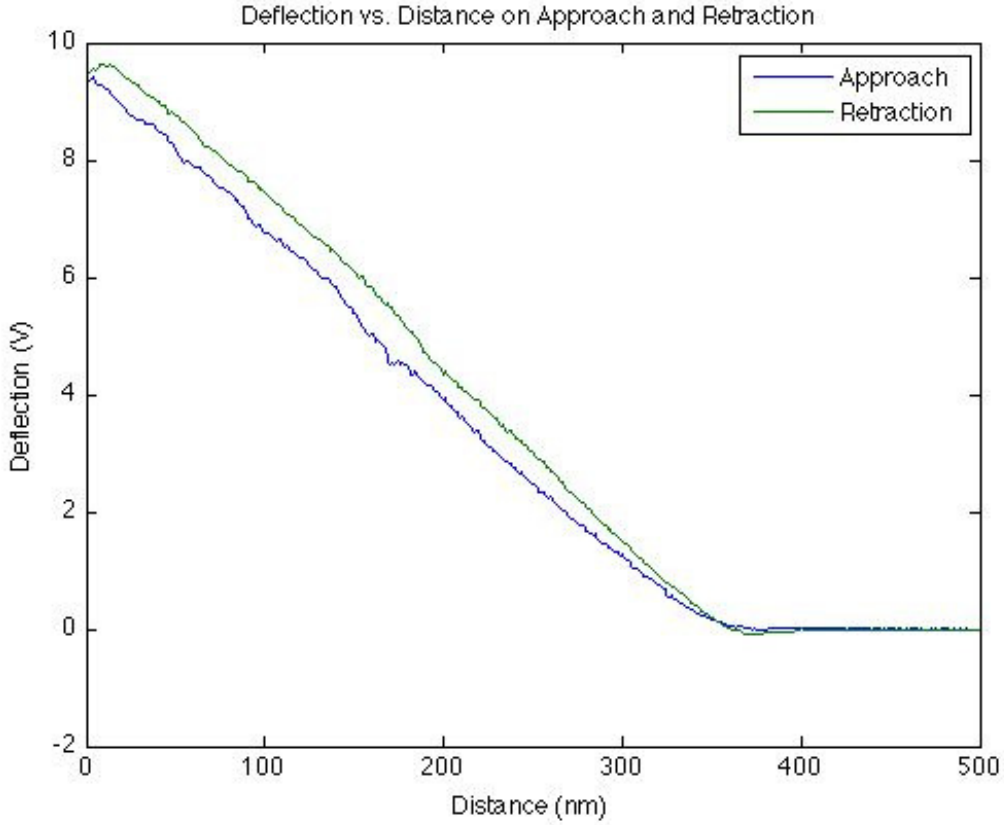
Deflection vs. Distance on Approach and Retraction
Approach
Retraction
Deflection (V)
Distance (nm)
10
8
6
4
2
0
-2
0
100
200
300
400
500

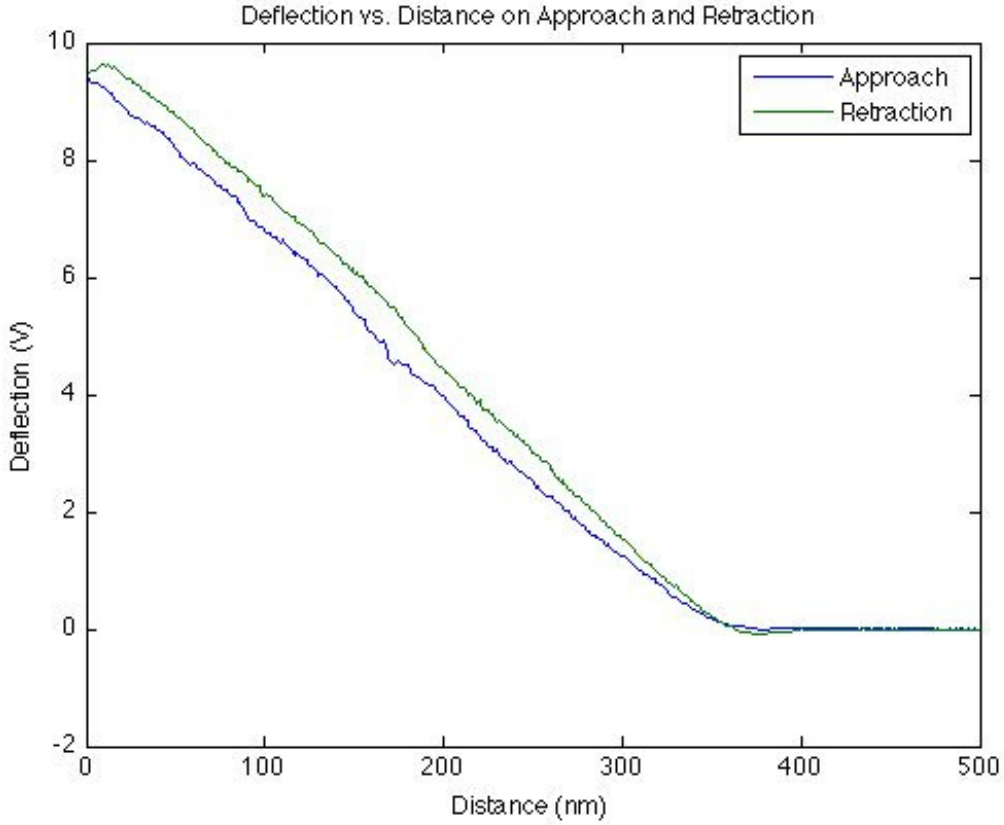
Deflection vs. Distance on Approach and Retraction
Approach
Retraction
Deflection (V)
Distance (nm)
10
8
6
4
2
0
-2
0
100
200
300
400
500

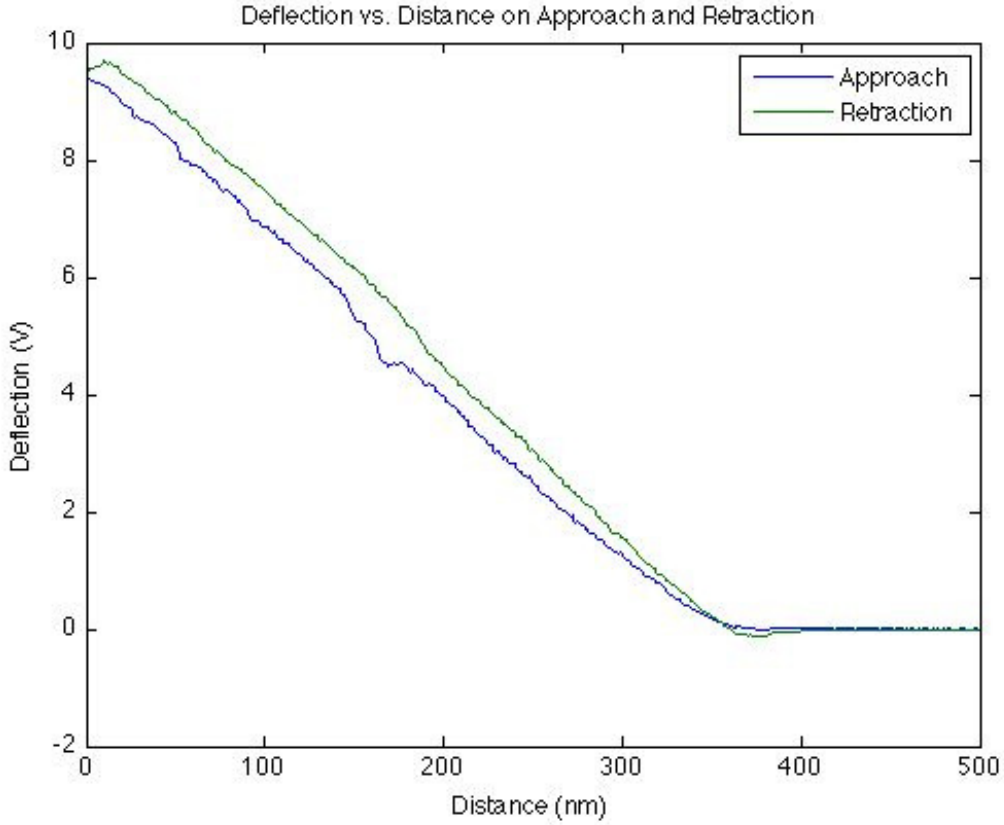
Deflection vs. Distance on Approach and Retraction
Approach
Retraction
Deflection (V)
Distance (nm)
10
8
6
4
2
0
-2
0
100
200
300
400
500

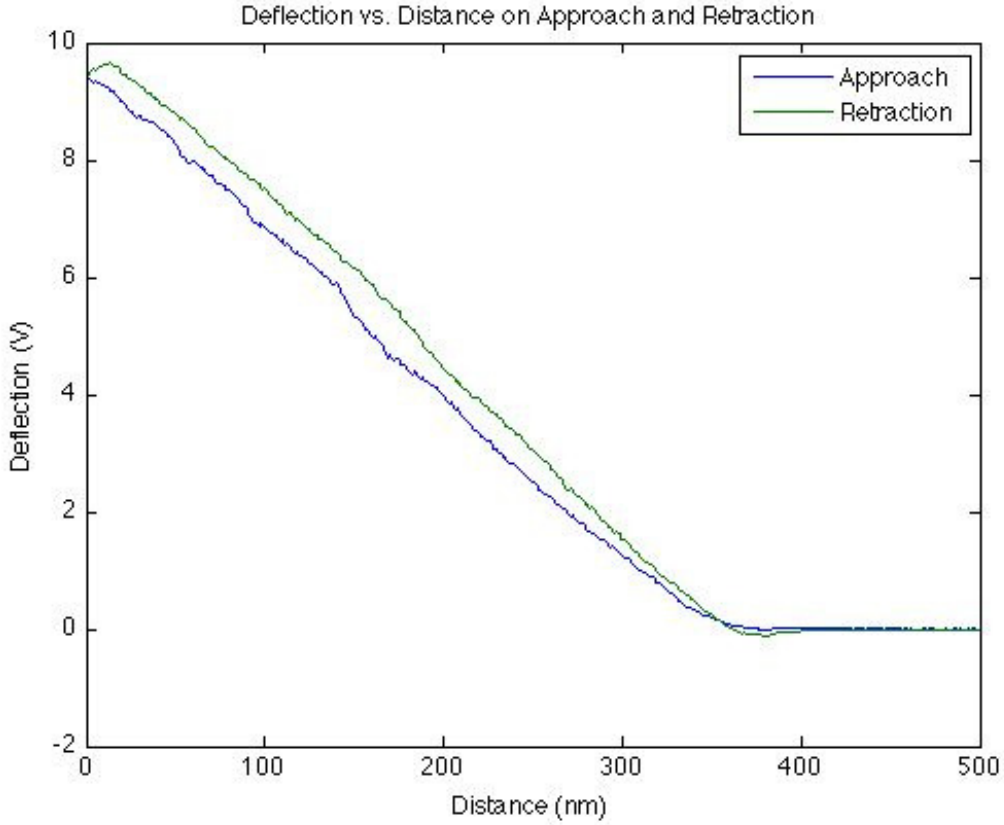
Deflection vs. Distance on Approach and Retraction
Approach
Retraction
Deflection (V)
Distance (nm)
10
8
6
4
2
0
-2
0
100
200
300
400
500

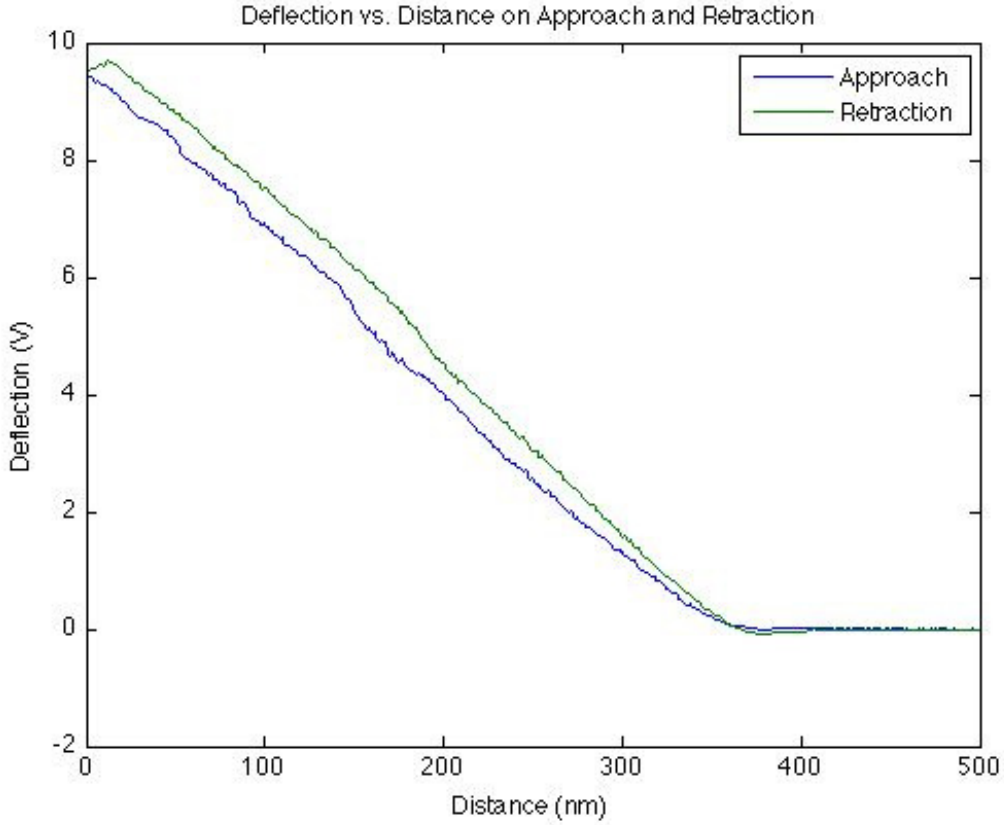
Deflection vs. Distance on Approach and Retraction
Approach
Retraction
Deflection (V)
Distance (nm)
10
8
6
4
2
0
-2
0
100
200
300
400
500

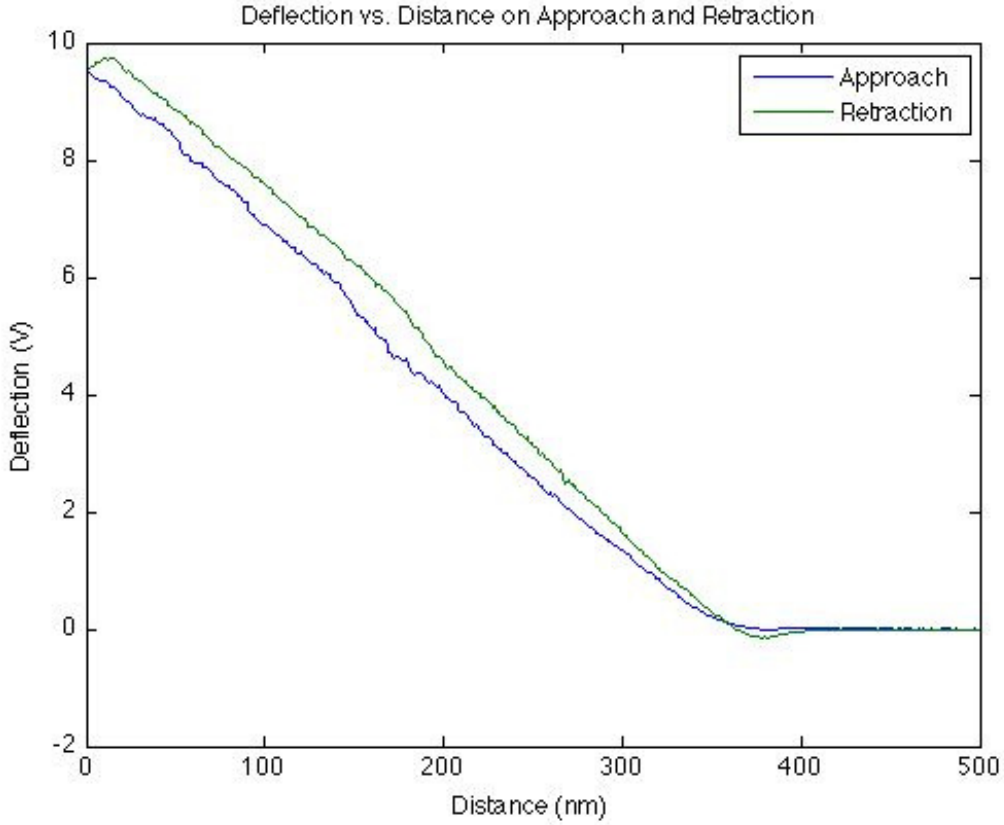
Deflection vs. Distance on Approach and Retraction
Approach
Retraction
Deflection (V)
Distance (nm)
10
8
6
4
2
0
-2
0
100
200
300
400
500

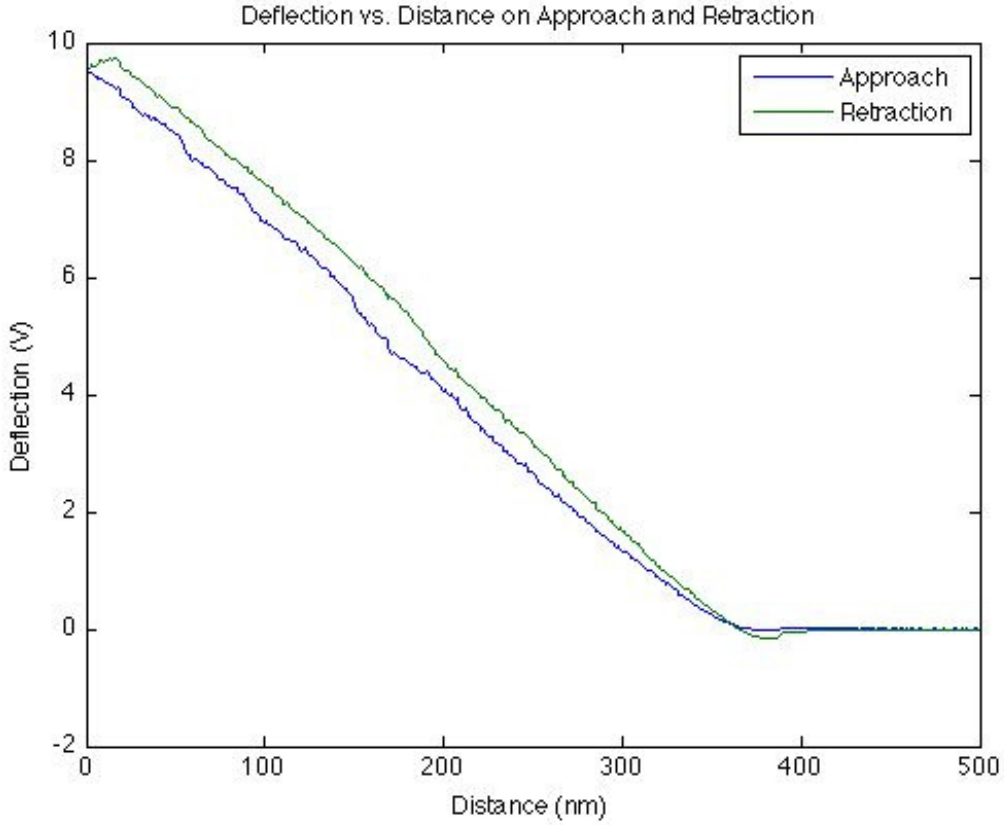
Deflection vs. Distance on Approach and Retraction
Approach
Retraction
Deflection (V)
Distance (nm)
10
8
6
4
2
0
-2
0
100
200
300
400
500

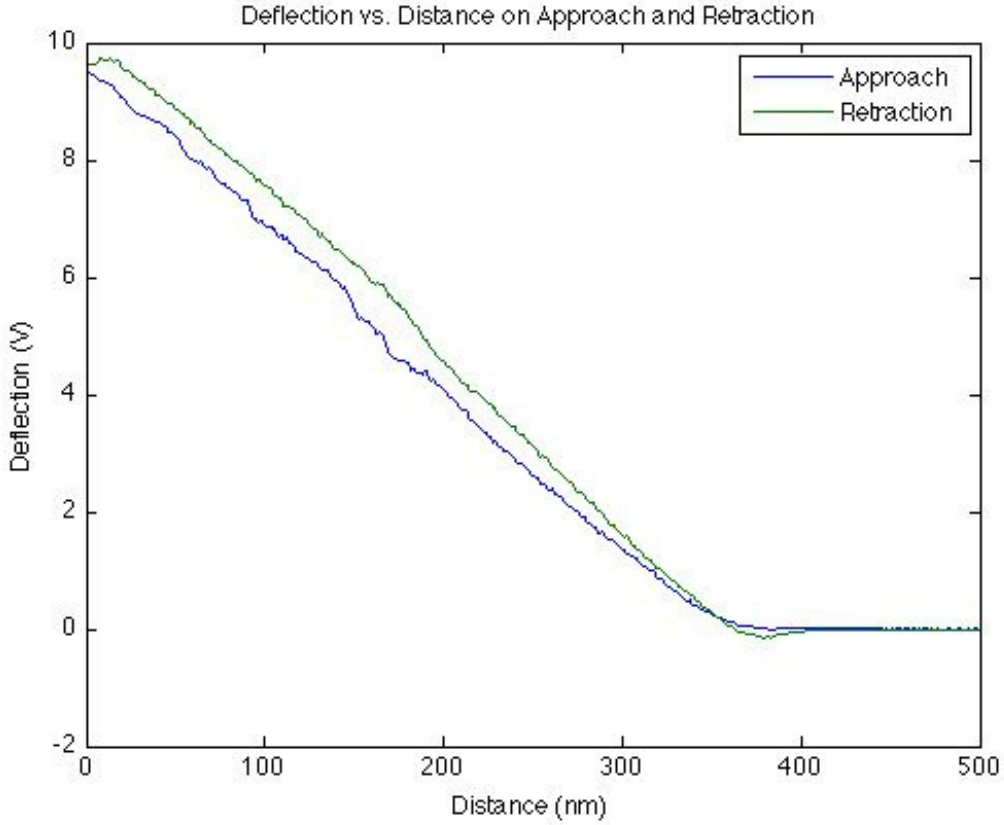
Deflection vs. Distance on Approach and Retraction
Approach
Retraction
Deflection (V)
Distance (nm)
10
8
6
4
2
0
-2
0
100
200
300
400
500

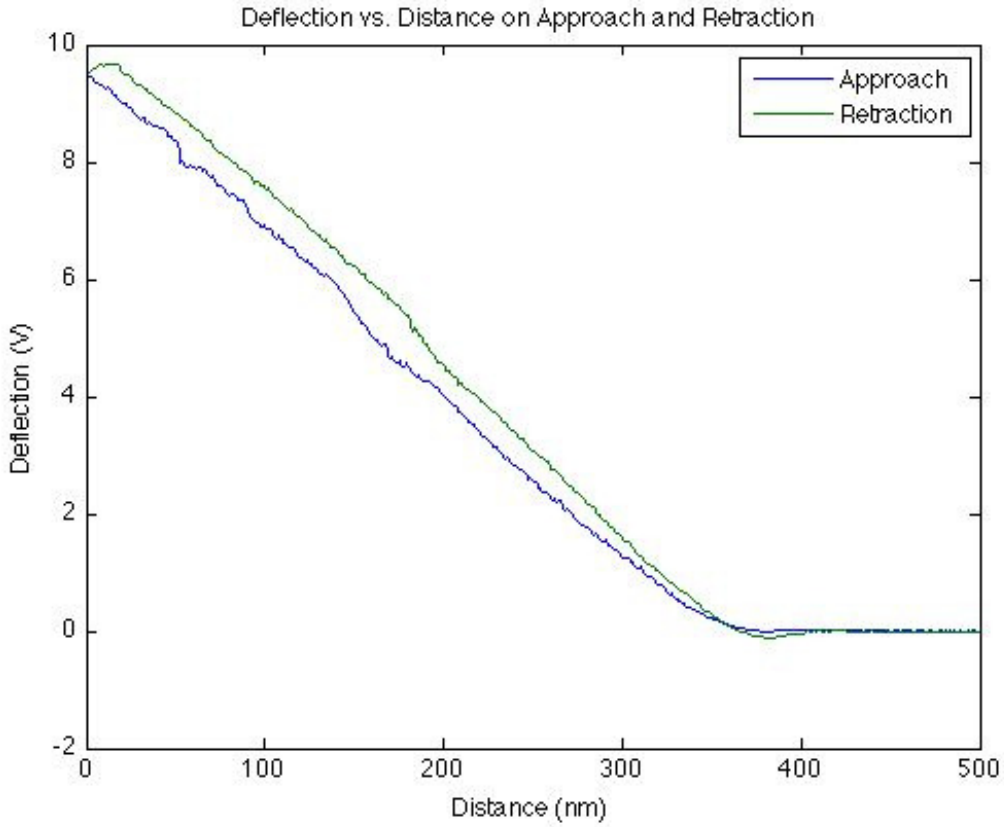
Deflection vs. Distance on Approach and Retraction
Approach
Retraction
Deflection (V)
Distance (nm)
10
8
6
4
2
0
-2
0
100
200
300
400
500

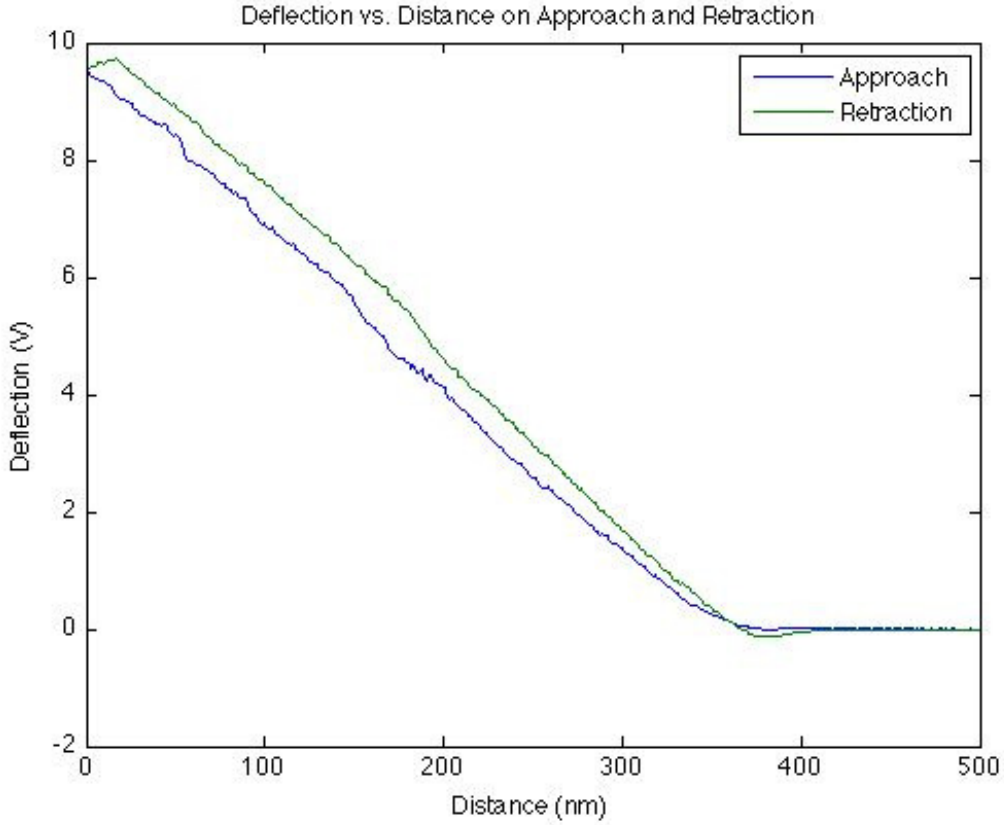
Deflection vs. Distance on Approach and Retraction
Approach
Retraction
Deflection (V)
Distance (nm)
10
8
6
4
2
0
-2
0
100
200
300
400
500

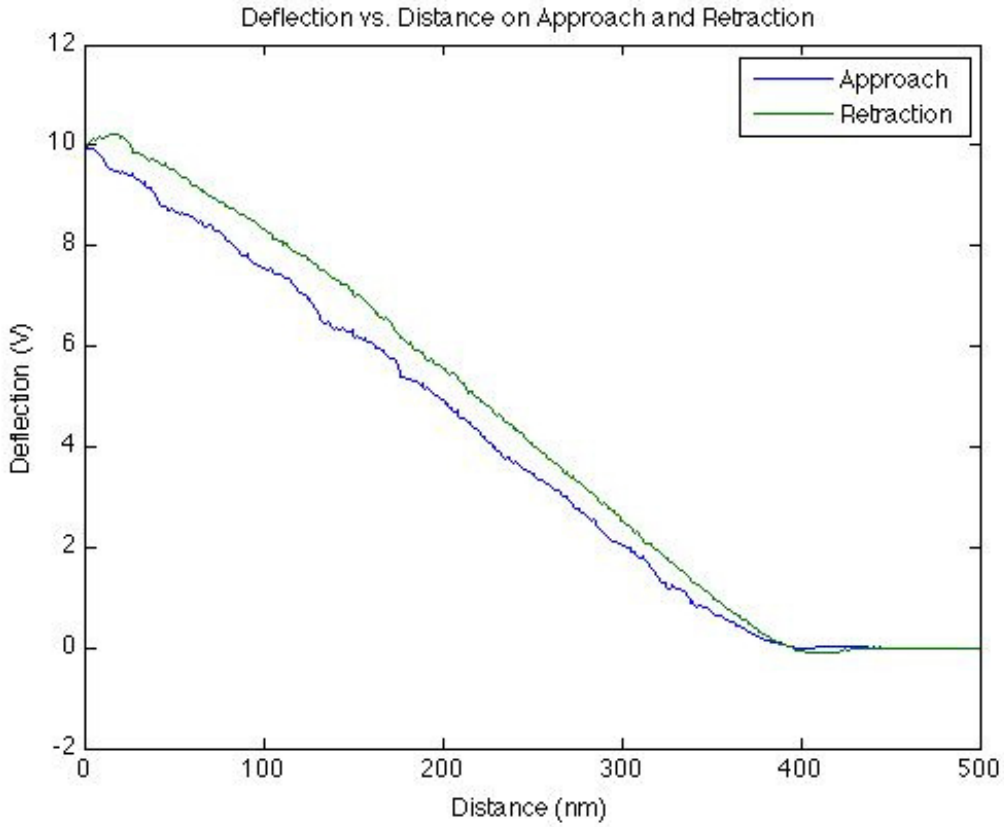
Deflection vs. Distance on Approach and Retraction
Approach
Retraction
Deflection (V)
Distance (nm)
12
10
8
6
4
2
0
-2
0
100
200
300
400
500

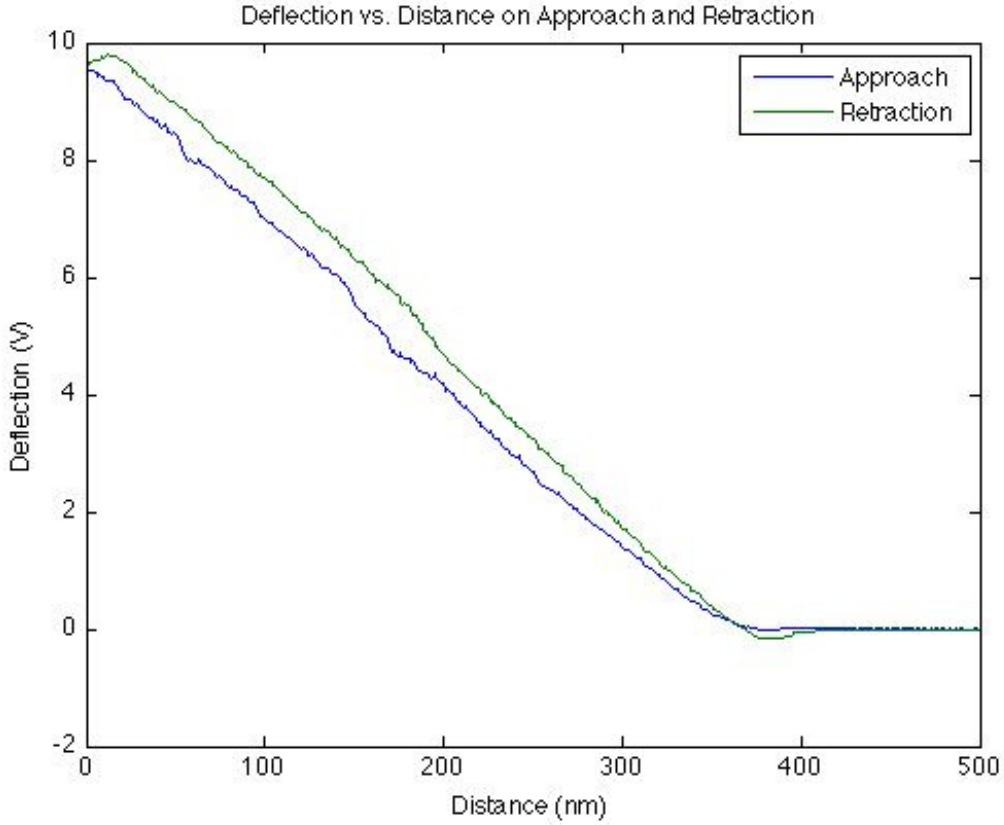
Deflection vs. Distance on Approach and Retraction
Approach
Retraction
Deflection (V)
Distance (nm)
10
8
6
4
2
0
-2
0
100
200
300
400
500

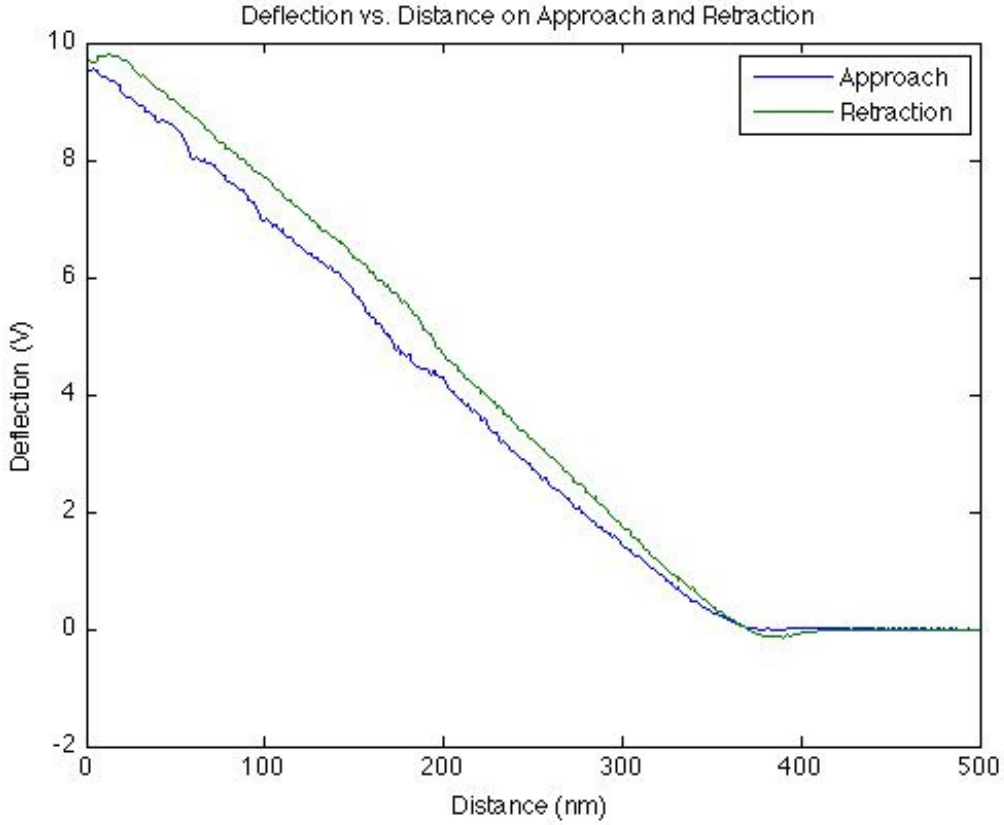
Deflection vs. Distance on Approach and Retraction
Approach
Retraction
Deflection (V)
Distance (nm)
10
8
6
4
2
0
-2
0
100
200
300
400
500

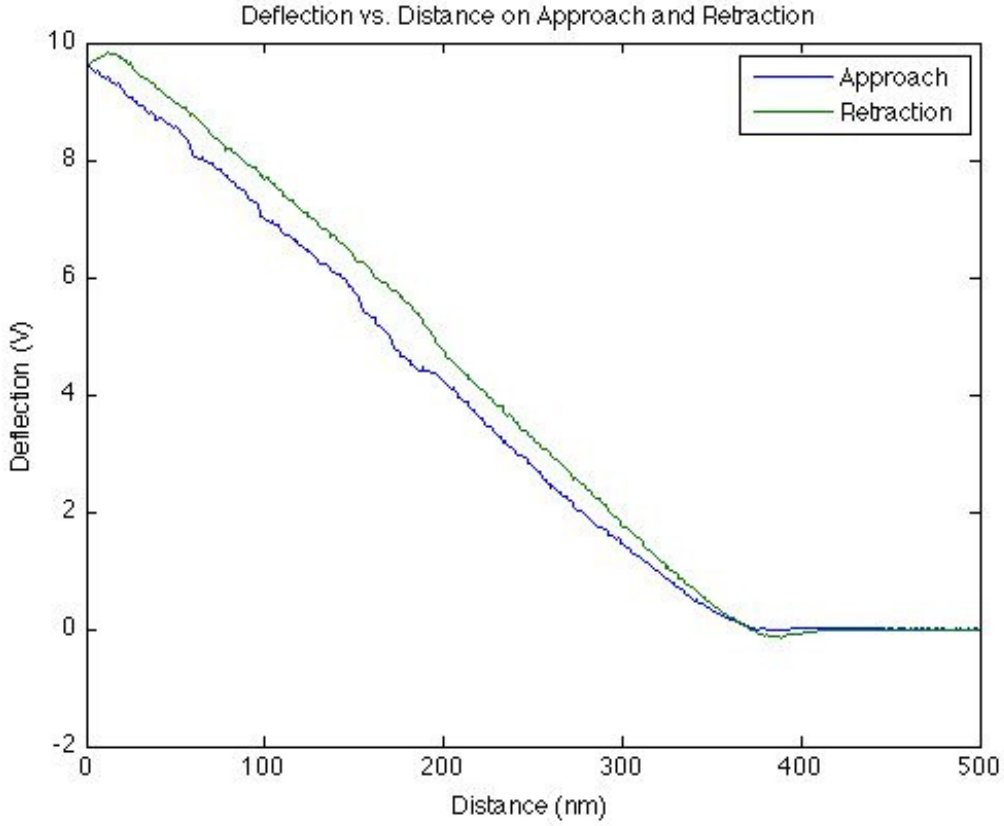
Deflection vs. Distance on Approach and Retraction
Approach
Retraction
Deflection (V)
Distance (nm)
10
8
6
4
2
0
-2
0
100
200
300
400
500

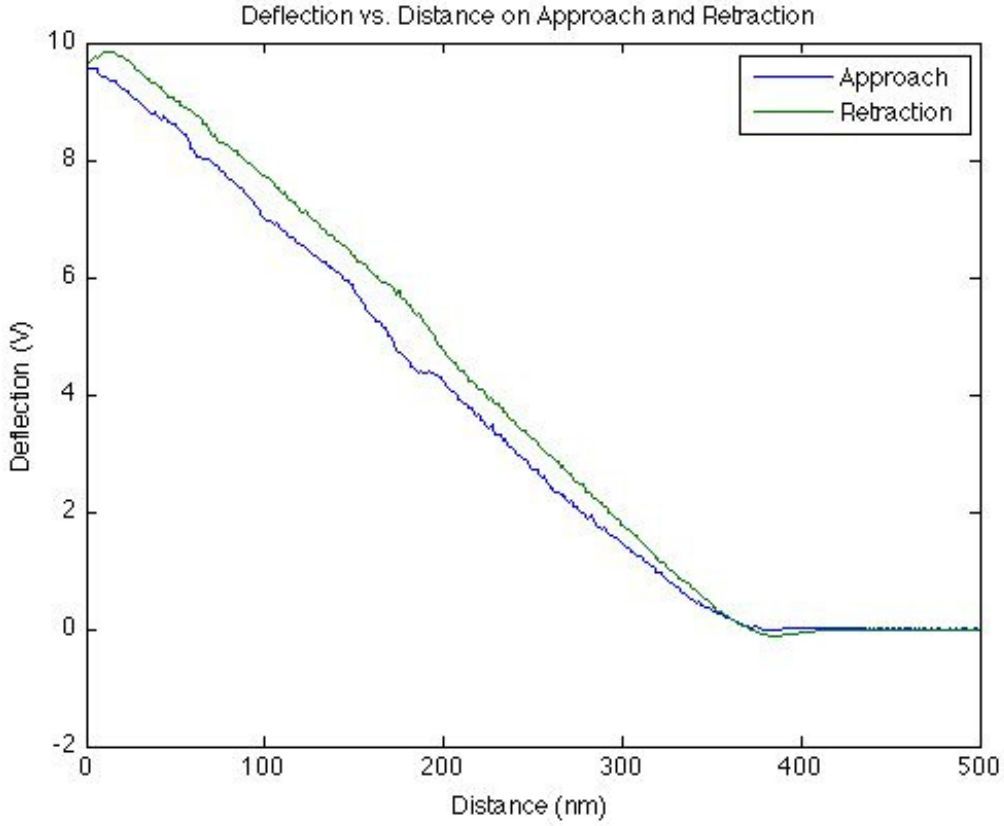
Deflection vs. Distance on Approach and Retraction
Approach
Retraction
Deflection (V)
Distance (nm)
10
8
6
4
2
0
-2
0
100
200
300
400
500

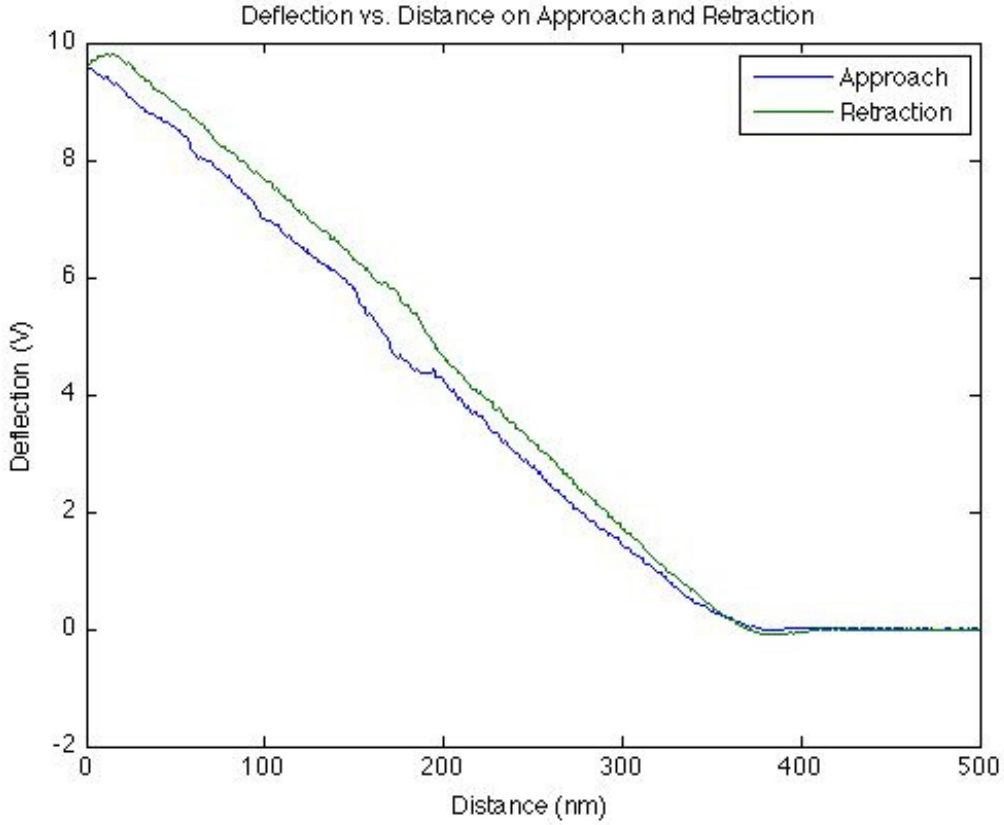
Deflection vs. Distance on Approach and Retraction
Approach
Retraction
Deflection (V)
Distance (nm)
10
8
6
4
2
0
-2
0
100
200
300
400
500

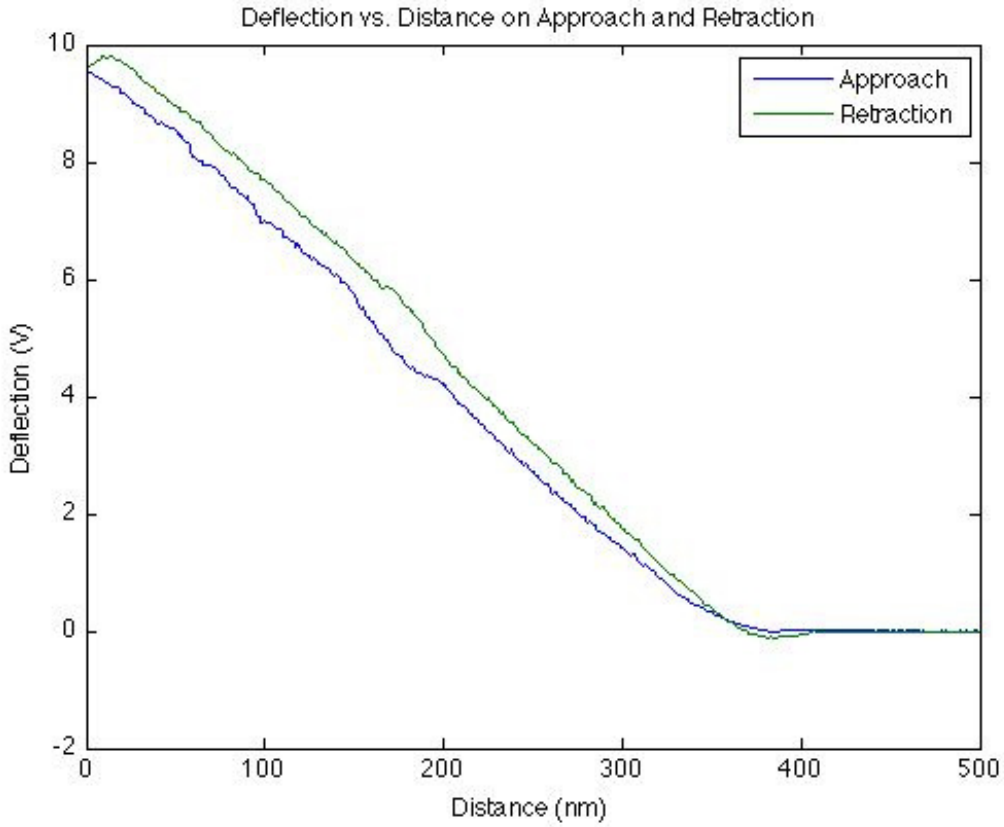
Deflection vs. Distance on Approach and Retraction
Approach
Retraction
Deflection (V)
Distance (nm)
10
8
6
4
2
0
-2
0
100
200
300
400
500

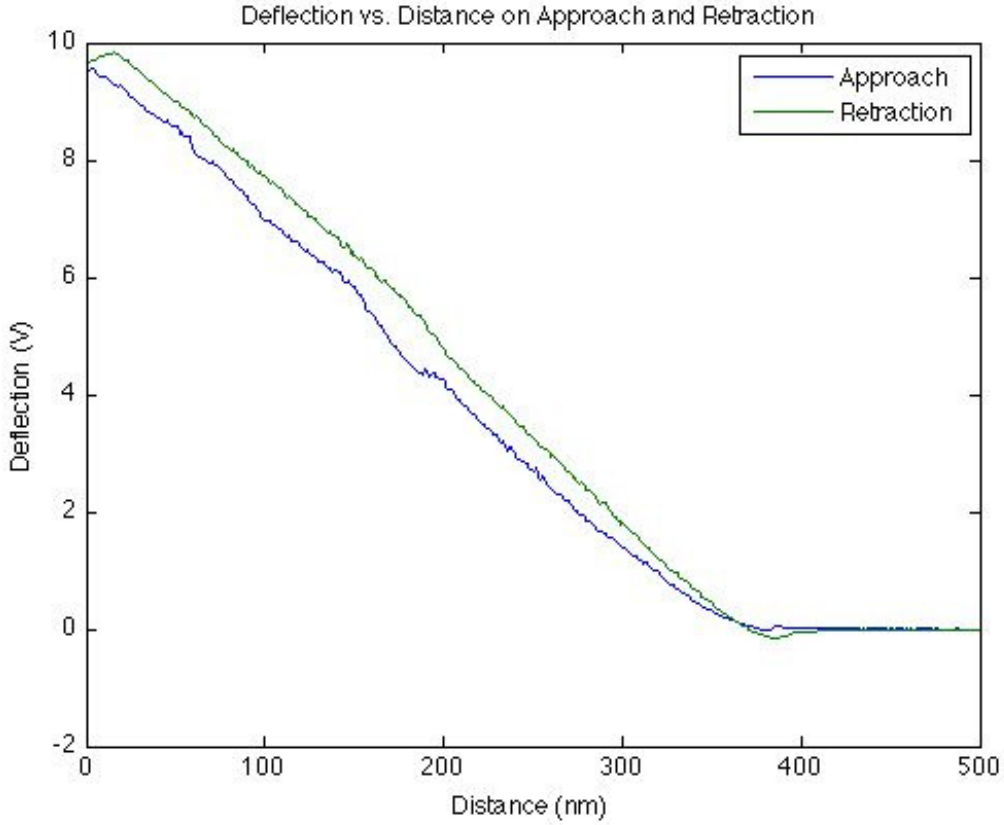
Deflection vs. Distance on Approach and Retraction
Approach
Retraction
Deflection (V)
Distance (nm)
10
8
6
4
2
0
-2
0
100
200
300
400
500

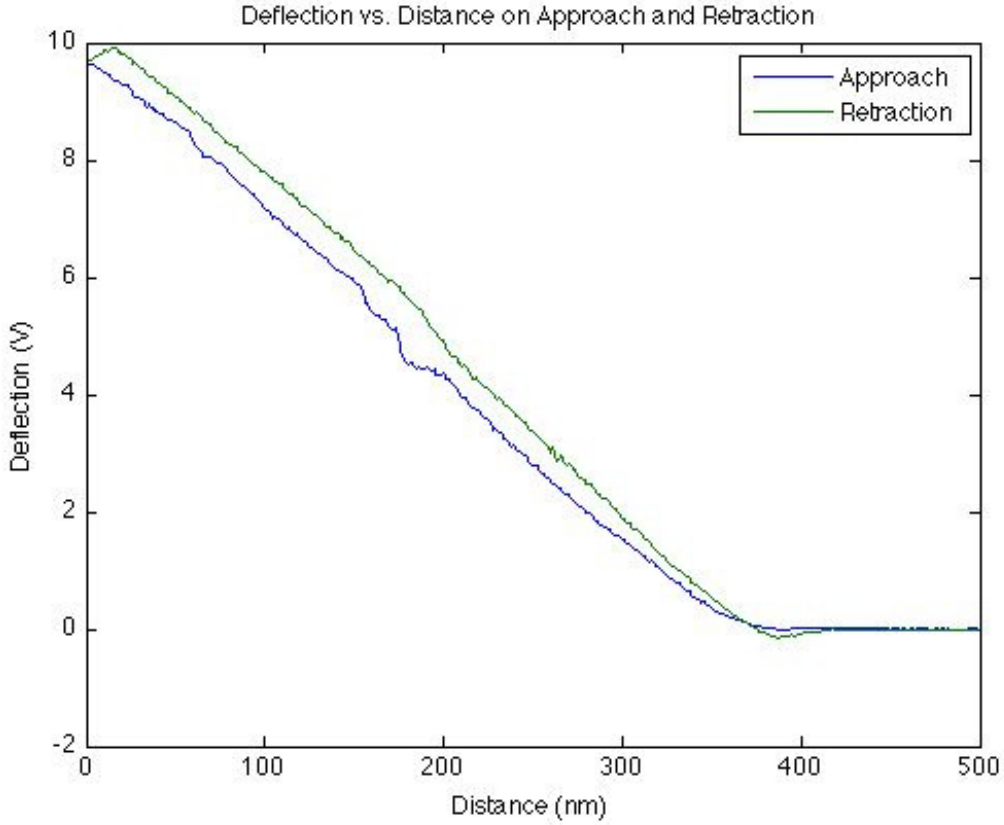
Deflection vs. Distance on Approach and Retraction
Approach
Retraction
Deflection (V)
Distance (nm)
10
8
6
4
2
0
-2
0
100
200
300
400
500

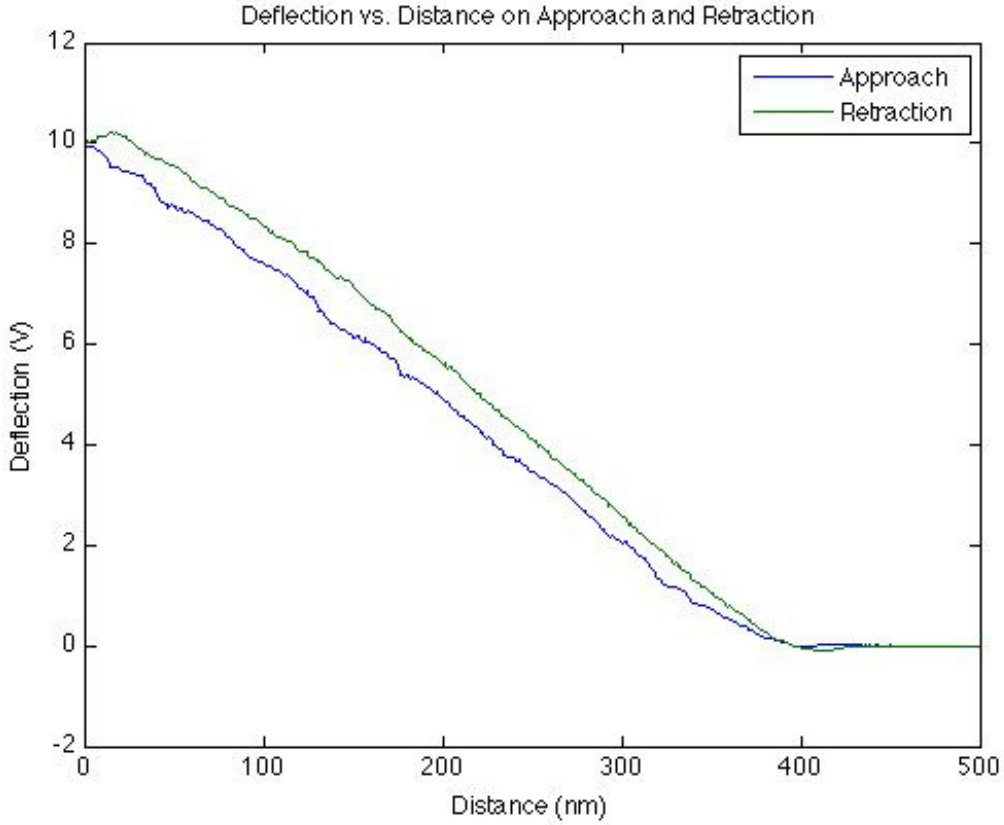
Deflection vs. Distance on Approach and Retraction
Approach
Retraction
Deflection (V)
Distance (nm)
12
10
8
6
4
2
0
-2
0
100
200
300
400
500

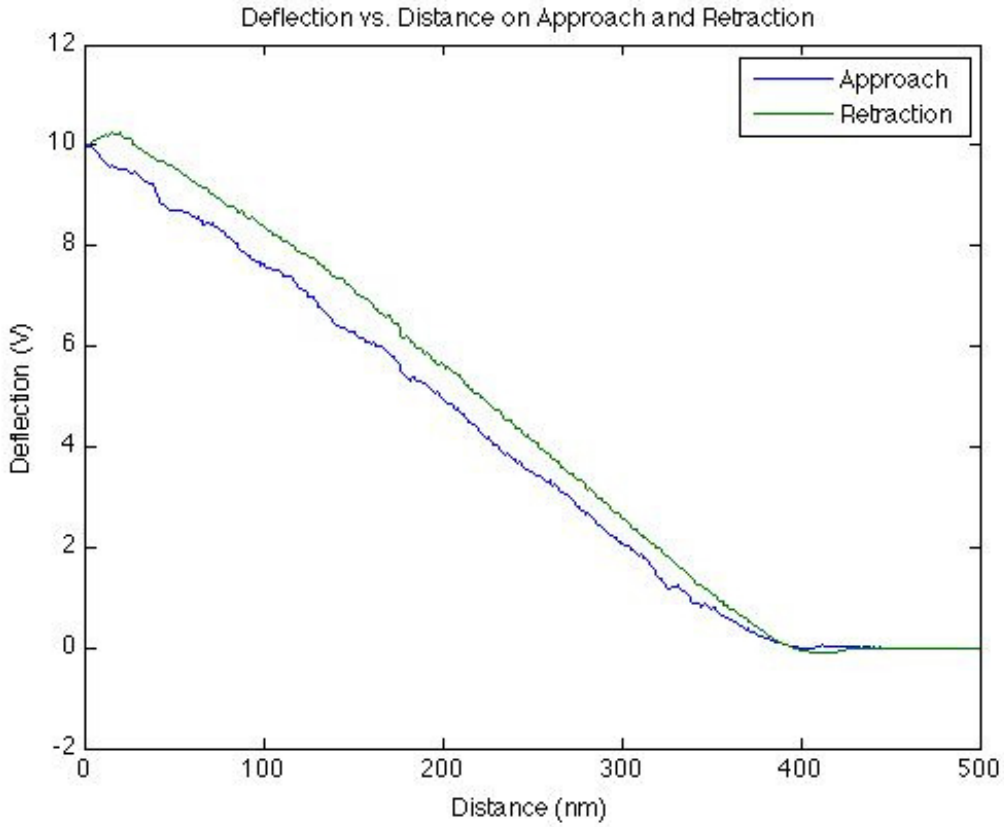
Deflection vs. Distance on Approach and Retraction
Approach
Retraction
Deflection (V)
Distance (nm)
12
10
8
6
4
2
0
-2
0
100
200
300
400
500

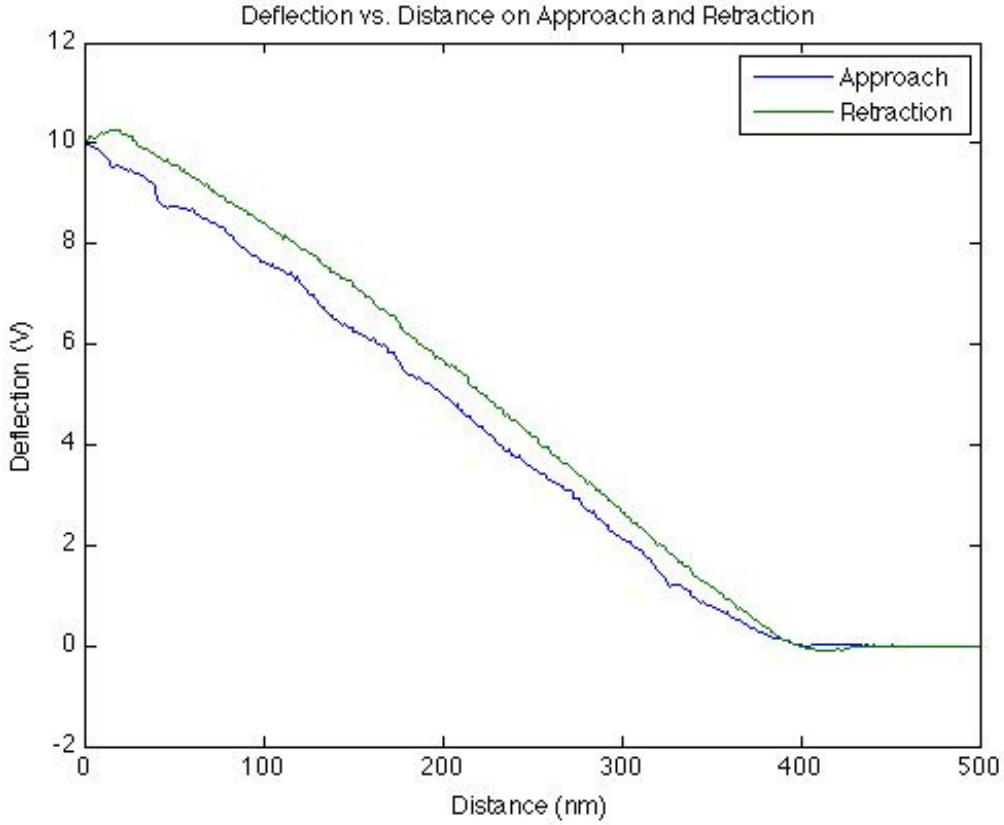
Deflection vs. Distance on Approach and Retraction
Approach
Retraction
Deflection (V)
Distance (nm)
12
10
8
6
4
2
0
-2
0
100
200
300
400
500

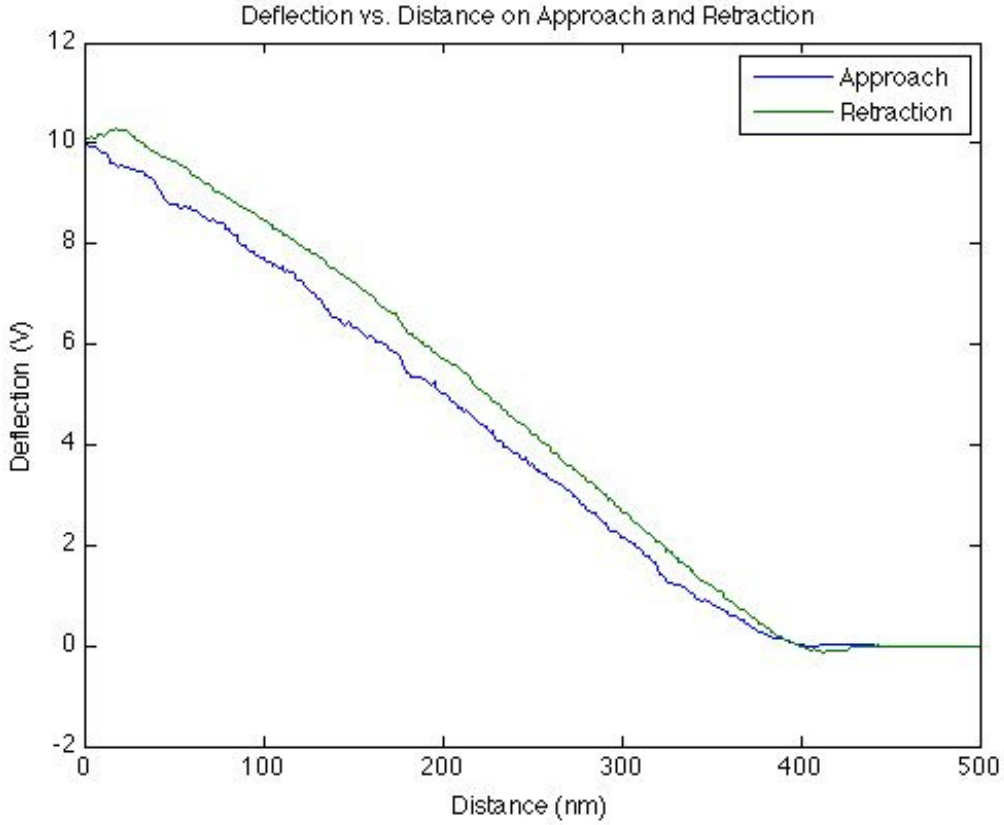
Deflection vs. Distance on Approach and Retraction
Approach
Retraction
Deflection (V)
Distance (nm)
12
10
8
6
4
2
0
-2
0
100
200
300
400
500

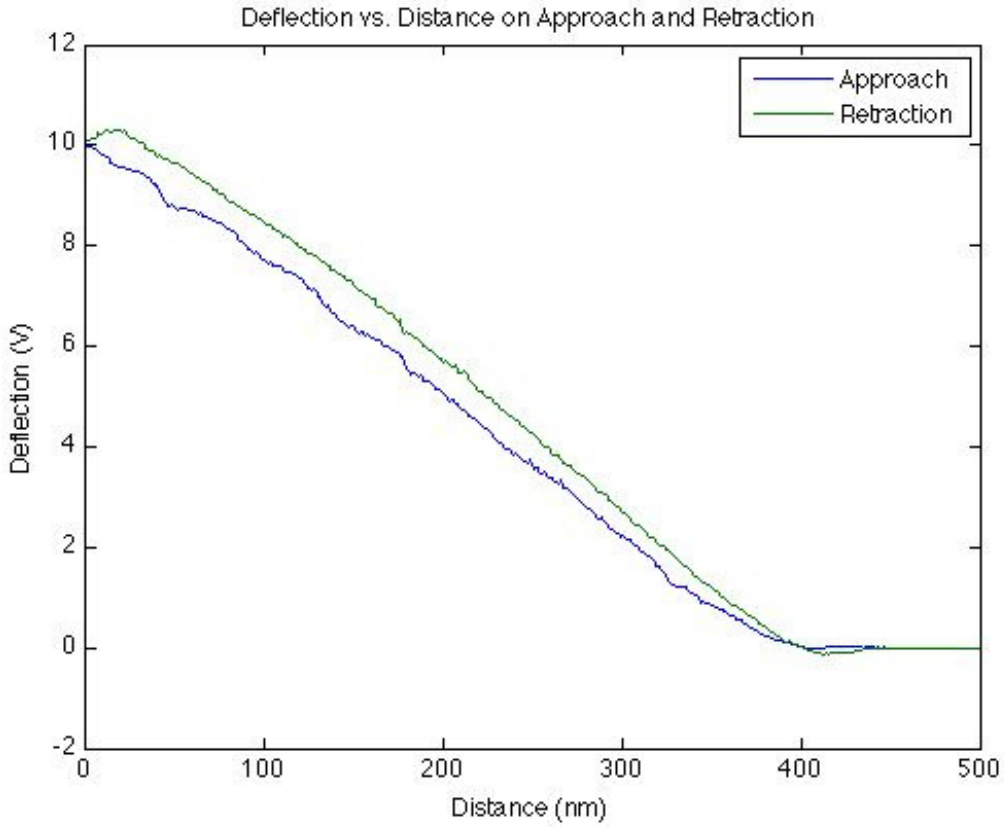
Deflection vs. Distance on Approach and Retraction
Approach
Retraction
Deflection (V)
Distance (nm)
12
10
8
6
4
2
0
-2
0
100
200
300
400
500

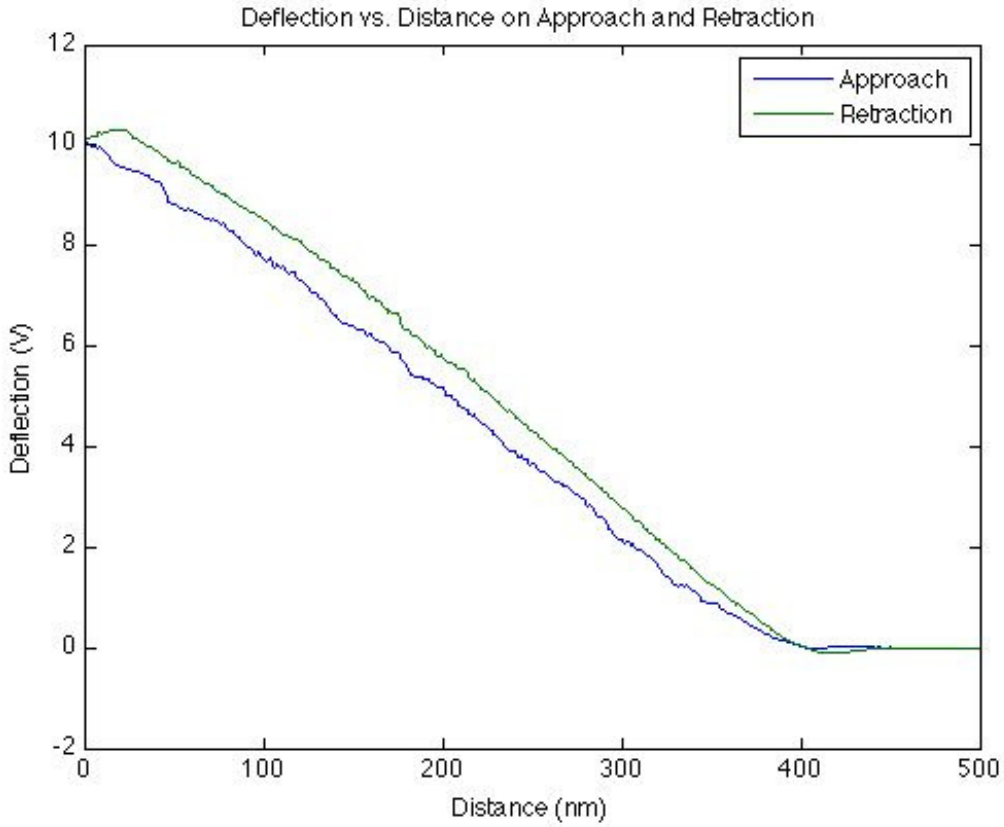
Deflection vs. Distance on Approach and Retraction
Approach
Retraction
Deflection (V)
Distance (nm)
12
10
8
6
4
2
0
-2
0
100
200
300
400
500

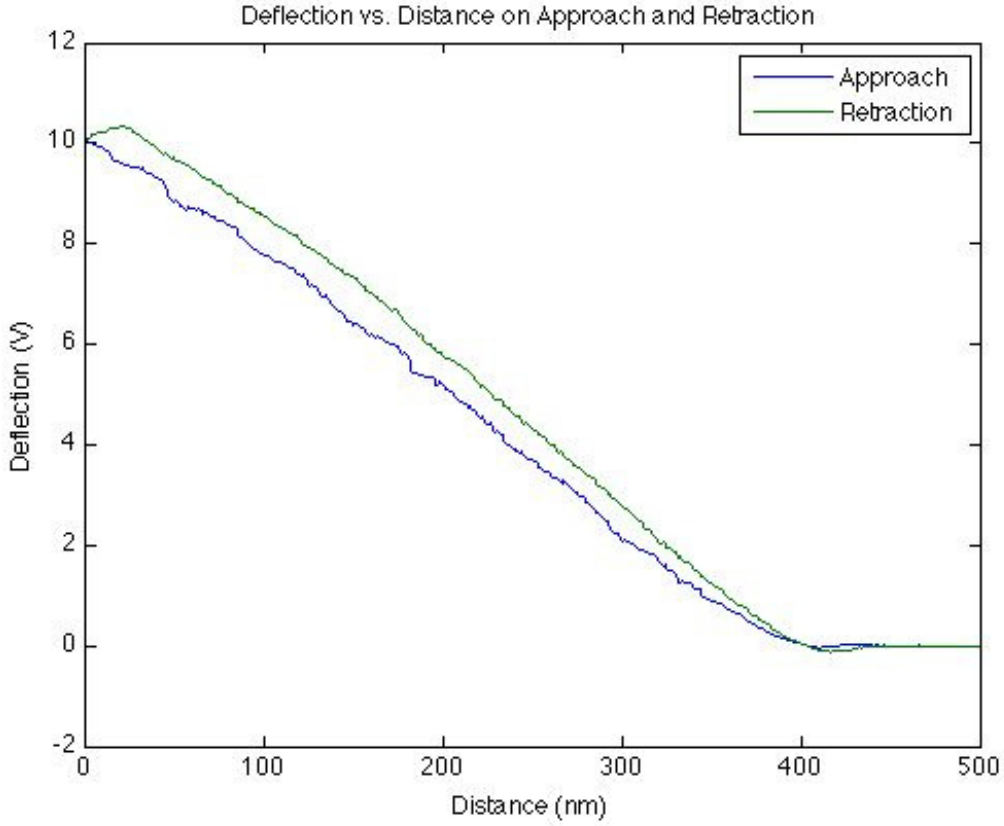
Deflection vs. Distance on Approach and Retraction
Approach
Retraction
Deflection (V)
Distance (nm)
12
10
8
6
4
2
0
-2
0
100
200
300
400
500

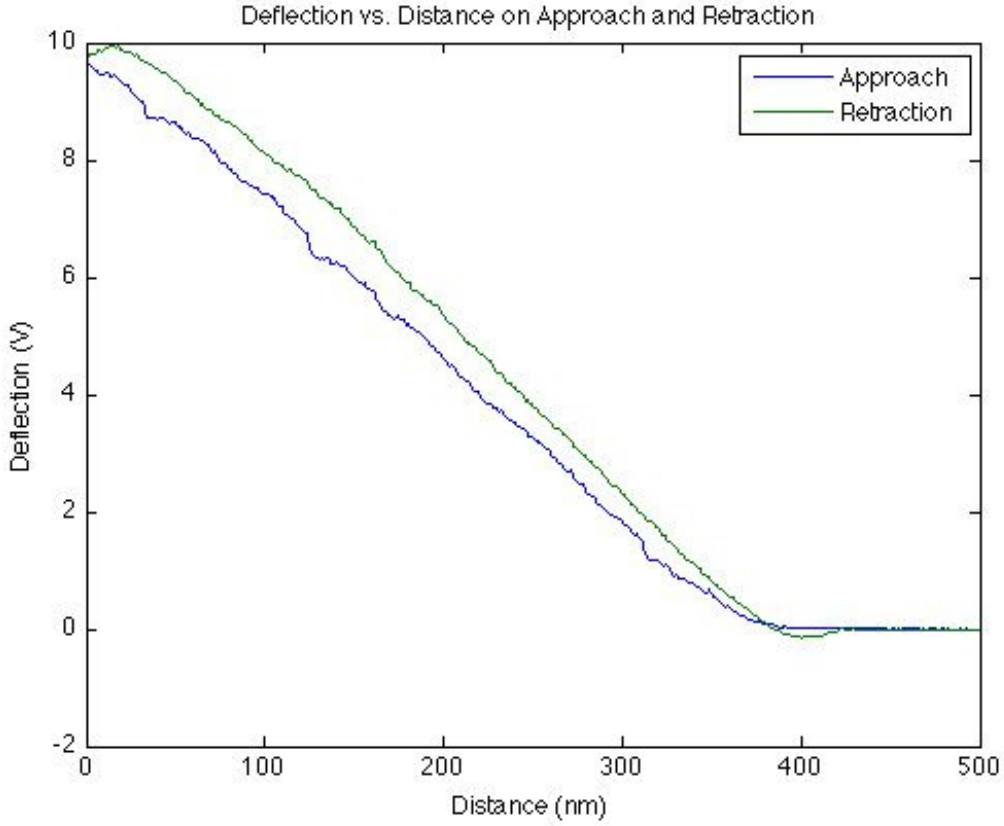
Deflection vs. Distance on Approach and Retraction
Approach
Retraction
Deflection (V)
Distance (nm)
10
8
6
4
2
0
-2
0
100
200
300
400
500

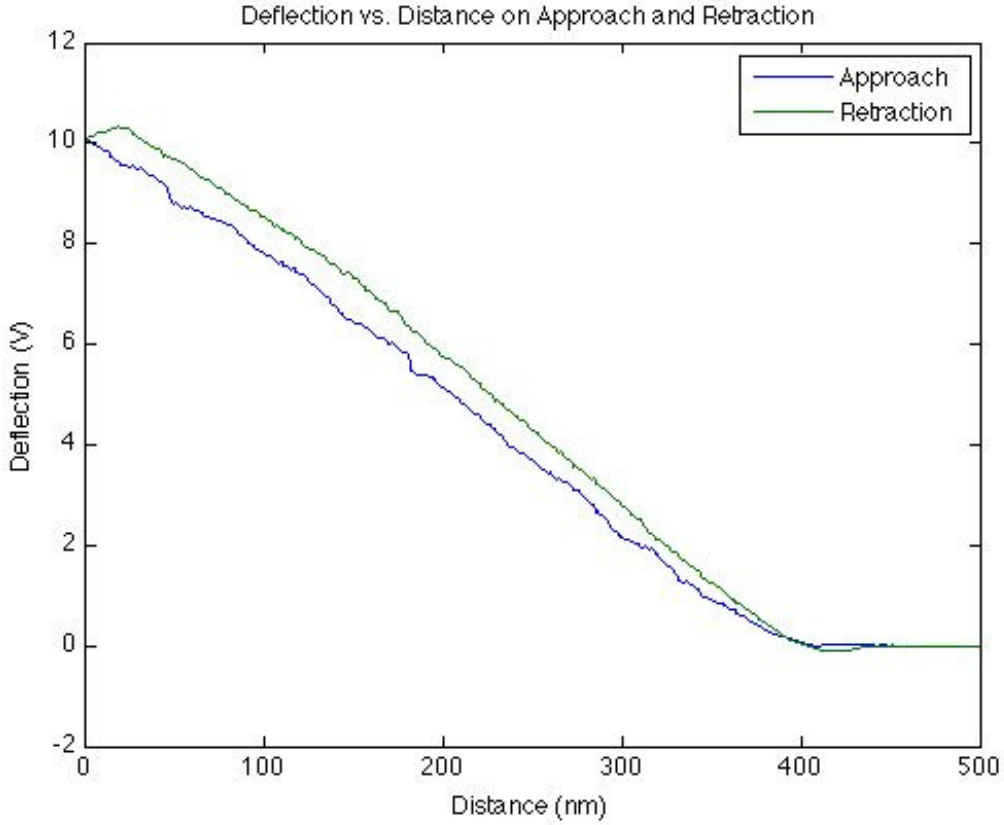
Deflection vs. Distance on Approach and Retraction
Approach
Retraction
Deflection (V)
Distance (nm)
12
10
8
6
4
2
0
-2
0
100
200
300
400
500

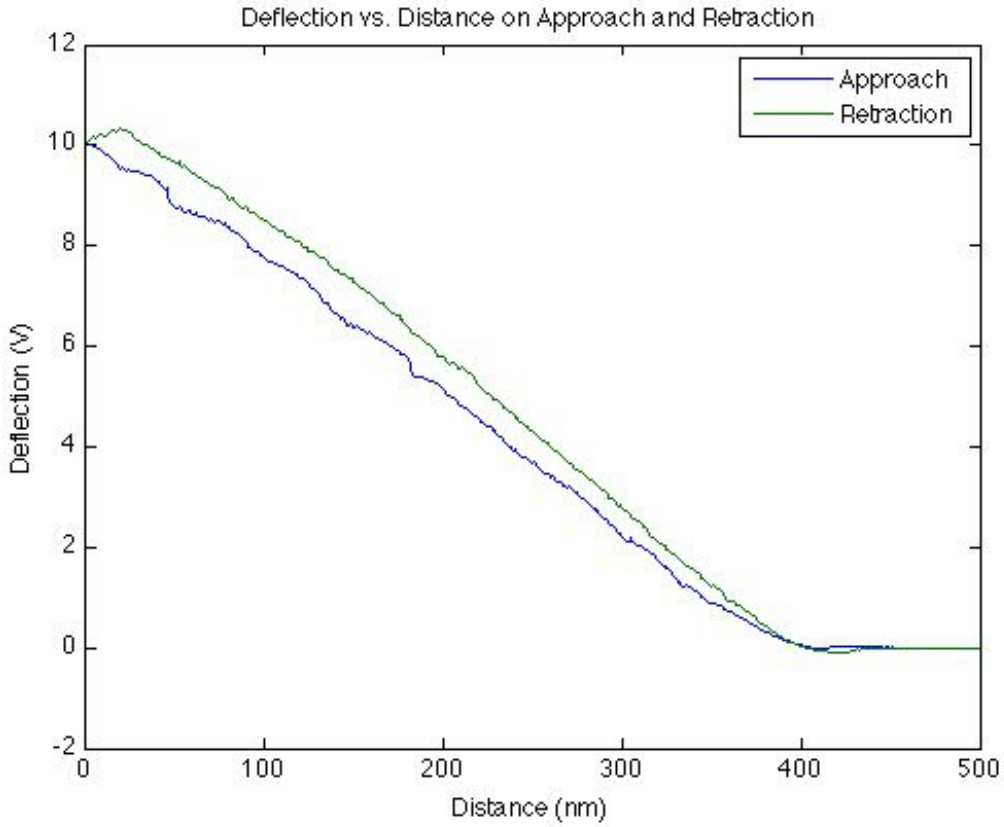
Deflection vs. Distance on Approach and Retraction
Approach
Retraction
Deflection (V)
Distance (nm)
12
10
8
6
4
2
0
-2
0
100
200
300
400
500

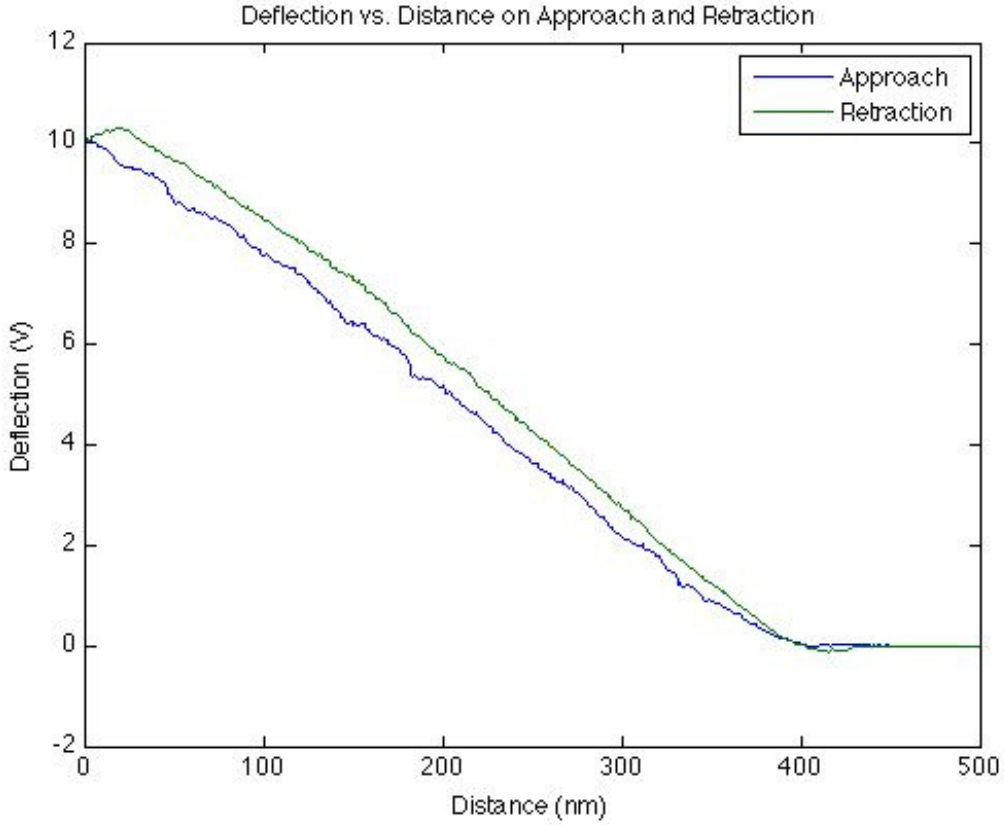
Deflection vs. Distance on Approach and Retraction
Approach
Retraction
Deflection (V)
Distance (nm)
12
10
8
6
4
2
0
-2
0
100
200
300
400
500

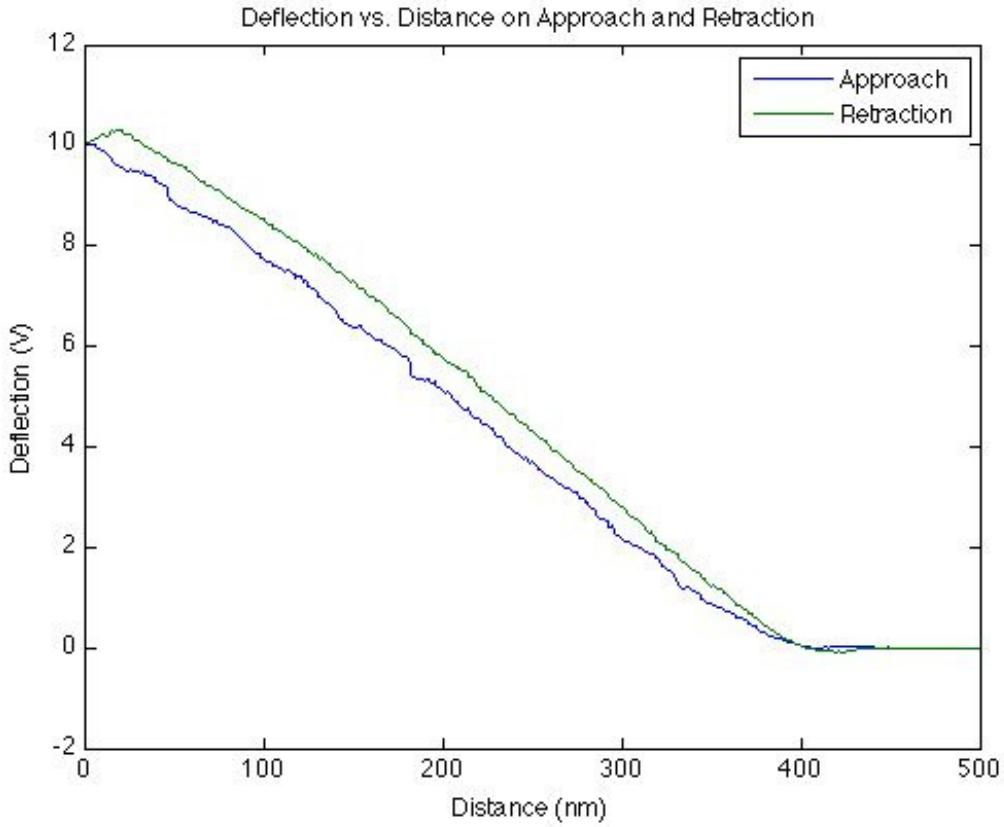
Deflection vs. Distance on Approach and Retraction
Approach
Retraction
Deflection (V)
Distance (nm)
12
10
8
6
4
2
0
-2
0
100
200
300
400
500

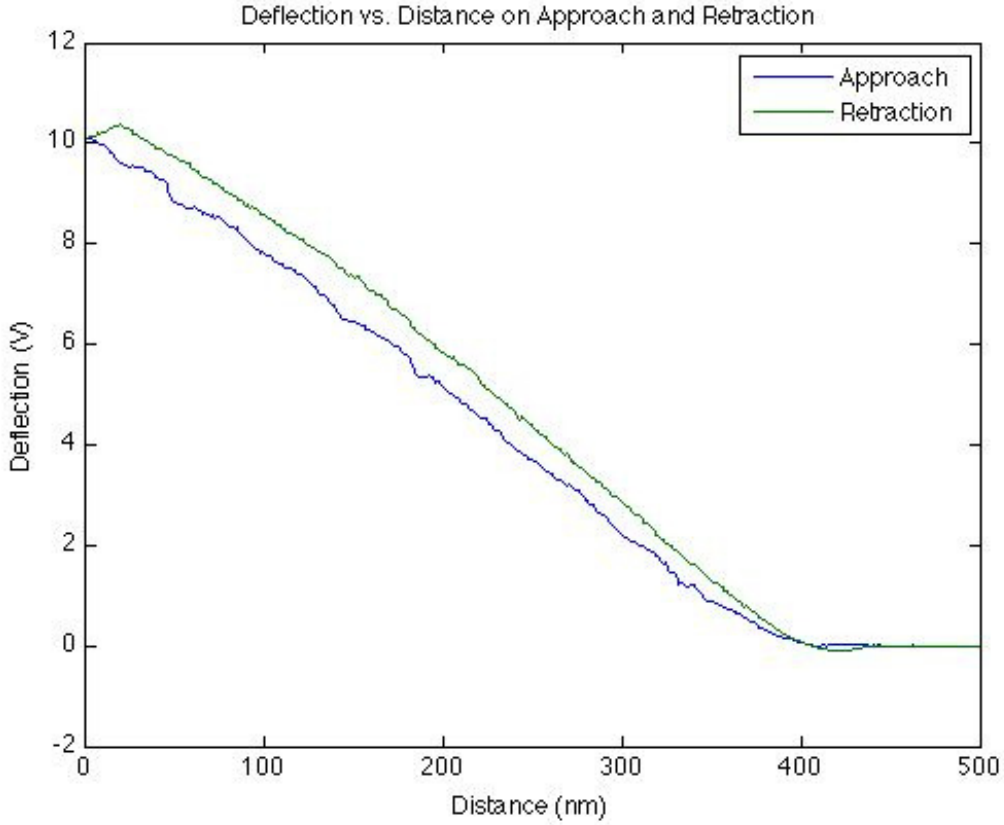
Deflection vs. Distance on Approach and Retraction
Approach
Retraction
Deflection (V)
Distance (nm)
12
10
8
6
4
2
0
-2
0
100
200
300
400
500

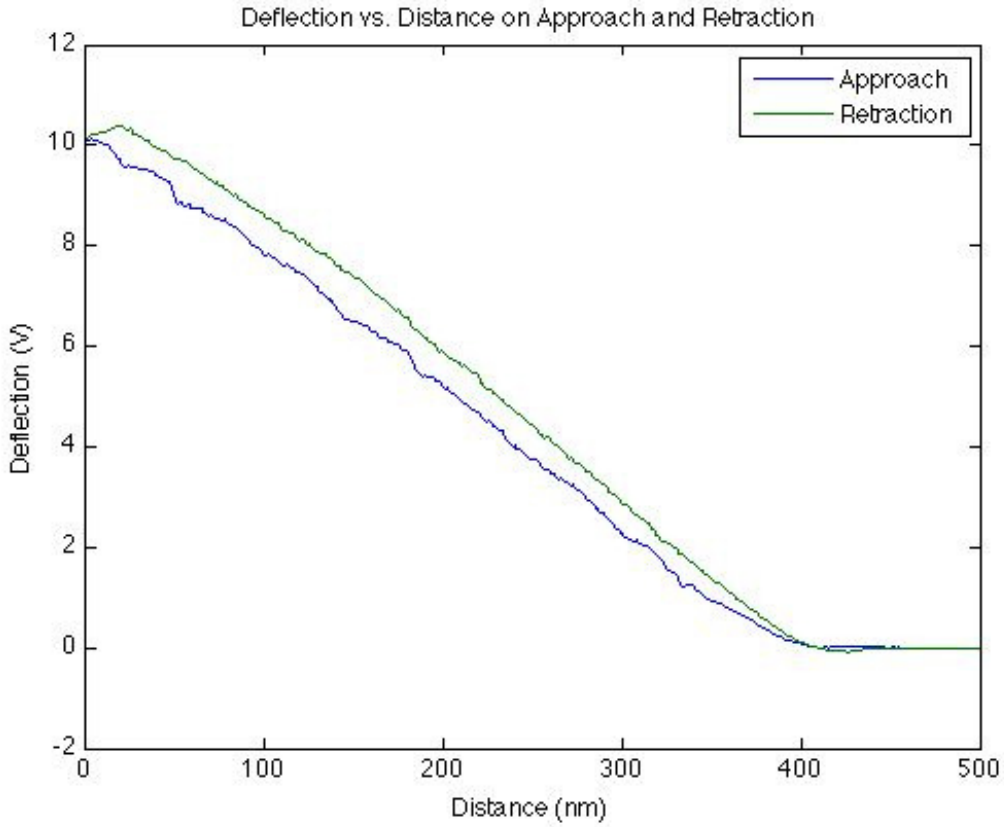
Deflection vs. Distance on Approach and Retraction
Approach
Retraction
Deflection (V)
Distance (nm)
12
10
8
6
4
2
0
-2
0
100
200
300
400
500

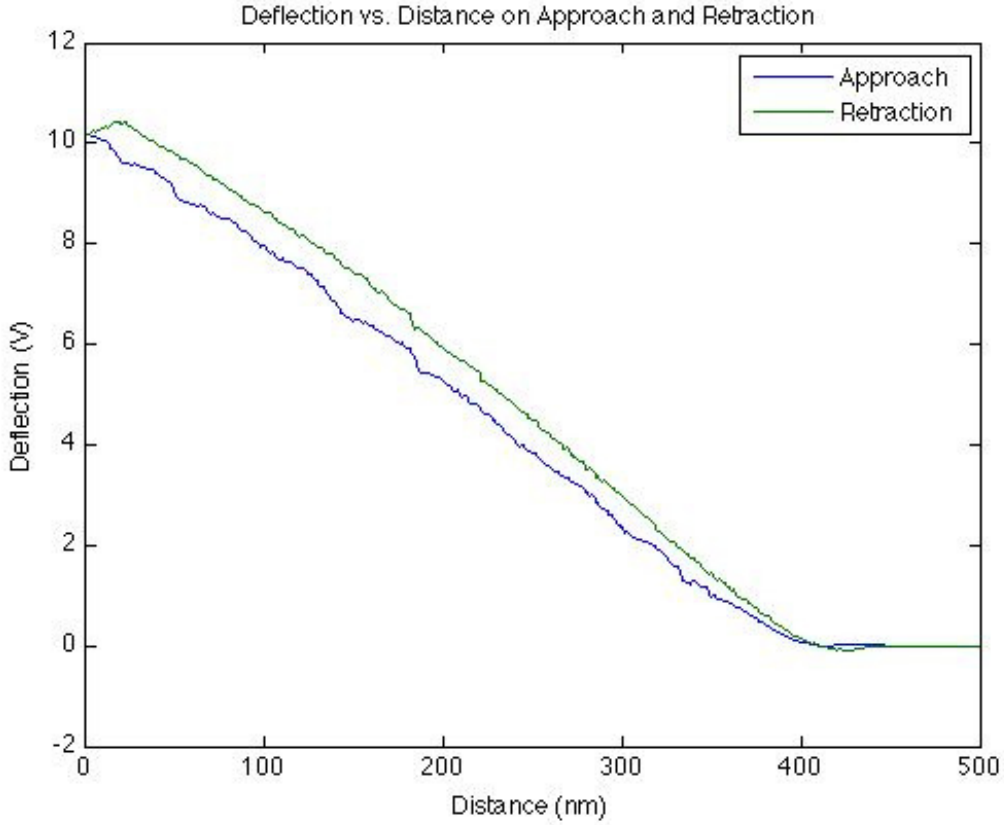
Deflection vs. Distance on Approach and Retraction
Approach
Retraction
Deflection (V)
Distance (nm)
12
10
8
6
4
2
0
-2
0
100
200
300
400
500

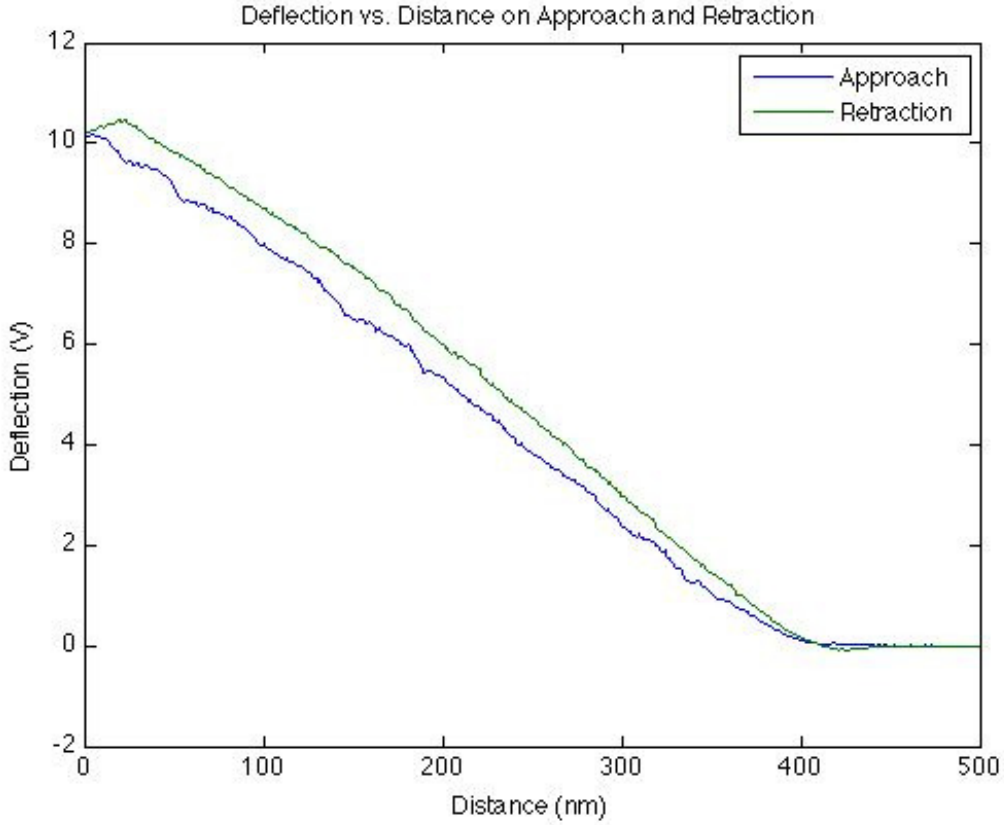
Deflection vs. Distance on Approach and Retraction
Approach
Retraction
Deflection (V)
Distance (nm)
12
10
8
6
4
2
0
-2
0
100
200
300
400
500

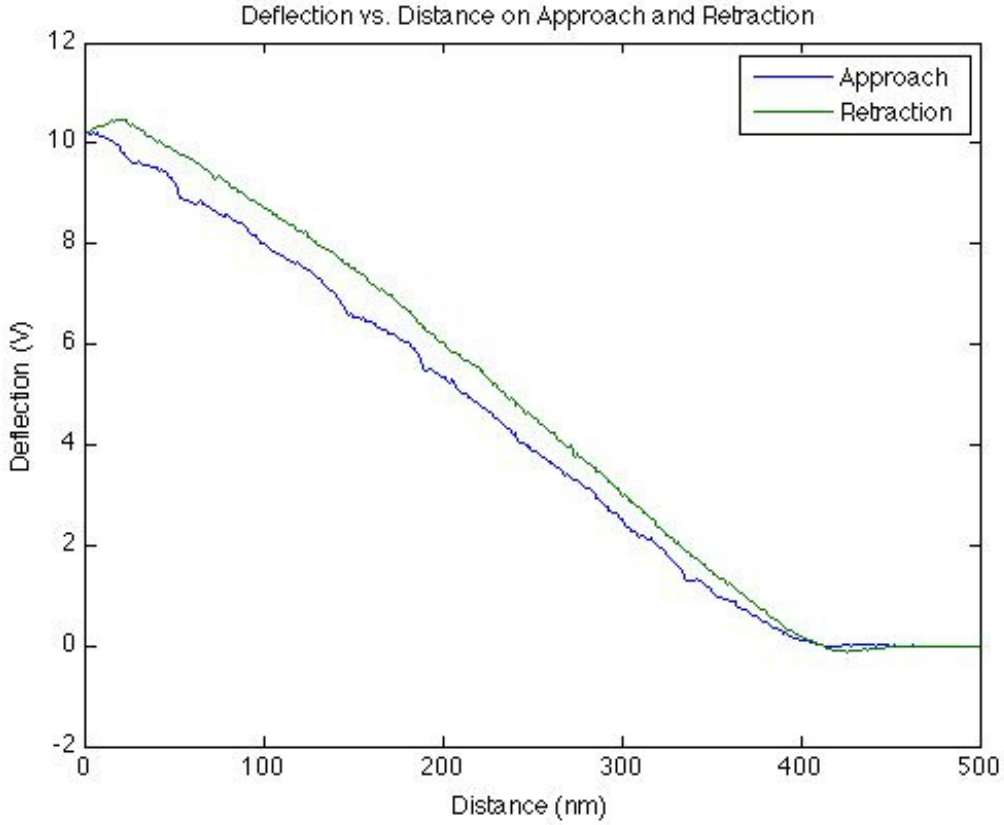
Deflection vs. Distance on Approach and Retraction
Approach
Retraction
Deflection (V)
Distance (nm)
12
10
8
6
4
2
0
-2
0
100
200
300
400
500

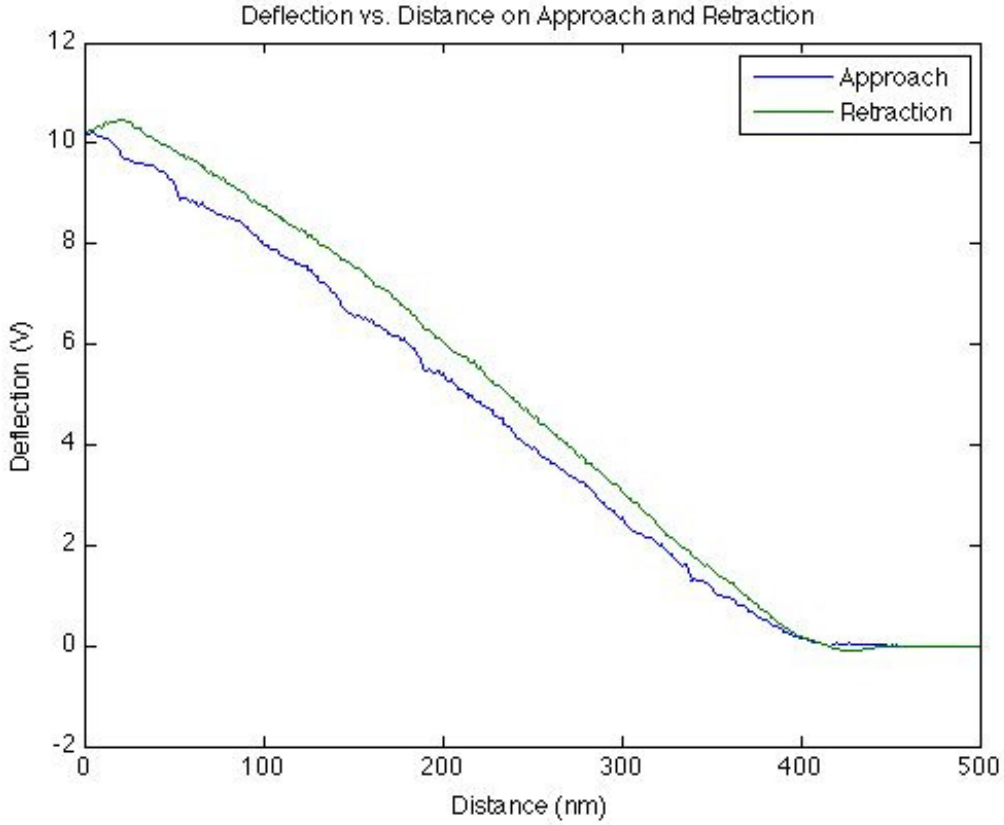
Deflection vs. Distance on Approach and Retraction
Approach
Retraction
Deflection (V)
Distance (nm)
12
10
8
6
4
2
0
-2
0
100
200
300
400
500

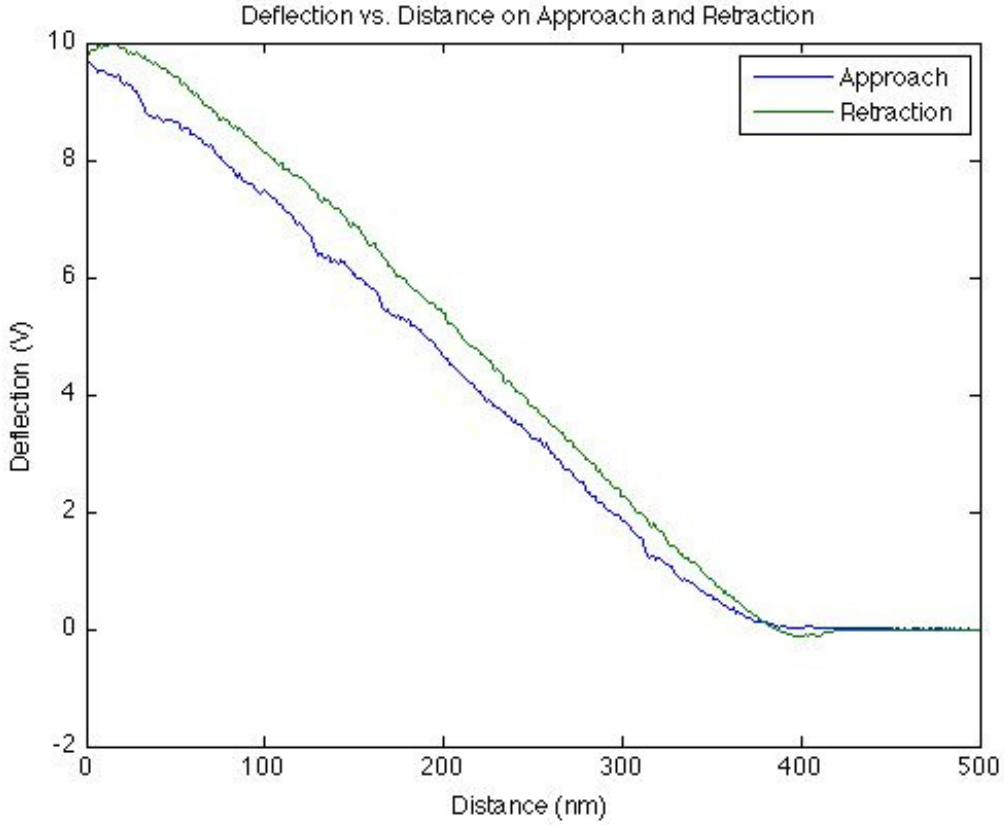
Deflection vs. Distance on Approach and Retraction
Approach
Retraction
Deflection (V)
Distance (nm)
10
8
6
4
2
0
-2
0
100
200
300
400
500

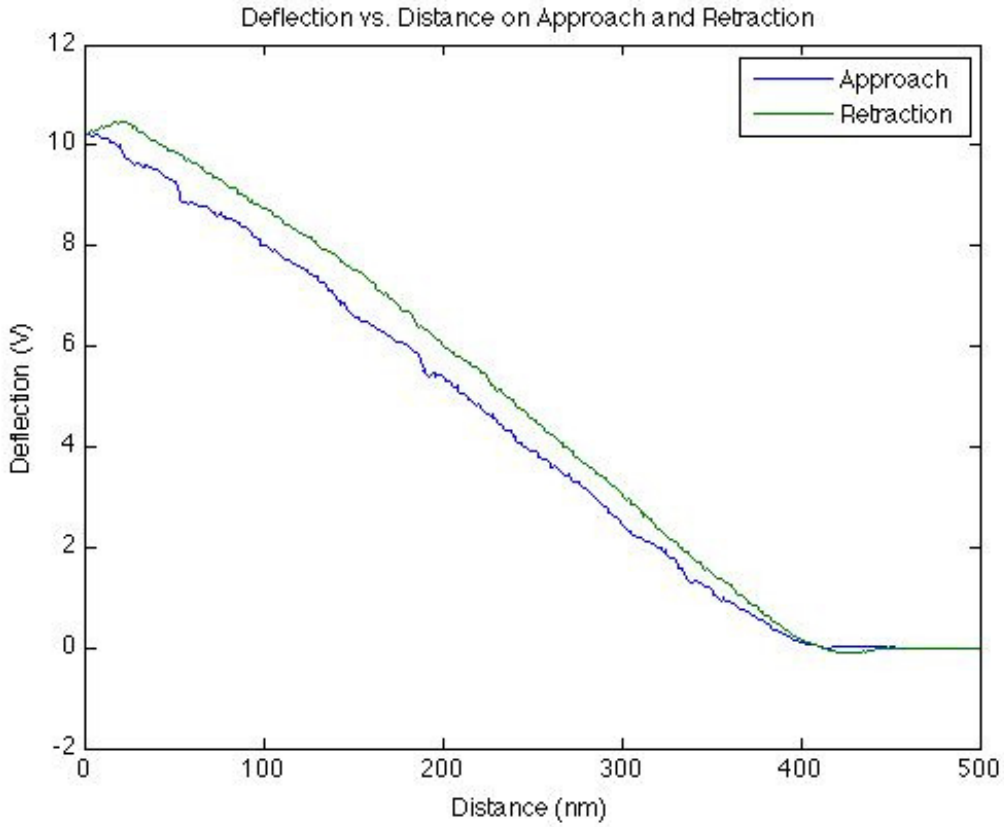
Deflection vs. Distance on Approach and Retraction
Approach
Retraction
Deflection (V)
Distance (nm)
12
10
8
6
4
2
0
-2
0
100
200
300
400
500

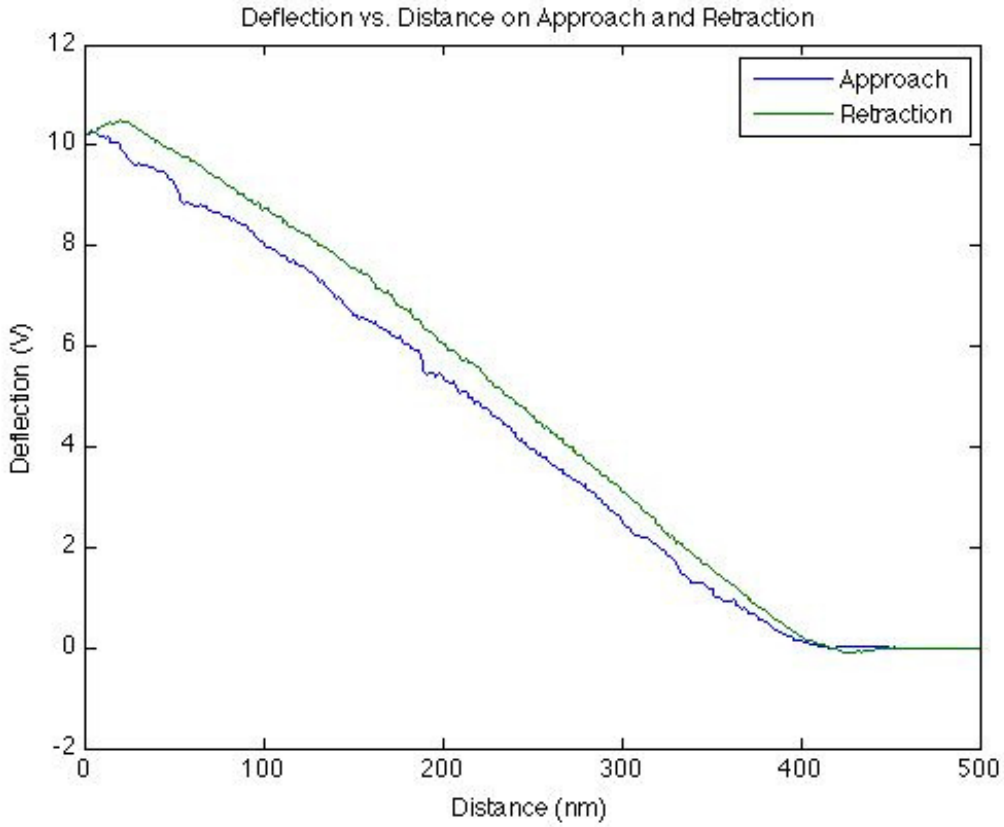
Deflection vs. Distance on Approach and Retraction
Approach
Retraction
Deflection (V)
Distance (nm)
12
10
8
6
4
2
0
-2
0
100
200
300
400
500

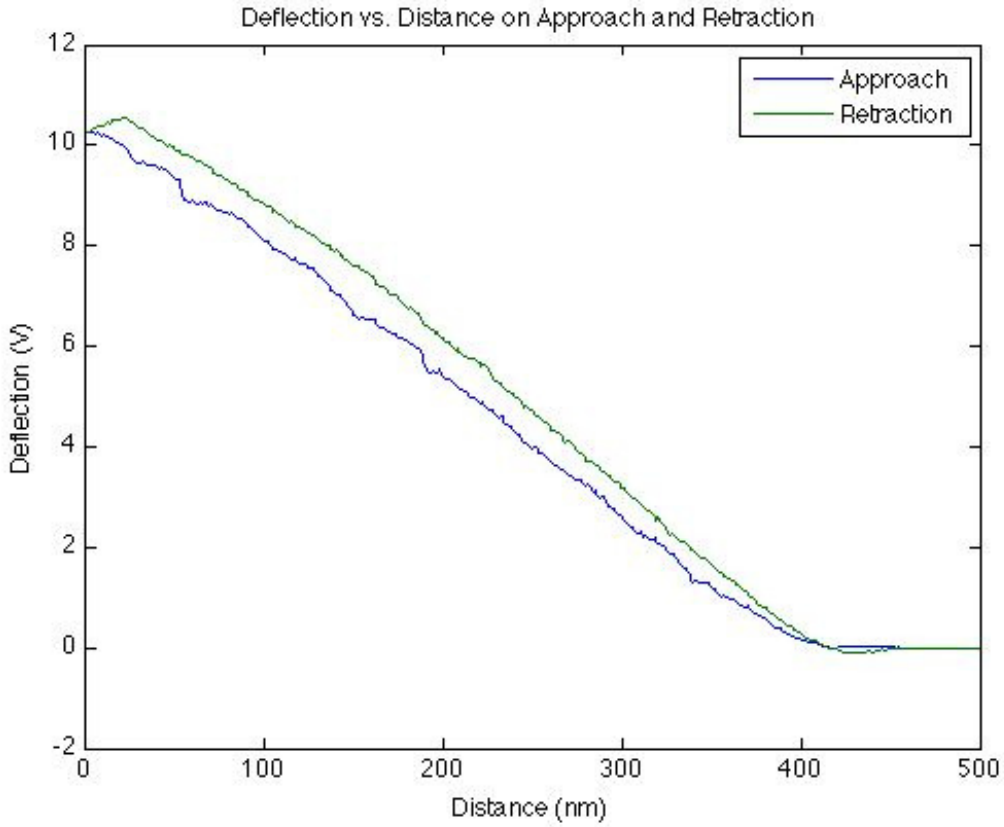
Deflection vs. Distance on Approach and Retraction
Approach
Retraction
Deflection (V)
Distance (nm)
12
10
8
6
4
2
0
-2
0
100
200
300
400
500

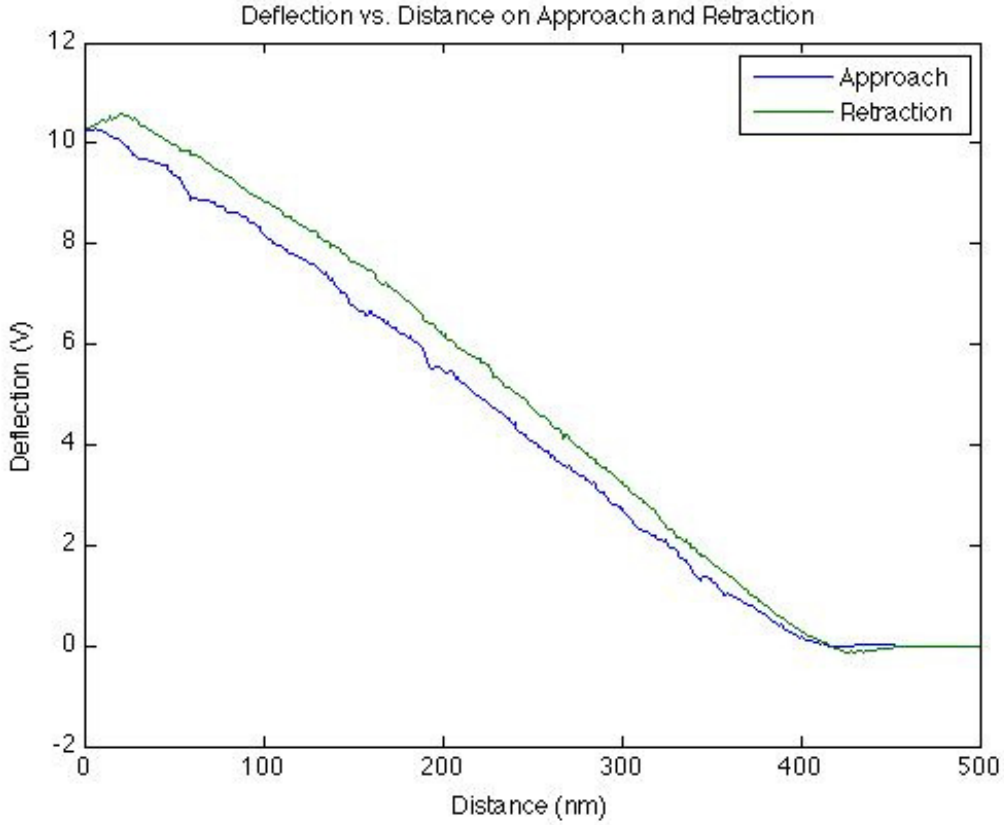
Deflection vs. Distance on Approach and Retraction
Approach
Retraction
Deflection (V)
Distance (nm)
12
10
8
6
4
2
0
-2
0
100
200
300
400
500

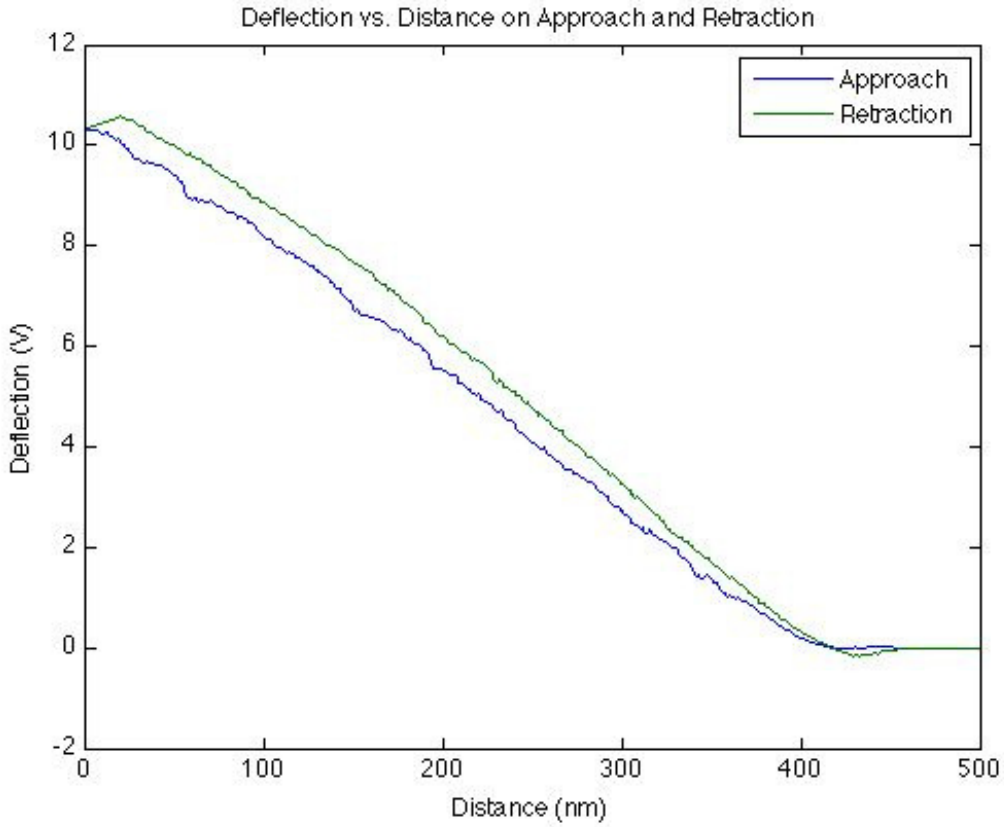
Deflection vs. Distance on Approach and Retraction
Approach
Retraction
Deflection (V)
Distance (nm)
12
10
8
6
4
2
0
-2
0
100
200
300
400
500

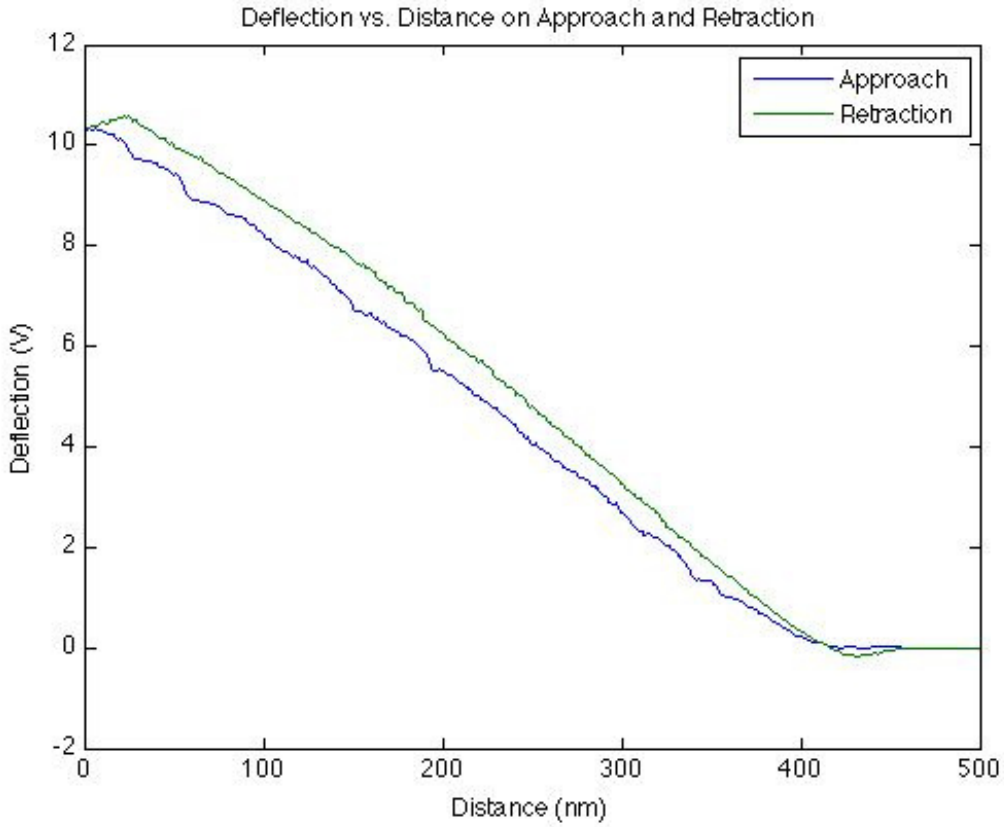
Deflection vs. Distance on Approach and Retraction
Approach
Retraction
Deflection (V)
Distance (nm)
12
10
8
6
4
2
0
-2
0
100
200
300
400
500

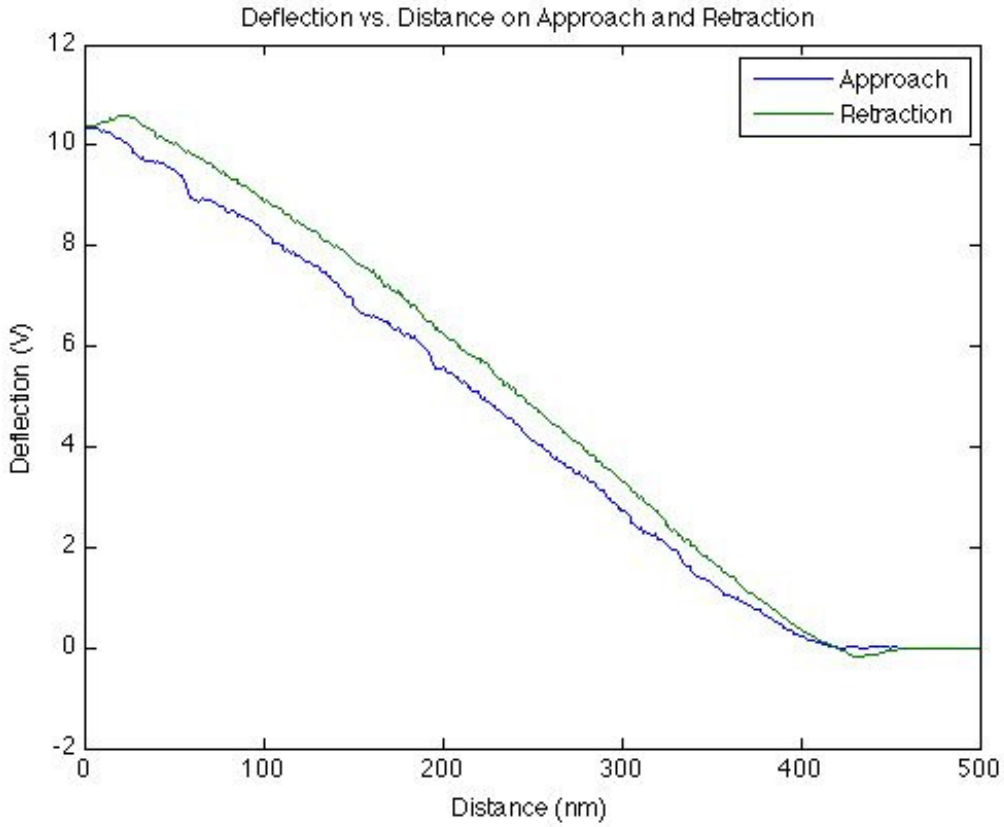
Deflection vs. Distance on Approach and Retraction
Approach
Retraction
Deflection (V)
Distance (nm)
12
10
8
6
4
2
0
-2
0
100
200
300
400
500

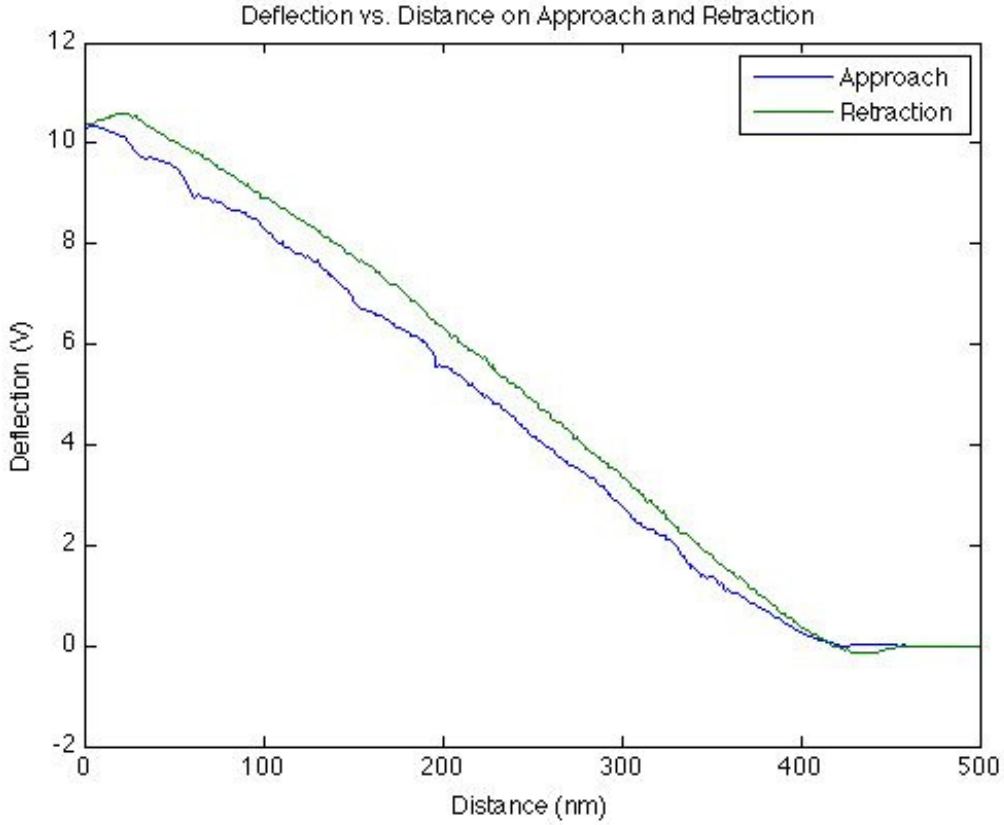
Deflection vs. Distance on Approach and Retraction
Approach
Retraction
Deflection (V)
Distance (nm)
12
10
8
6
4
2
0
-2
0
100
200
300
400
500

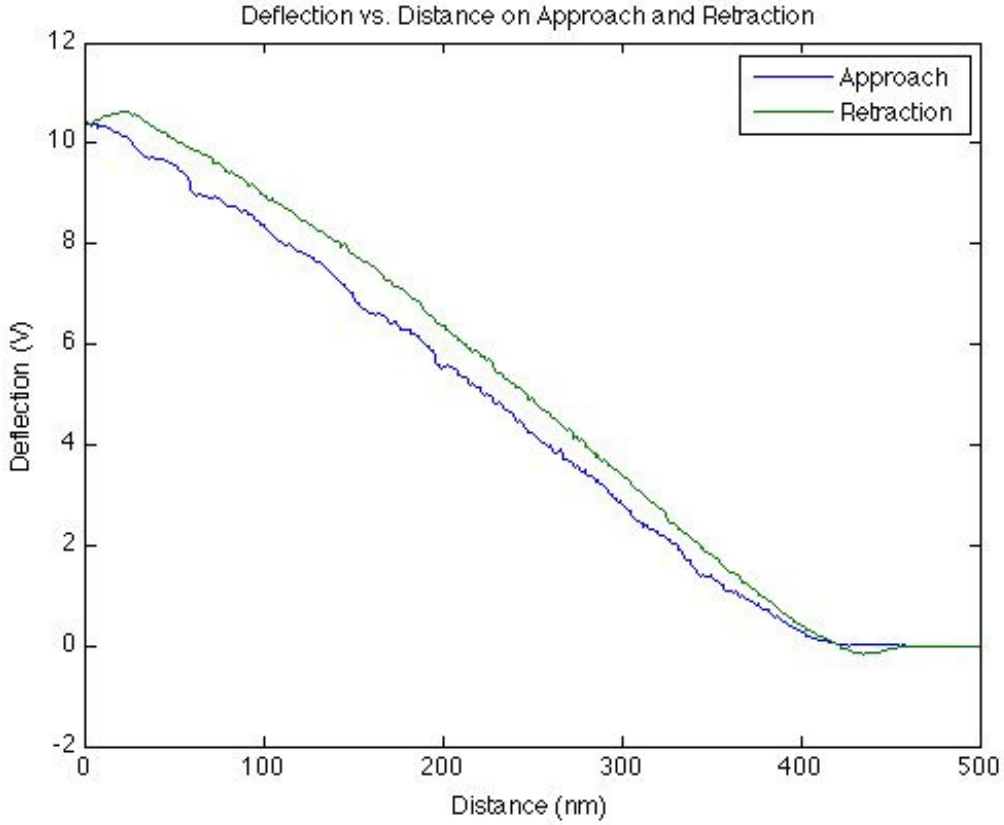
Deflection vs. Distance on Approach and Retraction
Approach
Retraction
Deflection (V)
Distance (nm)
12
10
8
6
4
2
0
-2
0
100
200
300
400
500

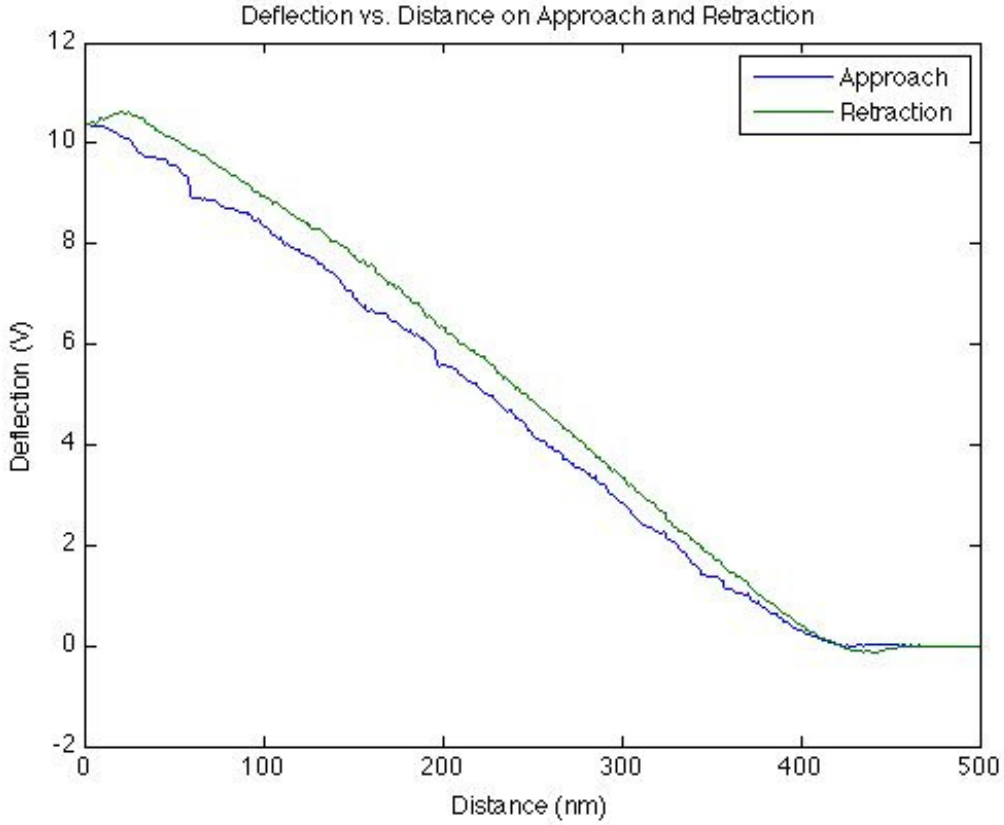
Deflection vs. Distance on Approach and Retraction
Approach
Retraction
Deflection (V)
Distance (nm)
12
10
8
6
4
2
0
-2
0
100
200
300
400
500

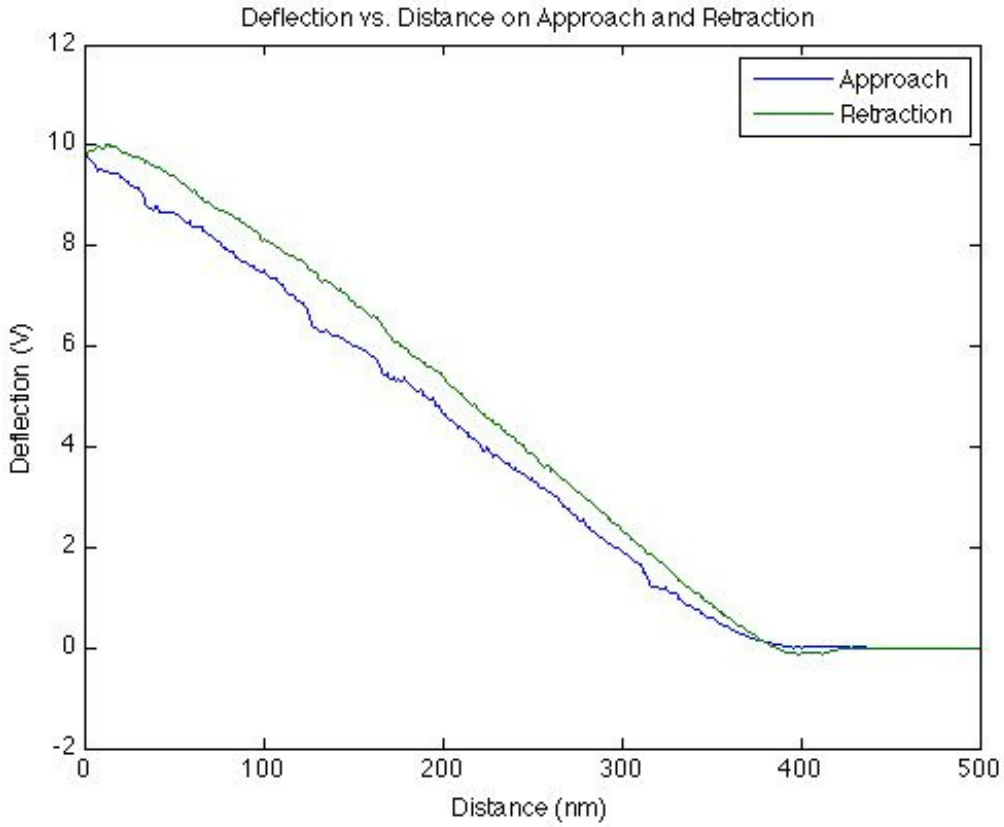
Deflection vs. Distance on Approach and Retraction
Approach
Retraction
Deflection (V)
Distance (nm)
12
10
8
6
4
2
0
-2
0
100
200
300
400
500

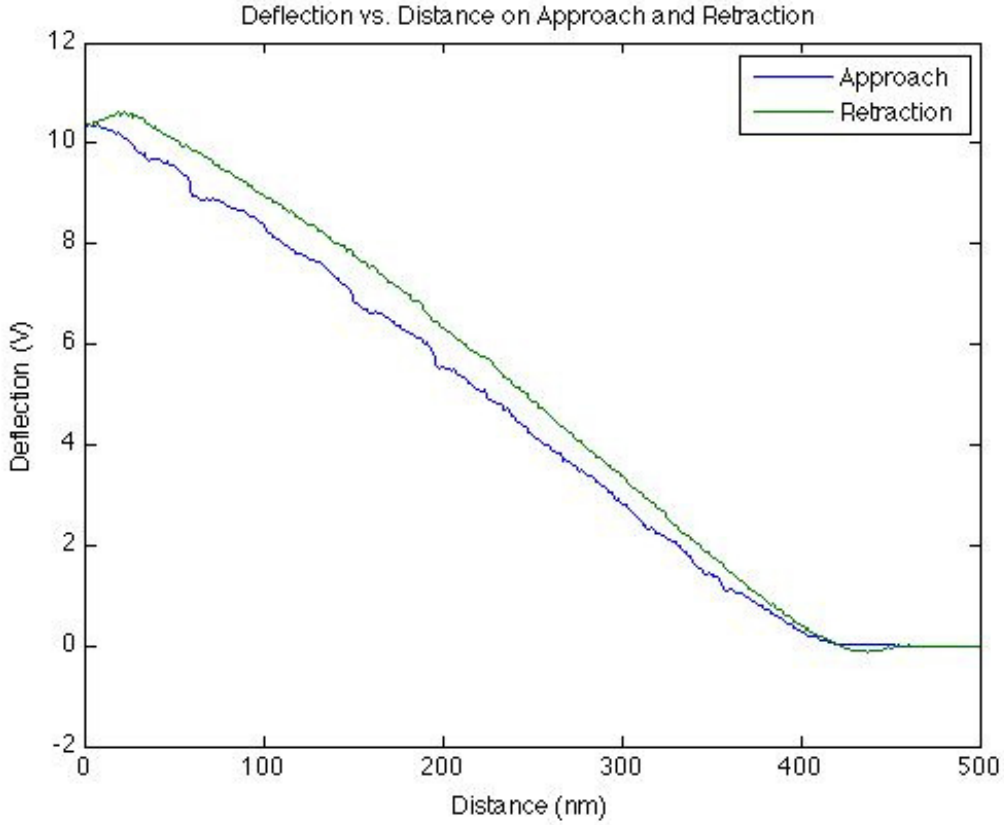
Deflection vs. Distance on Approach and Retraction
Approach
Retraction
Deflection (V)
Distance (nm)
12
10
8
6
4
2
0
-2
0
100
200
300
400
500

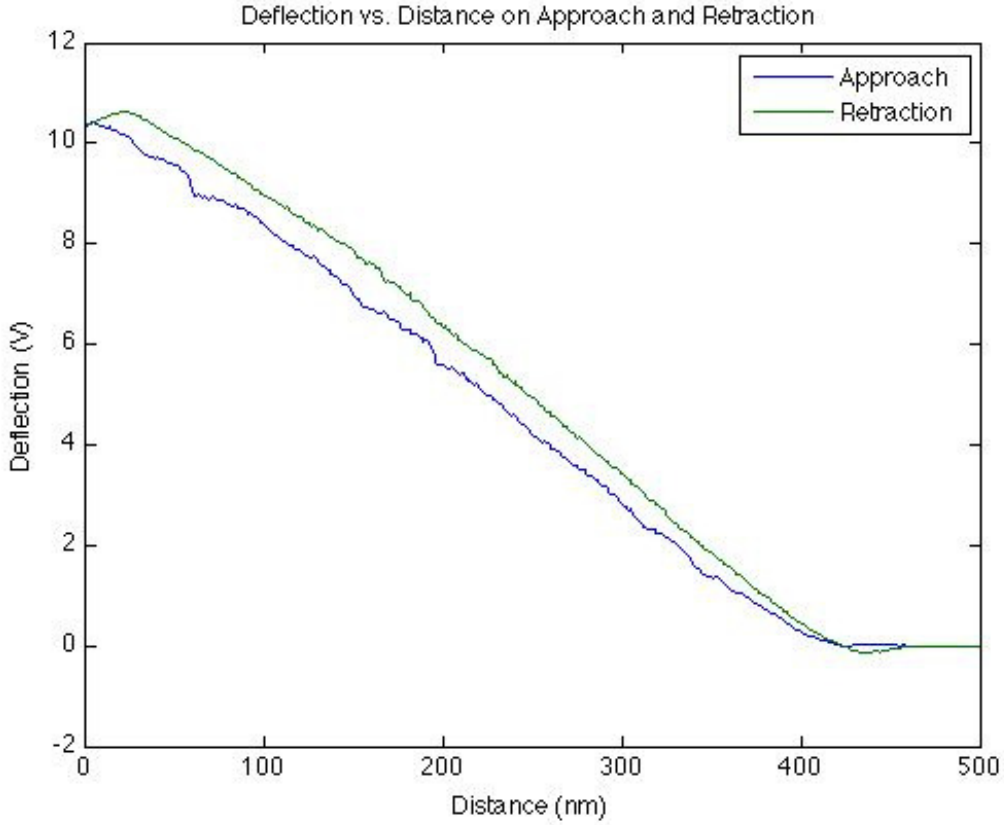
Deflection vs. Distance on Approach and Retraction
Approach
Retraction
Deflection (V)
Distance (nm)
12
10
8
6
4
2
0
-2
0
100
200
300
400
500

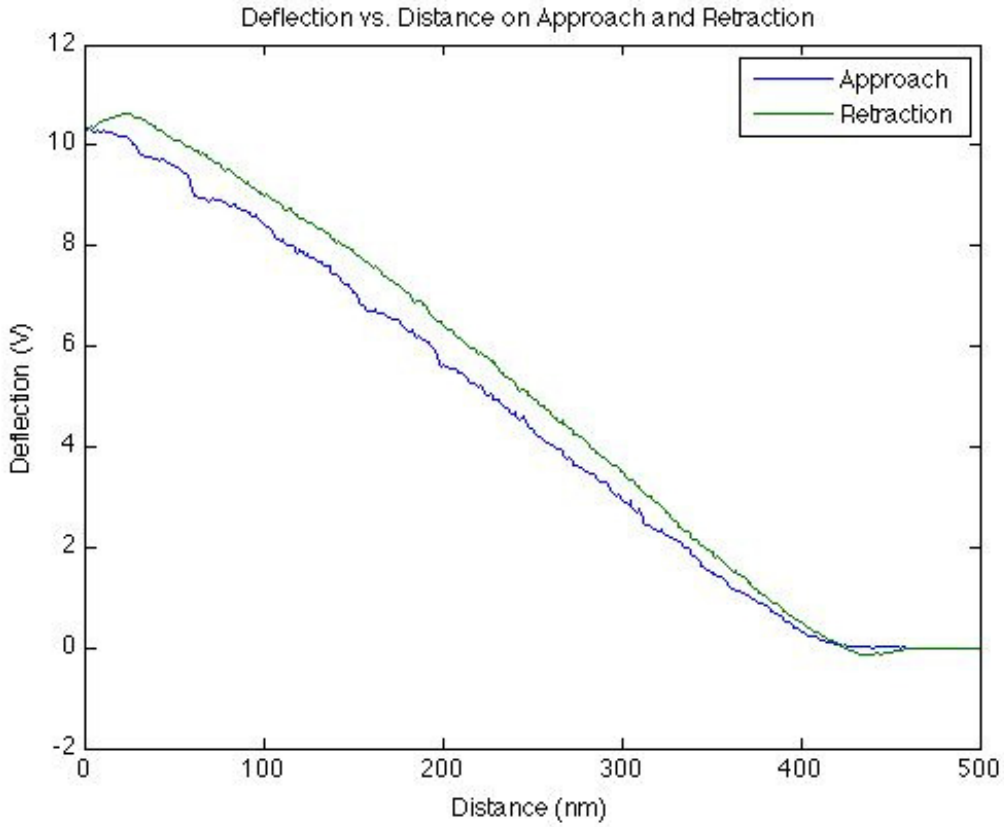
Deflection vs. Distance on Approach and Retraction
Approach
Retraction
Deflection (V)
Distance (nm)
12
10
8
6
4
2
0
-2
0
100
200
300
400
500

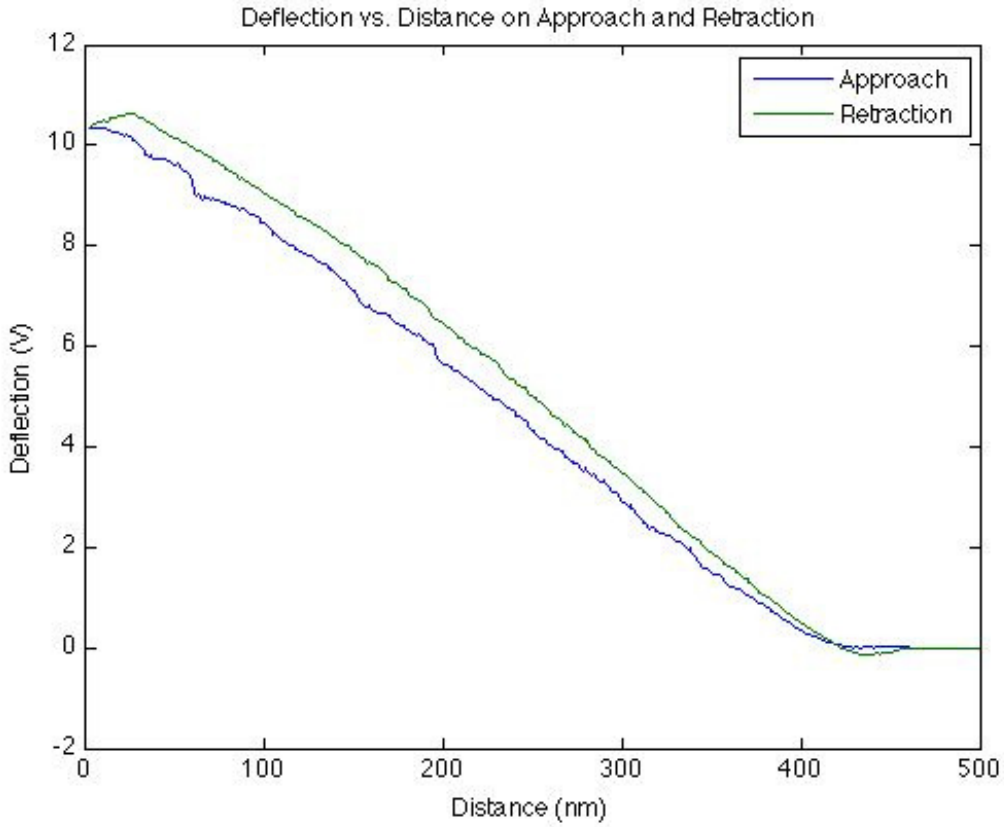
Deflection vs. Distance on Approach and Retraction
Approach
Retraction
Deflection (V)
Distance (nm)
12
10
8
6
4
2
0
-2
0
100
200
300
400
500

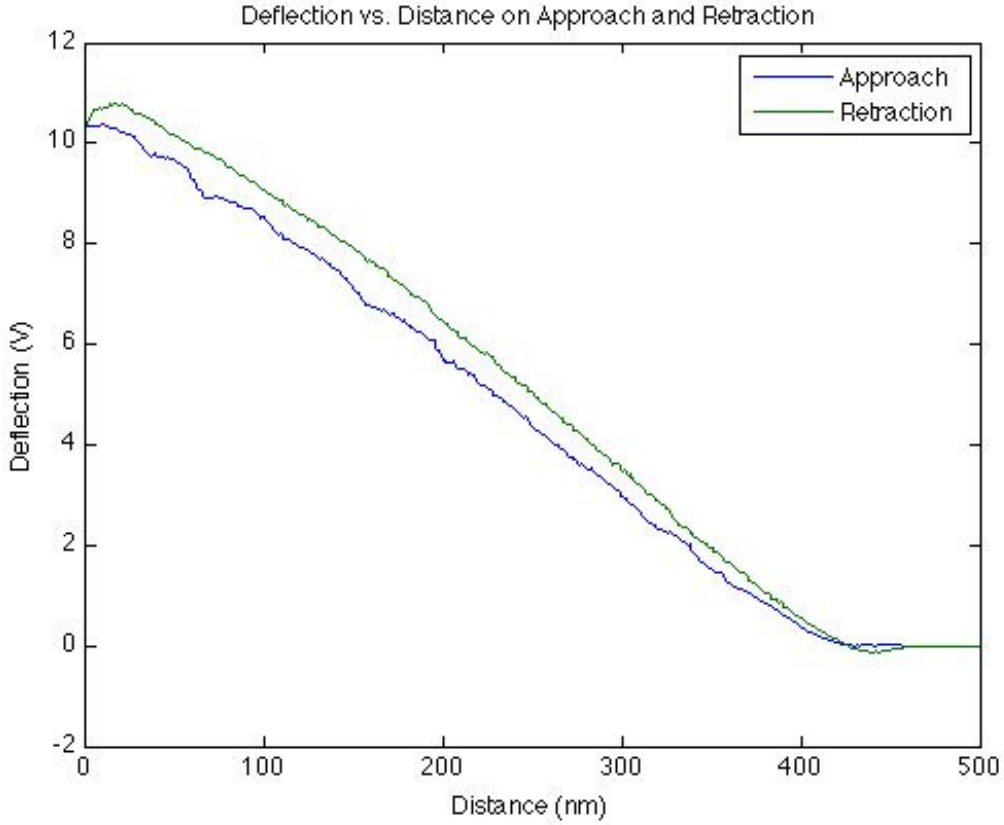
Deflection vs. Distance on Approach and Retraction
Approach
Retraction
Deflection (V)
Distance (nm)
12
10
8
6
4
2
0
-2
0
100
200
300
400
500

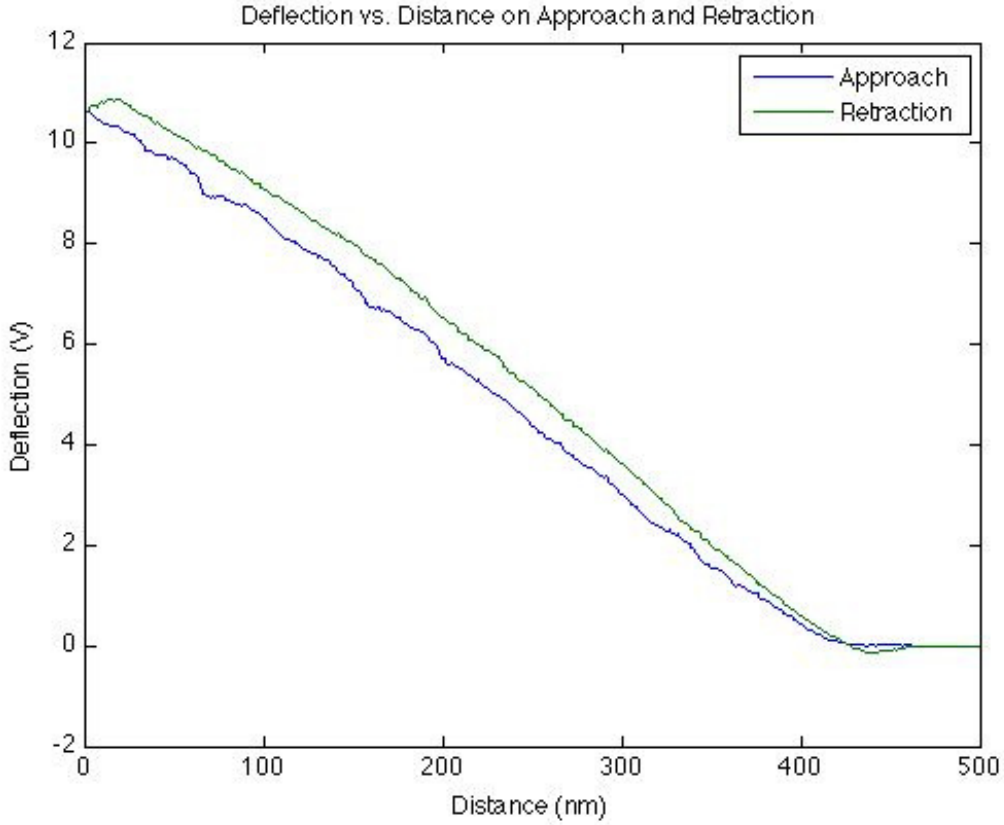
Deflection vs. Distance on Approach and Retraction
Approach
Retraction
Deflection (V)
Distance (nm)
12
10
8
6
4
2
0
-2
0
100
200
300
400
500

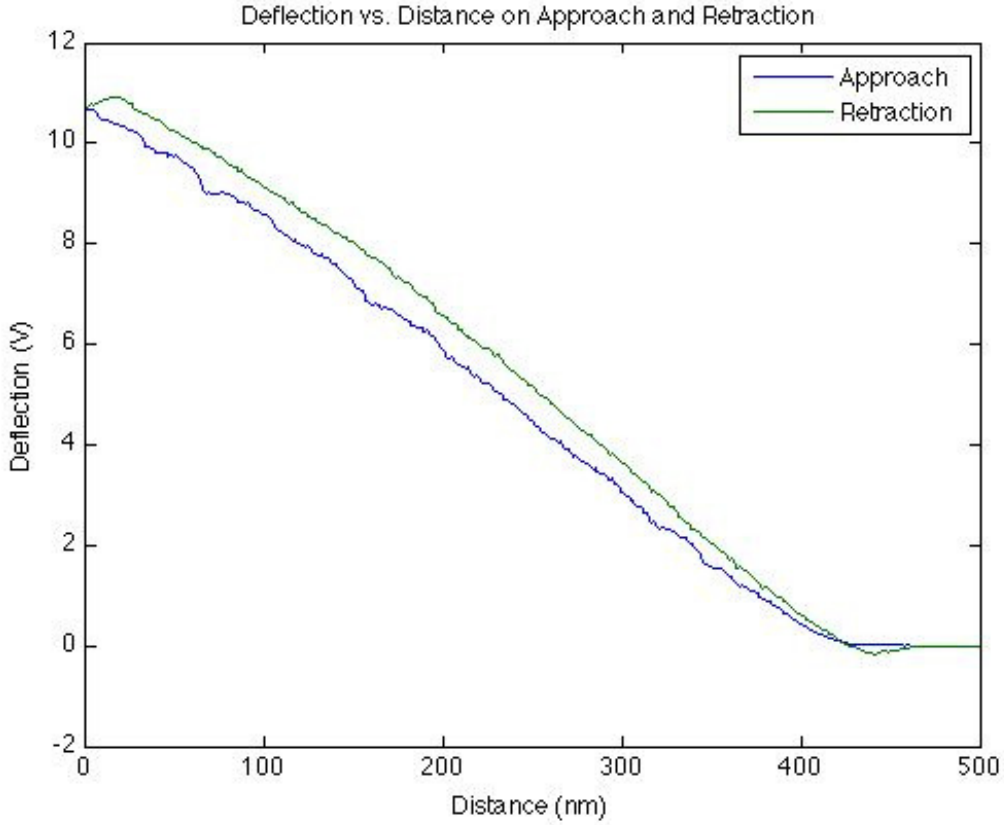
Deflection vs. Distance on Approach and Retraction
Approach
Retraction
Deflection (V)
Distance (nm)
12
10
8
6
4
2
0
-2
0
100
200
300
400
500

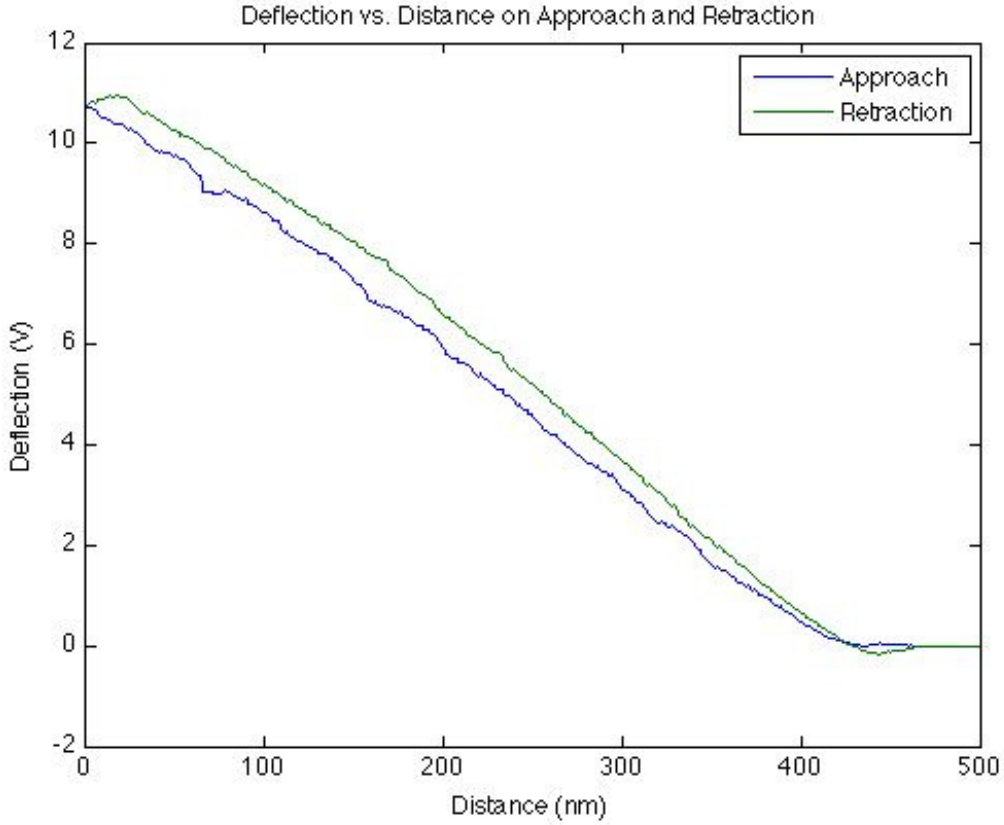
Deflection vs. Distance on Approach and Retraction
Approach
Retraction
Deflection (V)
Distance (nm)
12
10
8
6
4
2
0
-2
0
100
200
300
400
500

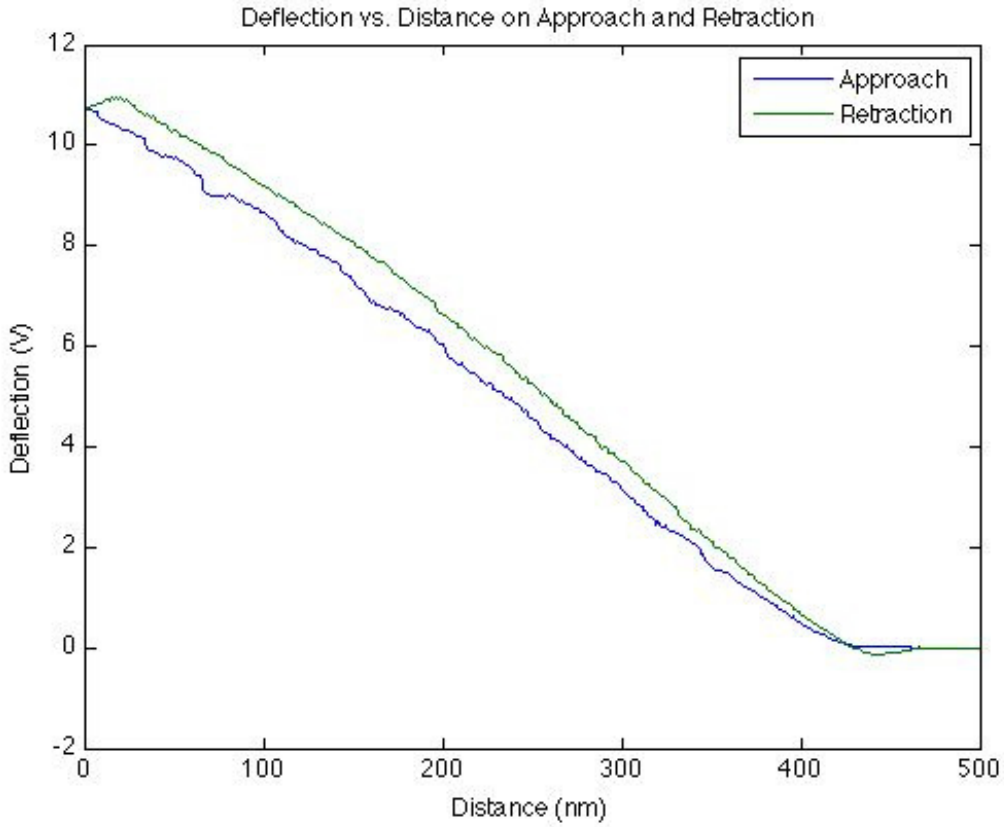
Deflection vs. Distance on Approach and Retraction
Approach
Retraction
Deflection (V)
Distance (nm)
12
10
8
6
4
2
0
-2
0
100
200
300
400
500

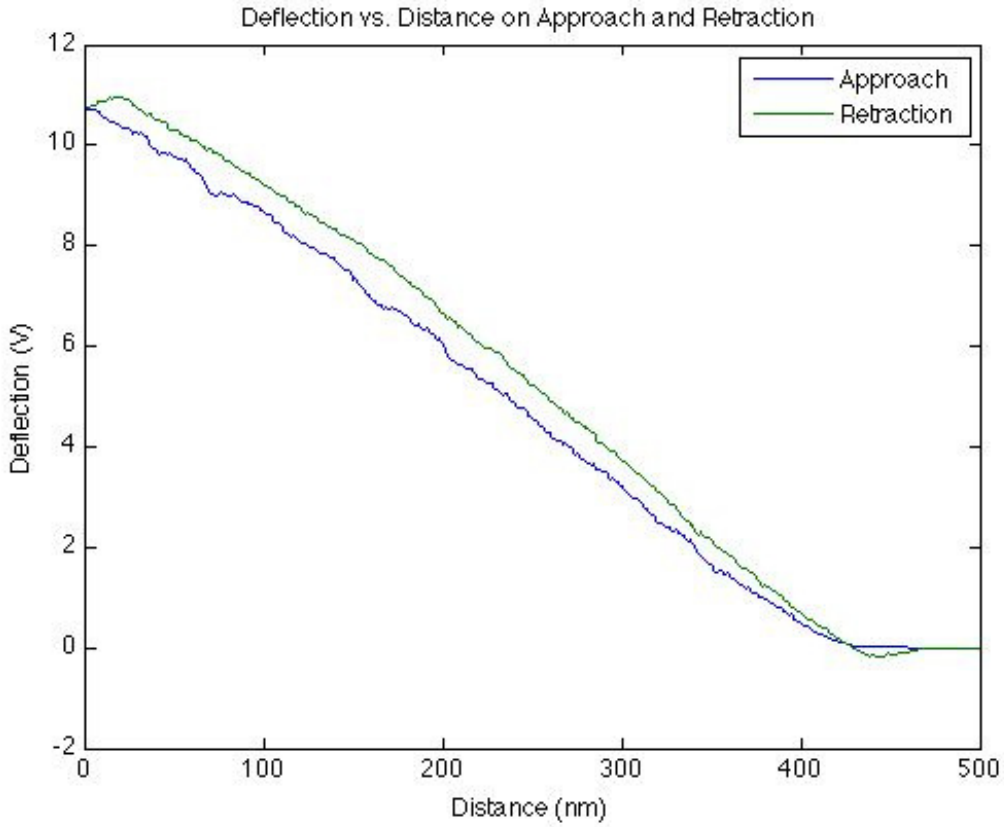
Deflection vs. Distance on Approach and Retraction
Approach
Retraction
Deflection (V)
Distance (nm)
12
10
8
6
4
2
0
-2
0
100
200
300
400
500

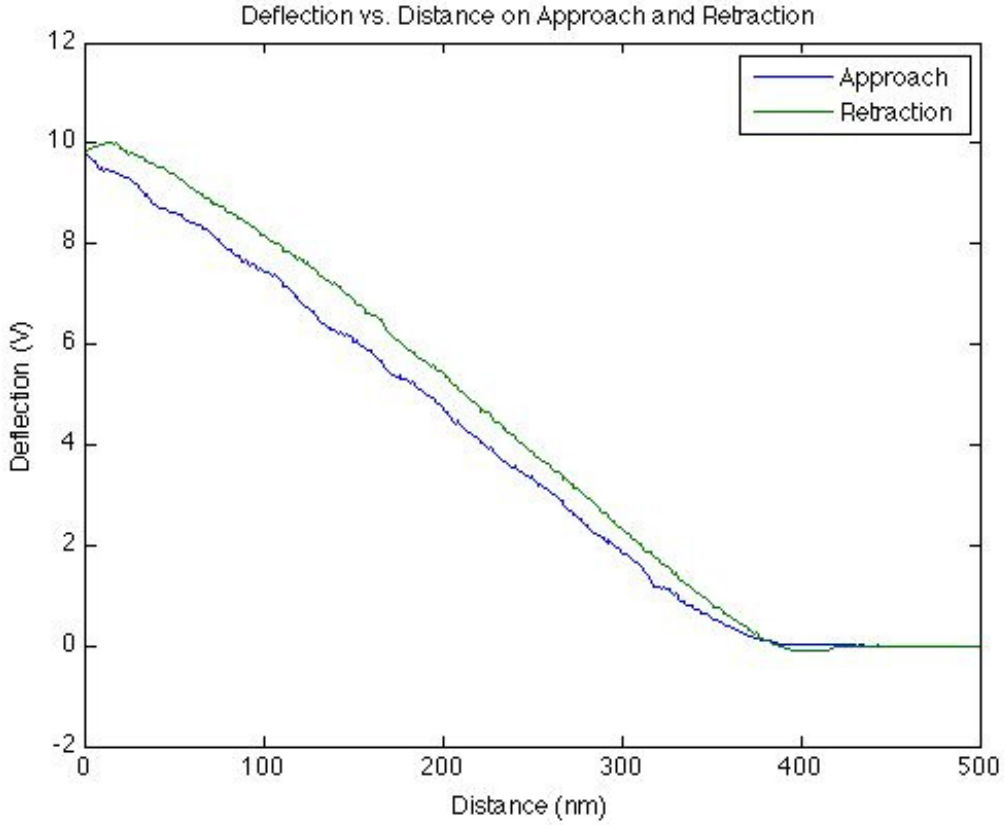
Deflection vs. Distance on Approach and Retraction
Approach
Retraction
Deflection (V)
Distance (nm)
12
10
8
6
4
2
0
-2
0
100
200
300
400
500

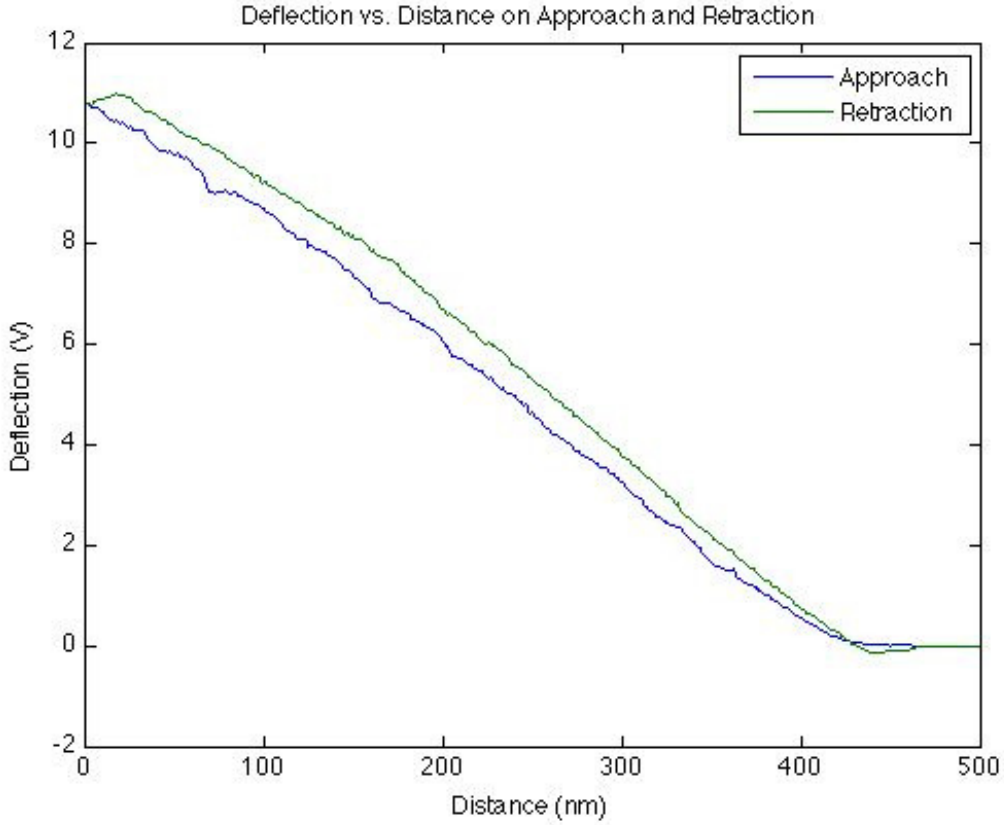
Deflection vs. Distance on Approach and Retraction
Approach
Retraction
Deflection (V)
Distance (nm)
12
10
8
6
4
2
0
-2
0
100
200
300
400
500

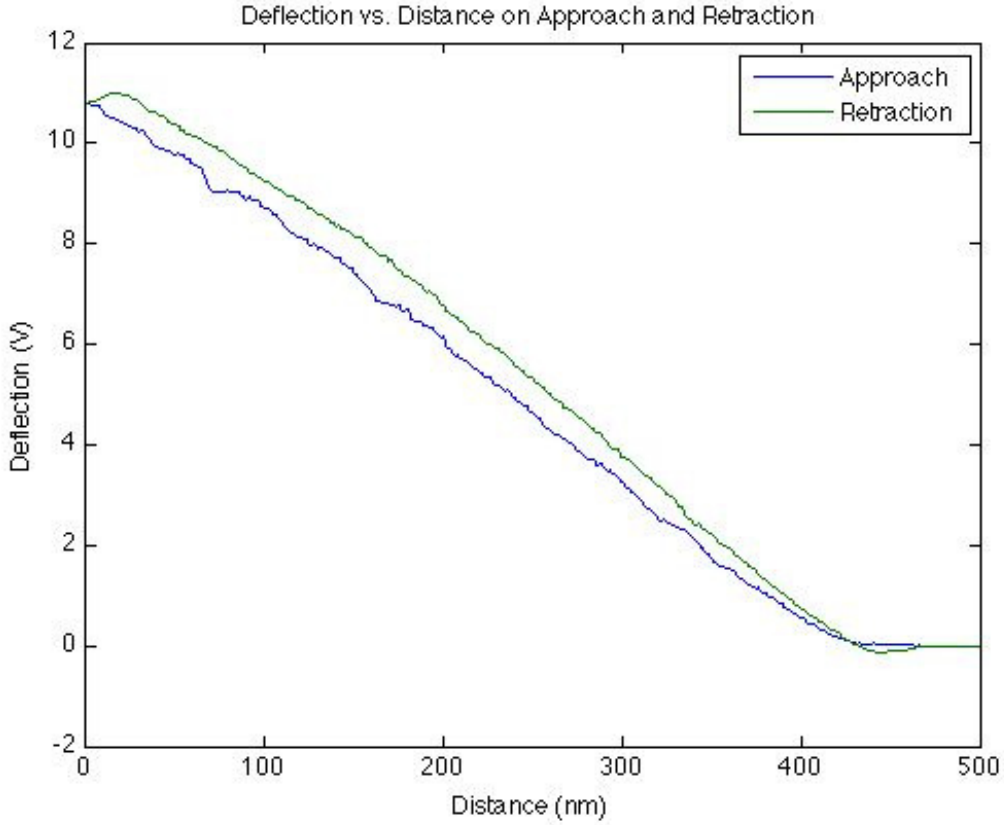
Deflection vs. Distance on Approach and Retraction
Approach
Retraction
Deflection (V)
Distance (nm)
12
10
8
6
4
2
0
-2
0
100
200
300
400
500

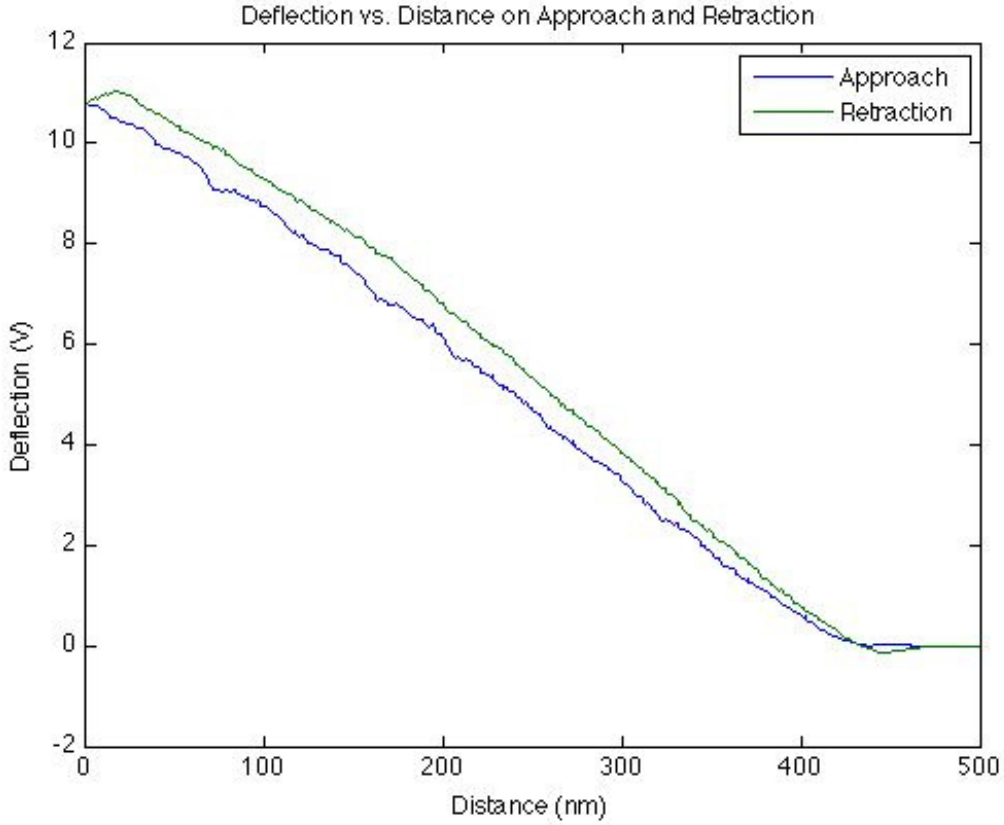
Deflection vs. Distance on Approach and Retraction
Approach
Retraction
Deflection (V)
Distance (nm)
12
10
8
6
4
2
0
-2
0
100
200
300
400
500

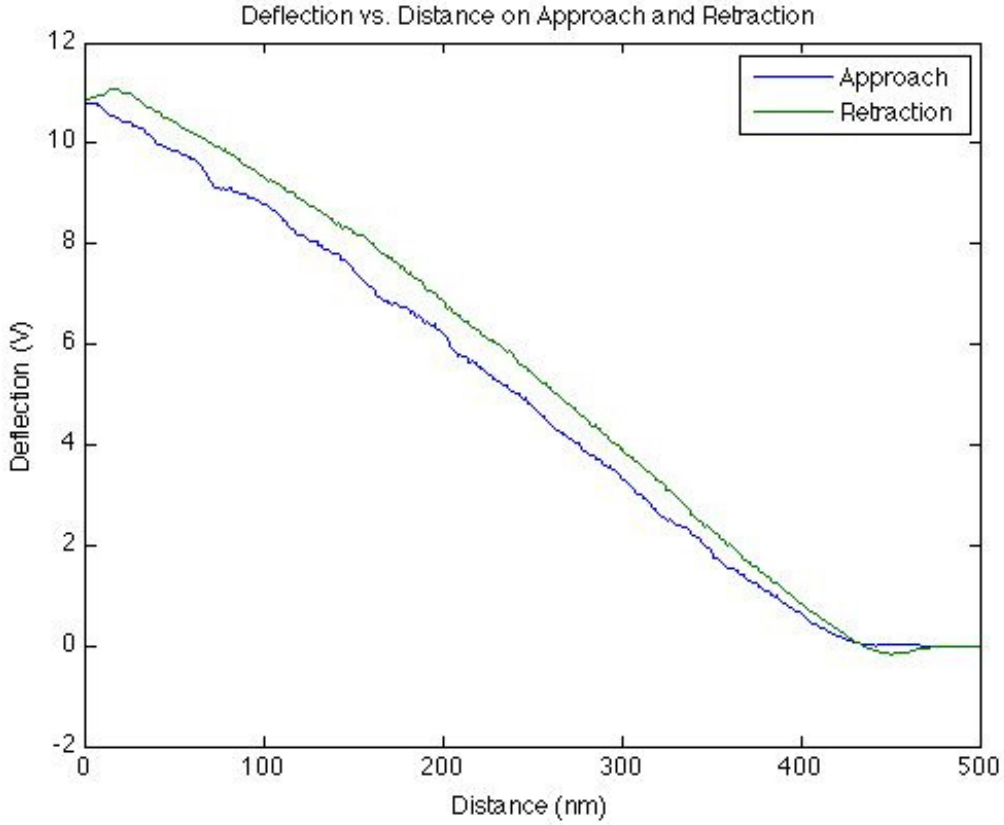
Deflection vs. Distance on Approach and Retraction
Approach
Retraction
Deflection (V)
Distance (nm)
12
10
8
6
4
2
0
-2
0
100
200
300
400
500

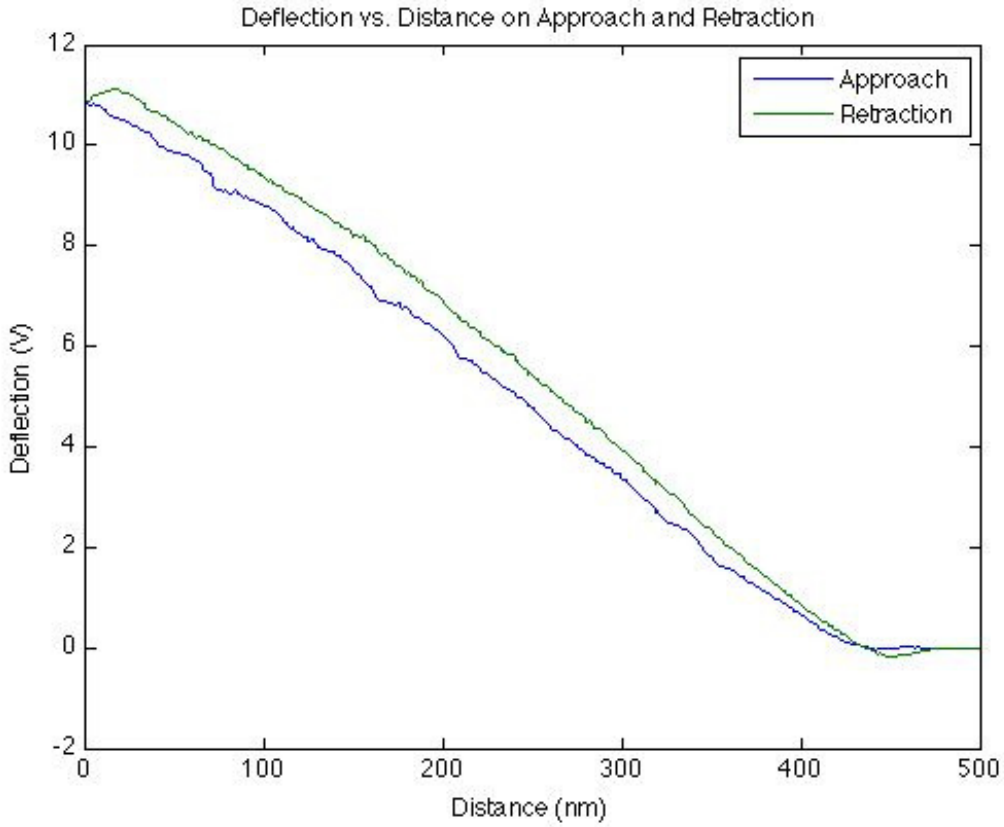
Deflection vs. Distance on Approach and Retraction
Approach
Retraction
Deflection (V)
Distance (nm)
12
10
8
6
4
2
0
-2
0
100
200
300
400
500

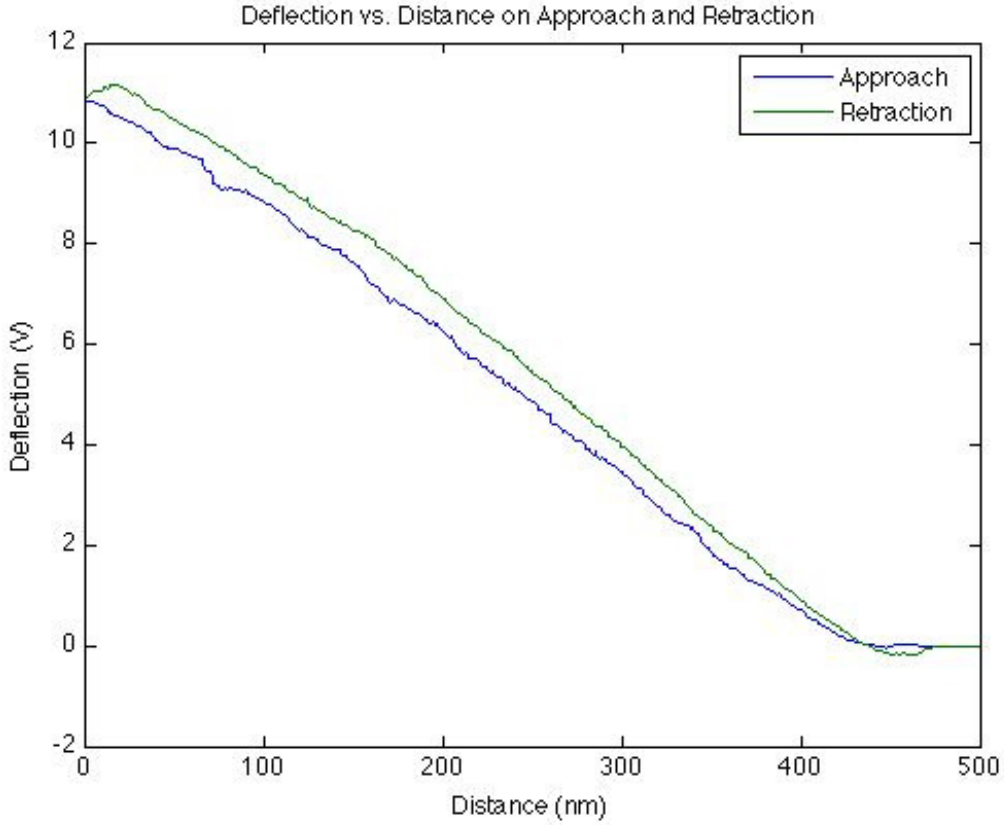
Deflection vs. Distance on Approach and Retraction
Approach
Retraction
Deflection (V)
Distance (nm)
12
10
8
6
4
2
0
-2
0
100
200
300
400
500

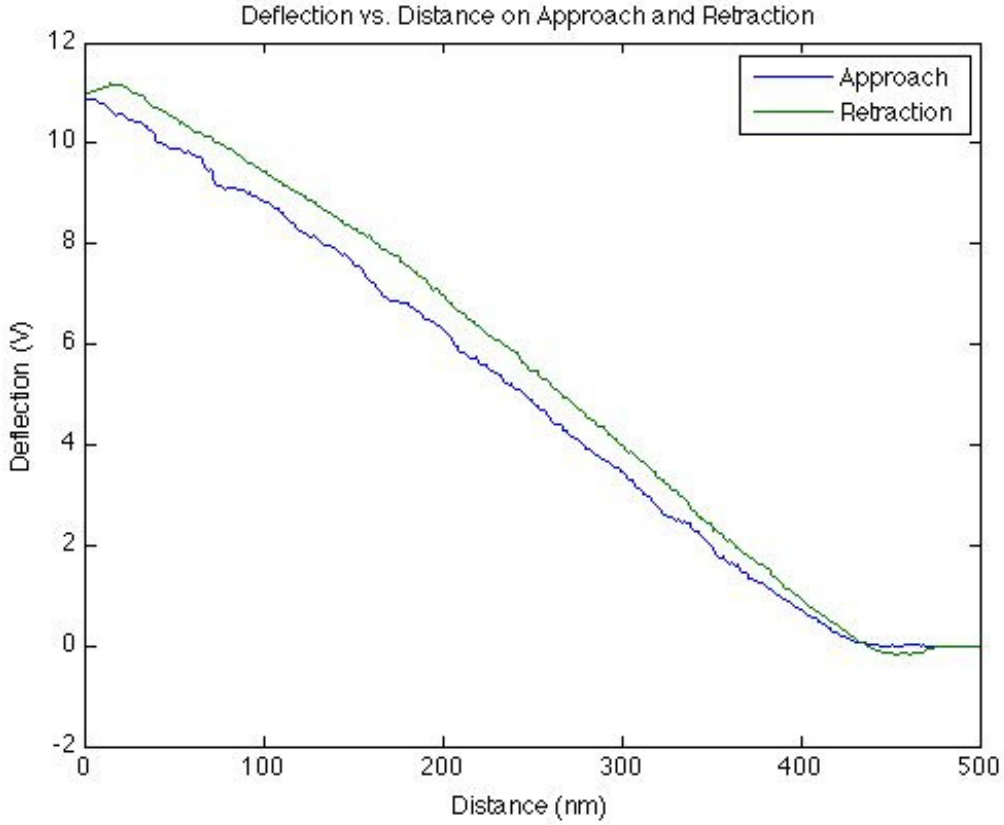
Deflection vs. Distance on Approach and Retraction
Approach
Retraction
Deflection (V)
Distance (nm)
12
10
8
6
4
2
0
-2
0
100
200
300
400
500

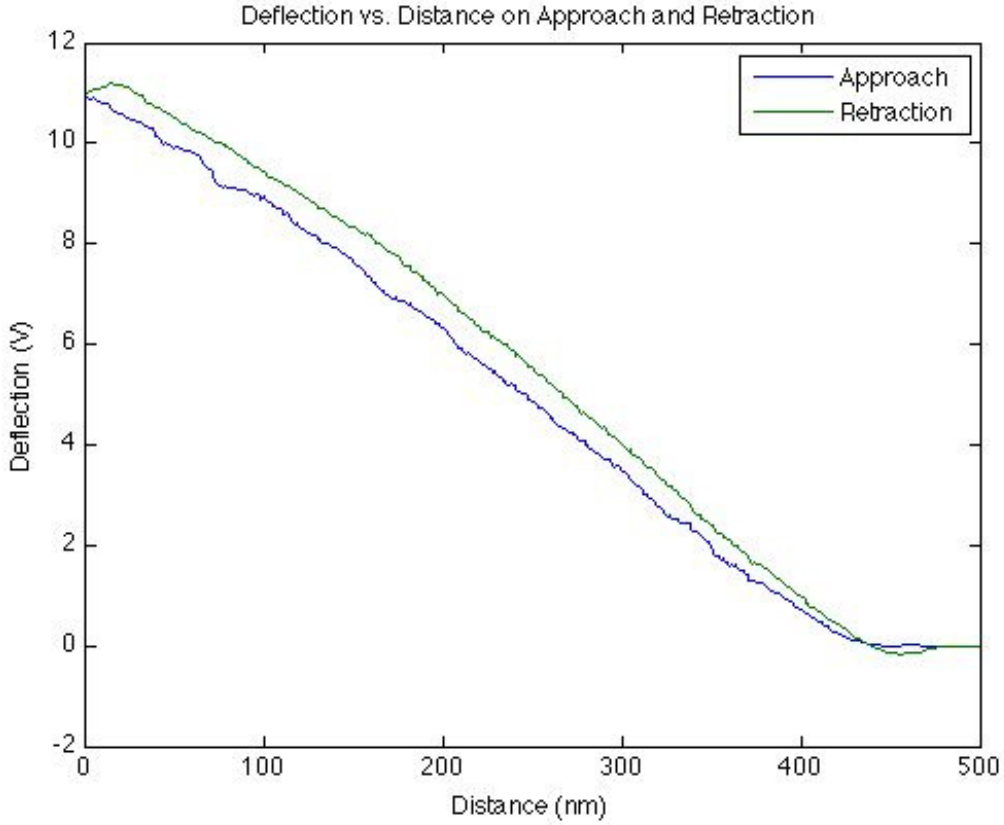
Deflection vs. Distance on Approach and Retraction
Approach
Retraction
Deflection (V)
Distance (nm)
12
10
8
6
4
2
0
-2
0
100
200
300
400
500

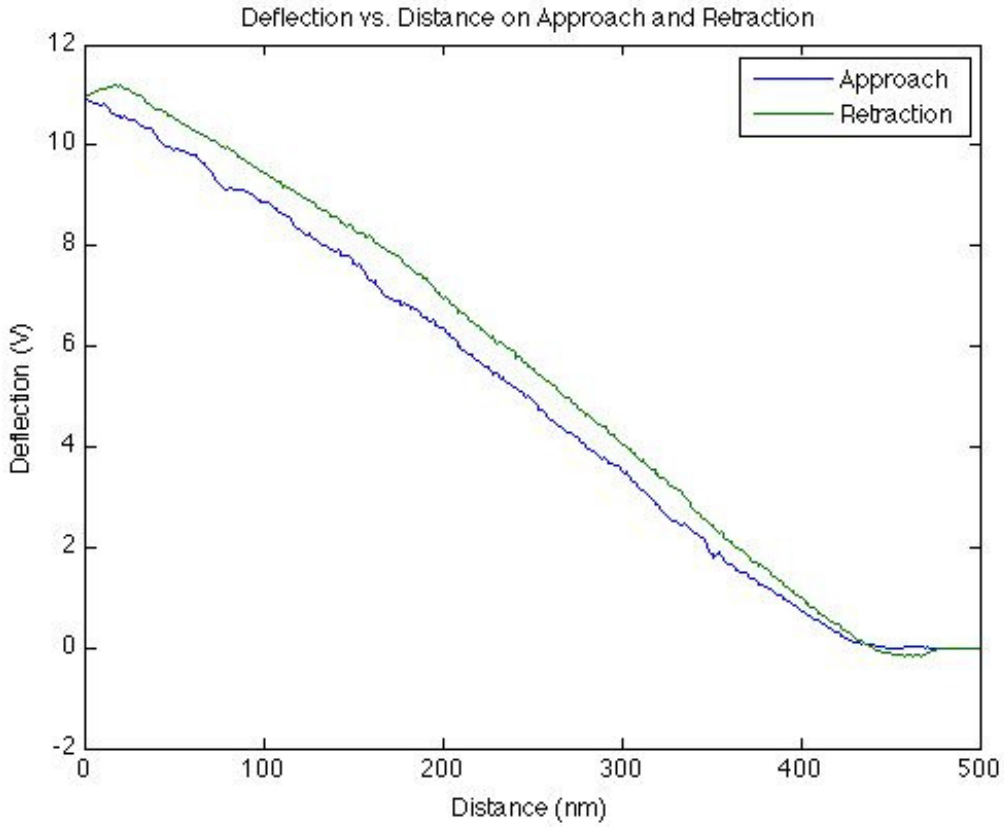
Deflection vs. Distance on Approach and Retraction
Approach
Retraction
Deflection (V)
Distance (nm)
12
10
8
6
4
2
0
-2
0
100
200
300
400
500

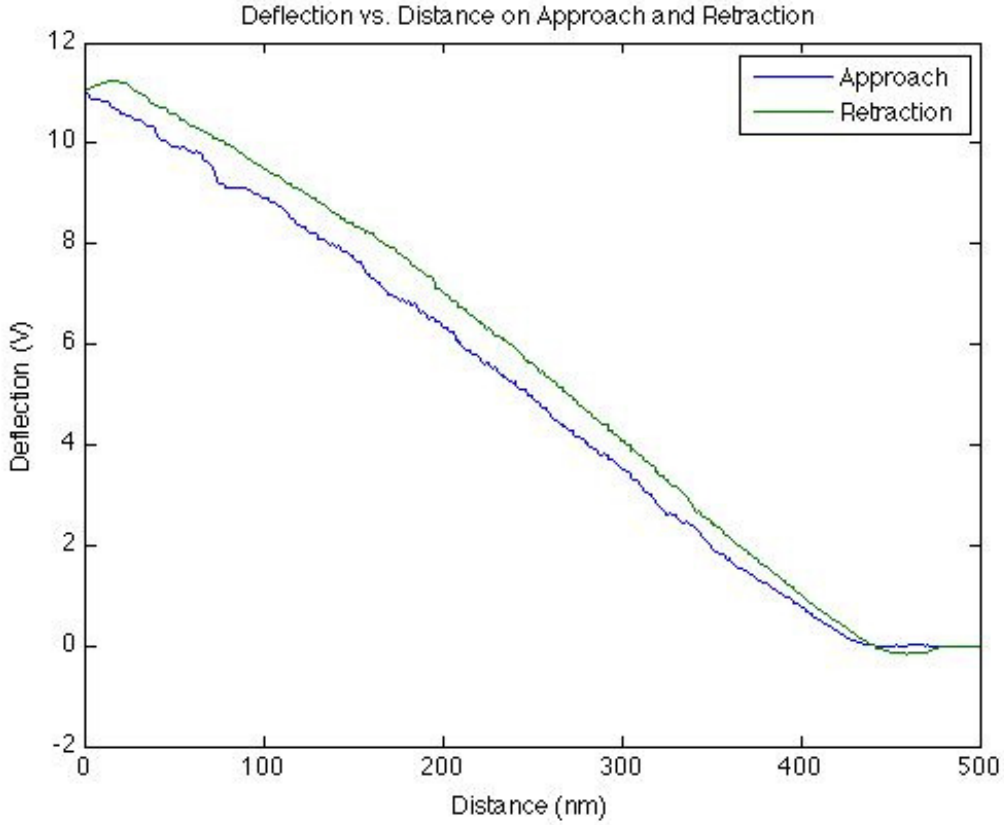
Deflection vs. Distance on Approach and Retraction
Approach
Retraction
Deflection (V)
Distance (nm)
12
10
8
6
4
2
0
-2
0
100
200
300
400
500

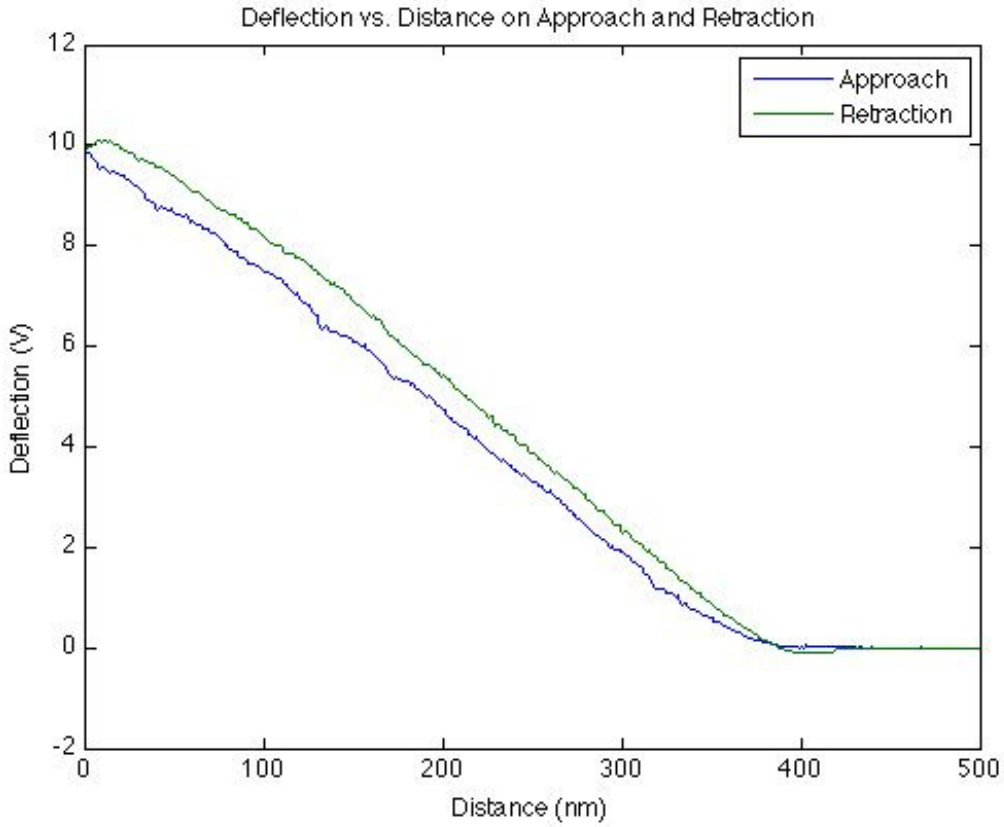
Deflection vs. Distance on Approach and Retraction
Approach
Retraction
Deflection (V)
Distance (nm)
12
10
8
6
4
2
0
-2
0
100
200
300
400
500

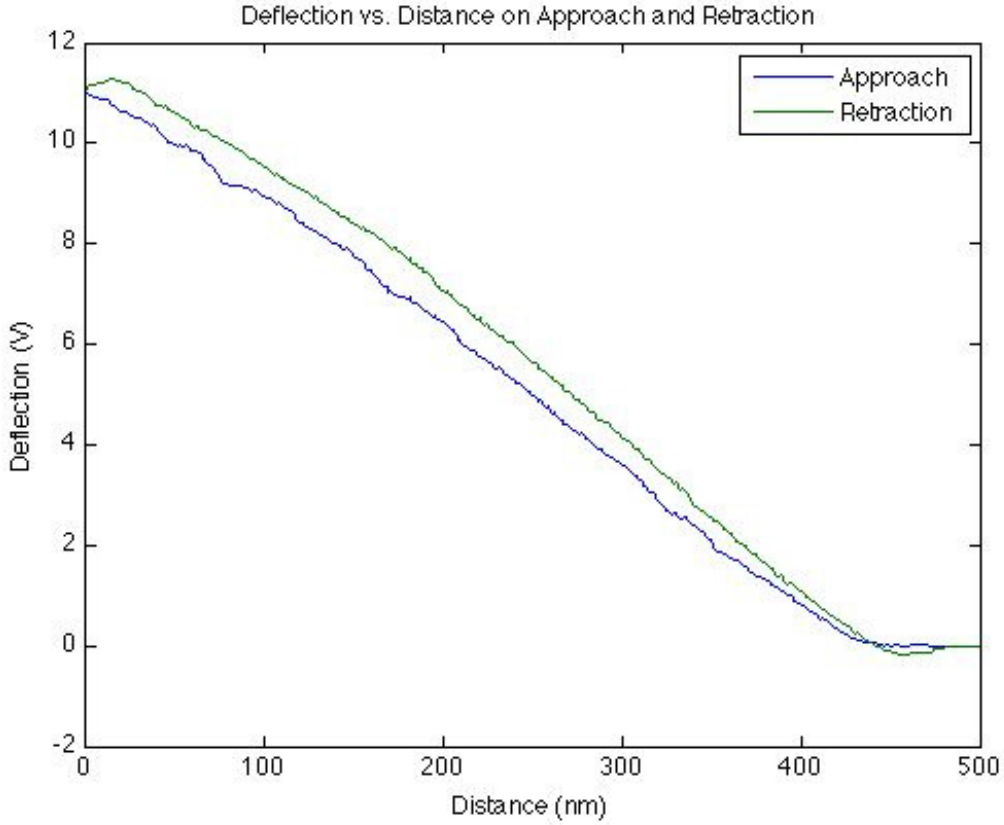
Deflection vs. Distance on Approach and Retraction
Approach
Retraction
Deflection (V)
Distance (nm)
12
10
8
6
4
2
0
-2
0
100
200
300
400
500

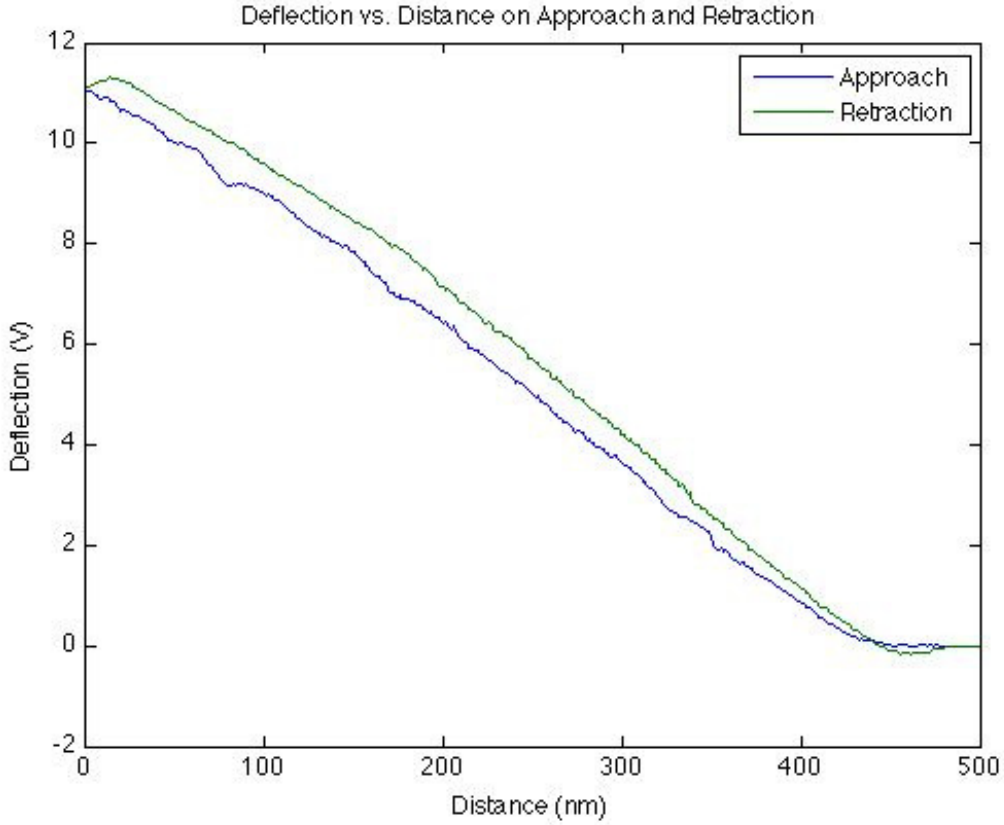
Deflection vs. Distance on Approach and Retraction
Approach
Retraction
Deflection (V)
Distance (nm)
12
10
8
6
4
2
0
-2
0
100
200
300
400
500

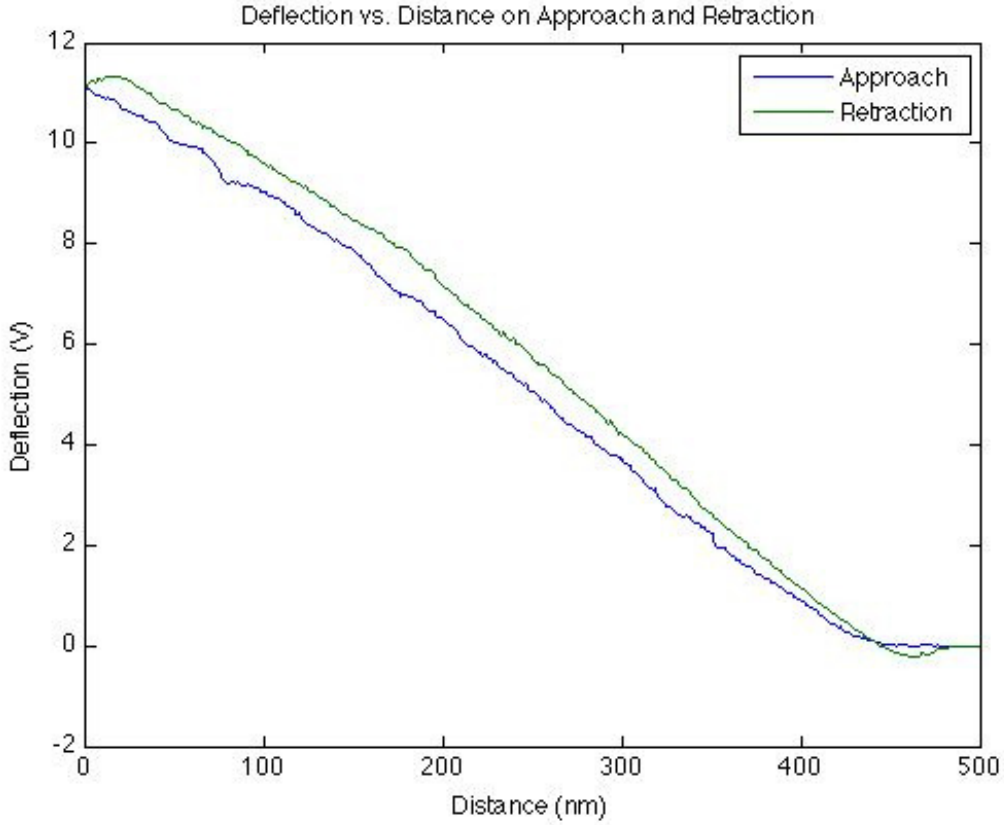
Deflection vs. Distance on Approach and Retraction
Approach
Retraction
Deflection (V)
Distance (nm)
12
10
8
6
4
2
0
-2
0
100
200
300
400
500

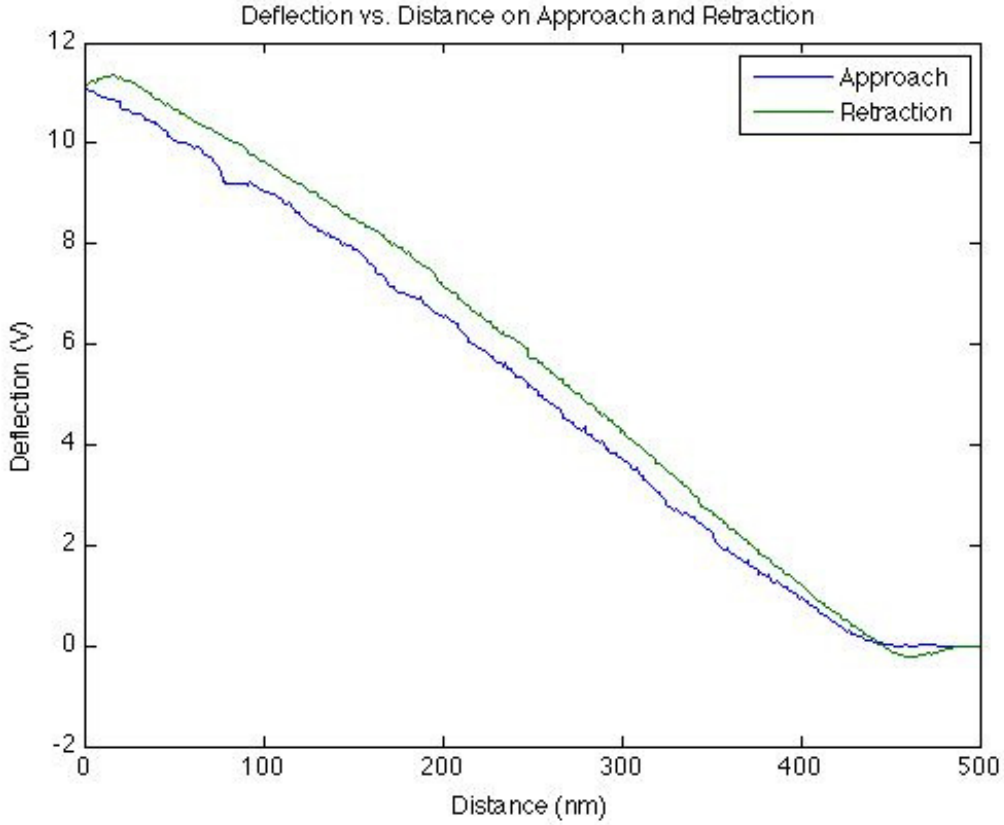
Deflection vs. Distance on Approach and Retraction
Approach
Retraction
Deflection (V)
Distance (nm)
12
10
8
6
4
2
0
-2
0
100
200
300
400
500

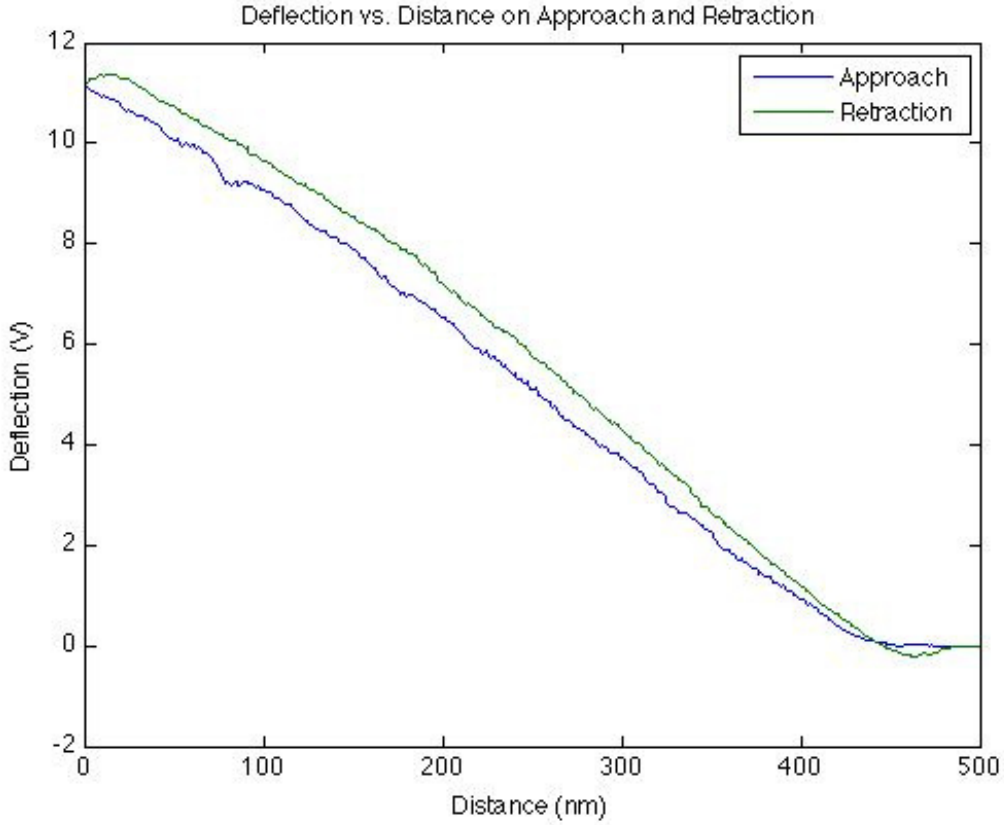
Deflection vs. Distance on Approach and Retraction
Approach
Retraction
Deflection (V)
Distance (nm)
12
10
8
6
4
2
0
-2
0
100
200
300
400
500

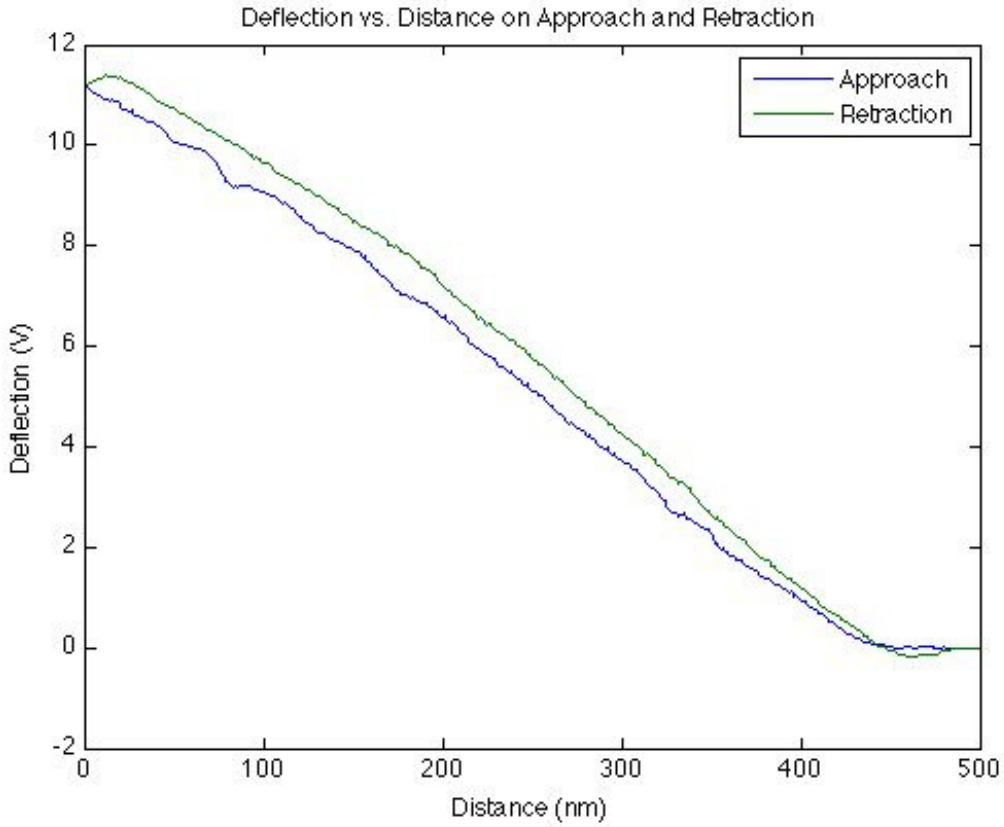
Deflection vs. Distance on Approach and Retraction
Approach
Retraction
Deflection (V)
Distance (nm)
12
10
8
6
4
2
0
-2
0
100
200
300
400
500

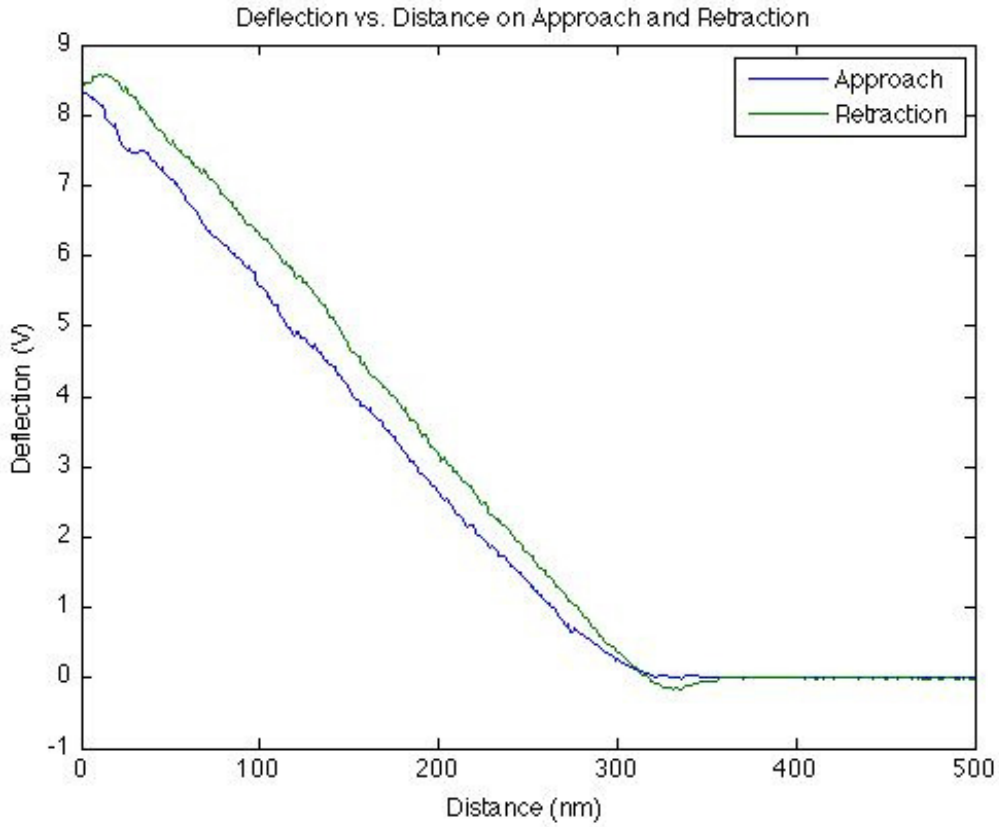
Deflection vs. Distance on Approach and Retraction
Approach
Retraction
Deflection (V)
Distance (nm)
9
8
7
6
5
4
3
2
1
0
-1
0
100
200
300
400
500

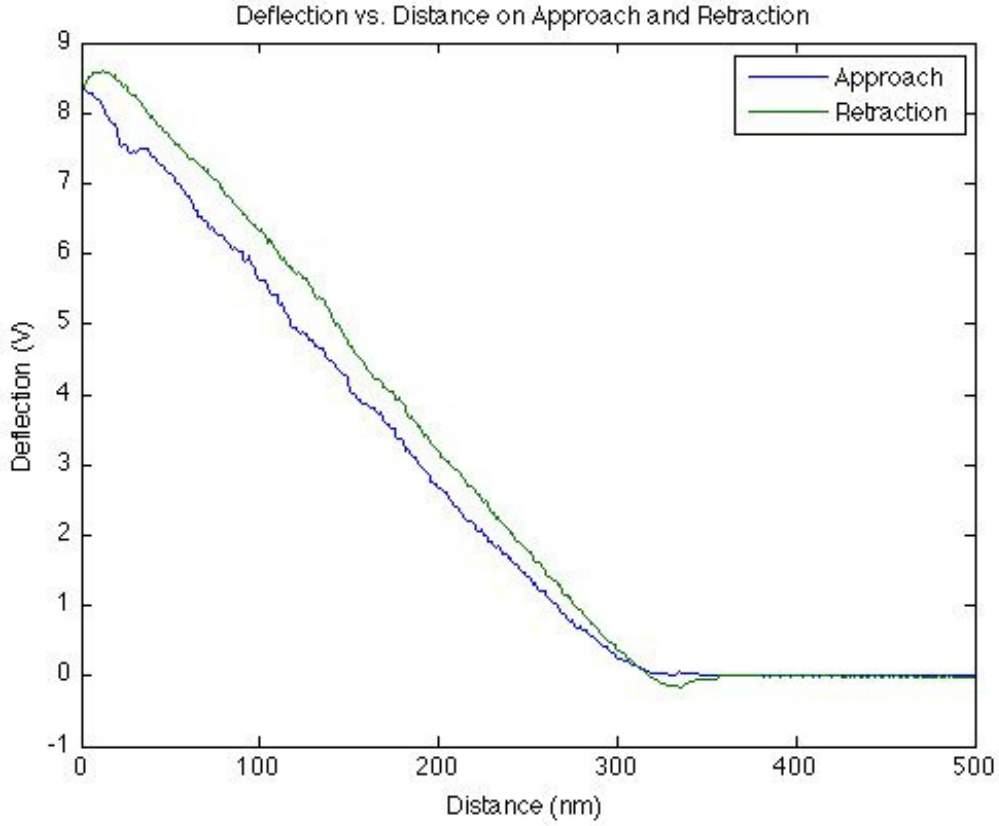
Deflection vs. Distance on Approach and Retraction
Approach
Retraction
Deflection (V)
Distance (nm)
9
8
7
6
5
4
3
2
1
0
-1
0
100
200
300
400
500

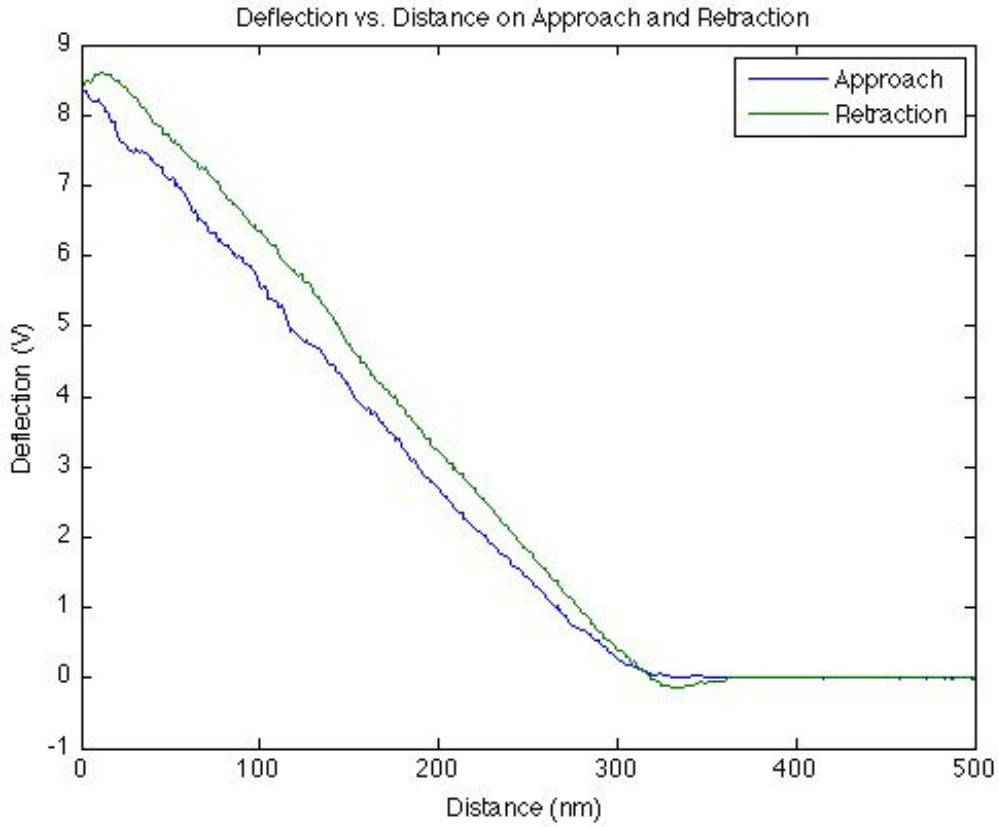
Deflection vs. Distance on Approach and Retraction
Approach
Retraction
Deflection (V)
Distance (nm)
9
8
7
6
5
4
3
2
1
0
-1
0
100
200
300
400
500

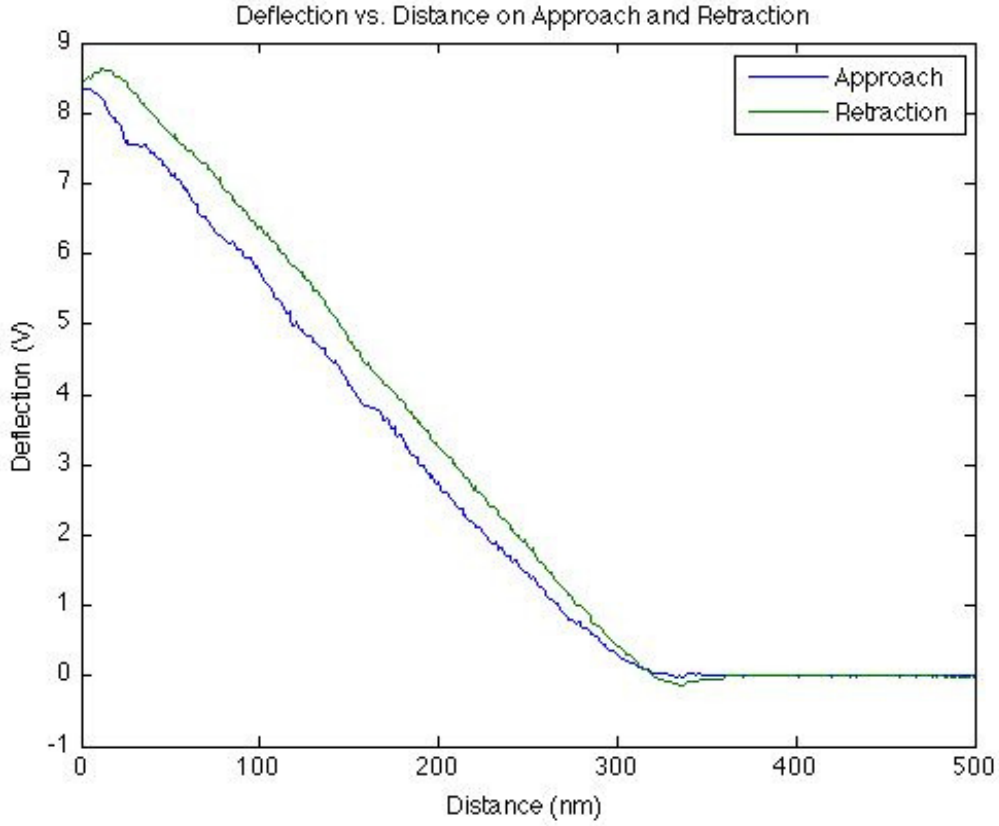
Deflection vs. Distance on Approach and Retraction
Approach
Retraction
Deflection (V)
Distance (nm)
9
8
7
6
5
4
3
2
1
0
-1
0
100
200
300
400
500

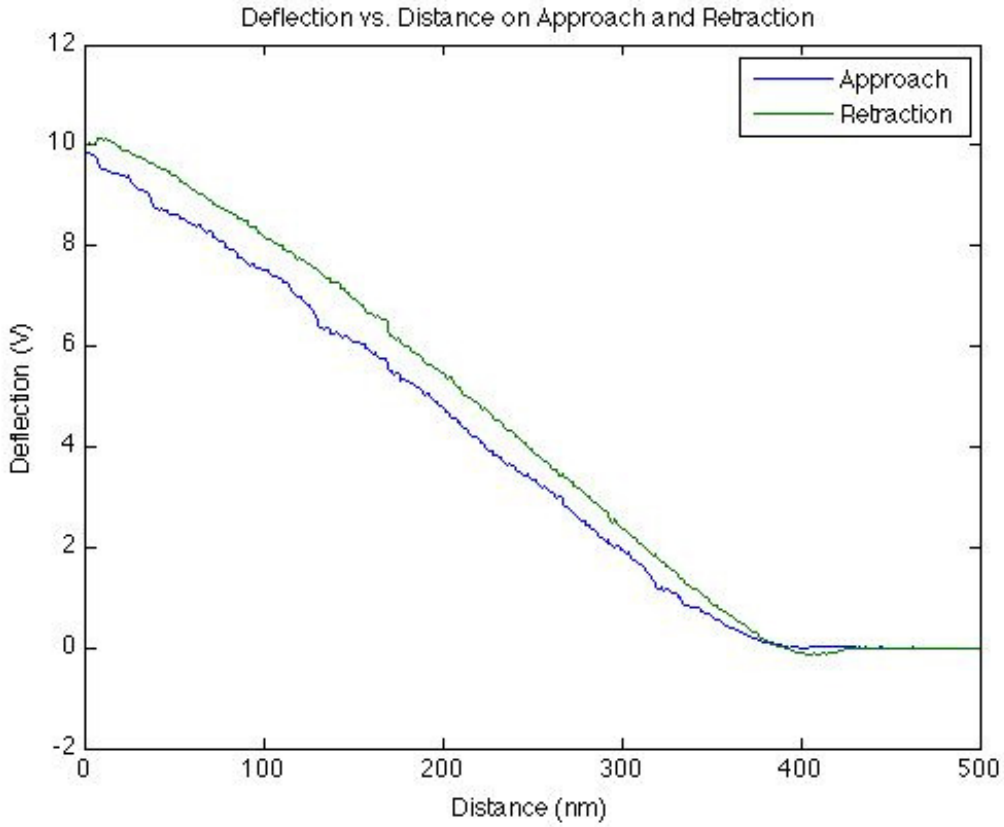
Deflection vs. Distance on Approach and Retraction
Approach
Retraction
Deflection (V)
Distance (nm)
12
10
8
6
4
2
0
-2
0
100
200
300
400
500

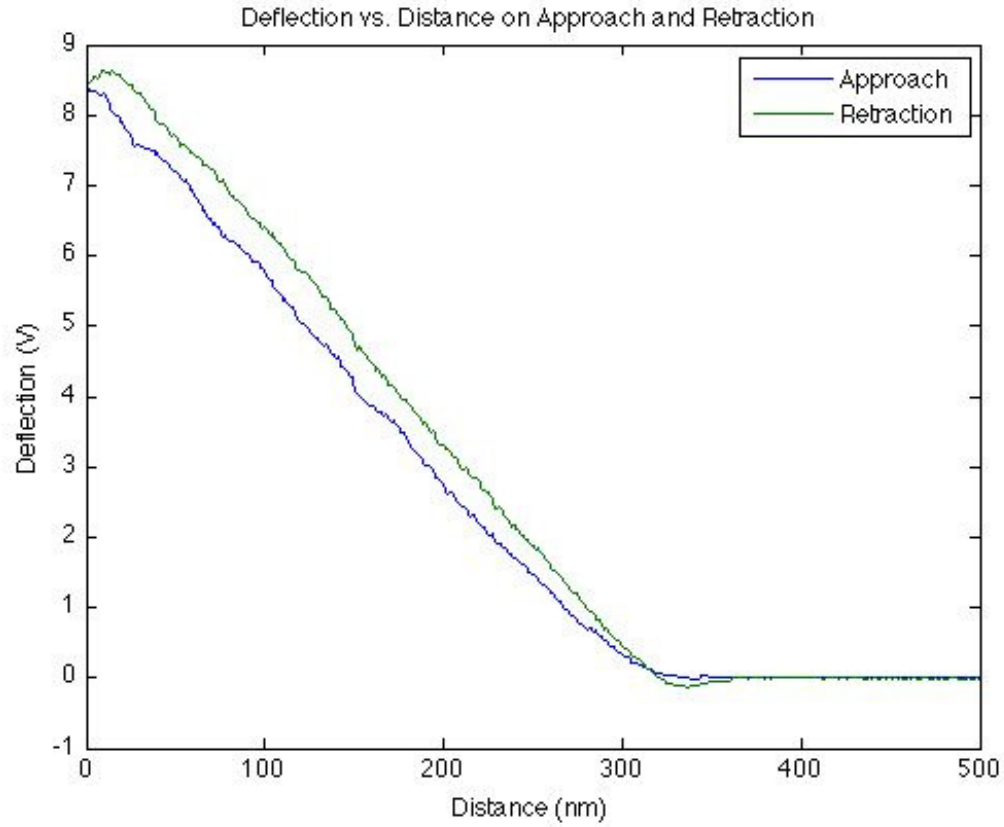
Deflection vs. Distance on Approach and Retraction
Approach
Retraction
Deflection (V)
Distance (nm)
9
8
7
6
5
4
3
2
1
0
-1
0
100
200
300
400
500

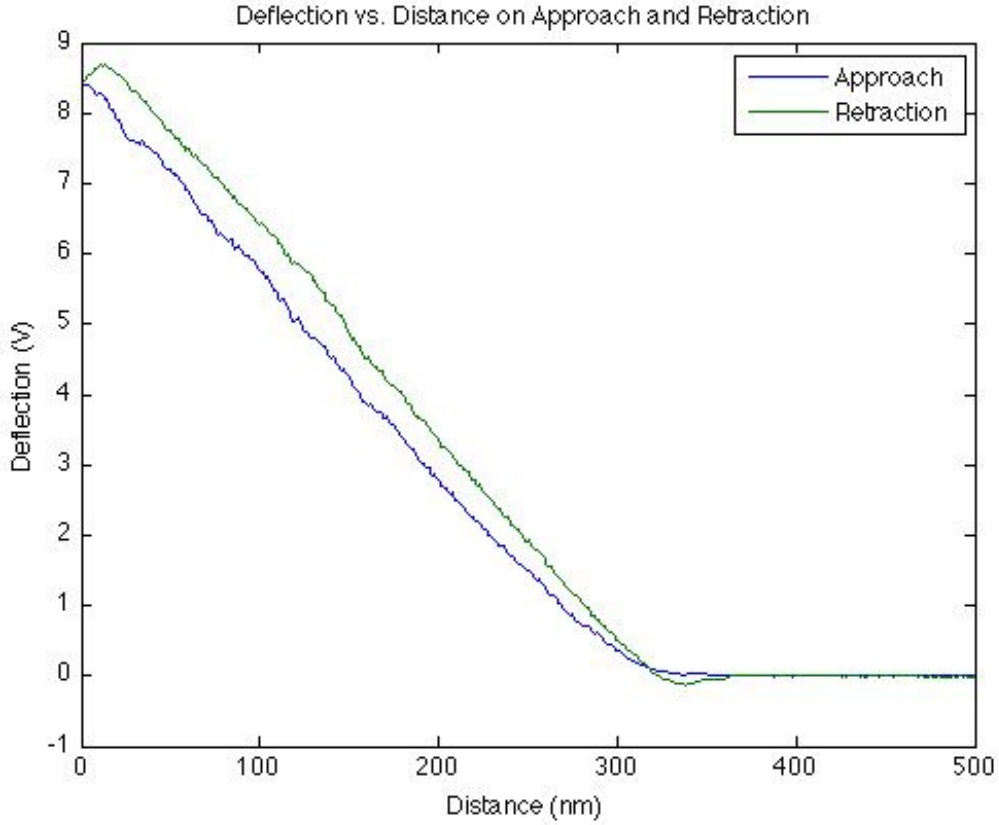
Deflection vs. Distance on Approach and Retraction
Approach
Retraction
Deflection (V)
Distance (nm)
9
8
7
6
5
4
3
2
1
0
-1
0
100
200
300
400
500

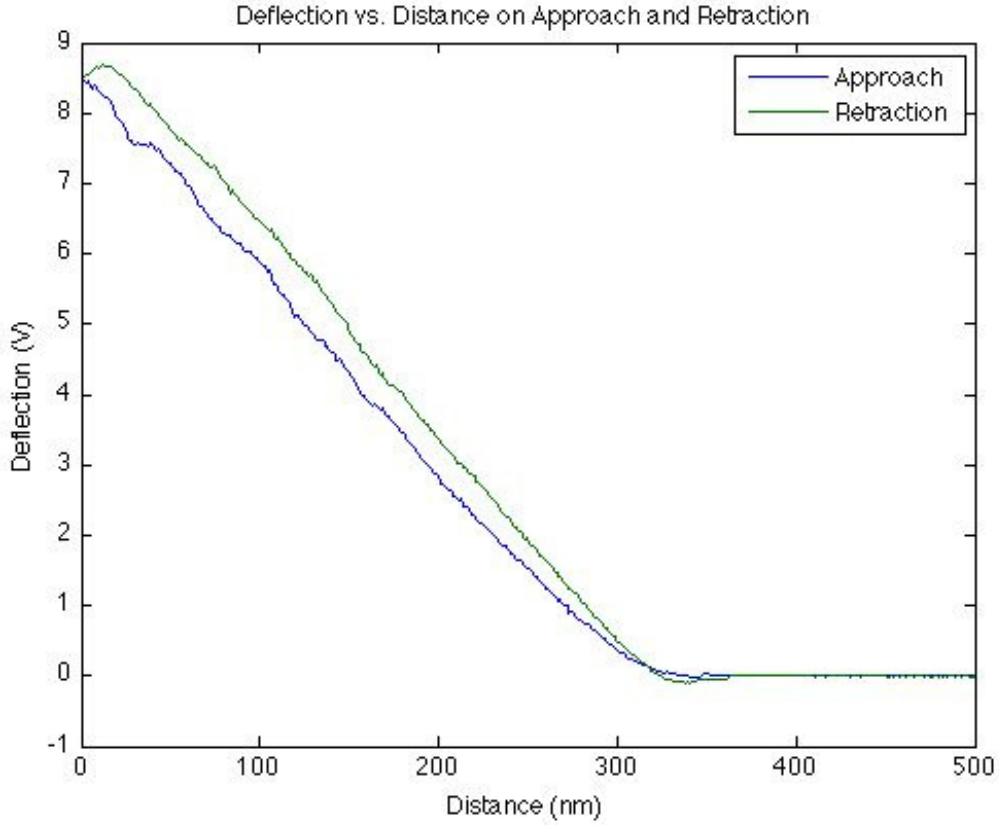
Deflection vs. Distance on Approach and Retraction
Approach
Retraction
Deflection (V)
Distance (nm)
9
8
7
6
5
4
3
2
1
0
-1
0
100
200
300
400
500

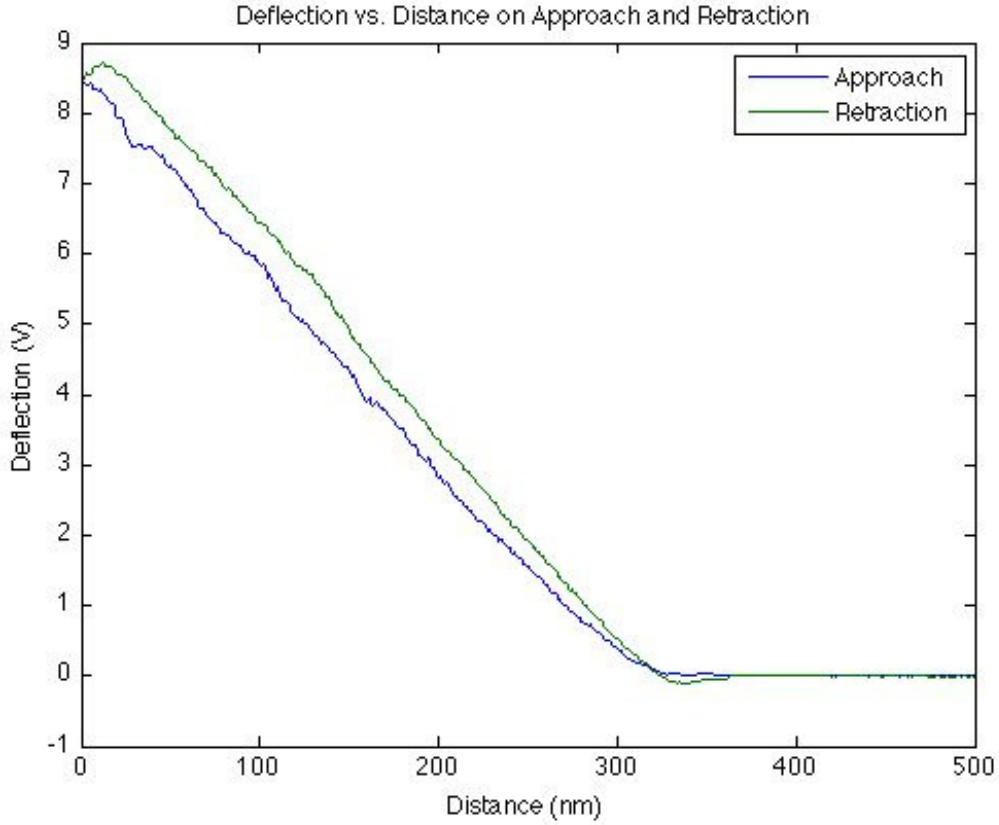
Deflection vs. Distance on Approach and Retraction
Approach
Retraction
Deflection (V)
Distance (nm)
9
8
7
6
5
4
3
2
1
0
-1
0
100
200
300
400
500

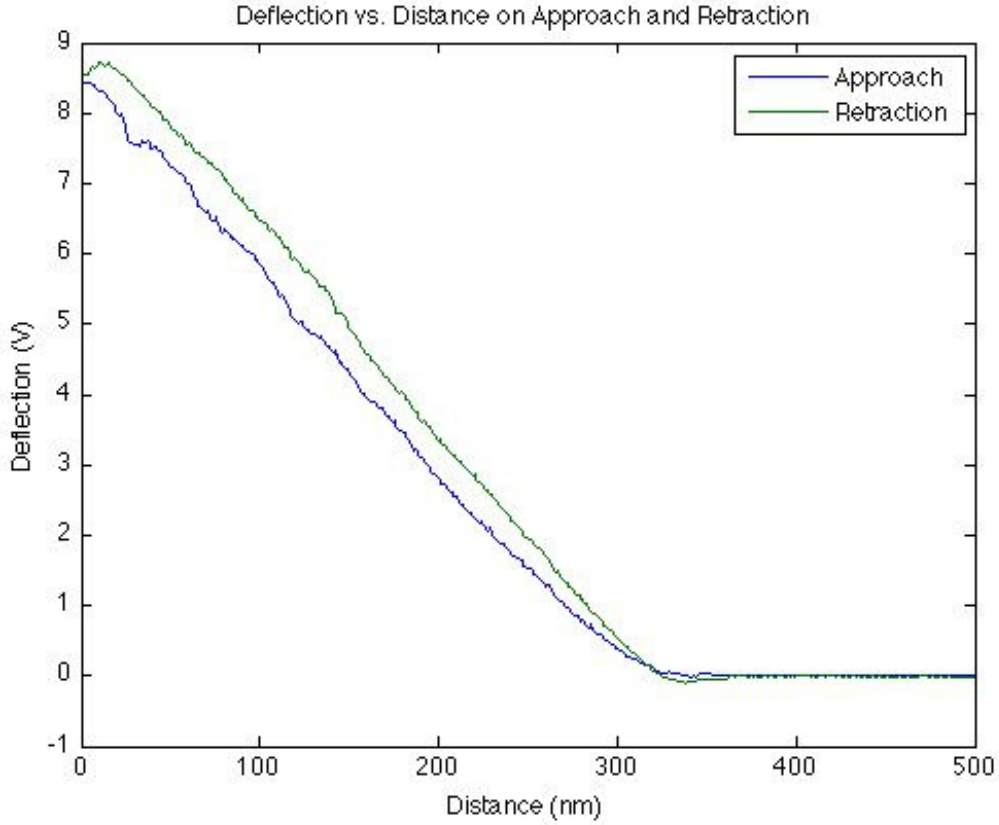
Deflection vs. Distance on Approach and Retraction
Approach
Retraction
Deflection (V)
Distance (nm)
9
8
7
6
5
4
3
2
1
0
-1
0
100
200
300
400
500

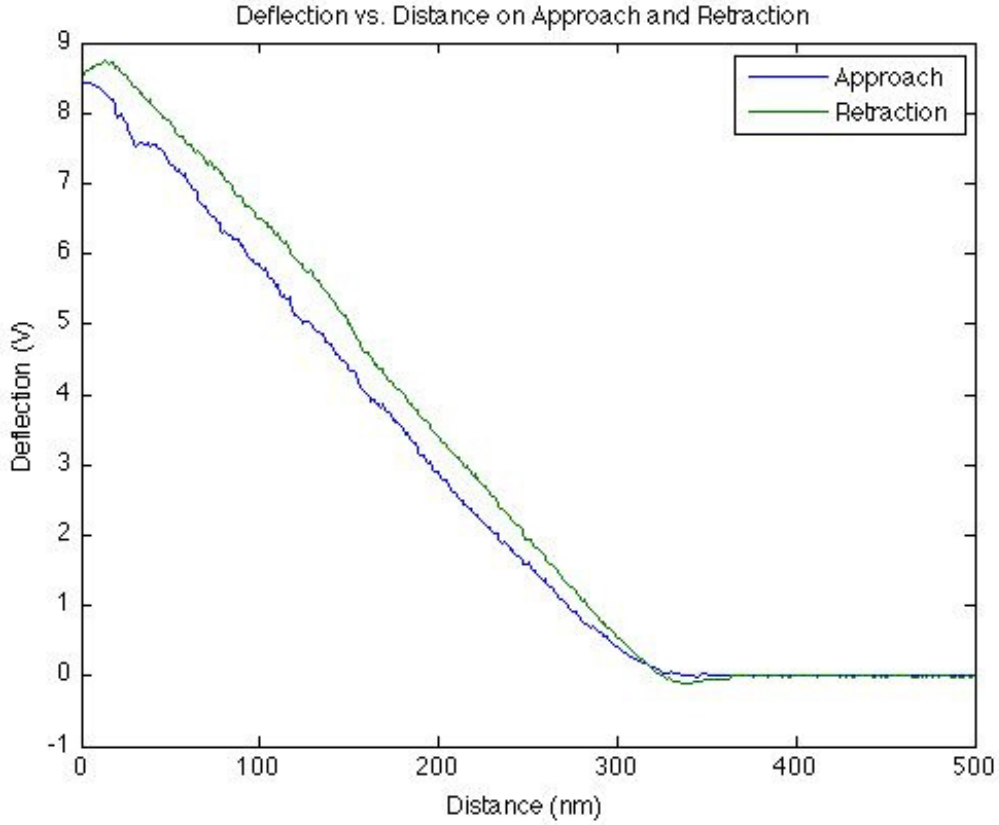
Deflection vs. Distance on Approach and Retraction
Approach
Retraction
Deflection (V)
Distance (nm)
9
8
7
6
5
4
3
2
1
0
-1
0
100
200
300
400
500

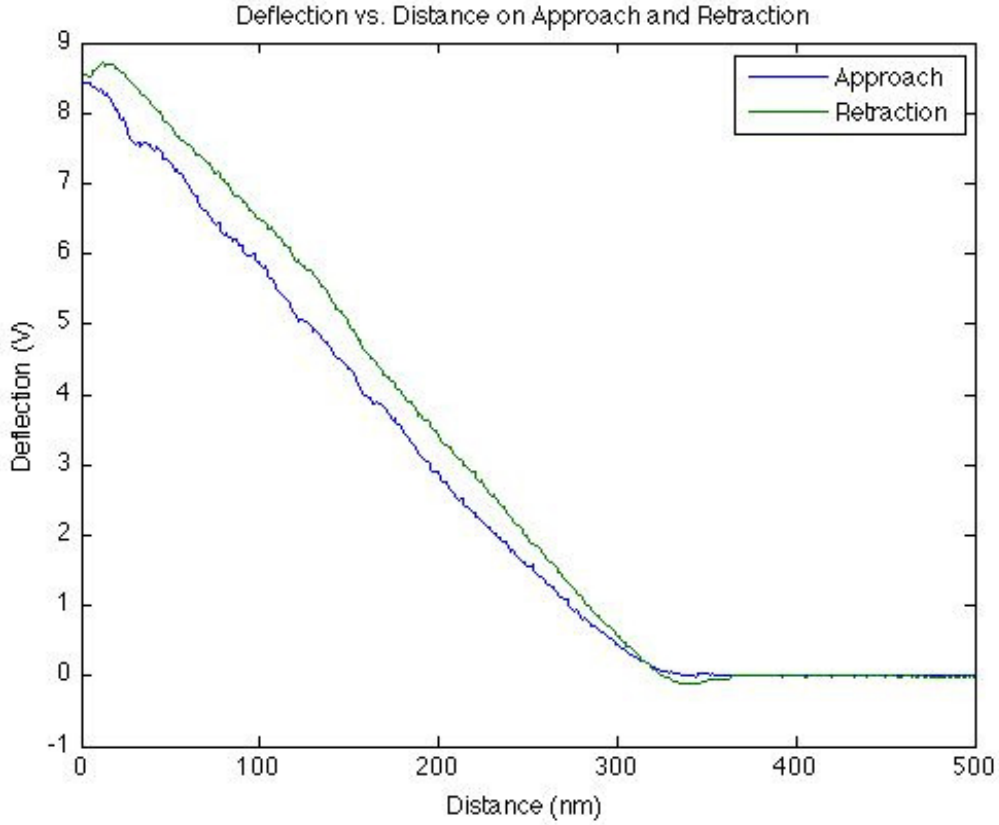
Deflection vs. Distance on Approach and Retraction
Approach
Retraction
Deflection (V)
Distance (nm)
9
8
7
6
5
4
3
2
1
0
-1
0
100
200
300
400
500

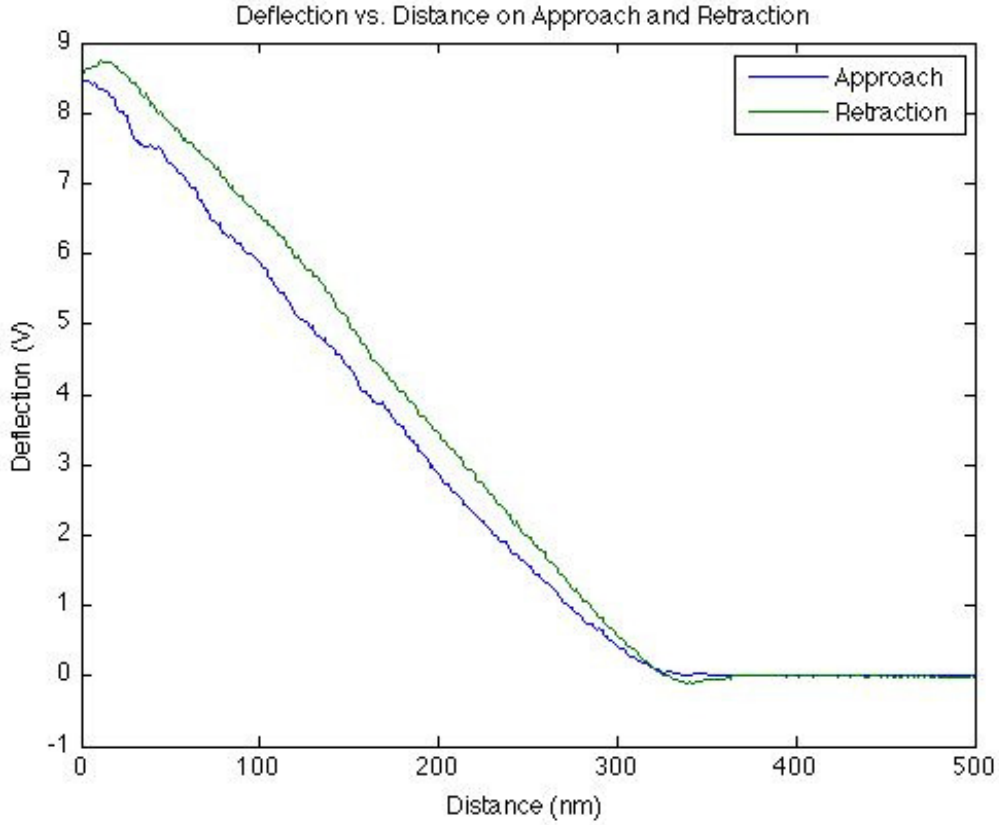
Deflection vs. Distance on Approach and Retraction
Approach
Retraction
Deflection (V)
Distance (nm)
9
8
7
6
5
4
3
2
1
0
-1
0
100
200
300
400
500

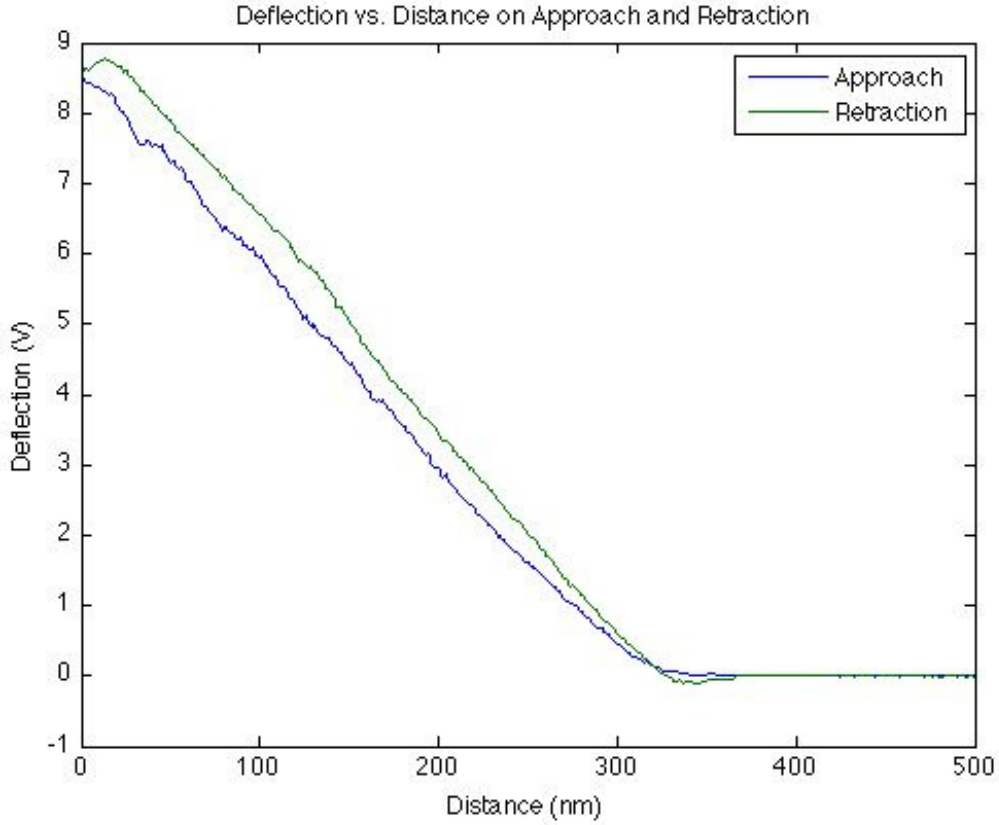
Deflection vs. Distance on Approach and Retraction
Approach
Retraction
Deflection (V)
Distance (nm)
9
8
7
6
5
4
3
2
1
0
-1
0
100
200
300
400
500

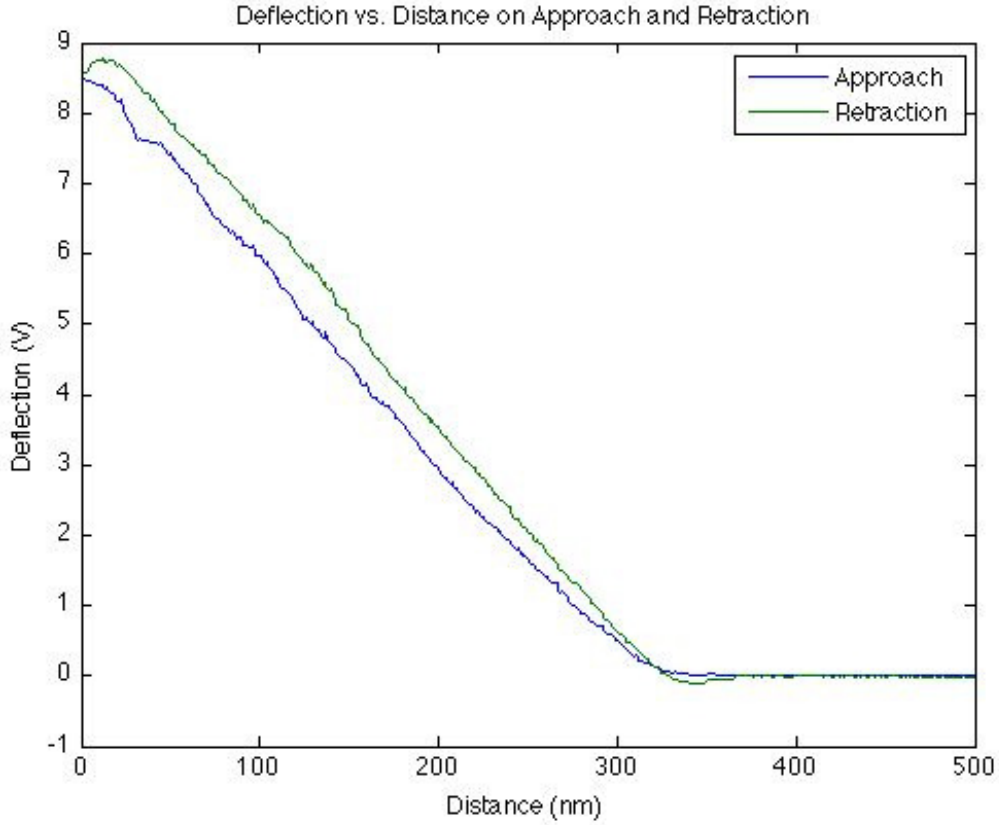
Deflection vs. Distance on Approach and Retraction
Approach
Retraction
Deflection (V)
Distance (nm)
9
8
7
6
5
4
3
2
1
0
-1
0
100
200
300
400
500

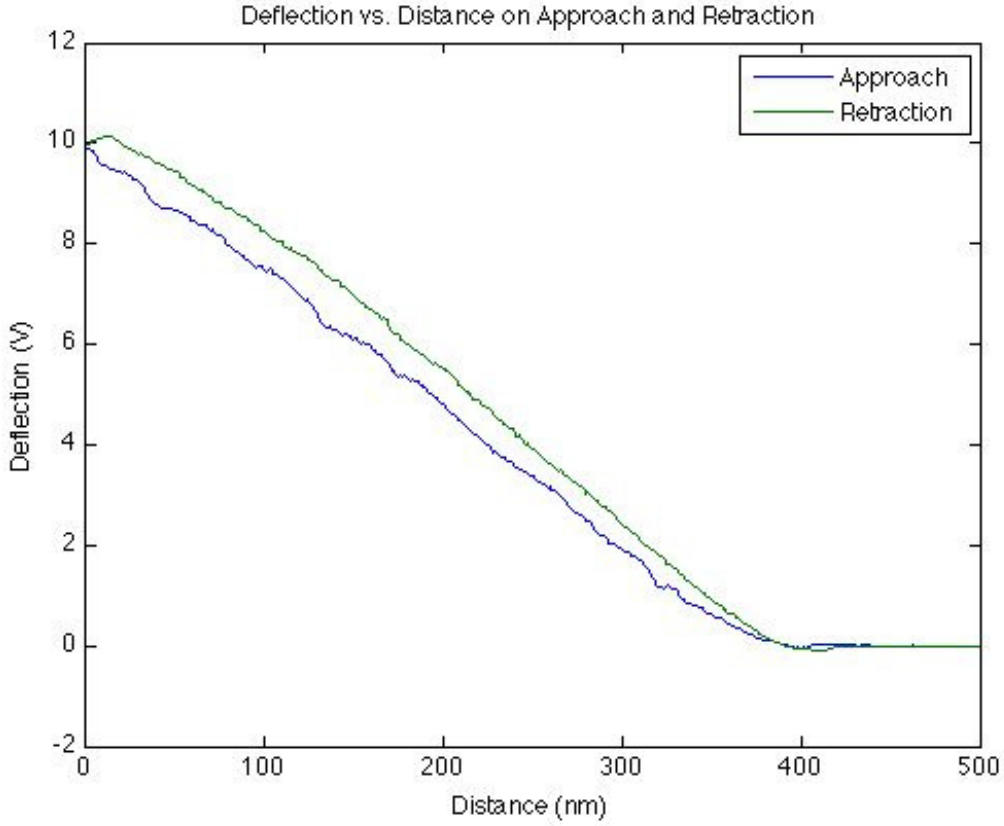
Deflection vs. Distance on Approach and Retraction
Approach
Retraction
Deflection (V)
Distance (nm)
12
10
8
6
4
2
0
-2
0
100
200
300
400
500

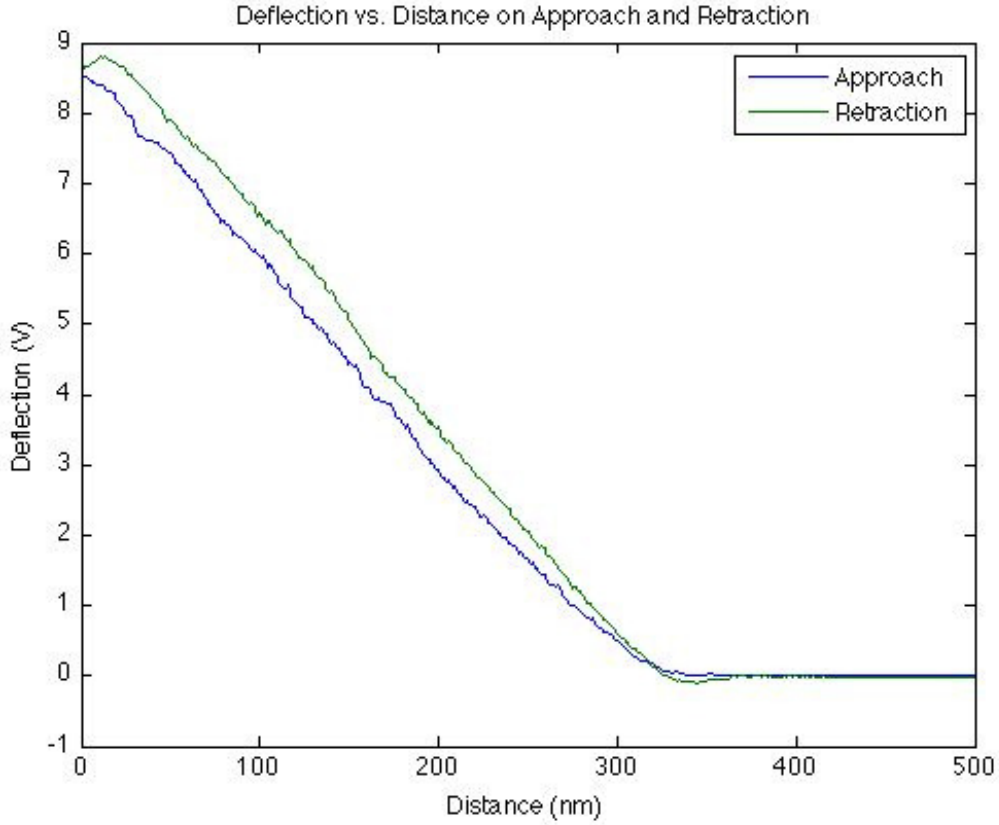
Deflection vs. Distance on Approach and Retraction
Approach
Retraction
Deflection (V)
Distance (nm)
9
8
7
6
5
4
3
2
1
0
-1
0
100
200
300
400
500

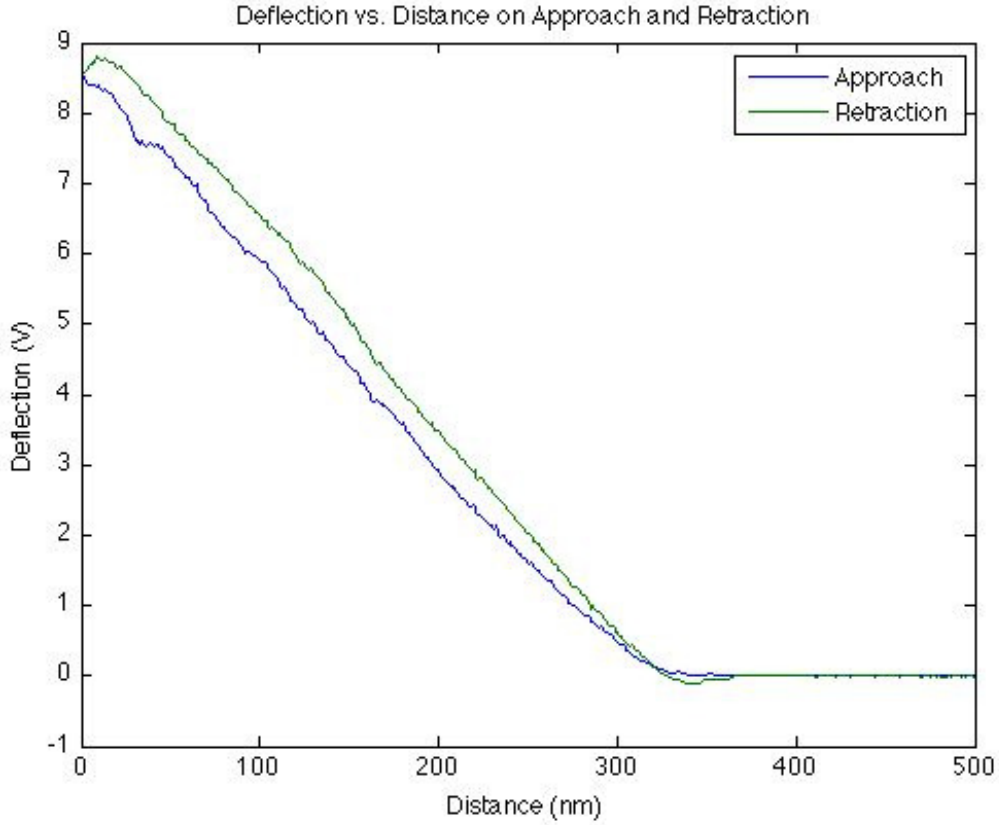
Deflection vs. Distance on Approach and Retraction
Approach
Retraction
Deflection (V)
Distance (nm)
9
8
7
6
5
4
3
2
1
0
-1
0
100
200
300
400
500

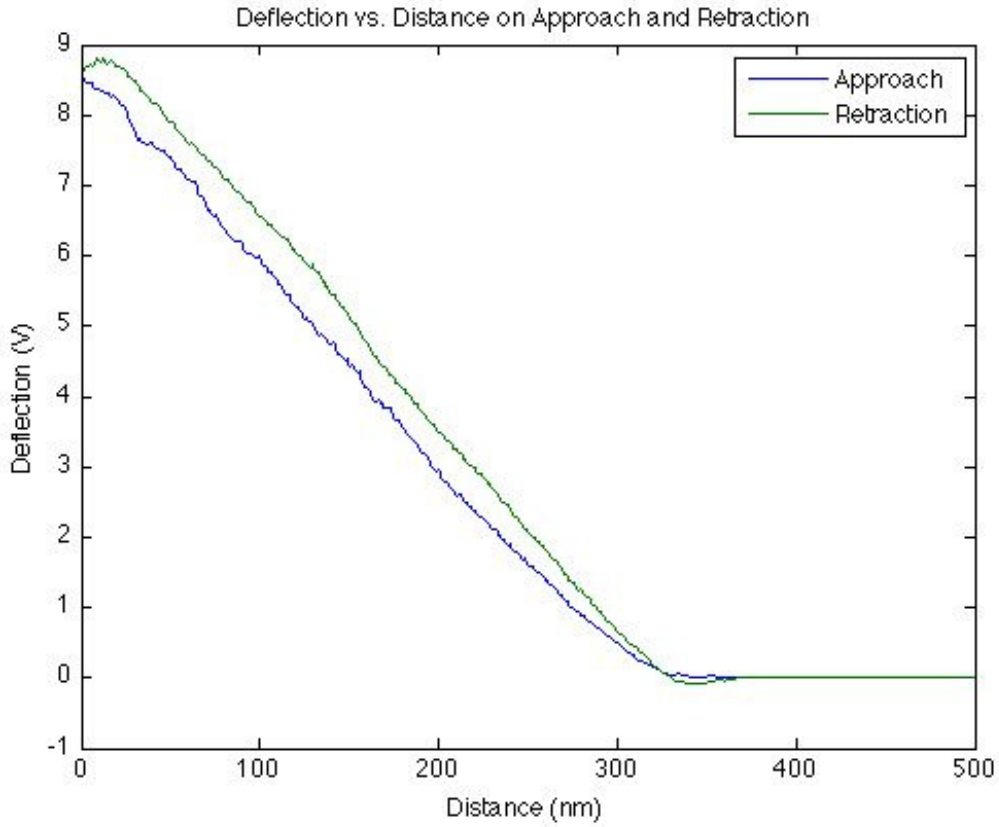
Deflection vs. Distance on Approach and Retraction
Approach
Retraction
Deflection (V)
Distance (nm)
9
8
7
6
5
4
3
2
1
0
-1
0
100
200
300
400
500

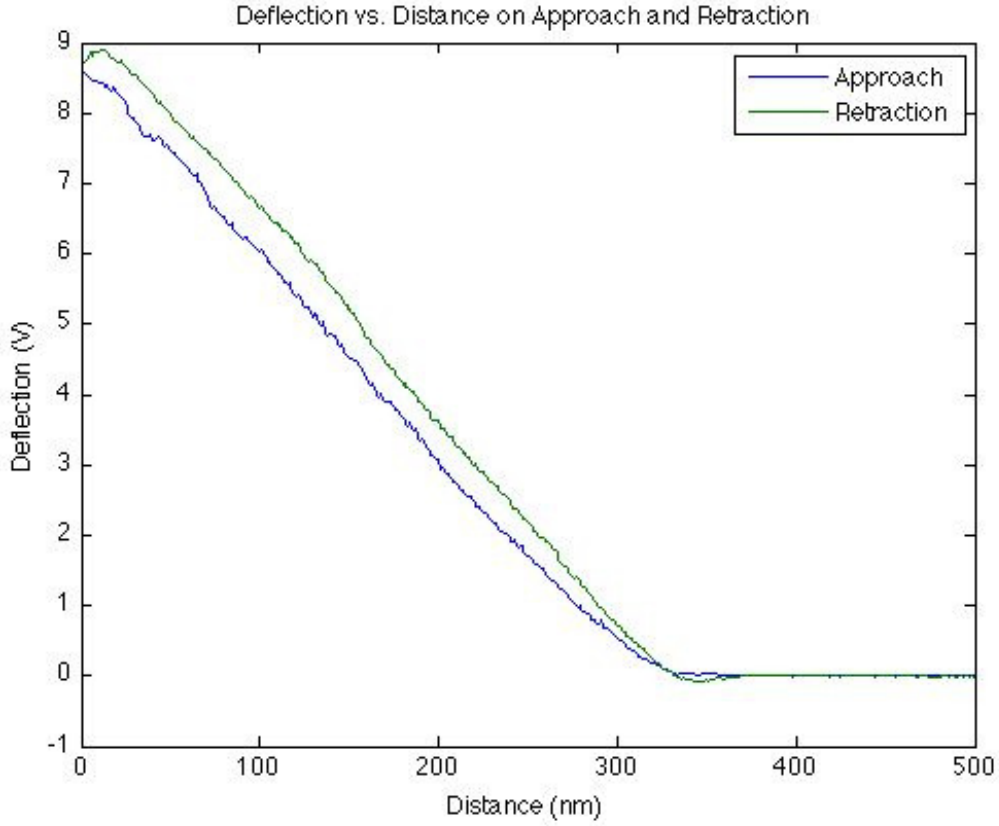
Deflection vs. Distance on Approach and Retraction
Approach
Retraction
Deflection (V)
Distance (nm)
9
8
7
6
5
4
3
2
1
0
-1
0
100
200
300
400
500

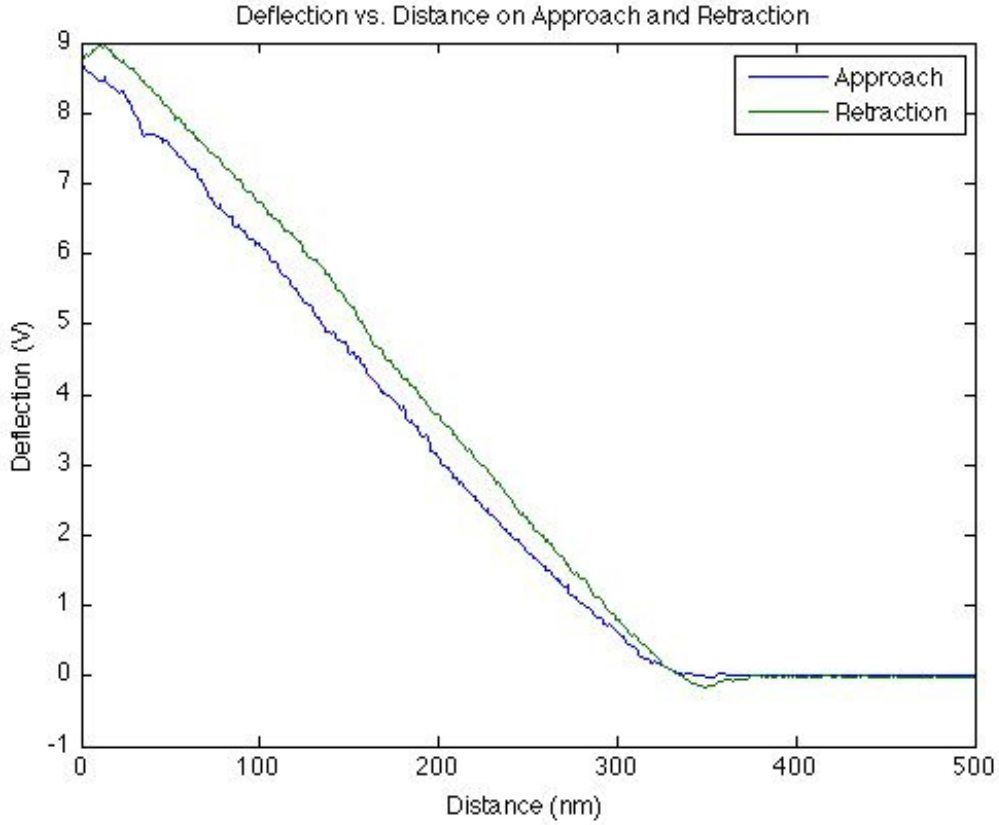
Deflection vs. Distance on Approach and Retraction
Approach
Retraction
Deflection (V)
Distance (nm)
9
8
7
6
5
4
3
2
1
0
-1
0
100
200
300
400
500

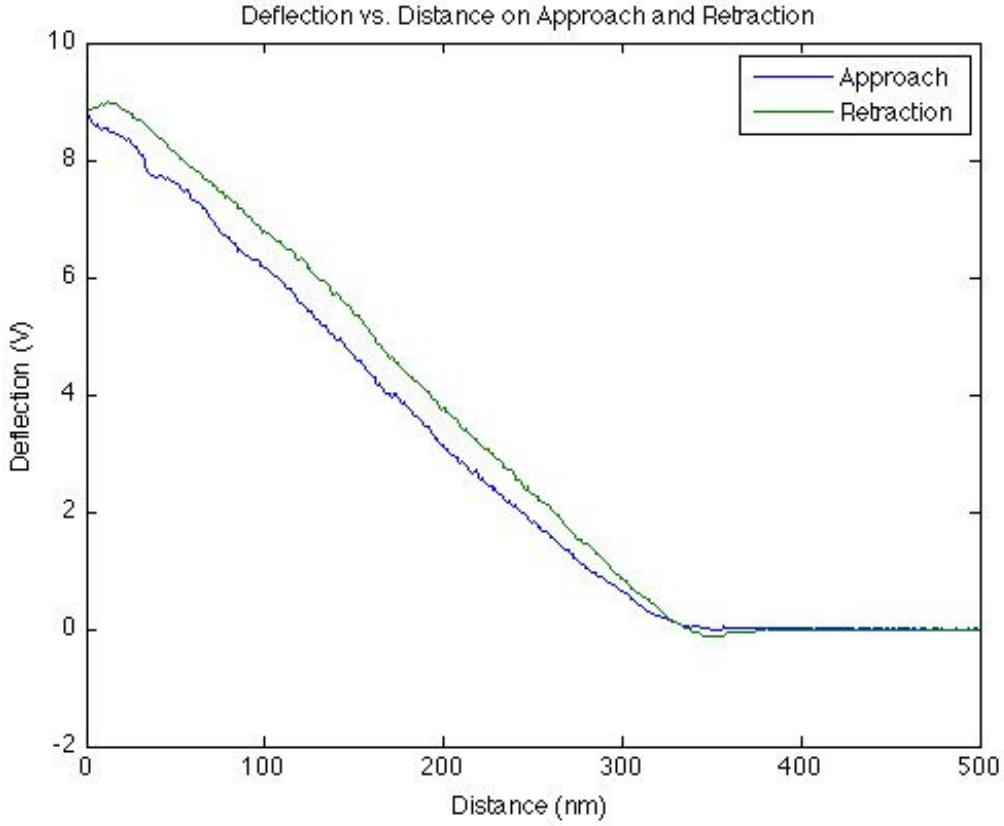
Deflection vs. Distance on Approach and Retraction
Approach
Retraction
Deflection (V)
Distance (nm)
10
8
6
4
2
0
-2
0
100
200
300
400
500

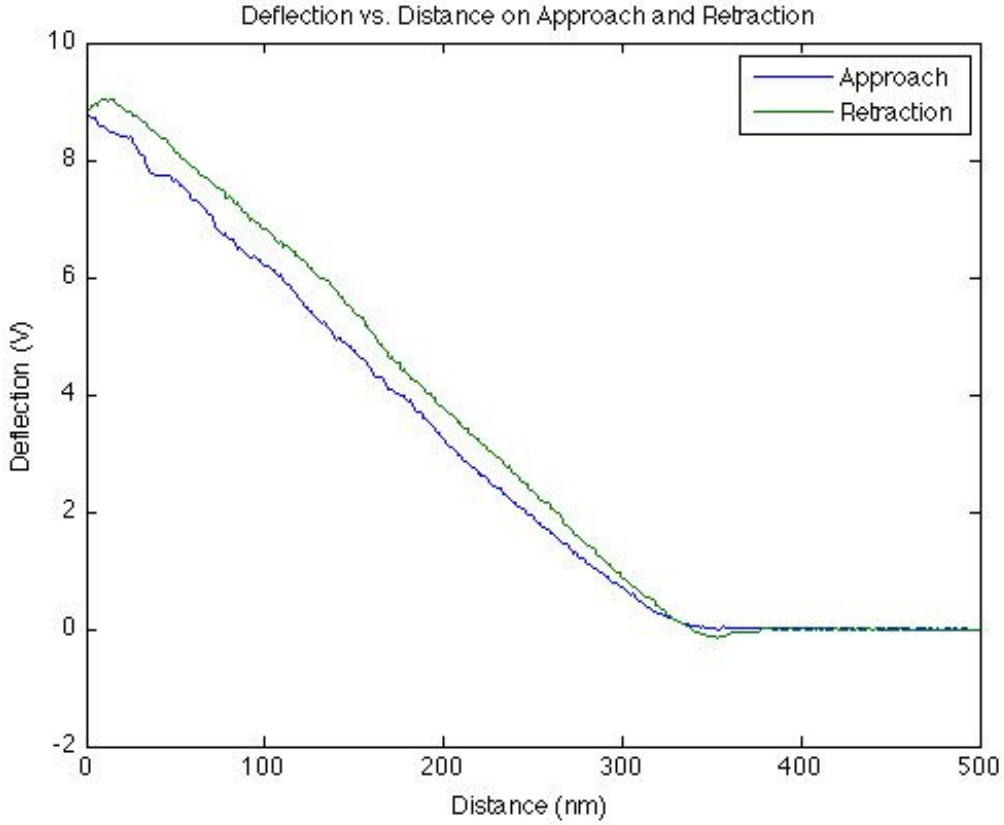
Deflection vs. Distance on Approach and Retraction
Approach
Retraction
Deflection (V)
Distance (nm)
10
8
6
4
2
0
-2
0
100
200
300
400
500

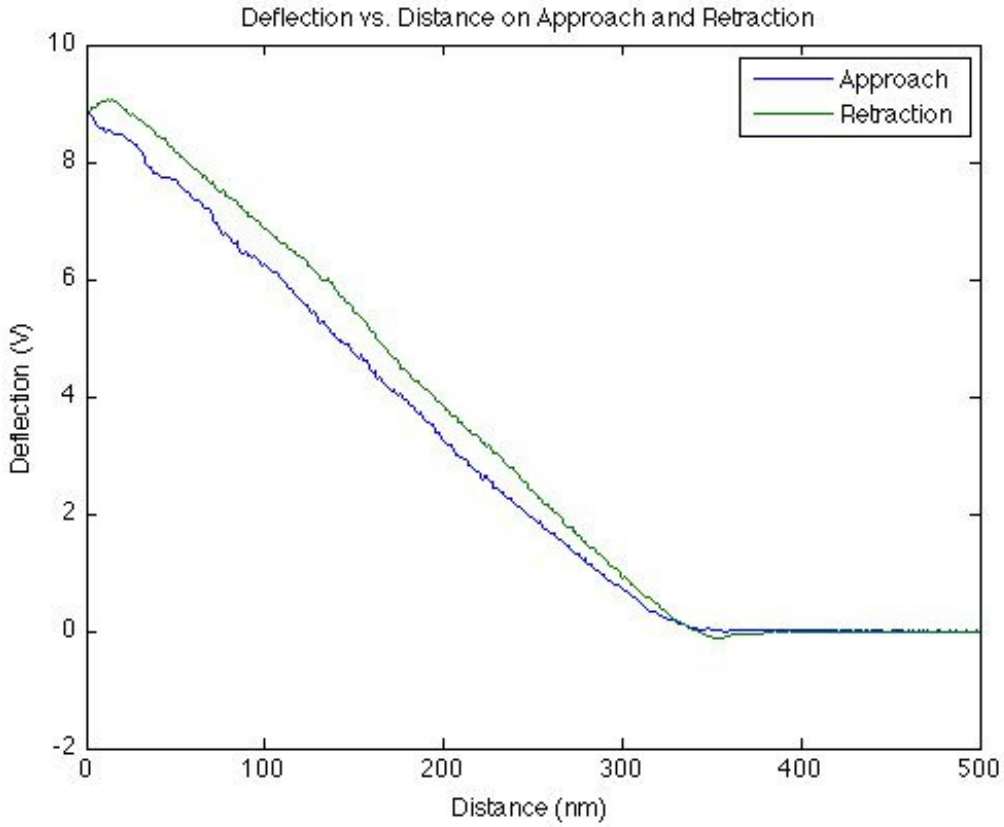
Deflection vs. Distance on Approach and Retraction
Approach
Retraction
Deflection (V)
Distance (nm)
10
8
6
4
2
0
-2
0
100
200
300
400
500

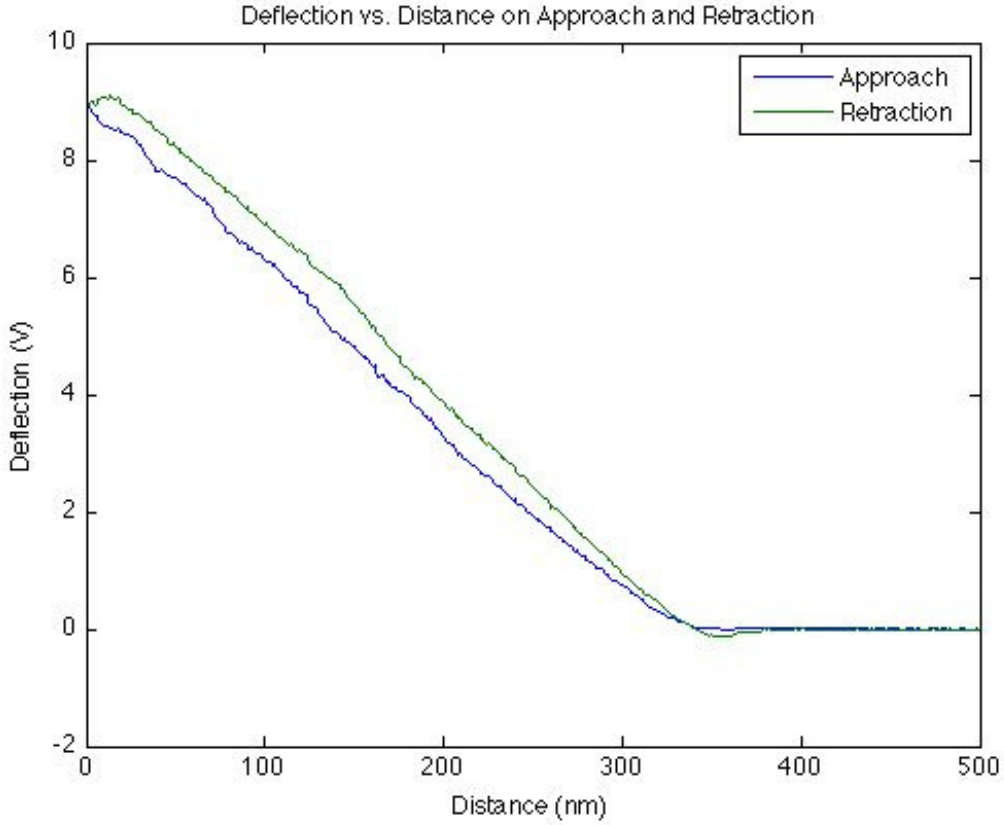
Deflection vs. Distance on Approach and Retraction
Approach
Retraction
Deflection (V)
Distance (nm)
10
8
6
4
2
0
-2
0
100
200
300
400
500

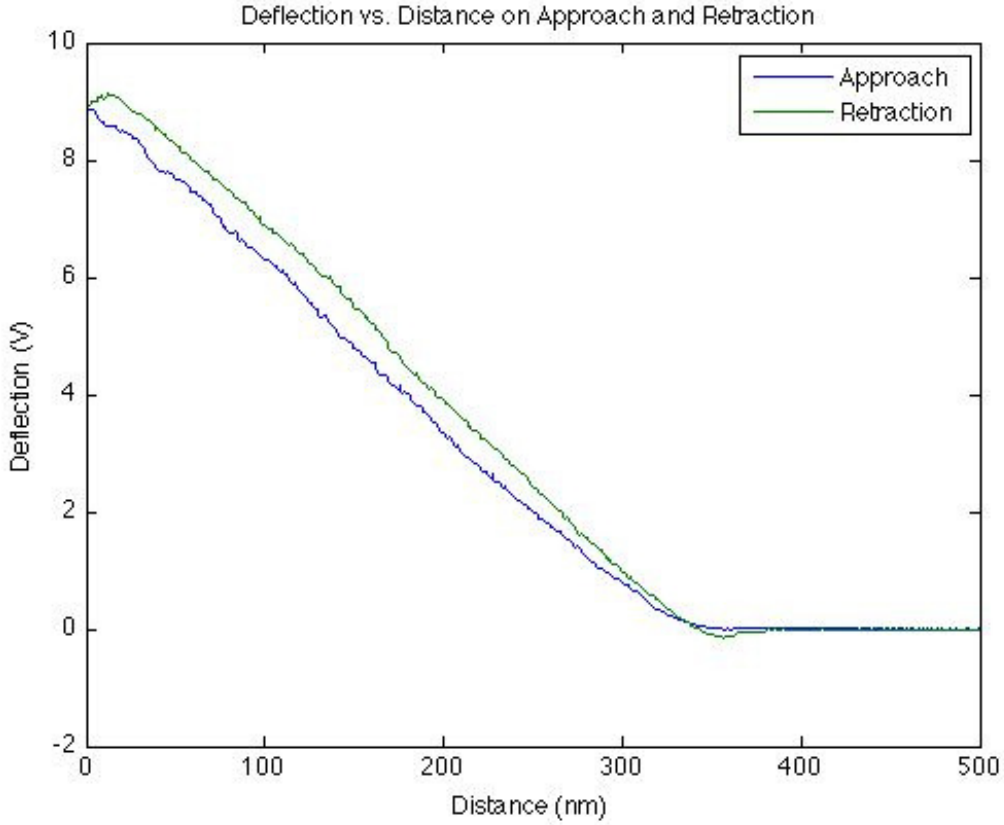
Deflection vs. Distance on Approach and Retraction
Approach
Retraction
Deflection (V)
Distance (nm)
10
8
6
4
2
0
-2
0
100
200
300
400
500

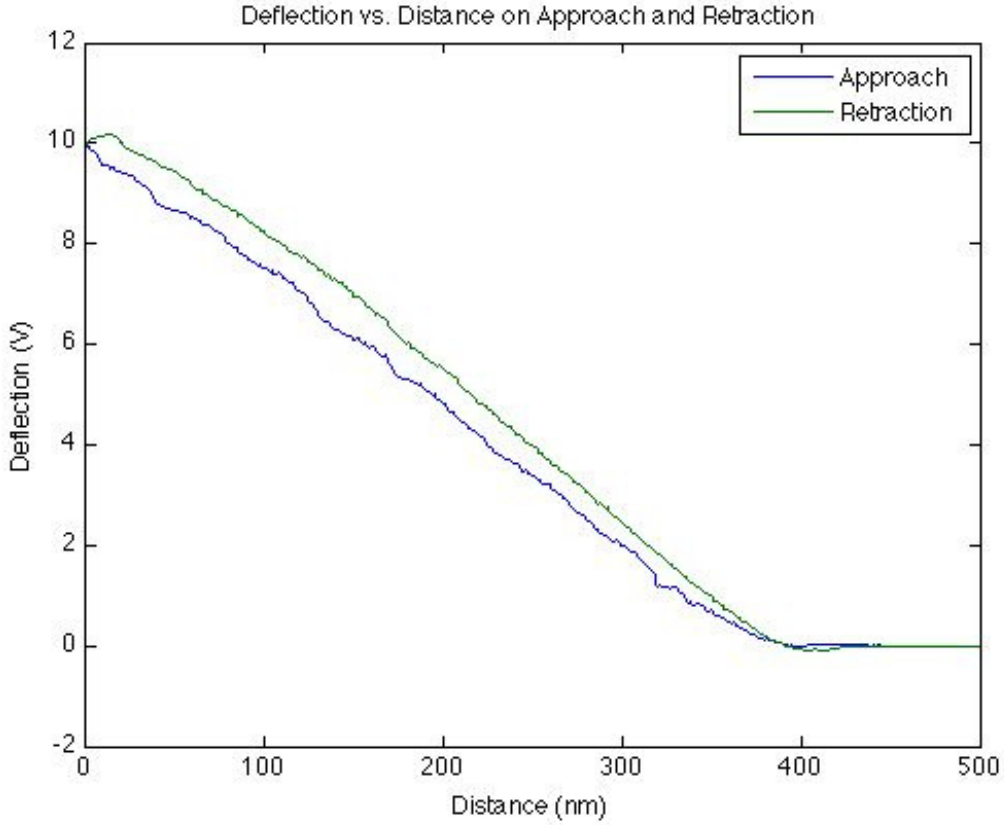
Deflection vs. Distance on Approach and Retraction
Approach
Retraction
Deflection (V)
Distance (nm)
12
10
8
6
4
2
0
-2
0
100
200
300
400
500

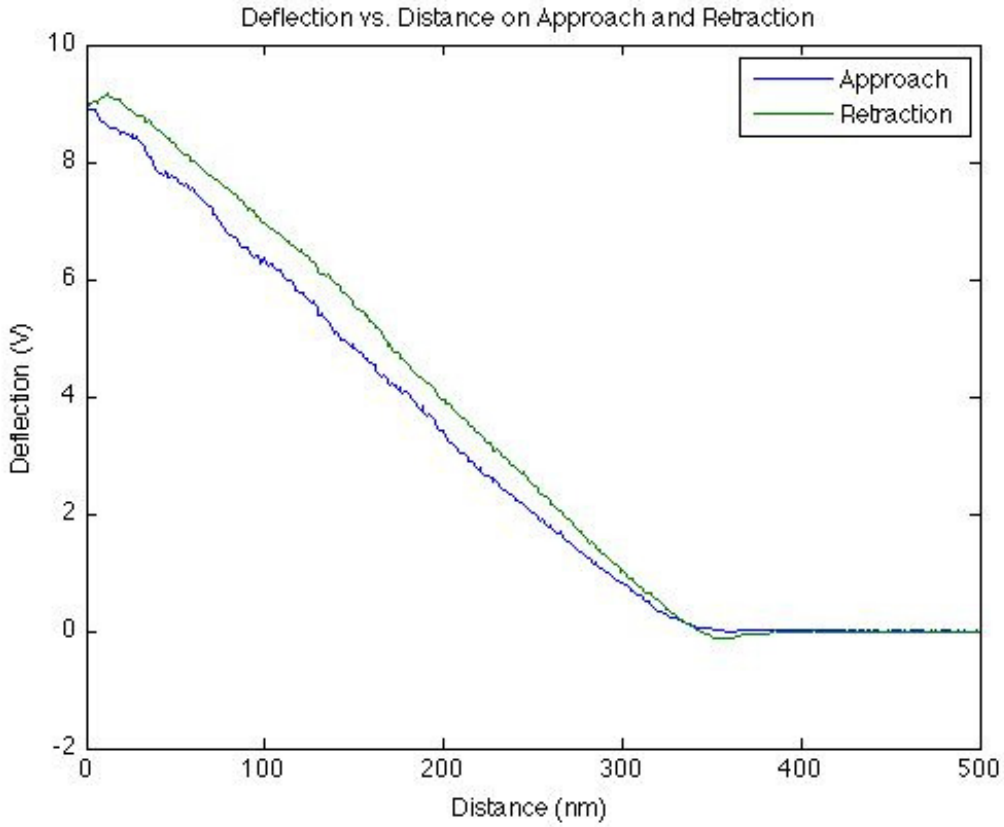
Deflection vs. Distance on Approach and Retraction
Approach
Retraction
Deflection (V)
Distance (nm)
10
8
6
4
2
0
-2
0
100
200
300
400
500

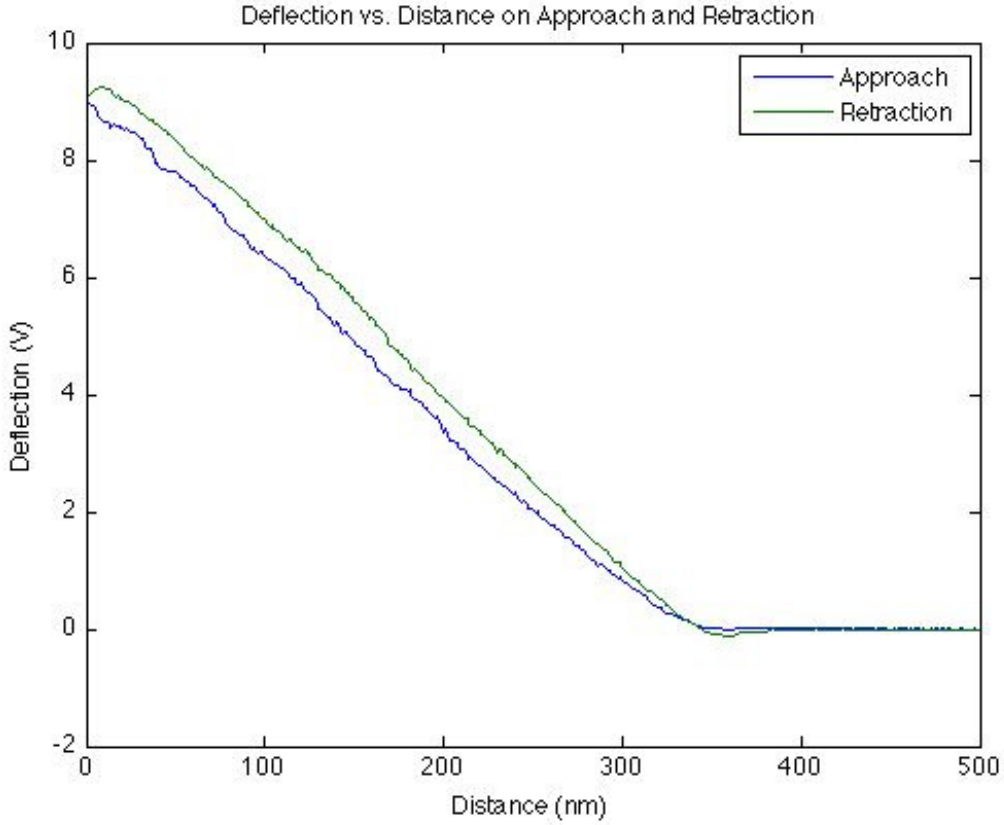
Deflection vs. Distance on Approach and Retraction
Approach
Retraction
Deflection (V)
Distance (nm)
10
8
6
4
2
0
-2
0
100
200
300
400
500

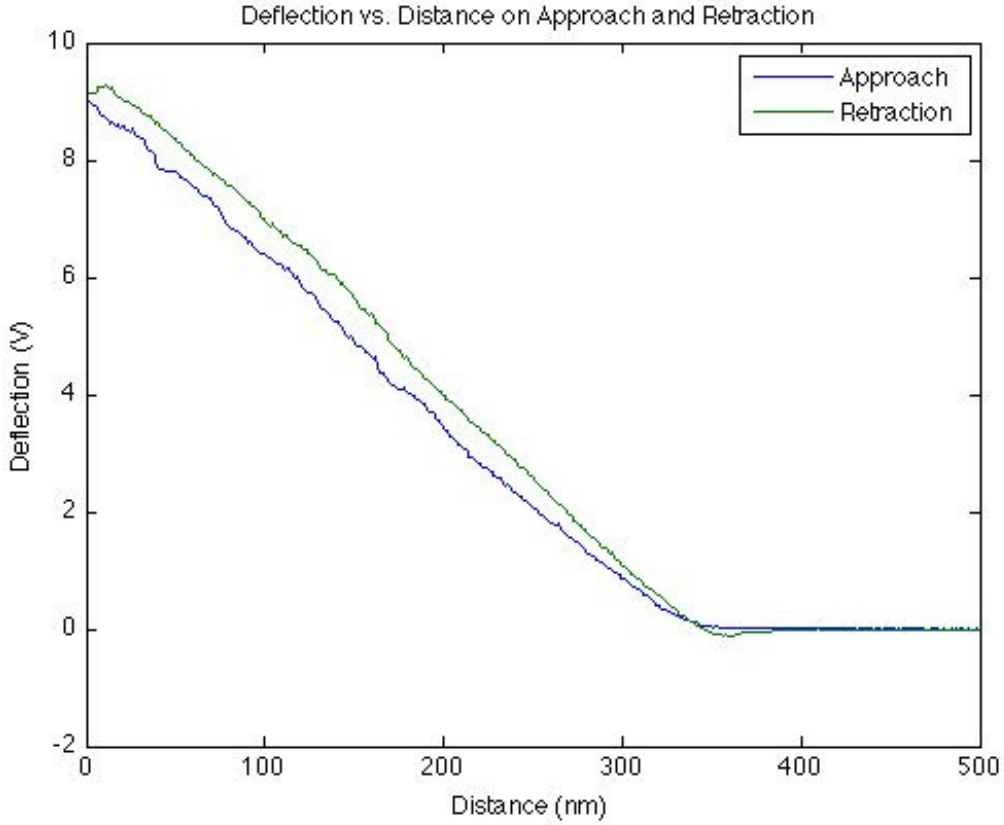
Deflection vs. Distance on Approach and Retraction
Approach
Retraction
Deflection (V)
Distance (nm)
10
8
6
4
2
0
-2
0
100
200
300
400
500

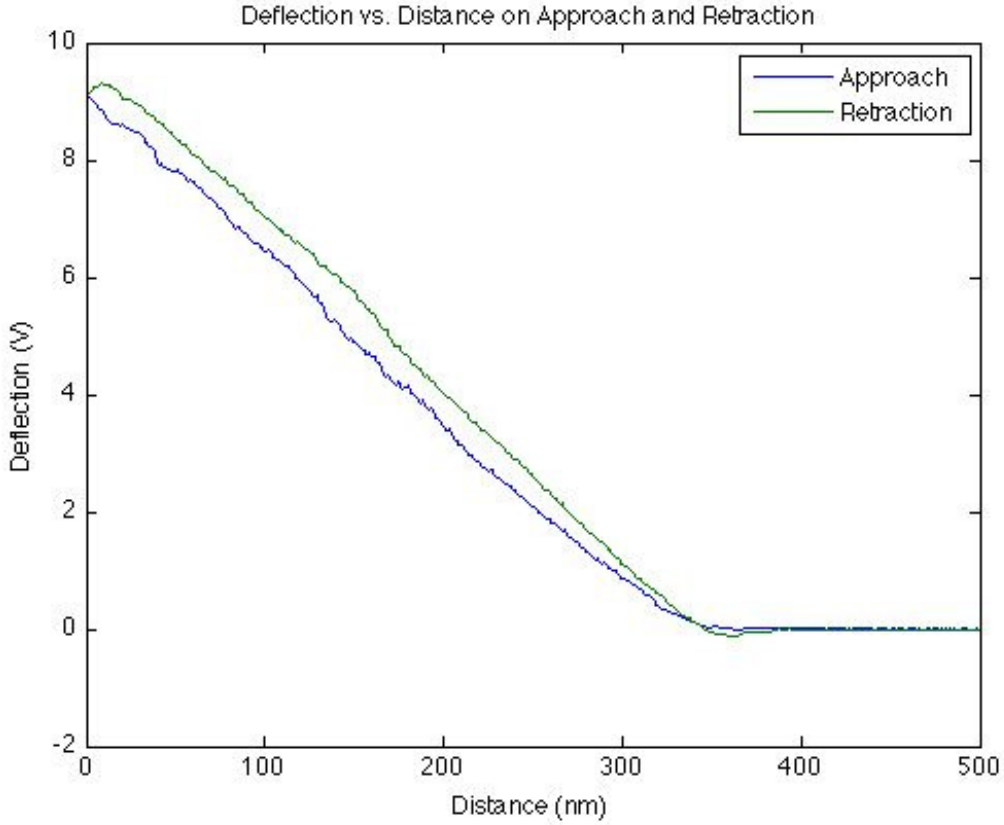
Deflection vs. Distance on Approach and Retraction
Approach
Retraction
Deflection (V)
Distance (nm)
10
8
6
4
2
0
-2
0
100
200
300
400
500

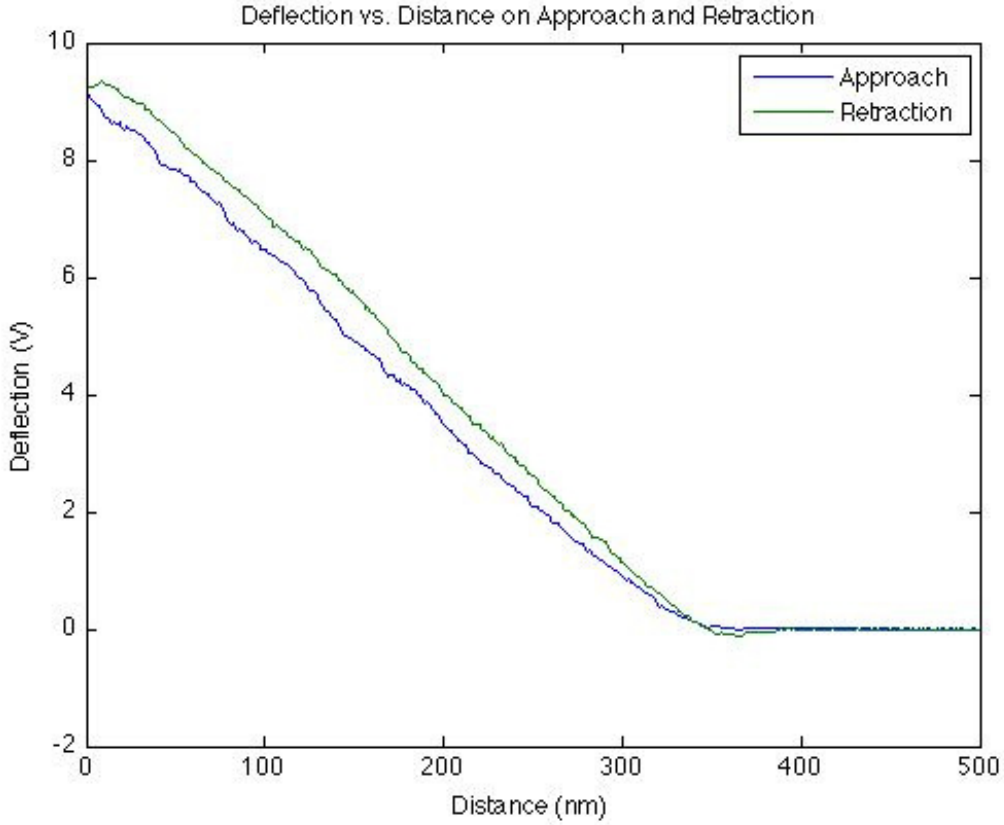
Deflection vs. Distance on Approach and Retraction
Approach
Retraction
Deflection (V)
Distance (nm)
10
8
6
4
2
0
-2
0
100
200
300
400
500

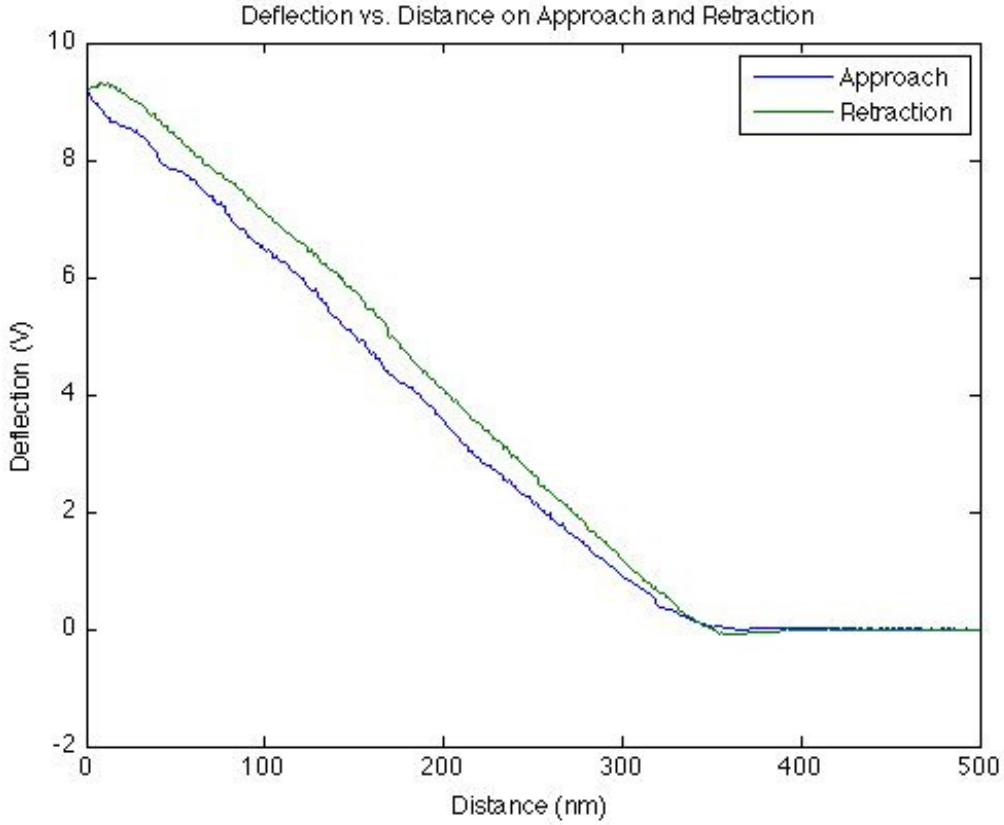
Deflection vs. Distance on Approach and Retraction
Approach
Retraction
Deflection (V)
Distance (nm)
10
8
6
4
2
0
-2
0
100
200
300
400
500

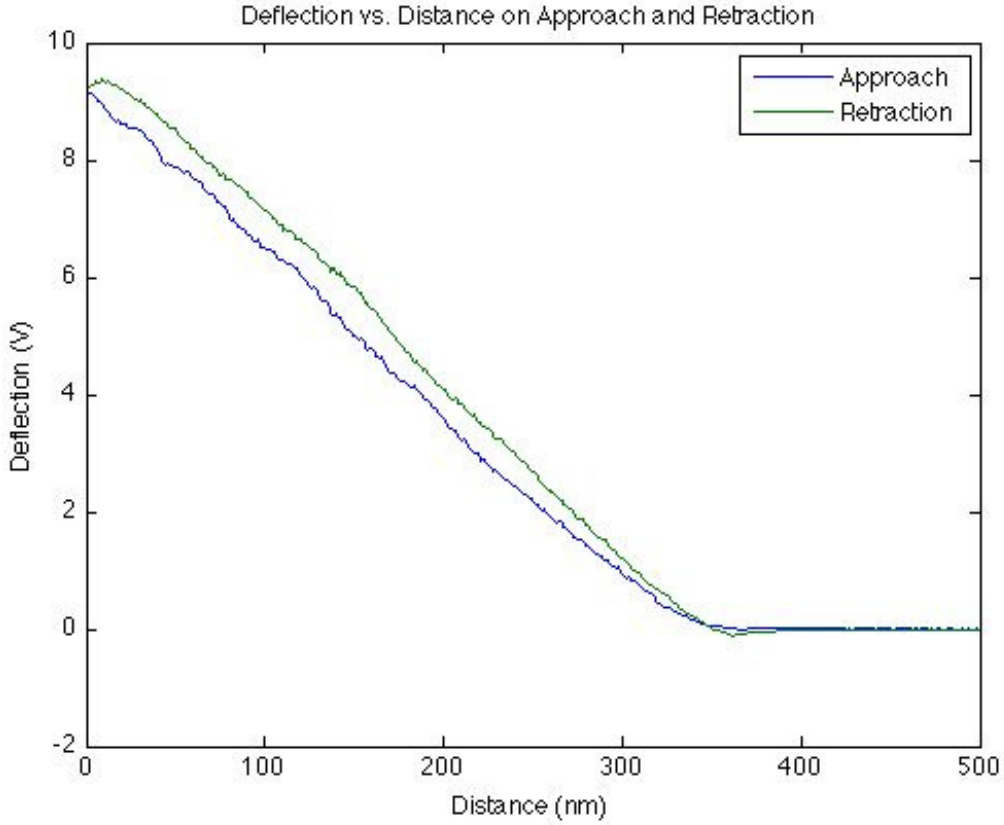
Deflection vs. Distance on Approach and Retraction
Approach
Retraction
Deflection (V)
Distance (nm)
10
8
6
4
2
0
-2
0
100
200
300
400
500

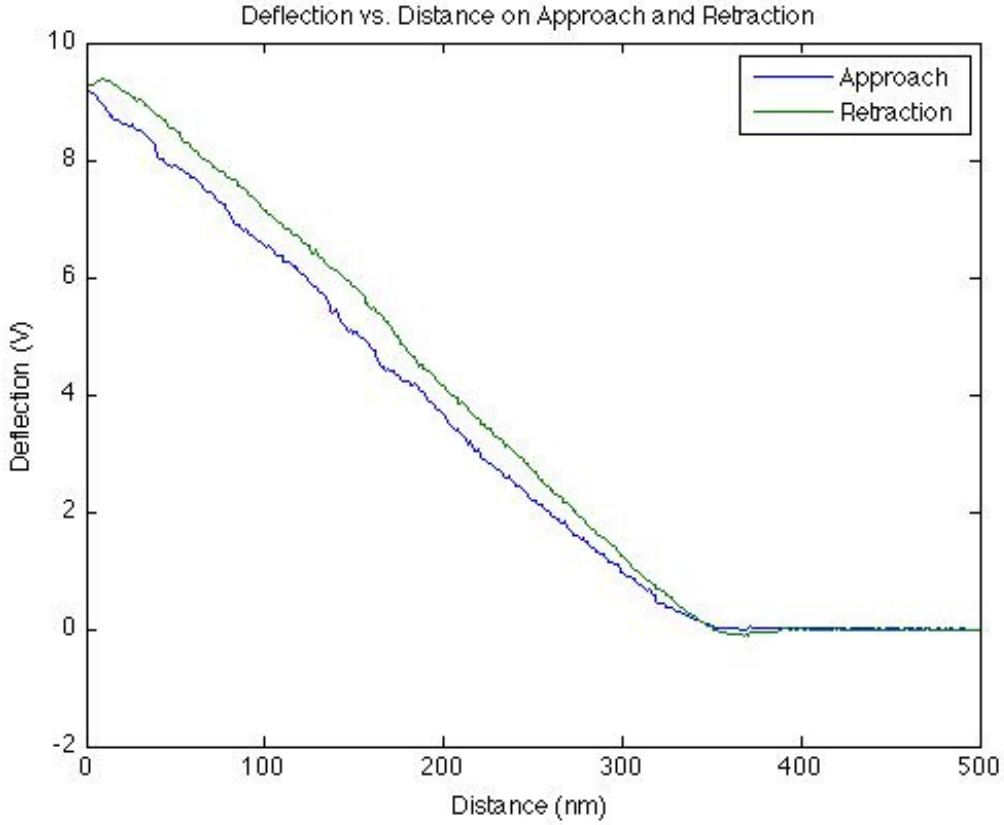
Deflection vs. Distance on Approach and Retraction
Approach
Retraction
Deflection (V)
Distance (nm)
10
8
6
4
2
0
-2
0
100
200
300
400
500

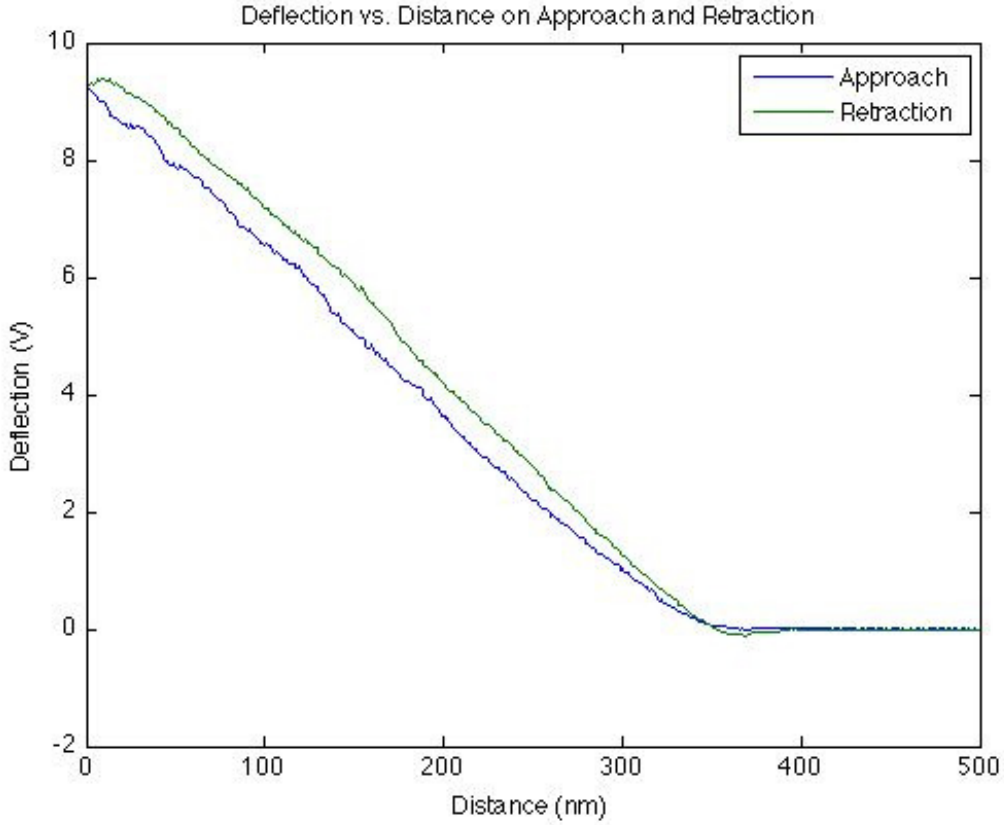
Deflection vs. Distance on Approach and Retraction
Approach
Retraction
Deflection (V)
Distance (nm)
10
8
6
4
2
0
-2
0
100
200
300
400
500

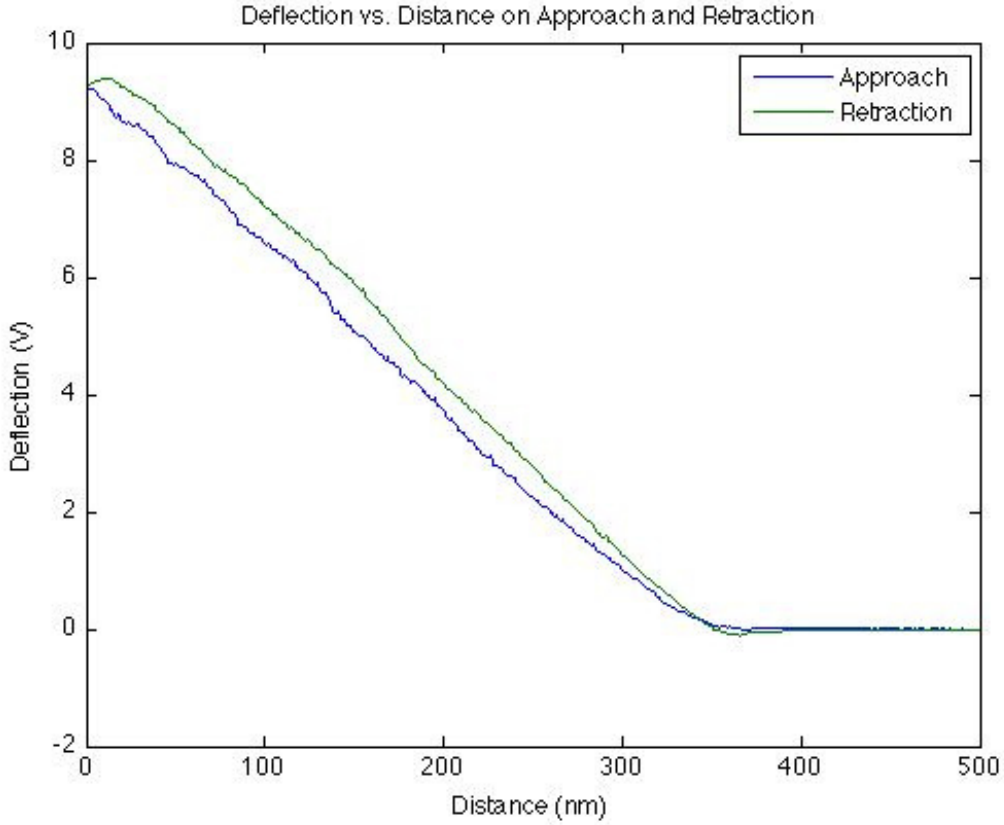
Deflection vs. Distance on Approach and Retraction
Approach
Retraction
Deflection (V)
Distance (nm)
10
8
6
4
2
0
-2
0
100
200
300
400
500

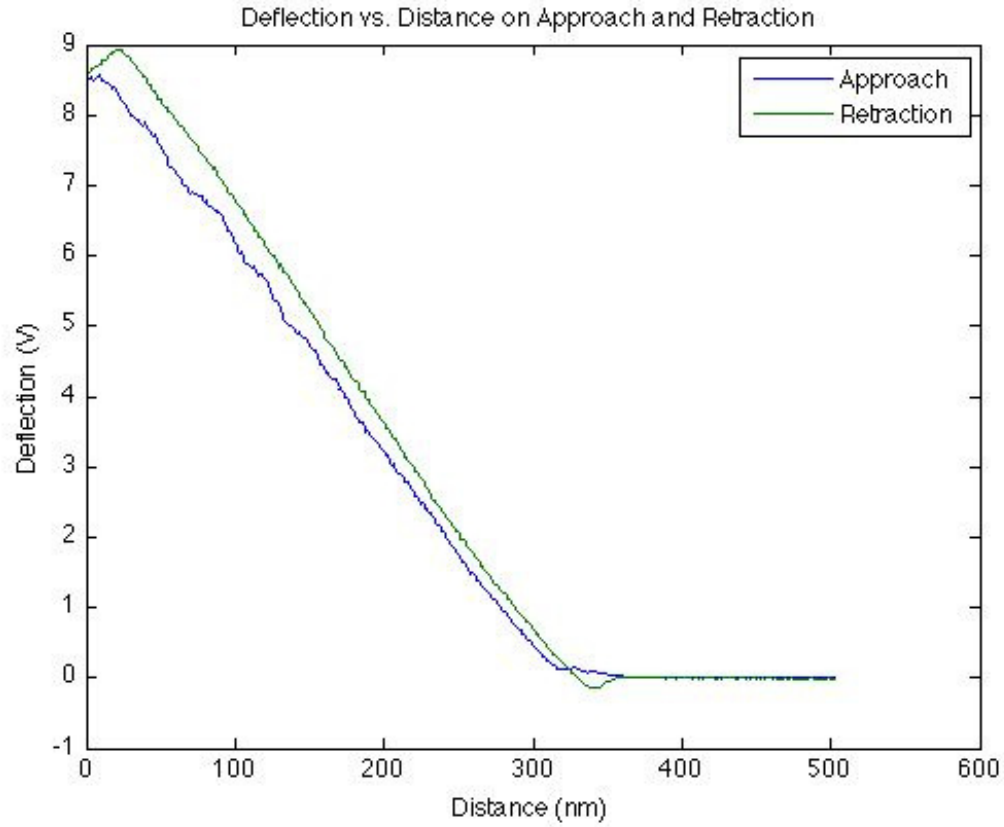
Deflection vs. Distance on Approach and Retraction
Approach
Retraction
Deflection (V)
Distance (nm)
9
8
7
6
5
4
3
2
1
0
-1
0
100
200
300
400
500
600

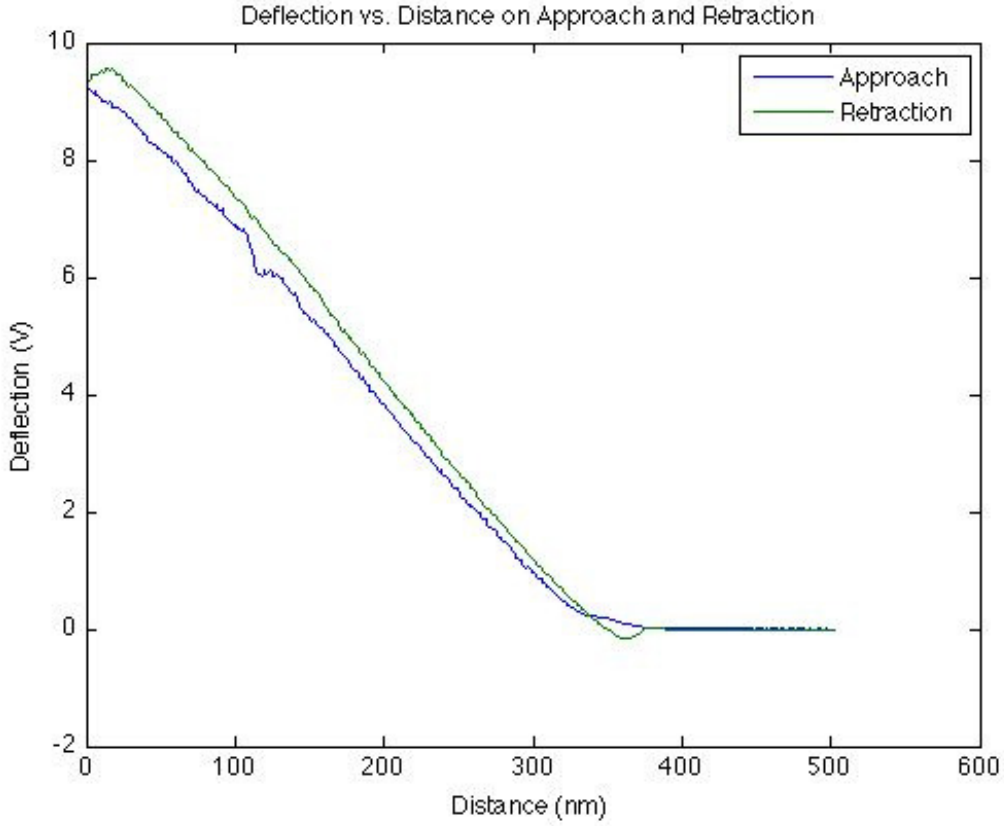
Deflection vs. Distance on Approach and Retraction
Approach
Retraction
Deflection (V)
Distance (nm)
10
8
6
4
2
0
-2
0
100
200
300
400
500
600

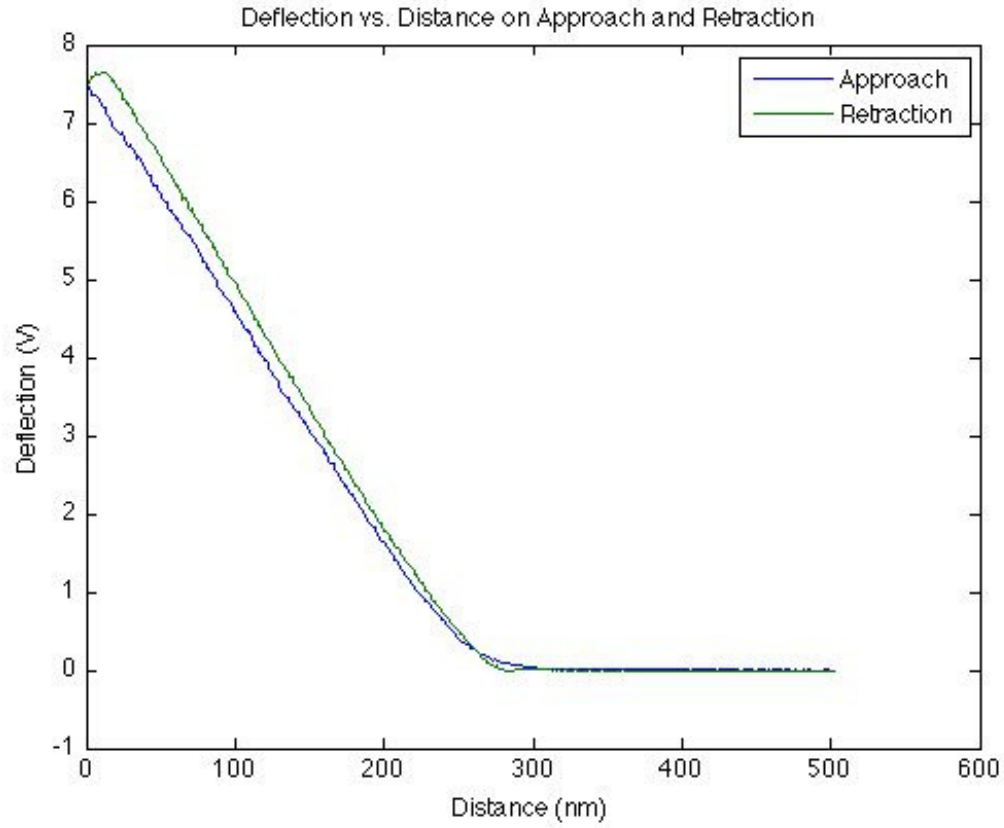
Deflection vs. Distance on Approach and Retraction
Approach
Retraction
Deflection (V)
Distance (nm)
8
7
6
5
4
3
2
1
0
-1
0
100
200
300
400
500
600

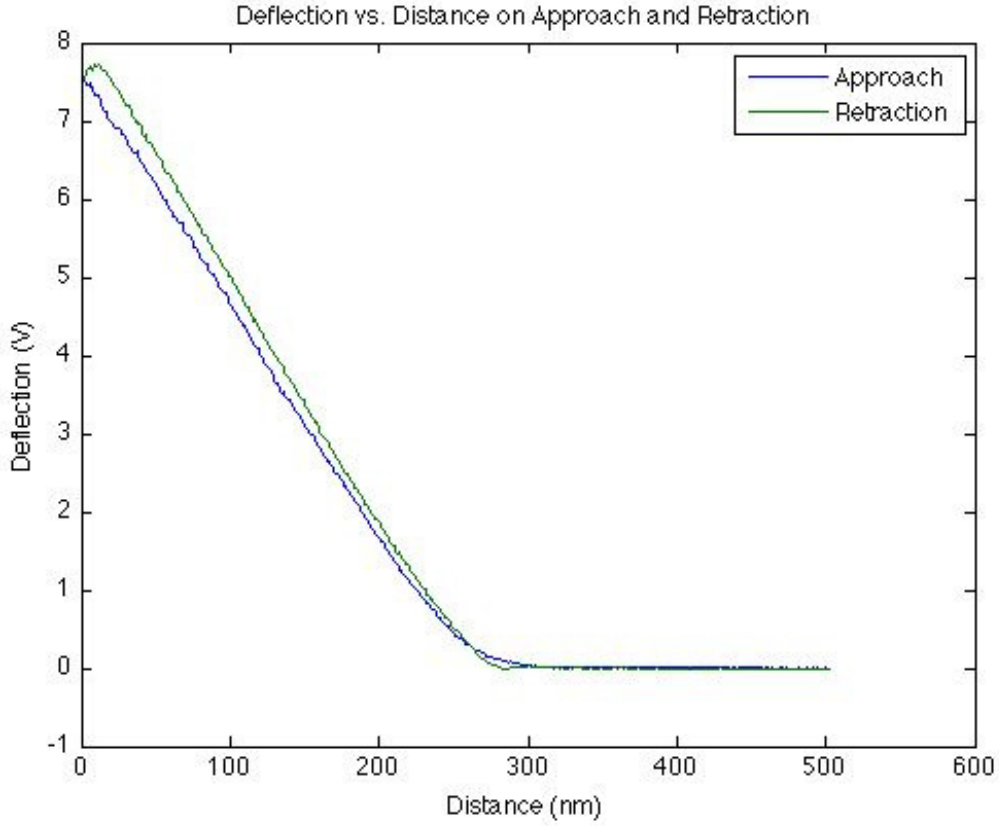
Deflection vs. Distance on Approach and Retraction
Approach
Retraction
Deflection (V)
Distance (nm)
8
7
6
5
4
3
2
1
0
-1
0
100
200
300
400
500
600

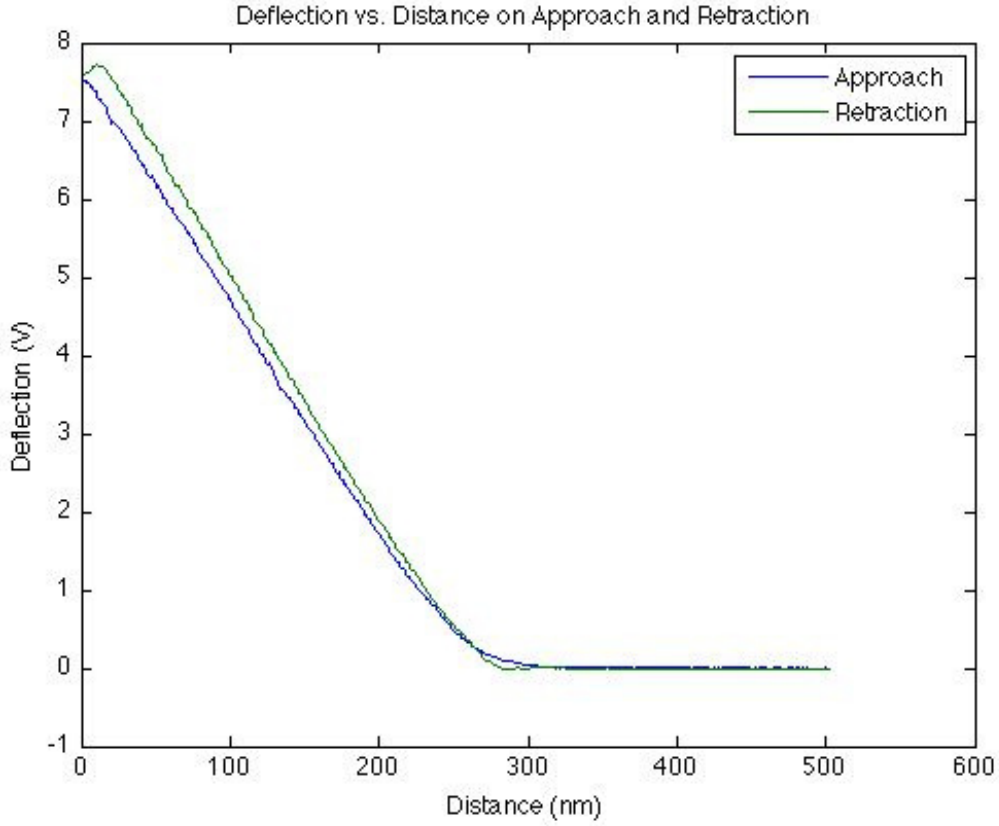
Deflection vs. Distance on Approach and Retraction
Approach
Retraction
Deflection (V)
Distance (nm)
8
7
6
5
4
3
2
1
0
-1
0
100
200
300
400
500
600

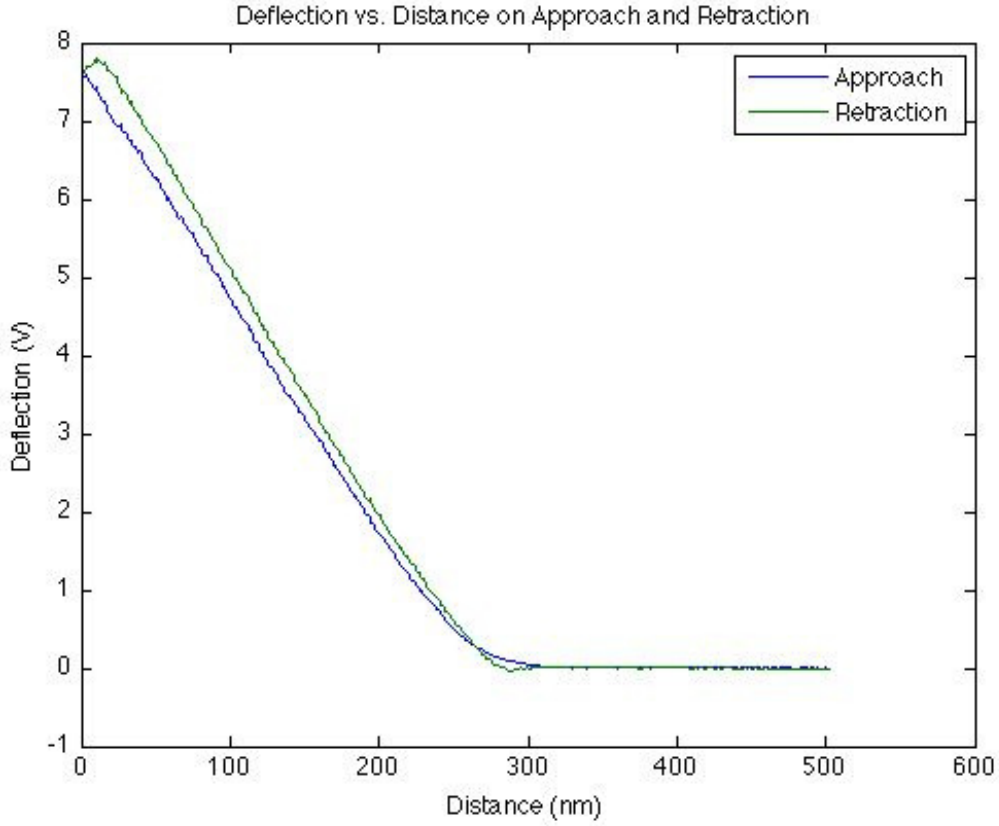
Deflection vs. Distance on Approach and Retraction
Approach
Retraction
Deflection (V)
Distance (nm)
8
7
6
5
4
3
2
1
0
-1
0
100
200
300
400
500
600

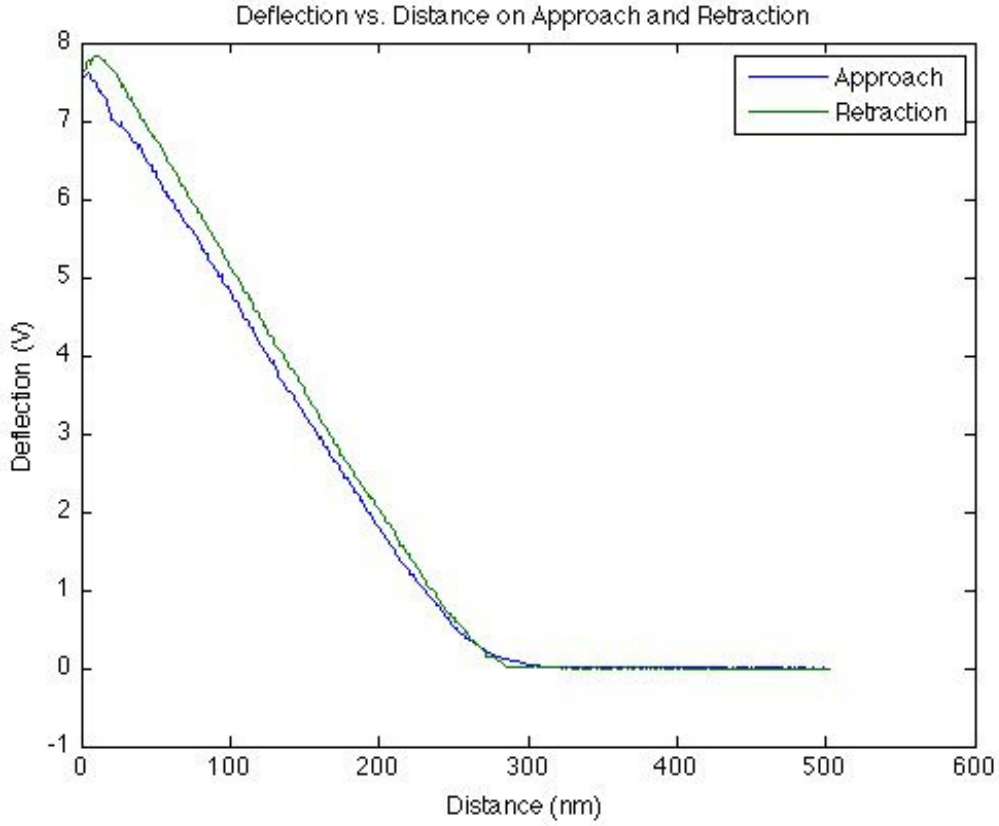
Deflection vs. Distance on Approach and Retraction
Approach
Retraction
Deflection (V)
Distance (nm)
8
7
6
5
4
3
2
1
0
-1
0
100
200
300
400
500
600

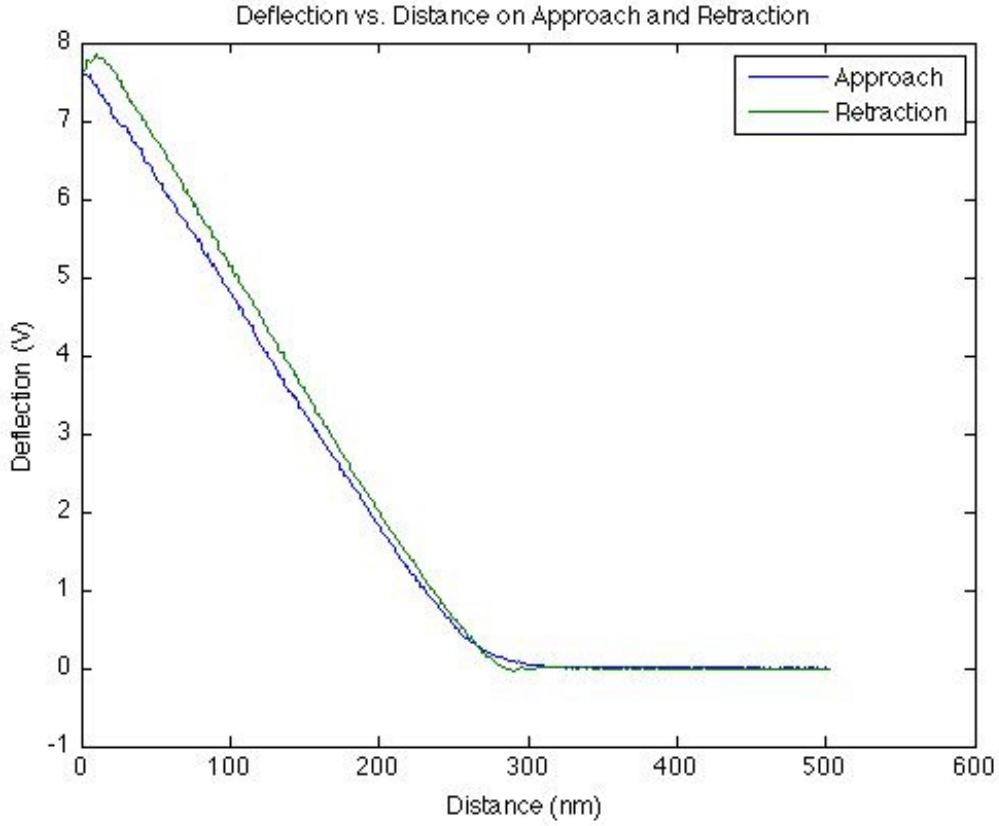
Deflection vs. Distance on Approach and Retraction
Approach
Retraction
Deflection (V)
Distance (nm)
8
7
6
5
4
3
2
1
0
-1
0
100
200
300
400
500
600

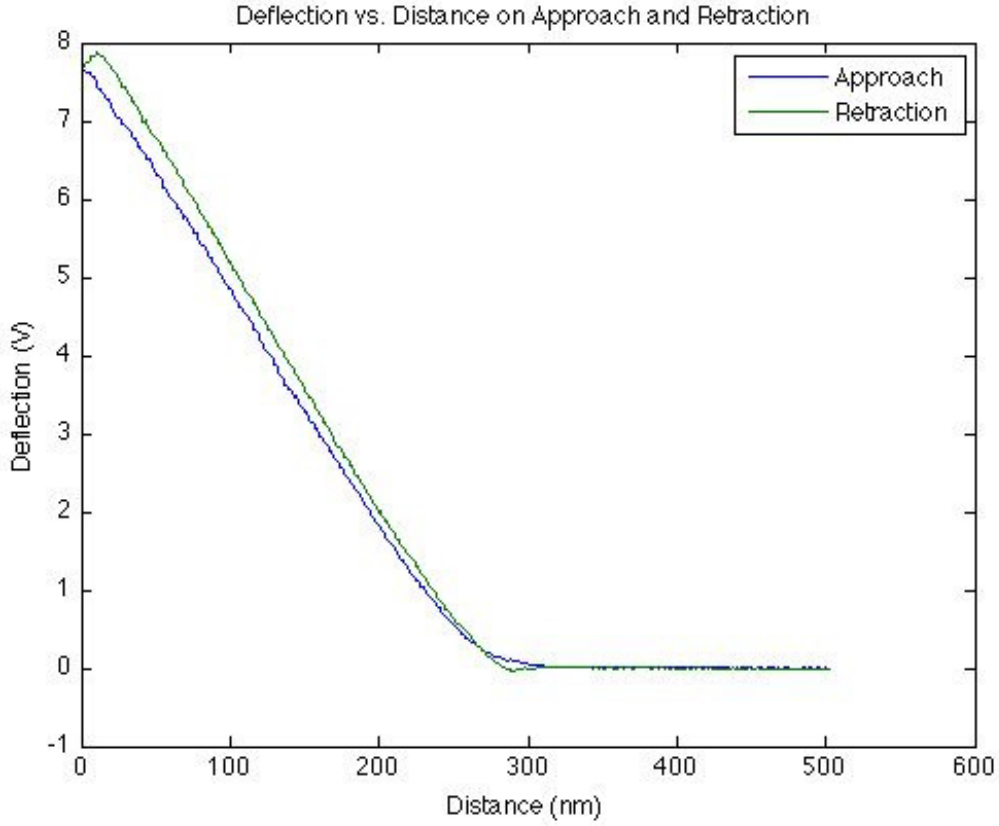
Deflection vs. Distance on Approach and Retraction
Approach
Retraction
Deflection (V)
Distance (nm)
8
7
6
5
4
3
2
1
0
-1
0
100
200
300
400
500
600

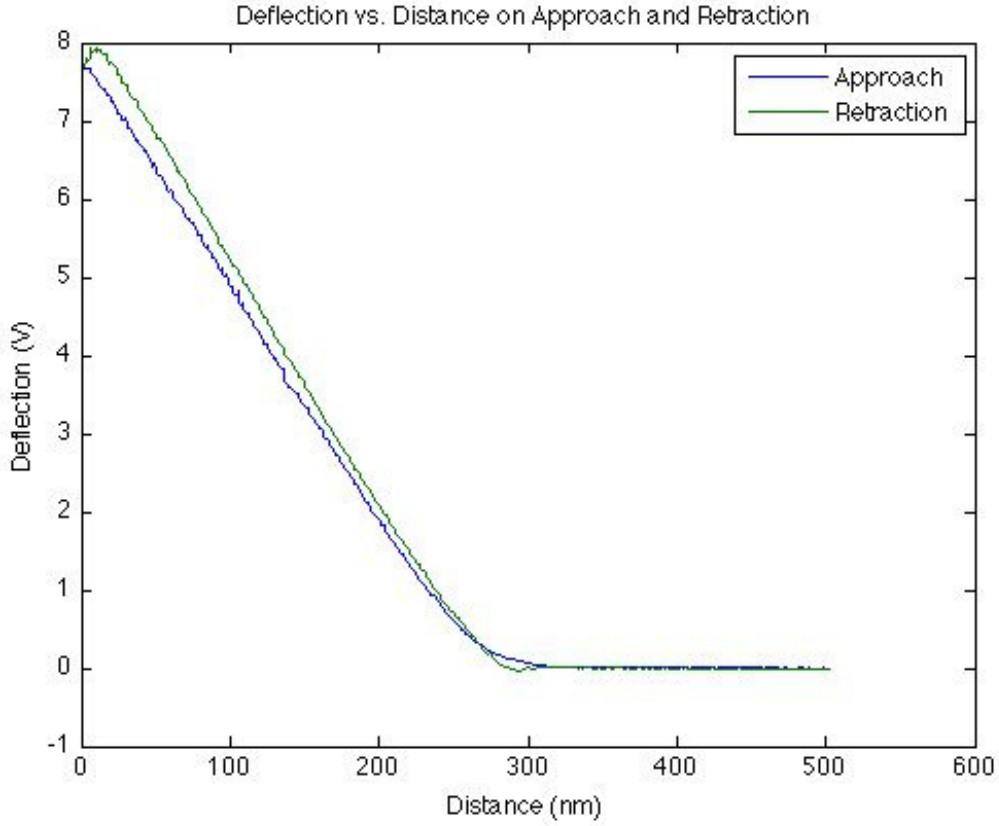
Deflection vs. Distance on Approach and Retraction
Approach
Retraction
Deflection (V)
Distance (nm)
8
7
6
5
4
3
2
1
0
-1
0
100
200
300
400
500
600

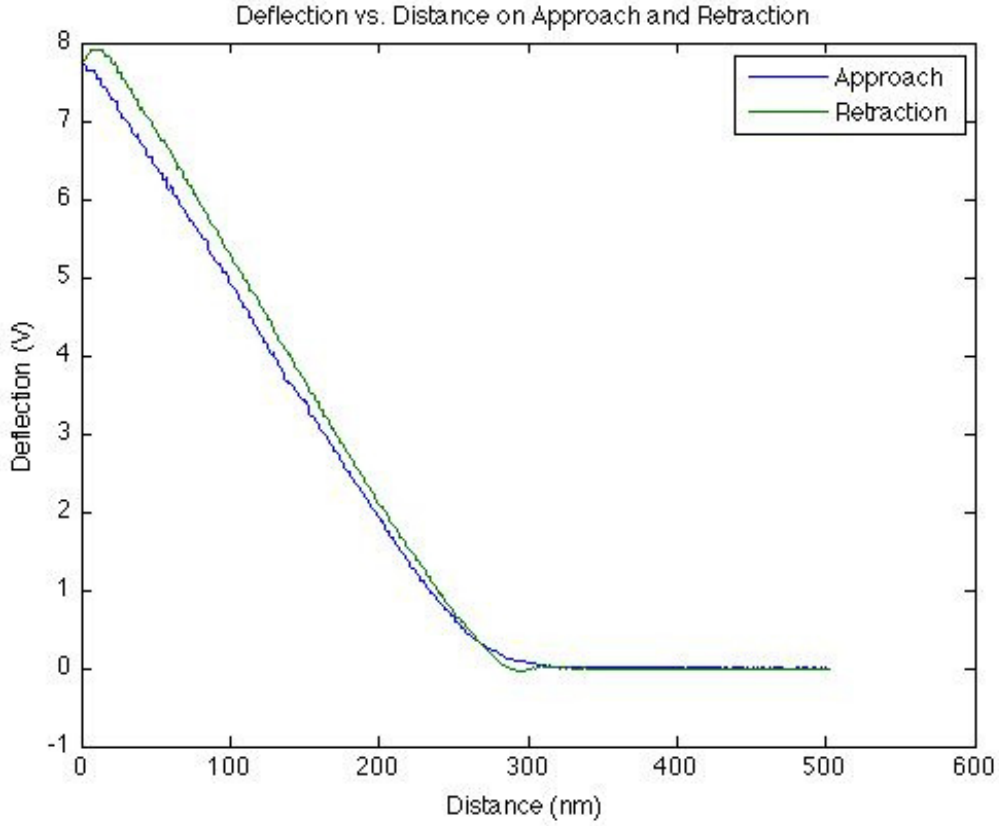
Deflection vs. Distance on Approach and Retraction
Approach
Retraction
Deflection (V)
Distance (nm)
8
7
6
5
4
3
2
1
0
-1
0
100
200
300
400
500
600

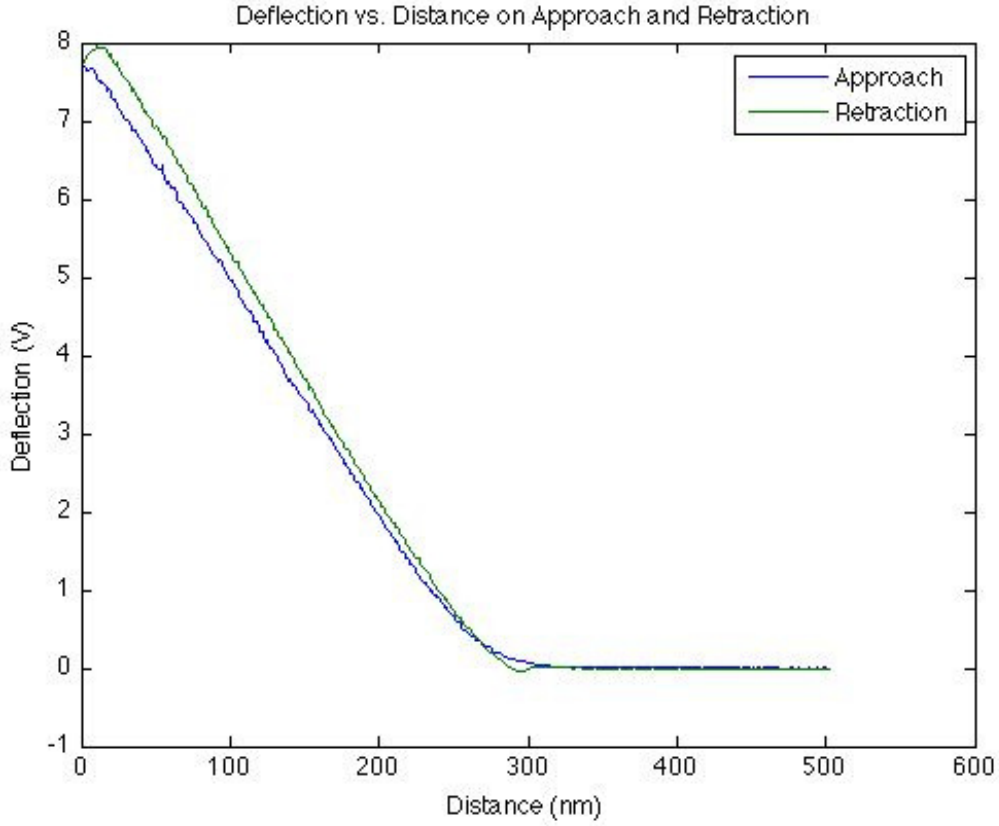
Deflection vs. Distance on Approach and Retraction
Approach
Retraction
Deflection (V)
Distance (nm)
8
7
6
5
4
3
2
1
0
-1
0
100
200
300
400
500
600

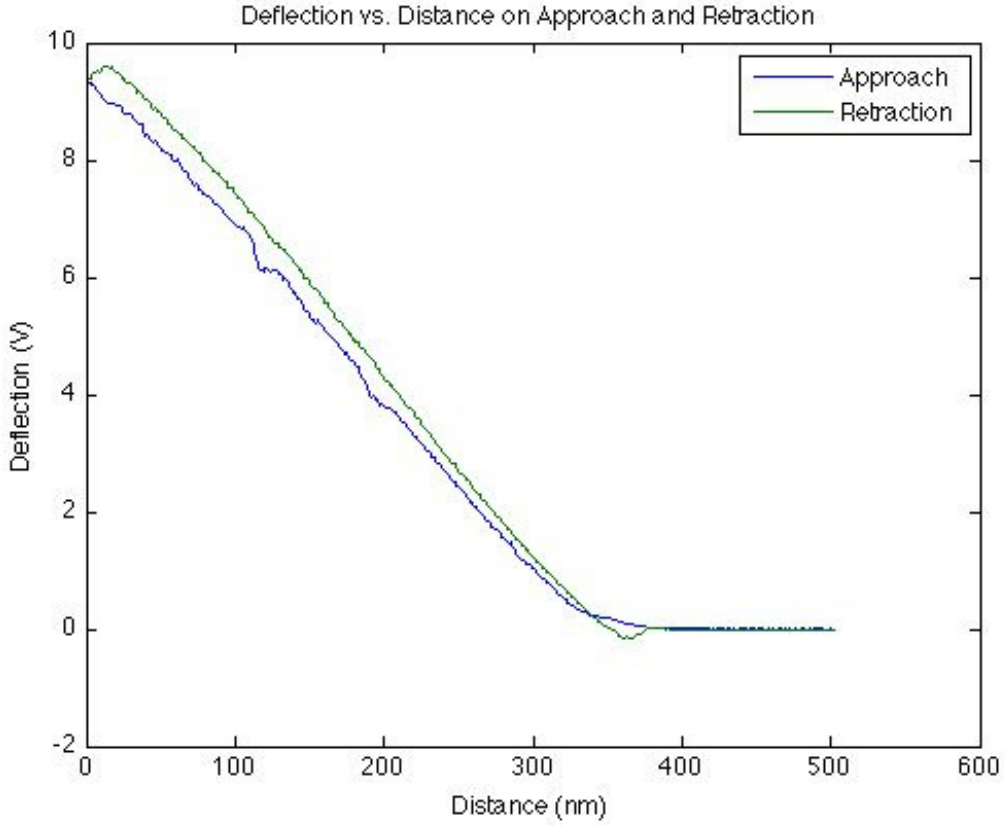
Deflection vs. Distance on Approach and Retraction
Approach
Retraction
Deflection (V)
Distance (nm)
10
8
6
4
2
0
-2
0
100
200
300
400
500
600

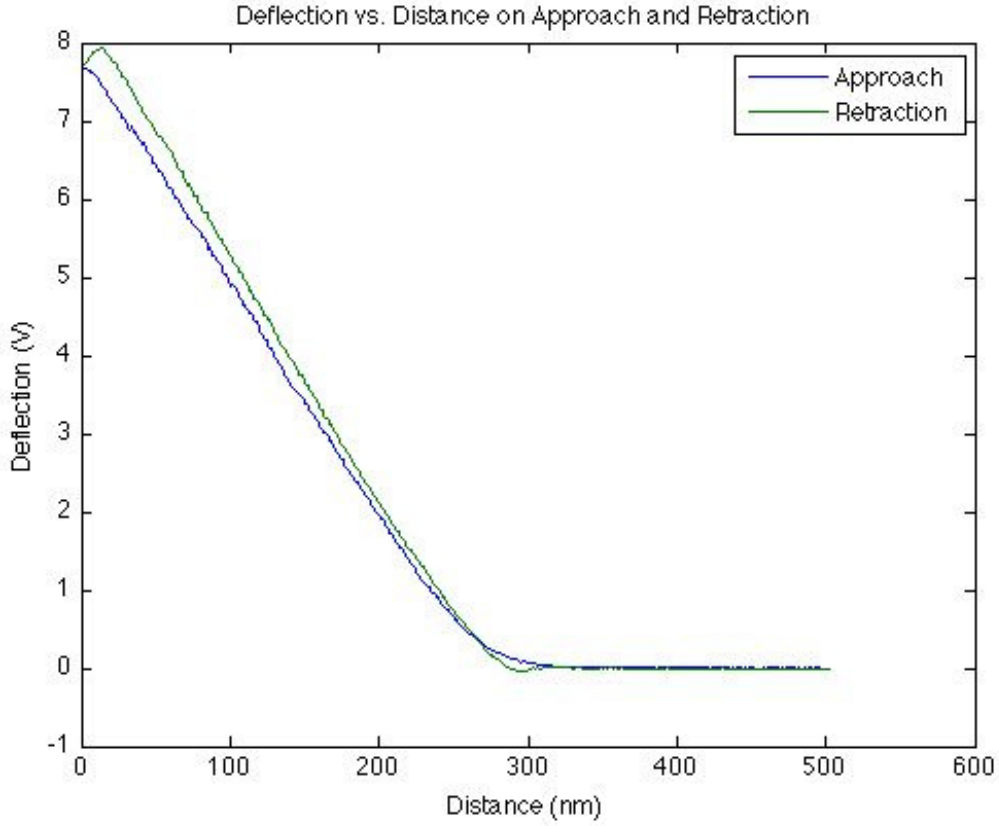
Deflection vs. Distance on Approach and Retraction
Approach
Retraction
Deflection (V)
Distance (nm)
8
7
6
5
4
3
2
1
0
-1
0
100
200
300
400
500
600

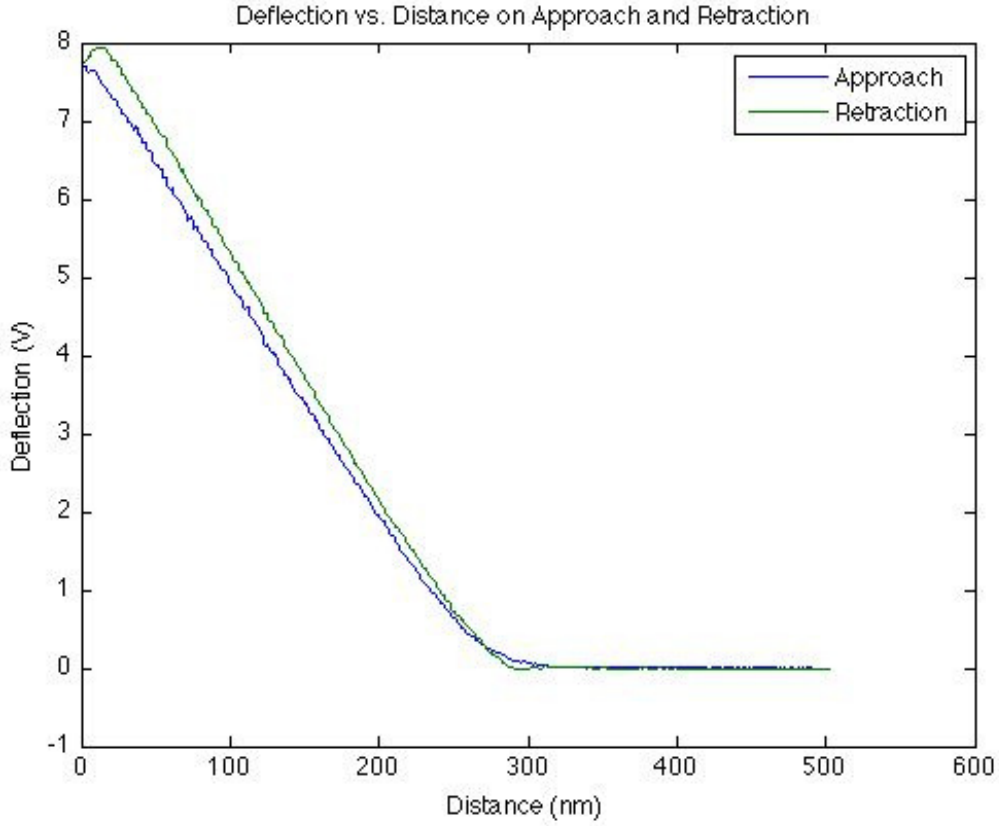
Deflection vs. Distance on Approach and Retraction
Approach
Retraction
Deflection (V)
Distance (nm)
8
7
6
5
4
3
2
1
0
-1
0
100
200
300
400
500
600

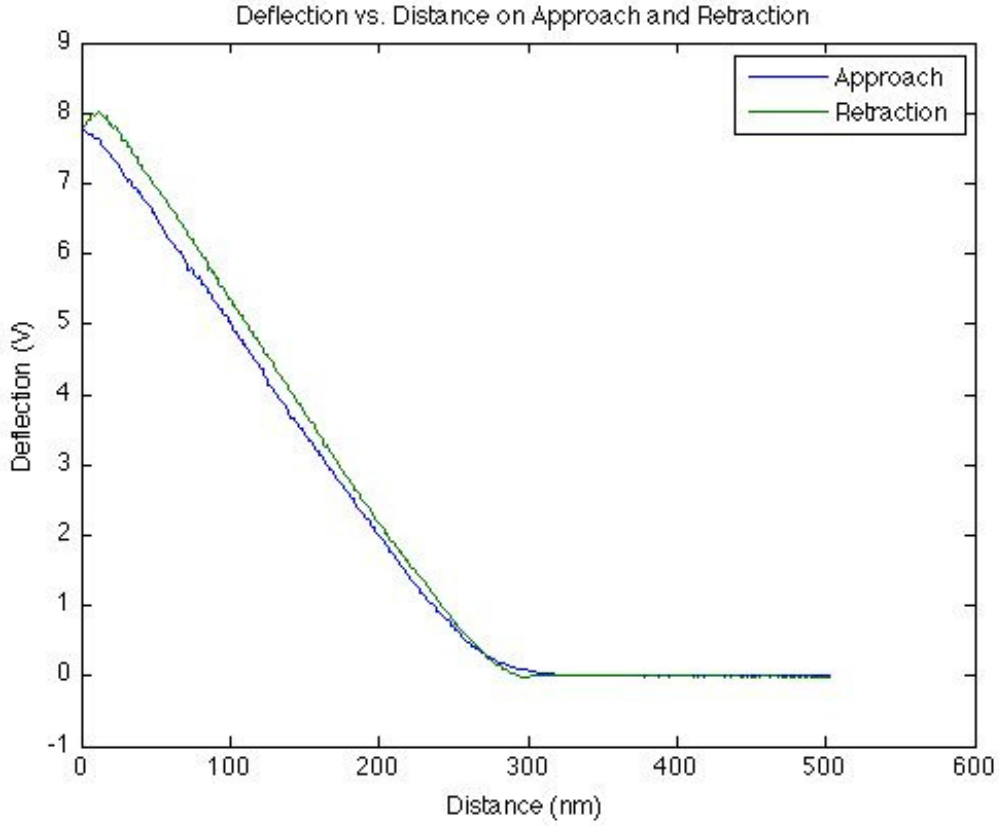
Deflection vs. Distance on Approach and Retraction
Approach
Retraction
Deflection (V)
Distance (nm)
9
8
7
6
5
4
3
2
1
0
-1
0
100
200
300
400
500
600

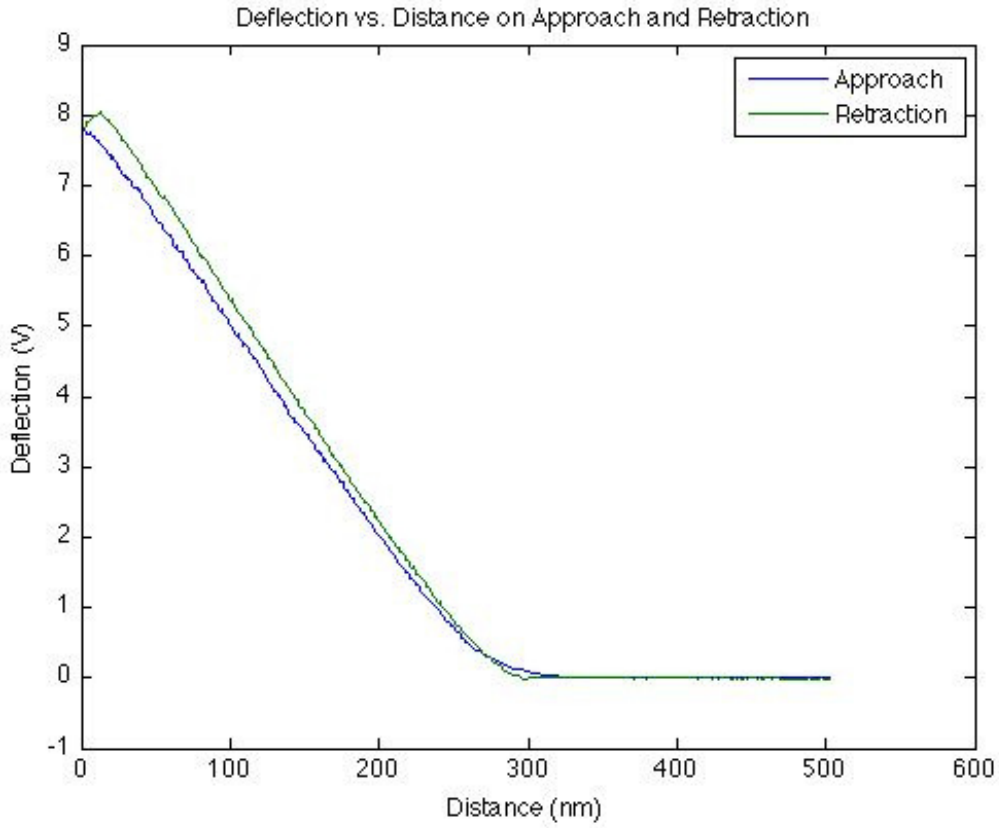
Deflection vs. Distance on Approach and Retraction
Approach
Retraction
Deflection (V)
Distance (nm)
9
8
7
6
5
4
3
2
1
0
-1
0
100
200
300
400
500
600

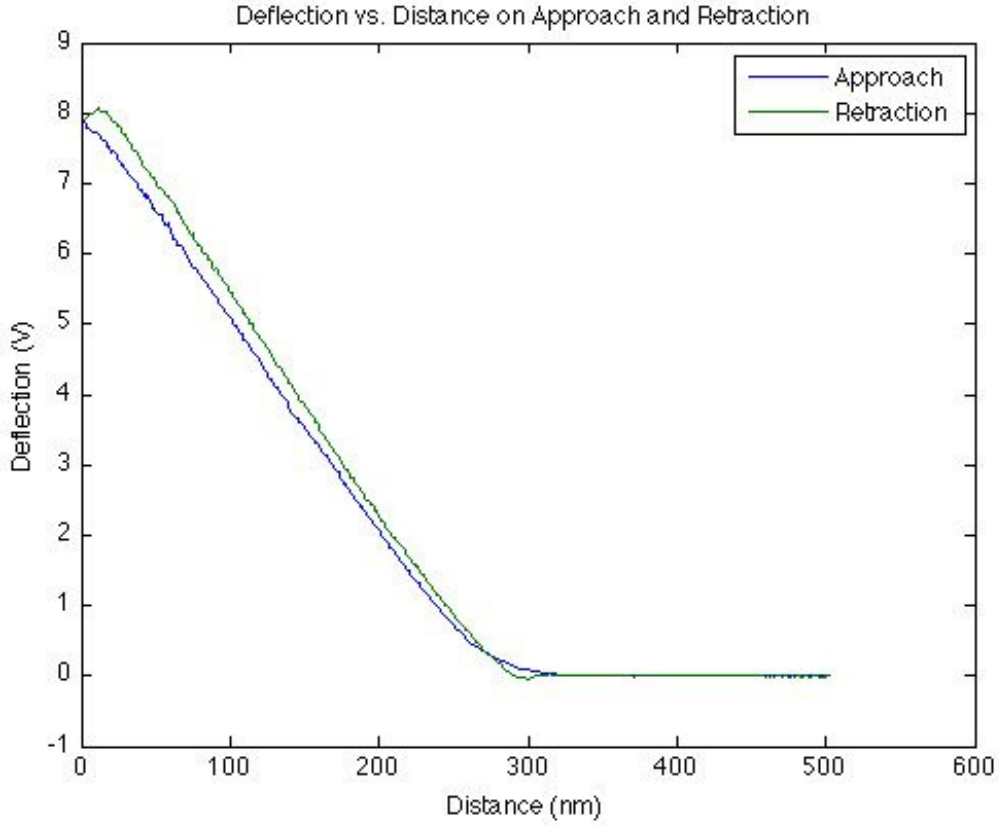
Deflection vs. Distance on Approach and Retraction
Approach
Retraction
Deflection (V)
Distance (nm)
9
8
7
6
5
4
3
2
1
0
-1
0
100
200
300
400
500
600

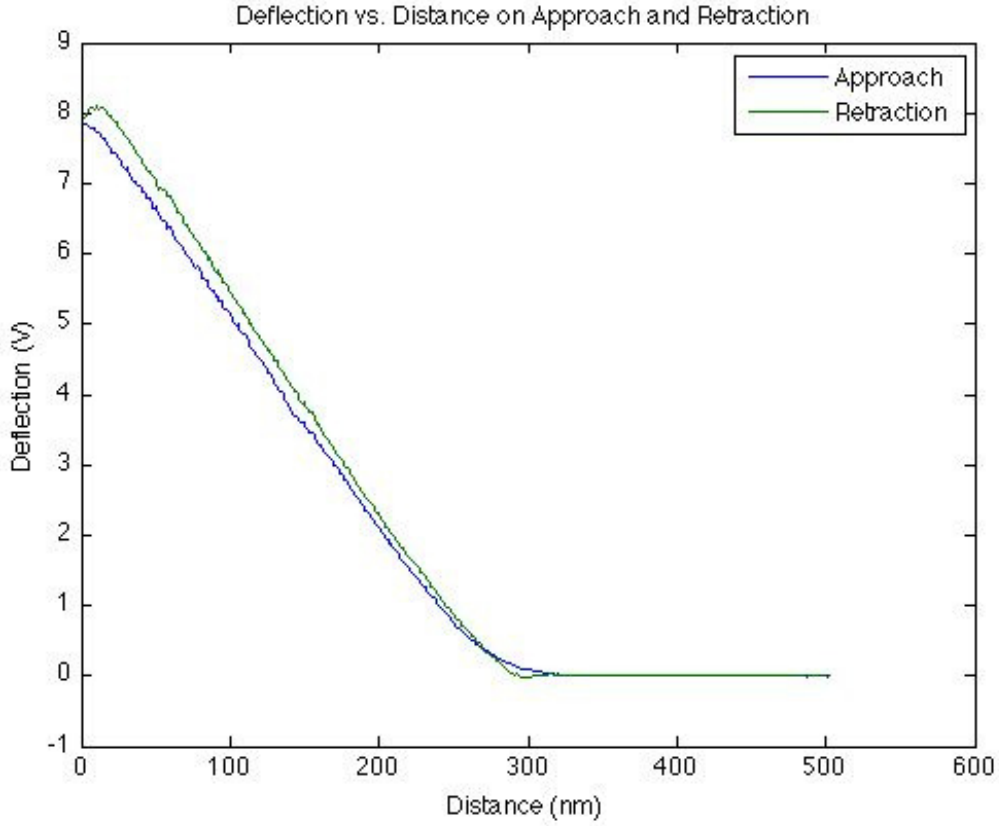
Deflection vs. Distance on Approach and Retraction
Approach
Retraction
Deflection (V)
Distance (nm)
9
8
7
6
5
4
3
2
1
0
-1
0
100
200
300
400
500
600

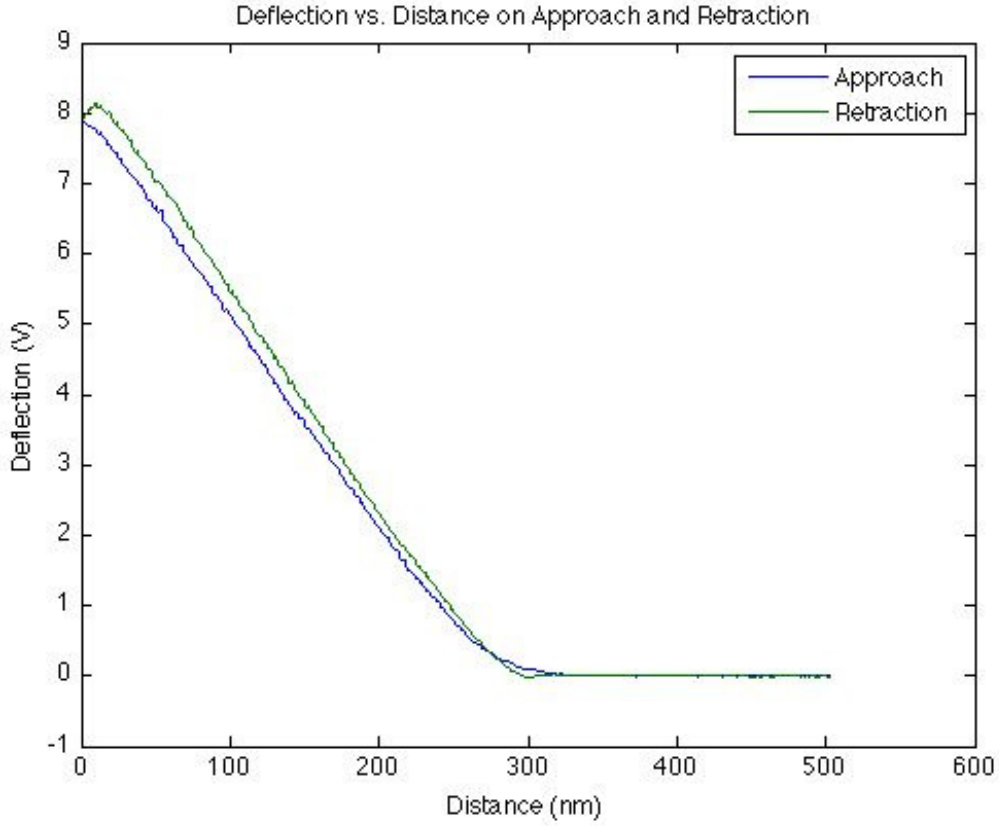
Deflection vs. Distance on Approach and Retraction
Approach
Retraction
Deflection (V)
Distance (nm)
9
8
7
6
5
4
3
2
1
0
-1
0
100
200
300
400
500
600

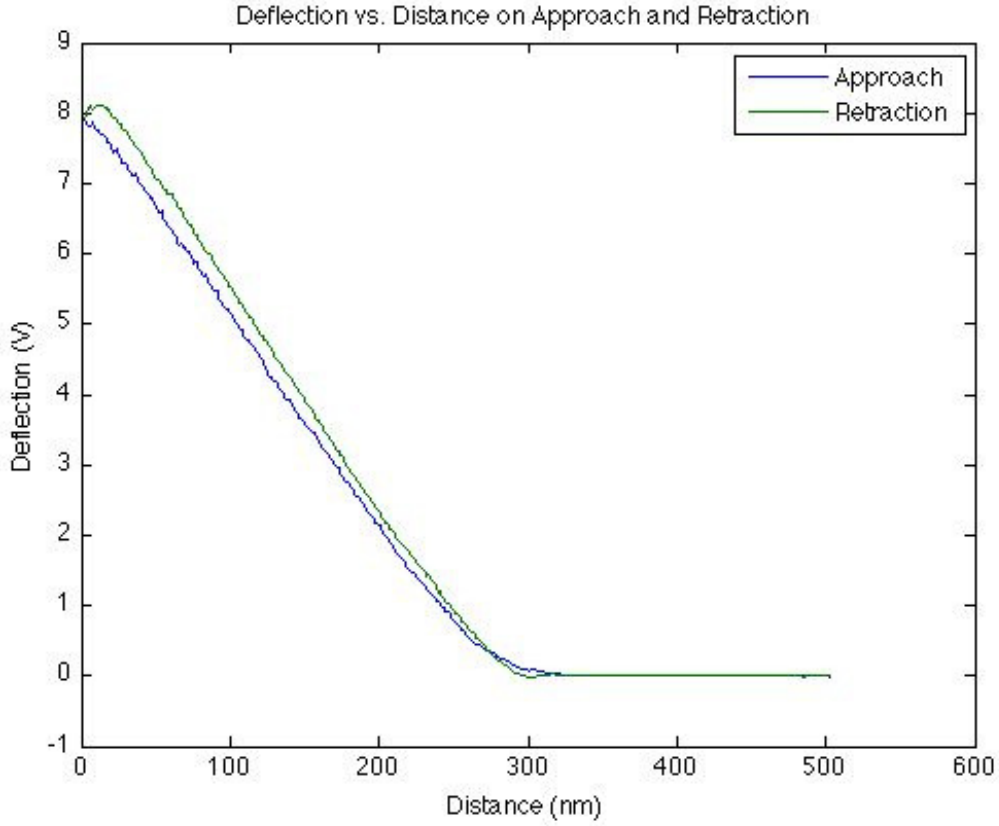
Deflection vs. Distance on Approach and Retraction
Approach
Retraction
Deflection (V)
Distance (nm)
9
8
7
6
5
4
3
2
1
0
-1
0
100
200
300
400
500
600

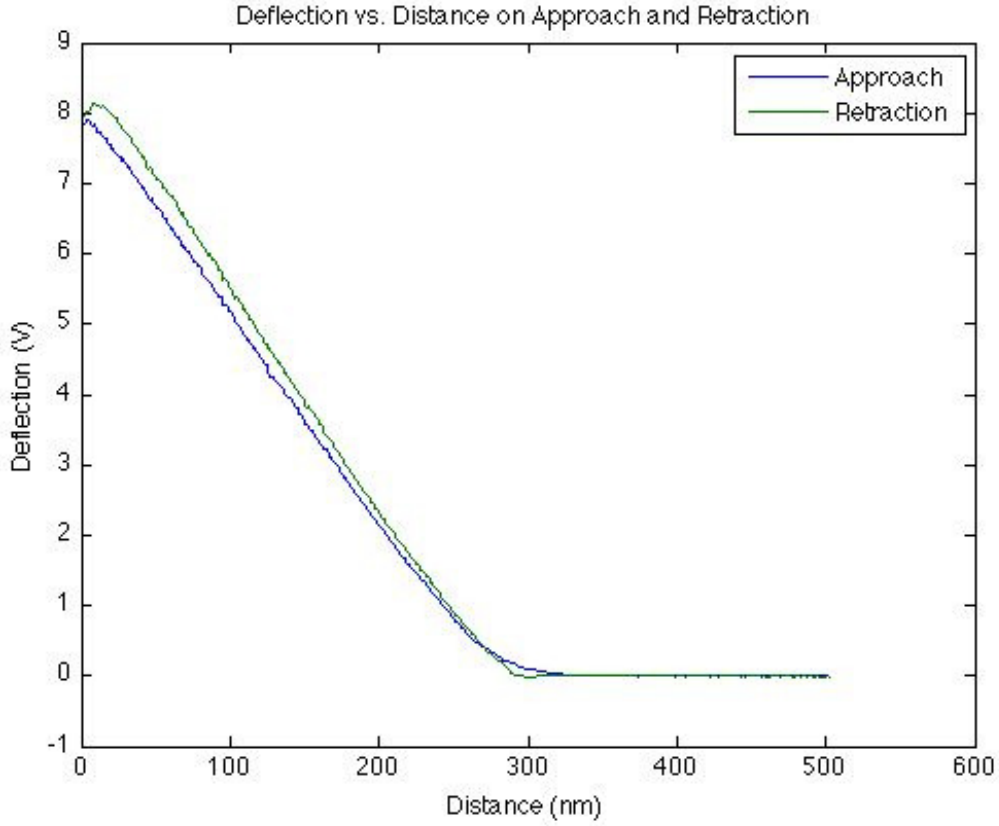
Deflection vs. Distance on Approach and Retraction
Approach
Retraction
Deflection (V)
Distance (nm)
9
8
7
6
5
4
3
2
1
0
-1
0
100
200
300
400
500
600

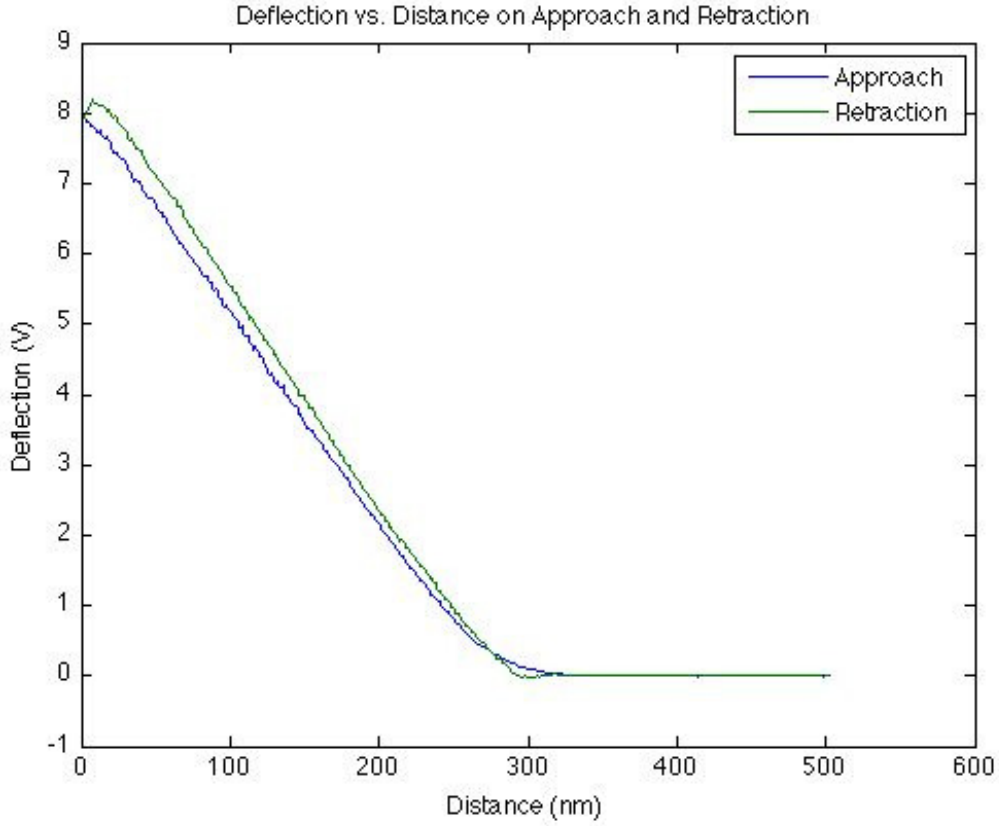
Deflection vs. Distance on Approach and Retraction
Approach
Retraction
Deflection (V)
Distance (nm)
9
8
7
6
5
4
3
2
1
0
-1
0
100
200
300
400
500
600

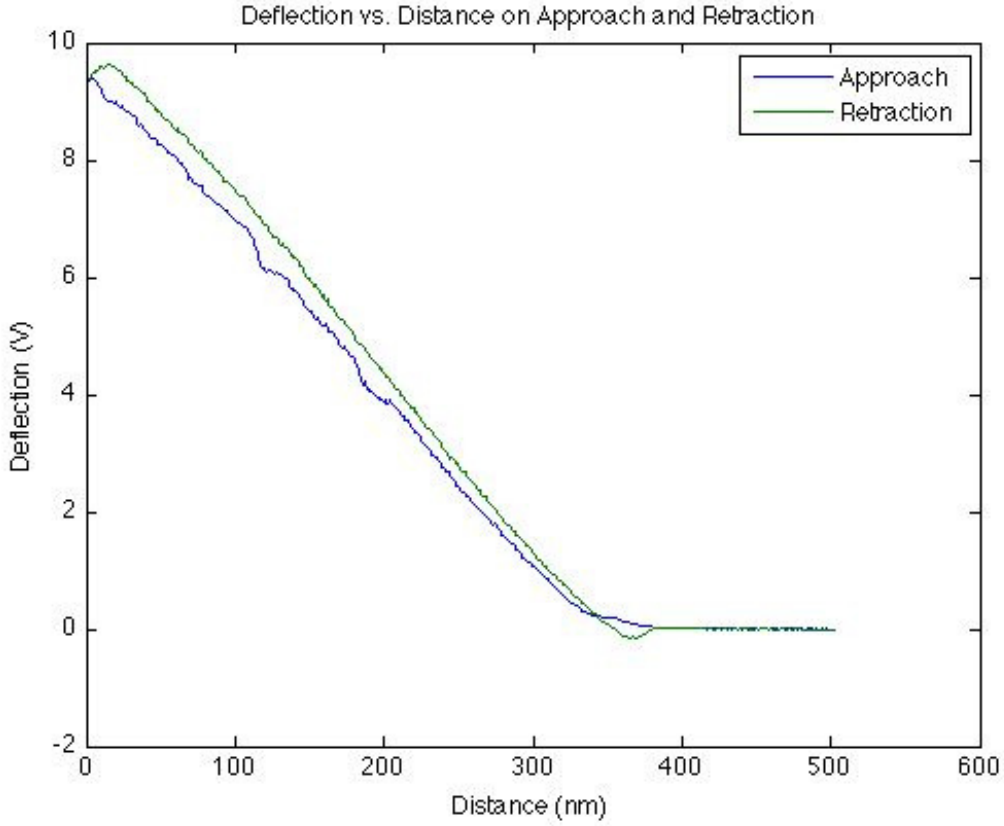
Deflection vs. Distance on Approach and Retraction
Approach
Retraction
Deflection (V)
Distance (nm)
10
8
6
4
2
0
-2
0
100
200
300
400
500
600

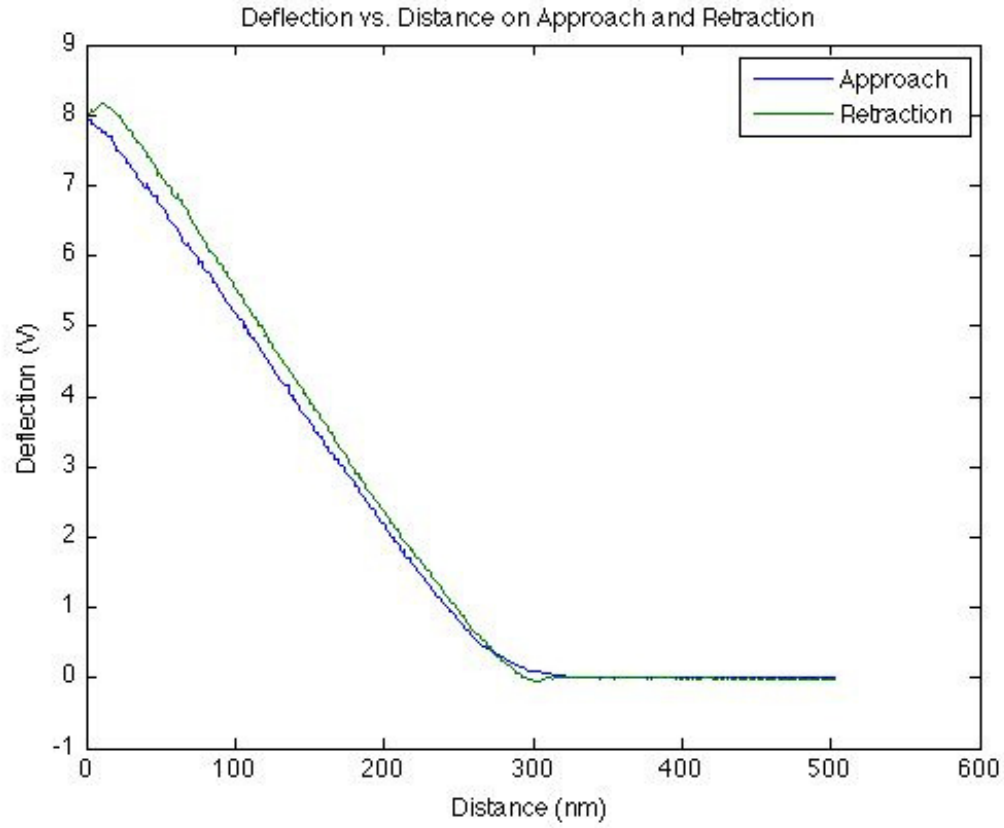
Deflection vs. Distance on Approach and Retraction
Approach
Retraction
Deflection (V)
Distance (nm)
9
8
7
6
5
4
3
2
1
0
-1
0
100
200
300
400
500
600

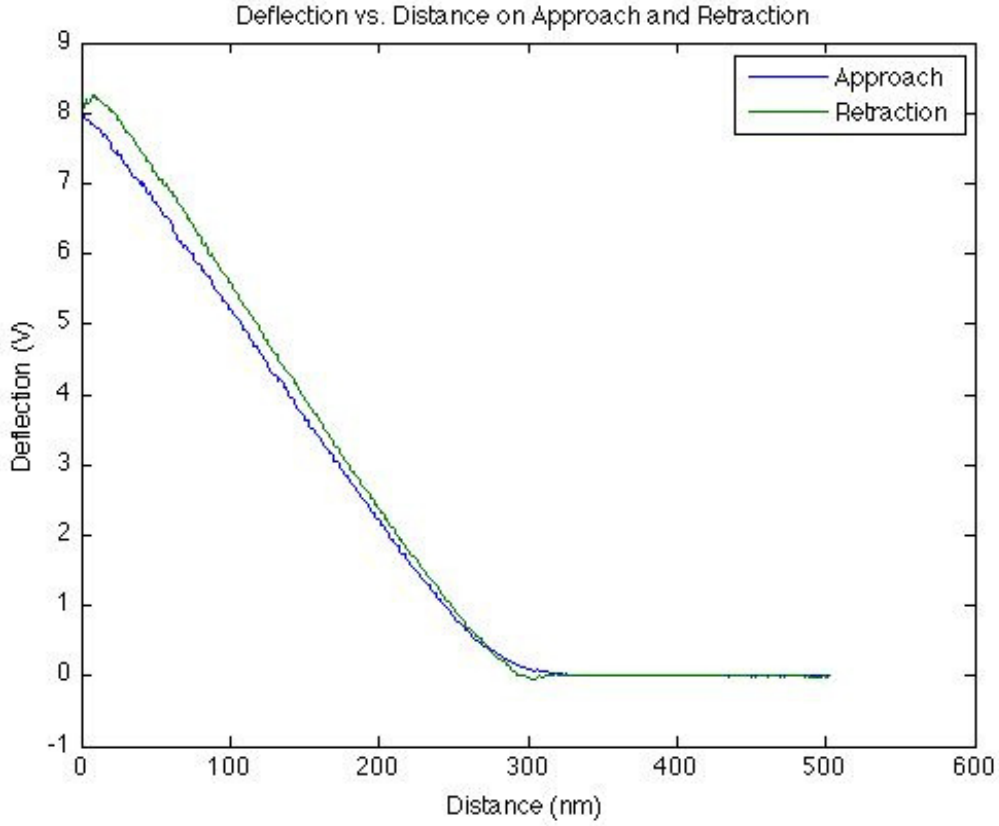
Deflection vs. Distance on Approach and Retraction
Approach
Retraction
Deflection (V)
Distance (nm)
9
8
7
6
5
4
3
2
1
0
-1
0
100
200
300
400
500
600

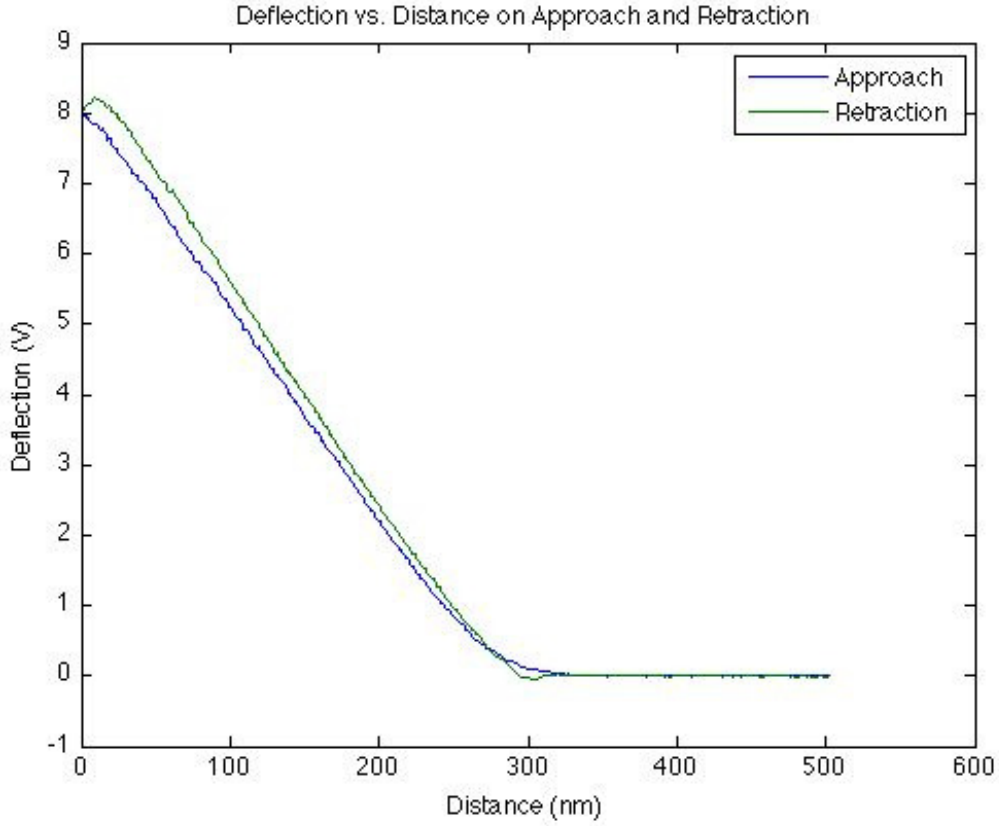
Deflection vs. Distance on Approach and Retraction
Approach
Retraction
Deflection (V)
Distance (nm)
9
8
7
6
5
4
3
2
1
0
-1
0
100
200
300
400
500
600

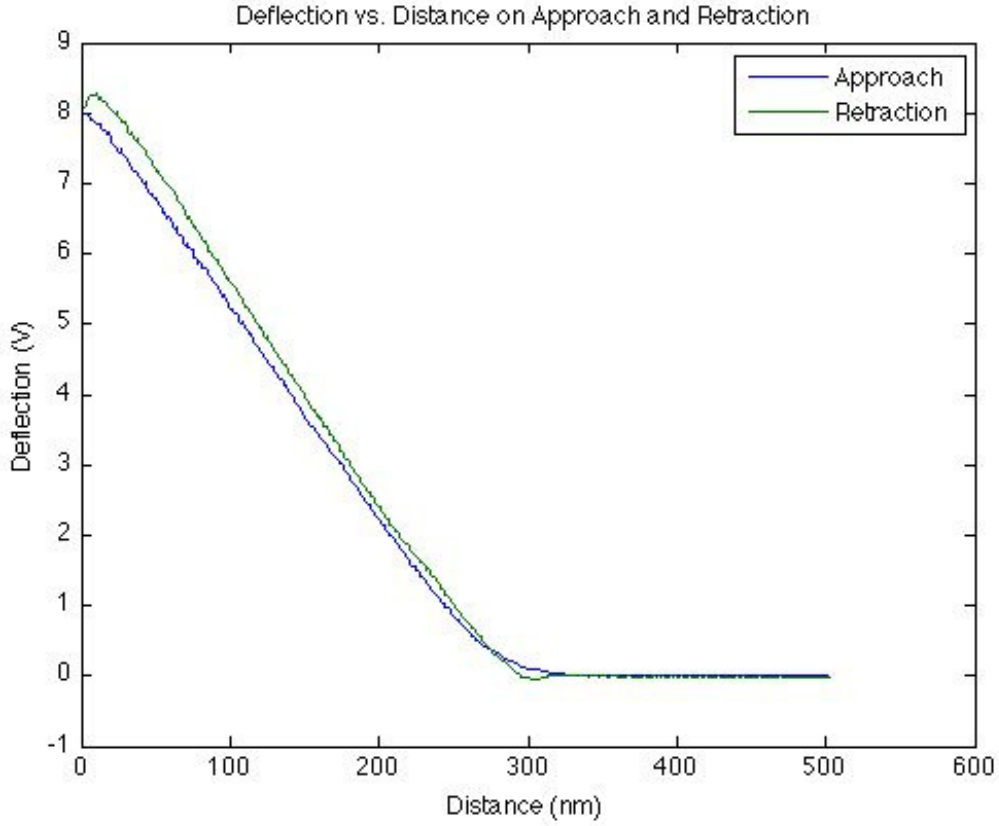
Deflection vs. Distance on Approach and Retraction
Approach
Retraction
Deflection (V)
Distance (nm)
9
8
7
6
5
4
3
2
1
0
-1
0
100
200
300
400
500
600

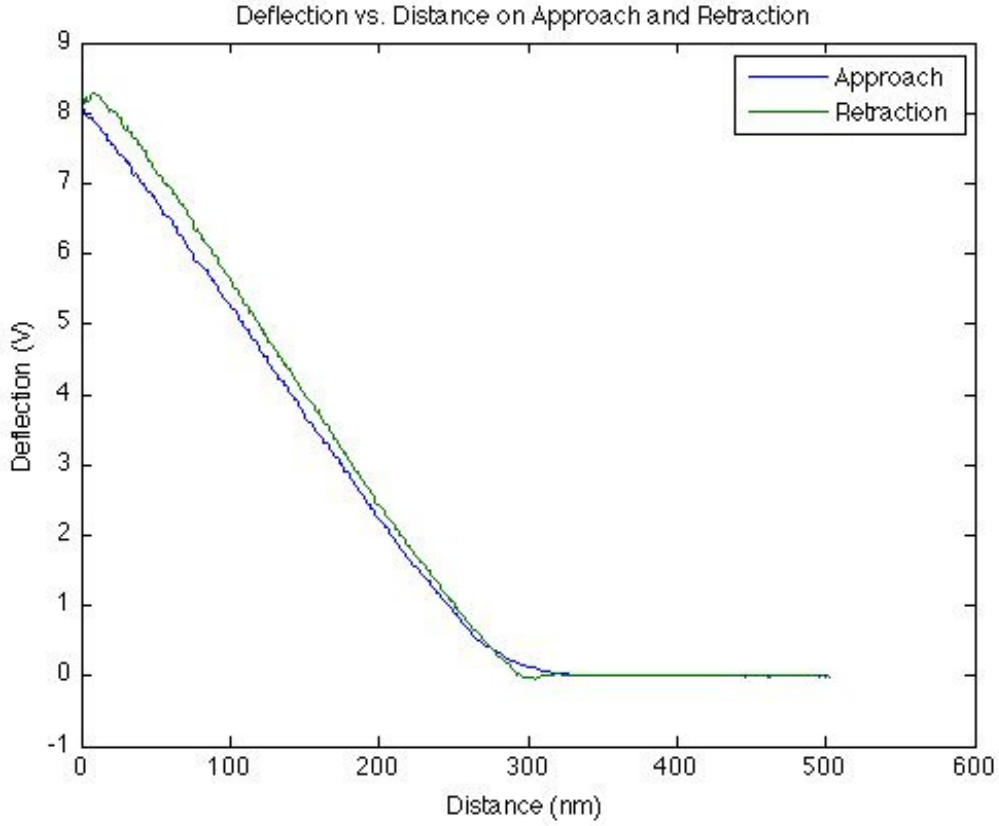
Deflection vs. Distance on Approach and Retraction
Approach
Retraction
Deflection (V)
Distance (nm)
9
8
7
6
5
4
3
2
1
0
-1
0
100
200
300
400
500
600

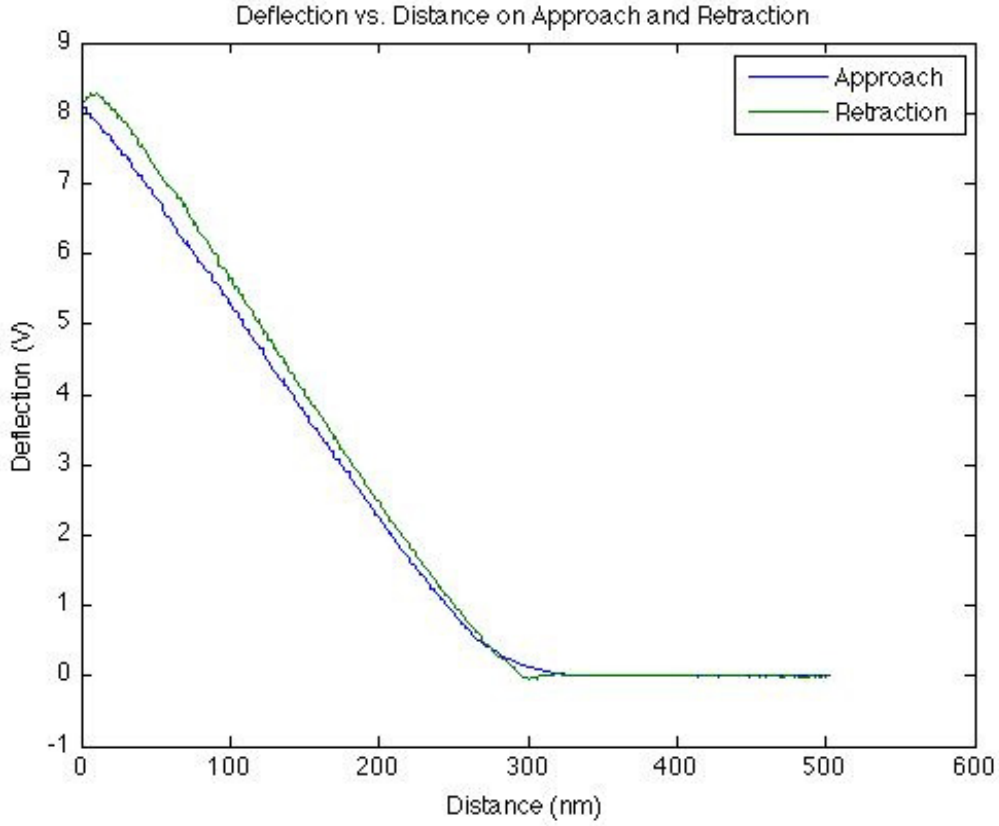
Deflection vs. Distance on Approach and Retraction
Approach
Retraction
Deflection (V)
Distance (nm)
9
8
7
6
5
4
3
2
1
0
-1
0
100
200
300
400
500
600

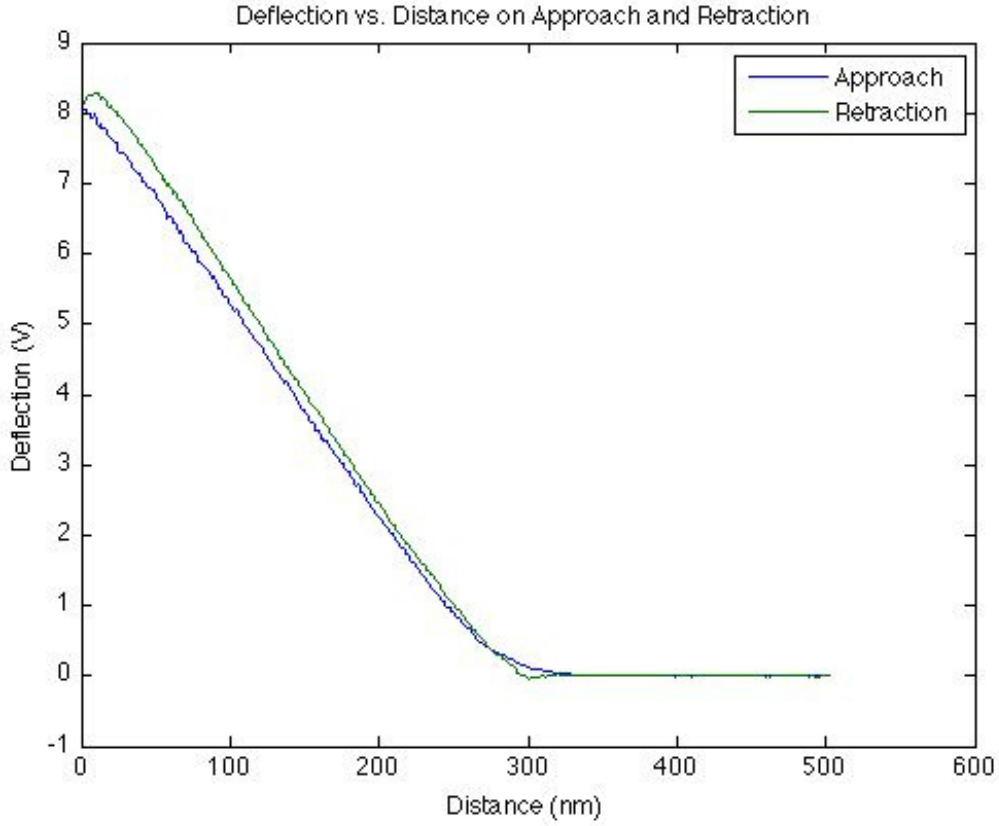
Deflection vs. Distance on Approach and Retraction
Approach
Retraction
Deflection (V)
Distance (nm)
9
8
7
6
5
4
3
2
1
0
-1
0
100
200
300
400
500
600

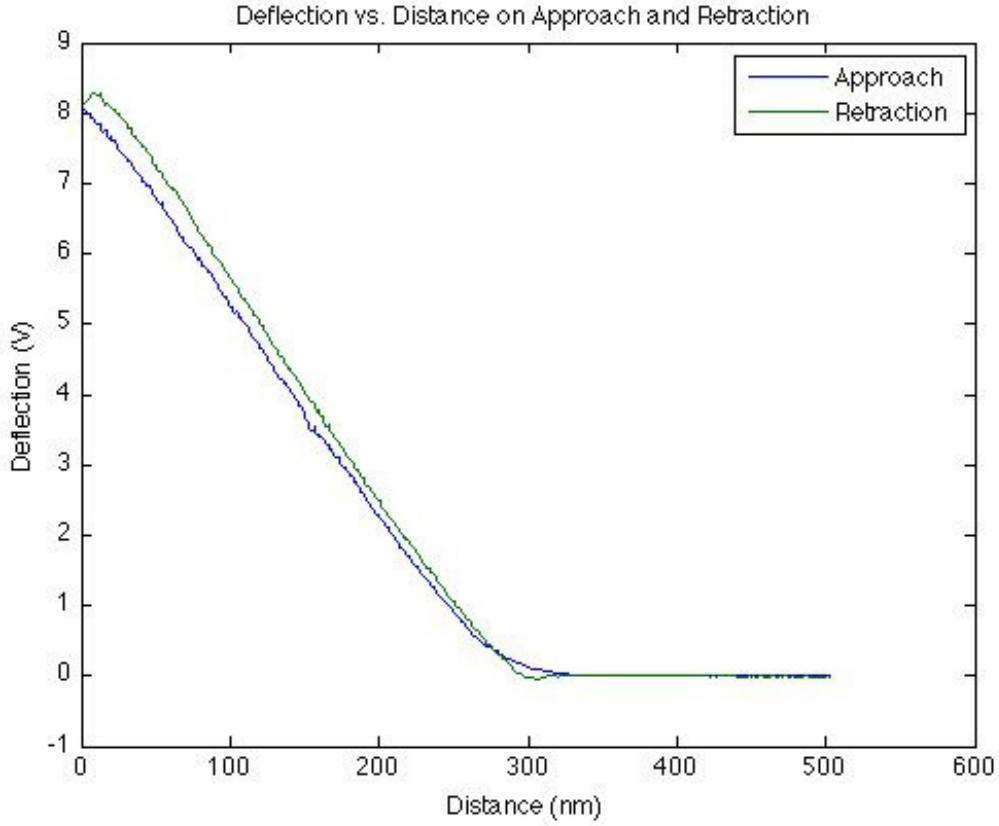
Deflection vs. Distance on Approach and Retraction
Approach
Retraction
Deflection (V)
Distance (nm)
9
8
7
6
5
4
3
2
1
0
-1
0
100
200
300
400
500
600

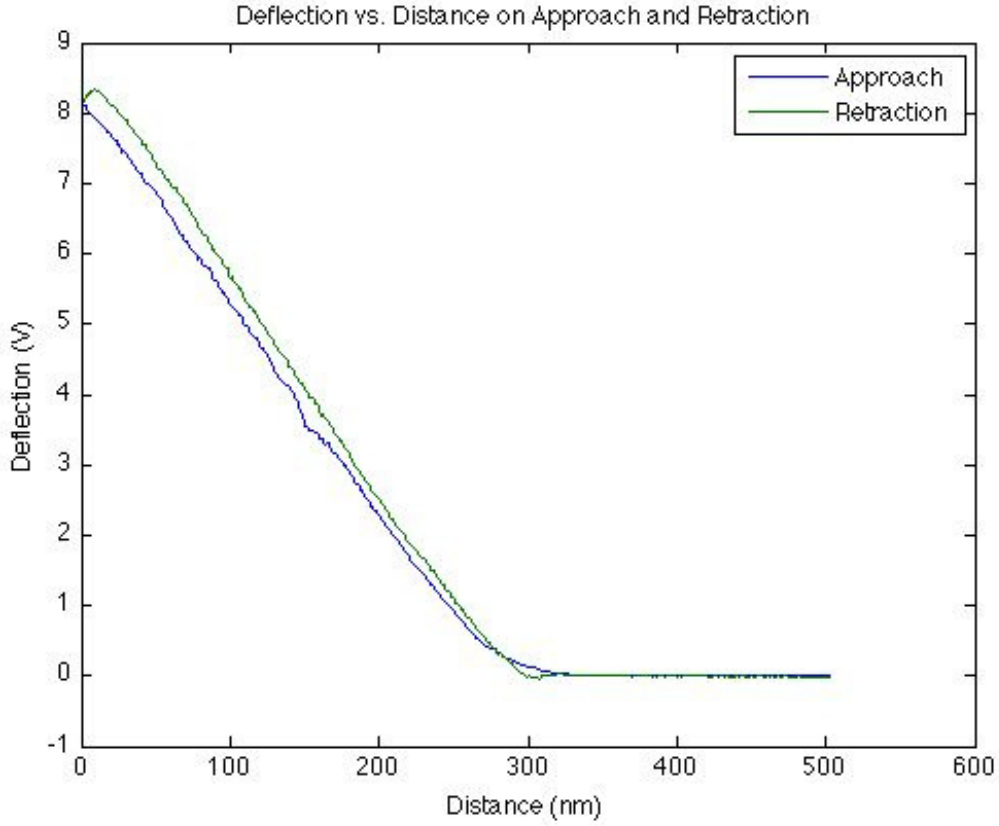
Deflection vs. Distance on Approach and Retraction
Approach
Retraction
Deflection (V)
Distance (nm)
9
8
7
6
5
4
3
2
1
0
-1
0
100
200
300
400
500
600

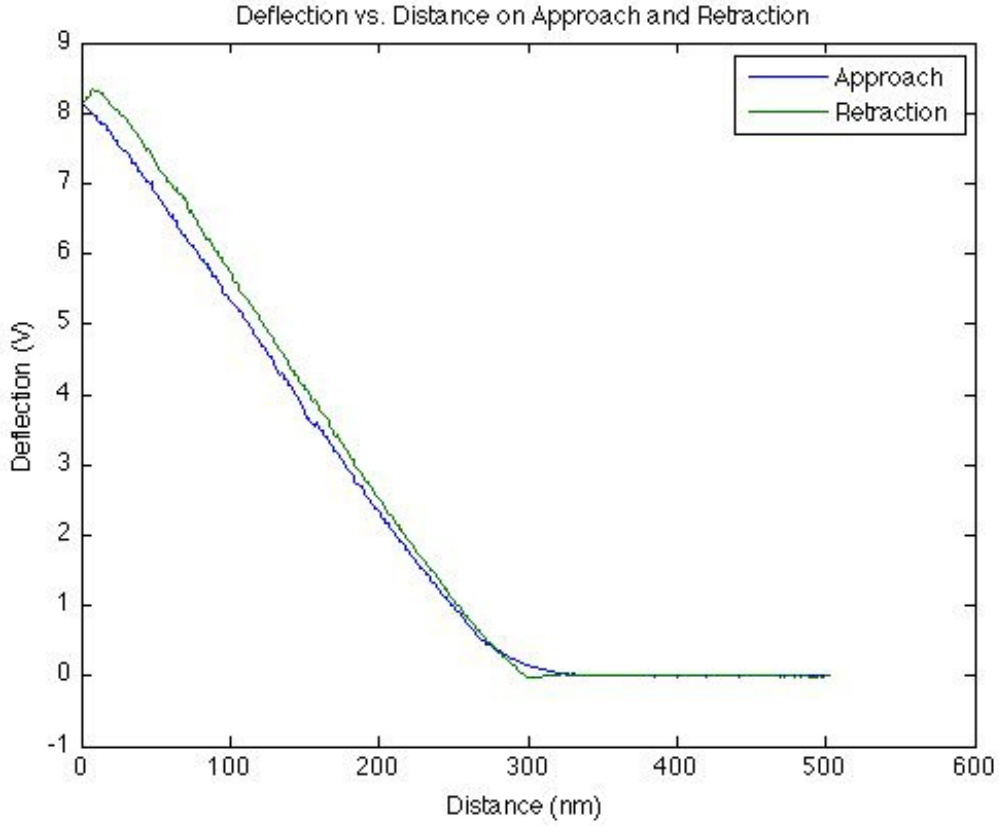
Deflection vs. Distance on Approach and Retraction
Approach
Retraction
Deflection (V)
Distance (nm)
9
8
7
6
5
4
3
2
1
0
-1
0
100
200
300
400
500
600

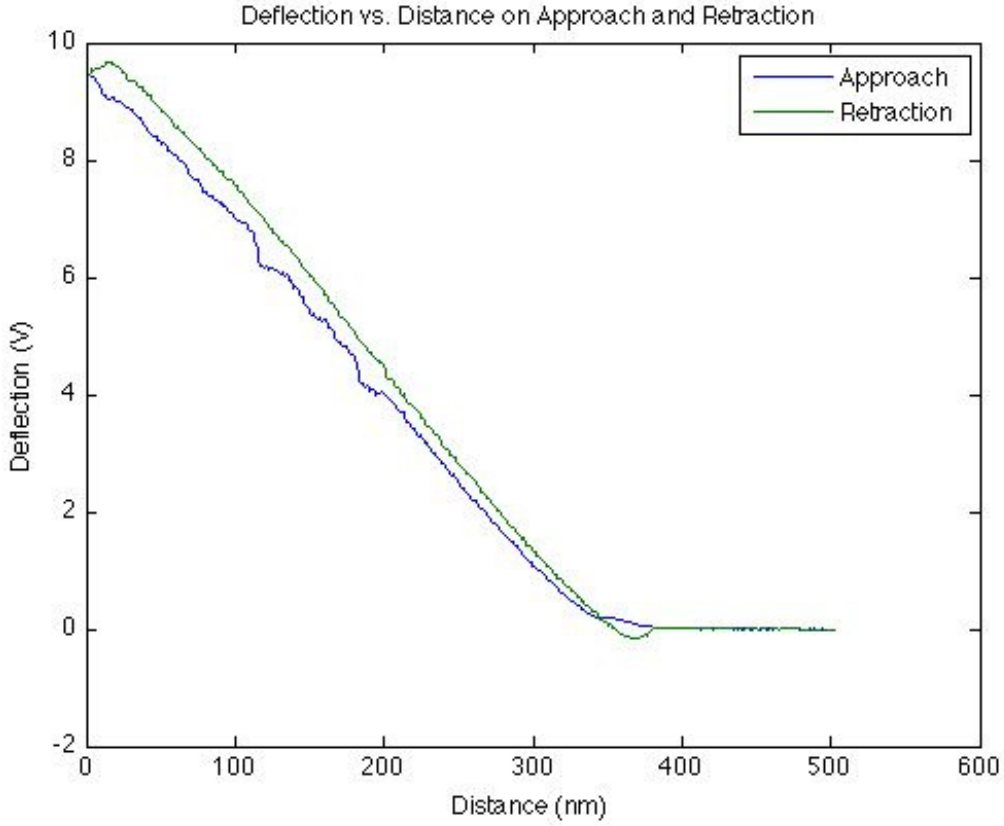
Deflection vs. Distance on Approach and Retraction
Approach
Retraction
Deflection (V)
Distance (nm)
10
8
6
4
2
0
-2
0
100
200
300
400
500
600

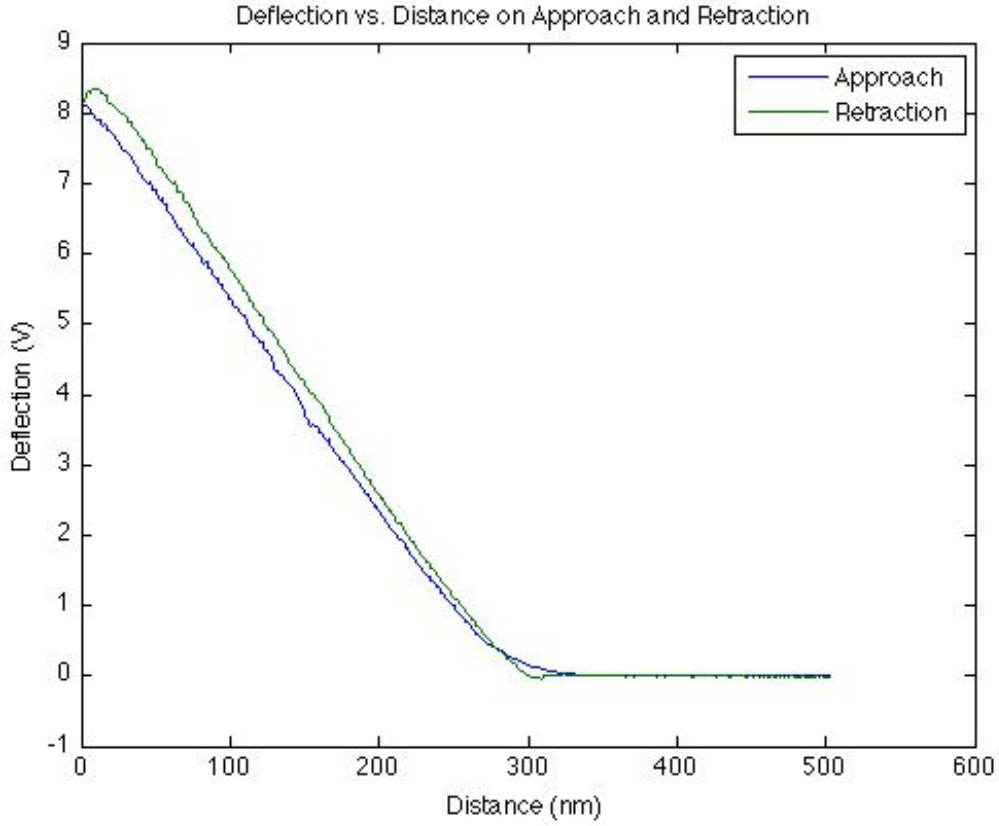
Deflection vs. Distance on Approach and Retraction
Approach
Retraction
Deflection (V)
Distance (nm)
9
8
7
6
5
4
3
2
1
0
-1
0
100
200
300
400
500
600

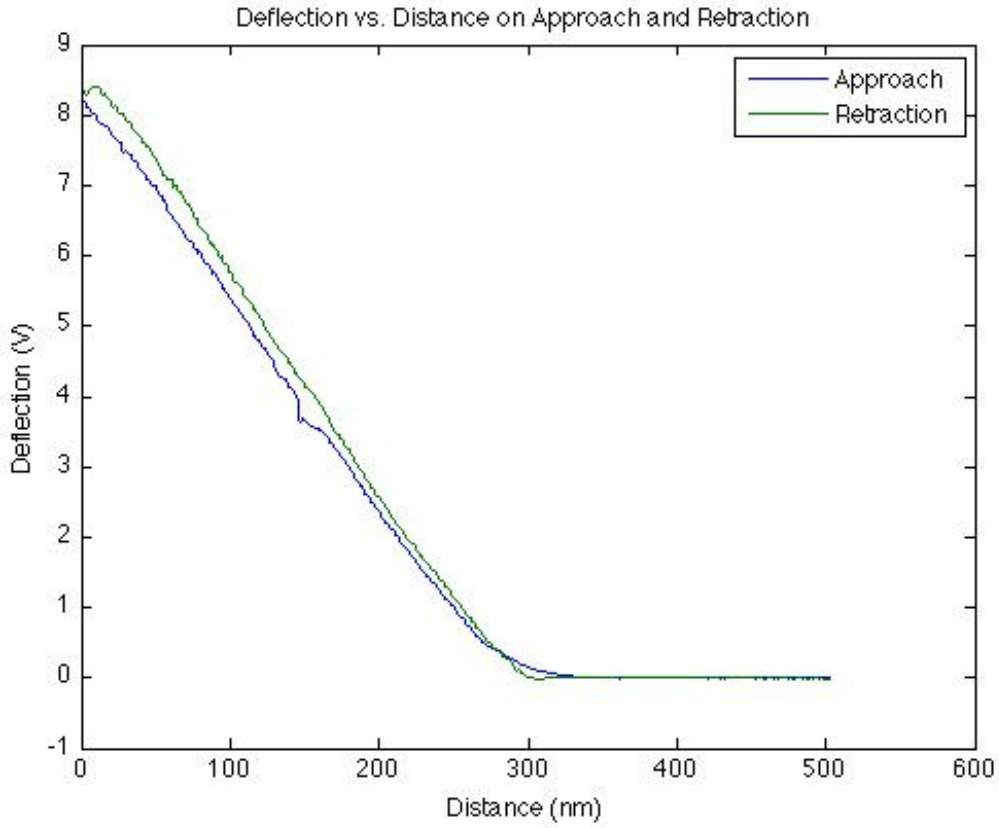
Deflection vs. Distance on Approach and Retraction
Approach
Retraction
Deflection (V)
Distance (nm)
9
8
7
6
5
4
3
2
1
0
-1
0
100
200
300
400
500
600

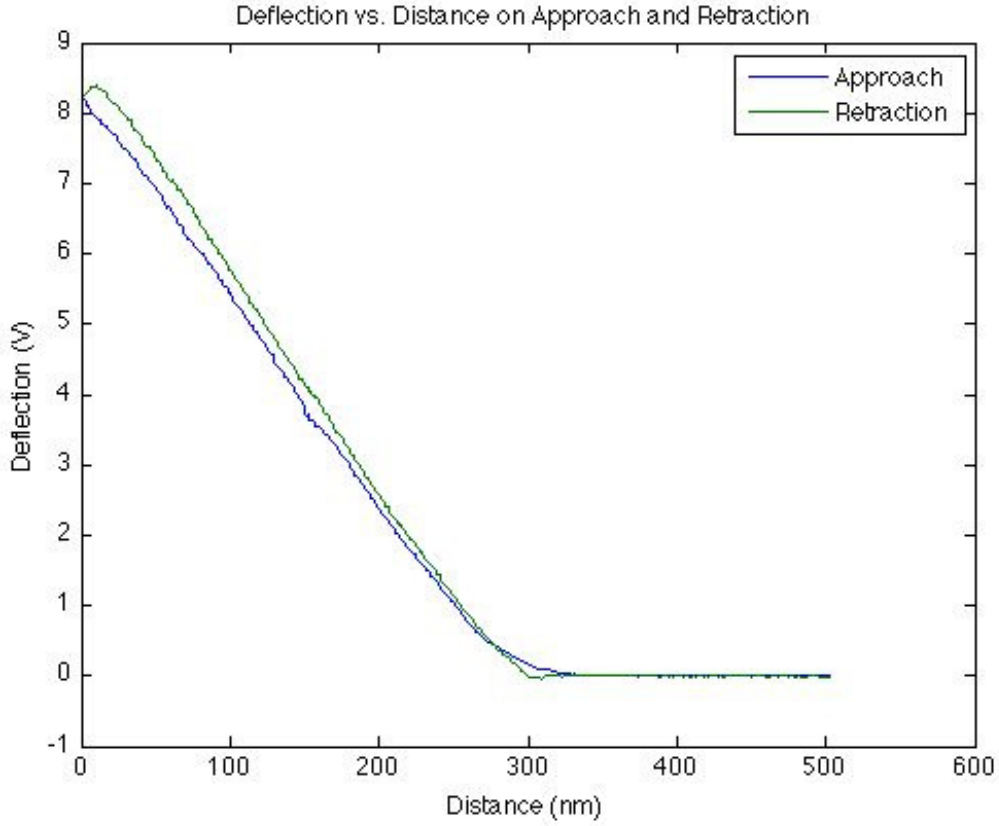
Deflection vs. Distance on Approach and Retraction
Approach
Retraction
Deflection (V)
Distance (nm)
9
8
7
6
5
4
3
2
1
0
-1
0
100
200
300
400
500
600

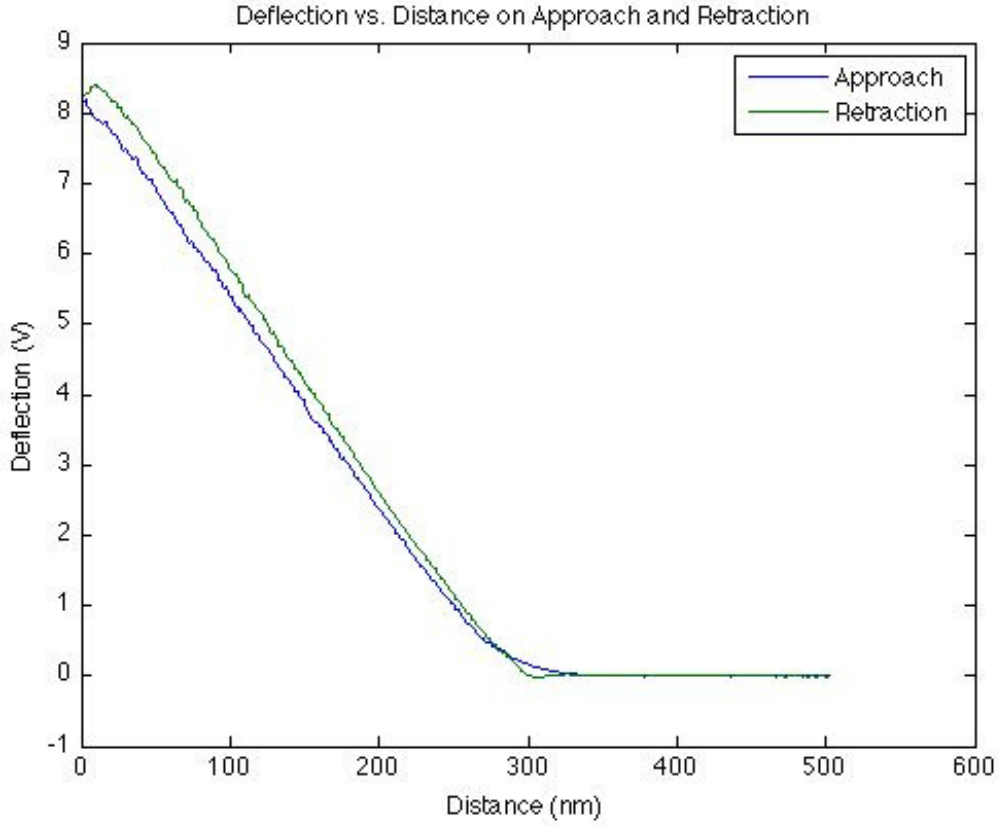
Deflection vs. Distance on Approach and Retraction
Approach
Retraction
Deflection (V)
Distance (nm)
9
8
7
6
5
4
3
2
1
0
-1
0
100
200
300
400
500
600

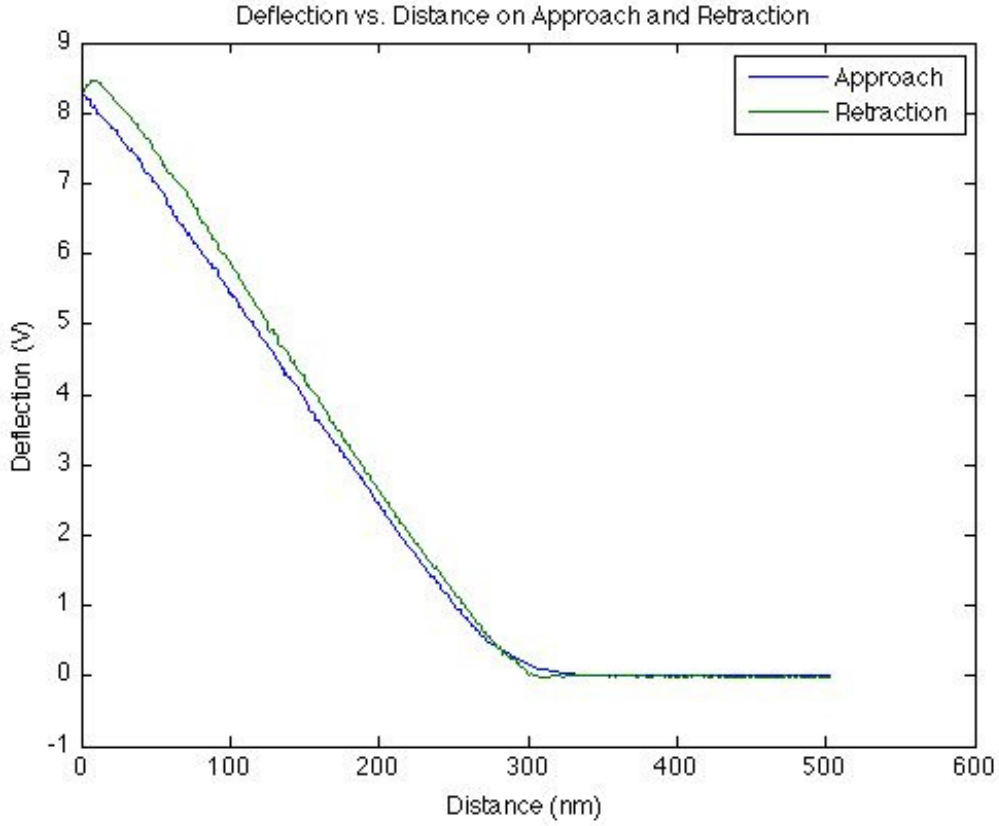
Deflection vs. Distance on Approach and Retraction
Approach
Retraction
Deflection (V)
Distance (nm)
9
8
7
6
5
4
3
2
1
0
-1
0
100
200
300
400
500
600

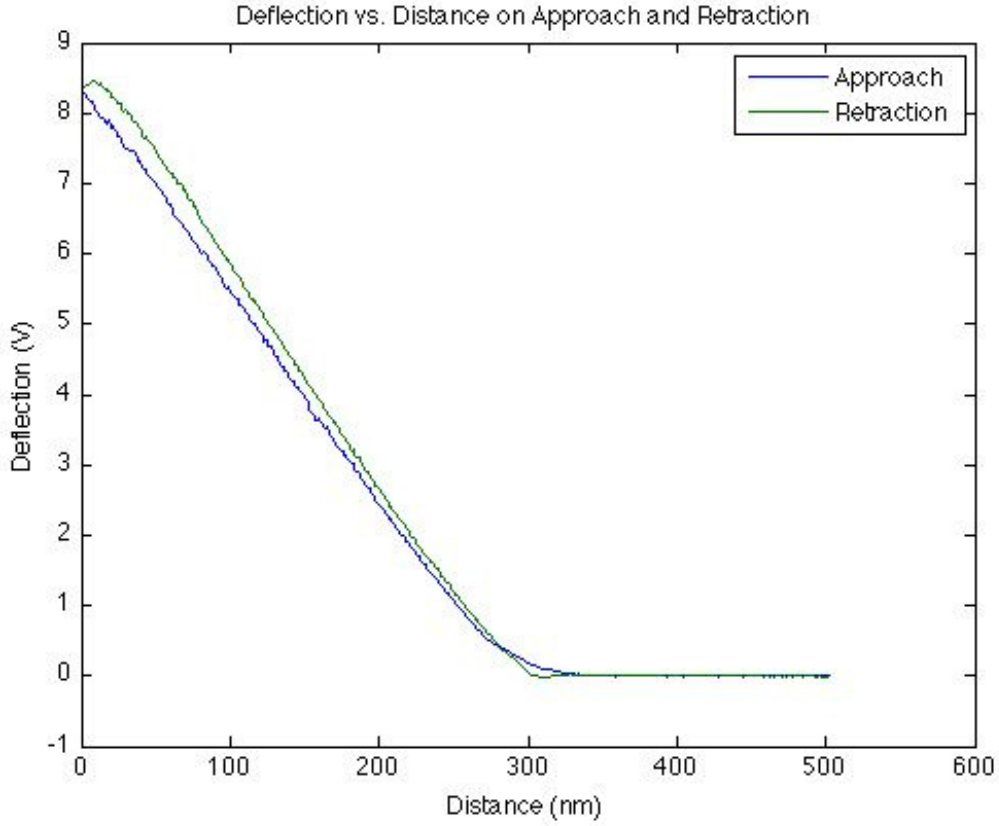
Deflection vs. Distance on Approach and Retraction
Approach
Retraction
Deflection (V)
Distance (nm)
9
8
7
6
5
4
3
2
1
0
-1
0
100
200
300
400
500
600

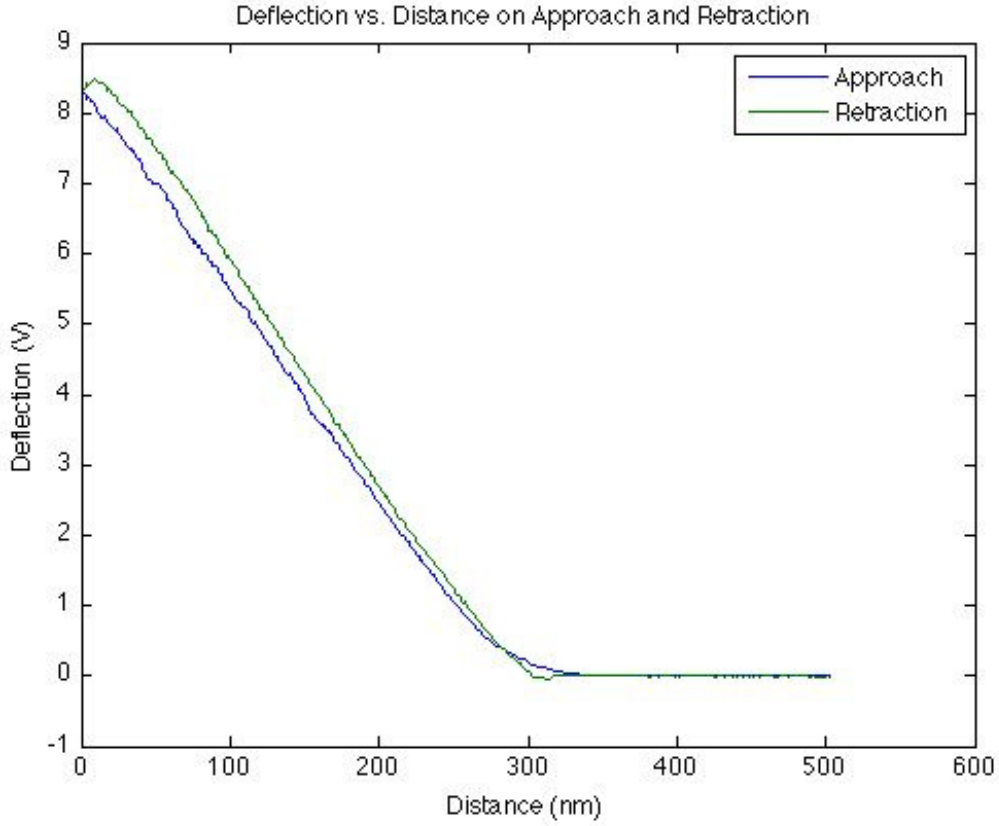
Deflection vs. Distance on Approach and Retraction
Approach
Retraction
Deflection (V)
Distance (nm)
9
8
7
6
5
4
3
2
1
0
-1
0
100
200
300
400
500
600

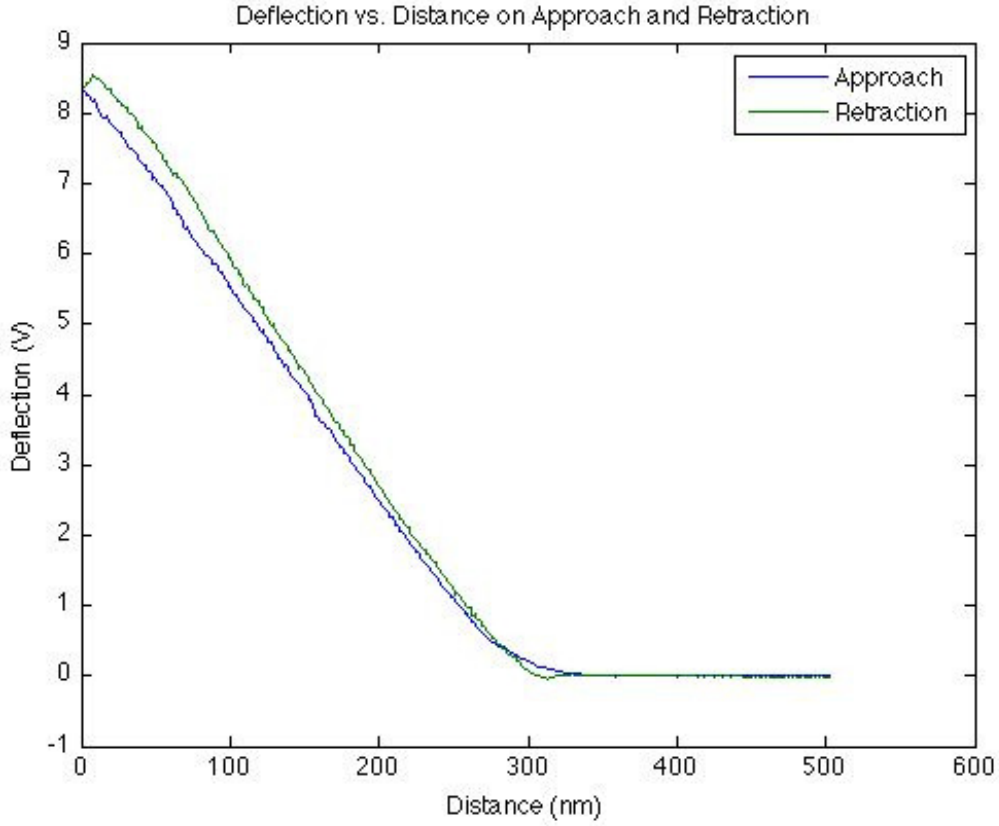
Deflection vs. Distance on Approach and Retraction
Approach
Retraction
Deflection (V)
Distance (nm)
9
8
7
6
5
4
3
2
1
0
-1
0
100
200
300
400
500
600

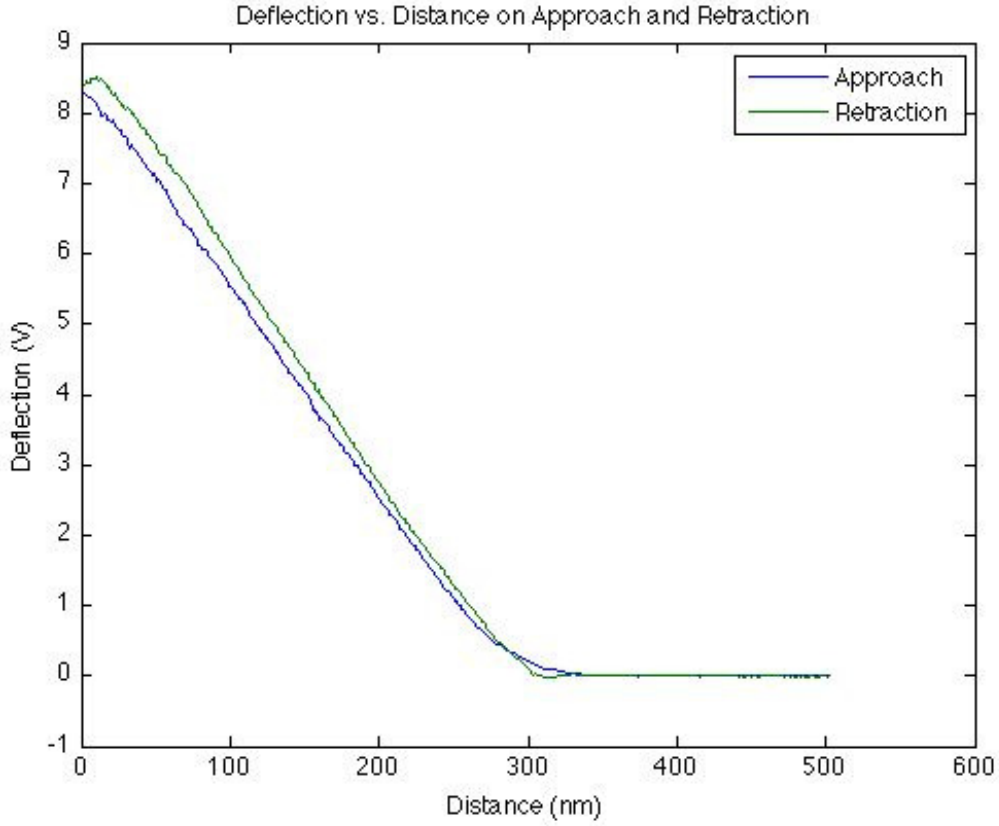
Deflection vs. Distance on Approach and Retraction
Approach
Retraction
Deflection (V)
Distance (nm)
9
8
7
6
5
4
3
2
1
0
-1
0
100
200
300
400
500
600

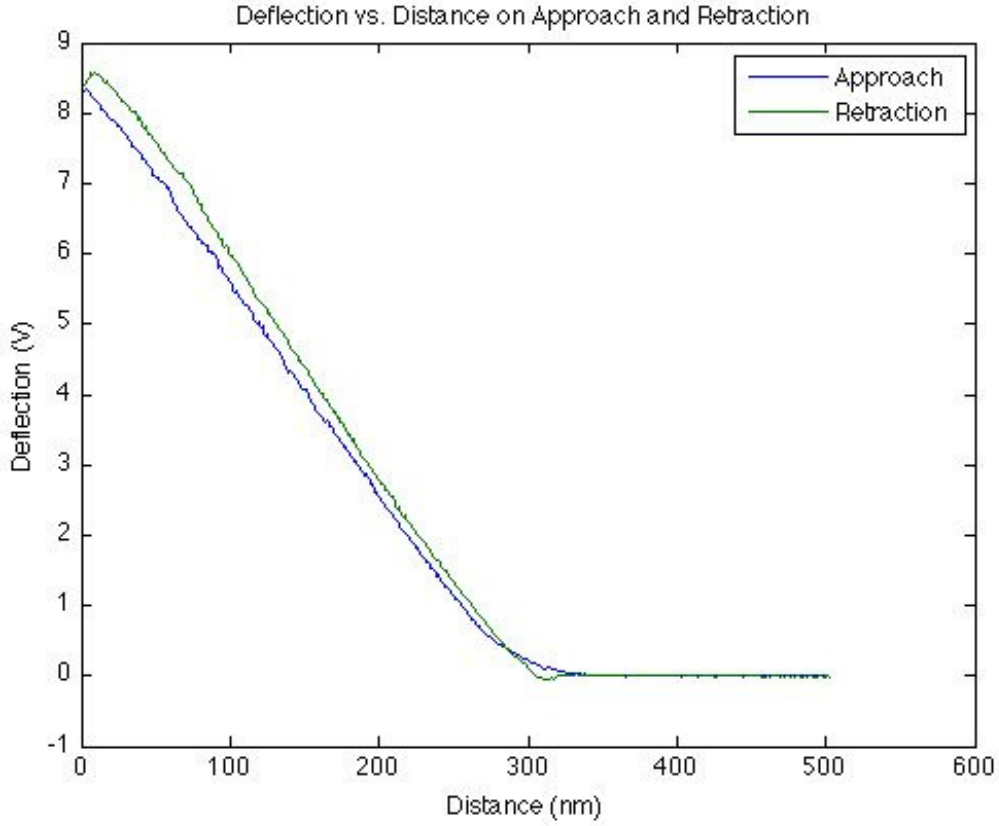
Deflection vs. Distance on Approach and Retraction
Approach
Retraction
Deflection (V)
Distance (nm)
9
8
7
6
5
4
3
2
1
0
-1
0
100
200
300
400
500
600

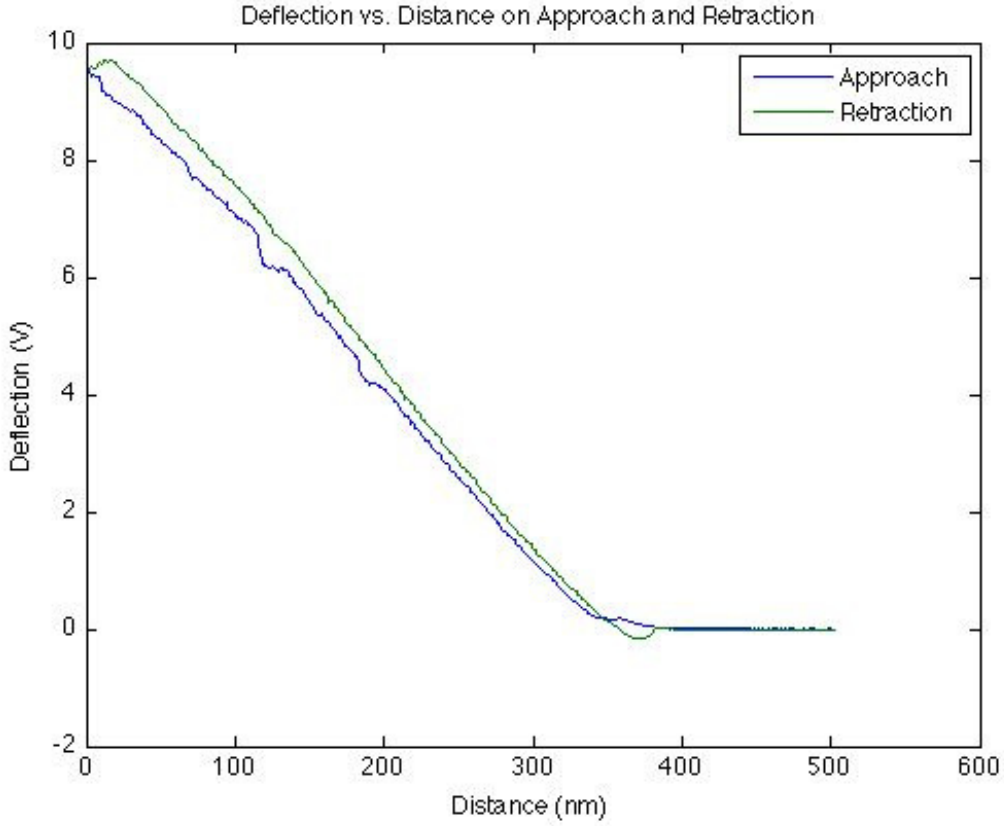
Deflection vs. Distance on Approach and Retraction
Approach
Retraction
Deflection (V)
Distance (nm)
10
8
6
4
2
0
-2
0
100
200
300
400
500
600

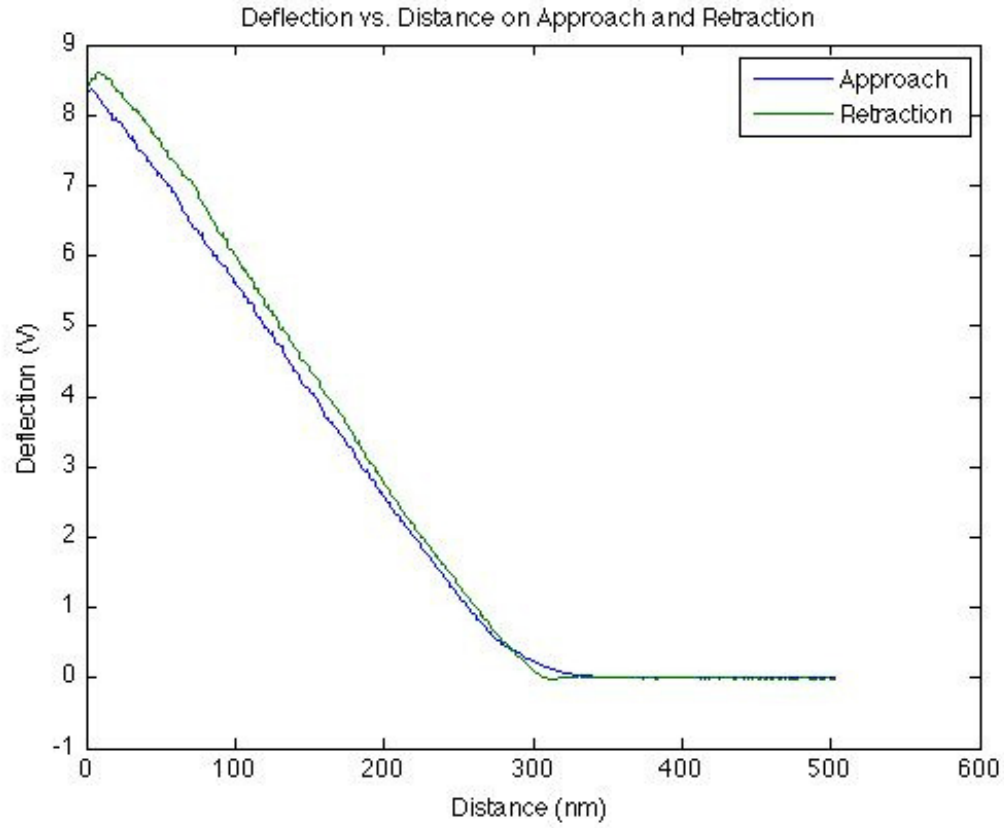
Deflection vs. Distance on Approach and Retraction
Approach
Retraction
Deflection (V)
Distance (nm)
9
8
7
6
5
4
3
2
1
0
-1
0
100
200
300
400
500
600

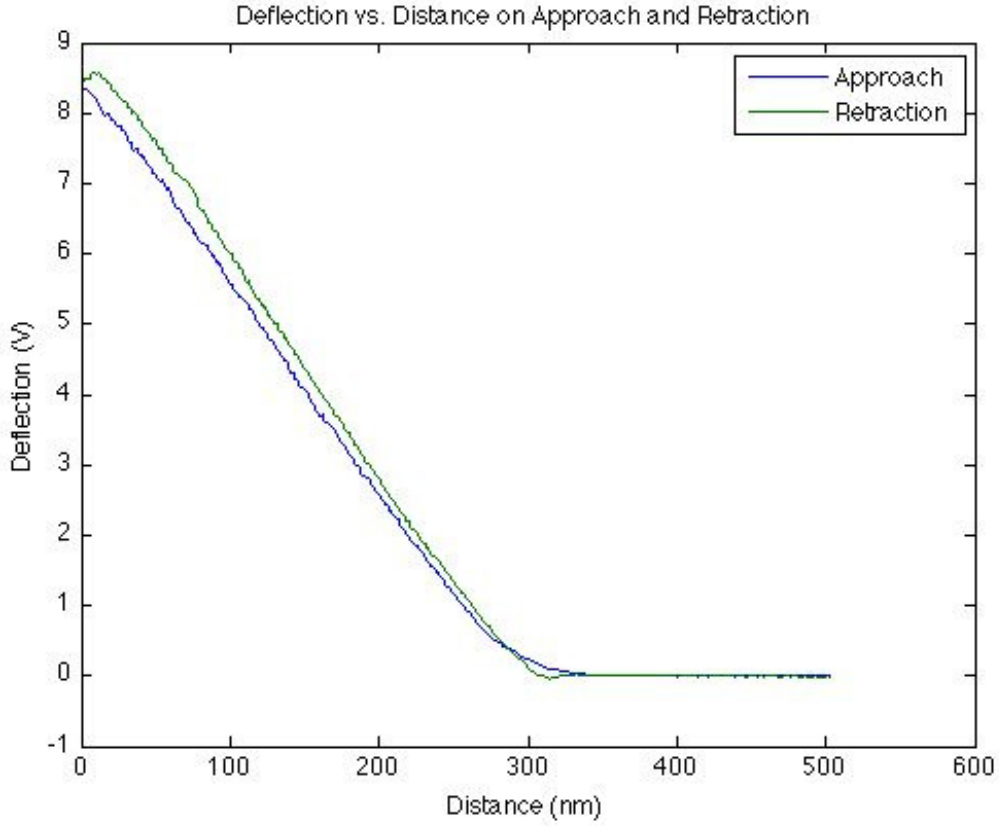
Deflection vs. Distance on Approach and Retraction
Approach
Retraction
Deflection (V)
Distance (nm)
9
8
7
6
5
4
3
2
1
0
-1
0
100
200
300
400
500
600

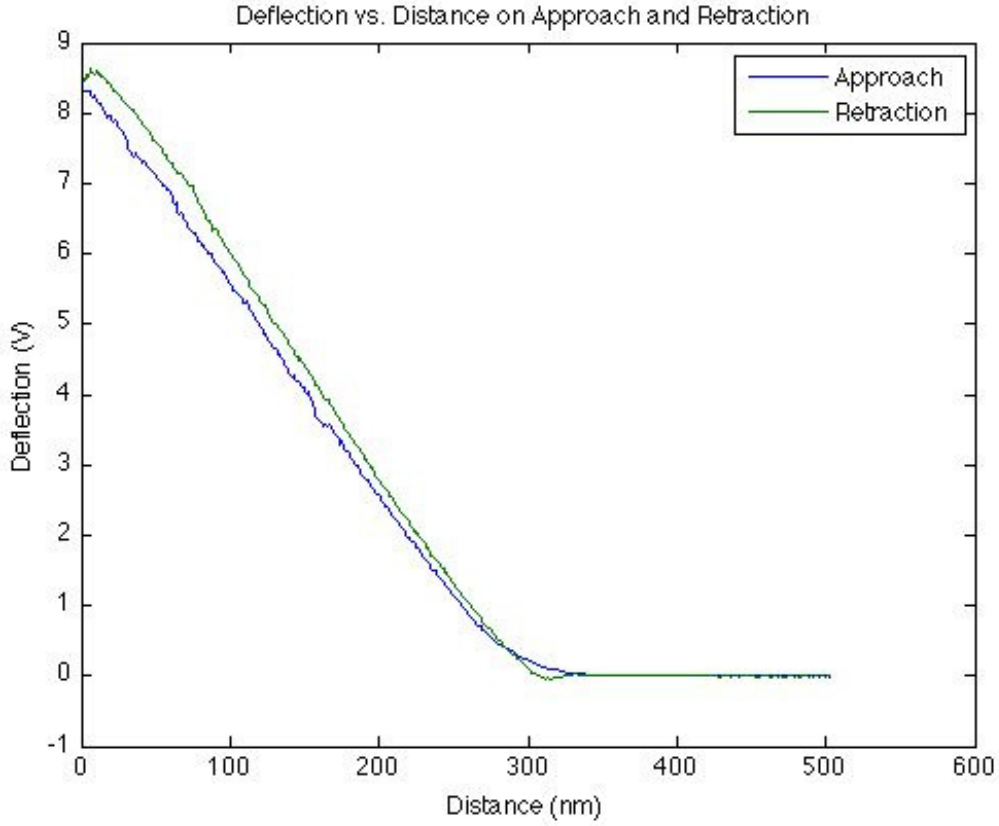
Deflection vs. Distance on Approach and Retraction
Approach
Retraction
Deflection (V)
Distance (nm)
9
8
7
6
5
4
3
2
1
0
-1
0
100
200
300
400
500
600

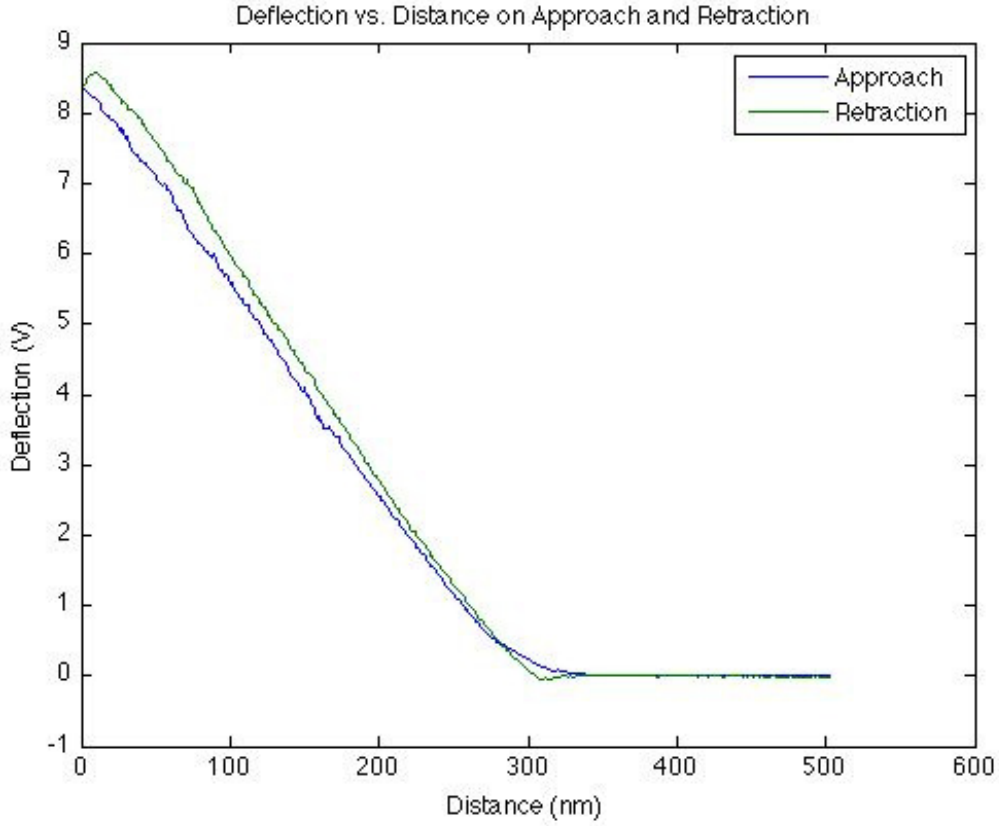
Deflection vs. Distance on Approach and Retraction
Approach
Retraction
Deflection (V)
Distance (nm)
9
8
7
6
5
4
3
2
1
0
-1
0
100
200
300
400
500
600

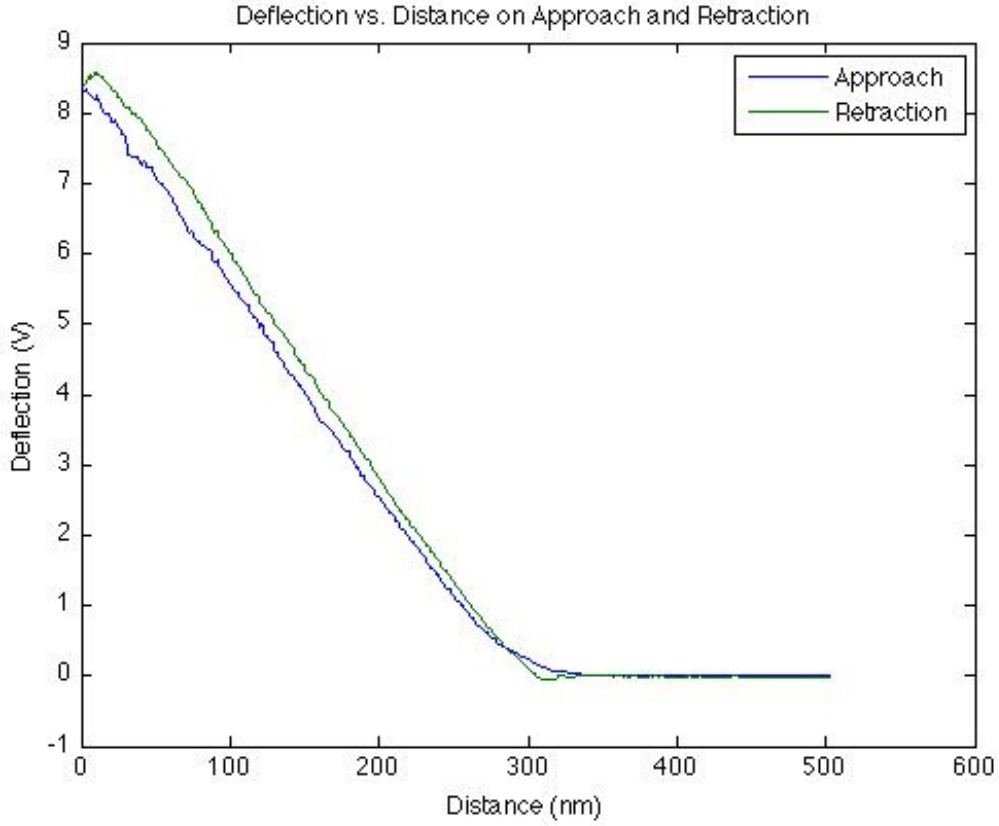
Deflection vs. Distance on Approach and Retraction
Approach
Retraction
Deflection (V)
Distance (nm)
9
8
7
6
5
4
3
2
1
0
-1
0
100
200
300
400
500
600

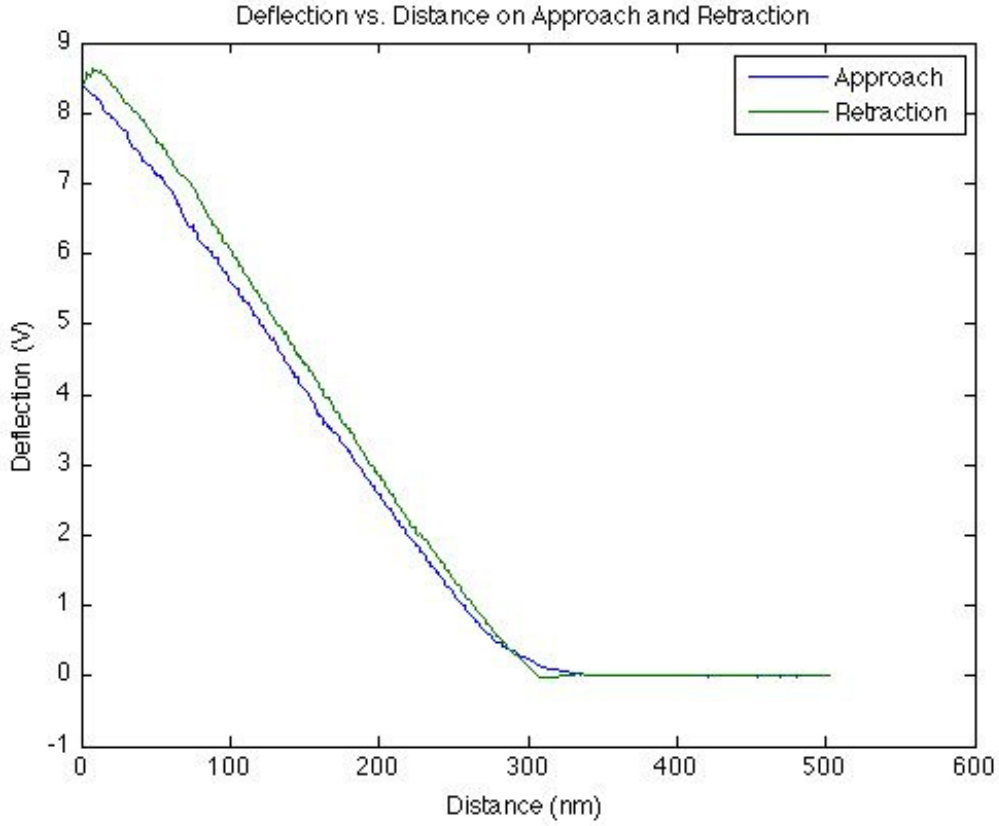
Deflection vs. Distance on Approach and Retraction
Approach
Retraction
Deflection (V)
Distance (nm)
9
8
7
6
5
4
3
2
1
0
-1
0
100
200
300
400
500
600

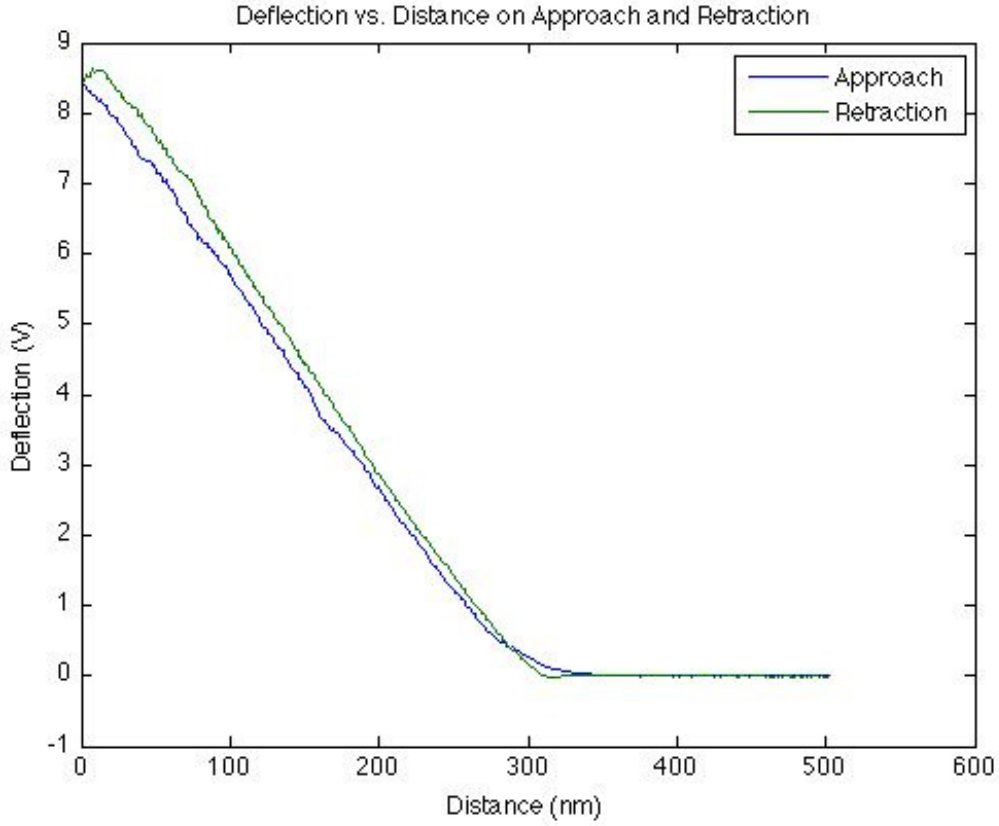
Deflection vs. Distance on Approach and Retraction
Approach
Retraction
Deflection (V)
Distance (nm)
9
8
7
6
5
4
3
2
1
0
-1
0
100
200
300
400
500
600

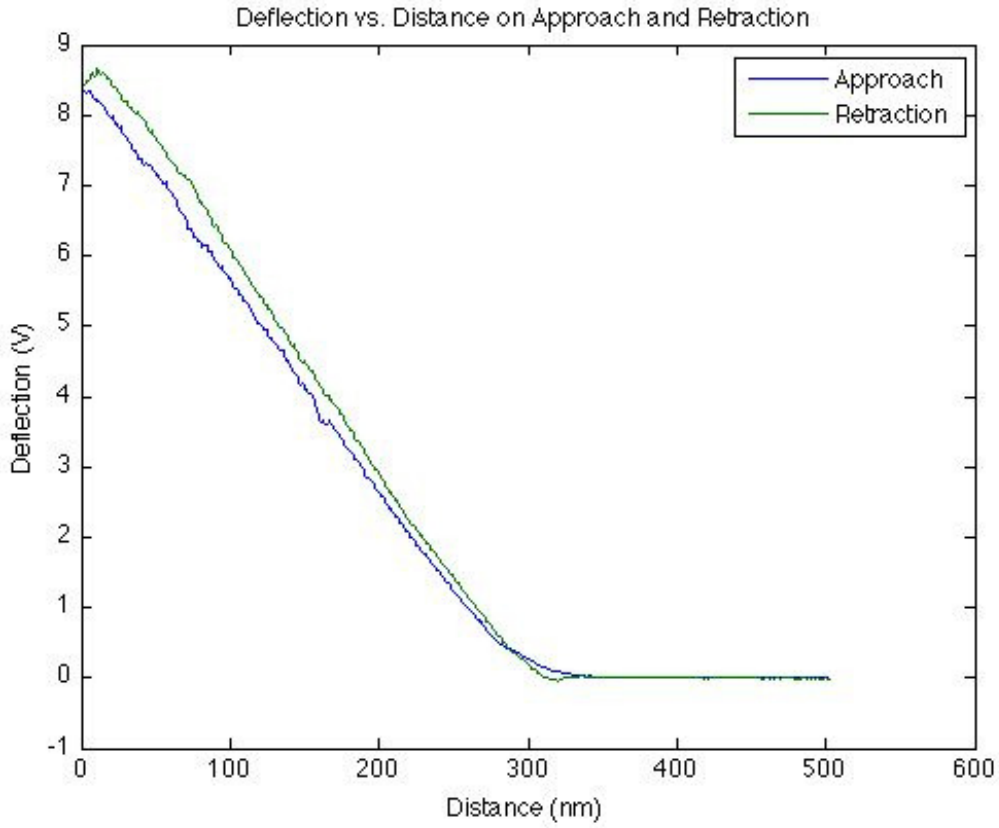
Deflection vs. Distance on Approach and Retraction
Approach
Retraction
Deflection (V)
Distance (nm)
9
8
7
6
5
4
3
2
1
0
-1
0
100
200
300
400
500
600

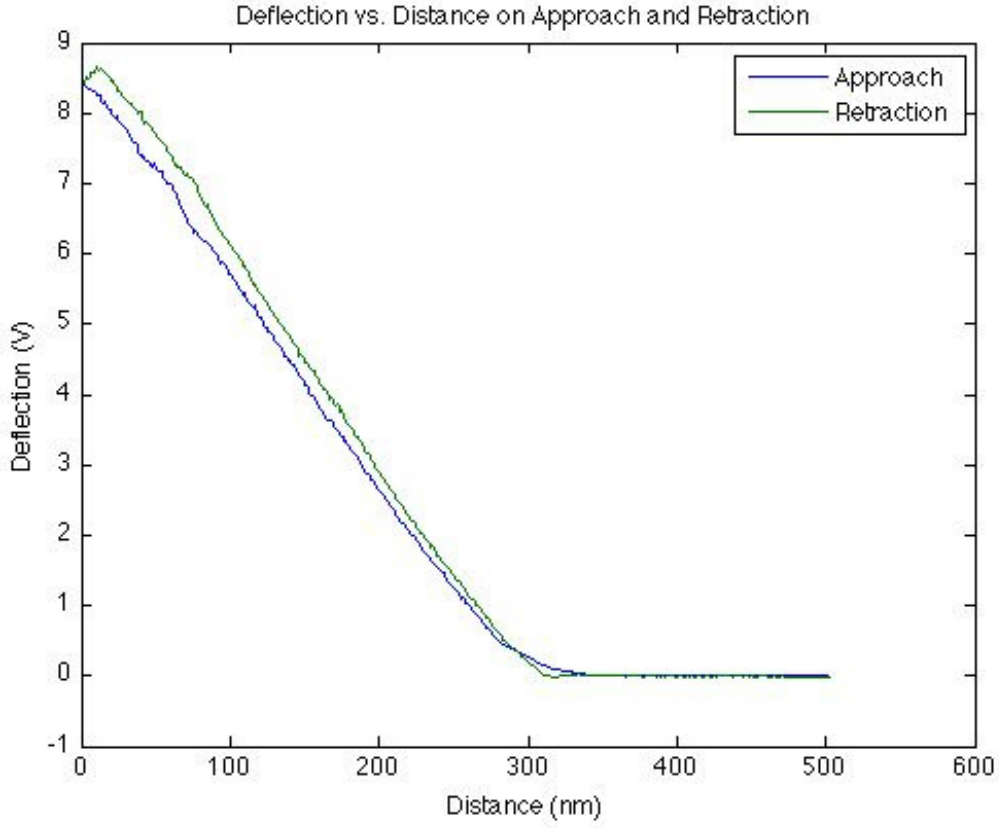
Deflection vs. Distance on Approach and Retraction
Approach
Retraction
Deflection (V)
Distance (nm)
9
8
7
6
5
4
3
2
1
0
-1
0
100
200
300
400
500
600

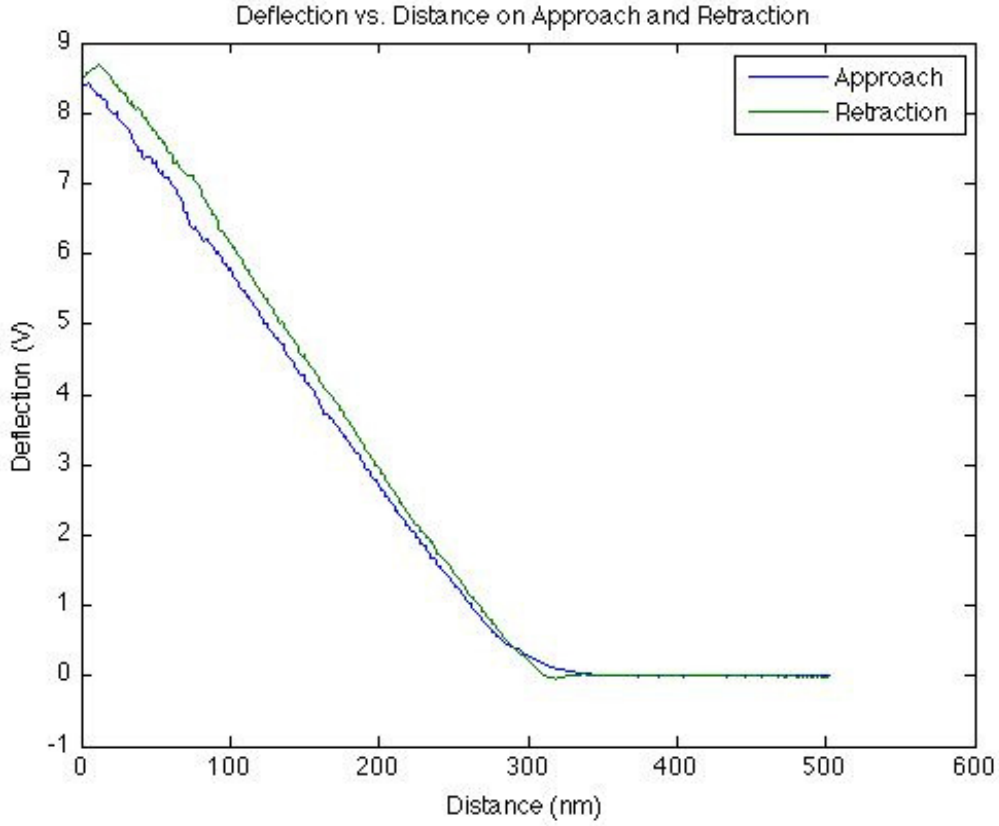
Deflection vs. Distance on Approach and Retraction
Approach
Retraction
Deflection (V)
Distance (nm)
9
8
7
6
5
4
3
2
1
0
-1
0
100
200
300
400
500
600

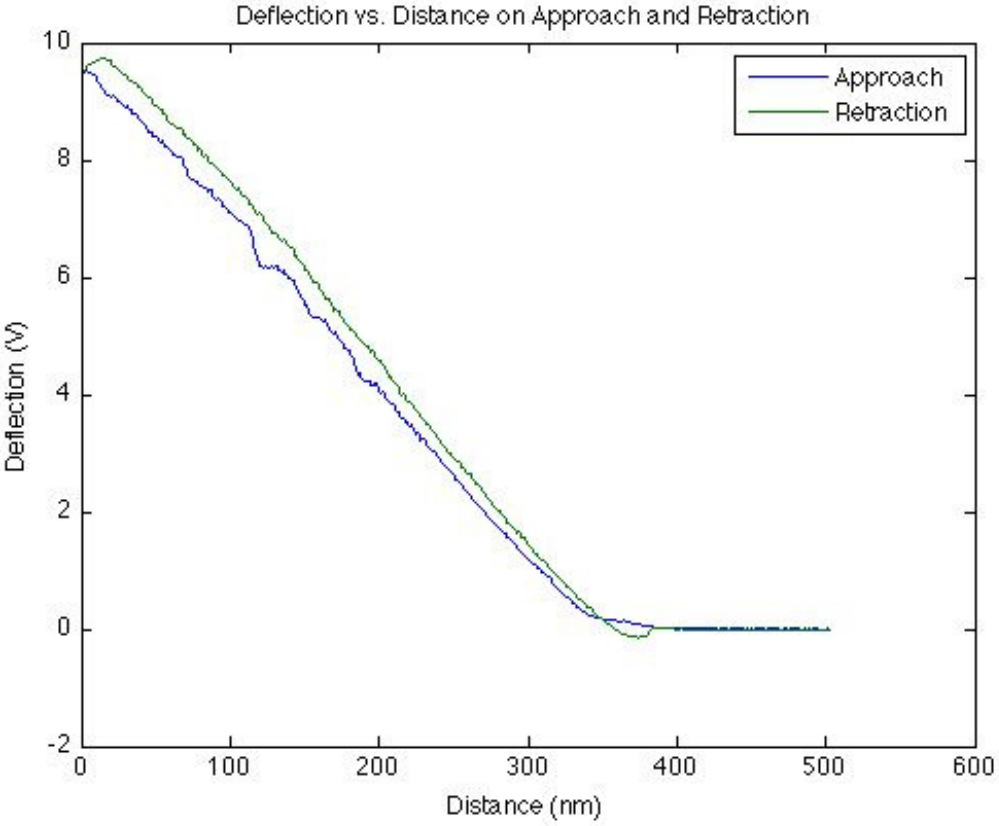
Deflection vs. Distance on Approach and Retraction
Approach
Retraction
Deflection (V)
Distance (nm)
10
8
6
4
2
0
-2
0
100
200
300
400
500
600

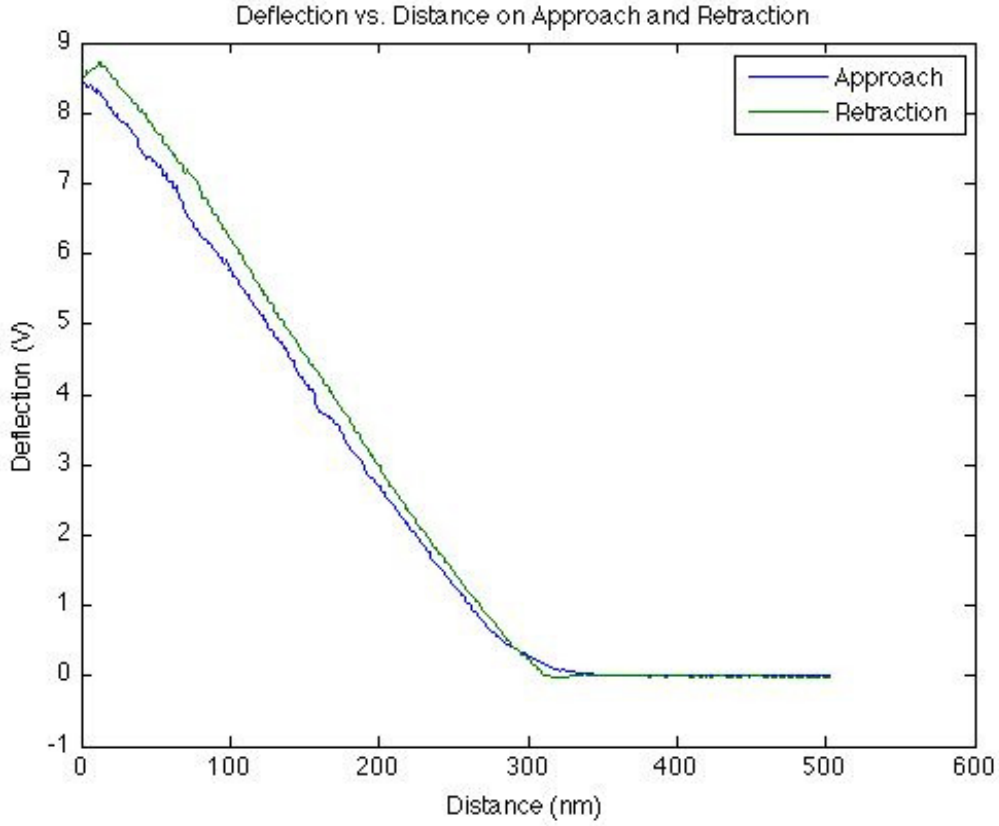
Deflection vs. Distance on Approach and Retraction
Approach
Retraction
Deflection (V)
Distance (nm)
9
8
7
6
5
4
3
2
1
0
-1
0
100
200
300
400
500
600

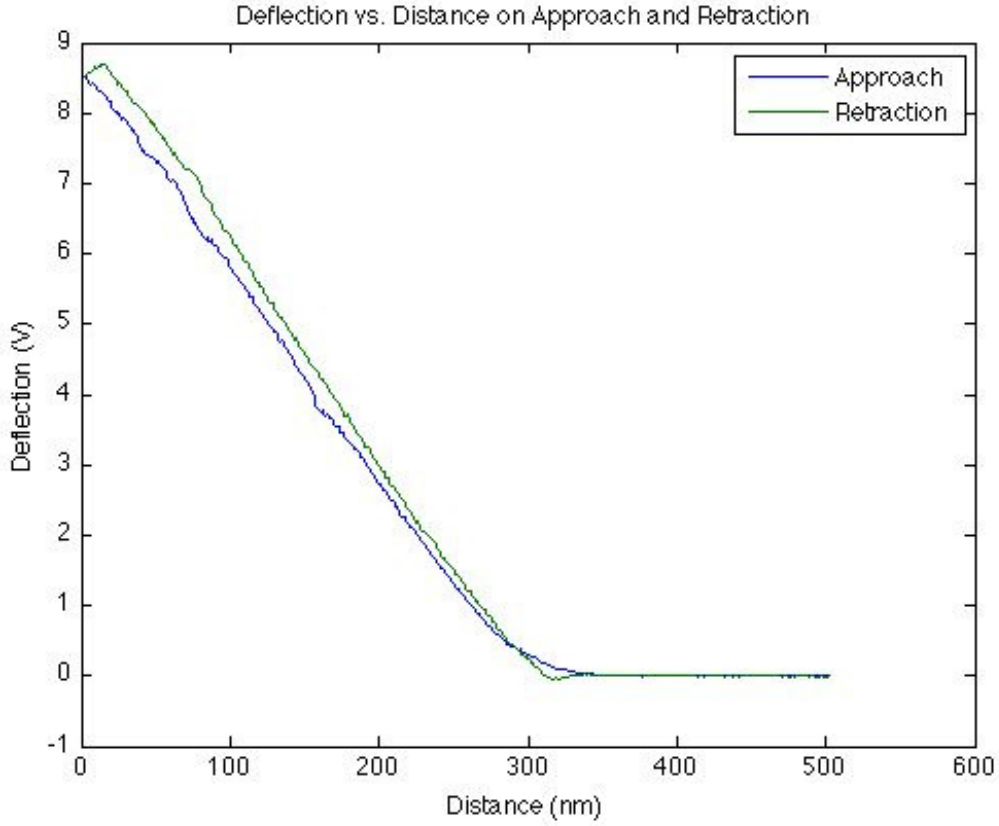
Deflection vs. Distance on Approach and Retraction
Approach
Retraction
Deflection (V)
Distance (nm)
9
8
7
6
5
4
3
2
1
0
-1
0
100
200
300
400
500
600

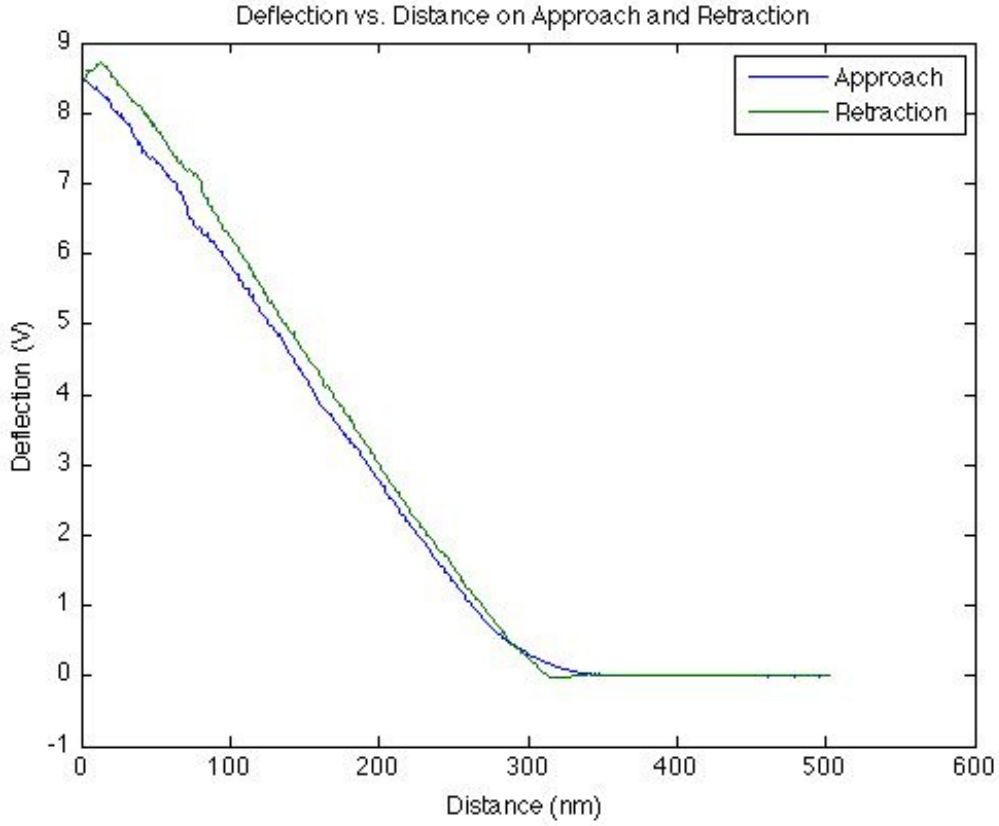
Deflection vs. Distance on Approach and Retraction
Approach
Retraction
Deflection (V)
Distance (nm)
9
8
7
6
5
4
3
2
1
0
-1
0
100
200
300
400
500
600

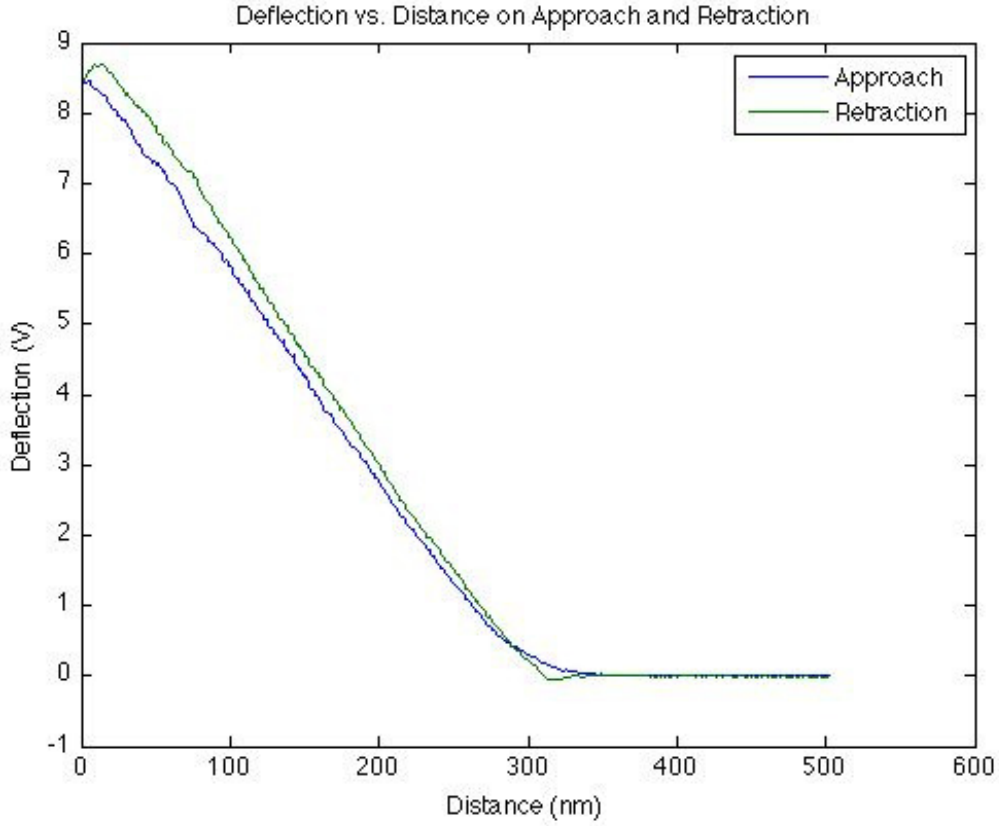
Deflection vs. Distance on Approach and Retraction
Approach
Retraction
Deflection (V)
Distance (nm)
9
8
7
6
5
4
3
2
1
0
-1
0
100
200
300
400
500
600

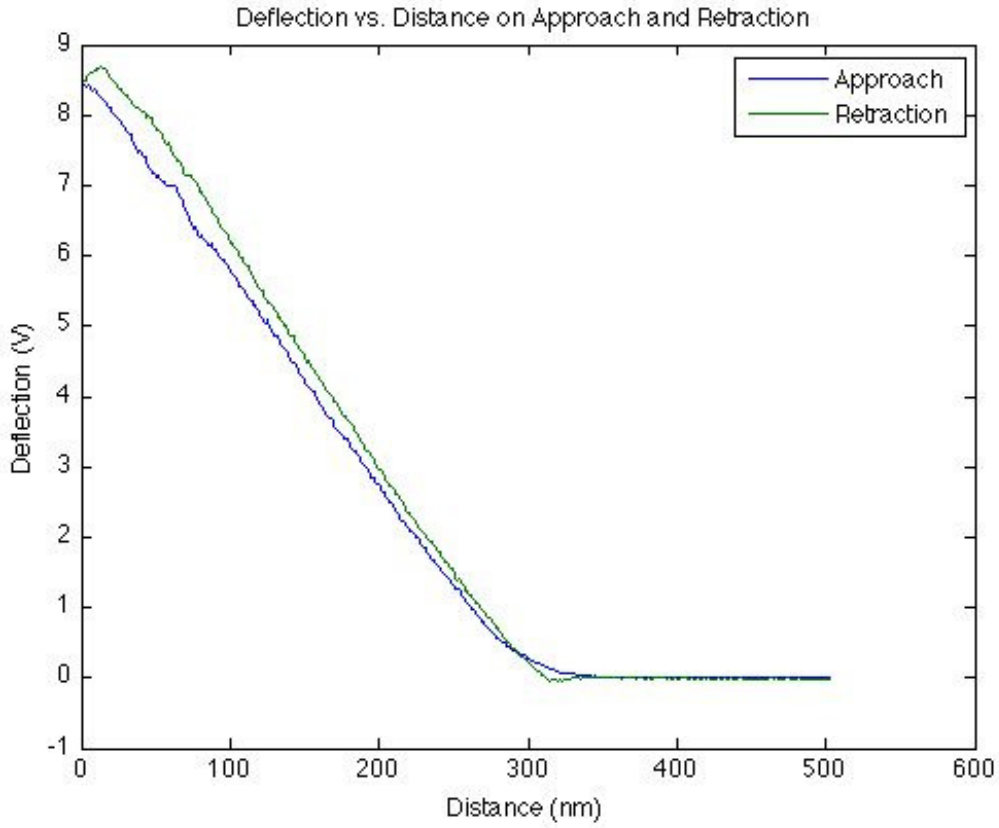
Deflection vs. Distance on Approach and Retraction
Approach
Retraction
Deflection (V)
Distance (nm)
9
8
7
6
5
4
3
2
1
0
-1
0
100
200
300
400
500
600

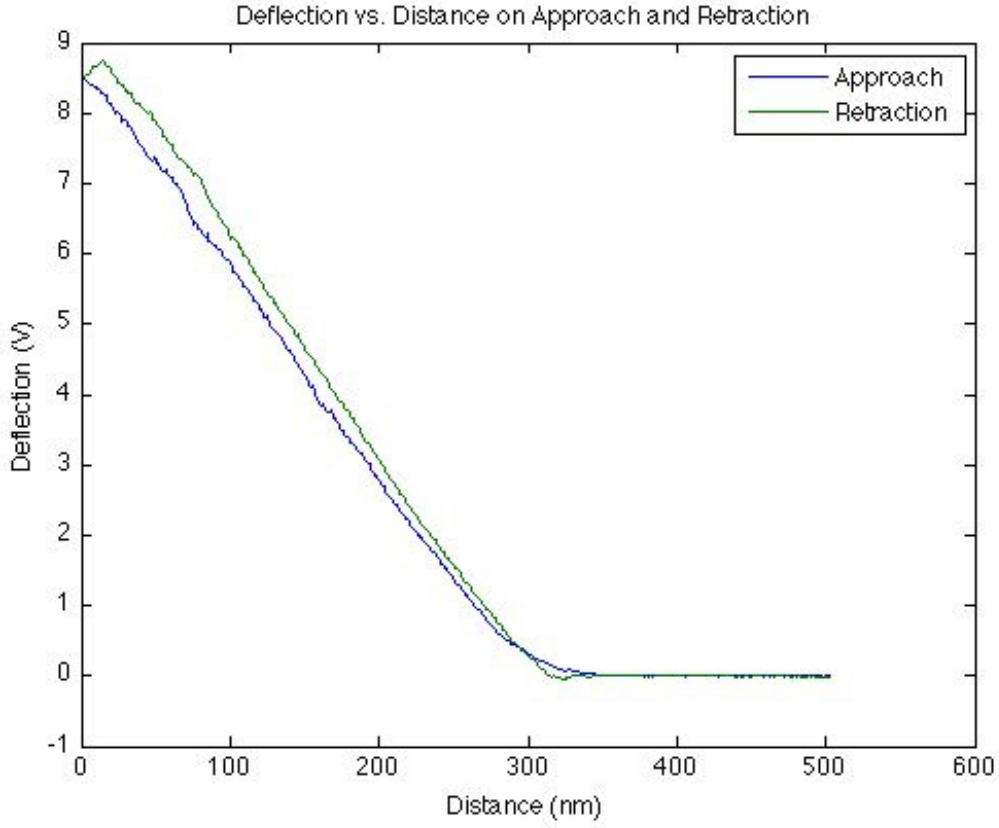
Deflection vs. Distance on Approach and Retraction
Approach
Retraction
Deflection (V)
Distance (nm)
9
8
7
6
5
4
3
2
1
0
-1
0
100
200
300
400
500
600

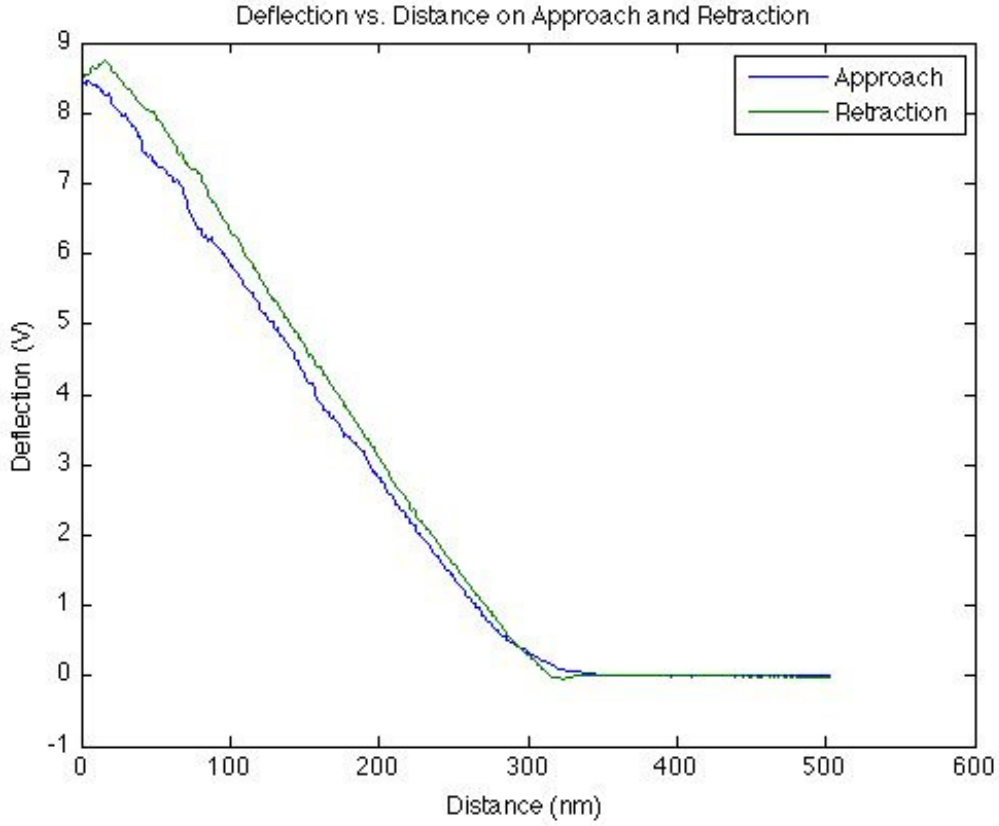
Deflection vs. Distance on Approach and Retraction
Approach
Retraction
Deflection (V)
Distance (nm)
9
8
7
6
5
4
3
2
1
0
-1
0
100
200
300
400
500
600

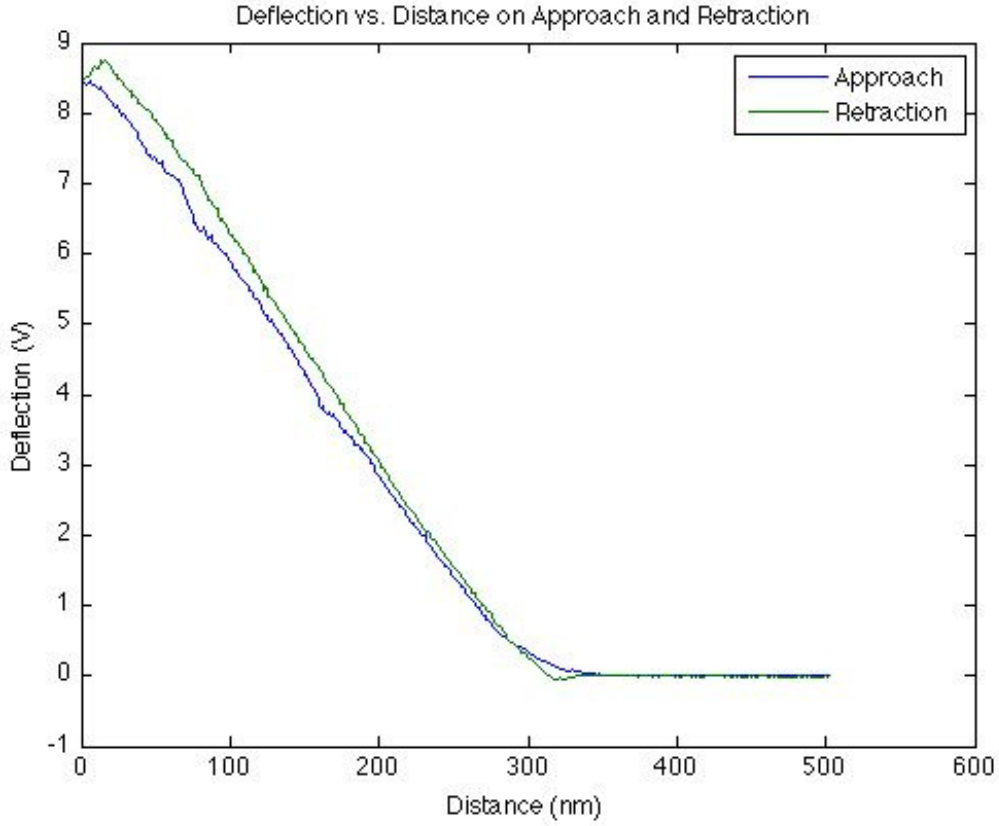
Deflection vs. Distance on Approach and Retraction
Approach
Retraction
Deflection (V)
Distance (nm)
9
8
7
6
5
4
3
2
1
0
-1
0
100
200
300
400
500
600

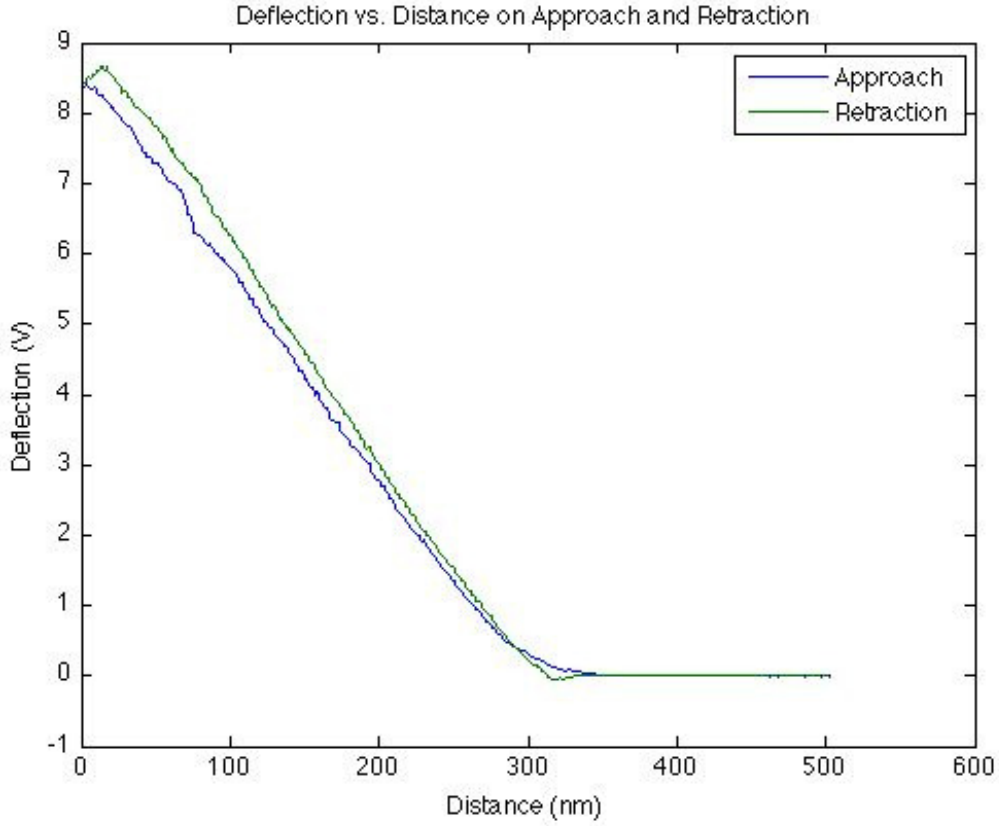
Deflection vs. Distance on Approach and Retraction
Approach
Retraction
Deflection (V)
Distance (nm)
9
8
7
6
5
4
3
2
1
0
-1
0
100
200
300
400
500
600

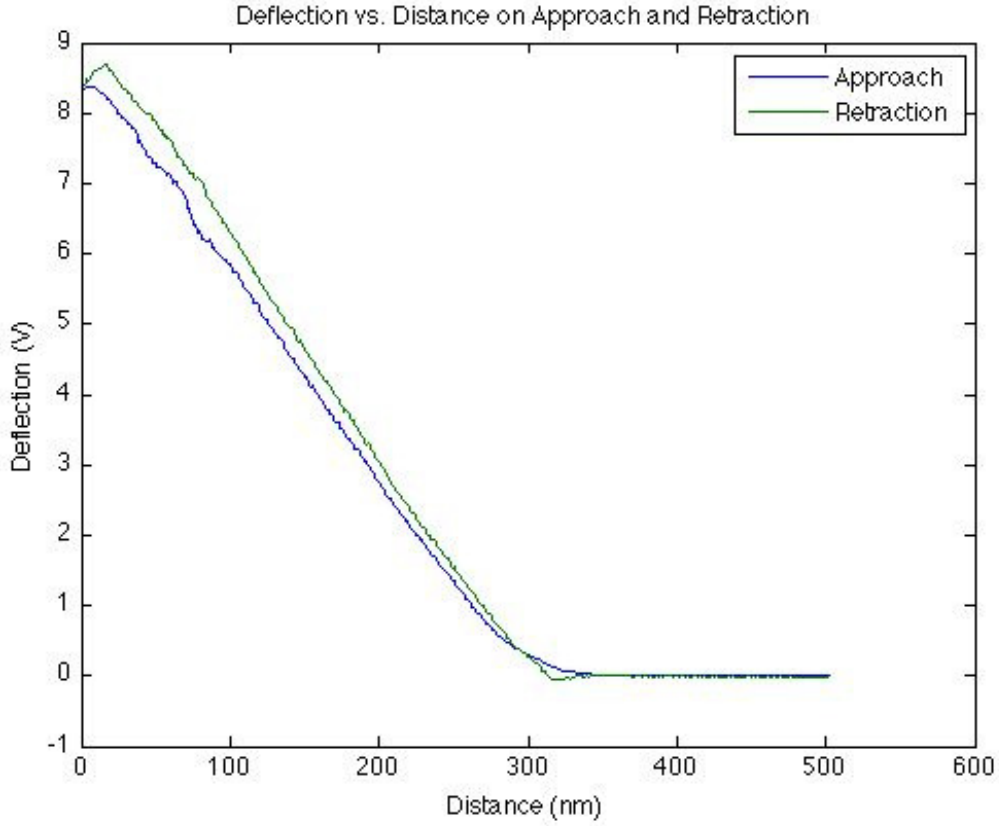
Deflection vs. Distance on Approach and Retraction
Approach
Retraction
Deflection (V)
Distance (nm)
9
8
7
6
5
4
3
2
1
0
-1
0
100
200
300
400
500
600

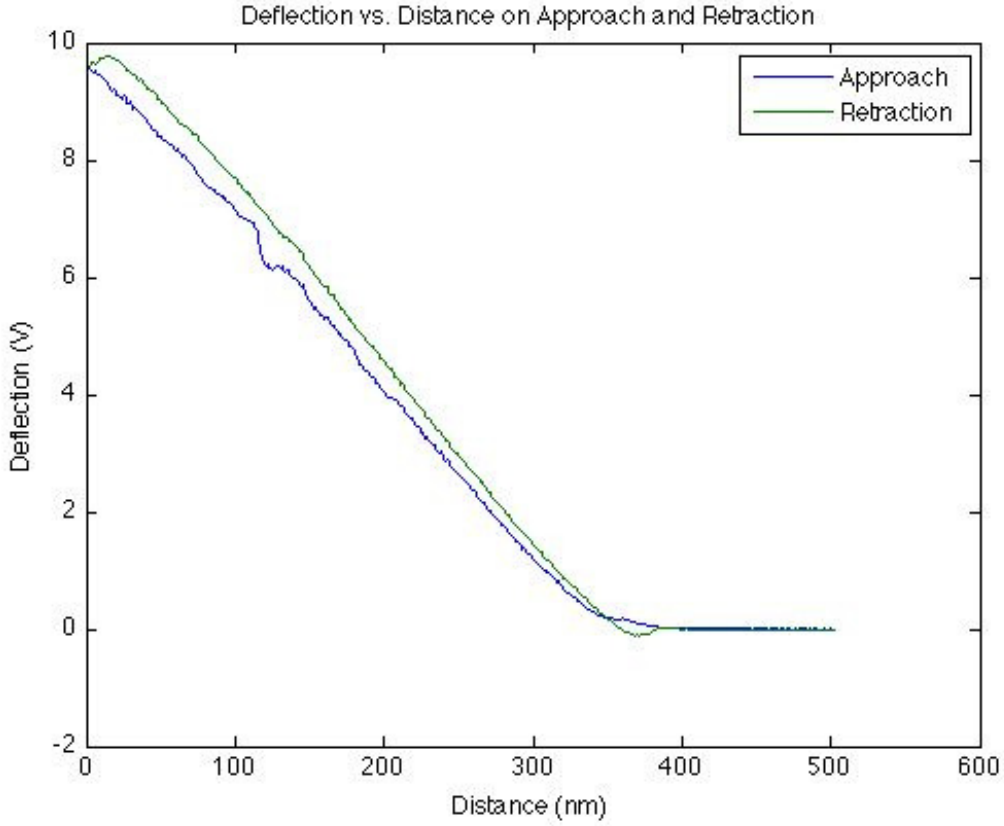
Deflection vs. Distance on Approach and Retraction
Approach
Retraction
Deflection (V)
Distance (nm)
10
8
6
4
2
0
-2
0
100
200
300
400
500
600

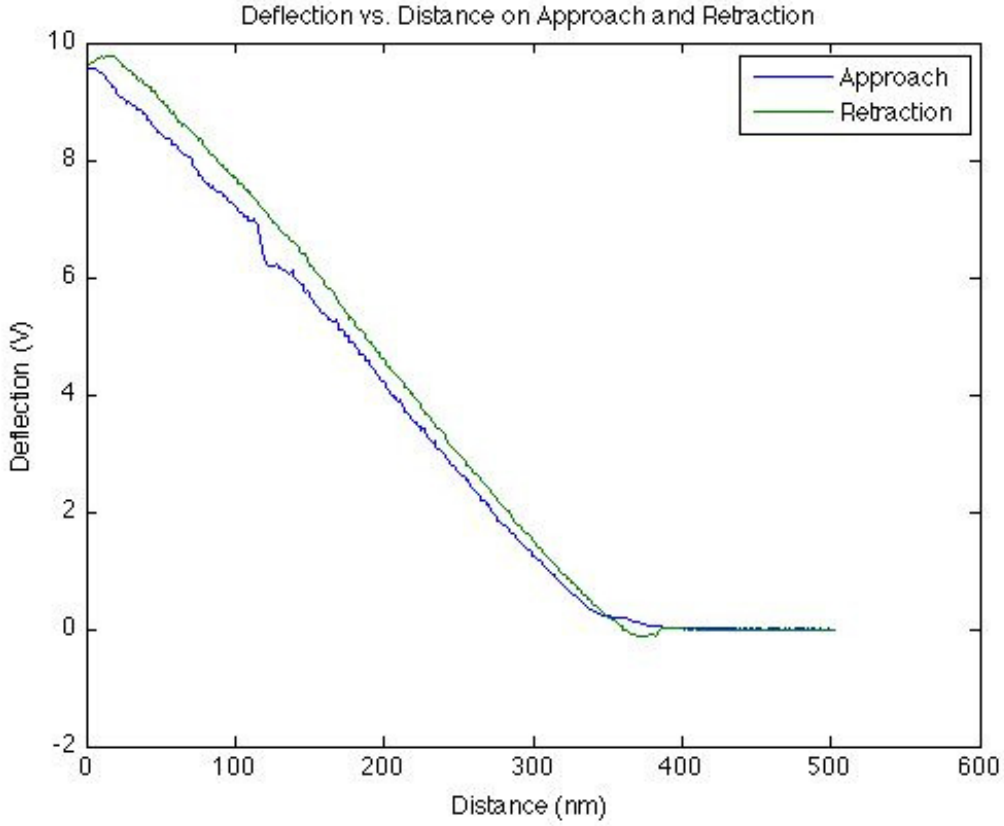
Deflection vs. Distance on Approach and Retraction
Approach
Retraction
Deflection (V)
Distance (nm)
10
8
6
4
2
0
-2
0
100
200
300
400
500
600

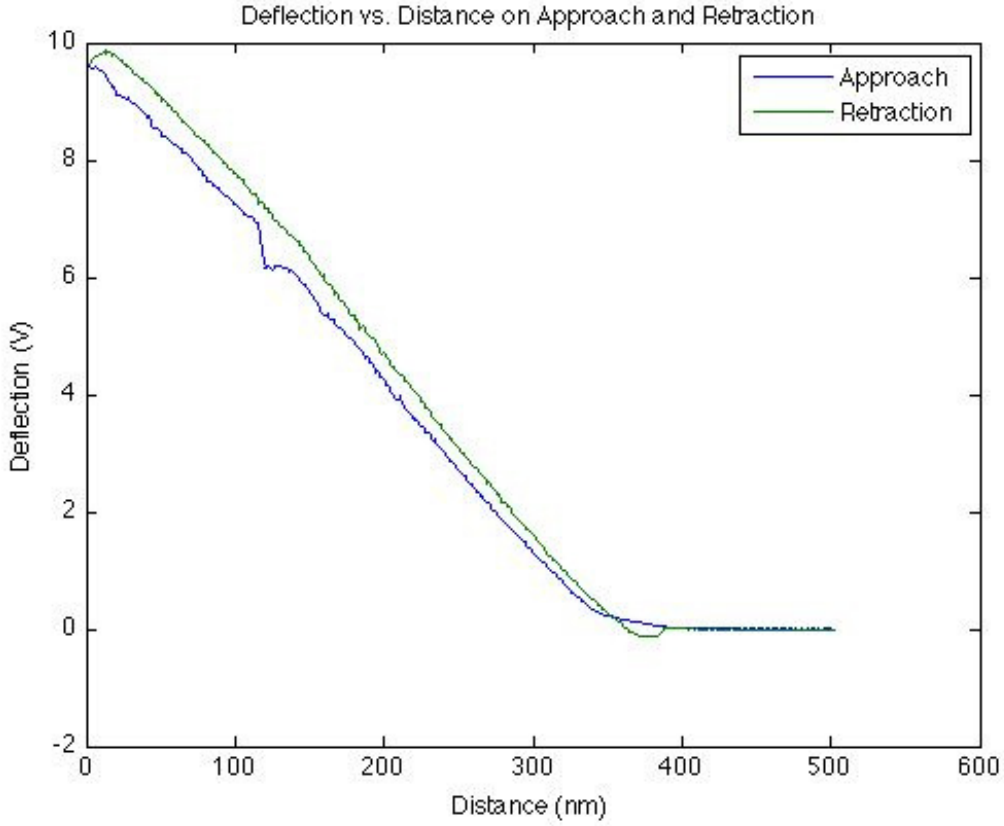
Deflection vs. Distance on Approach and Retraction
Approach
Retraction
Deflection (V)
Distance (nm)
10
8
6
4
2
0
-2
0
100
200
300
400
500
600

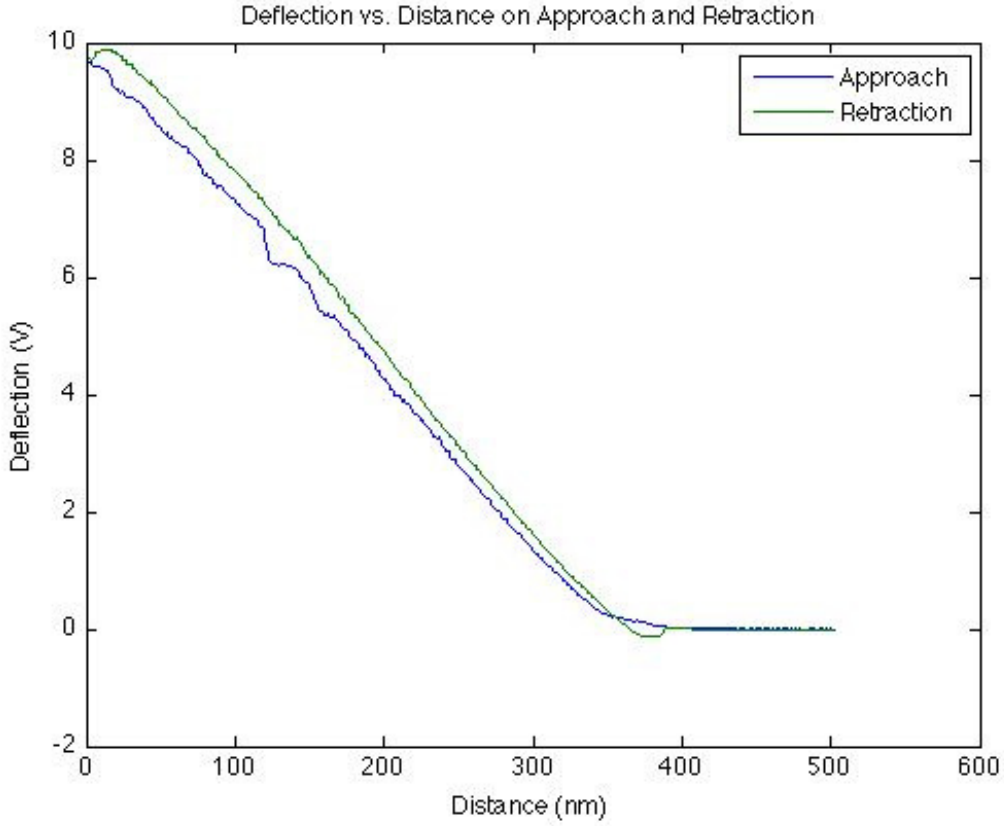
Deflection vs. Distance on Approach and Retraction
Approach
Retraction
Deflection (V)
Distance (nm)
10
8
6
4
2
0
-2
0
100
200
300
400
500
600

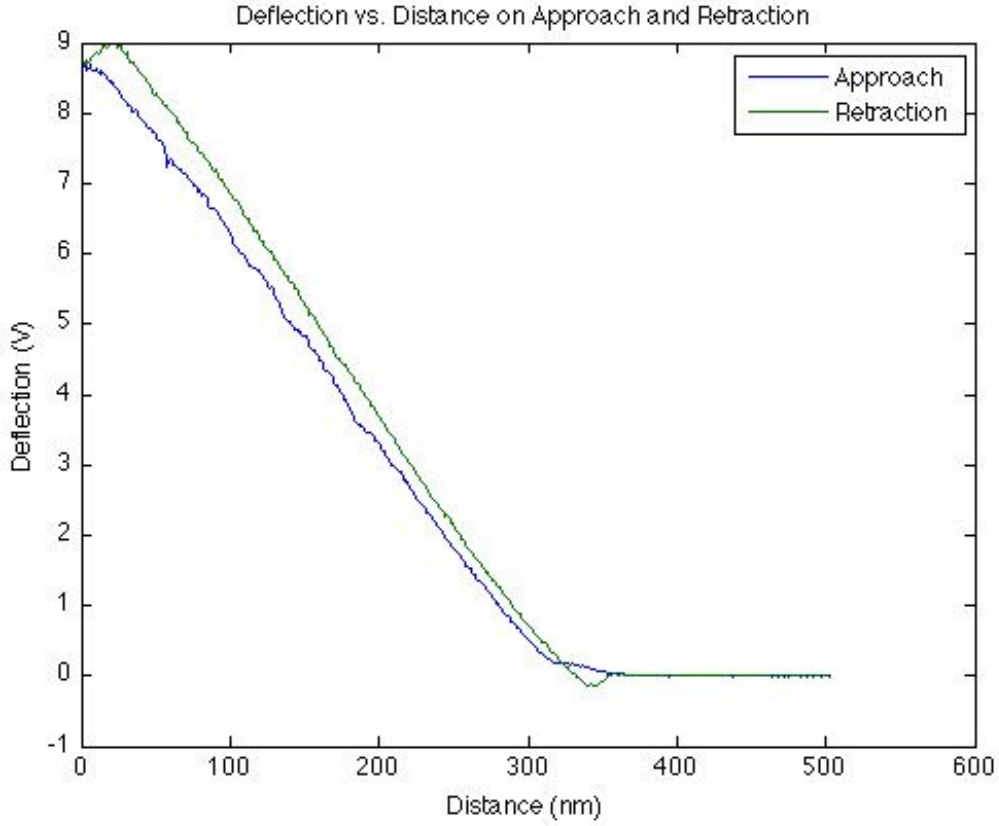
Deflection vs. Distance on Approach and Retraction
Approach
Retraction
Deflection (V)
Distance (nm)
9
8
7
6
5
4
3
2
1
0
-1
0
100
200
300
400
500
600

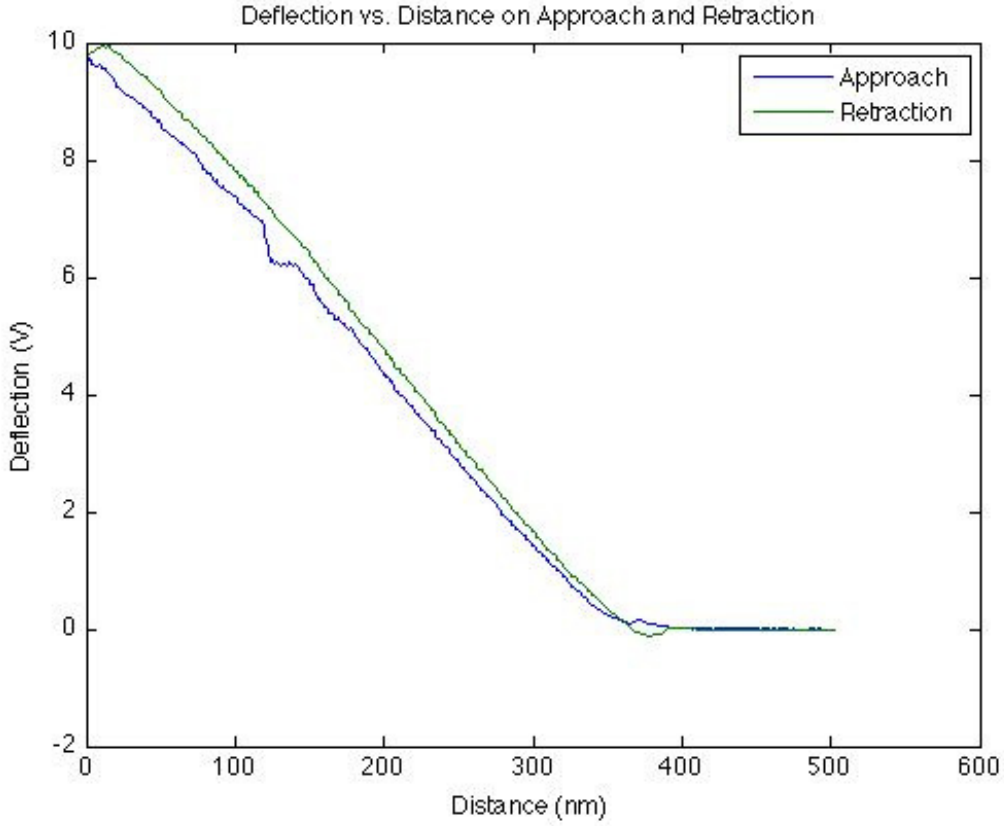
Deflection vs. Distance on Approach and Retraction
Approach
Retraction
Deflection (V)
Distance (nm)
10
8
6
4
2
0
-2
0
100
200
300
400
500
600

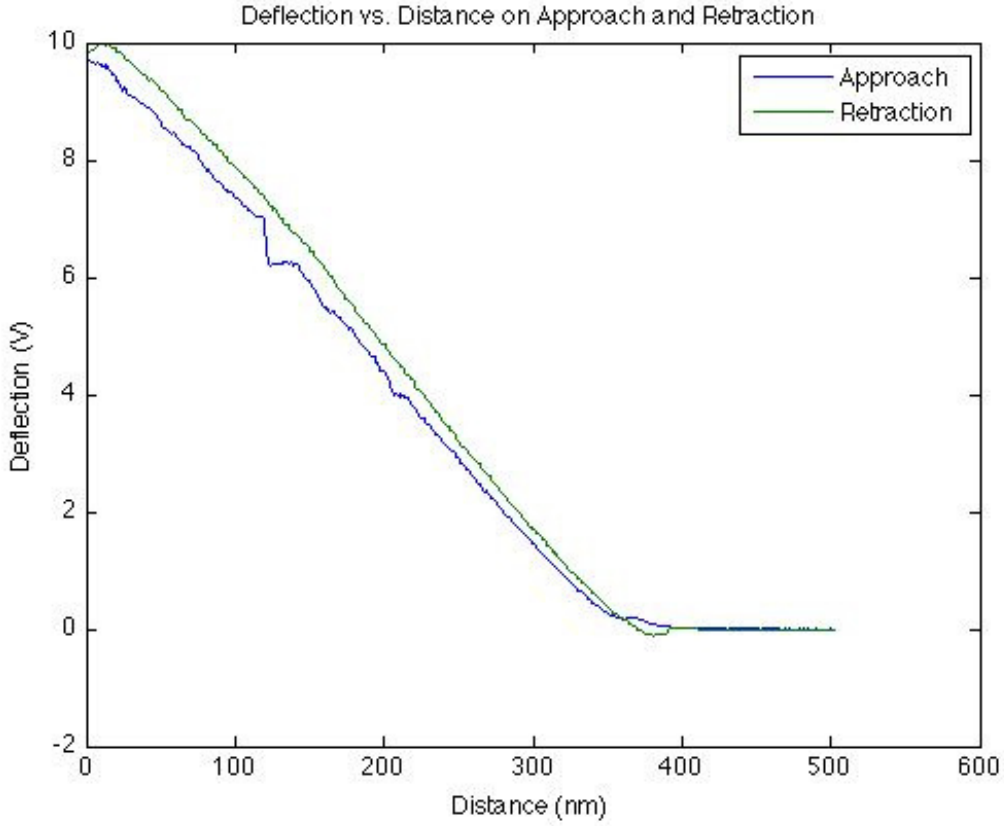
Deflection vs. Distance on Approach and Retraction
Approach
Retraction
Deflection (V)
Distance (nm)
10
8
6
4
2
0
-2
0
100
200
300
400
500
600

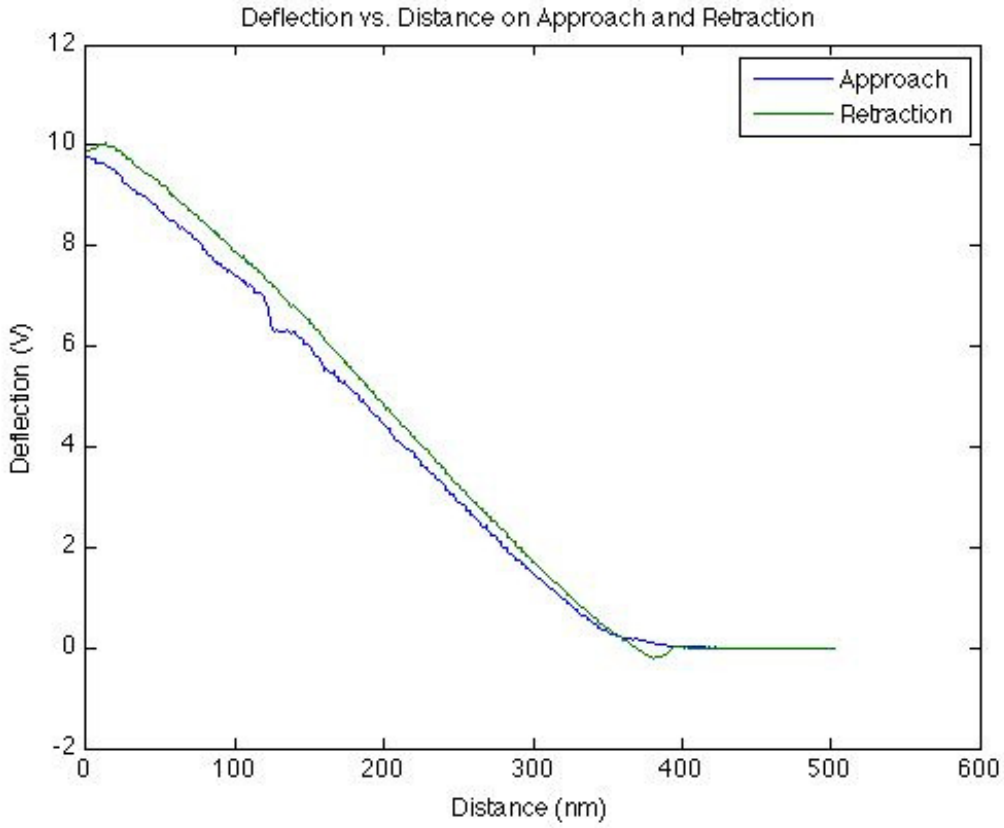
Deflection vs. Distance on Approach and Retraction
Approach
Retraction
Deflection (V)
Distance (nm)
12
10
8
6
4
2
0
-2
0
100
200
300
400
500
600

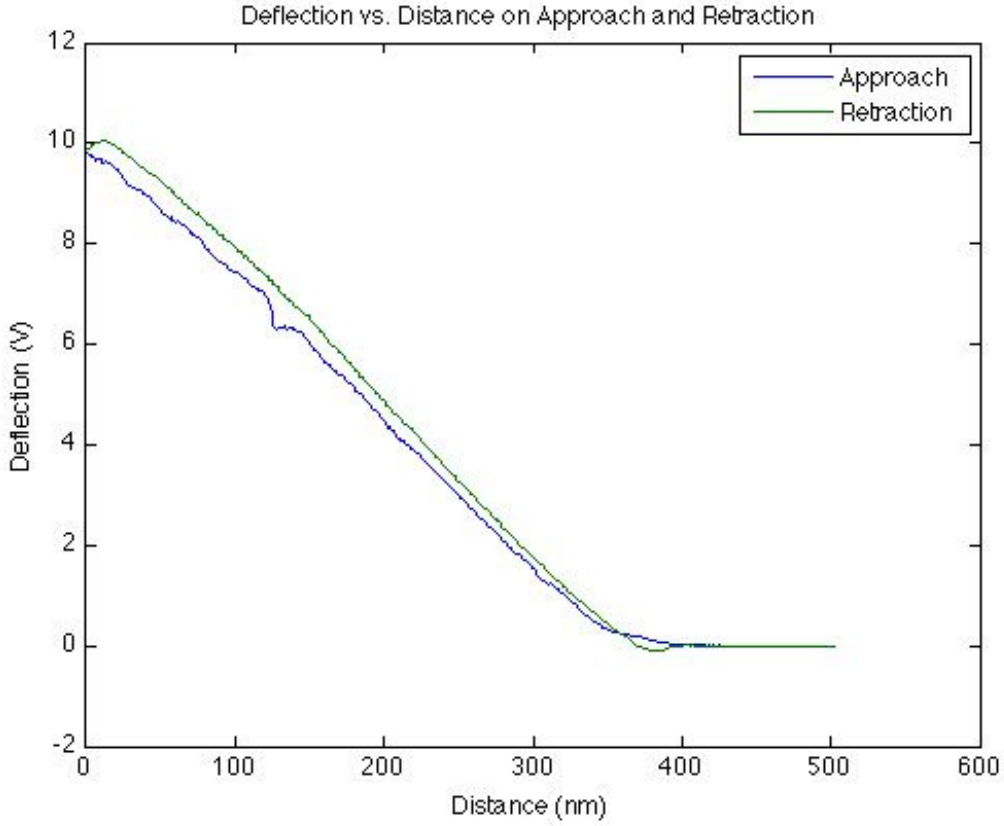
Deflection vs. Distance on Approach and Retraction
Approach
Retraction
Deflection (V)
Distance (nm)
12
10
8
6
4
2
0
-2
0
100
200
300
400
500
600

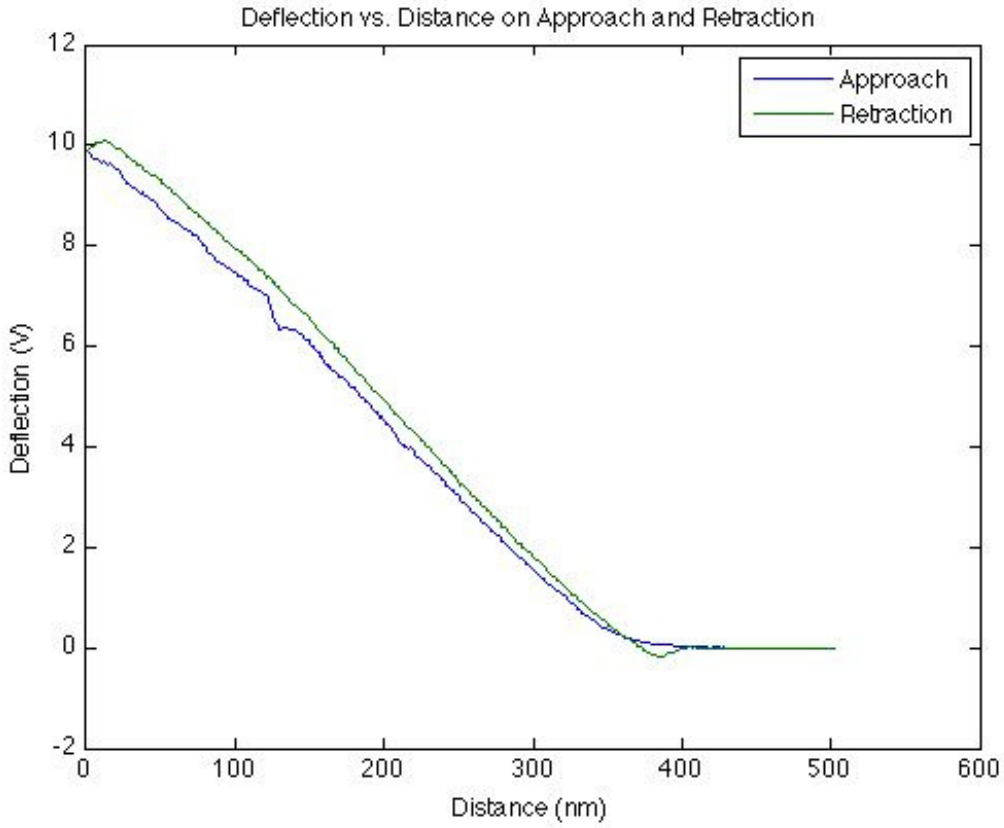
Deflection vs. Distance on Approach and Retraction
Approach
Retraction
Deflection (V)
Distance (nm)
12
10
8
6
4
2
0
-2
0
100
200
300
400
500
600

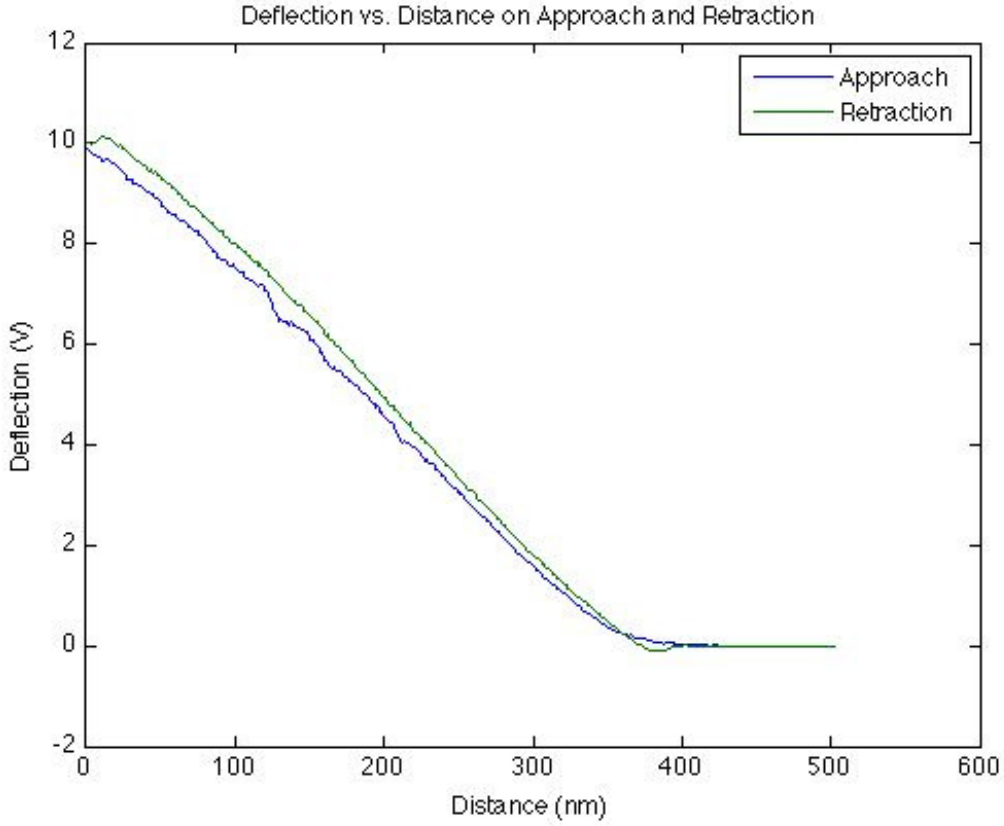
Deflection vs. Distance on Approach and Retraction
Approach
Retraction
Deflection (V)
Distance (nm)
12
10
8
6
4
2
0
-2
0
100
200
300
400
500
600

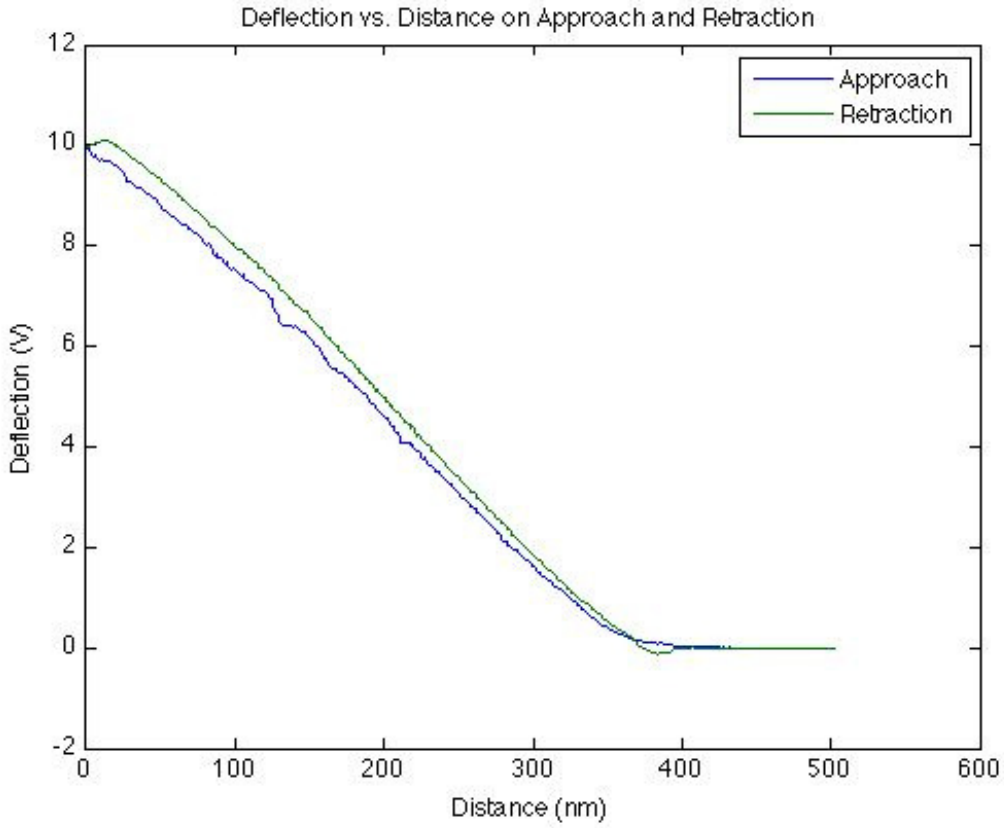
Deflection vs. Distance on Approach and Retraction
Approach
Retraction
Deflection (V)
Distance (nm)
12
10
8
6
4
2
0
-2
0
100
200
300
400
500
600

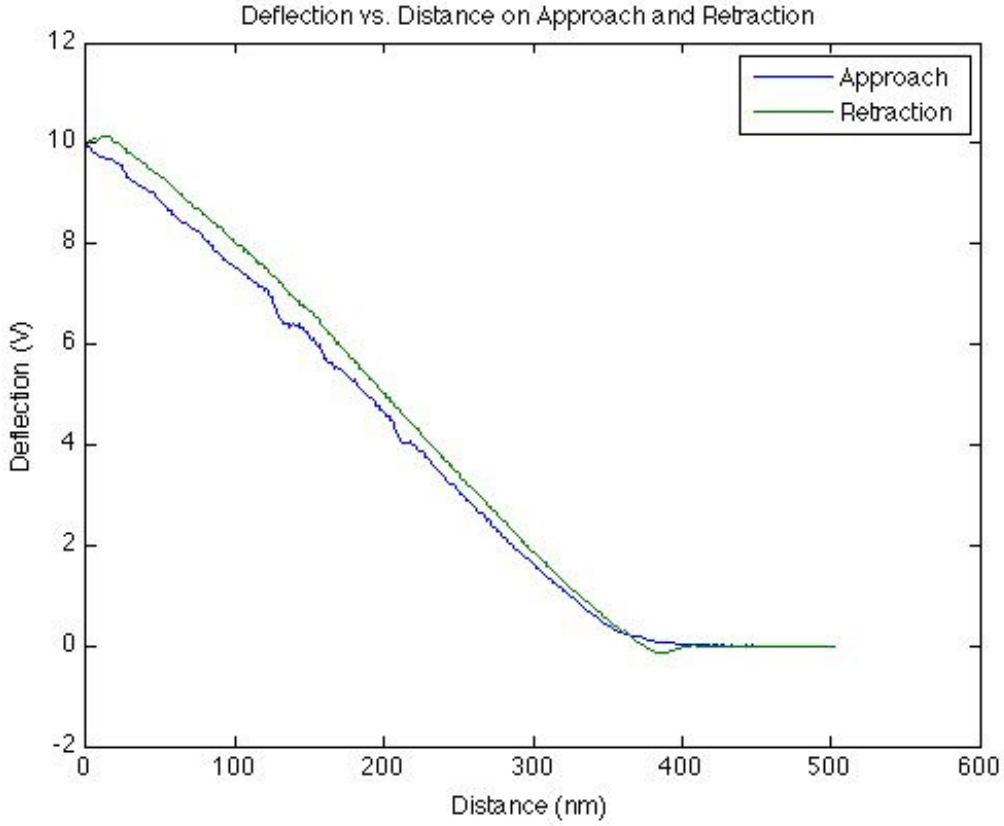
Deflection vs. Distance on Approach and Retraction
Approach
Retraction
Deflection (V)
Distance (nm)
12
10
8
6
4
2
0
-2
0
100
200
300
400
500
600

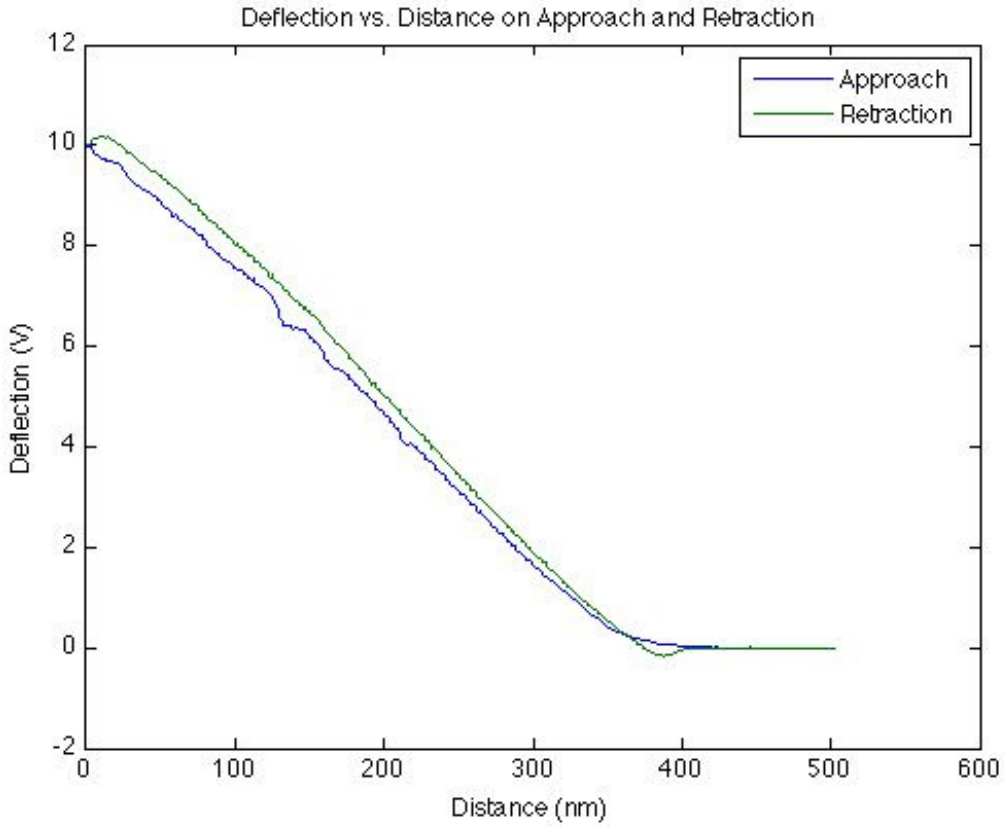
Deflection vs. Distance on Approach and Retraction
Approach
Retraction
Deflection (V)
Distance (nm)
12
10
8
6
4
2
0
-2
0
100
200
300
400
500
600

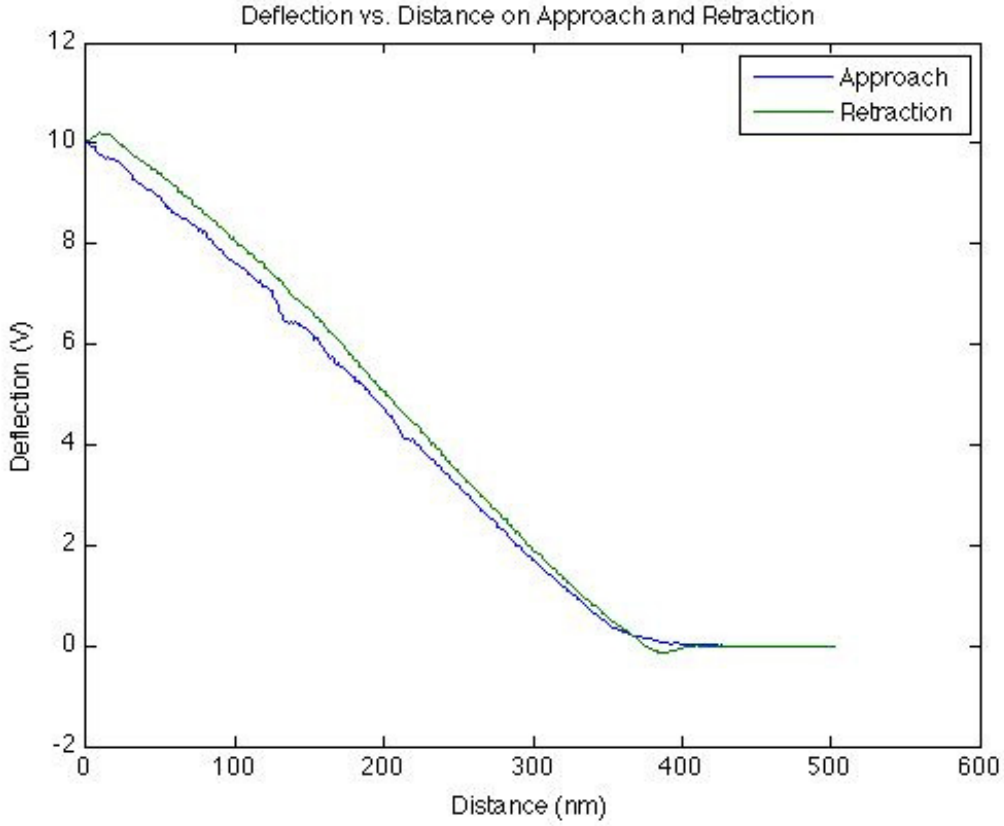
Deflection vs. Distance on Approach and Retraction
Approach
Retraction
Deflection (V)
Distance (nm)
12
10
8
6
4
2
0
-2
0
100
200
300
400
500
600

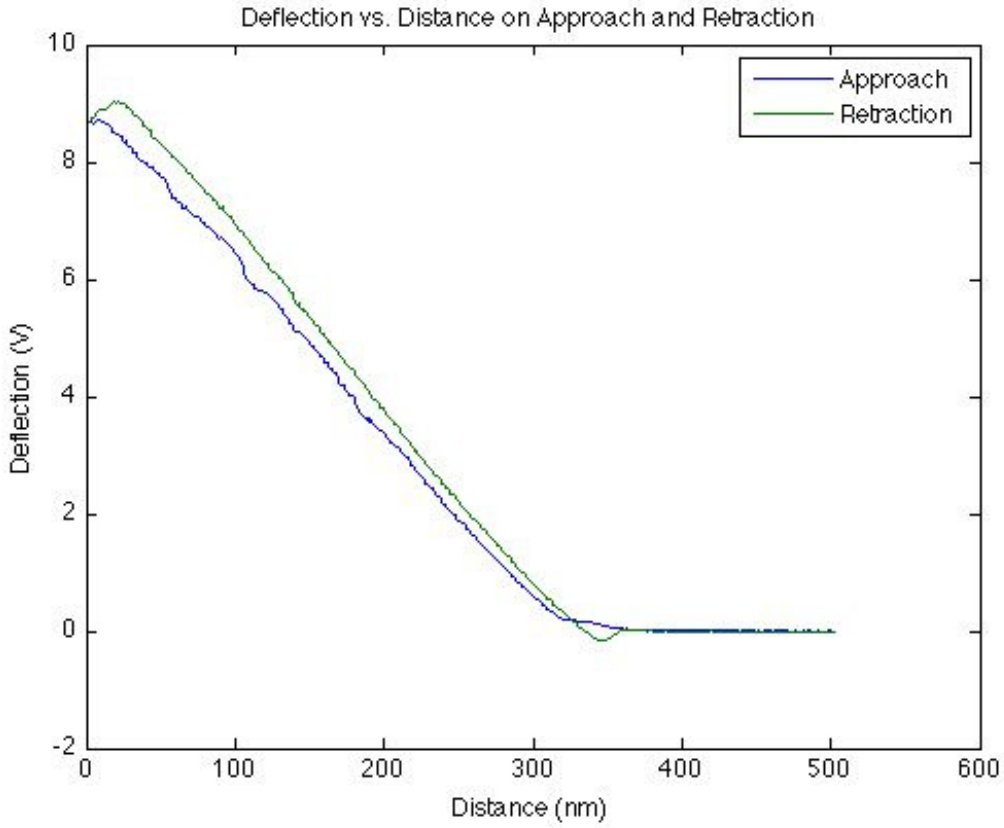
Deflection vs. Distance on Approach and Retraction
Approach
Retraction
Deflection (V)
Distance (nm)
10
8
6
4
2
0
-2
0
100
200
300
400
500
600

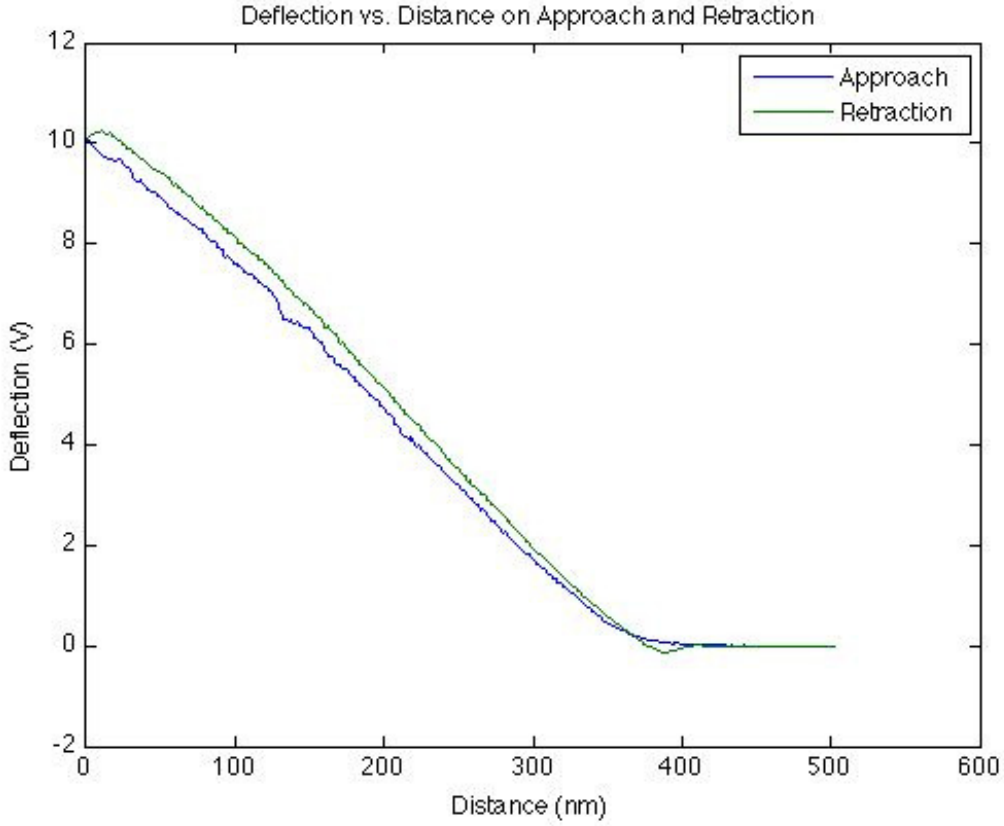
Deflection vs. Distance on Approach and Retraction
Approach
Retraction
Deflection (V)
Distance (nm)
12
10
8
6
4
2
0
-2
0
100
200
300
400
500
600

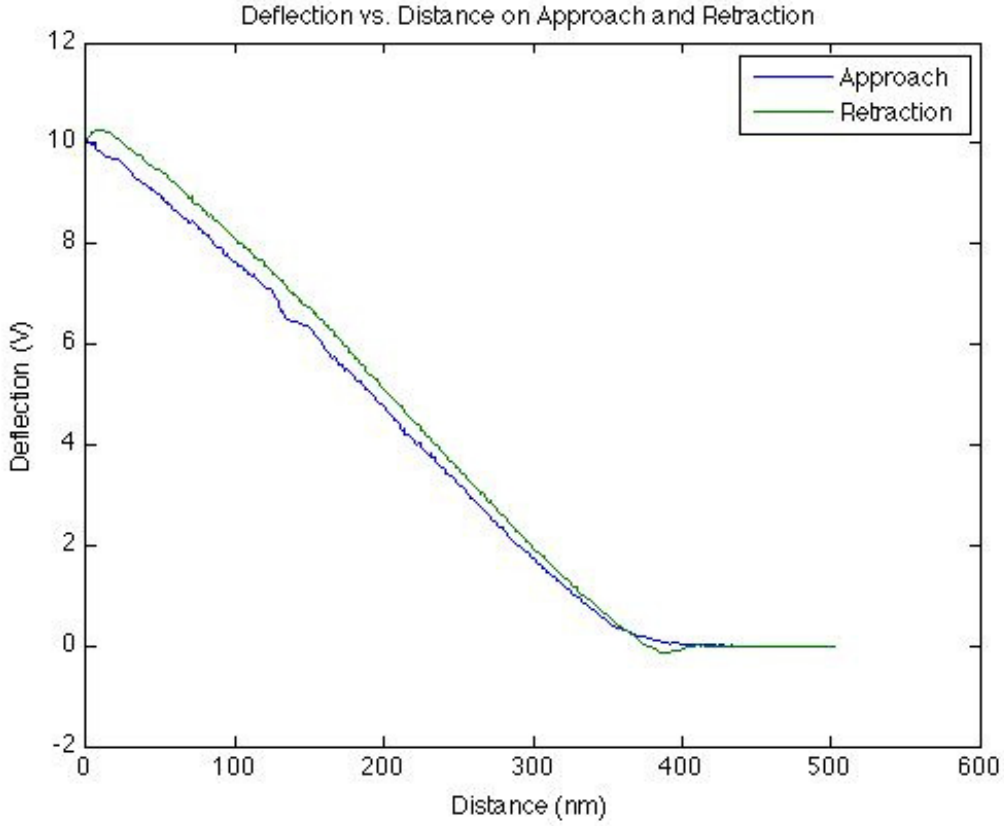
Deflection vs. Distance on Approach and Retraction
Approach
Retraction
Deflection (V)
Distance (nm)
12
10
8
6
4
2
0
-2
0
100
200
300
400
500
600

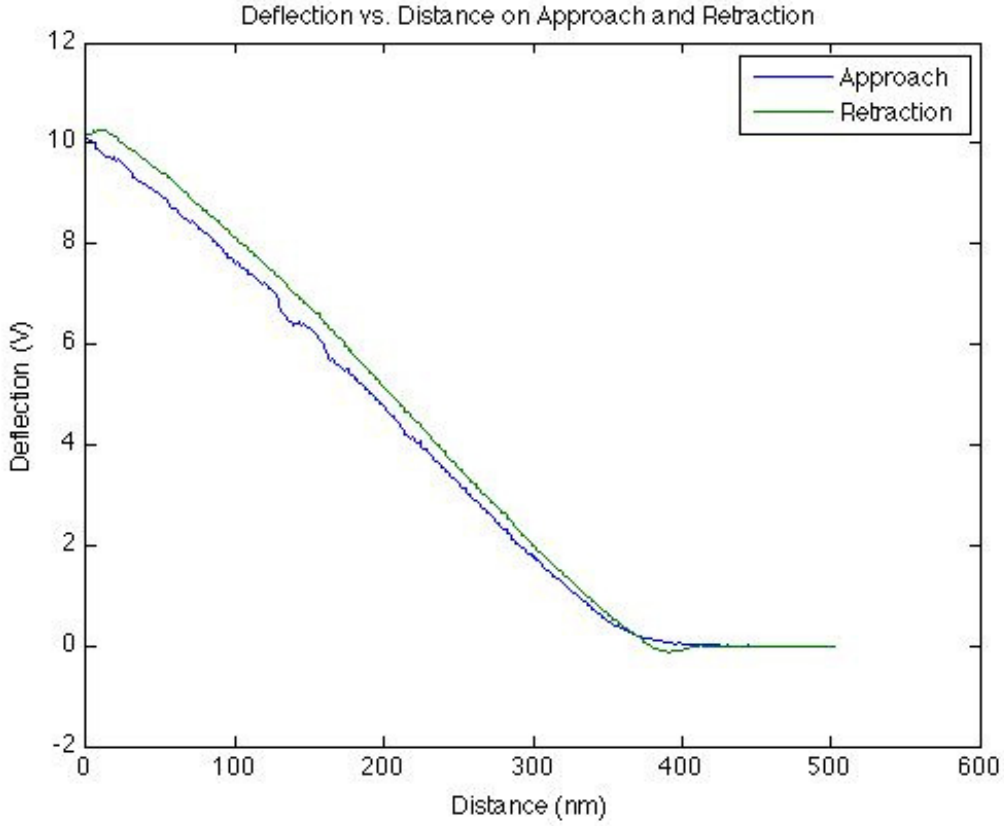
Deflection vs. Distance on Approach and Retraction
Approach
Retraction
Deflection (V)
Distance (nm)
12
10
8
6
4
2
0
-2
0
100
200
300
400
500
600

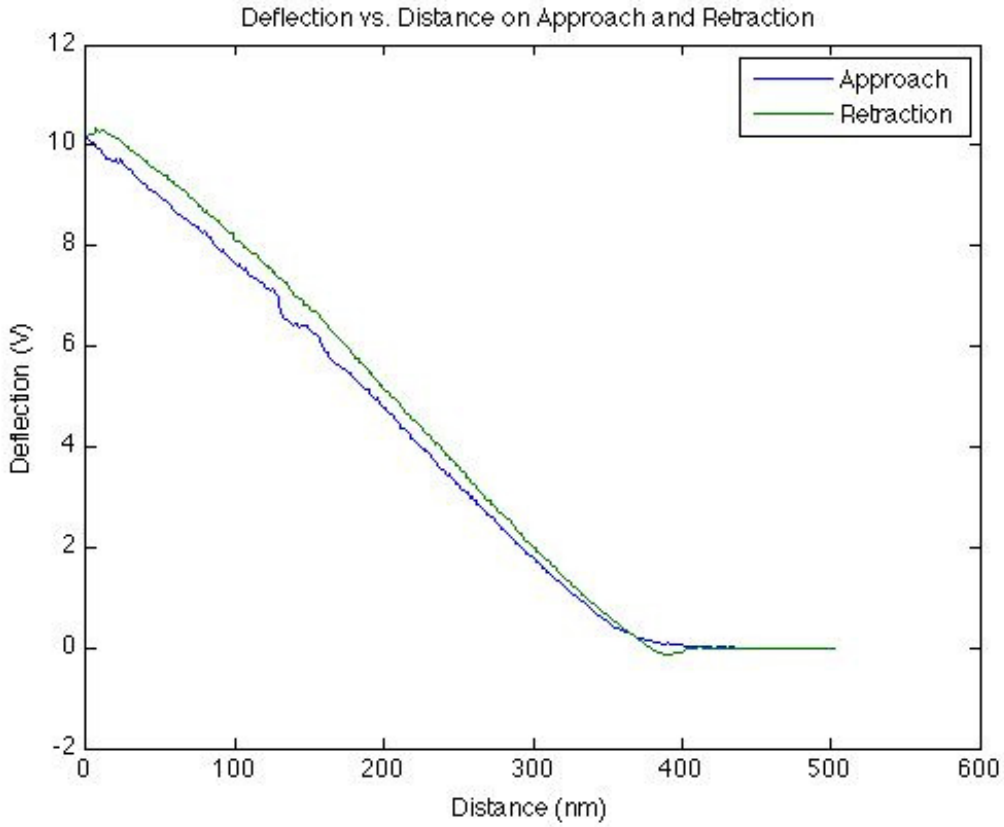
Deflection vs. Distance on Approach and Retraction
Approach
Retraction
Deflection (V)
Distance (nm)
12
10
8
6
4
2
0
-2
0
100
200
300
400
500
600

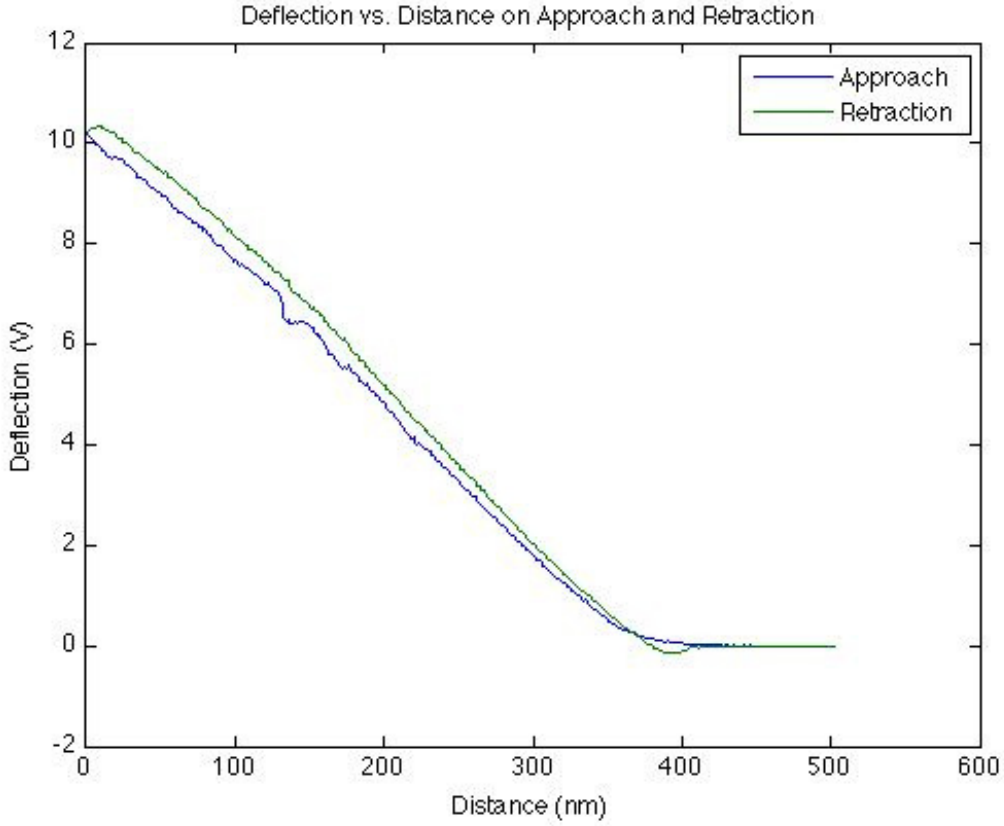
Deflection vs. Distance on Approach and Retraction
Approach
Retraction
Deflection (V)
Distance (nm)
12
10
8
6
4
2
0
-2
0
100
200
300
400
500
600

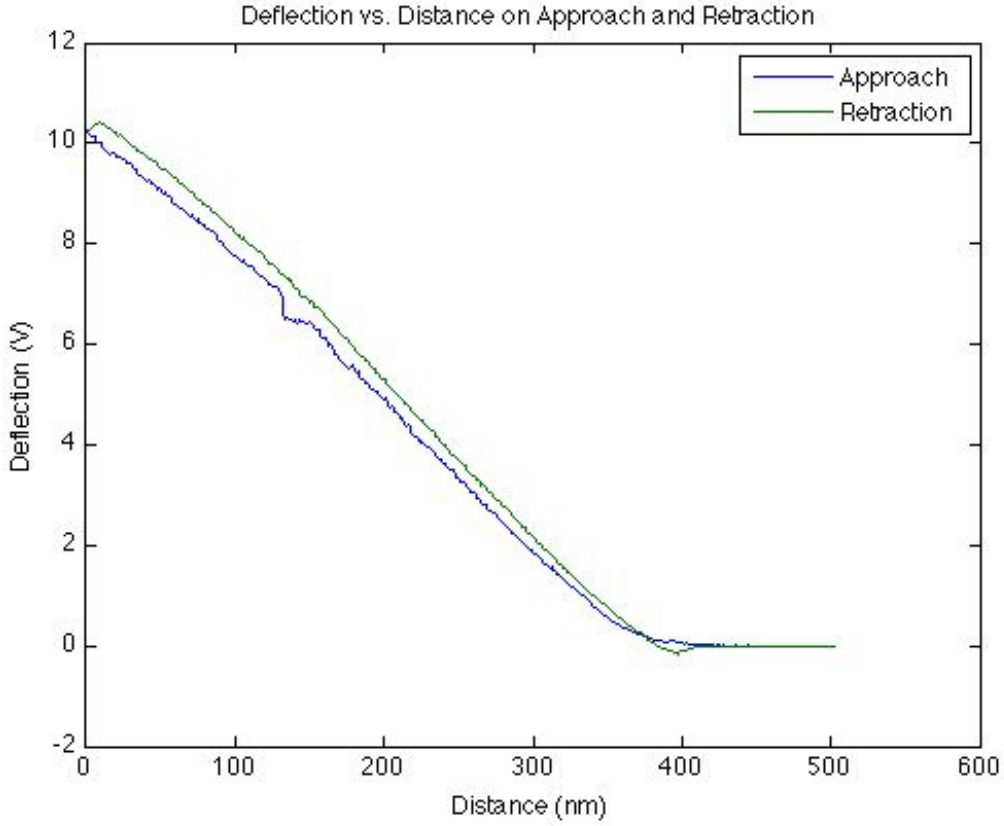
Deflection vs. Distance on Approach and Retraction
Approach
Retraction
Deflection (V)
Distance (nm)
12
10
8
6
4
2
0
-2
0
100
200
300
400
500
600

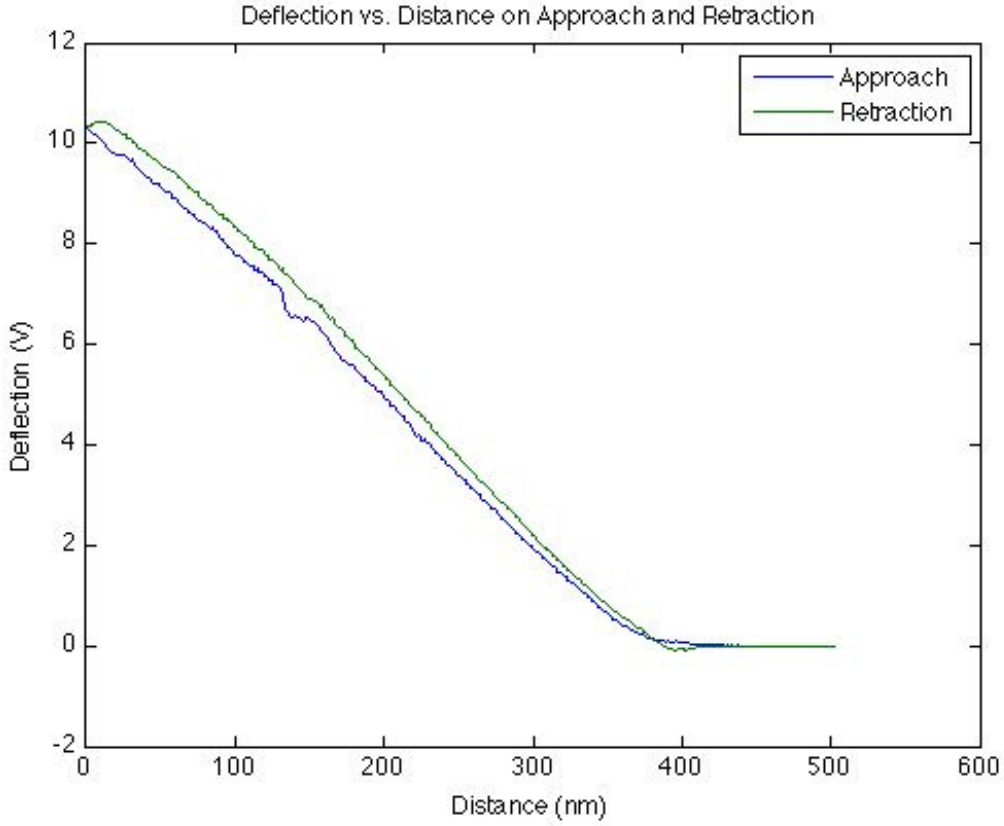
Deflection vs. Distance on Approach and Retraction
Approach
Retraction
Deflection (V)
Distance (nm)
12
10
8
6
4
2
0
-2
0
100
200
300
400
500
600

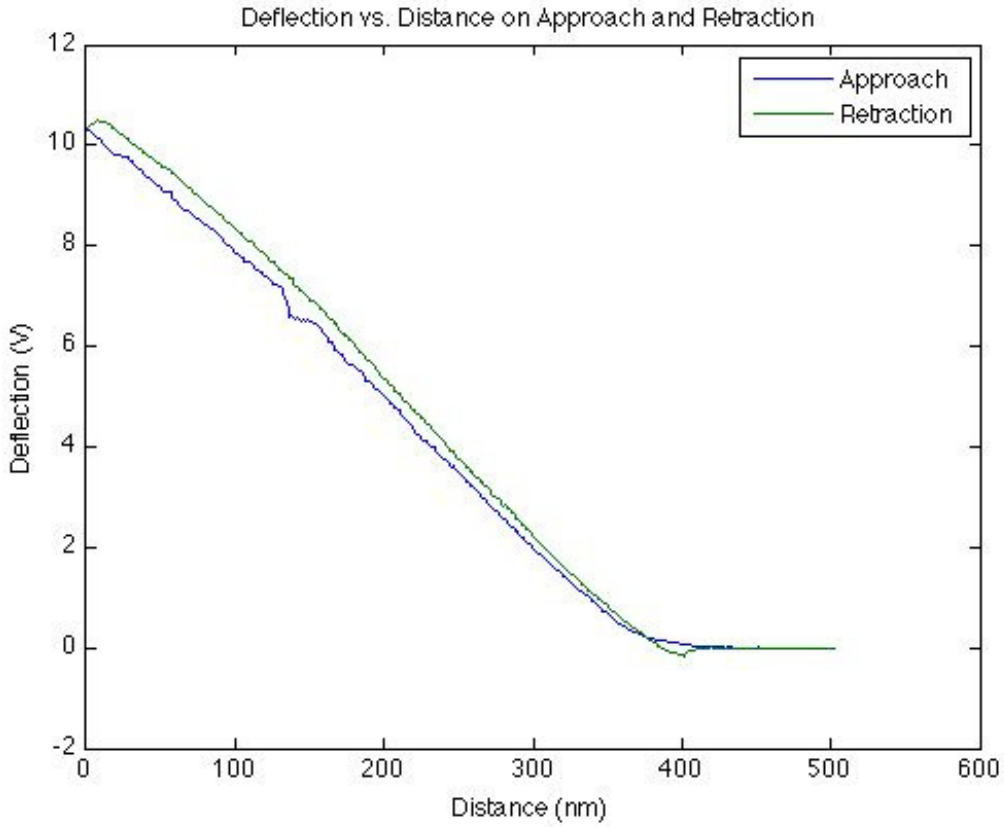
Deflection vs. Distance on Approach and Retraction
Approach
Retraction
Deflection (V)
Distance (nm)
12
10
8
6
4
2
0
-2
0
100
200
300
400
500
600

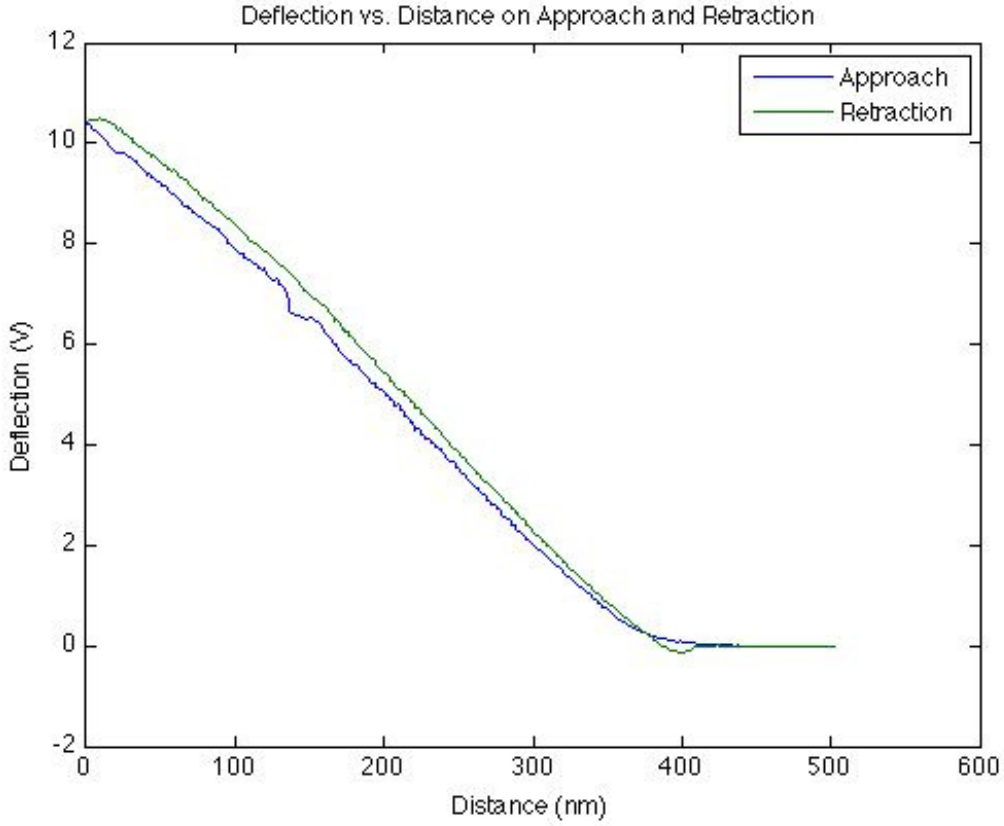
Deflection vs. Distance on Approach and Retraction
Approach
Retraction
Deflection (V)
Distance (nm)
12
10
8
6
4
2
0
-2
0
100
200
300
400
500
600

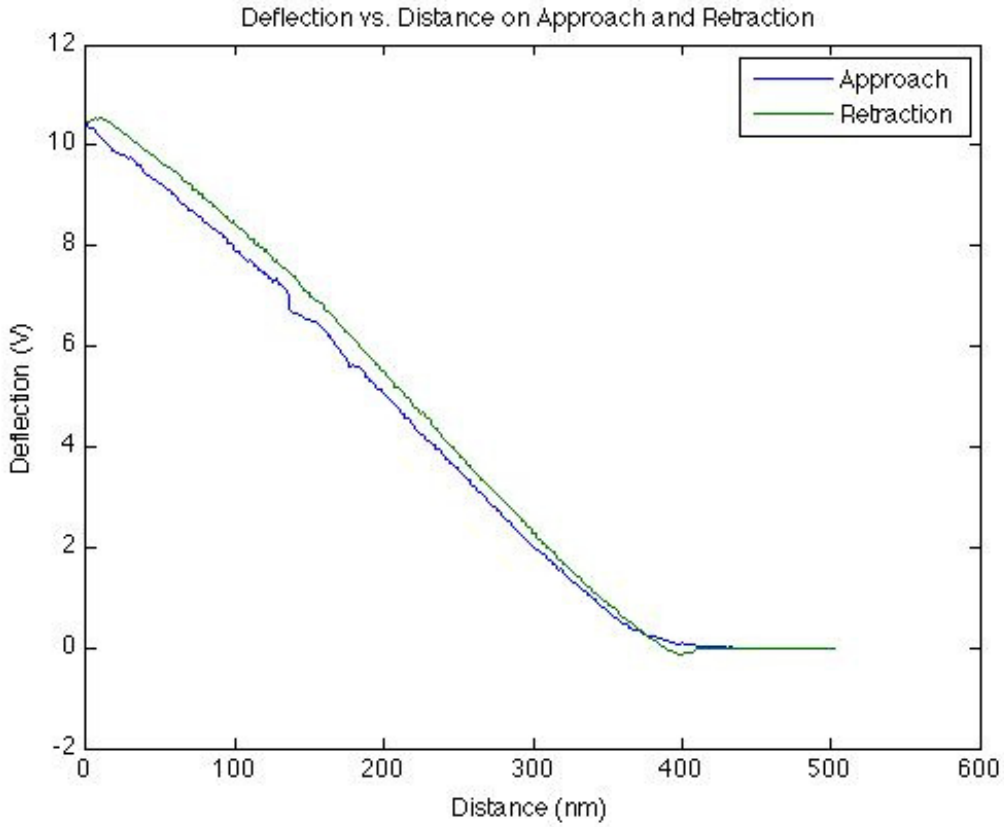
Deflection vs. Distance on Approach and Retraction
Approach
Retraction
Deflection (V)
Distance (nm)
12
10
8
6
4
2
0
-2
0
100
200
300
400
500
600

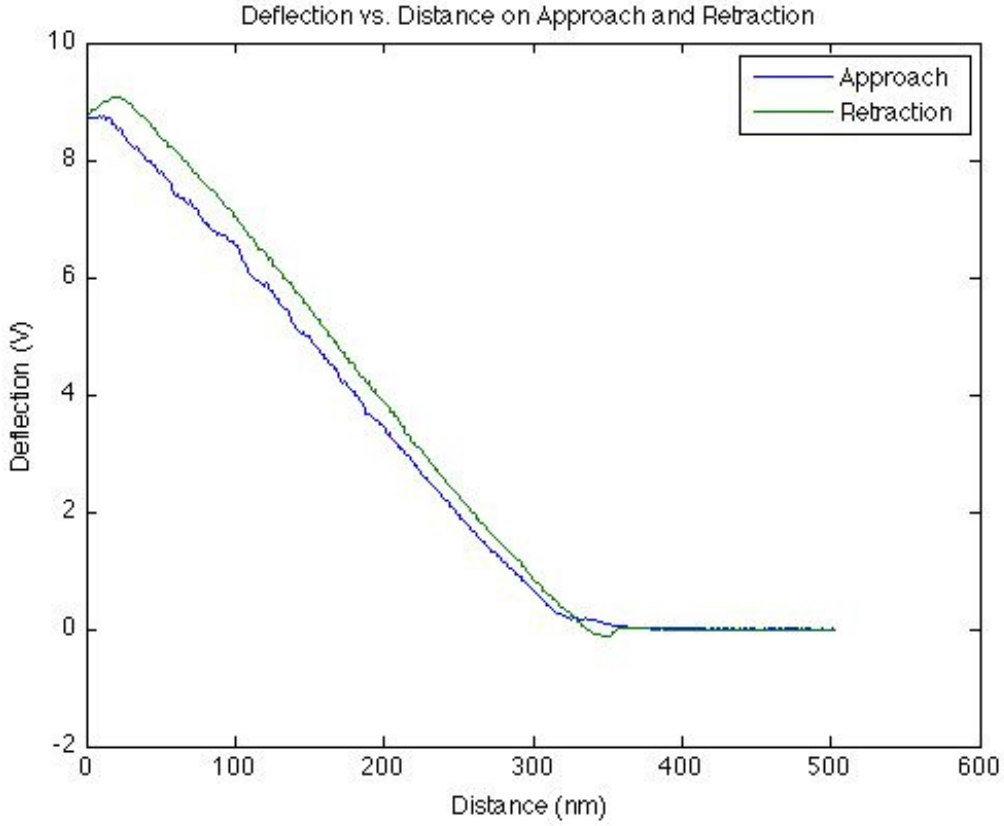
Deflection vs. Distance on Approach and Retraction
Approach
Retraction
Deflection (V)
Distance (nm)
10
8
6
4
2
0
-2
0
100
200
300
400
500
600

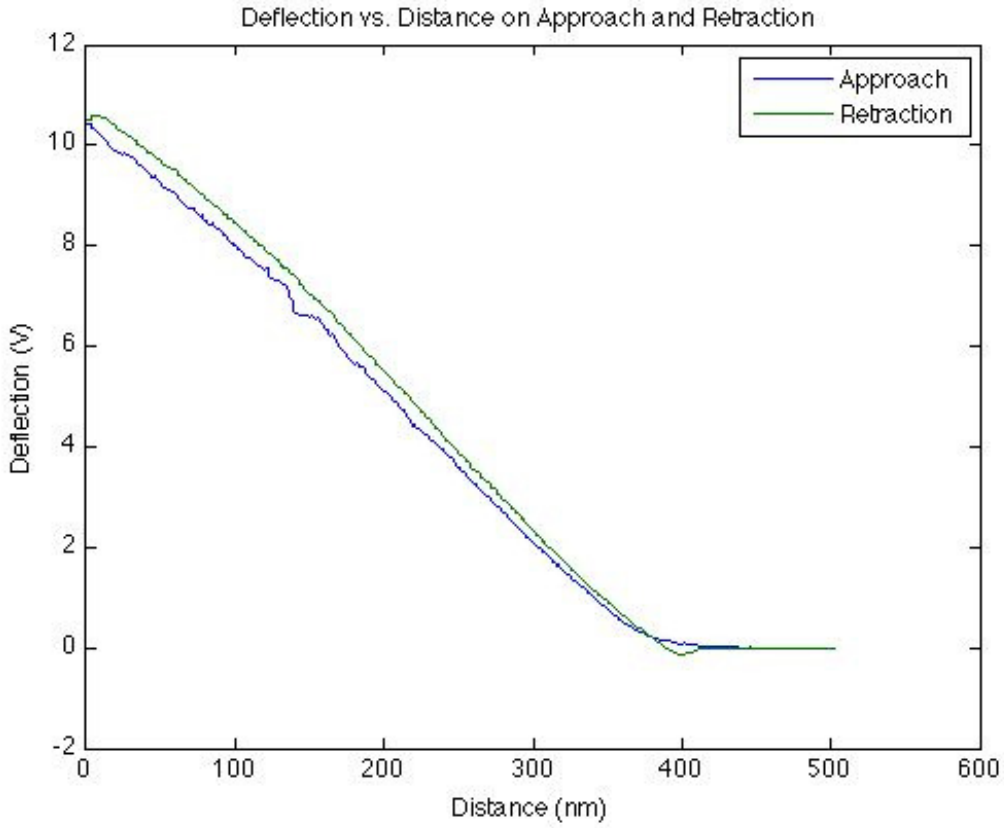
Deflection vs. Distance on Approach and Retraction
Approach
Retraction
Deflection (V)
Distance (nm)
12
10
8
6
4
2
0
-2
0
100
200
300
400
500
600

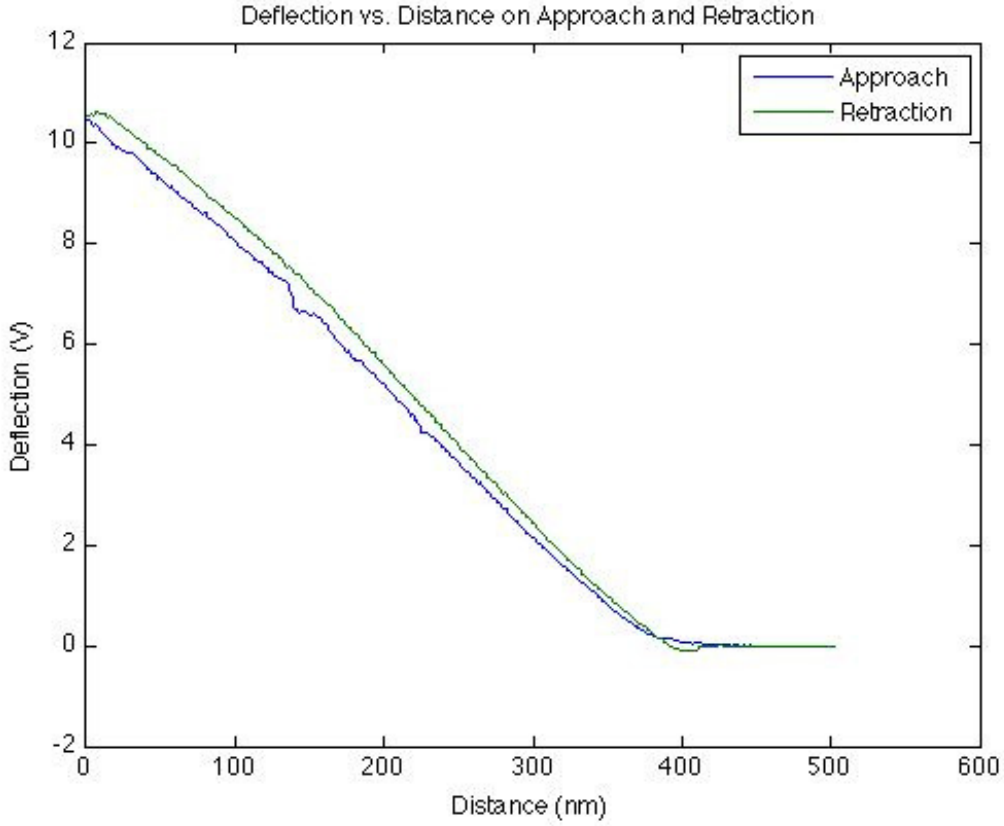
Deflection vs. Distance on Approach and Retraction
Approach
Retraction
Deflection (V)
Distance (nm)
12
10
8
6
4
2
0
-2
0
100
200
300
400
500
600

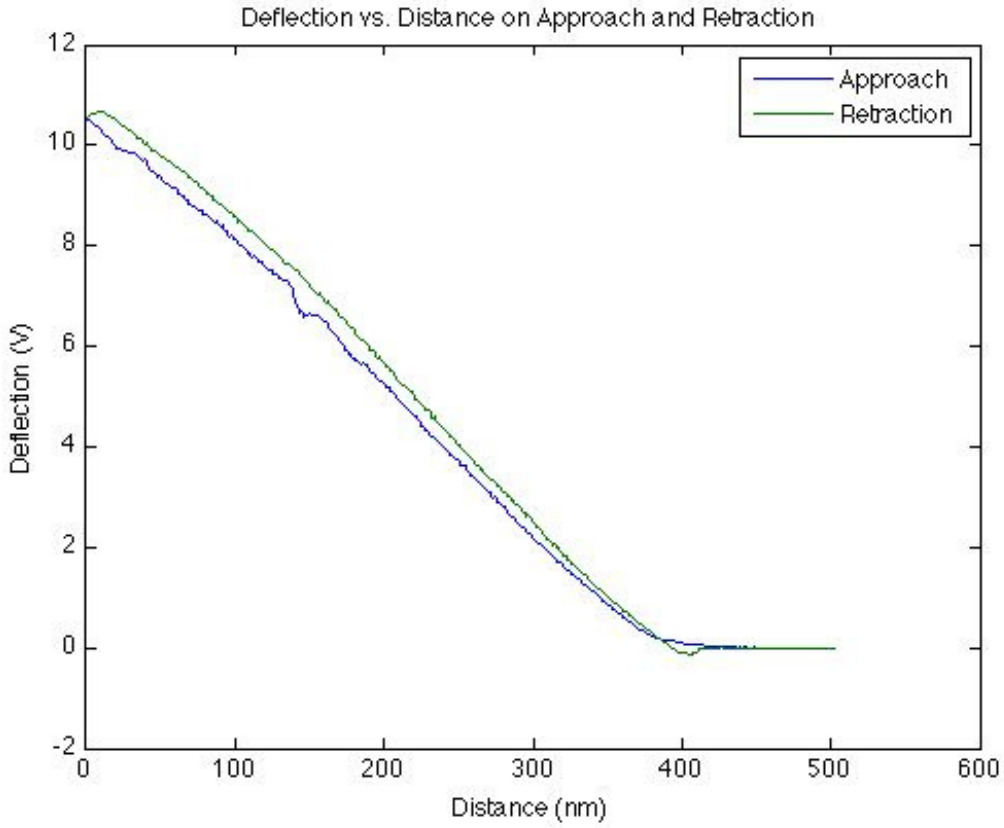
Deflection vs. Distance on Approach and Retraction
Approach
Retraction
Deflection (V)
Distance (nm)
12
10
8
6
4
2
0
-2
0
100
200
300
400
500
600

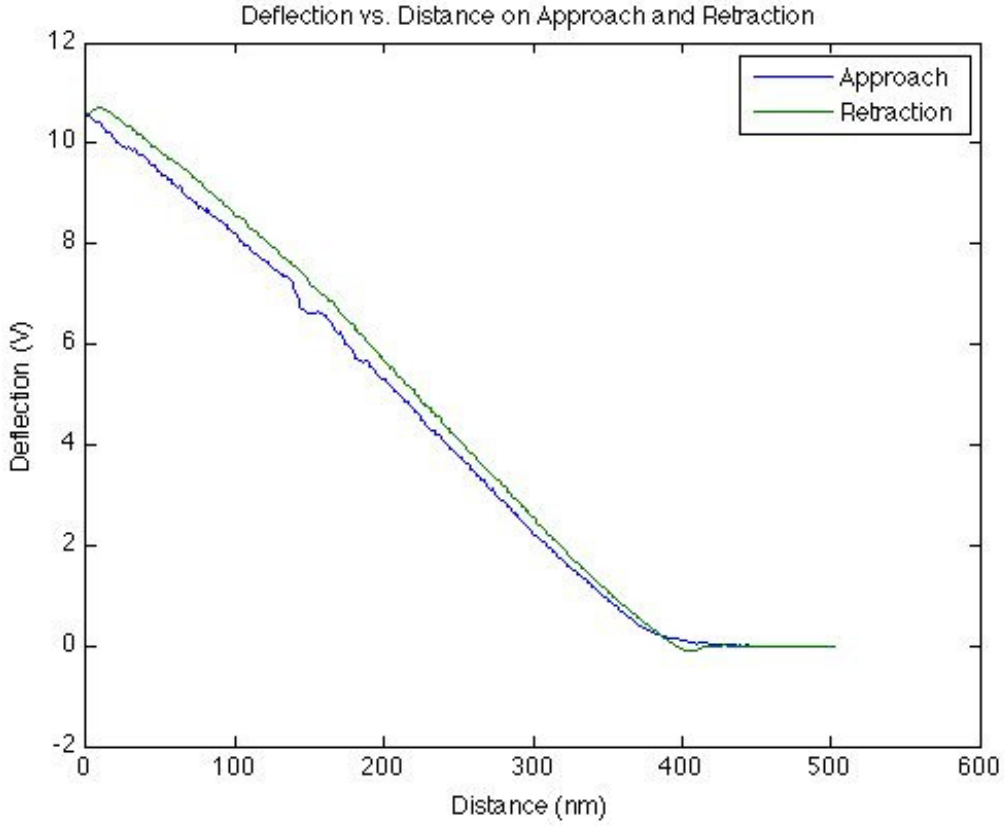
Deflection vs. Distance on Approach and Retraction
Approach
Retraction
Deflection (V)
Distance (nm)
12
10
8
6
4
2
0
-2
0
100
200
300
400
500
600

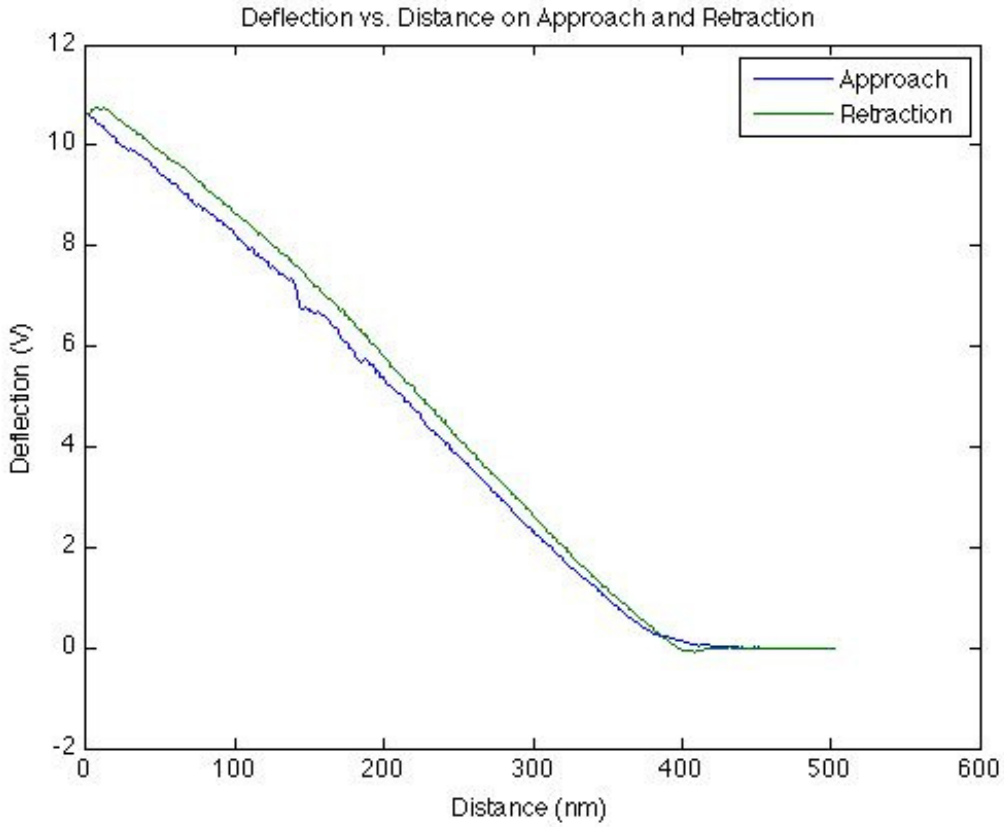
Deflection vs. Distance on Approach and Retraction
Approach
Retraction
Deflection (V)
Distance (nm)
12
10
8
6
4
2
0
-2
0
100
200
300
400
500
600

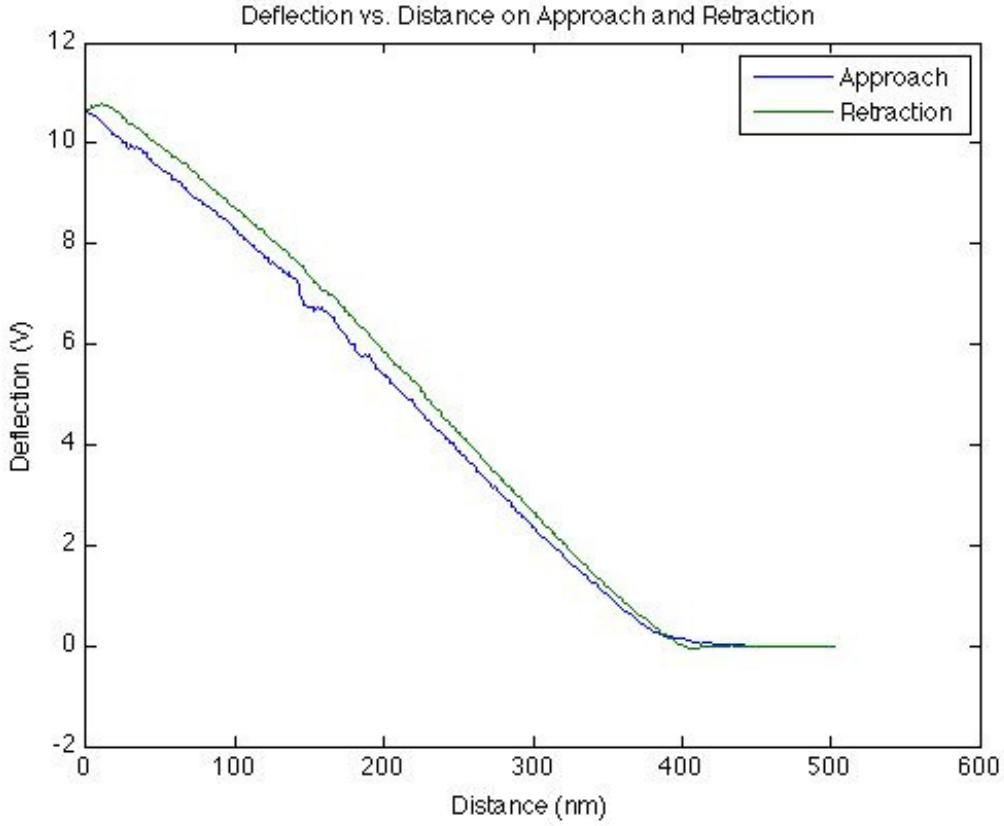
Deflection vs. Distance on Approach and Retraction
Approach
Retraction
Deflection (V)
Distance (nm)
12
10
8
6
4
2
0
-2
0
100
200
300
400
500
600

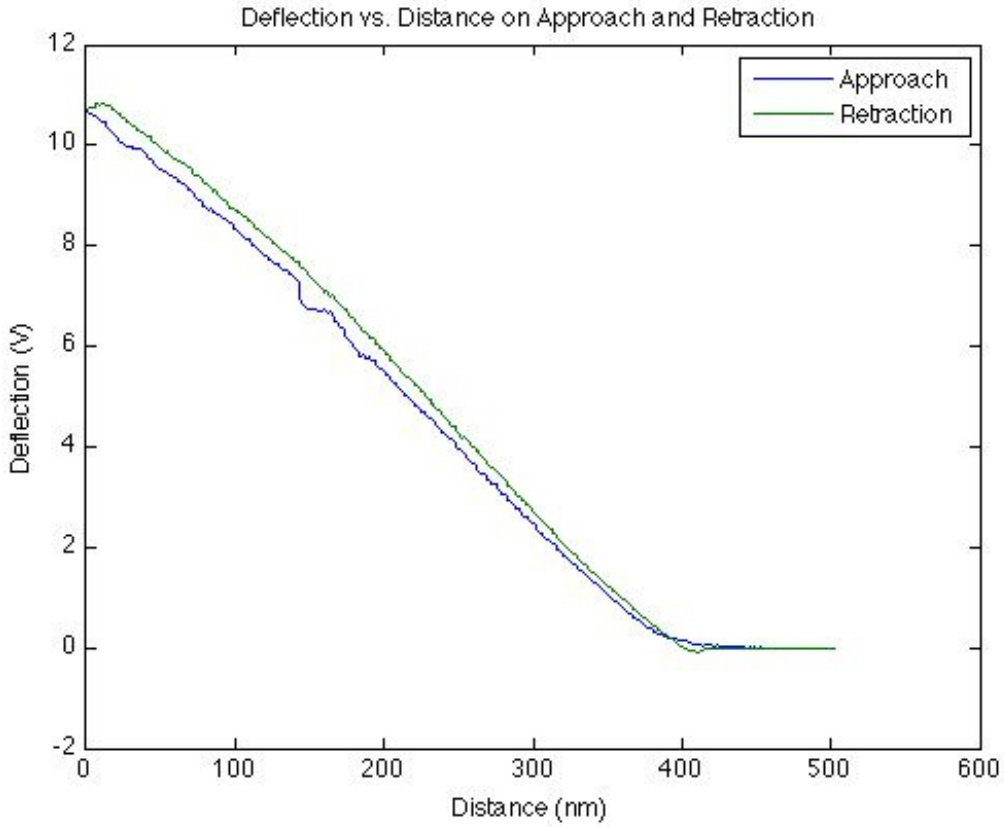
Deflection vs. Distance on Approach and Retraction
Approach
Retraction
Deflection (V)
Distance (nm)
12
10
8
6
4
2
0
-2
0
100
200
300
400
500
600

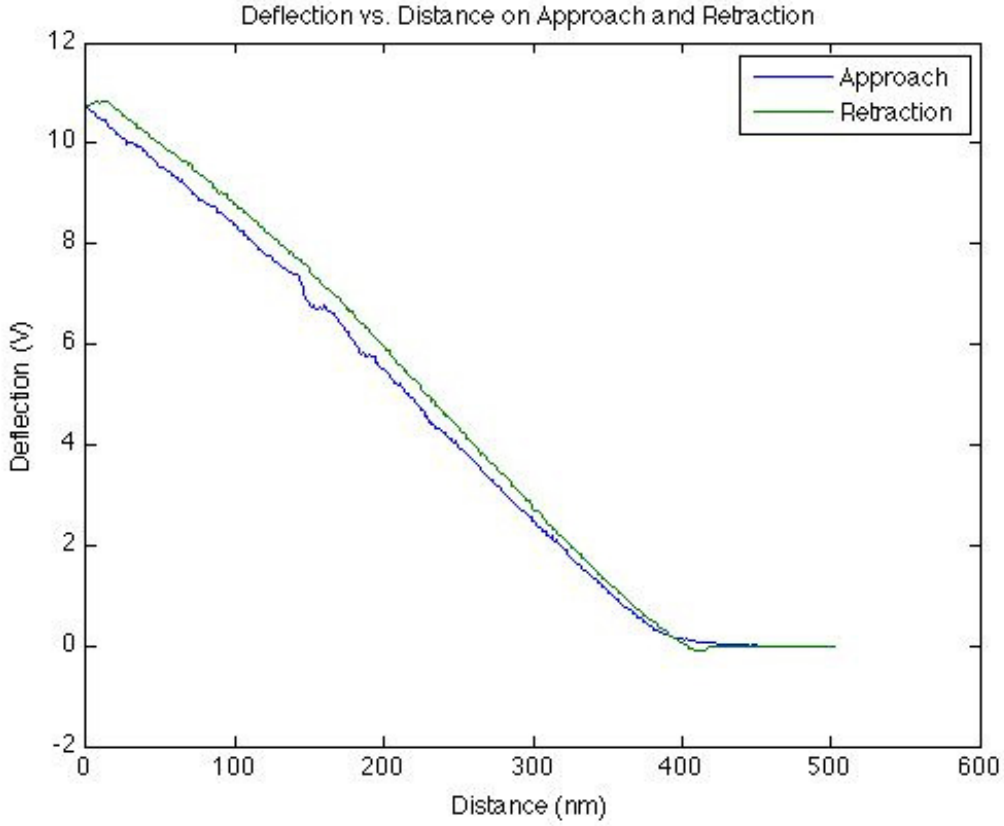
Deflection vs. Distance on Approach and Retraction
Approach
Retraction
Deflection (V)
Distance (nm)
12
10
8
6
4
2
0
-2
0
100
200
300
400
500
600

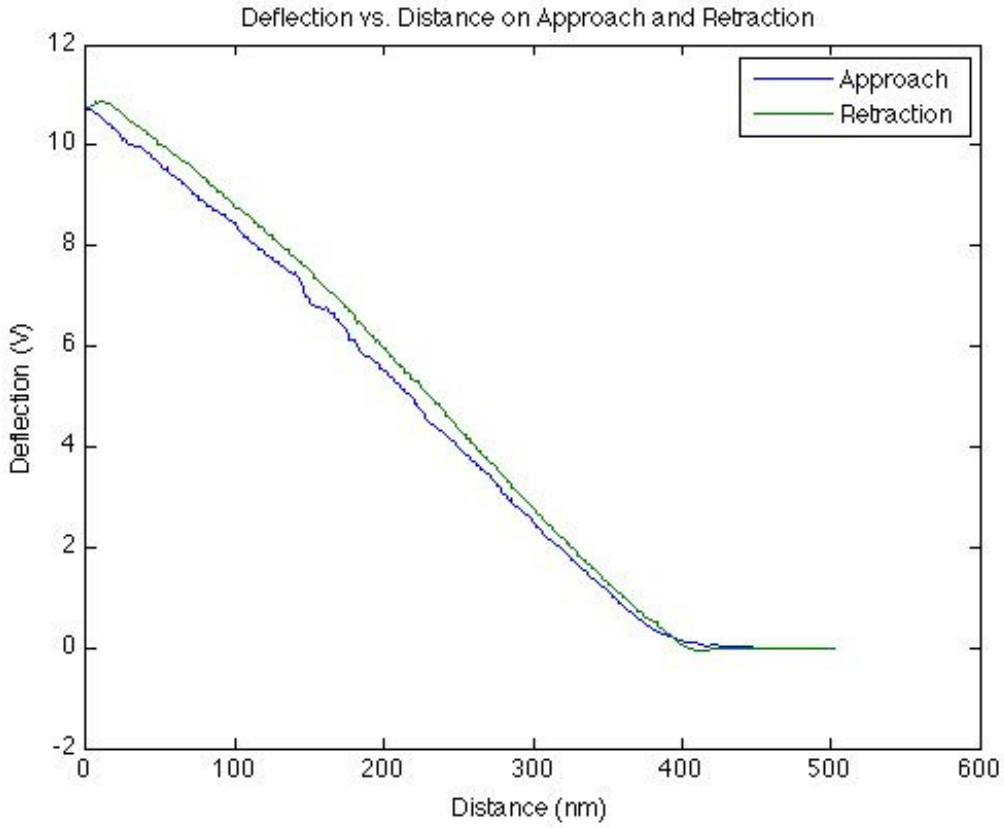
Deflection vs. Distance on Approach and Retraction
Approach
Retraction
Deflection (V)
Distance (nm)
12
10
8
6
4
2
0
-2
0
100
200
300
400
500
600

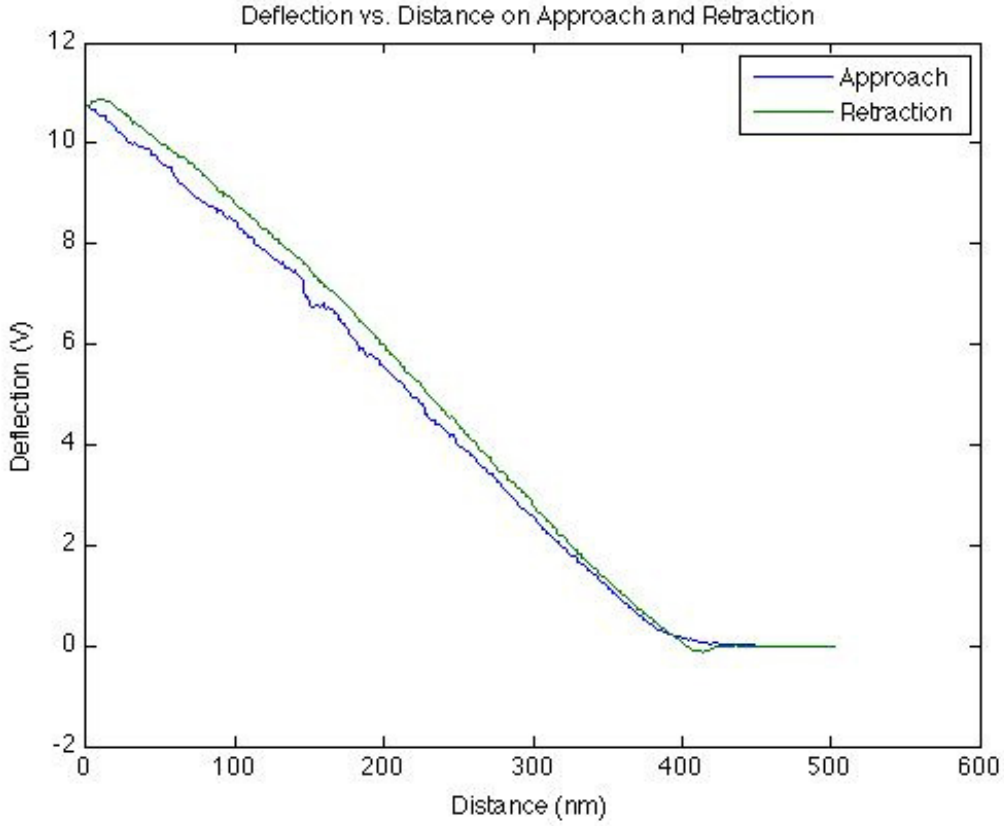
Deflection vs. Distance on Approach and Retraction
Approach
Retraction
Deflection (V)
Distance (nm)
12
10
8
6
4
2
0
-2
0
100
200
300
400
500
600

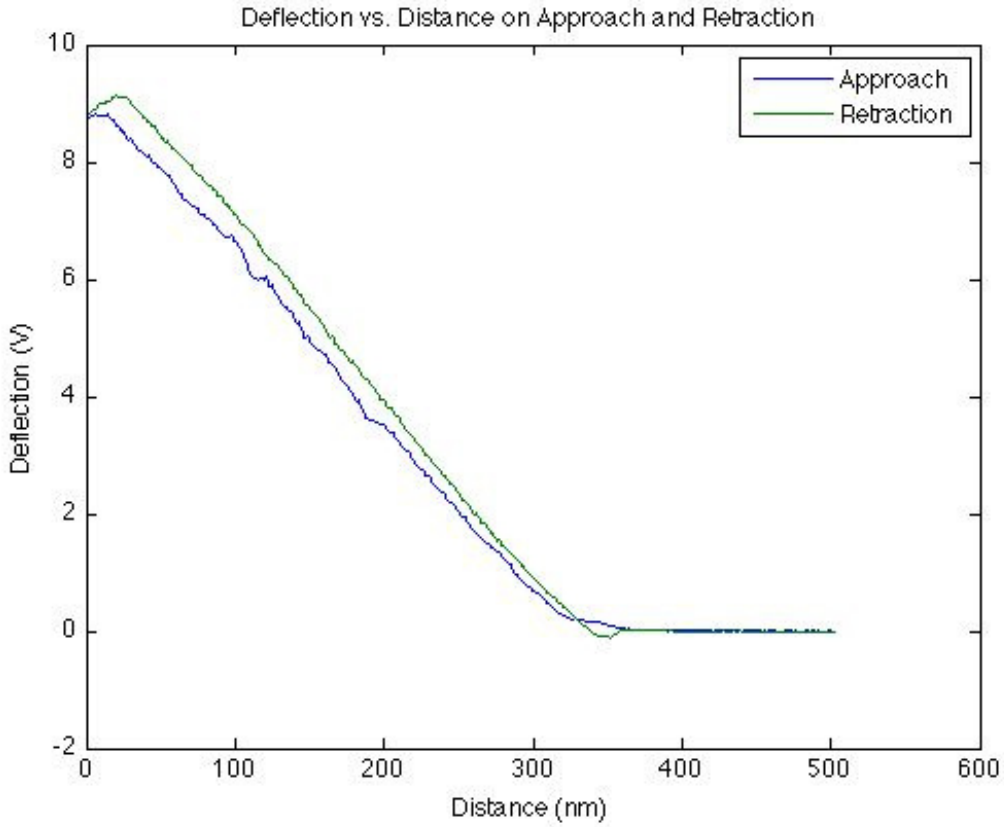
Deflection vs. Distance on Approach and Retraction
Approach
Retraction
Deflection (V)
Distance (nm)
10
8
6
4
2
0
-2
0
100
200
300
400
500
600

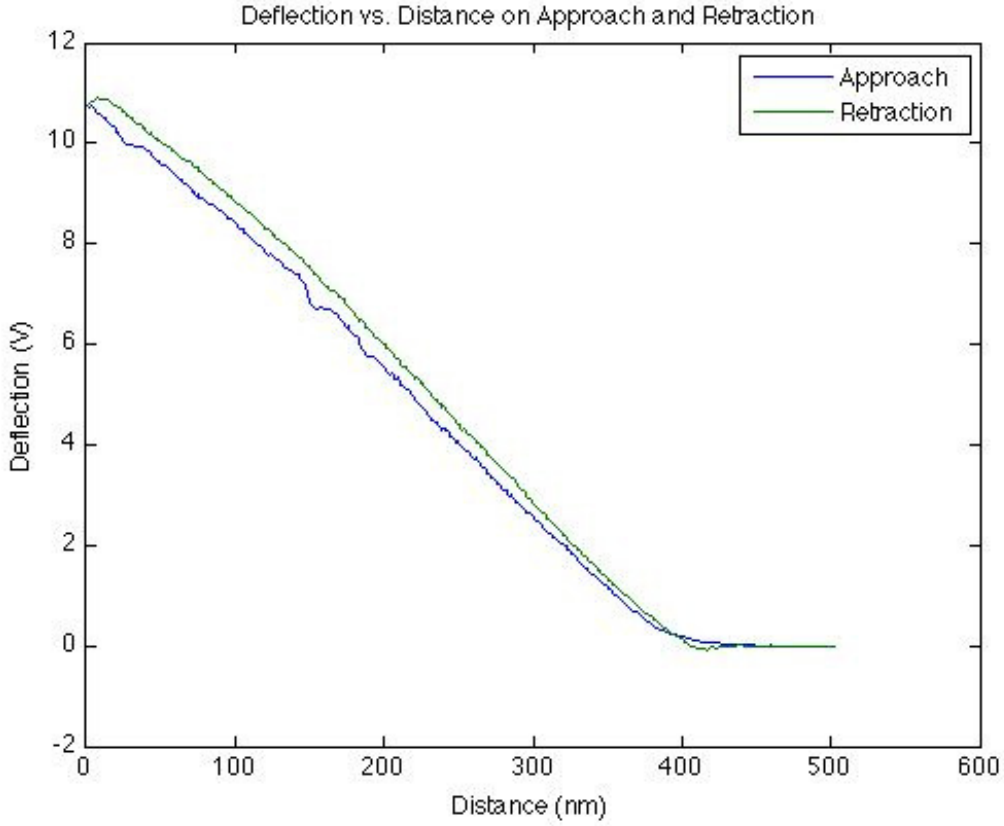
Deflection vs. Distance on Approach and Retraction
Approach
Retraction
Deflection (V)
Distance (nm)
12
10
8
6
4
2
0
-2
0
100
200
300
400
500
600

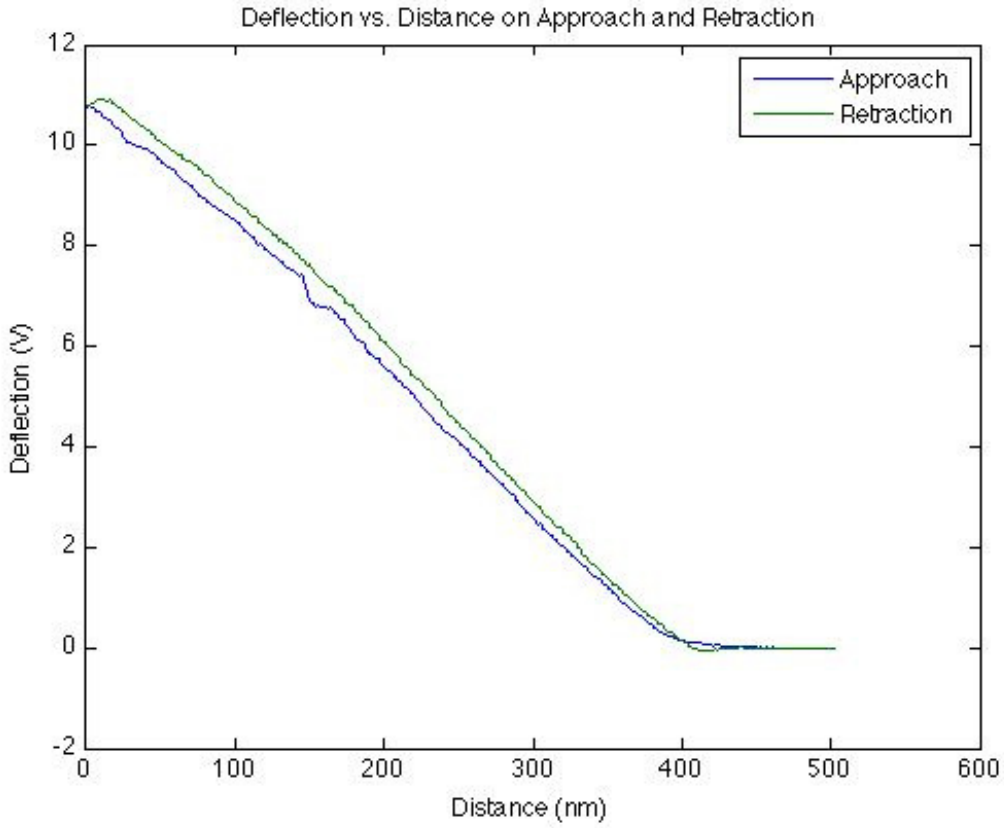
Deflection vs. Distance on Approach and Retraction
Approach
Retraction
Deflection (V)
Distance (nm)
12
10
8
6
4
2
0
-2
0
100
200
300
400
500
600

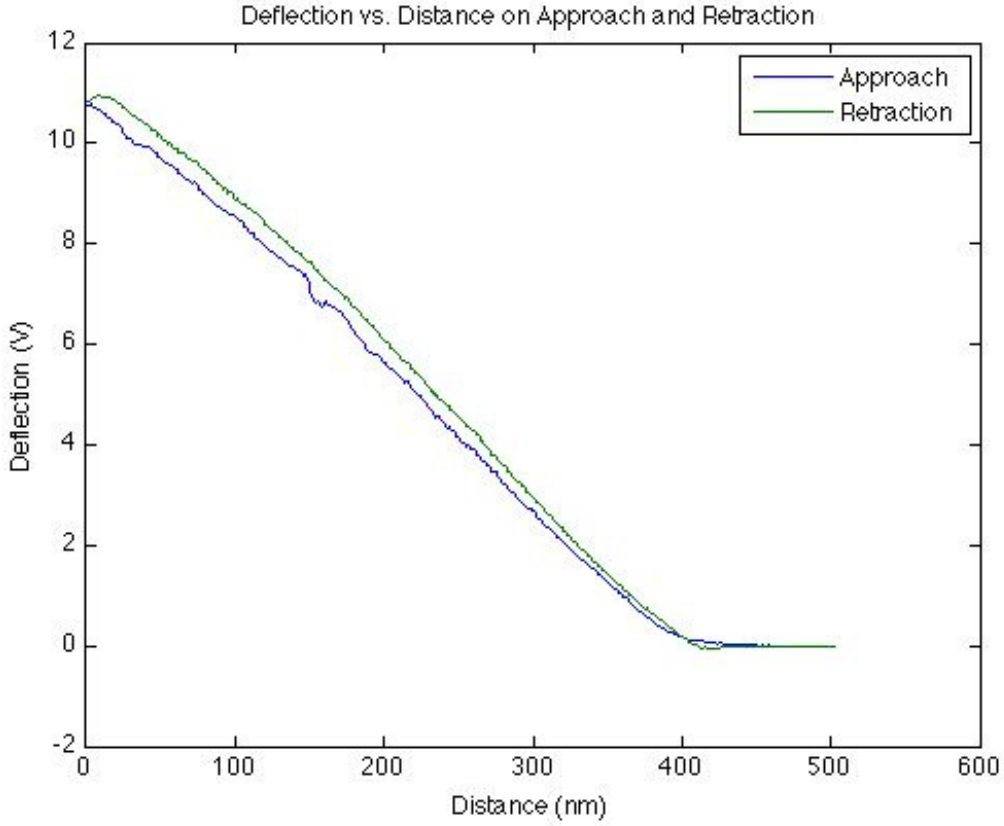
Deflection vs. Distance on Approach and Retraction
Approach
Retraction
Deflection (V)
Distance (nm)
12
10
8
6
4
2
0
-2
0
100
200
300
400
500
600

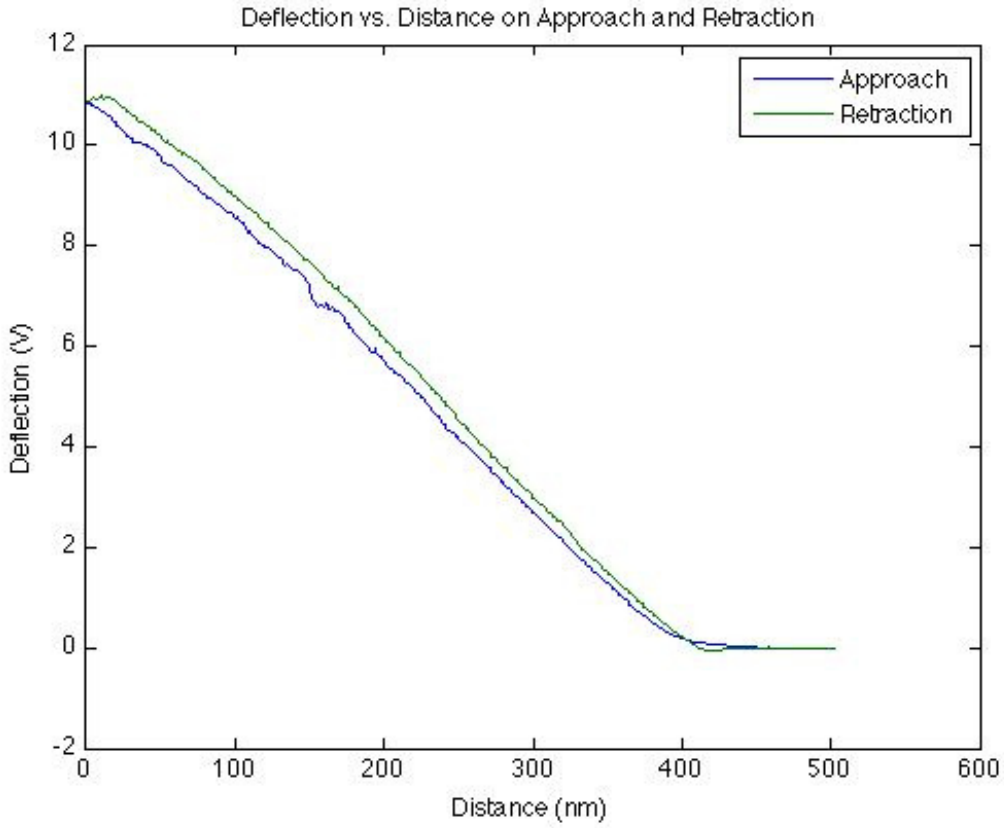
Deflection vs. Distance on Approach and Retraction
Approach
Retraction
Deflection (V)
Distance (nm)
12
10
8
6
4
2
0
-2
0
100
200
300
400
500
600

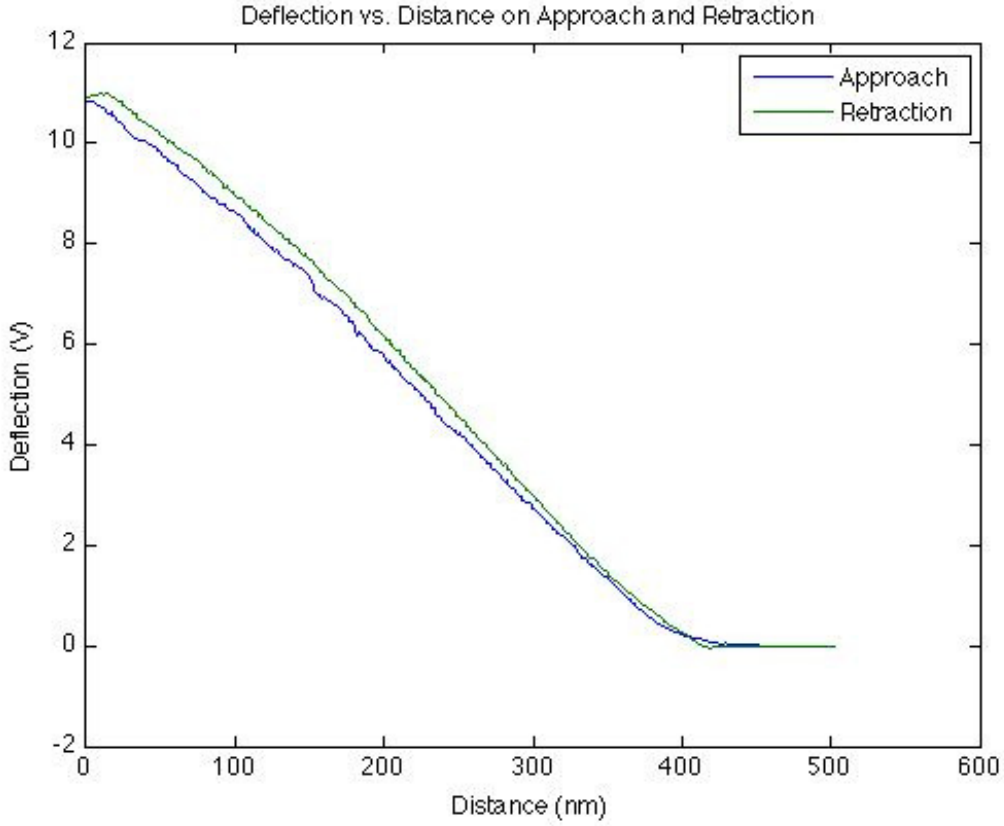
Deflection vs. Distance on Approach and Retraction
Approach
Retraction
Deflection (V)
Distance (nm)
12
10
8
6
4
2
0
-2
0
100
200
300
400
500
600

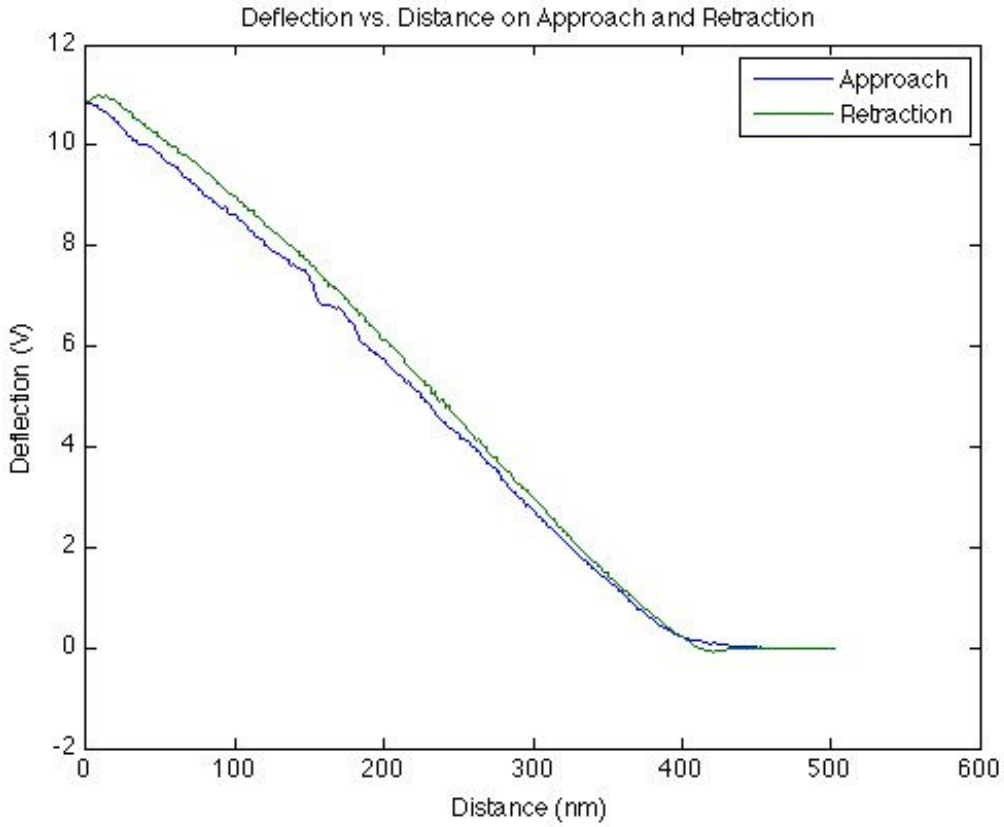
Deflection vs. Distance on Approach and Retraction
Approach
Retraction
Deflection (V)
Distance (nm)
12
10
8
6
4
2
0
-2
0
100
200
300
400
500
600

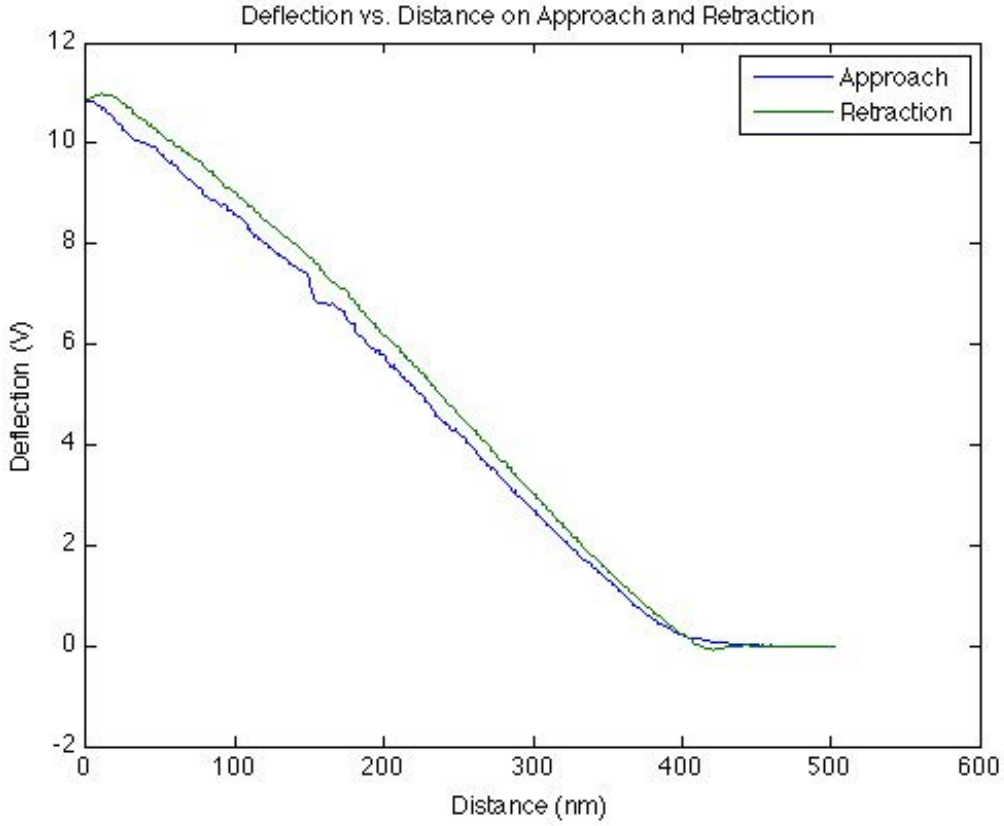
Deflection vs. Distance on Approach and Retraction
Approach
Retraction
Deflection (V)
Distance (nm)
12
10
8
6
4
2
0
-2
0
100
200
300
400
500
600

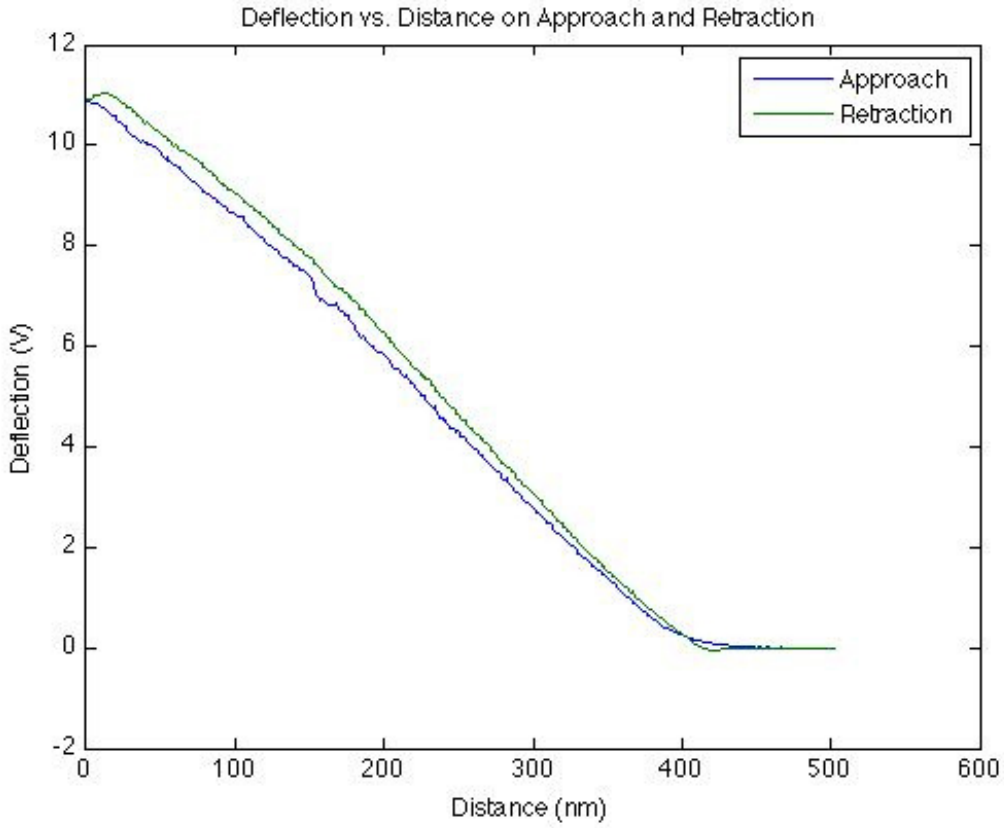
Deflection vs. Distance on Approach and Retraction
Approach
Retraction
Deflection (V)
Distance (nm)
12
10
8
6
4
2
0
-2
0
100
200
300
400
500
600

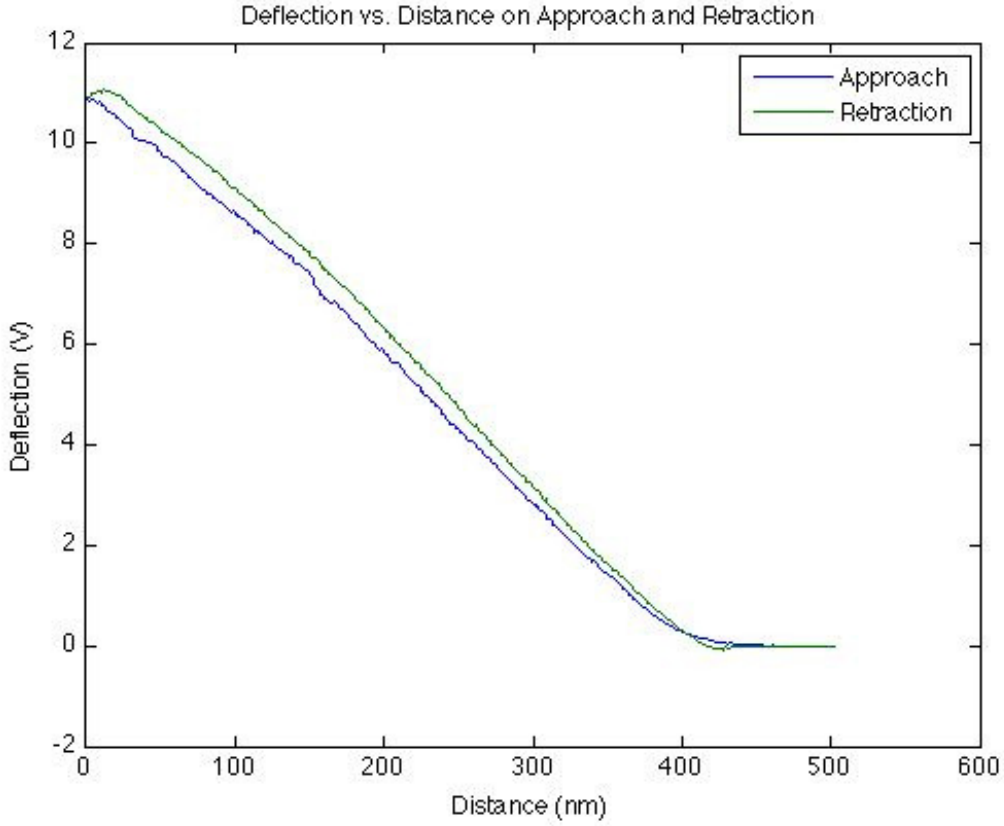
Deflection vs. Distance on Approach and Retraction
Approach
Retraction
Deflection (V)
Distance (nm)
12
10
8
6
4
2
0
-2
0
100
200
300
400
500
600

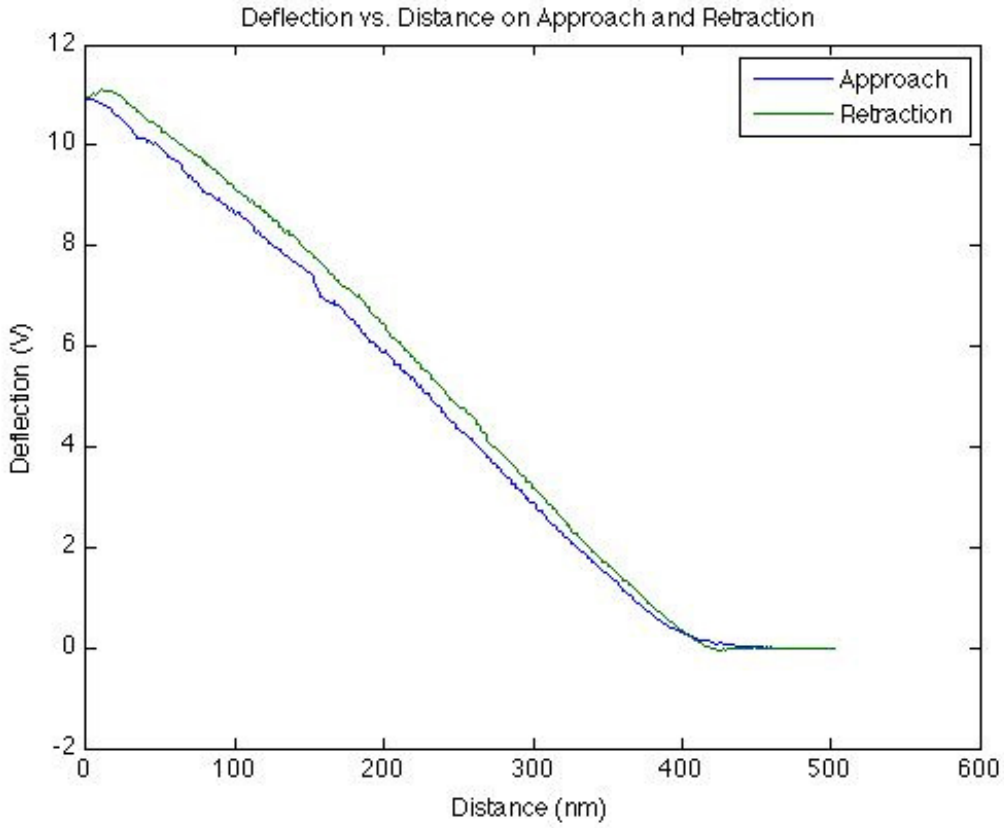
Deflection vs. Distance on Approach and Retraction
Approach
Retraction
Deflection (V)
Distance (nm)
12
10
8
6
4
2
0
-2
0
100
200
300
400
500
600

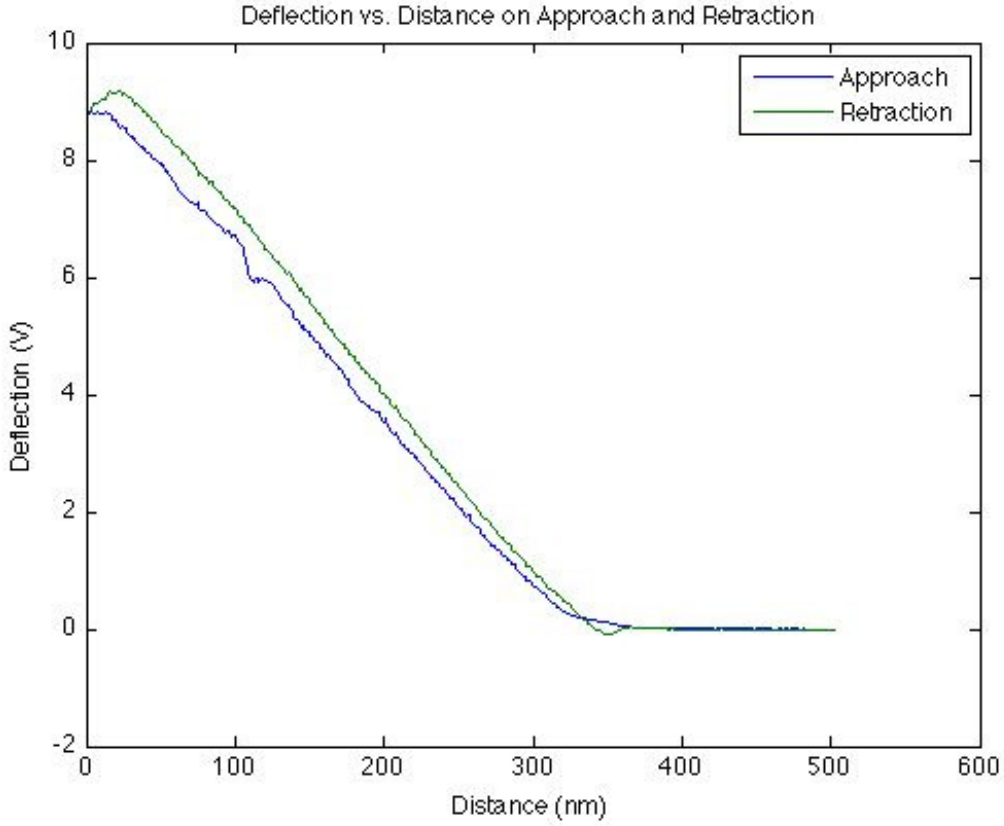
Deflection vs. Distance on Approach and Retraction
Approach
Retraction
Deflection (V)
Distance (nm)
10
8
6
4
2
0
-2
0
100
200
300
400
500
600

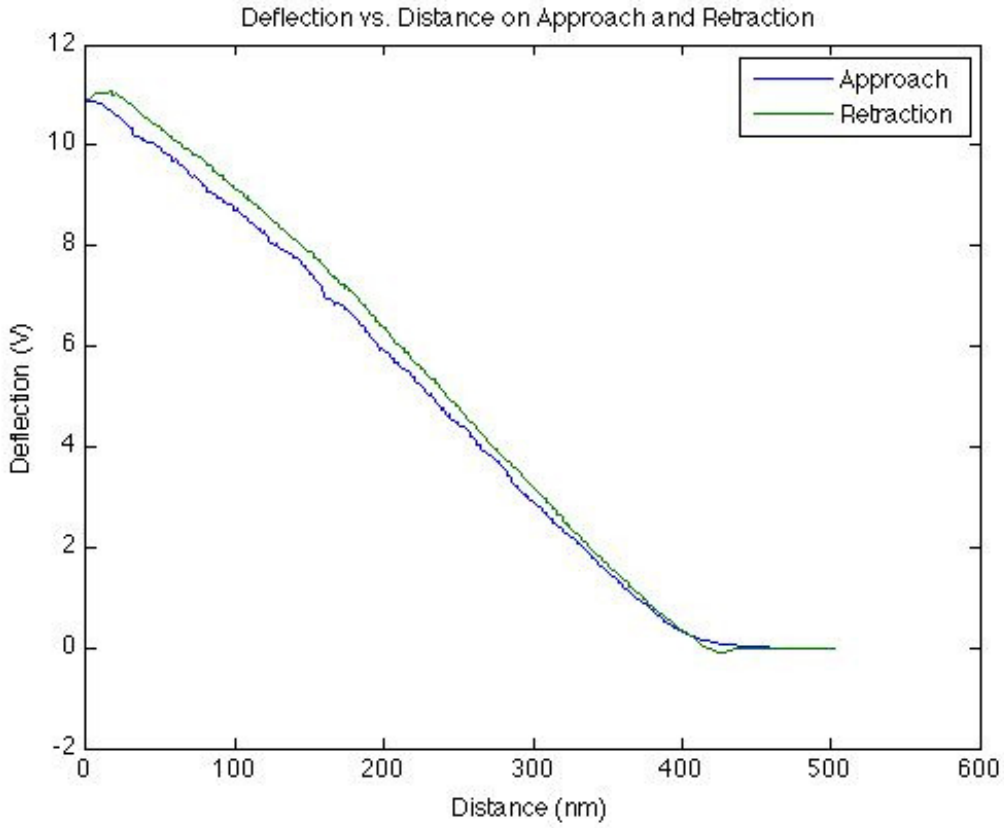
Deflection vs. Distance on Approach and Retraction
Approach
Retraction
Deflection (V)
Distance (nm)
12
10
8
6
4
2
0
-2
0
100
200
300
400
500
600

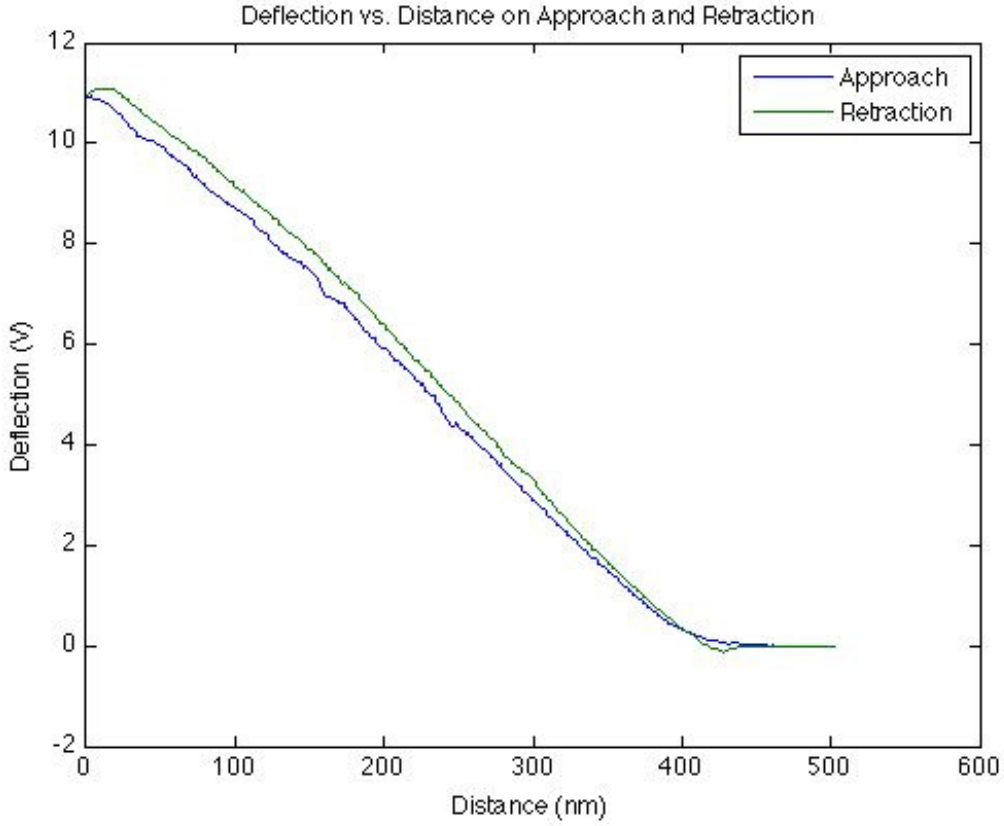
Deflection vs. Distance on Approach and Retraction
Approach
Retraction
Deflection (V)
Distance (nm)
12
10
8
6
4
2
0
-2
0
100
200
300
400
500
600

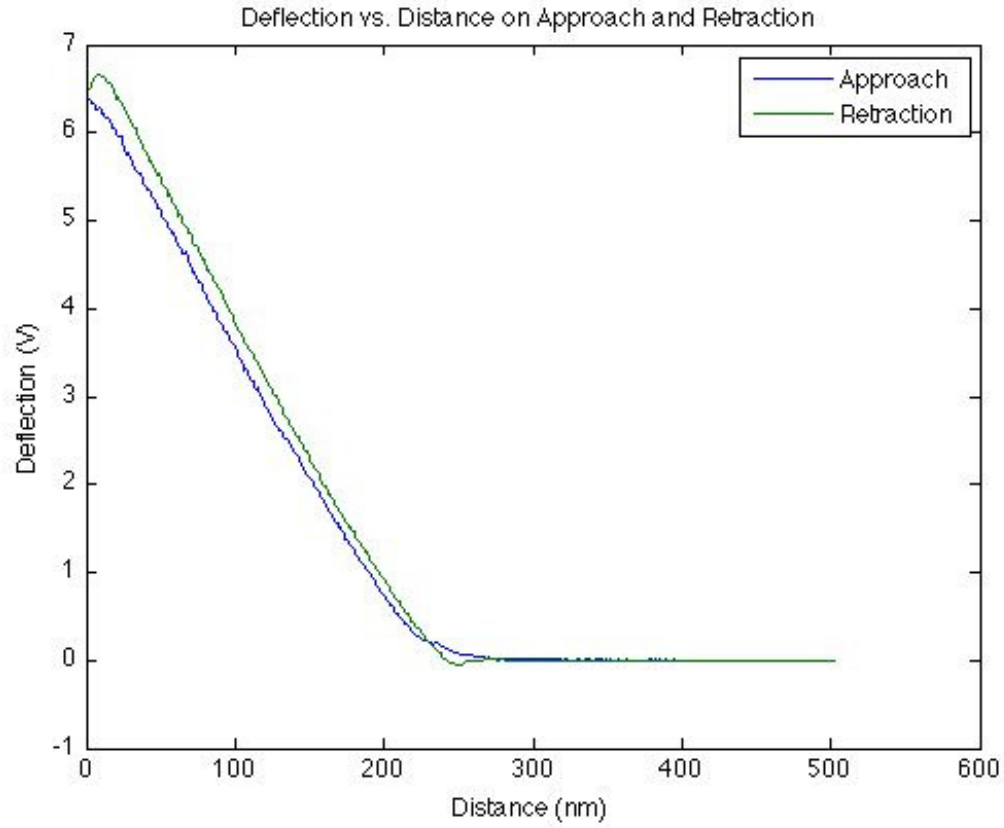
Deflection vs. Distance on Approach and Retraction
Approach
Retraction
Deflection (V)
Distance (nm)
7
6
5
4
3
2
1
0
-1
0
100
200
300
400
500
600

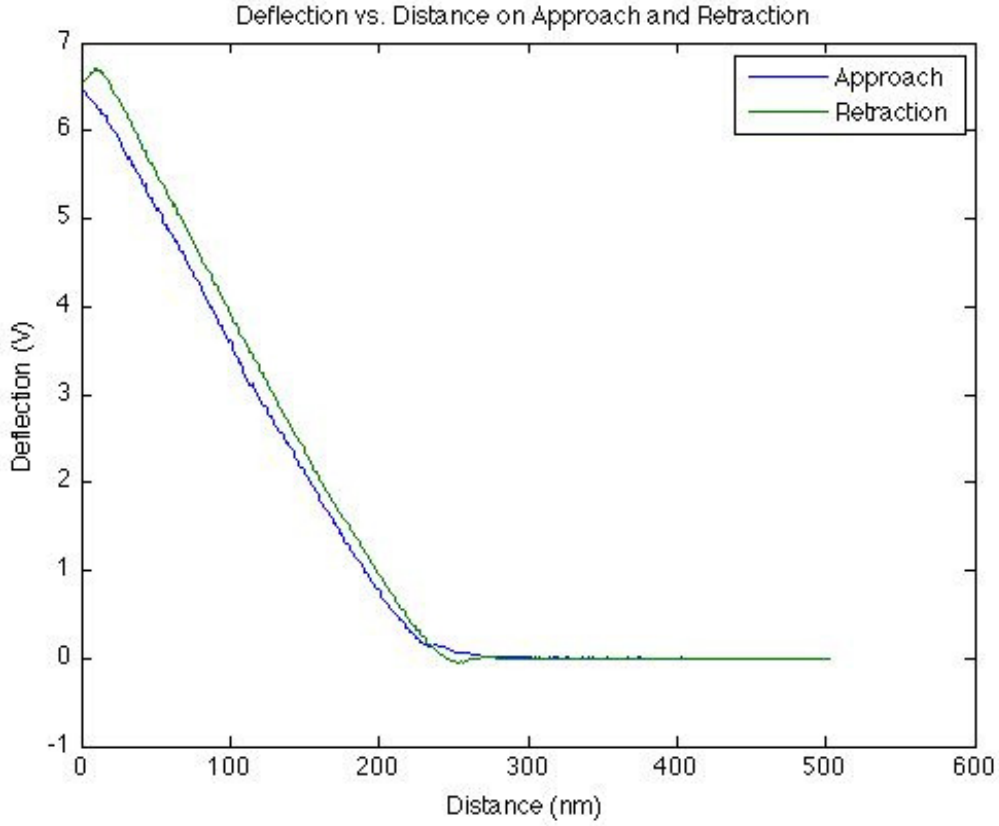
Deflection vs. Distance on Approach and Retraction
Approach
Retraction
Deflection (V)
Distance (nm)
7
6
5
4
3
2
1
0
-1
0
100
200
300
400
500
600

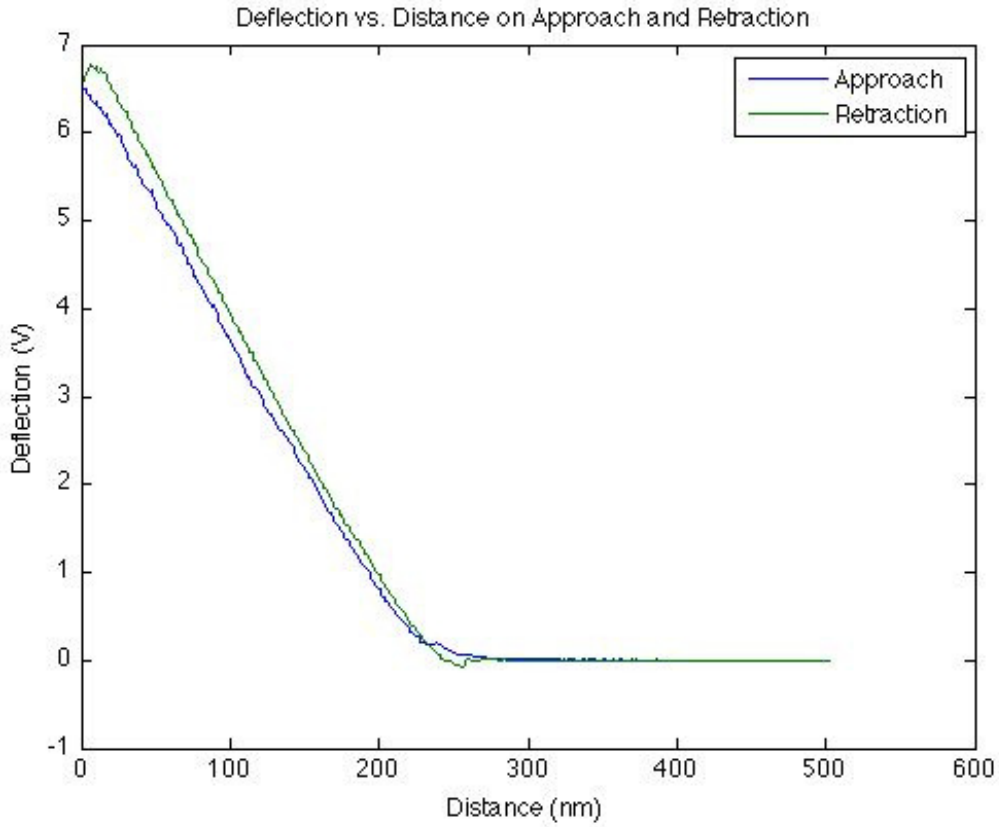
Deflection vs. Distance on Approach and Retraction
Approach
Retraction
Deflection (V)
Distance (nm)
7
6
5
4
3
2
1
0
-1
0
100
200
300
400
500
600

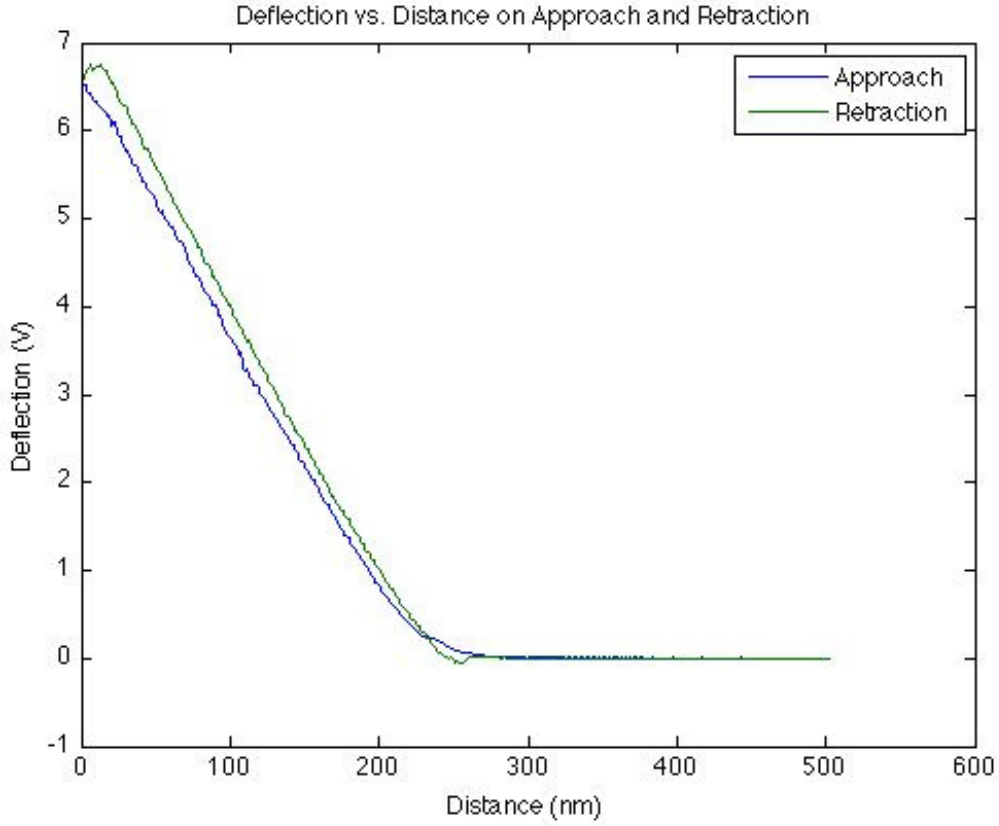
Deflection vs. Distance on Approach and Retraction
Approach
Retraction
Deflection (V)
Distance (nm)
7
6
5
4
3
2
1
0
-1
0
100
200
300
400
500
600

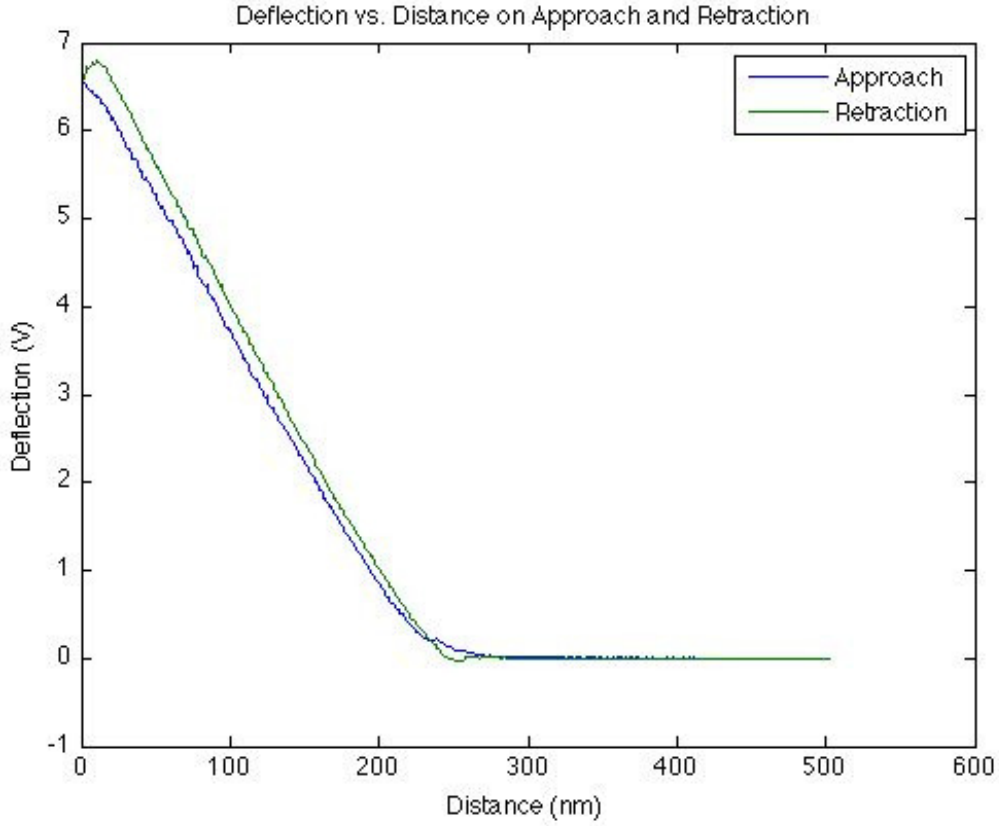
Deflection vs. Distance on Approach and Retraction
Approach
Retraction
Deflection (V)
Distance (nm)
7
6
5
4
3
2
1
0
-1
0
100
200
300
400
500
600

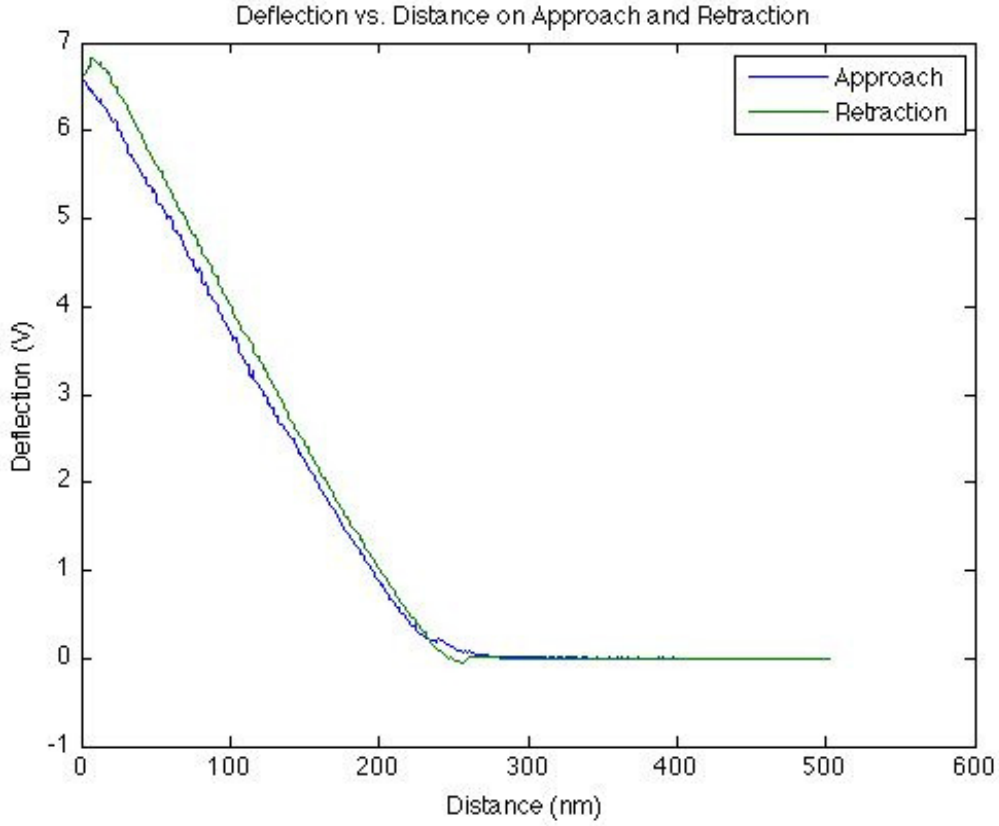
Deflection vs. Distance on Approach and Retraction
Approach
Retraction
Deflection (V)
Distance (nm)
7
6
5
4
3
2
1
0
-1
0
100
200
300
400
500
600

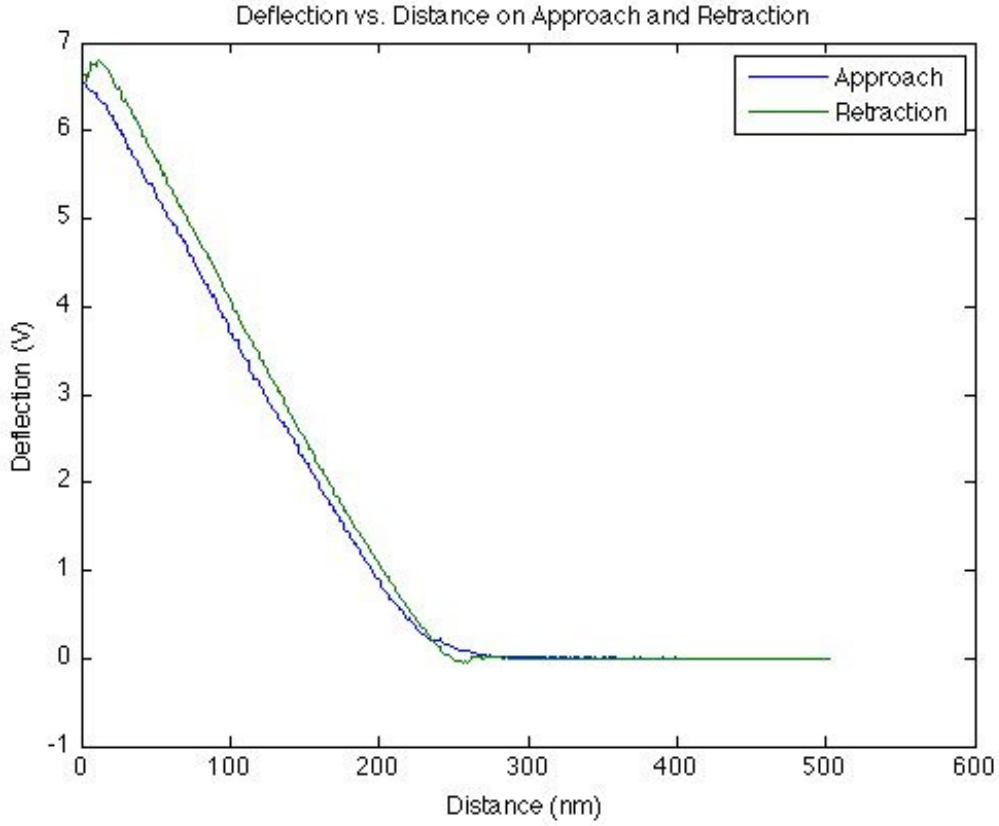
Deflection vs. Distance on Approach and Retraction
Approach
Retraction
Deflection (V)
Distance (nm)
7
6
5
4
3
2
1
0
-1
0
100
200
300
400
500
600

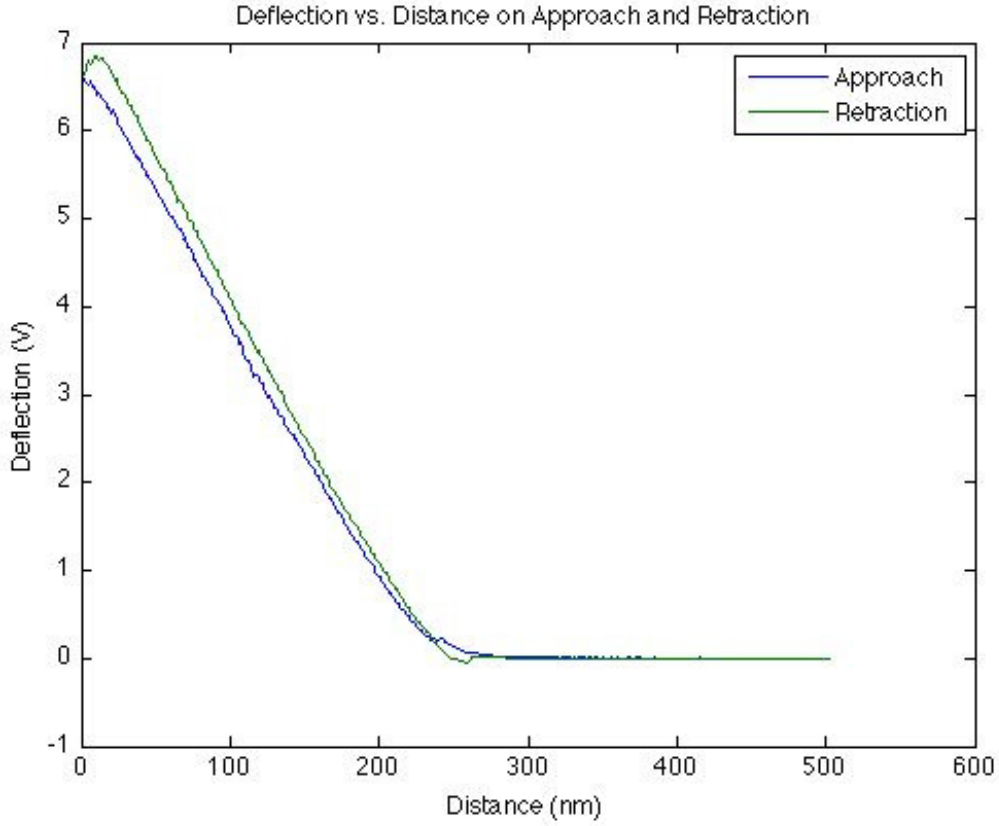
Deflection vs. Distance on Approach and Retraction
Approach
Retraction
Deflection (V)
Distance (nm)
7
6
5
4
3
2
1
0
-1
0
100
200
300
400
500
600

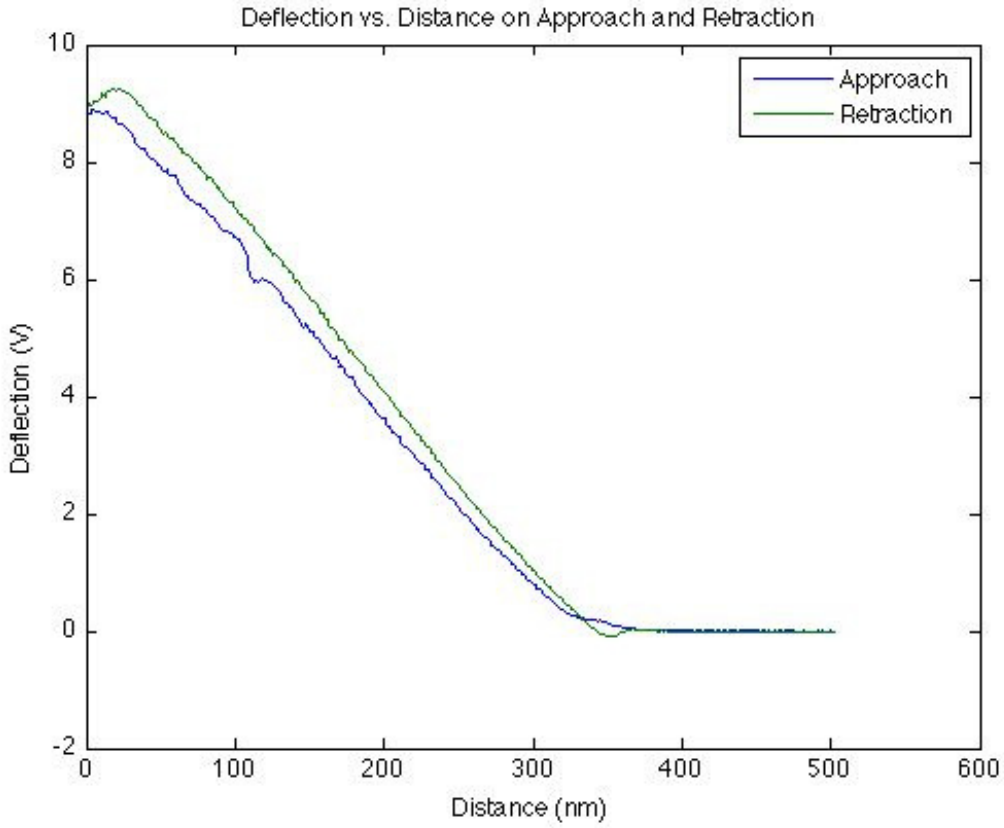
Deflection vs. Distance on Approach and Retraction
Approach
Retraction
Deflection (V)
Distance (nm)
10
8
6
4
2
0
-2
0
100
200
300
400
500
600

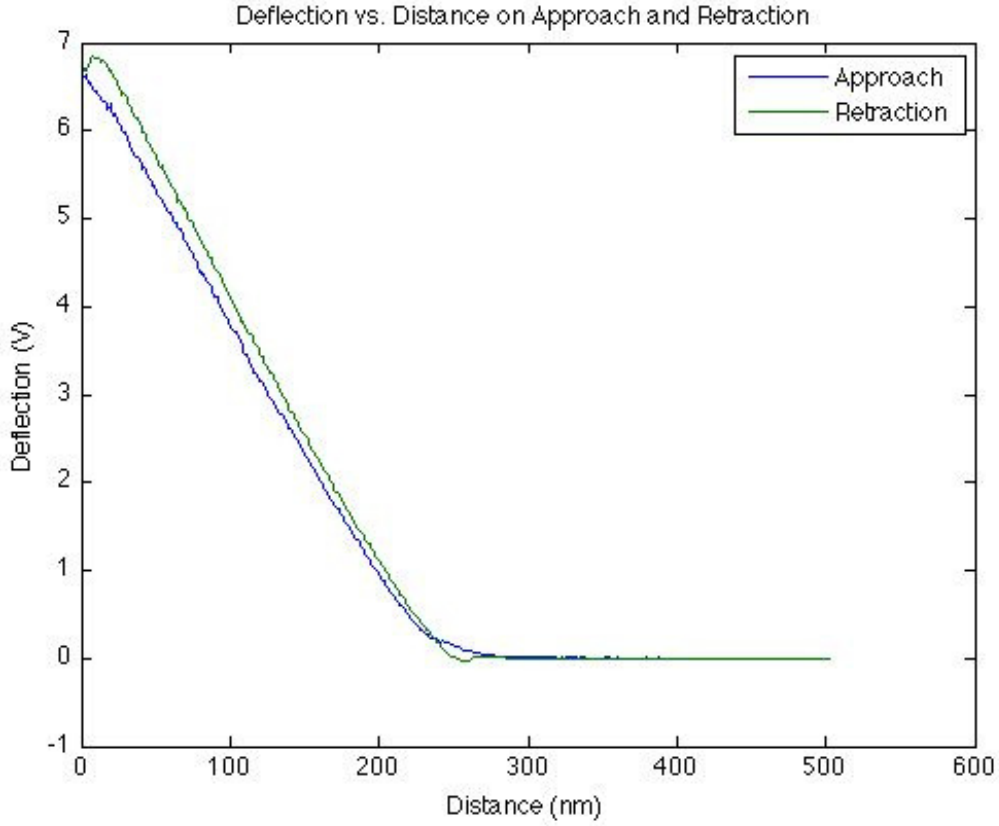
Deflection vs. Distance on Approach and Retraction
Approach
Retraction
Deflection (V)
Distance (nm)
7
6
5
4
3
2
1
0
-1
0
100
200
300
400
500
600

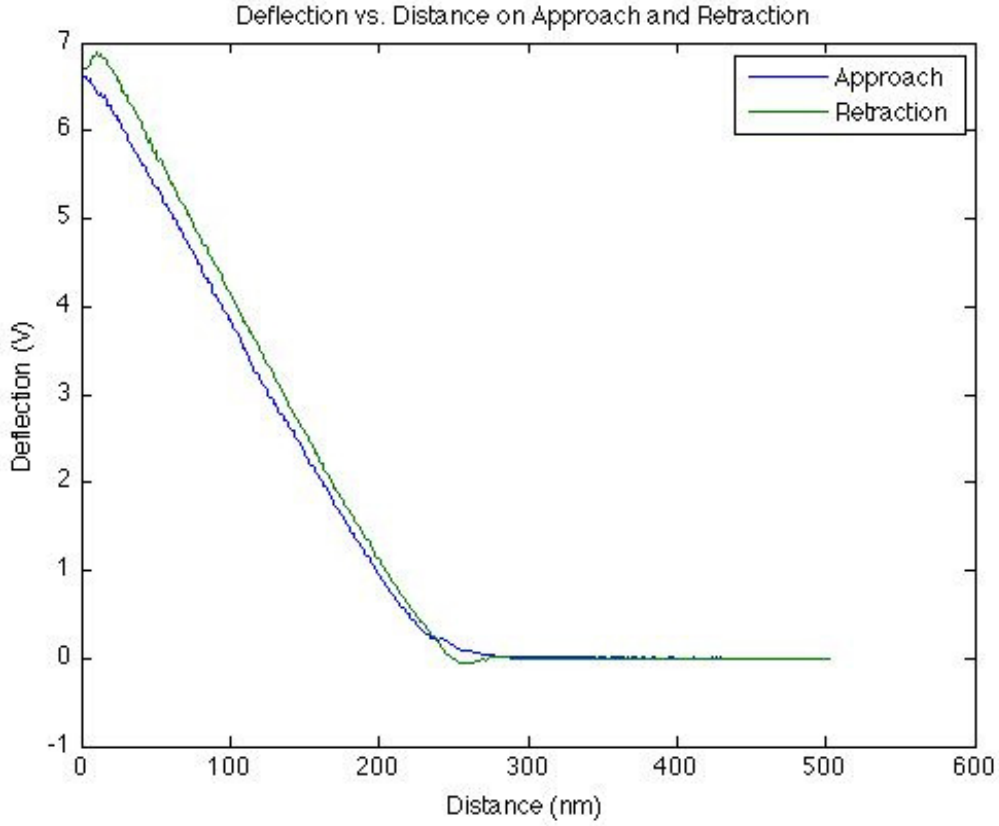
Deflection vs. Distance on Approach and Retraction
Approach
Retraction
Deflection (V)
Distance (nm)
7
6
5
4
3
2
1
0
-1
0
100
200
300
400
500
600

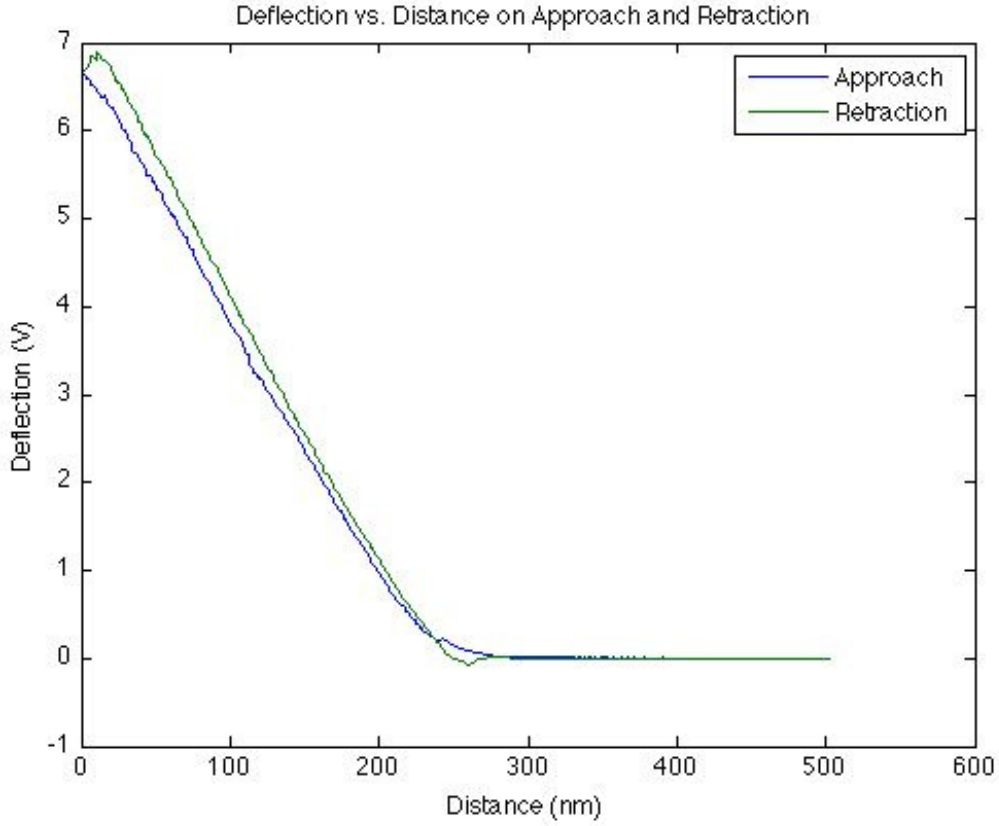
Deflection vs. Distance on Approach and Retraction
Approach
Retraction
Deflection (V)
Distance (nm)
7
6
5
4
3
2
1
0
-1
0
100
200
300
400
500
600

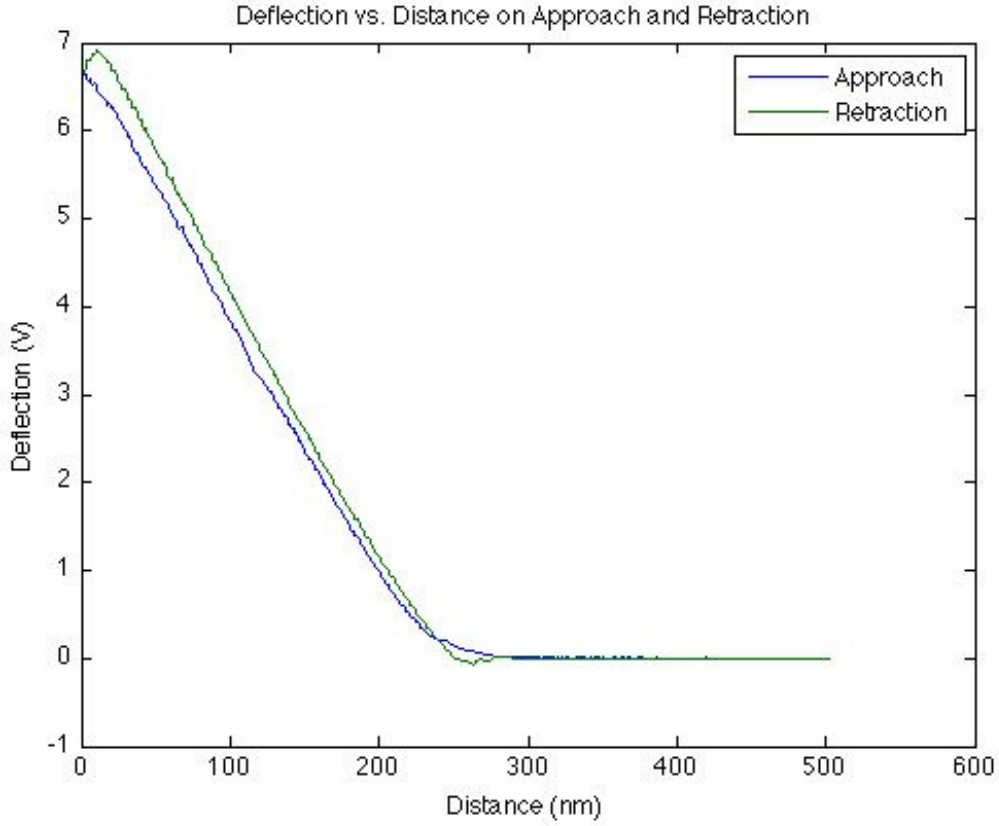
Deflection vs. Distance on Approach and Retraction
Approach
Retraction
Deflection (V)
Distance (nm)
7
6
5
4
3
2
1
0
-1
0
100
200
300
400
500
600

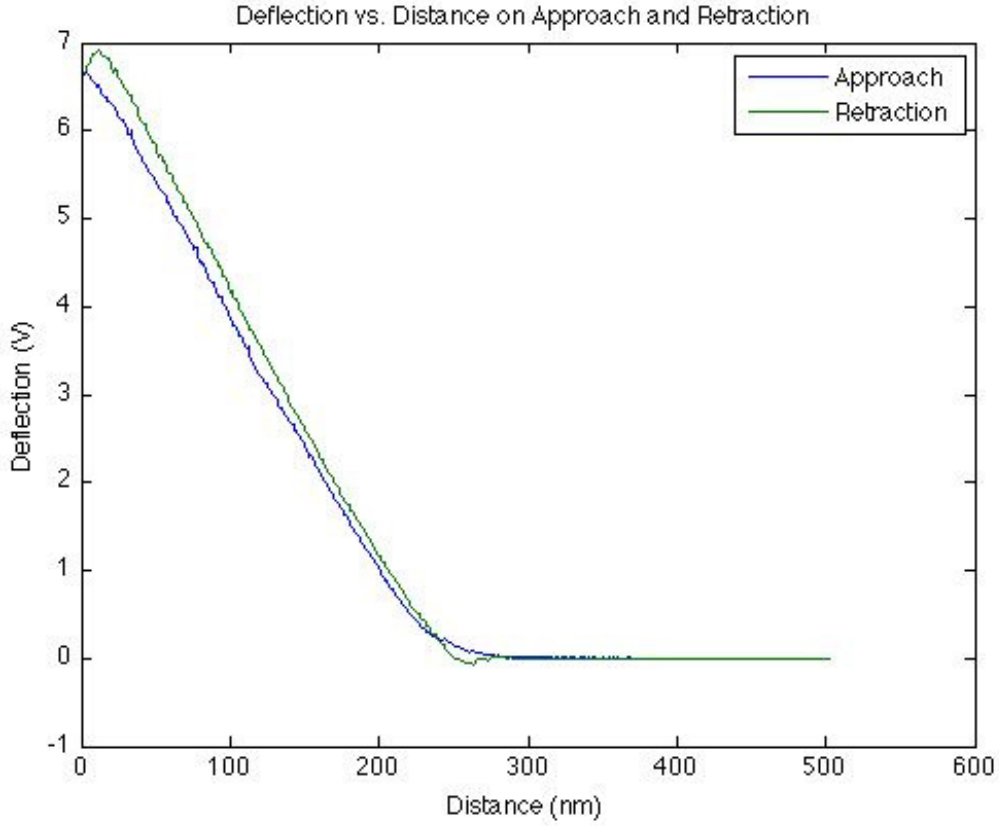
Deflection vs. Distance on Approach and Retraction
Approach
Retraction
Deflection (V)
Distance (nm)
7
6
5
4
3
2
1
0
-1
0
100
200
300
400
500
600

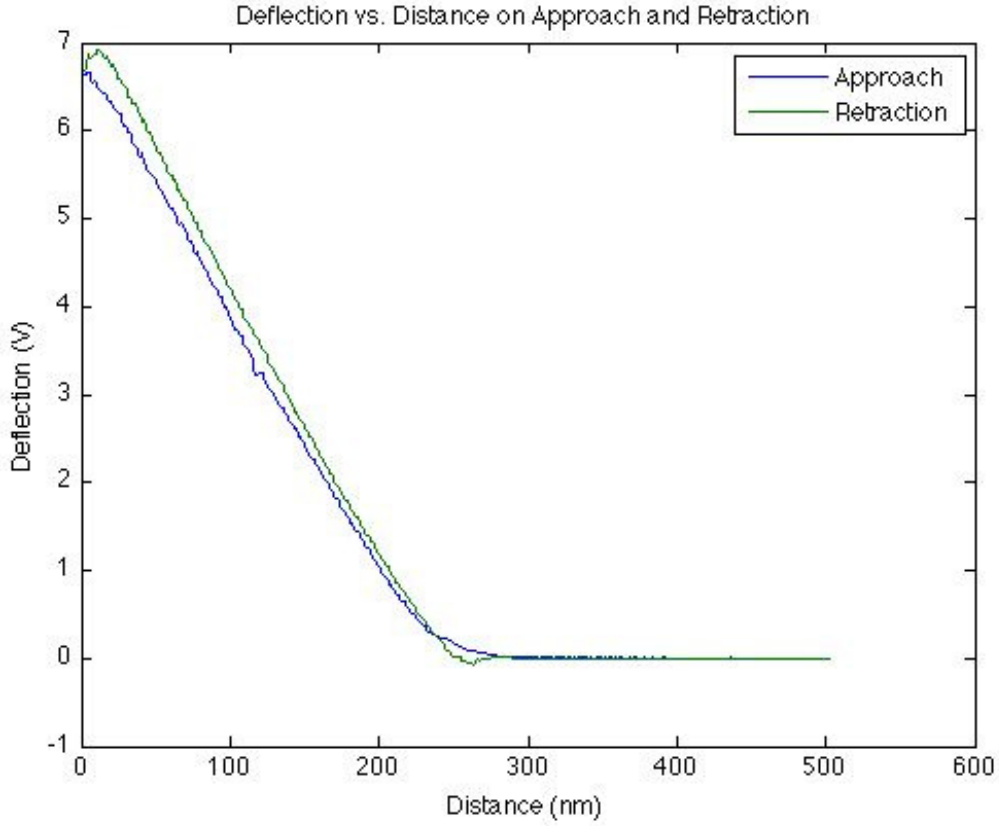
Deflection vs. Distance on Approach and Retraction
Approach
Retraction
Deflection (V)
Distance (nm)
7
6
5
4
3
2
1
0
-1
0
100
200
300
400
500
600

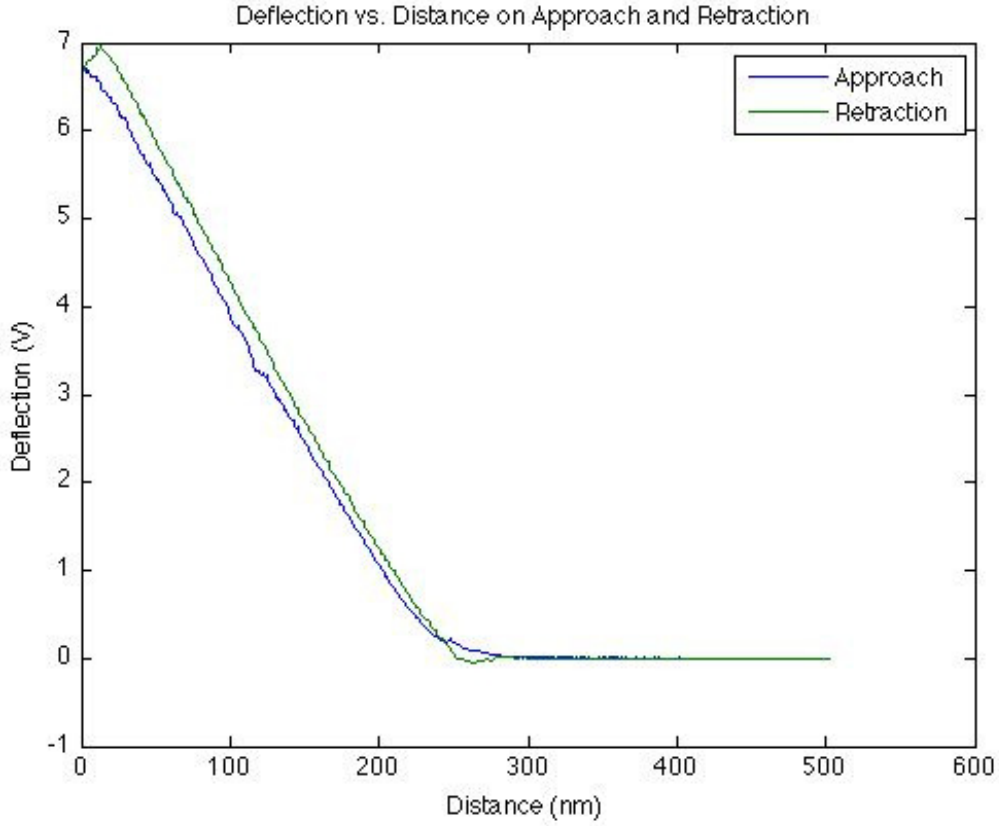
Deflection vs. Distance on Approach and Retraction
Approach
Retraction
Deflection (V)
Distance (nm)
7
6
5
4
3
2
1
0
-1
0
100
200
300
400
500
600

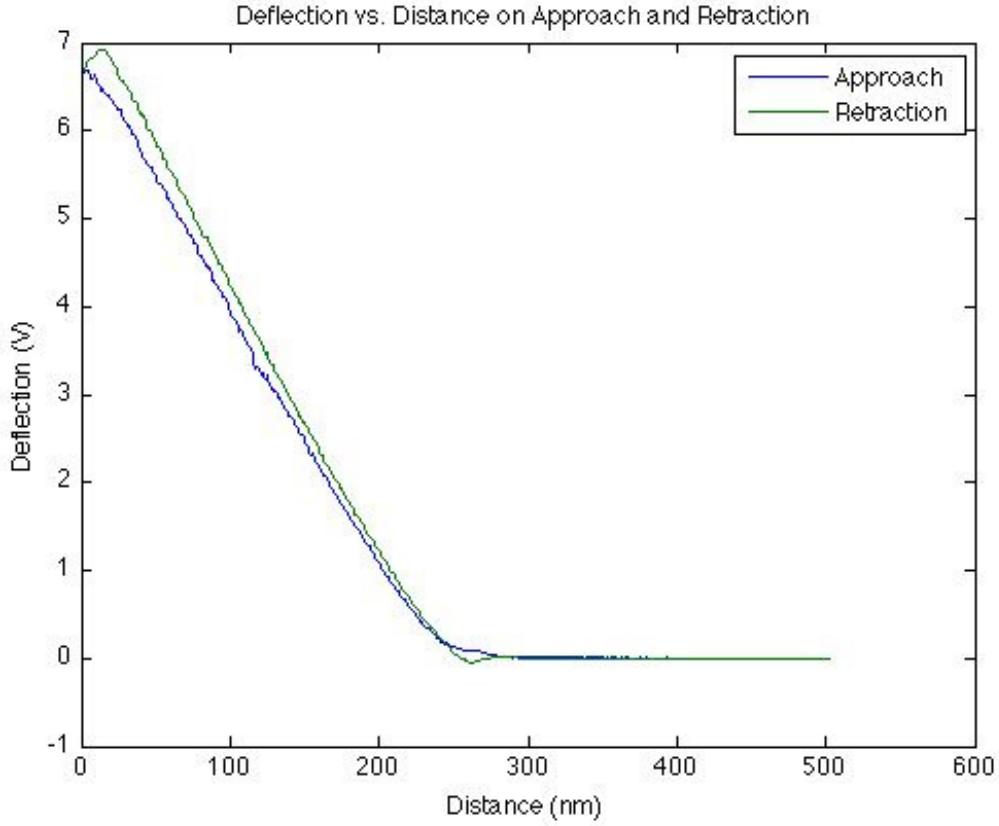
Deflection vs. Distance on Approach and Retraction
Approach
Retraction
Deflection (V)
Distance (nm)
7
6
5
4
3
2
1
0
-1
0
100
200
300
400
500
600

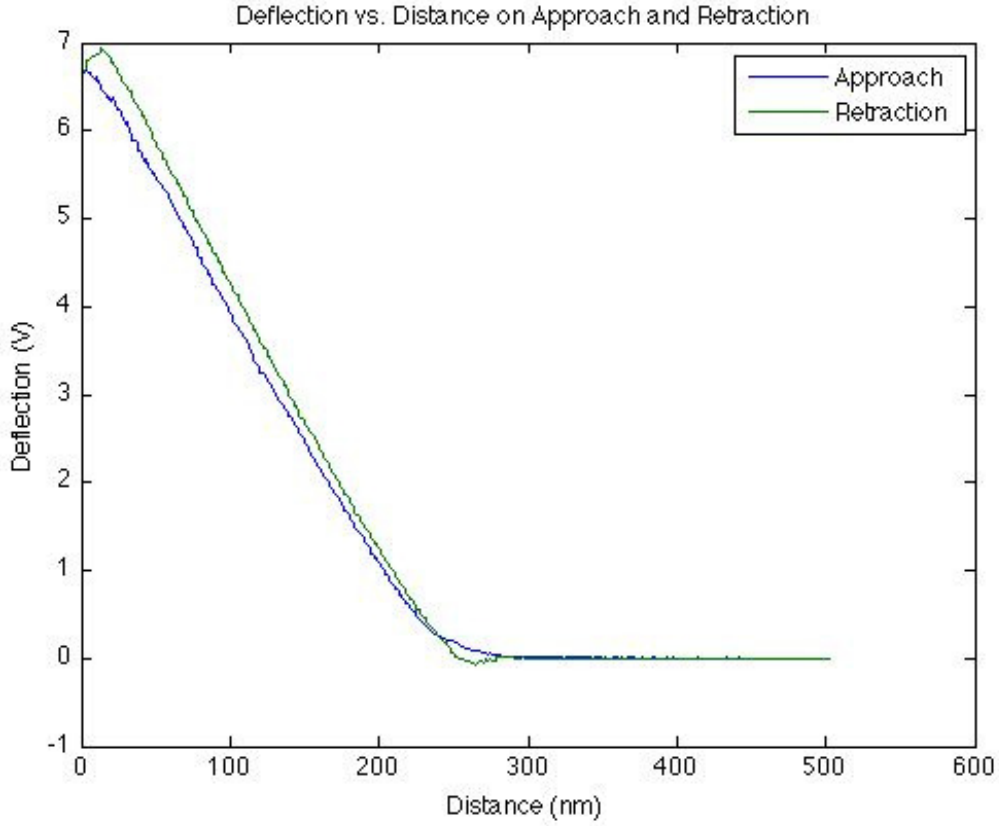
Deflection vs. Distance on Approach and Retraction
Approach
Retraction
Deflection (V)
Distance (nm)
7
6
5
4
3
2
1
0
-1
0
100
200
300
400
500
600

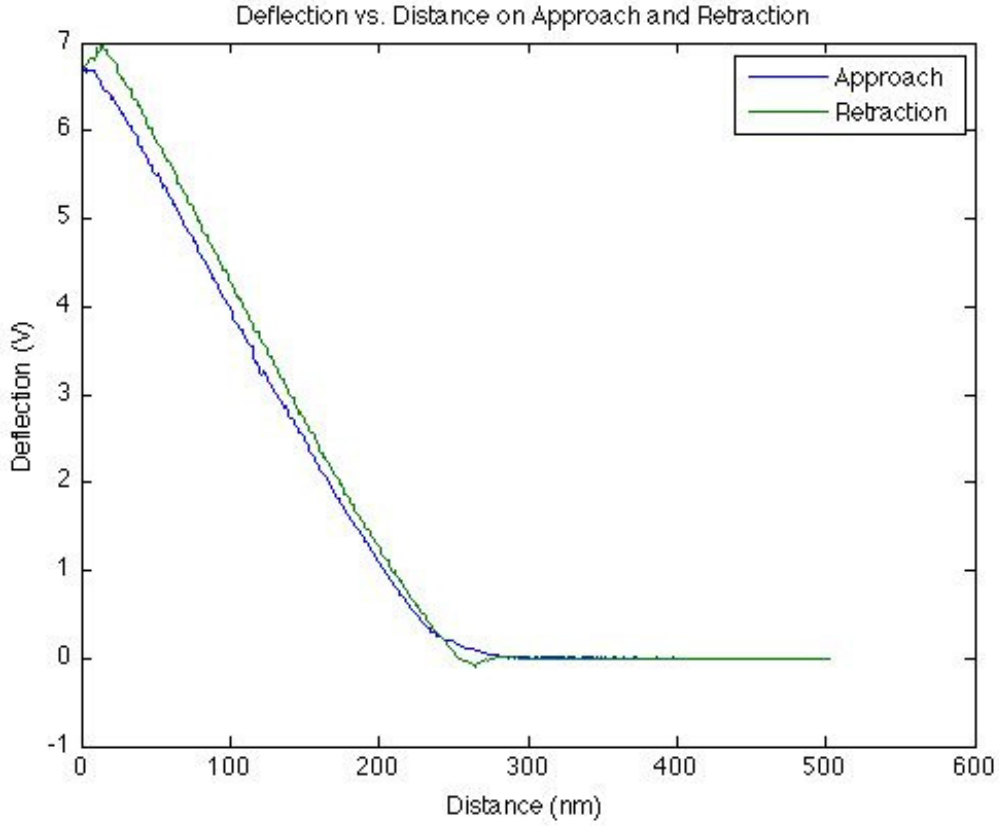
Deflection vs. Distance on Approach and Retraction
Approach
Retraction
Deflection (V)
Distance (nm)
7
6
5
4
3
2
1
0
-1
0
100
200
300
400
500
600

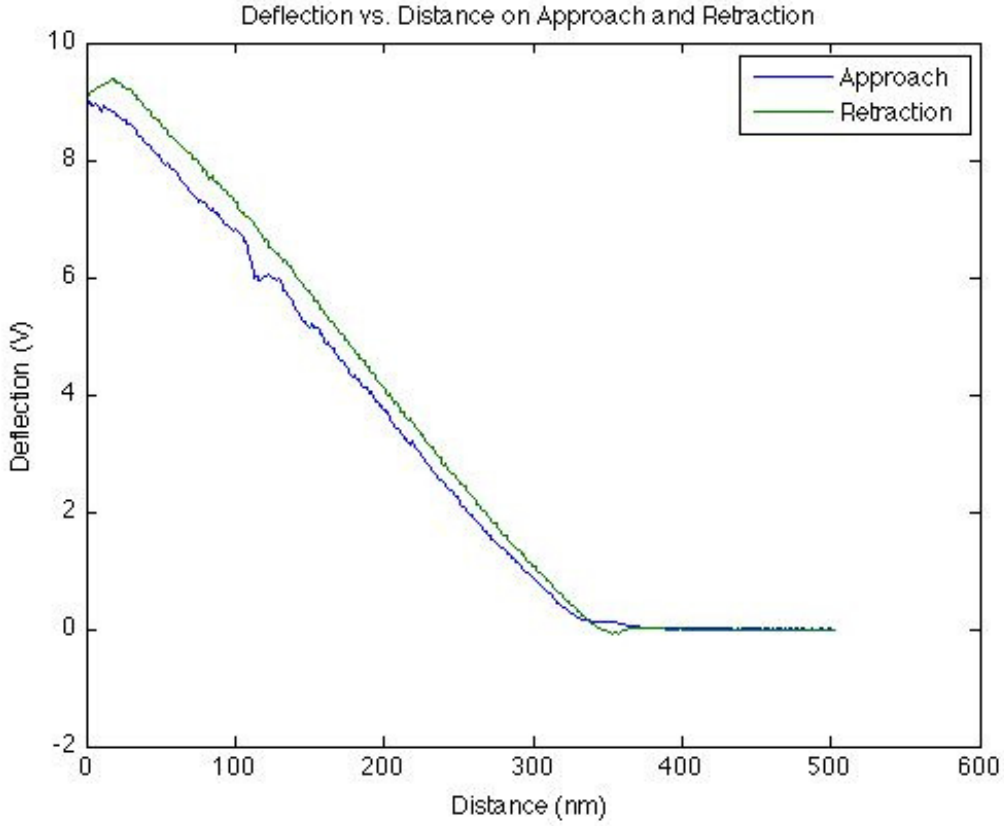
Deflection vs. Distance on Approach and Retraction
Approach
Retraction
Deflection (V)
Distance (nm)
10
8
6
4
2
0
-2
0
100
200
300
400
500
600

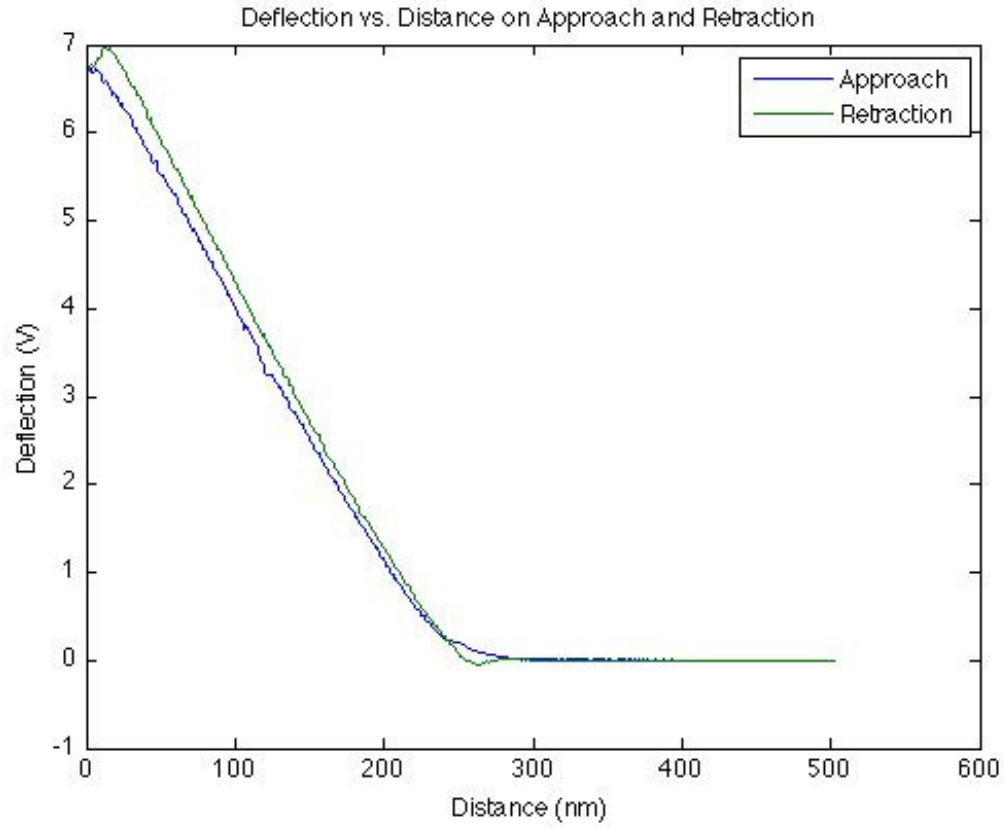
Deflection vs. Distance on Approach and Retraction
Approach
Retraction
Deflection (V)
Distance (nm)
7
6
5
4
3
2
1
0
-1
0
100
200
300
400
500
600

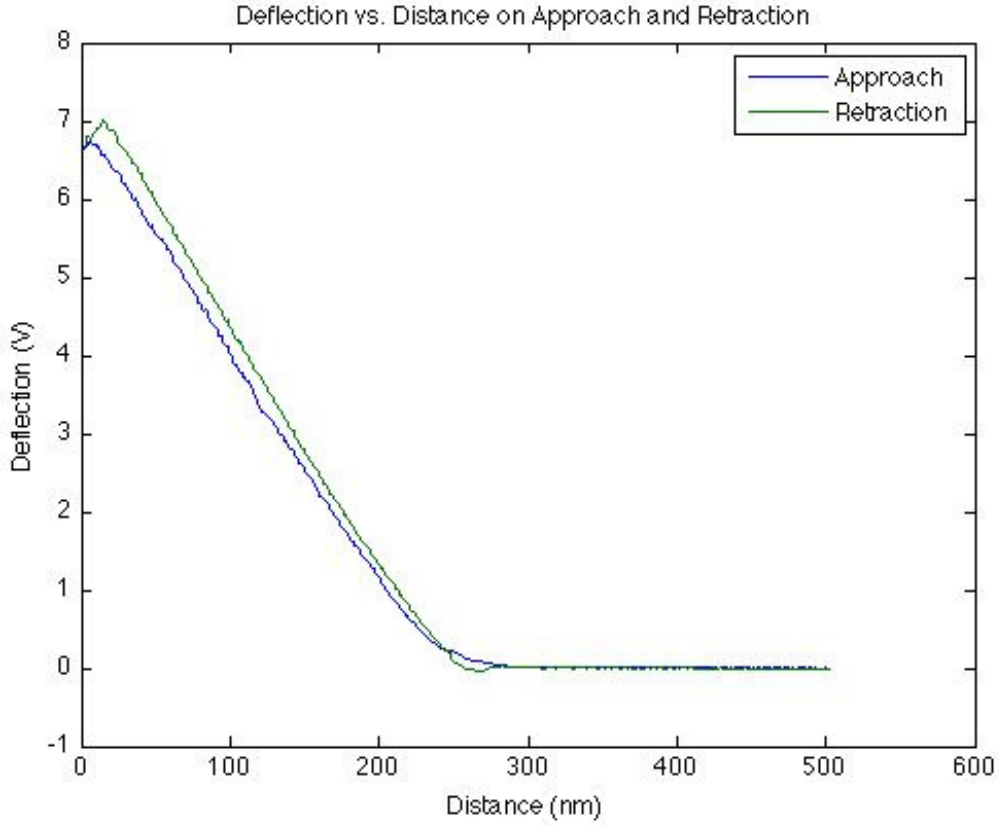
Deflection vs. Distance on Approach and Retraction
Approach
Retraction
Deflection (V)
Distance (nm)
8
7
6
5
4
3
2
1
0
-1
0
100
200
300
400
500
600

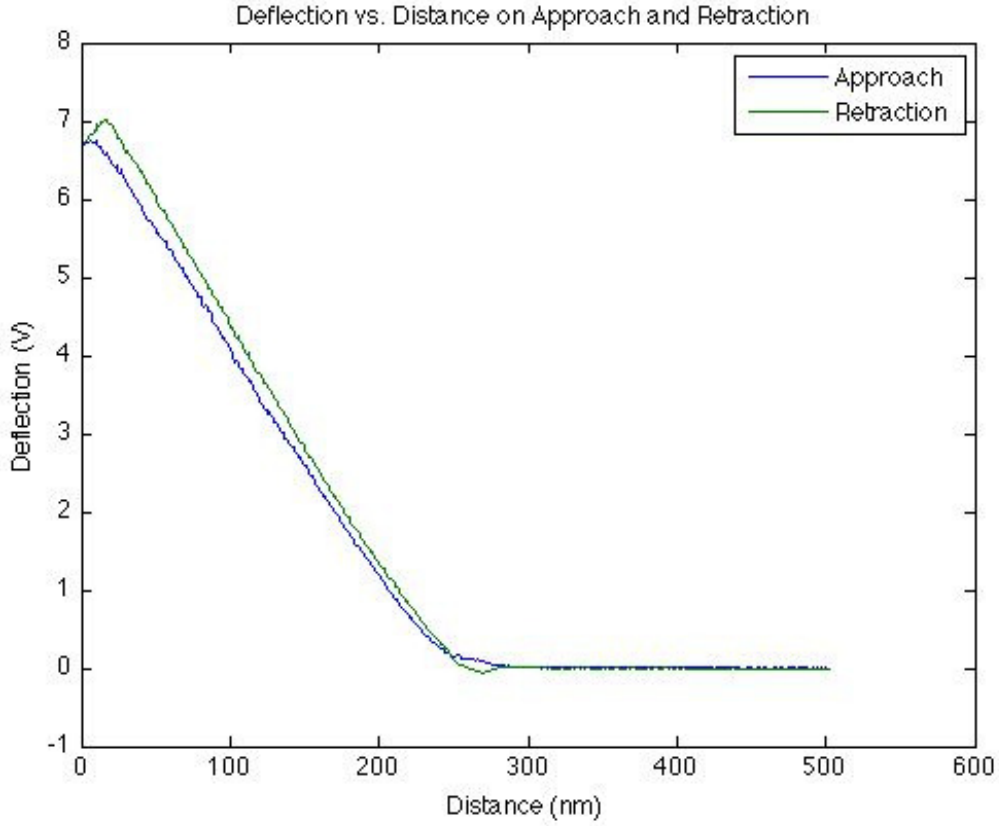
Deflection vs. Distance on Approach and Retraction
Approach
Retraction
Deflection (V)
Distance (nm)
8
7
6
5
4
3
2
1
0
-1
0
100
200
300
400
500
600

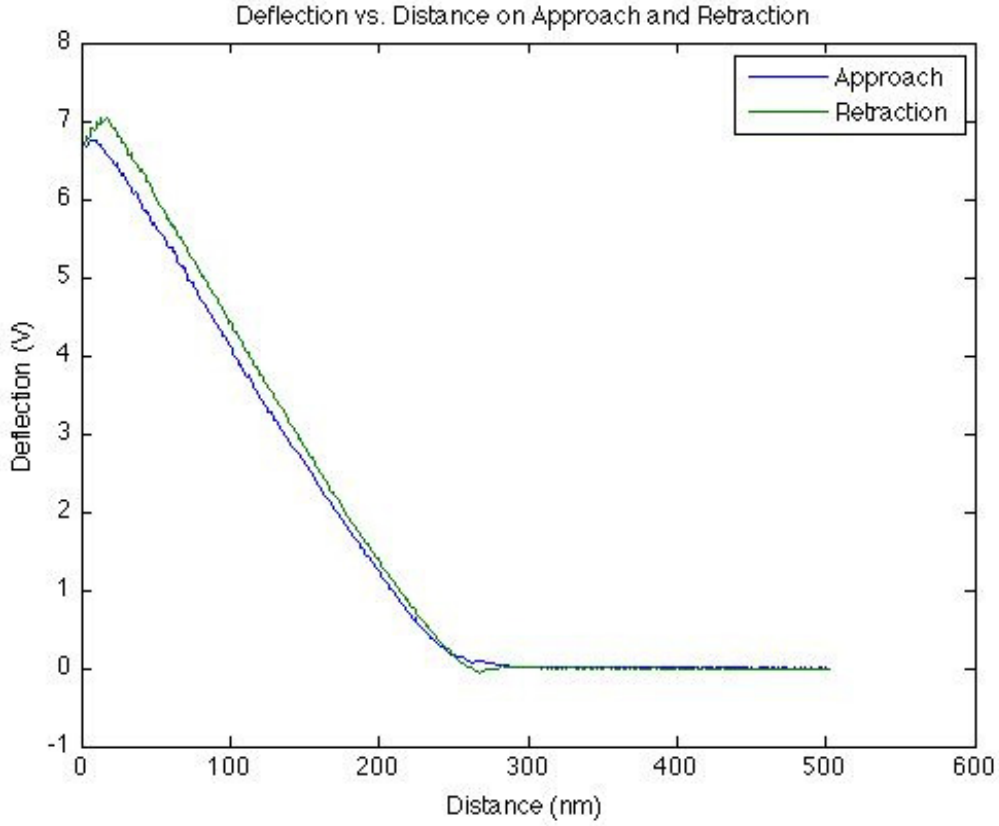
Deflection vs. Distance on Approach and Retraction
Approach
Retraction
Deflection (V)
Distance (nm)
8
7
6
5
4
3
2
1
0
-1
0
100
200
300
400
500
600

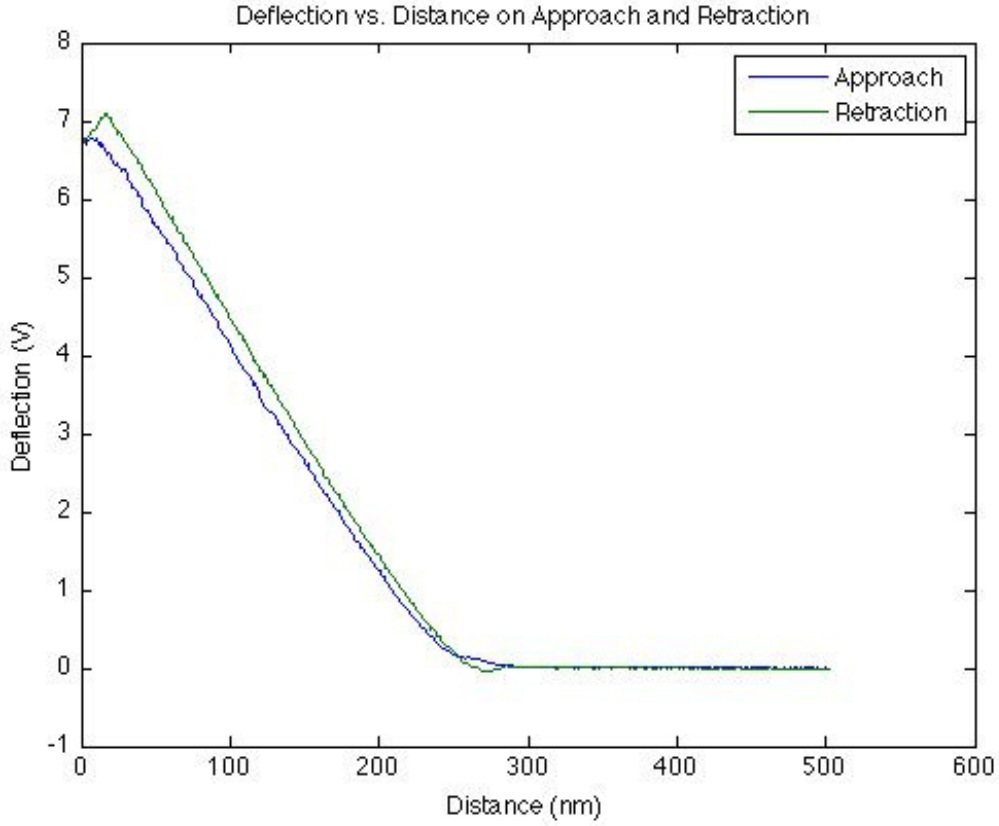
Deflection vs. Distance on Approach and Retraction
Approach
Retraction
Deflection (V)
Distance (nm)
8
7
6
5
4
3
2
1
0
-1
0
100
200
300
400
500
600

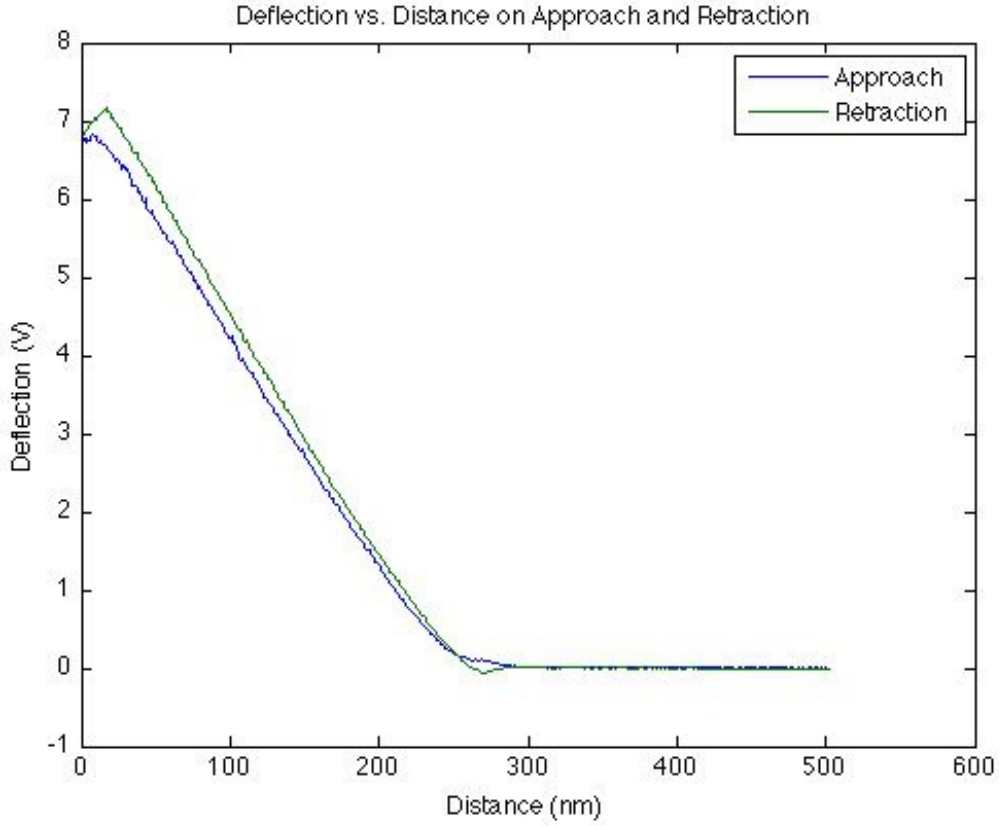
Deflection vs. Distance on Approach and Retraction
Approach
Retraction
Deflection (V)
Distance (nm)
8
7
6
5
4
3
2
1
0
-1
0
100
200
300
400
500
600

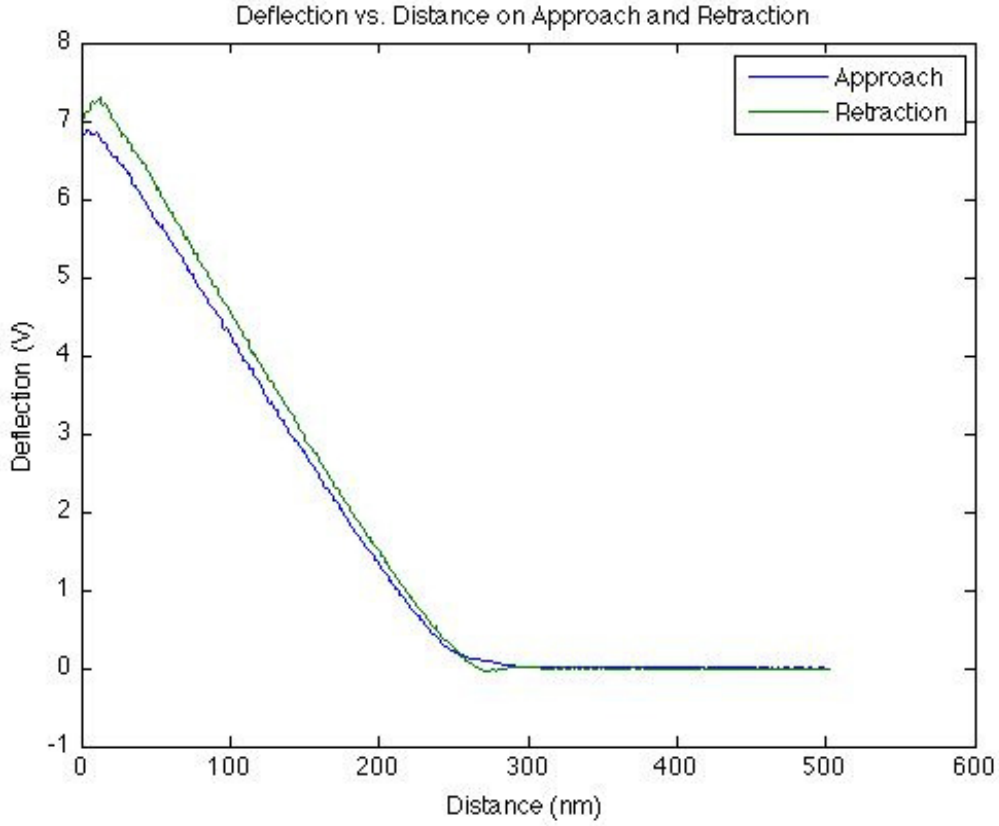
Deflection vs. Distance on Approach and Retraction
Approach
Retraction
Deflection (V)
Distance (nm)
8
7
6
5
4
3
2
1
0
-1
0
100
200
300
400
500
600

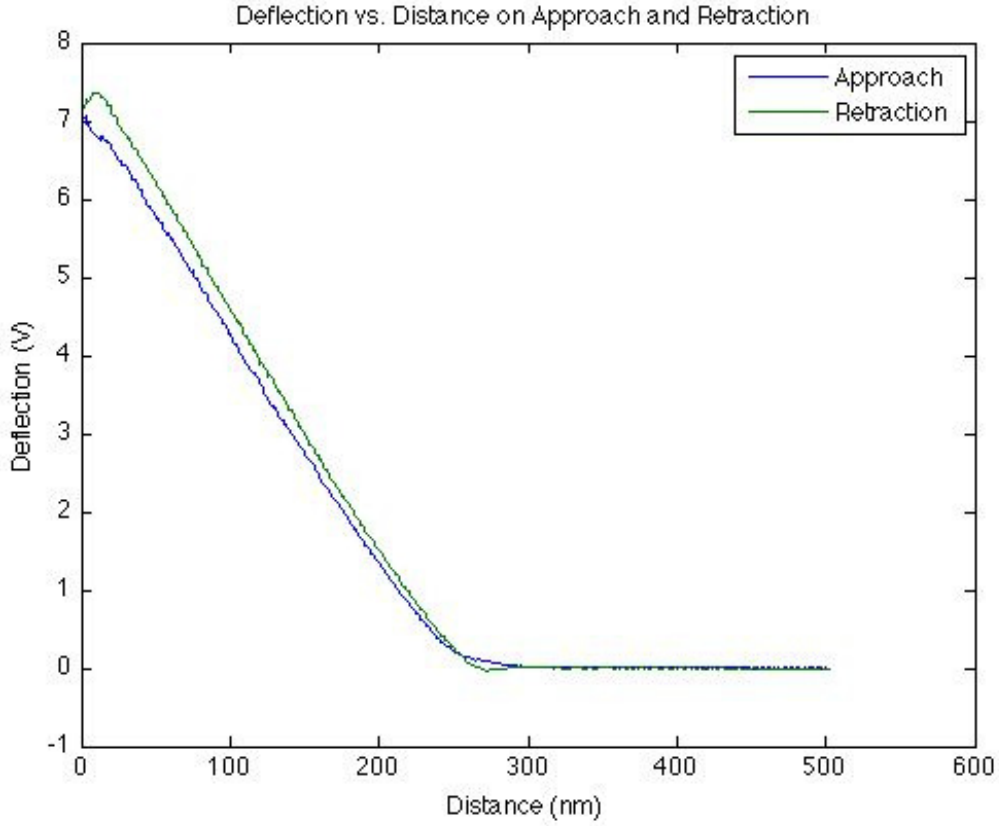
Deflection vs. Distance on Approach and Retraction
Approach
Retraction
Deflection (V)
Distance (nm)
8
7
6
5
4
3
2
1
0
-1
0
100
200
300
400
500
600

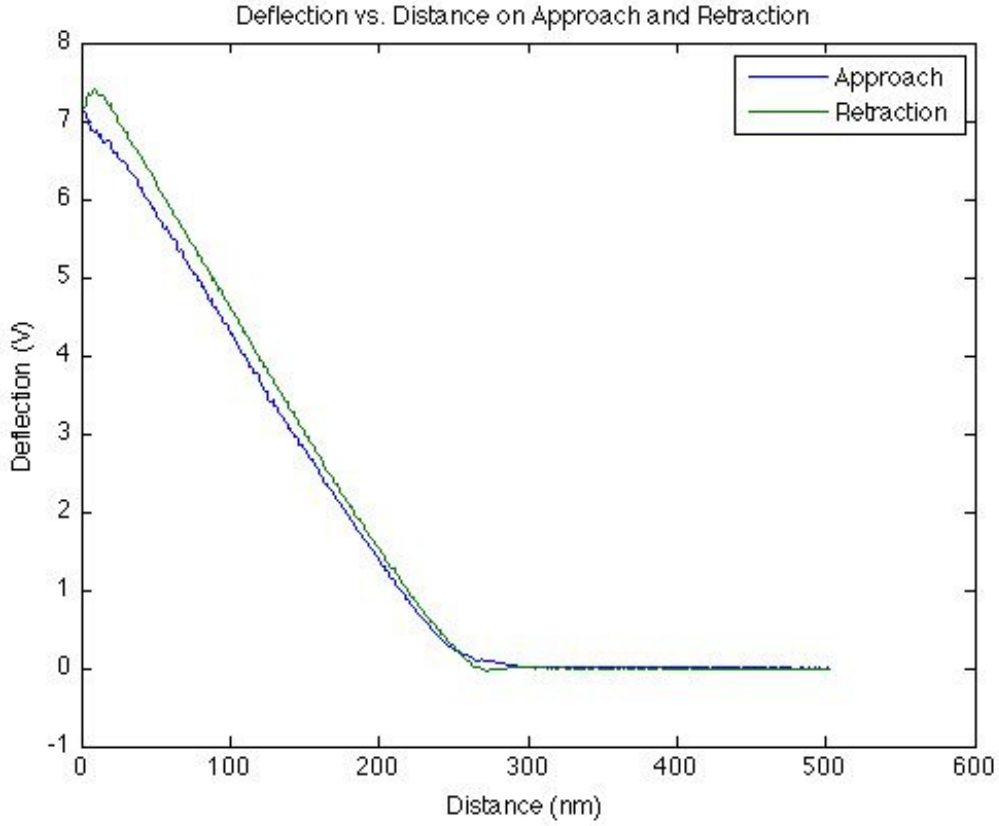
Deflection vs. Distance on Approach and Retraction
Approach
Retraction
Deflection (V)
Distance (nm)
8
7
6
5
4
3
2
1
0
-1
0
100
200
300
400
500
600

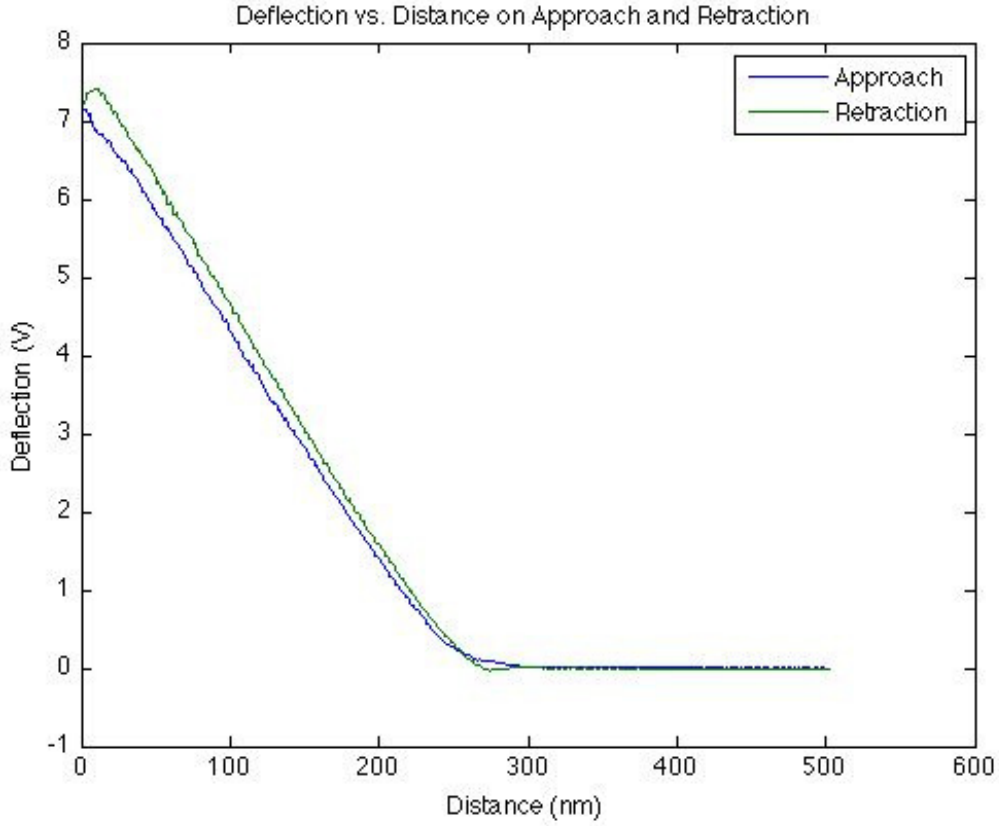
Deflection vs. Distance on Approach and Retraction
Approach
Retraction
Deflection (V)
Distance (nm)
8
7
6
5
4
3
2
1
0
-1
0
100
200
300
400
500
600

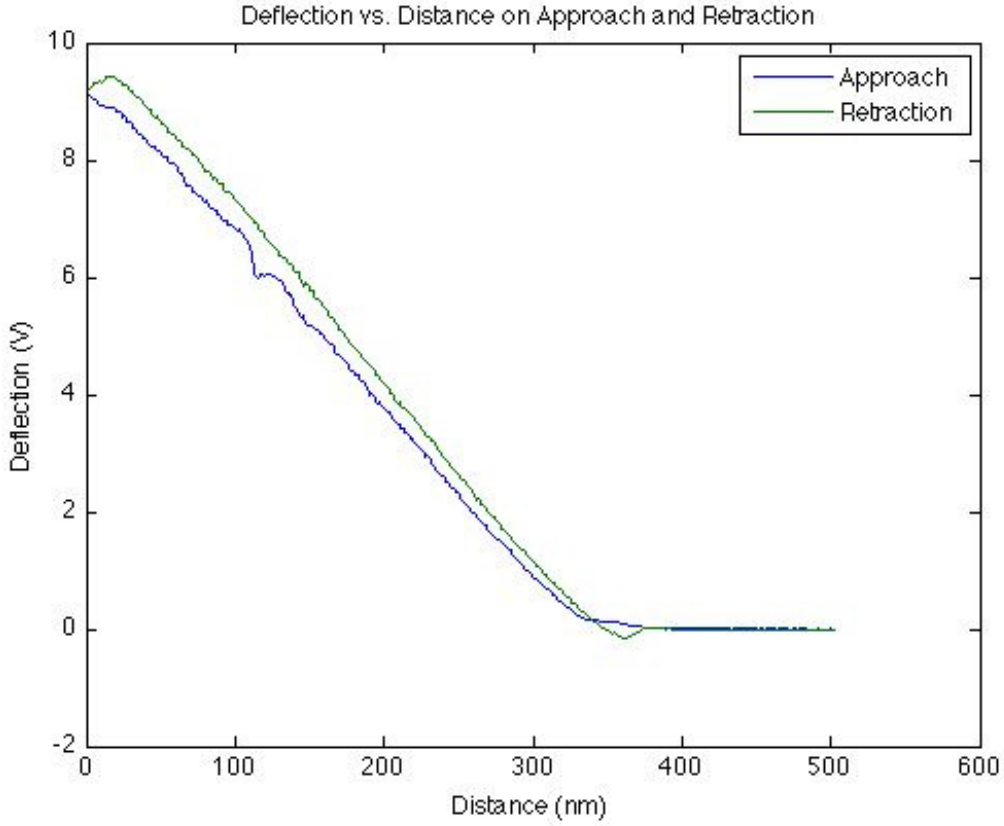
Deflection vs. Distance on Approach and Retraction
Approach
Retraction
Deflection (V)
Distance (nm)
10
8
6
4
2
0
-2
0
100
200
300
400
500
600

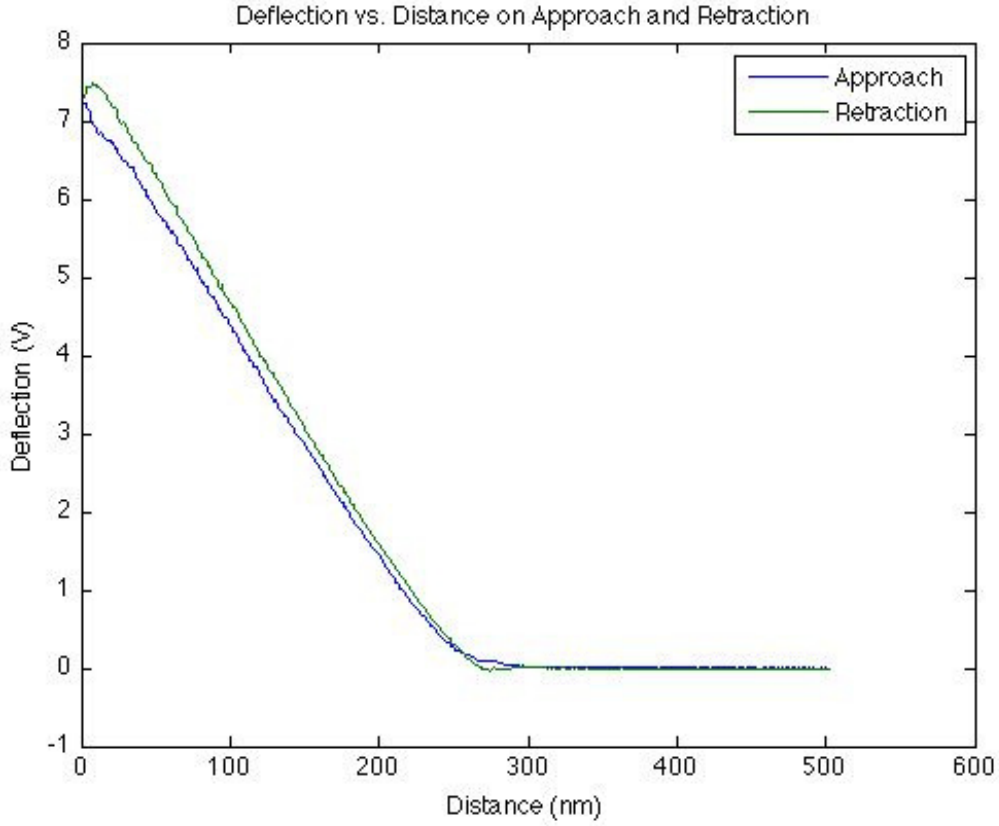
Deflection vs. Distance on Approach and Retraction
Approach
Retraction
Deflection (V)
Distance (nm)
8
7
6
5
4
3
2
1
0
-1
0
100
200
300
400
500
600

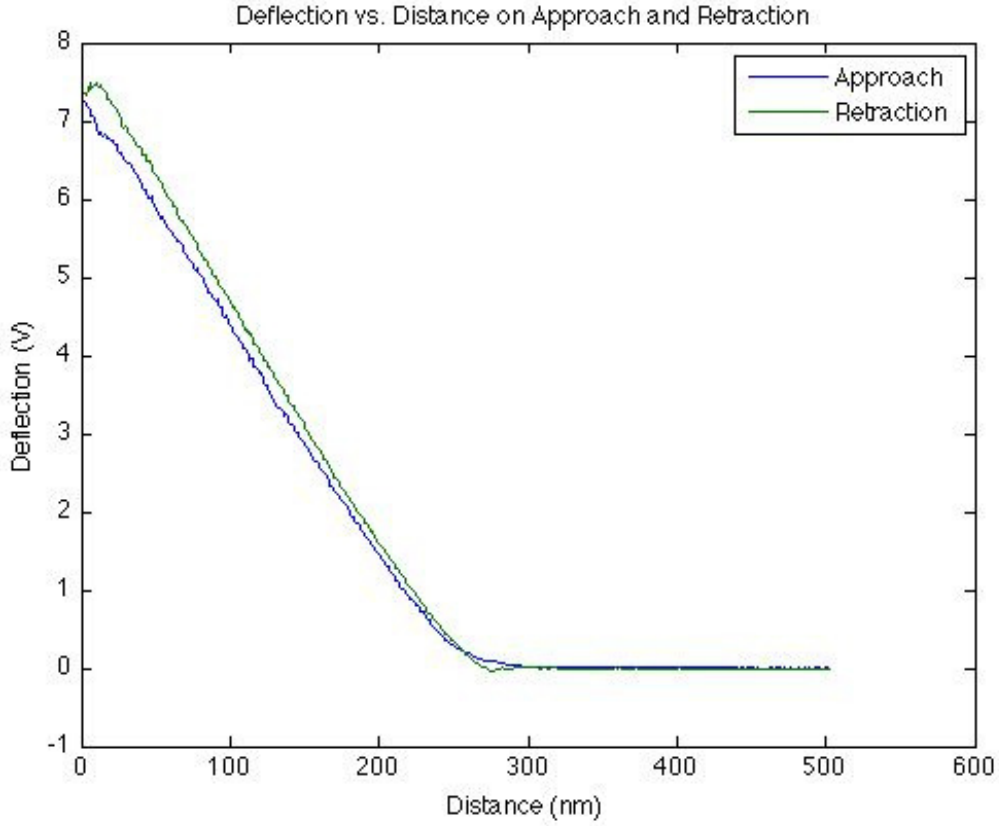
Deflection vs. Distance on Approach and Retraction
Approach
Retraction
Deflection (V)
Distance (nm)
8
7
6
5
4
3
2
1
0
-1
0
100
200
300
400
500
600

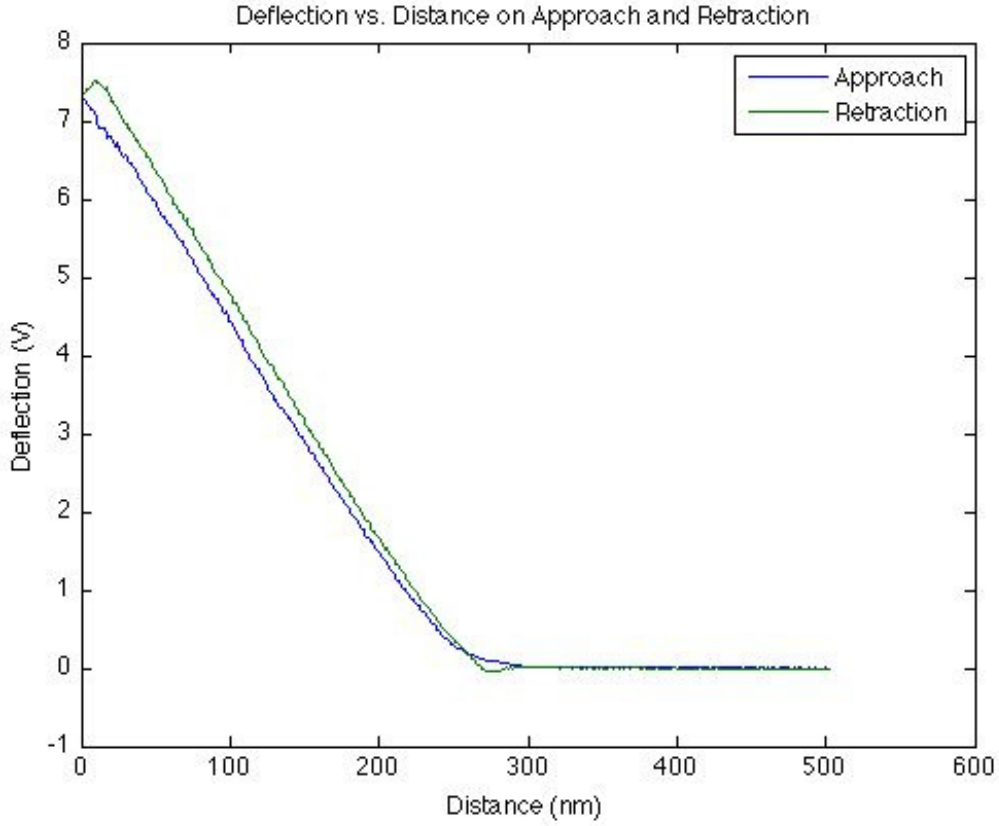
Deflection vs. Distance on Approach and Retraction
Approach
Retraction
Deflection (V)
Distance (nm)
8
7
6
5
4
3
2
1
0
-1
0
100
200
300
400
500
600

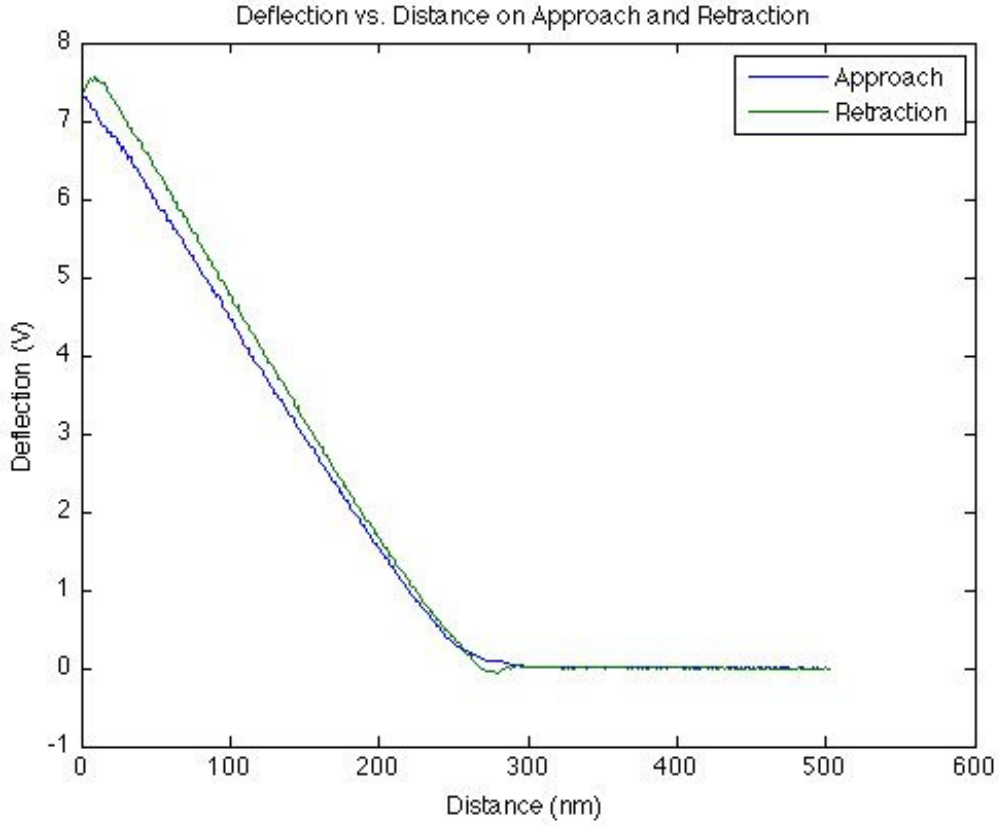
Deflection vs. Distance on Approach and Retraction
Approach
Retraction
Deflection (V)
Distance (nm)
8
7
6
5
4
3
2
1
0
-1
0
100
200
300
400
500
600

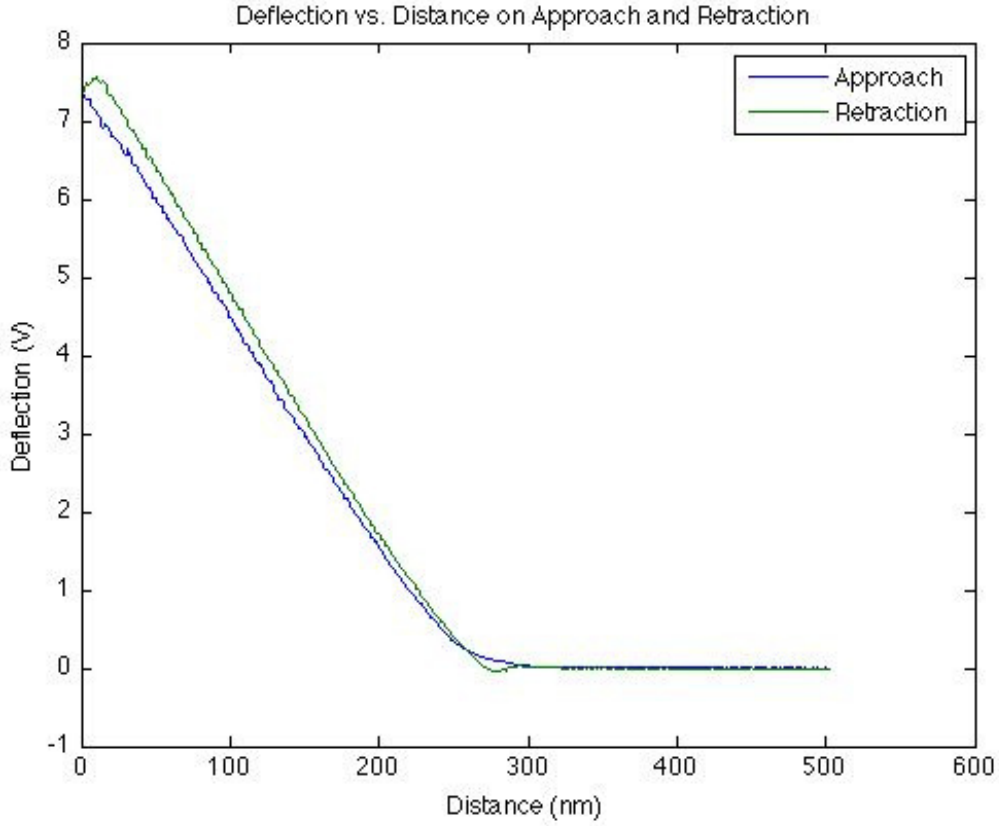
Deflection vs. Distance on Approach and Retraction
Approach
Retraction
Deflection (V)
Distance (nm)
8
7
6
5
4
3
2
1
0
-1
0
100
200
300
400
500
600

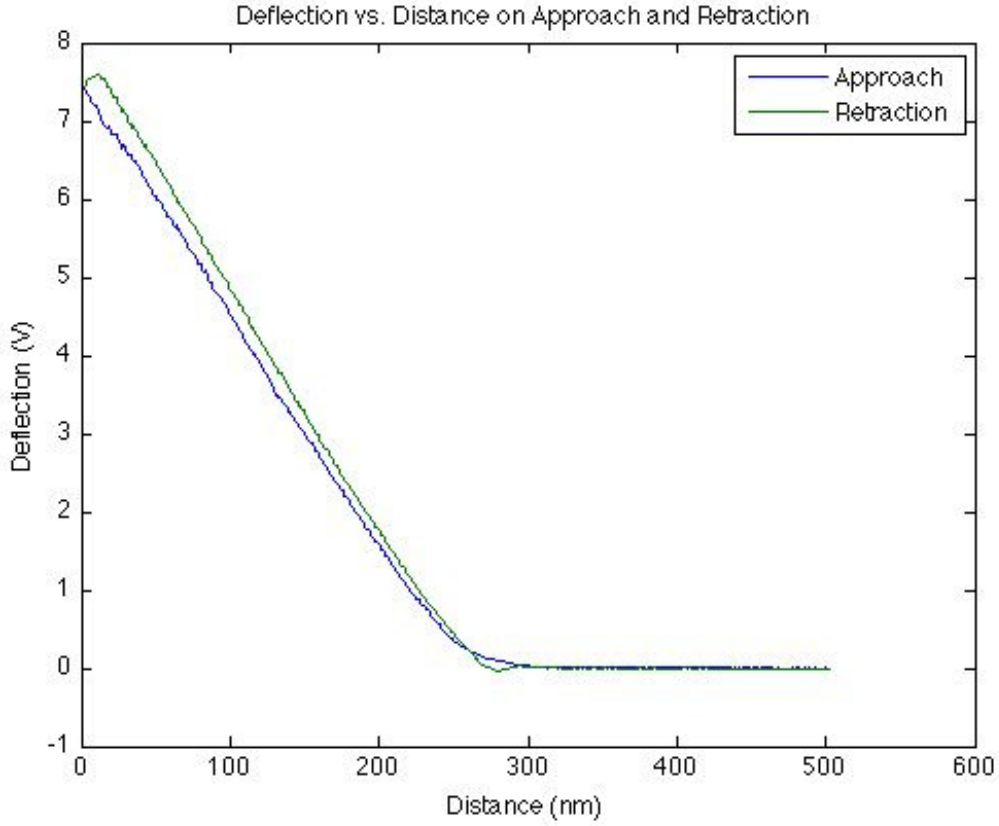
Deflection vs. Distance on Approach and Retraction
Approach
Retraction
Deflection (V)
Distance (nm)
8
7
6
5
4
3
2
1
0
-1
0
100
200
300
400
500
600

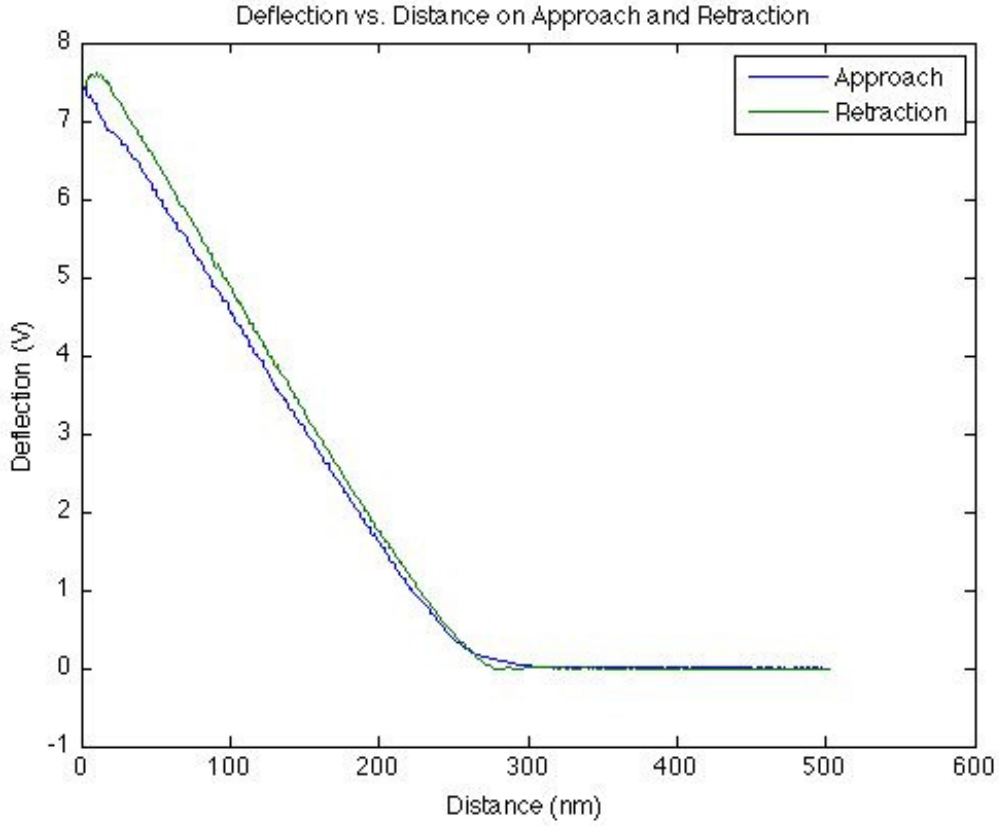
Deflection vs. Distance on Approach and Retraction
Approach
Retraction
Deflection (V)
Distance (nm)
8
7
6
5
4
3
2
1
0
-1
0
100
200
300
400
500
600

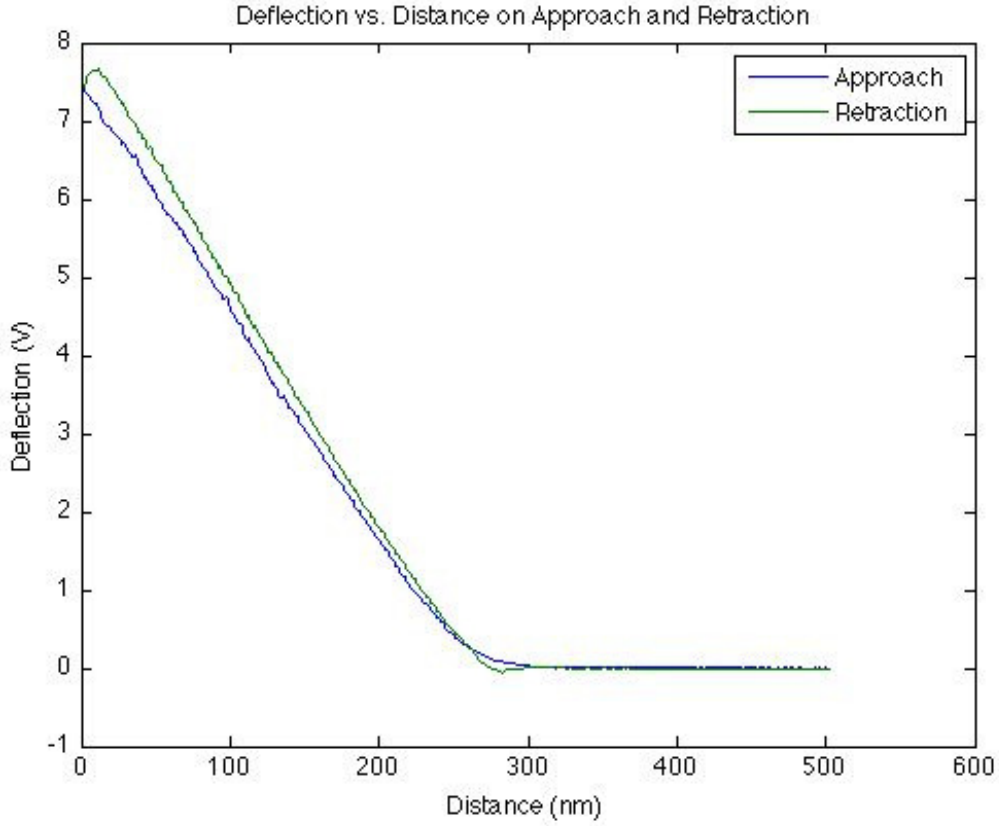
Deflection vs. Distance on Approach and Retraction
Approach
Retraction
Deflection (V)
Distance (nm)
8
7
6
5
4
3
2
1
0
-1
0
100
200
300
400
500
600

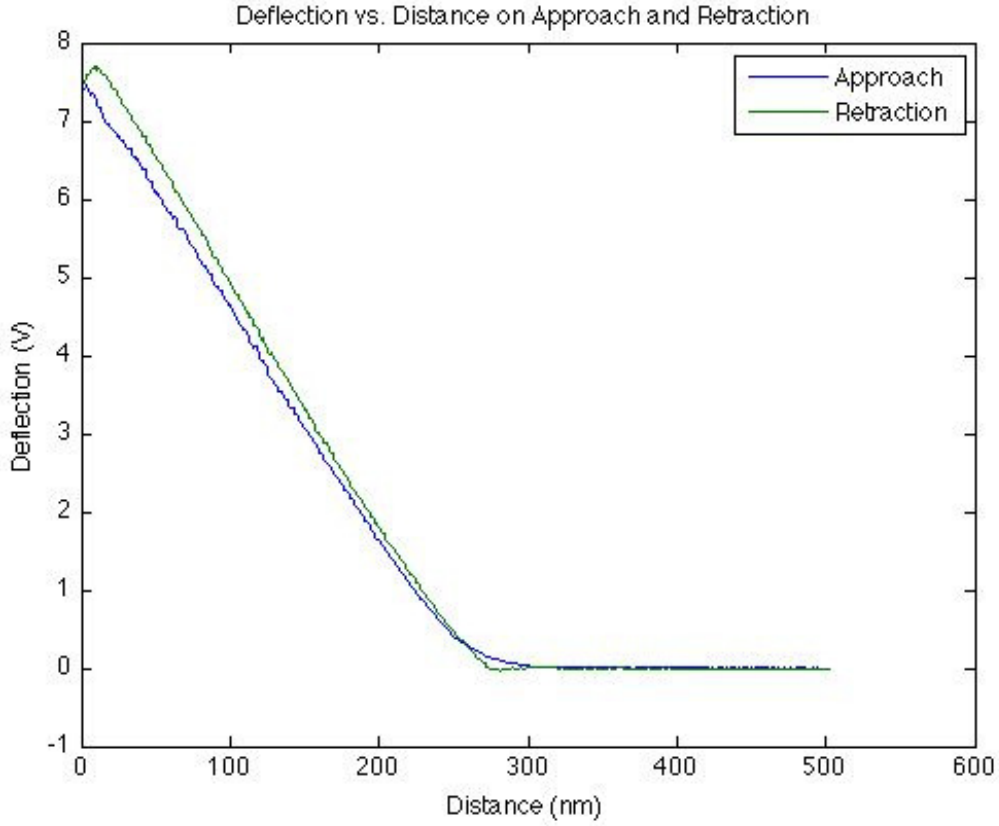
Deflection vs. Distance on Approach and Retraction
Approach
Retraction
Deflection (V)
Distance (nm)
8
7
6
5
4
3
2
1
0
-1
0
100
200
300
400
500
600

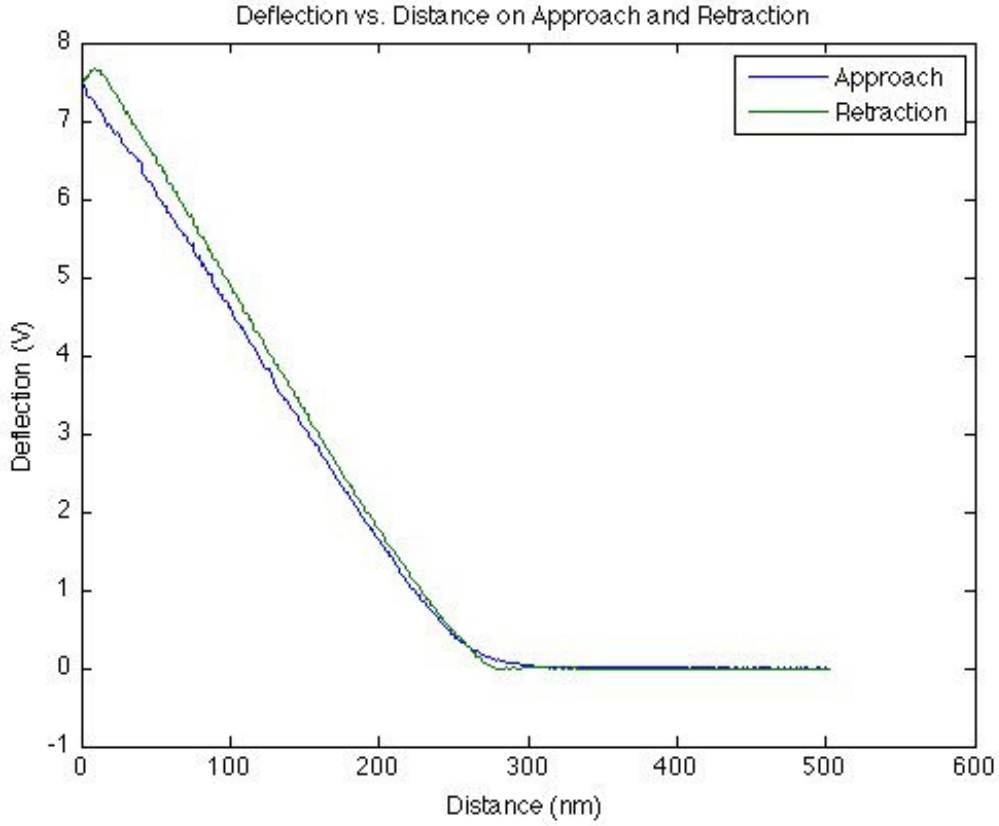
Deflection vs. Distance on Approach and Retraction
Approach
Retraction
Deflection (V)
Distance (nm)
8
7
6
5
4
3
2
1
0
-1
0
100
200
300
400
500
600

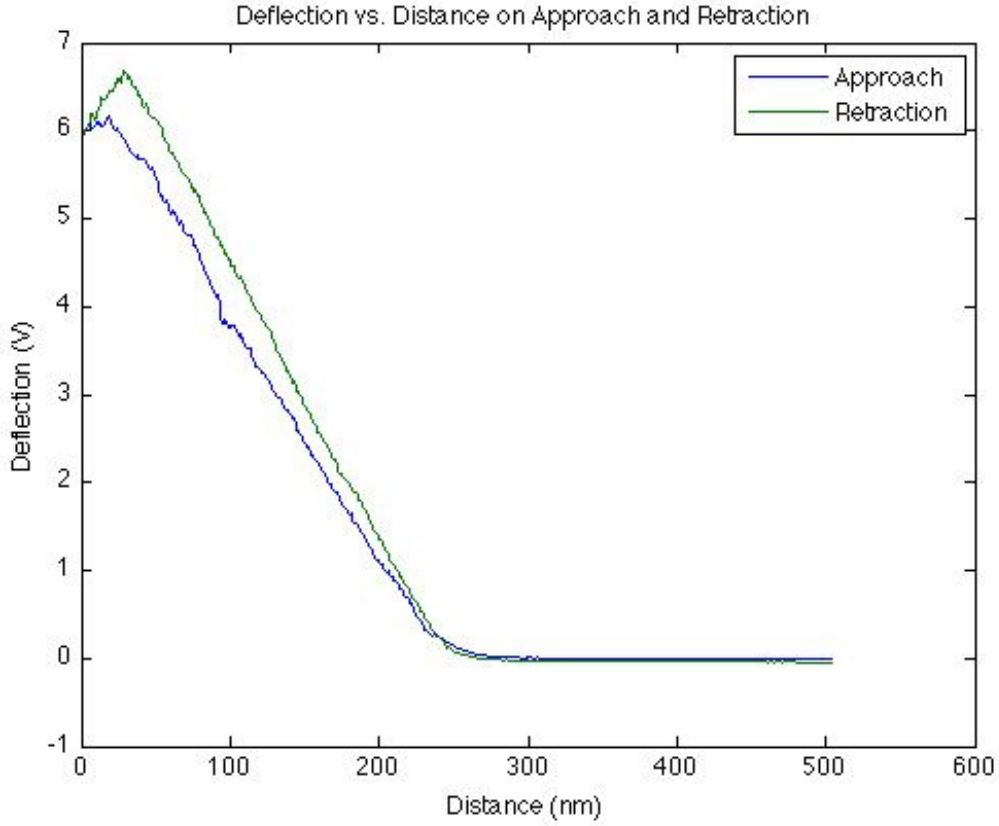
Deflection vs. Distance on Approach and Retraction
Approach
Retraction
Deflection (V)
Distance (nm)
7
6
5
4
3
2
1
0
-1
0
100
200
300
400
500
600

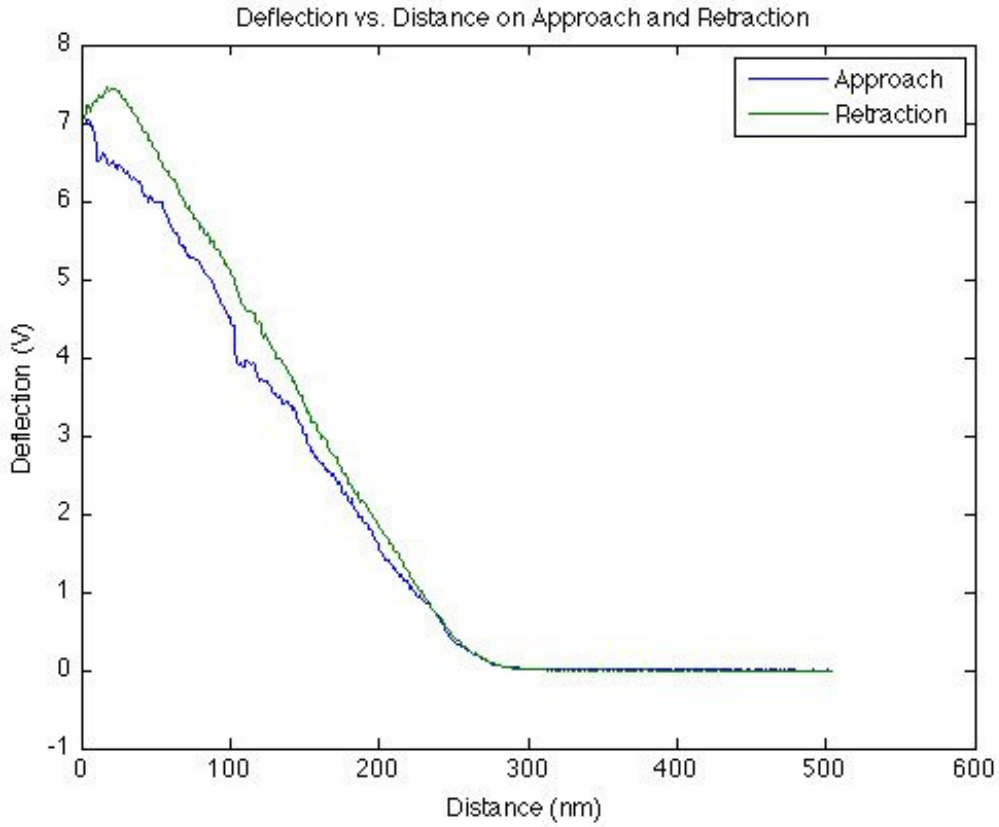
Deflection vs. Distance on Approach and Retraction
Approach
Retraction
Deflection (V)
Distance (nm)
8
7
6
5
4
3
2
1
0
-1
0
100
200
300
400
500
600

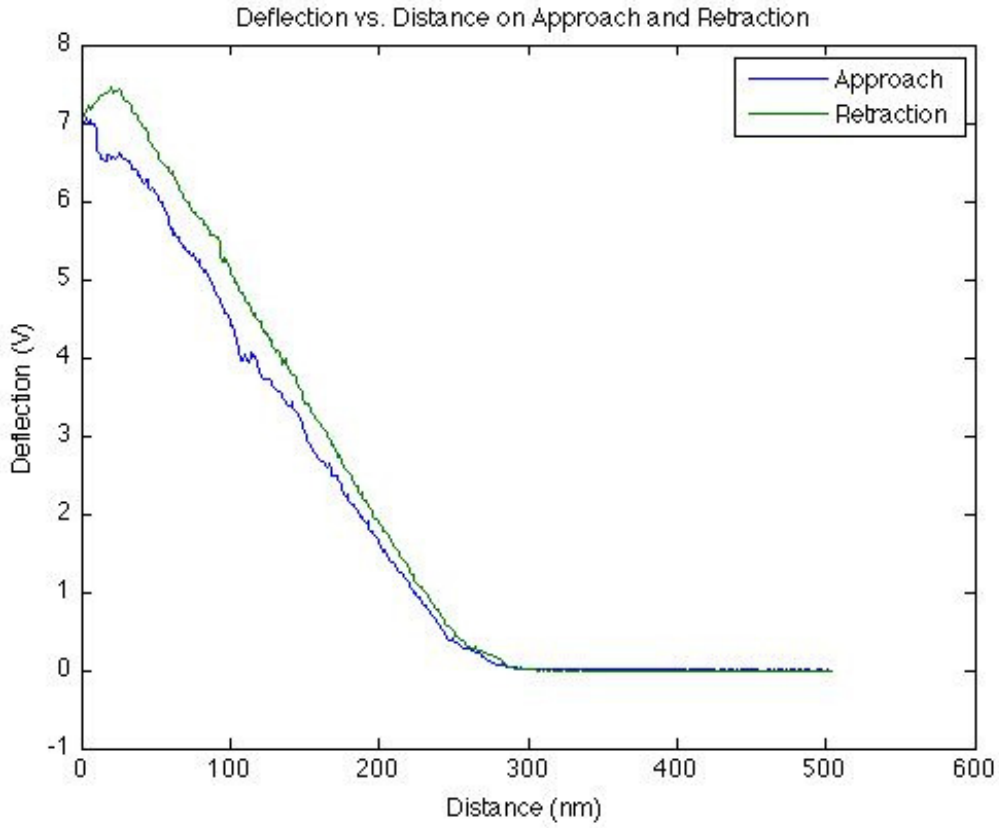
Deflection vs. Distance on Approach and Retraction
Approach
Retraction
Deflection (V)
Distance (nm)
8
7
6
5
4
3
2
1
0
-1
0
100
200
300
400
500
600

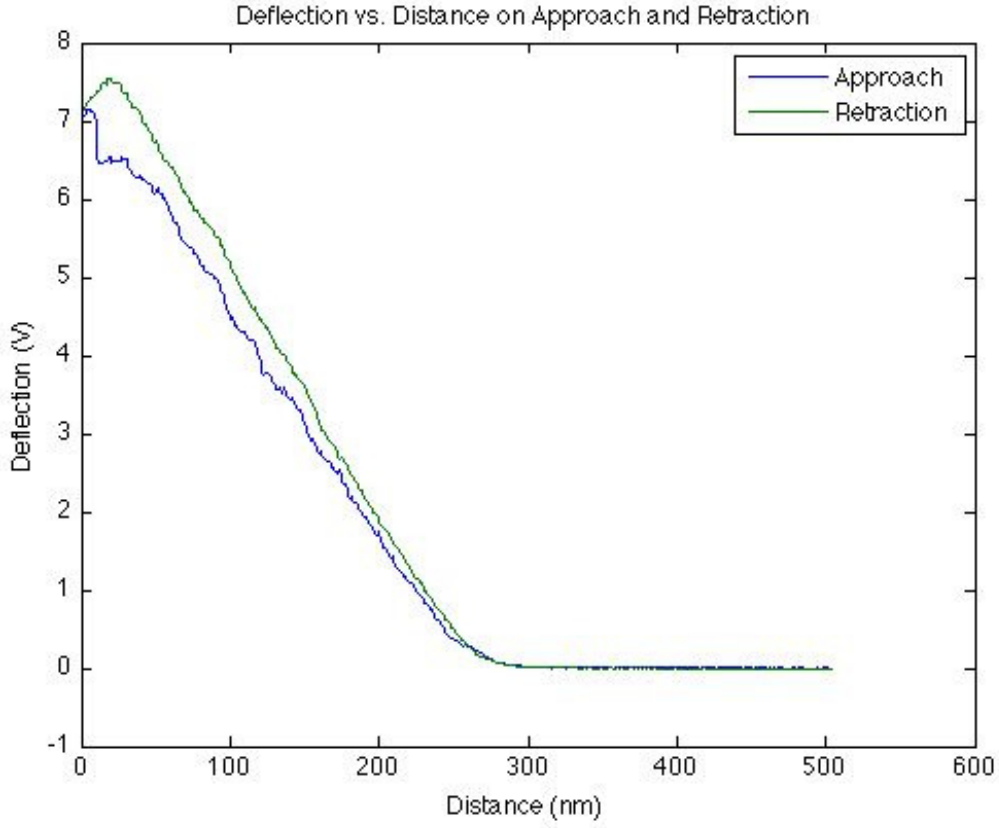
Deflection vs. Distance on Approach and Retraction
Approach
Retraction
Deflection (V)
Distance (nm)
8
7
6
5
4
3
2
1
0
-1
0
100
200
300
400
500
600

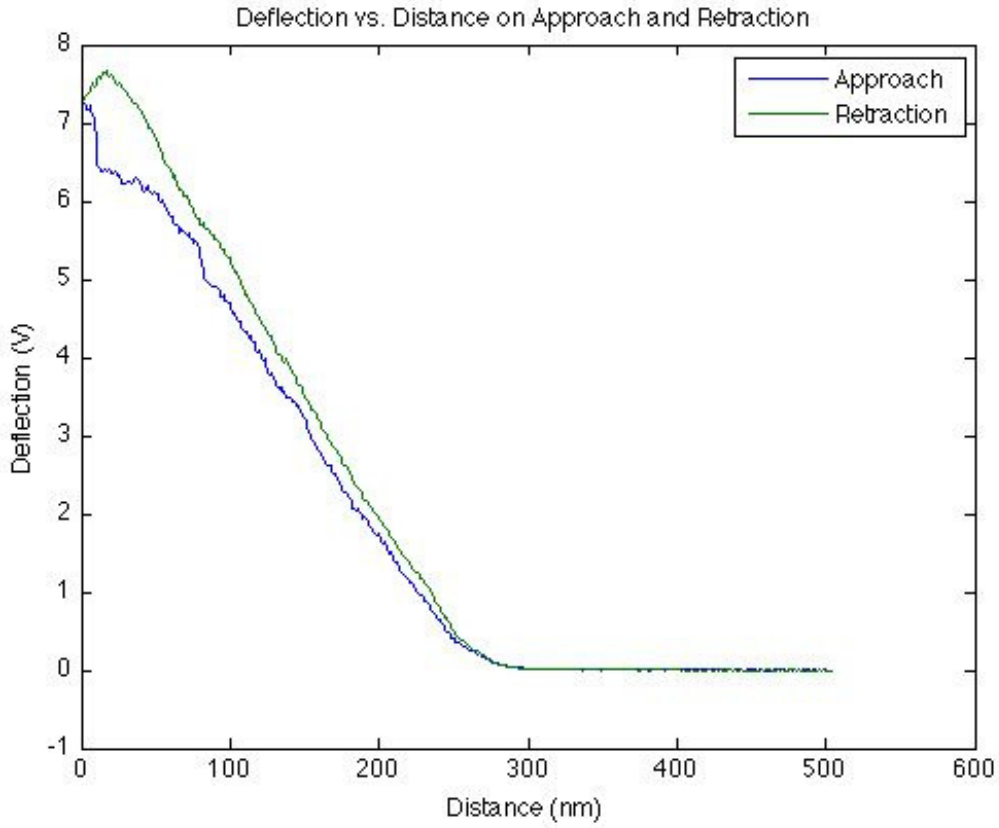
Deflection vs. Distance on Approach and Retraction
Approach
Retraction
Deflection (V)
Distance (nm)
8
7
6
5
4
3
2
1
0
-1
0
100
200
300
400
500
600

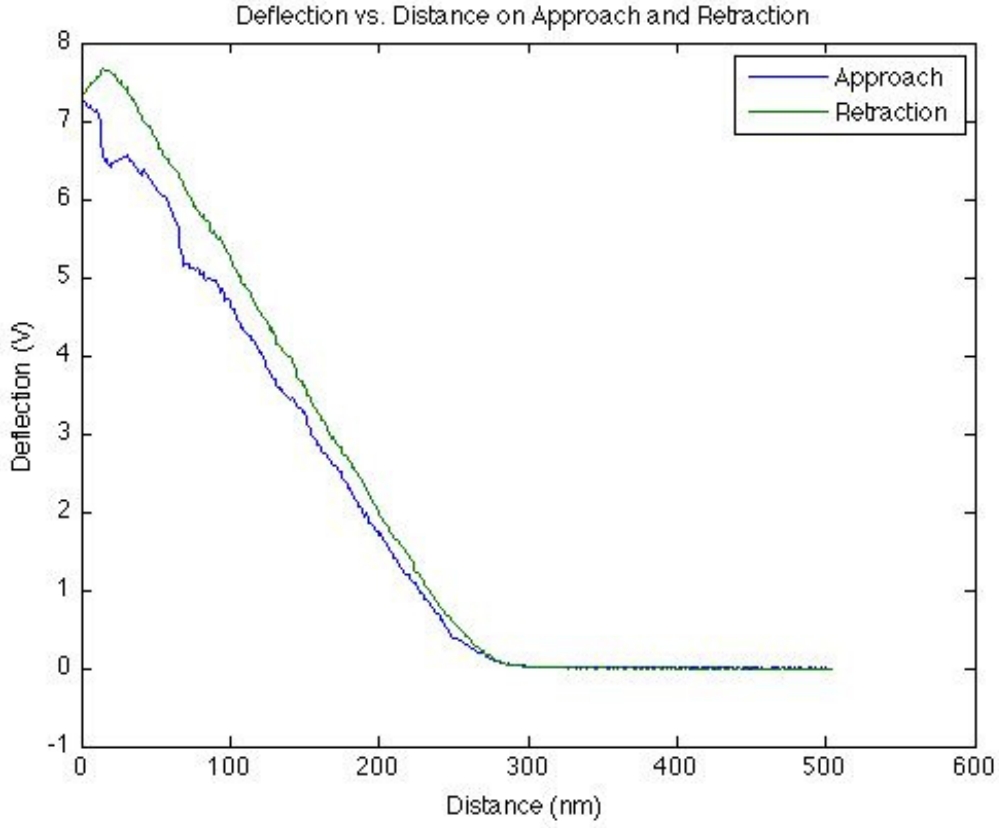
Deflection vs. Distance on Approach and Retraction
Approach
Retraction
Deflection (V)
Distance (nm)
8
7
6
5
4
3
2
1
0
-1
0
100
200
300
400
500
600

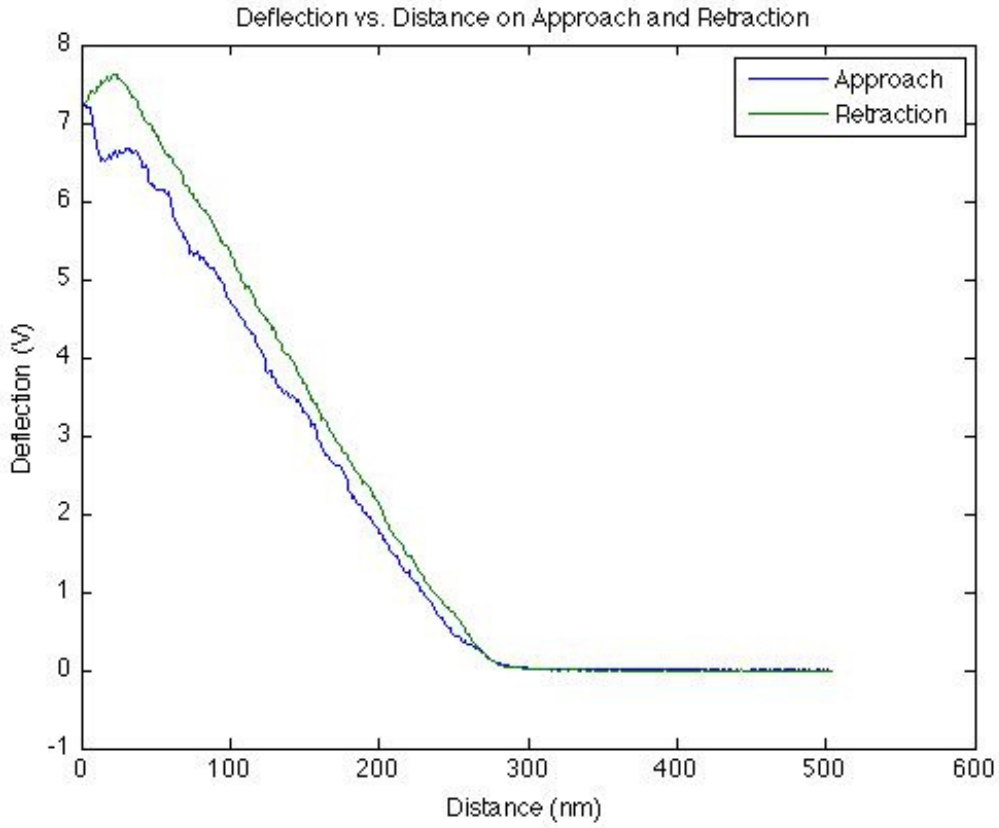
Deflection vs. Distance on Approach and Retraction
Approach
Retraction
Deflection (V)
Distance (nm)
8
7
6
5
4
3
2
1
0
-1
0
100
200
300
400
500
600

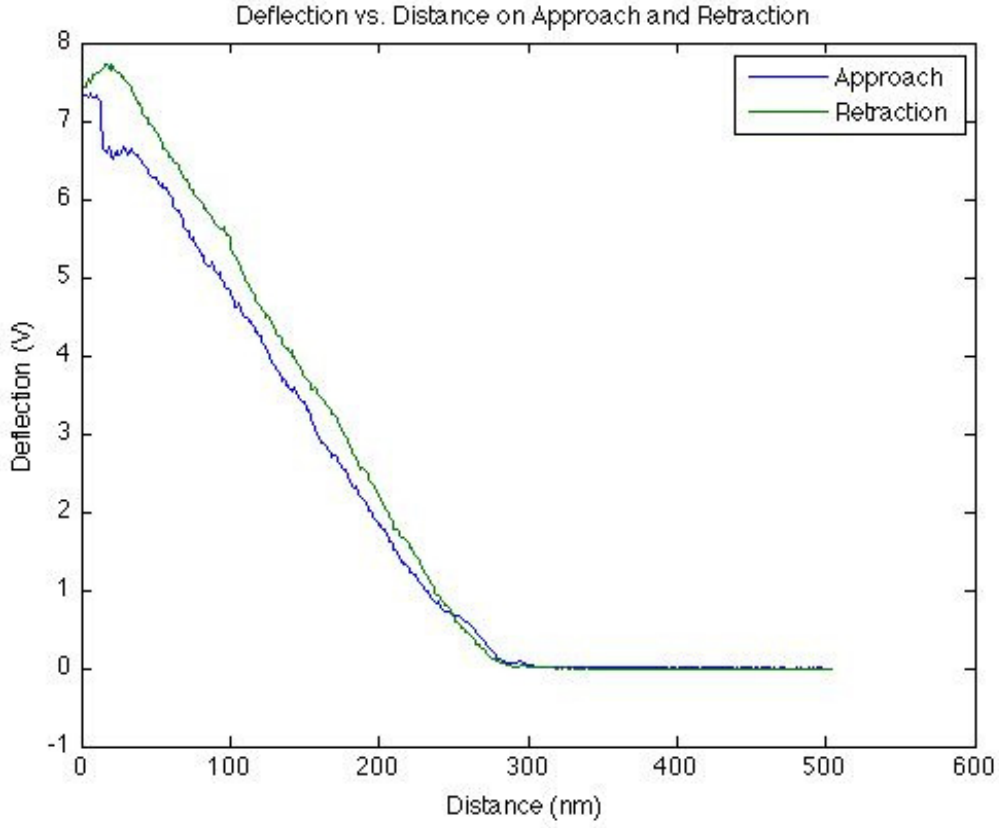
Deflection vs. Distance on Approach and Retraction
Approach
Retraction
Deflection (V)
Distance (nm)
8
7
6
5
4
3
2
1
0
-1
0
100
200
300
400
500
600

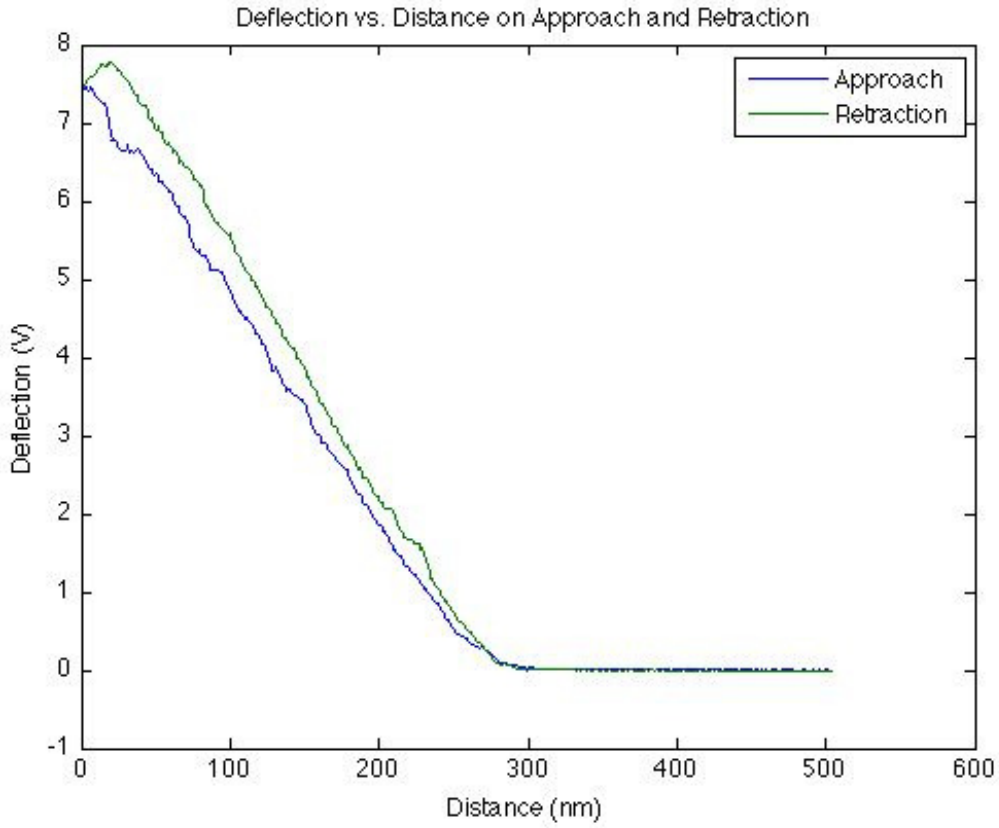
Deflection vs. Distance on Approach and Retraction
Approach
Retraction
Deflection (V)
Distance (nm)
8
7
6
5
4
3
2
1
0
-1
0
100
200
300
400
500
600

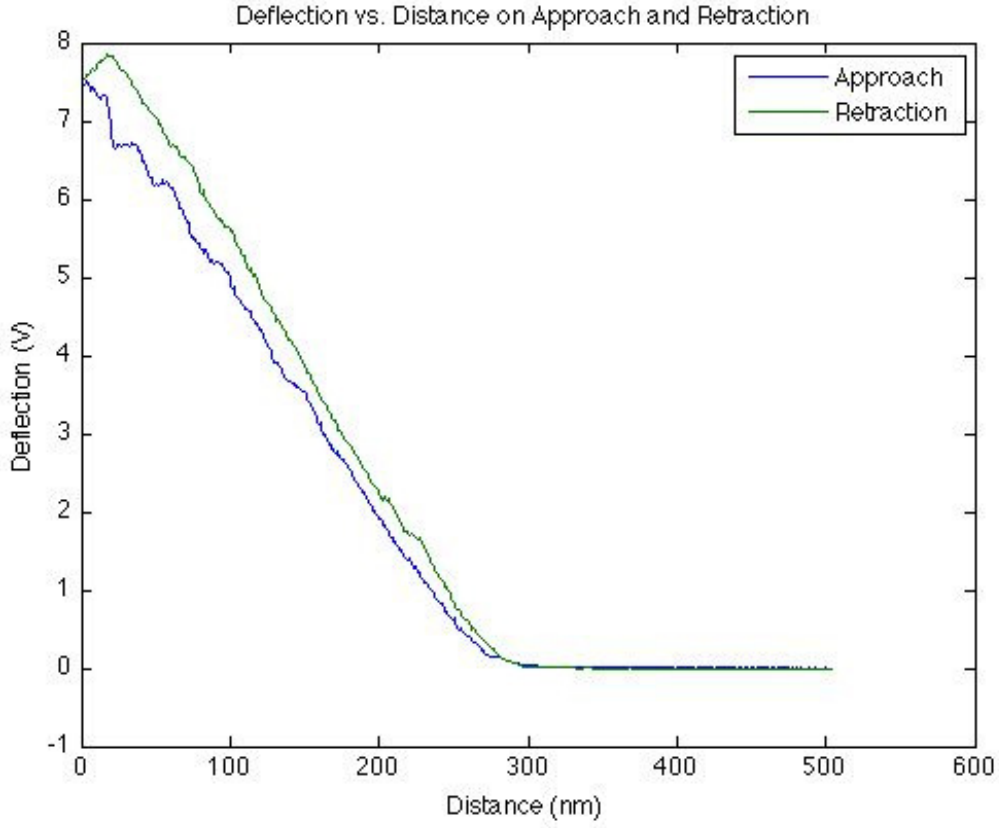
Deflection vs. Distance on Approach and Retraction
Approach
Retraction
Deflection (V)
Distance (nm)
8
7
6
5
4
3
2
1
0
-1
0
100
200
300
400
500
600

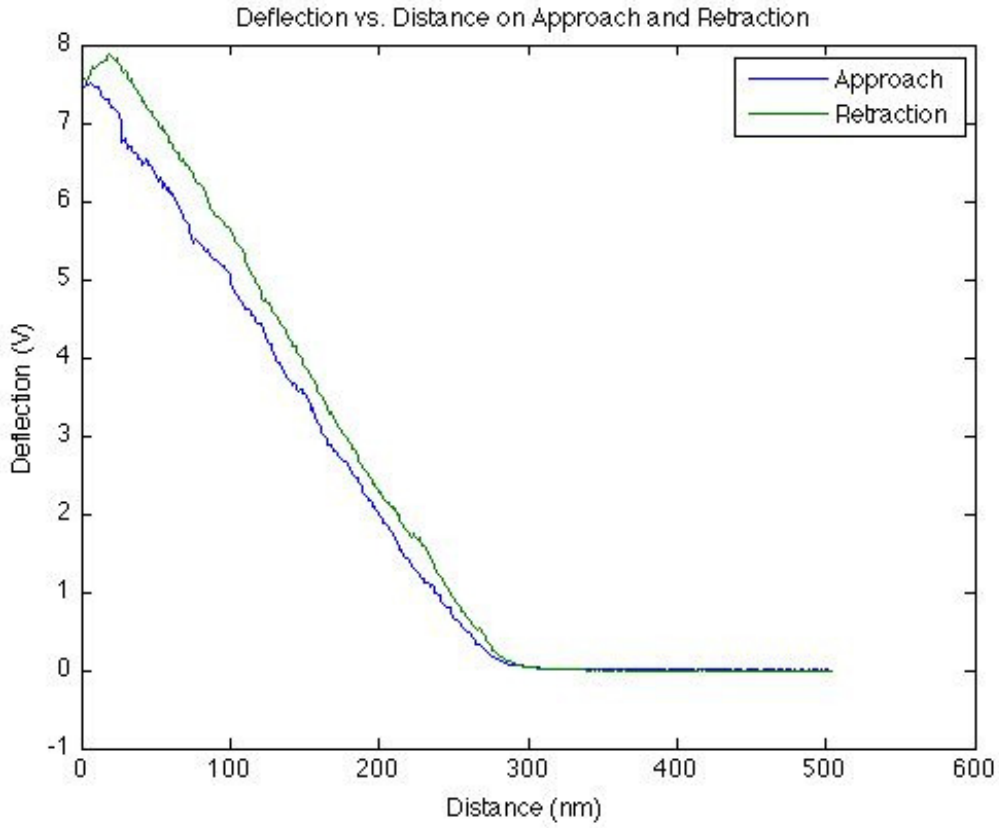
Deflection vs. Distance on Approach and Retraction
Approach
Retraction
Deflection (V)
Distance (nm)
8
7
6
5
4
3
2
1
0
-1
0
100
200
300
400
500
600

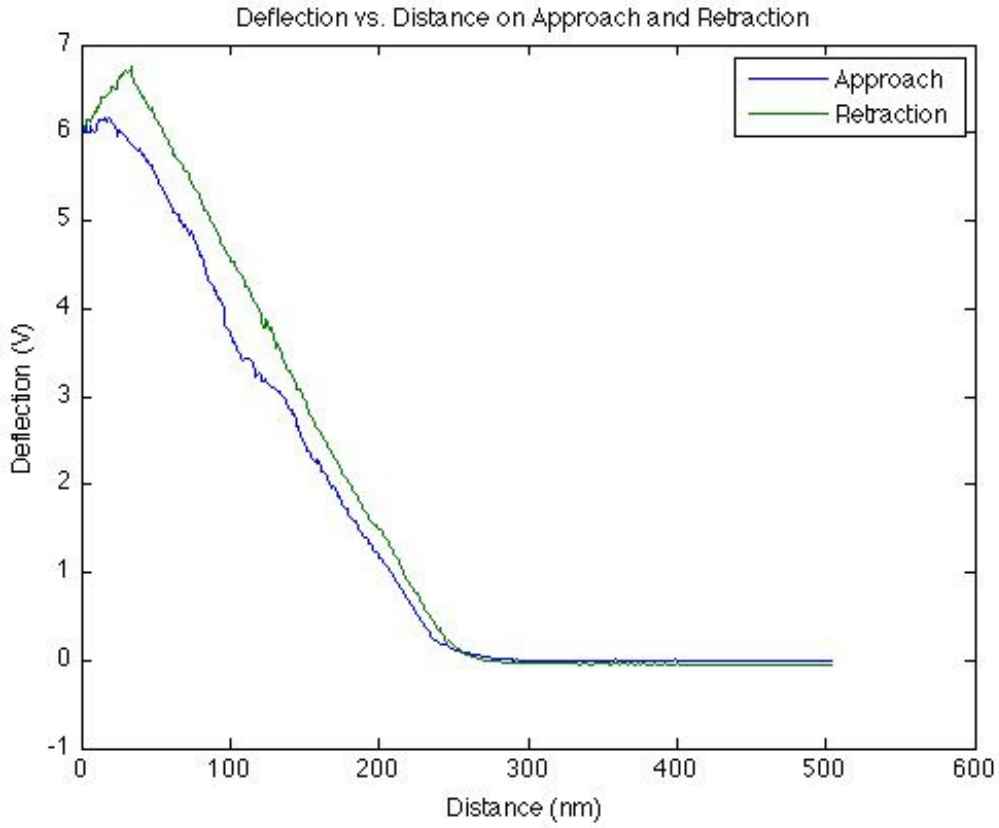
Deflection vs. Distance on Approach and Retraction
Approach
Retraction
Deflection (V)
Distance (nm)
7
6
5
4
3
2
1
0
-1
0
100
200
300
400
500
600

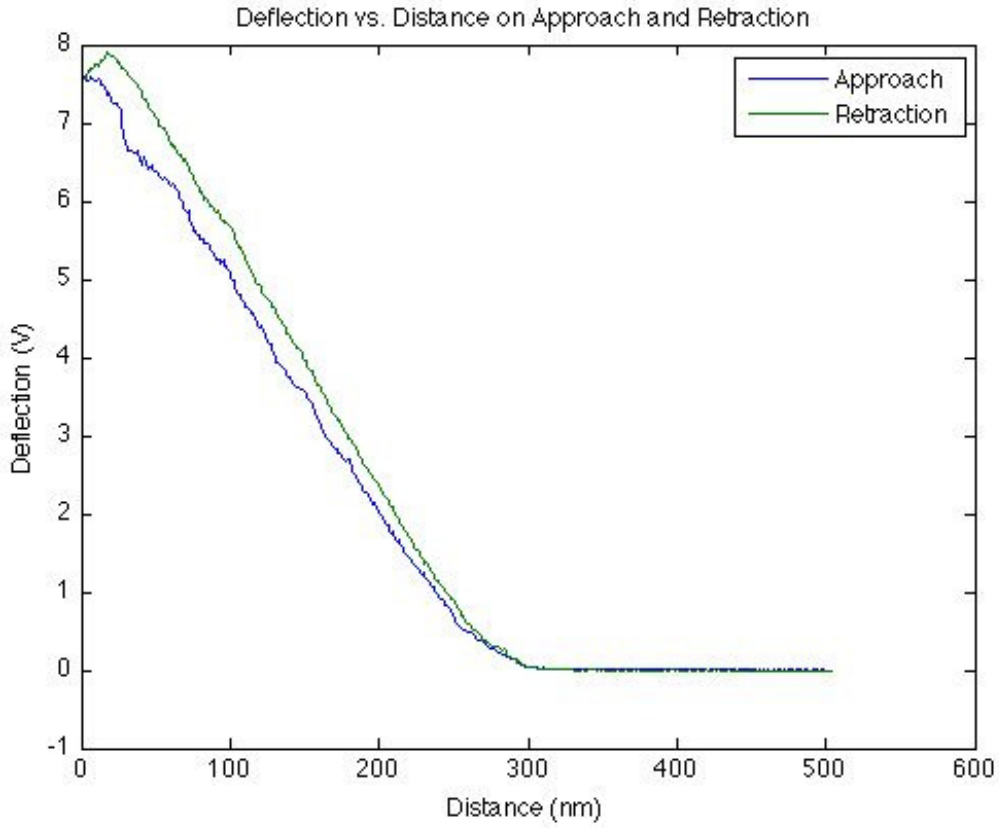
Deflection vs. Distance on Approach and Retraction
Approach
Retraction
Deflection (V)
Distance (nm)
8
7
6
5
4
3
2
1
0
-1
0
100
200
300
400
500
600

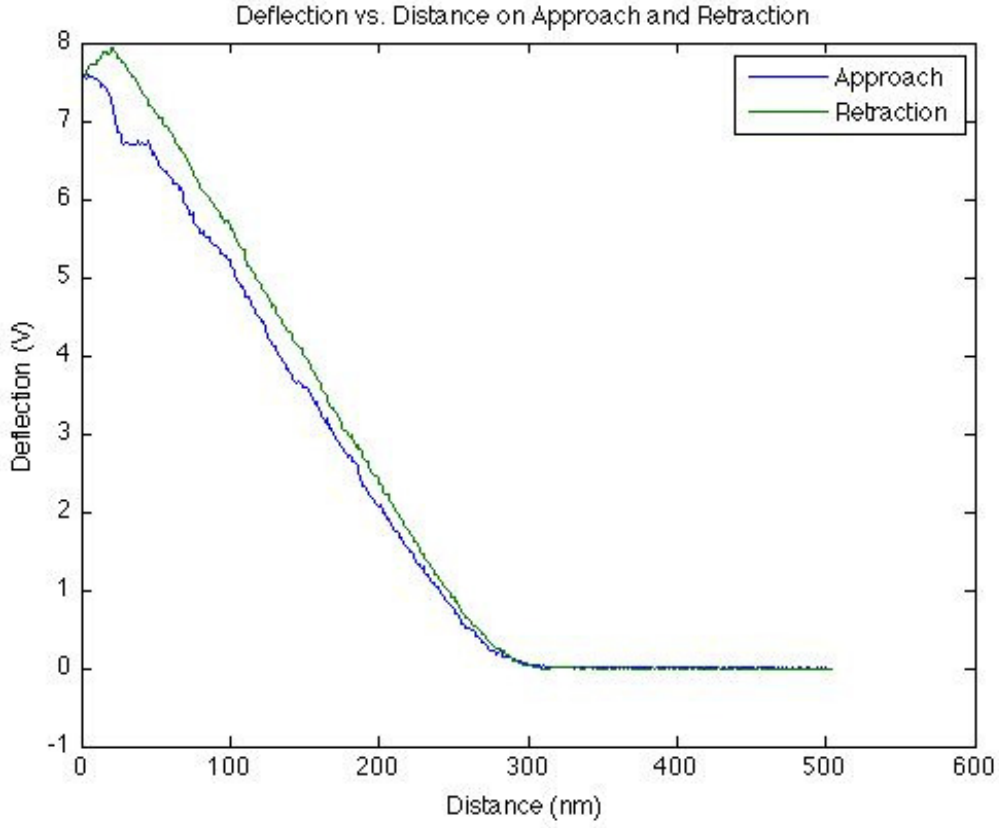
Deflection vs. Distance on Approach and Retraction
Approach
Retraction
Deflection (V)
Distance (nm)
8
7
6
5
4
3
2
1
0
-1
0
100
200
300
400
500
600

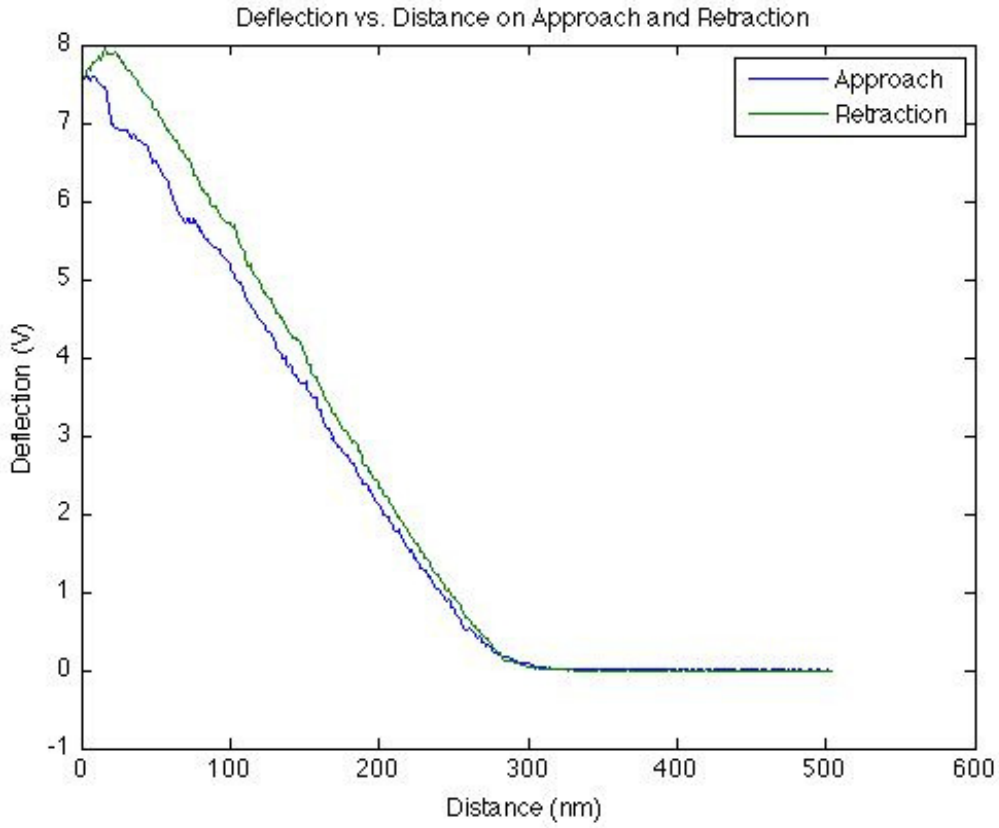
Deflection vs. Distance on Approach and Retraction
Approach
Retraction
Deflection (V)
Distance (nm)
8
7
6
5
4
3
2
1
0
-1
0
100
200
300
400
500
600

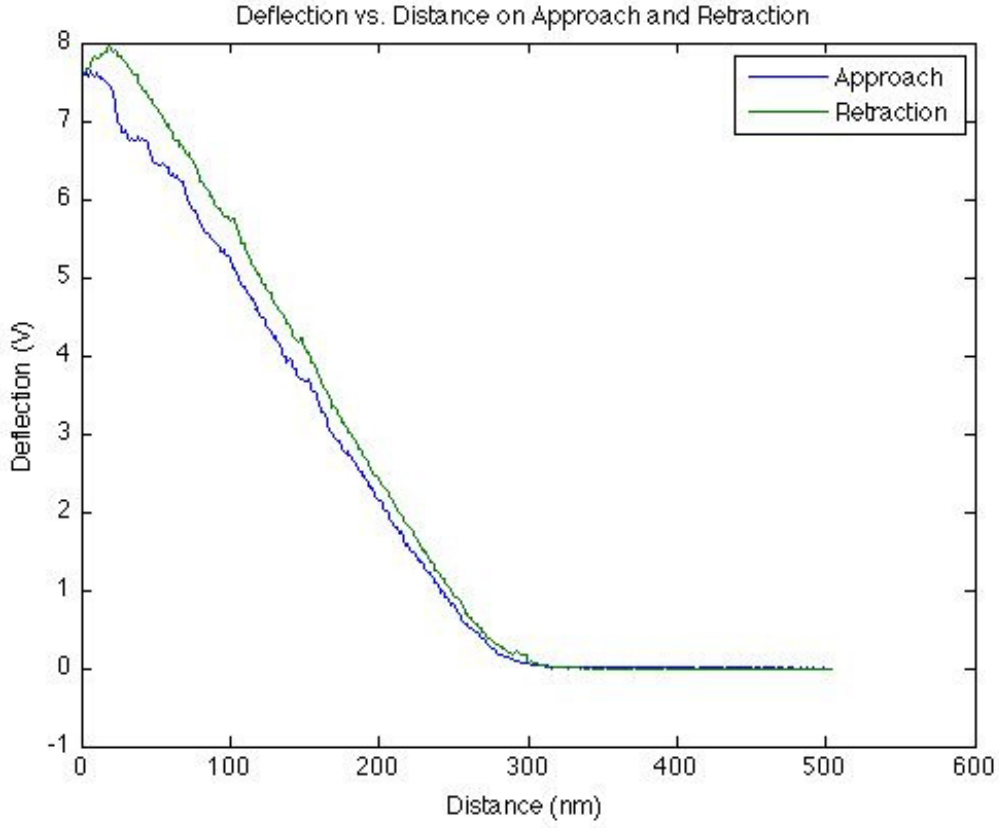
Deflection vs. Distance on Approach and Retraction
Approach
Retraction
Deflection (V)
Distance (nm)
8
7
6
5
4
3
2
1
0
-1
0
100
200
300
400
500
600

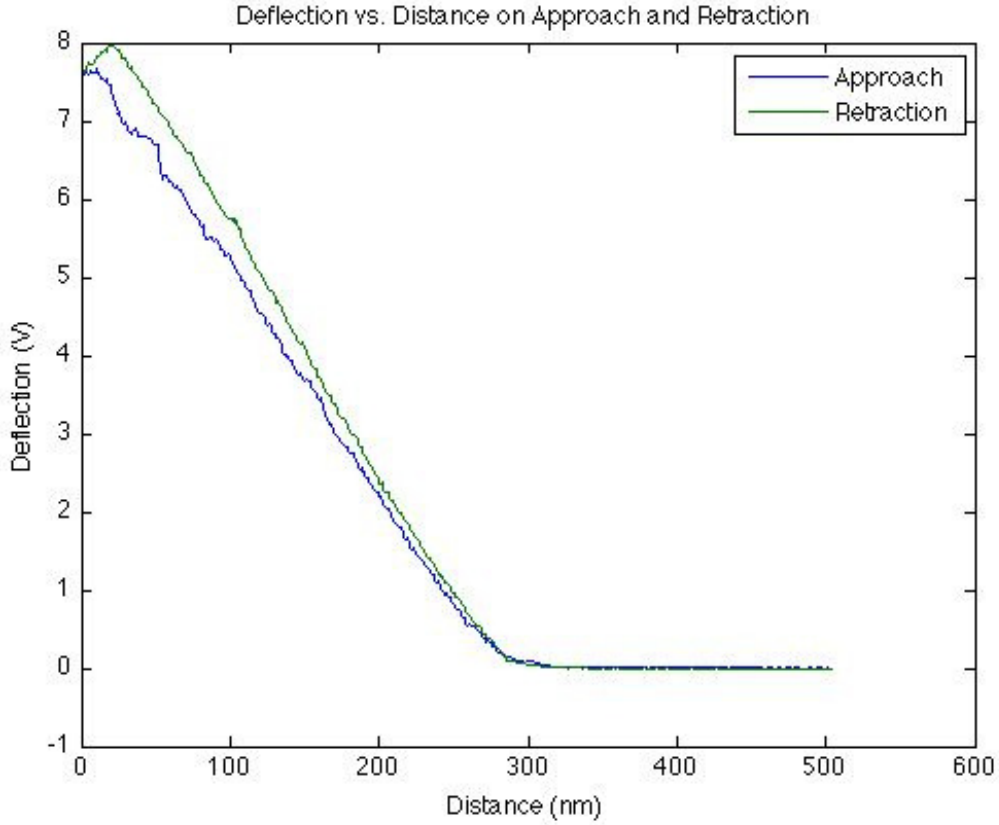
Deflection vs. Distance on Approach and Retraction
Approach
Retraction
Deflection (V)
Distance (nm)
8
7
6
5
4
3
2
1
0
-1
0
100
200
300
400
500
600

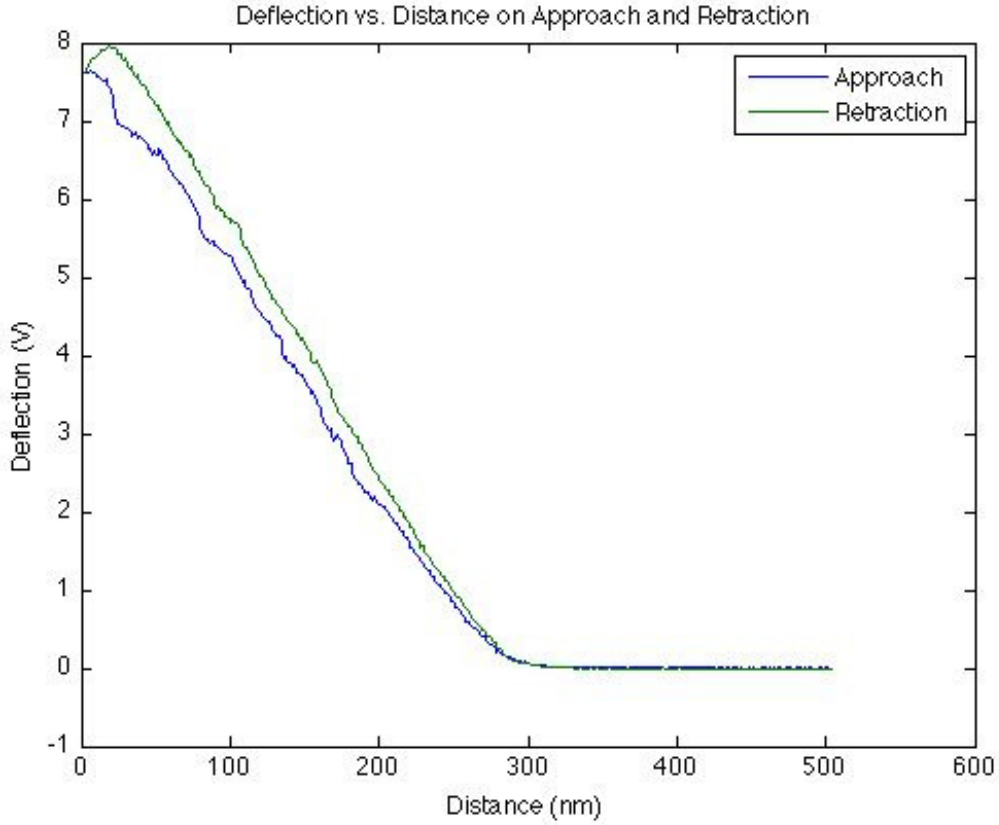
Deflection vs. Distance on Approach and Retraction
Approach
Retraction
Deflection (V)
Distance (nm)
8
7
6
5
4
3
2
1
0
-1
0
100
200
300
400
500
600

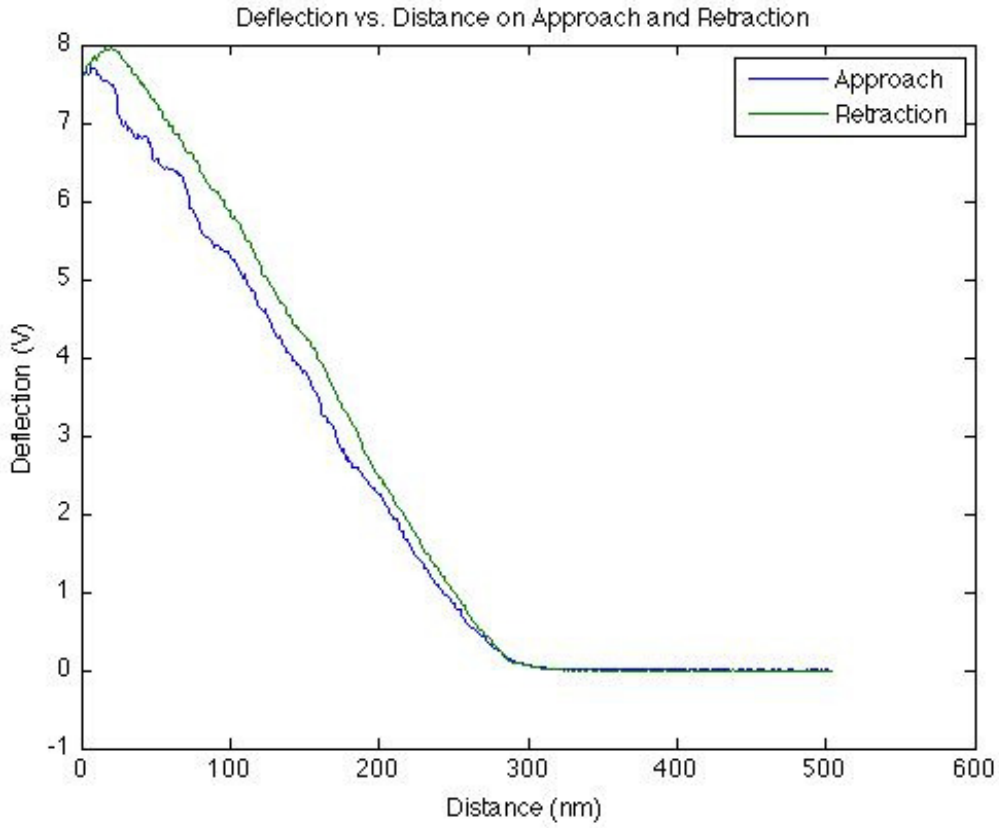
Deflection vs. Distance on Approach and Retraction
Approach
Retraction
Deflection (V)
Distance (nm)
8
7
6
5
4
3
2
1
0
-1
0
100
200
300
400
500
600

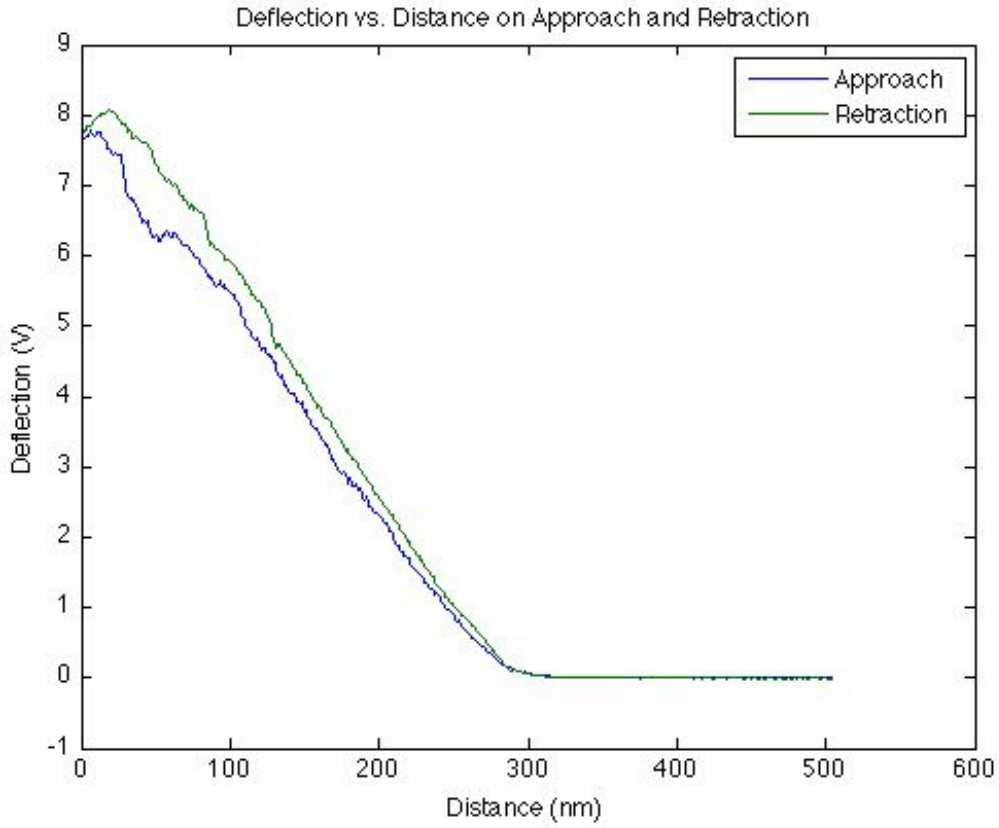
Deflection vs. Distance on Approach and Retraction
Approach
Retraction
Deflection (V)
Distance (nm)
9
8
7
6
5
4
3
2
1
0
-1
0
100
200
300
400
500
600

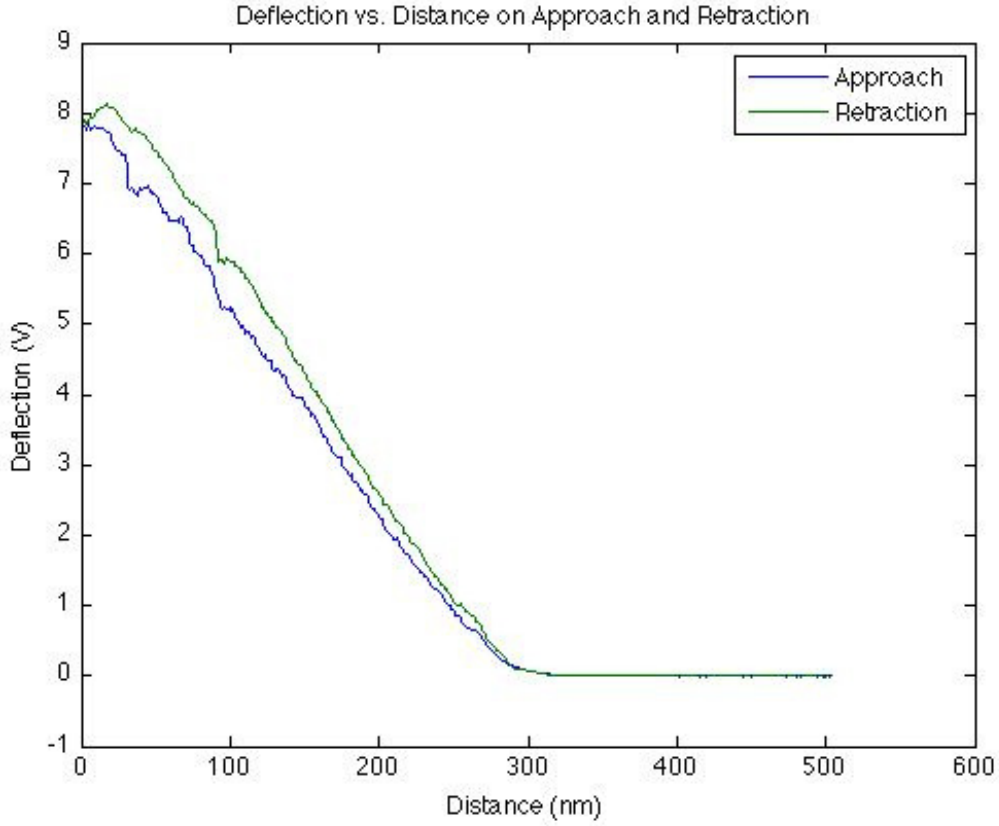
Deflection vs. Distance on Approach and Retraction
Approach
Retraction
Deflection (V)
Distance (nm)
9
8
7
6
5
4
3
2
1
0
-1
0
100
200
300
400
500
600

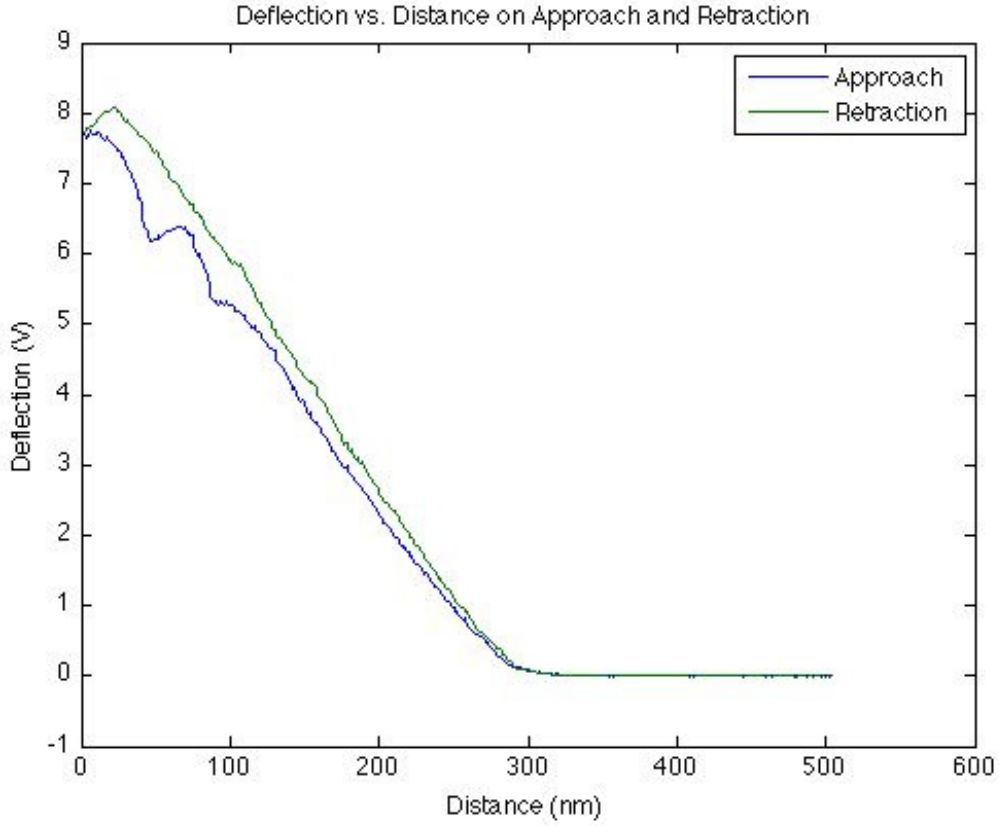
Deflection vs. Distance on Approach and Retraction
Approach
Retraction
Deflection (V)
Distance (nm)
9
8
7
6
5
4
3
2
1
0
-1
0
100
200
300
400
500
600

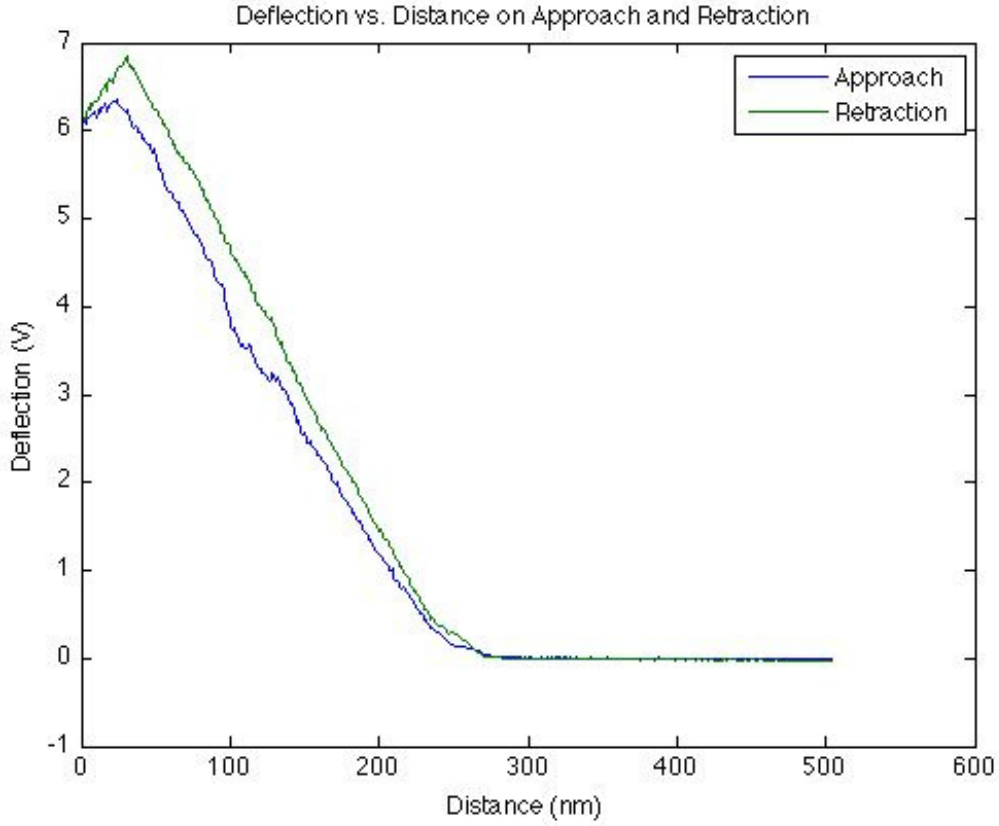
Deflection vs. Distance on Approach and Retraction
Approach
Retraction
Deflection (V)
Distance (nm)
7
6
5
4
3
2
1
0
-1
0
100
200
300
400
500
600

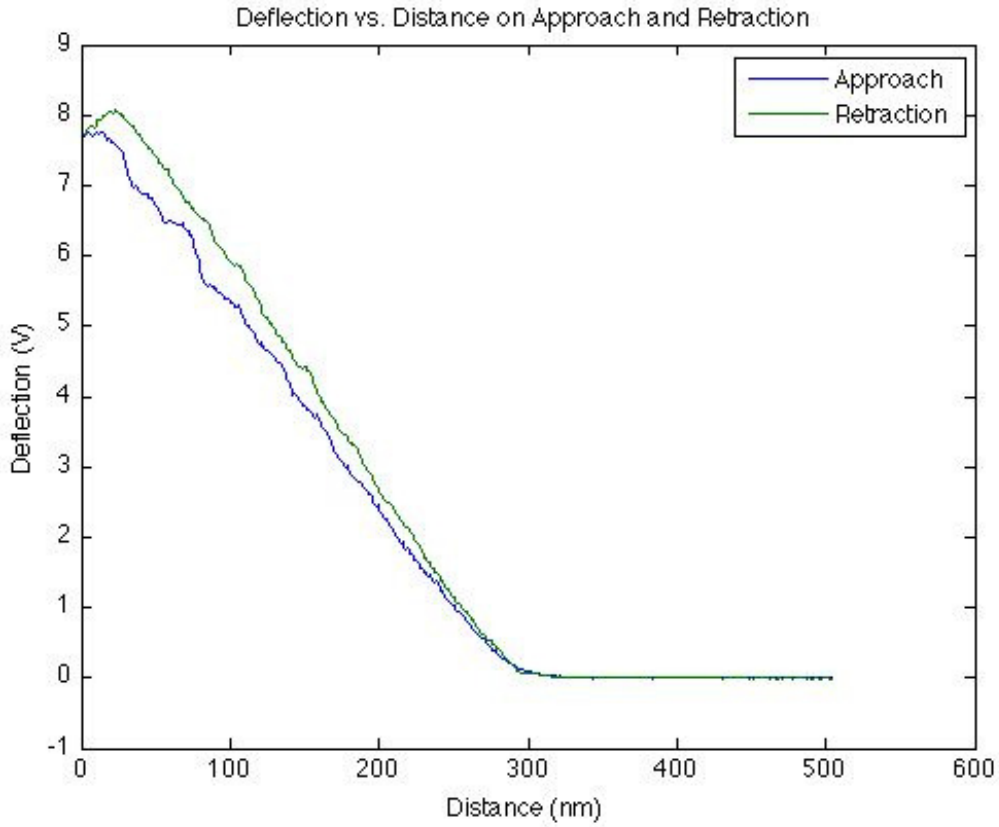
Deflection vs. Distance on Approach and Retraction
Approach
Retraction
Deflection (V)
Distance (nm)
9
8
7
6
5
4
3
2
1
0
-1
0
100
200
300
400
500
600

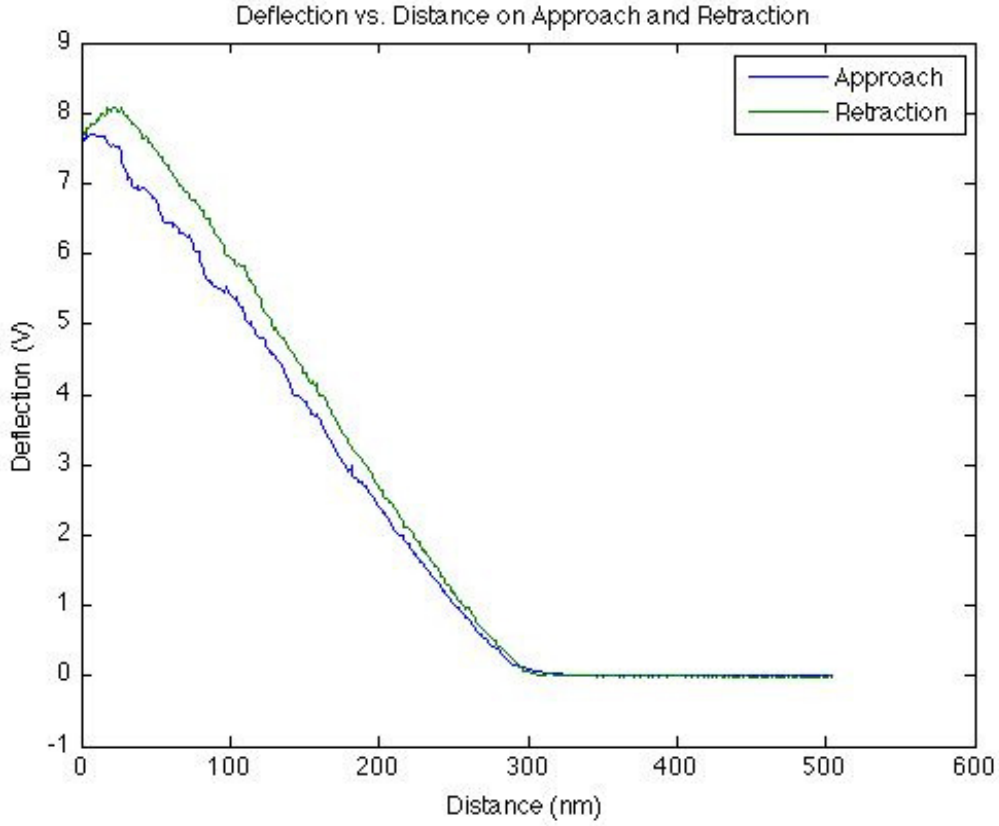
Deflection vs. Distance on Approach and Retraction
Approach
Retraction
Deflection (V)
Distance (nm)
9
8
7
6
5
4
3
2
1
0
-1
0
100
200
300
400
500
600

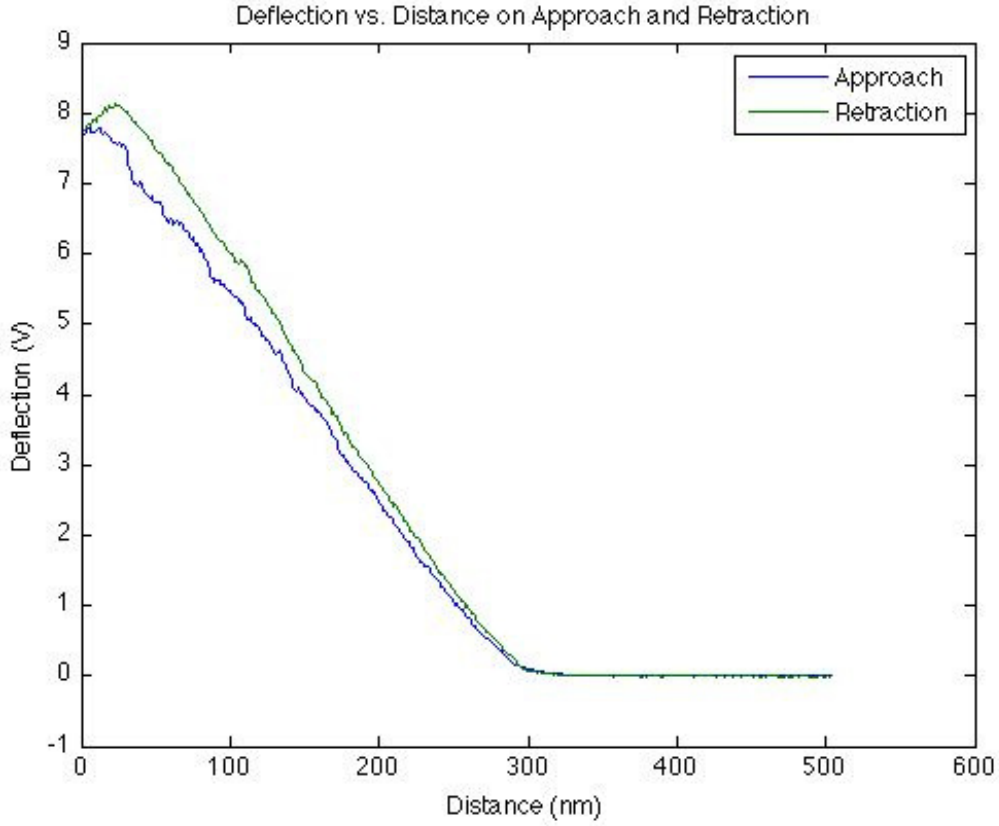
Deflection vs. Distance on Approach and Retraction
Approach
Retraction
Deflection (V)
Distance (nm)
9
8
7
6
5
4
3
2
1
0
-1
0
100
200
300
400
500
600

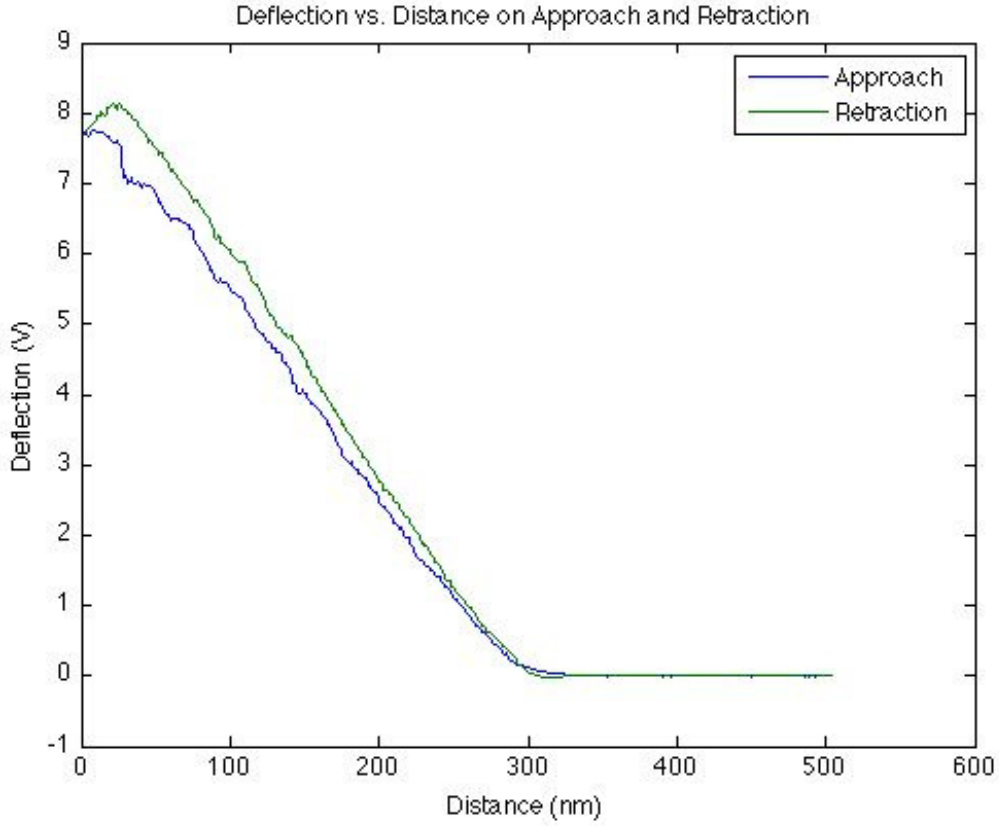
Deflection vs. Distance on Approach and Retraction
Approach
Retraction
Deflection (V)
Distance (nm)
9
8
7
6
5
4
3
2
1
0
-1
0
100
200
300
400
500
600

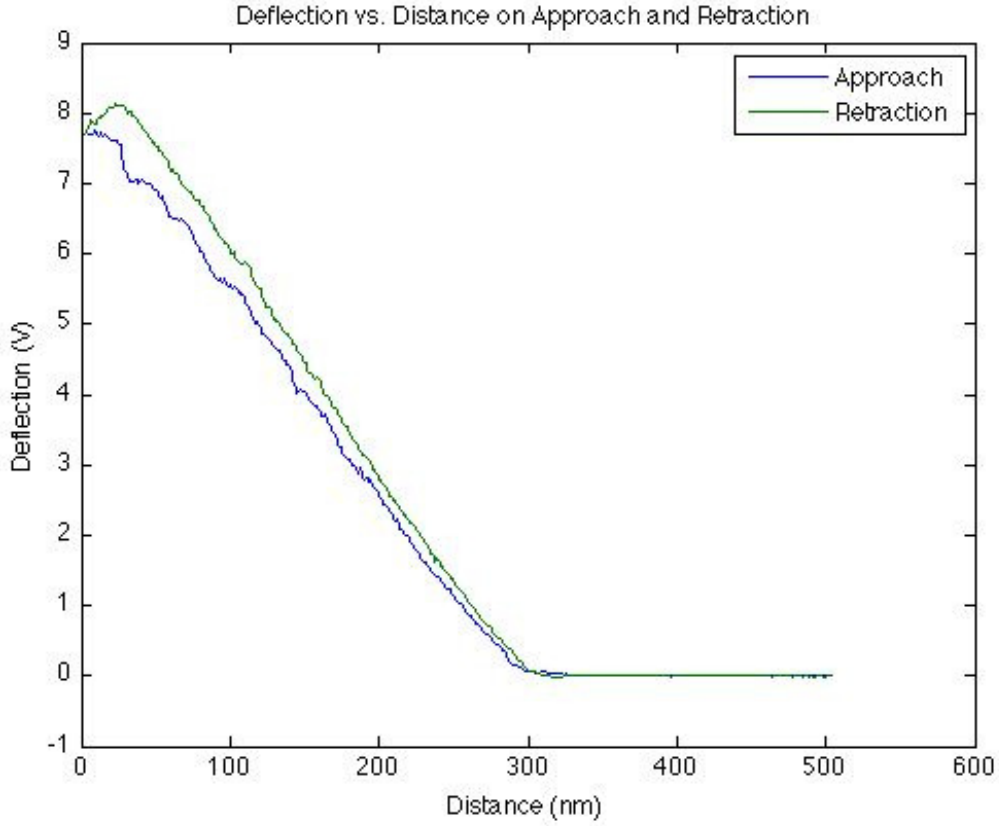
Deflection vs. Distance on Approach and Retraction
Approach
Retraction
Deflection (V)
Distance (nm)
9
8
7
6
5
4
3
2
1
0
-1
0
100
200
300
400
500
600

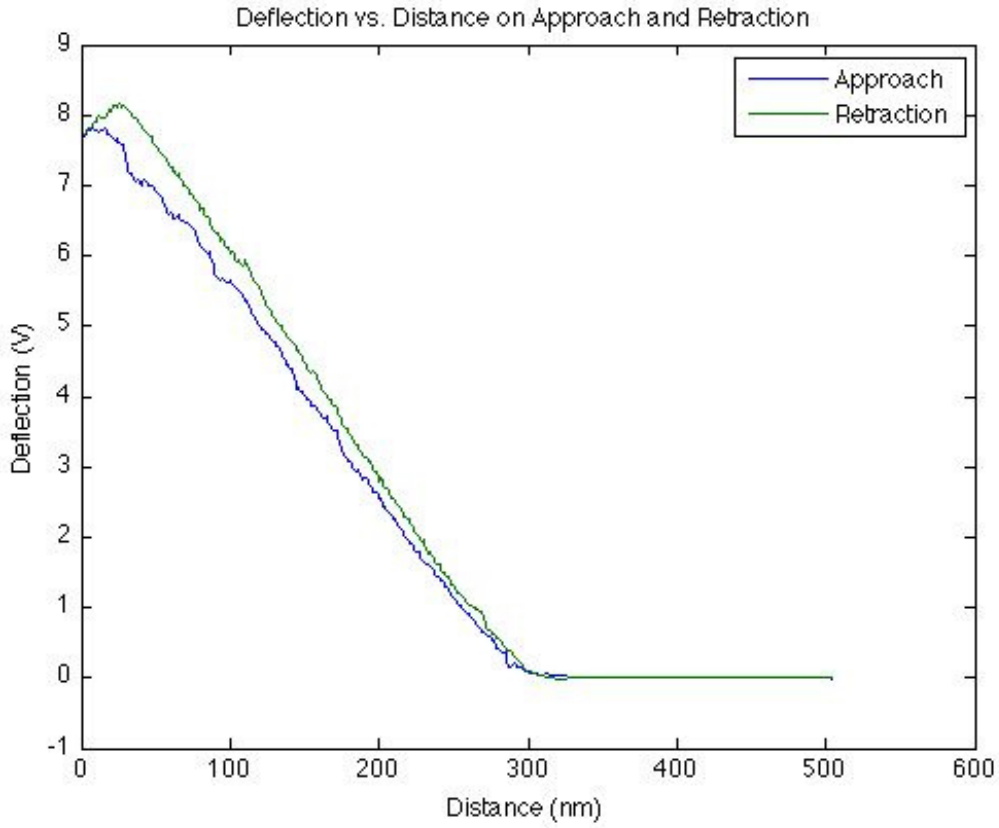
Deflection vs. Distance on Approach and Retraction
Approach
Retraction
Deflection (V)
Distance (nm)
9
8
7
6
5
4
3
2
1
0
-1
0
100
200
300
400
500
600

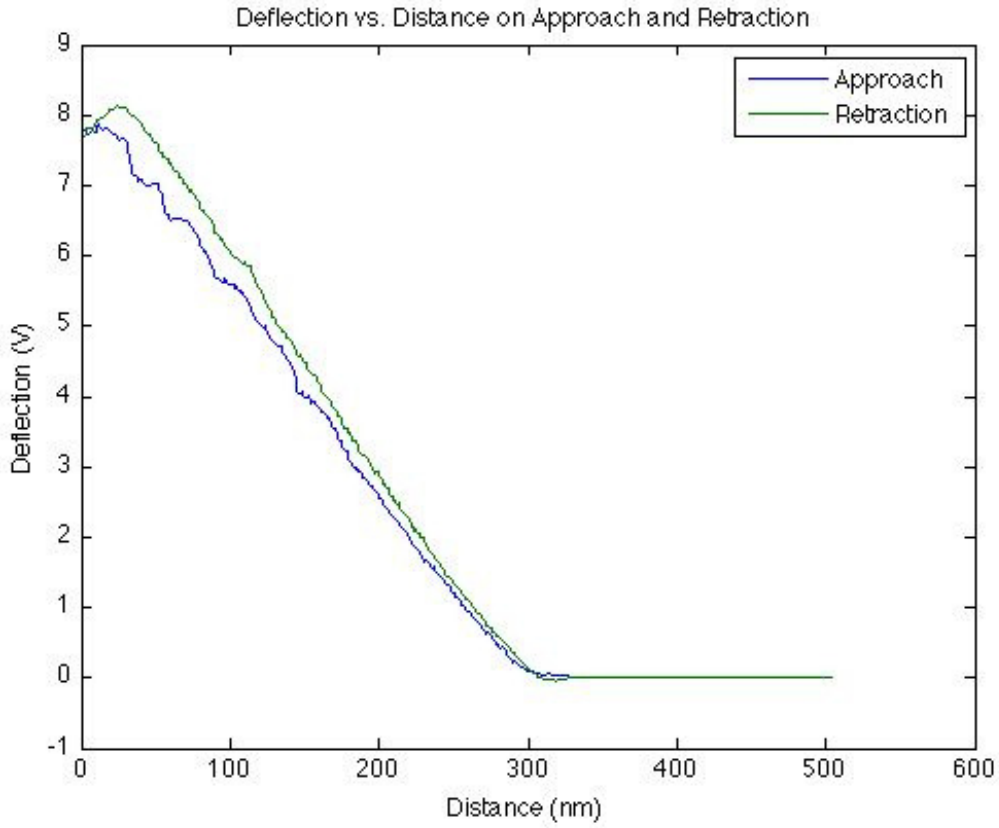
Deflection vs. Distance on Approach and Retraction
Approach
Retraction
Deflection (V)
Distance (nm)
9
8
7
6
5
4
3
2
1
0
-1
0
100
200
300
400
500
600

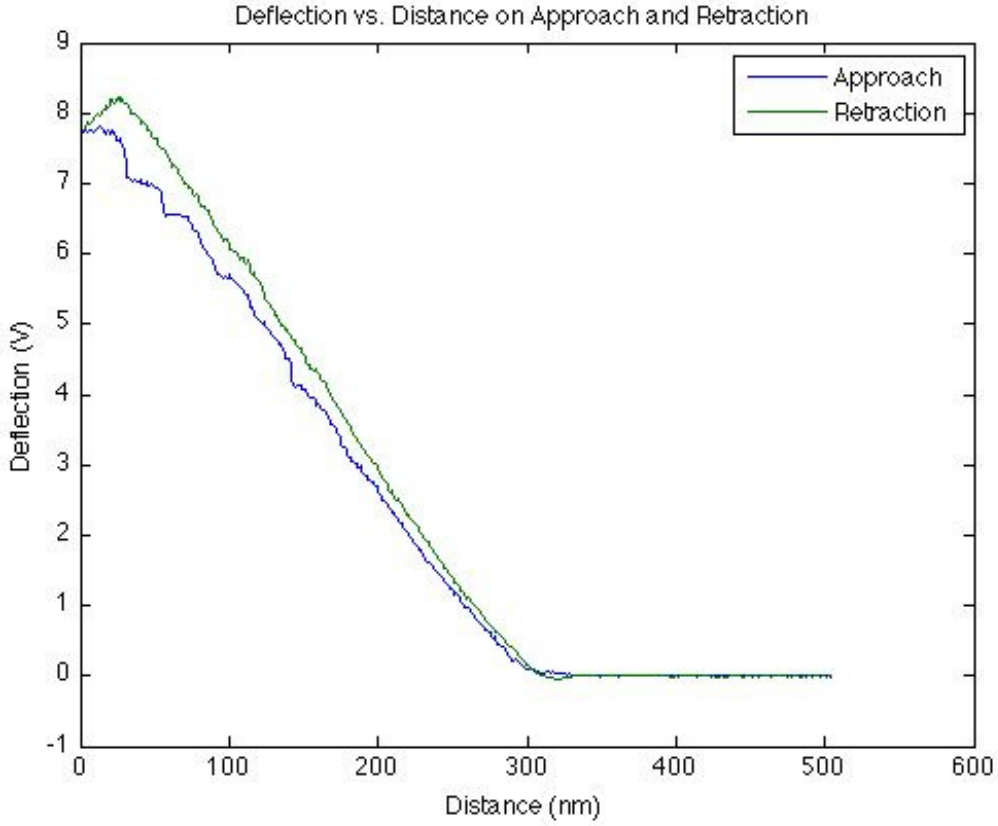
Deflection vs. Distance on Approach and Retraction
Approach
Retraction
Deflection (V)
Distance (nm)
9
8
7
6
5
4
3
2
1
0
-1
0
100
200
300
400
500
600

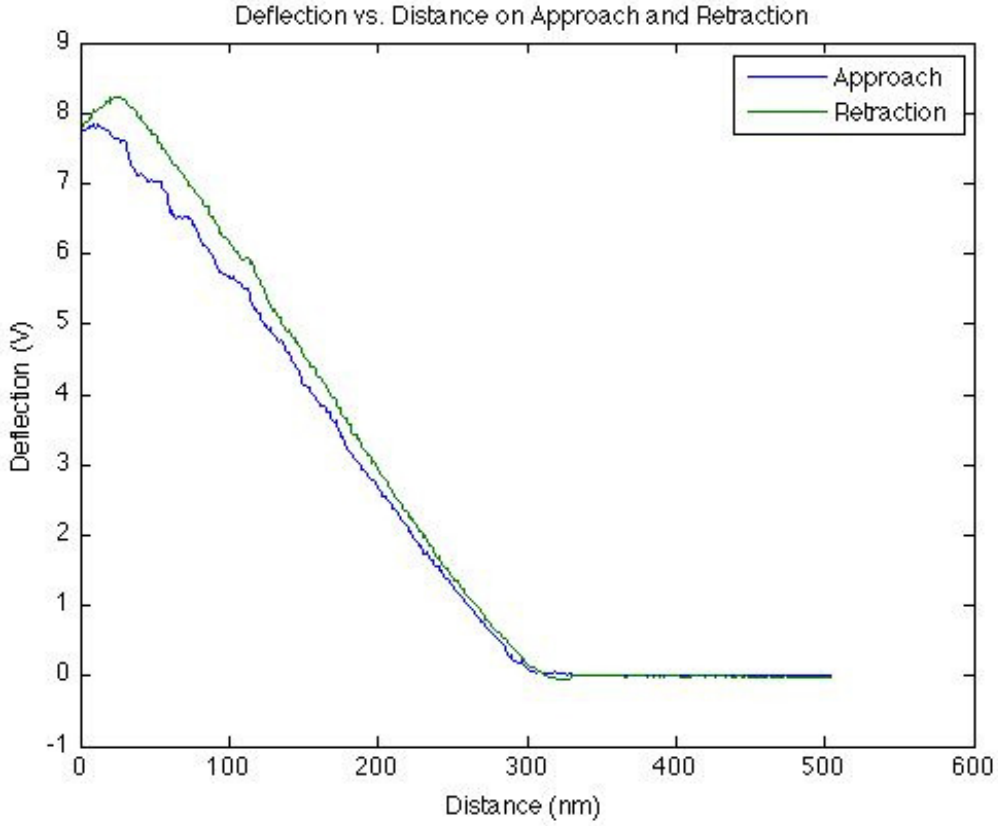
Deflection vs. Distance on Approach and Retraction
Approach
Retraction
Deflection (V)
Distance (nm)
9
8
7
6
5
4
3
2
1
0
-1
0
100
200
300
400
500
600

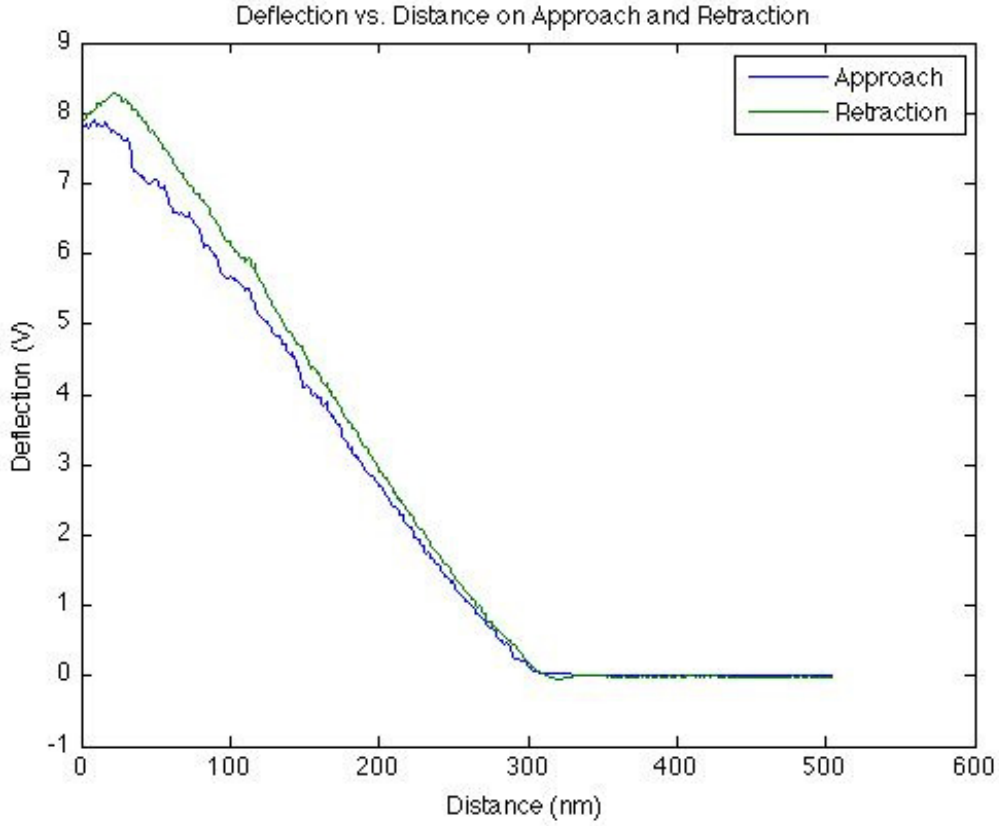
Deflection vs. Distance on Approach and Retraction
Approach
Retraction
Deflection (V)
Distance (nm)
9
8
7
6
5
4
3
2
1
0
-1
0
100
200
300
400
500
600

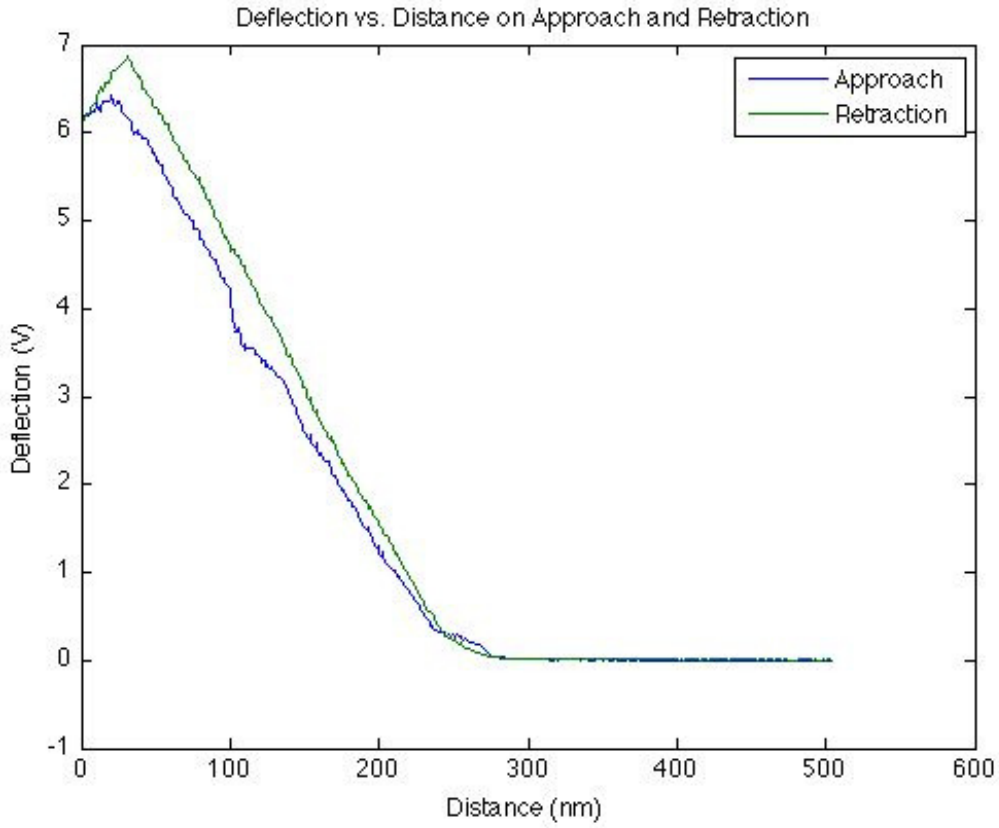
Deflection vs. Distance on Approach and Retraction
Approach
Retraction
Deflection (V)
Distance (nm)
7
6
5
4
3
2
1
0
-1
0
100
200
300
400
500
600

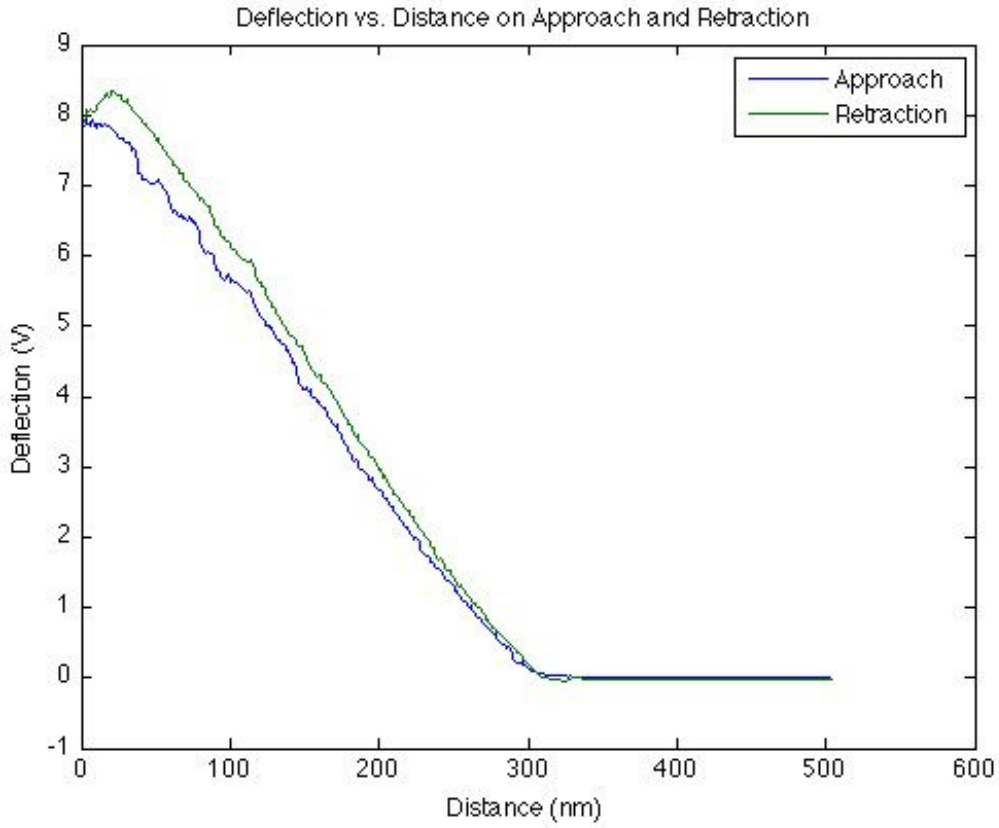
Deflection vs. Distance on Approach and Retraction
Approach
Retraction
Deflection (V)
Distance (nm)
9
8
7
6
5
4
3
2
1
0
-1
0
100
200
300
400
500
600

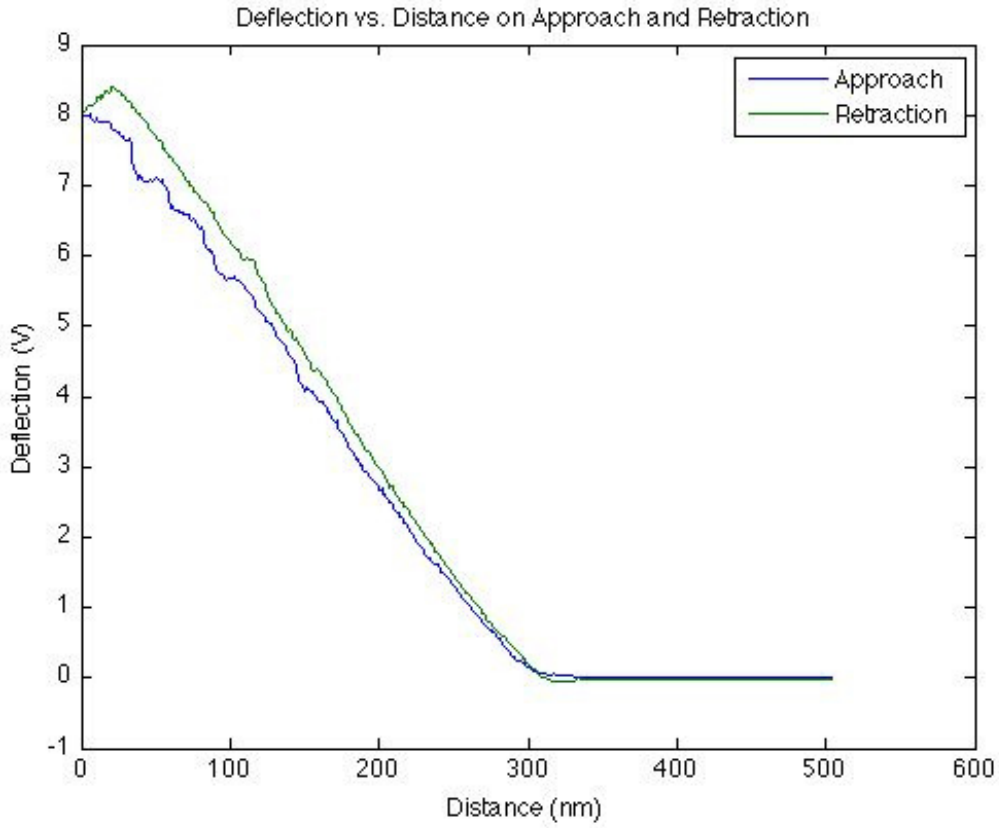
Deflection vs. Distance on Approach and Retraction
Approach
Retraction
Deflection (V)
Distance (nm)
9
8
7
6
5
4
3
2
1
0
-1
0
100
200
300
400
500
600

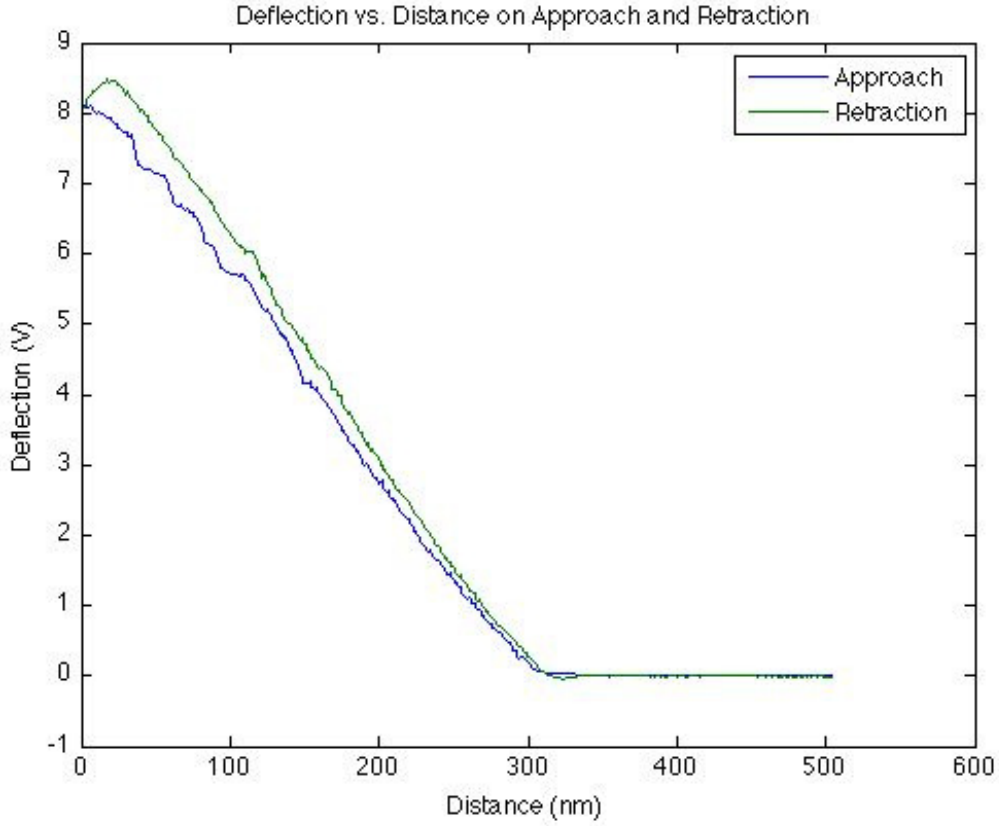
Deflection vs. Distance on Approach and Retraction
Approach
Retraction
Deflection (V)
Distance (nm)
9
8
7
6
5
4
3
2
1
0
-1
0
100
200
300
400
500
600

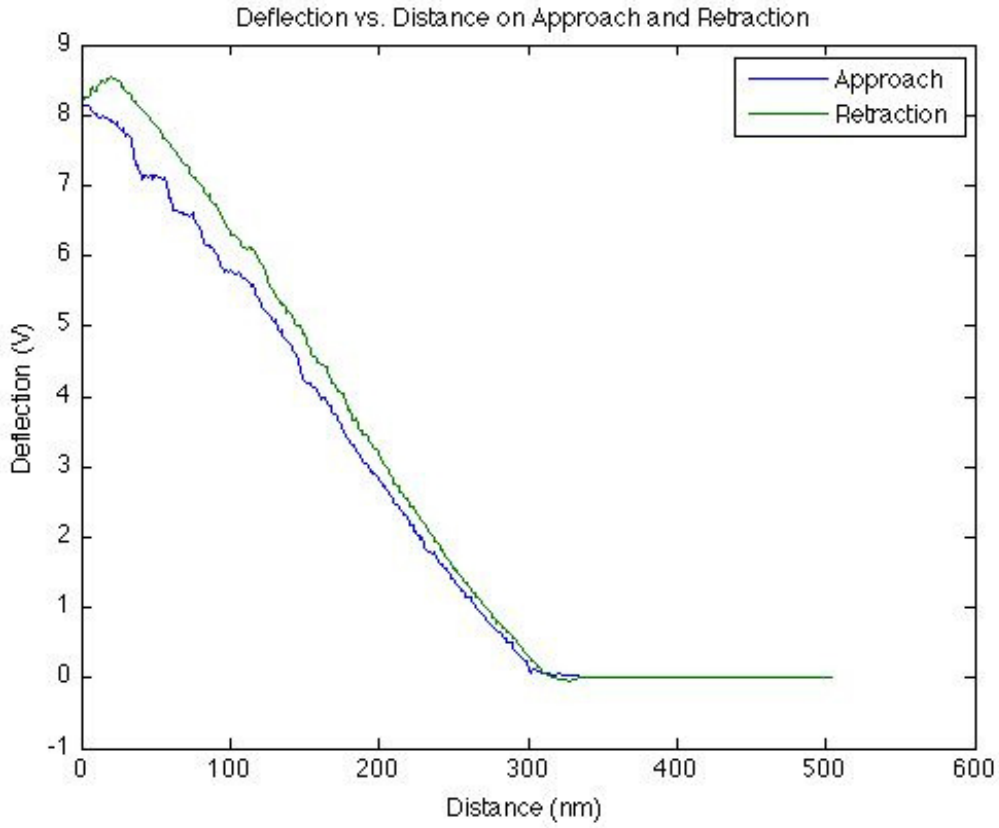
Deflection vs. Distance on Approach and Retraction
Approach
Retraction
Deflection (V)
Distance (nm)
9
8
7
6
5
4
3
2
1
0
-1
0
100
200
300
400
500
600

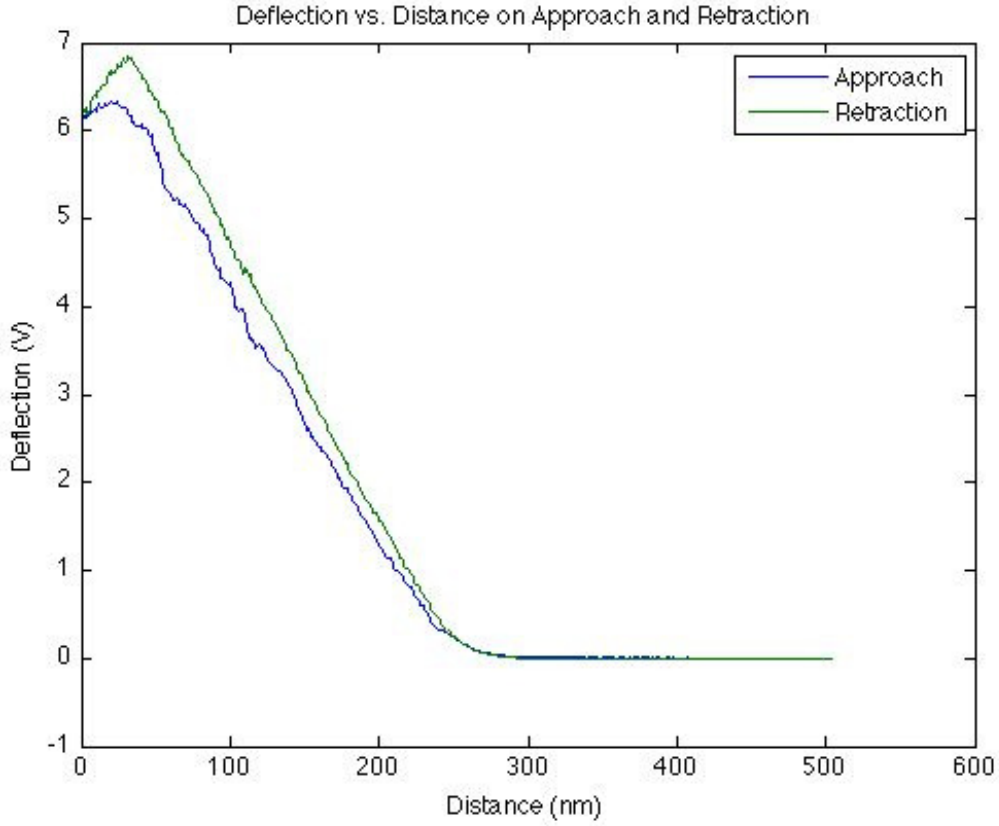
Deflection vs. Distance on Approach and Retraction
Approach
Retraction
Deflection (V)
Distance (nm)
7
6
5
4
3
2
1
0
-1
0
100
200
300
400
500
600

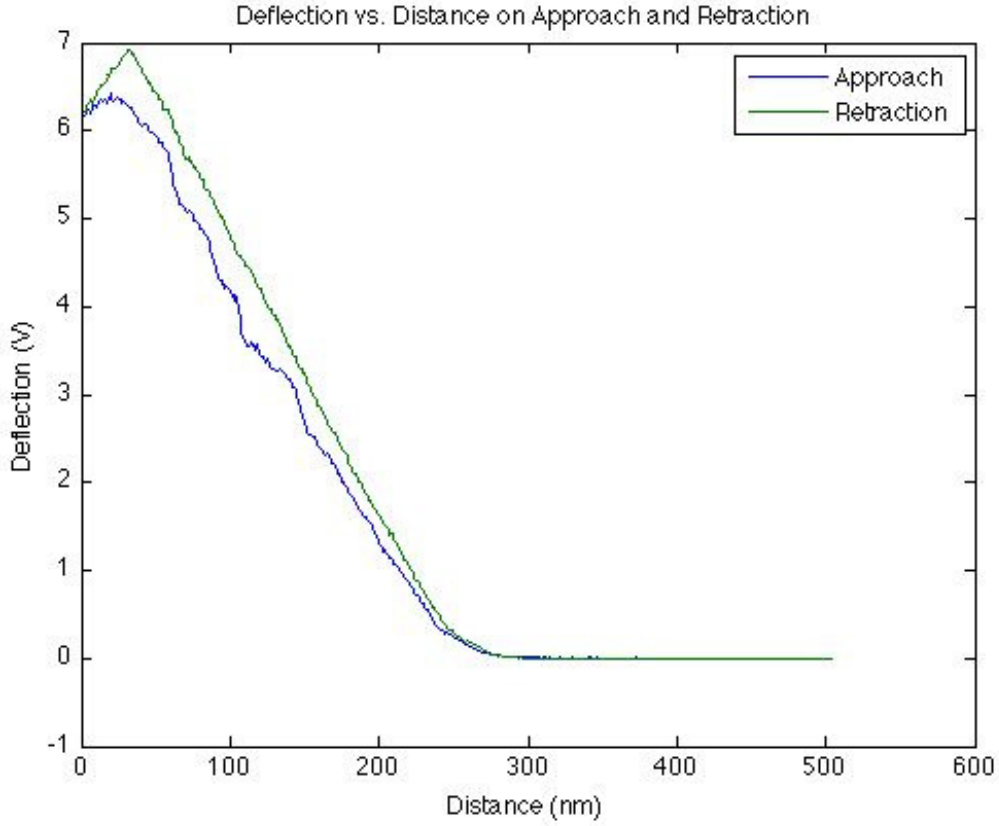
Deflection vs. Distance on Approach and Retraction
Approach
Retraction
Deflection (V)
Distance (nm)
7
6
5
4
3
2
1
0
-1
0
100
200
300
400
500
600

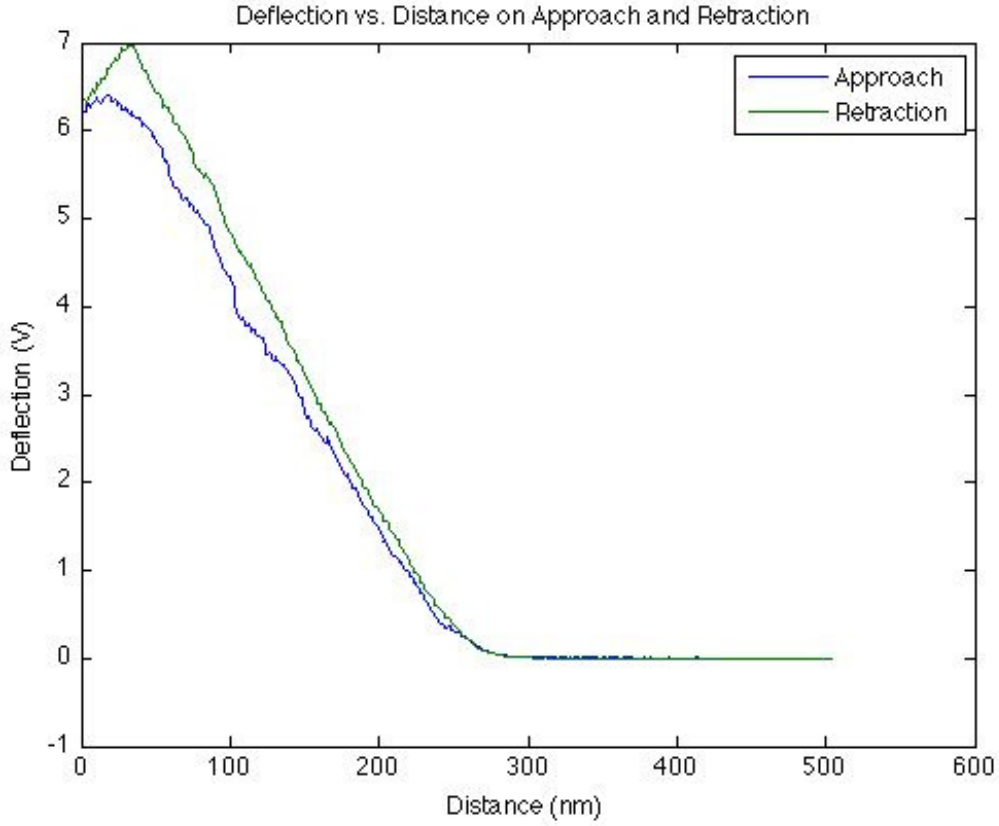
Deflection vs. Distance on Approach and Retraction
Approach
Retraction
Deflection (V)
Distance (nm)
7
6
5
4
3
2
1
0
-1
0
100
200
300
400
500
600

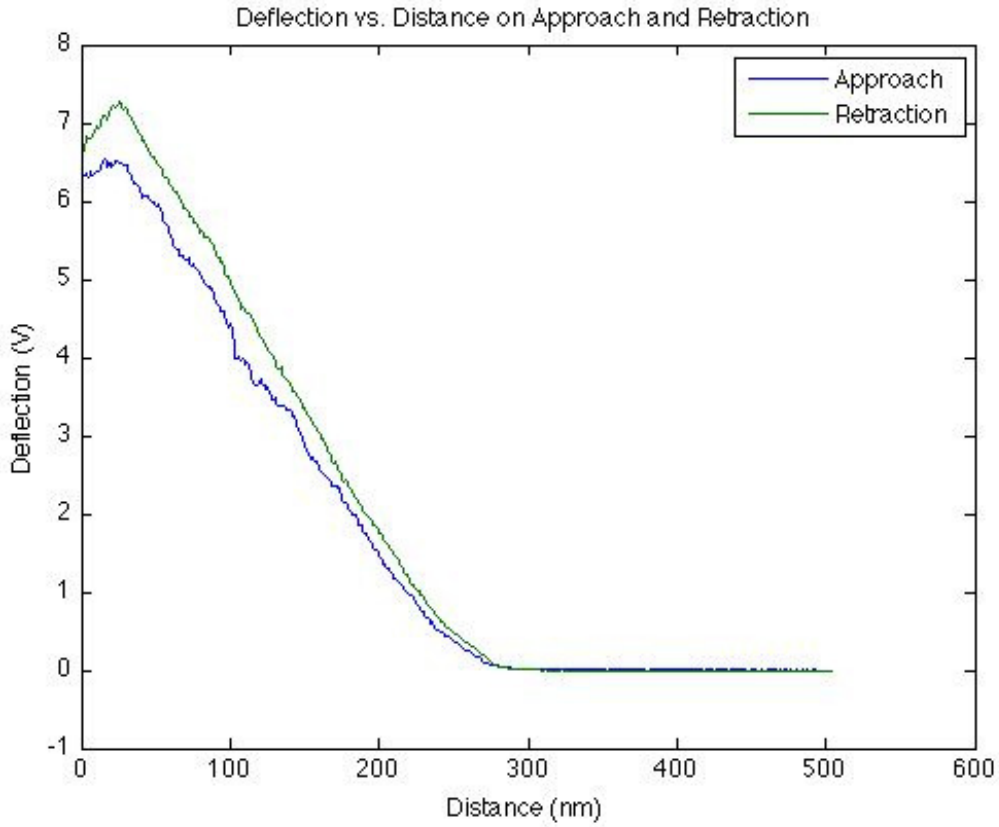
Deflection vs. Distance on Approach and Retraction
Approach
Retraction
Deflection (V)
Distance (nm)
8
7
6
5
4
3
2
1
0
-1
0
100
200
300
400
500
600

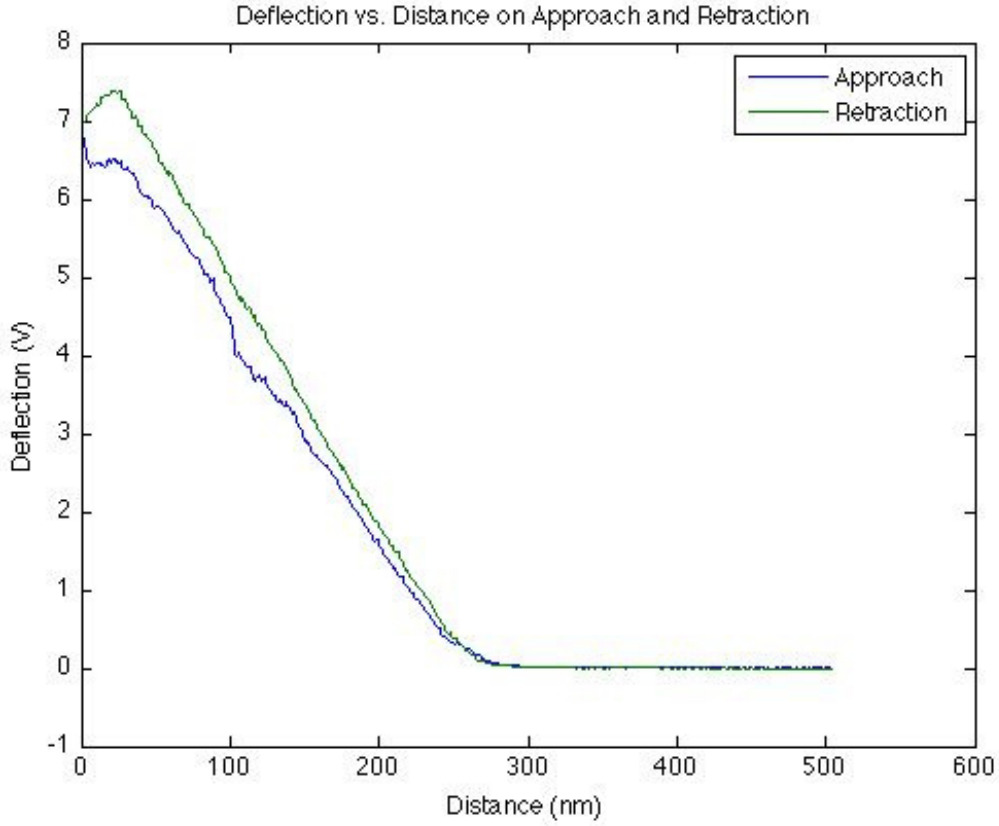
Deflection vs. Distance on Approach and Retraction
Approach
Retraction
Deflection (V)
Distance (nm)
8
7
6
5
4
3
2
1
0
-1
0
100
200
300
400
500
600

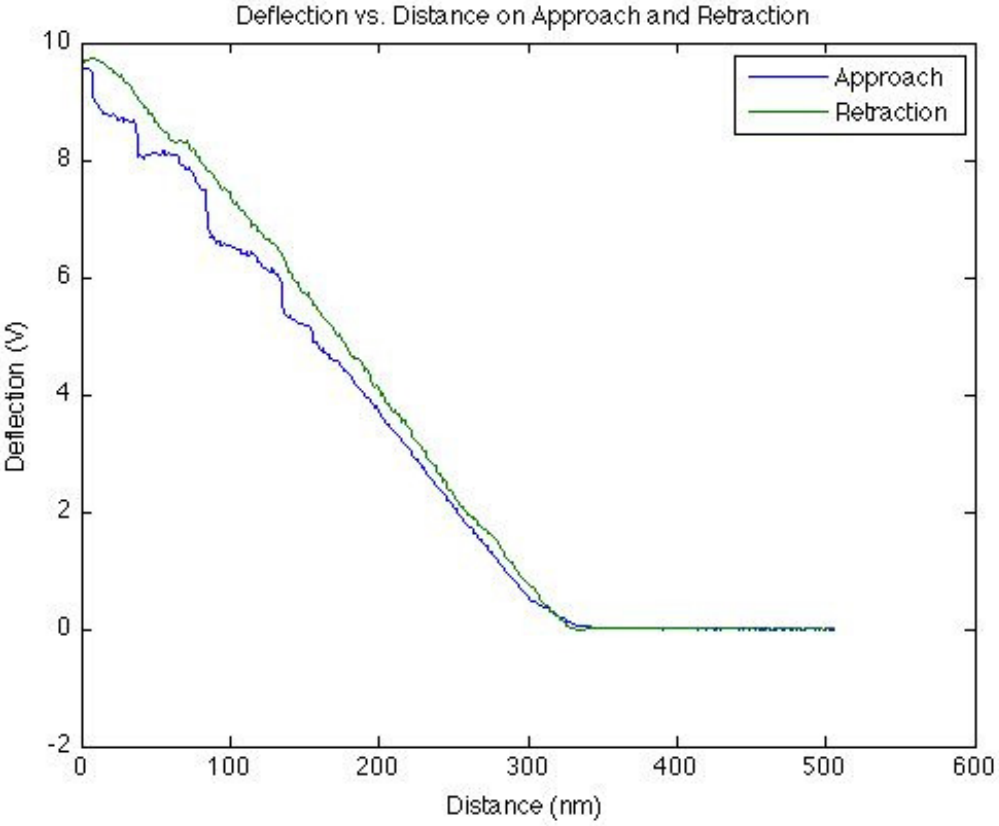
Deflection vs. Distance on Approach and Retraction
Approach
Retraction
Deflection (V)
Distance (nm)
10
8
6
4
2
0
-2
0
100
200
300
400
500
600

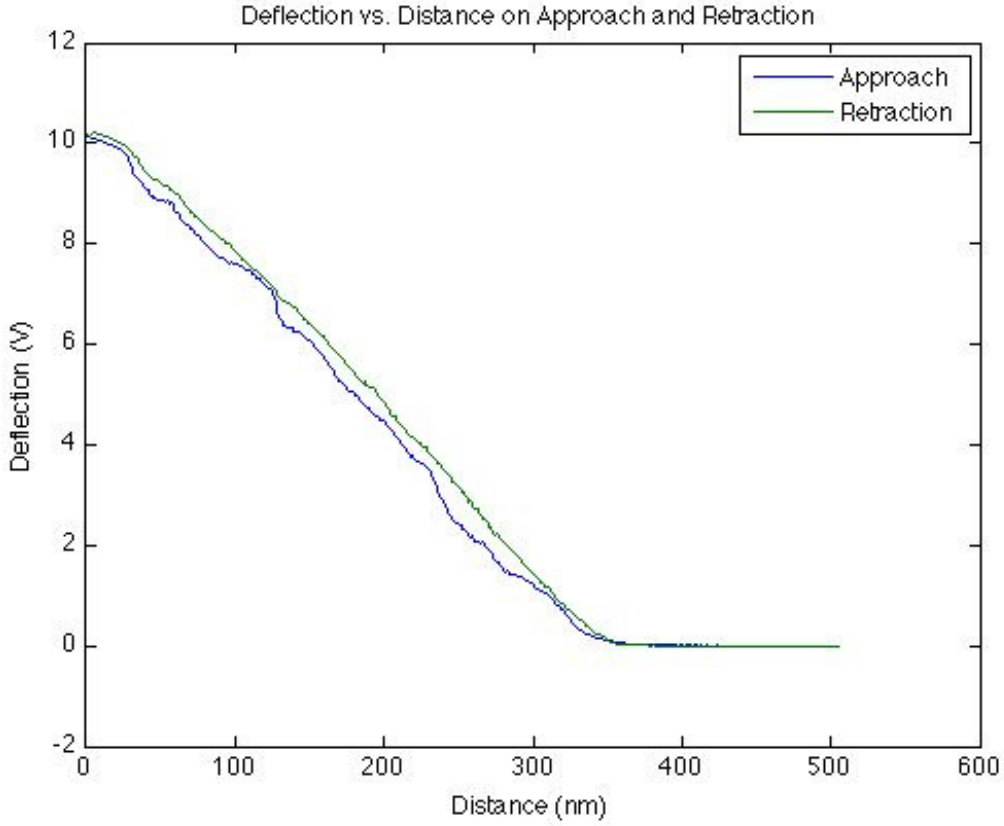
Deflection vs. Distance on Approach and Retraction
Approach
Retraction
Deflection (V)
Distance (nm)
12
10
8
6
4
2
0
-2
0
100
200
300
400
500
600

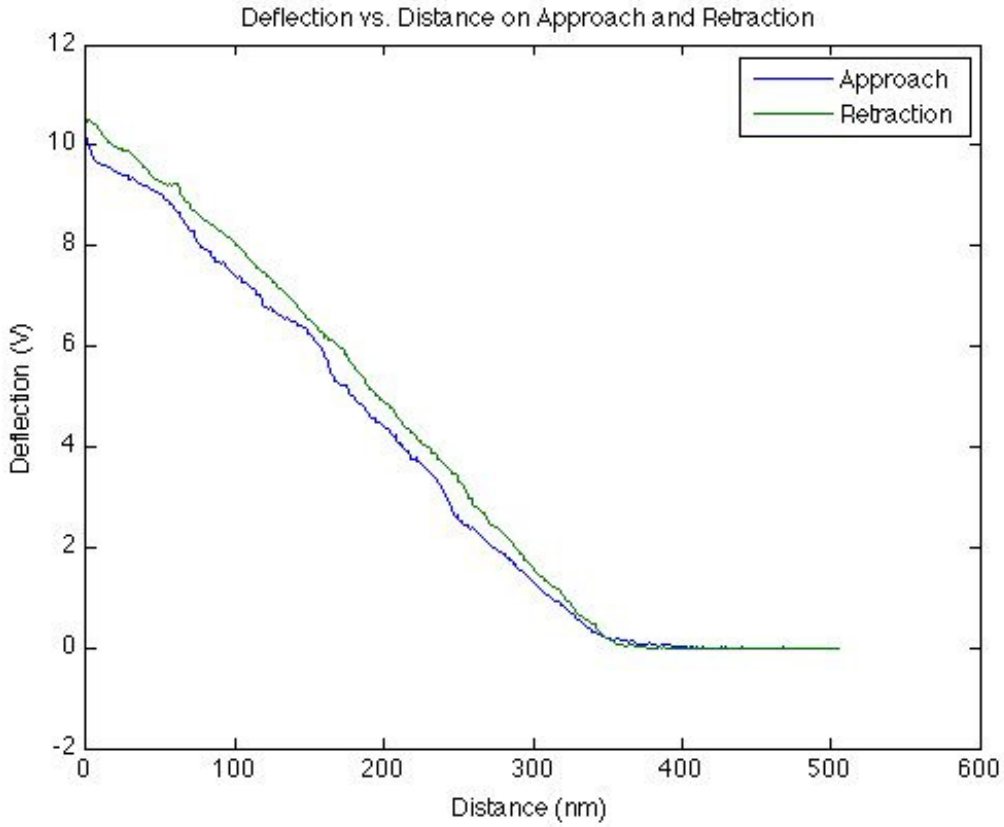
Deflection vs. Distance on Approach and Retraction
Approach
Retraction
Deflection (V)
Distance (nm)
12
10
8
6
4
2
0
-2
0
100
200
300
400
500
600

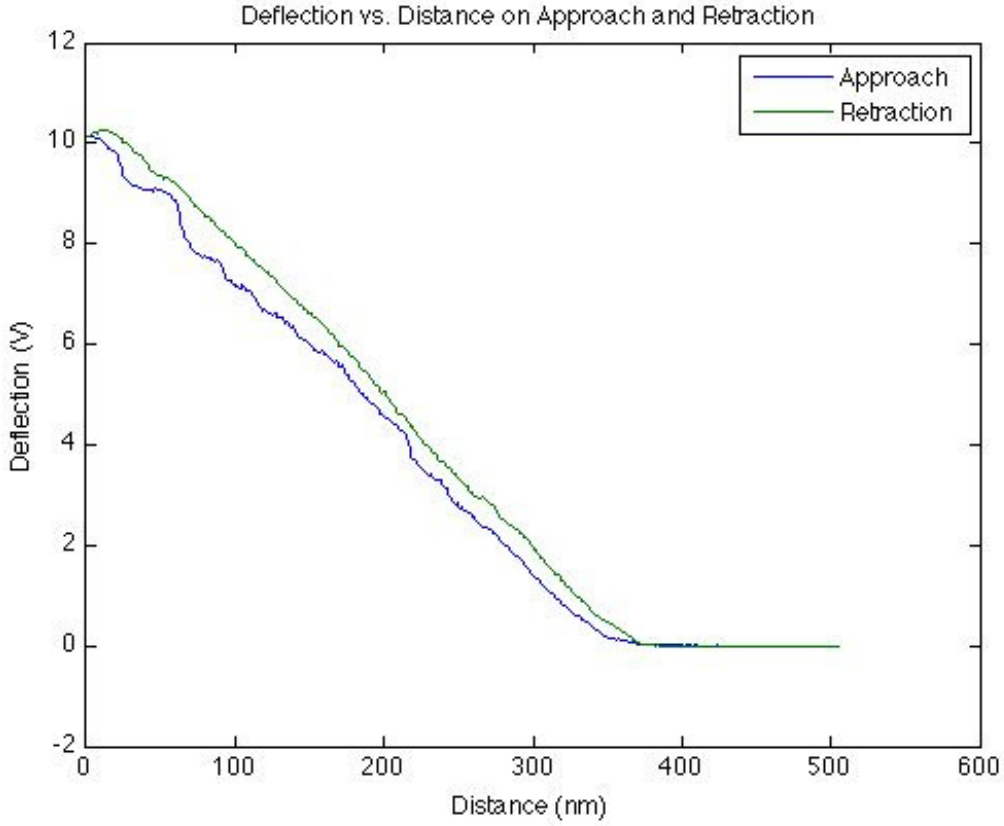
Deflection vs. Distance on Approach and Retraction
Approach
Retraction
Deflection (V)
Distance (nm)
12
10
8
6
4
2
0
-2
0
100
200
300
400
500
600

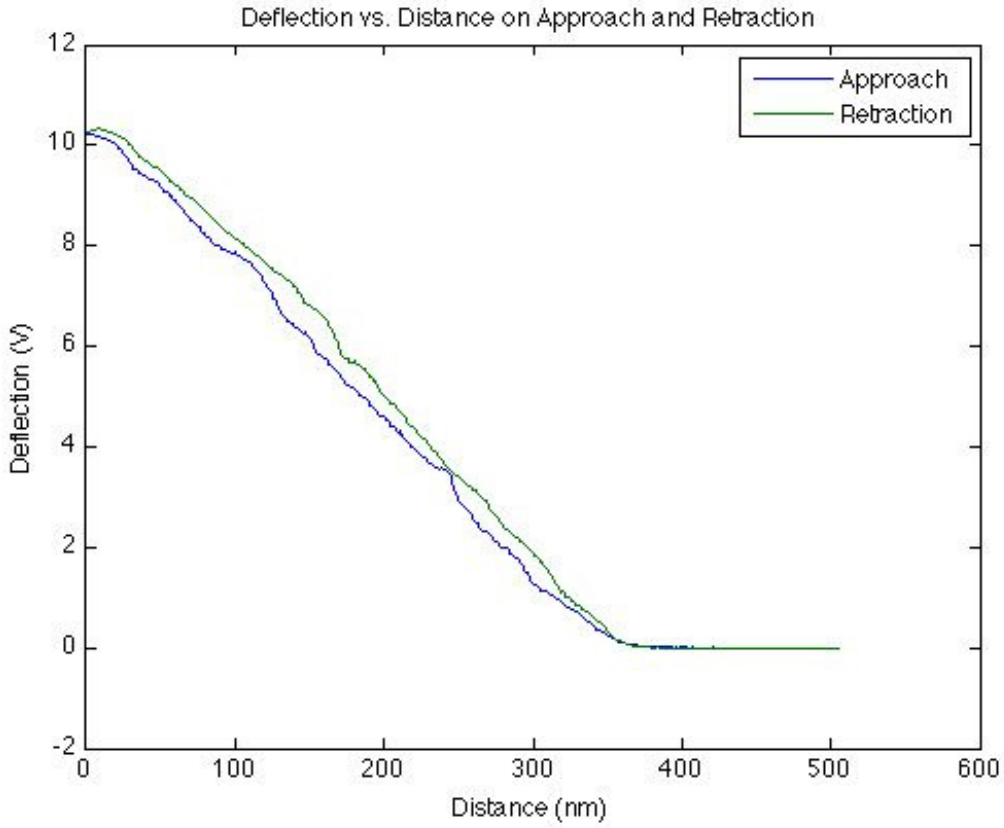
Deflection vs. Distance on Approach and Retraction
Approach
Retraction
Deflection (V)
Distance (nm)
12
10
8
6
4
2
0
-2
0
100
200
300
400
500
600

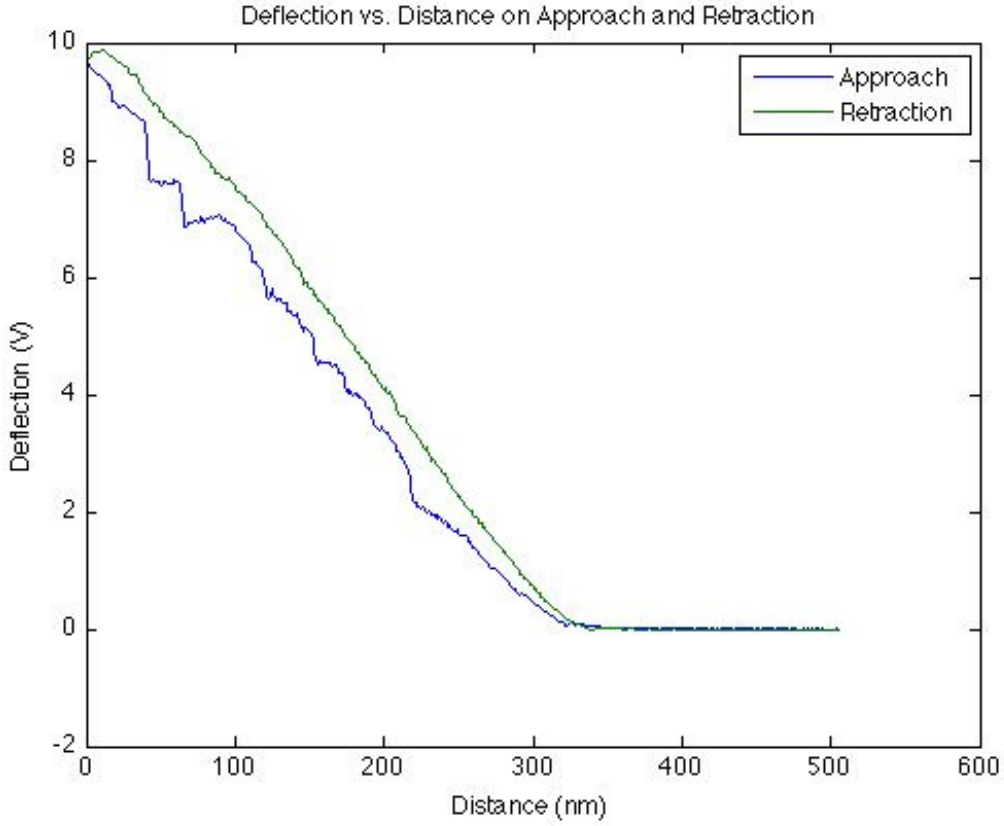
Deflection vs. Distance on Approach and Retraction
Approach
Retraction
Deflection (V)
Distance (nm)
10
8
6
4
2
0
-2
0
100
200
300
400
500
600

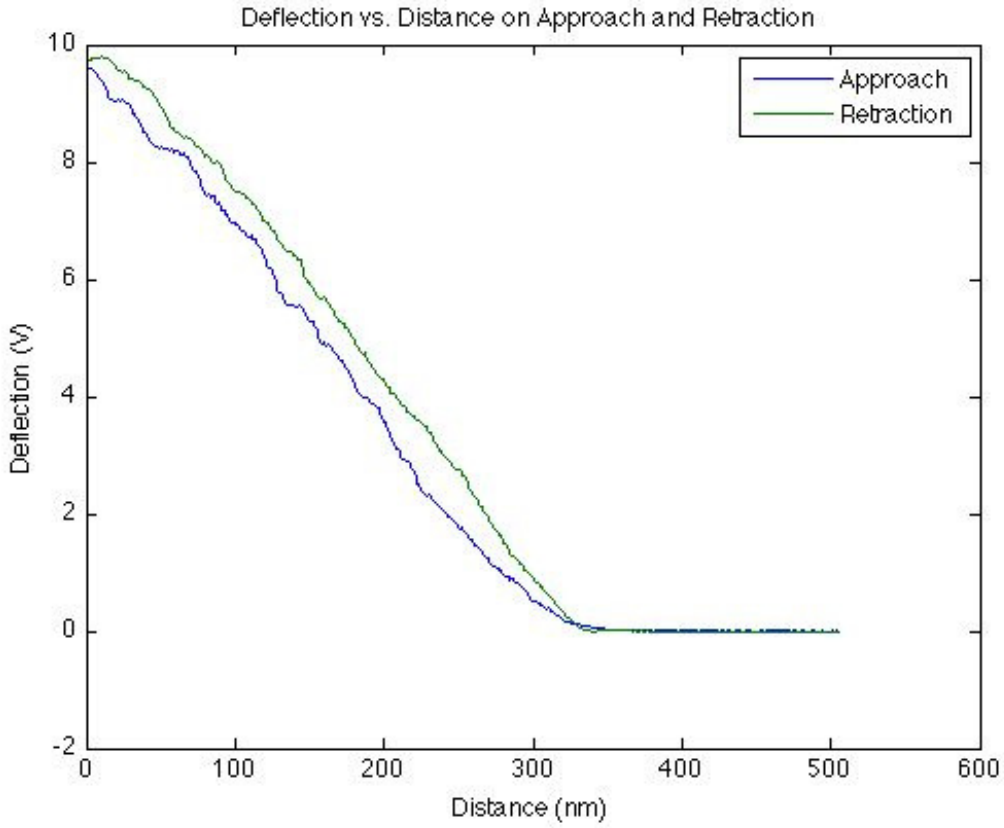
Deflection vs. Distance on Approach and Retraction
Approach
Retraction
Deflection (V)
Distance (nm)
10
8
6
4
2
0
-2
0
100
200
300
400
500
600

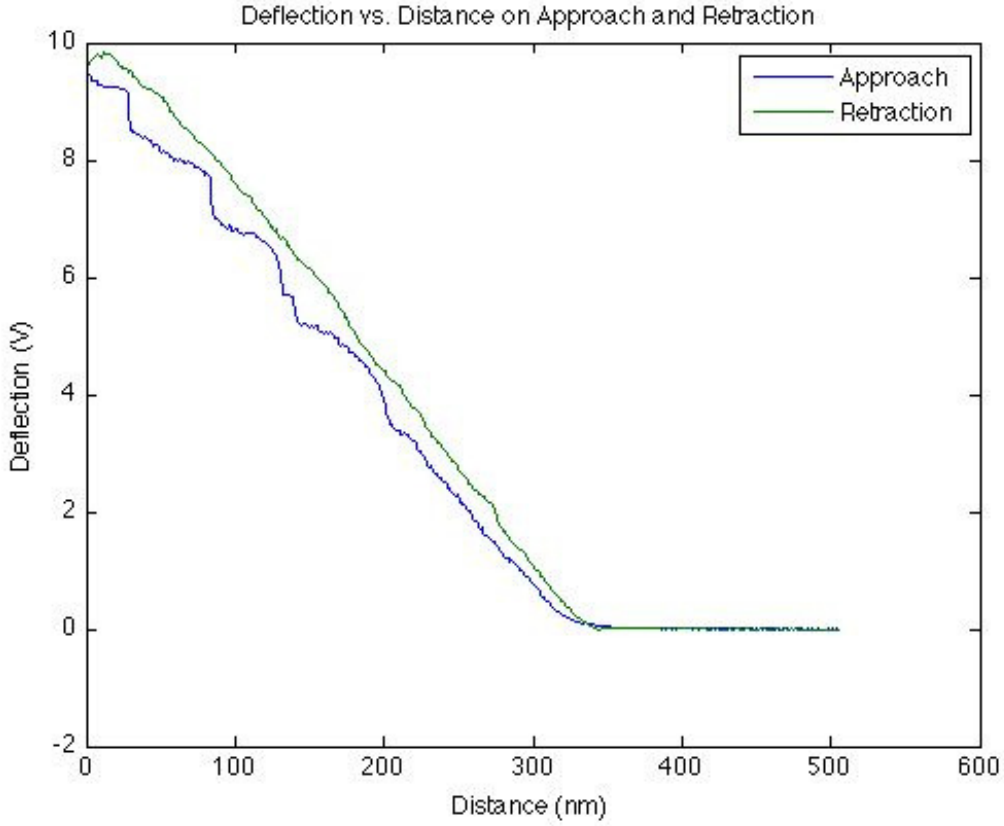
Deflection vs. Distance on Approach and Retraction
Approach
Retraction
Deflection (V)
Distance (nm)
10
8
6
4
2
0
-2
0
100
200
300
400
500
600

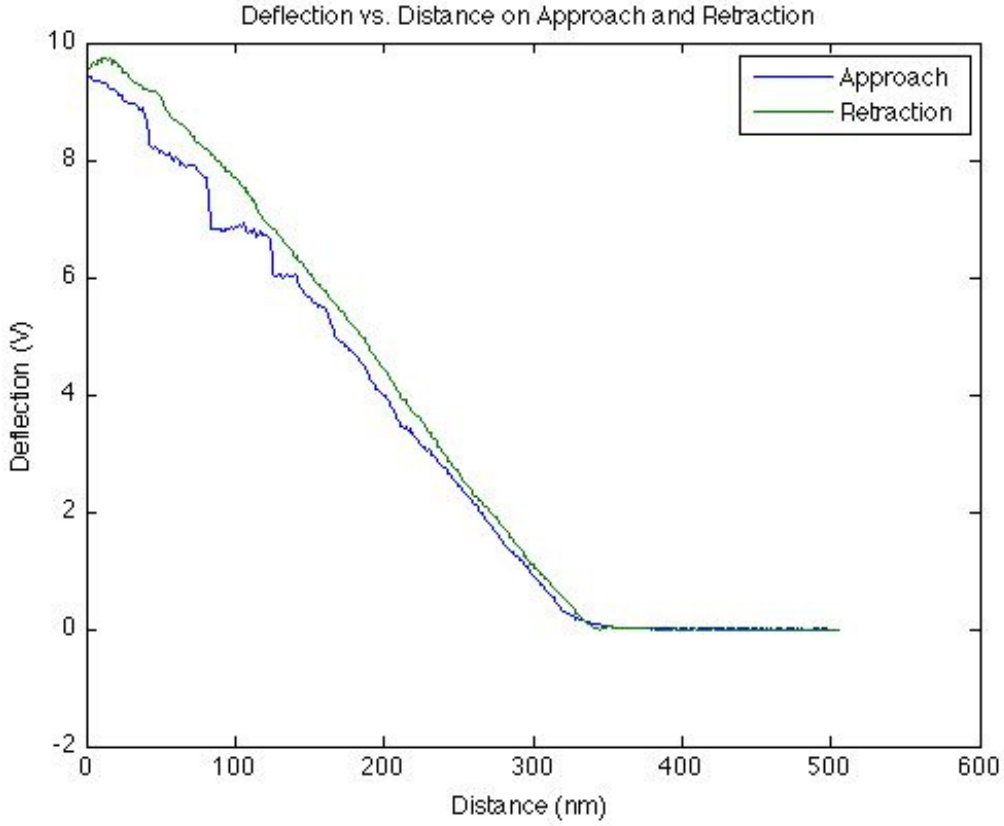
Deflection vs. Distance on Approach and Retraction
Approach
Retraction
Deflection (V)
Distance (nm)
10
8
6
4
2
0
-2
0
100
200
300
400
500
600

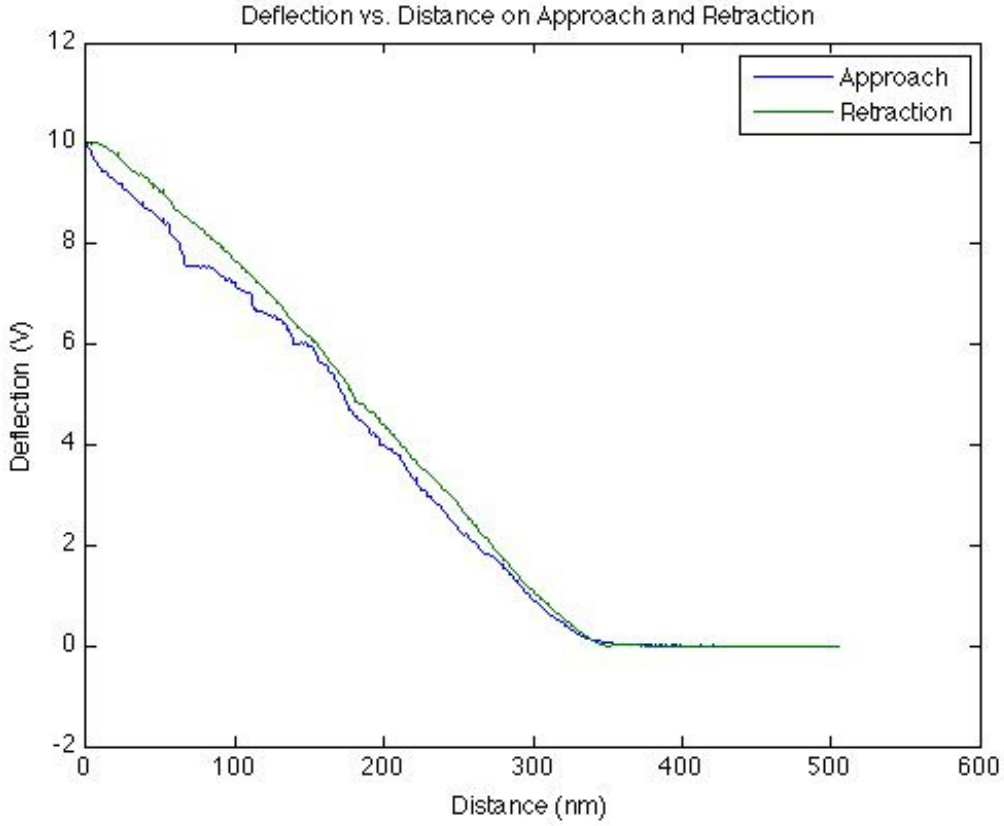
Deflection vs. Distance on Approach and Retraction
Approach
Retraction
Deflection (V)
Distance (nm)
12
10
8
6
4
2
0
-2
0
100
200
300
400
500
600

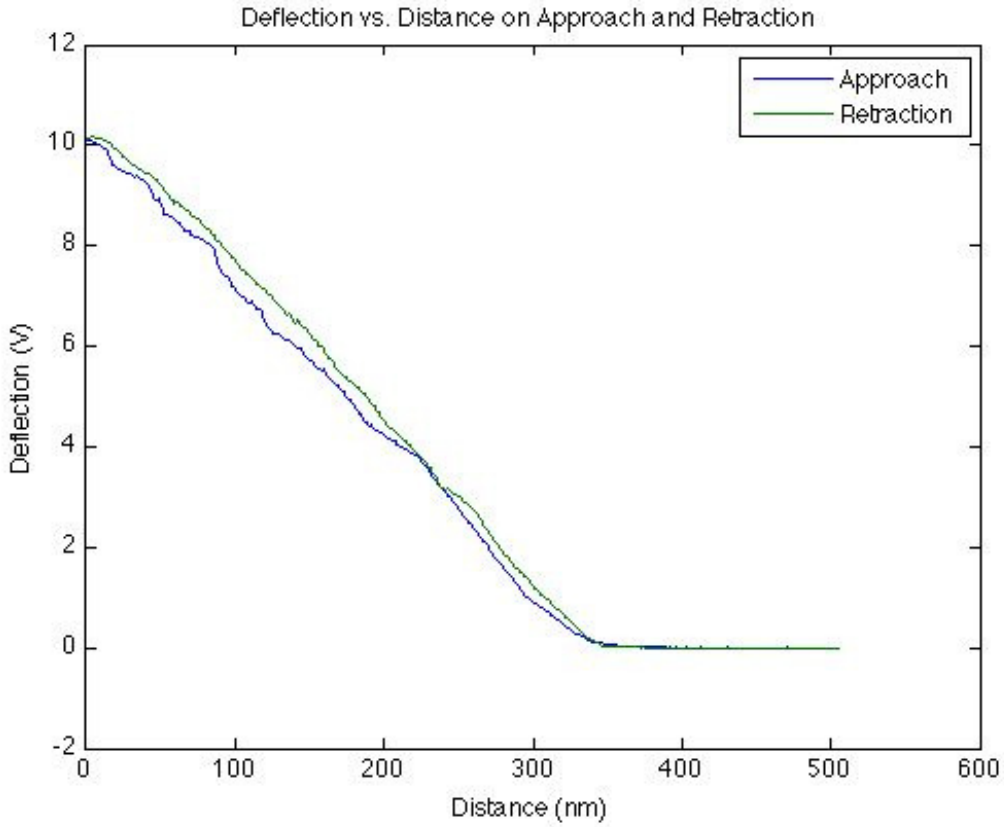
Deflection vs. Distance on Approach and Retraction
Approach
Retraction
Deflection (V)
Distance (nm)
12
10
8
6
4
2
0
-2
0
100
200
300
400
500
600

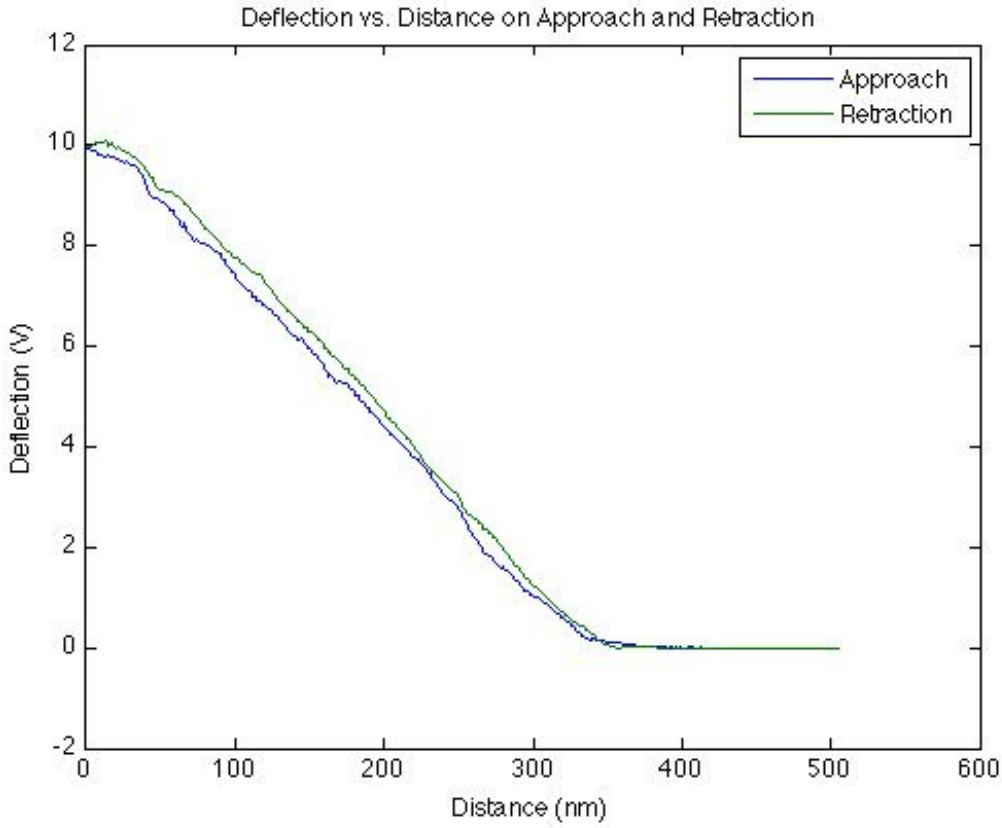
Deflection vs. Distance on Approach and Retraction
Approach
Retraction
Deflection (V)
Distance (nm)
12
10
8
6
4
2
0
-2
0
100
200
300
400
500
600

Appendix G

Calcium-saturated Wet Montmorillonite Deflection-Distance Curves

The deflection-distance curves contained in this section were obtained using the clay-coated glass probe and clay-coated glass substrate in an aqueous environment.

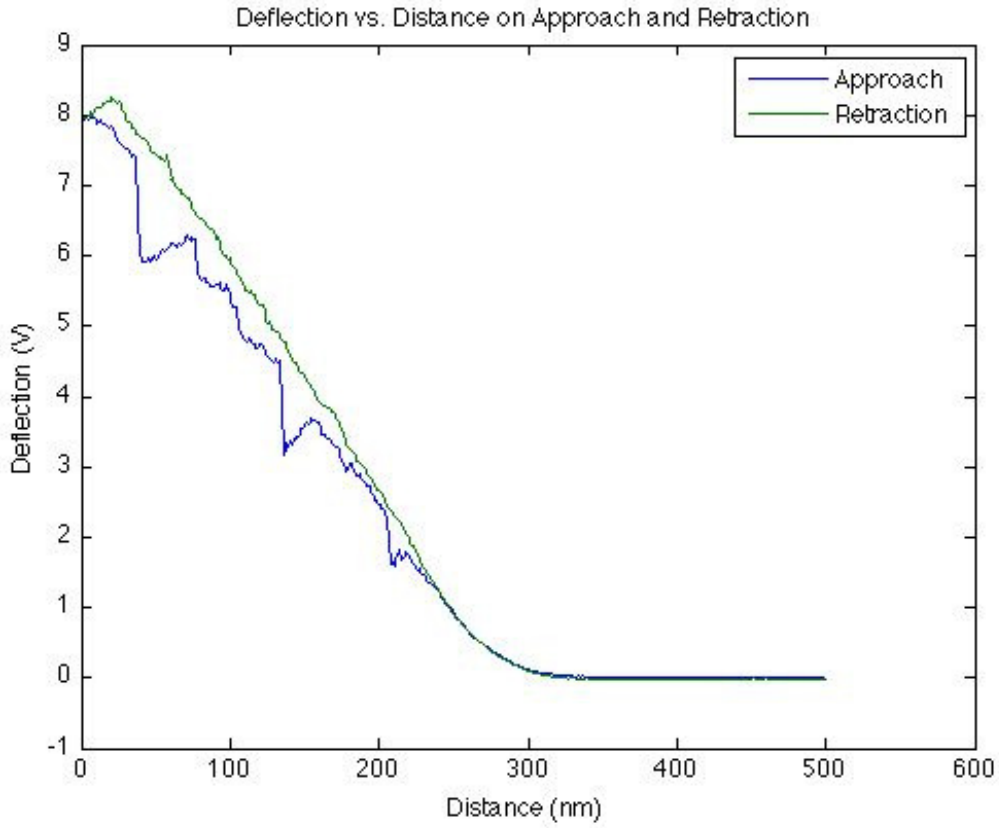
Deflection vs. Distance on Approach and Retraction
Approach
Retraction
Deflection (V)
Distance (nm)
9
8
7
6
5
4
3
2
1
0
-1
0
100
200
300
400
500
600

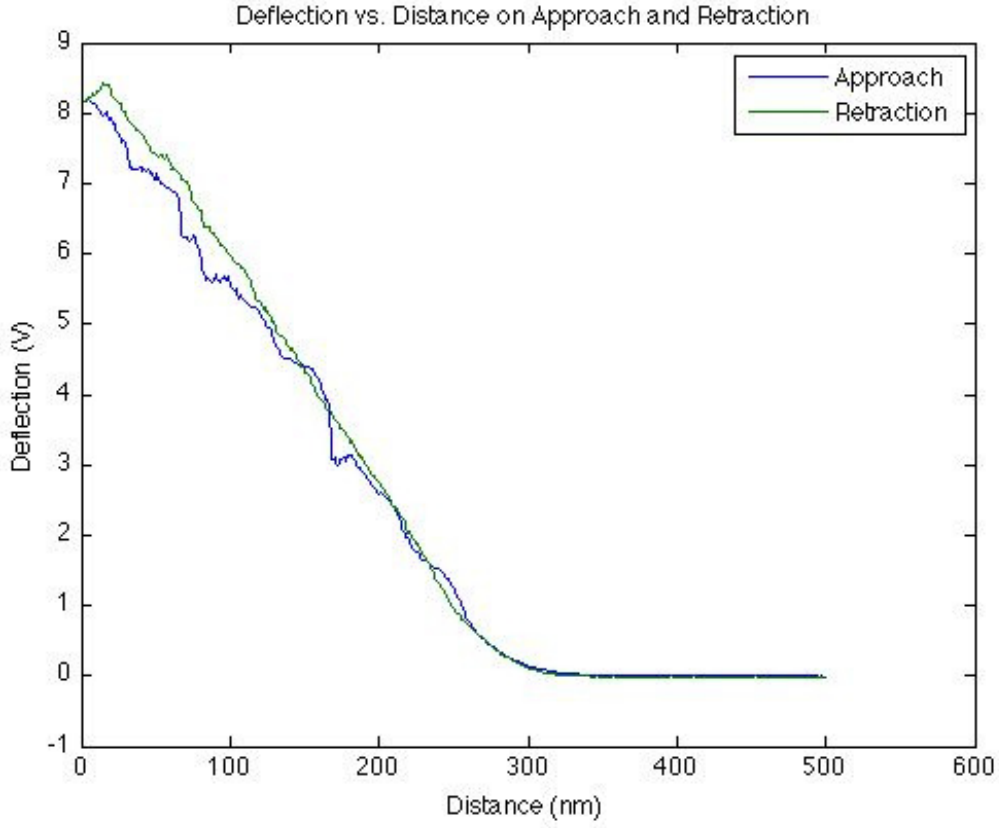
Deflection vs. Distance on Approach and Retraction
Approach
Retraction
Deflection (V)
Distance (nm)
9
8
7
6
5
4
3
2
1
0
-1
0
100
200
300
400
500
600

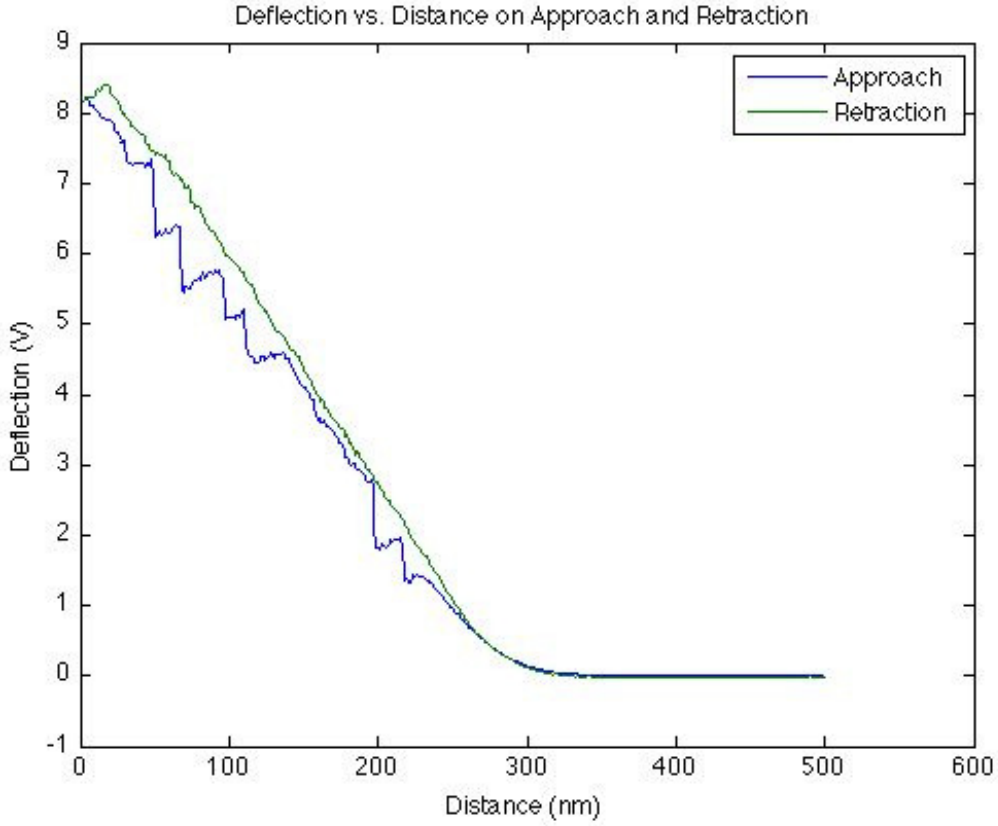
Deflection vs. Distance on Approach and Retraction
Approach
Retraction
Deflection (V)
Distance (nm)
9
8
7
6
5
4
3
2
1
0
-1
0
100
200
300
400
500
600

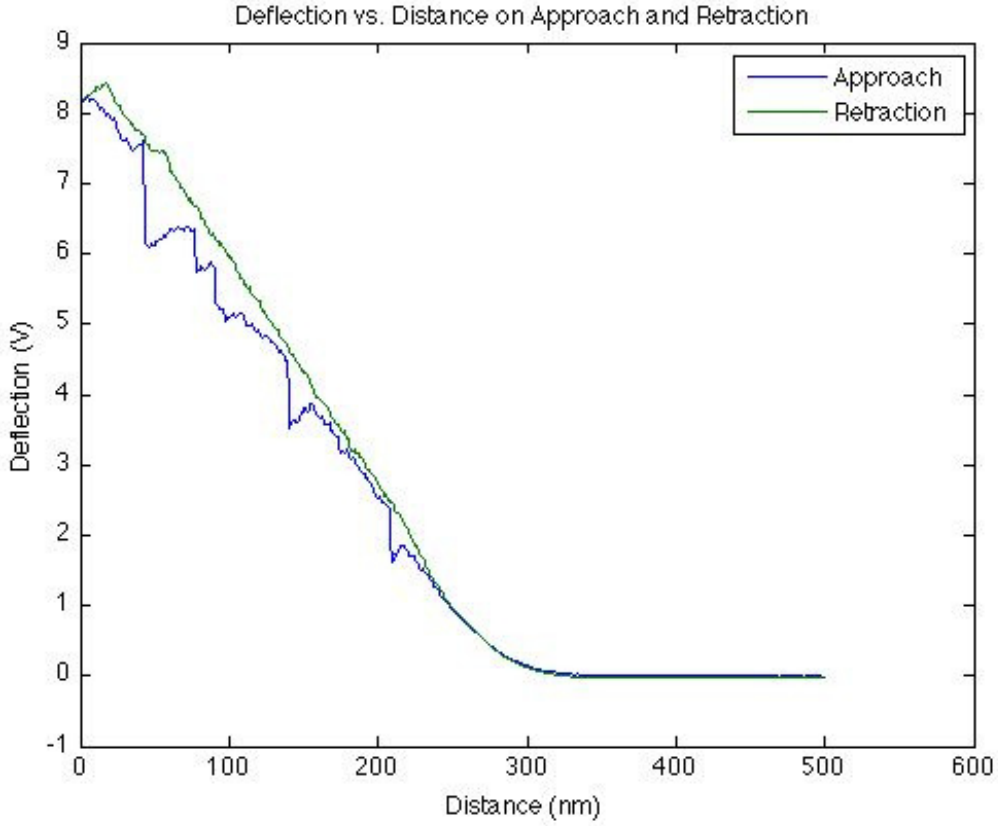
Deflection vs. Distance on Approach and Retraction
Approach
Retraction
Deflection (V)
Distance (nm)
9
8
7
6
5
4
3
2
1
0
-1
0
100
200
300
400
500
600

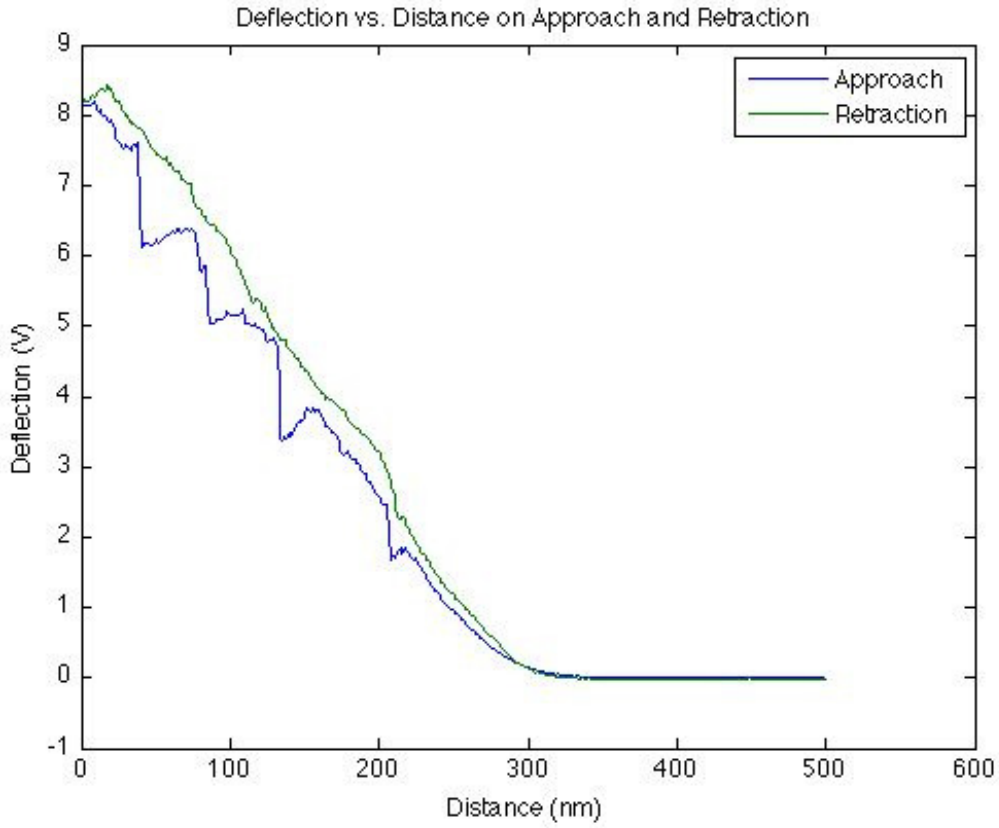
Deflection vs. Distance on Approach and Retraction
Approach
Retraction
Deflection (V)
Distance (nm)
9
8
7
6
5
4
3
2
1
0
-1
0
100
200
300
400
500
600

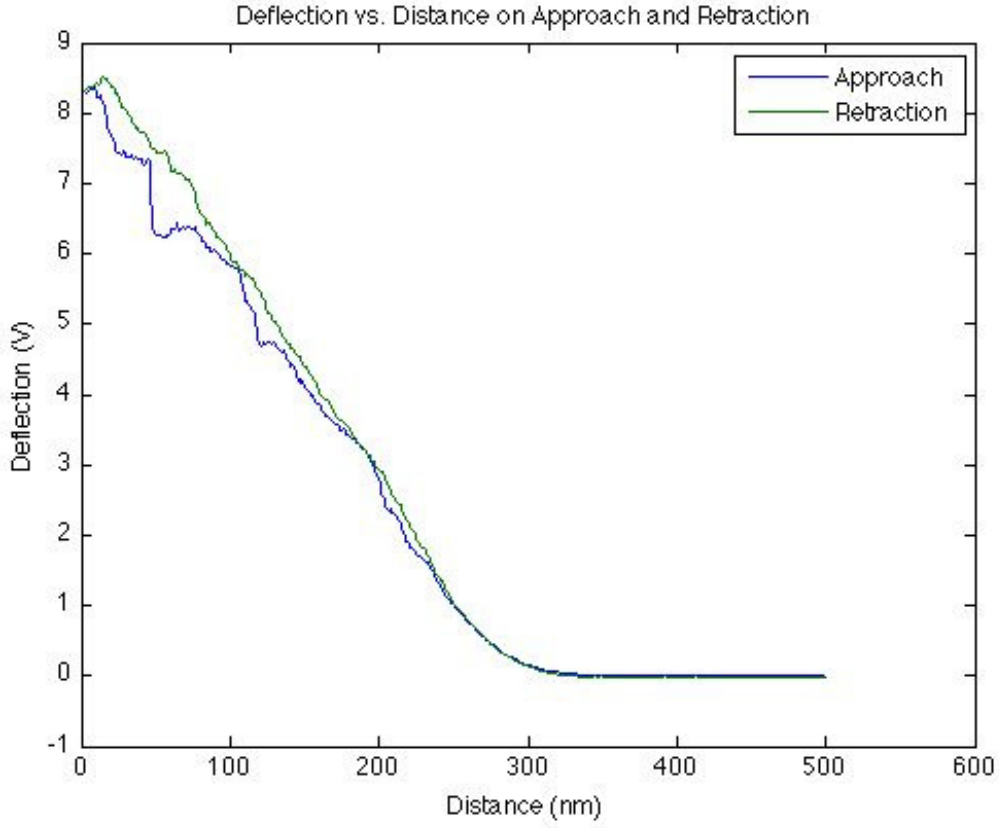
Deflection vs. Distance on Approach and Retraction
Approach
Retraction
Deflection (V)
Distance (nm)
9
8
7
6
5
4
3
2
1
0
-1
0
100
200
300
400
500
600

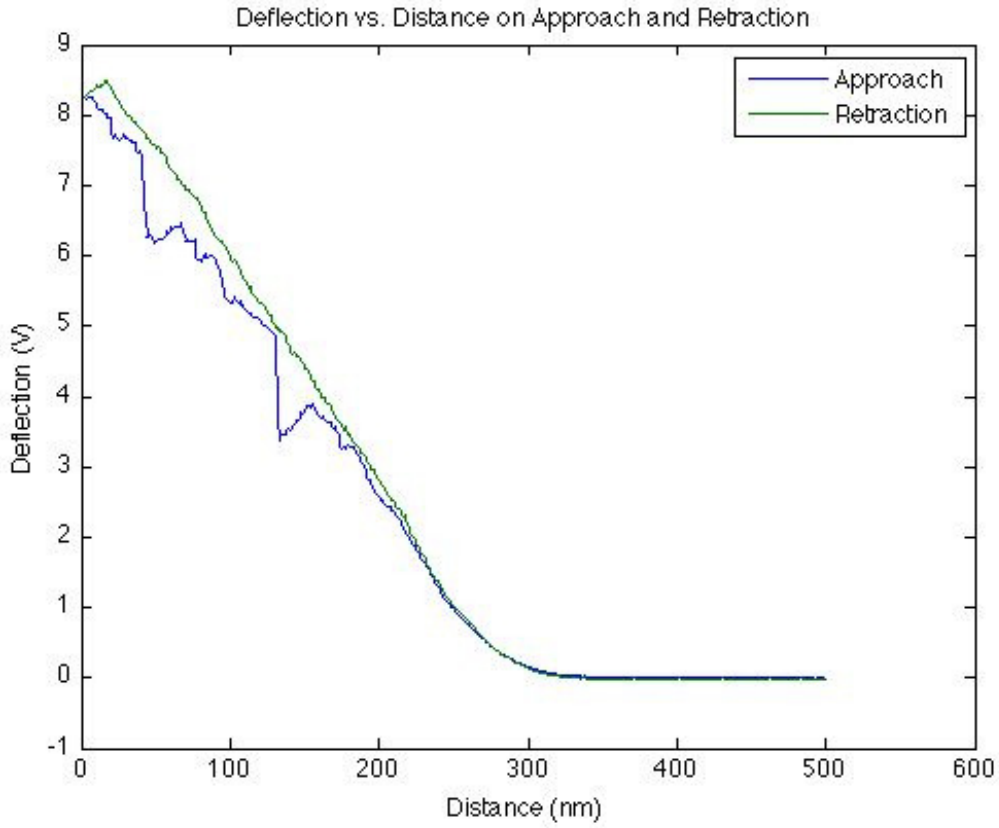
Deflection vs. Distance on Approach and Retraction
Approach
Retraction
Deflection (V)
Distance (nm)
9
8
7
6
5
4
3
2
1
0
-1
0
100
200
300
400
500
600

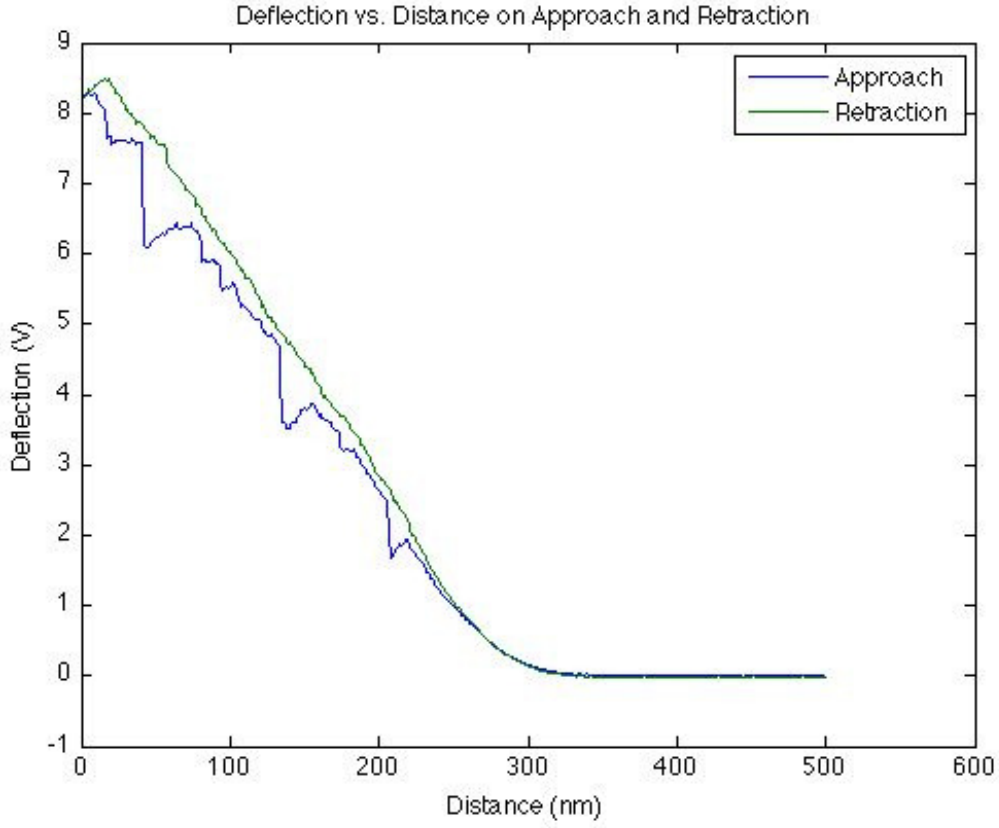
Deflection vs. Distance on Approach and Retraction
Approach
Retraction
Deflection (V)
Distance (nm)
9
8
7
6
5
4
3
2
1
0
-1
0
100
200
300
400
500
600

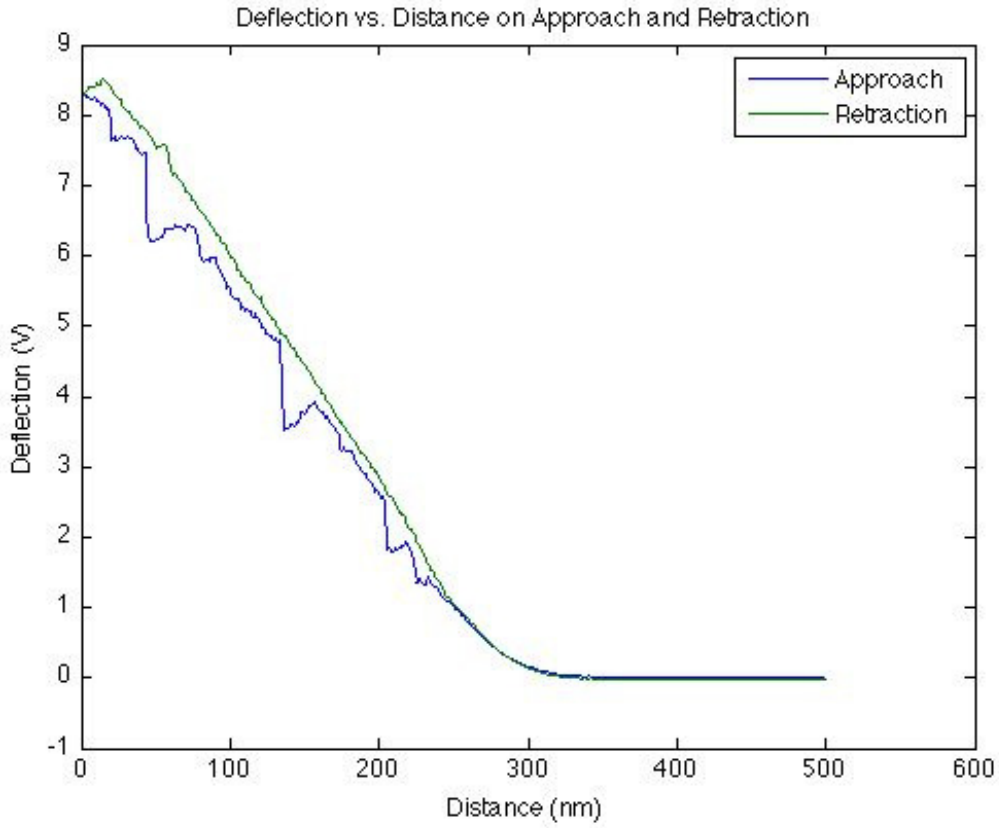
Deflection vs. Distance on Approach and Retraction
Approach
Retraction
Deflection (V)
Distance (nm)
9
8
7
6
5
4
3
2
1
0
-1
0
100
200
300
400
500
600

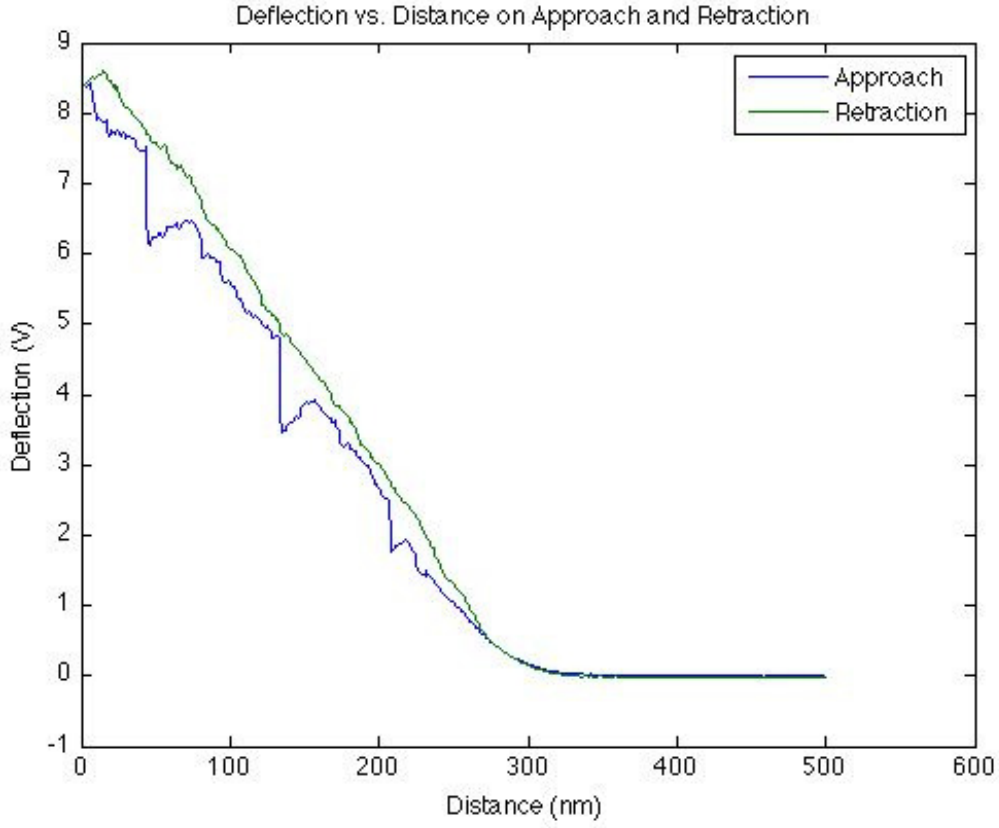
Deflection vs. Distance on Approach and Retraction
Approach
Retraction
Deflection (V)
Distance (nm)
9
8
7
6
5
4
3
2
1
0
-1
0
100
200
300
400
500
600

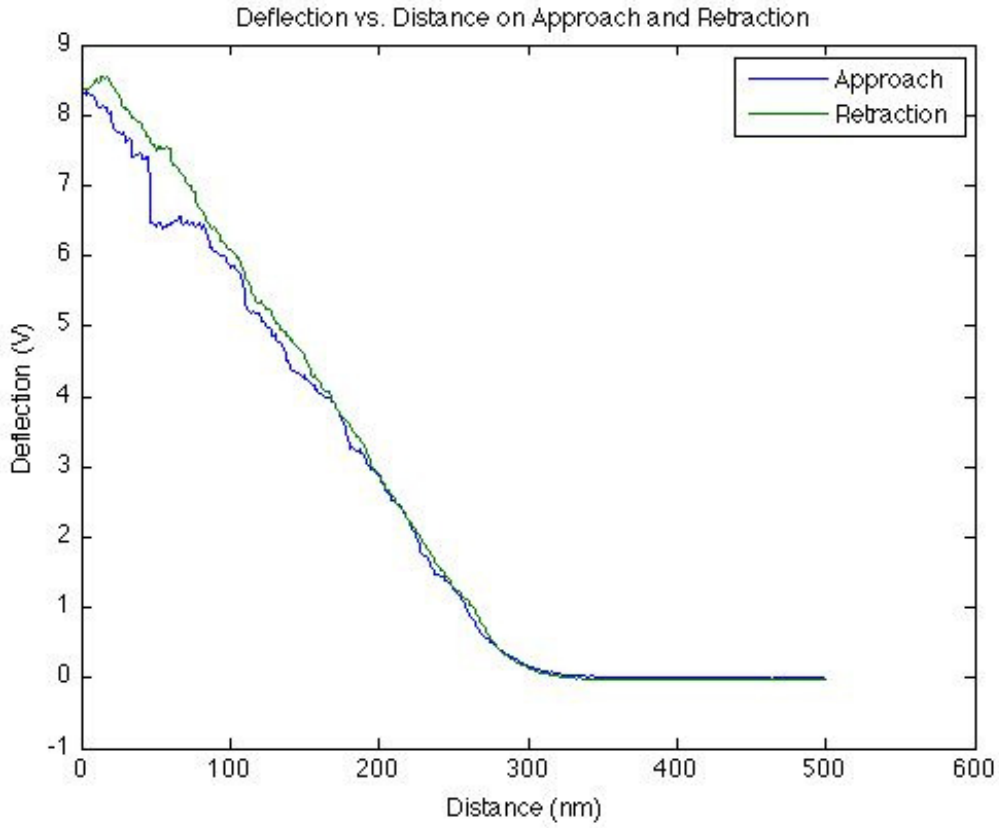
Deflection vs. Distance on Approach and Retraction
Approach
Retraction
Deflection (V)
Distance (nm)
9
8
7
6
5
4
3
2
1
0
-1
0
100
200
300
400
500
600

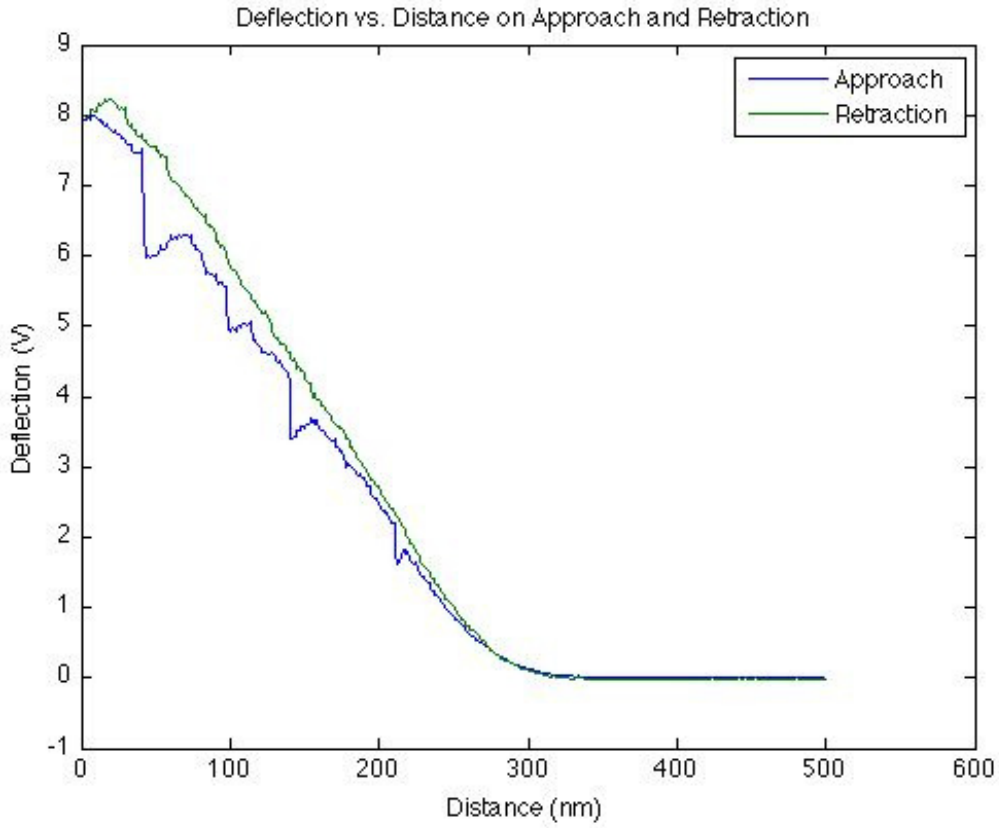
Deflection vs. Distance on Approach and Retraction
Approach
Retraction
Deflection (V)
Distance (nm)
9
8
7
6
5
4
3
2
1
0
-1
0
100
200
300
400
500
600

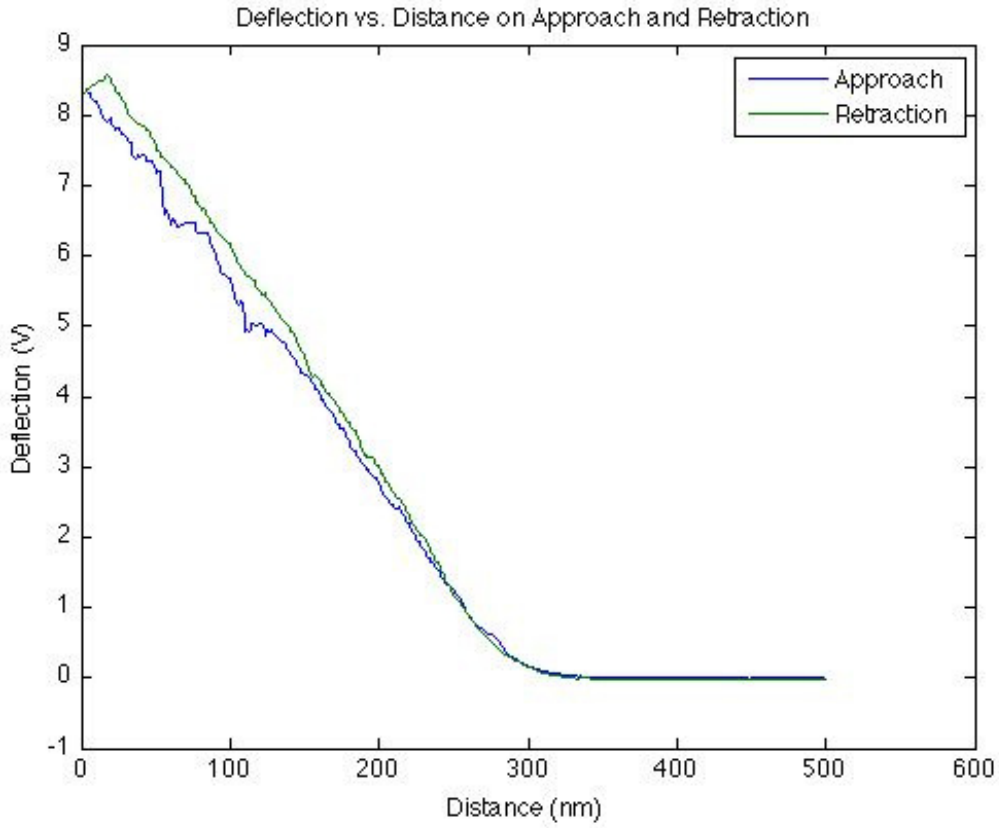
Deflection vs. Distance on Approach and Retraction
Approach
Retraction
Deflection (V)
Distance (nm)
9
8
7
6
5
4
3
2
1
0
-1
0
100
200
300
400
500
600

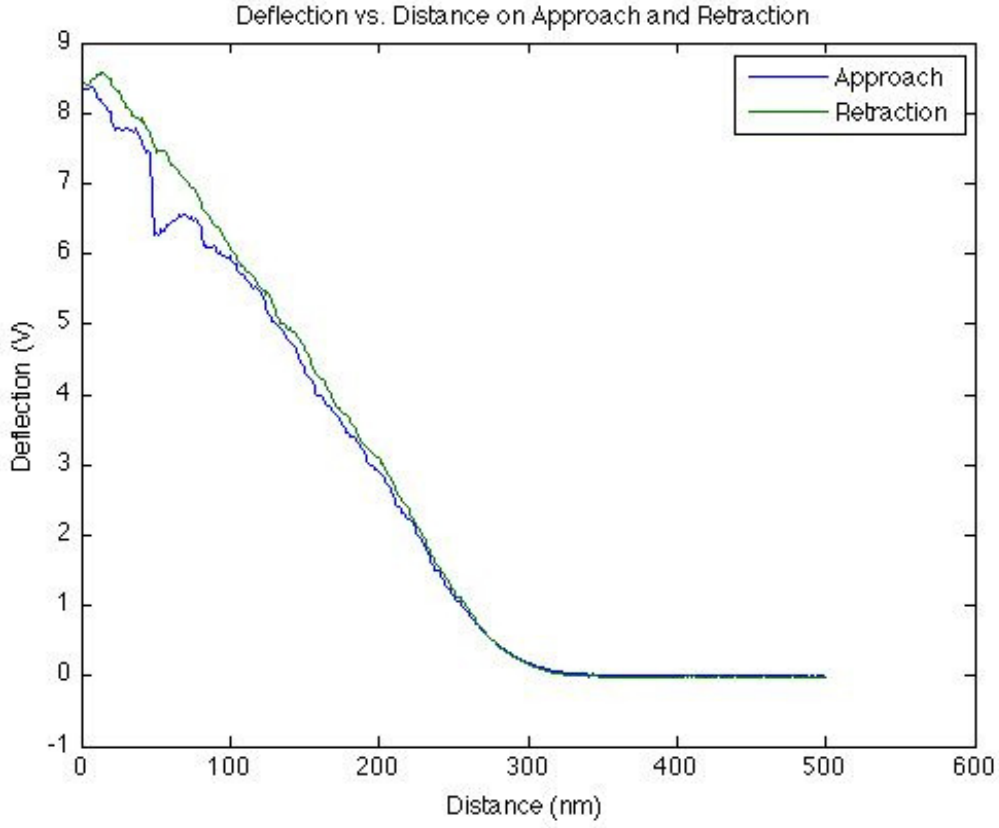
Deflection vs. Distance on Approach and Retraction
Approach
Retraction
Deflection (V)
Distance (nm)
9
8
7
6
5
4
3
2
1
0
-1
0
100
200
300
400
500
600

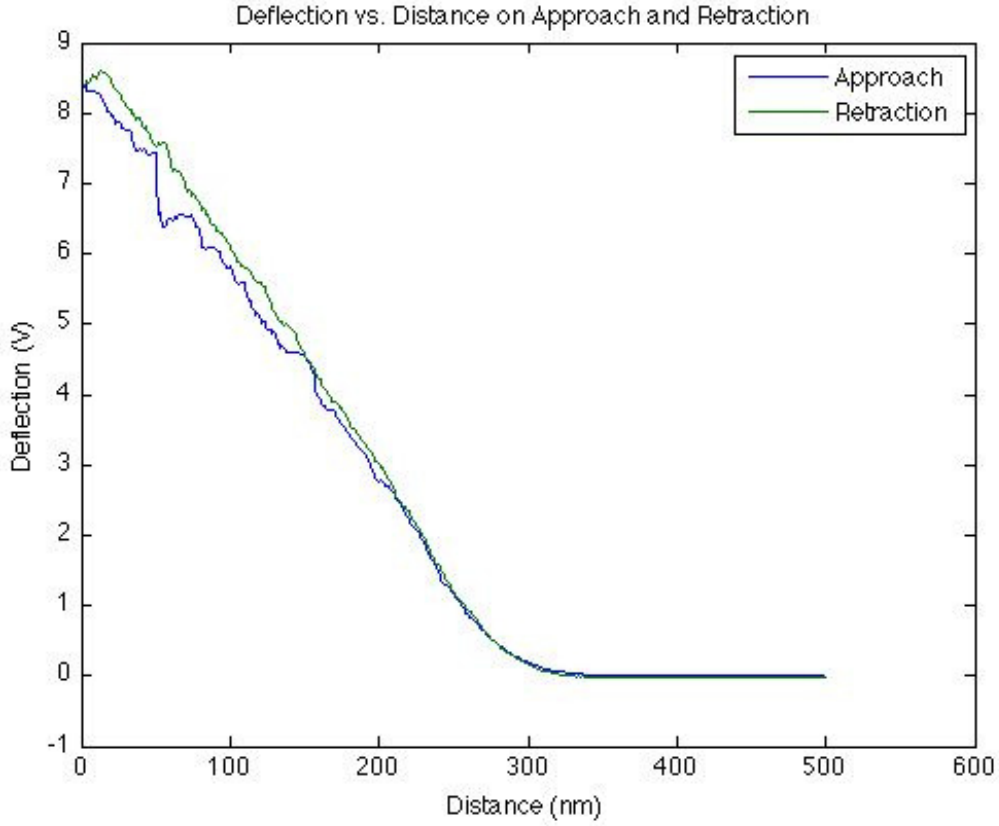
Deflection vs. Distance on Approach and Retraction
Approach
Retraction
Deflection (V)
Distance (nm)
9
8
7
6
5
4
3
2
1
0
-1
0
100
200
300
400
500
600

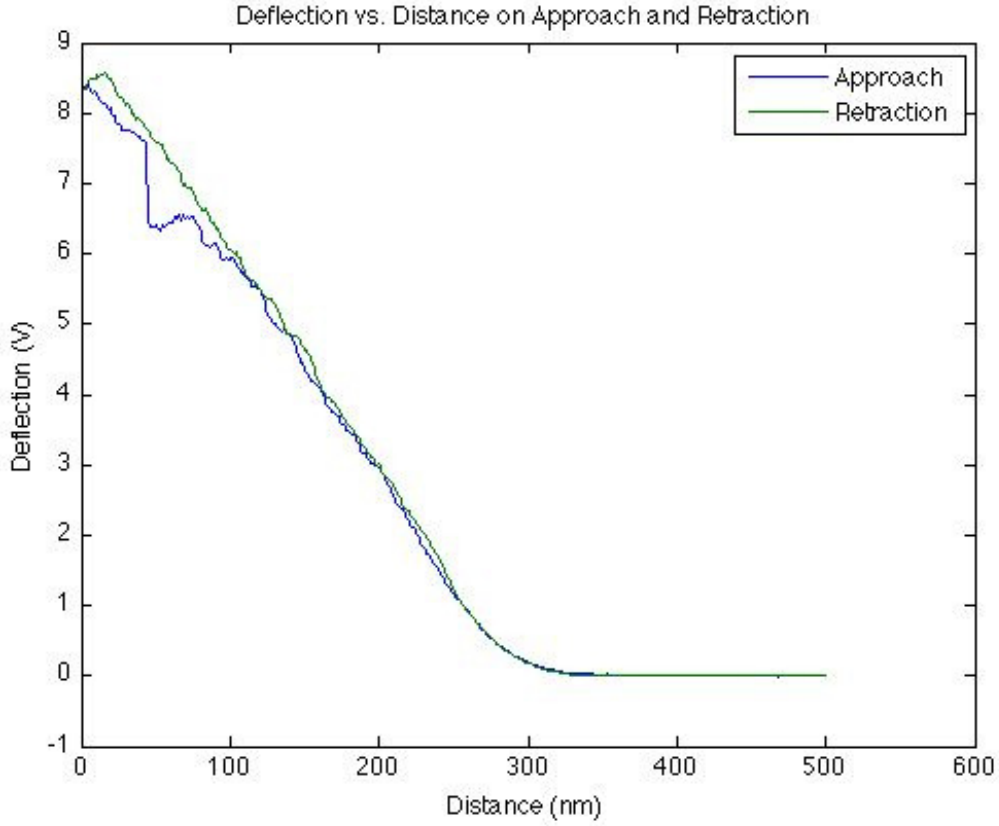
Deflection vs. Distance on Approach and Retraction
Approach
Retraction
Deflection (V)
Distance (nm)
9
8
7
6
5
4
3
2
1
0
-1
0
100
200
300
400
500
600

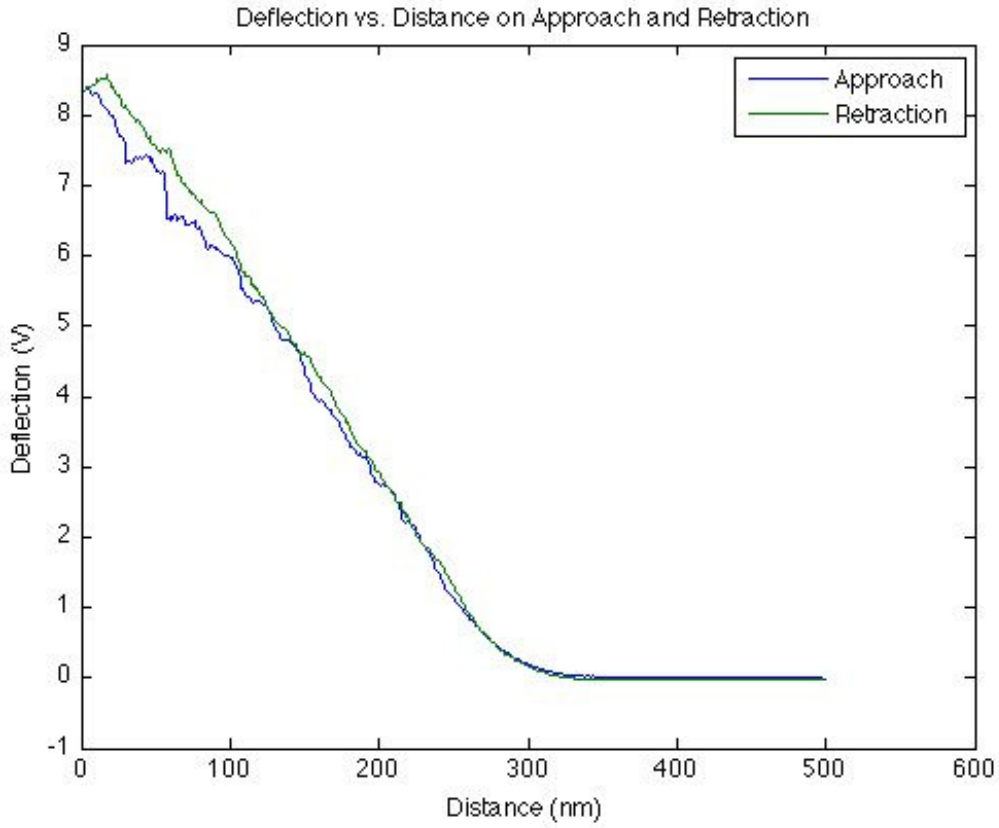
Deflection vs. Distance on Approach and Retraction
Approach
Retraction
Deflection (V)
Distance (nm)
9
8
7
6
5
4
3
2
1
0
-1
0
100
200
300
400
500
600

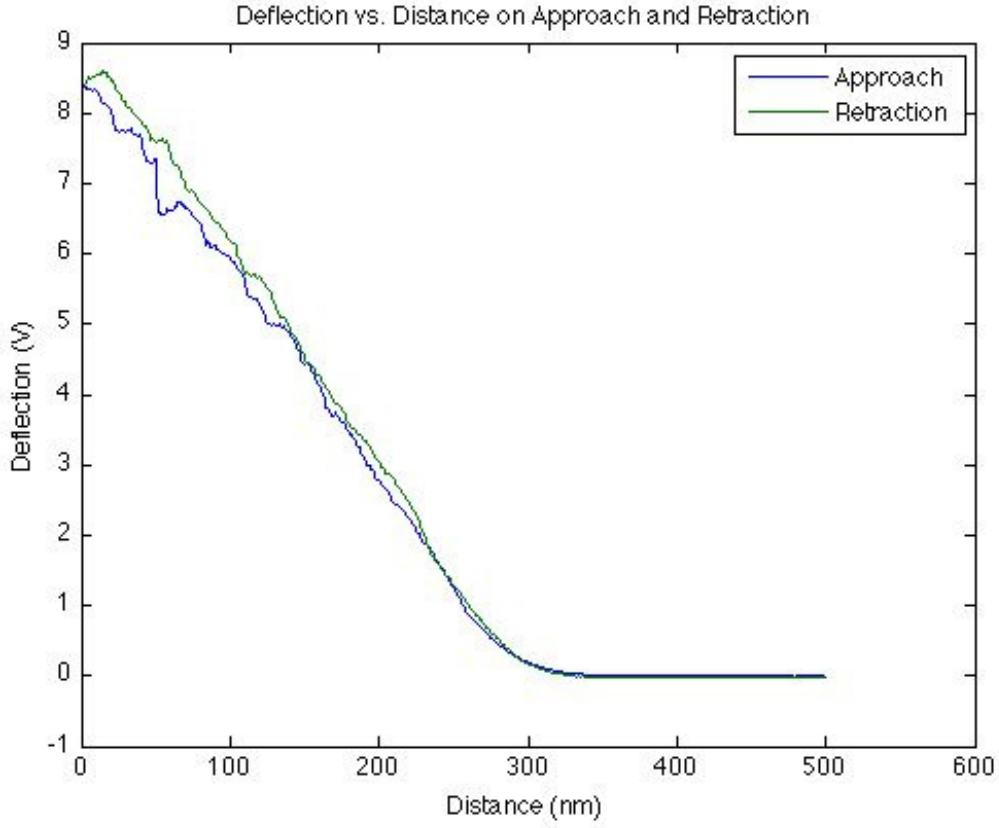
Deflection vs. Distance on Approach and Retraction
Approach
Retraction
Deflection (V)
Distance (nm)
9
8
7
6
5
4
3
2
1
0
-1
0
100
200
300
400
500
600

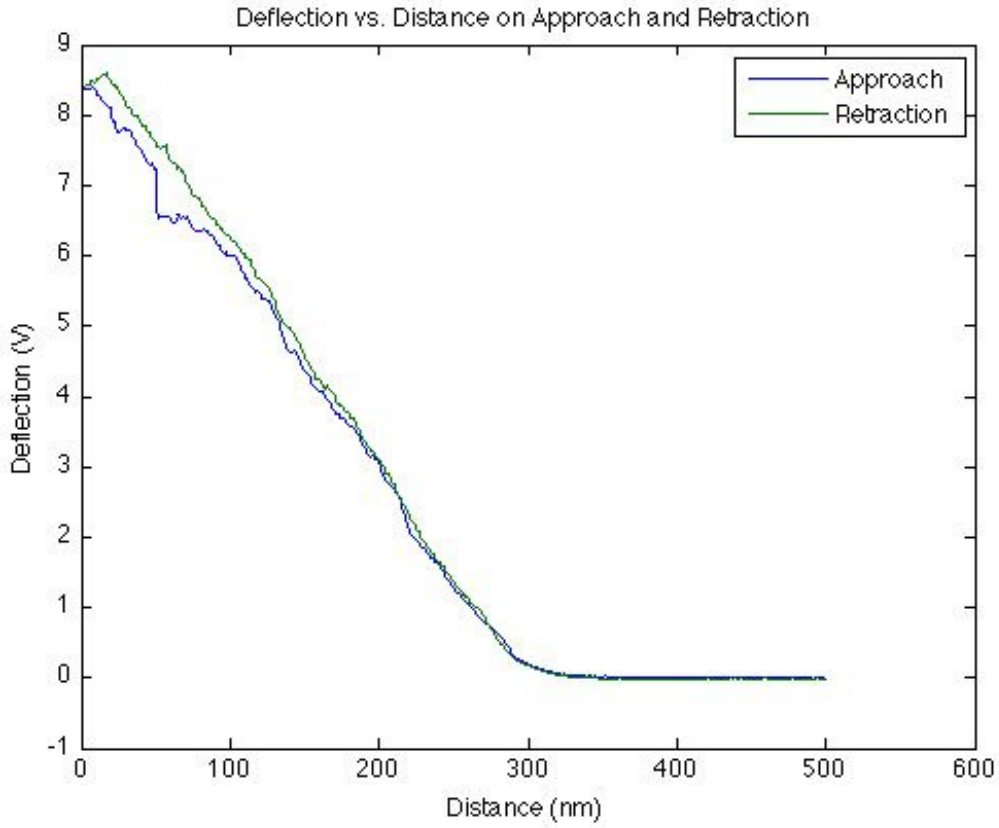
Deflection vs. Distance on Approach and Retraction
Approach
Retraction
Deflection (V)
Distance (nm)
9
8
7
6
5
4
3
2
1
0
-1
0
100
200
300
400
500
600

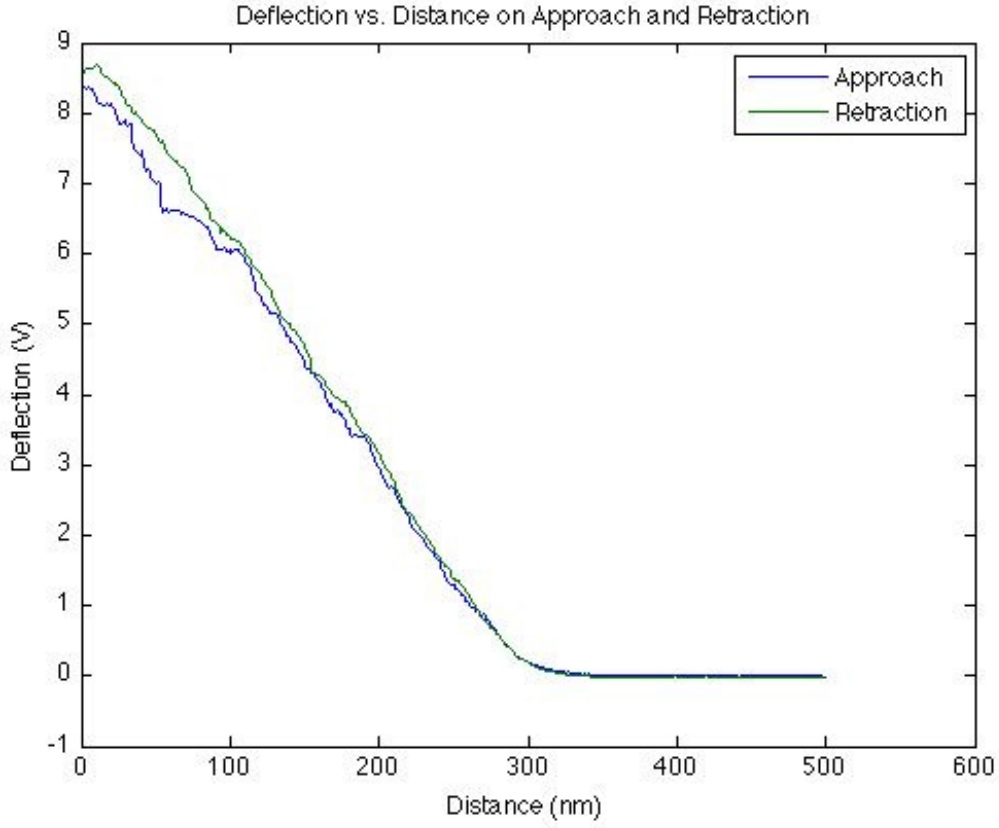
Deflection vs. Distance on Approach and Retraction
Approach
Retraction
Deflection (V)
Distance (nm)
9
8
7
6
5
4
3
2
1
0
-1
0
100
200
300
400
500
600

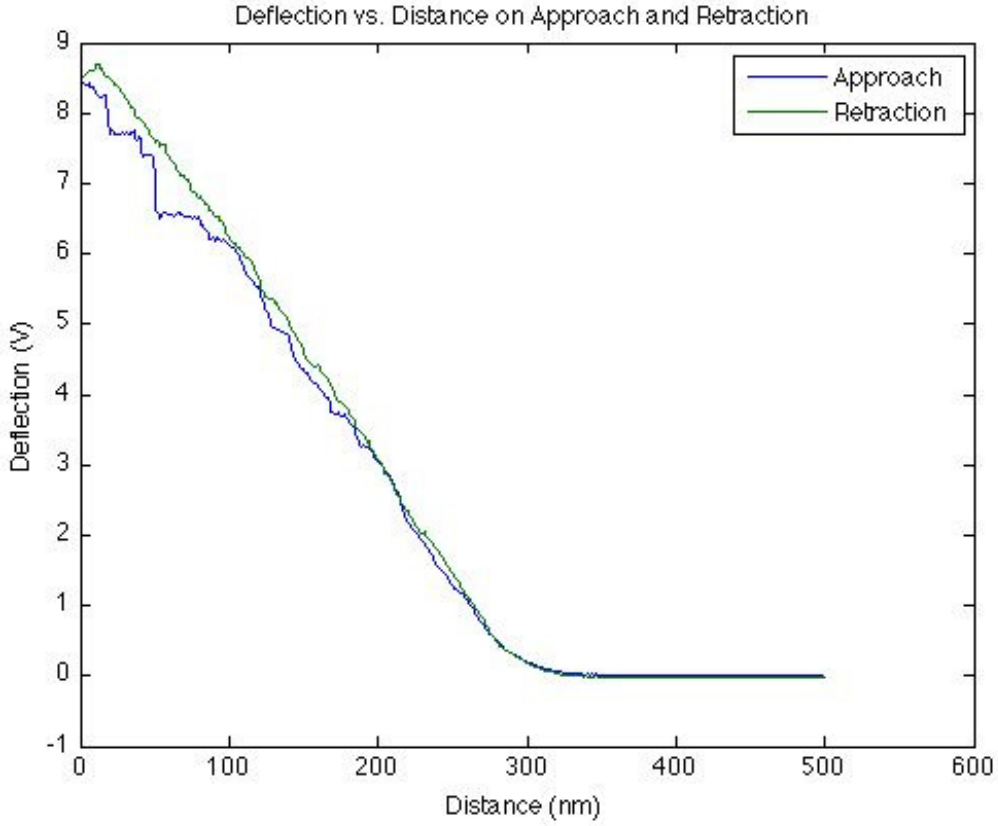
Deflection vs. Distance on Approach and Retraction
Approach
Retraction
Deflection (V)
Distance (nm)
9
8
7
6
5
4
3
2
1
0
-1
0
100
200
300
400
500
600

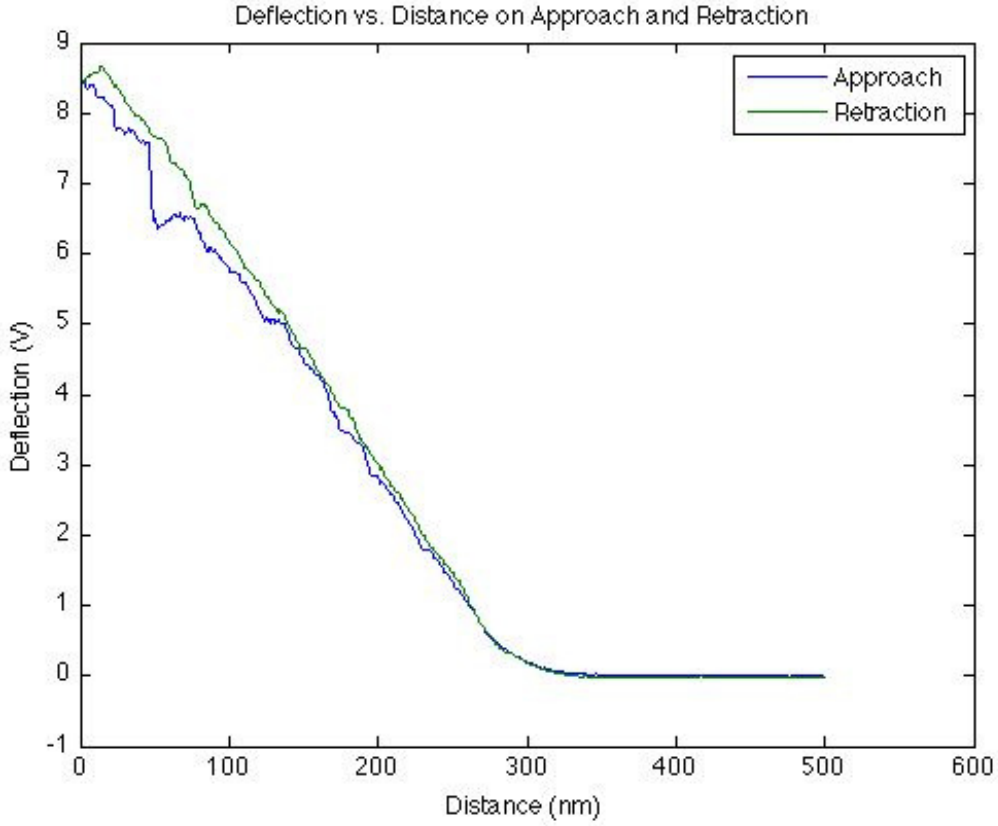
Deflection vs. Distance on Approach and Retraction
Approach
Retraction
Deflection (V)
Distance (nm)
9
8
7
6
5
4
3
2
1
0
-1
0
100
200
300
400
500
600

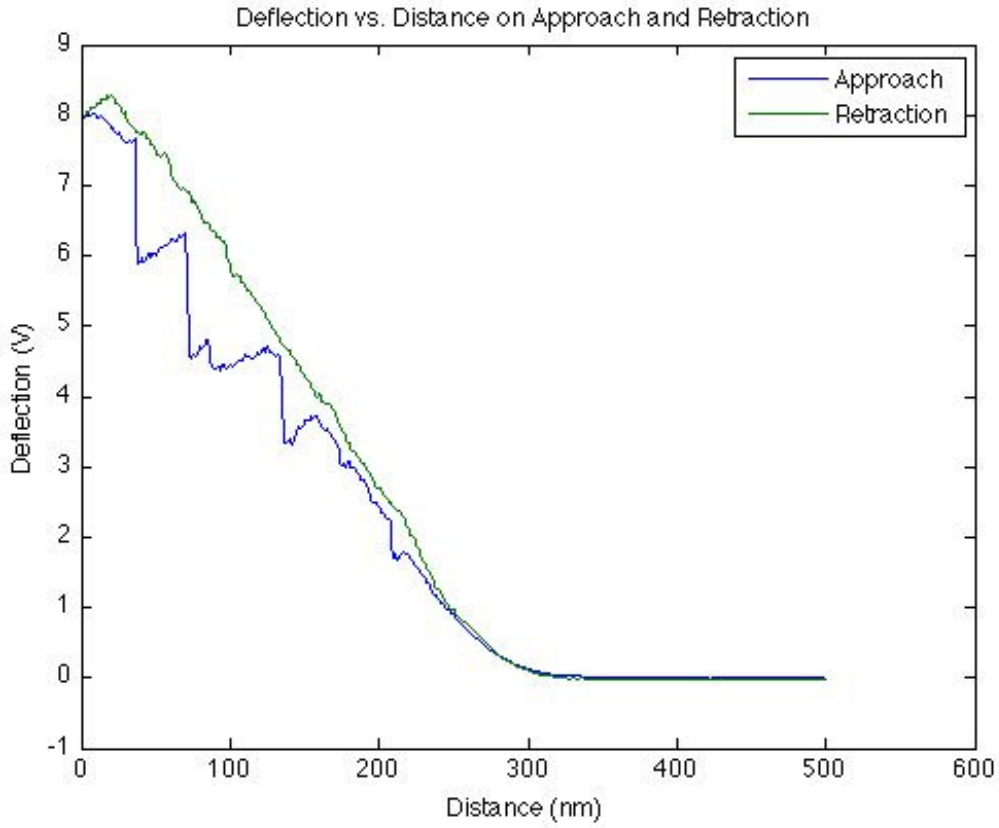
Deflection vs. Distance on Approach and Retraction
Approach
Retraction
Deflection (V)
Distance (nm)
9
8
7
6
5
4
3
2
1
0
-1
0
100
200
300
400
500
600

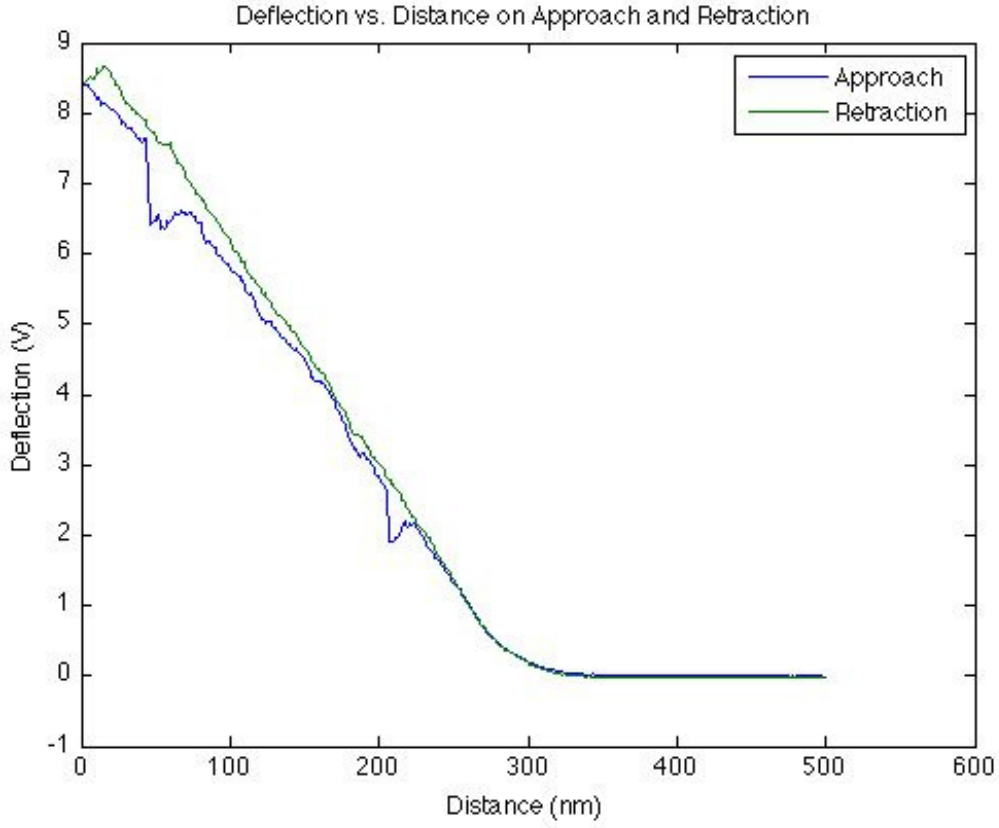
Deflection vs. Distance on Approach and Retraction
Approach
Retraction
Deflection (V)
Distance (nm)
9
8
7
6
5
4
3
2
1
0
-1
0
100
200
300
400
500
600

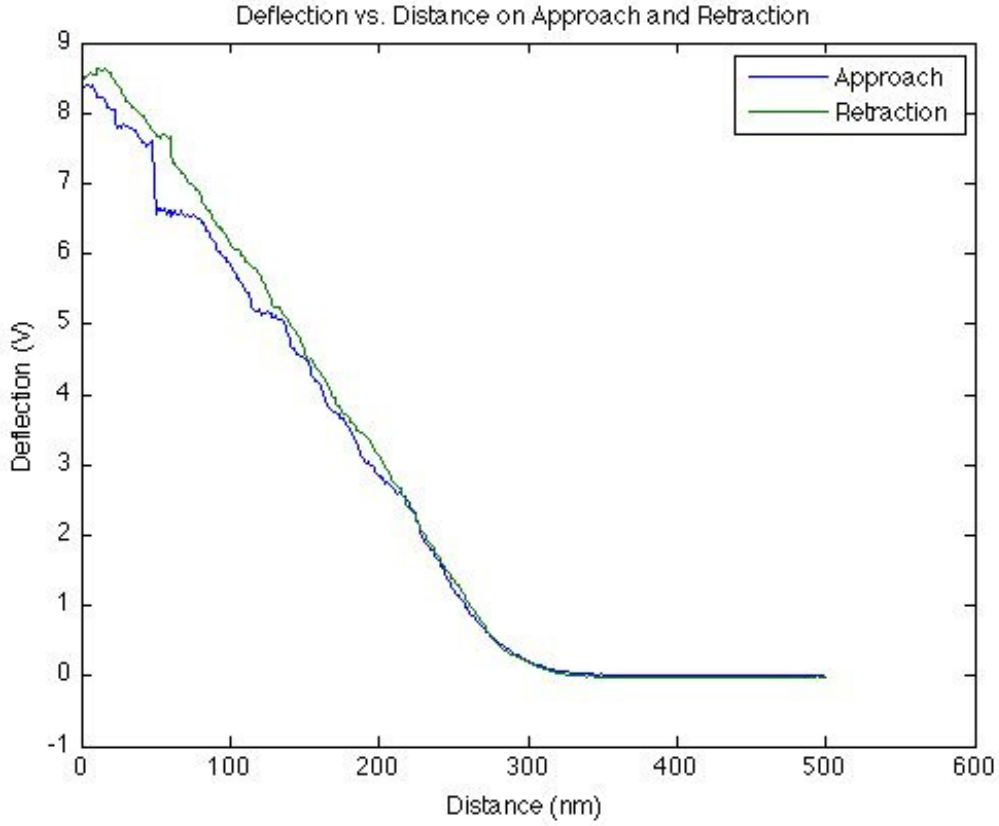
Deflection vs. Distance on Approach and Retraction
Approach
Retraction
Deflection (V)
Distance (nm)
9
8
7
6
5
4
3
2
1
0
-1
0
100
200
300
400
500
600

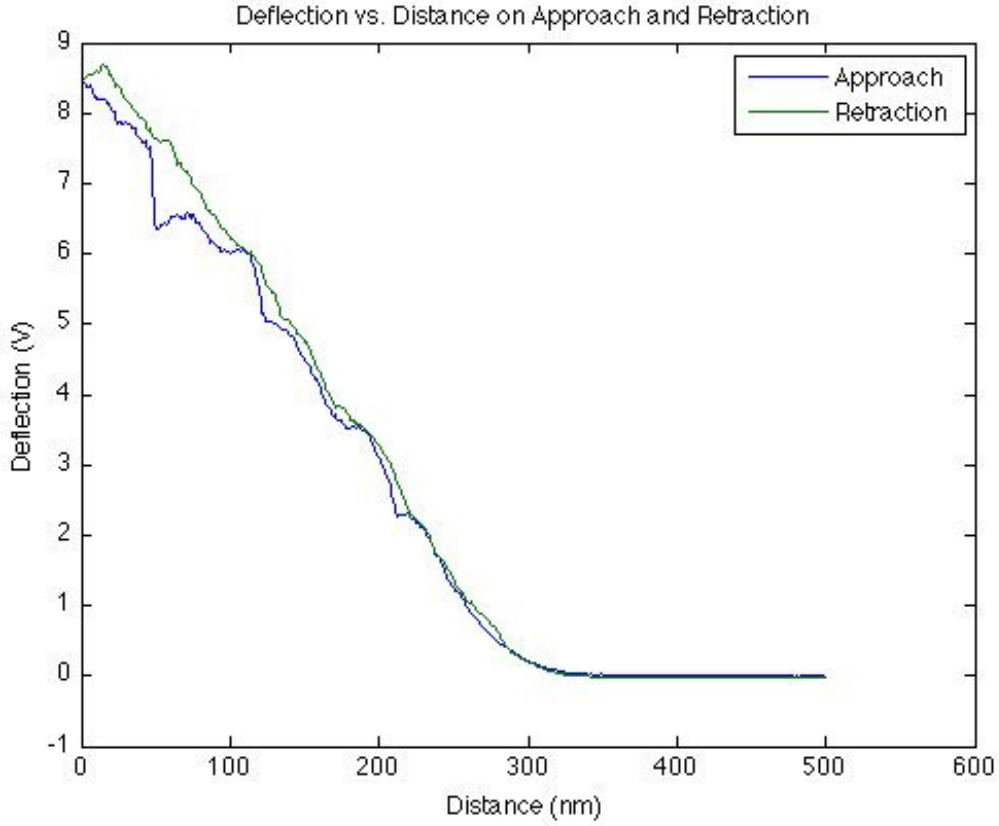
Deflection vs. Distance on Approach and Retraction
Approach
Retraction
Deflection (V)
Distance (nm)
9
8
7
6
5
4
3
2
1
0
-1
0
100
200
300
400
500
600

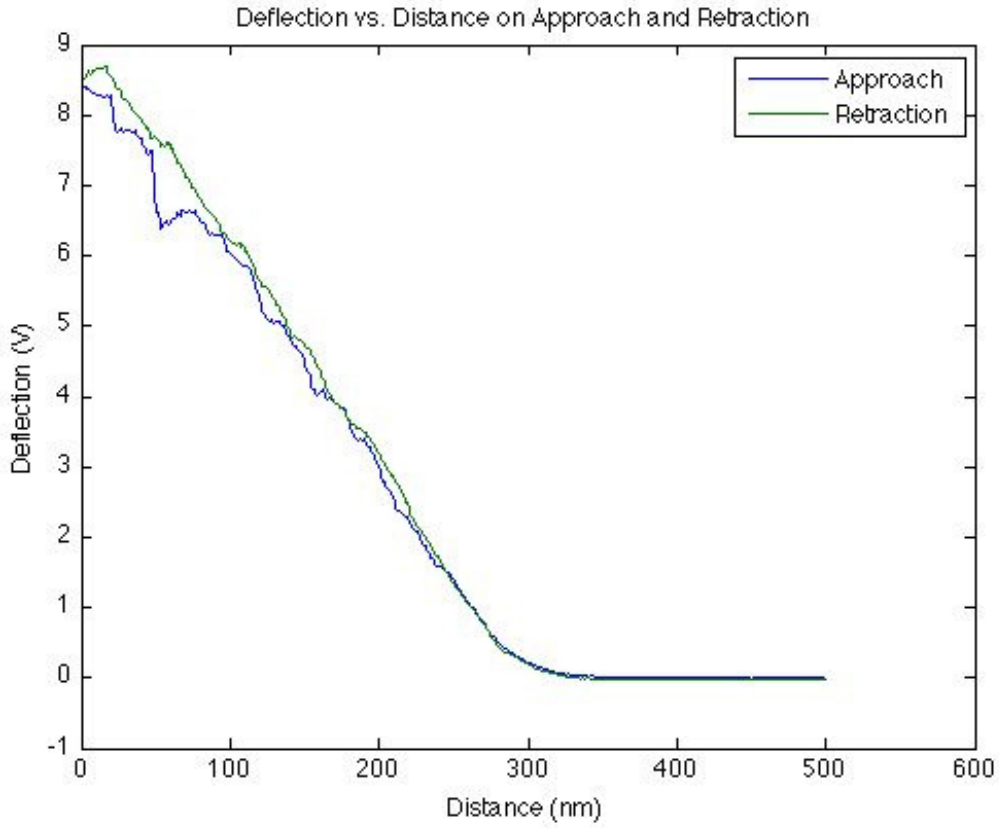
Deflection vs. Distance on Approach and Retraction
Approach
Retraction
Deflection (V)
Distance (nm)
9
8
7
6
5
4
3
2
1
0
-1
0
100
200
300
400
500
600

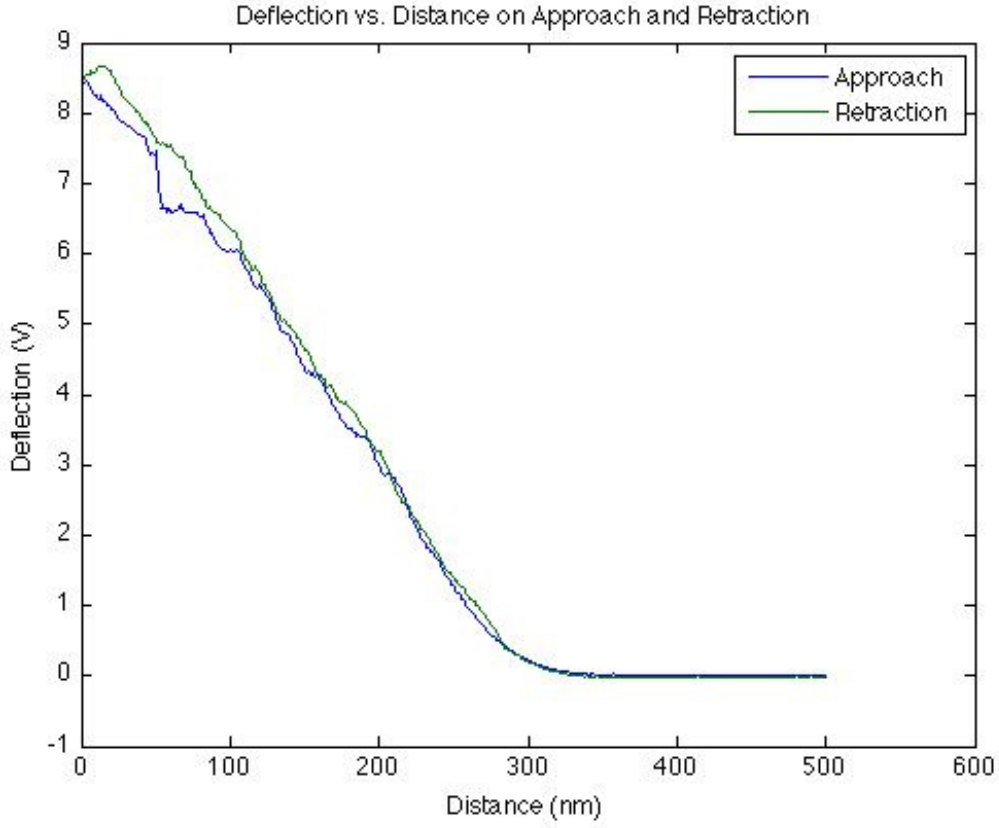
Deflection vs. Distance on Approach and Retraction
Approach
Retraction
Deflection (V)
Distance (nm)
9
8
7
6
5
4
3
2
1
0
-1
0
100
200
300
400
500
600

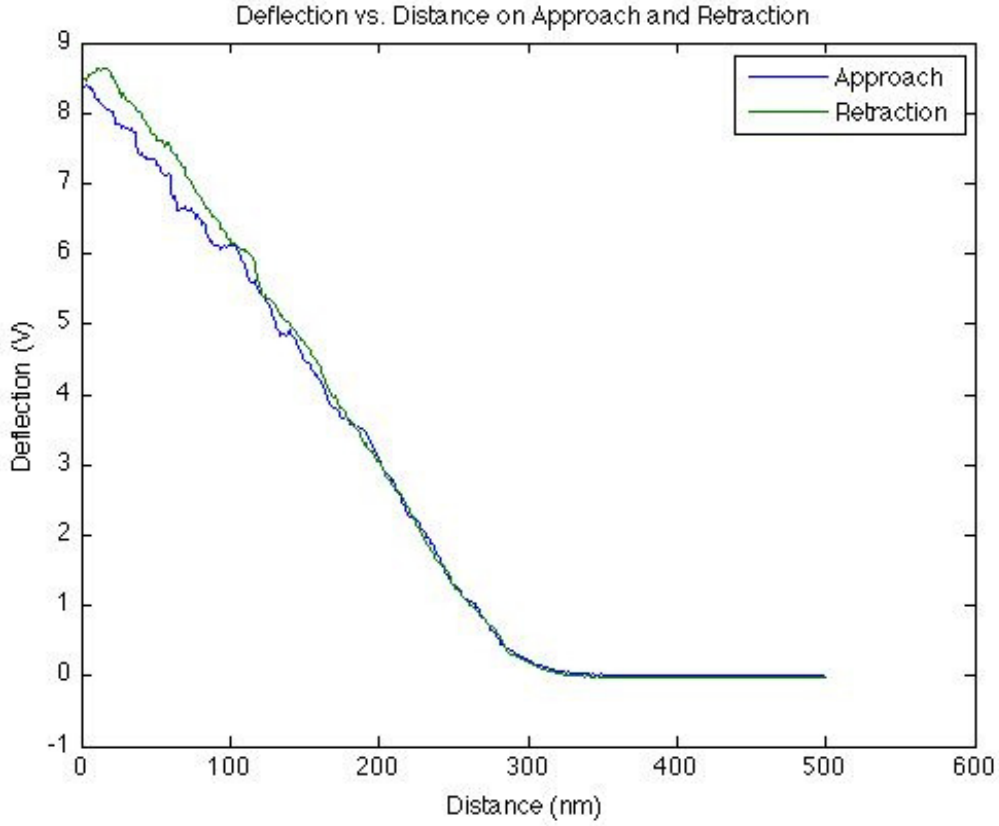
Deflection vs. Distance on Approach and Retraction
Approach
Retraction
Deflection (V)
Distance (nm)
9
8
7
6
5
4
3
2
1
0
-1
0
100
200
300
400
500
600

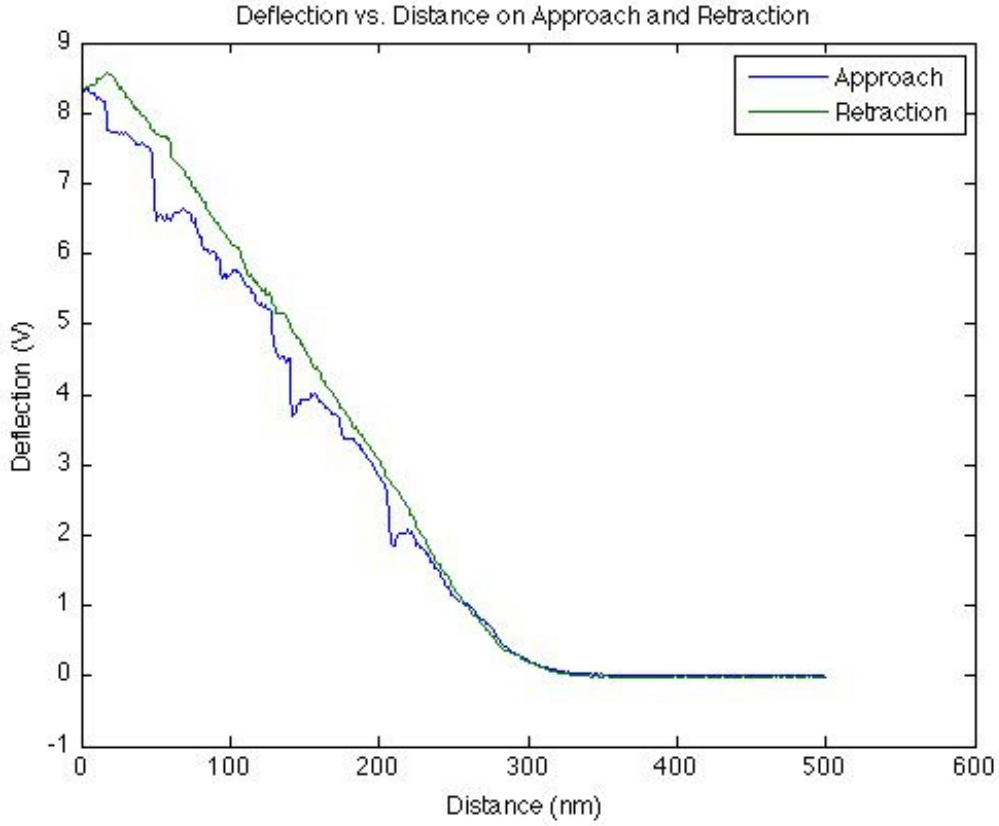
Deflection vs. Distance on Approach and Retraction
Approach
Retraction
Deflection (V)
Distance (nm)
9
8
7
6
5
4
3
2
1
0
-1
0
100
200
300
400
500
600

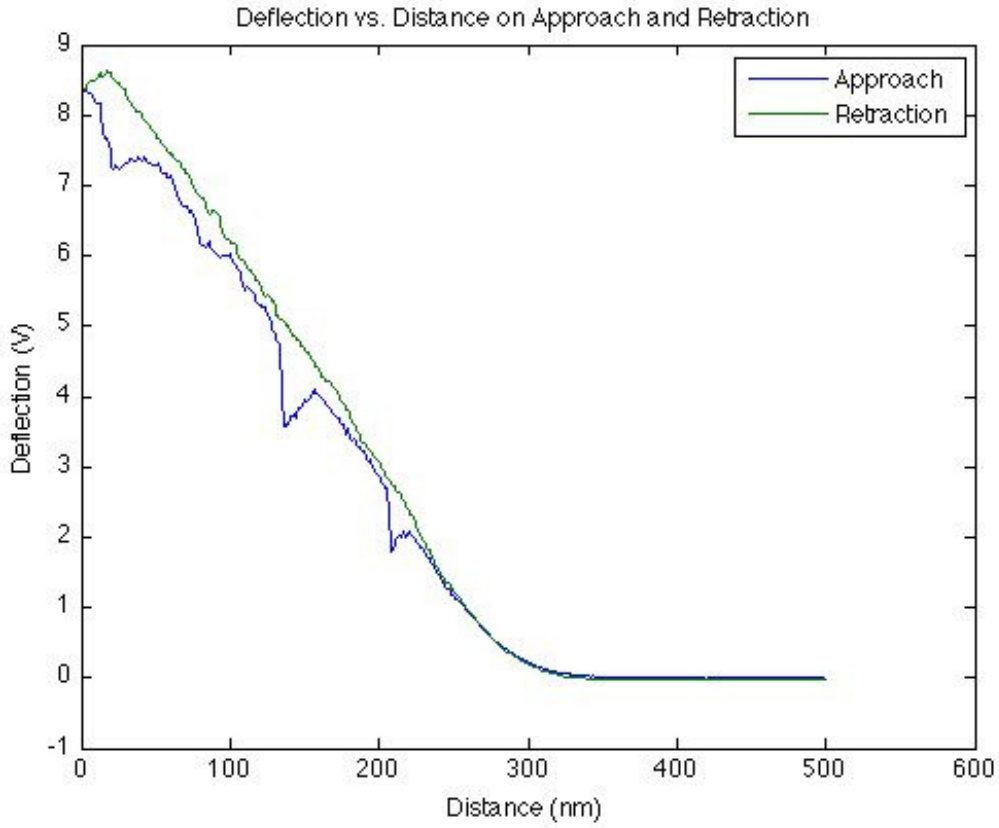
Deflection vs. Distance on Approach and Retraction
Approach
Retraction
Deflection (V)
Distance (nm)
9
8
7
6
5
4
3
2
1
0
-1
0
100
200
300
400
500
600

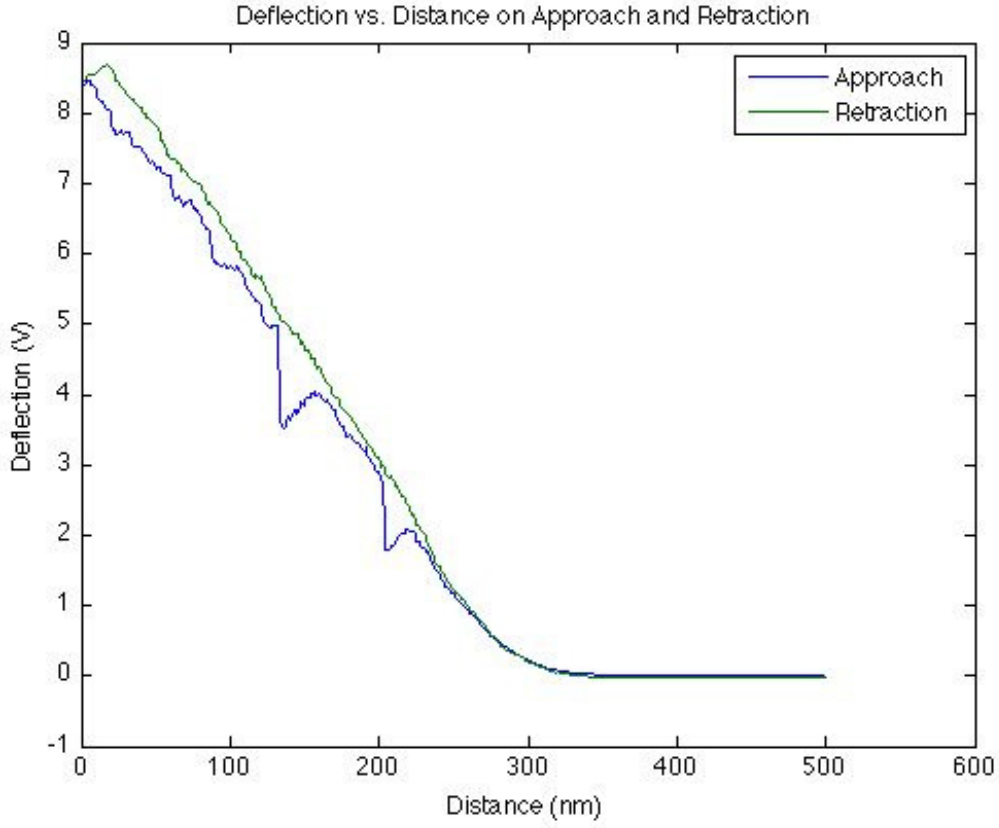
Deflection vs. Distance on Approach and Retraction
Approach
Retraction
Deflection (V)
Distance (nm)
9
8
7
6
5
4
3
2
1
0
-1
0
100
200
300
400
500
600

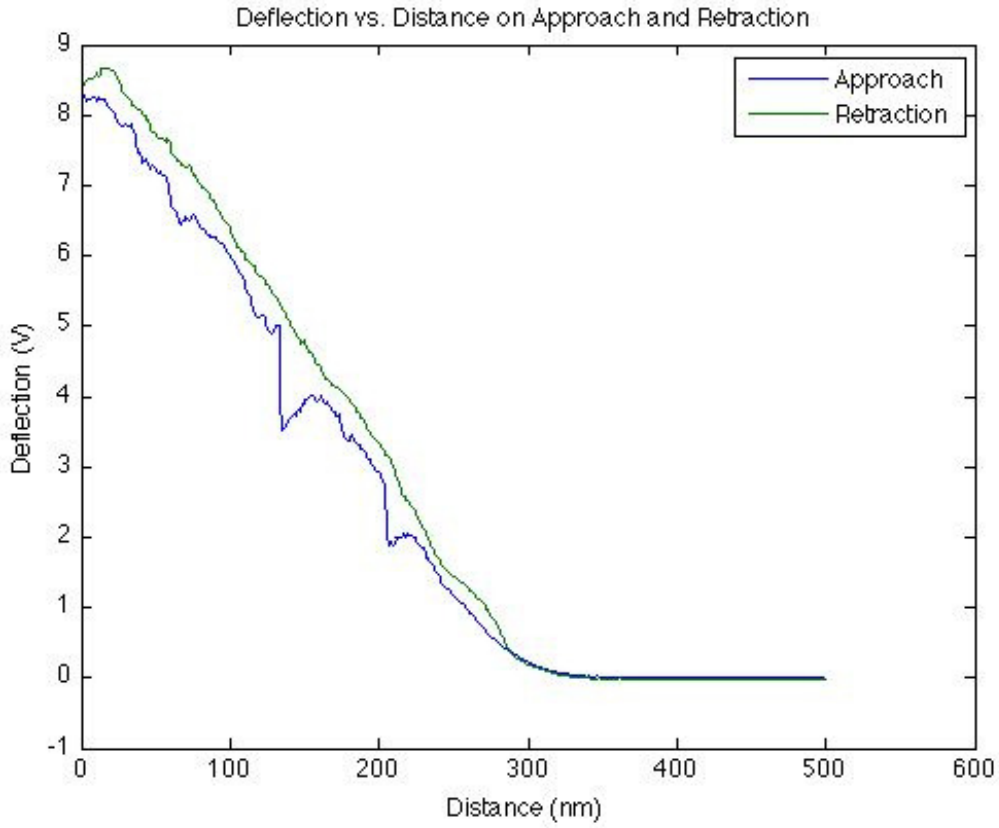
Deflection vs. Distance on Approach and Retraction
Approach
Retraction
Deflection (V)
Distance (nm)
9
8
7
6
5
4
3
2
1
0
-1
0
100
200
300
400
500
600

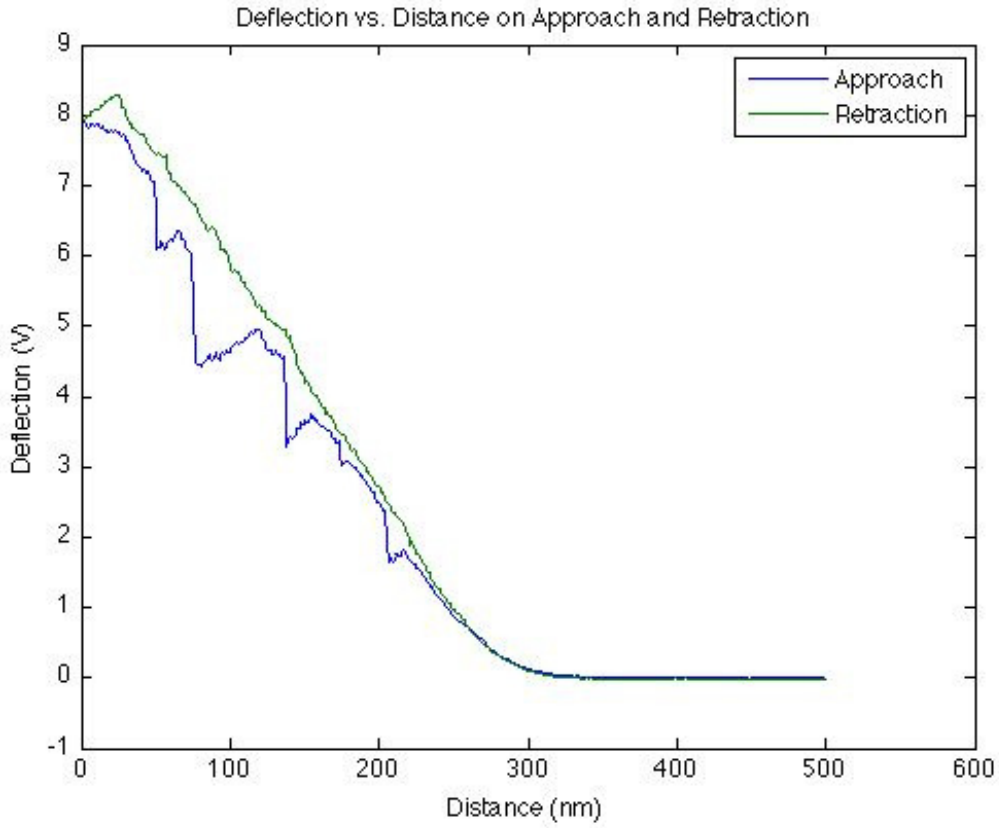
Deflection vs. Distance on Approach and Retraction
Approach
Retraction
Deflection (V)
Distance (nm)
9
8
7
6
5
4
3
2
1
0
-1
0
100
200
300
400
500
600

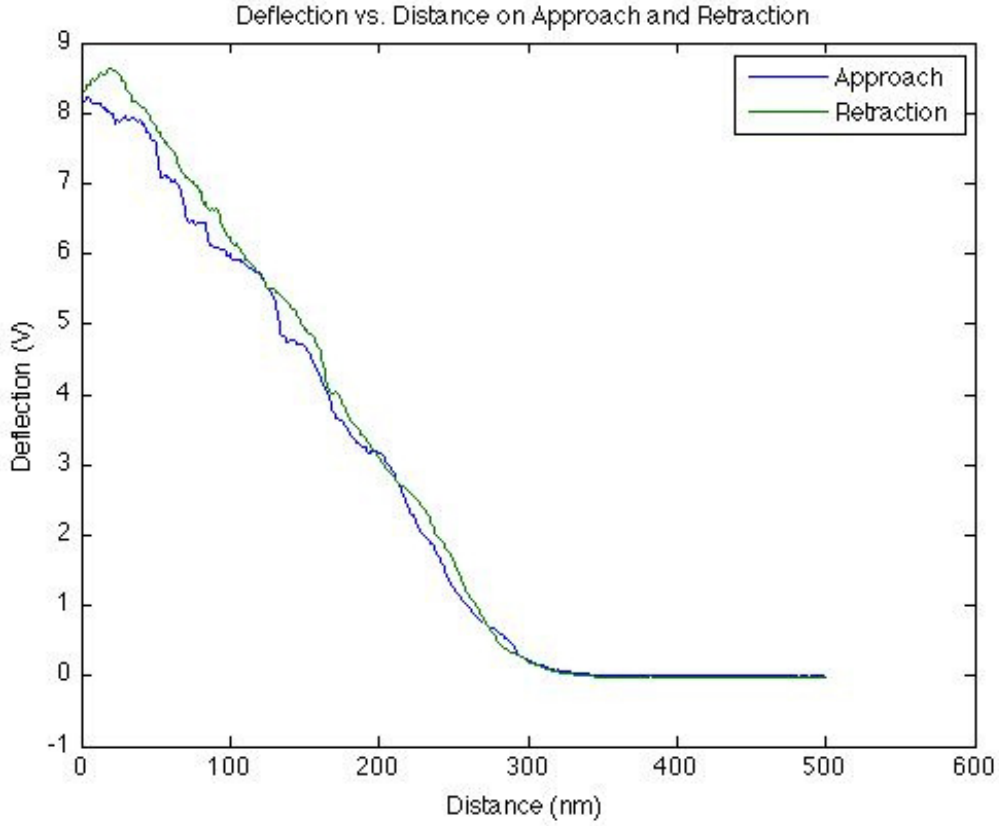
Deflection vs. Distance on Approach and Retraction
Approach
Retraction
Deflection (V)
Distance (nm)
9
8
7
6
5
4
3
2
1
0
-1
0
100
200
300
400
500
600

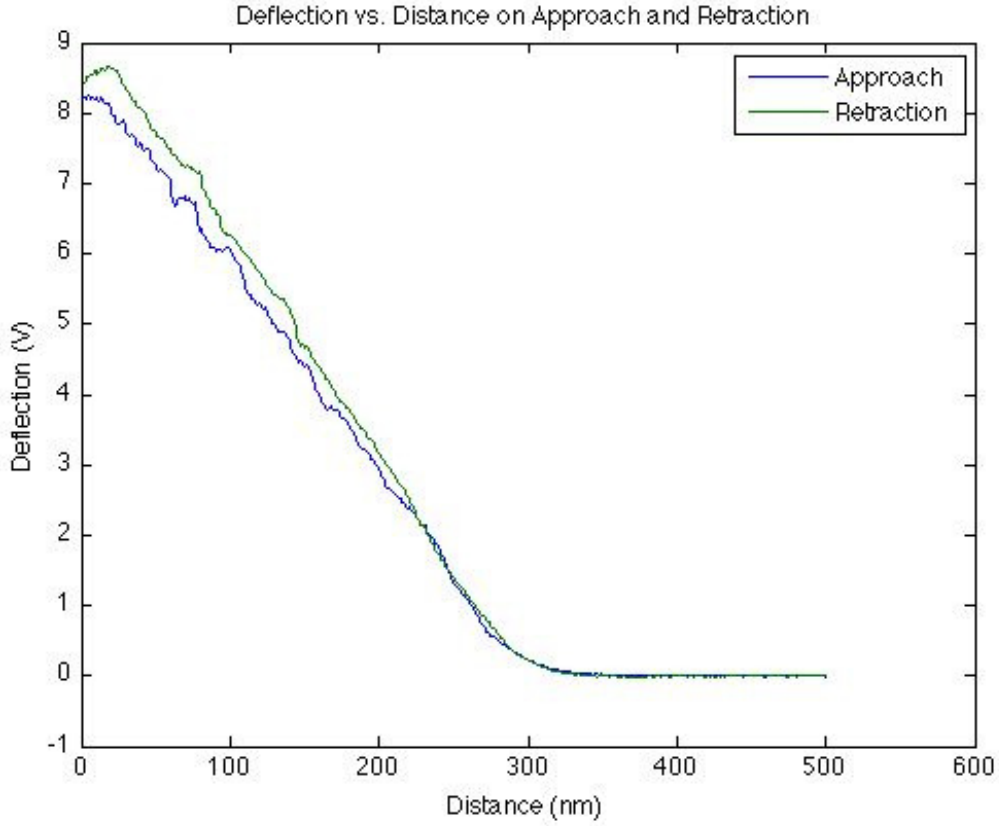
Deflection vs. Distance on Approach and Retraction
Approach
Retraction
Deflection (V)
Distance (nm)
9
8
7
6
5
4
3
2
1
0
-1
0
100
200
300
400
500
600

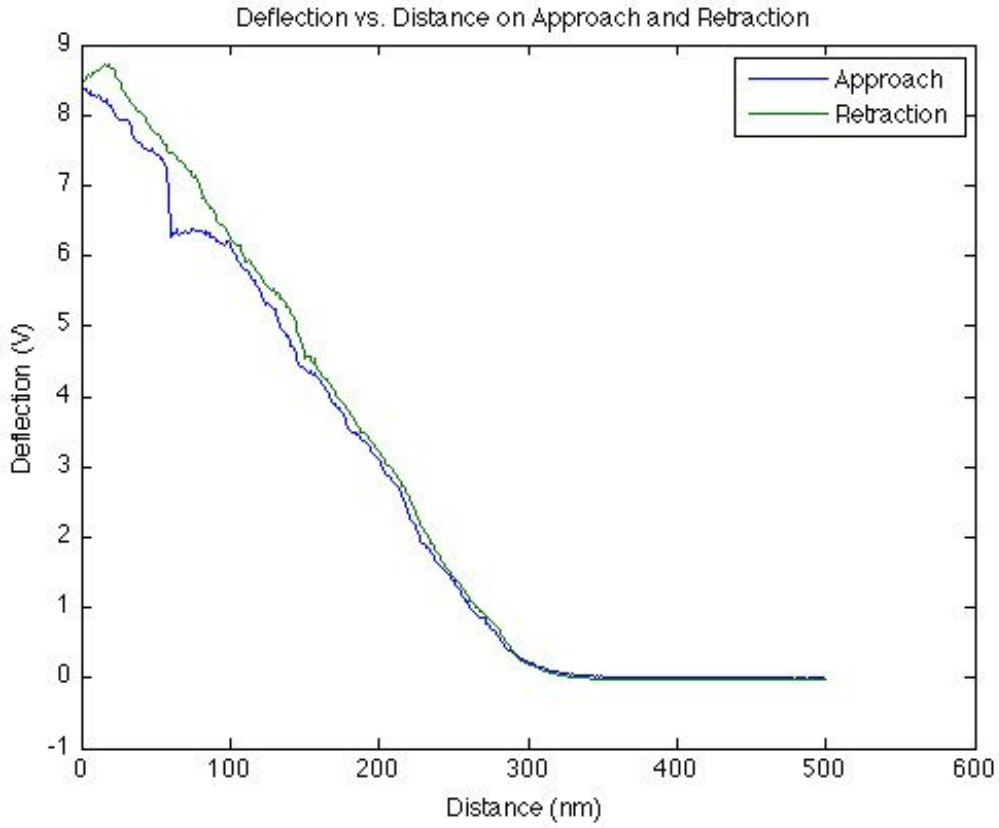
Deflection vs. Distance on Approach and Retraction
Approach
Retraction
Deflection (V)
Distance (nm)
9
8
7
6
5
4
3
2
1
0
-1
0
100
200
300
400
500
600

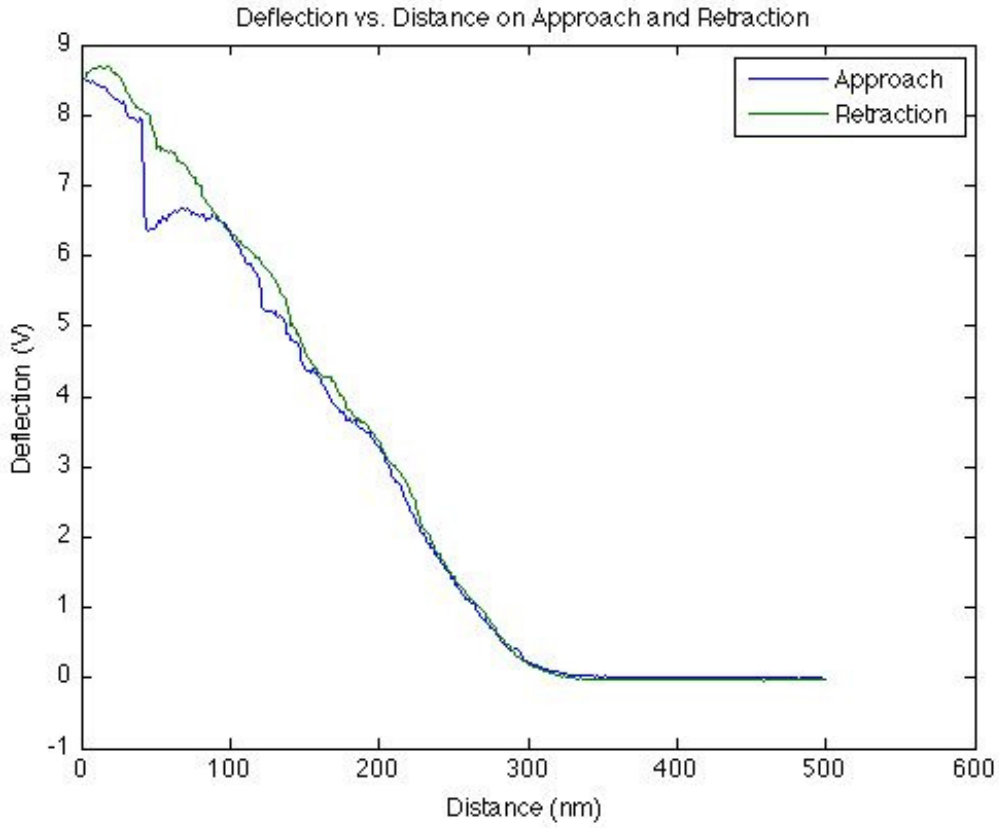
Deflection vs. Distance on Approach and Retraction
Approach
Retraction
Deflection (V)
Distance (nm)
9
8
7
6
5
4
3
2
1
0
-1
0
100
200
300
400
500
600

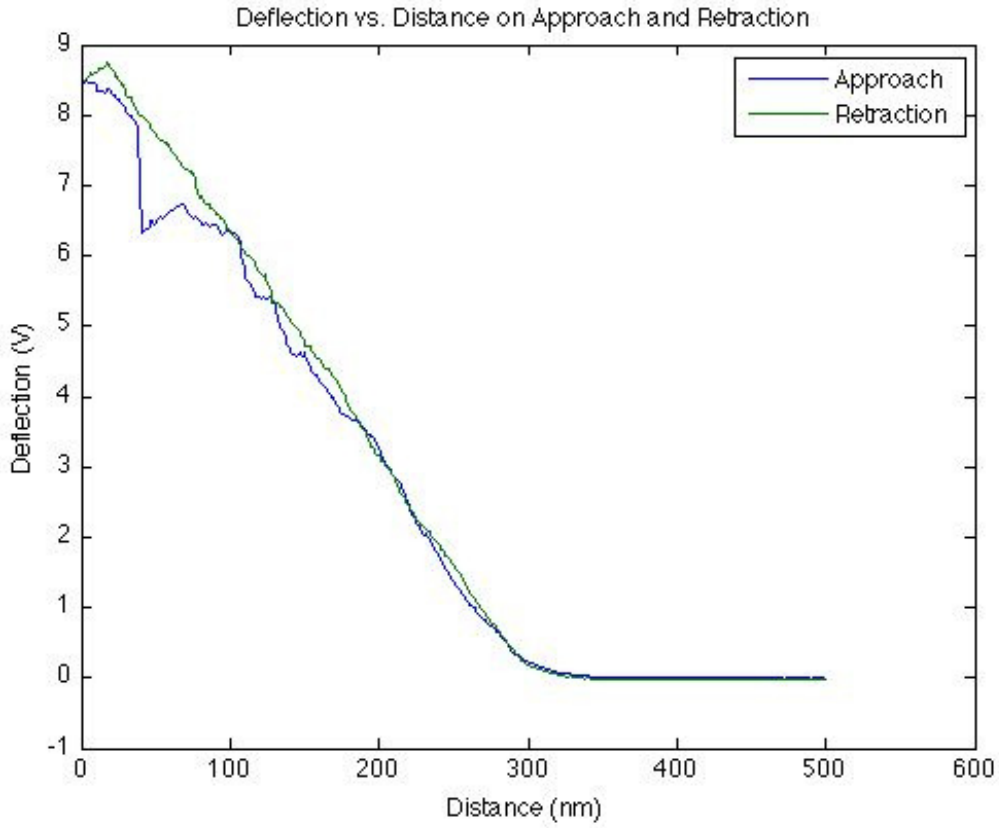
Deflection vs. Distance on Approach and Retraction
Approach
Retraction
Deflection (V)
Distance (nm)
9
8
7
6
5
4
3
2
1
0
-1
0
100
200
300
400
500
600

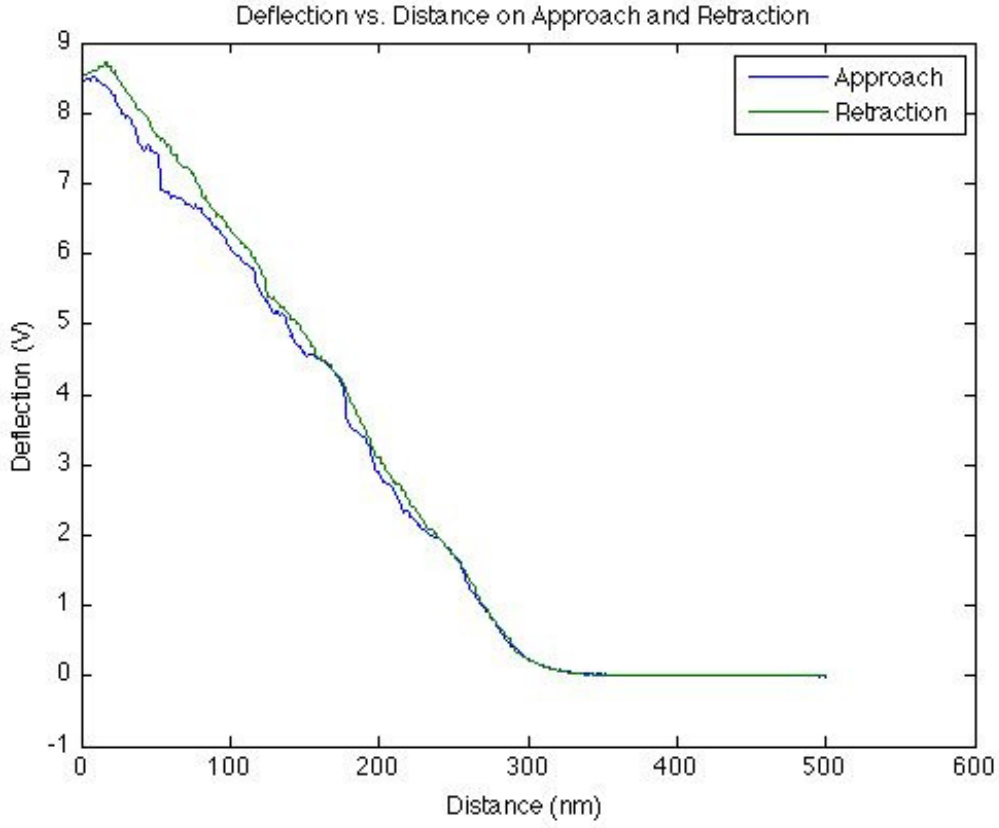
Deflection vs. Distance on Approach and Retraction
Approach
Retraction
Deflection (V)
Distance (nm)
9
8
7
6
5
4
3
2
1
0
-1
0
100
200
300
400
500
600

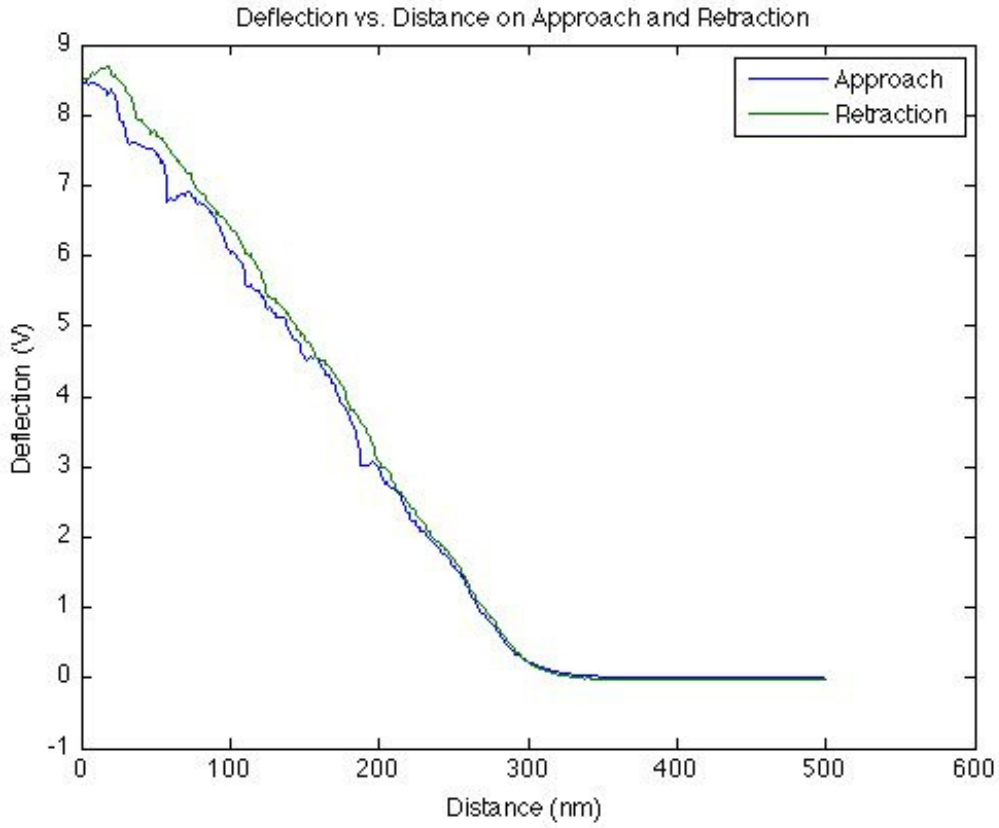
Deflection vs. Distance on Approach and Retraction
Approach
Retraction
Deflection (V)
Distance (nm)
9
8
7
6
5
4
3
2
1
0
-1
0
100
200
300
400
500
600

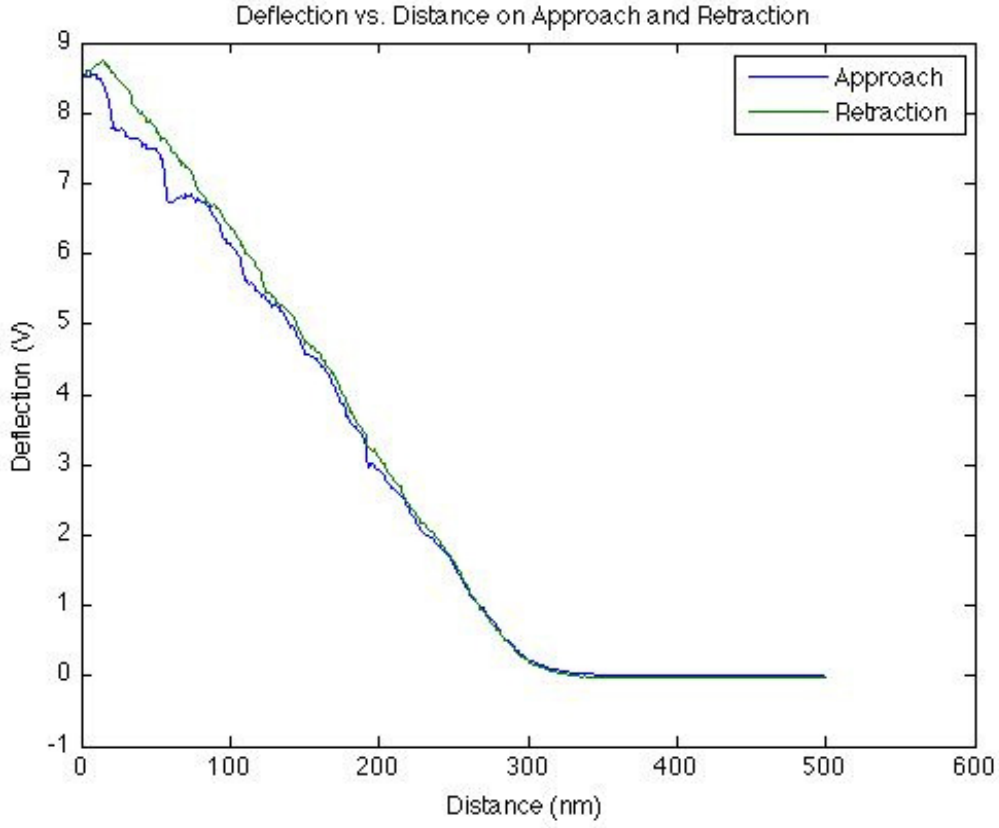
Deflection vs. Distance on Approach and Retraction
Approach
Retraction
Deflection (V)
Distance (nm)
9
8
7
6
5
4
3
2
1
0
-1
0
100
200
300
400
500
600

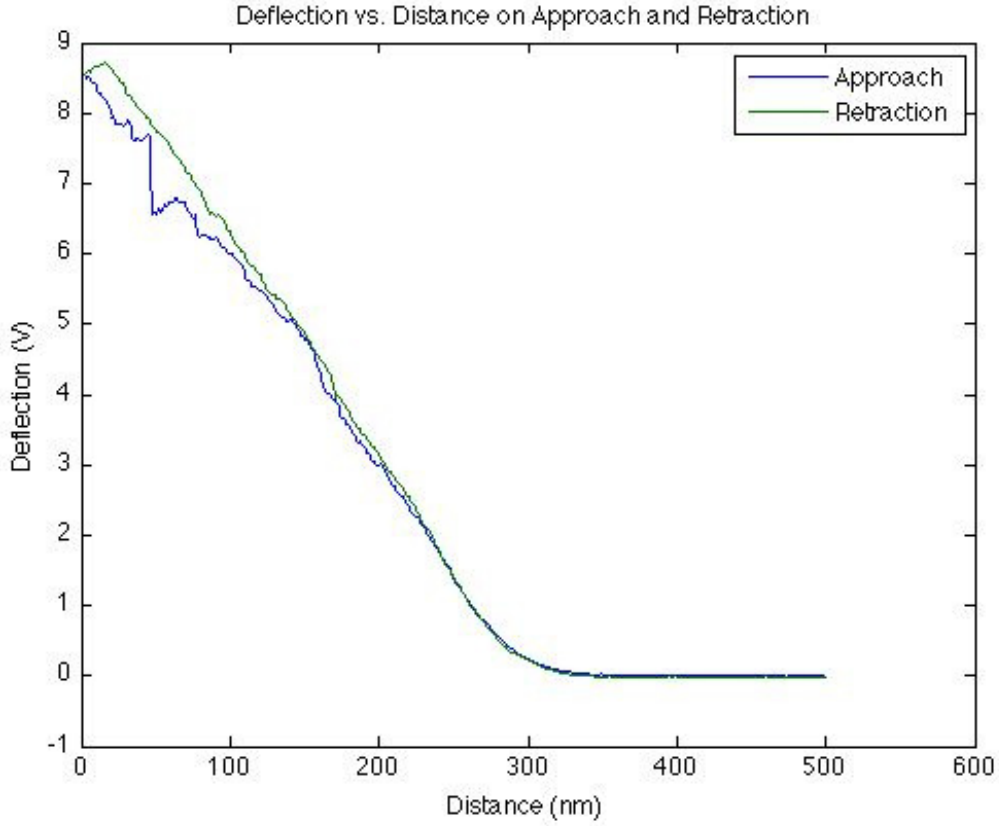
Deflection vs. Distance on Approach and Retraction
Approach
Retraction
Deflection (V)
Distance (nm)
9
8
7
6
5
4
3
2
1
0
-1
0
100
200
300
400
500
600

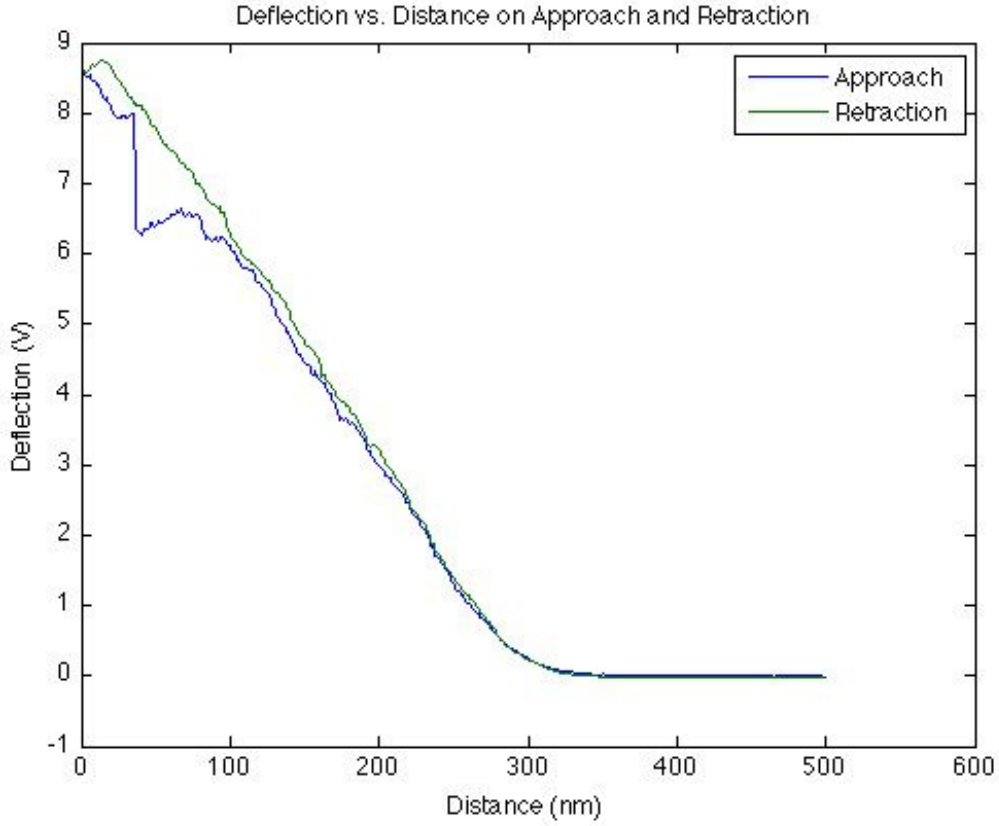
Deflection vs. Distance on Approach and Retraction
Approach
Retraction
Deflection (V)
Distance (nm)
9
8
7
6
5
4
3
2
1
0
-1
0
100
200
300
400
500
600

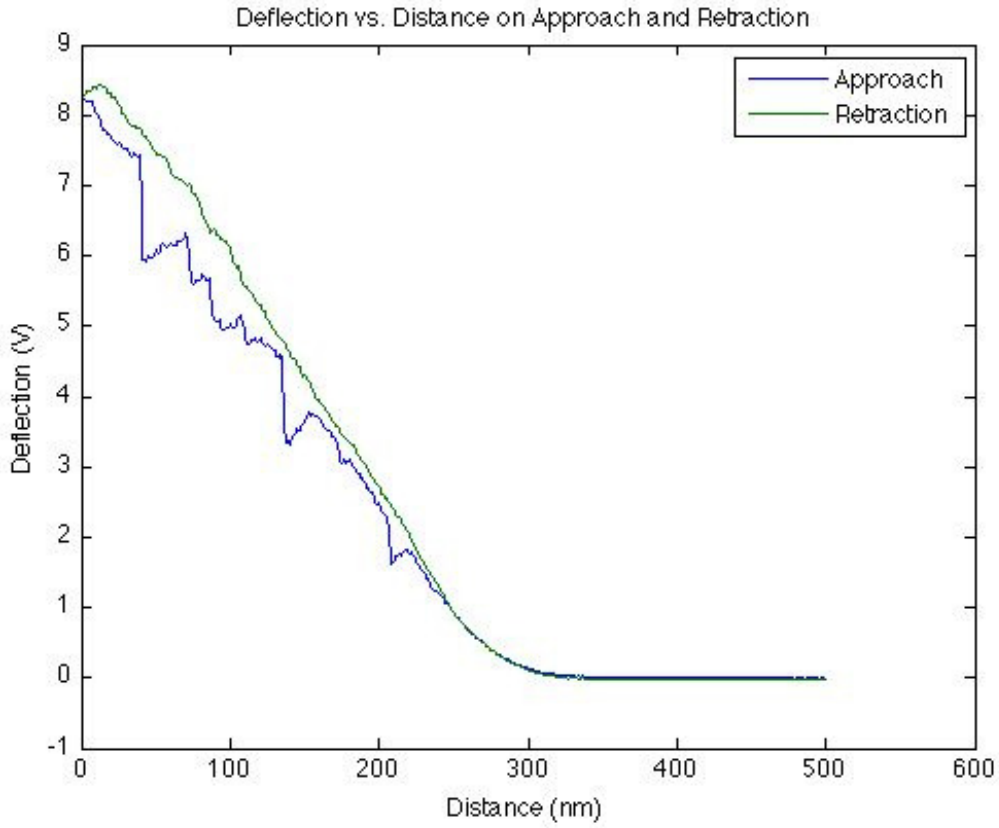
Deflection vs. Distance on Approach and Retraction
Approach
Retraction
Deflection (V)
Distance (nm)
9
8
7
6
5
4
3
2
1
0
-1
0
100
200
300
400
500
600

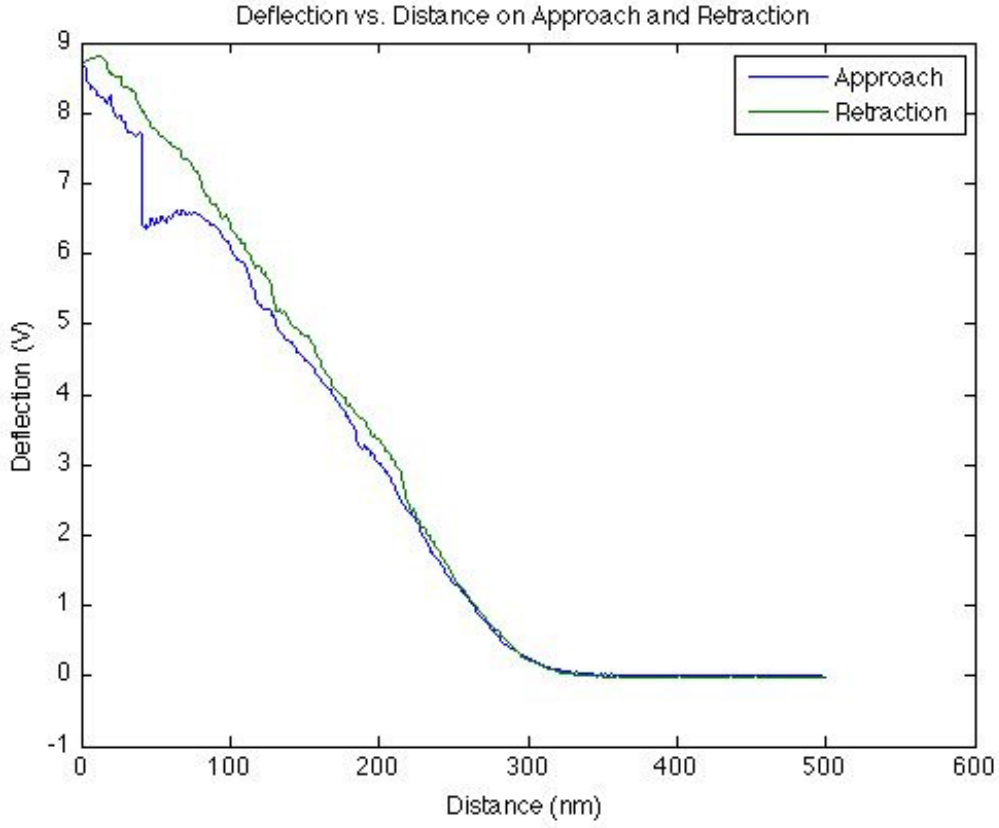
Deflection vs. Distance on Approach and Retraction
Approach
Retraction
Deflection (V)
Distance (nm)
9
8
7
6
5
4
3
2
1
0
-1
0
100
200
300
400
500
600

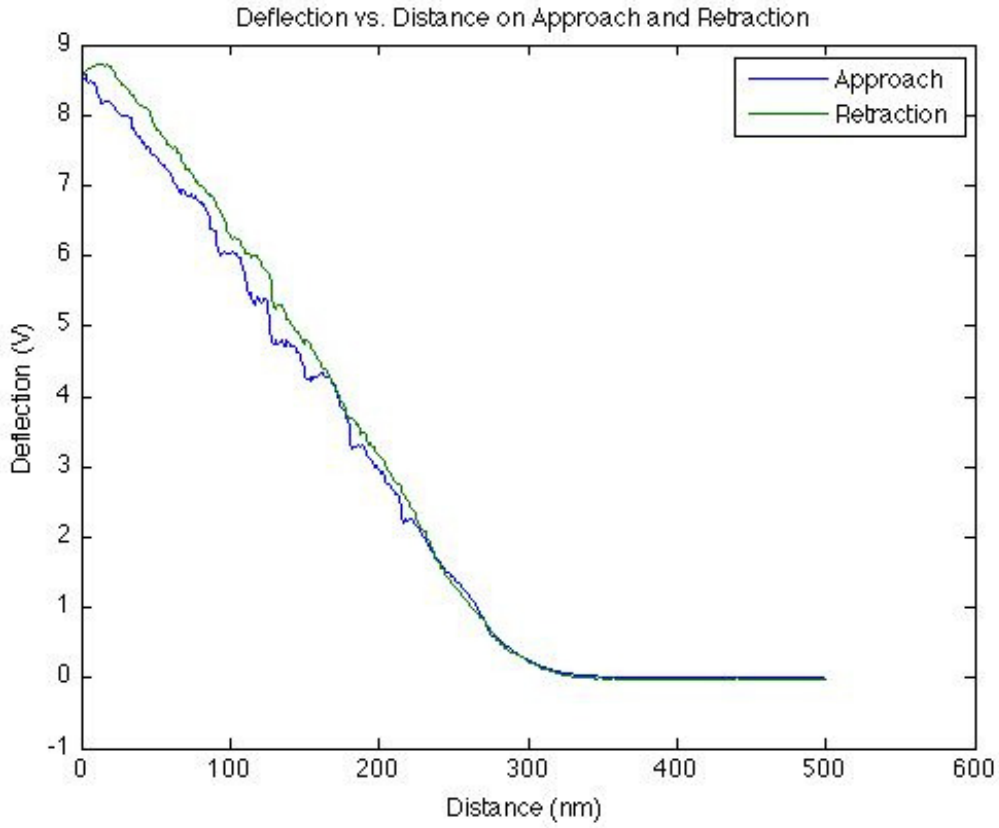
Deflection vs. Distance on Approach and Retraction
Approach
Retraction
Deflection (V)
Distance (nm)
9
8
7
6
5
4
3
2
1
0
-1
0
100
200
300
400
500
600

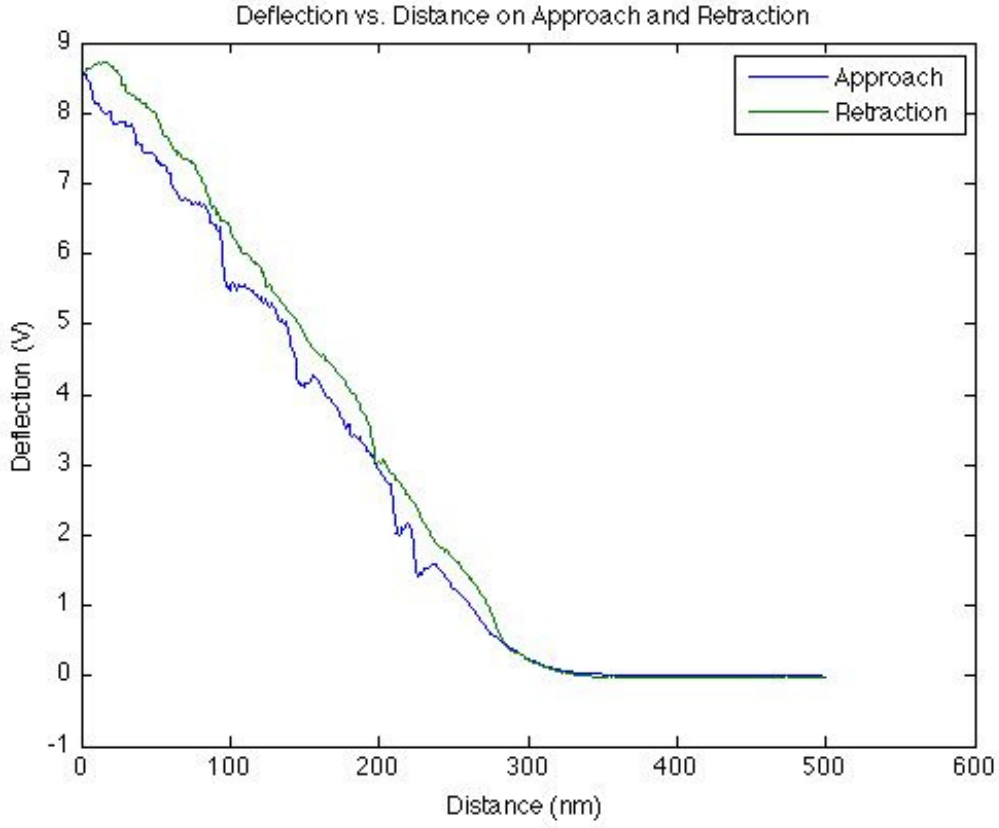
Deflection vs. Distance on Approach and Retraction
Approach
Retraction
Deflection (V)
Distance (nm)
9
8
7
6
5
4
3
2
1
0
-1
0
100
200
300
400
500
600

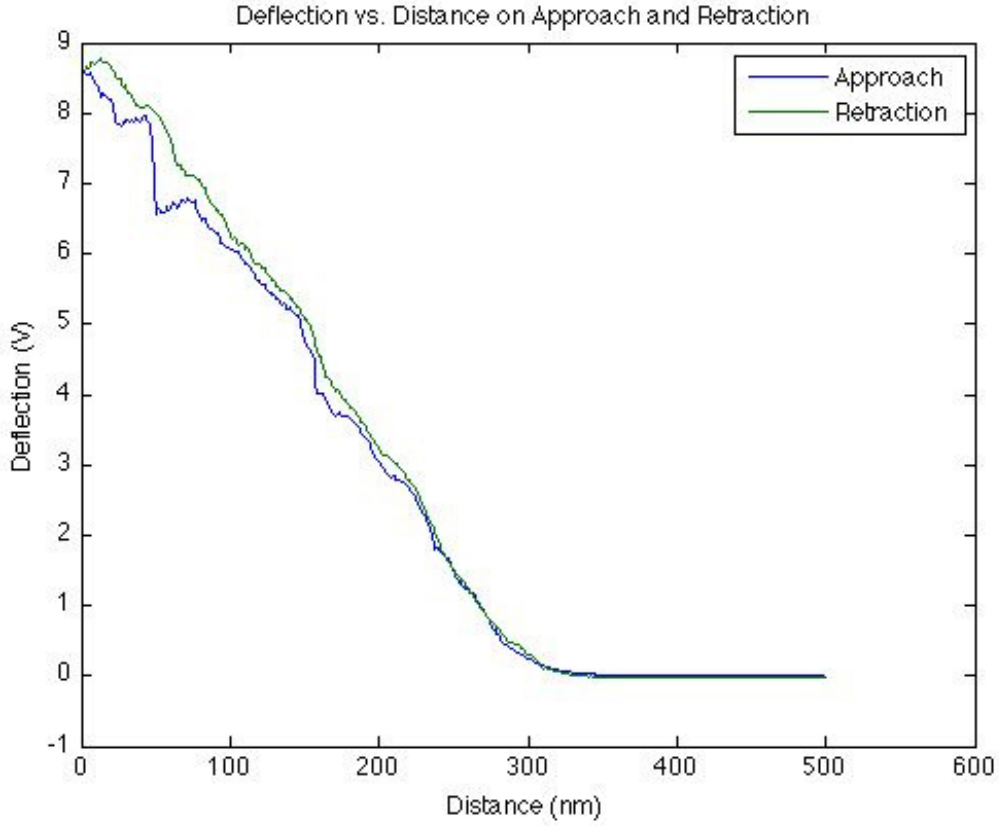
Deflection vs. Distance on Approach and Retraction
Approach
Retraction
Deflection (V)
Distance (nm)
9
8
7
6
5
4
3
2
1
0
-1
0
100
200
300
400
500
600

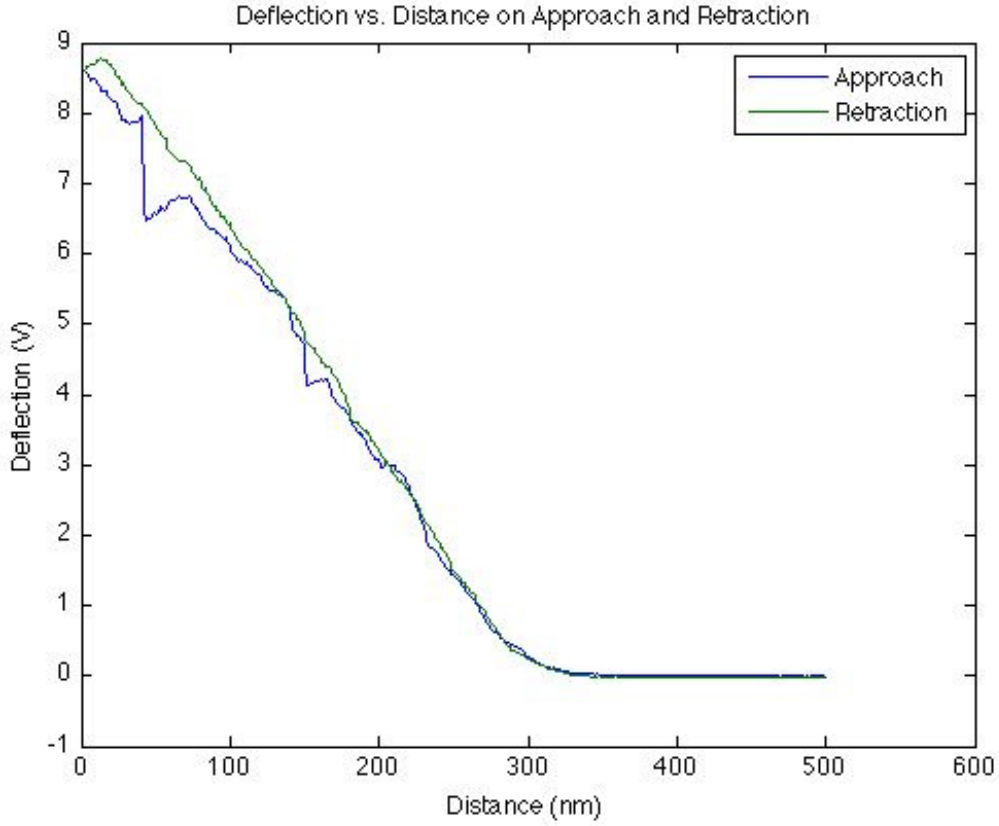
Deflection vs. Distance on Approach and Retraction
Approach
Retraction
Deflection (V)
Distance (nm)
9
8
7
6
5
4
3
2
1
0
-1
0
100
200
300
400
500
600

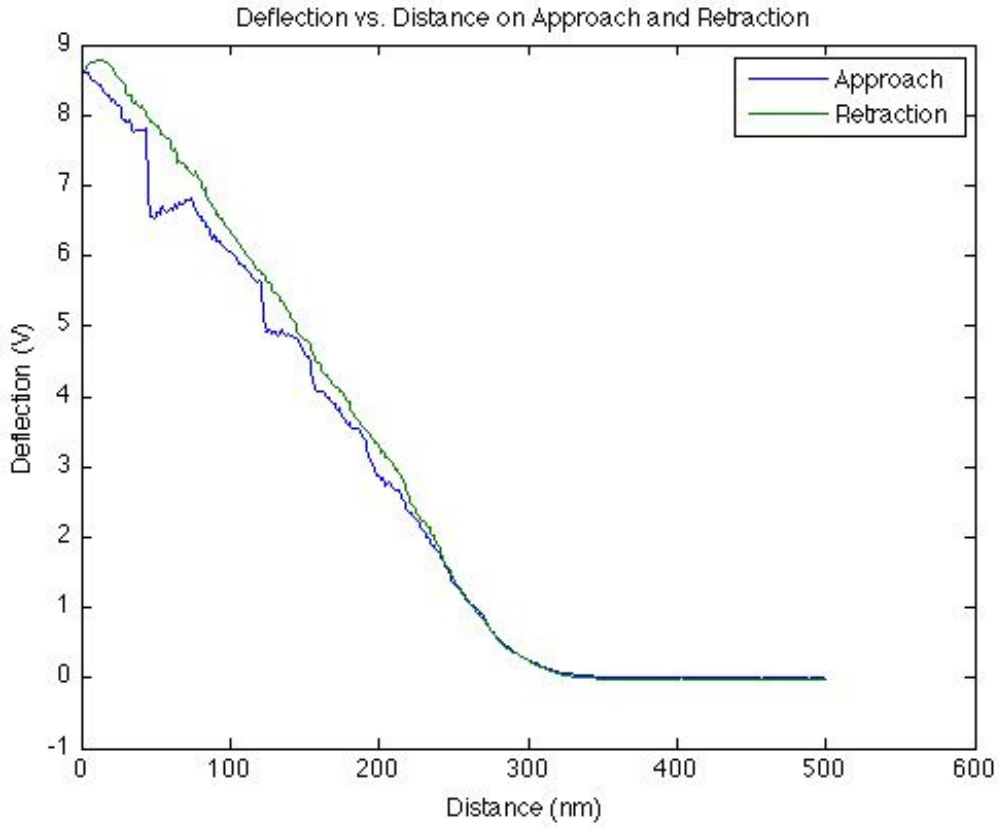
Deflection vs. Distance on Approach and Retraction
Approach
Retraction
Deflection (V)
Distance (nm)
9
8
7
6
5
4
3
2
1
0
-1
0
100
200
300
400
500
600

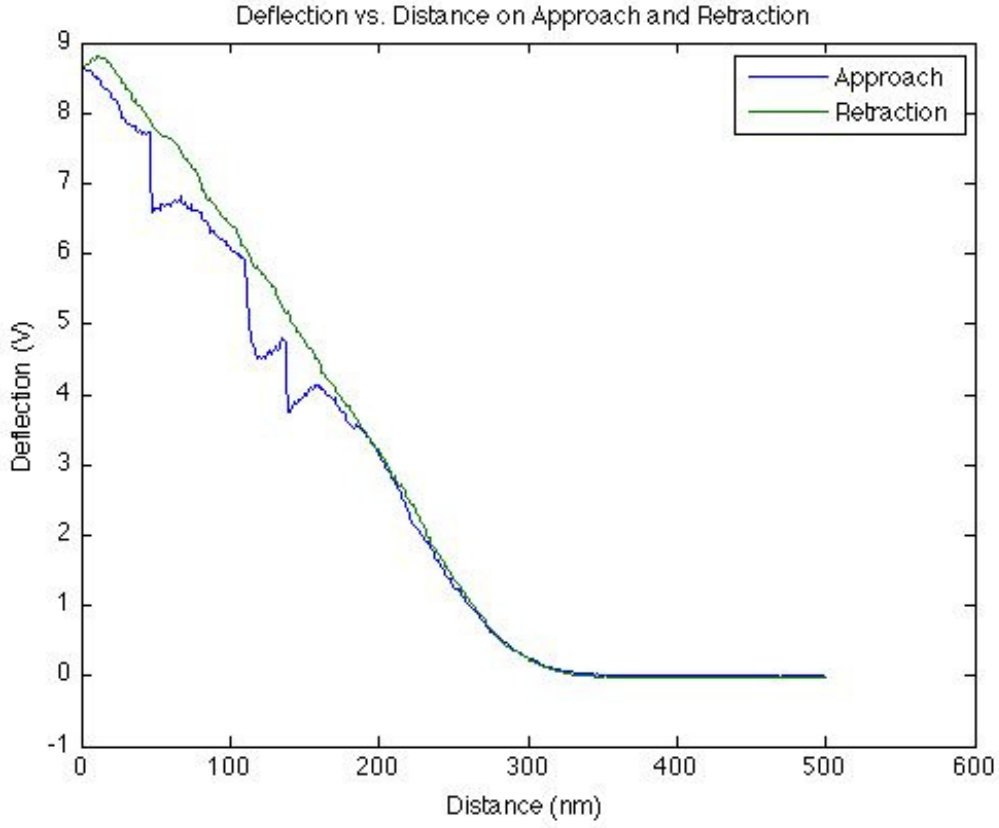
Deflection vs. Distance on Approach and Retraction
Approach
Retraction
Deflection (V)
Distance (nm)
9
8
7
6
5
4
3
2
1
0
-1
0
100
200
300
400
500
600

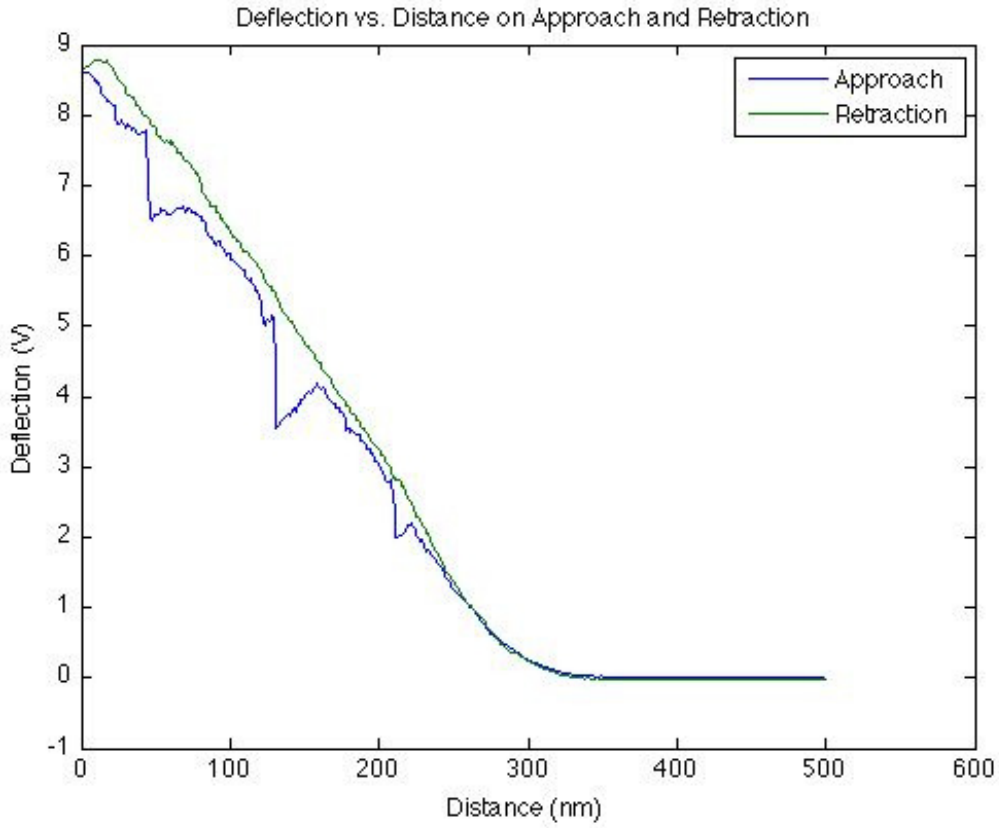
Deflection vs. Distance on Approach and Retraction
Approach
Retraction
Deflection (V)
Distance (nm)
9
8
7
6
5
4
3
2
1
0
-1
0
100
200
300
400
500
600

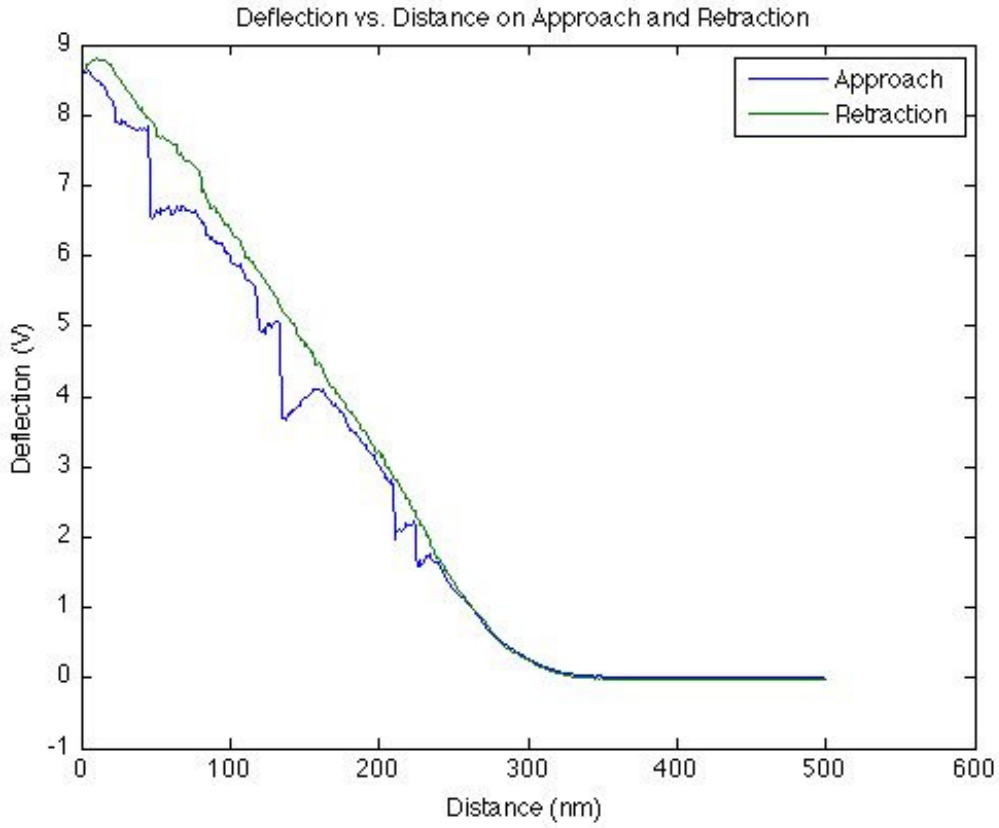
Deflection vs. Distance on Approach and Retraction
Approach
Retraction
Deflection (V)
Distance (nm)
9
8
7
6
5
4
3
2
1
0
-1
0
100
200
300
400
500
600

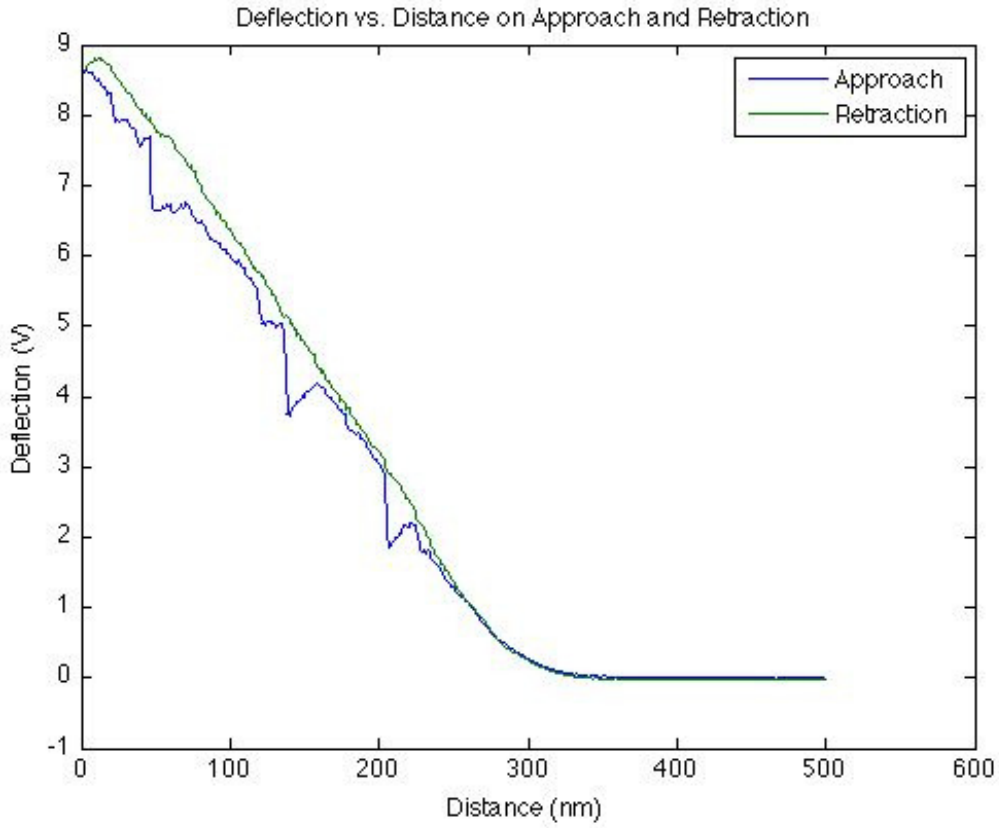
Deflection vs. Distance on Approach and Retraction
Approach
Retraction
Deflection (V)
Distance (nm)
9
8
7
6
5
4
3
2
1
0
-1
0
100
200
300
400
500
600

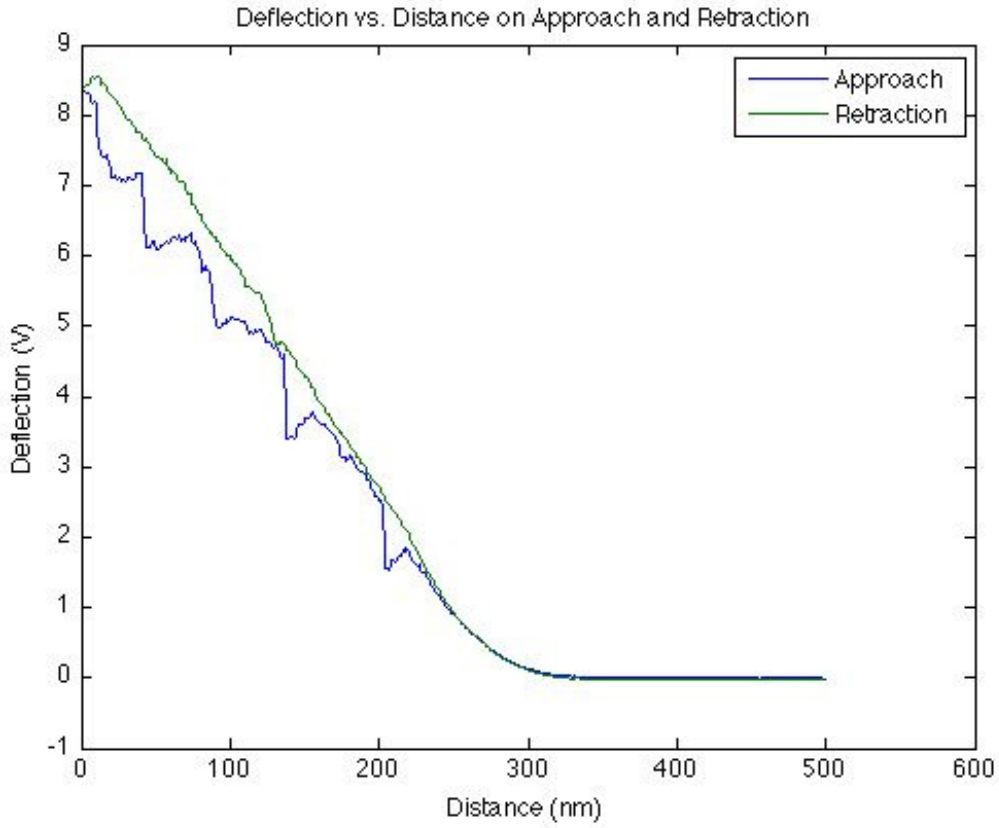
Deflection vs. Distance on Approach and Retraction
Approach
Retraction
Deflection (V)
Distance (nm)
9
8
7
6
5
4
3
2
1
0
-1
0
100
200
300
400
500
600

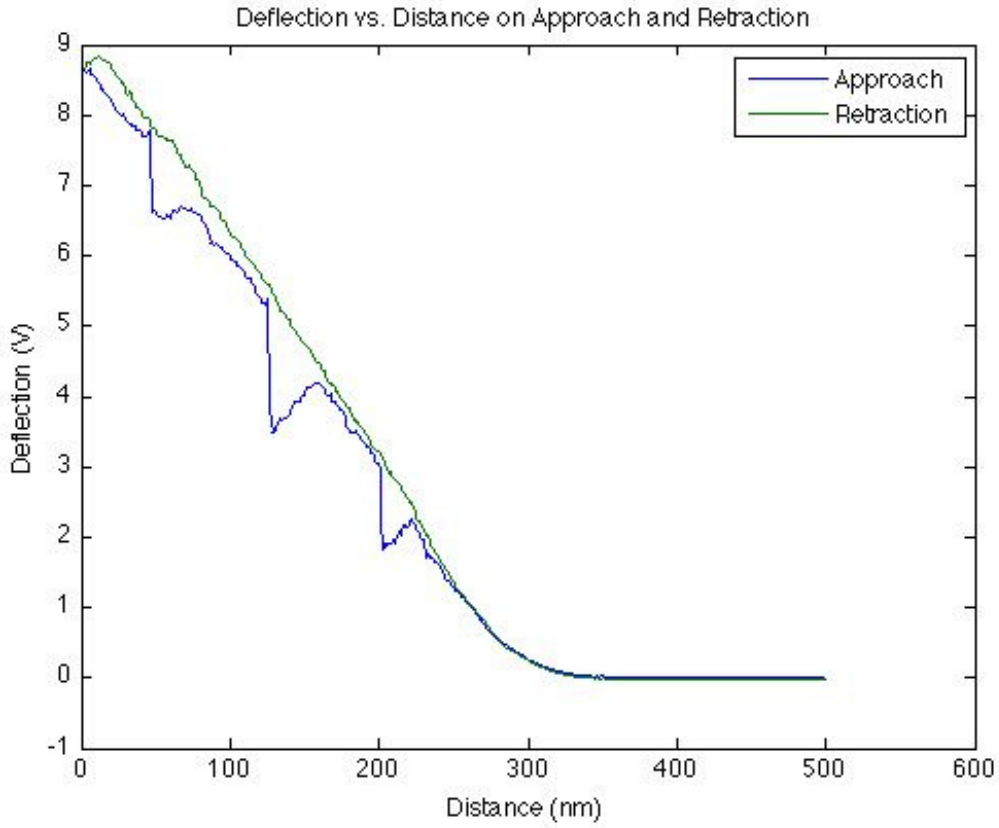
Deflection vs. Distance on Approach and Retraction
Approach
Retraction
Deflection (V)
Distance (nm)
9
8
7
6
5
4
3
2
1
0
-1
0
100
200
300
400
500
600

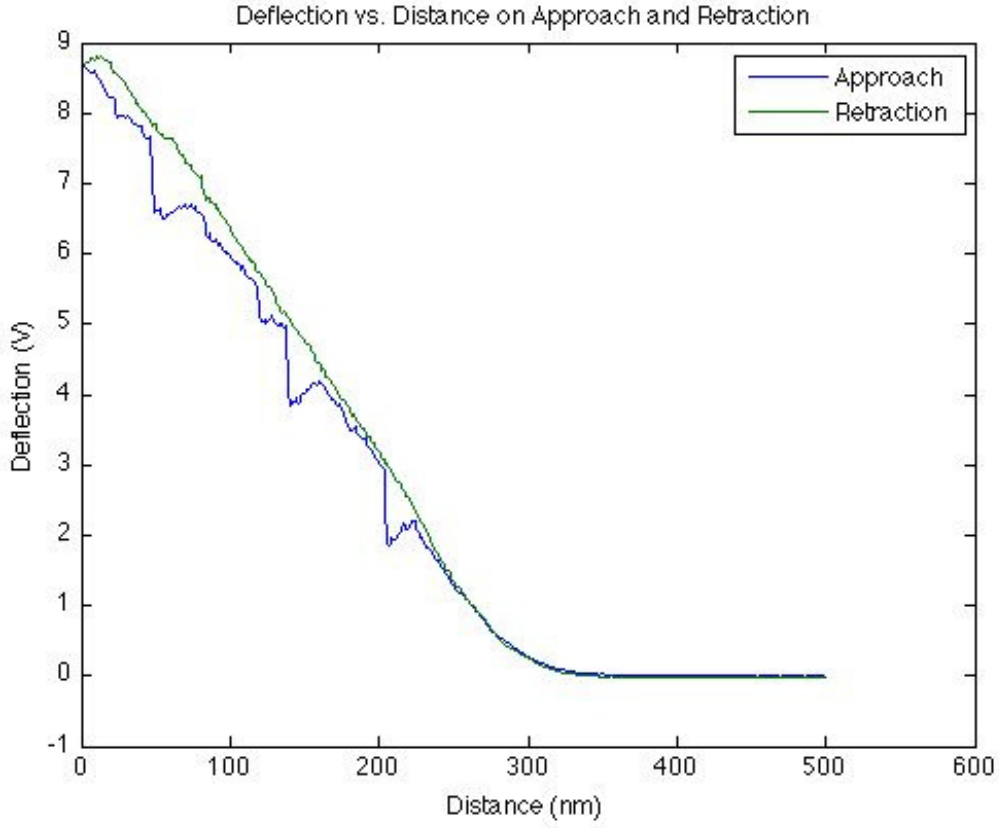
Deflection vs. Distance on Approach and Retraction
Approach
Retraction
Deflection (V)
Distance (nm)
9
8
7
6
5
4
3
2
1
0
-1
0
100
200
300
400
500
600

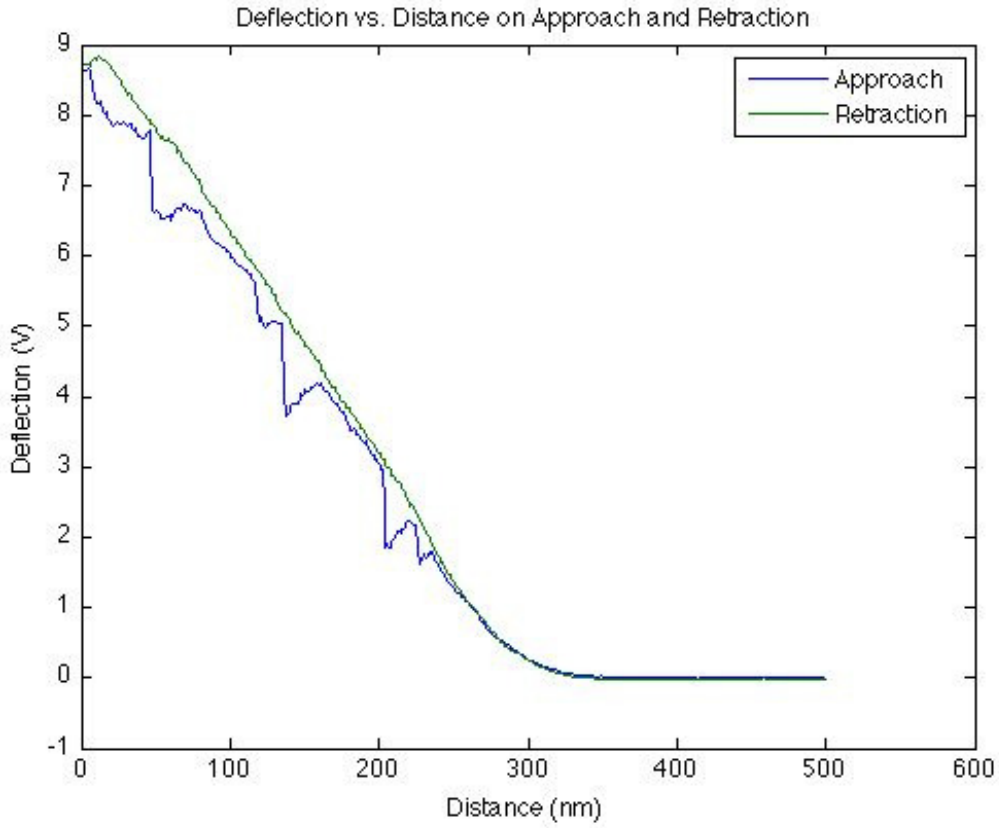
Deflection vs. Distance on Approach and Retraction
Approach
Retraction
Deflection (V)
Distance (nm)
9
8
7
6
5
4
3
2
1
0
-1
0
100
200
300
400
500
600

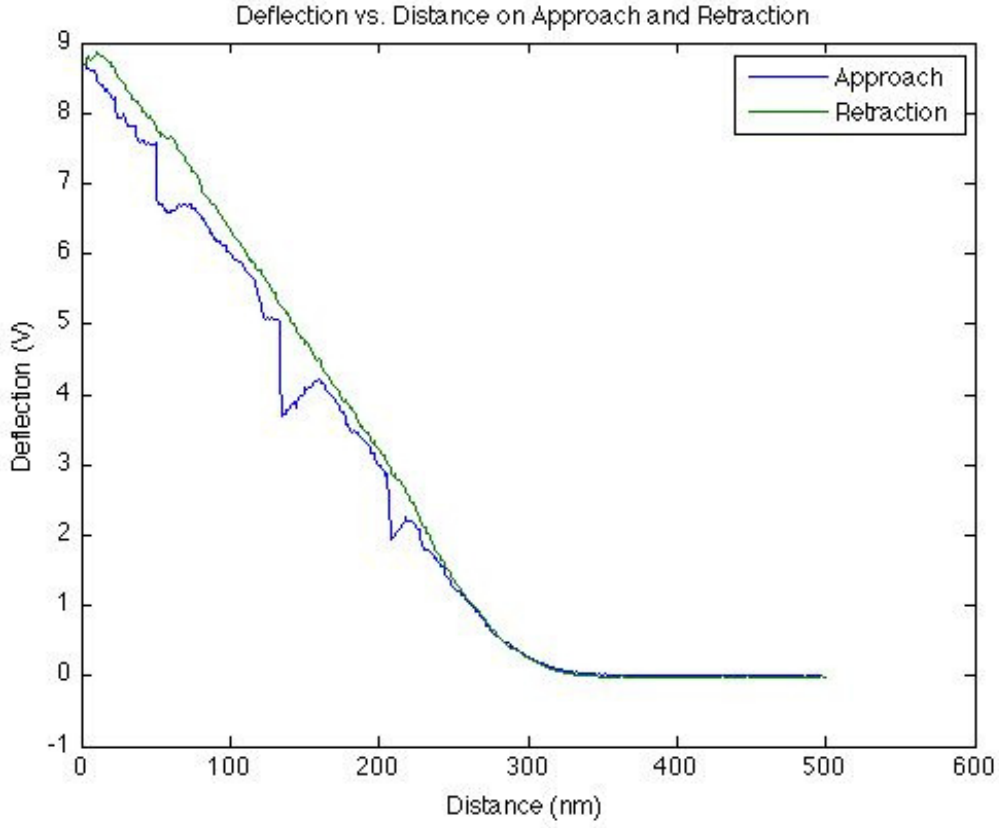
Deflection vs. Distance on Approach and Retraction
Approach
Retraction
Deflection (V)
Distance (nm)
9
8
7
6
5
4
3
2
1
0
-1
0
100
200
300
400
500
600

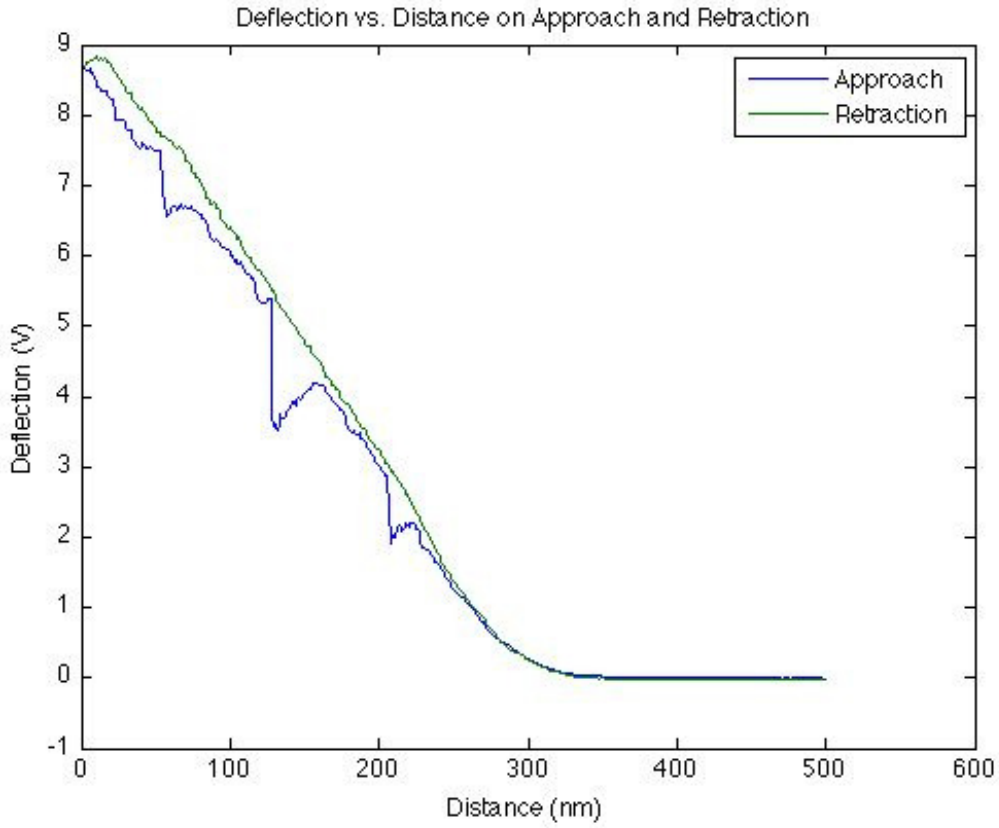
Deflection vs. Distance on Approach and Retraction
Approach
Retraction
Deflection (V)
Distance (nm)
9
8
7
6
5
4
3
2
1
0
-1
0
100
200
300
400
500
600

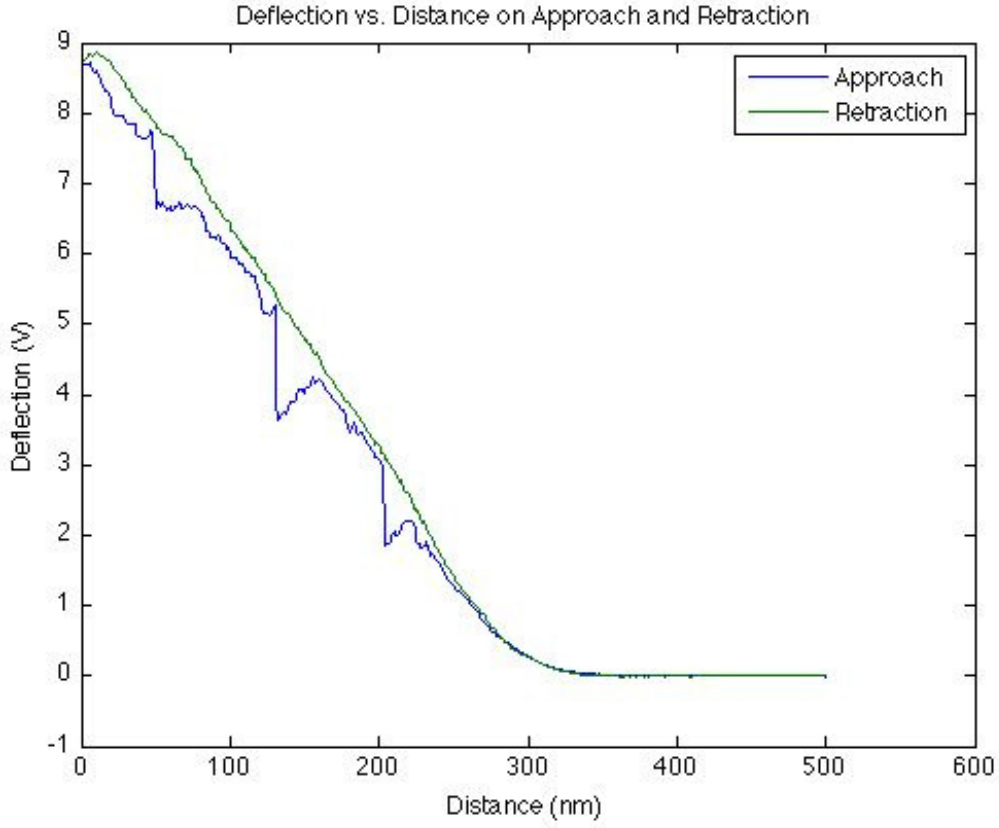
Deflection vs. Distance on Approach and Retraction
Approach
Retraction
Deflection (V)
Distance (nm)
9
8
7
6
5
4
3
2
1
0
-1
0
100
200
300
400
500
600

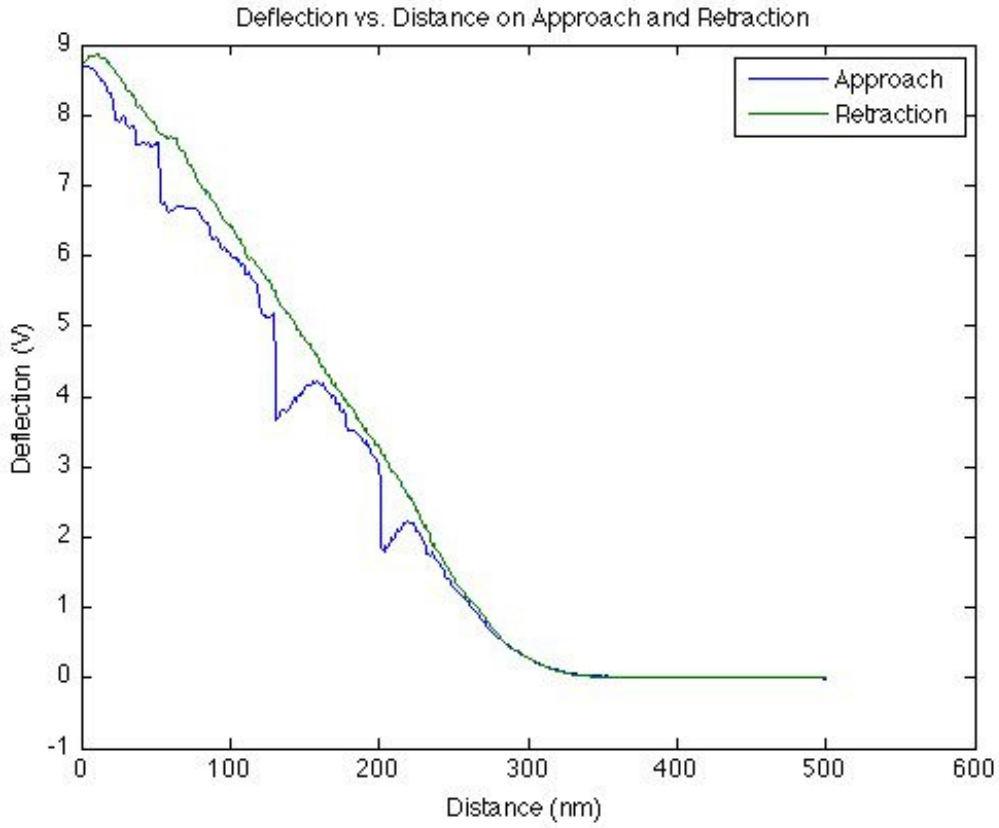
Deflection vs. Distance on Approach and Retraction
Approach
Retraction
Deflection (V)
Distance (nm)
9
8
7
6
5
4
3
2
1
0
-1
0
100
200
300
400
500
600

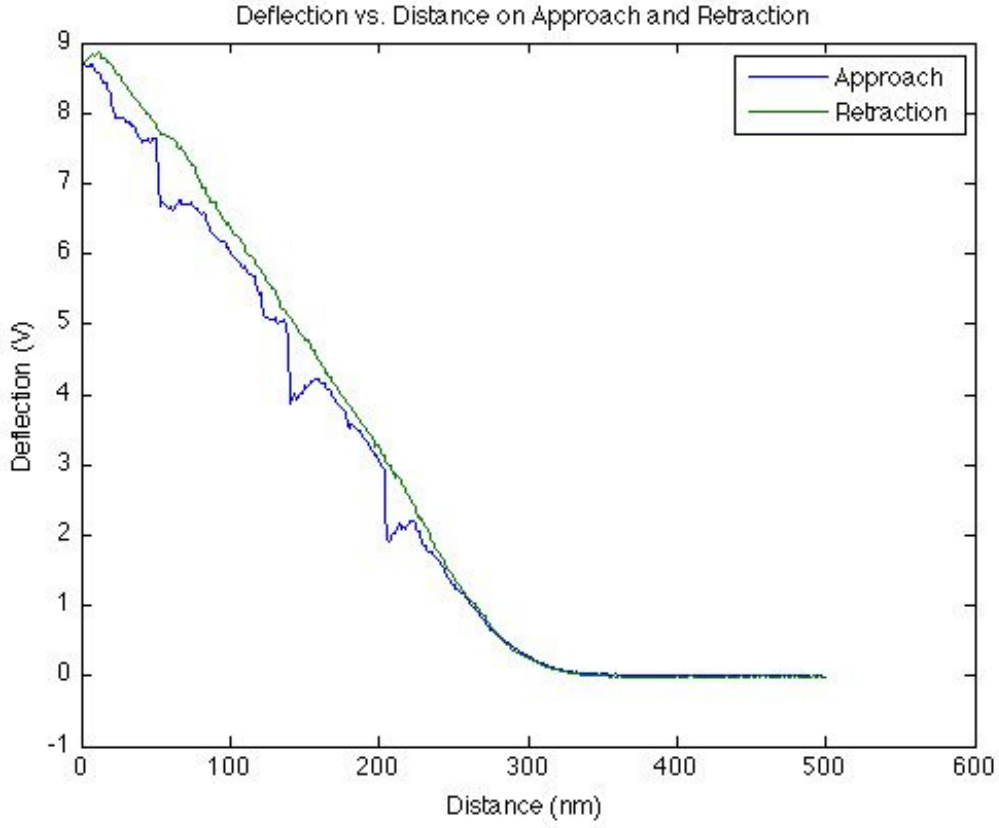
Deflection vs. Distance on Approach and Retraction
Approach
Retraction
Deflection (V)
Distance (nm)
9
8
7
6
5
4
3
2
1
0
-1
0
100
200
300
400
500
600

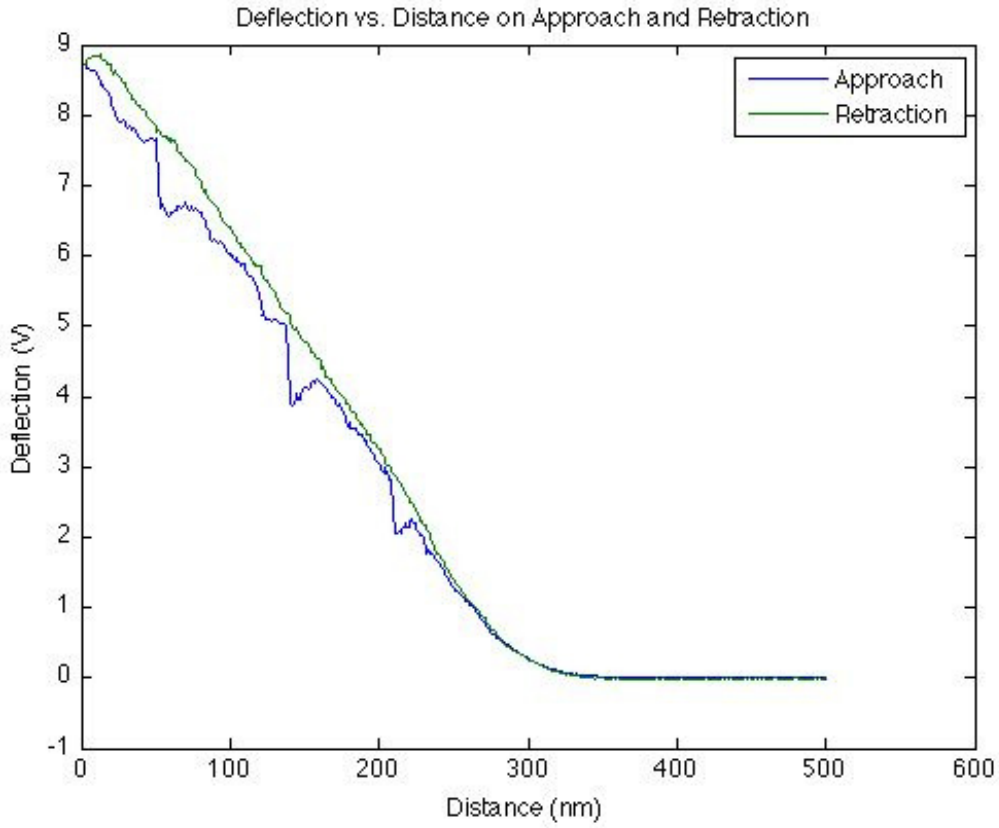
Deflection vs. Distance on Approach and Retraction
Approach
Retraction
Deflection (V)
Distance (nm)
9
8
7
6
5
4
3
2
1
0
-1
0
100
200
300
400
500
600

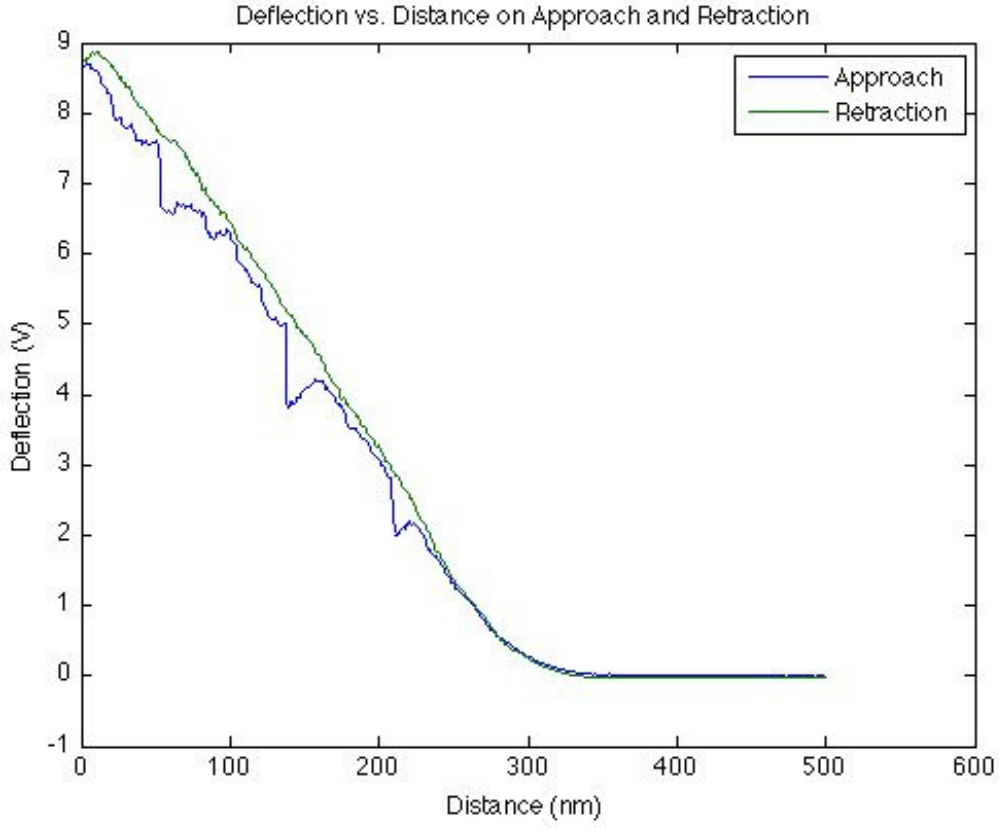
Deflection vs. Distance on Approach and Retraction
Approach
Retraction
Deflection (V)
Distance (nm)
9
8
7
6
5
4
3
2
1
0
-1
0
100
200
300
400
500
600

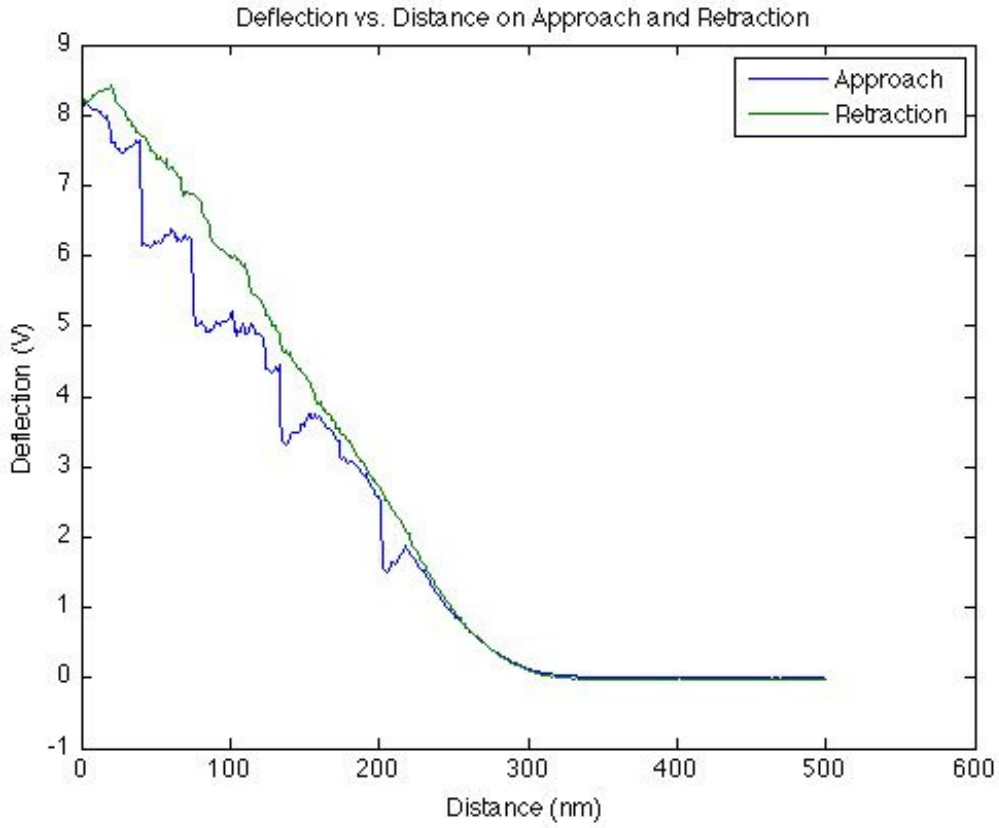
Deflection vs. Distance on Approach and Retraction
Approach
Retraction
Deflection (V)
Distance (nm)
9
8
7
6
5
4
3
2
1
0
-1
0
100
200
300
400
500
600

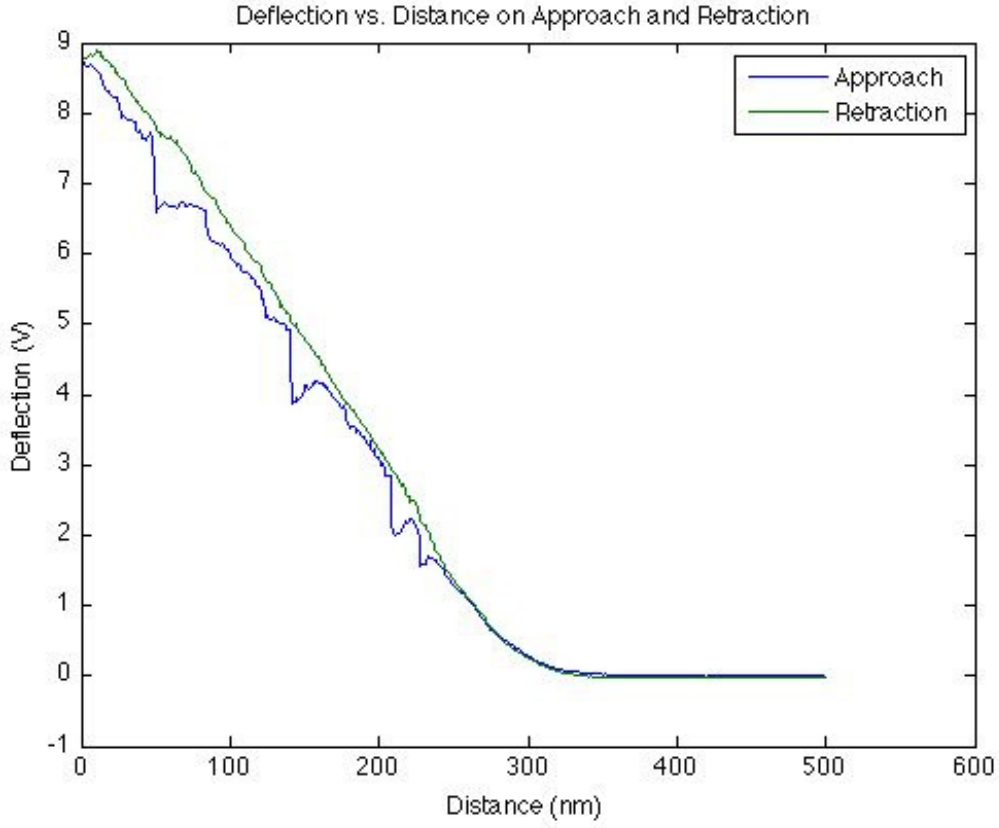
Deflection vs. Distance on Approach and Retraction
Approach
Retraction
Deflection (V)
Distance (nm)
9
8
7
6
5
4
3
2
1
0
-1
0
100
200
300
400
500
600

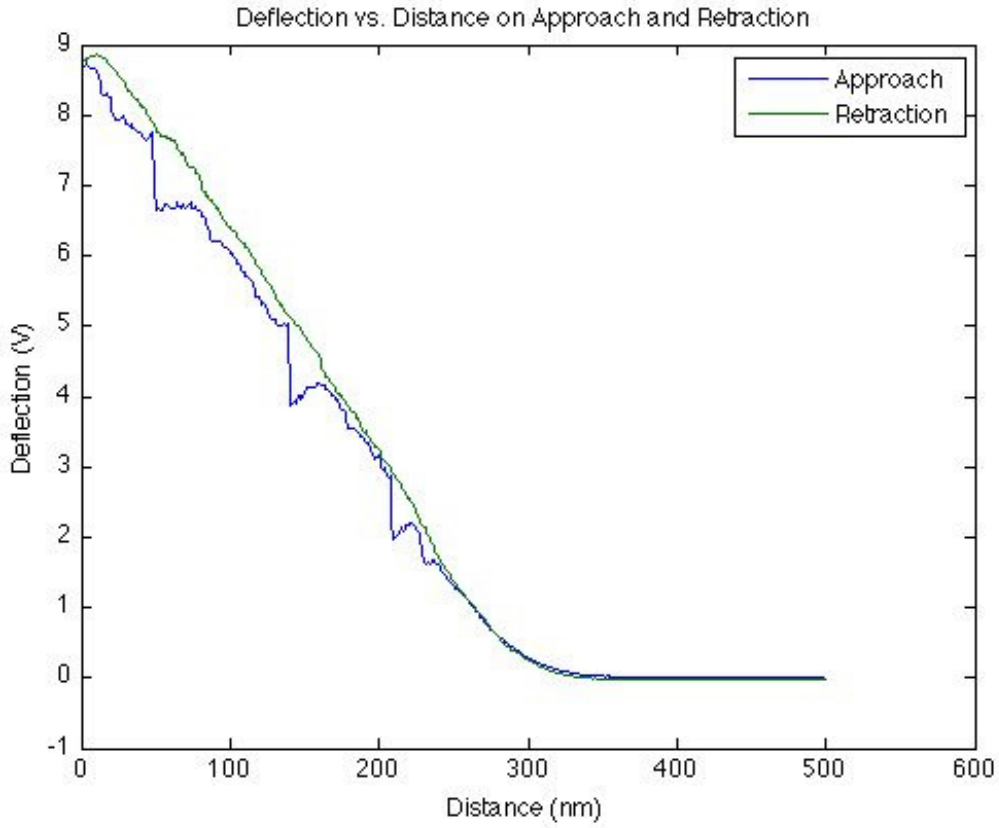
Deflection vs. Distance on Approach and Retraction
Approach
Retraction
Deflection (V)
Distance (nm)
9
8
7
6
5
4
3
2
1
0
-1
0
100
200
300
400
500
600

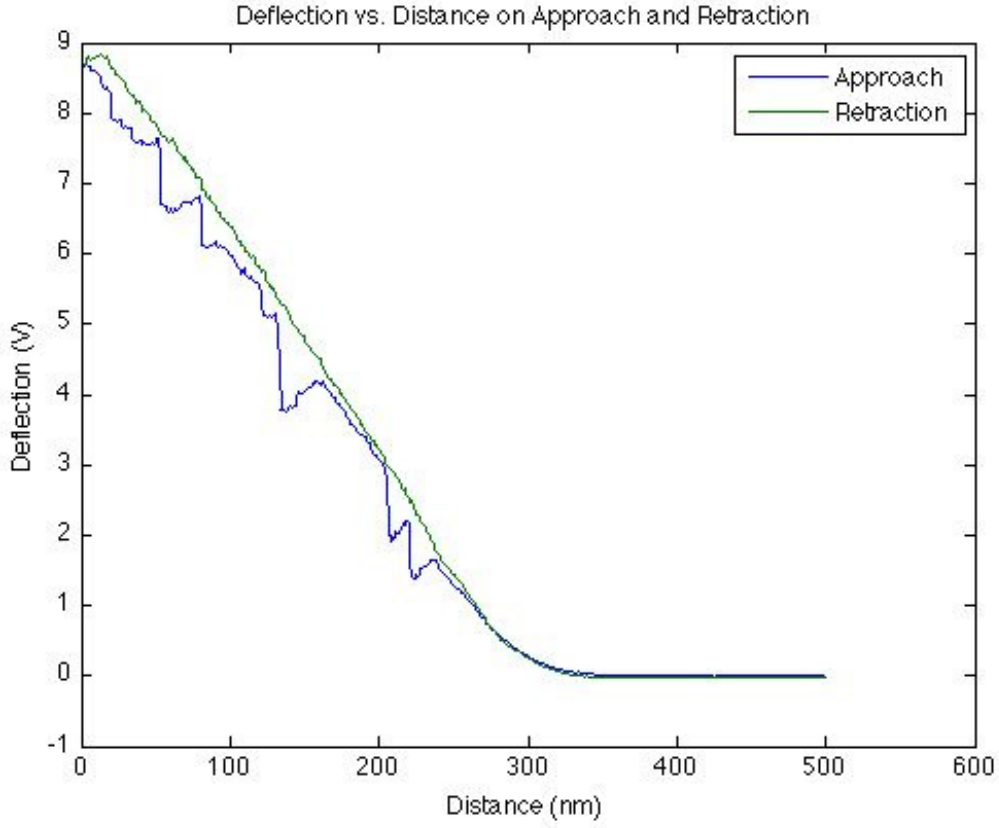
Deflection vs. Distance on Approach and Retraction
Approach
Retraction
Deflection (V)
Distance (nm)
9
8
7
6
5
4
3
2
1
0
-1
0
100
200
300
400
500
600

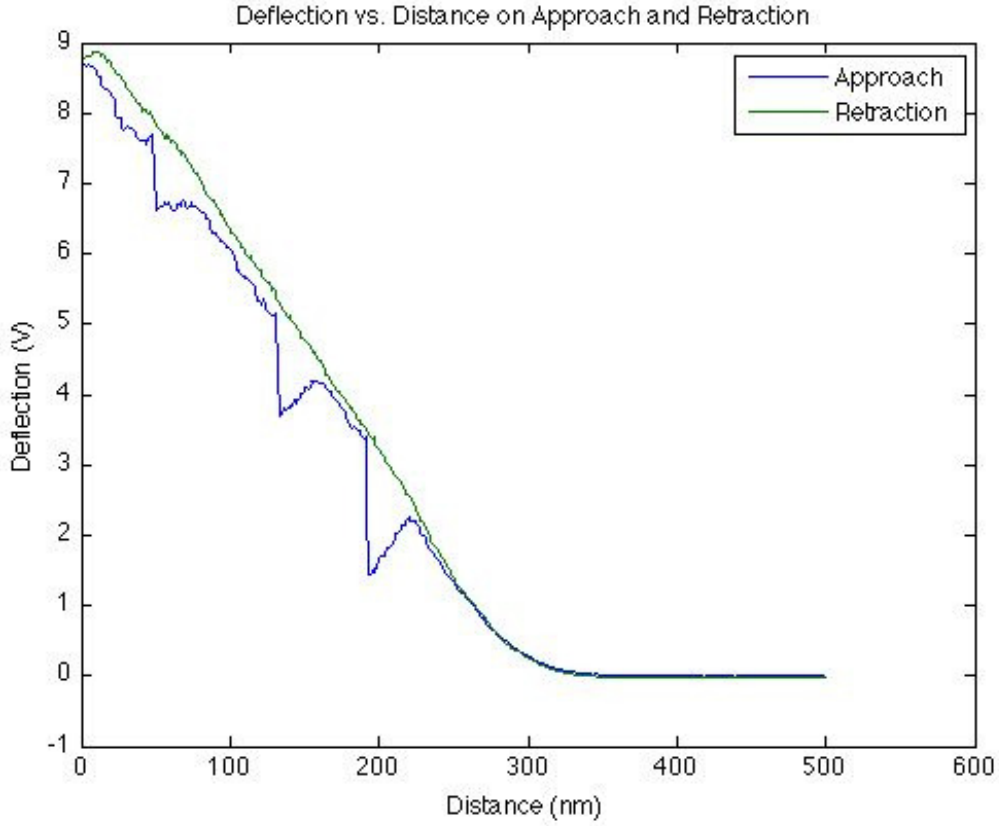
Deflection vs. Distance on Approach and Retraction
Approach
Retraction
Deflection (V)
Distance (nm)
9
8
7
6
5
4
3
2
1
0
-1
0
100
200
300
400
500
600

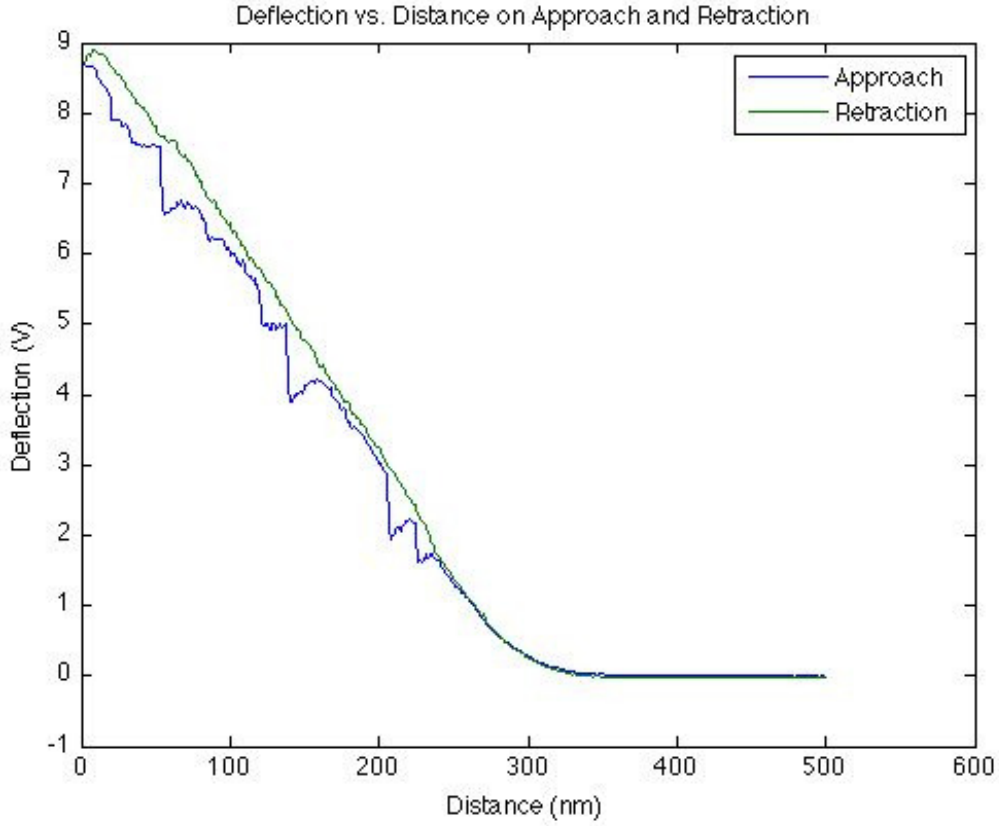
Deflection vs. Distance on Approach and Retraction
Approach
Retraction
Deflection (V)
Distance (nm)
9
8
7
6
5
4
3
2
1
0
-1
0
100
200
300
400
500
600

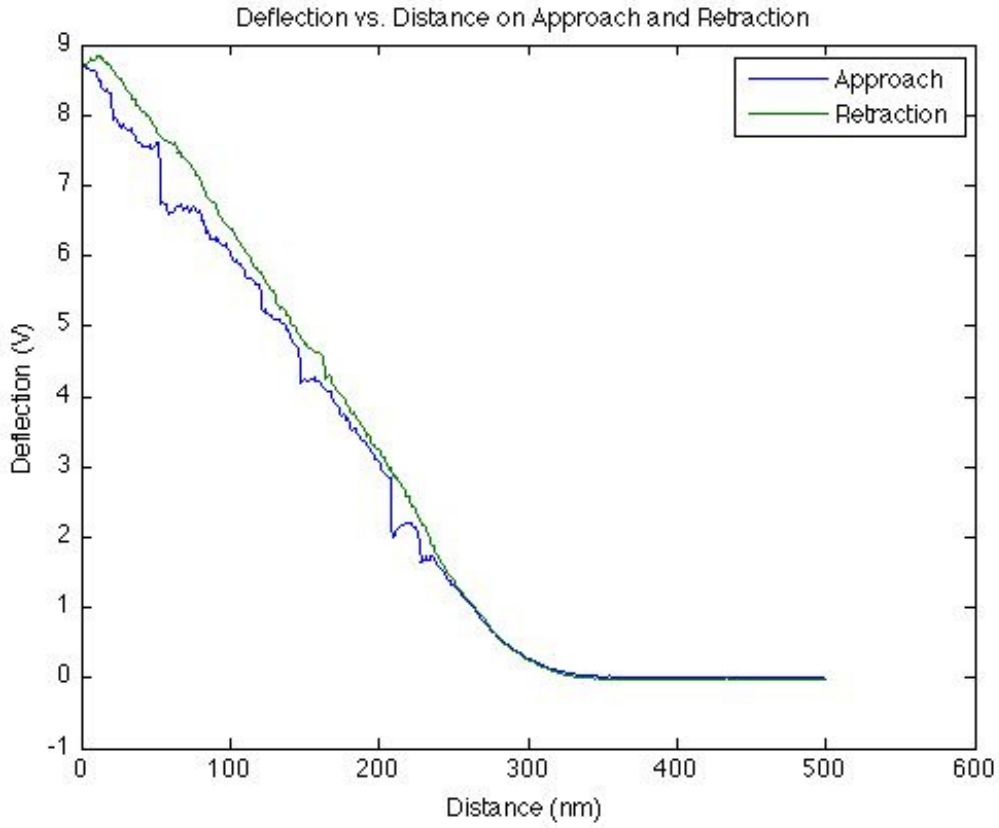
Deflection vs. Distance on Approach and Retraction
Approach
Retraction
Deflection (V)
Distance (nm)
9
8
7
6
5
4
3
2
1
0
-1
0
100
200
300
400
500
600

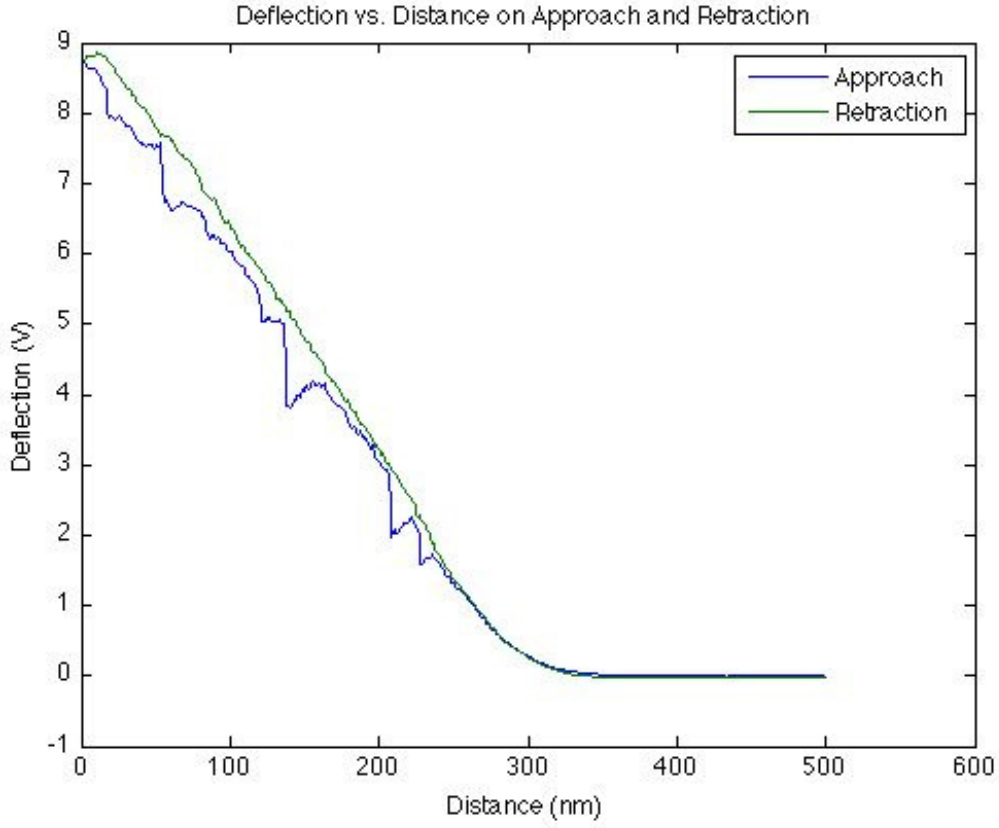
Deflection vs. Distance on Approach and Retraction
Approach
Retraction
Deflection (V)
Distance (nm)
9
8
7
6
5
4
3
2
1
0
-1
0
100
200
300
400
500
600

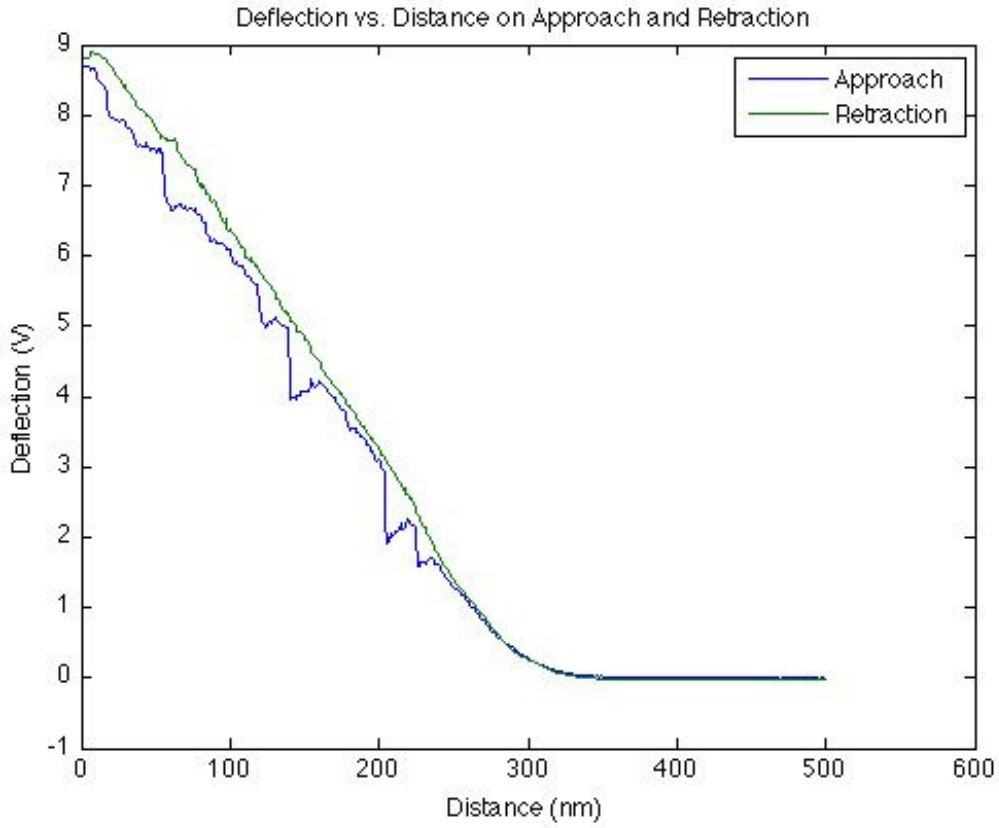
Deflection vs. Distance on Approach and Retraction
Approach
Retraction
Deflection (V)
Distance (nm)
9
8
7
6
5
4
3
2
1
0
-1
0
100
200
300
400
500
600

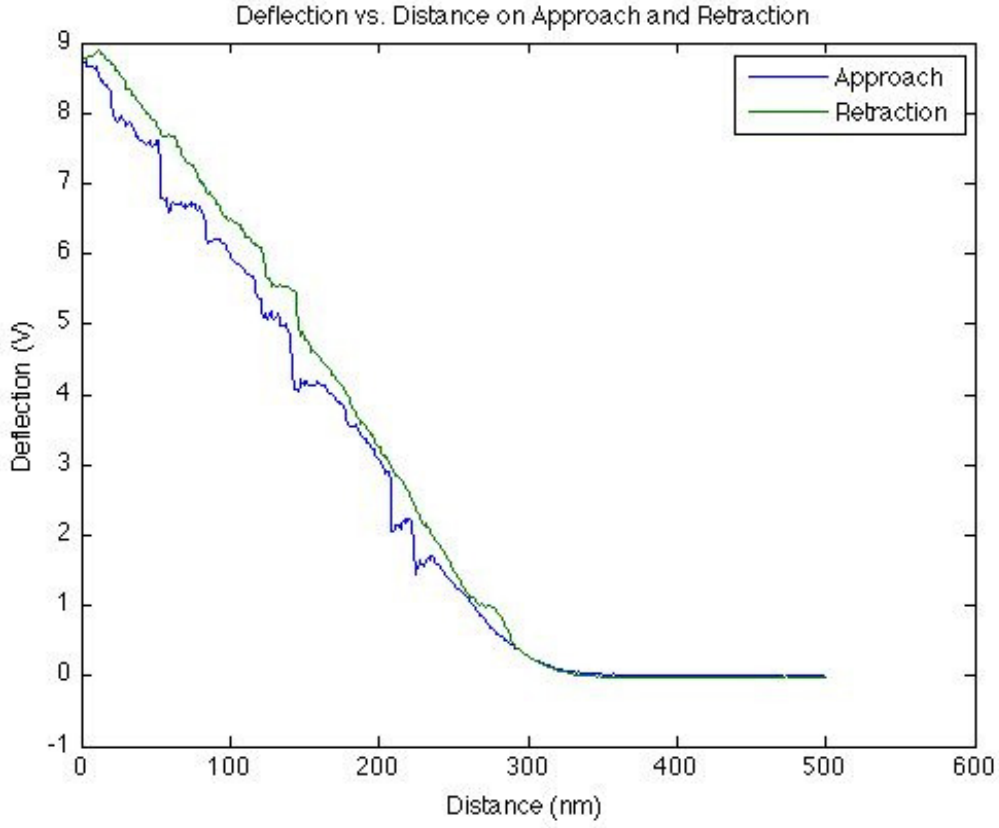
Deflection vs. Distance on Approach and Retraction
Approach
Retraction
Deflection (V)
Distance (nm)
9
8
7
6
5
4
3
2
1
0
-1
0
100
200
300
400
500
600

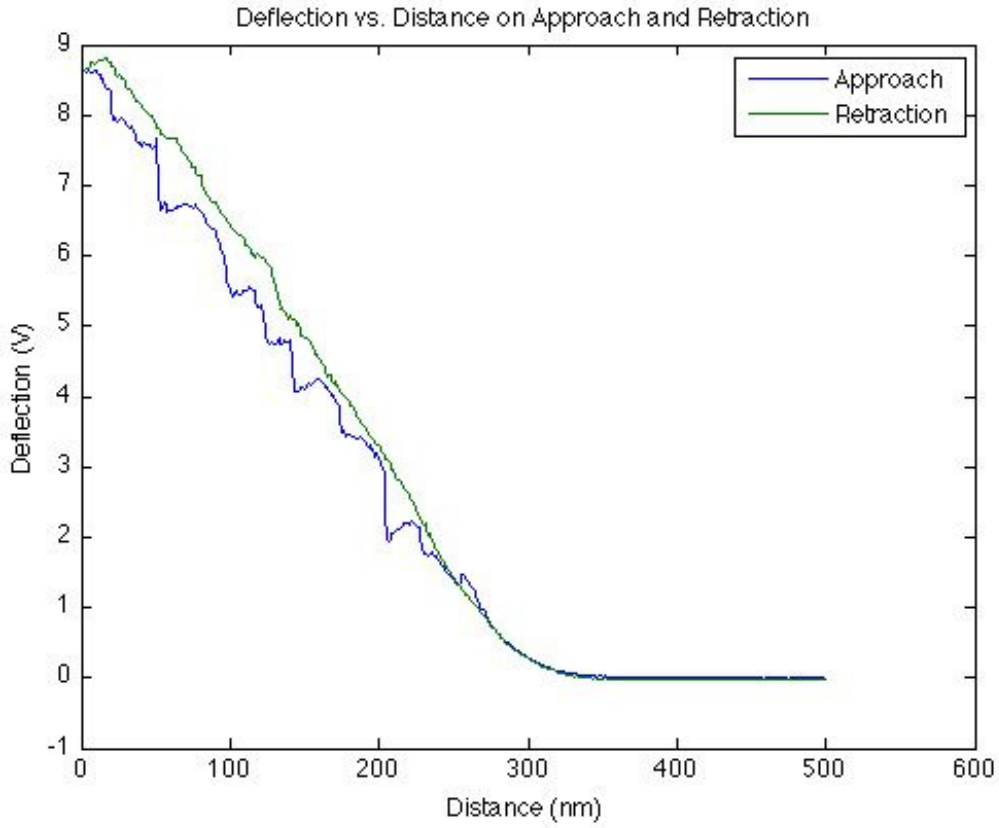
Deflection vs. Distance on Approach and Retraction
Approach
Retraction
Deflection (V)
Distance (nm)
9
8
7
6
5
4
3
2
1
0
-1
0
100
200
300
400
500
600

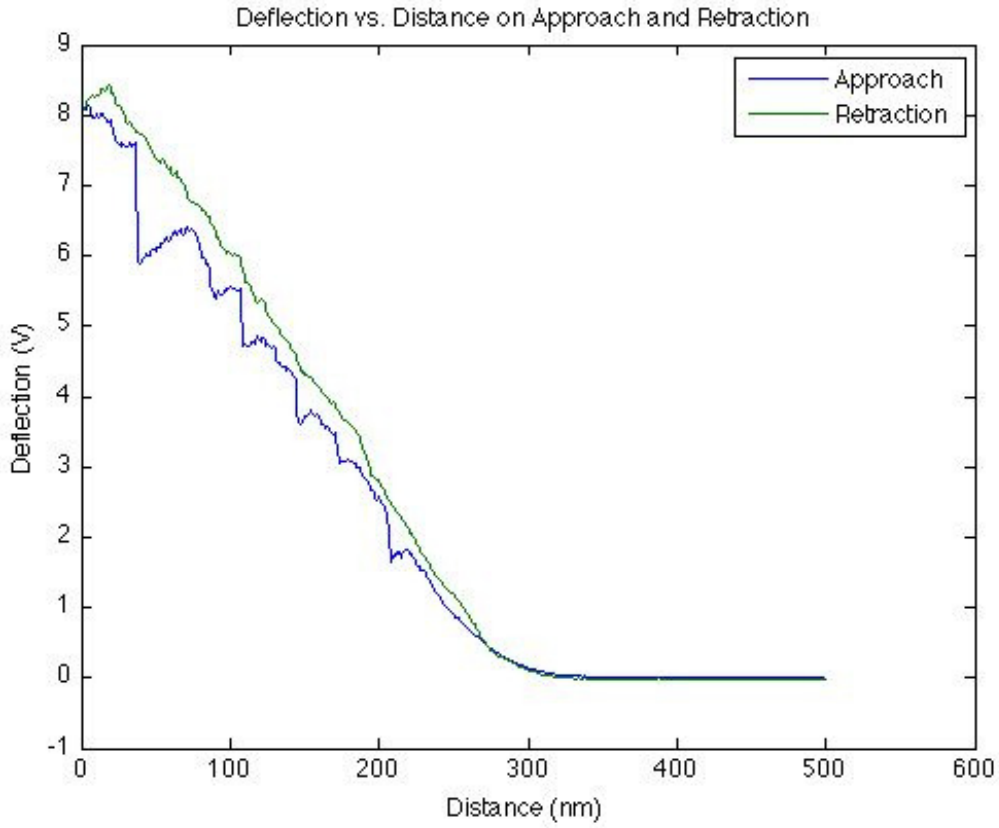
Deflection vs. Distance on Approach and Retraction
Approach
Retraction
Deflection (V)
Distance (nm)
9
8
7
6
5
4
3
2
1
0
-1
0
100
200
300
400
500
600

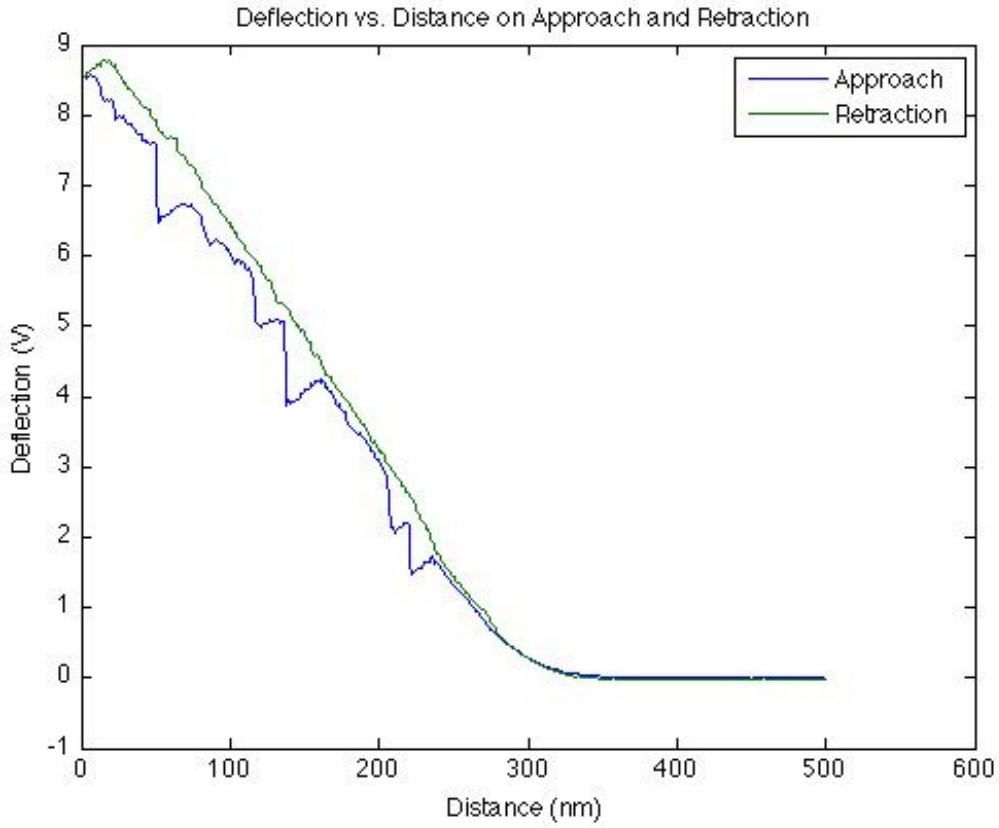
Deflection vs. Distance on Approach and Retraction
Approach
Retraction
Deflection (V)
Distance (nm)
9
8
7
6
5
4
3
2
1
0
-1
0
100
200
300
400
500
600

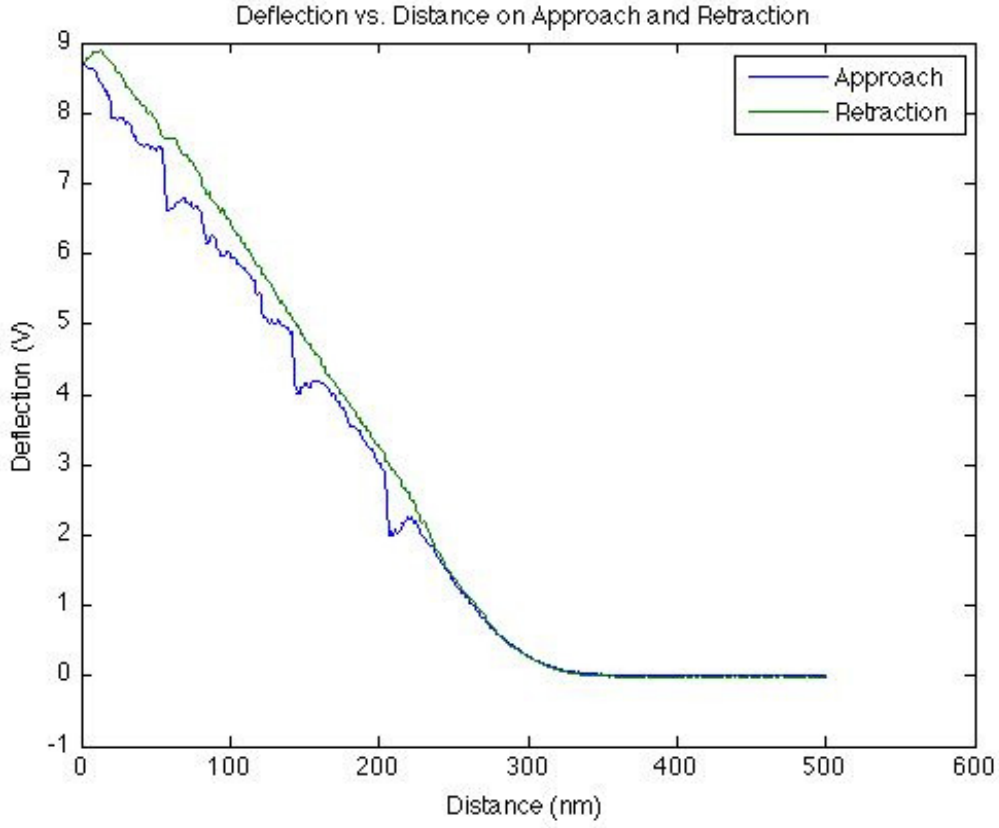
Deflection vs. Distance on Approach and Retraction
Approach
Retraction
Deflection (V)
Distance (nm)
9
8
7
6
5
4
3
2
1
0
-1
0
100
200
300
400
500
600

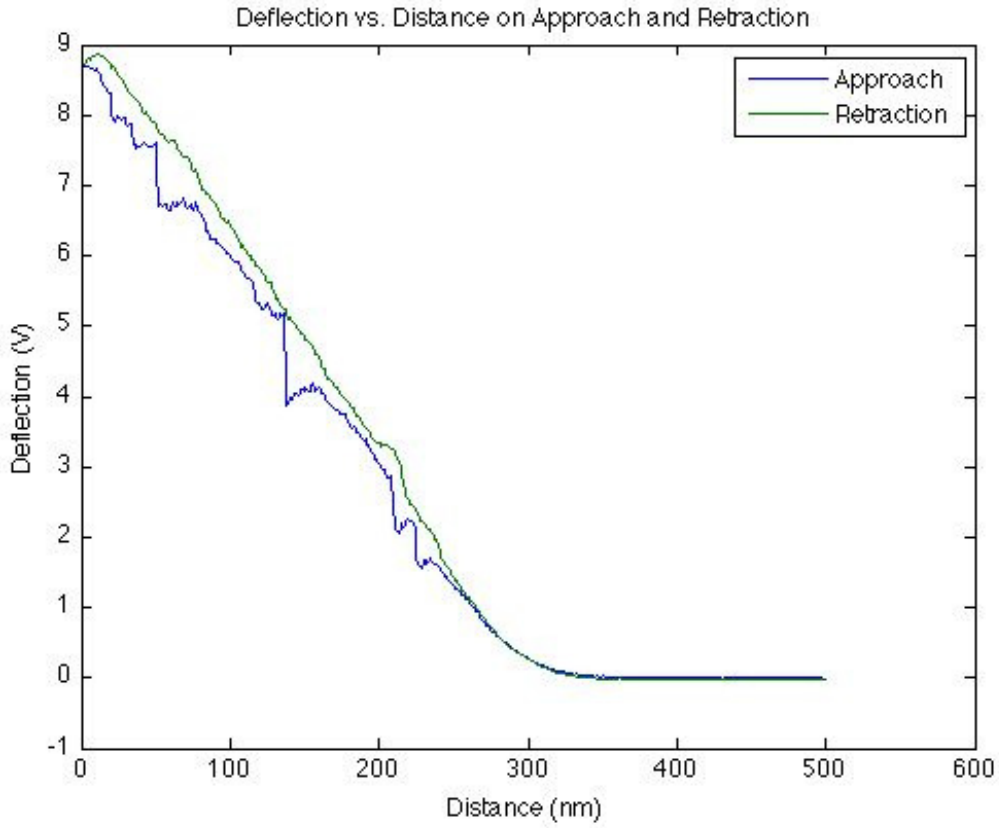
Deflection vs. Distance on Approach and Retraction
Approach
Retraction
Deflection (V)
Distance (nm)
9
8
7
6
5
4
3
2
1
0
-1
0
100
200
300
400
500
600

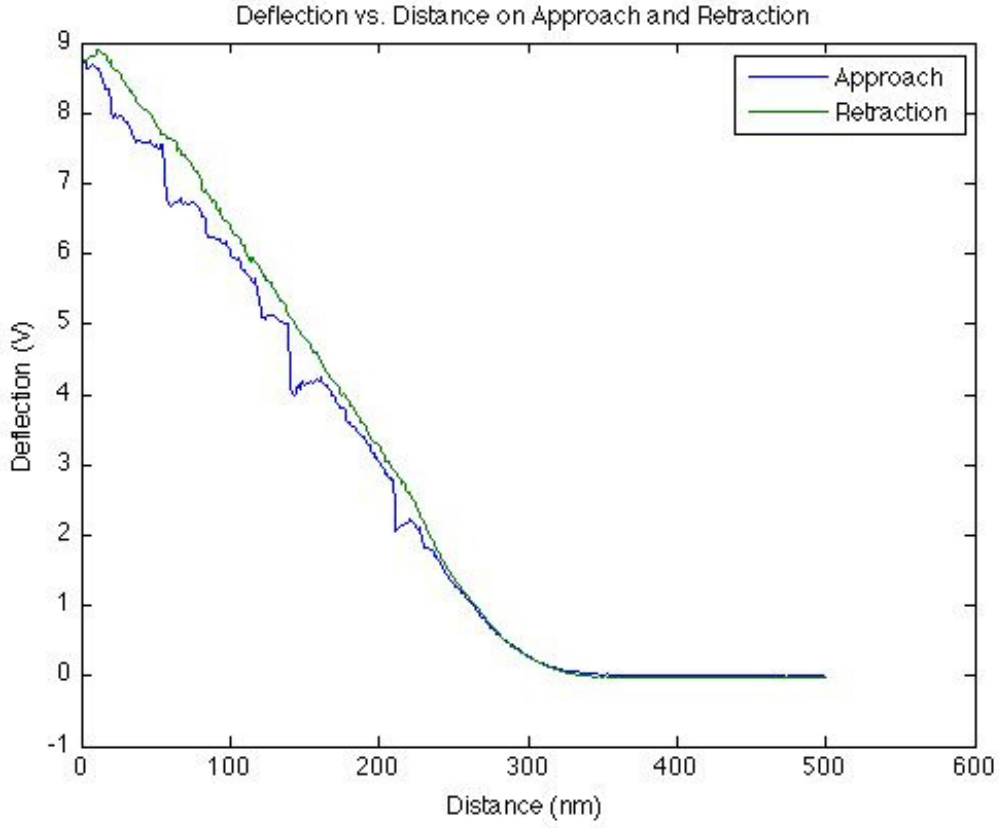
Deflection vs. Distance on Approach and Retraction
Approach
Retraction
Deflection (V)
Distance (nm)
9
8
7
6
5
4
3
2
1
0
-1
0
100
200
300
400
500
600

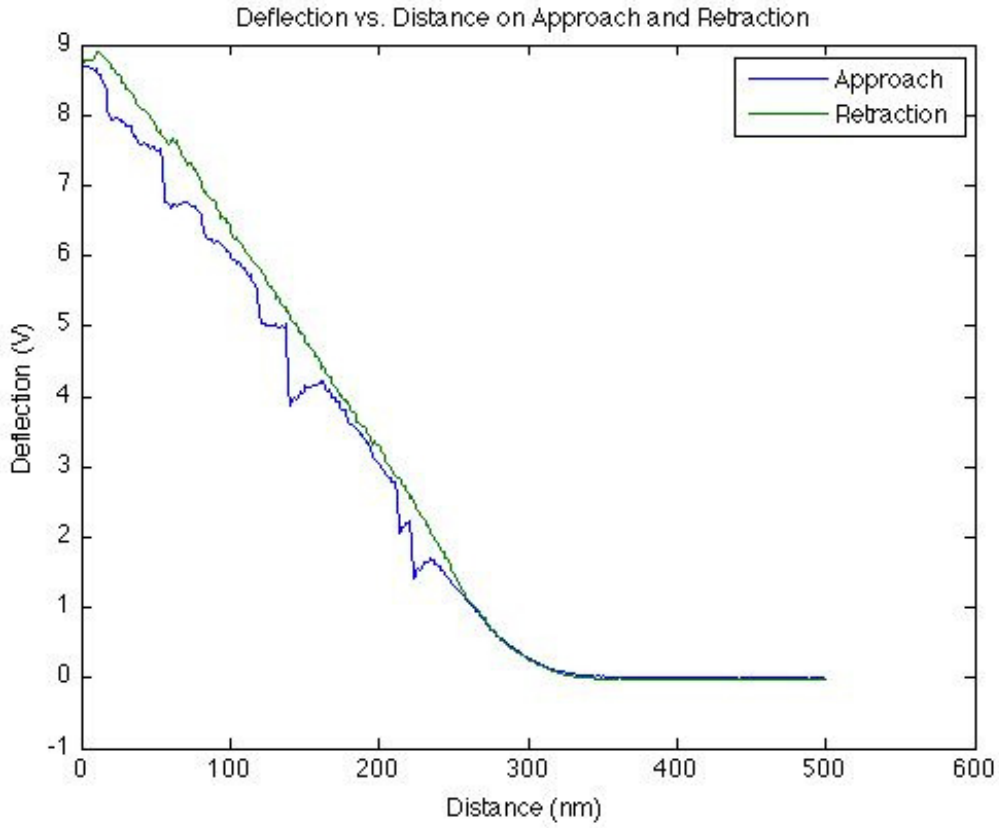
Deflection vs. Distance on Approach and Retraction
Approach
Retraction
Deflection (V)
Distance (nm)
9
8
7
6
5
4
3
2
1
0
-1
0
100
200
300
400
500
600

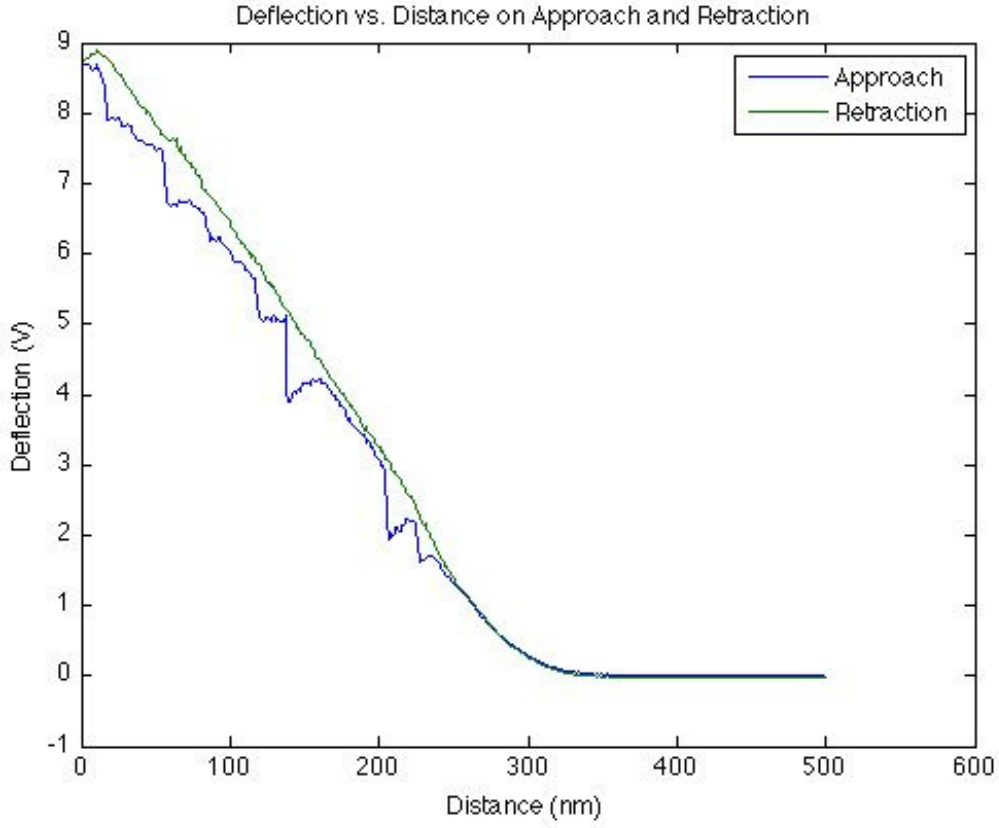
Deflection vs. Distance on Approach and Retraction
Approach
Retraction
Deflection (V)
Distance (nm)
9
8
7
6
5
4
3
2
1
0
-1
0
100
200
300
400
500
600

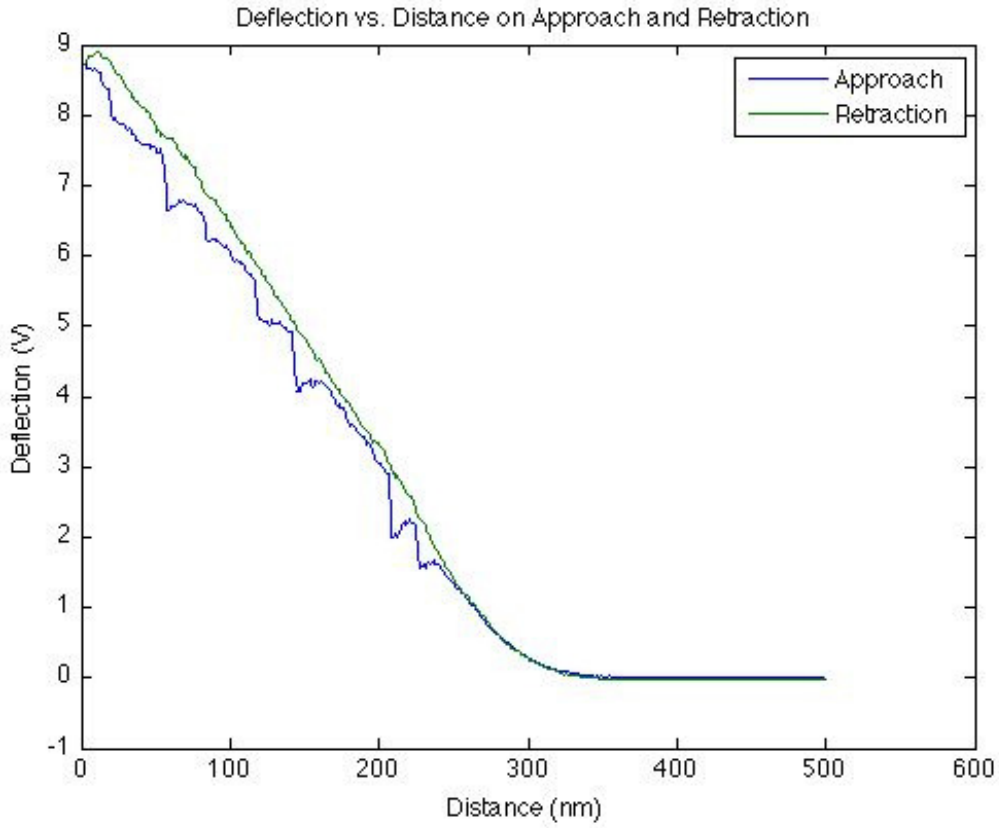
Deflection vs. Distance on Approach and Retraction
Approach
Retraction
Deflection (V)
Distance (nm)
9
8
7
6
5
4
3
2
1
0
-1
0
100
200
300
400
500
600

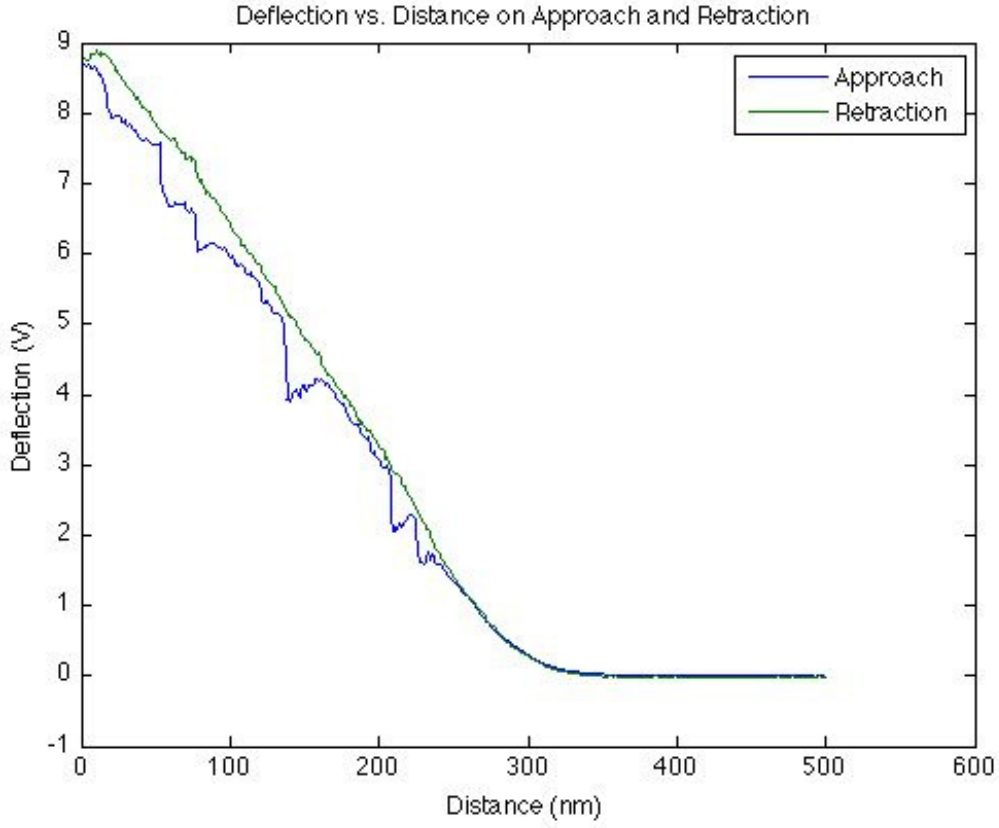
Deflection vs. Distance on Approach and Retraction
Approach
Retraction
Deflection (V)
Distance (nm)
9
8
7
6
5
4
3
2
1
0
-1
0
100
200
300
400
500
600

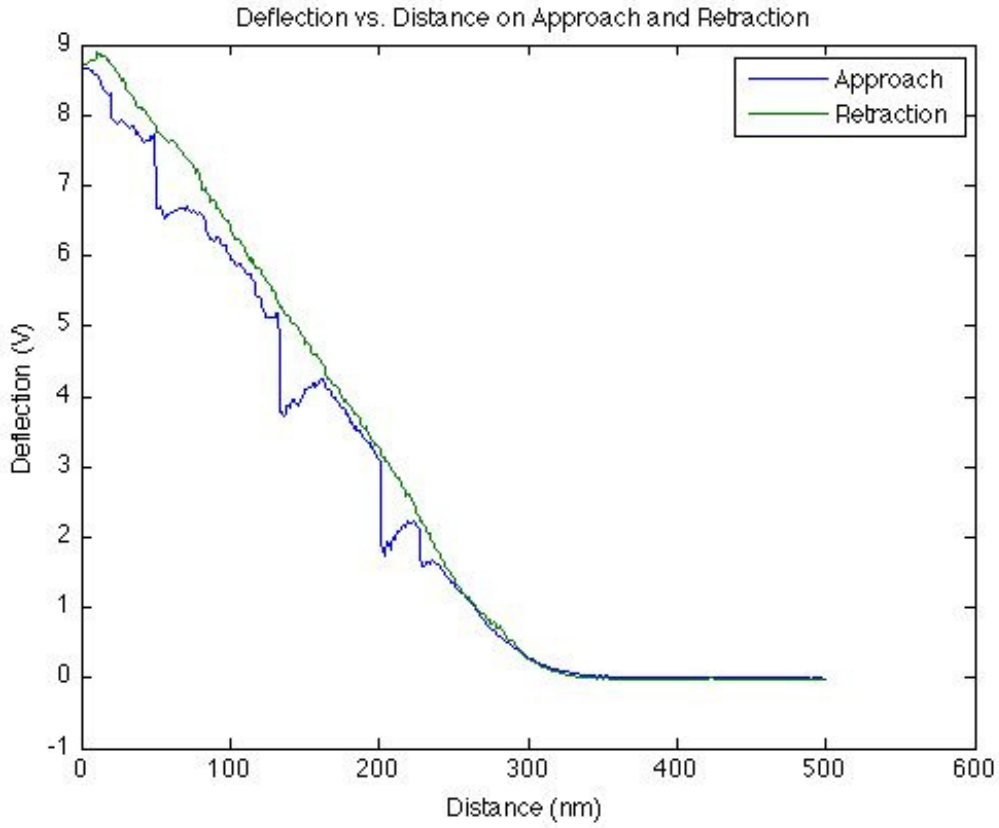
Deflection vs. Distance on Approach and Retraction
Approach
Retraction
Deflection (V)
Distance (nm)
9
8
7
6
5
4
3
2
1
0
-1
0
100
200
300
400
500
600

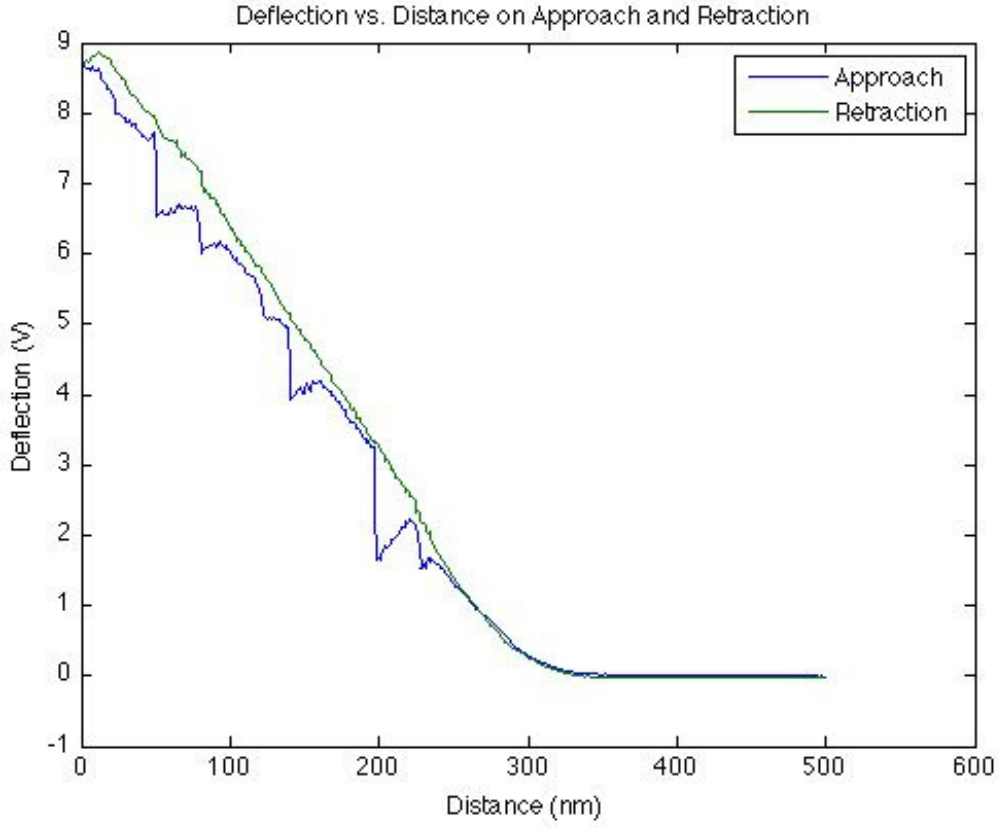
Deflection vs. Distance on Approach and Retraction
Approach
Retraction
Deflection (V)
Distance (nm)
9
8
7
6
5
4
3
2
1
0
-1
0
100
200
300
400
500
600

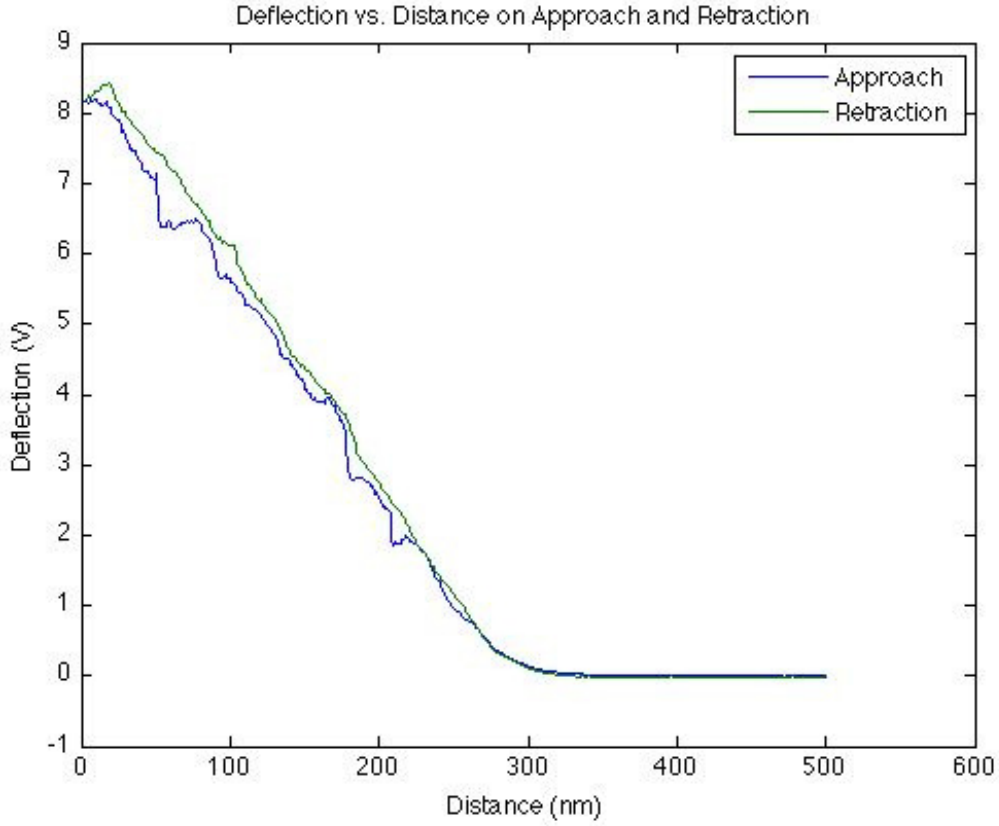
Deflection vs. Distance on Approach and Retraction
Approach
Retraction
Deflection (V)
Distance (nm)
9
8
7
6
5
4
3
2
1
0
-1
0
100
200
300
400
500
600

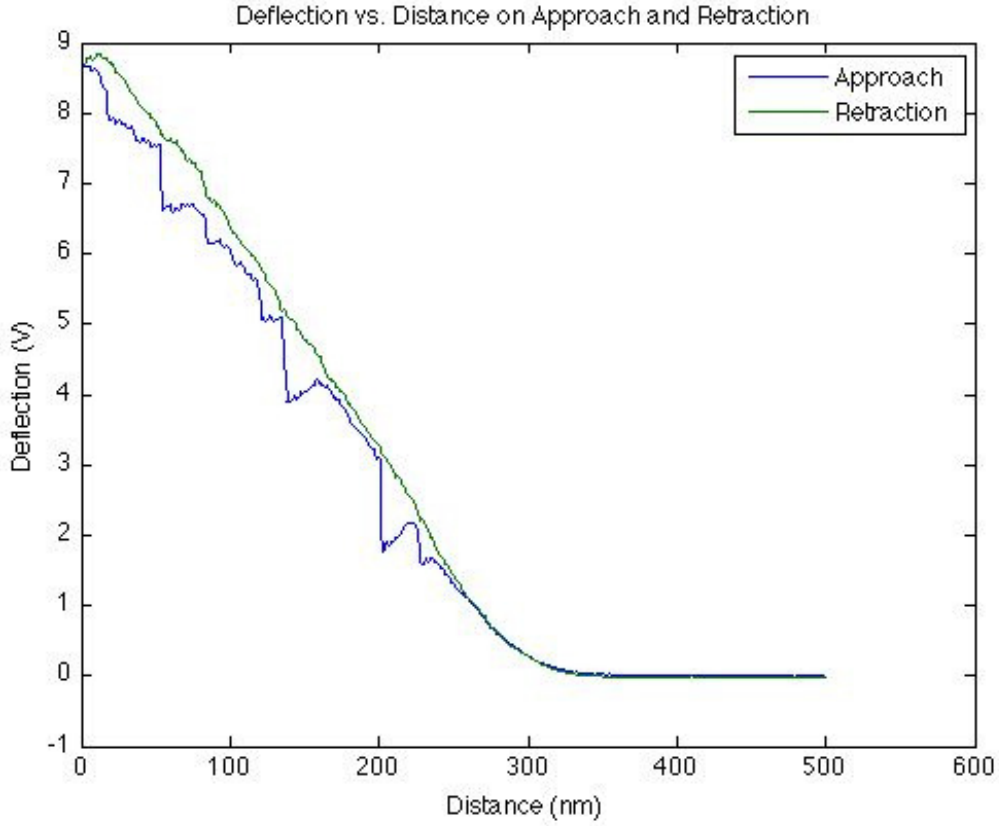
Deflection vs. Distance on Approach and Retraction
Approach
Retraction
Deflection (V)
Distance (nm)
9
8
7
6
5
4
3
2
1
0
-1
0
100
200
300
400
500
600

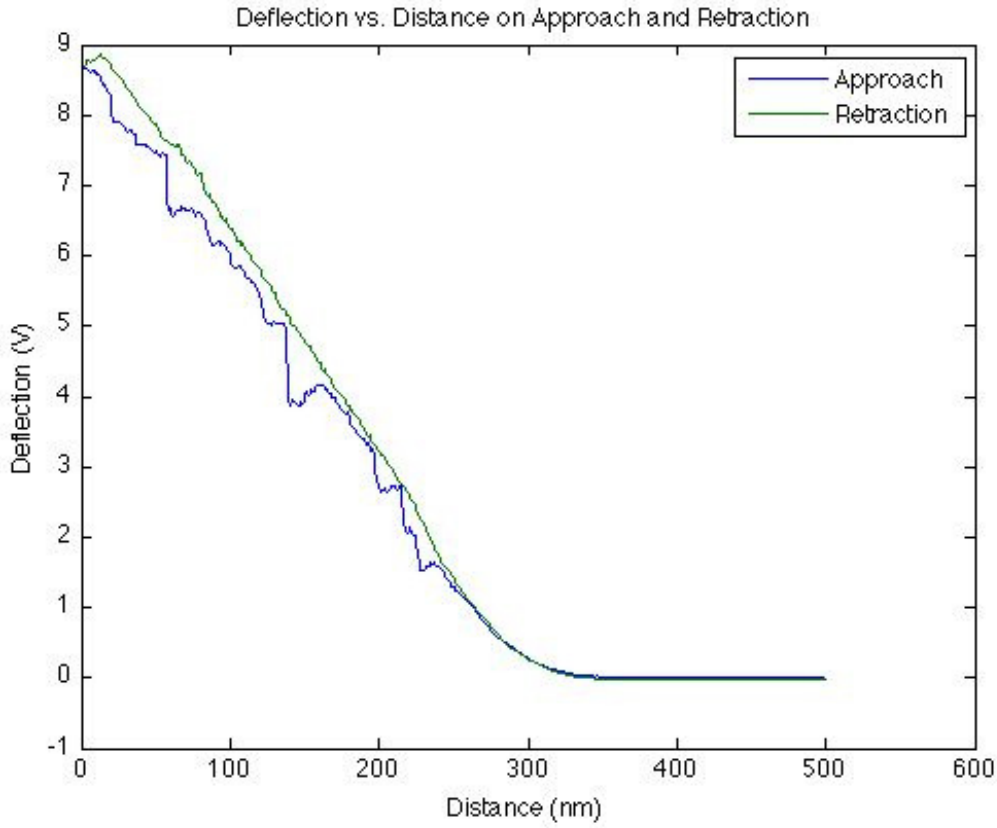
Deflection vs. Distance on Approach and Retraction
Approach
Retraction
Deflection (V)
Distance (nm)
9
8
7
6
5
4
3
2
1
0
-1
0
100
200
300
400
500
600

Appendix H

Potassium-saturated Wet Montmorillonite Deflection-Distance Curves

The deflection-distance curves contained in this section were obtained using the clay-coated glass probe and clay-coated glass substrate in an aqueous environment.

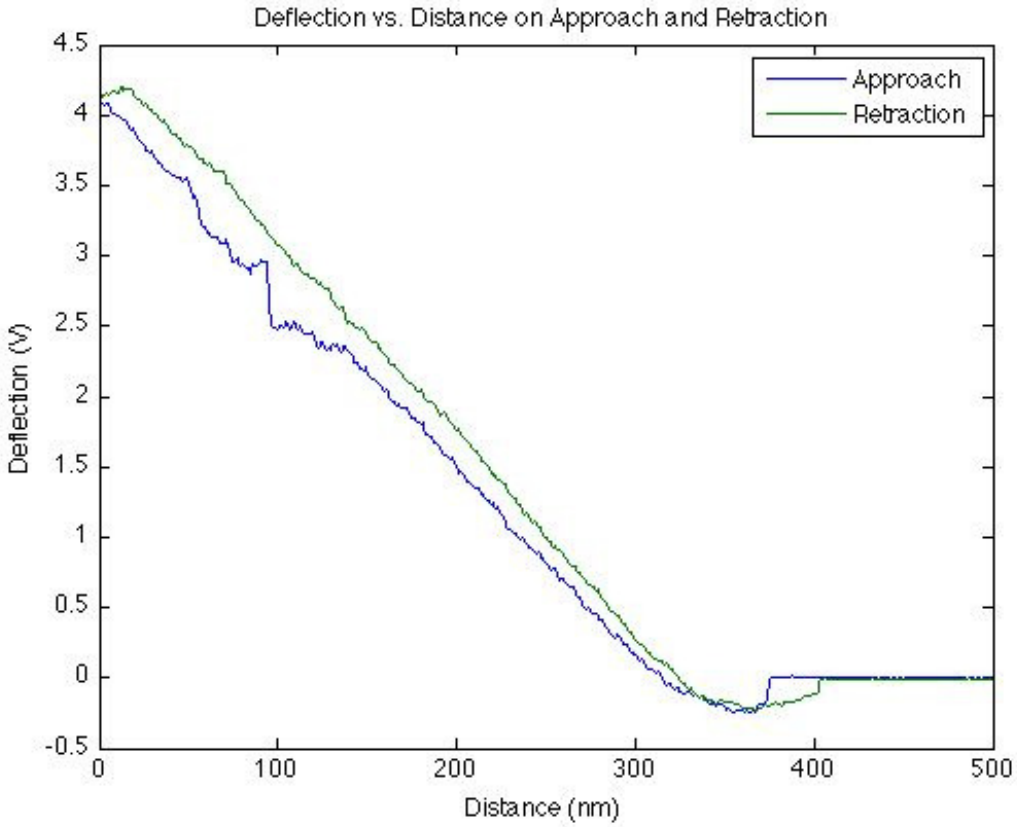
Deflection vs. Distance on Approach and Retraction
Approach
Retraction
Deflection (V)
Distance (nm)
4.5
4
3.5
3
2.5
2
1.5
1
0.5
0
-0.5
0
100
200
300
400
500

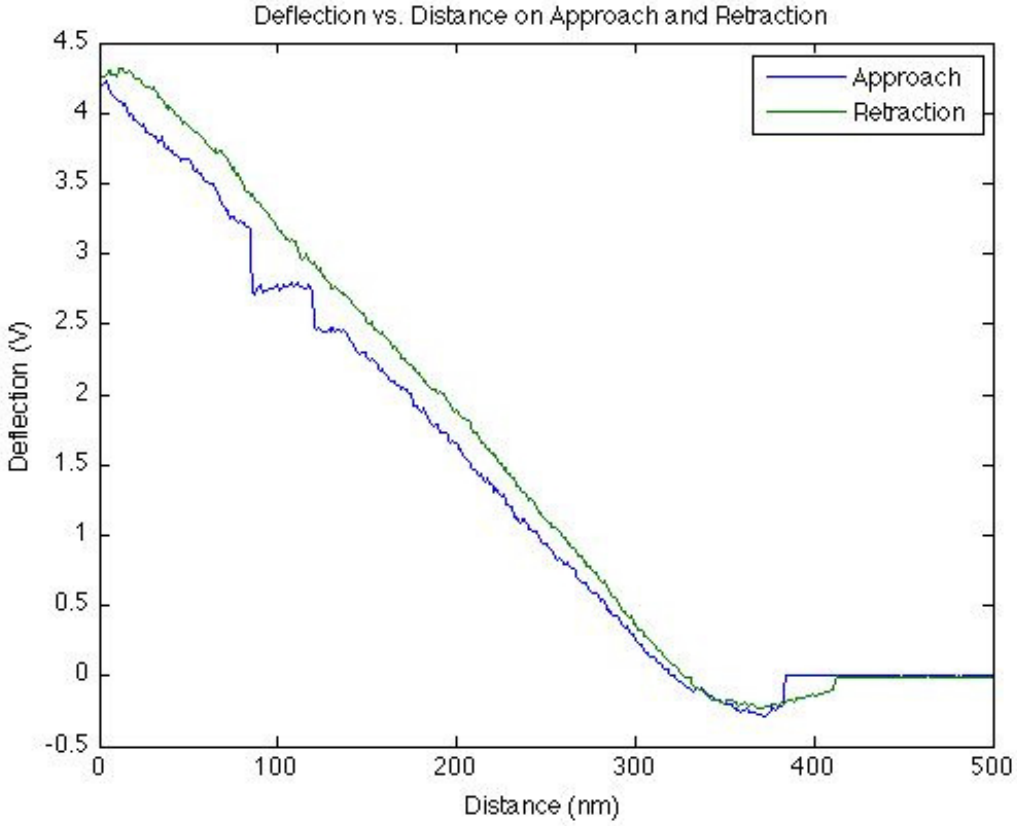
Deflection vs. Distance on Approach and Retraction
Approach
Retraction
Deflection (V)
Distance (nm)
4.5
4
3.5
3
2.5
2
1.5
1
0.5
0
-0.5
0
100
200
300
400
500

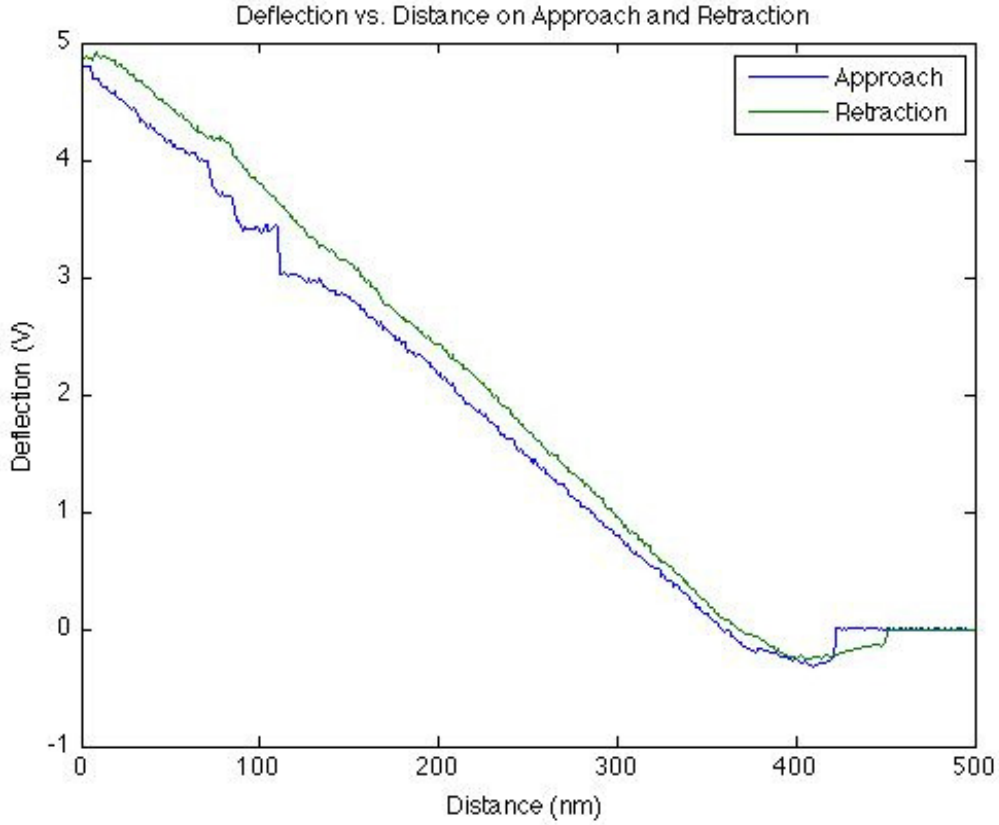
Deflection vs. Distance on Approach and Retraction
Approach
Retraction
Deflection (V)
Distance (nm)
5
4
3
2
1
0
-1
0
100
200
300
400
500

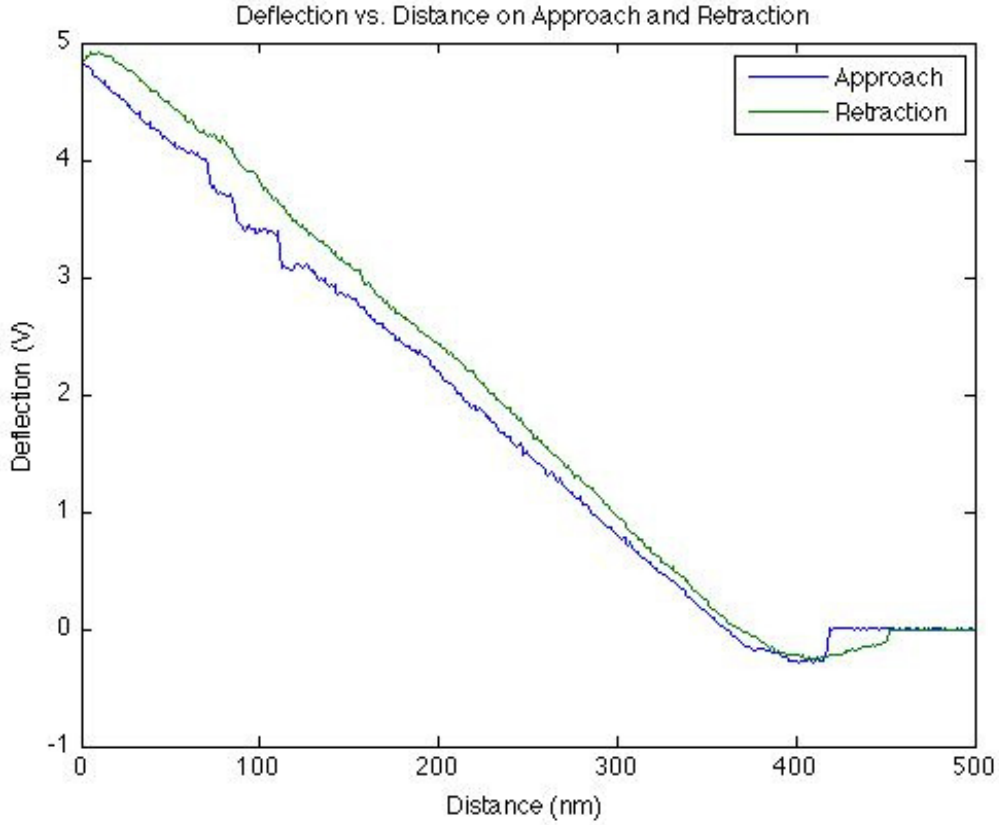
Deflection vs. Distance on Approach and Retraction
Approach
Retraction
Deflection (V)
Distance (nm)
5
4
3
2
1
0
-1
0
100
200
300
400
500

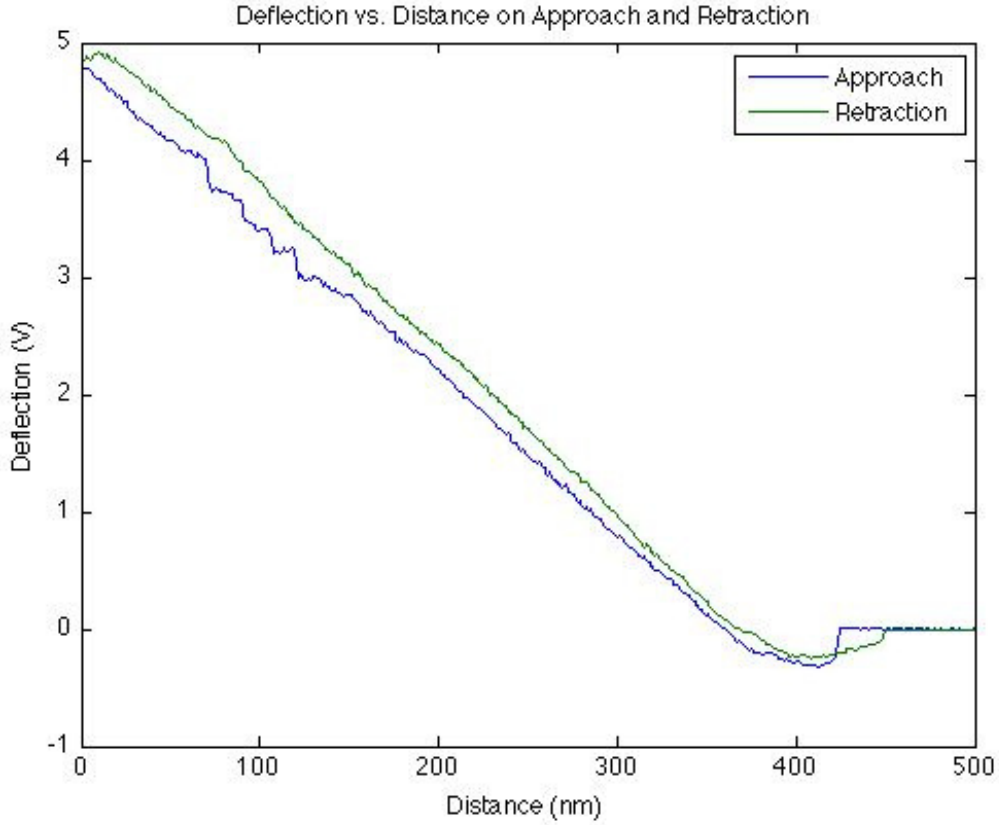
Deflection vs. Distance on Approach and Retraction
Approach
Retraction
Deflection (V)
Distance (nm)
5
4
3
2
1
0
-1
0
100
200
300
400
500

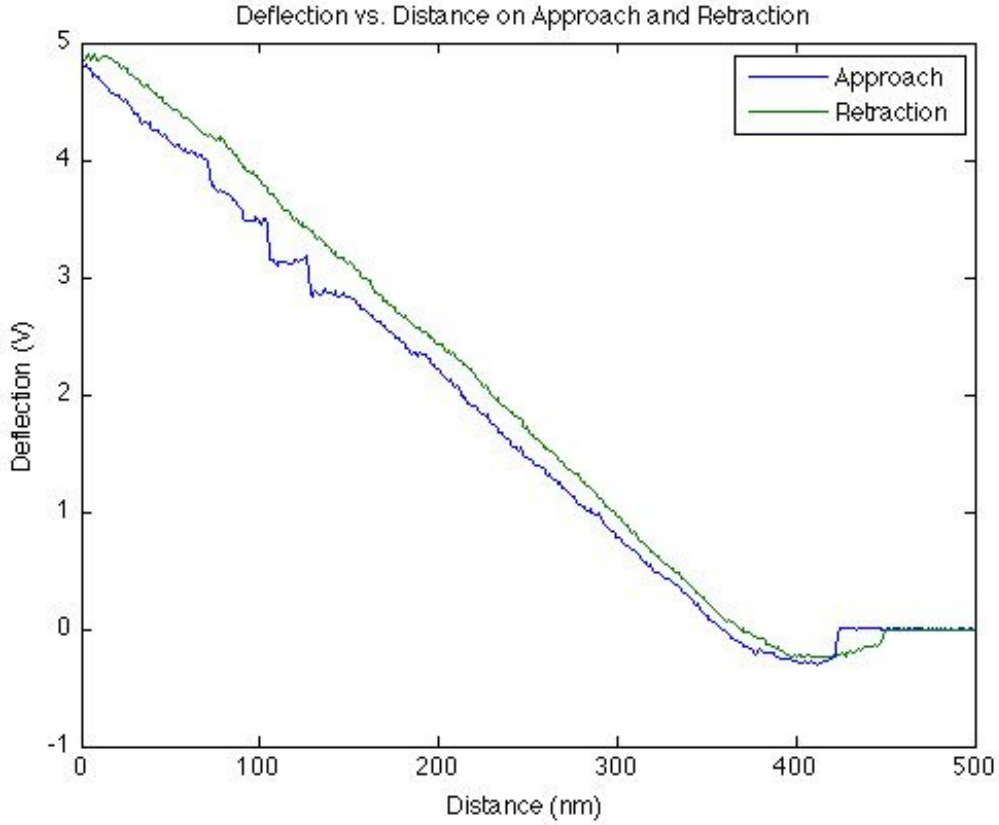
Deflection vs. Distance on Approach and Retraction
Approach
Retraction
Deflection (V)
Distance (nm)
5
4
3
2
1
0
-1
0
100
200
300
400
500

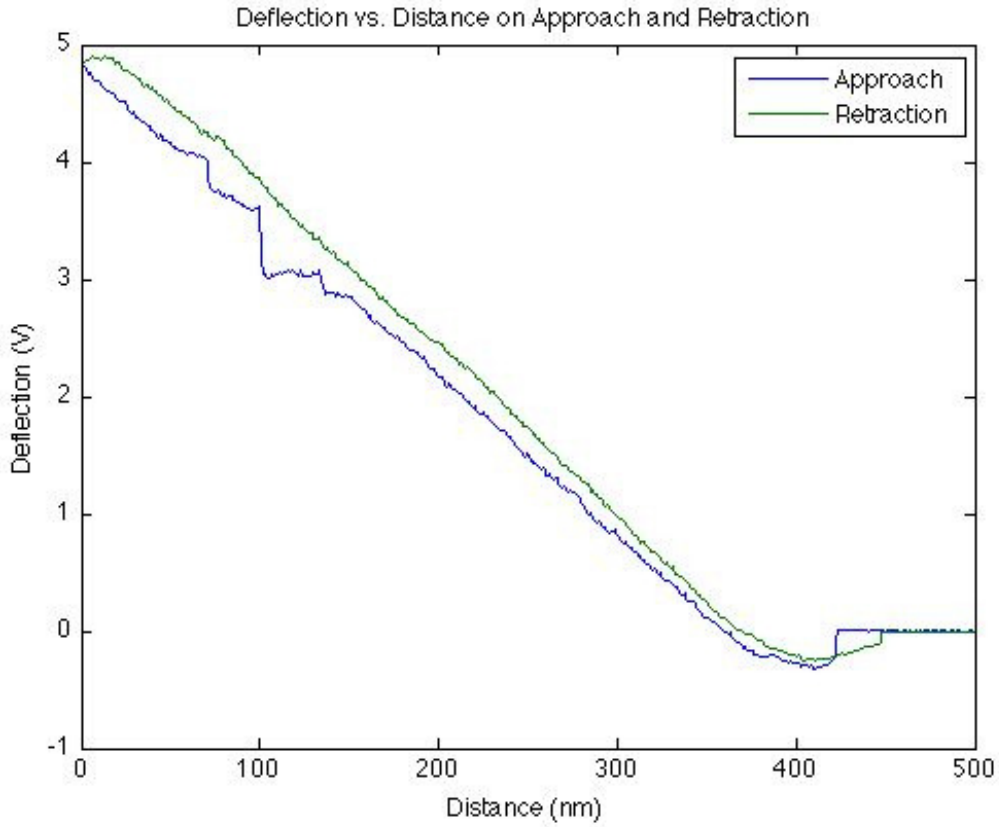
Deflection vs. Distance on Approach and Retraction
Approach
Retraction
Deflection (V)
Distance (nm)
5
4
3
2
1
0
-1
0
100
200
300
400
500

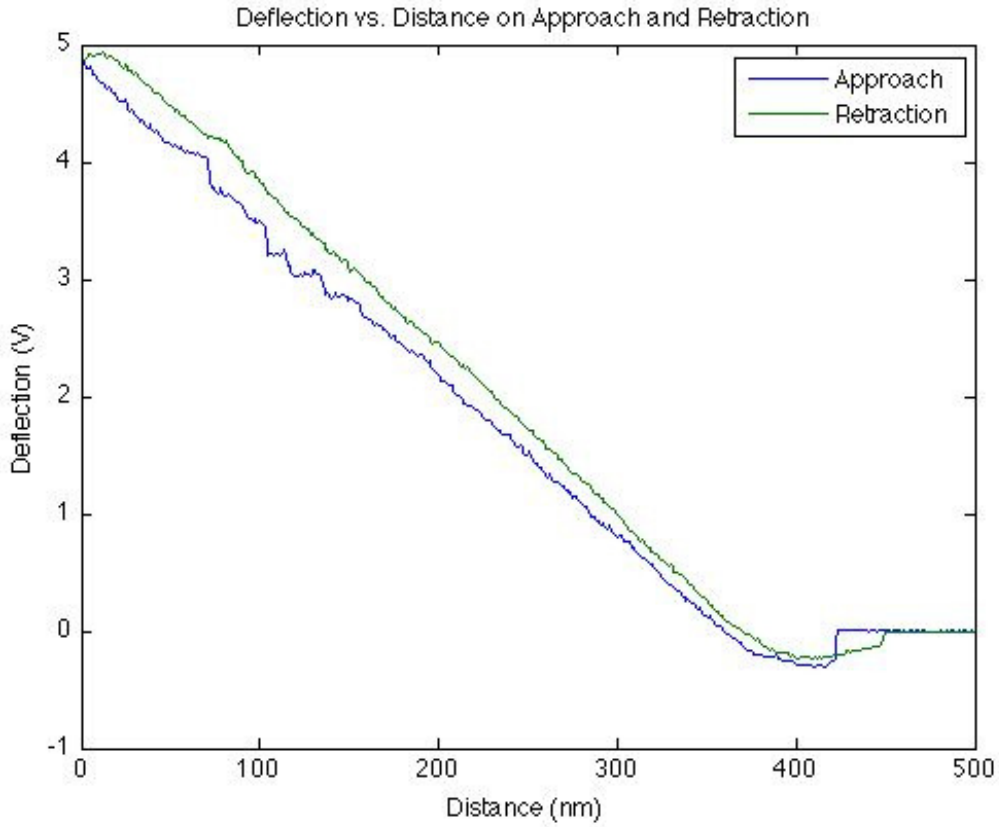
Deflection vs. Distance on Approach and Retraction
Approach
Retraction
Deflection (V)
Distance (nm)
5
4
3
2
1
0
-1
0
100
200
300
400
500

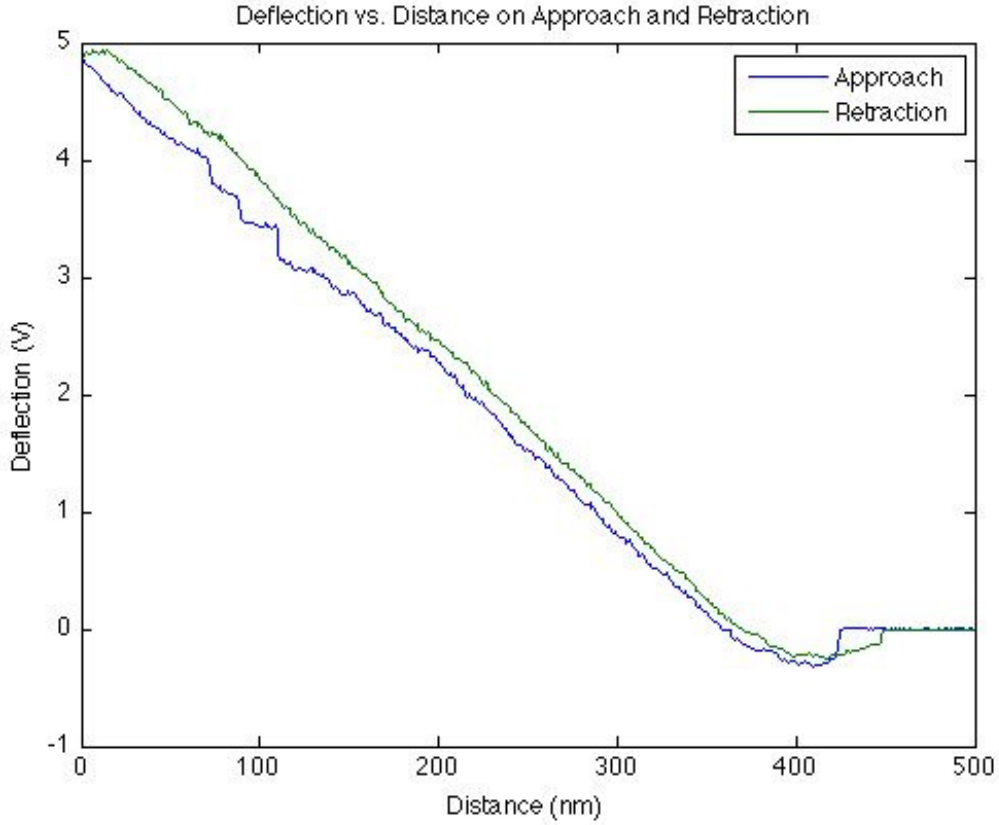
Deflection vs. Distance on Approach and Retraction
Approach
Retraction
Deflection (V)
Distance (nm)
5
4
3
2
1
0
-1
0
100
200
300
400
500

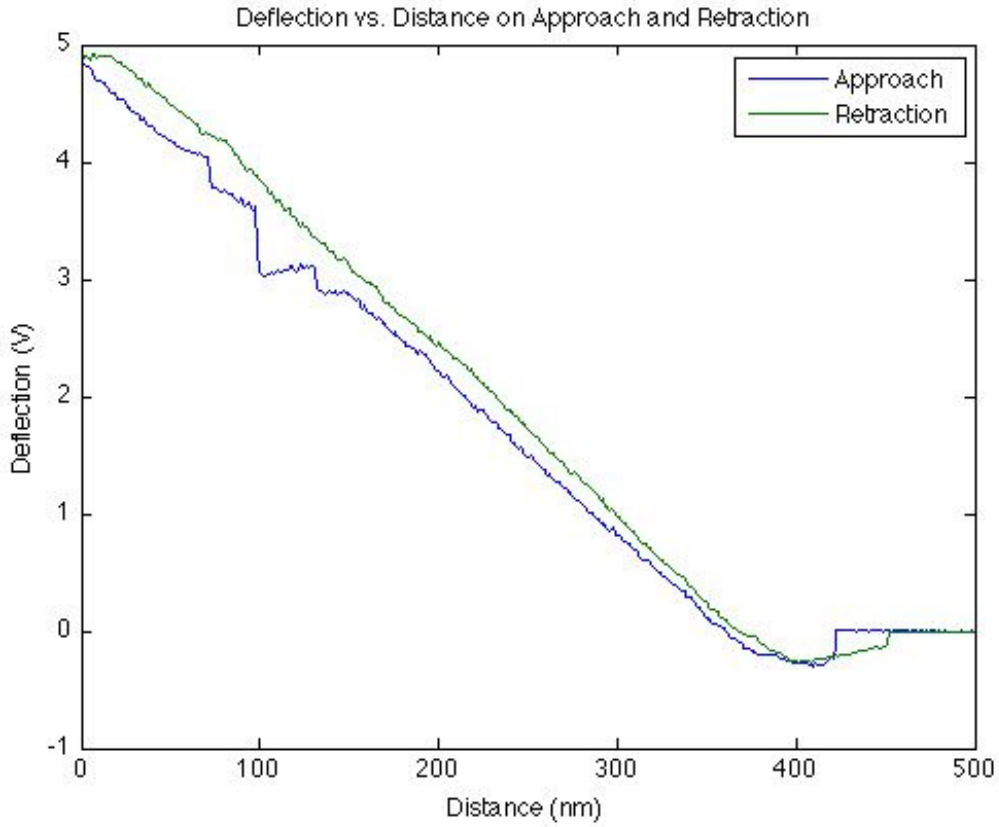
Deflection vs. Distance on Approach and Retraction
Approach
Retraction
Deflection (V)
Distance (nm)
5
4
3
2
1
0
-1
0
100
200
300
400
500

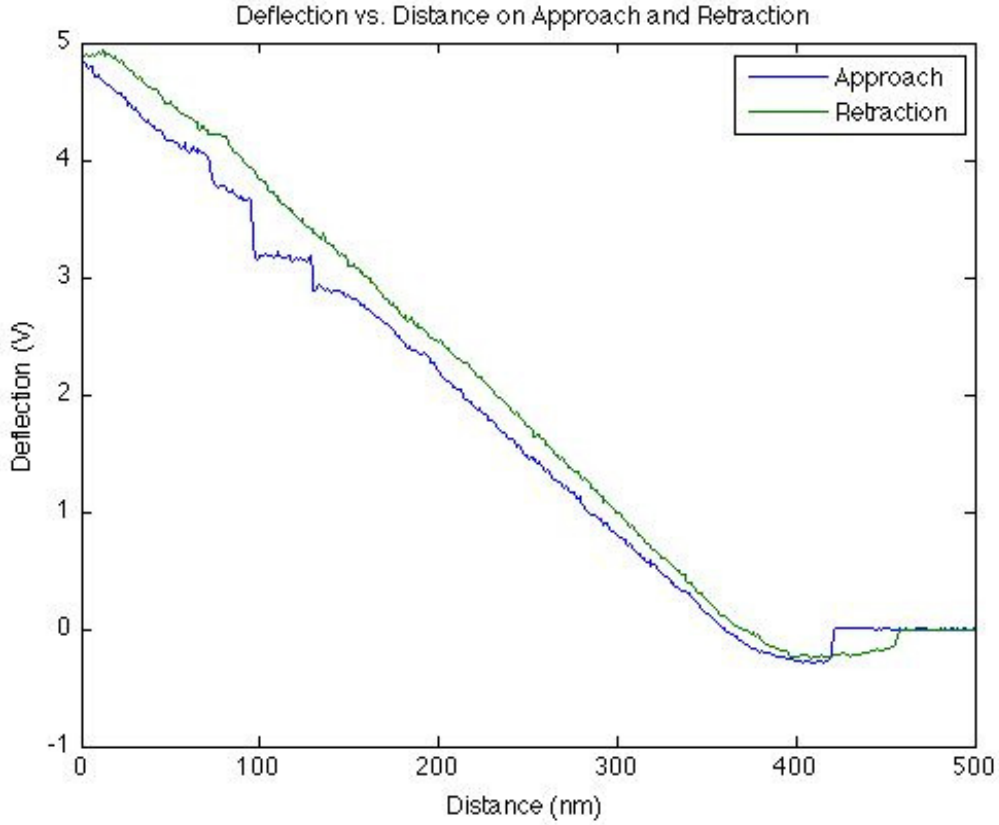
Deflection vs. Distance on Approach and Retraction
Approach
Retraction
Deflection (V)
Distance (nm)
5
4
3
2
1
0
-1
0
100
200
300
400
500

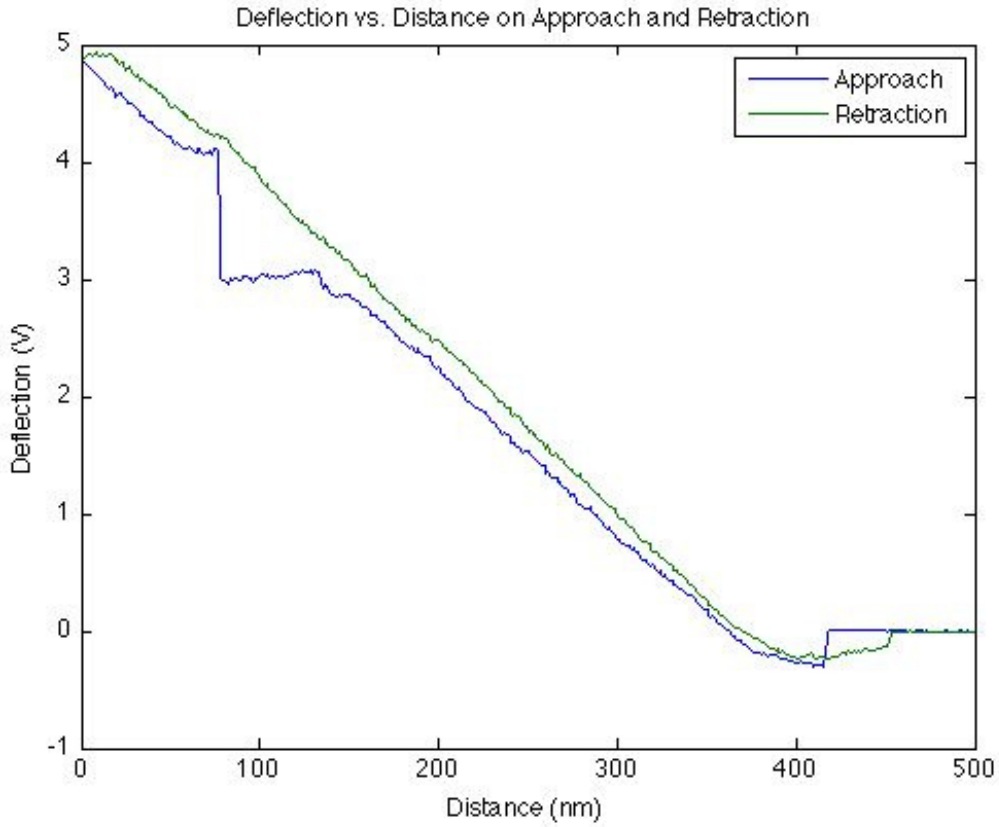
Deflection vs. Distance on Approach and Retraction
Approach
Retraction
Deflection (V)
Distance (nm)
5
4
3
2
1
0
-1
0
100
200
300
400
500

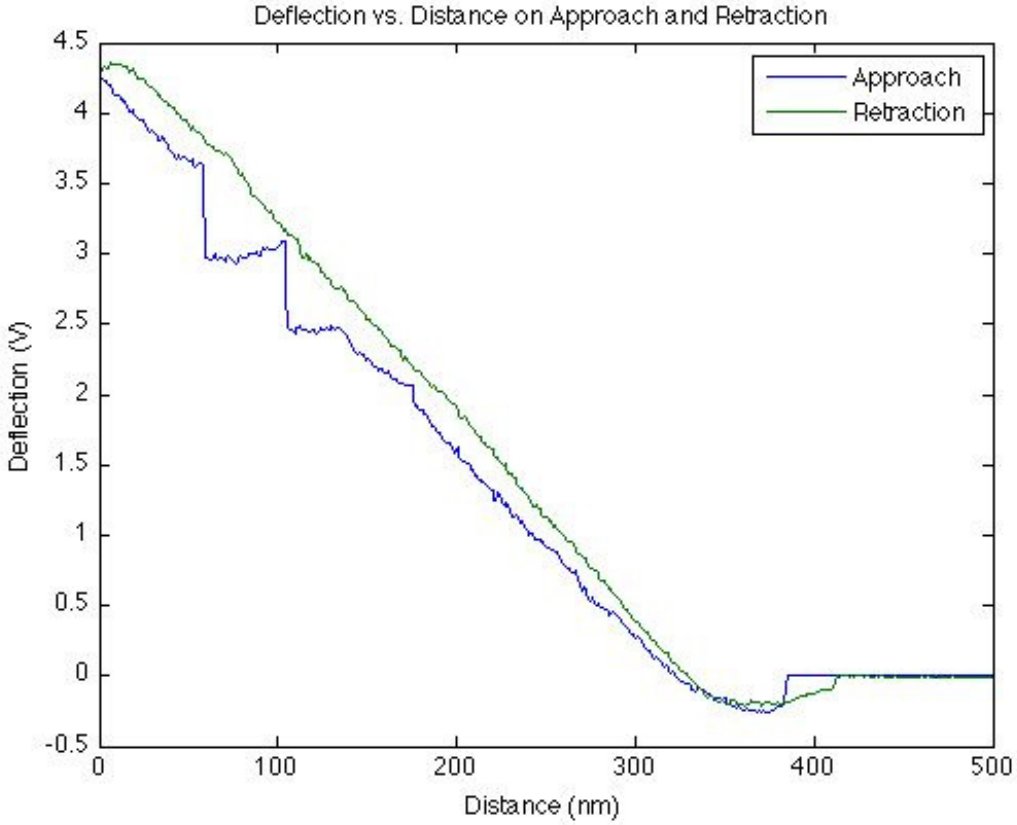
Deflection vs. Distance on Approach and Retraction
Approach
Retraction
Deflection (V)
Distance (nm)
4.5
4
3.5
3
2.5
2
1.5
1
0.5
0
-0.5
0
100
200
300
400
500

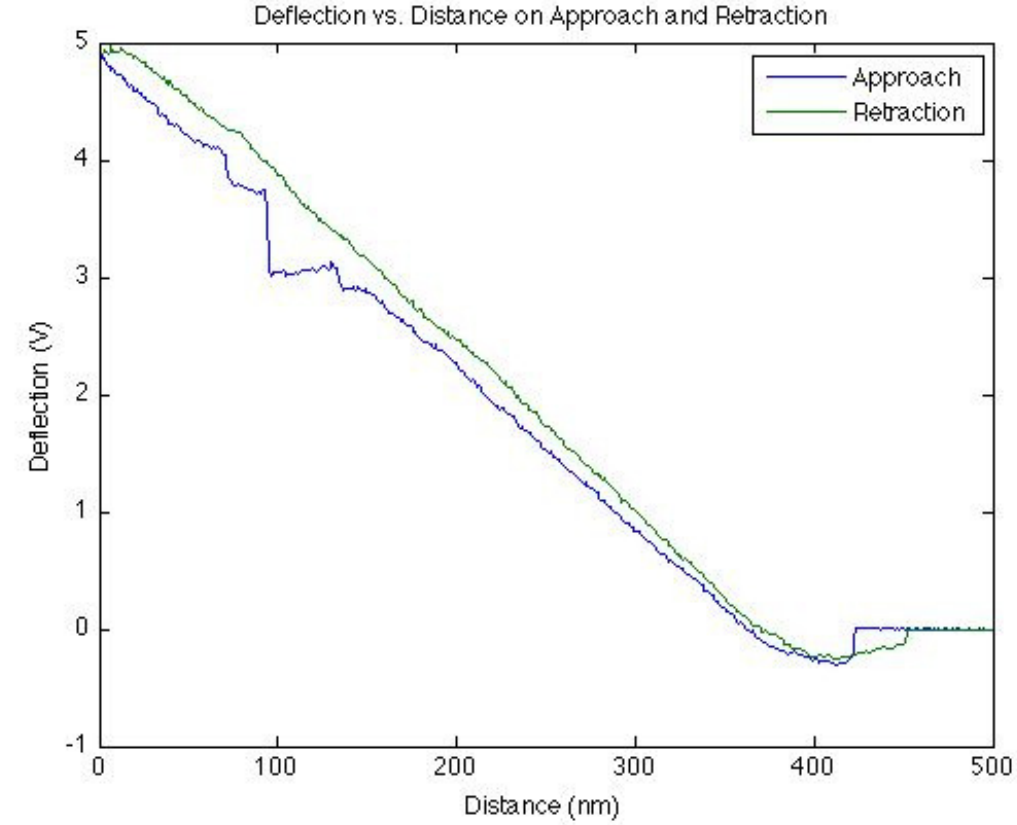
Deflection vs. Distance on Approach and Retraction
Approach
Retraction
Deflection (V)
Distance (nm)
5
4
3
2
1
0
-1
0
100
200
300
400
500

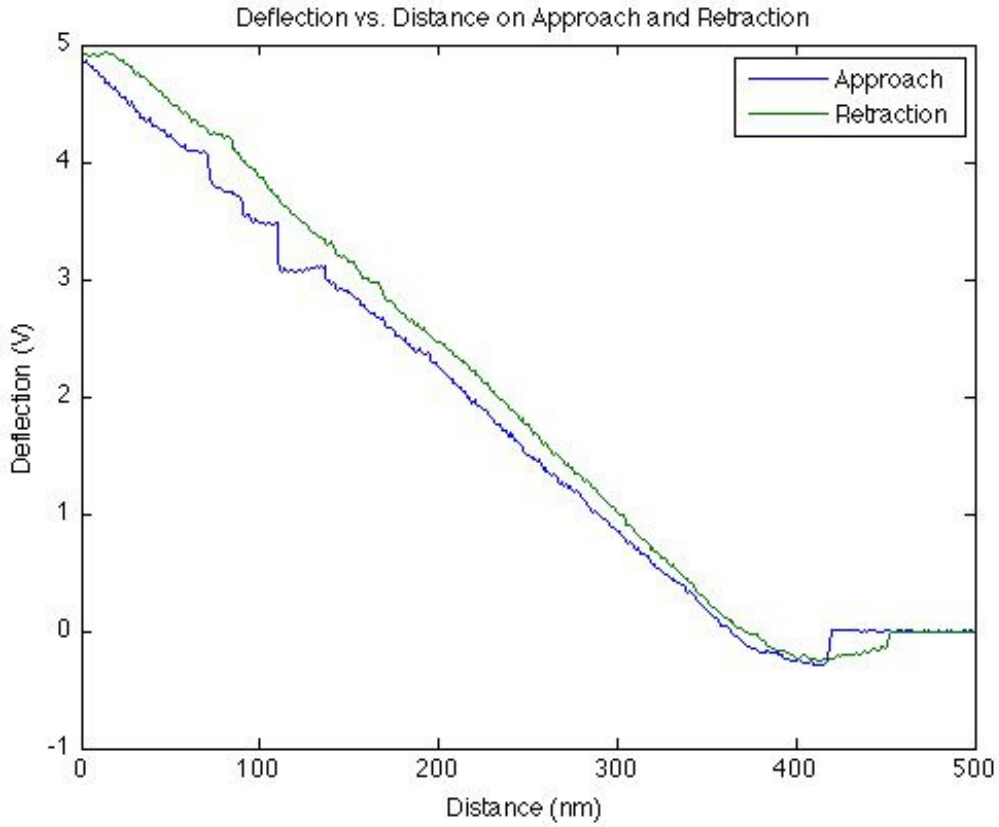
Deflection vs. Distance on Approach and Retraction
Approach
Retraction
Deflection (V)
Distance (nm)
5
4
3
2
1
0
-1
0
100
200
300
400
500

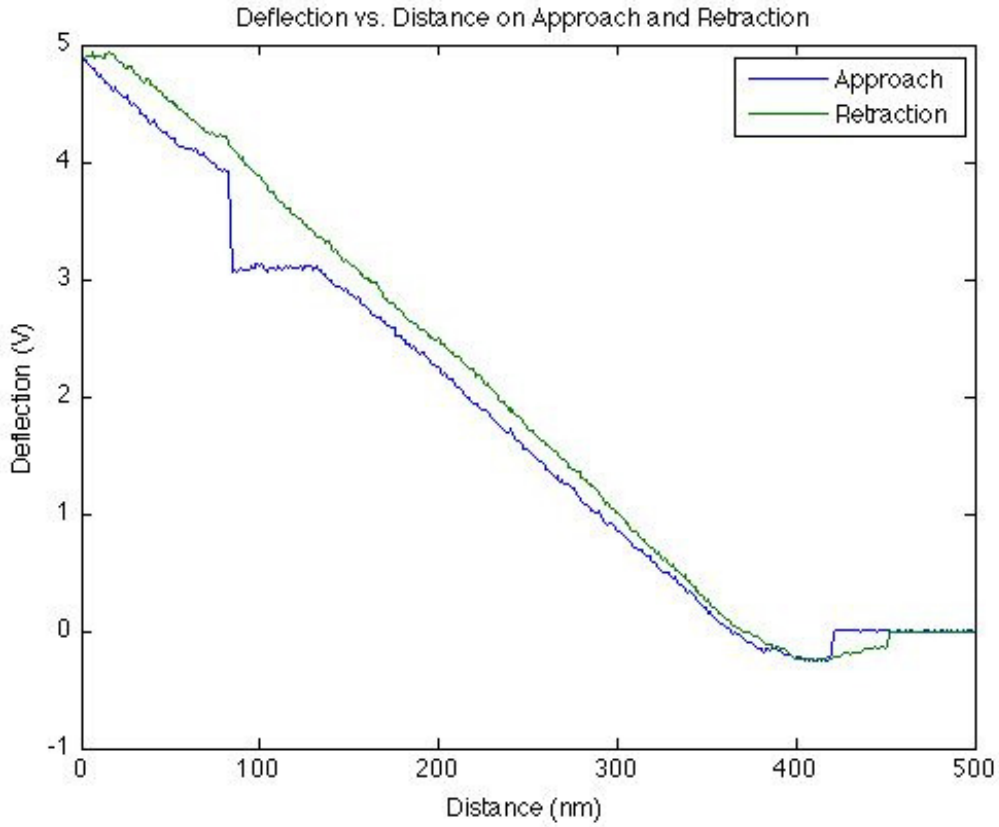
Deflection vs. Distance on Approach and Retraction
Approach
Retraction
Deflection (V)
Distance (nm)
5
4
3
2
1
0
-1
0
100
200
300
400
500

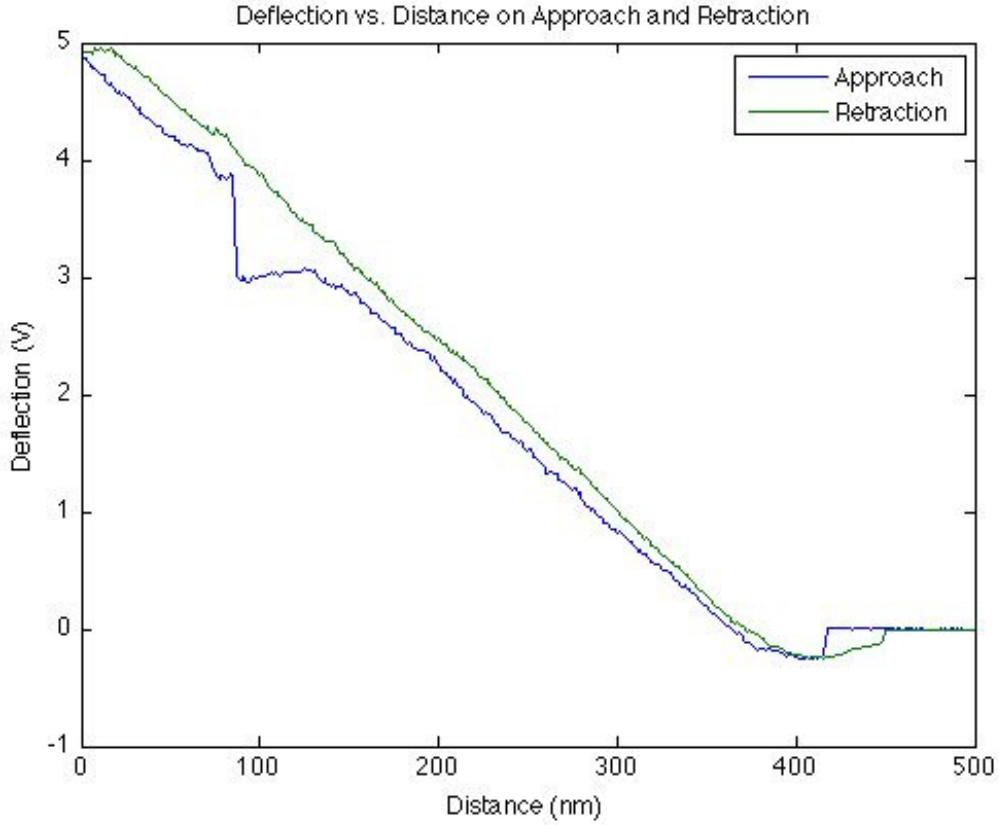
Deflection vs. Distance on Approach and Retraction
Approach
Retraction
Deflection (V)
Distance (nm)
5
4
3
2
1
0
-1
0
100
200
300
400
500

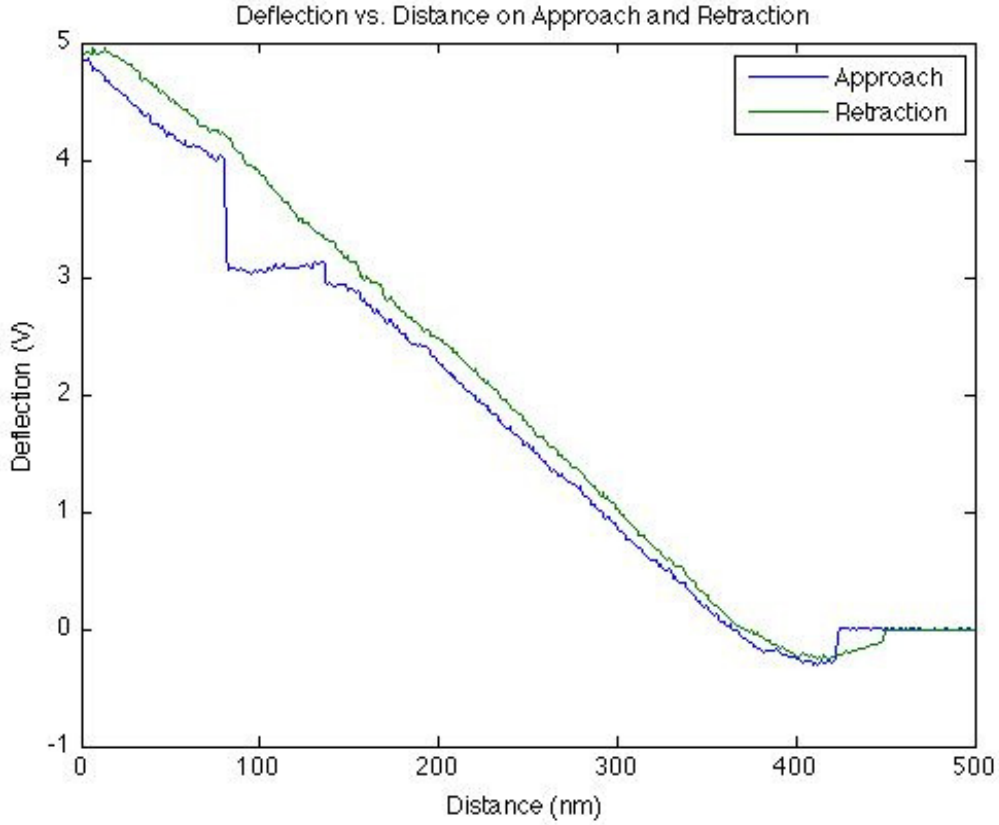
Deflection vs. Distance on Approach and Retraction
Approach
Retraction
Deflection (V)
Distance (nm)
5
4
3
2
1
0
-1
0
100
200
300
400
500

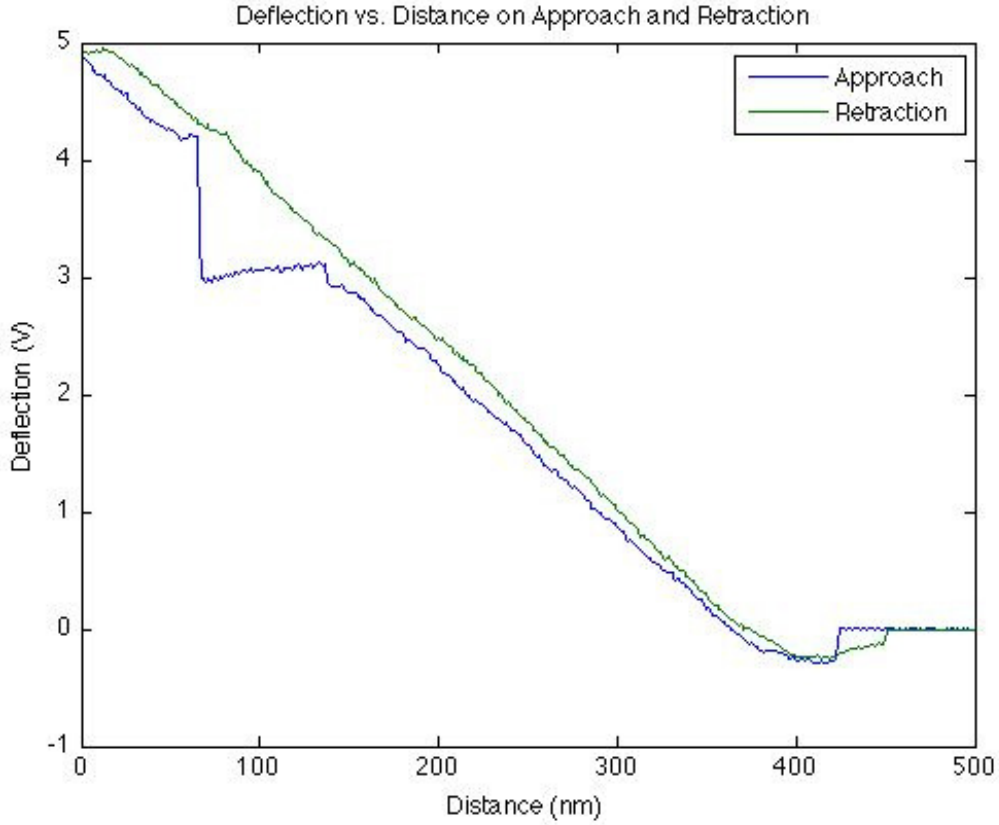
Deflection vs. Distance on Approach and Retraction
Approach
Retraction
Deflection (V)
Distance (nm)
5
4
3
2
1
0
-1
0
100
200
300
400
500

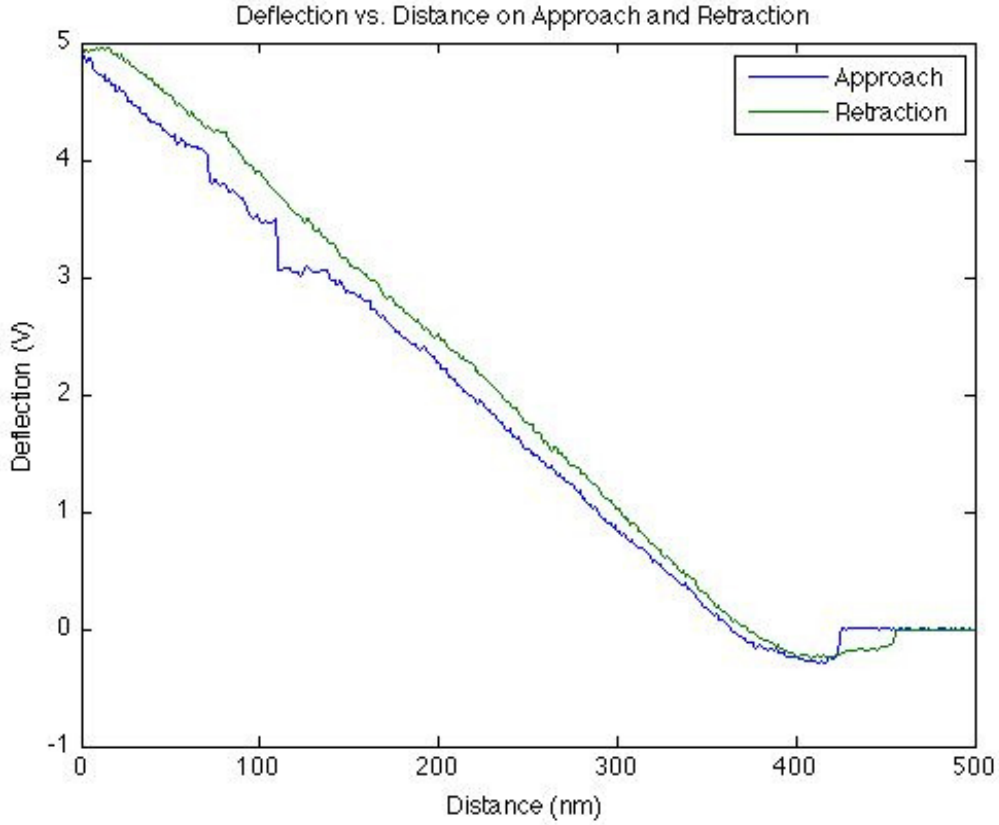
Deflection vs. Distance on Approach and Retraction
Approach
Retraction
Deflection (V)
Distance (nm)
5
4
3
2
1
0
-1
0
100
200
300
400
500

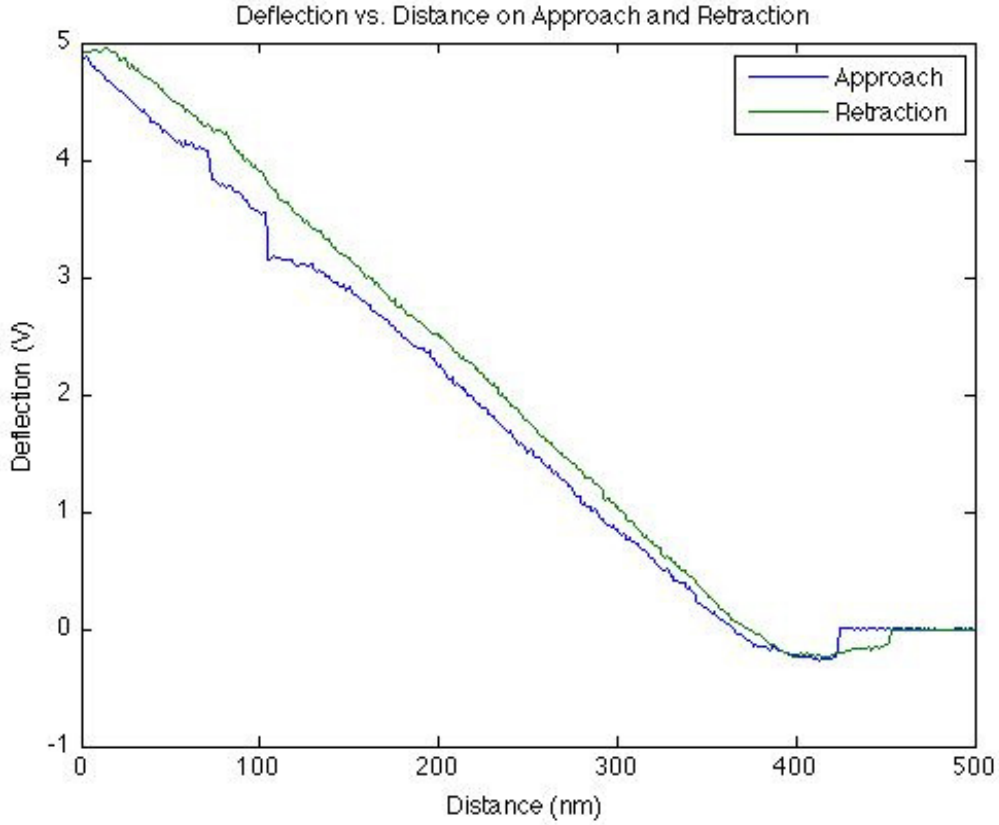
Deflection vs. Distance on Approach and Retraction
Approach
Retraction
Deflection (V)
Distance (nm)
5
4
3
2
1
0
-1
0
100
200
300
400
500

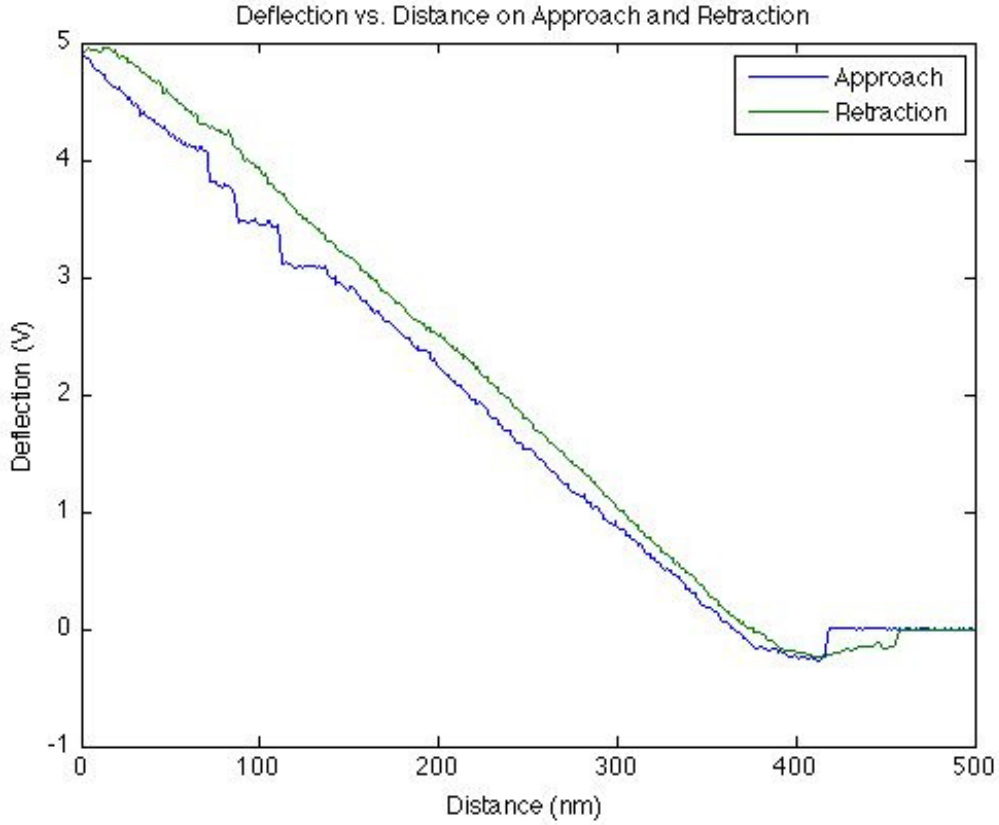
Deflection vs. Distance on Approach and Retraction
Approach
Retraction
Deflection (V)
Distance (nm)
5
4
3
2
1
0
-1
0
100
200
300
400
500

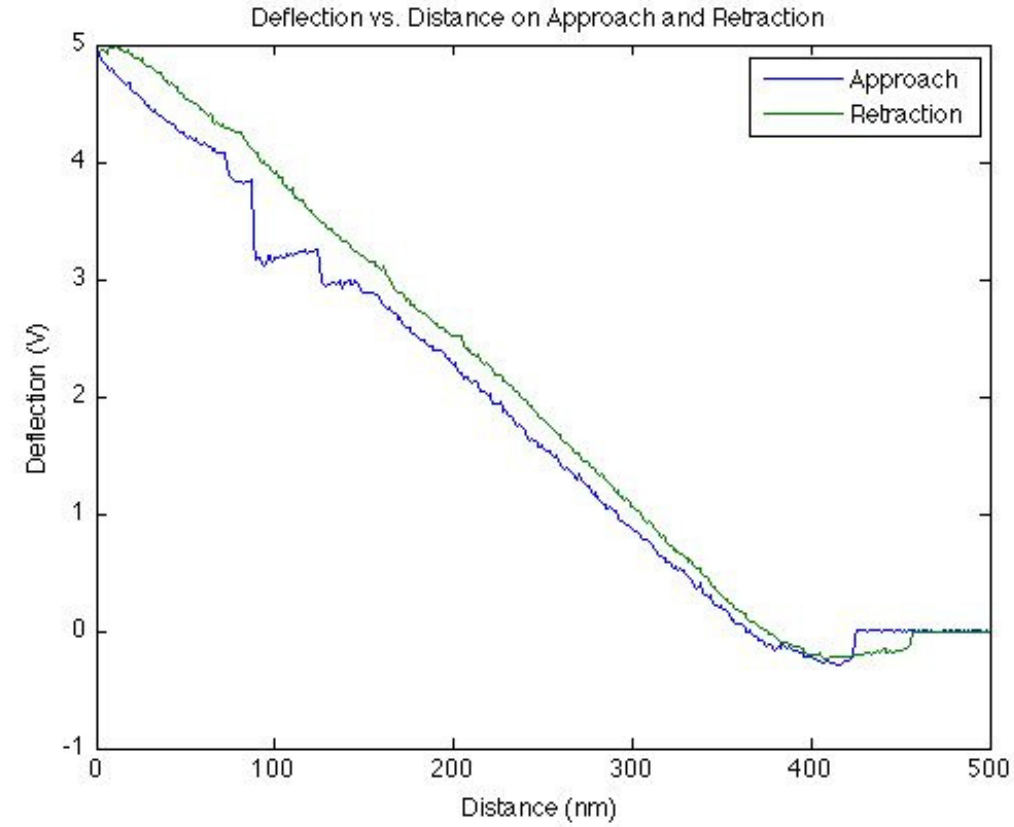
Deflection vs. Distance on Approach and Retraction
Approach
Retraction
Deflection (V)
Distance (nm)
5
4
3
2
1
0
-1
0
100
200
300
400
500

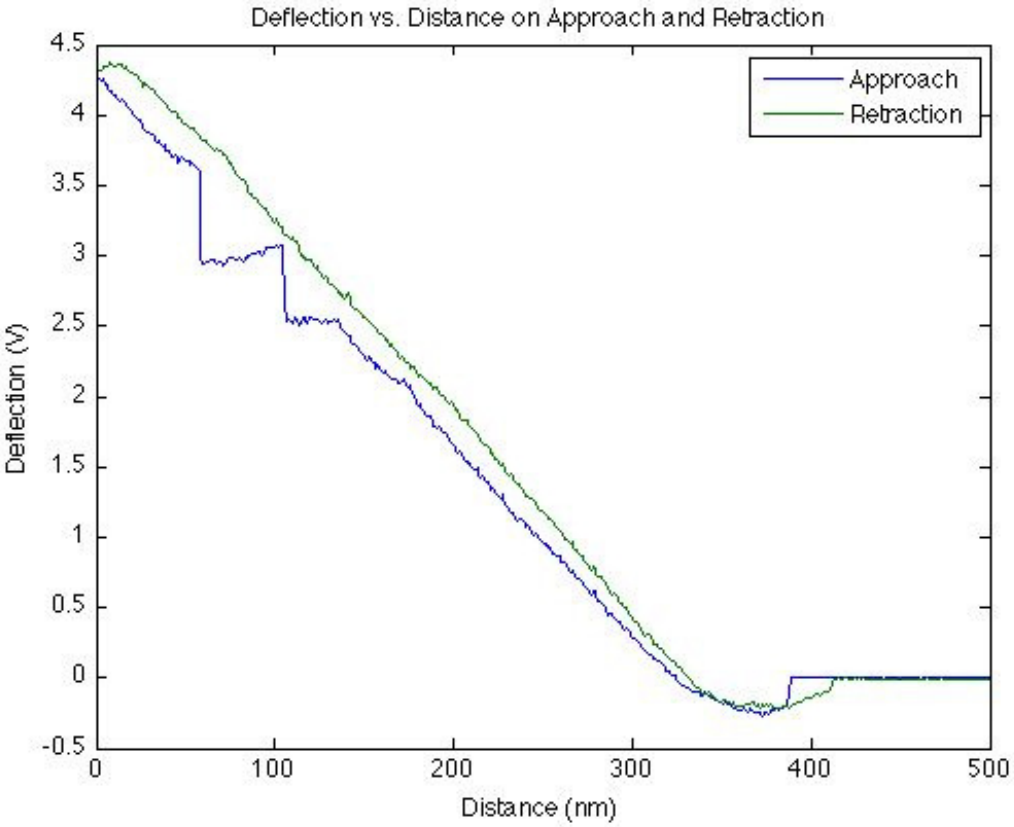
Deflection vs. Distance on Approach and Retraction
Approach
Retraction
Deflection (V)
Distance (nm)
4.5
4
3.5
3
2.5
2
1.5
1
0.5
0
-0.5
0
100
200
300
400
500

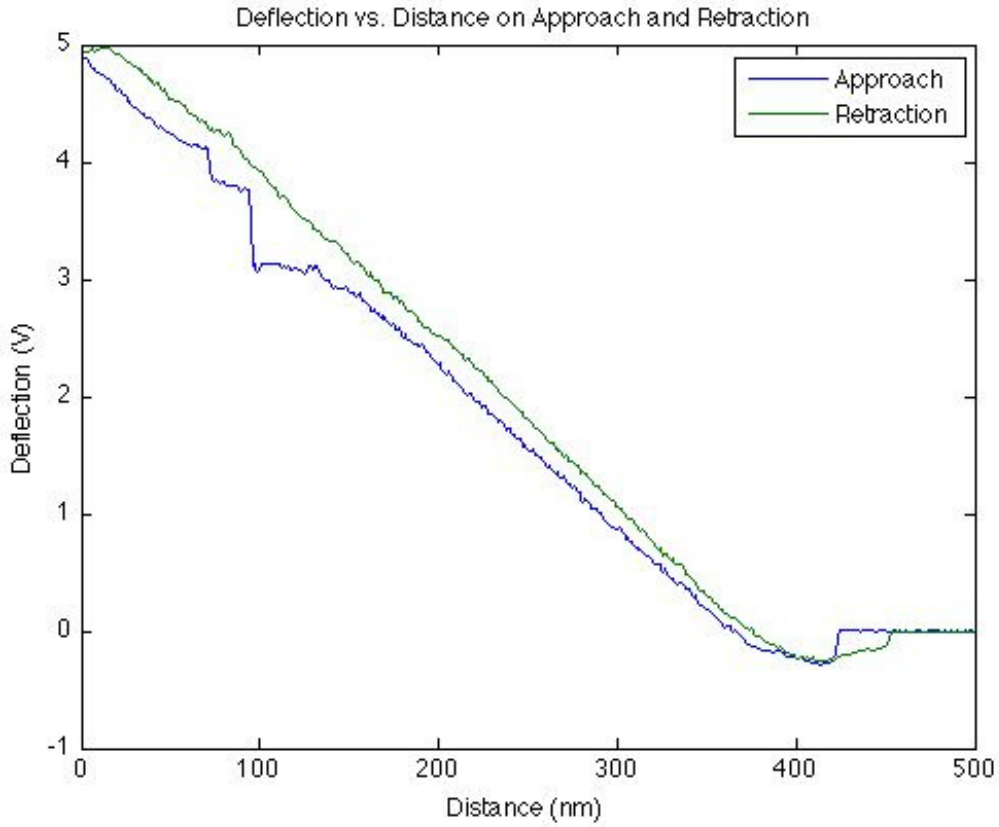
Deflection vs. Distance on Approach and Retraction
Approach
Retraction
Deflection (V)
Distance (nm)
5
4
3
2
1
0
-1
0
100
200
300
400
500

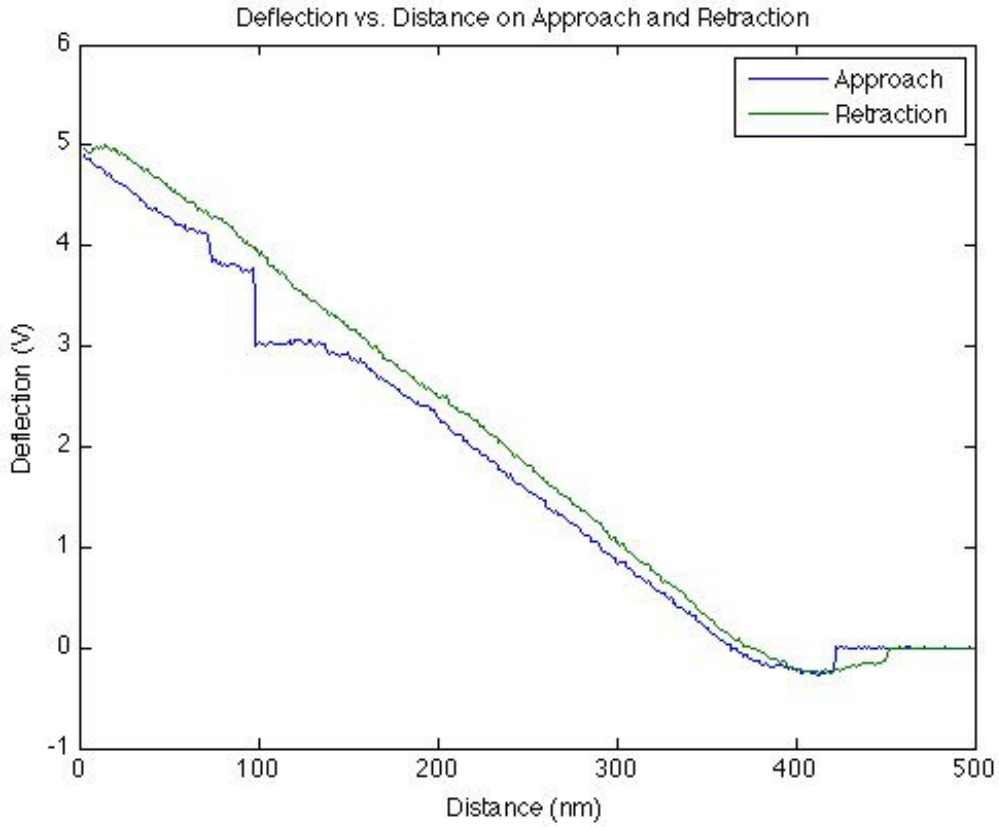
Deflection vs. Distance on Approach and Retraction
Approach
Retraction
Deflection (V)
Distance (nm)
6
5
4
3
2
1
0
-1
0
100
200
300
400
500

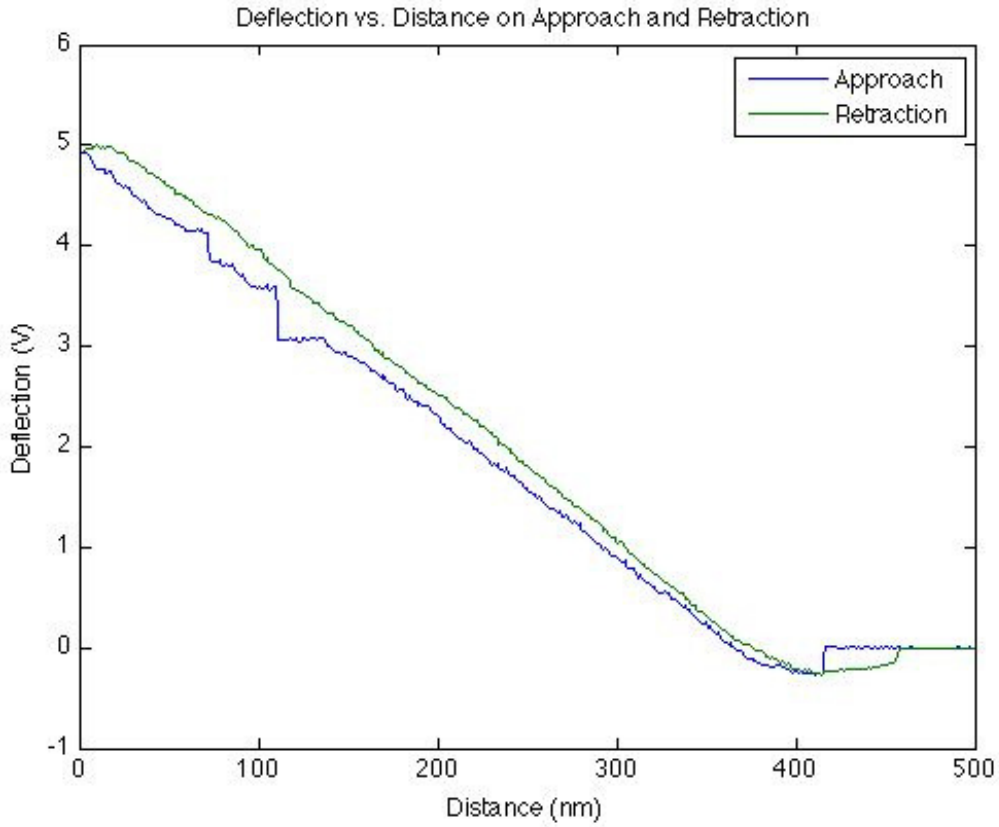
Deflection vs. Distance on Approach and Retraction
Approach
Retraction
Deflection (V)
Distance (nm)
6
5
4
3
2
1
0
-1
0
100
200
300
400
500

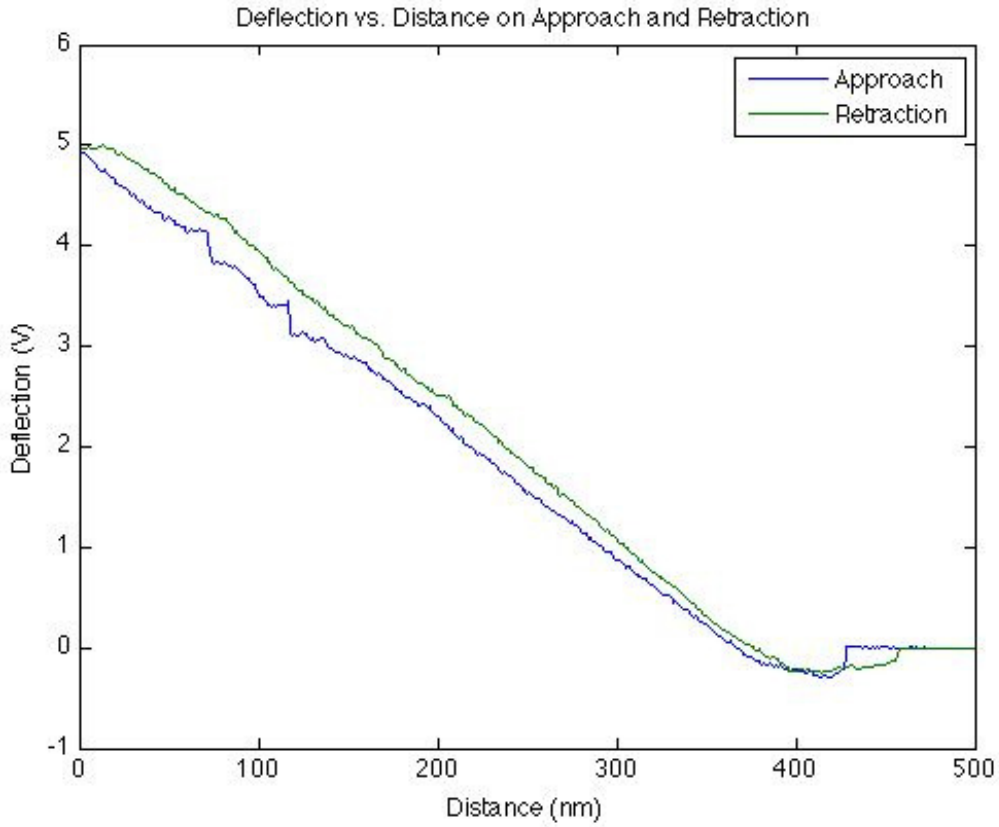
Deflection vs. Distance on Approach and Retraction
Approach
Retraction
Deflection (V)
Distance (nm)
6
5
4
3
2
1
0
-1
0
100
200
300
400
500

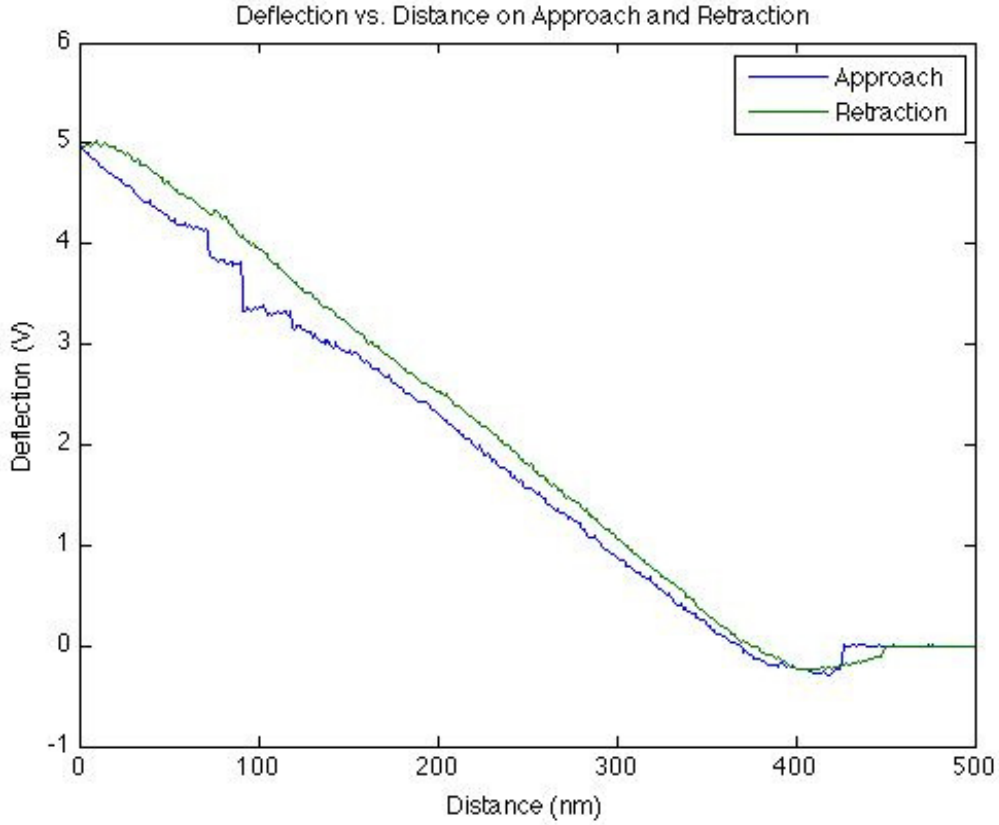
Deflection vs. Distance on Approach and Retraction
Approach
Retraction
Deflection (V)
Distance (nm)
6
5
4
3
2
1
0
-1
0
100
200
300
400
500

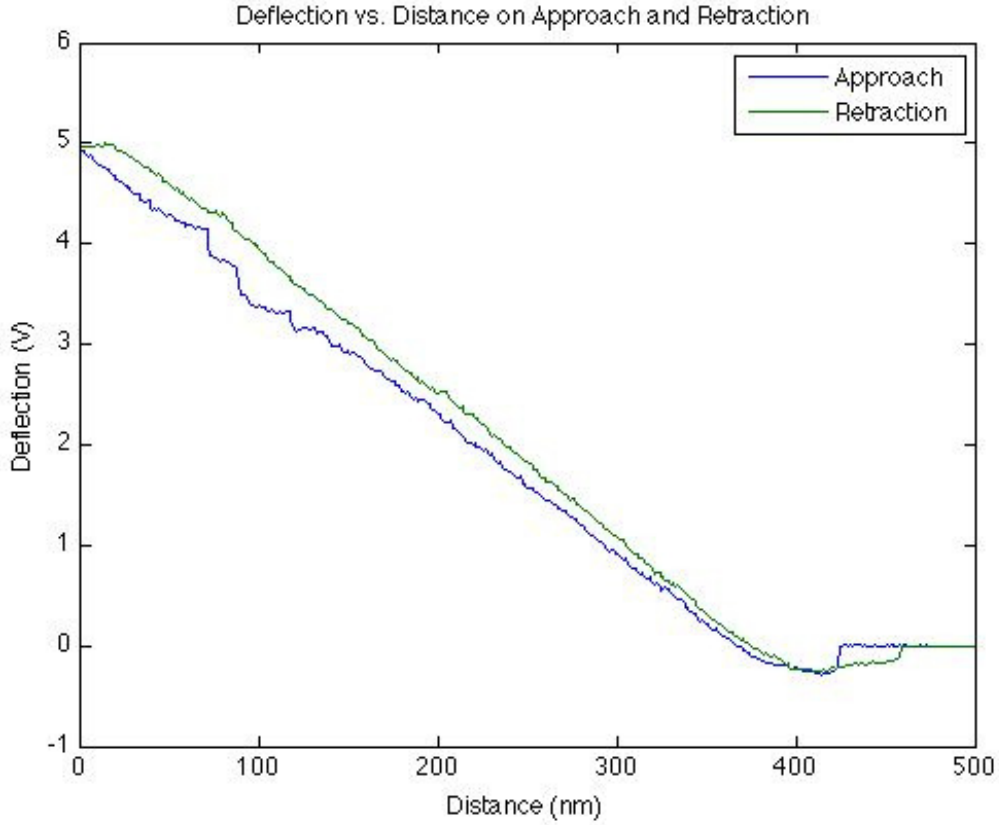
Deflection vs. Distance on Approach and Retraction
Approach
Retraction
Deflection (V)
Distance (nm)
6
5
4
3
2
1
0
-1
0
100
200
300
400
500

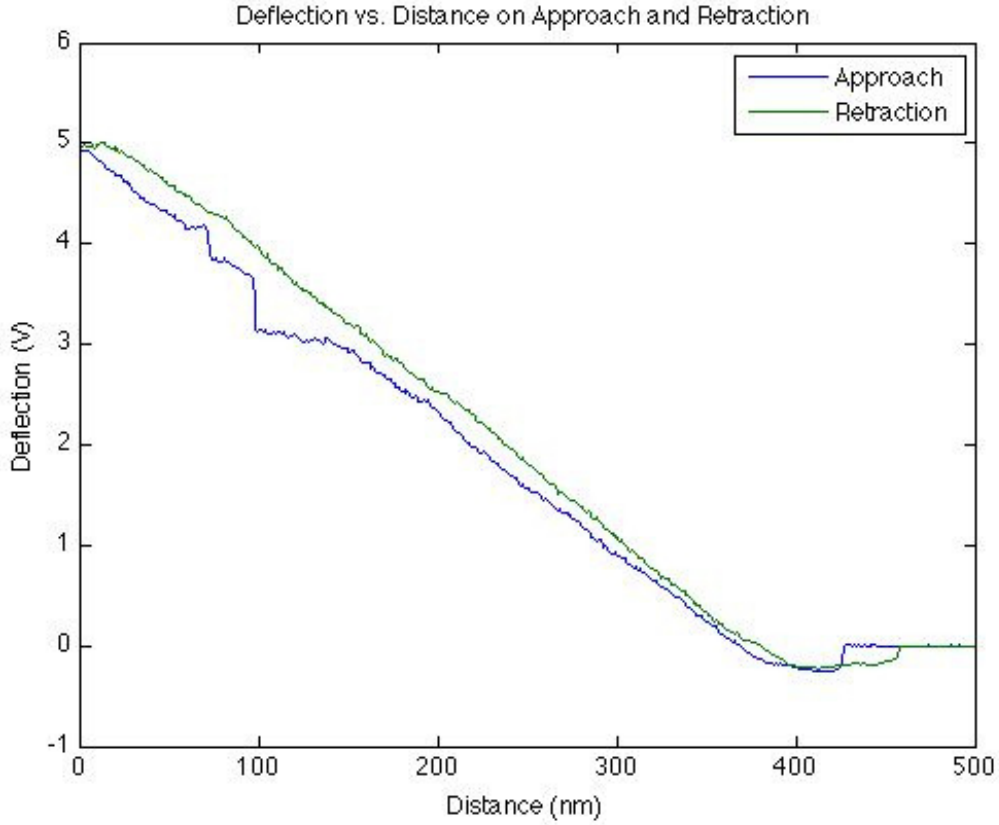
Deflection vs. Distance on Approach and Retraction
Approach
Retraction
Deflection (V)
Distance (nm)
6
5
4
3
2
1
0
-1
0
100
200
300
400
500

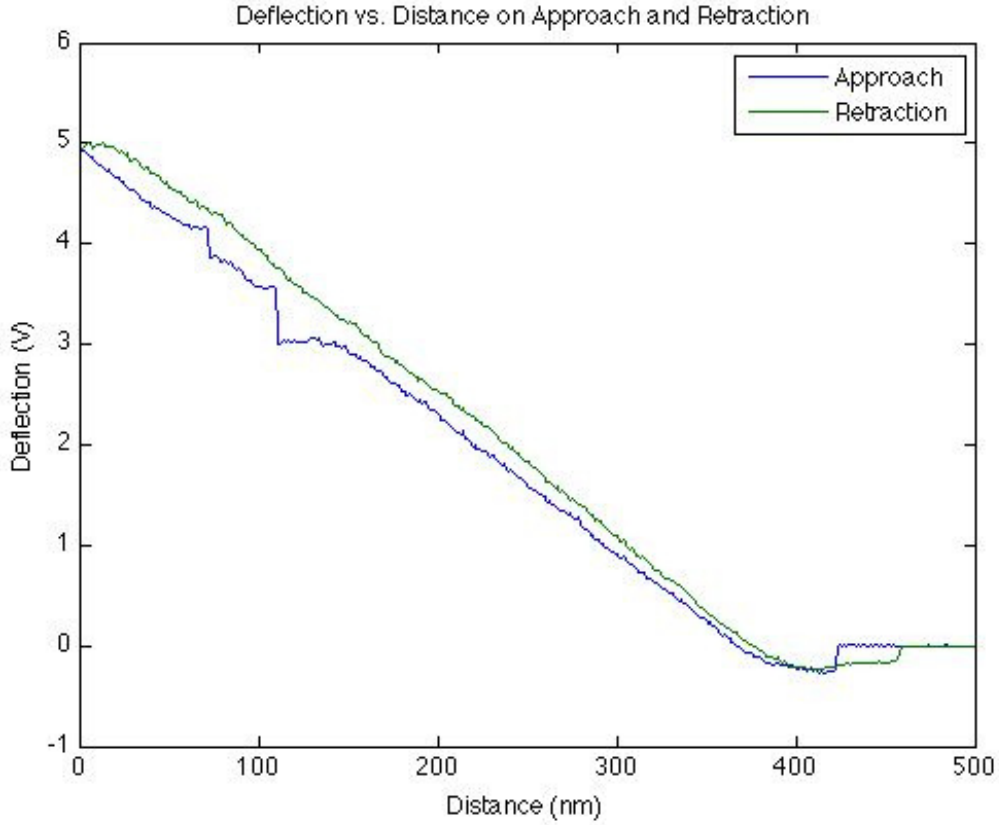
Deflection vs. Distance on Approach and Retraction
Approach
Retraction
Deflection (V)
Distance (nm)
6
5
4
3
2
1
0
-1
0
100
200
300
400
500

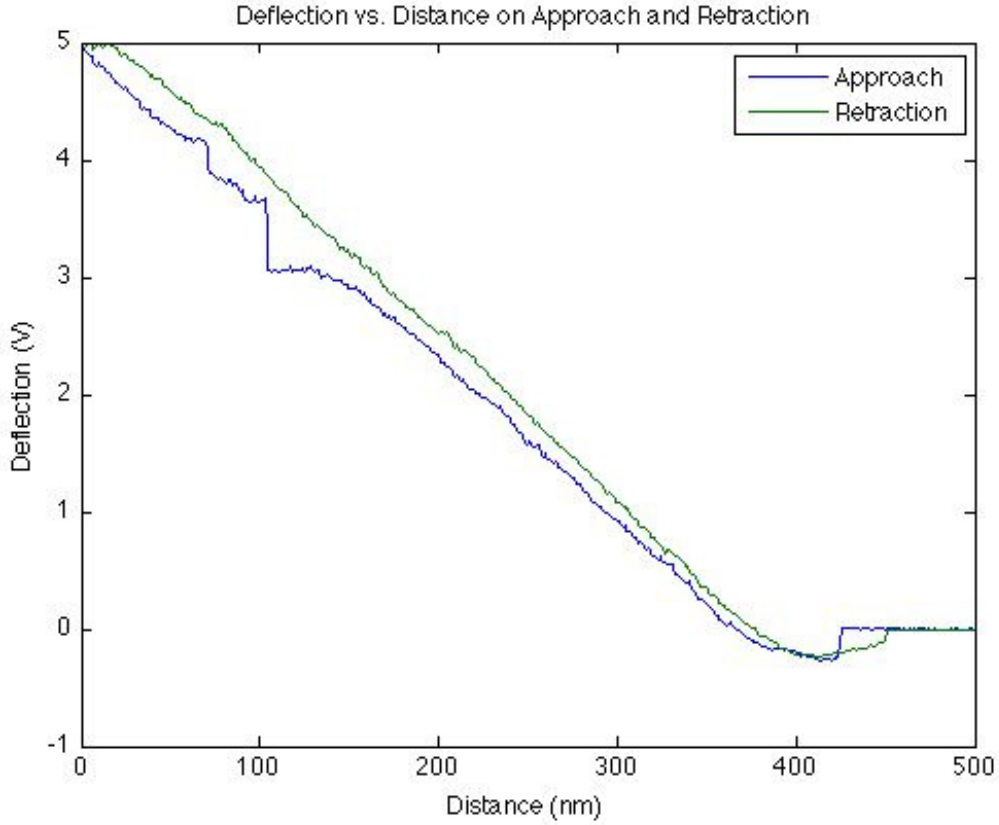
Deflection vs. Distance on Approach and Retraction
Approach
Retraction
Deflection (V)
Distance (nm)
5
4
3
2
1
0
-1
0
100
200
300
400
500

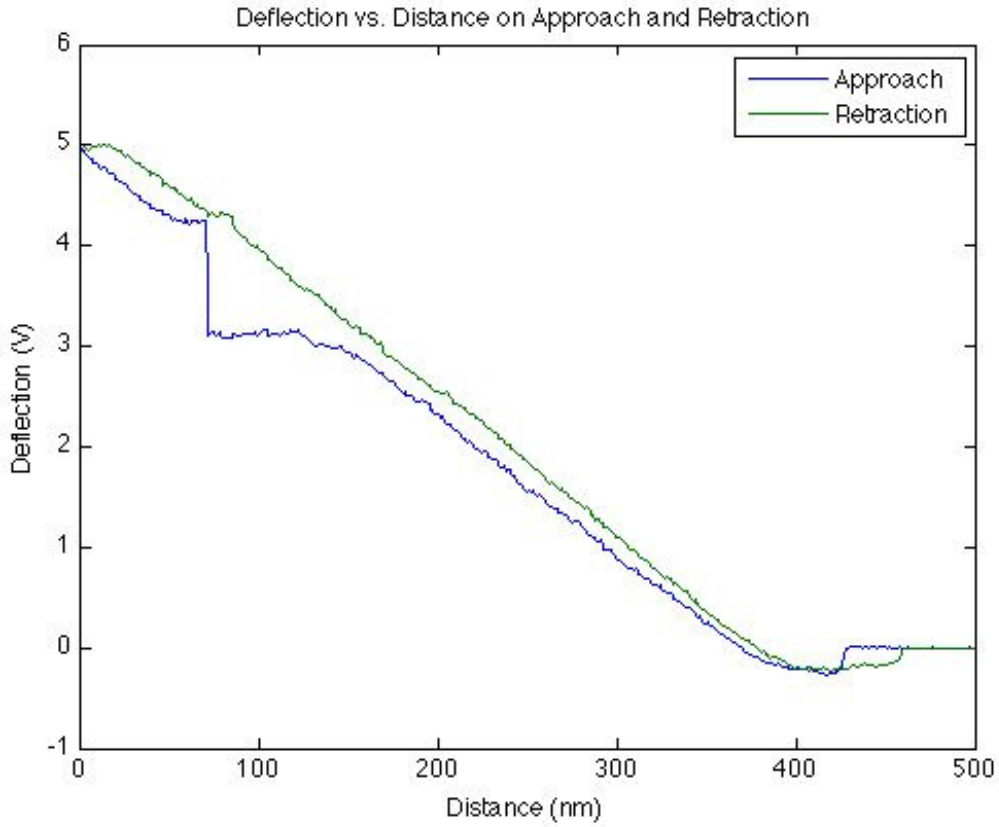
Deflection vs. Distance on Approach and Retraction
Approach
Retraction
Deflection (V)
Distance (nm)
6
5
4
3
2
1
0
-1
0
100
200
300
400
500

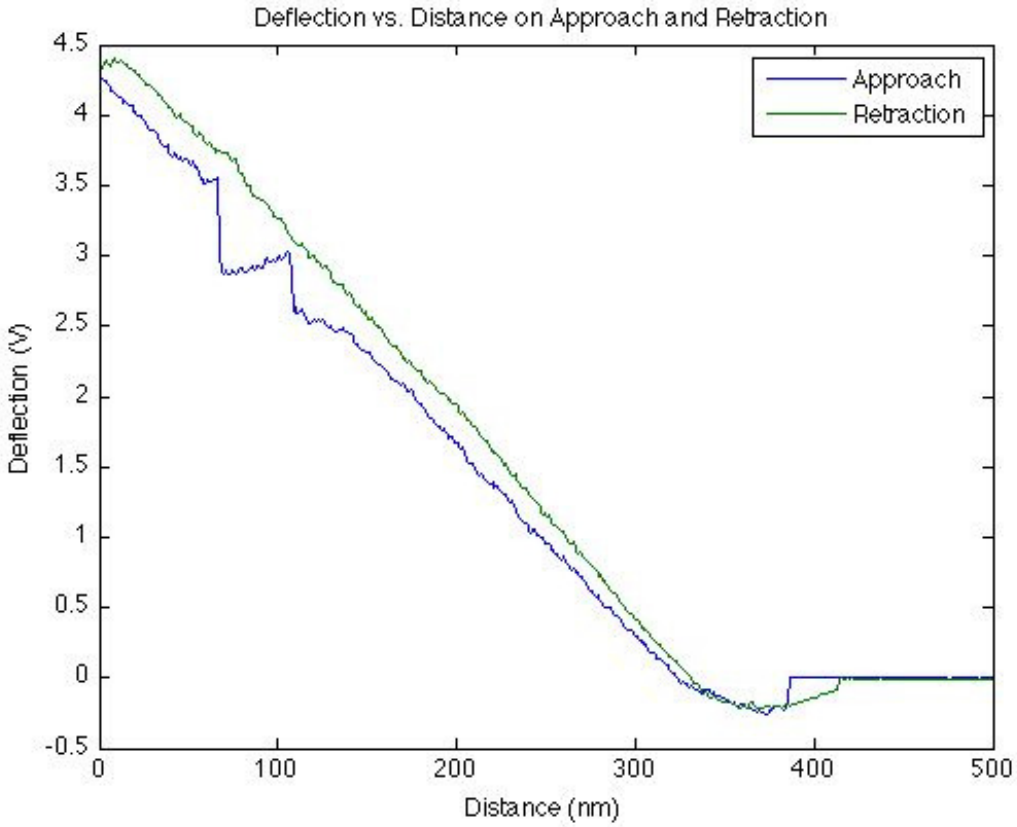
Deflection vs. Distance on Approach and Retraction
Approach
Retraction
Deflection (V)
Distance (nm)
4.5
4
3.5
3
2.5
2
1.5
1
0.5
0
-0.5
0
100
200
300
400
500

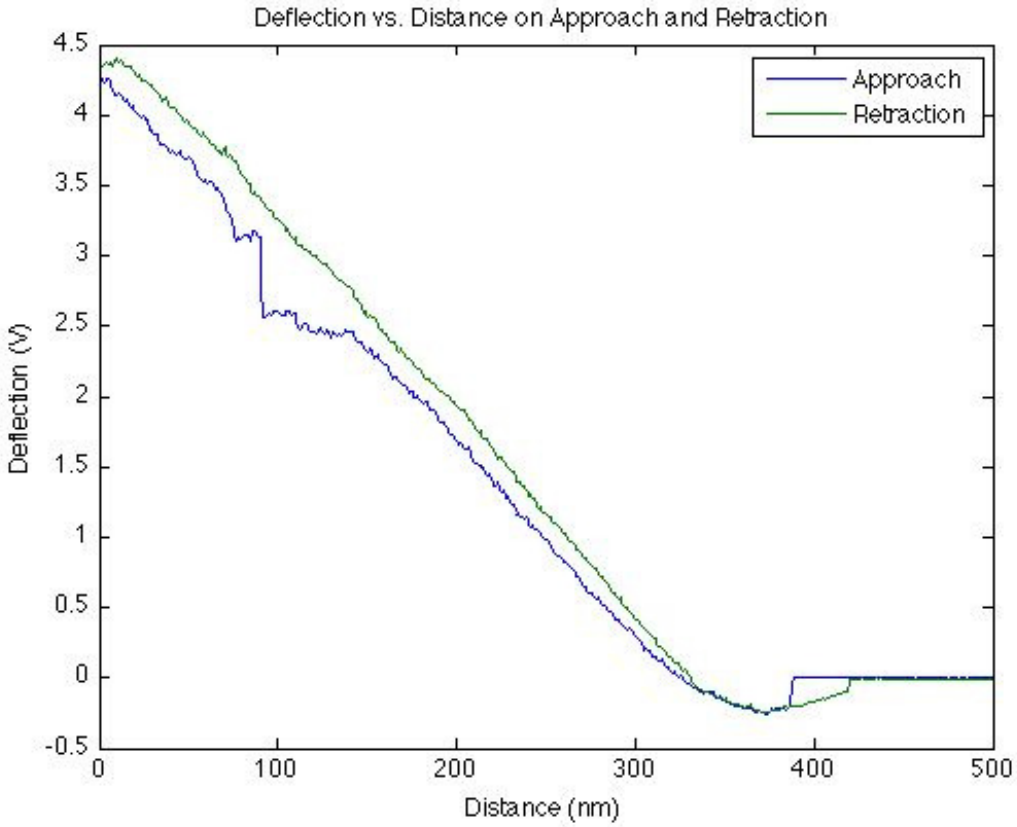
Deflection vs. Distance on Approach and Retraction
Approach
Retraction
Deflection (V)
Distance (nm)
4.5
4
3.5
3
2.5
2
1.5
1
0.5
0
-0.5
0
100
200
300
400
500

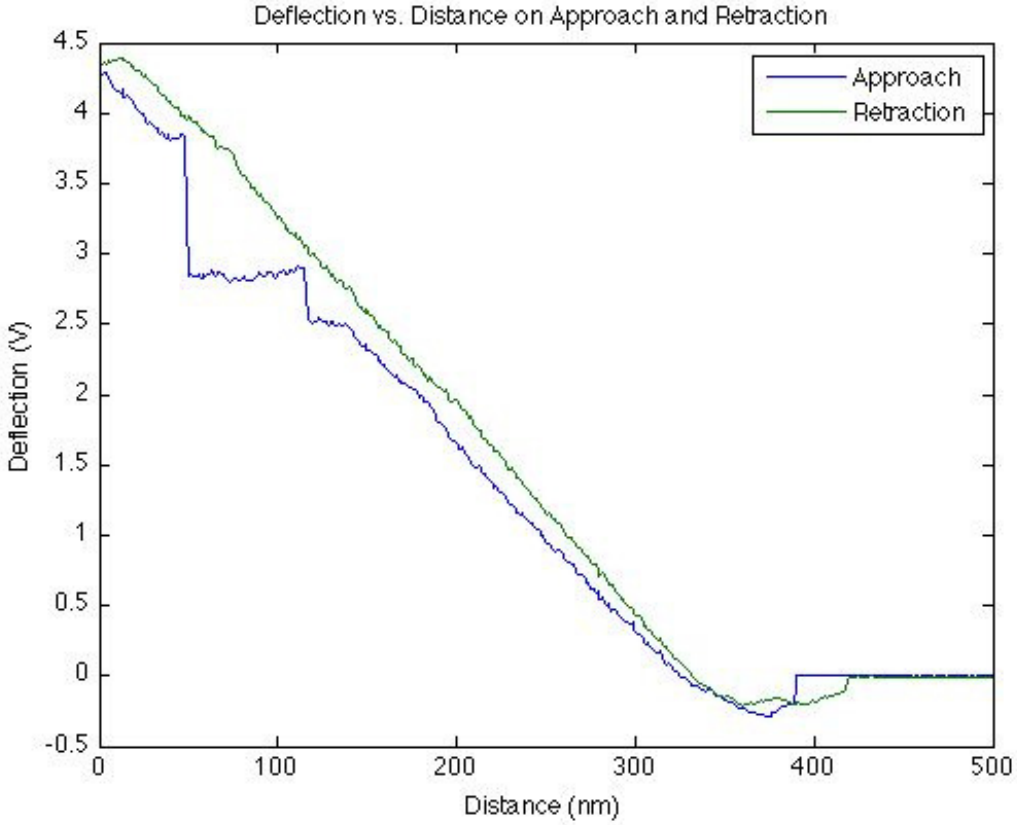
Deflection vs. Distance on Approach and Retraction
Approach
Retraction
Deflection (V)
Distance (nm)
4.5
4
3.5
3
2.5
2
1.5
1
0.5
0
-0.5
0
100
200
300
400
500

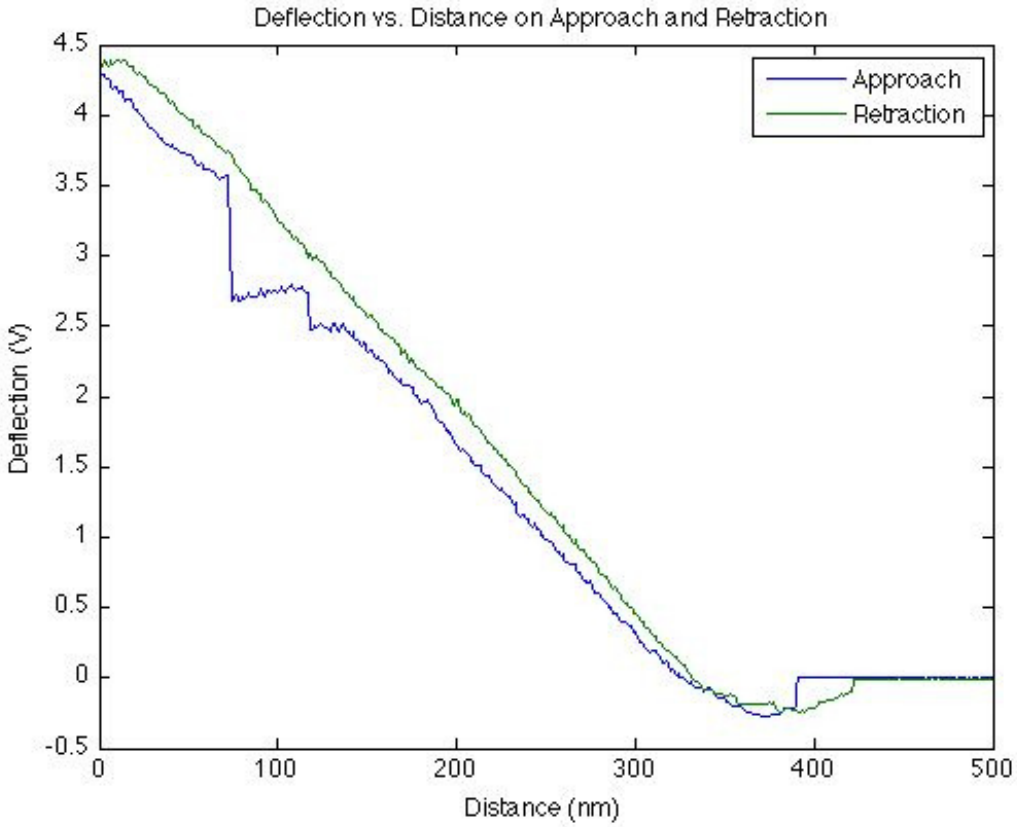
Deflection vs. Distance on Approach and Retraction
Approach
Retraction
Deflection (V)
Distance (nm)
4.5
4
3.5
3
2.5
2
1.5
1
0.5
0
-0.5
0
100
200
300
400
500

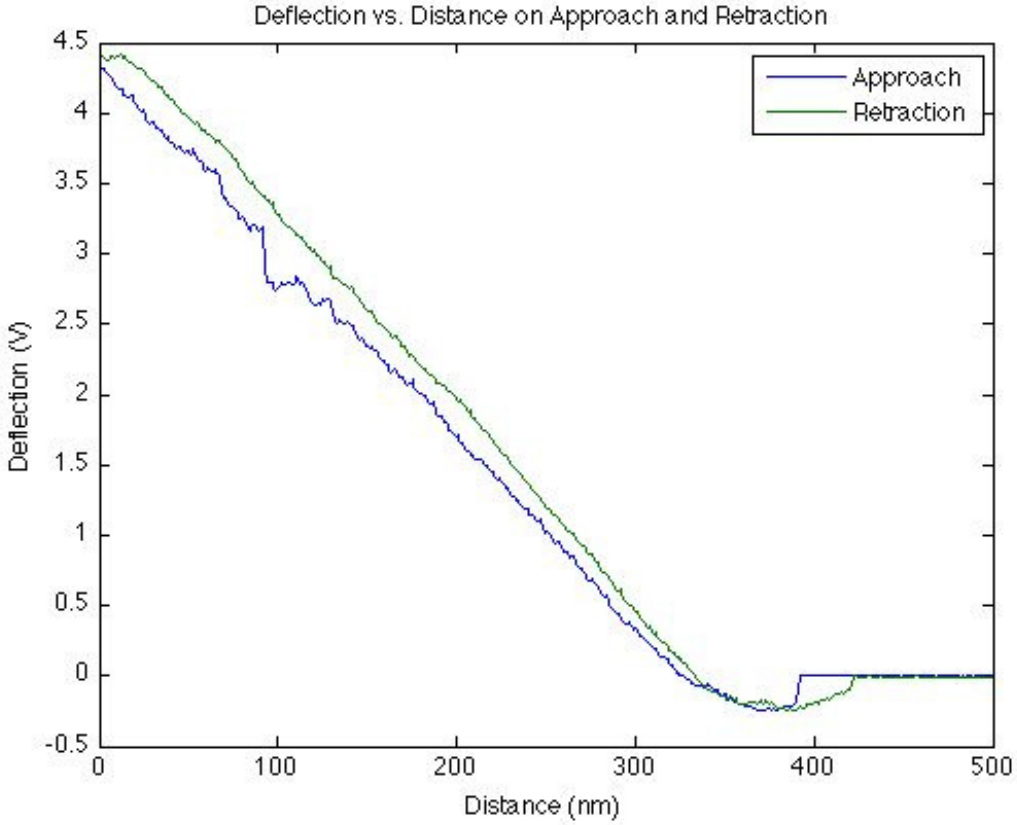
Deflection vs. Distance on Approach and Retraction
Approach
Retraction
Deflection (V)
Distance (nm)
4.5
4
3.5
3
2.5
2
1.5
1
0.5
0
-0.5
0
100
200
300
400
500

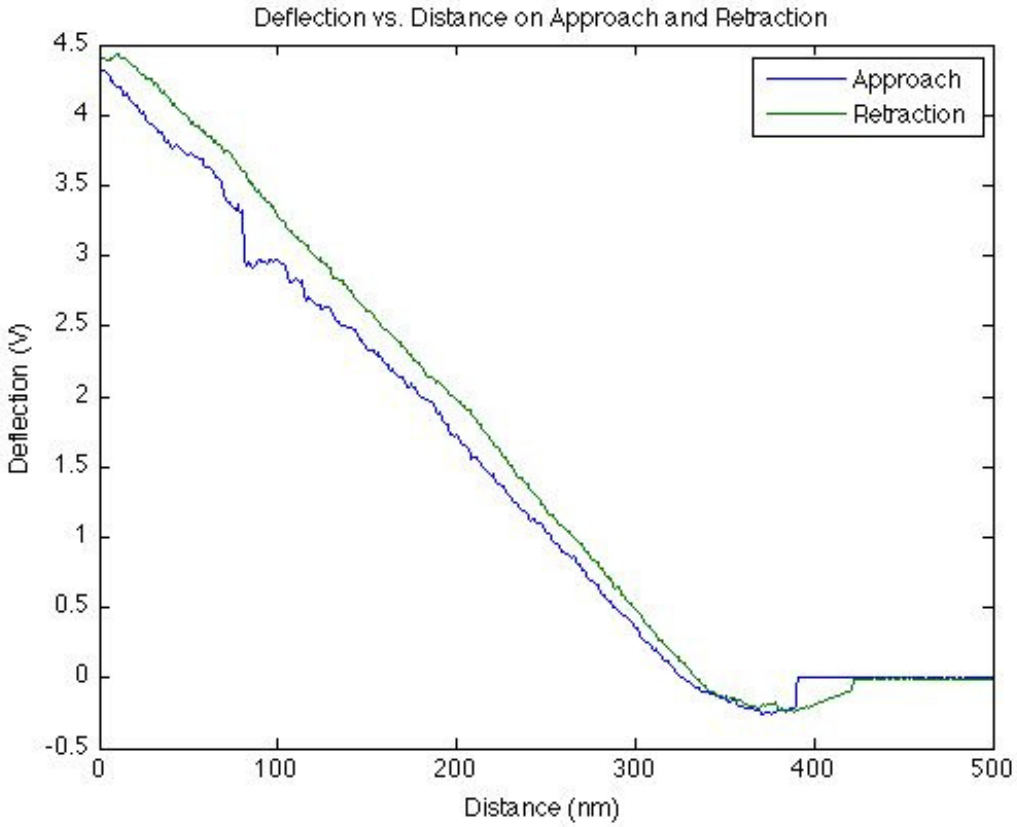
Deflection vs. Distance on Approach and Retraction
Approach
Retraction
Deflection (V)
Distance (nm)
4.5
4
3.5
3
2.5
2
1.5
1
0.5
0
-0.5
0
100
200
300
400
500

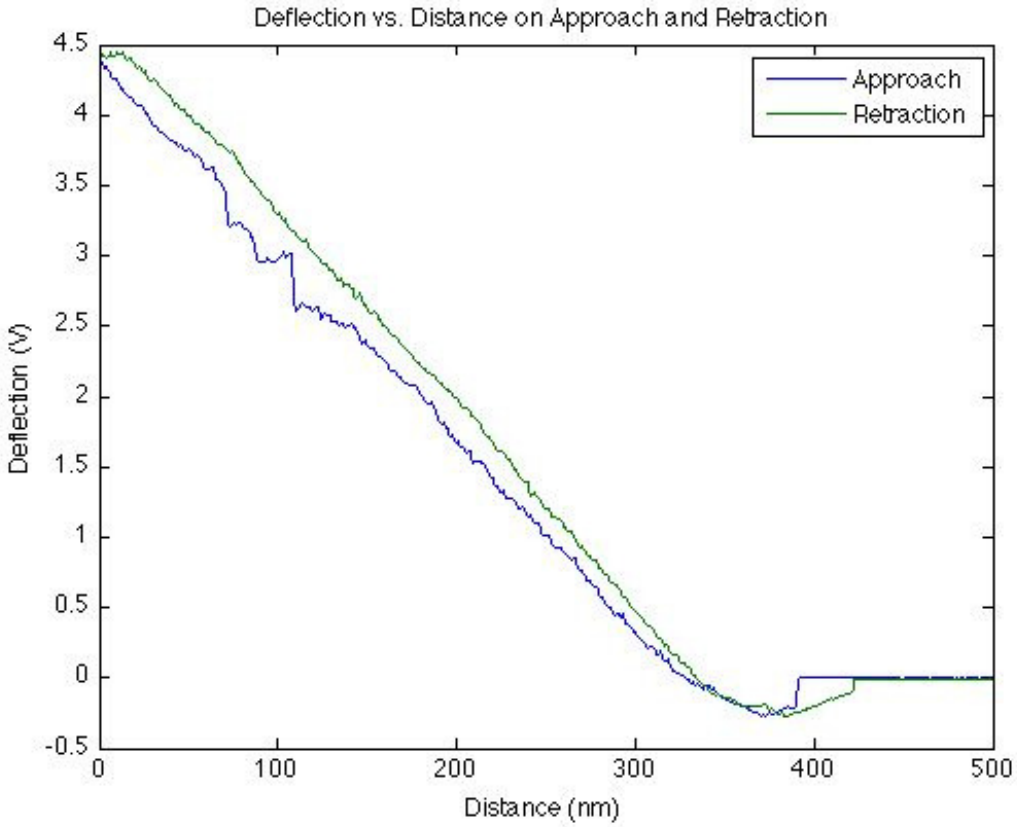
Deflection vs. Distance on Approach and Retraction
Approach
Retraction
Deflection (V)
Distance (nm)
4.5
4
3.5
3
2.5
2
1.5
1
0.5
0
-0.5
0
100
200
300
400
500

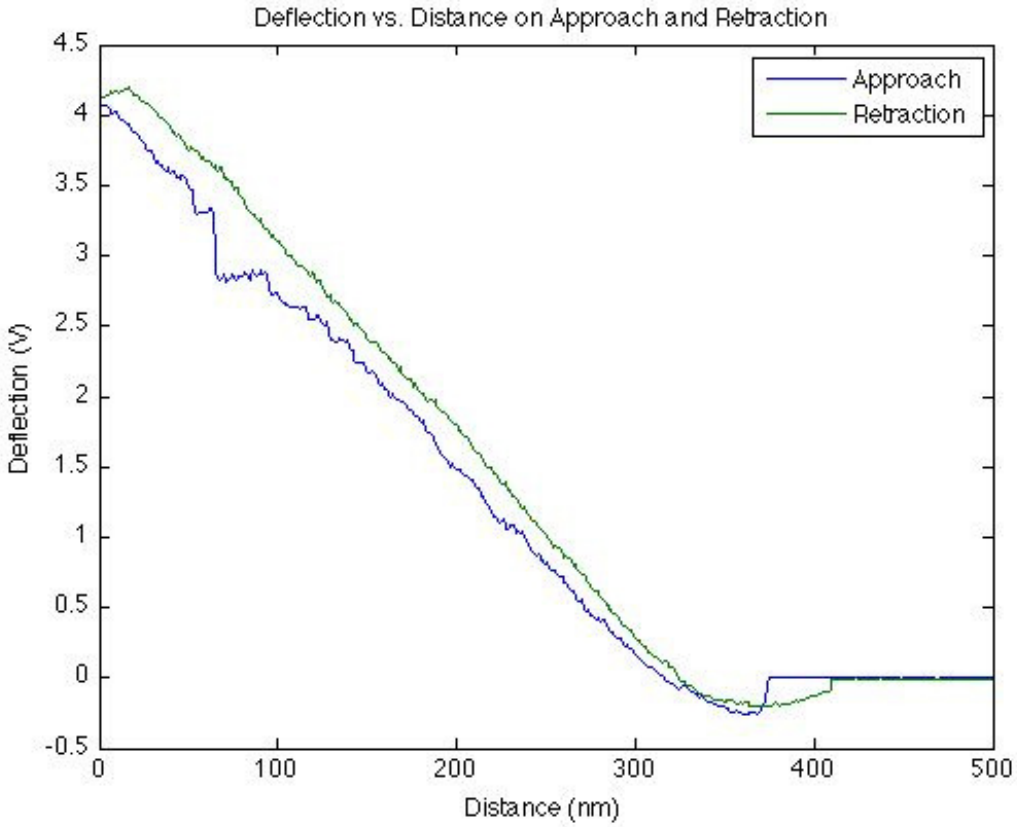
Deflection vs. Distance on Approach and Retraction
Approach
Retraction
Deflection (V)
Distance (nm)
4.5
4
3.5
3
2.5
2
1.5
1
0.5
0
-0.5
0
100
200
300
400
500

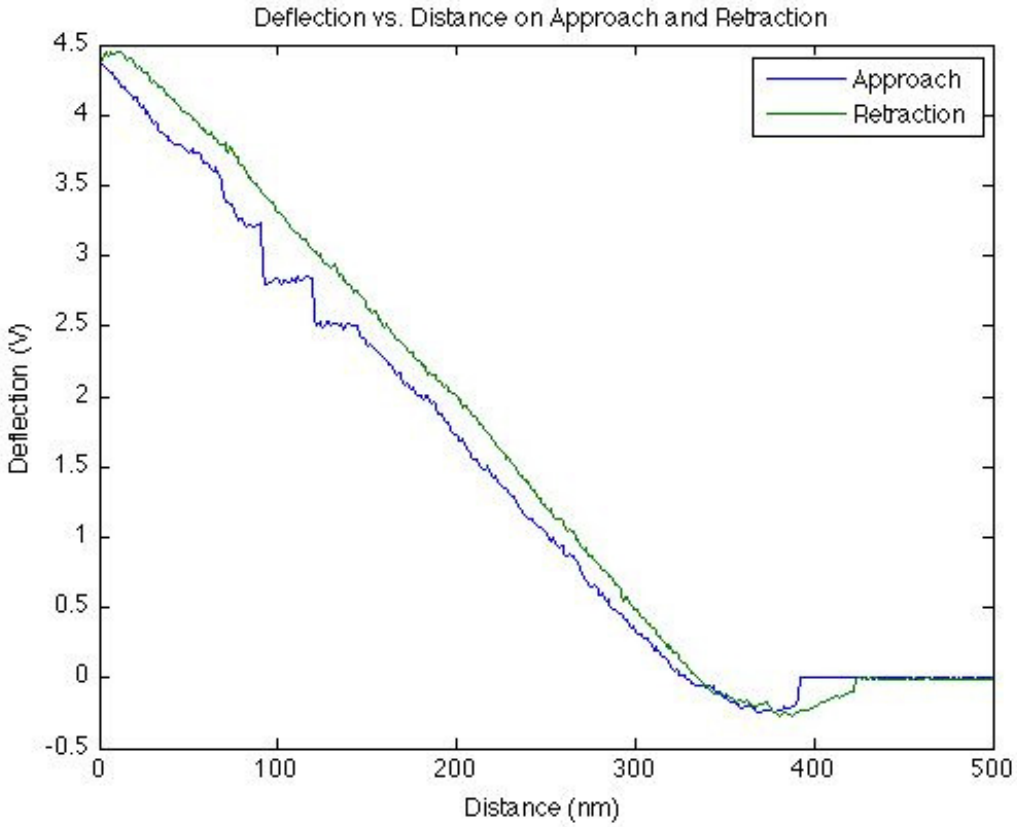
Deflection vs. Distance on Approach and Retraction
Approach
Retraction
Deflection (V)
Distance (nm)
4.5
4
3.5
3
2.5
2
1.5
1
0.5
0
-0.5
0
100
200
300
400
500

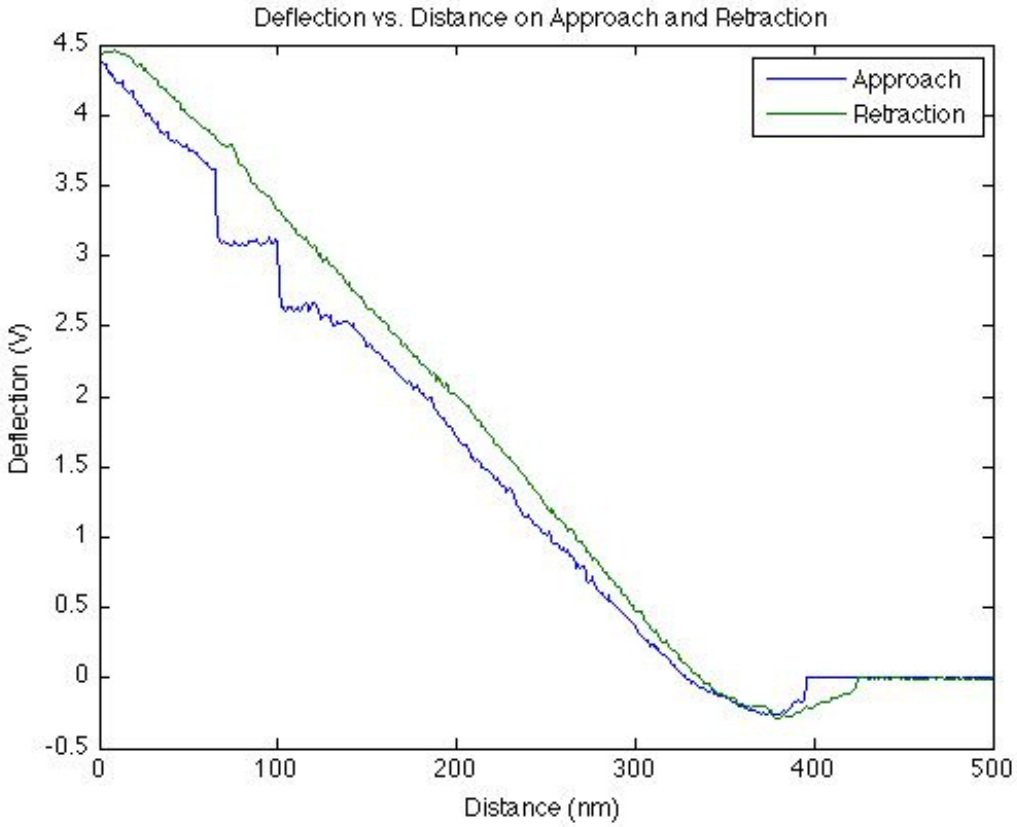
Deflection vs. Distance on Approach and Retraction
Approach
Retraction
Deflection (V)
Distance (nm)
4.5
4
3.5
3
2.5
2
1.5
1
0.5
0
-0.5
0
100
200
300
400
500

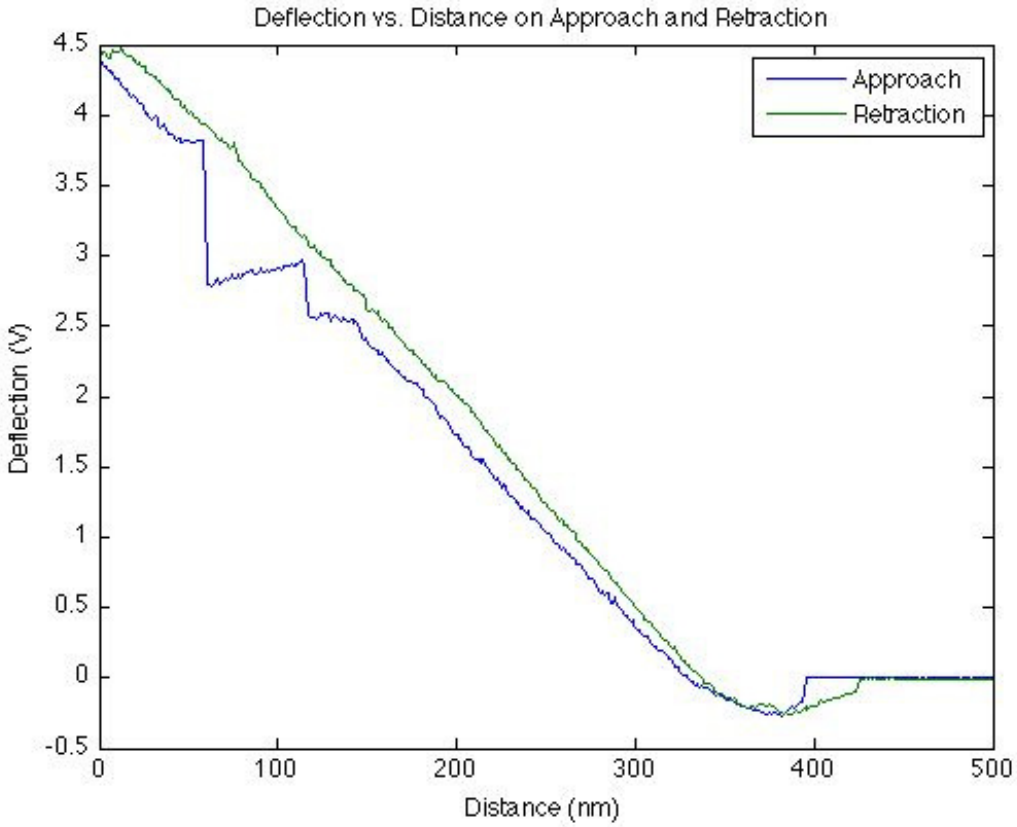
Deflection vs. Distance on Approach and Retraction
Approach
Retraction
Deflection (V)
Distance (nm)
4.5
4
3.5
3
2.5
2
1.5
1
0.5
0
-0.5
0
100
200
300
400
500

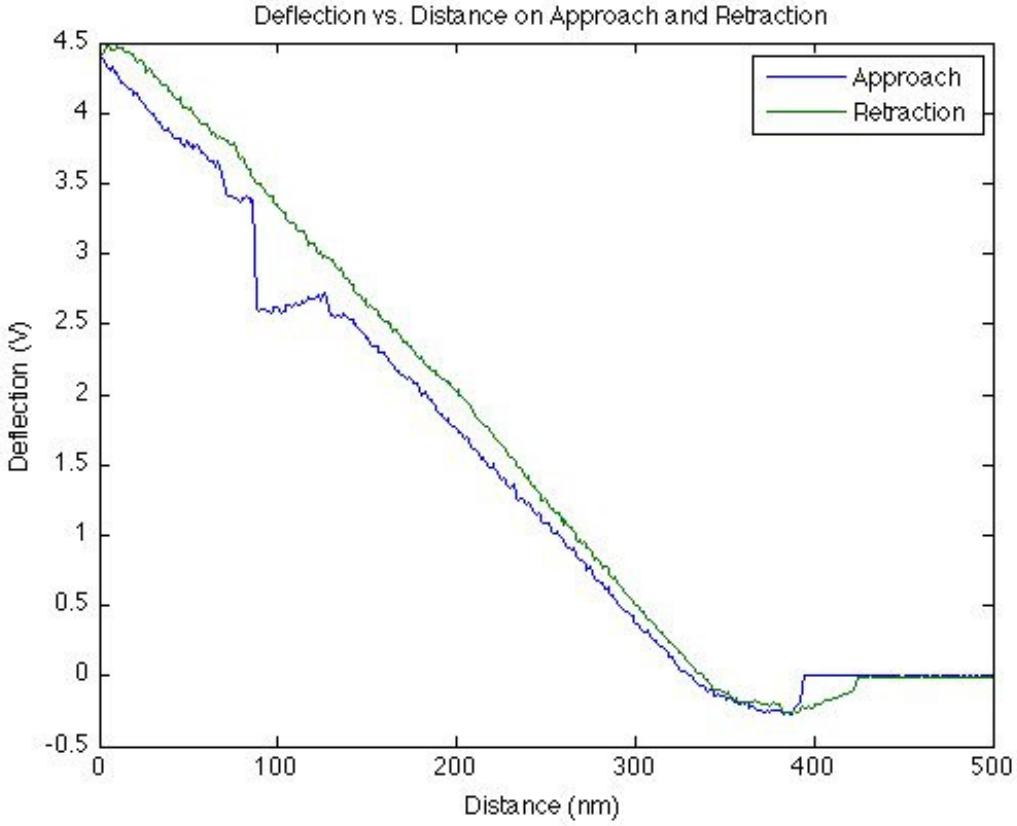
Deflection vs. Distance on Approach and Retraction
Approach
Retraction
Deflection (V)
Distance (nm)
4.5
4
3.5
3
2.5
2
1.5
1
0.5
0
-0.5
0
100
200
300
400
500

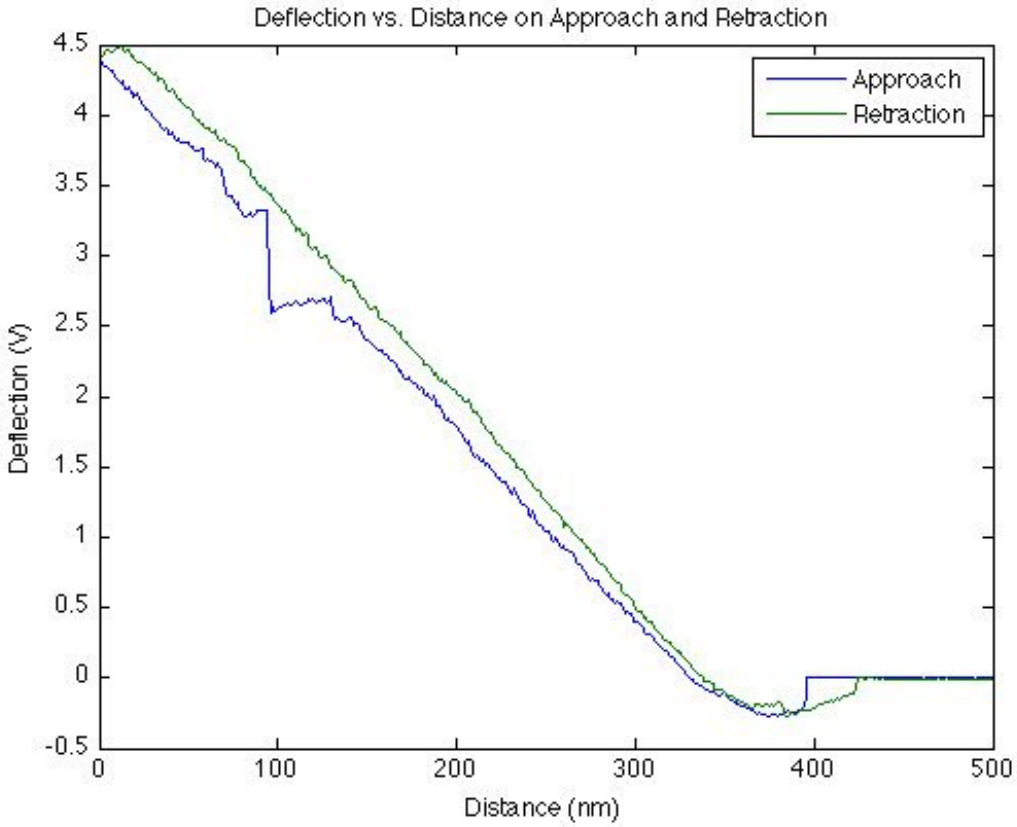
Deflection vs. Distance on Approach and Retraction
Approach
Retraction
Deflection (V)
Distance (nm)
4.5
4
3.5
3
2.5
2
1.5
1
0.5
0
-0.5
0
100
200
300
400
500

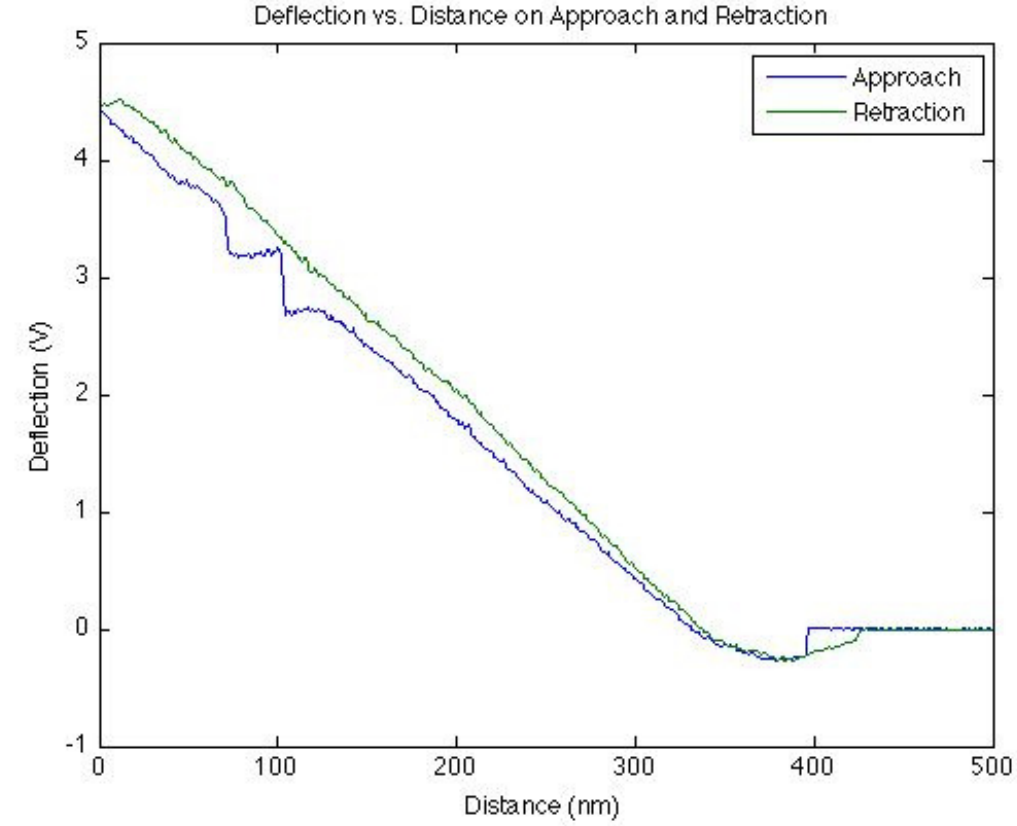
Deflection vs. Distance on Approach and Retraction
Approach
Retraction
Deflection (V)
Distance (nm)
5
4
3
2
1
0
-1
0
100
200
300
400
500

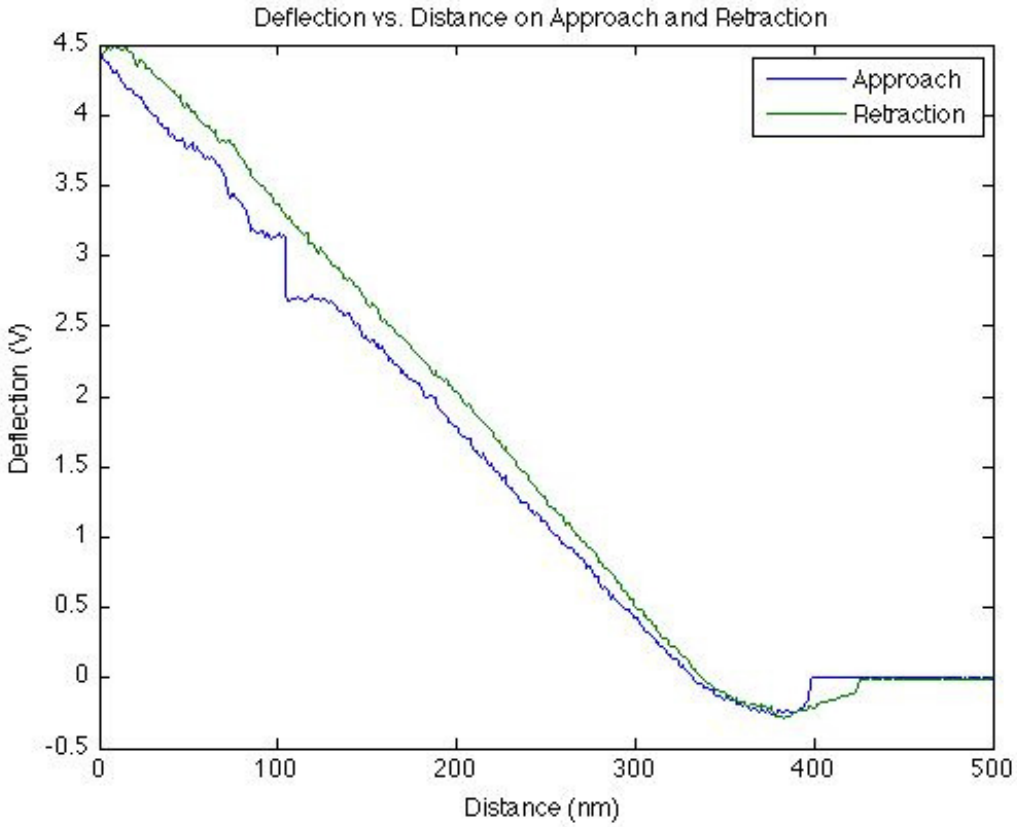
Deflection vs. Distance on Approach and Retraction
Approach
Retraction
Deflection (V)
Distance (nm)
4.5
4
3.5
3
2.5
2
1.5
1
0.5
0
-0.5
0
100
200
300
400
500

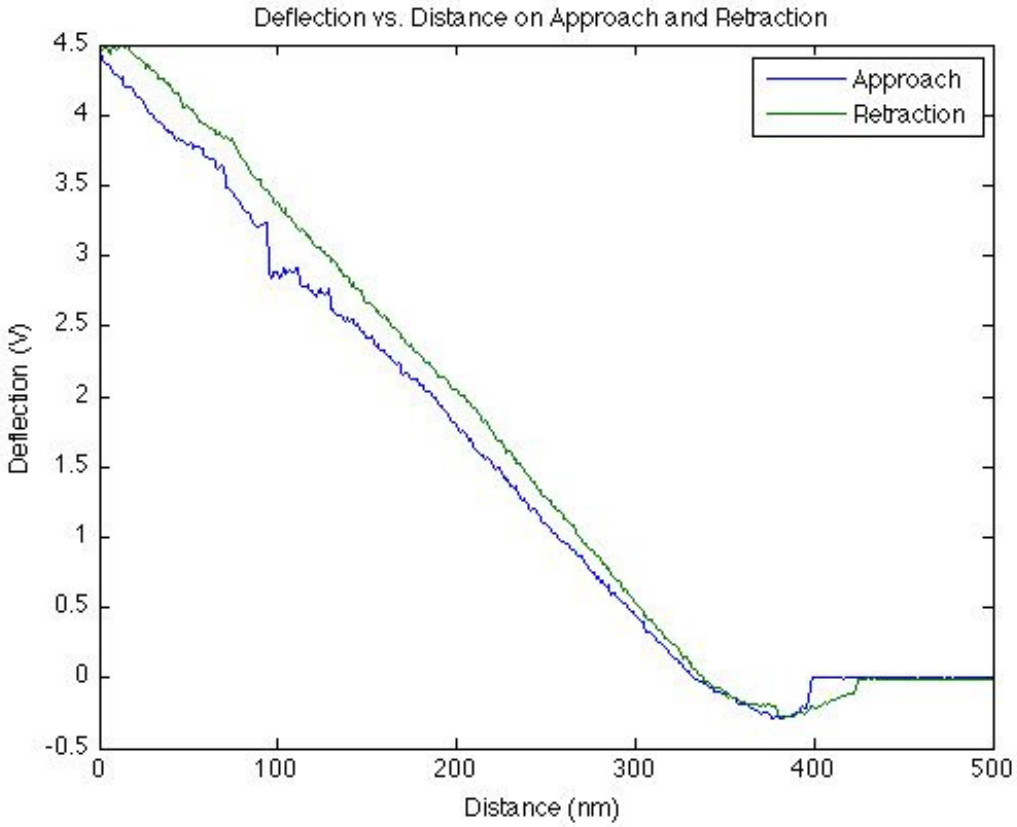
Deflection vs. Distance on Approach and Retraction
Approach
Retraction
Deflection (V)
Distance (nm)
4.5
4
3.5
3
2.5
2
1.5
1
0.5
0
-0.5
0
100
200
300
400
500

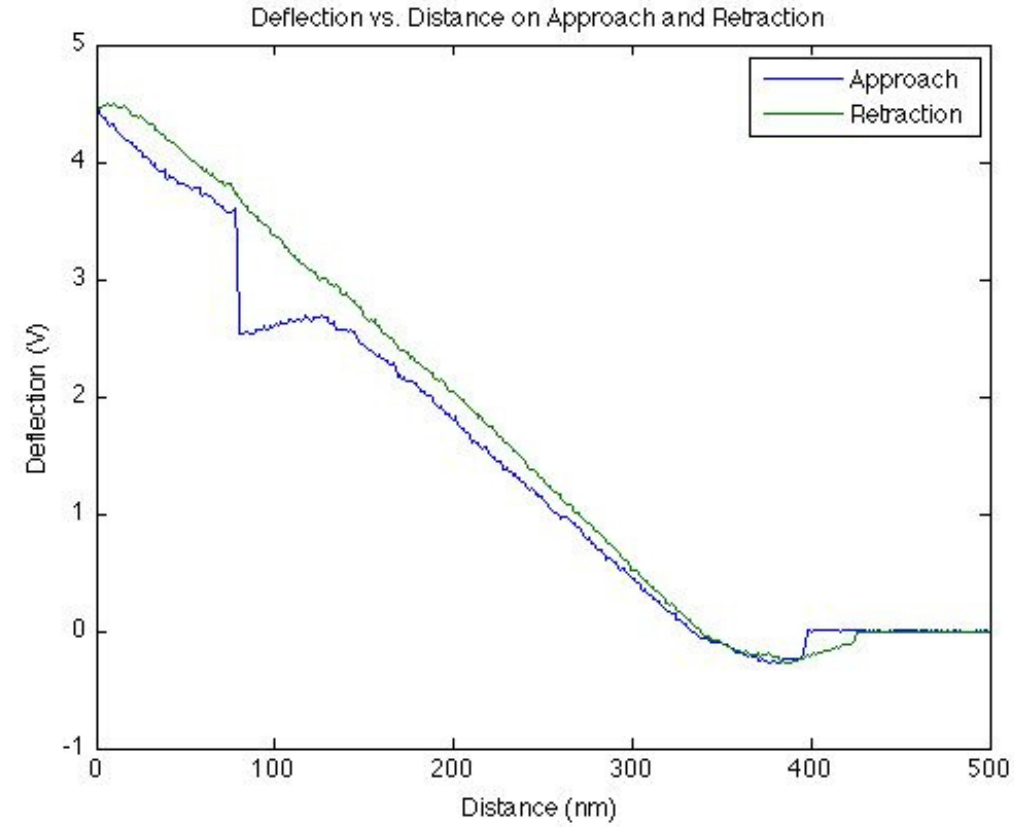
Deflection vs. Distance on Approach and Retraction
Approach
Retraction
Deflection (V)
Distance (nm)
5
4
3
2
1
0
-1
0
100
200
300
400
500

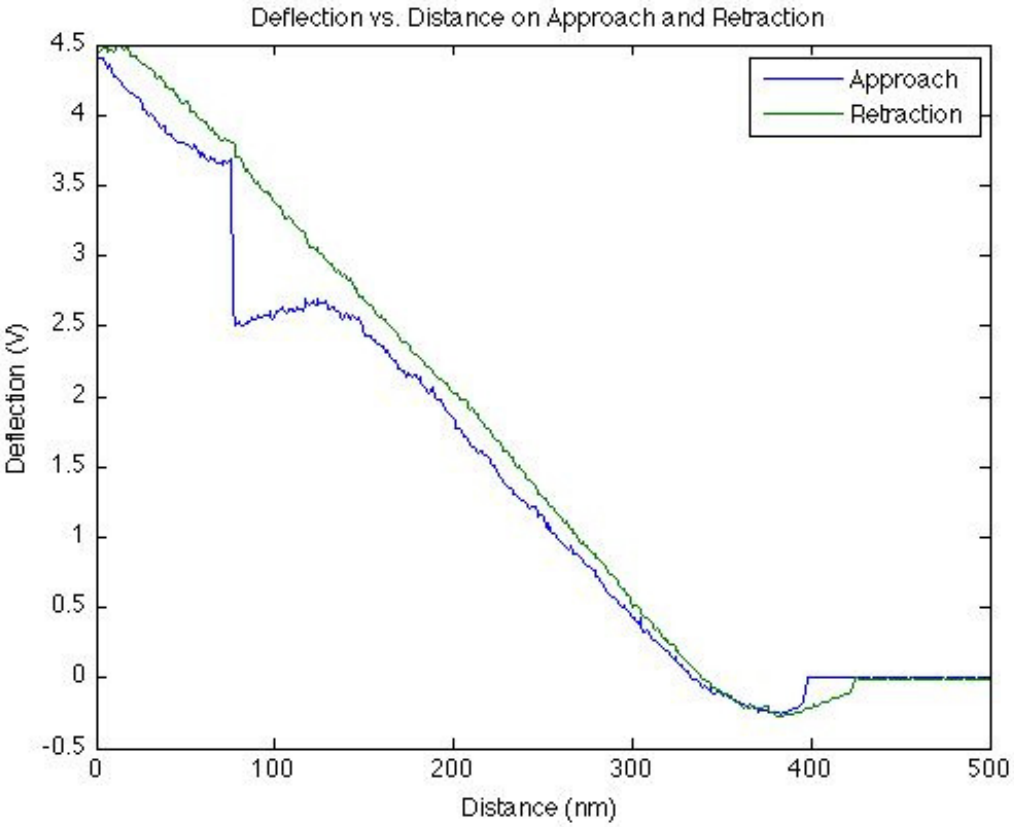
Deflection vs. Distance on Approach and Retraction
Approach
Retraction
Deflection (V)
Distance (nm)
4.5
4
3.5
3
2.5
2
1.5
1
0.5
0
-0.5
0
100
200
300
400
500

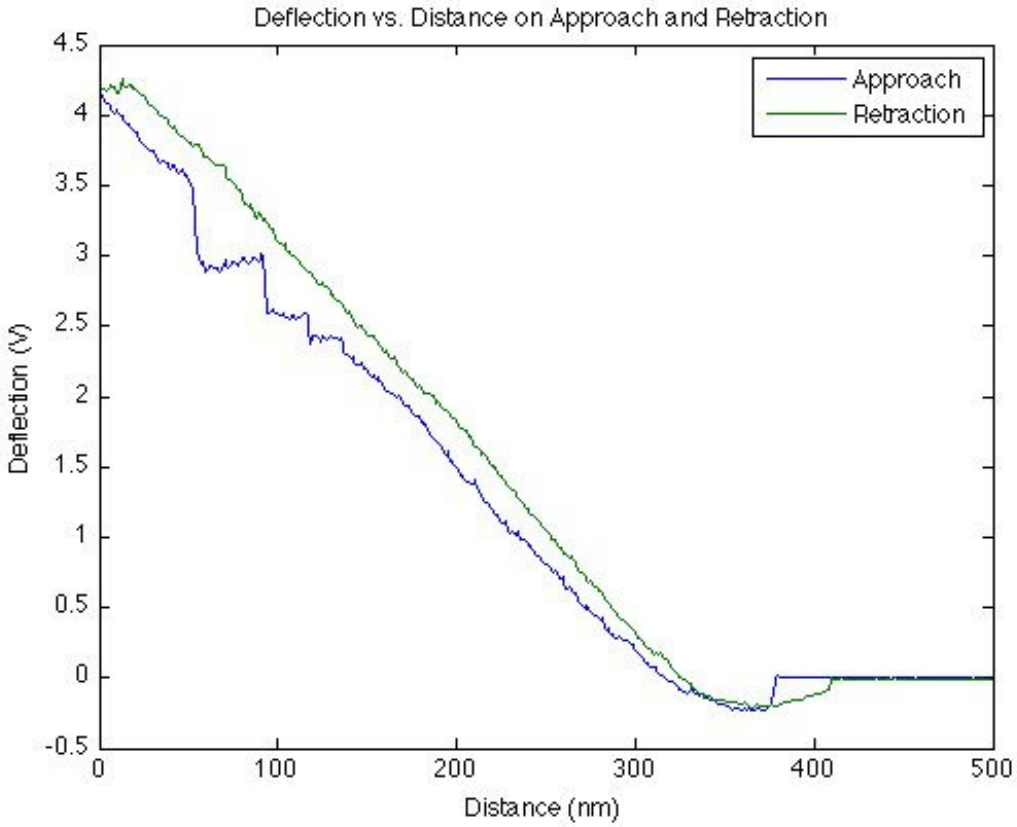
Deflection vs. Distance on Approach and Retraction
Approach
Retraction
Deflection (V)
Distance (nm)
4.5
4
3.5
3
2.5
2
1.5
1
0.5
0
-0.5
0
100
200
300
400
500

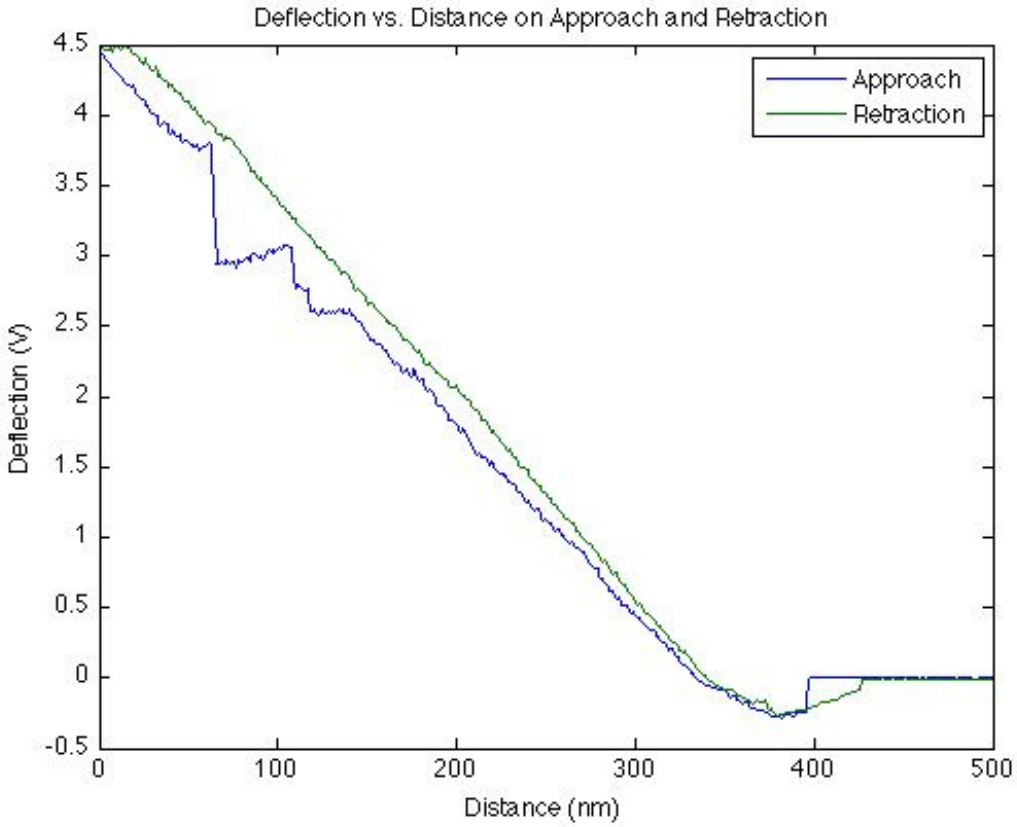
Deflection vs. Distance on Approach and Retraction
Approach
Retraction
Deflection (V)
Distance (nm)
4.5
4
3.5
3
2.5
2
1.5
1
0.5
0
-0.5
0
100
200
300
400
500

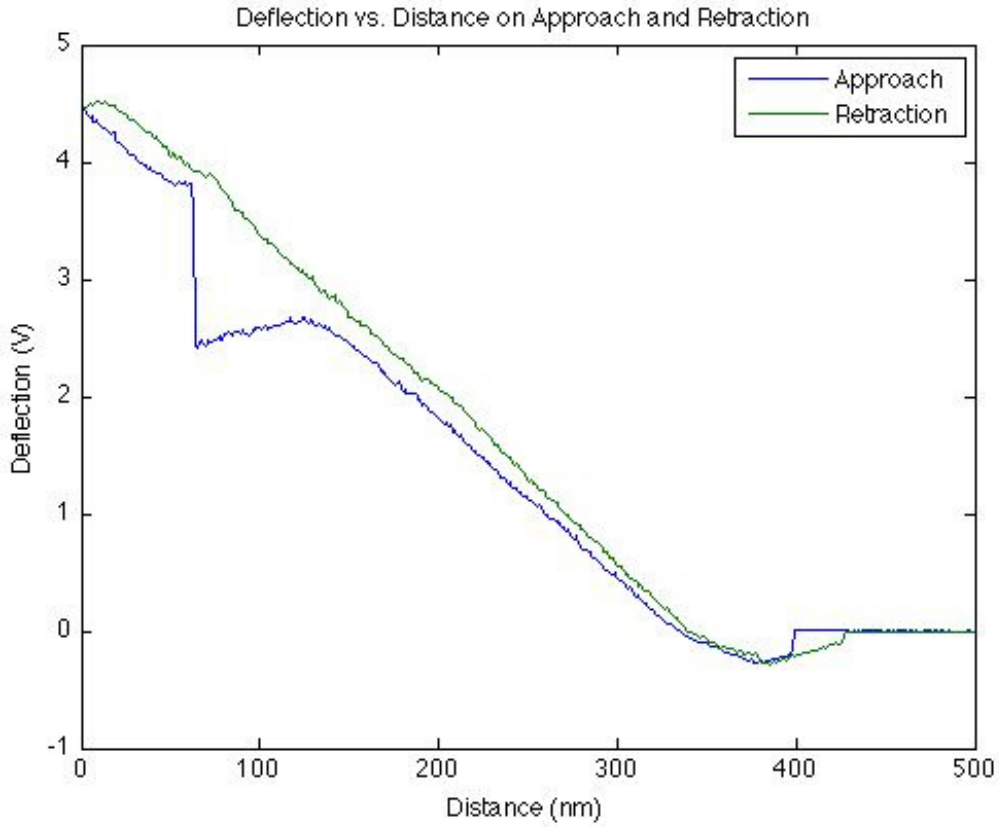
Deflection vs. Distance on Approach and Retraction
Approach
Retraction
Deflection (V)
Distance (nm)
5
4
3
2
1
0
-1
0
100
200
300
400
500

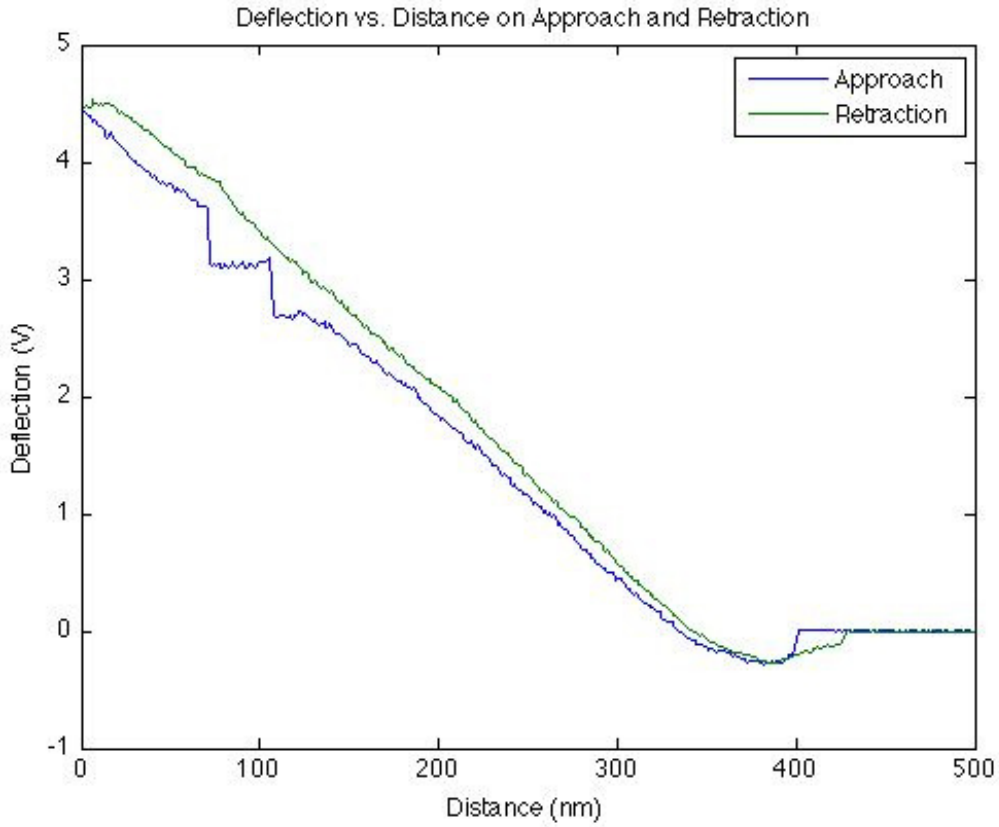
Deflection vs. Distance on Approach and Retraction
Approach
Retraction
Deflection (V)
Distance (nm)
5
4
3
2
1
0
-1
0
100
200
300
400
500

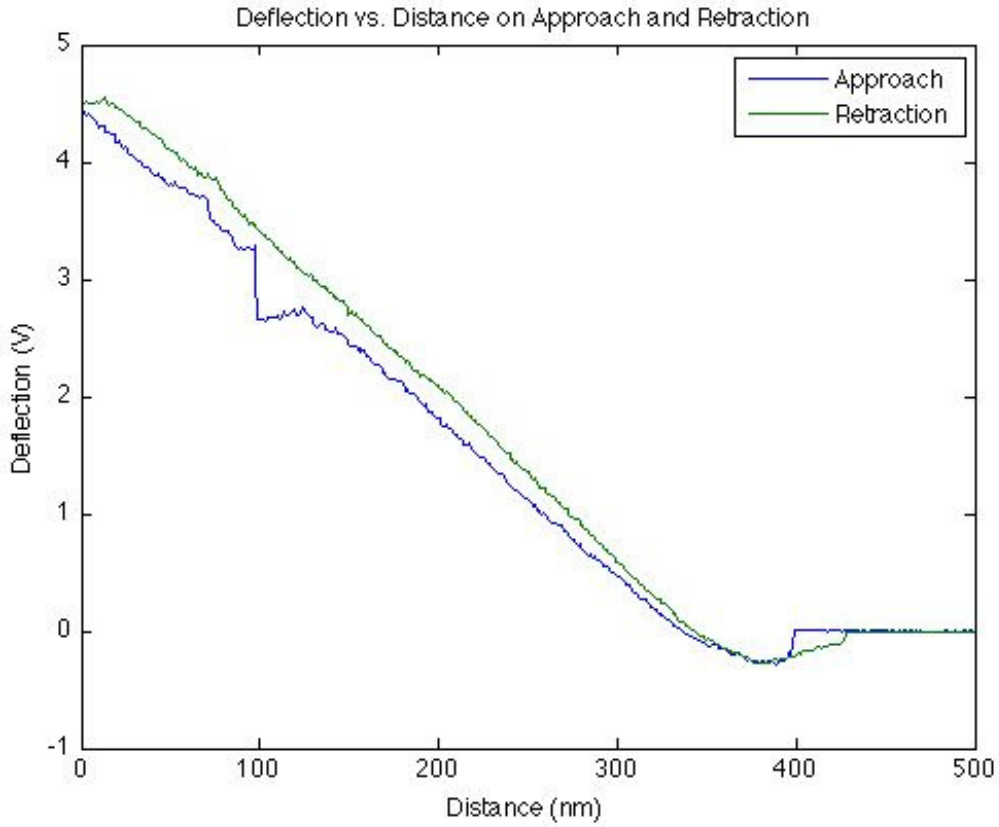
Deflection vs. Distance on Approach and Retraction
Approach
Retraction
Deflection (V)
Distance (nm)
5
4
3
2
1
0
-1
0
100
200
300
400
500

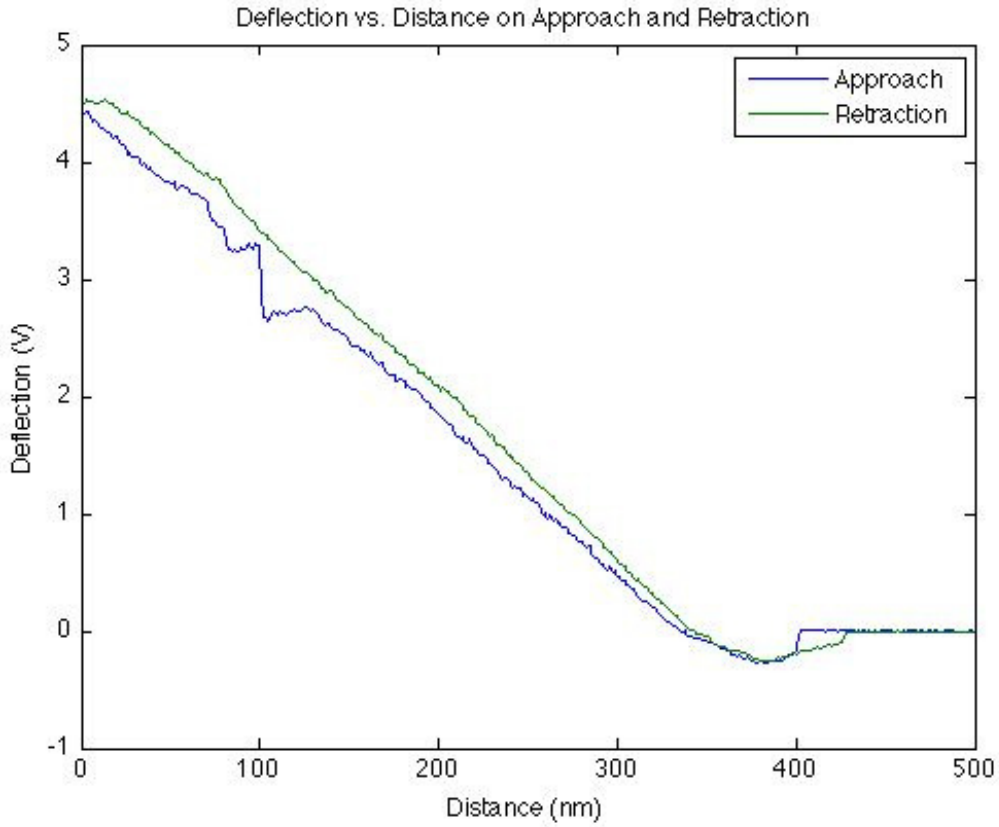
Deflection vs. Distance on Approach and Retraction
Approach
Retraction
Deflection (V)
Distance (nm)
5
4
3
2
1
0
-1
0
100
200
300
400
500

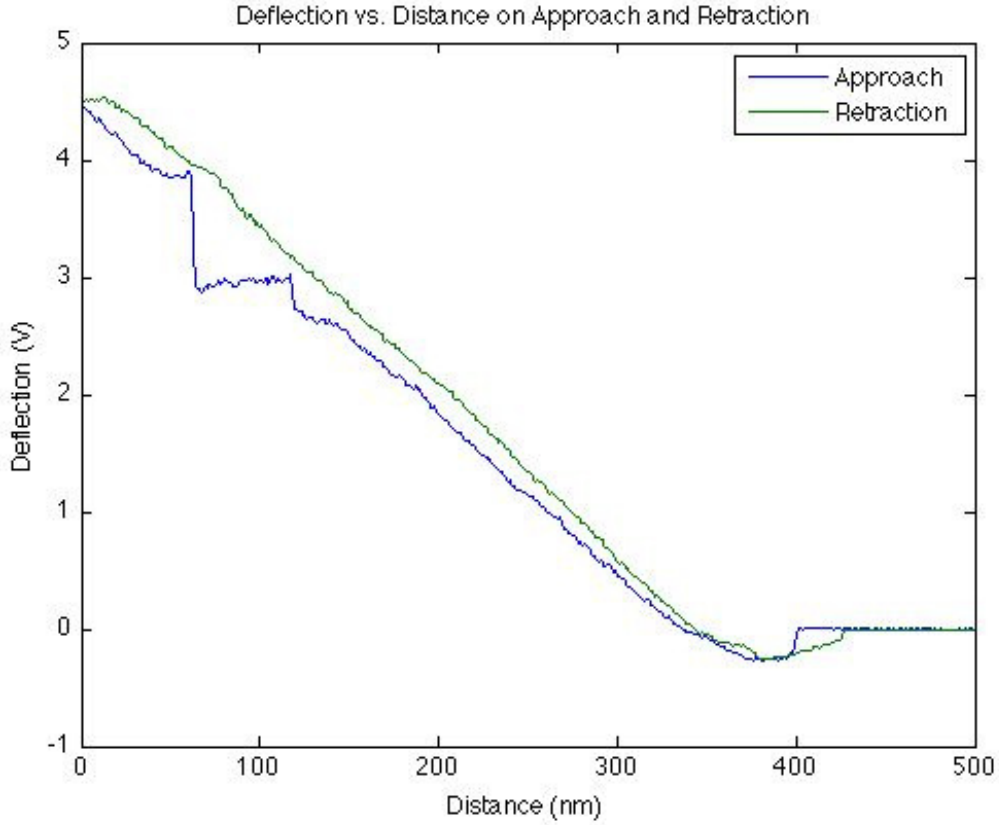
Deflection vs. Distance on Approach and Retraction
Approach
Retraction
Deflection (V)
Distance (nm)
5
4
3
2
1
0
-1
0
100
200
300
400
500

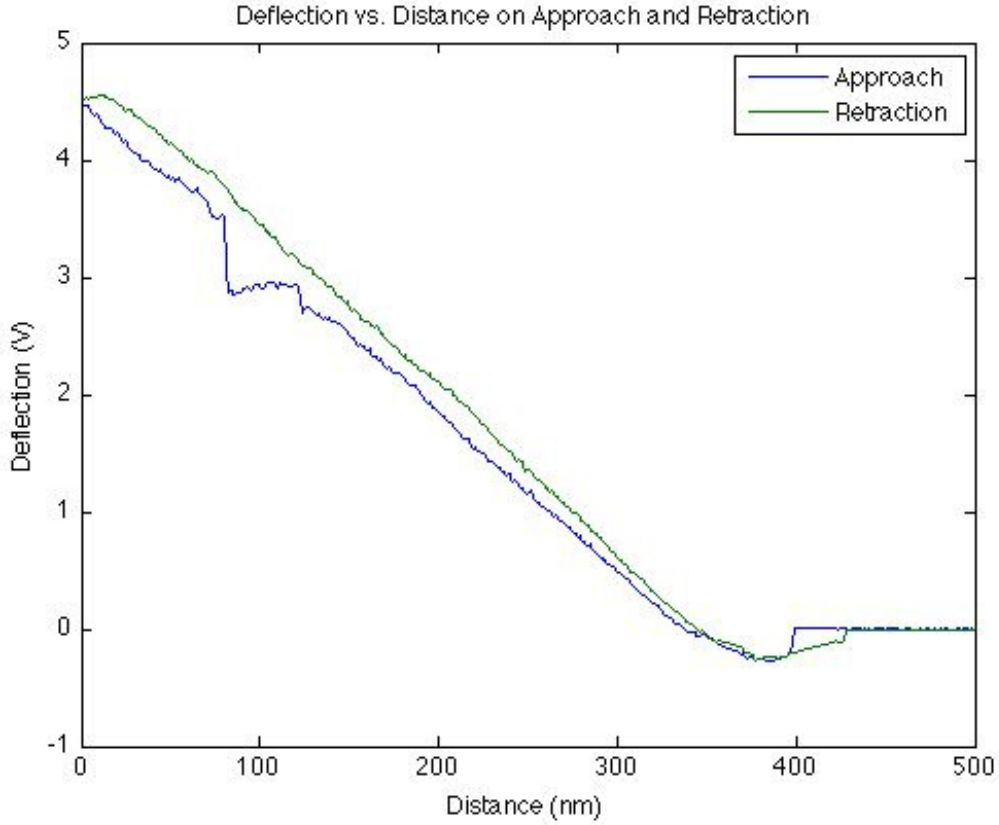
Deflection vs. Distance on Approach and Retraction
Approach
Retraction
Deflection (V)
Distance (nm)
5
4
3
2
1
0
-1
0
100
200
300
400
500

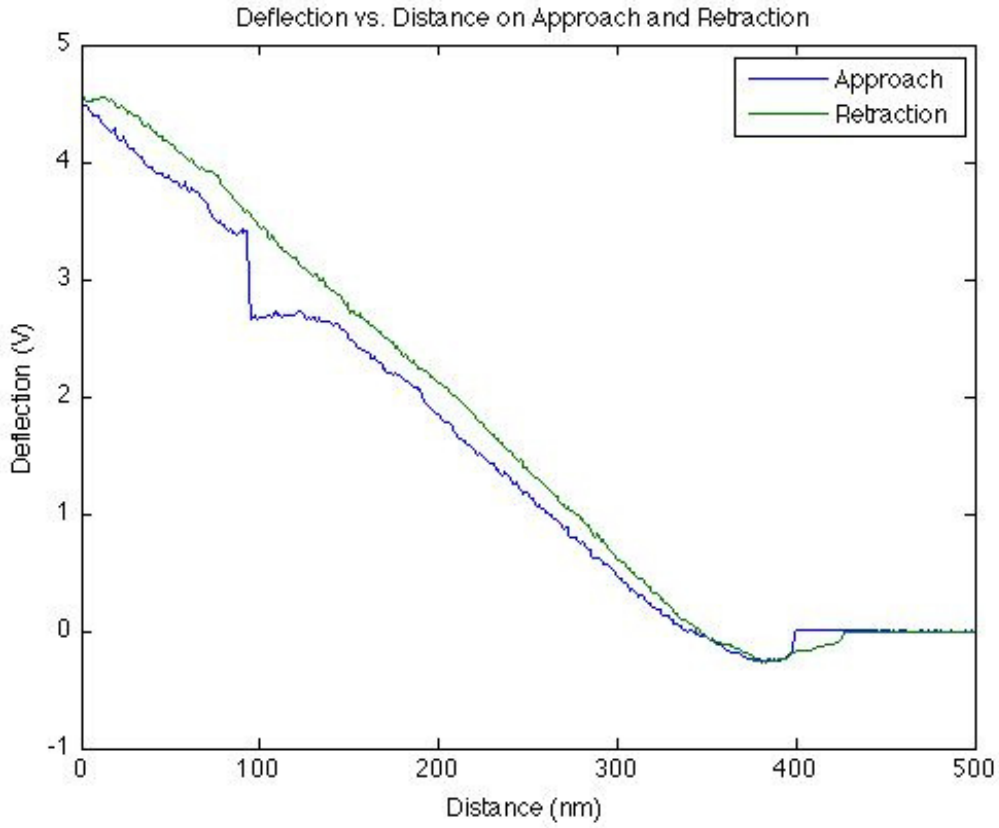
Deflection vs. Distance on Approach and Retraction
Approach
Retraction
Deflection (V)
Distance (nm)
5
4
3
2
1
0
-1
0
100
200
300
400
500

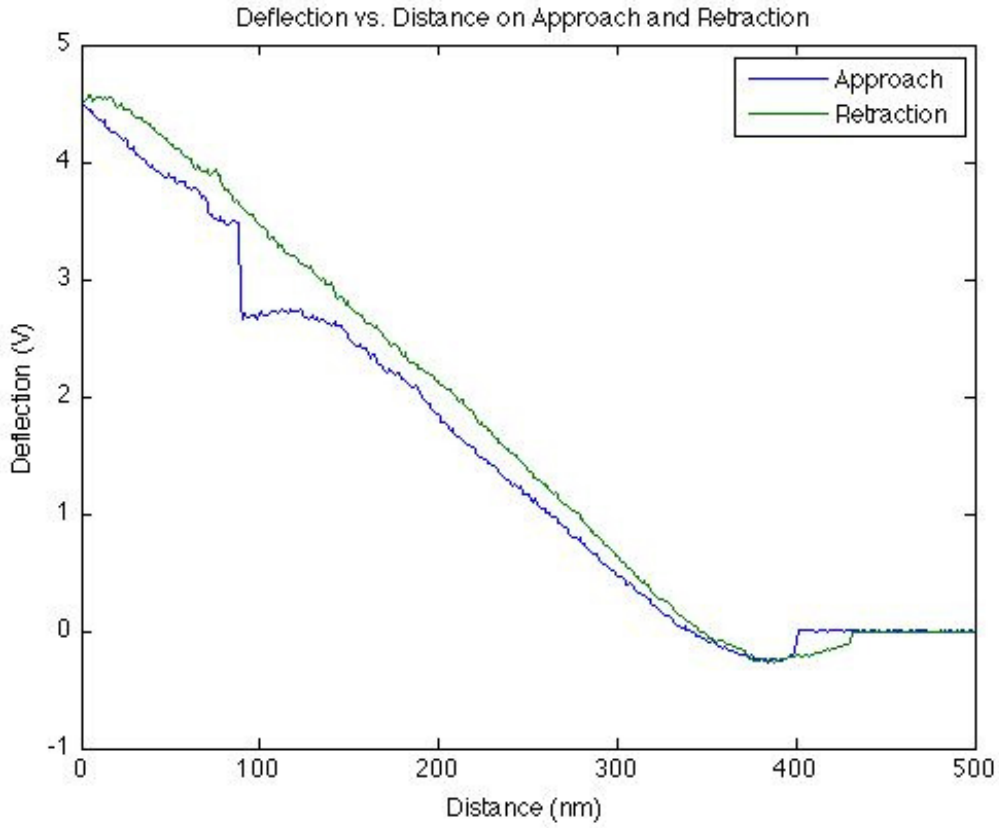
Deflection vs. Distance on Approach and Retraction
Approach
Retraction
Deflection (V)
Distance (nm)
5
4
3
2
1
0
-1
0
100
200
300
400
500

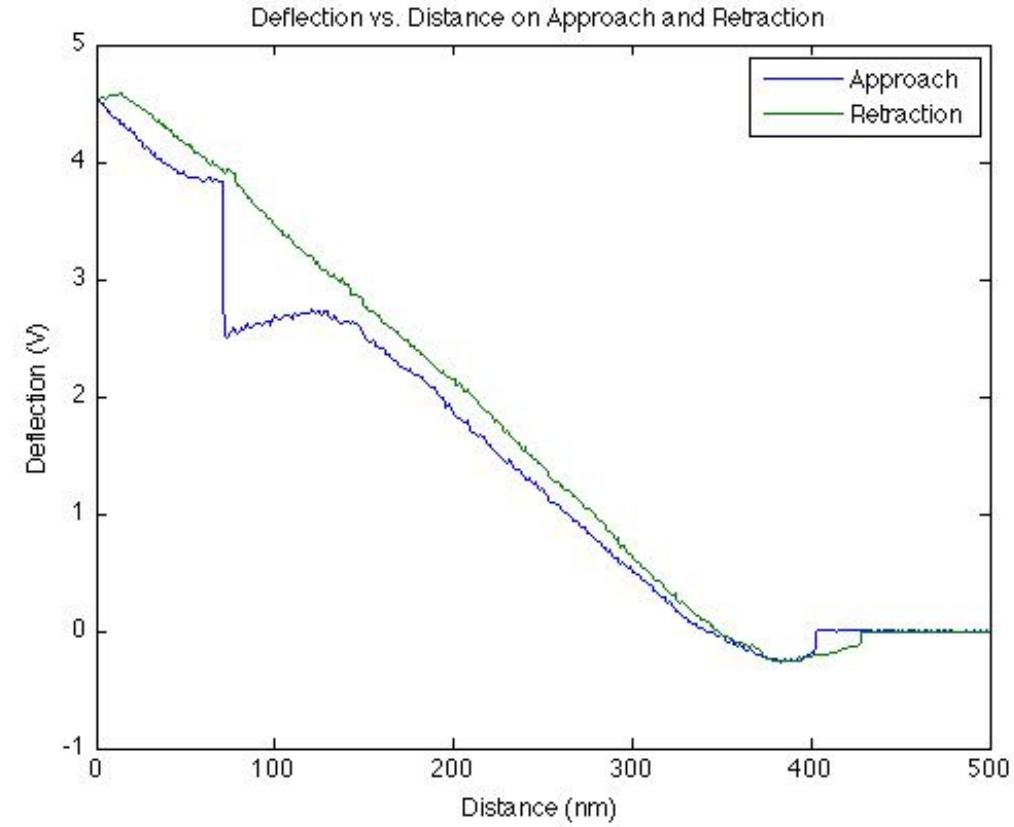
Deflection vs. Distance on Approach and Retraction
Approach
Retraction
Deflection (V)
Distance (nm)
5
4
3
2
1
0
-1
0
100
200
300
400
500

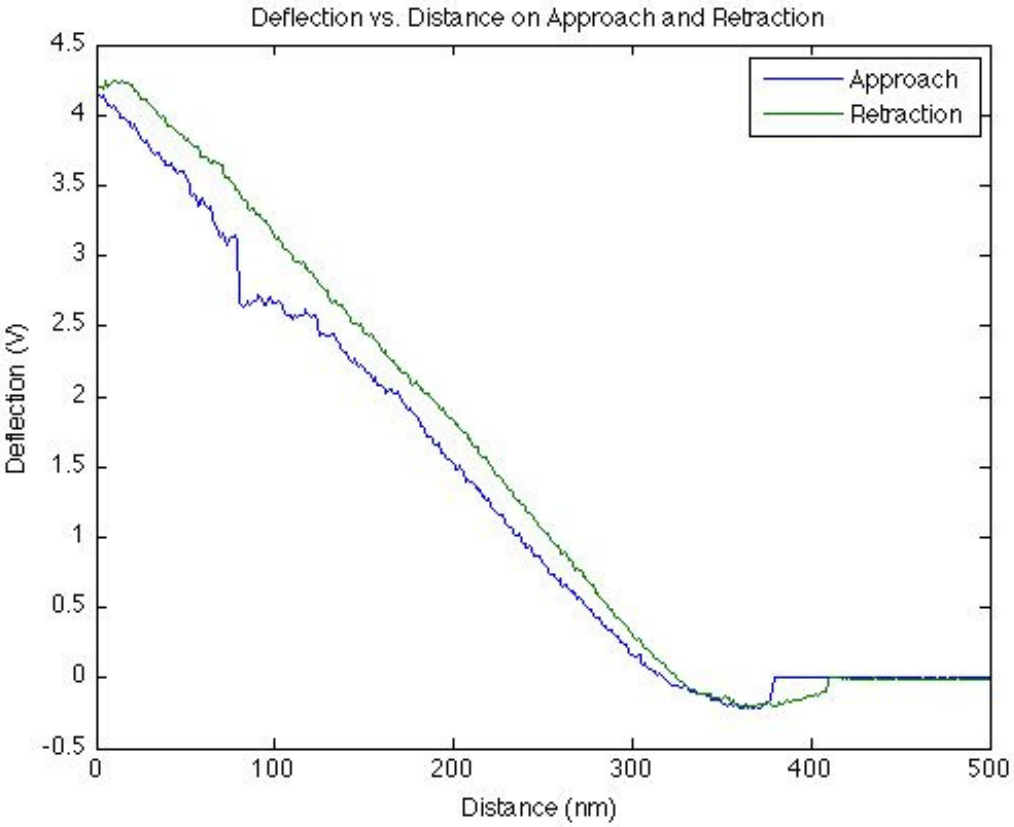
Deflection vs. Distance on Approach and Retraction
Approach
Retraction
Deflection (V)
Distance (nm)
4.5
4
3.5
3
2.5
2
1.5
1
0.5
0
-0.5
0
100
200
300
400
500

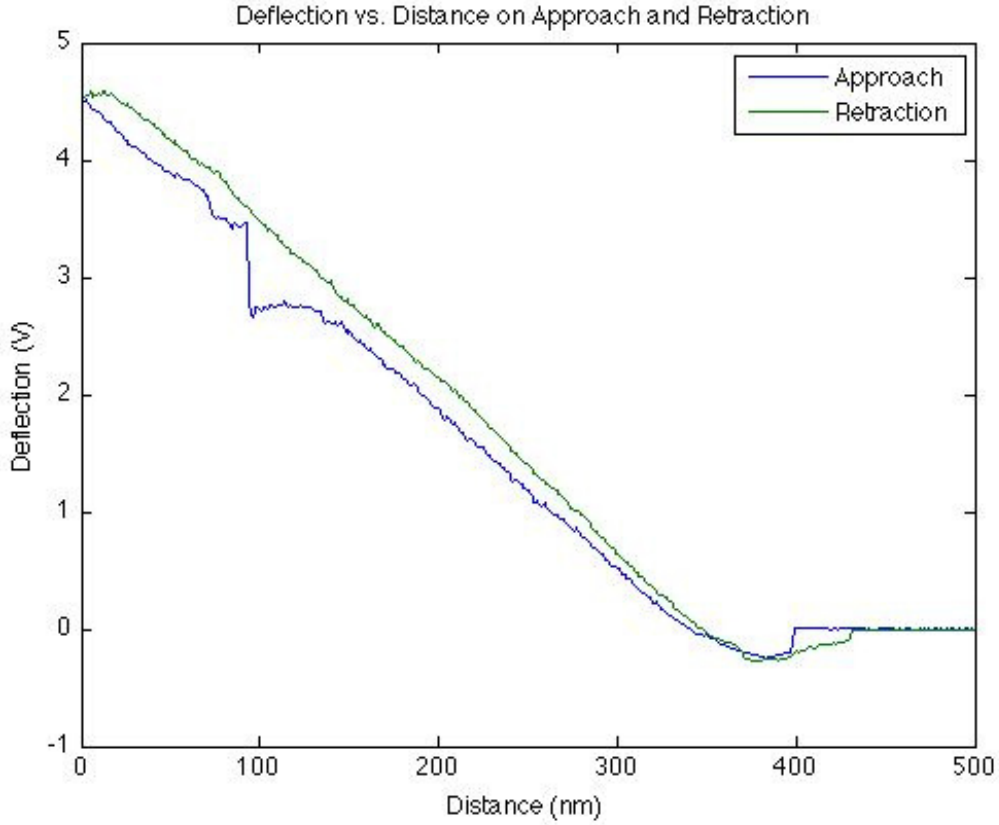
Deflection vs. Distance on Approach and Retraction
Approach
Retraction
Deflection (V)
Distance (nm)
5
4
3
2
1
0
-1
0
100
200
300
400
500

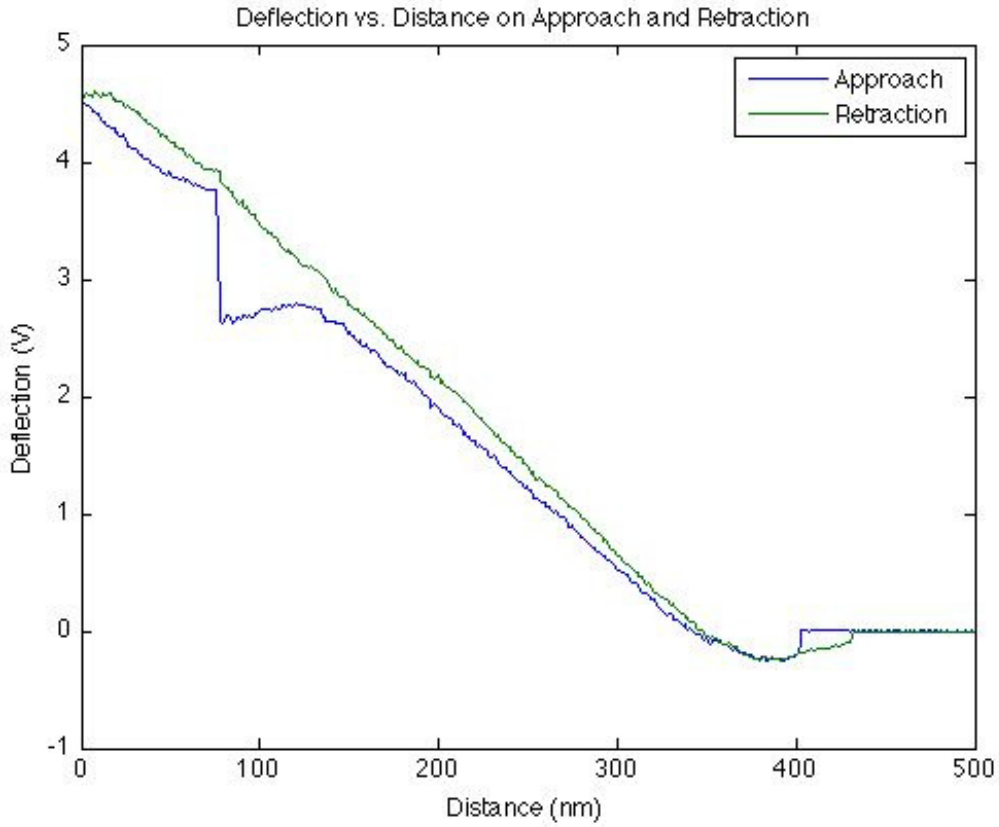
Deflection vs. Distance on Approach and Retraction
Approach
Retraction
Deflection (V)
Distance (nm)
5
4
3
2
1
0
-1
0
100
200
300
400
500

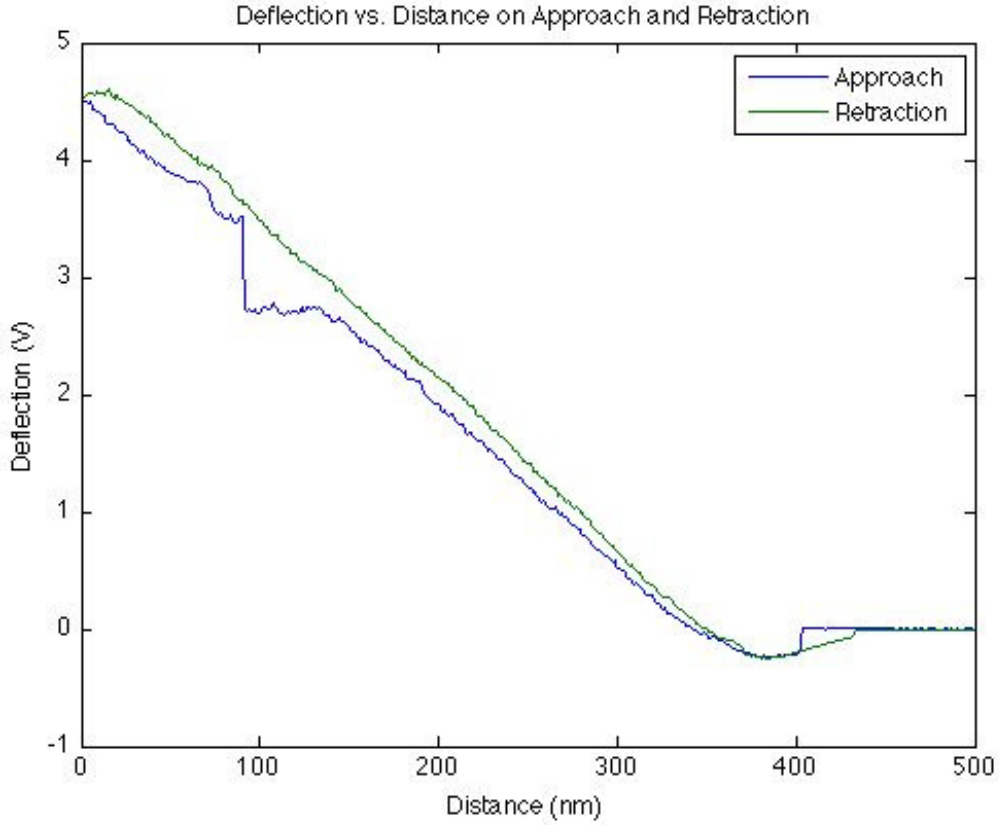
Deflection vs. Distance on Approach and Retraction
Approach
Retraction
Deflection (V)
Distance (nm)
5
4
3
2
1
0
-1
0
100
200
300
400
500

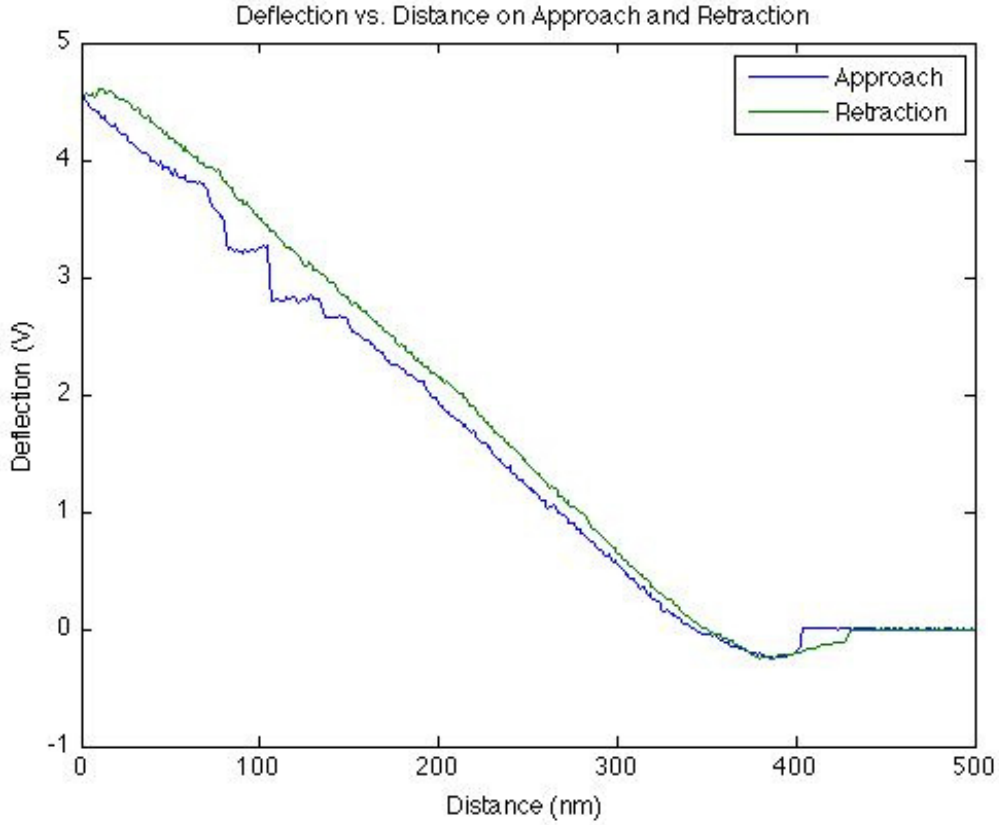
Deflection vs. Distance on Approach and Retraction
Approach
Retraction
Deflection (V)
Distance (nm)
5
4
3
2
1
0
-1
0
100
200
300
400
500

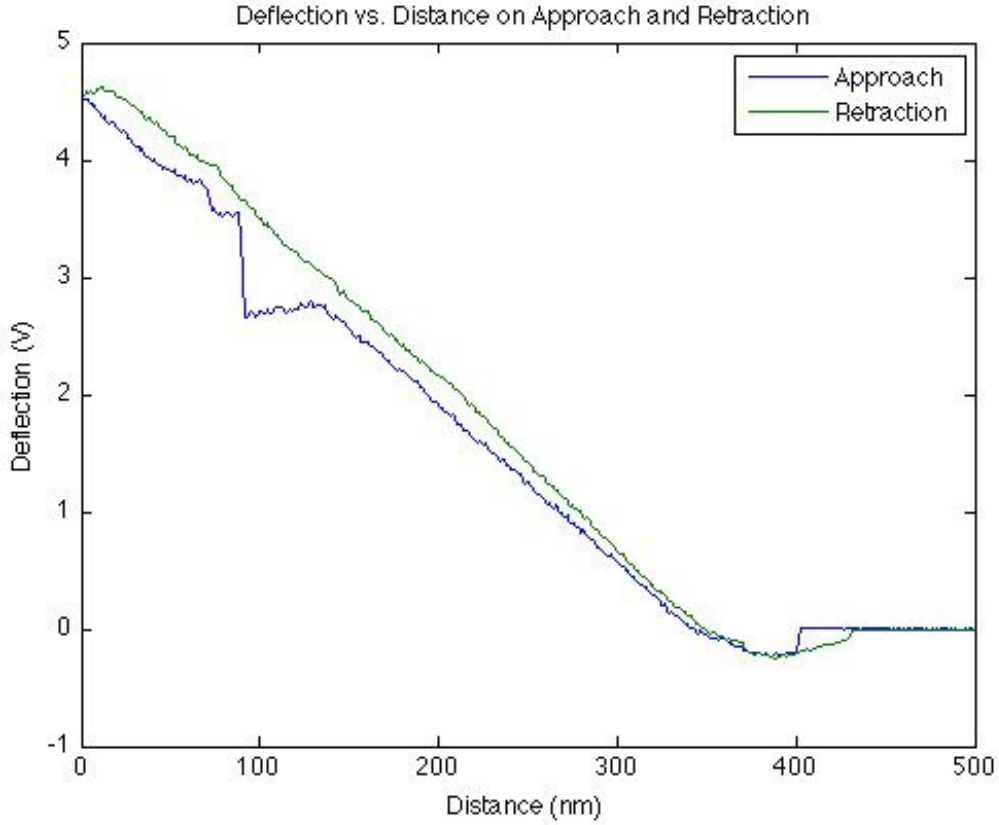
Deflection vs. Distance on Approach and Retraction
Approach
Retraction
Deflection (V)
Distance (nm)
5
4
3
2
1
0
-1
0
100
200
300
400
500

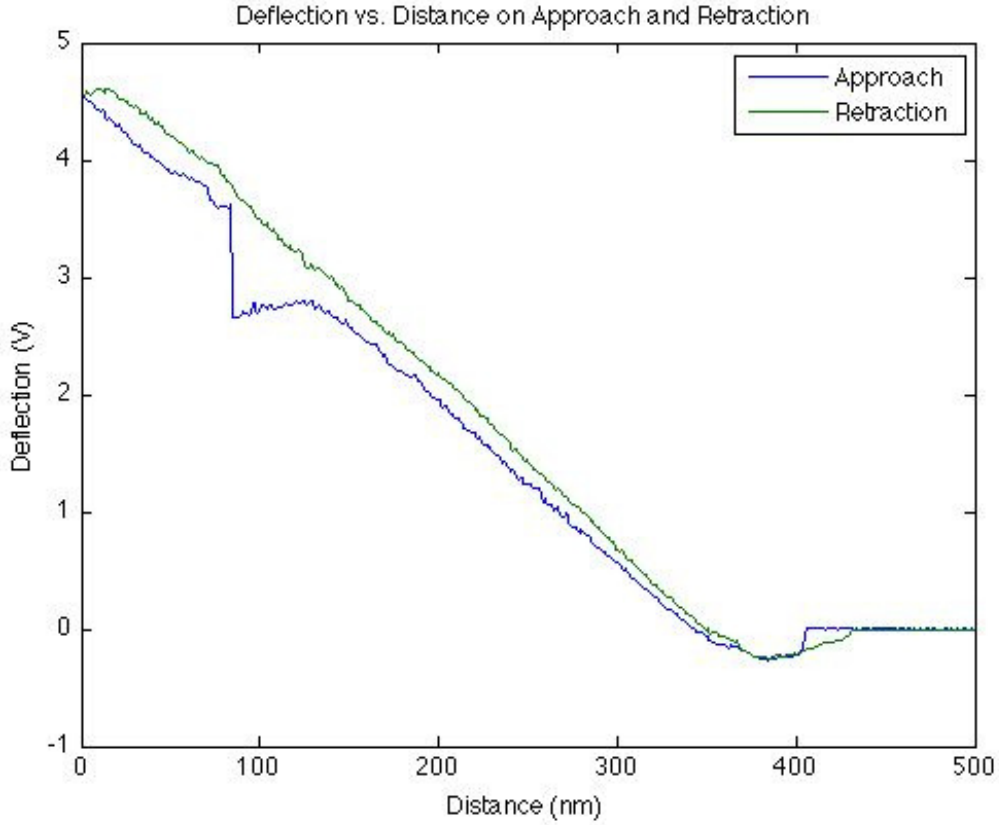
Deflection vs. Distance on Approach and Retraction
Approach
Retraction
Deflection (V)
Distance (nm)
5
4
3
2
1
0
-1
0
100
200
300
400
500

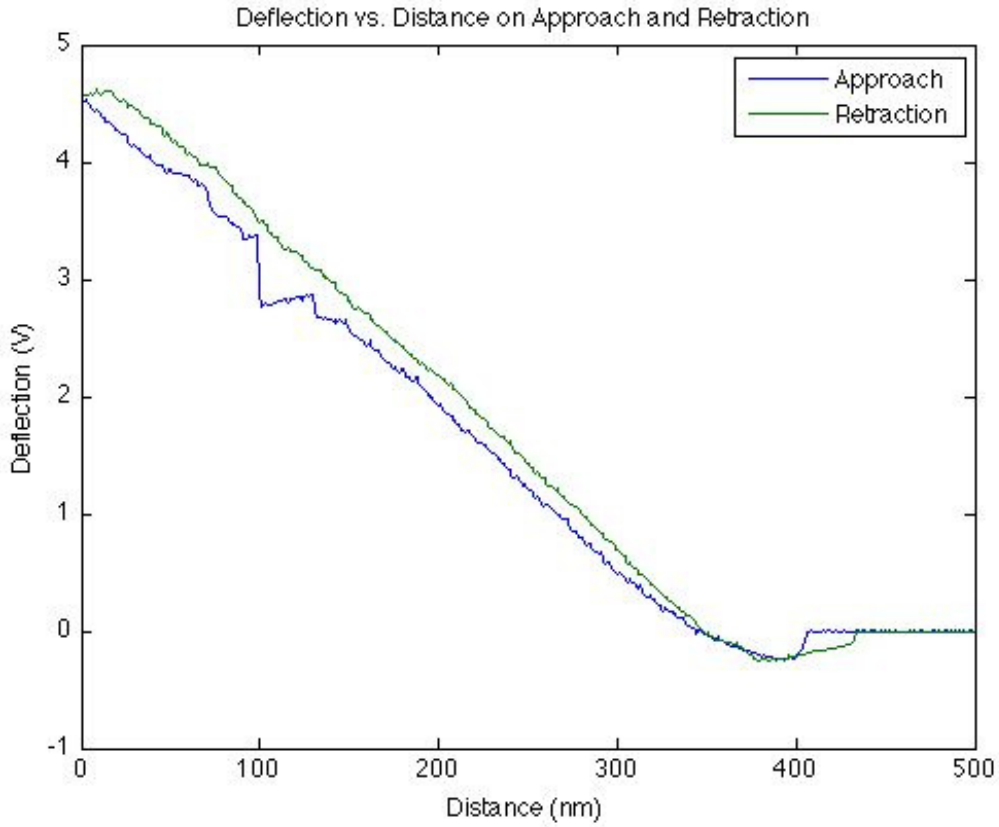
Deflection vs. Distance on Approach and Retraction
Approach
Retraction
Deflection (V)
Distance (nm)
5
4
3
2
1
0
-1
0
100
200
300
400
500

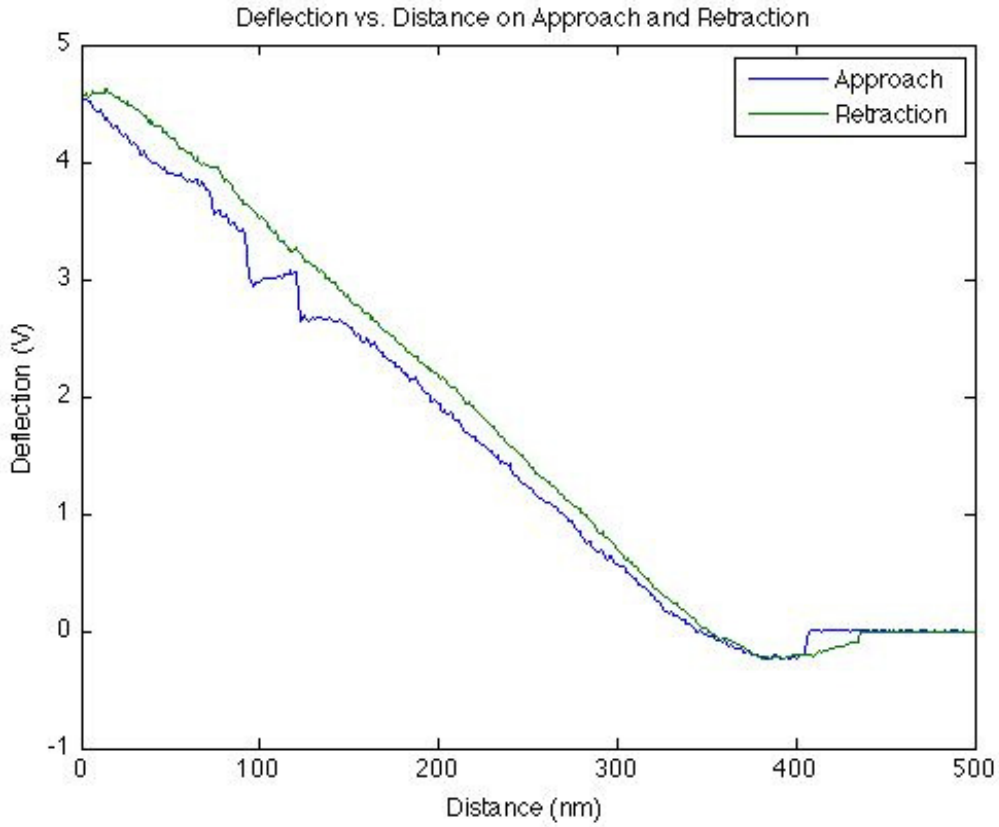
Deflection vs. Distance on Approach and Retraction
Approach
Retraction
Deflection (V)
Distance (nm)
5
4
3
2
1
0
-1
0
100
200
300
400
500

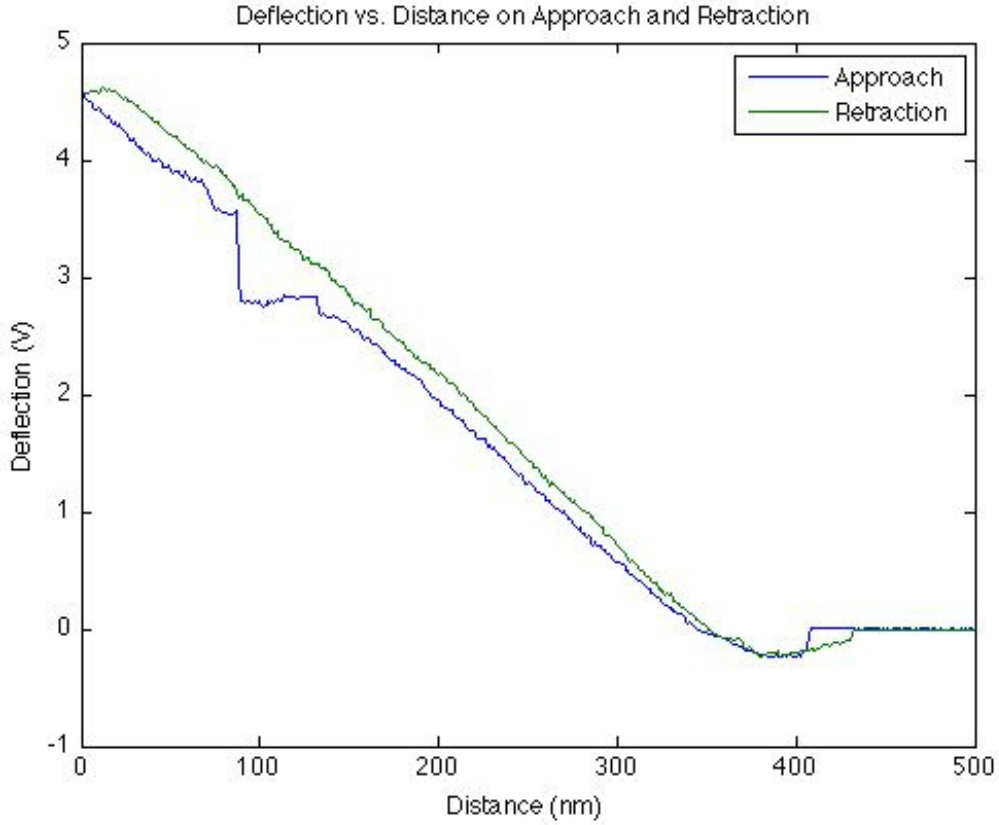
Deflection vs. Distance on Approach and Retraction
Approach
Retraction
Deflection (V)
Distance (nm)
5
4
3
2
1
0
-1
0
100
200
300
400
500

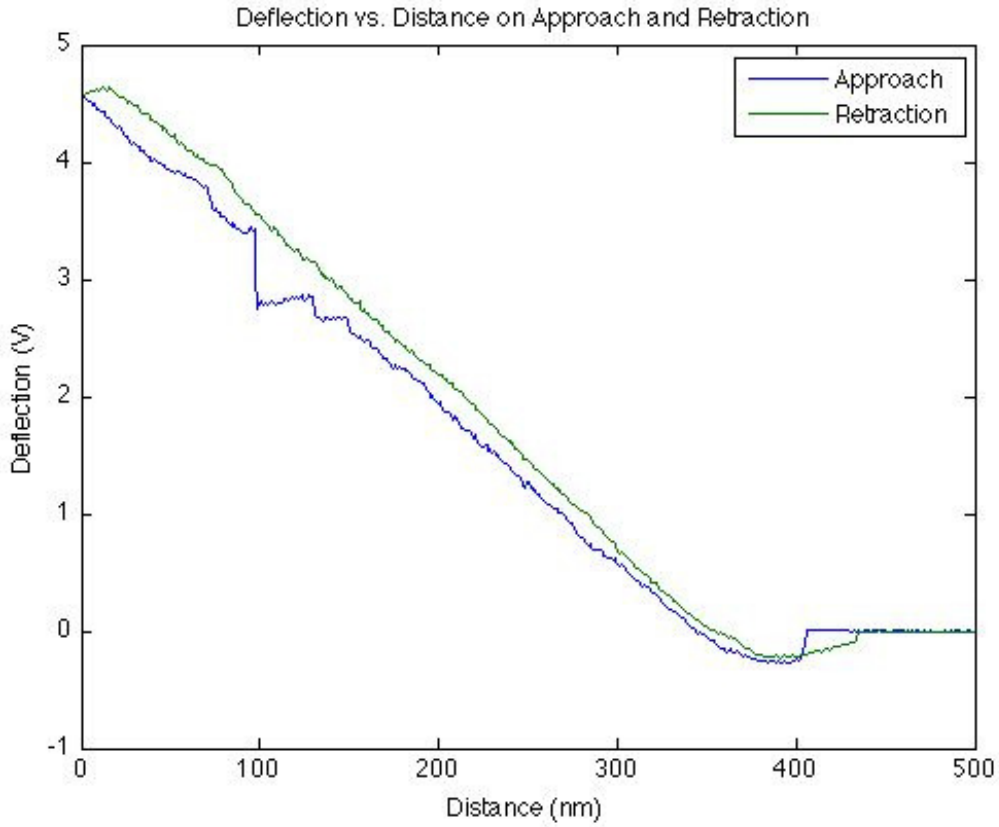
Deflection vs. Distance on Approach and Retraction
Approach
Retraction
Deflection (V)
Distance (nm)
5
4
3
2
1
0
-1
0
100
200
300
400
500

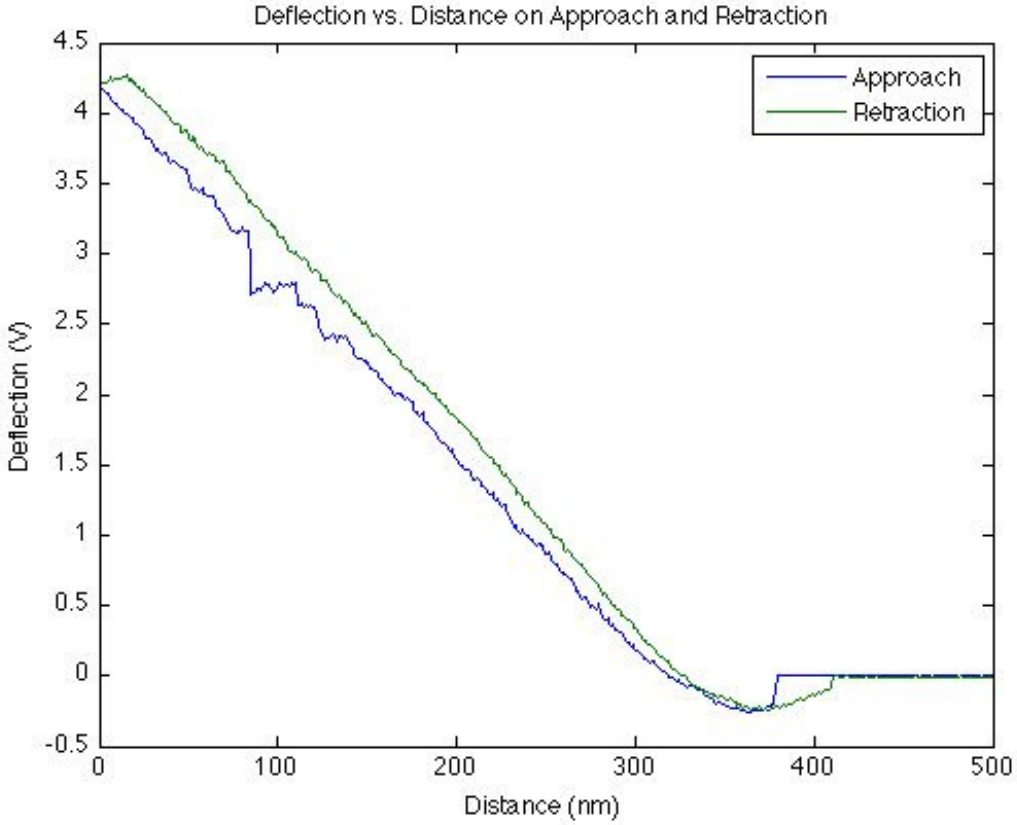
Deflection vs. Distance on Approach and Retraction
Approach
Retraction
Deflection (V)
Distance (nm)
4.5
4
3.5
3
2.5
2
1.5
1
0.5
0
-0.5
0
100
200
300
400
500

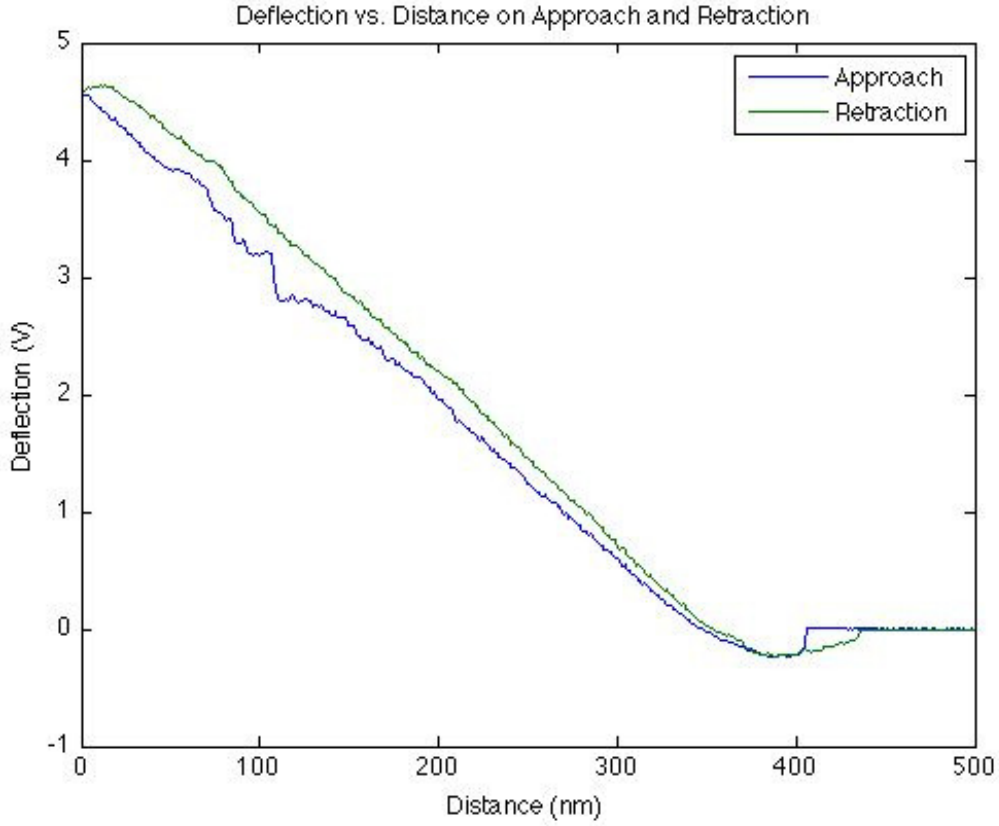
Deflection vs. Distance on Approach and Retraction
Approach
Retraction
Deflection (V)
Distance (nm)
5
4
3
2
1
0
-1
0
100
200
300
400
500

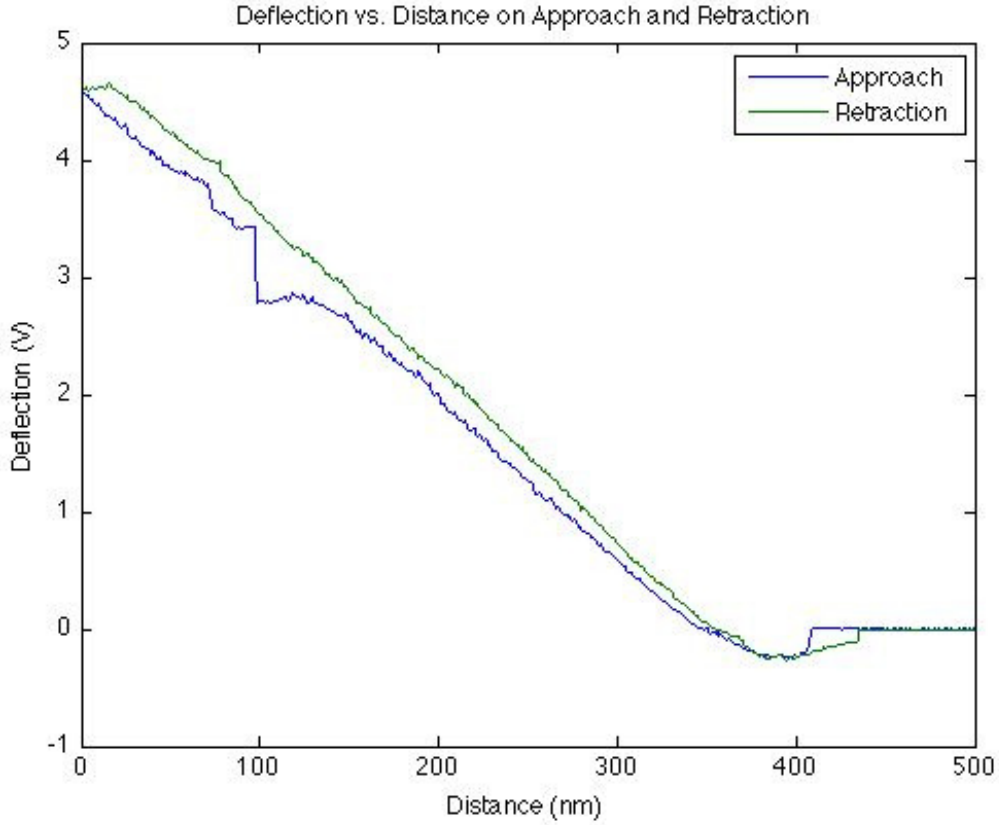
Deflection vs. Distance on Approach and Retraction
Approach
Retraction
Deflection (V)
Distance (nm)
5
4
3
2
1
0
-1
0
100
200
300
400
500

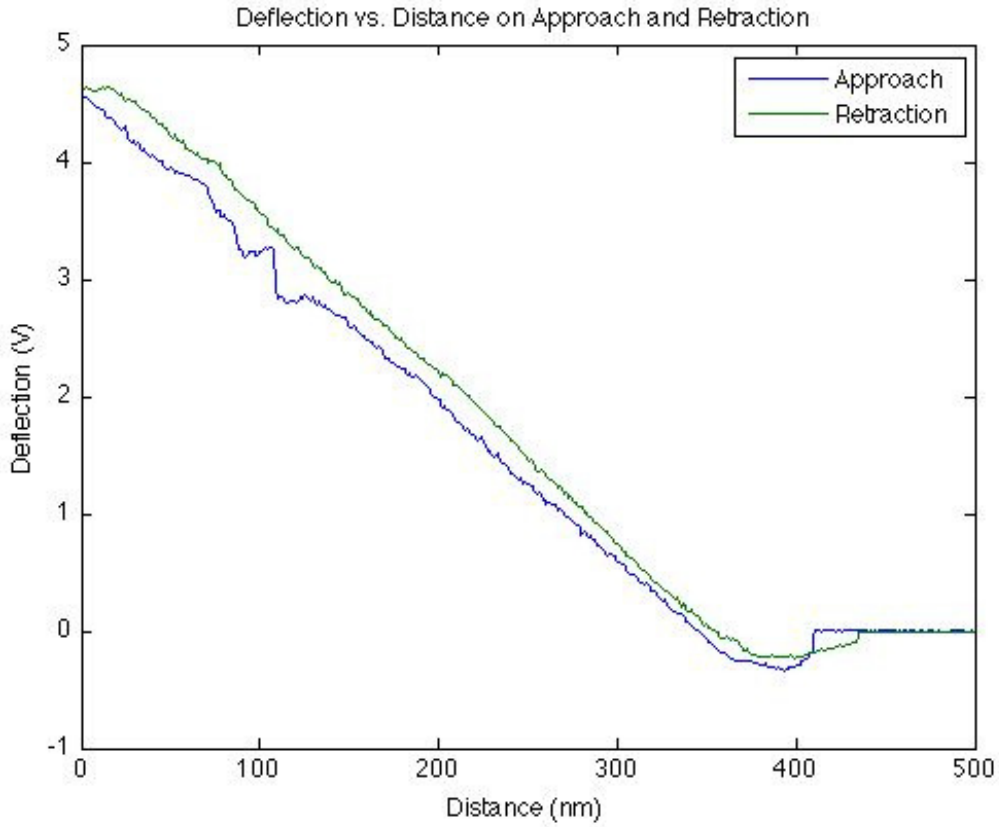
Deflection vs. Distance on Approach and Retraction
Approach
Retraction
Deflection (V)
Distance (nm)
5
4
3
2
1
0
-1
0
100
200
300
400
500

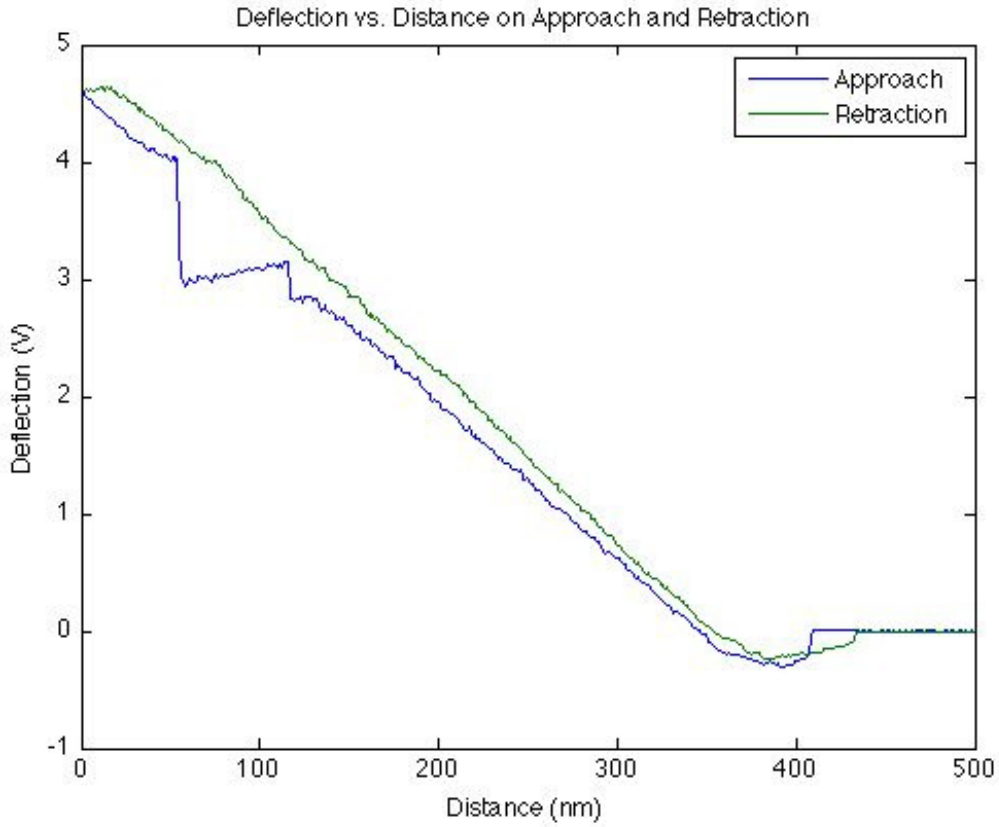
Deflection vs. Distance on Approach and Retraction
Approach
Retraction
Deflection (V)
Distance (nm)
5
4
3
2
1
0
-1
0
100
200
300
400
500

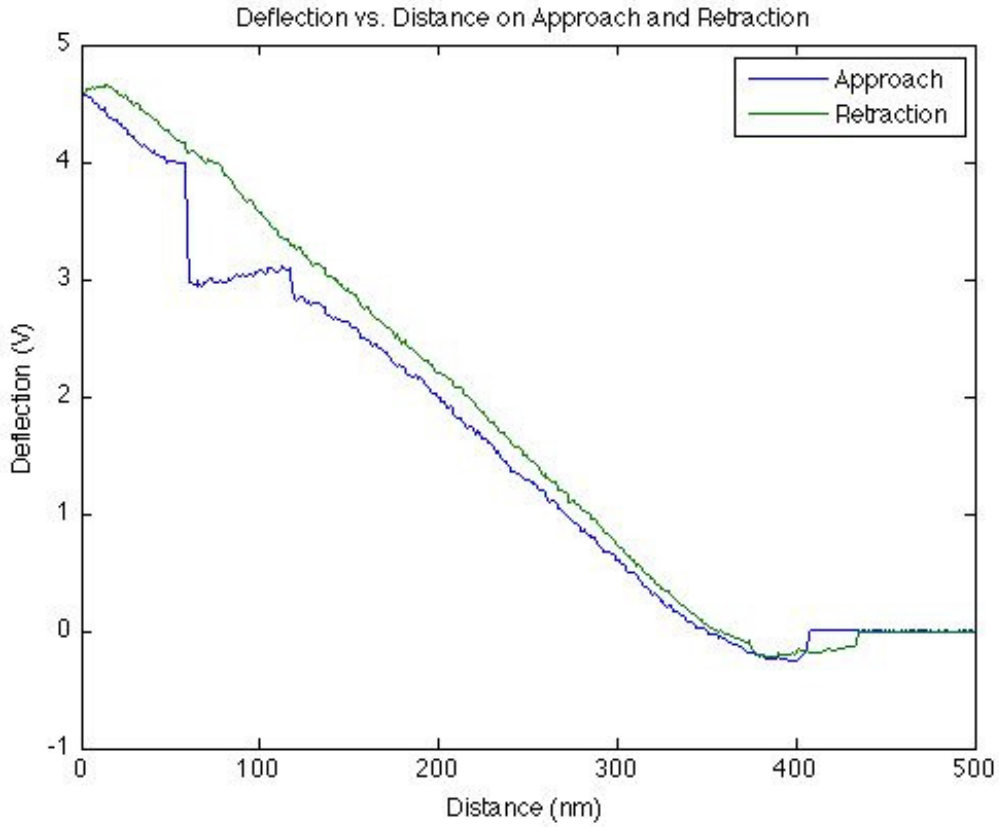
Deflection vs. Distance on Approach and Retraction
Approach
Retraction
Deflection (V)
Distance (nm)
5
4
3
2
1
0
-1
0
100
200
300
400
500

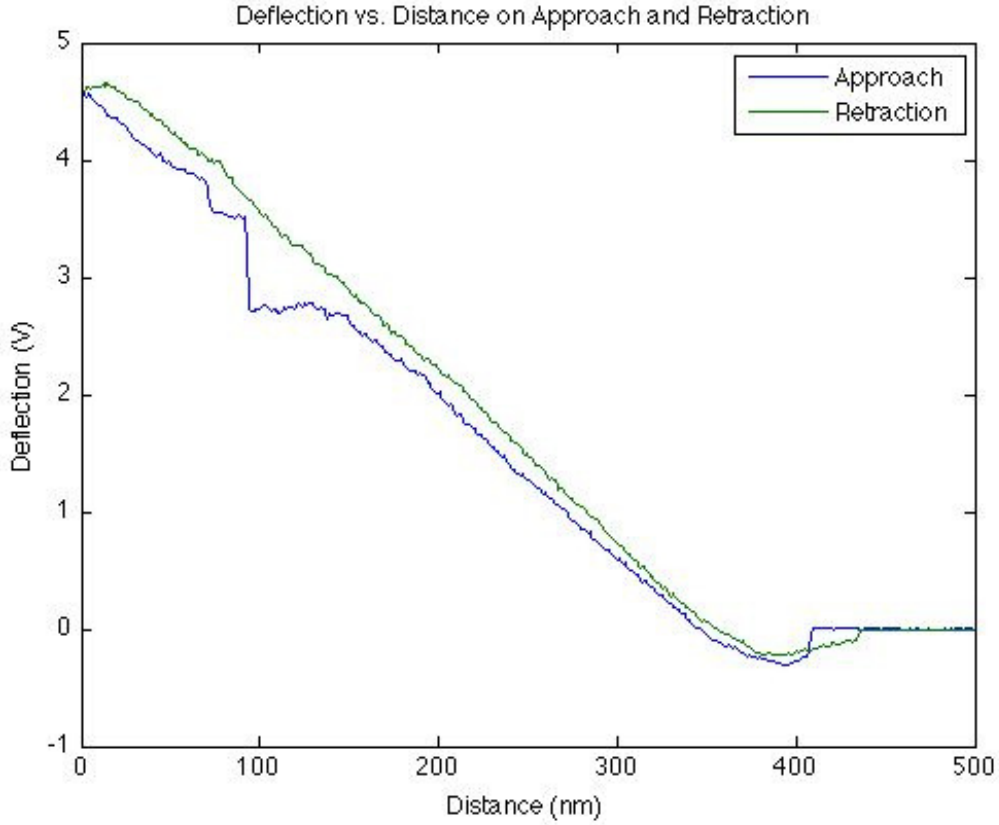
Deflection vs. Distance on Approach and Retraction
Approach
Retraction
Deflection (V)
Distance (nm)
5
4
3
2
1
0
-1
0
100
200
300
400
500

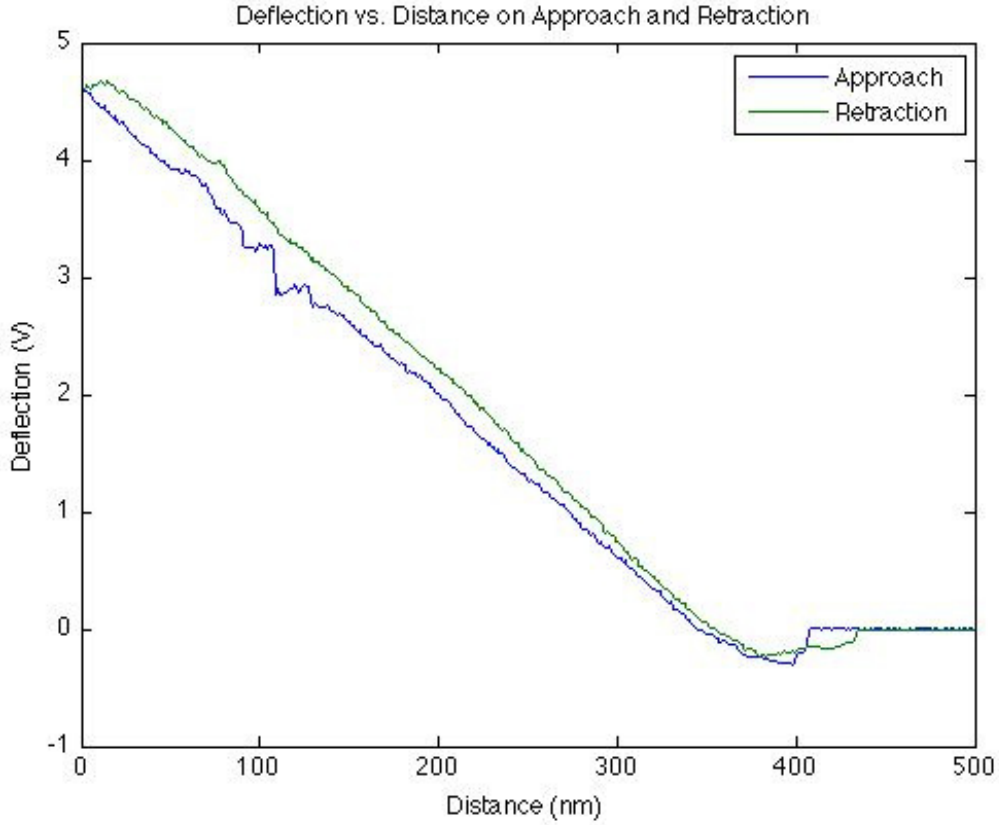
Deflection vs. Distance on Approach and Retraction
Approach
Retraction
Deflection (V)
Distance (nm)
5
4
3
2
1
0
-1
0
100
200
300
400
500

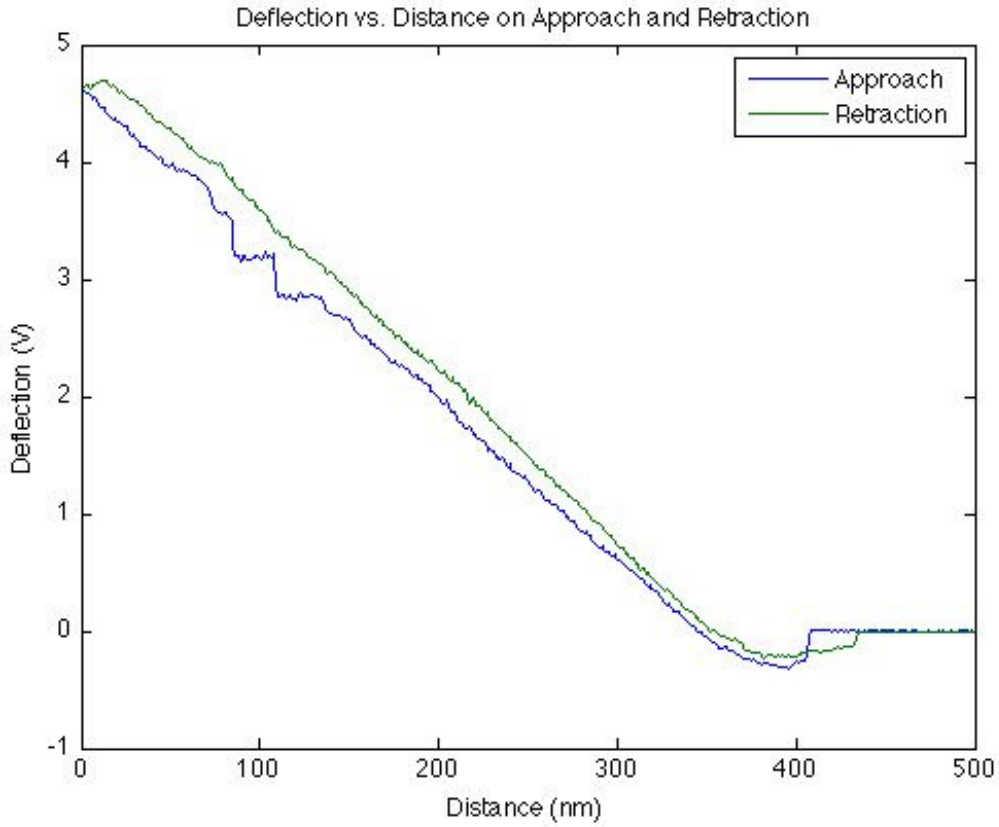
Deflection vs. Distance on Approach and Retraction
Approach
Retraction
Deflection (V)
Distance (nm)
5
4
3
2
1
0
-1
0
100
200
300
400
500

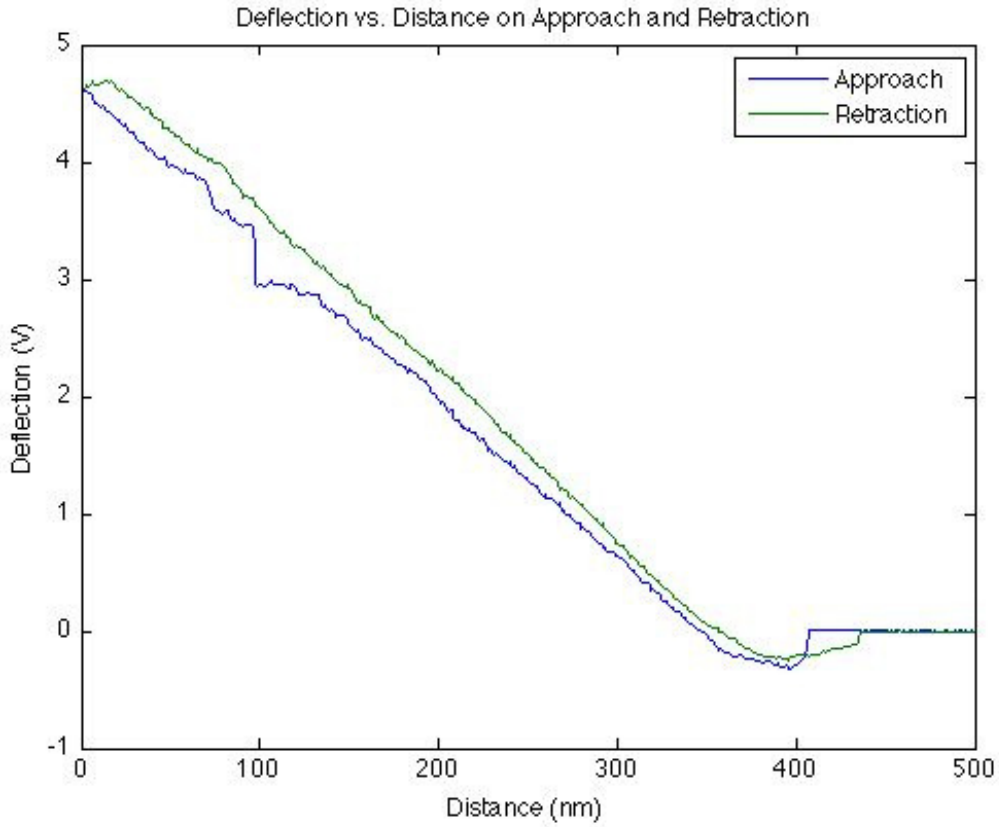
Deflection vs. Distance on Approach and Retraction
Approach
Retraction
Deflection (V)
Distance (nm)
5
4
3
2
1
0
-1
0
100
200
300
400
500

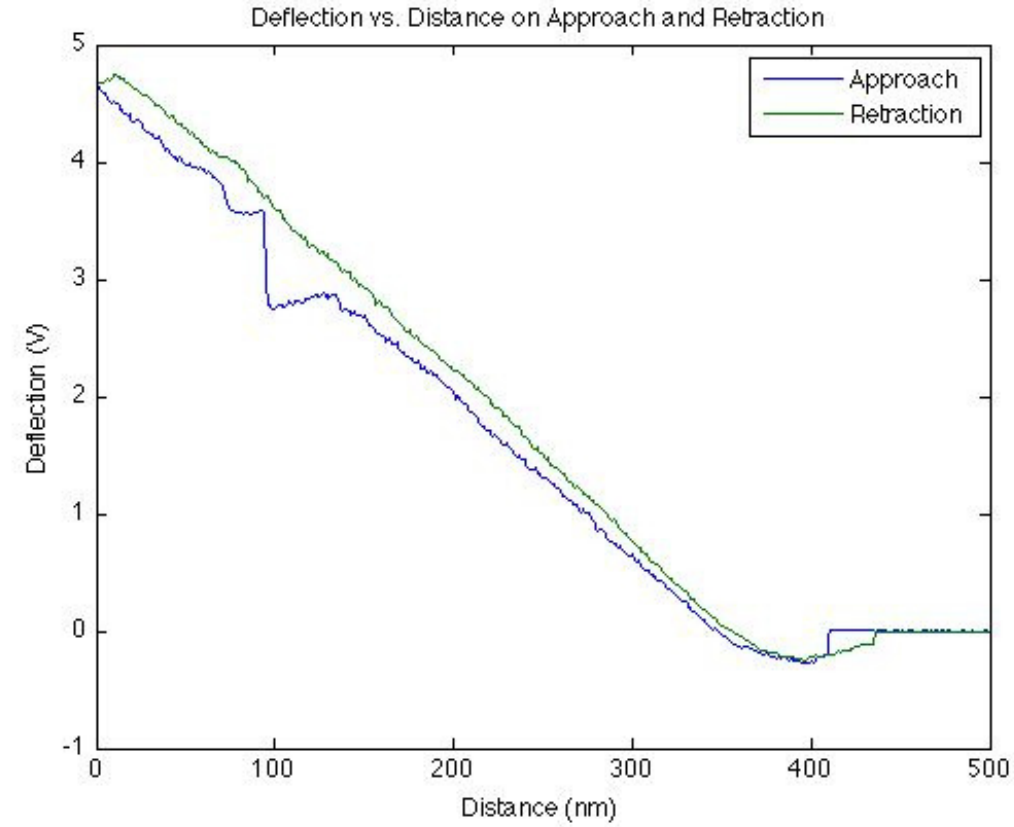
Deflection vs. Distance on Approach and Retraction
Approach
Retraction
Deflection (V)
Distance (nm)
5
4
3
2
1
0
-1
0
100
200
300
400
500

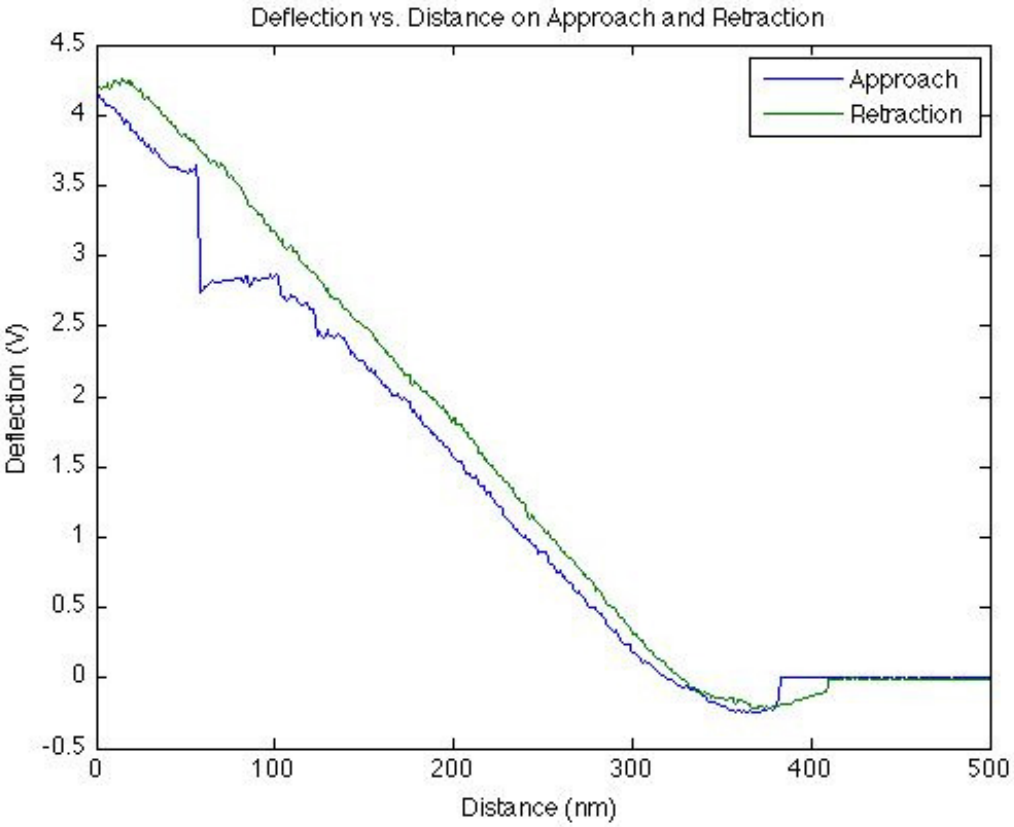
Deflection vs. Distance on Approach and Retraction
Approach
Retraction
Deflection (V)
Distance (nm)
4.5
4
3.5
3
2.5
2
1.5
1
0.5
0
-0.5
0
100
200
300
400
500

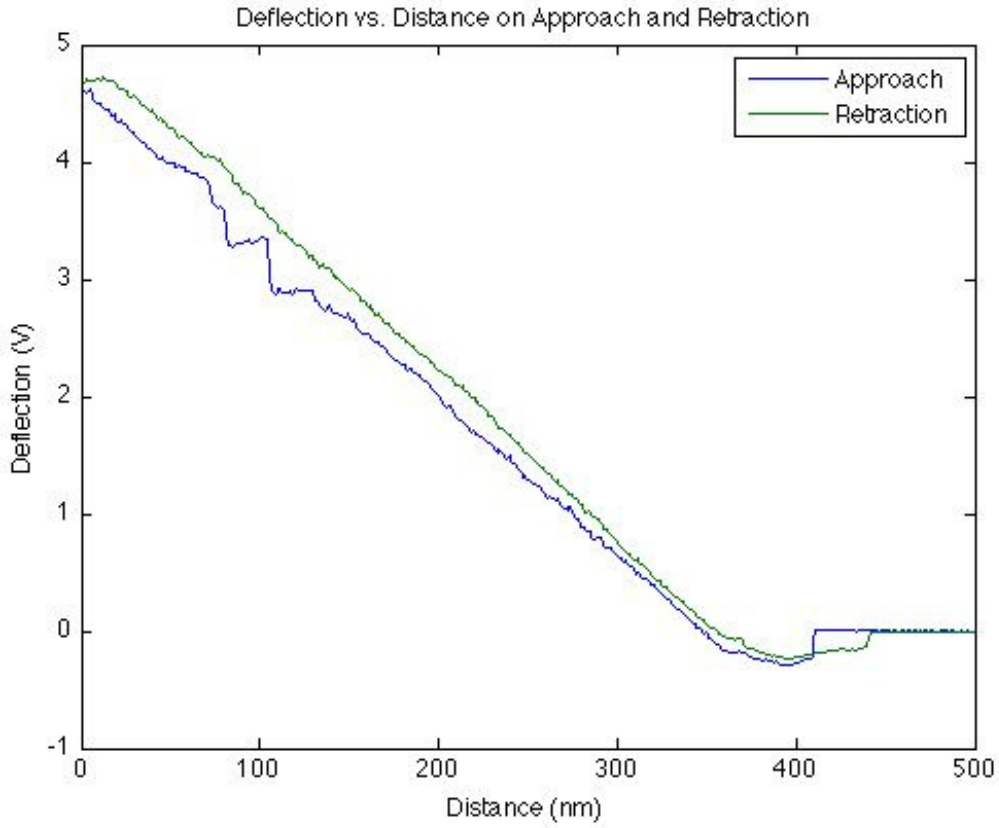
Deflection vs. Distance on Approach and Retraction
Approach
Retraction
Deflection (V)
Distance (nm)
5
4
3
2
1
0
-1
0
100
200
300
400
500

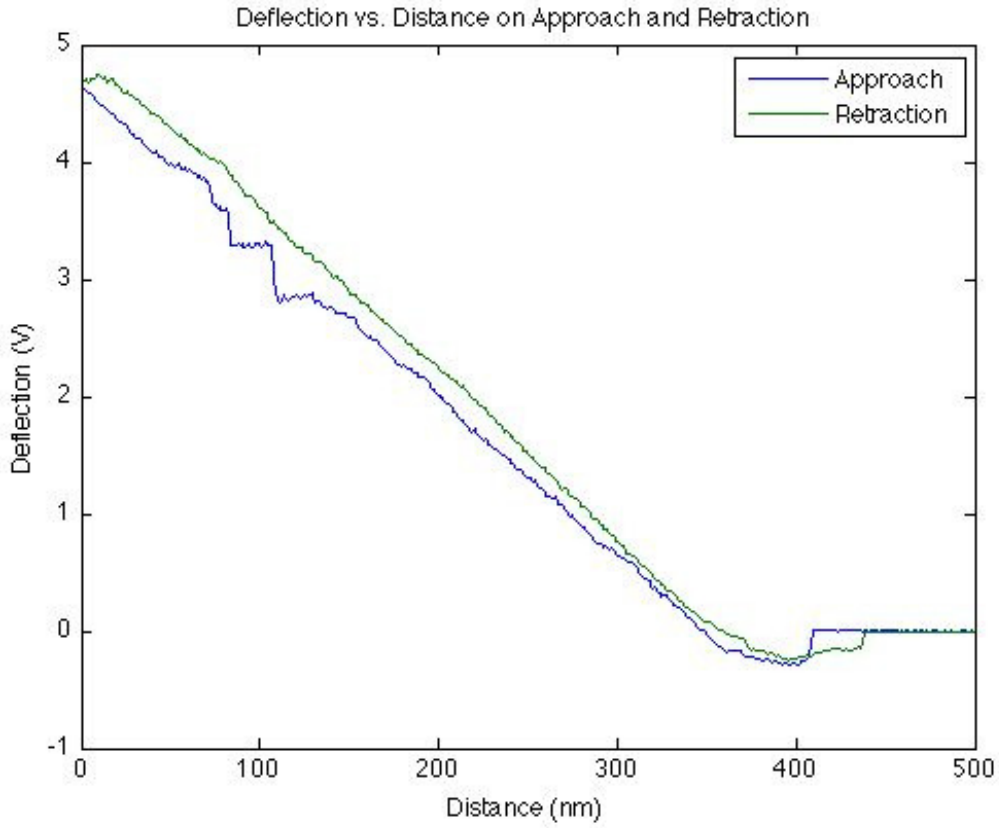
Deflection vs. Distance on Approach and Retraction
Approach
Retraction
Deflection (V)
Distance (nm)
5
4
3
2
1
0
-1
0
100
200
300
400
500

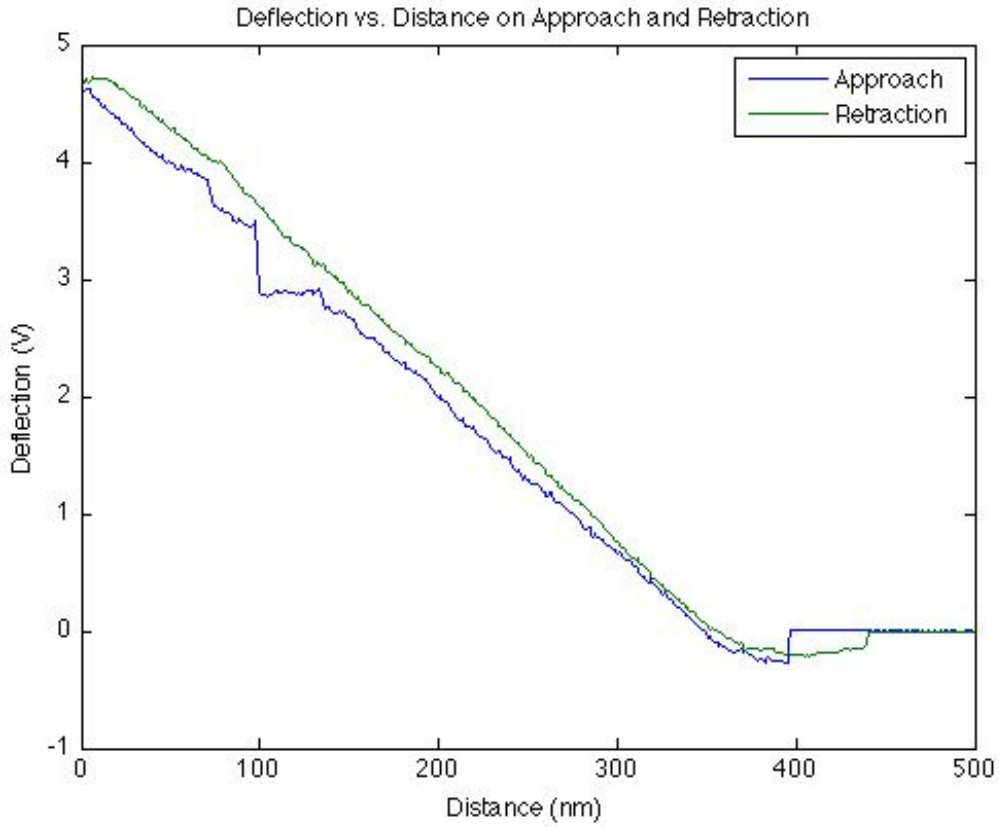
Deflection vs. Distance on Approach and Retraction
Approach
Retraction
Deflection (V)
Distance (nm)
5
4
3
2
1
0
-1
0
100
200
300
400
500

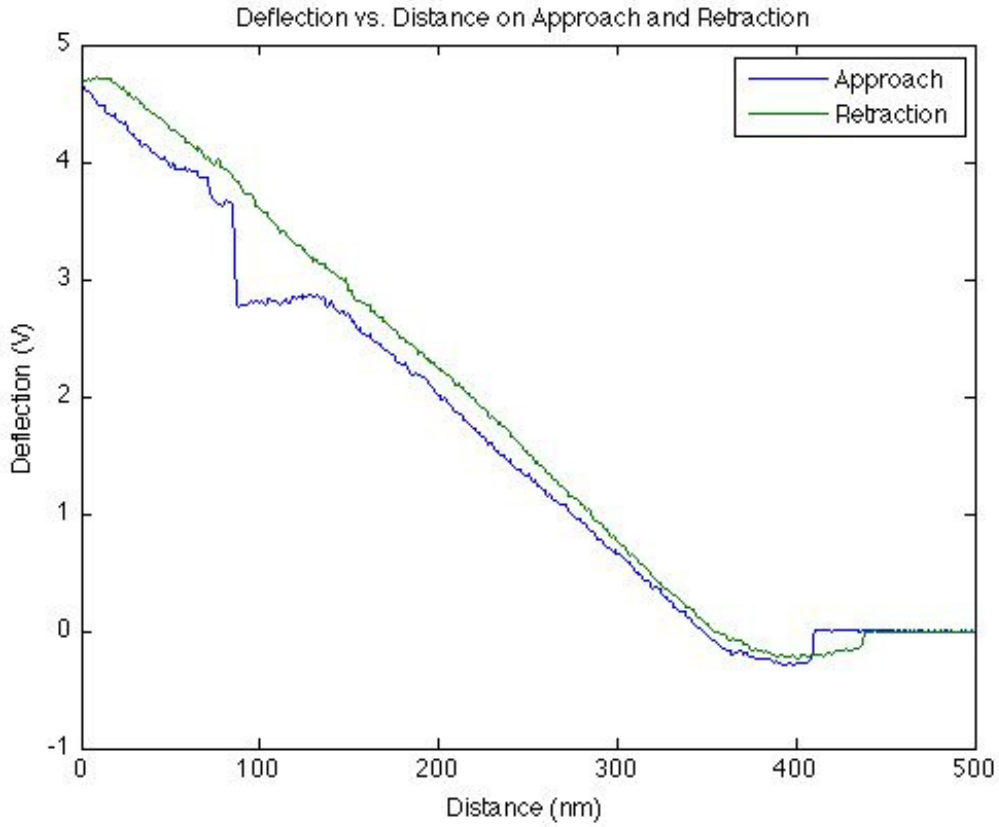
Deflection vs. Distance on Approach and Retraction
Approach
Retraction
Deflection (V)
Distance (nm)
5
4
3
2
1
0
-1
0
100
200
300
400
500

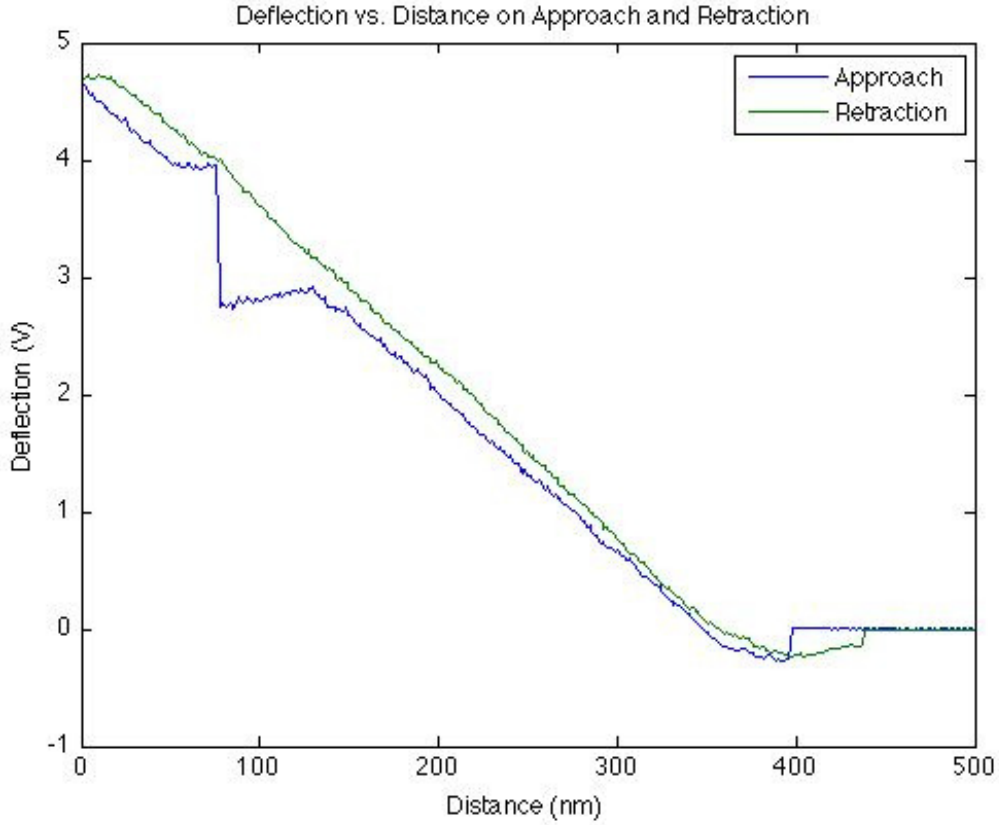
Deflection vs. Distance on Approach and Retraction
Approach
Retraction
Deflection (V)
Distance (nm)
5
4
3
2
1
0
-1
0
100
200
300
400
500

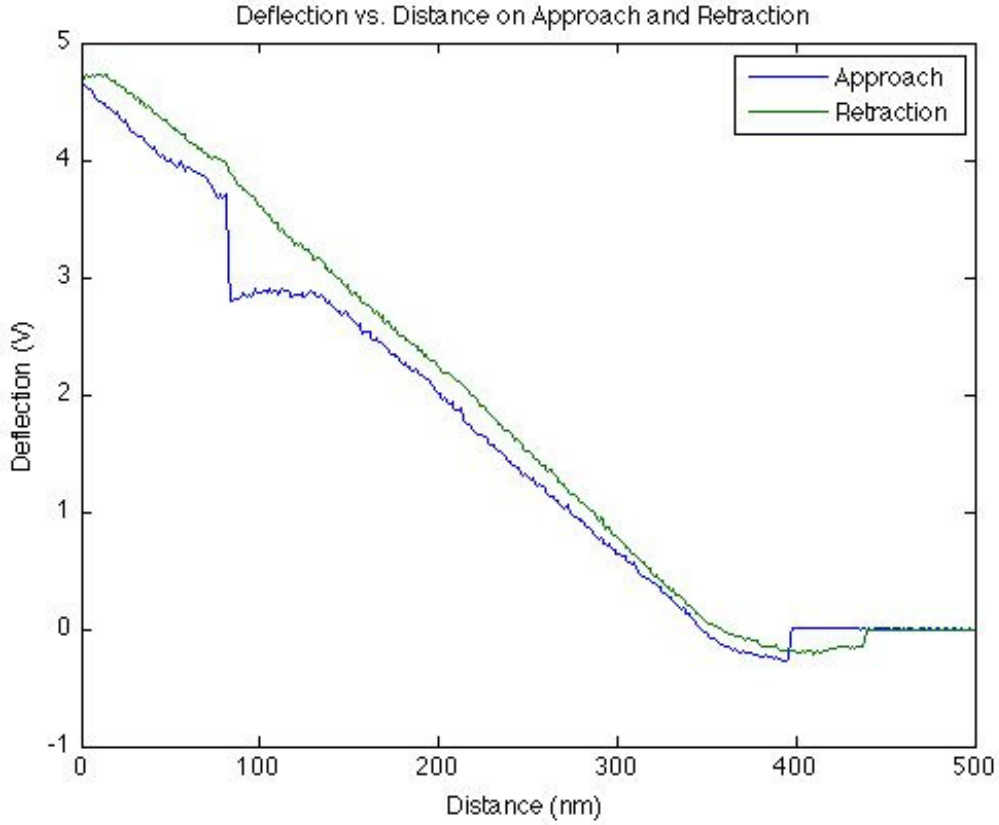
Deflection vs. Distance on Approach and Retraction
Approach
Retraction
Deflection (V)
Distance (nm)
5
4
3
2
1
0
-1
0
100
200
300
400
500

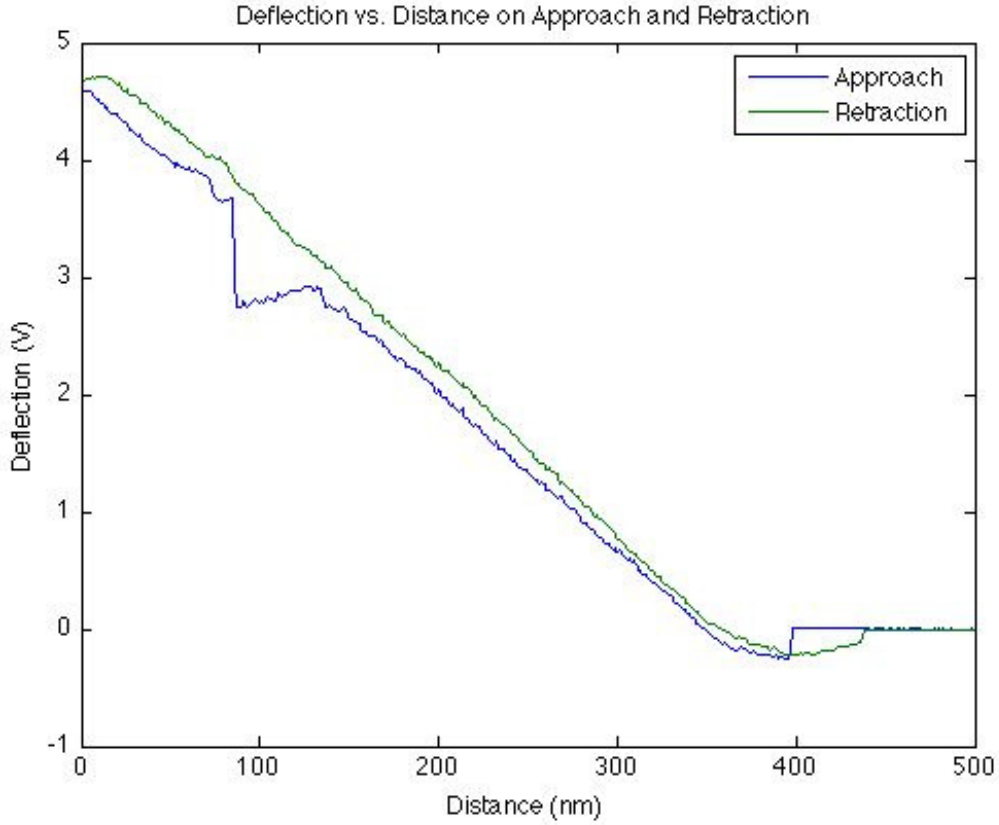
Deflection vs. Distance on Approach and Retraction
Approach
Retraction
Deflection (V)
Distance (nm)
5
4
3
2
1
0
-1
0
100
200
300
400
500

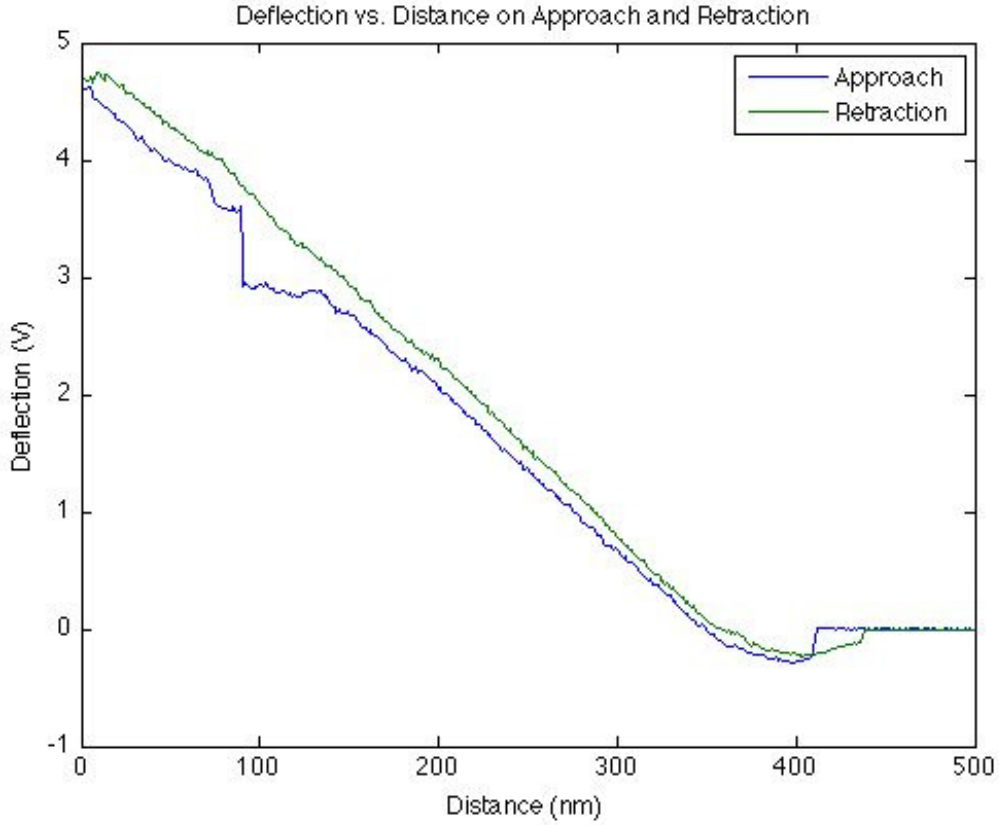
Deflection vs. Distance on Approach and Retraction
Approach
Retraction
Deflection (V)
Distance (nm)
5
4
3
2
1
0
-1
0
100
200
300
400
500

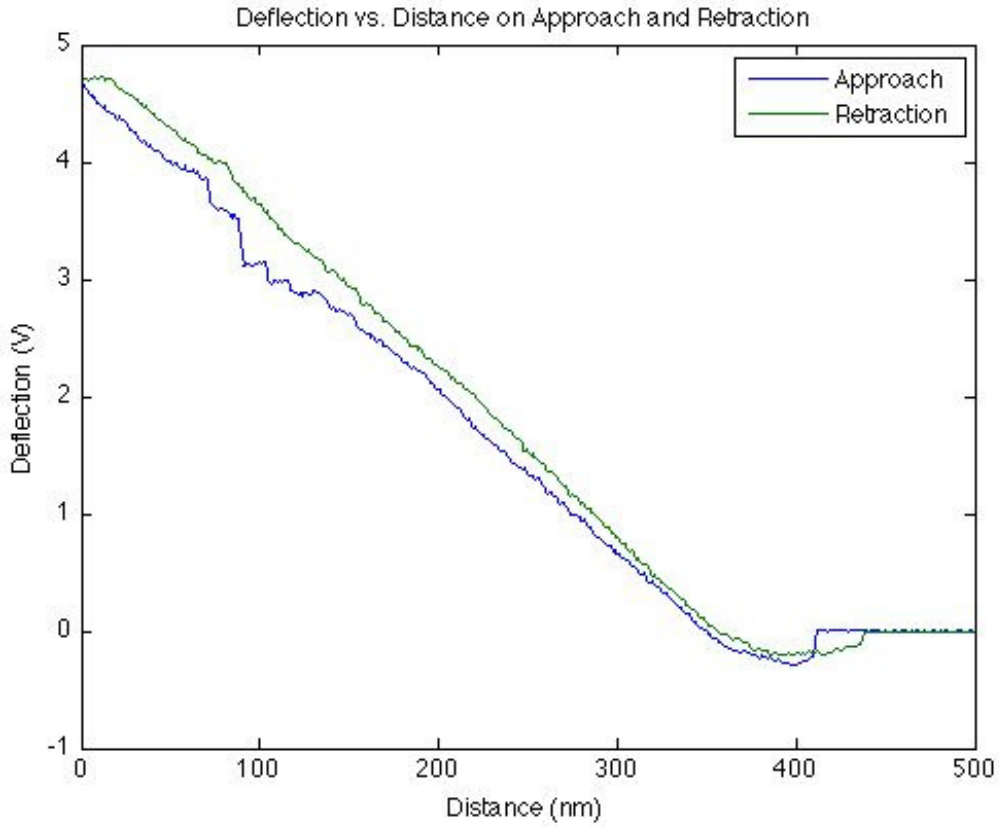
Deflection vs. Distance on Approach and Retraction
Approach
Retraction
Deflection (V)
Distance (nm)
5
4
3
2
1
0
-1
0
100
200
300
400
500

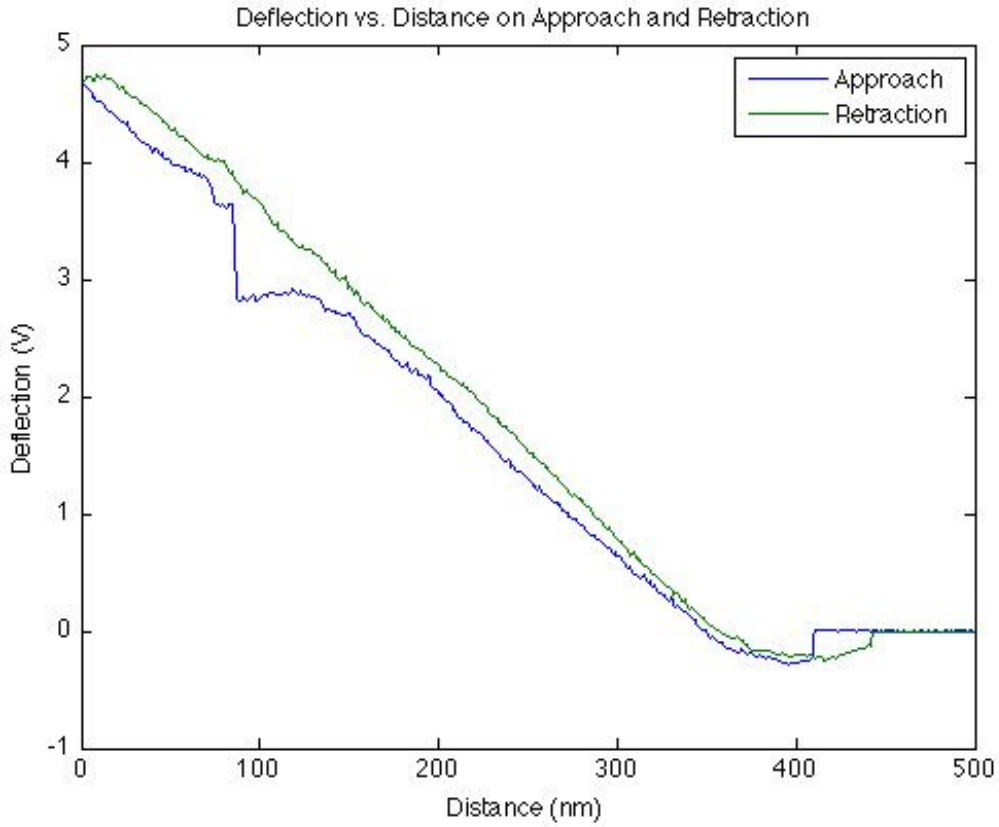
Deflection vs. Distance on Approach and Retraction
Approach
Retraction
Deflection (V)
Distance (nm)
5
4
3
2
1
0
-1
0
100
200
300
400
500

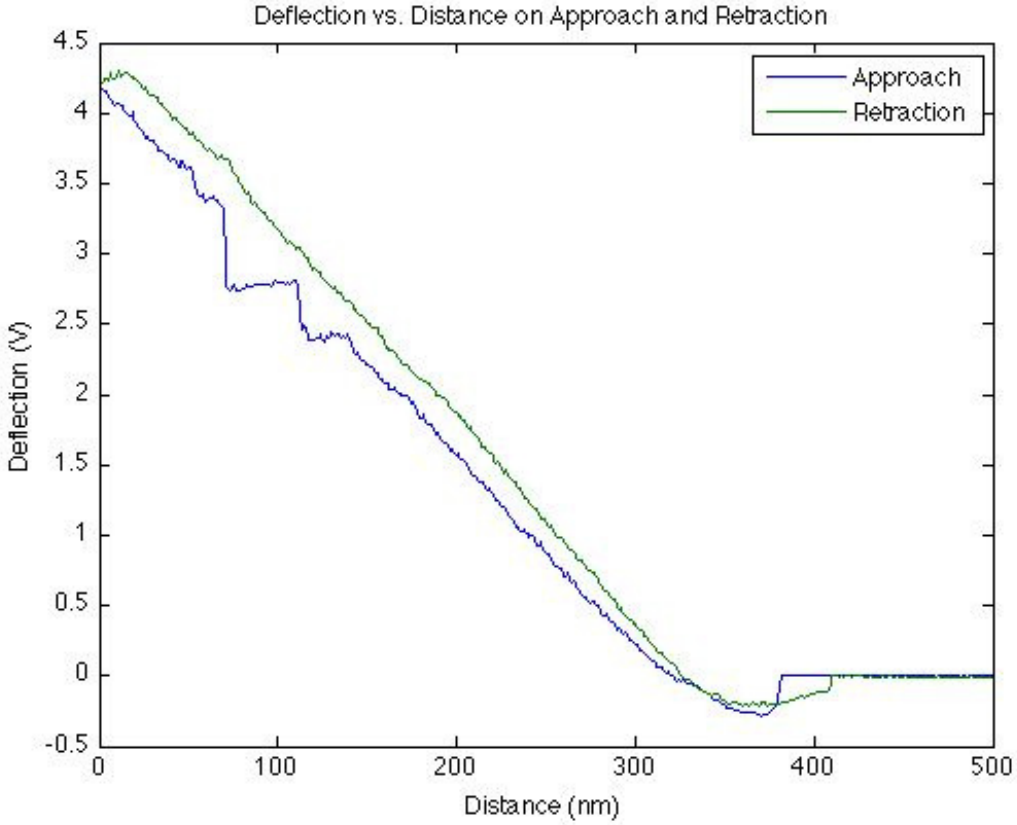
Deflection vs. Distance on Approach and Retraction
Approach
Retraction
Deflection (V)
Distance (nm)
4.5
4
3.5
3
2.5
2
1.5
1
0.5
0
-0.5
0
100
200
300
400
500

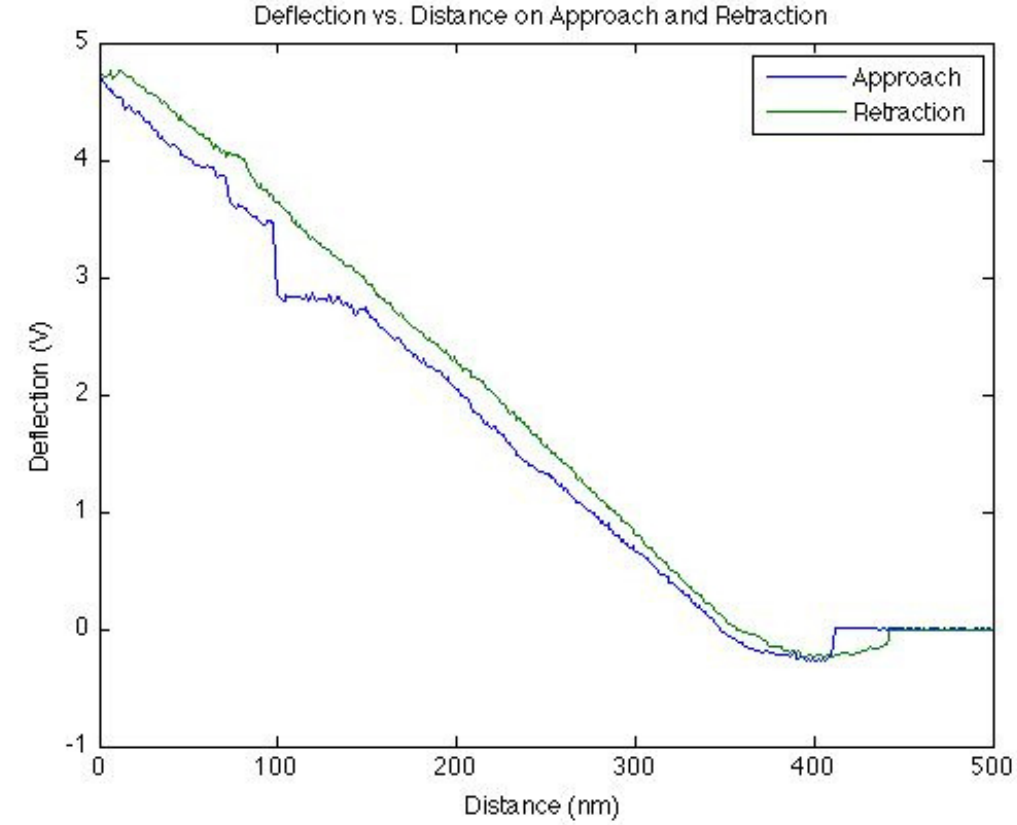
Deflection vs. Distance on Approach and Retraction
Approach
Retraction
Deflection (V)
Distance (nm)
5
4
3
2
1
0
-1
0
100
200
300
400
500

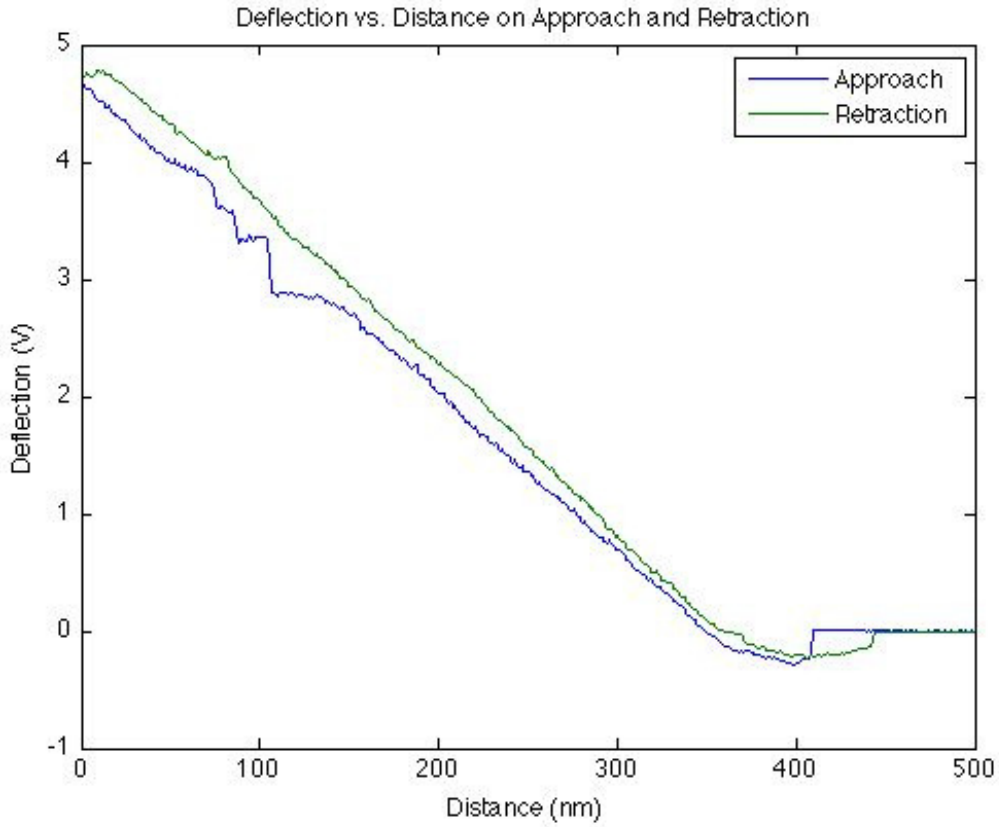
Deflection vs. Distance on Approach and Retraction
Approach
Retraction
Deflection (V)
Distance (nm)
5
4
3
2
1
0
-1
0
100
200
300
400
500

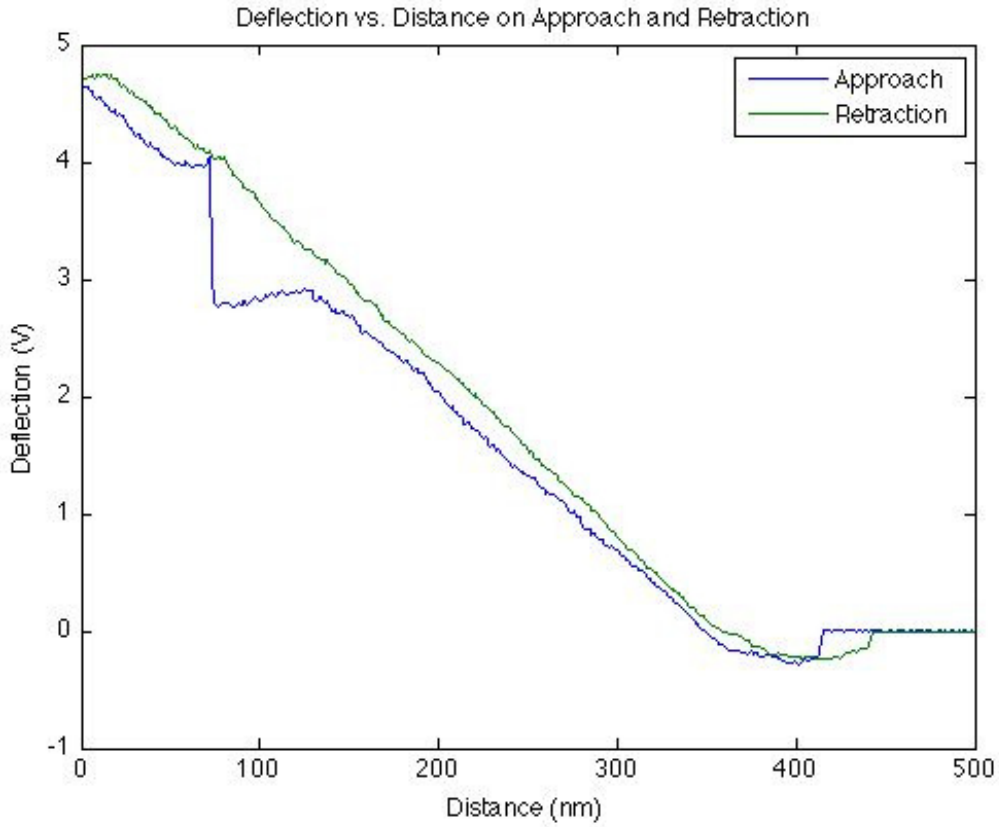
Deflection vs. Distance on Approach and Retraction
Approach
Retraction
Deflection (V)
Distance (nm)
5
4
3
2
1
0
-1
0
100
200
300
400
500

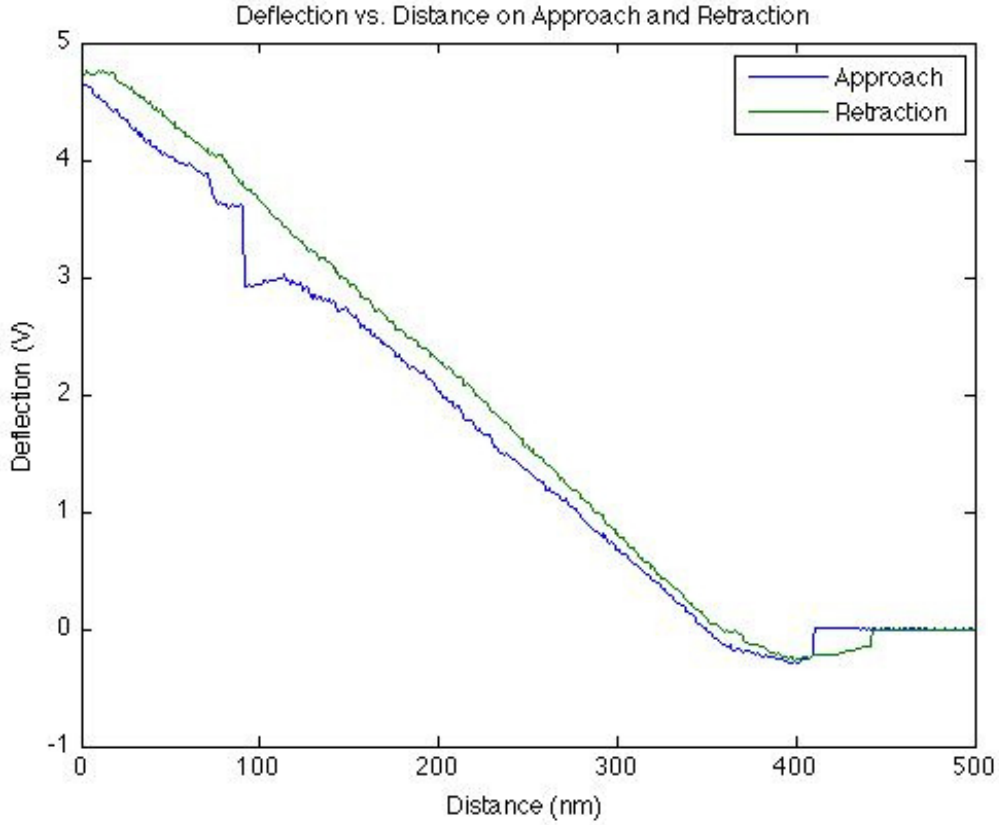
Deflection vs. Distance on Approach and Retraction
Approach
Retraction
Deflection (V)
Distance (nm)
5
4
3
2
1
0
-1
0
100
200
300
400
500

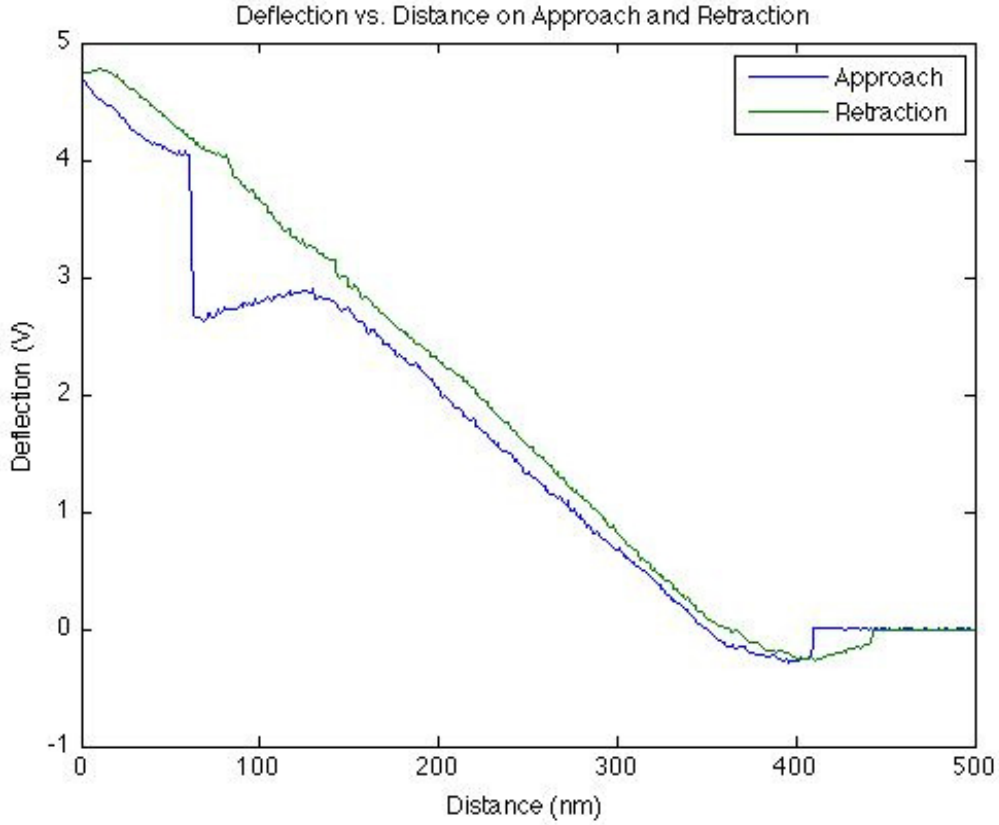
Deflection vs. Distance on Approach and Retraction
Approach
Retraction
Deflection (V)
Distance (nm)
5
4
3
2
1
0
-1
0
100
200
300
400
500

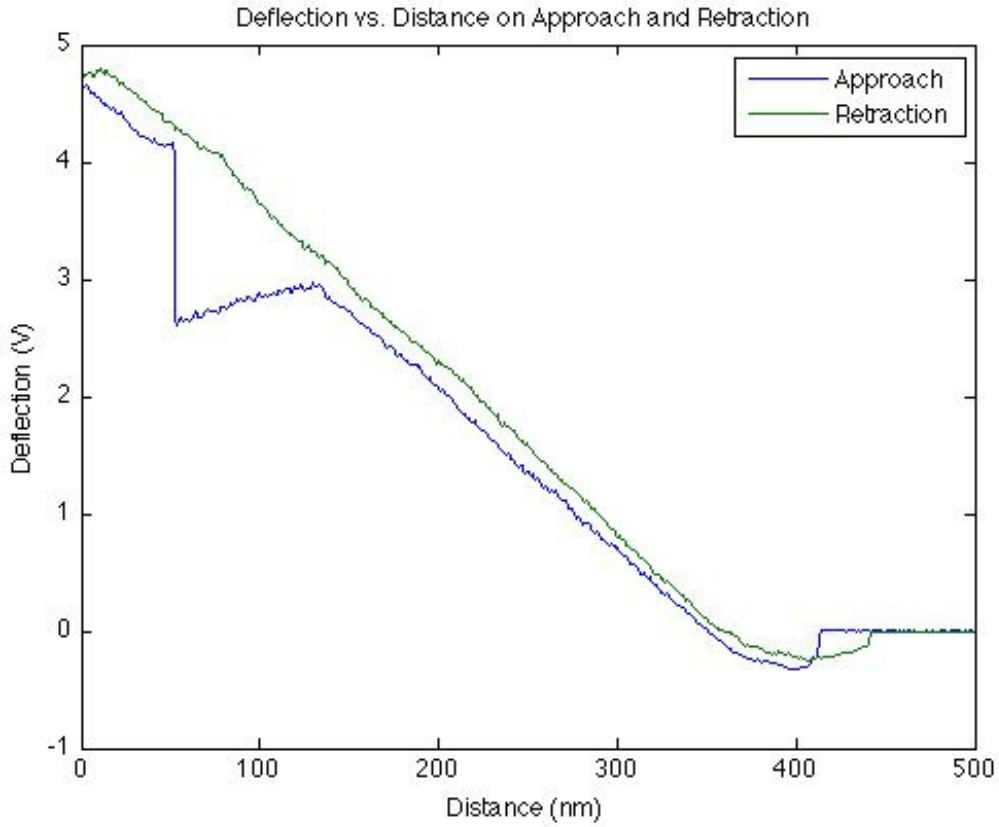
Deflection vs. Distance on Approach and Retraction
Approach
Retraction
Deflection (V)
Distance (nm)
5
4
3
2
1
0
-1
0
100
200
300
400
500

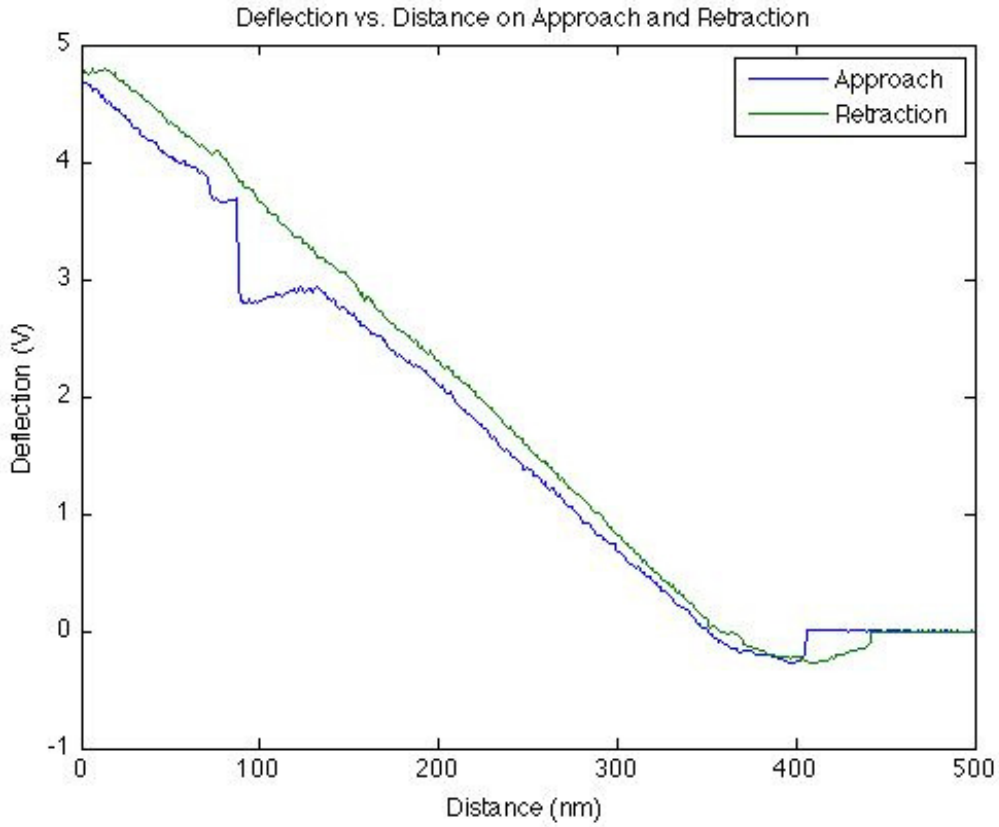
Deflection vs. Distance on Approach and Retraction
Approach
Retraction
Deflection (V)
Distance (nm)
5
4
3
2
1
0
-1
0
100
200
300
400
500

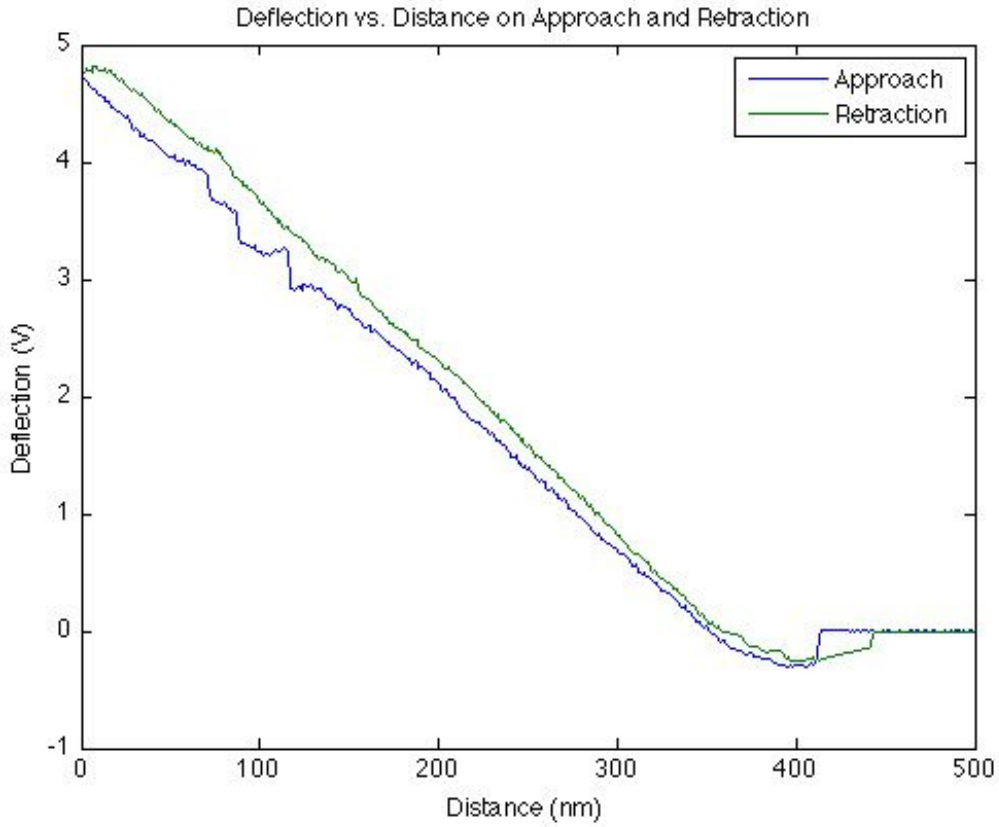
Deflection vs. Distance on Approach and Retraction
Approach
Retraction
Deflection (V)
Distance (nm)
5
4
3
2
1
0
-1
0
100
200
300
400
500

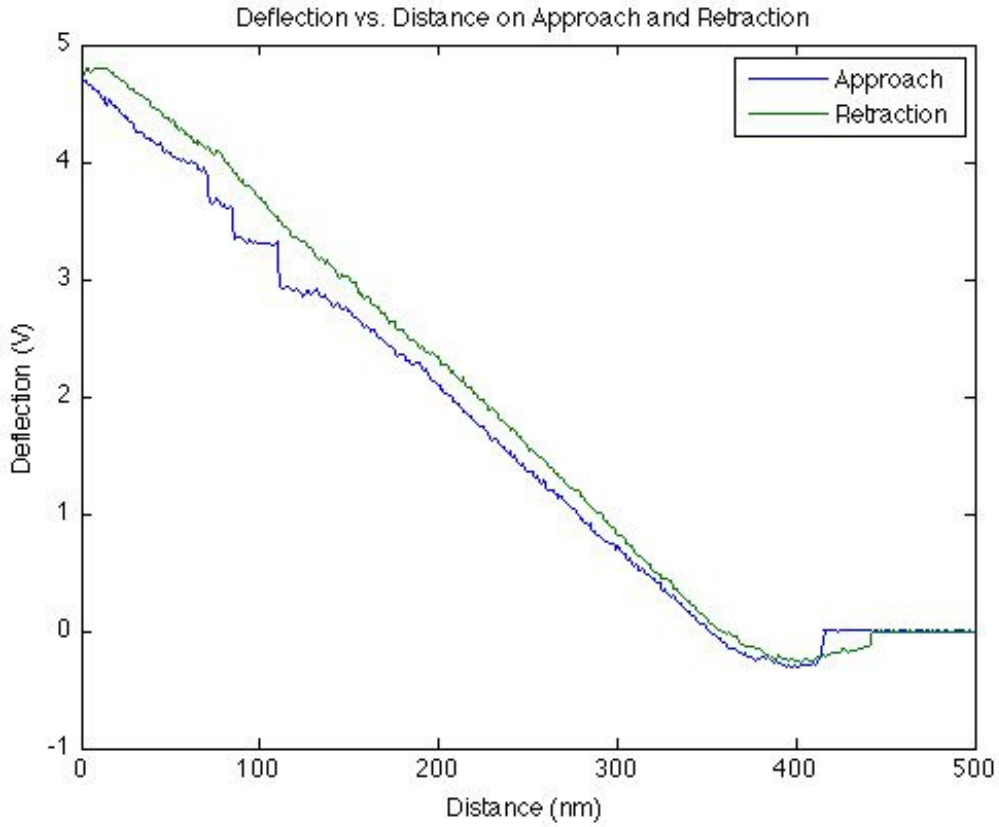
Deflection vs. Distance on Approach and Retraction
Approach
Retraction
Deflection (V)
Distance (nm)
5
4
3
2
1
0
-1
0
100
200
300
400
500

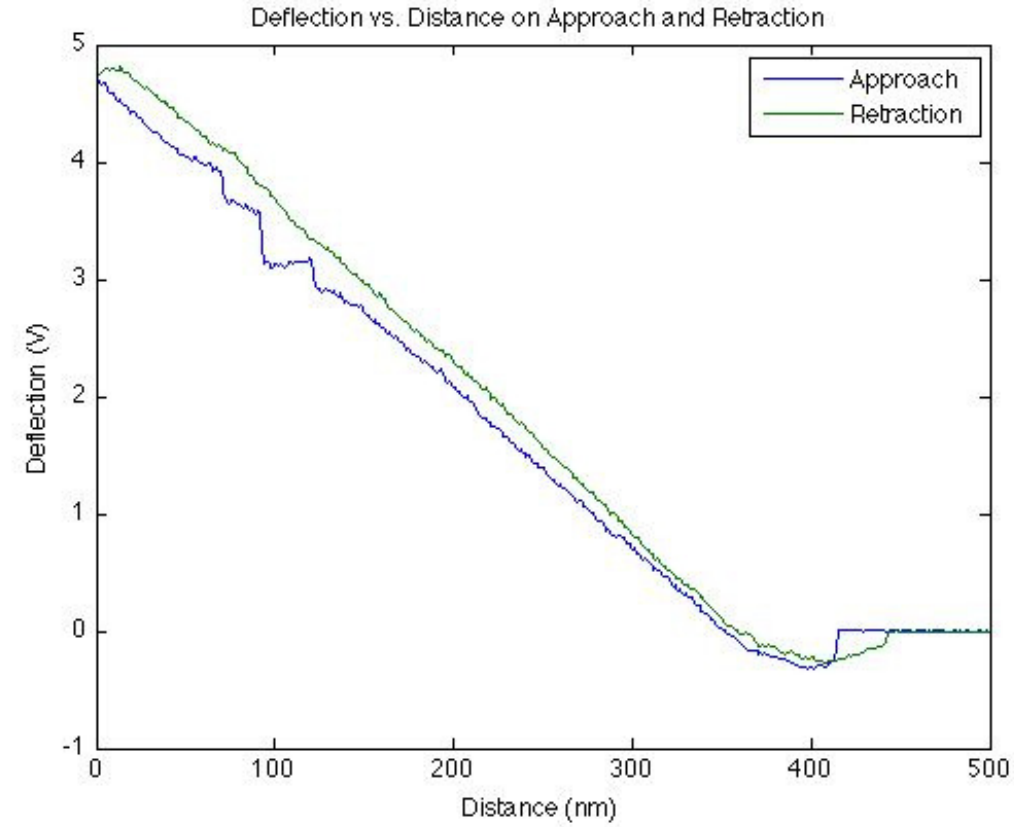
Deflection vs. Distance on Approach and Retraction
Approach
Retraction
Deflection (V)
Distance (nm)
5
4
3
2
1
0
-1
0
100
200
300
400
500

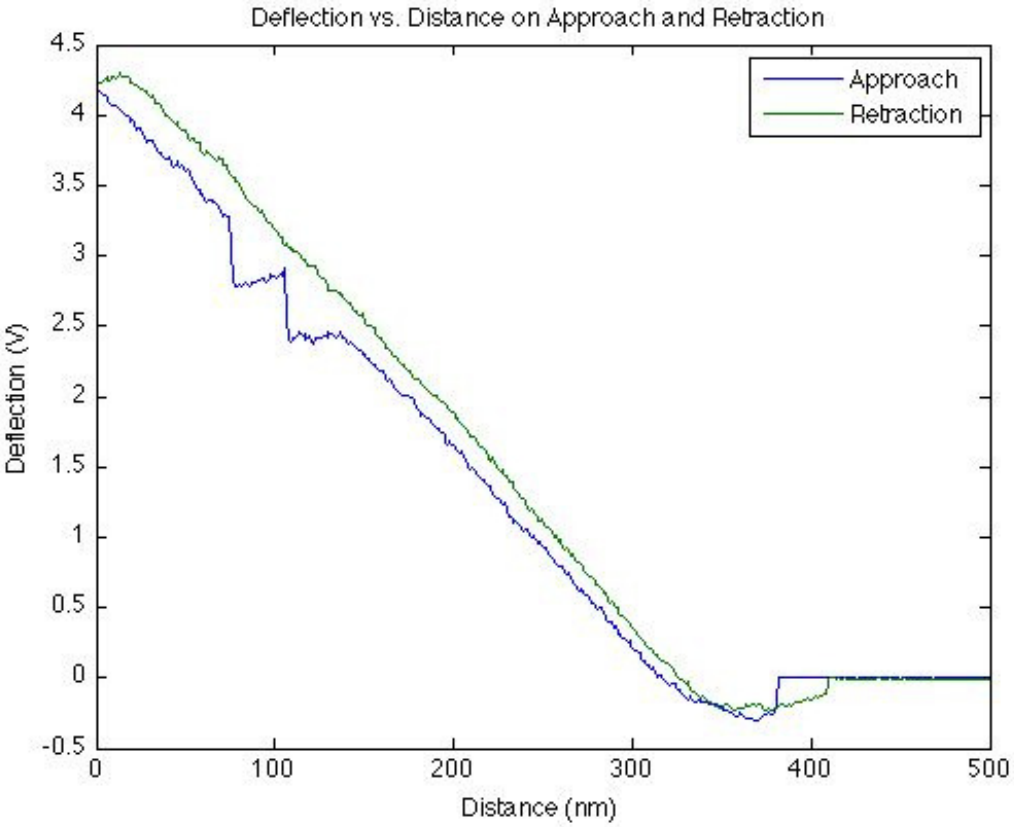
Deflection vs. Distance on Approach and Retraction
Approach
Retraction
Deflection (V)
Distance (nm)
4.5
4
3.5
3
2.5
2
1.5
1
0.5
0
-0.5
0
100
200
300
400
500

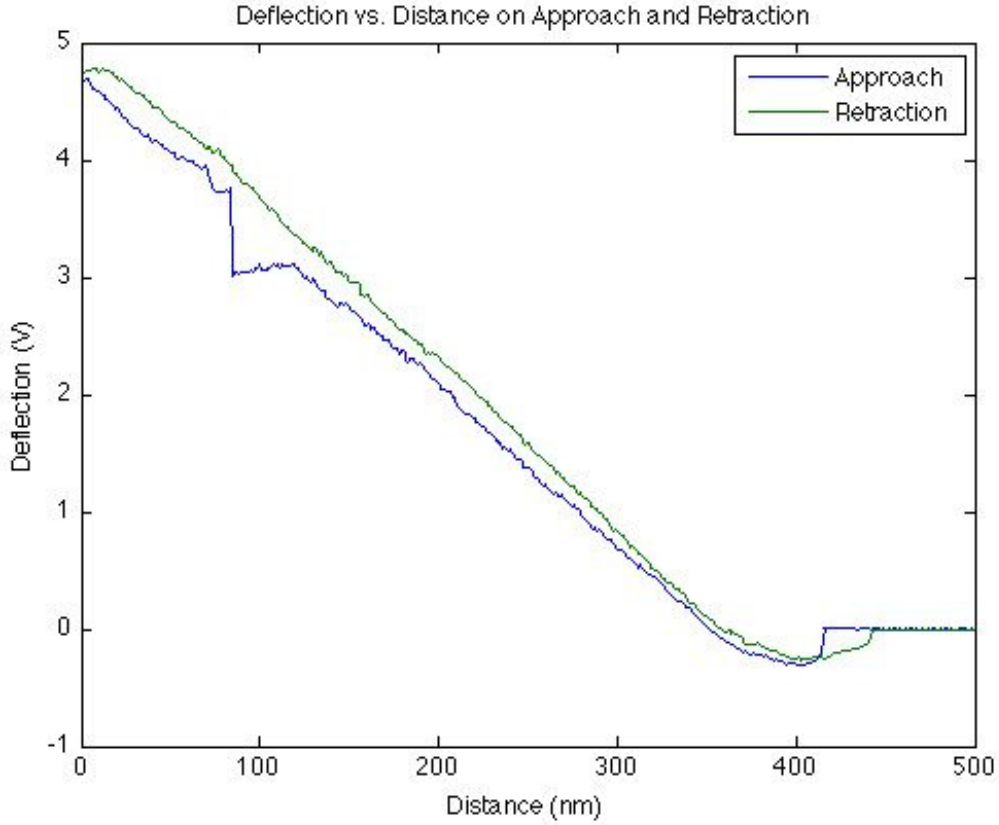
Deflection vs. Distance on Approach and Retraction
Approach
Retraction
Deflection (V)
Distance (nm)
5
4
3
2
1
0
-1
0
100
200
300
400
500

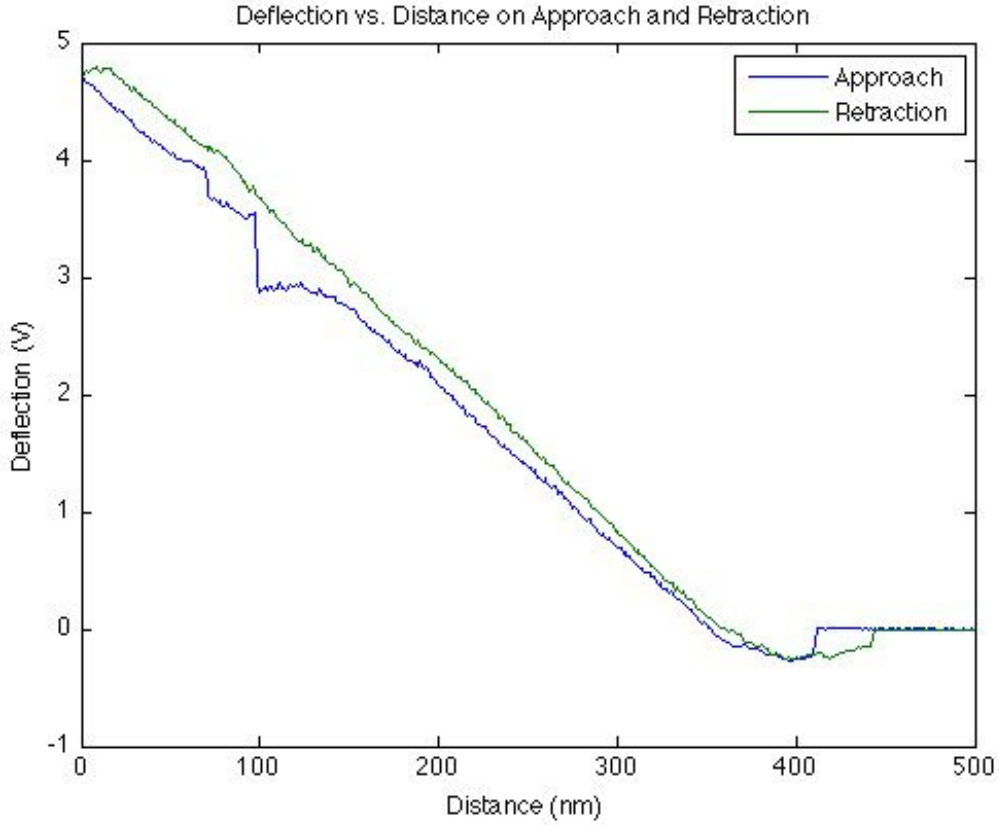
Deflection vs. Distance on Approach and Retraction
Approach
Retraction
Deflection (V)
Distance (nm)
5
4
3
2
1
0
-1
0
100
200
300
400
500

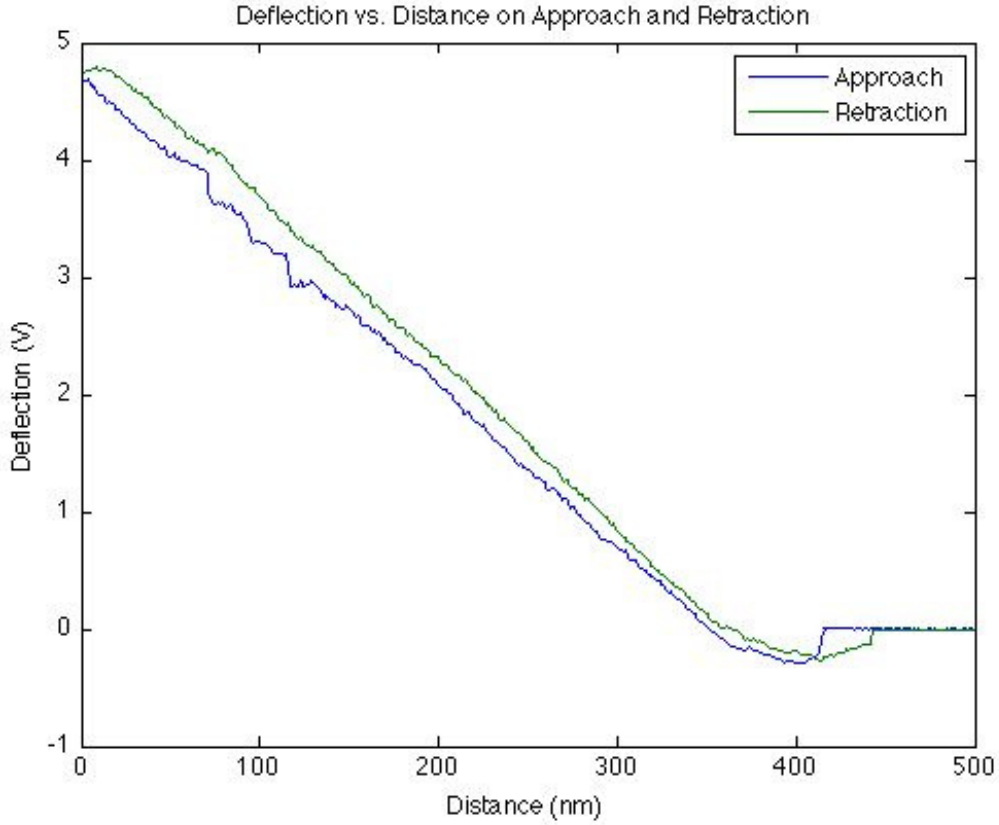
Deflection vs. Distance on Approach and Retraction
Approach
Retraction
Deflection (V)
Distance (nm)
5
4
3
2
1
0
-1
0
100
200
300
400
500

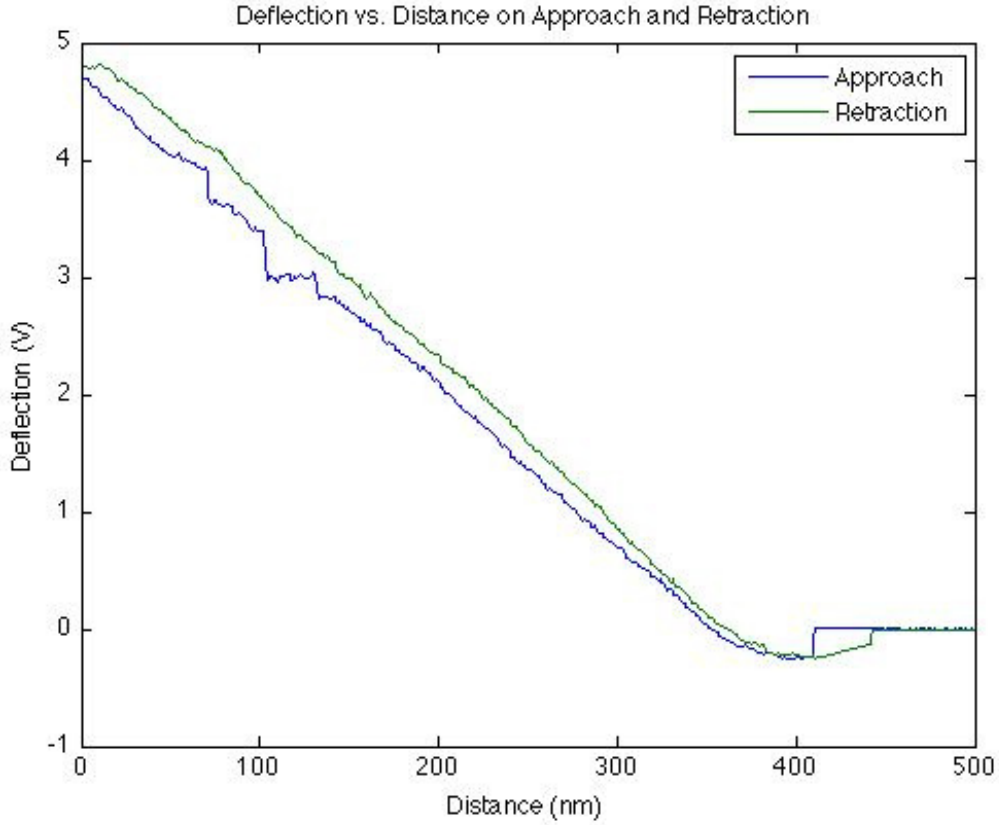
Deflection vs. Distance on Approach and Retraction
Approach
Retraction
Deflection (V)
Distance (nm)
5
4
3
2
1
0
-1
0
100
200
300
400
500

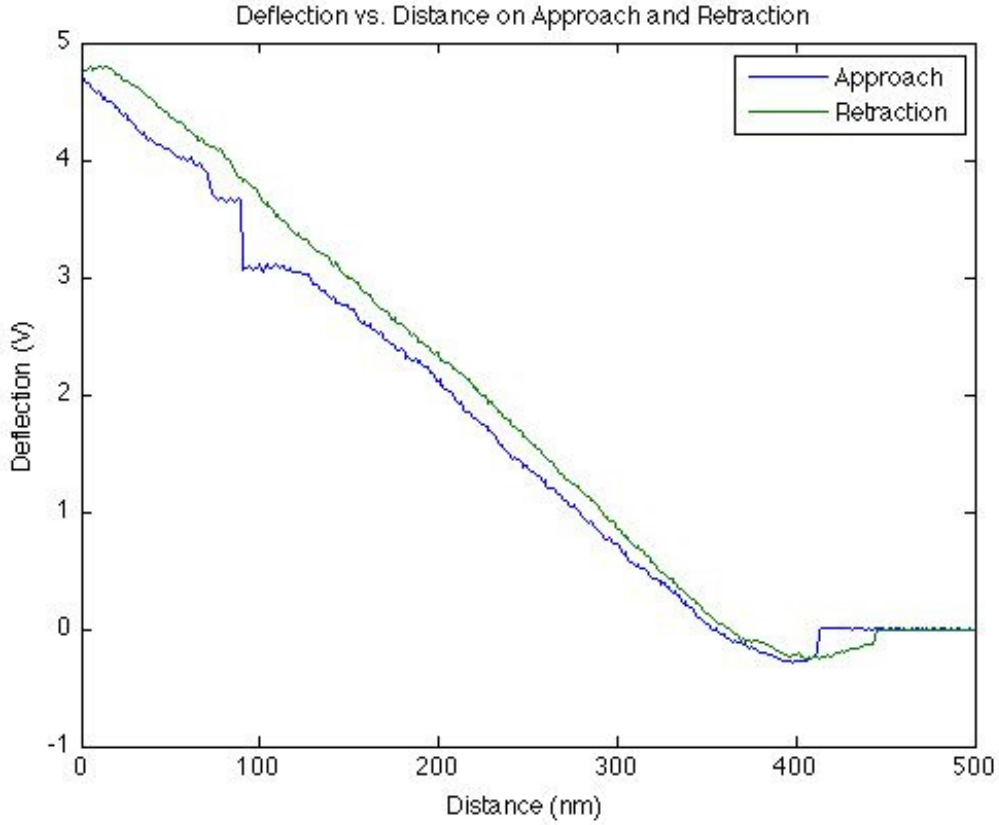
Deflection vs. Distance on Approach and Retraction
Approach
Retraction
Deflection (V)
Distance (nm)
5
4
3
2
1
0
-1
0
100
200
300
400
500

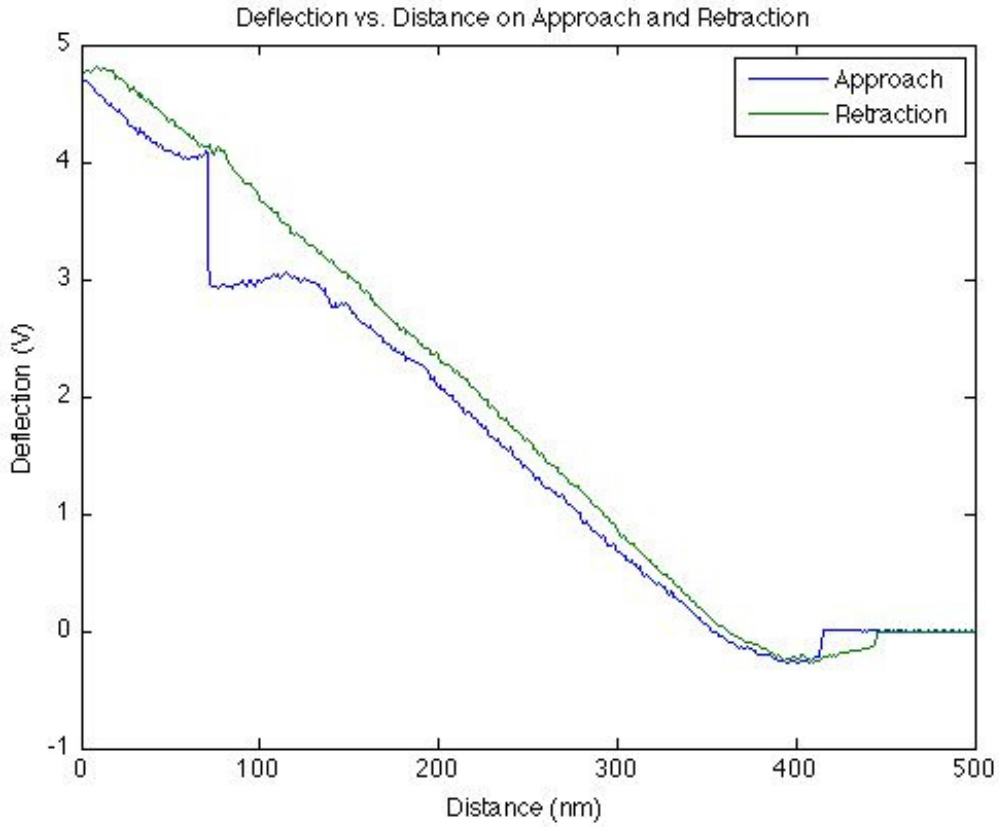
Deflection vs. Distance on Approach and Retraction
Approach
Retraction
Deflection (V)
Distance (nm)
5
4
3
2
1
0
-1
0
100
200
300
400
500

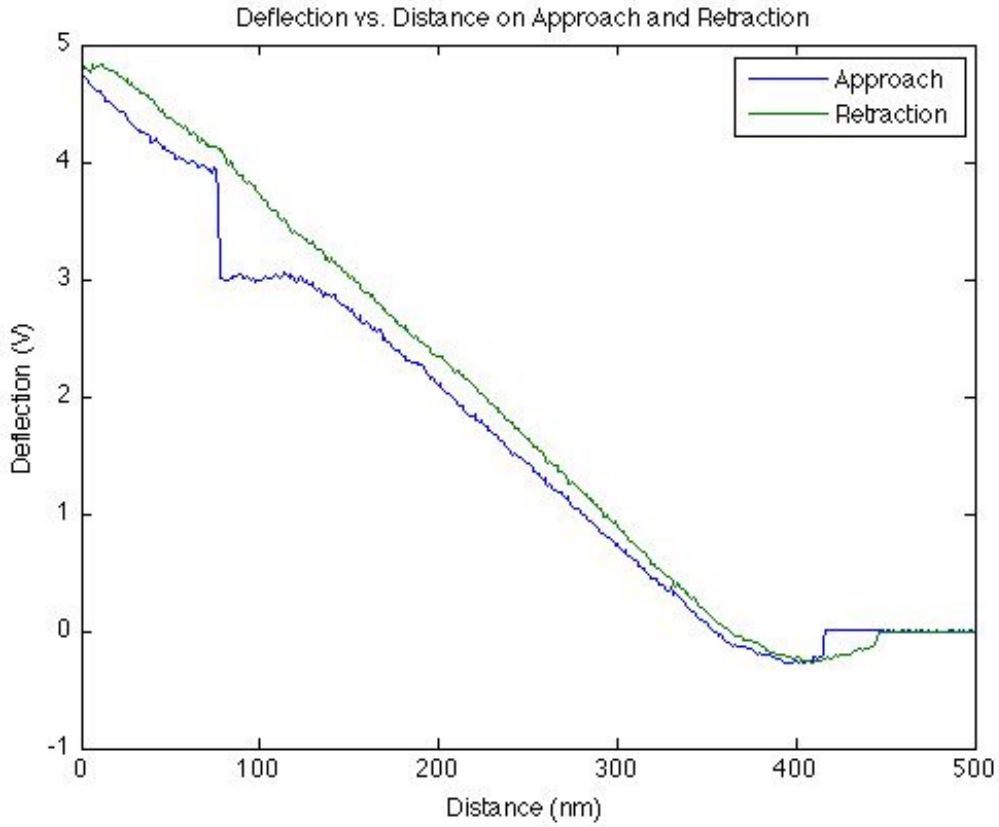
Deflection vs. Distance on Approach and Retraction
Approach
Retraction
Deflection (V)
Distance (nm)
5
4
3
2
1
0
-1
0
100
200
300
400
500

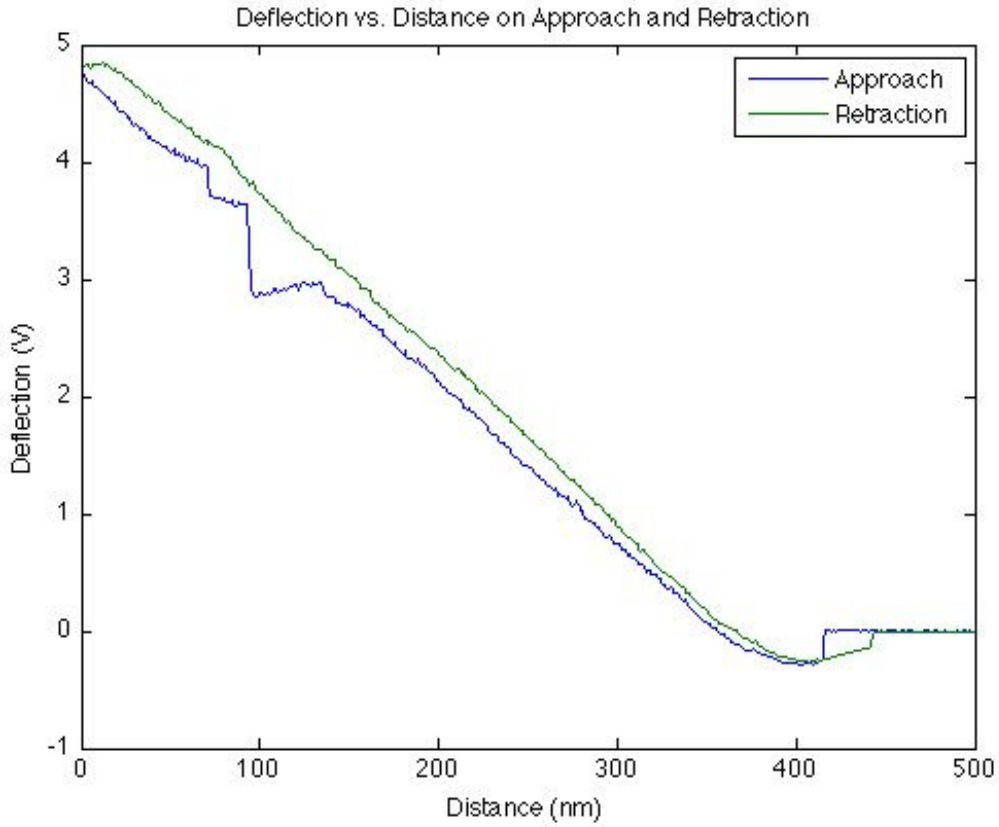
Deflection vs. Distance on Approach and Retraction
Approach
Retraction
Deflection (V)
Distance (nm)
5
4
3
2
1
0
-1
0
100
200
300
400
500

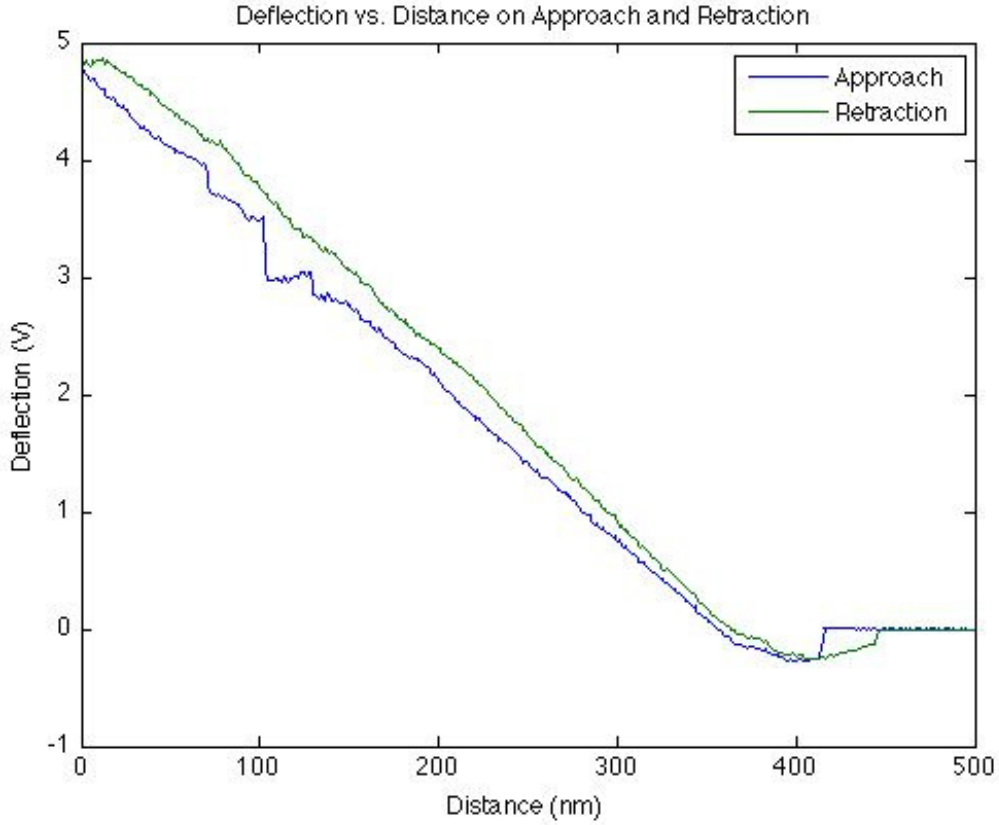
Deflection vs. Distance on Approach and Retraction
Approach
Retraction
Deflection (V)
Distance (nm)
5
4
3
2
1
0
-1
0
100
200
300
400
500

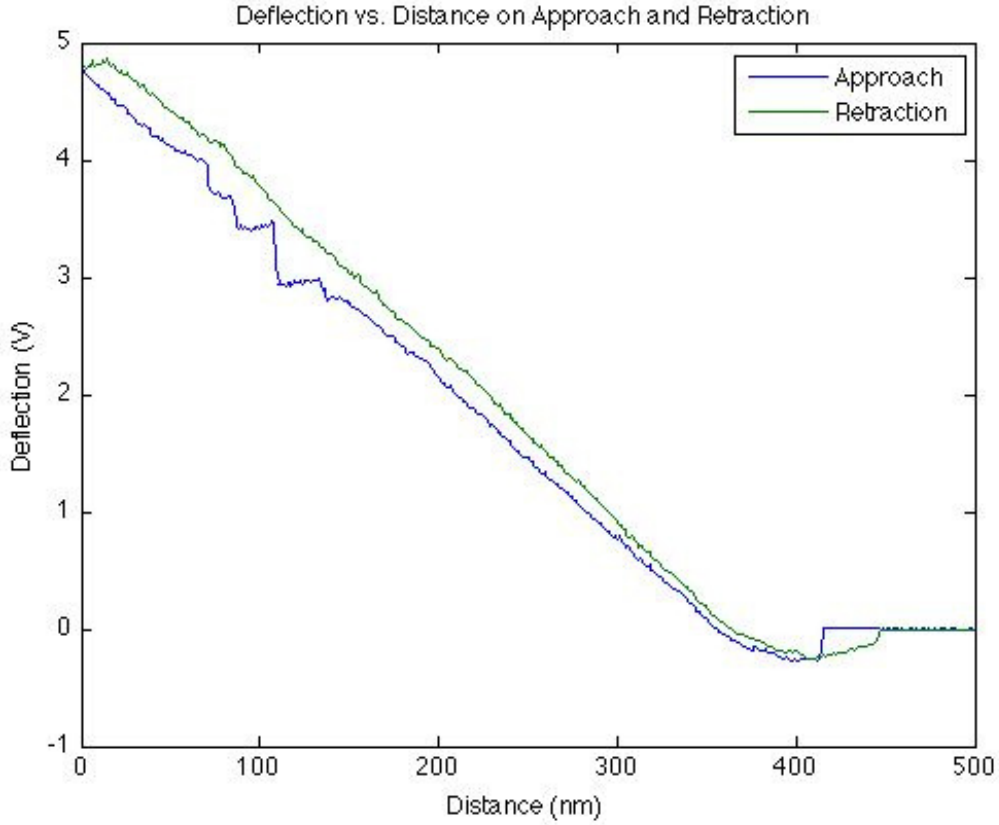
Deflection vs. Distance on Approach and Retraction
Approach
Retraction
Deflection (V)
Distance (nm)
5
4
3
2
1
0
-1
0
100
200
300
400
500

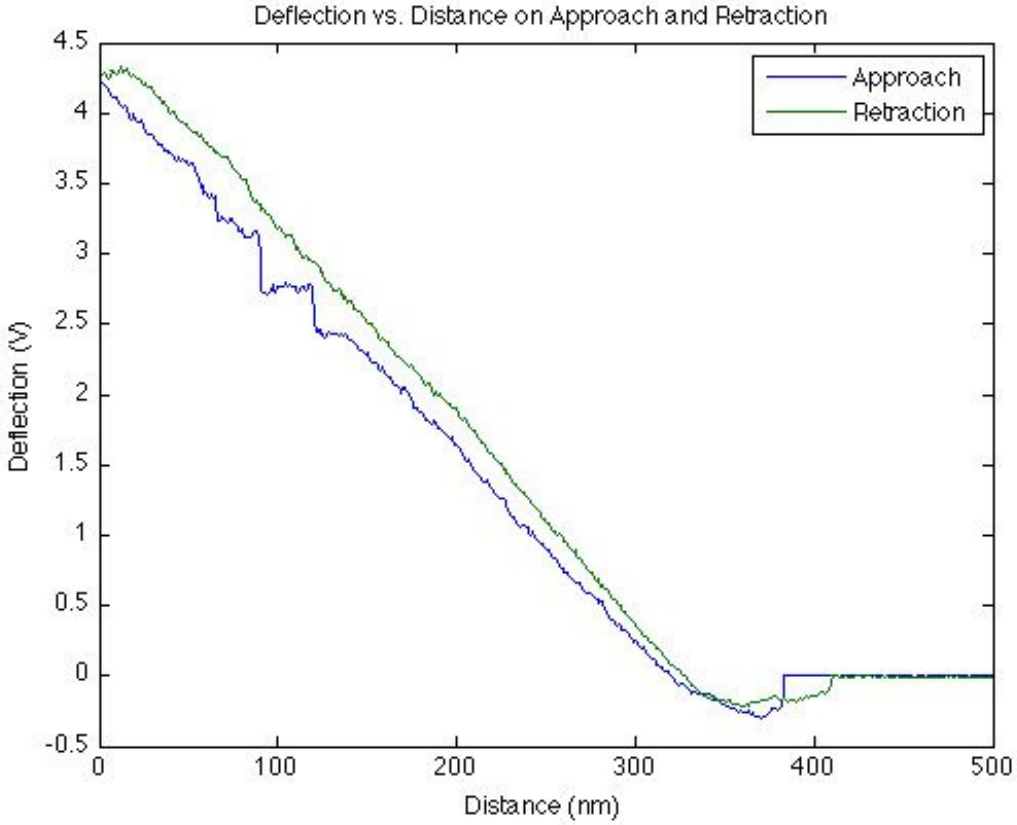
Deflection vs. Distance on Approach and Retraction
Approach
Retraction
Deflection (V)
Distance (nm)
4.5
4
3.5
3
2.5
2
1.5
1
0.5
0
-0.5
0
100
200
300
400
500

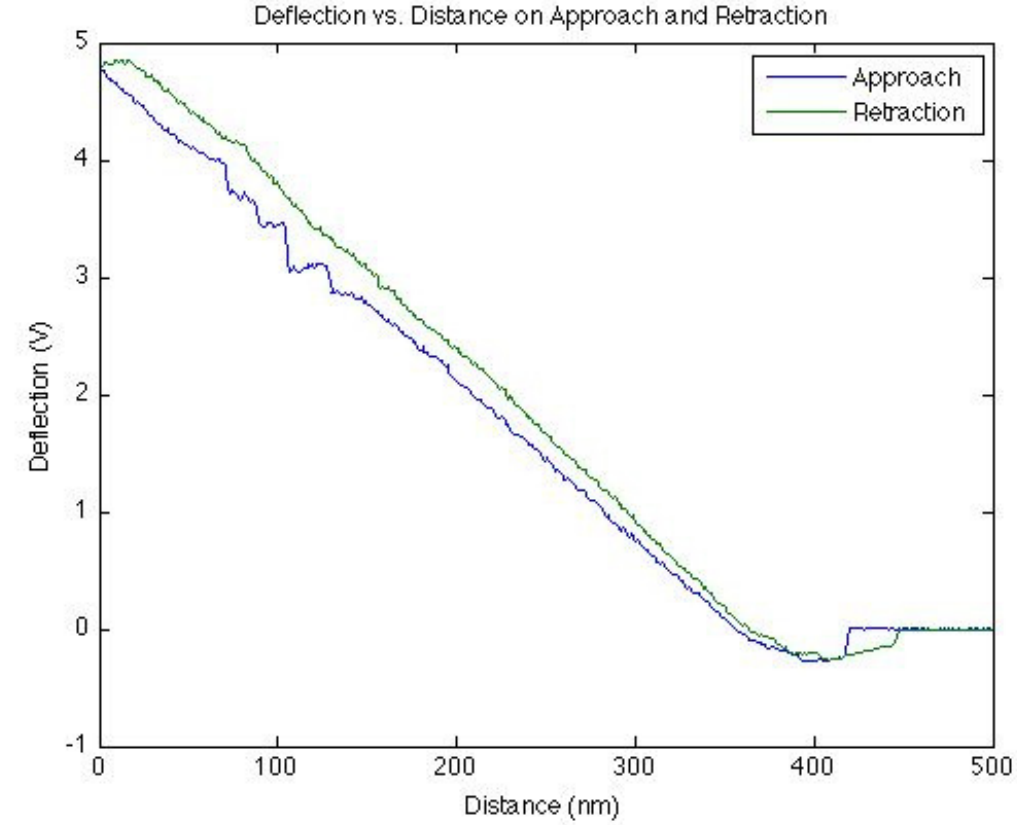
Deflection vs. Distance on Approach and Retraction
Approach
Retraction
Deflection (V)
Distance (nm)
5
4
3
2
1
0
-1
0
100
200
300
400
500

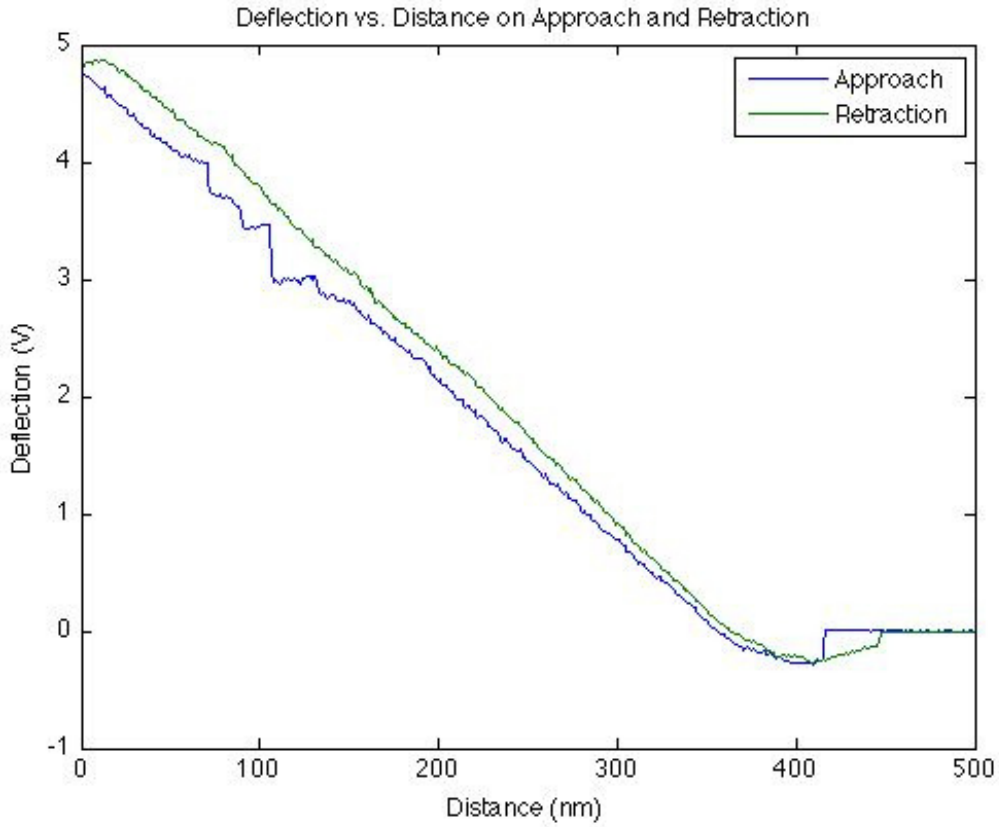
Deflection vs. Distance on Approach and Retraction
Approach
Retraction
Deflection (V)
Distance (nm)
5
4
3
2
1
0
-1
0
100
200
300
400
500

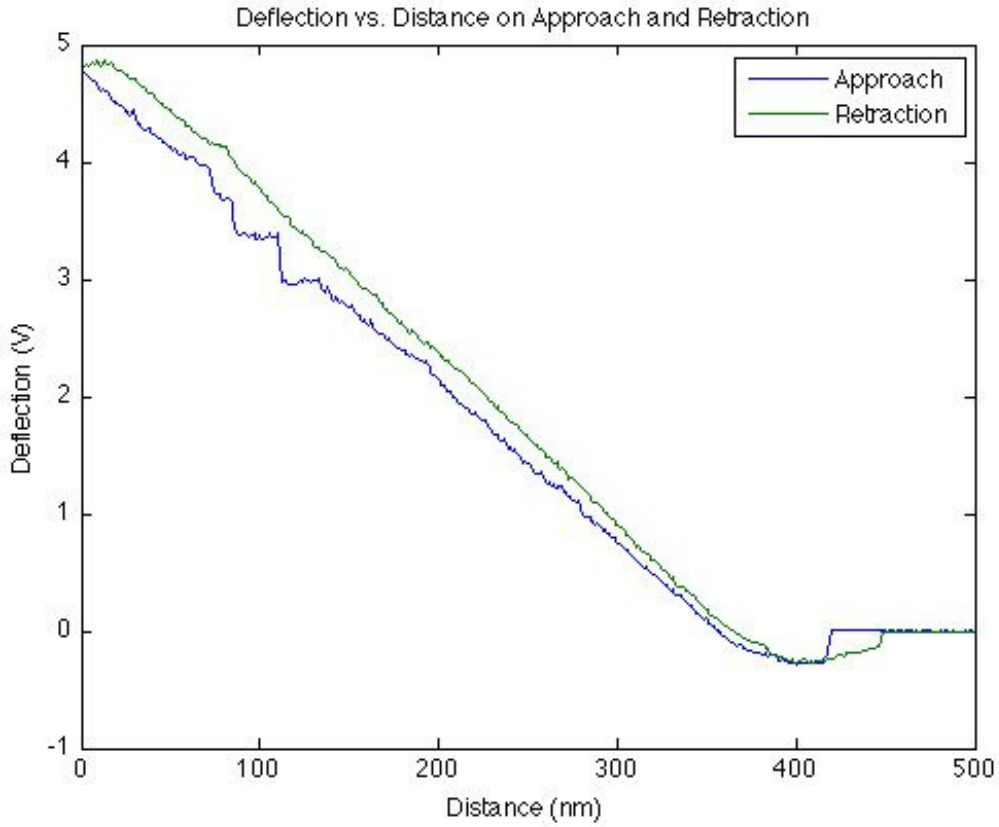
Deflection vs. Distance on Approach and Retraction
Approach
Retraction
Deflection (V)
Distance (nm)
5
4
3
2
1
0
-1
0
100
200
300
400
500

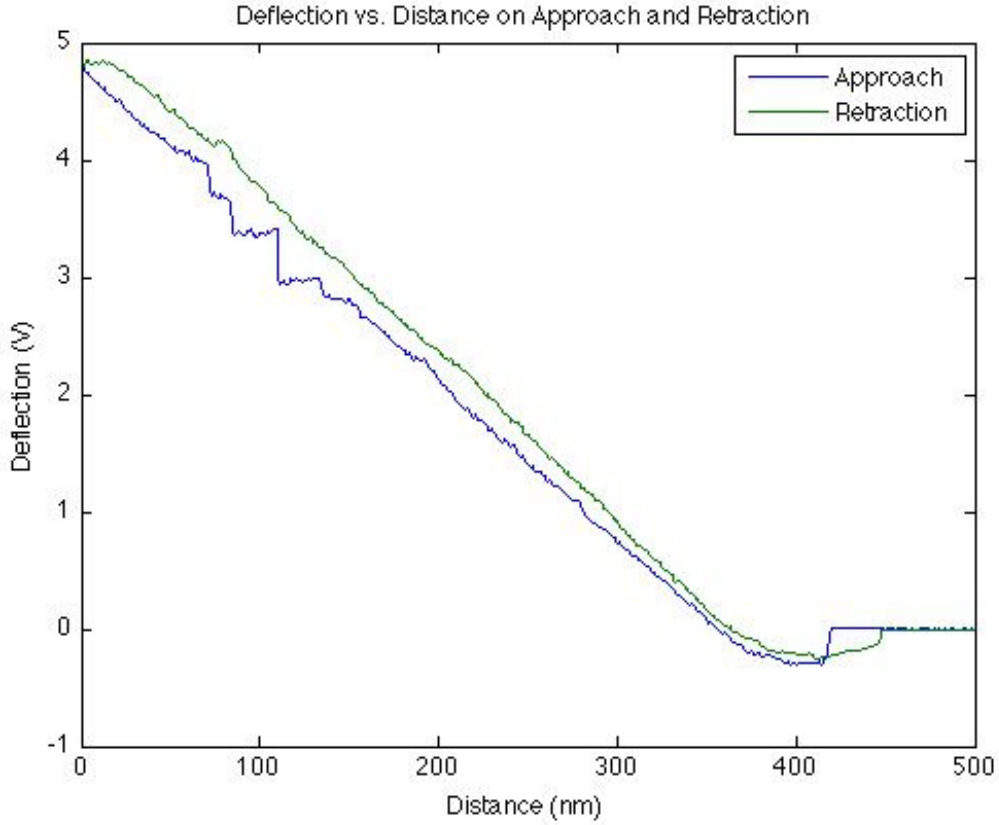
Deflection vs. Distance on Approach and Retraction
Approach
Retraction
Deflection (V)
Distance (nm)
5
4
3
2
1
0
-1
0
100
200
300
400
500

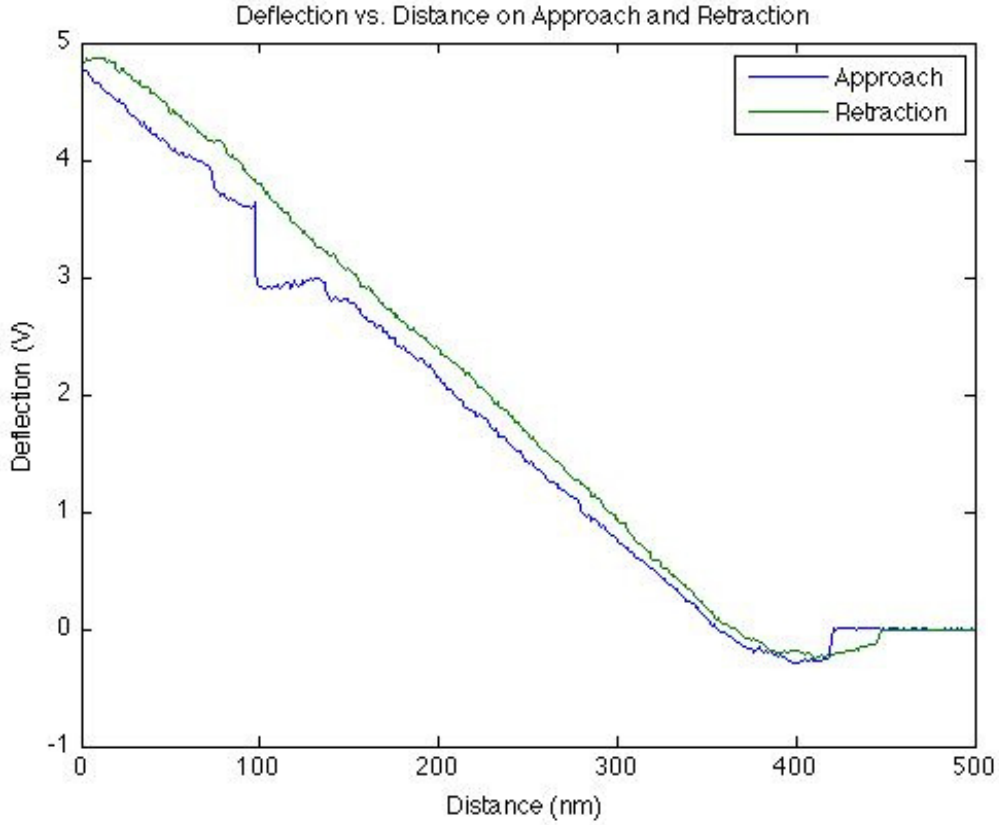
Deflection vs. Distance on Approach and Retraction
Approach
Retraction
Deflection (V)
Distance (nm)
5
4
3
2
1
0
-1
0
100
200
300
400
500

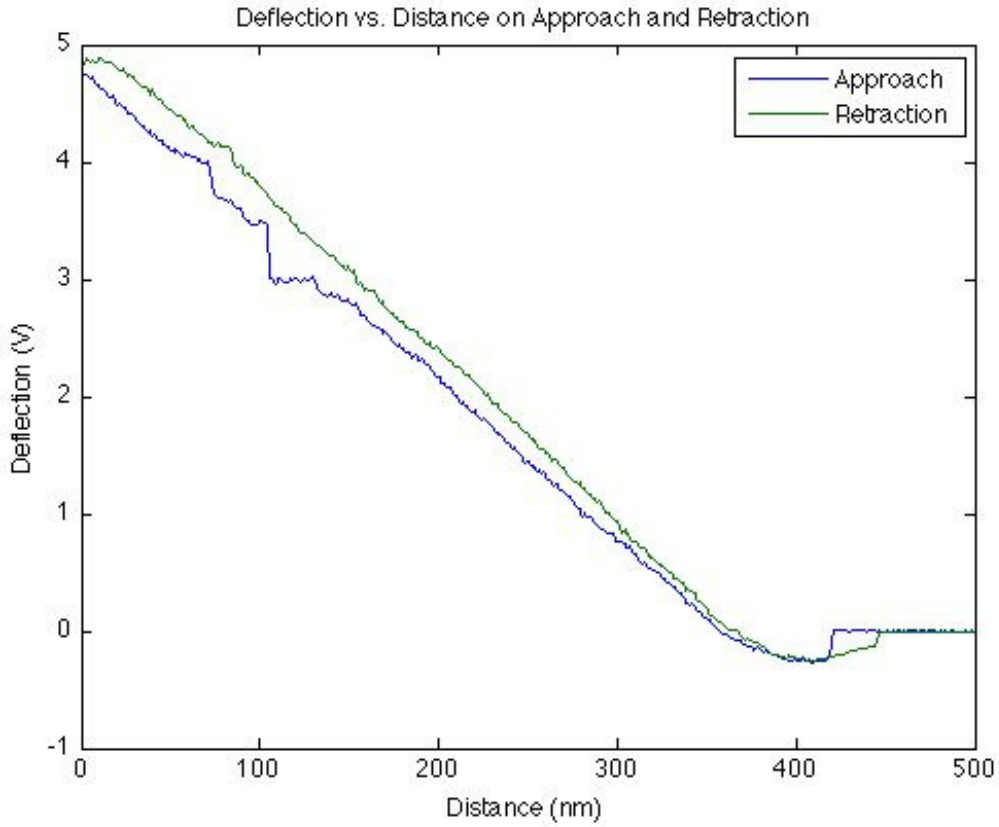
Deflection vs. Distance on Approach and Retraction
Approach
Retraction
Deflection (V)
Distance (nm)
5
4
3
2
1
0
-1
0
100
200
300
400
500

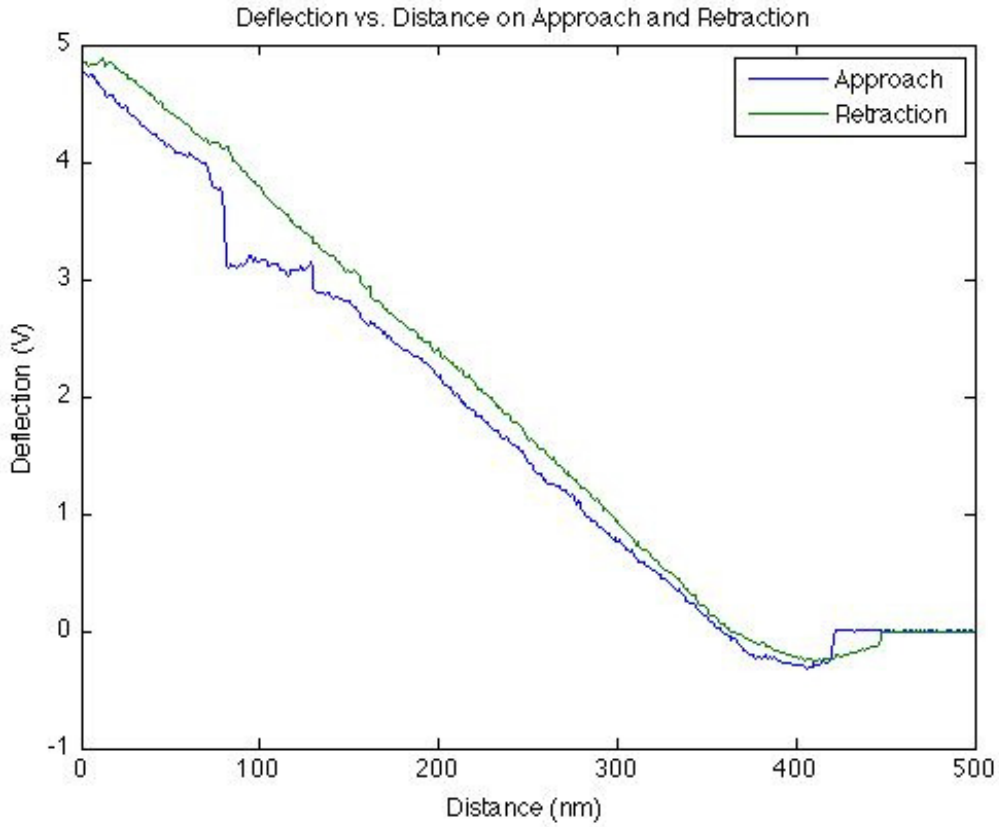
Deflection vs. Distance on Approach and Retraction
Approach
Retraction
Deflection (V)
Distance (nm)
5
4
3
2
1
0
-1
0
100
200
300
400
500

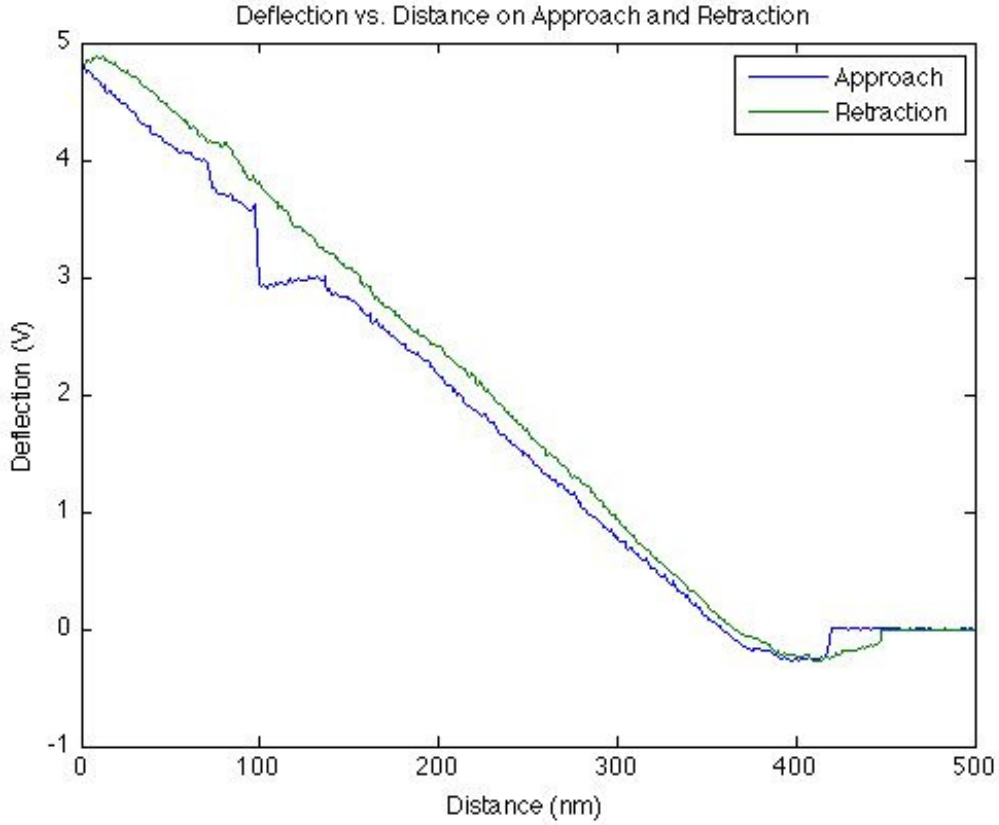
Deflection vs. Distance on Approach and Retraction
Approach
Retraction
Deflection (V)
Distance (nm)
5
4
3
2
1
0
-1
0
100
200
300
400
500

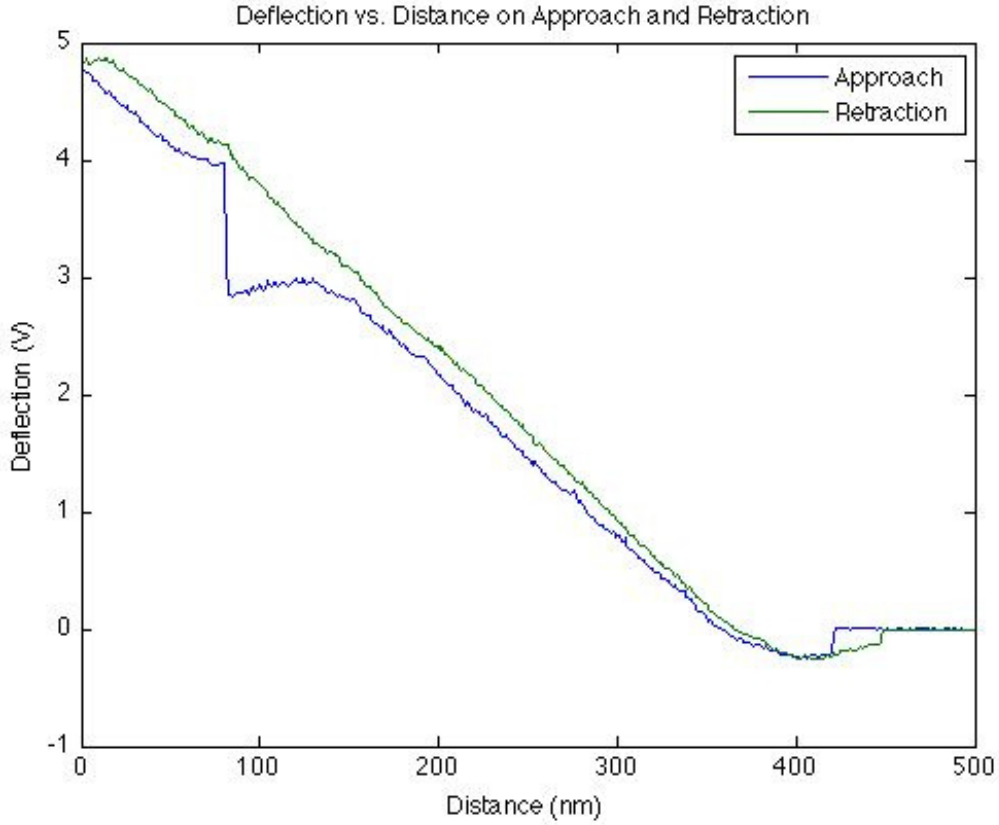
Deflection vs. Distance on Approach and Retraction
Approach
Retraction
Deflection (V)
Distance (nm)
5
4
3
2
1
0
-1
0
100
200
300
400
500

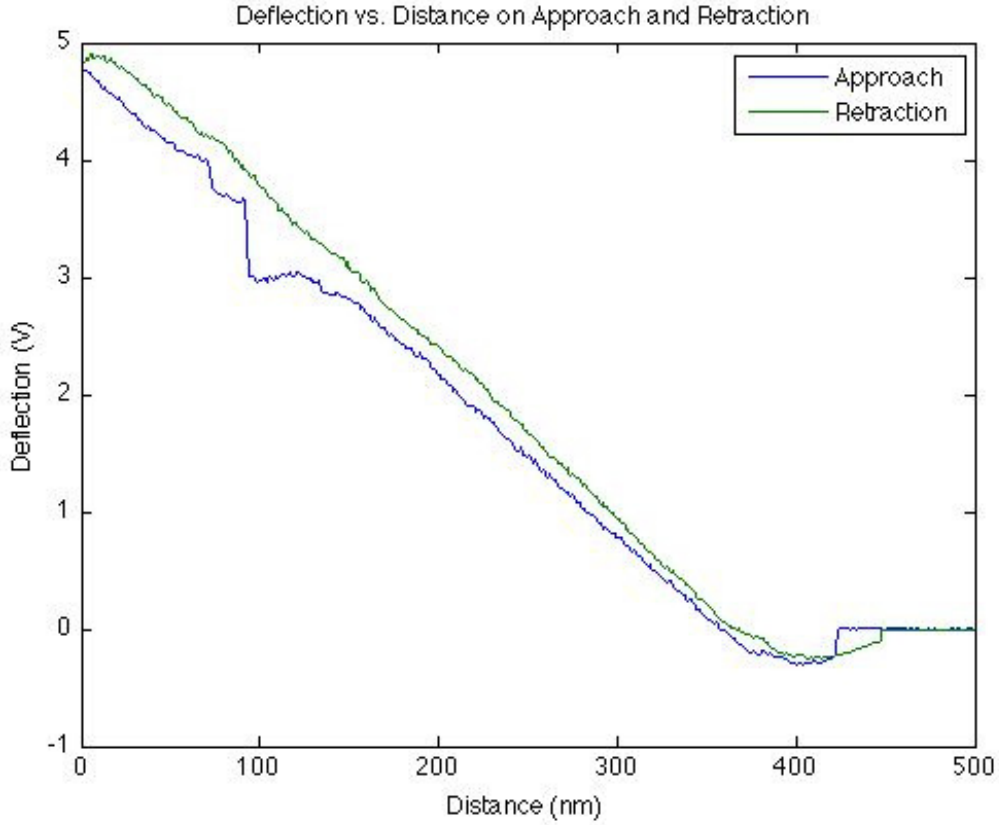
Deflection vs. Distance on Approach and Retraction
Approach
Retraction
Deflection (V)
Distance (nm)
5
4
3
2
1
0
-1
0
100
200
300
400
500

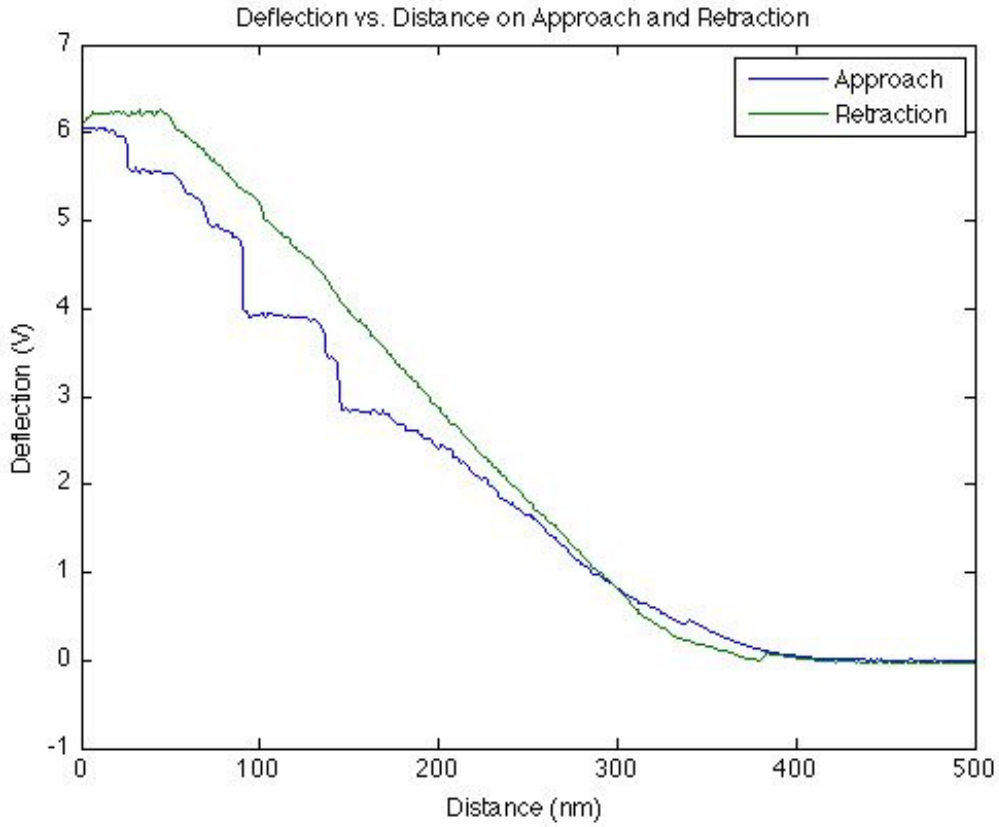
Deflection vs. Distance on Approach and Retraction
Approach
Retraction
Deflection (V)
Distance (nm)
7
6
5
4
3
2
1
0
-1
0
100
200
300
400
500

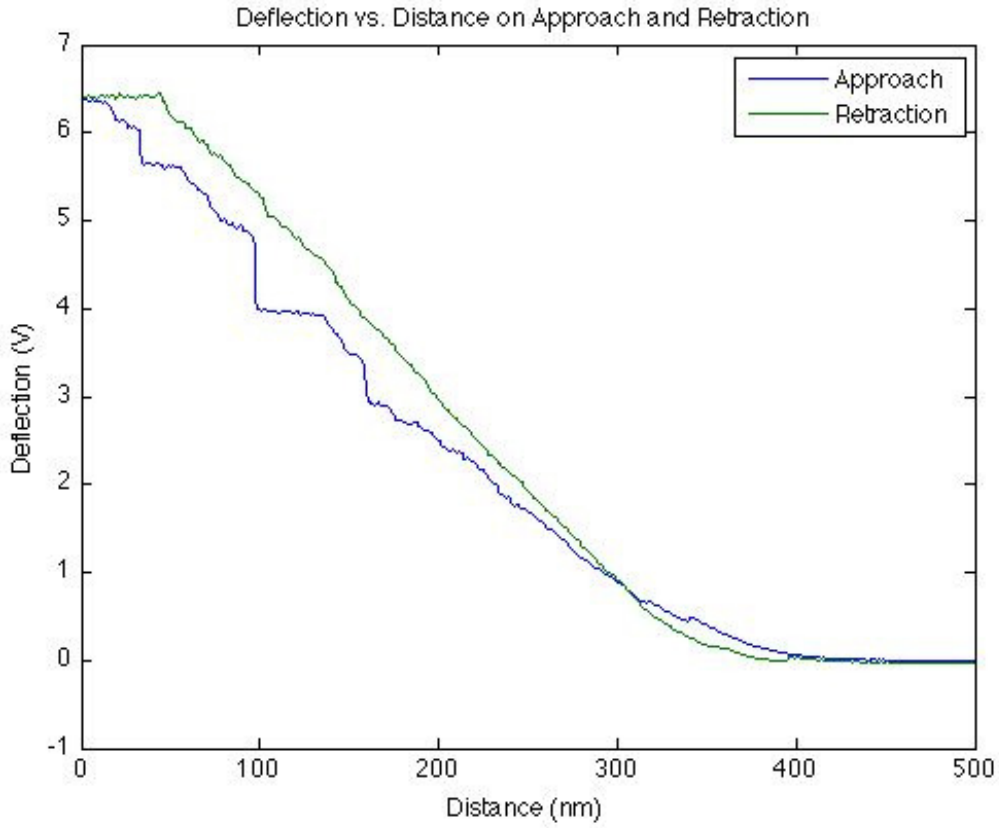
Deflection vs. Distance on Approach and Retraction
Approach
Retraction
Deflection (V)
Distance (nm)
7
6
5
4
3
2
1
0
-1
0
100
200
300
400
500

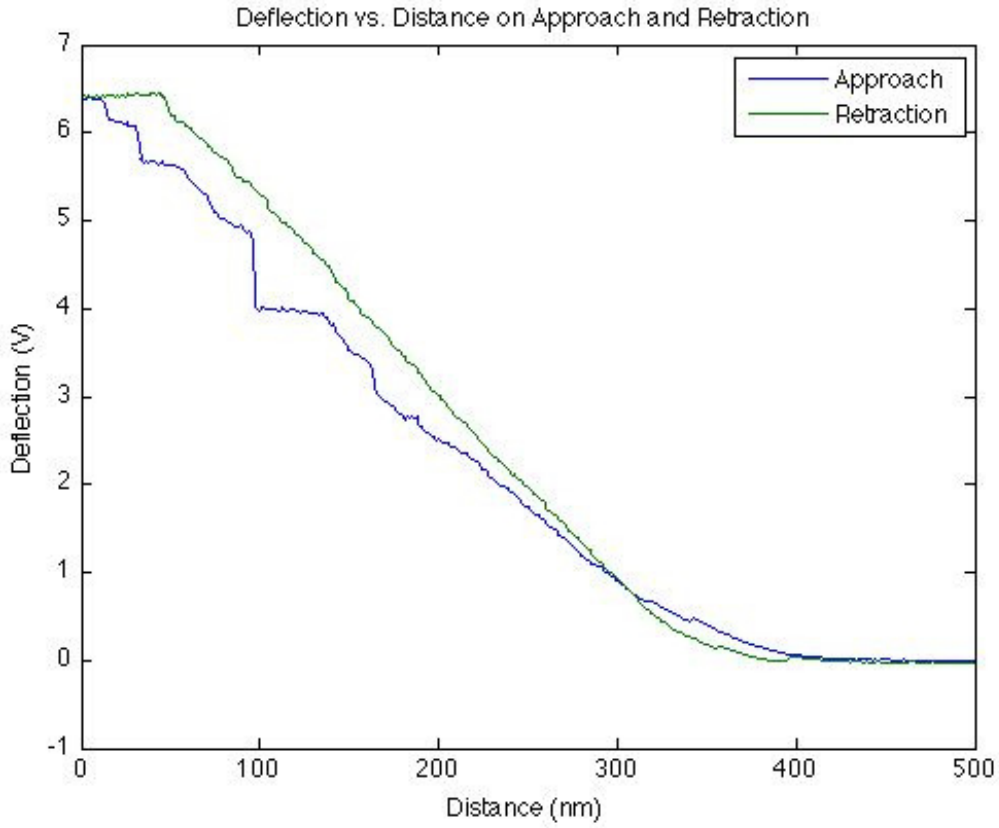
Deflection vs. Distance on Approach and Retraction
Approach
Retraction
Deflection (V)
Distance (nm)
7
6
5
4
3
2
1
0
-1
0
100
200
300
400
500

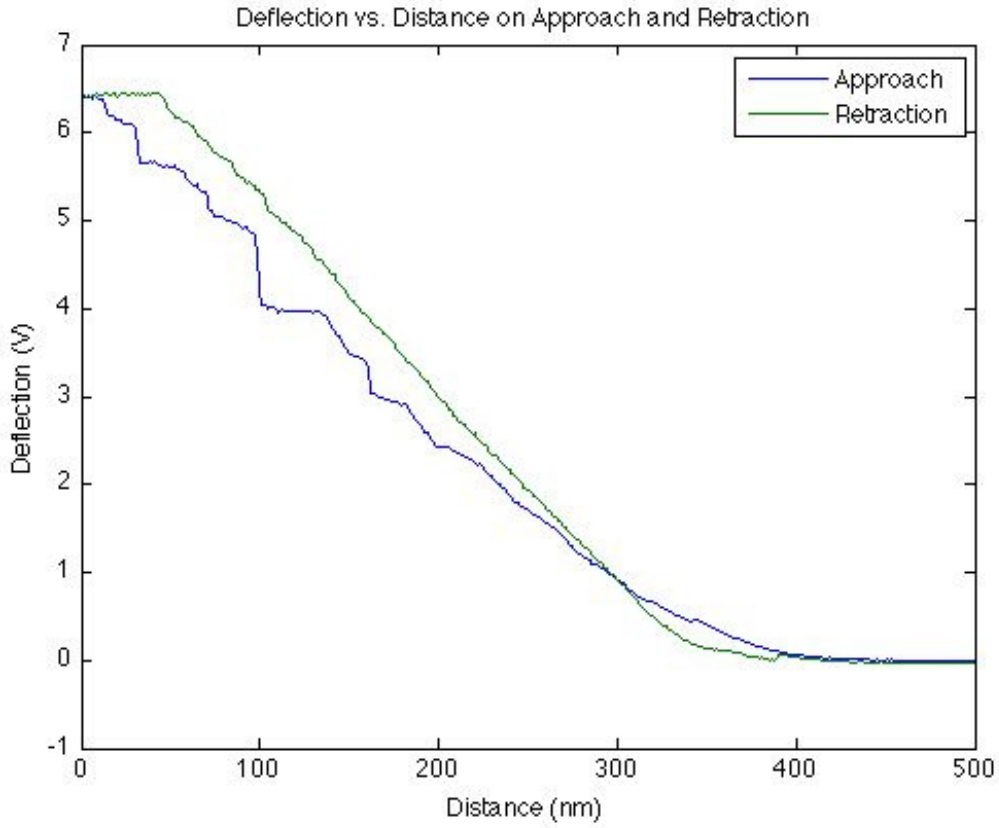
Deflection vs. Distance on Approach and Retraction
Approach
Retraction
Deflection (V)
Distance (nm)
7
6
5
4
3
2
1
0
-1
0
100
200
300
400
500

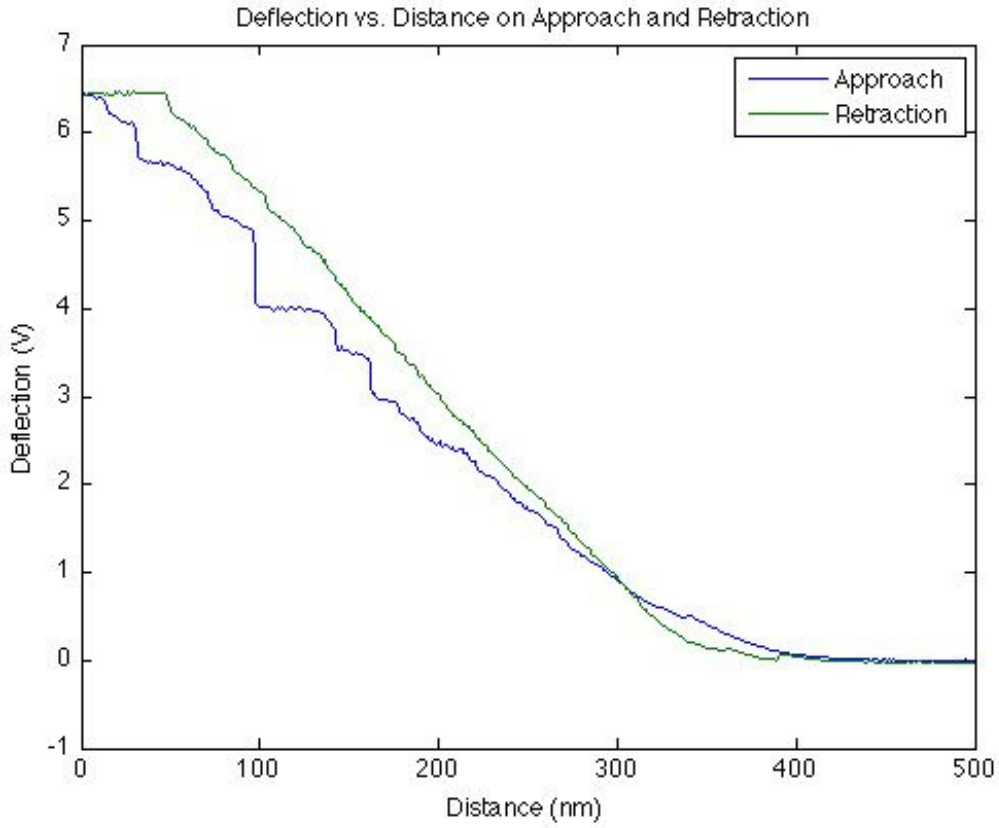
Deflection vs. Distance on Approach and Retraction
Approach
Retraction
Deflection (V)
Distance (nm)
7
6
5
4
3
2
1
0
-1
0
100
200
300
400
500

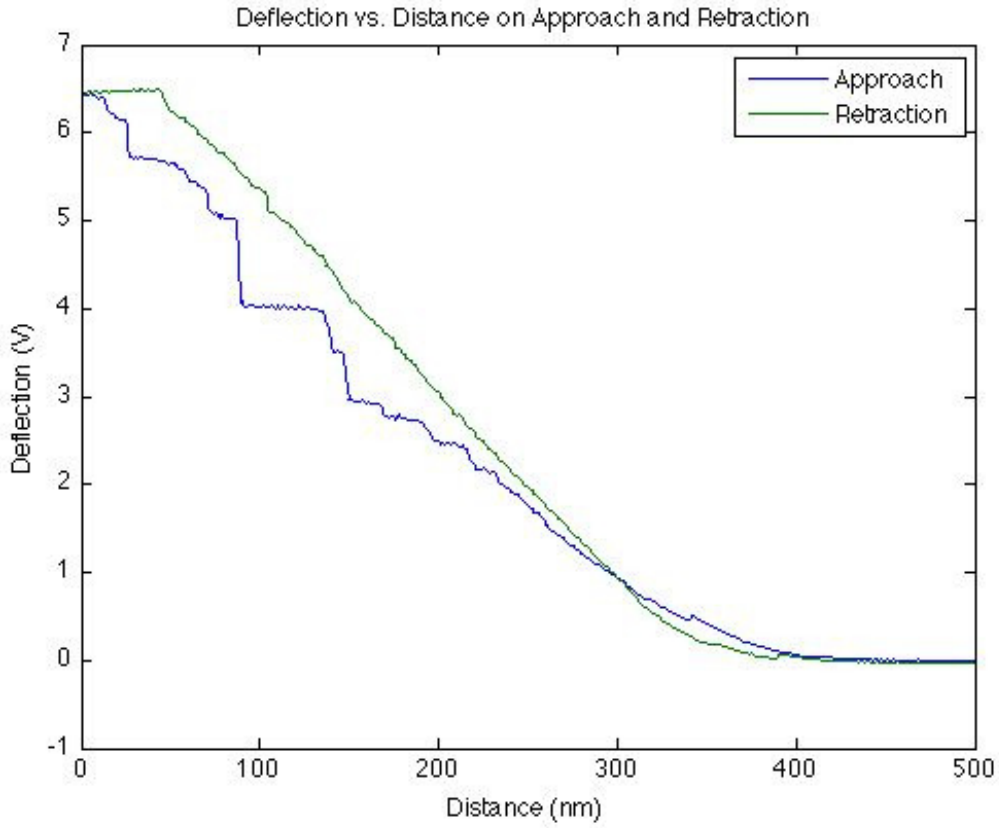
Deflection vs. Distance on Approach and Retraction
Approach
Retraction
Deflection (V)
Distance (nm)
7
6
5
4
3
2
1
0
-1
0
100
200
300
400
500

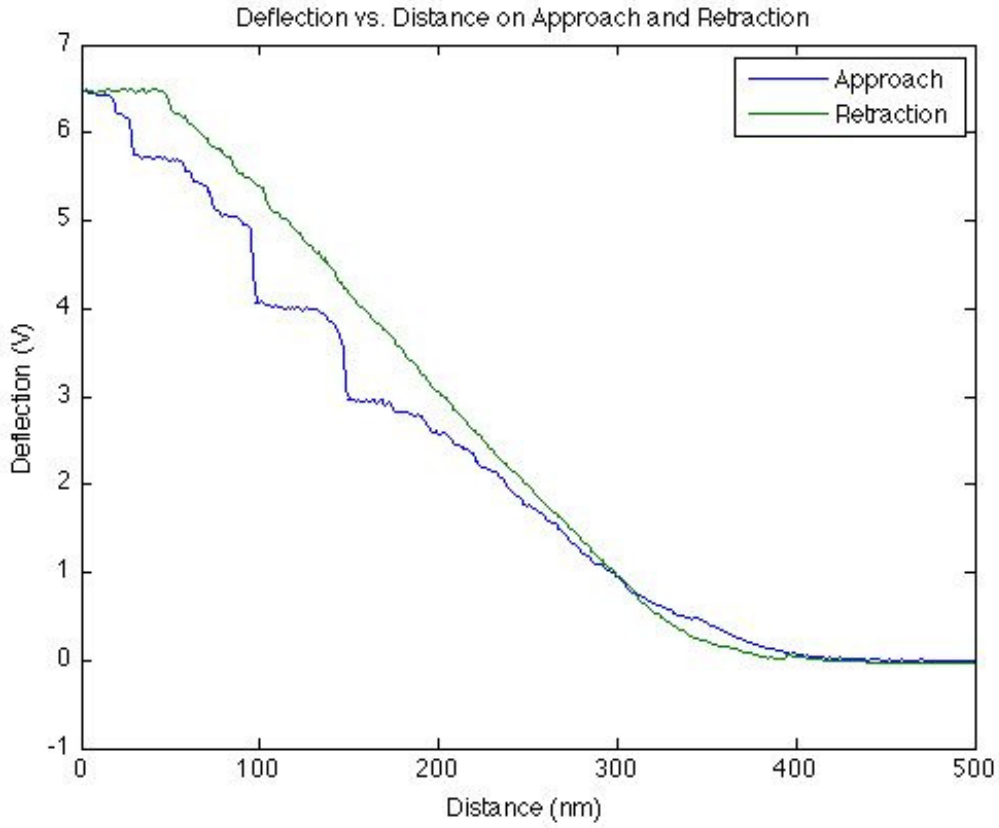
Deflection vs. Distance on Approach and Retraction
Approach
Retraction
Deflection (V)
Distance (nm)
7
6
5
4
3
2
1
0
-1
0
100
200
300
400
500

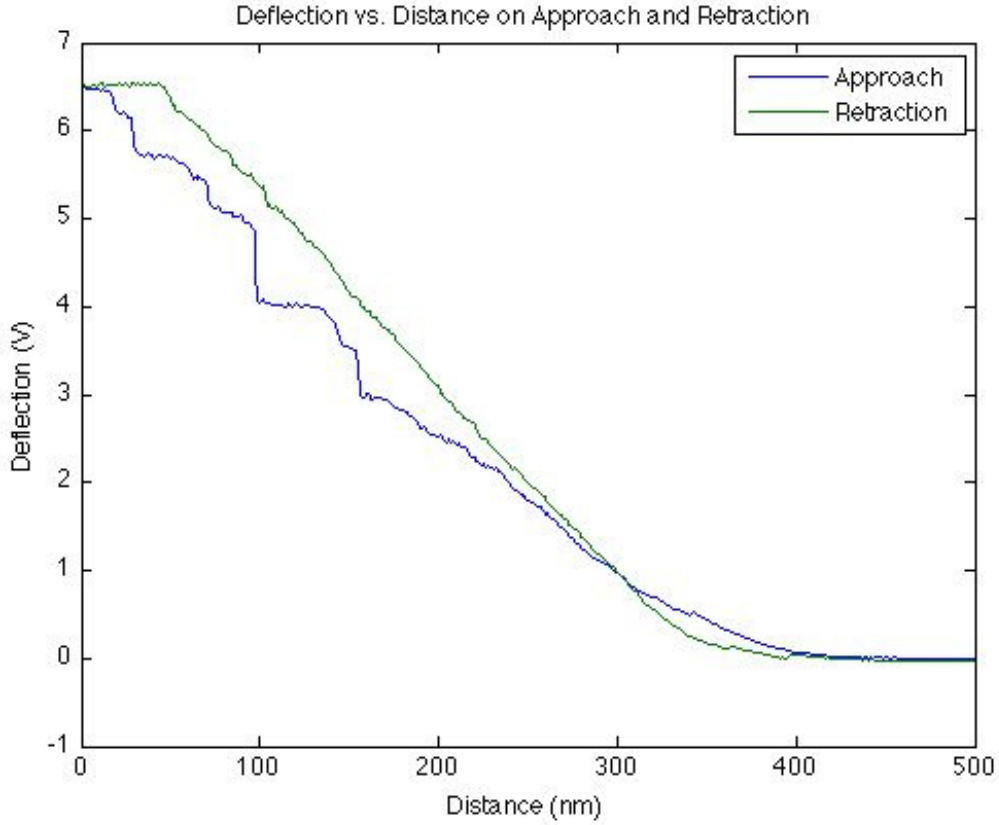
Deflection vs. Distance on Approach and Retraction
Approach
Retraction
Deflection (V)
Distance (nm)
7
6
5
4
3
2
1
0
-1
0
100
200
300
400
500

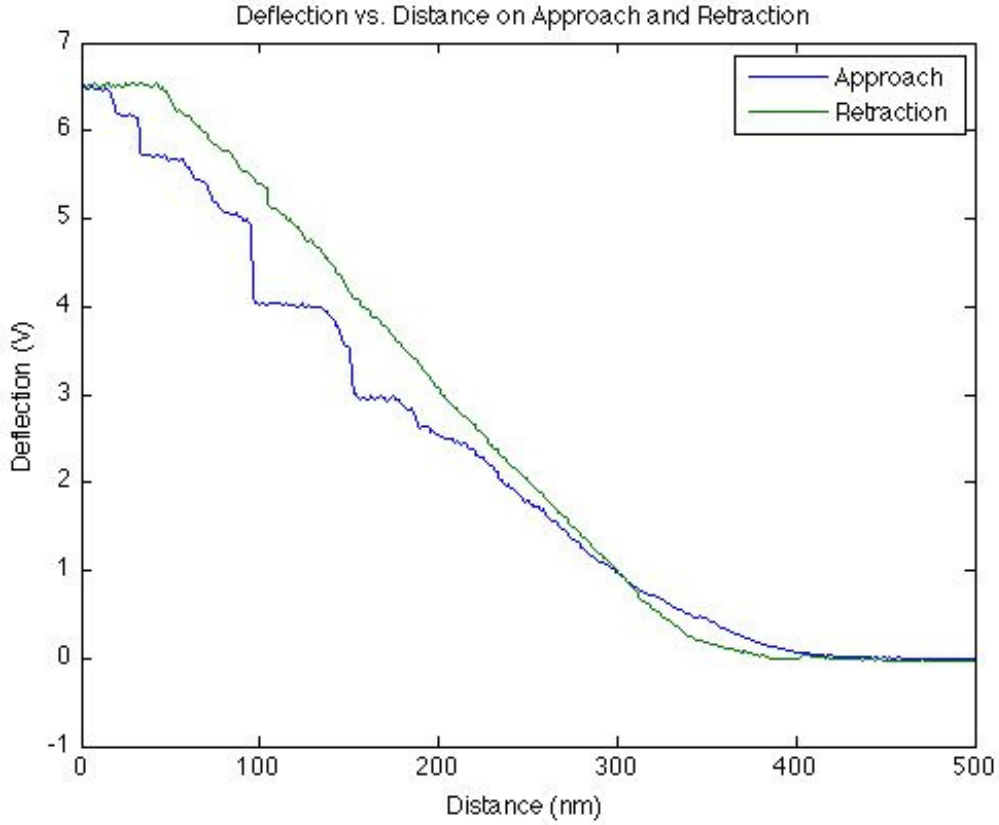
Deflection vs. Distance on Approach and Retraction
Approach
Retraction
Deflection (V)
Distance (nm)
7
6
5
4
3
2
1
0
-1
0
100
200
300
400
500

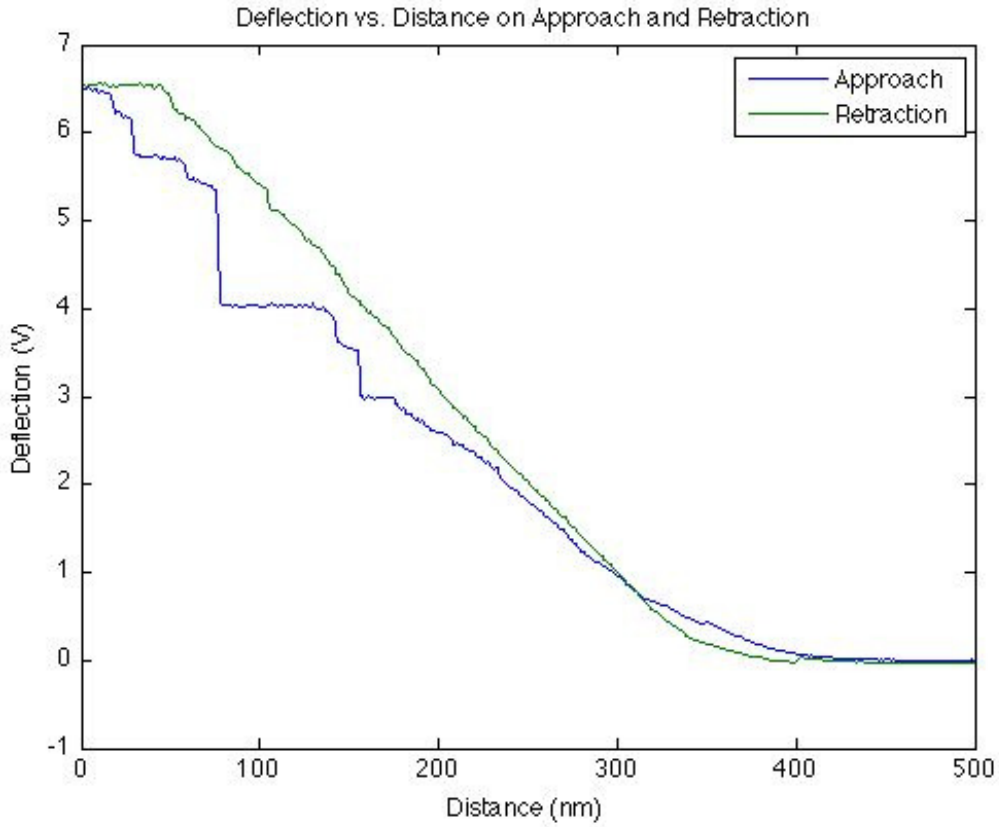
Deflection vs. Distance on Approach and Retraction
Approach
Retraction
Deflection (V)
Distance (nm)
7
6
5
4
3
2
1
0
-1
0
100
200
300
400
500

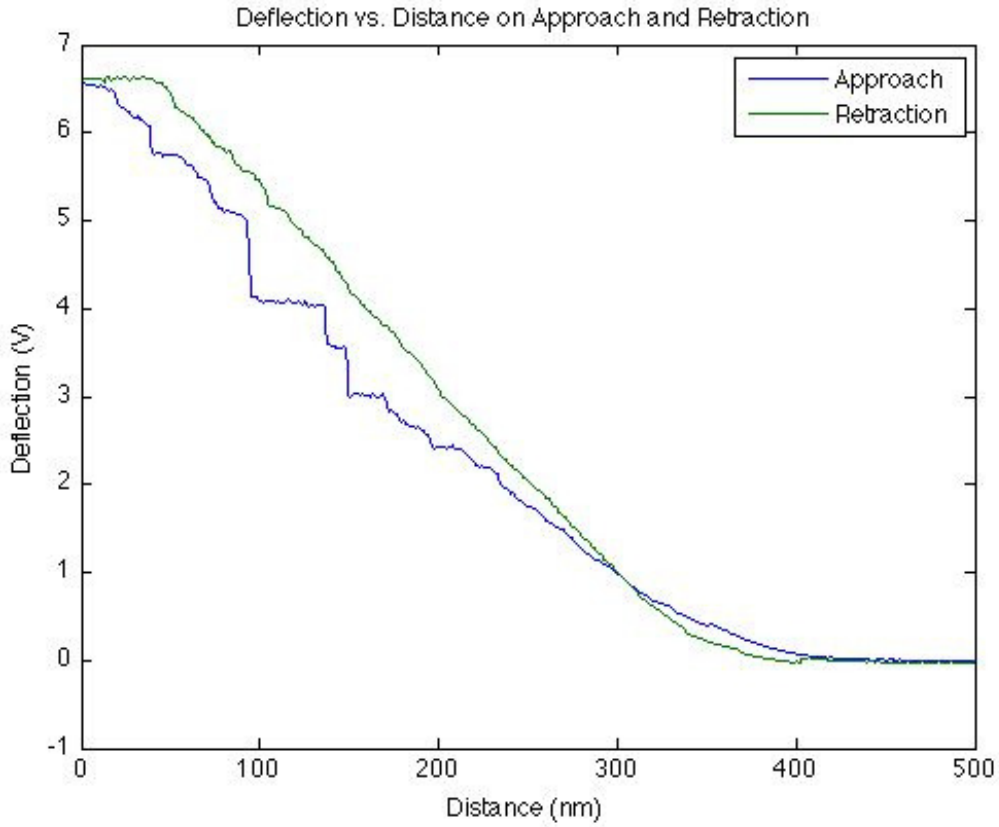
Deflection vs. Distance on Approach and Retraction
Approach
Retraction
Deflection (V)
Distance (nm)
7
6
5
4
3
2
1
0
-1
0
100
200
300
400
500

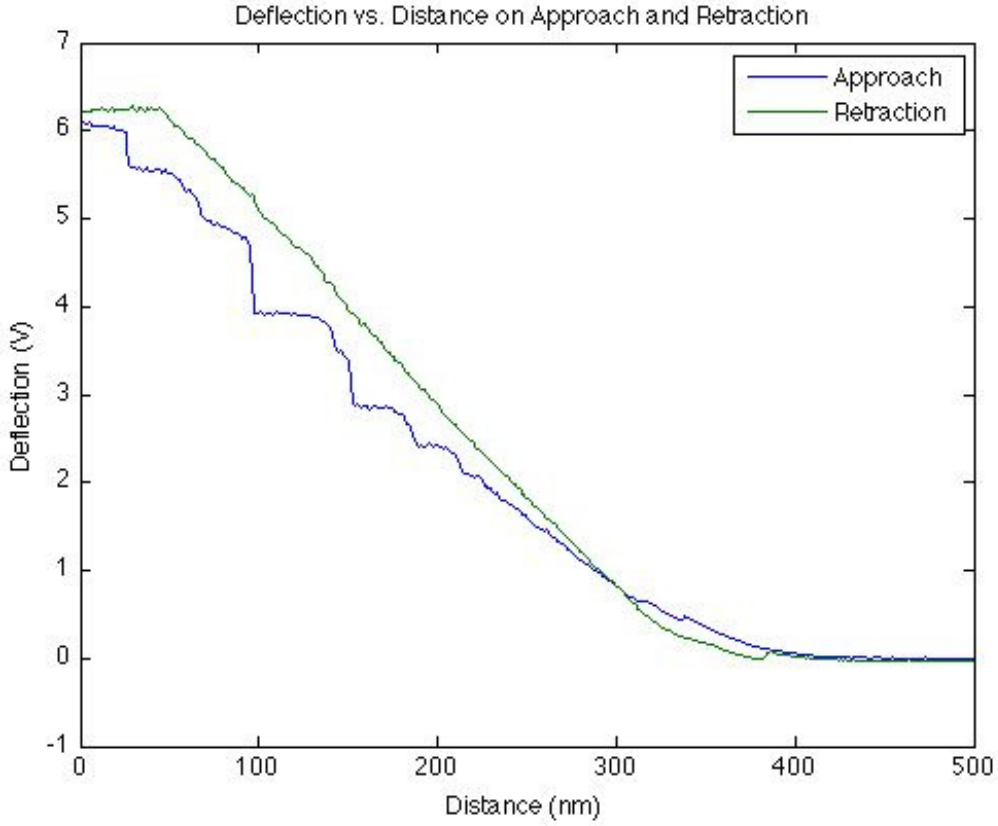
Deflection vs. Distance on Approach and Retraction
Approach
Retraction
Deflection (V)
Distance (nm)
7
6
5
4
3
2
1
0
-1
0
100
200
300
400
500

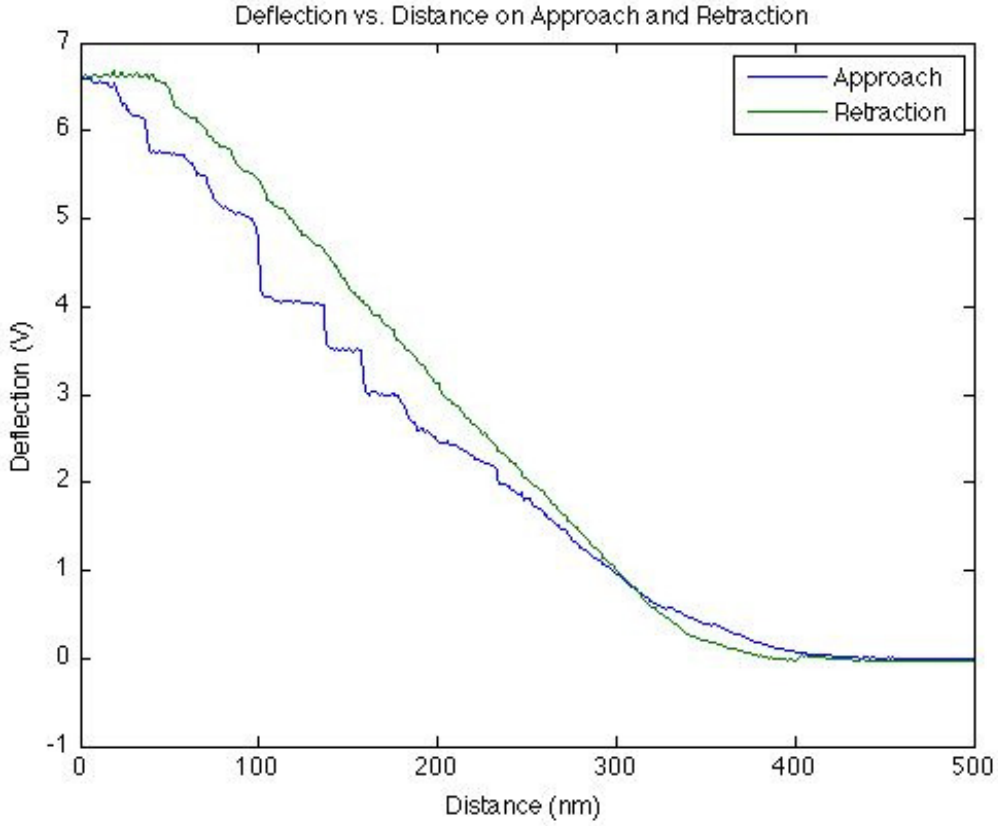
Deflection vs. Distance on Approach and Retraction
Approach
Retraction
Deflection (V)
Distance (nm)
7
6
5
4
3
2
1
0
-1
0
100
200
300
400
500

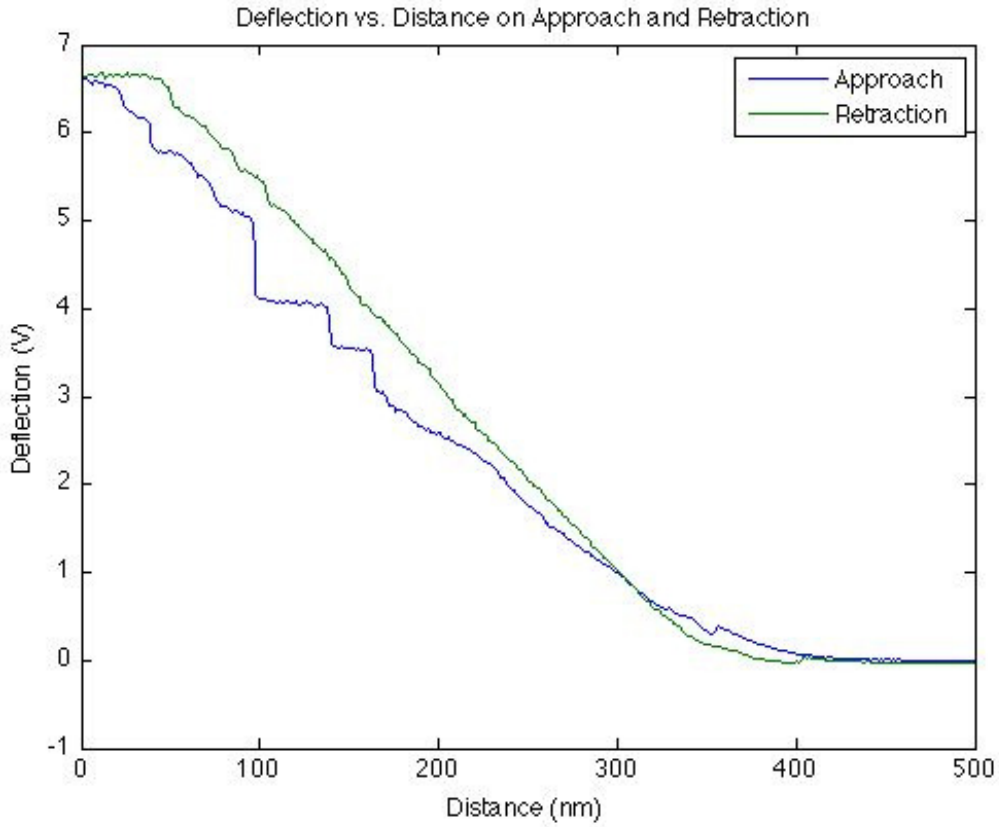
Deflection vs. Distance on Approach and Retraction
Approach
Retraction
Deflection (V)
Distance (nm)
7
6
5
4
3
2
1
0
-1
0
100
200
300
400
500

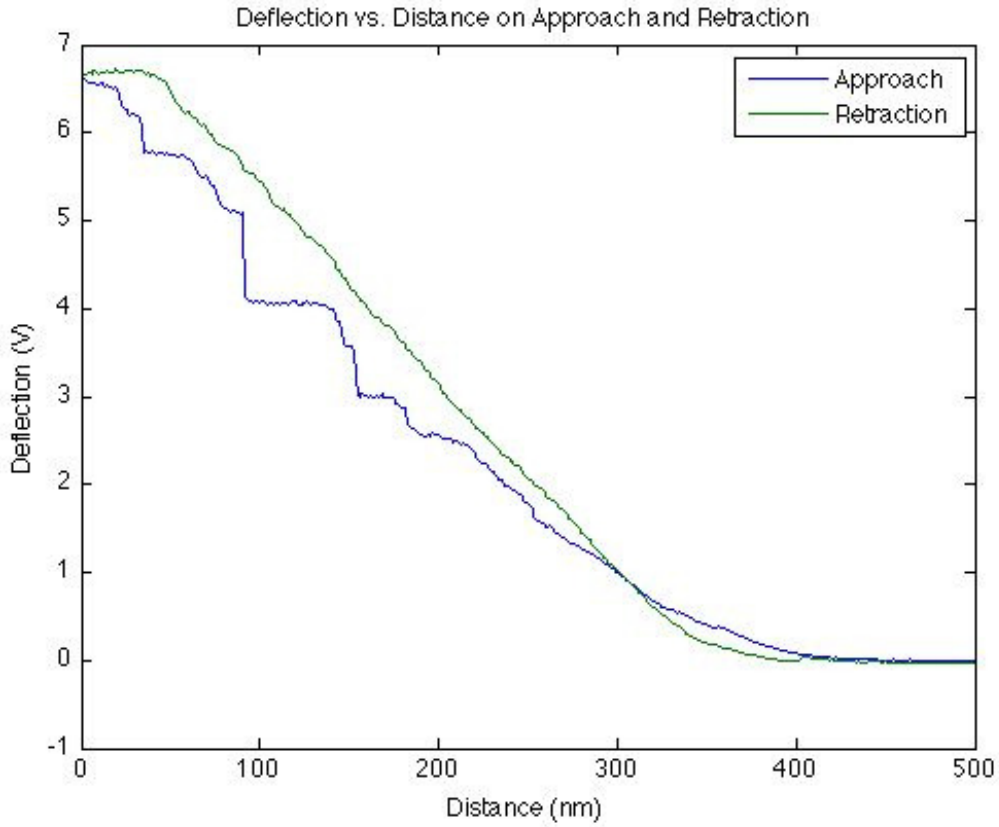
Deflection vs. Distance on Approach and Retraction
Approach
Retraction
Deflection (V)
Distance (nm)
7
6
5
4
3
2
1
0
-1
0
100
200
300
400
500

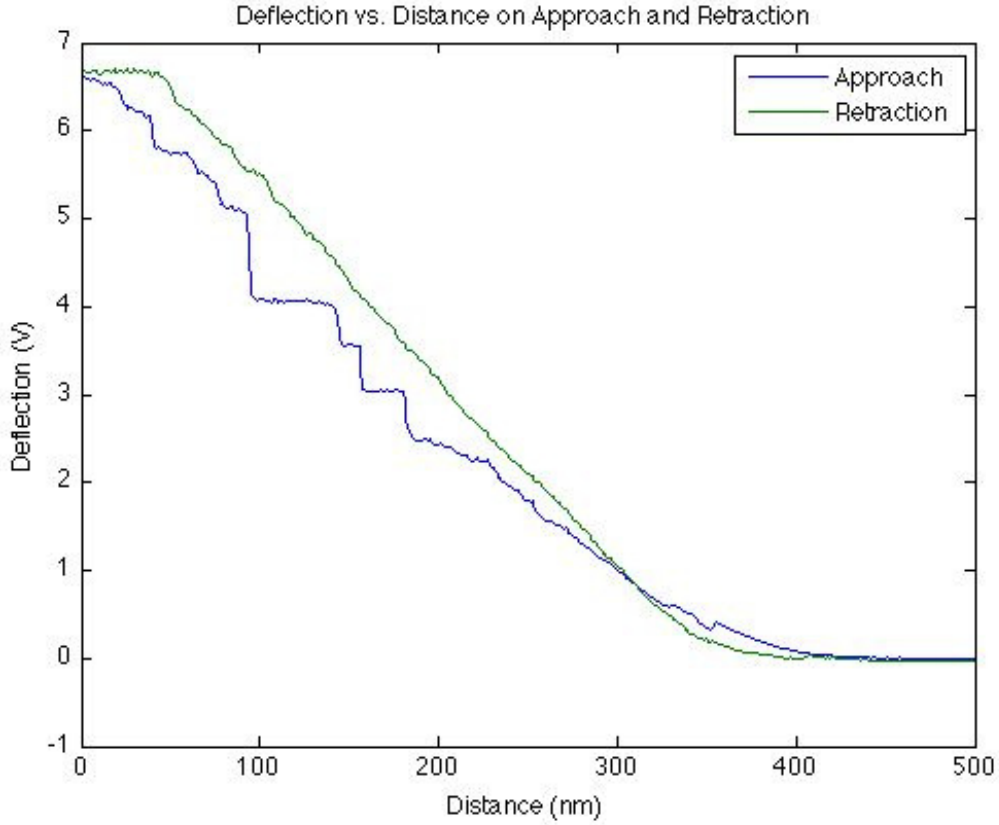
Deflection vs. Distance on Approach and Retraction
Approach
Retraction
Deflection (V)
Distance (nm)
7
6
5
4
3
2
1
0
-1
0
100
200
300
400
500

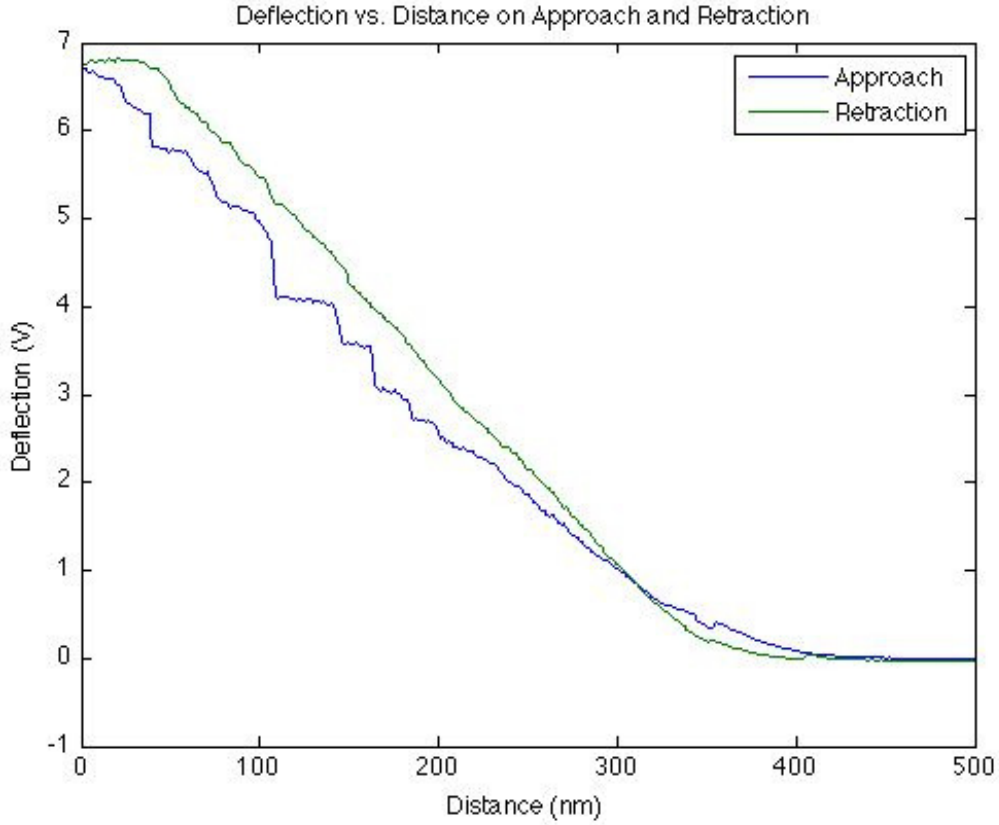
Deflection vs. Distance on Approach and Retraction
Approach
Retraction
Deflection (V)
Distance (nm)
7
6
5
4
3
2
1
0
-1
0
100
200
300
400
500

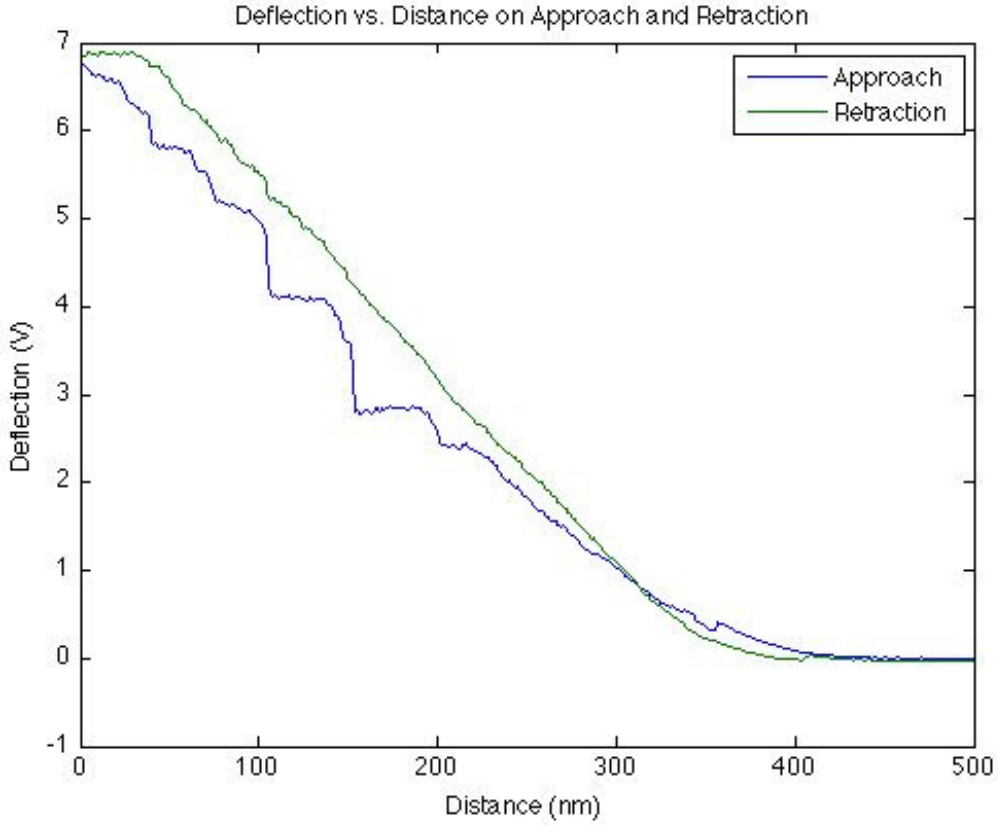
Deflection vs. Distance on Approach and Retraction
Approach
Retraction
Deflection (V)
Distance (nm)
7
6
5
4
3
2
1
0
-1
0
100
200
300
400
500

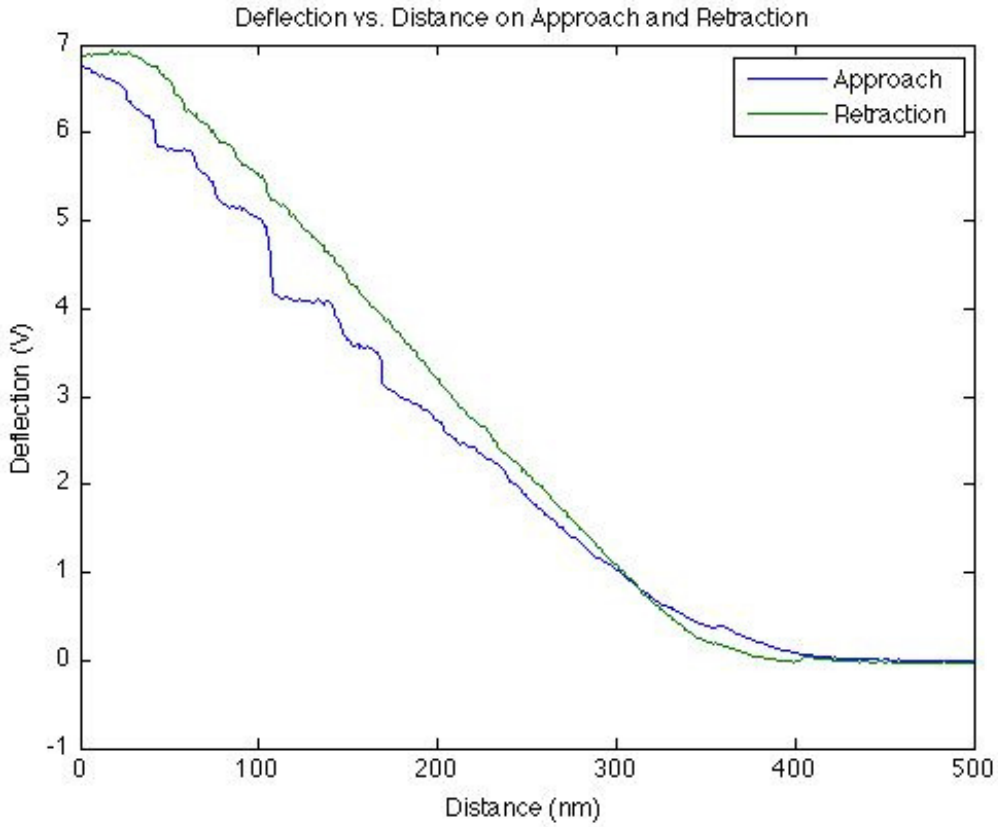
Deflection vs. Distance on Approach and Retraction
Approach
Retraction
Deflection (V)
Distance (nm)
7
6
5
4
3
2
1
0
-1
0
100
200
300
400
500

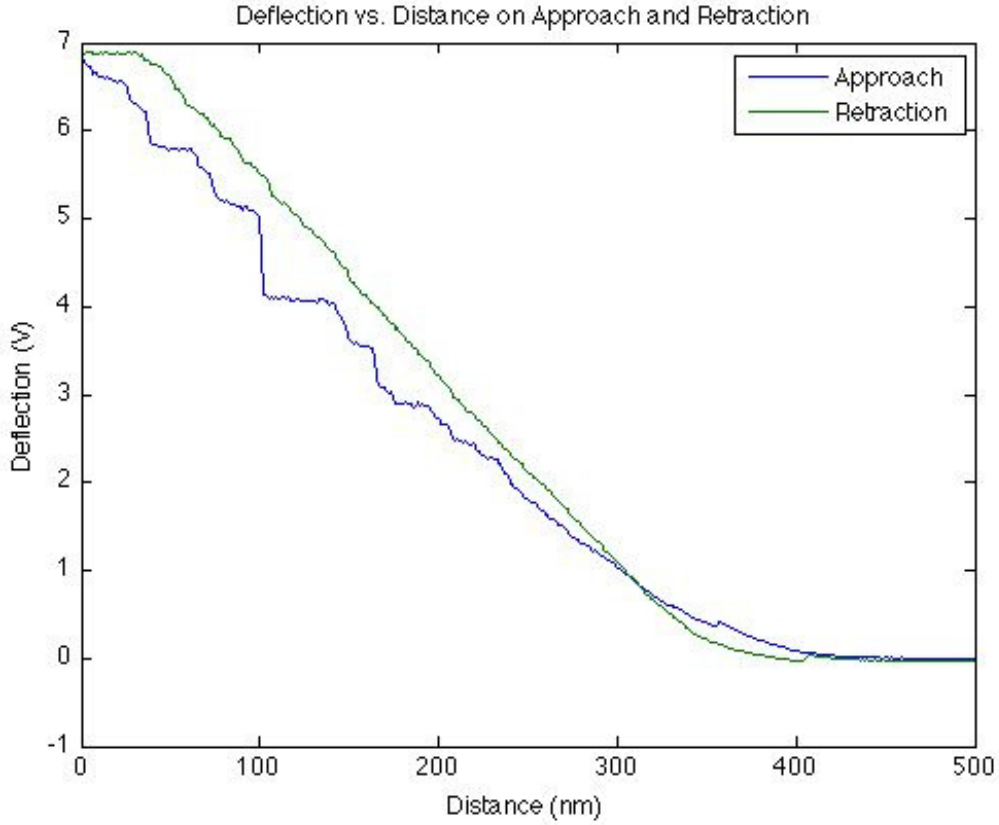
Deflection vs. Distance on Approach and Retraction
Approach
Retraction
Deflection (V)
Distance (nm)
7
6
5
4
3
2
1
0
-1
0
100
200
300
400
500

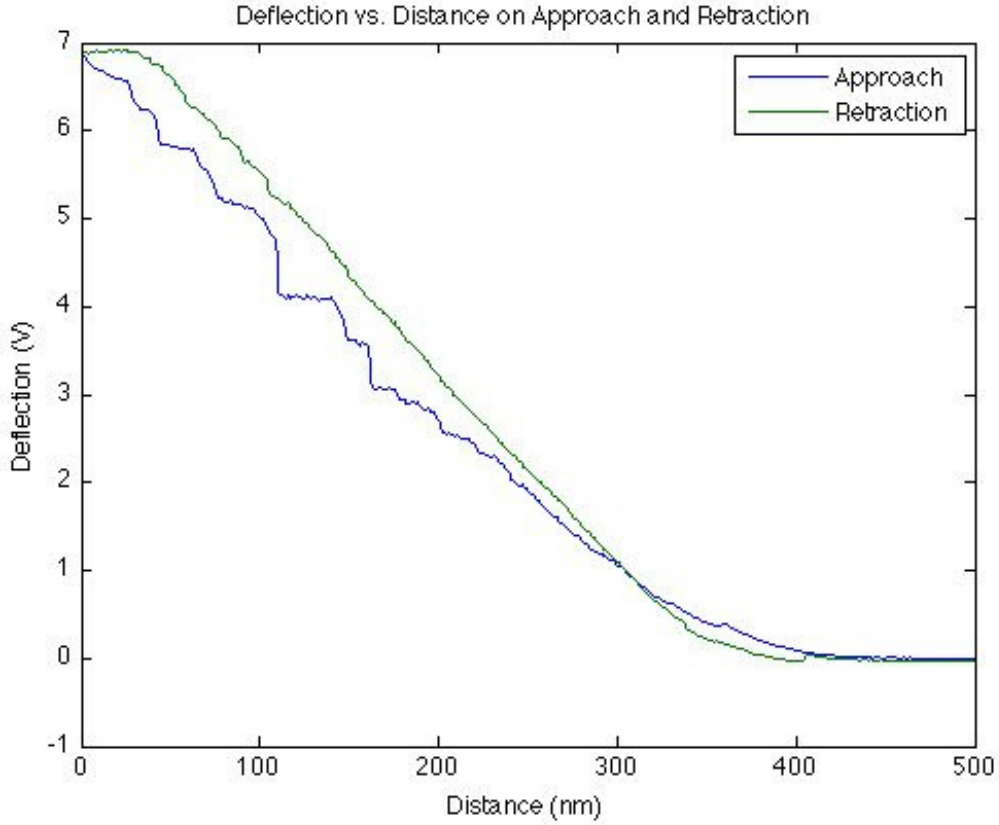
Deflection vs. Distance on Approach and Retraction
Approach
Retraction
Deflection (V)
Distance (nm)
7
6
5
4
3
2
1
0
-1
0
100
200
300
400
500

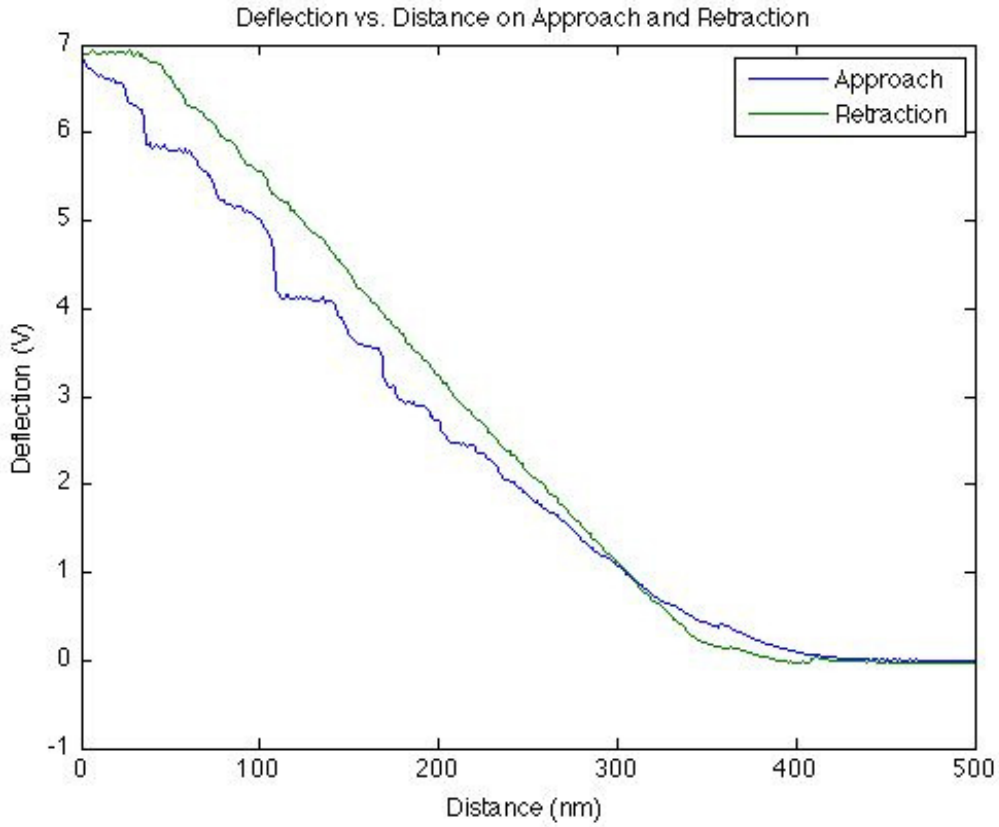
Deflection vs. Distance on Approach and Retraction
Approach
Retraction
Deflection (V)
Distance (nm)
7
6
5
4
3
2
1
0
-1
0
100
200
300
400
500

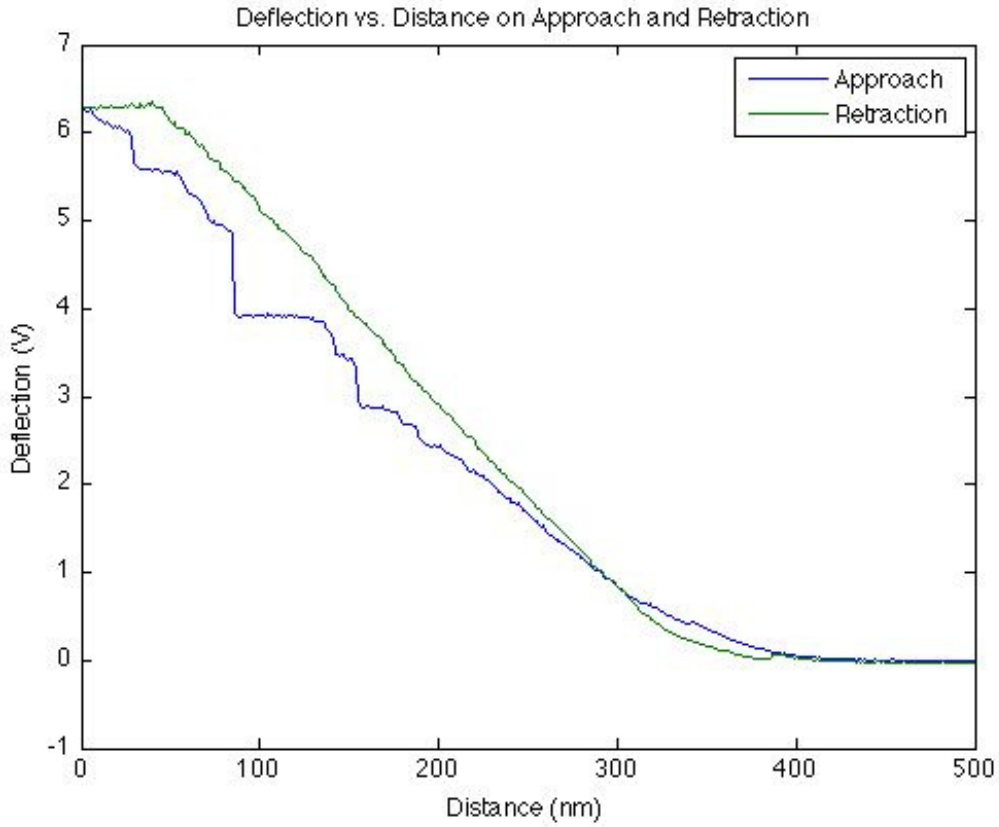
Deflection vs. Distance on Approach and Retraction
Approach
Retraction
Deflection (V)
Distance (nm)
7
6
5
4
3
2
1
0
-1
0
100
200
300
400
500

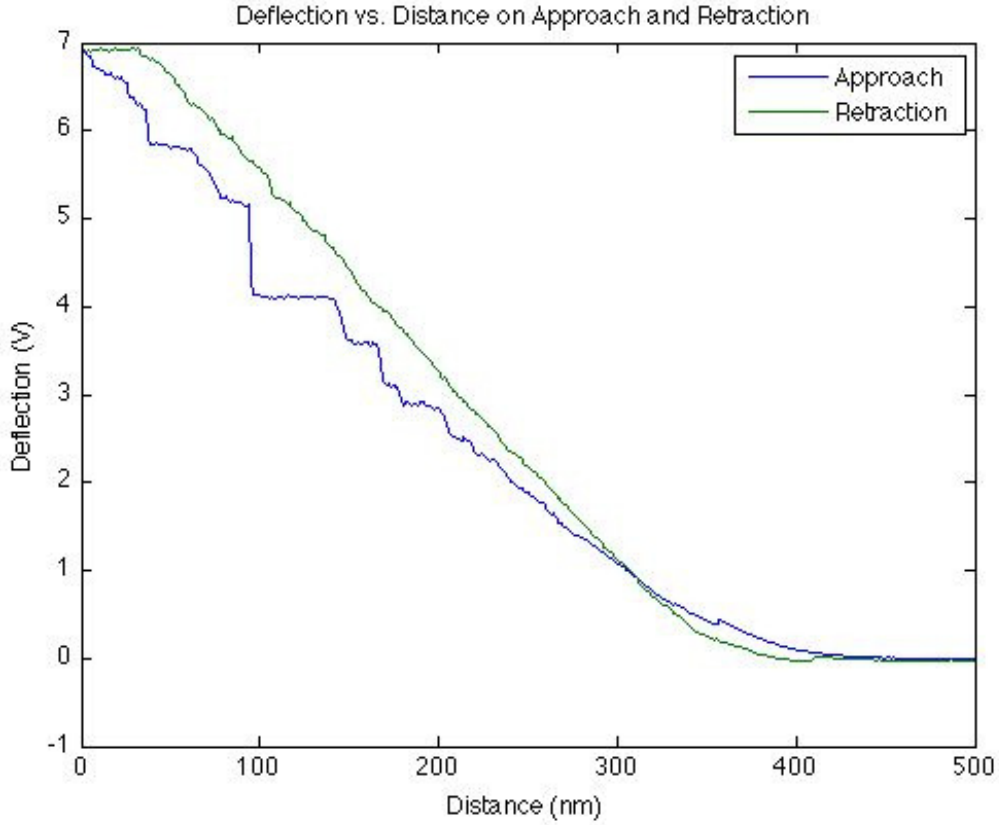
Deflection vs. Distance on Approach and Retraction
Approach
Retraction
Deflection (V)
Distance (nm)
7
6
5
4
3
2
1
0
-1
0
100
200
300
400
500

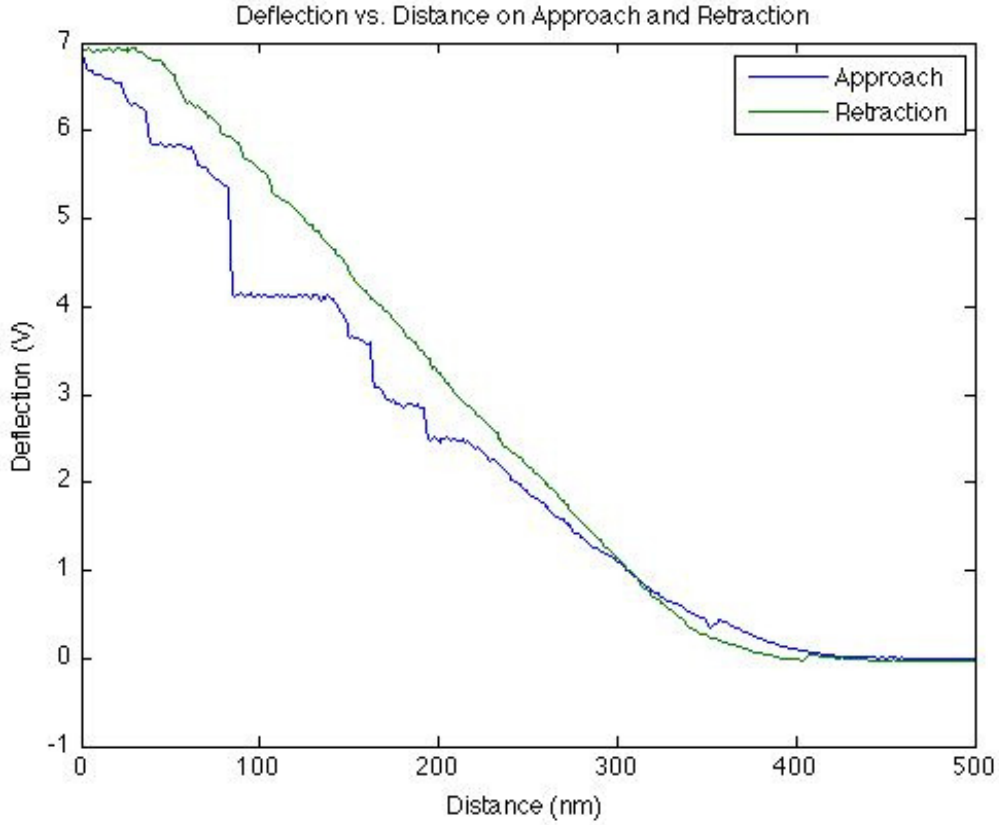
Deflection vs. Distance on Approach and Retraction
Approach
Retraction
Deflection (V)
Distance (nm)
7
6
5
4
3
2
1
0
-1
0
100
200
300
400
500

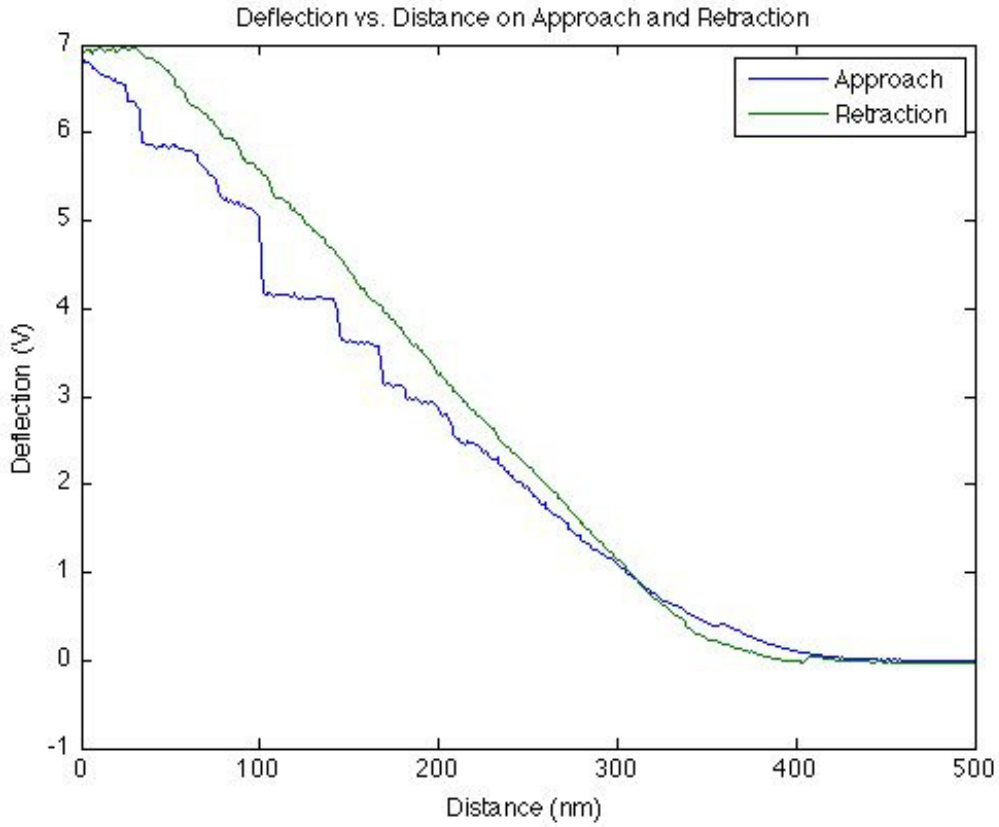
Deflection vs. Distance on Approach and Retraction
Approach
Retraction
Deflection (V)
Distance (nm)
7
6
5
4
3
2
1
0
-1
0
100
200
300
400
500

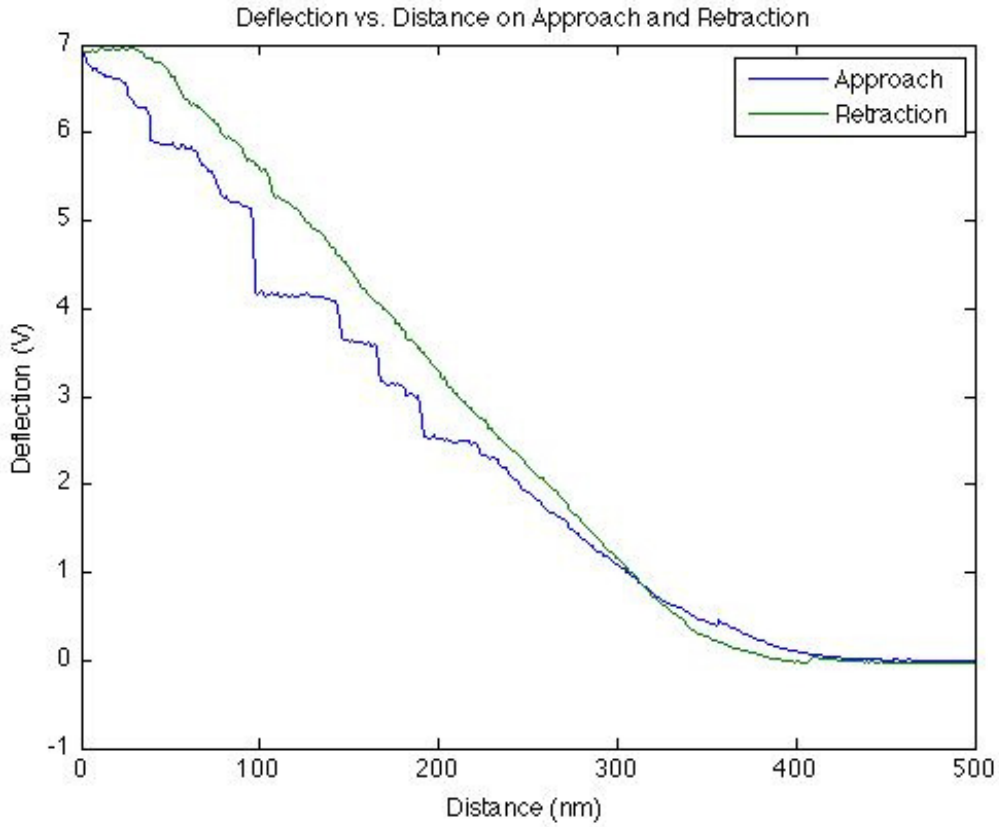
Deflection vs. Distance on Approach and Retraction
Approach
Retraction
Deflection (V)
Distance (nm)
7
6
5
4
3
2
1
0
-1
0
100
200
300
400
500

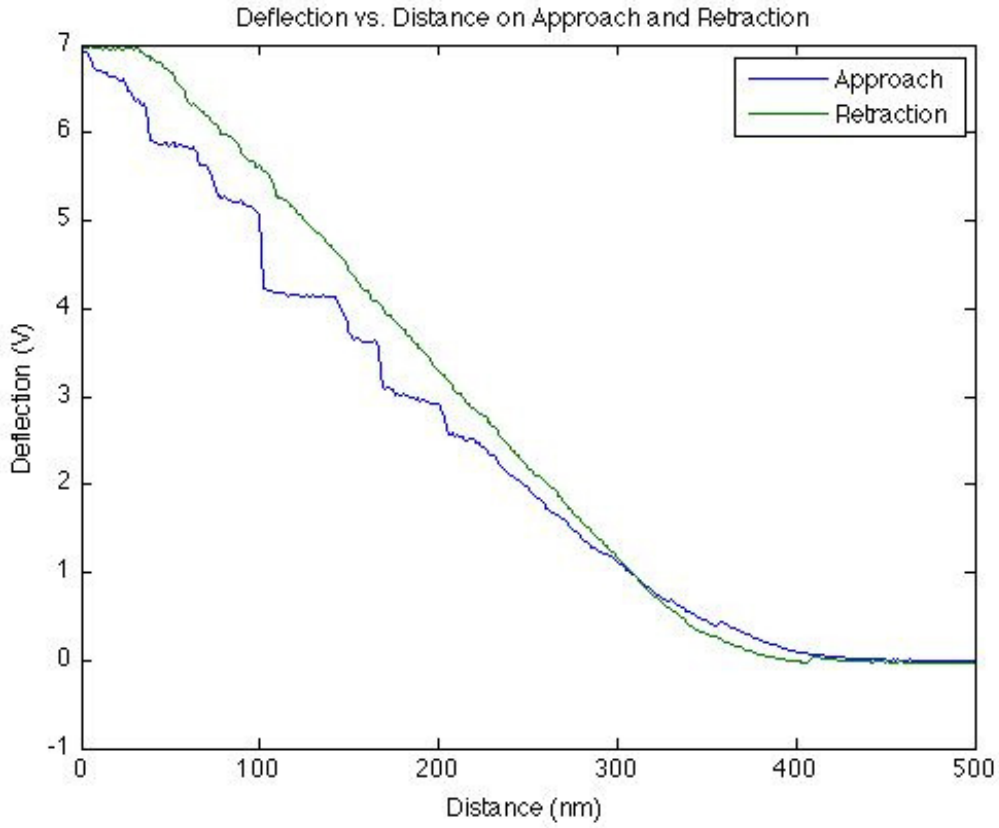
Deflection vs. Distance on Approach and Retraction
Approach
Retraction
Deflection (V)
Distance (nm)
7
6
5
4
3
2
1
0
-1
0
100
200
300
400
500

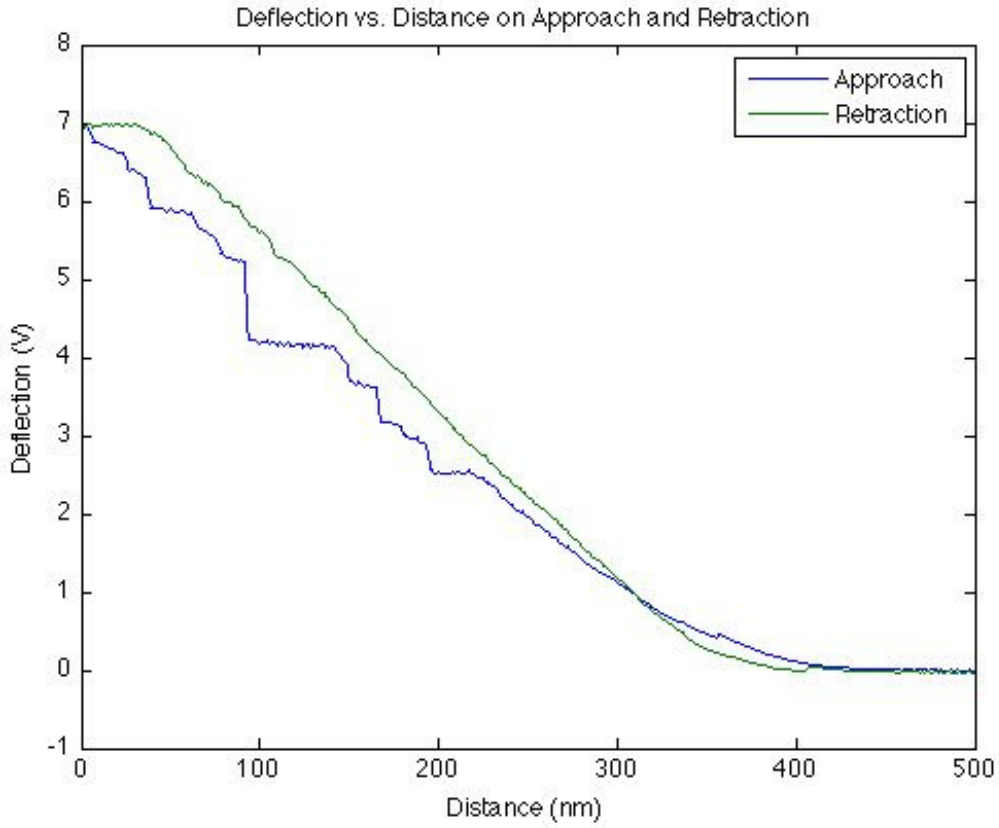
Deflection vs. Distance on Approach and Retraction
Approach
Retraction
Deflection (V)
Distance (nm)
8
7
6
5
4
3
2
1
0
-1
0
100
200
300
400
500

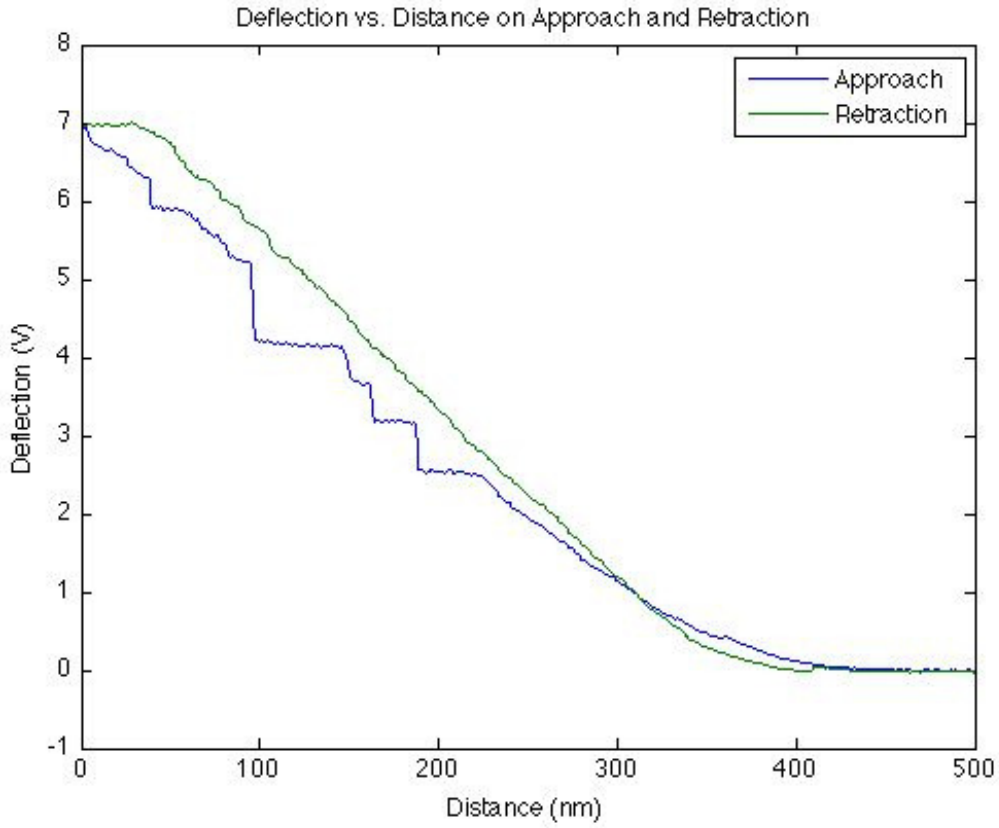
Deflection vs. Distance on Approach and Retraction
Approach
Retraction
Deflection (V)
Distance (nm)
8
7
6
5
4
3
2
1
0
-1
0
100
200
300
400
500

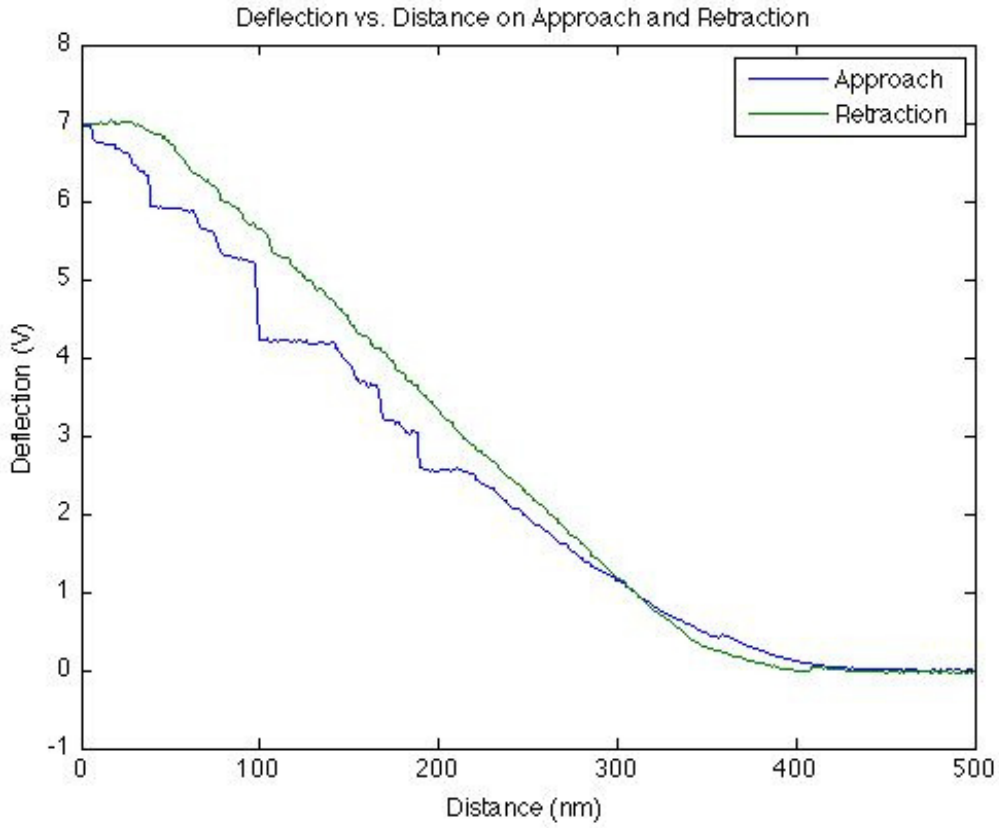
Deflection vs. Distance on Approach and Retraction
Approach
Retraction
Deflection (V)
Distance (nm)
8
7
6
5
4
3
2
1
0
-1
0
100
200
300
400
500

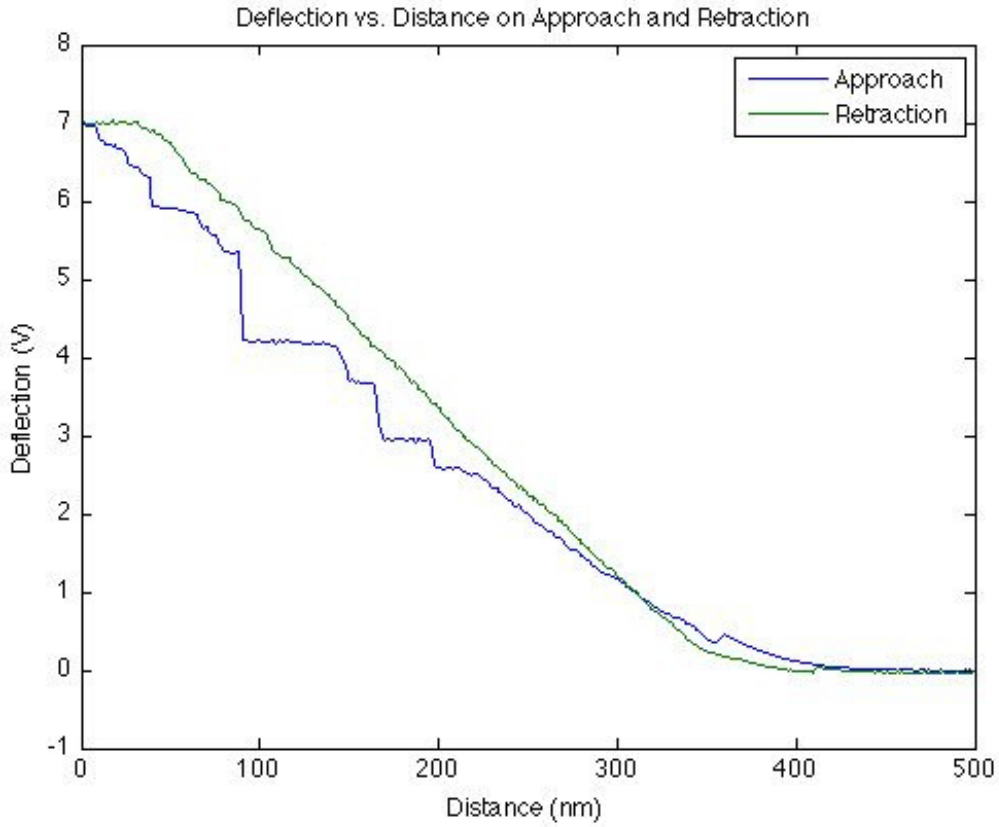
Deflection vs. Distance on Approach and Retraction
Approach
Retraction
Deflection (V)
Distance (nm)
8
7
6
5
4
3
2
1
0
-1
0
100
200
300
400
500

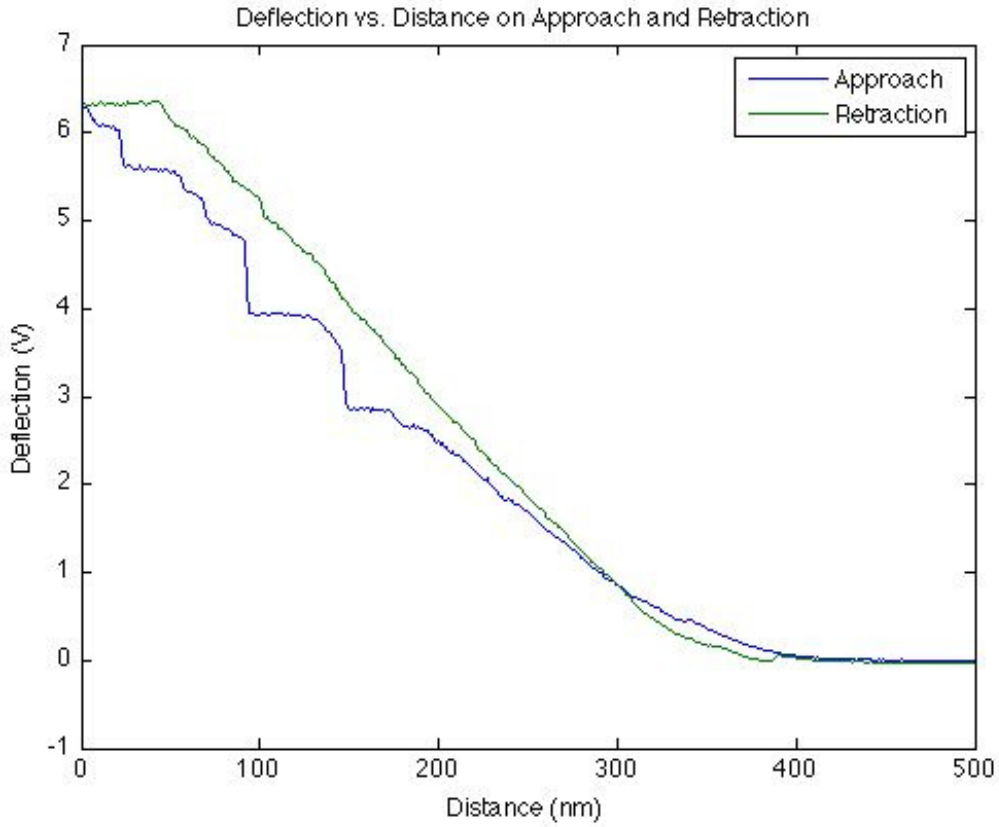
Deflection vs. Distance on Approach and Retraction
Approach
Retraction
Deflection (V)
Distance (nm)
7
6
5
4
3
2
1
0
-1
0
100
200
300
400
500

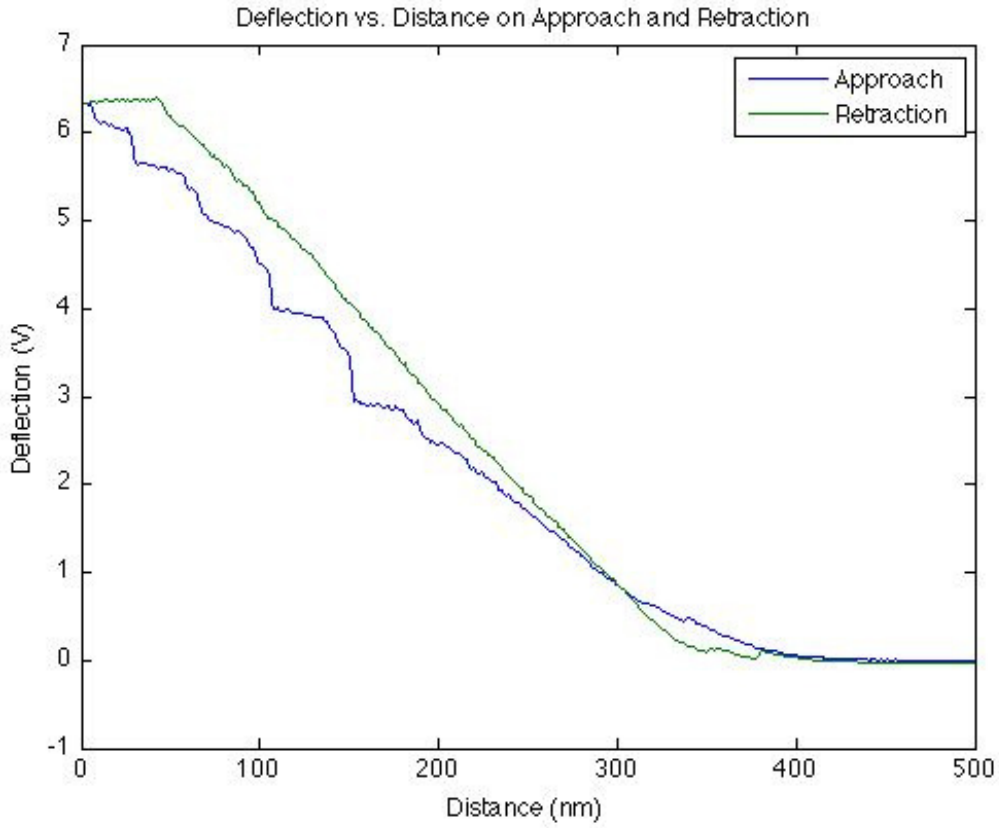
Deflection vs. Distance on Approach and Retraction
Approach
Retraction
Deflection (V)
Distance (nm)
7
6
5
4
3
2
1
0
-1
0
100
200
300
400
500

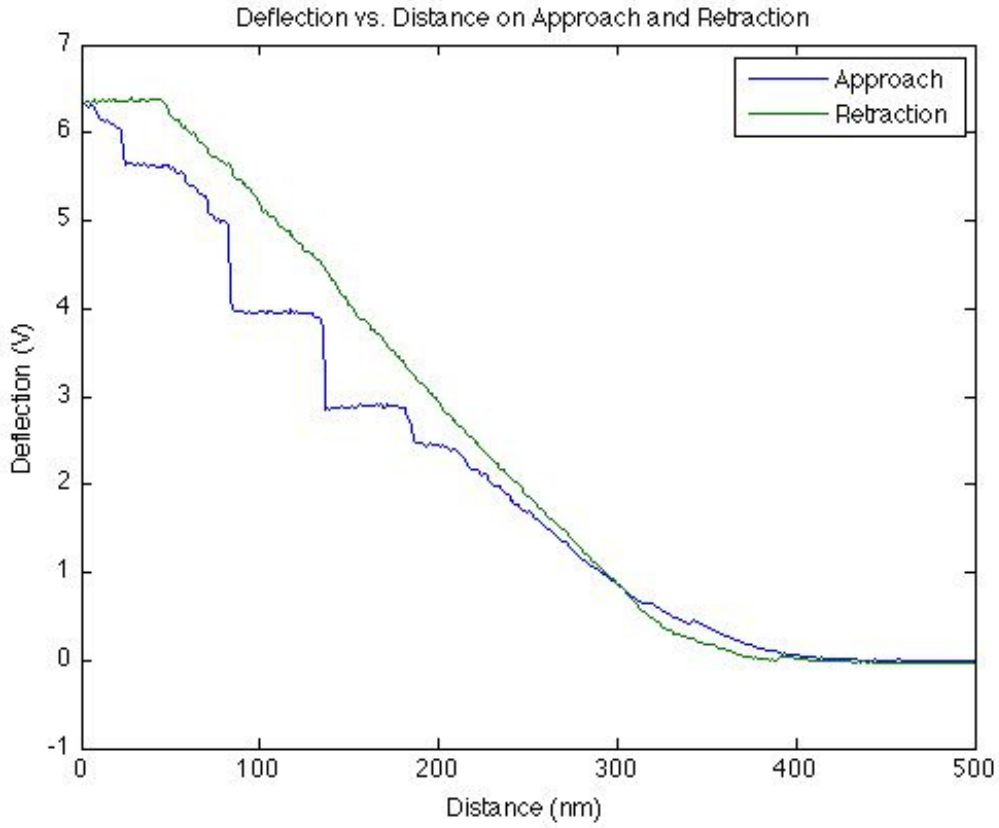
Deflection vs. Distance on Approach and Retraction
Approach
Retraction
Deflection (V)
Distance (nm)
7
6
5
4
3
2
1
0
-1
0
100
200
300
400
500

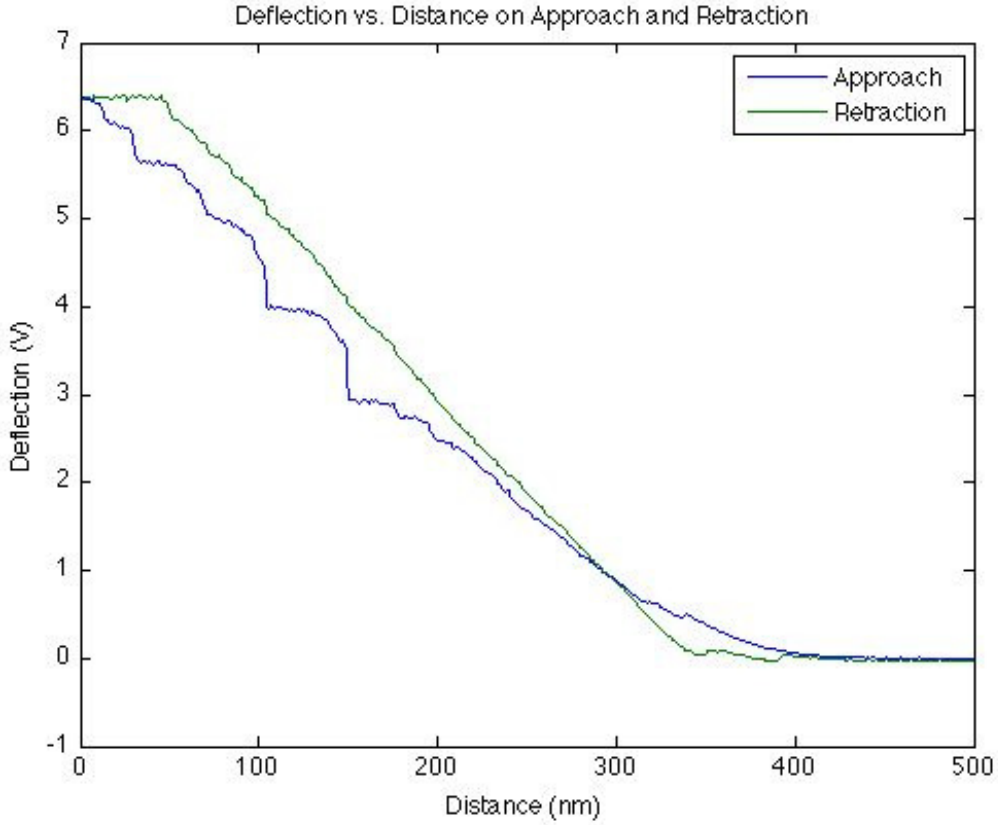
Deflection vs. Distance on Approach and Retraction
Approach
Retraction
Deflection (V)
Distance (nm)
7
6
5
4
3
2
1
0
-1
0
100
200
300
400
500

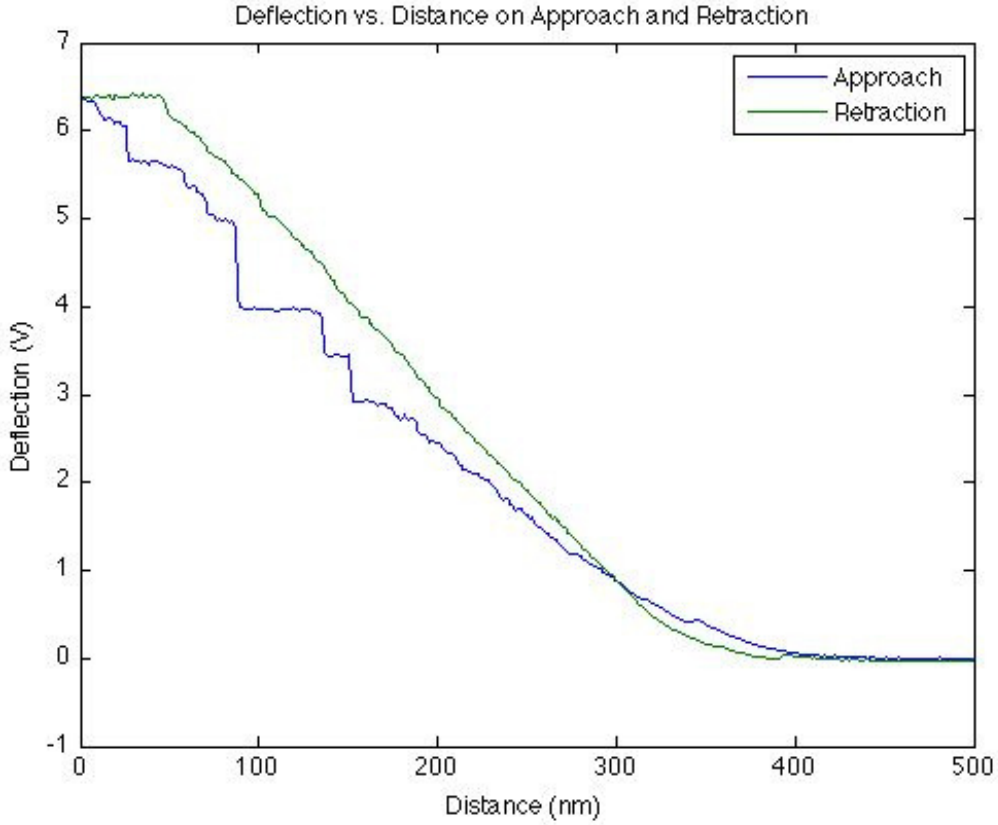
Deflection vs. Distance on Approach and Retraction
Approach
Retraction
Deflection (V)
Distance (nm)
7
6
5
4
3
2
1
0
-1
0
100
200
300
400
500

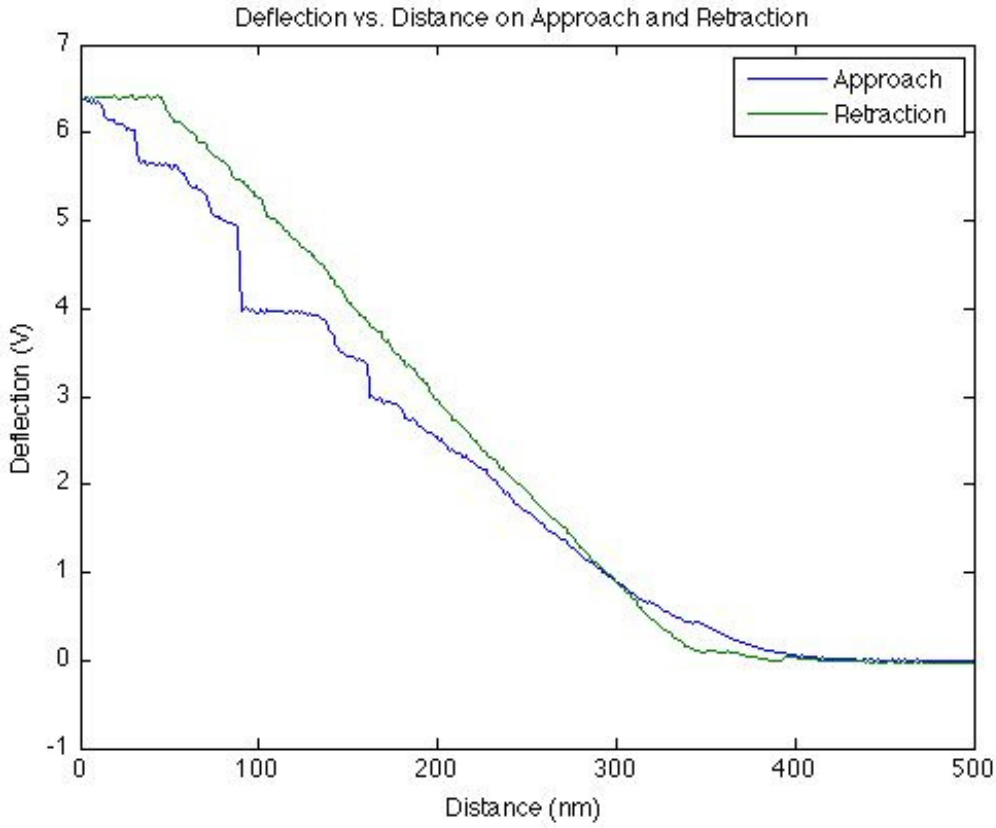
Deflection vs. Distance on Approach and Retraction
Approach
Retraction
Deflection (V)
Distance (nm)
7
6
5
4
3
2
1
0
-1
0
100
200
300
400
500